

**DISCOVERY OF NOVEL DRUGS WITH TISSUE AND CELL-TYPE
SELECTIVITY FOR CANCER AND INFLAMMATION**

A Dissertation
Presented to
The Academic Faculty

by

Bocheng Wu

In Partial Fulfillment
of the Requirements for the Degree
Doctor of Philosophy in the
School of Chemistry and Biochemistry

Georgia Institute of Technology
May 2021

COPYRIGHT © 2021 BY BOCHENG WU

NOVEL DRUG DISCOVERY LINK TO CANCER AND INFLAMMATION WITH TISSUE AND CELL-TYPE SELECTIVITY

Approved by:

Dr. Adegboyega Oyelere, Advisor
School of Chemistry and Biochemistry
Georgia Institute of Technology

Dr. Amit Reddi
School of Chemistry and Biochemistry
Georgia Institute of Technology

Dr. M.G. Finn
School of Chemistry and Biochemistry
Georgia Institute of Technology

Dr. Loren Williams
School of Chemistry and Biochemistry
Georgia Institute of Technology

Dr. Stefan France
School of Chemistry and Biochemistry
Georgia Institute of Technology

Date Approved: [Apr. 5th 2021]

To my lovely wife and my Families.

ACKNOWLEDGEMENTS

At the very beginning of my Ph.D. study, when I waited outside of the room of original proposal exam, I prayed to God to bless me on my road of research, guide me through all the challenges, lead me towards the mission of life-saving. Through 6 years of training in cancers and fibrosis related research, I deeply recognized that I was blessed, as we discovered many break-through outcomes that may prevent or reverse the development of the lethal diseases in patients. I am grateful to God's blessing in providing me all spiritual powers to persist on this road.

After the first time we met in Dr.Oyelere's office, I decided to join the lab with no hesitation because I believed he could be my first choice, with interesting research focuses and welcoming personality. I will never forget the words Dr.Oyelere spoke to me in my darkest time in the pursuit of my Ph.D. I must express my appreciation to Dr. Oyelere as my principal investigator in research and my close friend in my life. He supported me in my experiments based on his experience, and encouraged me spiritually on my innovative thoughts. Through his guidance, I gradually understood the process of drug discovery, developed my original ideas of drug discovery, and learned to write proposal and publications. He also gave me the warm-hearted cares in my life, prayed for me and my wife like we are families. With all his amazing supports, I confidently regard myself as a well-trained scientist. Thank you, Dr.Oyelere!

I would like to thank my Committees Dr. M.G. Finn, Dr. Amit Reddi, Dr. Stefan France, and Dr. Loren Williams for their valuable guidance and collaborations in research. Specifically, I want to thank Dr. Finn for his collaboration with us, and his recommendation in job position for me. I also want to thank Dr. France for the trust and patience in the COX project collaboration, and his effort in job searching for me. Dr.Reddi had supported me with a lot of encouragement and suggestions

in my class, my research, and my job searching. I would also thank Dr. Williams for his encouragement in my life. I will never forget the words you spoke to me in my original proposal.

My thanks go to Dr. Idris Raji, Dr. Subhasish Tapadar, Dr. Shay Fathi, and Dr. Berkley Gryder as my previous colleagues. Idris is a nice person that he is always very supportive, and provides good career advice. Shay always shared her experiences with me and guided me with advice regard my future as a postdoc research and immigration issues. Subhasish is a knowledgeable scientist with rich experience in synthesis. I could not complete the projects so efficiently without his help. Although I did not meet Berkley, we had virtual conversations and he recommended me to his colleagues as my future postdoc mentor. I sincerely thank you for your helps!

I want to thank my collaborators Dr. Jang and his lab members Mohiudin Mahir, Shannon Anderson, Jeong Gunjae, and Nanhee Lee for their efforts in guiding me with Western blot, PCR, *in vivo* experiments such as drug administration, tissue harvest, and histology studies. It has been the very important and precious experience in working with you all.

I want to give my deepest gratitude to my wife, Kaixin Yang. You are always with me, prays for me, encourages me, and never condemns me no matter how difficult our situation was. I know that I could never succeed without you. Supports and understandings from you is the most powerful motivation in every morning. Your love calm my heart in research and daily life. I regret that I did not spend much time with you in most of weekends. Thanks for your understanding and love!

Lastly, I want to give my special thanks to my families. My parents and grand parents shaped me as a open-minded person who loves science. I sincerely thank my parents for their financial and spirtual supports, which have significantly helped to guide and focus me in my quest for knowledge.

TABLE OF CONTENTS

ACKNOWLEDGEMENTS	4
LIST OF TABLES	10
LIST OF FIGURES	12
LIST OF SYMBOLS AND ABBREVIATIONS	16
SUMMARY OF RESEARCH	23
Chapter 1. Introduction of the linkage between tissue inflammation and cancer	26
1.1 Introduction :	26
1.2 Inflammation and its causes.	27
1.3 Inflammation and Tissue fibrosis	28
1.3.1 Idiopathic pulmonary fibrosis (IPF)	28
1.3.2 IPF Pathogenesis	29
1.4 Inflammation and tumorigenesis	30
1.4.1 Cancer types linked to chronic tissue inflammation	30
1.5 Major inflammation pathways in tumor progression and tissue fibrosis	34
1.5.1 TGF- β pathway and inflammation-induced carcinogenesis	34
1.5.2 TNF-alpha, NF- κ B pathway and inflammation	37
1.5.3 JAK-STAT pathway and inflammation	39
1.5.4 Arachidonic acid metabolism pathway and inflammation	43
1.5.5 Epigenetic pathway	47
1.6 Current medical challenges and novel solutions for targeting inflammation pathways:	50
1.6.1 Challenges with inhibition of TGF- β pathway	50
1.6.2 Challenges with NF- κ B pathway inhibition	51
1.6.3 Challenges with COX/LOX inhibition	52
1.6.4 Challenges with STAT3 inhibition	53
1.6.5 Challenges with HDAC inhibition:	53
1.7 Solutions investigated in this thesis:	54
1.7.1 Macrolides as templates for targeted delivery to liver and lung tissues	54
1.7.2 Novel STAT3 inhibitors	61
1.7.3 Novel HDAC inhibitors	62
1.8 Conclusion	65
Chapter 2. Macrolide-derived Anti-Fibrotic and Anti-inflammatory Agents	82
2.1 Introduction	84
2.2 Results	87
2.2.1 Design and molecular docking	87
2.2.2 Chemistry:	96
2.2.3 Cell cytotoxicity study	101
2.2.4 Effect of lead macrolide-PFD compounds on NF- κ B pathway	106

2.2.5	Effect of macrolide-PFD compounds on Pro-COL1A1 expression	108
2.2.6	Effect of lead macrolide-PFD compounds on TGF- β pathway	109
2.2.7	Intracellular target validation study	111
2.3	Conclusion	117
2.4	Materials and methods	119
2.4.1	Materials	119
2.4.2	Synthesis	119
2.4.3	Cell culture	150
2.4.4	MTS assay	151
2.4.5	Anti-inflammatory activity assay (NF- κ B inhibition assay)	151
2.4.6	Human Pro-collagen ELISA kit	152
2.4.7	Western blot	152
2.4.8	Bioassay (TGF- β pathway inhibition)	153
2.5	Reference:	154
2.6	Supporting Information	161

Chapter 3. Structural modification of antioxidants with macrolide conjugation enhanced anti-cancer and anti-fibrosis effect

3.1	Introduction	230
3.2	Results	232
3.2.1	Conjugation design	232
3.2.2	Cell cytotoxicity	244
3.2.3	Anti-fibrotic effects macrolide-antioxidant conjugates	249
3.2.4	Investigation of the mechanisms of the antiproliferative effects of macrolide-antioxidant conjugates.	256
3.3	Conclusion:	262
3.4	Materials and methods	263
3.4.1	Materials:	263
3.4.2	Synthesis:	264
3.4.3	Cell culture	288
3.4.4	MTS assay	289
3.4.5	Western blot	289
3.5	Reference:	290
3.6	Supporting information	293

Chapter 4. Discovery of a Novel Clarithromycin Derivative with Eukaryotic Ribosome Inhibition and Anti-cancer Activity

4.1	Introduction:	338
4.2	Result and Discussion:	340
4.2.1	Chemistry	340
4.2.2	Effects of AO-02-63 on the prokaryotic and eukaryotic protein translation	346
4.2.3	Anti-cancer effects of AO-02-63	354
4.2.4	Anti-inflammation effect of AO-02-63	356
4.3	Conclusion:	359
4.4	Material and methods	360
4.4.1	Synthesis:	360
4.4.2	Cell culture and viability assay.	368

4.4.3	X-ray crystallography:	369
4.4.4	Translation inhibition assay:	369
4.4.5	Pull-down assay and mass spectroscopy:	371
4.5	Reference:	372
4.6	Supporting Information	376

Chapter 5. Pyrimethamine Conjugated Histone Deacetylase inhibitors: Design, Synthesis and Evidence for Triple Negative Breast Cancer Selective Cytotoxicity.

5.1	Introduction:	387
5.2	Results and discussion	390
5.2.1	Design of PYM-HDACi compounds	390
5.2.2	Molecular docking study	392
5.2.3	Chemistry	399
5.2.4	HDAC inhibition study	402
5.2.5	Anti-proliferative activity	403
5.2.6	Intracellular target validation	406
5.2.7	Flow Cytometry for Cell Cycle Analysis.	411
5.3	Conclusion	413
5.4	Experimental section	413
5.4.1	Materials and methods	413
5.4.2	Cell culture and viability assay	425
5.4.3	In vitro HDAC inhibition assay.	426
5.4.4	Western blots analysis.	426
5.4.5	Flow cytometry	427
5.5	References	427
5.6	Supporting Information	433

Chapter 6. Discovery of Novel STAT3 DNA Binding Domain Inhibitors.

6.1	Introduction	473
6.2	Results and Discussion	475
6.2.1	Design of PYM-based novel STAT3 inhibitors and molecular docking	475
6.2.2	Chemistry.	479
6.2.3	Cell cytotoxicity	484
6.2.4	Intracellular target validation	486
6.2.5	STAT3 DNA binding inhibition	488
6.2.6	Cell cycle analysis by flow cytometry	491
6.3	Conclusion	492
6.4	Material and methods	493
6.4.1	Materials:	493
6.4.2	Synthesis	495
6.4.3	Cell culture and viability assay	511
6.4.4	Western blots analysis	511
6.4.5	STAT3 DNA-Binding ELISA Assay	512
6.4.6	Flow cytometry	513
6.5	Reference	514
6.6	Supporting Information	520

Chapter 7. Novel Glycosylated Histone deacetylase Inhibitors for Targeted Treatment of Hepatocellular Carcinoma	566
7.1 Introduction	568
7.2 Result	571
7.2.1 Chemistry (The synthesis described in this section was performed by Dr. Subhasish Tapadar)	571
7.2.2 Molecular docking	578
7.2.3 Anti-proliferation activity.	580
7.2.4 Hep-G2 cell line uptake glycosylated HDACi via GLUT-2	583
7.2.5 Glycosylated HDACi showed intracellular HDAC inhibition	584
7.2.6 Glycosylated HDACi induce selective Hep-G2 cell apoptosis	586
7.2.7 STR-V-53 caused cell cycle arrest at S stage	588
7.2.8 Glycosylated HDACi suppress tumor growth in murine model (This experiment was performed in collaboration with Petros lab at Emory University)	590
7.3 Conclusion	593
7.4 Materials and Methods	594
7.4.1 Materials	594
7.4.2 Synthesis	596
7.4.3 Cell Culture:	612
7.4.4 Western blots analysis	612
7.4.5 GLUT-2 uptake competition test	613
7.4.6 Flow cytometry	614
7.5 Reference:	614
7.6 Supporting information	619
VITA	649

LIST OF TABLES

Table 1.1 Inflammation associated cancer types.	31
Table 1.2. The possible heterodimers and their inflammation activator and anti-inflammation activators.	41
Table 2.1. Effect of class I compounds on cell viability. Structures of class I compounds 10a-c and 11a-c are shown atop of the Table.	102
Table 2. 2. Effect of class II compounds on cell viability. Structures of class II compounds 12a-c and 13a-c are shown atop of the Table.	102
Table 2. 3. Effect of class III compounds on cell viability. Structures of class III compounds 14a-c and 15a-c are shown atop of the Table.	103
Table 2. 4. Effect of class IV compounds and controls (PFD, AZM, CLM, and combinational treatment of PFD+AZM or PFD+CLM) on cell viability.....	104
Table 2S.1. Docking scores of all candidates on ALK-5 (PDB:5USQ). All candidates showed highly enhanced binding affinity on interaction with ALK-5.....	226
Table 2S.2. Docking scores of all candidates on p-P38 γ (PDB:1CM8). All candidates showed highly enhanced binding affinity on interaction with p-P38 γ relative to PFD or macrolides. ...	226
Table 3.1. The effects of macrolide-ALA conjugates on cell proliferation.....	245
Table 3.2. The effects of macrolide-PIPE conjugates on cell proliferation.....	247
Table 3.3. The effects of macrolide-fumarate conjugates on cell proliferation.....	248
Table 4.1. Major proteins pulled down by Biotin-63 based on mass spectroscopy PSM score ranking.....	352
Table 4. 2. The list of all ribosomal proteins pulled down by Biotin-63.....	352
Table 4. 3. Cell growth inhibitory activity (IC ₅₀ in μ M) of AO-02-63 in selected cancer and healthy cell lines..	355
Table S4. 1. Compare of PSM scores on top ribosomal proteins pulled down by Biotin-CLM and Biotin-63.	377
Table 5.1: HDAC inhibition activities of PYM-HDACi compounds (IC ₅₀ in μ M).....	403

Table 5. 2. Anti-proliferative activity of PYM-HDACi compounds (IC ₅₀ in μ M).....	405
Table 6. 1. Cytotoxicity of the Novel PYM-derivatives.....	485
Table 6S.1. Docking score of 11b and controls on P1 and P2 postions of DBD domain.....	520
Table 7.1. IC ₅₀ of anti-proliferation effects of glycosylated HDACi.....	581

LIST OF FIGURES

Figure 1.1. The 5-year survival percentage of IPF relative to several types of cancers..	29
Figure 1.2. TGF- β pathway in cancer and inflammation.....	36
Figure 1.3. Cell signaling and pathways of NF- κ B-mediated inflammation.....	38
Figure 1.4. General cellular signaling for STAT protein activation and transcription	40
Figure 1.5. COX pathways and following prostaglandin products.....	44
Figure 1.6. HDACs and HATs mechanism of action in chromatin.	47
Figure 1.7. Selected HDACi.	49
Figure 1.8. General structures of macrolide-based PFD-like compounds.	57
Figure 1.9. Structures of ALA derivatives investigated..	59
Figure 1.10. Structures of macrolide-derived PPA and FMA agents..	59
Figure 1.11 Structure of AO-02-63 and clarithromycin (CLM).	61
Figure 1.12. Dual-acting STAT3-HDACi based on PYM.....	63
Figure 1.13. Glycosylated HDAC inhibitors structures.....	64
Figure 2.1. Designed macrolide- PFD compounds.....	88
Figure 2.2. AZM representative structures of class I-IV for molecular docking.....	90
Figure 2.3. Molecular docking analysis of macrolide-PFD compounds	93
Figure 2.4 Molecular docking analysis of macrolide-PFD compounds at the active site of ALK-5 (5USQ).	95
Figure 2.5. Effect of tested agents on NF- κ B transcriptional activity at 5 μ M	107
Figure 2.6.Effect of macrolide-PFD compounds on the production of soluble pro-collagen at various concentrations.	109
Figure 2.7. Effect of macrolide-PFD compounds on TGF- β activity using Luciferase Gene-reporter assay kit.	111

Figure 2.8. Effects of representative macrolide-PFD compounds on the expression status of COL1A1 and α -smooth actin.....	114
Figure 2.9. Compound 15c demonstrates strong anti-fibrosis effect in TGF- β stimulated MRC-5 cell line.....	117
Figure 3.1 The designed macrolide-ALA conjugates.....	234
Figure 3.2. Designed macrolide-PIPE Conjugates.....	238
Figure 3.3. Designed macrolide-fumarate conjugates.....	241
Figure 3.4. Anti-fibrotic effects of macrolide-ALA conjugates.....	252
Figure 3.5. Anti-fibrotic effects of macrolide-PIPE conjugates.....	253
Figure 3.6. Anti-fibrotic effects of macrolide-fumarate conjugates.....	255
Figure 3.7. Anti-cancer effects of ALA and its derivatives towards MDA-MB-231.....	258
Figure 3.8. The HO-1 is upregulated by the macrolide derivatives of PPA, but not Macrolide alone or PPA alone.....	260
Figure 3.9. The HO-1 is upregulated by the macrolide derivatives of MMF.....	261
Figure 4.1. Structures of representative clinically useful macrolide antibiotics, new macrolide (AO-02-63) and EM201.....	339
Figure 4.2. X-ray structure of the AO-02-63.....	343
Figure 4.3. Proposed mechanism of the conversion of CLM to AO-02-63.....	344
Figure 4.4. Translation inhibition of AO-02-63 and control inhibitors.....	348
Figure 4.5. AO-02-63 inhibits the growth of B. subtilis in disk diffusion test (disk diffusion assay).....	349
Figure 4.6. Cell growth inhibitory activity (GI_{50} in μ M) of AO-02-63 in NCI-60 panel.....	356
Figure 4.7. Anti-inflammation effect of AO-02-63 based on inhibition of ECM components production.....	358
Figure 4.8. Effects of AO-02-63 and CLM on intracellular HDAC2 activity.....	359
Figure 5.1. Structure of pyrimethamine.....	387

Figure 5.2. Structures of approved HDACi.	390
Figure 5.3. Pharmacophoric model and designs of HDACi using SAHA as a prototypical HDACi.	392
Figure 5.4. Molecular docking of PYM and class I PYM-HDACi compound B to STAT3 (PDB:1BG1).	394
Figure 5.5. Docked poses of PYM-HDACi at the active sites of HDAC 1 (PDB:5ICN).	397
Figure 5.6. Docked poses of PYM-HDACi at the active sites of HDAC 6 (PDB:5G0G).	398
Figure 5.7. The Western blot analysis of HDAC inhibition	407
Figure 5.8. The Western blot analysis of STAT3 pathway inhibition in MDA-MB-231 cells. .	409
Figure 5.9. Western blot analysis of 12c on the cyclin D1 expression MDA-MB-231 cells.. ...	410
Figure 5.10. Effect of selected agent 12c for MDA-MB-231 cell cycle progression.	413
Figure 5S.1. Docking outputs of PYM and class I compound B and class II compound E on hDHFR (PDB:1U72).	434
Figure 5S.2. The docking of 12d on the DBD region of STAT3 protein..	435
Figure 5S.3. Effect of 12b on MDA-MB-231 cell cycle progression.	436
Figure 6.1 Demonstration of pyrimethamine and our PYM-derivative agents.	477
Figure 6.2. <i>In silico</i> interrogation of the interaction of 11b with the STAT3 DBD (PDB:1BG1)	479
Figure 6.3. Western blot data of the effect of selected compounds on STAT3 signaling.	488
Figure 6.4. DNA binding of p-STAT3 was inhibited by the novel STAT3i.	489
Figure 6.5. Cell Cycle arrest analysis.	492
Figure 6S.1. Western blot gels for Compound 11c and 11d	563
Figure 6S.2. Western blot gels for Compound 11b and 15a	564
Figure 6S.3. Absorbance of NADPH without DHFR reduction.	565
Figure 6S.4. Novel STAT3 inhibitor candidates do not inhibit DHFR activities.	565

Figure 7.1. Models and designs of the glycosylated HDACi	572
Figure 7.2. Molecular docking of selected candidate STR-V-53 on HDAC2 (PDB:4LXZ), HDAC6 (PDB:5G0G), and GLUT-1 (PDB:4PYP)	579
Figure 7.3. Blockage of GLUT-2 attenuates the cytotoxicity of STR-V-53 against Hep-G2....	584
Figure 7.4. Hep-G2 induced up-regulation of acetylated H4 and acetylated α -Tubulin.	585
Figure 7.5. Evidence of caspase 3 cleavage and p21 up-regulation in Hep-G2 cell by glycosylated HDACi.....	587
Figure 7.6. No evidence of cleavage of caspase 3 in Vero cell treated with STR-V-53 or STR-I-195	588
Figure 7.7. The effect of STR-V-53 on cell cycle progression.....	589
Figure 7.8. Compound STR-V-53 significantly suppressed liver tumor growth and liver tissue accumulation with no toxicity based on mice body weight indication.	591
Figure S7. 1. Table of NCI-60 panel of STR-V-53 in 10 μ M dosage screening.....	648

LIST OF SYMBOLS AND ABBREVIATIONS

AA	Amino acid
Å	Angstrom
α -SMA	α -Smooth muscle actin
Ac	Acetylated
ALA (Chemical)	α -(R)-Lipoic acid
ALA (amino acid)	Alanine
ALK-5	TGF-(beta) type I receptor
APT	Adenosine triphosphate
ARG (amino acid)	Arginine
ASN (amino acid)	Asparagine
ASP (amino acid)	Aspartic acid
AZM	Azithromycin
BC	Breast cancer
Bcl-2	B-cell lymphoma 2
Bcl-Xl	B-cell lymphoma-extra large
Boc	tert-butyloxycarbonyl protecting group
C	Carbon
°C	Celsius
Caspase	Cysteine-aspartic proteases
CDCl ₃	Deuterated chloroform
CD ₃ OD	Deuterated methanol
CAC	Colitis associated cancer
COL1A1	Collagen I A1

CLM	Clarithromycin
COX	Cyclooxygenase
CRC	Colorectal Cancer
CSF	Cancer-associated fibroblasts
CTCL	Cutaneous T-cell lymphoma
CTGF	Connective tissue growth factor
CuAAC	copper(I)-catalyzed alkyne-azide cycloaddition
CyclinD1	a protein that in humans is encoded by the CCND1 gene
d	Doublet
dd	Doublet of doublet
ddd	Doublet of doublet of doublet
DMEM	Dulbecco's Modified Eagle Medium
DBD	DNA binding domain
DCM	Dichloromethane
DCC	1,3-Dicyclohexylcarboimide
DHFR	Dihydrofolate reductase
DNA	Deoxyribonucleic acid
DMF (Chemical)	Dimethyl fumarate
DMF (Organic solvent)	N,N-Dimethylformamide
DMSO	Dimethyl sulfoxide
EGF	Epidermal growth factor
EMEM	Minimum essential medium Eagle
EMT	Endothelial-mesenchymal transition
EndoMT	Endothelial-mesenchymal transition
ECM	Extracellular matrix

EDCI	1-Ethyl-3-(3-dimethylaminopropyl) carbodiimide
EtOAc	Ethyl acetate
ERK	Extracellular regulated kinase
ERM	Erythromycin
FDA	Food and drug administration
FN-1	Fibronectin-1
GAPDH	Glyceraldehyde 3-phosphate dehydrogenase
GLY (amino acid)	Glycine
GLU (amino acid)	Glutamic acid
GLN (amino acid)	Glutamine
GI	Gastrointestinal
GLUT	Glucose transporter
hnRNP	Heterogenous nuclear Ribonucleoprotein
H	Proton
HAT	Histone Acetyltransferase
HDAC	Histone Deacetylase
HETEs	Hydroxyeicosatetraenoic acids
HBV	Hepatitis B Virus
HCC	Hepatocellular carcinoma
HCV	Hepatitis C Virus
HIS (amino acid)	Histidine
HO-1	Heme oxygenase-1
HPLC	High performance liquid chromatography
HSC	Hepatocyte stellate cell
Hz	Hertz

IBD	inflammatory bowel disease
IC ₅₀	Half-maximal inhibitory concentration
IG	Immunoglobulin
IP	Intraperitoneal
IV	Intravenous
IL	Interleukin
ILE (amino acid)	Isoleucine
ILD	Interstitial lung disease
IPF	Idiopathic pulmonary fibrosis
<i>J</i>	Coupling constant
JAK	Janus kinase
L	liter
LAP	Latency associated peptide
LC/MS	Liquid chromatography–mass spectrometry
Leu (amino acid)	Leucine
LLC	large latent complex
LOX	Lysyl oxidase
LT	leukotriene
LTBP	latent TGF- β -binding proteins
m	multiplet
mg	milligram
mL	milliliter
mM	millimolar
μ M	micromolar
μ g	microgram

μL	microliter
MAPK	mitogen-activated protein kinase
Met	Methionine
MeOH	Methanol
Mg	Magnesium
MMF	Monomethyl fumarate
MMP	Matrix metalloproteinases
MMT	Macrophage-to-myofibroblast transition
MS	Mass spectroscopy
MTS	an assay for cell cytotoxicity, viability and proliferation test.
m/z	Mass to charge ratio
nM	Nanomolar
NAPDH	Nicotinamide adenine dinucleotide phosphate
NF-κB	Nuclear factor kappa-light-chain-enhancer of activated B cells
NI	No inhibition
NMR	Nuclear magnetic resonance
NRF-2	Nuclear factor erythroid 2-related factor 2
NSAID	Non-steroid anti-Inflammation Drug
NT	Not tested
O-trityl	O-Triphenylmethyl
O/N	Overnight
p21	a cyclin dependent kinase inhibitor
p38	a mitogen-activated protein kinases
p53	a tumor suppressor protein
ppm	Parts per million

PDB	Protein data base
PDH	Pyruvate dehydrogenase
PDK	Pyruvate dehydrogenase kinase
PD-1	Programmed cell-death protein-1
PD-L1	Programmed death-ligand 1
PEG	Polyethylene glycol
PFD	Pirfenidone
PGE2	Prostaglandin E2
Ph	Phloretin
PHE (amino acid)	Phenylalanine
PIPE	Piperine
PPA	Piperic acid
PRO (amino acid)	Proline
PVDF	Polyvinylidene fluoride
PSM	Peptide spectral matches
PYM	Pyrimethamine
Q	quartet
R.T.	Room temperature
RIPA	Radioimmunoprecipitation assay buffer
RNA	Ribonucleic acid
RNP	Ribonucleoprotein
ROS	Reactive oxygen species
s	singlet
STAT	Signal transducer and activator of transcription
SAHA	Suberoyl anilide hydroxamic acid

SAR	Structure-activity relationship
SER (amino acid)	Serine
SIRT	Sirtuin
SLC	Small latent complex
TEA	Triethylamine
TNBC	Triple negative breast cancer
TGF- β	Transforming-growth factor β
TFA	Trifluoroacetic acid
THF	Tetrahydrofuran
THR	Threonine
TIPS	Triisopropylsilane
TLC	Thin-layer chromatography
TLR	Toll-like receptors
TNF- α	Tissue necrosis factor α
TRP (amino acid)	Tryptophan
TYR (amino acid)	Tyrosine
TXA2	Thromboxane A2
Th2	T helper cell 2
VAL (amino acid)	Valine
VEGF	Vascular endothelial growth factor
WCL	Whole cell lysate
Zn ²⁺	Zinc ion
ZBG	Zinc binding group

SUMMARY

Uncontrolled inflammation is a key factor in multiple disease types, including tissue fibrosis and cancers. The underlying mechanisms and treatment of several of these diseases are still unsolved medical challenges. The studies described in this thesis focused on developing novel cell-type and tissue-selective anti-inflammation and anti-cancer agents that target microinjuries, fibroblast hyperplasia exaggerated extracellular matrix (ECM) deposition and epigenetic dysfunctions.

Idiopathic pulmonary fibrosis (IPF) is a life-threatening interstitial lung disease (ILD) of ambiguous cause. IPF is sustained by inflammation caused by chronic injury that promotes inflammatory cytokines release and the accumulation of these cytokines in the bronchial tubes and airways. IPF is a chronic and fatal disease that progressively declines the lung function. Till date, IPF remains untreatable. The FDA approved drugs - pirfenidone (PFD) and nintedanib – are suboptimal in the management of IPF due to their toxic side effects, low potency, cost ineffectiveness and minimal beneficial effect on the patients' survival rate. In chapter 2 of this thesis, I described four classes of macrolide-based anti-fibrotic agents (28 final compounds) designed to exploit the excellent PK and selective lungs and/or liver tissues distribution activities of the macrolide templates to arrive at novel anti-fibrotic agents that may selectively accumulate within these tissues. I investigated the effects of these compounds on the viability of four cell lines (MRC-5, A549 Hep-G2 and VERO), NF- κ B and TGF- β pathways and the levels of fibrosis markers (FN-1, MMP-9, COL1A1, α -SMA). A cohort of these compounds elicit anti-proliferative and anti-inflammatory effects with potency enhancement as high as 1000-fold relative to the standard of care PFD. Based on the data from these experiments, compound **15c** was identified as a lead based while the next best compounds are **10c**, **11c** and **20e**.

Inspired by the study described in chapter 2, I designed and synthesized macrolide (azithromycin (AZM) and clarithromycin (CLM)) conjugates of three antioxidants – alpha lipoic acid (ALA), fumarate and piperic acid (PIPE) – in chapter 3. After investigation of the cytotoxicity of these macrolide-antioxidant conjugates against cancer cells, normal kidney cell line, and fibroblast cell line, I observed that most of novel compounds showed significant enhancement (more than 100-fold) in cytotoxicity and stronger anti-fibrotic effects relative to their unconjugated antioxidants. Specifically, ALA derivatives showed strong STAT3 inhibition and extracellular matrix (ECM) components production inhibition effects with attenuation of TGF- β stimulation. Fumarate and PIPE derivatives also demonstrated strong anti-fibrotic effects and Nrf-2 activation.

In Chapter 4, I report the discovery that macrolide antibiotic clarithromycin (CLM) undergoes tandem dehydration- cyclization-dehydration reactions, involving C-11 and C-12 hydroxyl groups and the C-9 keto moiety, to furnish a dihydrofuranyl macrolide **AO-02-63**. I observed that **AO-02-63** inhibits the activities of prokaryotic and eukaryotic ribosomes and possibly disrupts the activity of hnRNPs. **AO-02-63** also inhibits the proliferation of all cell lines in the NCI-60 panel with low micromolar IC₅₀s and elicits anti-inflammatory activity similar to CLM, although with a 10-fold potency enhancement. The broad anti-cancer activity of **AO-02-63** could be due to its inhibition of protein synthesis and mRNA processing, two processes that are vital for the survival of cells.

The potential of STAT3 pathway inhibition as an anticancer and anti-inflammatory strategy is under active investigation in preclinical and clinical settings. Chapter 5 of this thesis focused on validating our hypothesis that simultaneous STAT3 and histone deacetylase (HDAC) inhibition will lead to more durable anti-proliferative effects in STAT3-addicted cancer cells. Toward this end, I synthesized 5 pyrimethamine (PYM)-derived compounds and tested them against Hep-G2,

A549, VERO, MDA-MB-231, and MCF-7 cell lines. I noticed that these compounds inhibited both HDAC and STAT3 pathway intracellularly. Interestingly, compounds **12b** and **12c** showed 6- to 10-fold cell-type selectivity for a STAT3-dependent, TNBC cell line MDA-MB-231. In Chapter 6, I used an *in silico* molecular docking tool (Autodock vina) to design three classes of PYM derivatives (total of 12 compounds) as putative STAT3 inhibitors that function by blocking the DNA binding domain of STAT3. I synthesized these compounds and profiled their STAT3 inhibition in a cell free assay. Subsequently, they were analyzed against Hep-G2, A549, VERO, MDA-MB-231, and MCF-7 cell line. I found that class II compounds **11b-d** showed 100-fold enhanced cytotoxicity relative to PYM and are also 100-fold better STAT3 pathway inhibitors. Using a p-STAT3 DNA binding assay, I found that the STAT3 inhibition activities of these PYM derivatives are largely due to their direct STAT3 DNA binding interruption. These PYM-HDAC inhibitors and STAT3 DNA domain inhibitors could be novel anticancer agents that are selective for STAT3-addicted cancer cells.

In chapter 7, I described results from characterization of the anti-proliferative activities and mechanism of action of 19 glycosylated HDAC inhibitors (HDACi). I found that these compounds are selectively cytotoxic to several HCC cell lines possibly due to GLUT2-mediated uptake with lead compound **STR-V-53** significantly more selective for HCC cells. In collaboration with the Petros Lab at Emory University, we found that **STR-V-53** is non-toxic to healthy mice (MTD > 100 mg/kg) and effectively suppressed tumor growth in orthotopic murine model of HCC. In addition, we identified **STR-V-165** and **STR-I-195** as back-up compounds. Collectively, these glycosylated HDACi are promising anti-HCC agents.

CHAPTER 1. INTRODUCTION OF THE LINKAGE BETWEEN TISSUE INFLAMMATION AND CANCER

1.1 Introduction :

Uncontrolled inflammation is a salient factor in multiple disease types, including several chronic diseases and cancers. Inflammation can be directly link to tissue injury, fibrosis and necrosis, and it can be life threatening.¹ In fact, treatment of tissue fibrosis is still an unsolved medical challenge as there are currently no tools to effectively overturn the progression of tissue fibrosis and necrosis. Idiopathic pulmonary fibrosis, an example of tissue inflammation, remain unsolvable and irreversible once diagnosed, with a 5-year survival rate lower than many types of cancer.² A direct connection between inflammation and cancers is that tissue injury, and the concomitantly produced inflammatory factors, promote cancer cell growth via dysfunction in chemokines and cytokines signaling.³ It is known that some cancer types rely on inflammation signals for their progression, angiogenesis, proliferation and survival, invasiveness, and metastasis.⁴⁻⁶ Therefore, targeting inflammation is a promising therapeutic option for many types of cancers. However, challenges including low potency with poor drug distribution at disease sites, and off-target effects, which result in overt toxicity, remain unsolved in anti-inflammation and anti-cancer drug development. The studies described in this thesis focused on developing novel cell-type and tissue-selective anti-inflammation and anti-cancer agents that target microinjuries, fibroblast hyperplasia exaggerated extracellular matrix (ECM, mainly collagens) deposition, and epigenetic dysfunctions.

1.2 Inflammation and causes.

Inflammation involves upregulation of pro-inflammatory signals and it serves dual roles in biology. Controlled inflammation could protect infection and tissue injury while uncontrolled inflammation sustains autoimmunity and malignant transformations.⁷ Reactive oxidative stress (ROS) produced in response to tissue injury, bacteria or virus infections, chemical stimulation, hypoxia, or within the tumor microenvironment (TME) can stimulate the tissue epithelial cells.⁸ The stimulated epithelial cells further release ROS species and pro-inflammatory cytokines to trigger the immune system response.⁹ The pro-inflammatory cytokines, which include but not limited to TGF- β , TNF- α , IL-1, IL-6, IL-8, IL-10,¹⁰ bind to their respective receptors and cause pro-inflammatory signals within the cell. These signals may induce the activation of inflammation pathways such as TGF- β pathway, STAT3 pathway, NF- κ B pathway and epigenetic pathways. These pathways could promote the expressions of different proteins to either resolve the inflammation, or progress the pathogen and cause chronic injury, tissue fibrosis, or tumorigenic transformation.¹¹ In some cases, the expressed proteins could be components of the extracellular matrix (ECM) that is supposed to heal and repair the tissue.¹² However, due to the excess tissue damage or injury, ECM production could be out of control.¹³ The accumulation of ECM causes tissue stiffness, necrosis, and dysfunction. In other cases, proteins like anti-apoptotic STAT and Bcl-2 family proteins could be activated with the stimulation of cytokines. These proteins could induce anti-apoptosis in cells and promote cell proliferation.¹⁴ NF- κ B pathway could be activated by these proteins, resulting in the inhibition of the tumor suppressor p53.¹⁵ Therefore, inflammation strongly links tumor progression with tissue/cell damage caused by injuries, infections, and other stimuli.

1.3 Inflammation and Tissue Fibrosis

Fibrosis is the thickening and scarring of the connective tissues in organs, which could be induced by injuries from environmental stimuli, biohazards exposure, radiation, or infection, or could be triggered by gene mutation or other unclear intracellular disorder. The abnormally stressed microenvironment of the tissue may cause the upregulation of cytokine expression to modulate the stage of inflammation. Immunity responses will be triggered to protect the tissue from further attacks by the pathogenic sources such as bacteria and virus. However, the process could be overregulated when the injuries tend to be continuous over time. For example, liver cirrhosis can be triggered by HCV infection.¹⁶ Due to the continuous infection and inflammation, immune system response augments the process of healing and induce overexpression of ECM. The deposition of ECM could thicken the tissue which will deteriorate with sustained inflammation and finally induce liver fibrosis. One of my major focus in this thesis is on Idiopathic pulmonary fibrosis (IPF), induced by chronic inflammation and for which there is a significant unmet medical need.

1.3.1 *Idiopathic pulmonary fibrosis (IPF)*

IPF is the most common and most severe disease type of interstitial lung disease (ILD).¹⁷ IPF is a chronic and fatal disease which progressively declines the lung function. The cause of the IPF is ambiguous, and the disease infects 5 per 10,000 people worldwide.¹⁸ In the US, 40,000 patients die of IPF every year.¹⁹ The prognosis of the IPF is the worst of all ILDs, as its median survival is about 2-5 years from diagnosis (Fig. 1.1).²⁰

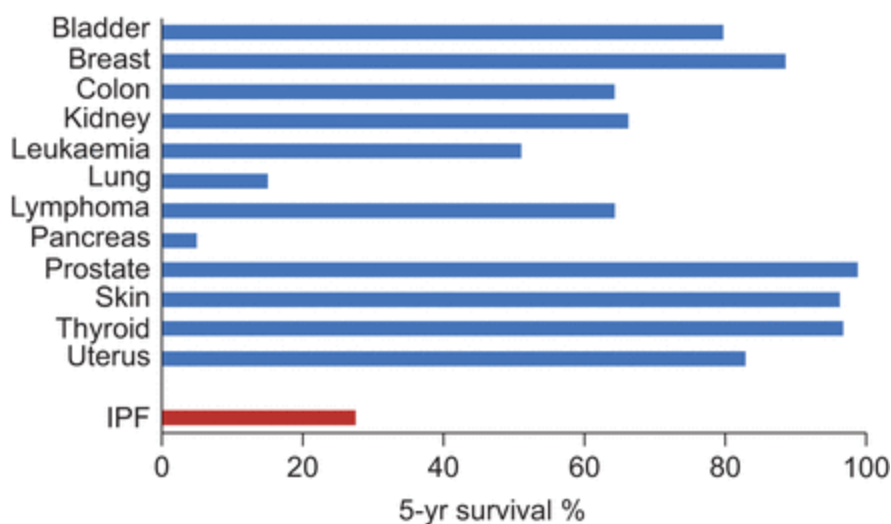


Figure 1.1. The 5-year survival percentage of IPF relative to several types of cancers.² The data suggested that IPF has higher mortality rate than several cancers.²⁰

1.3.2 IPF Pathogenesis

The IPF can be related to the excessive accumulation of extracellular matrix (ECM) components. Fibronectin, tenascin-C, collagen type I and III are the ECM secreted by fibroblasts in the process of fibrosis.²¹⁻²³ Fibroblast, the most common cell to produce ECM, is activated by cytokines, growth factors, and fibrotic factors to continuously generate ECM.

During IPF, many cells secrete cytokines to activate fibroblasts to become myofibroblasts which are key cells that overregulate the ECM remodeling through combination of synthesizing features of fibroblasts with cytoskeletal contractile characteristics of smooth muscle cells (α -SMA).²⁴ During this process, other cells are transformed as well. Specifically, endothelial cell, which lines blood vessel, can transform to fibroblasts. Once the endothelial injury occurs, the endothelial cells can go under a process call endothelial-mesenchymal transition (EMT) when stimulated by inflammatory cytokines such as TGF- β_1 .²⁵ The mesenchymal cell is the primitive fibroblast which can transition to fibroblast cell and induce the fibrosis. Therefore, the EMT process is one of the

major sources of the fibrosis, as it supplies more amounts of fibroblasts and support for the ECM production later.

Lymphocyte can also induce the activation of fibroblast via the Th2 polarized response. The Th2 (T cell helper 2) response is an immune response against helminths and other extracellular injuries. This Th2 polarization is induced by adhesion between endothelial cell and lymphocytes. The response secretes pro-inflammatory cytokines IL-4, IL-5, IL-6, IL-10, IL-13 which activate the fibroblasts and transform them to the myofibroblasts.²⁶ The next important activation of fibroblasts is through the macrophage. The polarization of monocyte turns it into M1 or M2 Macrophage. In IPF, M2 macrophage is the major polarized phenotype of macrophage, as the endothelial cell injury paracrine the cytokines IL-4, IL-10-IL-13 and TGF- β to the monocytes on the purpose of anti-inflammation. However, the M2 macrophage phenotype over-regulates the expression of TGF- β signal, connective tissue growth factor (CTGF), platelet-derived growth factor (PDGF), epidermal growth factor (EGF) and IL-1 α , which continuously activate the fibroblasts and induce tissue fibrosis. On the other hand, the M1 macrophage (inflammation phenotype) can also induce the EMT by secreting TNF- α , IL-8 and ROS signals to endothelial cell and cause tissue necrosis and fibrosis.²⁷ This process is called macrophage to myofibroblast transition (MMT).

Based on the a forementioned literature observations, the main pathway towards IPF is the activation and proliferation of fibroblasts, as the ECM components can only be over-expressed when myofibroblasts are formed. Thus, inhibition of the activation and proliferation of fibroblasts could be an effective strategy in preventing or slowing fibrosis progression.

1.4 Inflammation and tumorigenesis

1.4.1 Cancer types linked to chronic tissue inflammation

Several studies have shown that dysregulation of inflammatory signals caused by chronic injuries could progress into malignant transformation. For example, chronic liver tissue injury caused by hepatitis infection predisposes hepatitis patients to higher risks of cirrhosis and hepatocyte carcinoma (HCC). Colitis associated cancer (CAC) is a subtype of colorectal cancer that is known to be associated with inflammatory bowel disease (IBD).²⁸ Additionally, IPF patients also have higher risks of lung cancer.^{29, 30} Table 1.1 summarizes inflammation associated cancer types and their inducers.

Table 1. 1 Inflammation associated cancer types.³¹⁻³³

Inflammation conditions	Cancer type	Inducer
Asbestosis	Lung carcinoma	Silica
Chronic Bronchitis	Lung carcinoma	Silica
IPF	Lung carcinoma	Unclear
Tuberculosis	Lung carcinoma	Mycobacterium tuberculosis
Liver cirrhosis	HCC	Hepatitis infection, alcoholic, genetic
IBD, Crohn's disease, chronic ulcerative colitis	Colorectal cancer	Gut pathogens

Table 1.1 continued.

Chronic gastric inflammation	Gastric cancer	<i>Helicobacter pylori</i>
Reflux oesophagitis, Barrett's oesophagus	Oesophageal carcinoma	Gastric acids
Skin inflammation	Melanoma	UV light
Chronic pancreatitis hereditary pancreatitis	Pancreatic carcinoma	Alcohol, gene mutation
Schistosomiasis	Bladder carcinoma	Gram-uropathogens
Cervicitis	Cervical cancer	Human papilloma virus
chronic prostatitis	Prostate cancer	Bacterial infection
Sialadenitis	Salivary gland carcinoma	Bacterial infection
Sjögrensyndrome, Hashimoto's thyroiditis	MALT lymphoma	unclear
Gingivitis, lichen planus	Oral squamous cell carcinoma	Bacterial infection
Chronic cholecystitis	Gall bladder cancer	Bacteria, gall bladder stones

Bacterial and virus infections are one cause of chronic tissue injuries. HCC is linked to liver cirrhosis that could result from infections by hepatitis virus, including hepatitis B virus (HBV) and hepatitis C virus (HCV). The cytokines (TGF- β and IL-6) released as a result of these infections activate the hepatocyte stellate cells (HSCs), triggering immune response and inflammation.³⁴ Also, the failure of anti-viral treatment could induce chronic inflammation and liver tissue fibrosis in response to the overexpression of supposedly protective TGF- β . These events ultimately result in accumulation of ECM and liver cirrhosis.³⁵ The chronic inflammation triggered ROS production is the main cause of genetic mutation, which is responsible for carcinogenic event to take place.³⁶

Recent studies found that the *Helicobacter pylori* is the key pathogenic factor for chronic gastric inflammation. *H. pylori* resides in the host for a lifetime as the host's immune system is incapable of clearing it out. *H. pylori* infects 50% of the world population and its infection can cause the duodenal and gastric ulcer disease.³⁷ *H. pylori*-infected cells release IL-8, IL-10, TNF- α to cause tissue inflammation as superficial gastritis. These cytokines directly stimulate immune cell. In addition to contributions from other factors, such as smoking and high salt consumption, chronic inflammation caused by *H. pylori* infection could induce the gastric cancer.³⁸

Exposure to chemicals is another inducer of chronic inflammation. Lungs tissues are most susceptible to the effects of chemical exposure which could cause chronic injuries such as Bronchitis and idiopathic pulmonary fibrosis. Smoking, silica exposure, inhalation of hazardous chemicals are the major sources of irritants that could cause chronic lung tissues inflammation linked to lung carcinoma. The lung tissue injuries induced by these chemical irritants could cause integrins $\alpha\text{v}\beta 6$ and $\alpha\text{v}\beta 8$ to stimulate and induce overexpression of TGF- β .³⁹ The binding of TGF- β to TGF- β R in epithelial cells or fibroblasts causes EMT or myofibroblast differentiation^{40, 41} which induces an over-expression of ECM and change of metabolism in cells – from aerobic

glycolysis to anaerobic glycolysis – to support extra energy for ECM production and migration. Stiffness and lung tissue necrosis occur when ECM is overproduced. Lung cancer could be triggered in this circumstance.⁴²

1.5 Major inflammation pathways in tumor progression and tissue fibrosis

1.5.1 TGF- β pathway and inflammation-induced carcinogenesis

In current understanding, TGF- β plays a double-edged sword role in inflammation and cancer. In case of common acute injury, TGF- β is regarded as an important anti-inflammatory cytokine that can protect tissue from injury. It plays an essential role in tissue repair as well. However, TGF- β could also be a pro-inflammatory cytokine in the chronic injured condition and tumor microenvironment. The activation of TGF- β usually caused by tissue inflammation, ROS up-regulation, and immune response. TGF- β has three isoforms, which are TGF- β 1-3, and TGF- β 1 plays the critical role to induce inflammation.⁴³ In most of cases, TGF- β is secreted by cells in a large latent complex (LLC) in which the TGF- β is protected by latency associated peptide (LAP) and covalently bond to a family member of the ‘latent TGF-b-binding proteins’ (LTBPs).^{44, 45} Upon cleavage, the small latent complex (SLC) will be formed. However, TGF- β needs to be activated via the release of LAP. Only a few of cell types can secrete the SLC form of TGF- β . And the SLC form can be activated by non-integrin activation,⁴⁵ including low pH (pH<4),⁴⁶ protease activity (MMPs),⁴⁷ ROS,⁴⁸ and thrombospondin-1⁴⁹ (TSP-1) induced LAP transformation. Integrin $\alpha\beta$ 6 and $\alpha\beta$ 8 play roles in TGF- β activation via different mechanism. Specifically, LLC form of TGF- β bind to $\alpha\beta$ 6 or $\alpha\beta$ 8 of the other cell on the membrane. For $\alpha\beta$ 6, cell traction and pulling induce conformational change in LAP to release the TGF- β in the active form. The integrin $\alpha\beta$ 8 induces MT-1 MMP into the LAP interaction, and therefore a proteolytical cleavage between

LAP and TGF- β .⁵⁰ The released TGF- β binds to TGF- β Rs to induce inflammation pathways. With the TGF- β ligand-receptor binding, SMAD2/3, PI3K, JNK and MAPK pathways could be activated. SMAD pathway activation induces pro-inflammatory cytokines and ECM production.⁵¹ Activated PI3K pathway induces cell proliferation and invasiveness, while JNK and MAPK pathways induce cell stress, inflammation and tissue necrosis;⁵² The TGF- β activation and overregulation could also induce process of EMT through transcriptional regulation and expression of Snail families, ZEB families, and bHLH families,⁴⁹ which could induce malignant tumor growth.^{53, 54} In addition, Angiogenesis could also be promoted through TGF- β through expression of ID-1 and ID-3 in terms of SMADs transcriptional regulation.^{55, 56} Overall, TGF- β pathway is central to the connection between chronic inflammation and tumorigenesis (Fig. 1.2).

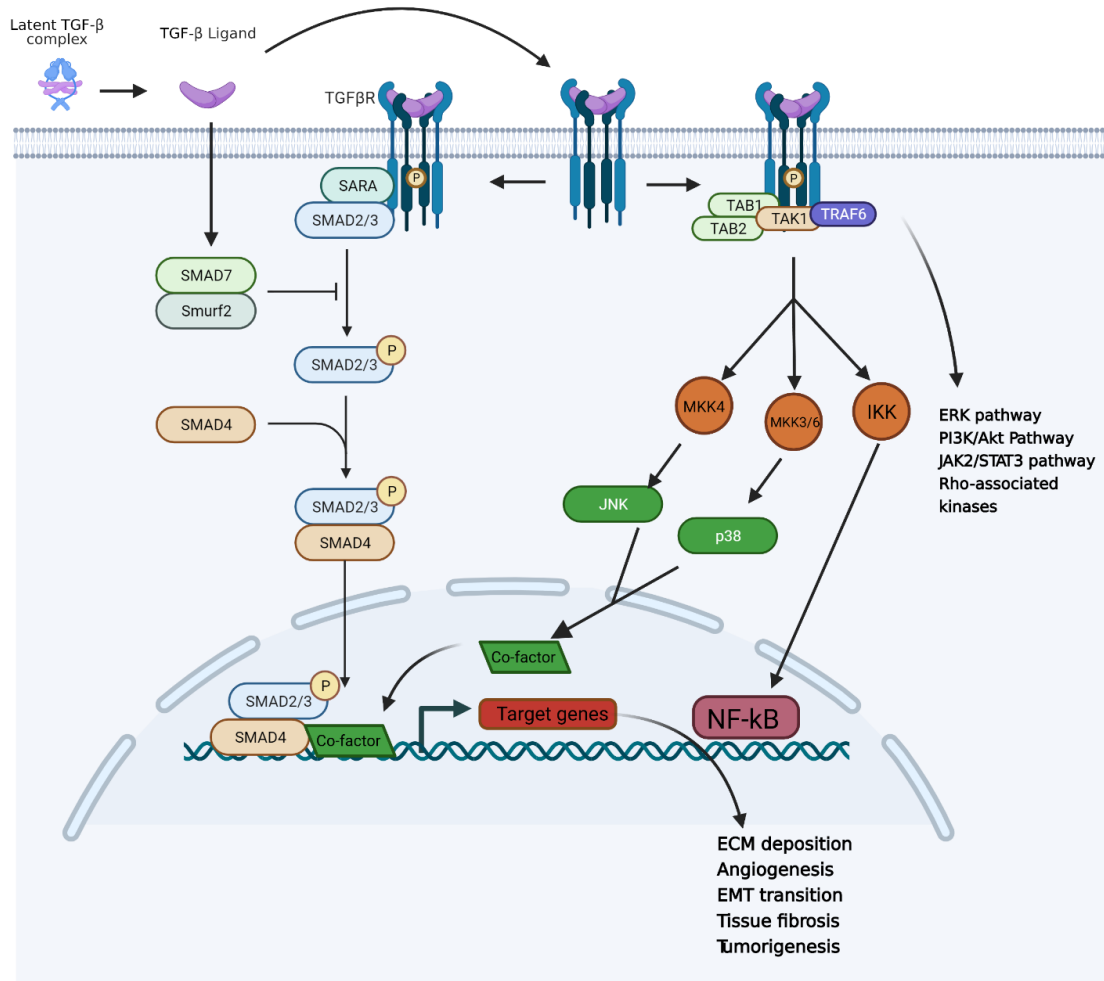


Figure 1.2. TGF- β pathway in cancer and inflammation.⁵⁷⁻⁵⁹

The acidic tumor microenvironment promotes TGF- β activation that assists in building fibrosis environment around the tumor. Within the microenvironment, cancer-associated fibroblasts (CSF) are the major producer of TGF- β cytokines⁶⁰ that will stimulate excessive ECM deposition and form desmoplasia, a term to indicate fibrosis microenvironment around the tumor. Desmoplastic reaction shields the tumor from exposure to chemotherapeutic agents and significantly increases tumor growth, angiogenesis, and promotes cancer cell invasiveness and metastasis.⁶¹ Pancreatic and triple negative breast cancers are especially prone to desmoplasia formation. Once desmoplasia is built, it is hard to treat the cancer with small molecule drugs.⁶²⁻⁶³

TGF- β pathway inhibition is a promising strategy for managing/treating fibrosis, inflammation, and cancer. Therapeutic targets within the TGF- β pathway includes integrin, TGF- β R, TGF- β R kinase, SMAD2/3 phosphorylation, and TGF- β expression. Anti-integrin antibody can block integrin $\alpha\beta$ 6 binding with LAP-TGF- β and so prevent the release of activated TGF- β . On the other hand, MT-1 MMP antibody can also effectively reduce the activation of TGF- β by inhibiting the function of $\alpha\beta$ 8. The strategies to inhibit the TGF- β R including ligand traps, TGF- β RI kinase inhibitor, TGF- β RII kinase inhibitors. For the TGF- β ligand trap, small molecules such as pirfenidone (PFD) and its derivatives have been found to be a ligand for the receptor. PFD has been approved by FDA for the treatment of IPF.^{64, 65} In addition, PFD is also known to be a potential anti-tumor agent due to its TGF- β pathway inhibition.⁶⁶ Peptides probes, which demonstrated selective inhibition effects on integrin and TGF- β Rs, have been reported.^{67, 68} For Kinase inhibition, selective TGF- β R kinase inhibitors such as SB-431542 and galunisertib have shown to potently inhibit both cancer growth and inflammation. On the other hand, inhibition of p38 and SMAD phosphorylation, which suppresses TGF- β up-regulation, has been achieved with small molecule inhibitors PD169316 and SB203580.⁶⁹

1.5.2 TNF- α , NF- κ B pathway and inflammation

The transcription factor NF- κ B is a regulator of inflammation and immune response. NF- κ B pathway is crucial to the survival of several cancer cells as it prevents cell death and promote cell proliferation by inhibiting the tumor suppressors such as p53. Several pro-inflammatory ligands and their receptors (cytokine receptors, pattern-recognition receptors (PRRs), TNF receptor, T-cell receptors) activate NF- κ B pathway, including TNFR for TNF- α , TLRs for LPS and IL-1 β , IL-6R for IL-6, etc.²¹ It has been shown that NF- κ B signaling has two separate pathways. The ‘canonical’ pathway is stimulated by TNF- α and IL-1 or TLR, to cause induction of I κ B α phosphorylation by

IKK (Fig. 1.3). I κ B α is a protein associated with and inactivated by p50/Rel-A or p50/c-Rel dimers. The phosphorylation of I κ B α promotes its degradation by ubiquitin-proteasome degradation pathway; the consequently released Rel-A/p50 will translocate into the nucleus and promote the expression of pro-inflammatory cytokines, anti-apoptosis proteins, chemokines, cell cycle regulators. The downstream effect of this signaling cascade is induction of tissue inflammation, necrosis, or tumorigenesis. For the other non-canonical NF- κ B pathway, the stimulation from LTs, CD40L, or BAFF, causes IKK α activation and the release of the p100/Rel-B dimer into the nucleus (Fig.1.3).⁷⁰ Both pathways are responsible for inflammation, tissue necrosis, and tumorigenesis.

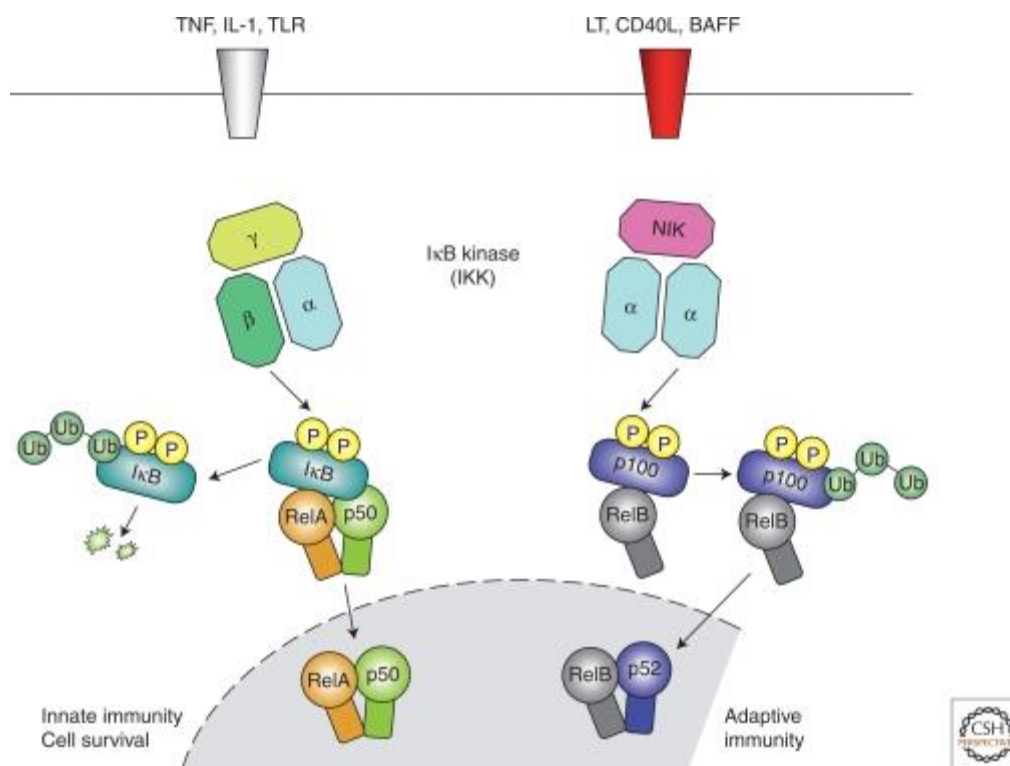


Figure 1.3. Cell signaling and pathways of NF- κ B-mediated inflammation.⁷⁰

Upregulation of NF- κ B pathway in several cancer cells promotes proliferation, invasiveness, metastasis, and angiogenesis through the expression of NF- κ B target genes.⁷¹ For example, the

expressions of Bcl-2 families of apoptosis regulators,⁷² caspase-8 inhibitor FLIP⁷³ and VEGF⁷⁴ are regulated by NF- κ B. In addition, NF- κ B also induces EMT which directly contributes to cancer metastasis.⁷⁵ Thus, a targeted inhibition of NF- κ B by pharmacological agents is considered a promising cancer therapy strategy.

Approaches that have been investigated to achieve NF- κ B inhibition include receptor inhibition, IKK complex inhibition, I κ B degradation inhibitor, NF- κ B DNA binding inhibitors, NF- κ B translocation inhibitors, p53 induction, p65 acetylation and Nrf-2 activation. Receptor inhibitors such as TNFR inhibitor SGT-11 and IL-6R inhibitor Tocilizumab; IKK inhibitors such as TPCA 1,⁷⁶ BOT-64,⁷⁷ BMS 345541,⁷⁸ and IMD 0354⁷⁹; I κ B degradation inhibitors such as BAY 11-7082,⁸⁰ Parthenolide,⁸¹ Lactacystin,⁸² MG-132,⁸³ and MG-115;^{82, 84} NF- κ B DNA binding inhibitors such as GYY 4137⁸⁵ and p-XSC,⁸⁶ are all promising NF- κ B pathway inhibitors. In addition to these pathway specific agents, NF- κ B pathway could also be inhibited by corticosteroid Dexamethasone⁸⁷ and anti-ROS agents such as lipoic acid⁸⁸ and Dimethyl fumarate.⁸⁹

1.5.3 JAK-STAT pathway and inflammation

Signal Transducer and activator of transcription (STAT) is an essential regulator of inflammation signal in the tissue inflammation. STAT family consists of seven sub-members: STAT1, STAT2, STAT3, STAT4, STAT5a, STAT5b and STAT6. Each member plays different role in regulating inflammation, proliferation, survival, and tumorigenic activities.⁹⁰ In general, STAT proteins are activated through the receptors-ligands (Interleukins, interferon, etc) interaction that stimulates Janus kinases (JAKs) phosphorylation. The activated JAKs phosphorylate STAT; the dimerization of the phosphorylated STAT (p-STAT) results in the translocation of the p-STAT dimer into the nucleus where induces the transcription of STAT-target genes.

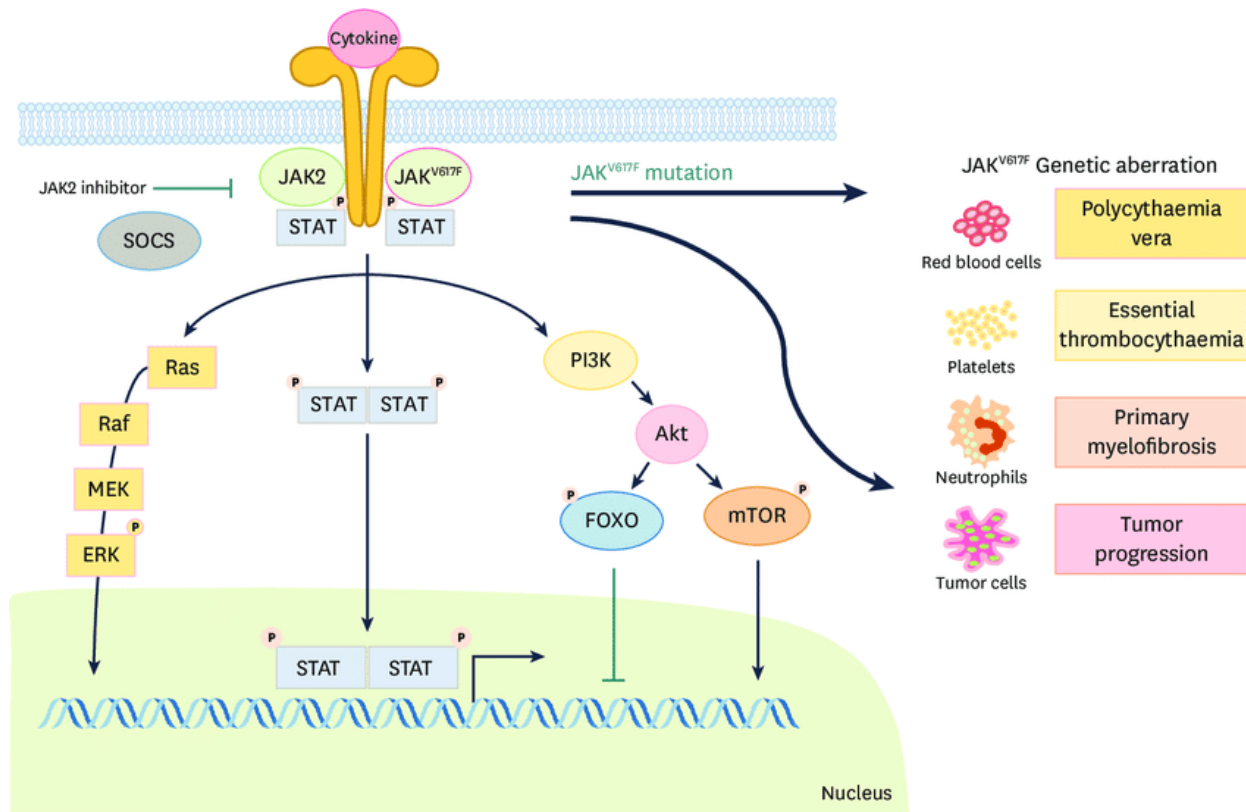


Figure 1.4. General cellular signaling for STAT protein activation and transcription.⁹¹

Heterodimerization of STAT sub-members occurs in the cell and these heterodimers have different cellular activities (Table 1.2). Specifically, STAT1-STAT2 dimer (also STAT1-STAT1 and STAT2-STAT2 dimers) induces the transcription of pro-inflammatory and immunoregulation genes in interferon stimulated cells in response to virus and bacterial infections;^{92, 93} STAT1-STAT3 dimer induces cytokine production and inflammation or blocks the STAT1-STAT1 activity. On the other hand, STAT3-STAT3 dimerization induces cell proliferation, anti-apoptosis, and invasion. STAT3-STAT3 dimerization (signaling) is upregulated in difficult to treat cancers such as the triple negative breast cancer (TNBC),⁹⁰ HCC; lung, breast, renal, and ovarian cancers, and lymphomas, are STAT3-dependent.⁹⁴⁻⁹⁹ STAT3-STAT5 heterodimer also promotes inflammation and tumorigenesis (to be discussed more below). In comparing to others, STAT4

may not directly link to inflammation and cancer. Rather, it connects with immune response for tissue inflammation. STAT4 could be activated by IL-12, IL-2 IL-23, IL-32, IFN-1, IL-18, IL-21 and induce tissue inflammation and disease through immune response.¹⁰⁰ The known inflammatory diseases that can be induced by STAT4 are IBDs, HBV, type-1 Diabetes etc.¹⁰⁰ In addition to promoting pro-inflammatory cytokines production, STAT5-STAT5 dimer up-regulates Akt proteins, p85 and p110 for PI3K pathway to induce tumorigenesis and mutagenesis in several cancers including breast cancer, acute myeloid leukemia, prostate cancer and melanoma.^{101,43} STAT3-STAT5 could act similarly as inflammation promoter with cytokine activations¹⁰² while by IL-4 and IL-13 activation of STAT6 promotes its involvement in inflammatory airway hyperresponsiveness,¹⁰³ eosinophilic infiltration,¹⁰⁴ and responses of mast cells.^{105, 106}

Table 1.2. The possible heterodimers and their inflammation activator and anti-inflammation activators.¹⁰²

STAT protein types	Stimulators (Inflammation)	Stimulators (Anti-inflammation)	Heterodimerization
STAT1	Type I IFN	IL-10	STAT2
	Type II IFN	IL-27	STAT3
	IL-6	IL-35	STAT4
STAT2	Type I IFN		STAT1 STAT6
STAT3	IL-2	IL-10	STAT1
	IL-5	IL-27	STAT4
	IL-6		STAT5
	IL-23		
	M-CSF		
	G-CSF		
	Type-I IFN		
STAT4	IL-12	IL-35	STAT1
	IL-23		STAT3
STAT5	IL-2-7, IL-9, IL-15		STAT3
	IL-21		
	M-CSF		
	GM,-CSF		
STAT6	TypeI IFN		STAT2
	IL-3		
	IL-4		
	IL-13		

Among all STAT sub-members, STAT3 is the most important regulator of inflammatory factors that feed cancer progression. Specifically, STAT3-mediated up-regulation of anti-apoptotic proteins Bcl-2 families and Mcl-1 resists cell death, while its upregulation of Cyclin D1 and c-Myc causes increase cell proliferation. Over-active p-STAT3 helps cancer cells evade the immune system through upregulation of PD-L1 expression.¹⁰⁸ In addition, STAT3 enhances cancer cell directional migration by regulating Rac1 activity¹⁰⁹ while it promotes angiogenesis by transcriptionally regulating VEGF activity.¹¹⁰

Therapeutic agents targeting STAT3 pathway have been well-studied as treatment modalities for cancers but none has been approved by FDA. Representative STAT3 inhibitors so far investigated include JAK kinase inhibitors, STAT3 SH2 domain phosphorylation inhibitors, nuclear

translocation inhibitors, DNA binding domain inhibitors, and transcription inhibitors. JAK kinase inhibitors include AZD-1480¹¹⁰; SH2 domain inhibitors include Bt354,¹¹¹ Osthole,¹¹² and KYZ3;¹¹³ STAT3 translocation inhibitor; STAT3 DBD inhibitor methylsulfonylmethane¹¹⁴ as the VEGF promoter inhibitor, CPA-1, CPA-7¹¹⁵ to prevent DNA binding; Chemical inS3-54A18¹¹⁶ binds to Cyclin D1 promoter and Salidroside as the MMP-2 promoter inhibitor.¹¹⁷

1.5.4 Arachidonic acid metabolism pathway and inflammation

Arachidonic acid is a precursor of the metabolite Prostanoids which are the lipid mediators of inflammatory response. Prostanoids include prostaglandins (PGs), prostacyclin (PGI), and Thromboxane (TX). PGs act as signals for cell-cell communications and control inflammation status via intracellular and intercellular signaling. There are types of PGs with different functions. For example, Prostaglandin E2 (PGE₂) acts as a pro-inflammatory mediator which may trigger pain, swelling, redness and other immune responses in the injured region.¹¹⁸ Prostacyclin (prostaglandin I₂, or PGI) is another prostanoid that prevents platelet formation and attenuate vascular contraction.¹¹⁹ Recently, PGI has been shown to be an anti-inflammatory mediator which could modulate immune system and attenuate inflammation in tissues.¹²⁰ On the other hand, Thromboxane (TXA₂) acts in the opposite direction as it promotes platelet formation,¹²¹ vasoconstrictor,¹²² and causes Prinzmetal's angina.¹²³ In addition, TXA₂ could promote inflammation, progression and metastasis in multiple tumors.¹²⁴

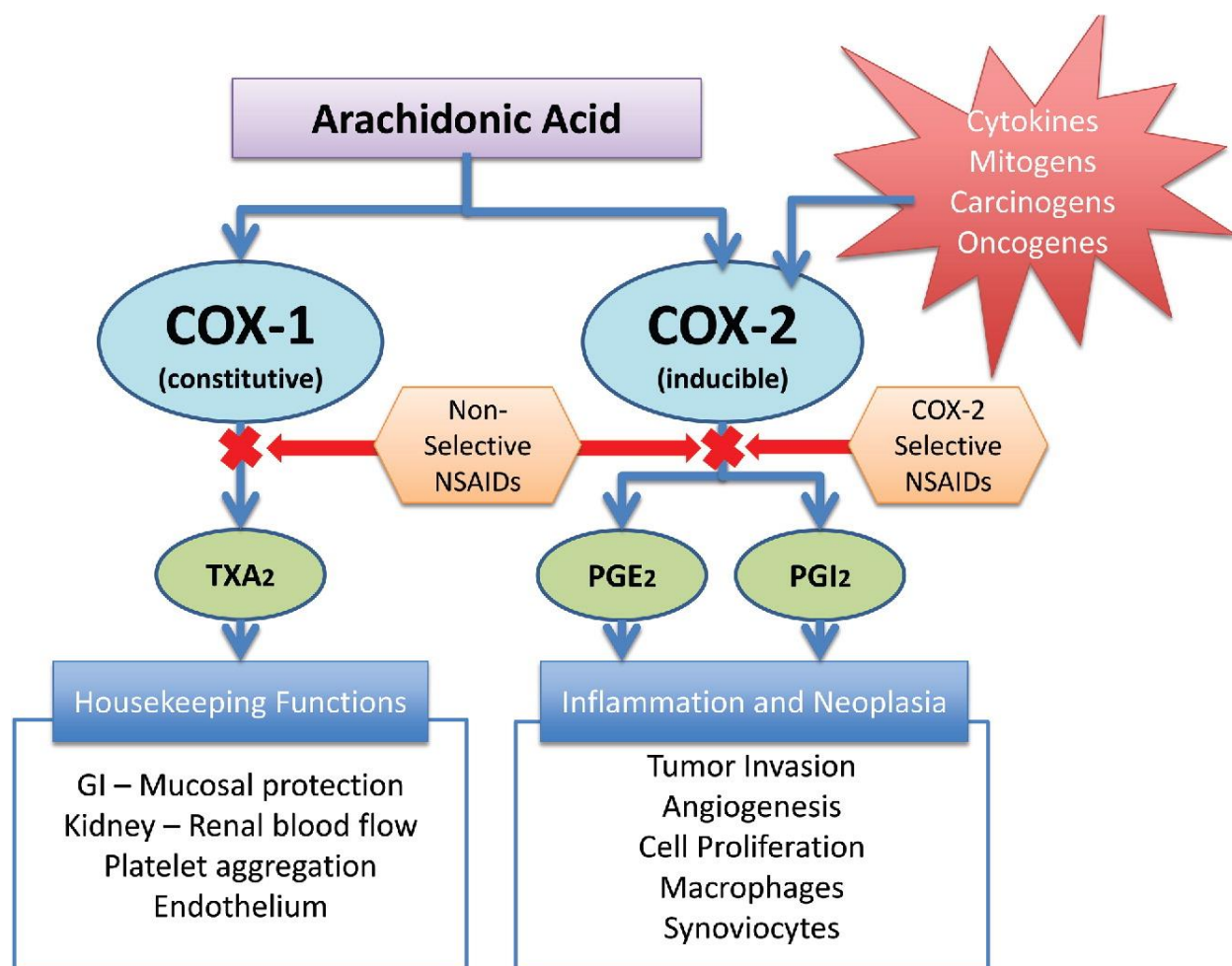


Figure 1. 5. COX pathways and following prostaglandin products.¹²⁵

Drugs, such as corticosteroid, which inhibit PGE₂ receptors, have been found to effectively block the inflammation process. Other PG EP4 receptor antagonists like GW627368X,¹²⁶ CJ-023,423,¹²⁷ and AH23848¹²⁸ have shown promising efficacy in blocking the synthesis of PGE₂ or TXA₂.

Enzymes such as cyclooxygenases (COX) that control the metabolism of arachidonic acid have attracted attention as therapeutic targets. COX families include COX-1, COX-2, COX-3 and COX-IV. In this family, COX-1 and COX-2 are the ones that have been well-studied as targets of inflammation and cancer treatment. COX-1 is a constitutively expressed enzyme with critical roles

in tissue protection such that it guards gastrointestinal tract with synthesis of prostaglandins essential for the maintenance of mucosal integrity.¹²⁹ Recently however, studies found that COX-1 is over-expressed and highly relevant to the etiology of ovarian cancer. COX-1 intersects multiple pro-tumorigenic pathways in high-grade serous ovarian cancer.¹³⁰ In breast cancer, stromal cells demonstrated with a highly overexpressed COX-1 level, which may lead to Tumorigenesis.¹³¹ In Cervical cancer, highly expressed COX-1 was known to regulate COX-2, PGE2 receptors, and angiogenic factors.¹³² Therefore, inhibition of COX-1 may be a chemoprevention strategy for cancers. COX-2 is widely regarded as a destructive enzyme that is not active in normal conditions. COX-2 overexpression and high activities are found in injured tissues, fibrotic tissues and tumors. COX-2 is known to be highly active in multiple cancers including breast,¹³³ prostate,¹³⁴ and liver cancers.¹³⁵ COX-2 promotes tumor growth, apoptosis resistance, and angiogenesis.¹³⁶⁻¹³⁸ Thus, COX-2 inhibition is favorable in drug discovery for anti-inflammation and anti-cancer purposes.

Lipoxygenases (LOXs), a class of iron-containing metalloproteins, are other enzymes that regulate the arachidonic acid metabolisms. LOXs catalyze the transformation of arachidonic acid to three types of hydroxyeicosatetraenoic acids (HETEs) –5-HPETE or 5-HETE by 5-LOX, 12-HETEs by 12-LOX, 15-HETEs by 15-LOX. 5-HETE is the precursor of Leukotriene LTA₄, which is converted to lipid mediators LTB₄, LTC₄, LTD₄, LTE₄ that induce asthma and inflammation.^{139, 140} Studies have found that 5-HETE and 5-HPETE stimulate the generation of superoxide in human neutrophils, and trigger the ROS stress.¹⁴¹ The product LTs are complementary pro-inflammatory factors to the PGE₂. Like COX, 5-LOX contributes to tumorigenesis by directly promoting tumor cell proliferation, growth, and survival through up-regulation of LTs.¹⁴² For example, in a colon cancer study, 5-LOX expression was found to be positively correlated with polyp size,

intraepithelial neoplasia and adenoma, suggesting that LOX may contribute to the early stage of colon cancer.¹⁴³ On the other hand, 12-LOX expression was found to be correlated with advanced stages of prostate cancer,¹⁴⁴ and an elevation of urinary levels of 12-HETE has been found prostate cancer patients.¹⁴⁵ Therefore, LOXs represent another target in arachidonic acid pathway for the discovery in anti-inflammation and anti-cancer agents.

Current strategy for the inhibition of arachidonic acid metabolism pathway focuses on PGs receptor inhibition, PGE₂ production inhibition, COX inhibition, LOX inhibition. Specifically, PGs receptor antagonists have been widely used for anti-inflammation treatment. For example, Timapiprant is a prostanoid receptor 2 (DP₂) inhibitor that has been used for lung inflammation (atopic eosinophilic asthma) and eye allergy;¹⁴⁶ Iloprost is a PG receptor inhibitor used for treatment of pulmonary arterial hypertension (PAH);¹⁴⁷ Fevipiprant is a PG DP₂ receptor inhibitor currently in Phase III clinical trial (NCT02555683) for the treatment of asthma.¹⁴⁸ Bimatoprost is a PG analog that acts to prevent the progression of glaucoma and manage the ocular hypertension.¹⁴⁹ Inhibition of PGE₂ production by non-steroidal anti-inflammatory drugs (NSAIDs) is also effective, however, several early NSAIDs are non-selective COX inhibitors. For example, Ibuprofen, Indomethacin, and Aspirin are NSAIDs with no COX-1/2 selective index.¹⁵⁰ New generation of NSAIDs showing COX-2 inhibition have been developed. For example celecoxib is a COX-2 selective inhibitor,¹⁵⁰ which is still in use as anti-inflammatory drug for the purpose relieving pain, swelling and rheumatoid arthritis. More recently, LOX inhibitors are attracting more attention for application in anti-inflammation and anti-cancer treatment. 5-LOX inhibitors include Meclofenamate sodium, Zileuton and Myxochelins/ pseudochelin. Meclofenamate sodium effectively suppresses the production of LTD₄ via and attenuates Asthma.¹⁵¹ Zileuton to downregulates several LTs and is also used for managing asthma.¹⁵²

Myxochelins/pseudochelins are newly discovered 5-LOX inhibitors that significantly suppress LTs production as well.¹⁵³

1.5.5 Epigenetic pathway

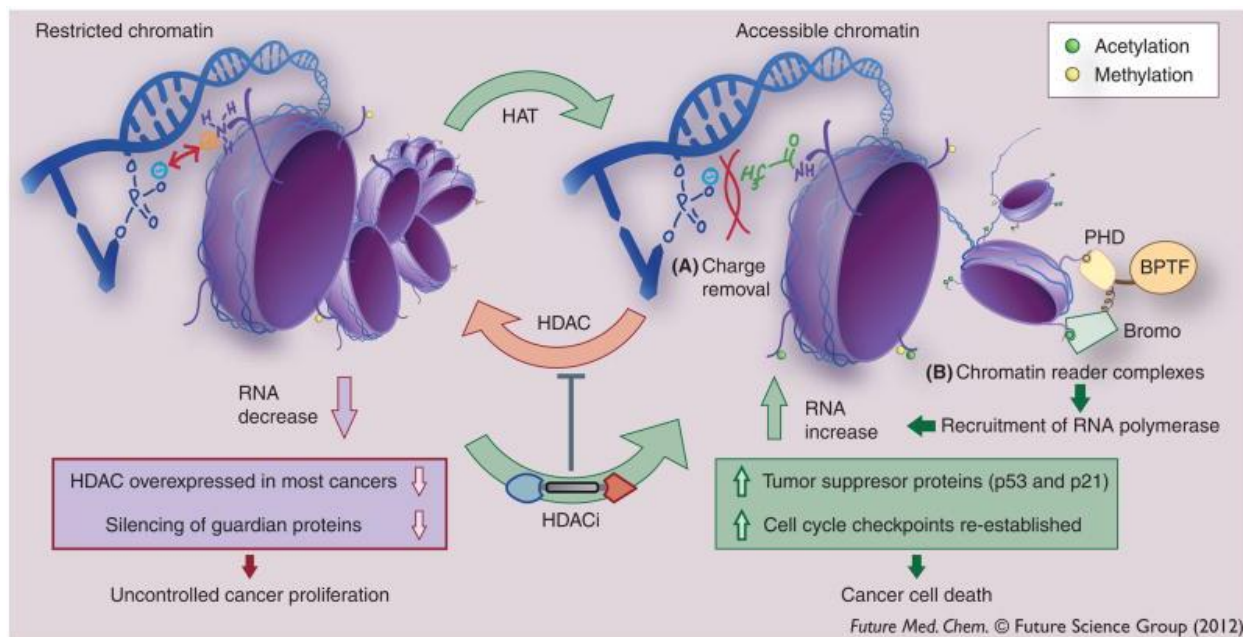


Figure 1.6. HDACs and HATs mechanism of action in chromatin.¹⁵⁴

Histone acetyltransferases (HATs) and Deacetylases (HDACs) are key epigenetic enzymes that regulate chromatin dynamics.¹⁵⁵ HATs acetylate the lysine residue of histones to generate 'open' form of chromatin that is accessible to transcription factors. Nuclear HDACs promote the reverse reaction to generate restricted chromatin. HDACs deacetylate other nonhistone proteins as well. There are eighteen HDAC isoforms grouped into four classes.¹⁵⁶ Classes I, II and IV are zinc-dependent amidohydrolases while class III are NAD^+ -dependent deacetylases. Class I consists of HDACs 1, 2, 3, and 8, which are mostly located in the nucleus; class IIa comprises of HDACs 4, 5, 7, 9, and they can shuttle between the nucleus and cytoplasm. Class IIb members are HDACs 6

and 10, and are found in cytoplasm while the only member of class IV is HDAC 11. Class III are Sirtuins, consisting of SIRT1-7.

Dysfunctions in HDACs activities could promote inflammation and immune response. For example, upregulation of HDAC1 and 2 activity stimulates TGF- β pathway, induces EMT,¹⁵⁷ ECM overproduction; and promotes fibroblast-myofibroblast transformation, and cell migration. Also, HDACs promote the expression of cytokines such as TNF- α , IL-6, and IL-1 β . HDAC3 specifically recruit the NF- κ B/p65 signal through epigenetic regulation of IL-1 expression, and thus TNF- α induced inflammation.^{158, 159} HDAC1 and HDAC2 are evidenced in responsible for positive regulation IL-6 and STAT3 induced gene expression.¹⁶⁰ Aberrant HDACs activities have also be implicated in fibrosis including liver cirrhosis, cardiac fibrosis, pulmonary fibrosis, renal fibrosis, and other inflammation diseases.¹⁶¹ HDAC inhibitors (HDACi) MS-275 and TSA suppress the TGF- β -mediated MAPK and PI3K pathway inflammation signals with demonstrable downregulation of biomarkers of p-ERK and p-Akt.¹⁶² TSA also attenuates tissue inflammation and prevents further damage.^{163, 164} HDAC inhibition also regulates the STAT pathway by hyperacetylation of STAT proteins.¹⁶⁵ Specifically, acetylation of STAT3 accelerates the STAT3 translocation towards the mitochondria where the acetylated STAT3 bind to E1 subunit of pyruvate dehydrogenase (PDH) stimulates the conversion of pyruvate to acetyl coA to increase metabolic flux through the TCA cycle that will consequently stimulate energy production via oxidative phosphorylation.¹⁶⁵ HDAC inhibition can also suppress tissue inflammation through inhibition of COX activation and PGE production.¹⁶⁶

The FDA and other non-US regulatory authorities have so far approved five HDACi to treat hematological malignancies. Vorinostat (SAHA) is approved for cutaneous T-cell lymphoma.¹⁶⁷ Belinostat, Chidamide, and Romidepsin are approved for peripheral T-cell lymphoma,¹⁶⁸⁻¹⁷⁰ while

Panobinostat is approved for multiple myeloma¹⁷¹ (Fig. 1.7). The standard pharmacophoric model of zinc-dependent HDACi consists of a zinc-binding group (ZBG), a hydrophobic linker, and a recognition cap group. Common ZBGs include carboxylic acid, hydroxamic acid, thiol, trifluoroketones and benzamide.¹⁷² To address the pharmacokinetic and pharmacodynamics issues plaguing early ZBGs, there has been sustained interest in identifying novel ZBGs.¹⁷³ In this regard, natural products flavonoids (Genistein, chrysin, etc.) have been reported as HDACi with novel ZBGs.¹⁷⁴

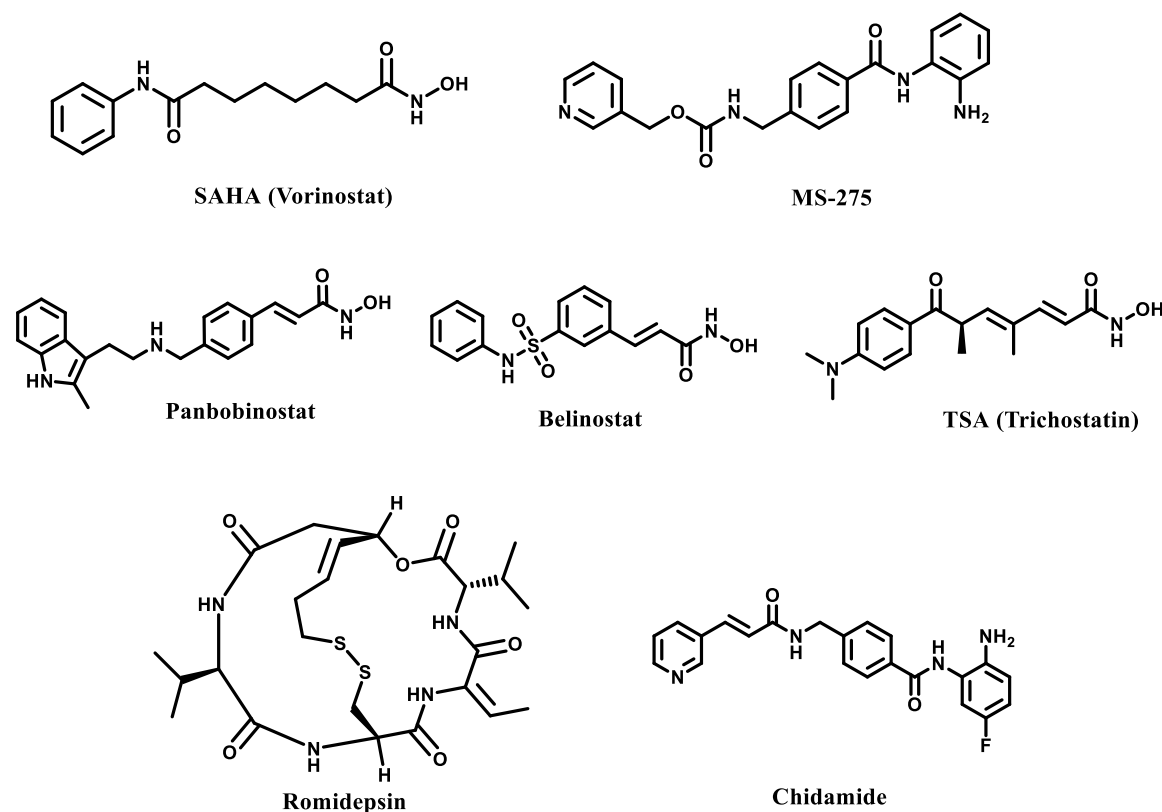


Figure 1.7. Selected HDACis.

Other researchers have reported novel ZGs as well.^{172, 175, 176} These new ZBGs are promising templates for the design of new generation of HDACi may possess targeted anti-inflammation and anti-cancer activities with reduced systemic toxicity.

1.6 Current medical challenges and novel solutions for targeting inflammation pathways:

1.6.1 Challenges with inhibition of TGF- β pathway

Inhibition of TGF- β pathway anti-inflammation and anti-cancer treatment strategy has encountered several challenges including overt toxicity, off-target effects, and low *in vivo* efficacy. The toxicity that results from TGF- β pathway inhibition is due to the vital multifaceted roles in normal biology. TGF- β pathway maintains tissue homeostasis and repair.¹⁷⁷ In normal tissue and organs, TGF- β promotes tissue regeneration and repair by recruiting stem/progenitor cells.¹⁷⁸ In another study, TGF- β pathway was shown to induce anti-oxidative effect via suppression of COX-2 activities in lung cancer cell.¹⁷⁹ Thus, inhibition of TGF- β may cause adverse effects.¹⁸⁰ Five drug candidates targeting the upstream of TGF- β pathway – the integrin inhibition – have been studied in the clinic for cancer treatment. Despite of promising data from preclinical animal models, the clinical outcomes have not been encouraging. Two trials (NCT01122888, NCT02337309) were terminated due to a lack positive outcome and the results from three trials (NCT00721669, NCT00284817, NCT00635193) have not disclosed to the public till date.¹⁸¹ Also, the integrin mechanism in TGF- β activation and cancer is not fully understood. Even though $\alpha\text{v}\beta 6$ Integrin activates TGF- β pathway and promote tumorigenesis, they seem to suppress pancreatic cancer progression.¹⁸² So, integrin inhibition as a cancer treatment strategy remains to be clinically validated.

As described in section **1.4.1** above, TGF- β pathway is regulated by several other pathways whose individual or collective inhibition could overcome the challenges noted with integrin inhibition. Pleiotropic small molecules that inhibit cohorts of TGF- β signaling mediators have been investigated. PFD, a notable example that suppresses TGF- β pathway through MAPK inhibition,

has been approved by FDA for the management of IPF.^{64, 65} The potential of PFD as anti-tumor agent is under active investigation.⁶⁶ However, PFD's systematic toxicity and low bioavailability have limited its efficacy in IPF treatment. PFD only slows long term IPF progression with 2.47 years life expectancy extension with no evidence of stopping the disease progression.¹⁸³

1.6.2 Challenges with NF- κ B pathway inhibition

NF- κ B pathway is important for both normal cell and diseased cell regulation and gain of function mutations within this pathway is relatively rare.^{184,185} This has contributed to the low therapeutic indices of NF- κ B-targeting agents. In addition, not all cancer cells are solely dependent on NF- κ B for survival, which makes most of NF- κ B inhibitors to only suppress cancer cell proliferation but not cause cancer cell death. Paradoxically, NF- κ B inhibition may even augment the invasiveness of certain cancer cells as it has been observed that ovarian cancer cells could become more invasive with NF- κ B inhibition.¹⁸⁶ Also, NF- κ B may play very important role in immunity, and NF- κ B inhibitors could induce the impairment of NF- κ B-dependent immune response and inflammation.¹⁸⁴

Nrf-2 activation is an alternative approach to achieve NF- κ B inhibition.¹⁸⁷ Activated Nrf-2 induces the transcription of anti-ROS genes such as HO-1, SOD, NQO1, catalase, and other anti-oxidant proteins. These proteins effectively suppress the signal of NF- κ B and attenuate inflammation progression. Most importantly, the Nrf-2 activation does not impair the normal NF- κ B pathway in the cell, and so effectively reduces inflammation with reduced adverse effects. Nrf-2 activation could be achieved through the inhibition of Kelch-like ECH-associated protein 1 (KEAP1). To date, known KEAP1 inhibitors, such as dimethyl fumarate (DMF), are electrophilic compounds

that form covalent bonds with its cysteine 288 and 289.^{89, 188, 189} DMF has been approved for the treatment of relapsing multiple sclerosis and psoriasis while clinical trials evaluating its potential application in other inflammatory disease and cancer are ongoing.¹⁹⁰ Piperic acid and its analog, piperine, are another examples of KEAP1 inhibitors whose mechanisms of action have not been firmly established.¹⁹¹ The PPA and DMF may work similarly to inhibit the KEAP1 activity. However, DMF and PPA lack tissue targeting and are widely distributed in the human body. The systemic distribution could be responsible for the adverse effects, such as abdominal pain, flushing, diarrhea, nausea, etc, which DMF has elicited in the clinic.¹⁹²

1.6.3 Challenges with COX/LOX inhibition

Recent efforts on achieving COX inhibition has mainly focused on COX-2 selective inhibition. Celecoxib, a lead FDA-approved COX-2 inhibitor, is being investigated in clinical trials for the treatment of several cancer types including head and neck cancer (NCT04162873), bladder cancer (NCT02885974), TNBC (NCT04081389), malignant pleural mesothelioma (NCT03710876); antiangiogenic therapy for medulloblastoma, ependymoma ATRT (NCT01356290) and others. In previous trials, Celecoxib has been studied as a combination therapy to cancer with chemotherapy, due to its efficiency of COX-2 inhibition. COX-2 overexpression had been found to increase cancer cell drug resistance to chemotherapy, and combination of celecoxib may induce drug sensitivity instead. However, in previous clinical trials, HER2 positive breast cancer patients that were treated with trastuzumab along with Celecoxib did not experience improved efficacy.¹⁹³ In a colorectal cancer chemoprevention study, cardiovascular risks (heart failure) was observed in patients taking high daily dosage of Celecoxib for a period of 3 years.¹⁹⁴ Another study also noticed

Celecoxib's cardiovascular risks.¹⁹⁵ Valdecoxib, another COX-2 selective inhibitor, was voluntarily withdrawn due to the cardiovascular concerns.¹⁹⁶

Although the roles of COX-2 in malignant transformations are well established, COX-1 also plays leading roles in tumorigenesis (see section **1.5.4** for details). Unfortunately, COX-1 selective inhibitors are few and have yet to be well-studied to decipher the roles of COX-1 in the pathophysiology of cancers.¹⁹⁷ The traditional NSAIDs COX-1 selective inhibitors encountered with elucidating gastrointestinal toxicity, and yet to solve the issue to date.¹⁹⁸ Tumor-targeting delivery or cell-type selective COX-1 inhibitors could potentially mitigate the GI adversary effect. Therefore, there is a significant need for novel COX-1 selective agents.

1.6.4 Challenges with STAT3 inhibition

Inhibition of multiple effectors, including JAK kinase, SH2 Domain, and DNA binding domain, have been investigated for inhibitions in STAT3 pathway.¹⁹⁹ However, the FDA has approved none of the drugs targeting these effectors. The failure of current STAT3 inhibitors is largely due to toxicity and lack of specificity for STAT3. Despite this frustration, STAT3 still remains a valuable target for the discovery of anti-inflammation and anti-cancer drugs.

1.6.5 Challenges with HDAC inhibition:

Although HDAC inhibition has been clinically validated for the treatment of hematological malignancies, it has so far not been effective against solid tumors. The reason for the lack of

efficacy of HDACi against solid tumors is not fully understood. However, the fact that most HDACi do not accumulate within the tumor interstitium at therapeutically efficacious concentrations is a major culprit.¹⁵⁴ Additionally, HDAC inhibition elicits a pleiotropic phenotype, primarily due to their nonselective inhibition of various HDAC isoforms and possibly other non-HDAC targets. This non-selectivity causes reduced *in vivo* potency and toxic side effects. Regardless, reactivation of tumor-suppressor genes by HDACi is still currently being pursued as a potentially broad cancer treatment option.²⁰⁰

1.7 Solutions investigated in this thesis:

Inhibition of the major inflammation pathways enumerated herein, as anti-inflammation and anti-cancer treatment strategy, still has great potential. Targeted inhibition – of tumor/cancer cells, or the inflamed tissues – could be a feasible solution to mitigate the off-target toxicity and systematic toxicity of drugs inhibiting these pathways. This thesis focused on developing cell- and tissue-selective anti-inflammatory and anti-cancer agents that have potential to overcome the shortcomings of the currently available drugs.

1.7.1 Macrolides as templates for targeted delivery to liver and lung tissues

Azithromycin (AZM) and clarithromycin (CLM) are two macrolactone antibiotics that is widely used to treat upper respiratory tract infections. AZM and CLM shared similar mechanism of action involving selective inhibition of bacterial ribosome to prevent protein synthesis.²⁰¹

AZM and CLM are highly effective in treating upper respiratory tract infections due to their outstanding pharmacokinetics (PK) properties and selective distributions to the disease sites. AZM and CLM selectively accumulate in lung resident macrophages and other immune cells which may accumulate in infectious tissues.^{202, 203, 204} AZM and CLM also accumulate in the liver tissues as well. These macrolides demonstrate more than 100-fold enrichment in these tissues relative to the bloodstream.²⁰⁵⁻²⁰⁷ Evidently, AZM and CLM have intrinsic anti-inflammatory activities. AZM facilitates the repair of tissue injury, downregulates leukocytes activities, and the expressions of pro-inflammatory cytokines.²⁰⁸⁻²¹³ CLM attenuates tissue fibrosis progression by downregulating the cytokines, and inhibiting the fibroblast migration through downregulation of inflammatory product TXA₂.^{214, 215} Third, AZM has been observed to selectively accumulates internally with epithelial cells, fibroblasts, lymphocyte, and hepatocyte.^{203, 216, 217} These evidences make AZM an excellent lung/liver targeting antibiotics with low systematic toxicity. In addition, AZM is well-tolerated by patients as a result of its safe metabolites.²⁰⁸ Currently, Macrolides have been recognized as potential anti-inflammatory candidates in respiratory disease.²¹⁸ Based on these attributes, AZM and CLM are ideal template molecules for the design of liver- and lung-tissues targeted anti-inflammation and anti-cancer agents.

1.7.1.1 Macrolide-based anti-fibrotic agents

As discussed above, PFD, as a TGF- β inhibitor, showed potential and possibility in attenuating tissue inflammation. Tissue targeted delivery may overcome challenges associated with PFD clinical application, such as off-target effects and systematic toxicity. We hypothesized that

integration of PFD-like moiety into AZM and CLM templates would afford novel TGF- β inhibiting anti-fibrotic agents that are selectively accumulated in the lungs and liver tissues.

In Chapter 2, I designed and synthesized four classes macrolide-based PFD-like compounds (total of 28 compounds) to test our hypothesis (Fig. 1.8). We found that the selected candidates showed significant anti-inflammatory and anti-fibrotic effects that are more than 1,000-fold more potent than PFD. Specifically, among five lead agents, compound **15c** is one of the most promising candidates based on its biological activity and chemical structure. Compound **15c** is 10-fold more potent in inhibition of NF- κ B pathway and 2,500-fold more cytotoxic to MRC5 cells than PFD. Also, **15c** showed over 1,000-fold more potent TGF- β pathway inhibition and about 1,000-fold more potent ECM production inhibition than PFD. From mechanism of action studies, we found that **15c** derived its bioactivities by targeting pathways responsible for the anti-fibrotic activities of PFD and AZM. Collectively, these macrolide-based PFD-like compounds are excellent candidates for more in-depth preclinical studies as therapeutic agents for IPF.

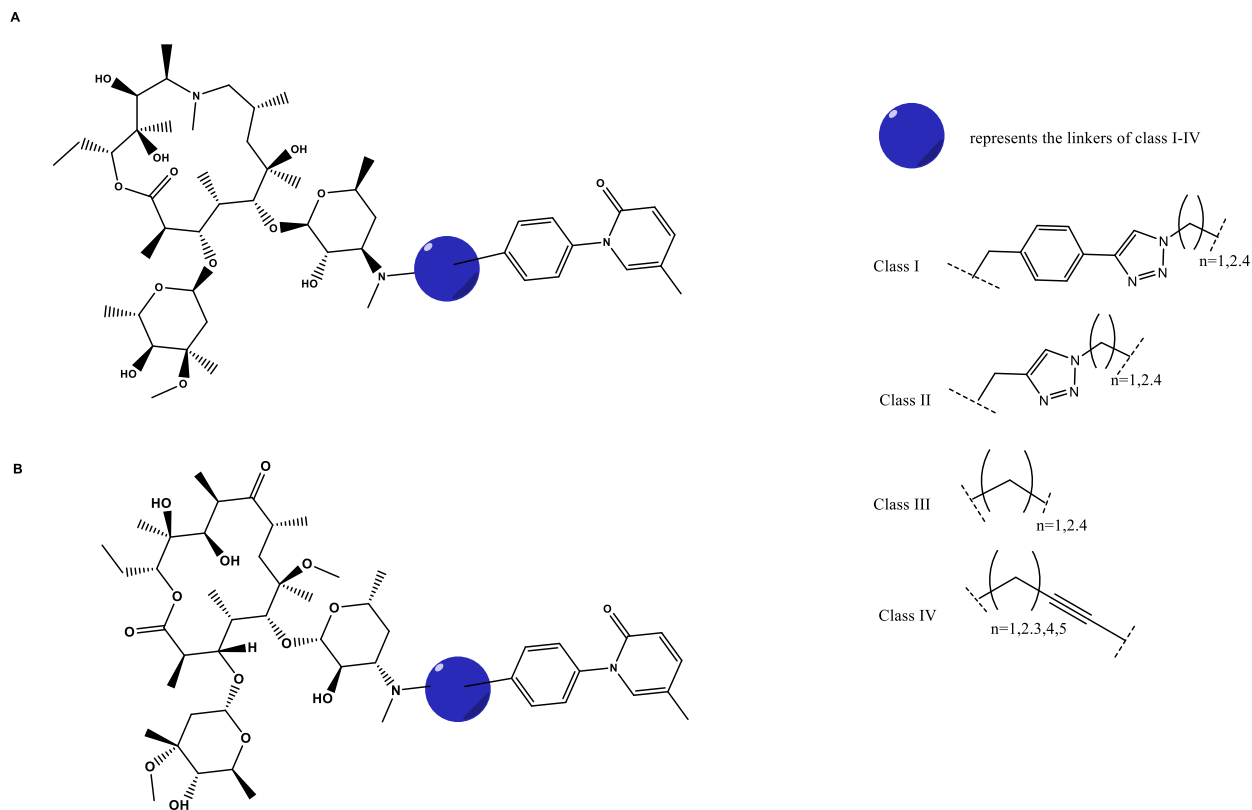


Figure 1.8. General structures of macrolide-based PFD-like compounds.

1.7.1.2 Macrolide conjugated with anti-oxidants as novel anti-inflammation and anti-cancer agents.

In Chapter 3, to follow-up on the promising anti-IPF activities that were observed with the macrolide-based PFD-like compounds, I co-opted AZM and CLM as templates for the design of other tissue selective anti-inflammatory drugs. I used R-alpha lipoic acid (ALA), piperic acid (PPA), and Fumaric acid (FMA) as a model anti-inflammatory drug in this follow-up project. ALA is a well-known anti-inflammation agent that is ubiquitously available in the in biological milieu due to its involvement as a co-factor in several metabolic processes. ALA has been touted to possess beneficial biological properties including anti-cancer, anti-aging, anti-diabetes and anti-

HIV activities. The anti-inflammatory activities of ALA have been made evident by its attenuation of PI3K/Akt pathway and inhibition of NF- κ B²¹⁹ and PDK1.²²⁰ PDK1 is a TCA cycle inhibitor which switches cell energy production from the mitochondrial respiration into aerobic glycolysis. In IPF or during tumor growth, the myofibroblasts or cancer cells sustain reprogramming to the glycolytic metabolism by elevating the PDK1.²²¹ Therefore, ALA has potential anti-fibrotic and anti-cancer activities. Literature evidence further supporting the bioactivity of ALA include its downregulation of Bcl-xL, Mcl-1, Bcl-2, and Bax in breast cancer cells, resulting in cell apoptosis.^{222, 223} However, presumably due to its weak efficacy, ALA has neither been approved by FDA, nor successfully used to treat any medical condition. We hypothesized that conjugation of ALA to AZM and CLM could enhance its potency and impart on the resulting agents lung tissue and liver selective distribution property.

Subsequently, I further extended this aspect of my research to include PPA and fumarate analogs, the two classes of electrophilic agents that act as NF- κ B pathway inhibitors and Nrf-2 activators. Again, my expectation here is that conjugation of PPA and FMA analogs would enhance their potency and furnish lung and liver tissue targeting anti-ROS agents. Toward this end, I designed and synthesized 12 macrolide-derived PPA and Fumarate agents. General structures of these compounds are shown in Figure 1.10.

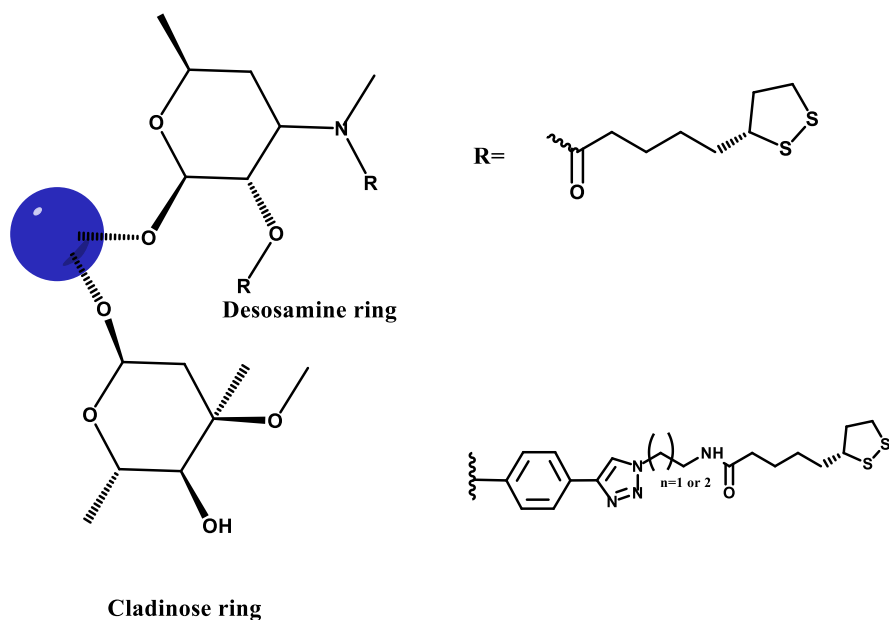


Figure 1.9. Structures of ALA derivatives investigated. Blue ball indicates macrolides (AZM and CLM). The glycosylated side arms desosamine may conjugate with lipoic acid in R position or the hydroxyl group with ALA in multiple types of conjugation. We also made de-cladinose derivatives (removal of cladinose) to investigate how this modification affects bioactivity of the synthesized agents.

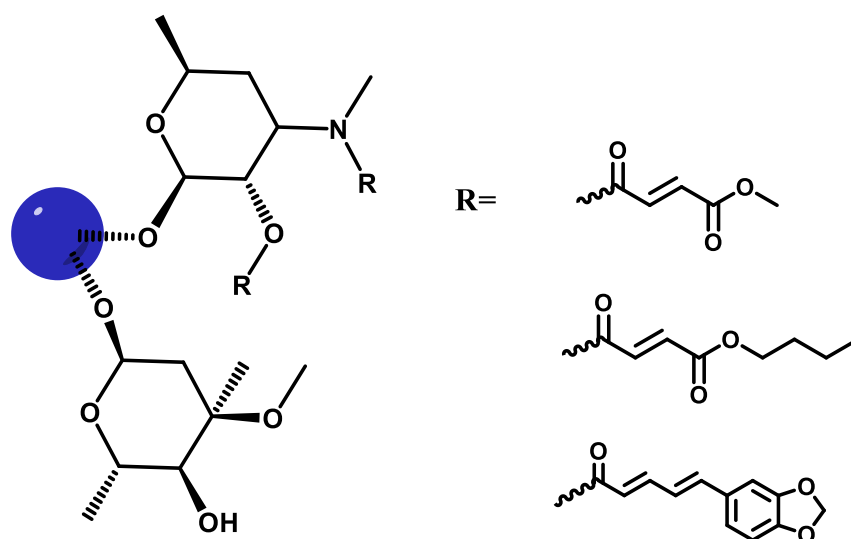
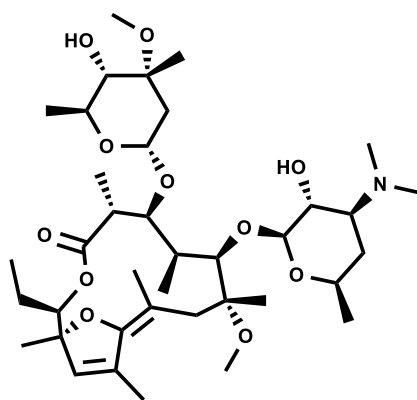


Figure 1.10. Structures of macrolide-derived PPA and FMA agents. Blue ball indicates macrolides, (AZM and CLM). The sugar moieties desosamine is conjugated with PPA or FMA analogs in positions R or the hydroxyl group. We also made de-cladinose derivatives (removal of cladinose) to investigate how this modification affects bioactivity of the synthesized agents.

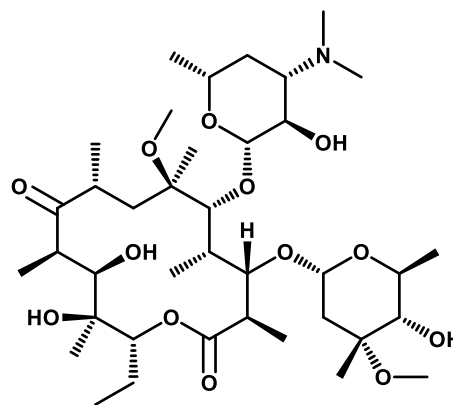
In chapter 3, I designed and synthesized three classes (total 12 candidates) of AZM and CLM conjugated ALA, PPA, and fumarate derivatives (Fig. 1.9 and 1.10). We observed that these compounds have significantly enhanced cytotoxicity against multiple cancer cells and fibroblast cell relative to unconjugated antioxidants. In addition, we noted that many candidates showed anti-fibrotic effects evidenced by the reduction in the ECM production. We also found that representative compounds in this series more potently inhibit STAT3 pathway relative to ALA. Targeted STAT3 inhibition is highly desirable as a therapeutic strategy for STAT3-addicted cancers such as triple negative breast cancer. To further investigate the electrophilic antioxidants, we investigated their effects on Nrf-2 activity and found that they induced Nrf-2 activation, evidenced by HO-1 upregulation within 6h of exposure to cells. Collectively, these data showed that macrolide-derived PPA and FMA agents are promising Nrf-2 activators and NF- κ B inhibitors.

1.7.1.3 A Novel anti-cancer macrolide.

In addition to the richness of their biological activities, several functional groups on macrolides, including AZM and CLM, also display unique reactivity, largely due to the unique steric effect of their macrolactone moiety. In Chapter 4, we have discovered that CLM undergoes a one-step dehydrative cyclization when treated with mildly acidic or neutral dehydration reagents, leading to a dihydrofuranyl analog, df-CLM (AO-02-63). This novel compound displayed a drastically reduced prokaryotic translation inhibition activity and an occurrence of eukaryotic translation inhibition relative to the parent CLM.



AO-02-63



clarithromycin

Figure 1.11 Structure of AO-02-63 and clarithromycin (CLM).

The new compound showed broad-spectrum anti-cancer activity in NCI-60 panel with low micromolar IC_{50} (~ 2.5 - $5\mu M$). Because AO-02-63 induces eukaryotic ribosome activity inhibition, we speculated that it could fit into the eukaryotic 80s ribosome exit tunnel, in an analogous manner to the interaction of CLM with the exit tunnel of the prokaryotic 50s ribosome, to block protein translation. More importantly, we noticed that AO-02-63 inherited the anti-fibrotic effects of CLM but with enhanced potency (10-fold enhancement). At 2.5 to $5\mu M$, it repressed the ECM production significantly, CLM requires $50\mu M$ to reach the same level ECM production repression. In further study, we noticed that AO-02-63 acts similarly to CLM to activate HDAC2 and downregulate the acetylation of H4.

1.7.2 Novel STAT3 inhibitors

The potential of STAT3 pathway inhibition as an anticancer strategy is being actively investigated in preclinical and clinical settings. Recently, pyrimethamine (PYM) was discovered

as a dihydrofolate reductase (DHFR) inhibitor which also has STAT3 inhibition activity.^{224, 225} PYM has been studied in clinical trials as an agent for leukemia treatment. Though no STAT3 inhibitor has been approved by the FDA, PYM could be a synthetically tractable template for the synthesis of less toxic STAT3 inhibitors since it is approved for the treatment of other human diseases such as toxoplasmosis, Isosporiasis, and cystoisosporiasis.²²⁶⁻²²⁹ The biological activities of PYM is tolerant of modifications at the chloride moiety of PYM. Therefore, modifications of this moiety could be pursued to design novel STAT3 inhibitors.

In Chapter 6, I describe the used of an *in silico* molecular docking tool (Autodock vina) to design three classes of PYM derivatives (total of 12 compounds) as putative STAT3 inhibitors that function by blocking the DNA binding domain of STAT3. I synthesized these compounds and profiled for their STAT3 inhibition in a cell free assay. Subsequently, they were analyzed in Hep-G2, A549, VERO, MDA-MB-231, and MCF-7 cell line. I found that class II compound **11b-d** showed 100-fold enhanced cytotoxicity relative to PYM. More significantly, they are also 100-fold better STAT3 pathway inhibitors. As hypothesized, the STAT3 inhibition activities of these compounds are largely due to their direct STAT3 DNA binding interruption.

1.7.3 Novel HDAC inhibitors

To overcome the challenges of HDACi, we have been optimizing the classic three pharmacophoric model – Cap group-linker-ZBG – that virtually all HDACi fit into. We have been incorporating into HDACi cap group chemotypes that have tissue and/or cell-type selectively. We have developed and reported different types of HDACi based on this method.^{230, 231, 232, 233} In this thesis, I developed and/or characterized novel HDACi that are selective for TNBC and HCC.

1.7.3.1 Dual-acting STAT3-HDACi based on PYM are selective for TNBC.

Premised on the well-established role of HDACs in the regulation of STAT3 signaling,^{234, 235} we had earlier hypothesized that simultaneous STAT3 and HDAC inhibition will lead to more durable anti-proliferative effects in STAT3-addicted cancer cells. To validate this hypothesis, I synthesized 5 compounds (Fig. 1.12) and tested them in the same set of cell lines that we tested in chapter 5. We noticed that these inhibited both HDAC and STAT3 pathway intracellularly. Interestingly, compounds **12b** and **12c** showed 6- to 10-fold cell-type selectivity for a STAT3-dependent, TNBC cell line MDA-MB-231. These data indicate that PYM-HDACi could be the bifunctional agent that are selective for STAT3-addicted cancer cells.

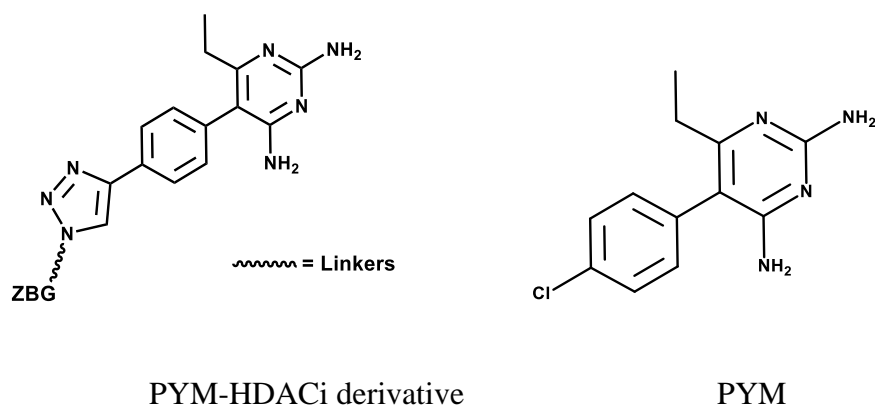


Figure 1. 12. Dual-acting STAT3-HDACi based on PYM. The linker groups are derived from methylene or cinnamic groups.

1.7.3.2 Glycosylated HDACi are selective for HCC.

Warburg effect is well-known as the main energy supply method for cancer cells. Since cancer cells favor metabolism via glycolysis rather than oxidative phosphorylation pathway, sugar uptake and consumption rate is much higher in cancer cells than normal cell lines. To take an advantage to this effect, we hypothesized that integration of glucose or mannose into the surface cap group (recognition group) of prototypical HDACi will furnish agents that will be selectively up-taken by cancer cells. GLUT2, a glucose transporter that is overexpressed in hepatocyte and liver cancer cell lines,^{236, 237} could facilitate a selective uptake of glycosylated HDACi into HCC cells to elicit selective HCC cells toxicity.

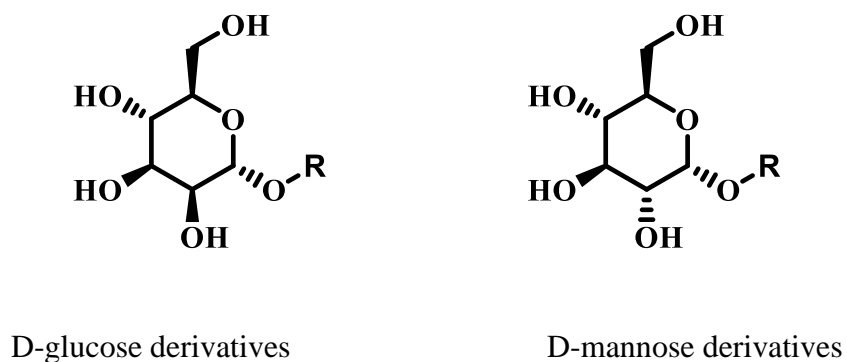


Figure 1.13. Glycosylated HDAC inhibitors structures. R stands for various types of HDAC inhibitors with different types of linkers.

In Chapter 7, I described results from characterization of the anti-proliferative activities and mechanism of action of 19 glucose-, mannose- and desosamine-derived HDACi. We found that these compounds are selectively cytotoxic to several HCC cell lines due to GLUT2-mediated uptake. Specifically, glucose derivative **STR-V-53** is significantly more selective for HCC cells. In collaboration with the Petros Lab at Emory University, we found that **STR-V-53** is non-toxic to healthy mice (MTD > 100 mg/kg) and effectively suppressed tumor growth in orthotopic murine model of HCC. In addition, we identified desosamine (STR-V-165) and mannose (STR-I-195)

derivatives as back-up compounds. Collectively, these glycosylated HDACi are promising anti-HCC agents.

1.8 Conclusion

Inflammation is strongly linked to several serious chronic diseases that remained to be effectively managed in the clinic. Death rates from several of these diseases, including IPF, liver cirrhosis, gastric inflammation, etc., are very high. There are copious evidences that implicate several of these diseases in malignant transformations as key pro-inflammatory signals, including TGF- β pathway, NF- κ B, STAT pathway, arachidonic acid metabolism, and epigenetic regulations, play essential roles in tumorigenesis. Several pharmacological agents that are currently in use for the treatments of chronic diseases and tumors are sub-optimal, as most are systemic agents that are plagued with overt toxicity and poor distribution at disease sites. In this thesis, I described plausible tissue targeted and/or pathways selective approaches may overcome the challenges the current agents. Cohorts of compounds disclosed in this work merit further investigation to elucidate their potential as new generation of targeted therapeutic agents for the treatment/management of fibrosis, inflammation, and cancers.

1.9 References:

1. Singh N, Baby D, Rajguru JP, Patil PB, Thakkannavar SS, Pujari VB. Inflammation and cancer. *Annals of African medicine*. 2019;18(3):121.
2. Vancheri C, du Bois RM. A progression-free end-point for idiopathic pulmonary fibrosis trials: lessons from cancer. *Eur Respir J*. 2013;41(2):262-9.

3. Kuraishy A, Karin M, Grivennikov SI. Tumor promotion via injury-and death-induced inflammation. *Immunity*. 2011;35(4):467-77.
4. Elliot A, Myllymäki H, Feng Y. Inflammatory Responses during Tumour Initiation: From Zebrafish Transgenic Models of Cancer to Evidence from Mouse and Man. *Cells*. 2020;9(4):1018.
5. Borsig L, Wolf MJ, Roblek M, Lorentzen A, Heikenwalder M. Inflammatory chemokines and metastasis—tracing the accessory. *Oncogene*. 2014;33(25):3217-24.
6. Coussens LM, Werb Z. Inflammation and cancer. *Nature*. 2002;420(6917):860-7.
7. Singh AK, Khare P, Obaid A, Conlon KP, Basrur V, DePinho RA, et al. SUMOylation of ROR- γ t inhibits IL-17 expression and inflammation via HDAC2. *Nature communications*. 2018;9(1):1-11.
8. Ranneh Y, Ali F, Akim AM, Hamid HA, Khazaai H, Fadel A. Crosstalk between reactive oxygen species and pro-inflammatory markers in developing various chronic diseases: a review. *Applied Biological Chemistry*. 2017;60(3):327-38.
9. Mittal M, Siddiqui MR, Tran K, Reddy SP, Malik AB. Reactive oxygen species in inflammation and tissue injury. *Antioxidants & redox signaling*. 2014;20(7):1126-67.
10. Zhang J-M, An J. Cytokines, inflammation and pain. *International anesthesiology clinics*. 2007;45(2):27.
11. Chen L, Deng H, Cui H, Fang J, Zuo Z, Deng J, et al. Inflammatory responses and inflammation-associated diseases in organs. *Oncotarget*. 2018;9(6):7204.
12. Midwood KS, Williams LV, Schwarzbauer JE. Tissue repair and the dynamics of the extracellular matrix. *The international journal of biochemistry & cell biology*. 2004;36(6):1031-7.
13. Herrera J, Henke CA, Bitterman PB. Extracellular matrix as a driver of progressive fibrosis. *The Journal of clinical investigation*. 2018;128(1):45-53.
14. Akl H, Vervloessem T, Kiviluoto S, Bittremieux M, Parys JB, De Smedt H, et al. A dual role for the anti-apoptotic Bcl-2 protein in cancer: mitochondria versus endoplasmic reticulum. *Biochim Biophys Acta*. 2014;1843(10):2240-52.
15. Schneider G, Henrich A, Greiner G, Wolf V, Lovas A, Wieczorek M, et al. Cross talk between stimulated NF-kappaB and the tumor suppressor p53. *Oncogene*. 2010;29(19):2795-806.
16. Chen SL, Morgan TR. The natural history of hepatitis C virus (HCV) infection. *Int J Med Sci*. 2006;3(2):47-52.
17. Sauleda J, Nunez B, Sala E, Soriano JB. Idiopathic Pulmonary Fibrosis: Epidemiology, Natural History, Phenotypes. *Med Sci (Basel)*. 2018;6(4).
18. Navaratnam V, Fleming KM, West J, Smith CJ, Jenkins RG, Fogarty A, et al. The rising incidence of idiopathic pulmonary fibrosis in the U.K. *Thorax*. 2011;66(6):462-7.
19. Health TNIo. Idiopathic pulmonary fibrosis. 2020.

20. Fernandez Perez ER, Daniels CE, Schroeder DR, St Sauver J, Hartman TE, Bartholmai BJ, et al. Incidence, prevalence, and clinical course of idiopathic pulmonary fibrosis: a population-based study. *Chest*. 2010;137(1):129-37.
21. Huard J, Li Y, Fu FH. Muscle injuries and repair: current trends in research. *J Bone Joint Surg Am*. 2002;84(5):822-32.
22. Heinemeier KM, Olesen JL, Haddad F, Langberg H, Kjaer M, Baldwin KM, et al. Expression of collagen and related growth factors in rat tendon and skeletal muscle in response to specific contraction types. *J Physiol*. 2007;582(Pt 3):1303-16.
23. Wolters PJ, Collard HR, Jones KD. Pathogenesis of idiopathic pulmonary fibrosis. *Annu Rev Pathol*. 2014;9:157-79.
24. Kramann R, DiRocco DP, Humphreys BD. Understanding the origin, activation and regulation of matrix-producing myofibroblasts for treatment of fibrotic disease. *J Pathol*. 2013;231(3):273-89.
25. Xu J, Lamouille S, Derynck R. TGF-beta-induced epithelial to mesenchymal transition. *Cell Res*. 2009;19(2):156-72.
26. Piera-Velazquez S, Li Z, Jimenez SA. Role of endothelial-mesenchymal transition (EndoMT) in the pathogenesis of fibrotic disorders. *Am J Pathol*. 2011;179(3):1074-80.
27. Bagnato G, Harari S. Cellular interactions in the pathogenesis of interstitial lung diseases. *Eur Respir Rev*. 2015;24(135):102-14.
28. Francescone R, Hou V, Grivennikov SI. Cytokines, IBD, and colitis-associated cancer. *Inflamm Bowel Dis*. 2015;21(2):409-18.
29. Park J, Kim DS, Shim TS, Lim CM, Koh Y, Lee SD, et al. Lung cancer in patients with idiopathic pulmonary fibrosis. *Eur Respir J*. 2001;17(6):1216-9.
30. Karampitsakos T, Tzilas V, Tringidou R, Steiropoulos P, Aidinis V, Papiris SA, et al. Lung cancer in patients with idiopathic pulmonary fibrosis. *Pulm Pharmacol Ther*. 2017;45:1-10.
31. Coussens LM, Werb Z. Inflammation and cancer. *Nature*. 2002;420(6917):860-7.
32. Multhoff G, Molls M, Radons J. Chronic inflammation in cancer development. *Front Immunol*. 2011;2:98.
33. Park J, Kim D, Shim T, Lim C, Koh Y, Lee S, et al. Lung cancer in patients with idiopathic pulmonary fibrosis. *European Respiratory Journal*. 2001;17(6):1216-9.
34. Pietras EM. Inflammation: a key regulator of hematopoietic stem cell fate in health and disease. *Blood*. 2017;130(15):1693-8.
35. Arrese M, Hernandez A, Astete L, Estrada L, Cabello-Verrugio C, Cabrera D. TGF-beta and Hepatocellular Carcinoma: When A Friend Becomes An Enemy. *Curr Protein Pept Sci*. 2018;19(12):1172-9.
36. Vescovo T, Refolo G, Vitagliano G, Fimia GM, Piacentini M. Molecular mechanisms of hepatitis C virus-induced hepatocellular carcinoma. *Clin Microbiol Infect*. 2016;22(10):853-61.

37. Salih BA. Helicobacter pylori infection in developing countries: the burden for how long? *Saudi J Gastroenterol*. 2009;15(3):201-7.
38. Wroblewski LE, Peek RM, Jr., Wilson KT. Helicobacter pylori and gastric cancer: factors that modulate disease risk. *Clin Microbiol Rev*. 2010;23(4):713-39.
39. Teoh CM, Tan SS, Tran T. Integrins as Therapeutic Targets for Respiratory Diseases. *Curr Mol Med*. 2015;15(8):714-34.
40. Phan SH. Biology of fibroblasts and myofibroblasts. *Proc Am Thorac Soc*. 2008;5(3):334-7.
41. Salton F, Volpe MC, Confalonieri M. Epithelial(-)Mesenchymal Transition in the Pathogenesis of Idiopathic Pulmonary Fibrosis. *Medicina (Kaunas)*. 2019;55(4).
42. Kinoshita T, Goto T. Molecular Mechanisms of Pulmonary Fibrogenesis and Its Progression to Lung Cancer: A Review. *Int J Mol Sci*. 2019;20(6).
43. Poniatowski ŁA, Wojdasiewicz P, Gasik R, Szukiewicz D. Transforming growth factor Beta family: insight into the role of growth factors in regulation of fracture healing biology and potential clinical applications. *Mediators of inflammation*. 2015;2015.
44. Munger JS, Sheppard D. Cross talk among TGF- β signaling pathways, integrins, and the extracellular matrix. *Cold Spring Harbor perspectives in biology*. 2011;3(11):a005017.
45. Annes JP, Chen Y, Munger JS, Rifkin DB. Integrin α V β 6-mediated activation of latent TGF- β requires the latent TGF- β binding protein-1. *The Journal of cell biology*. 2004;165(5):723-34.
46. Lyons RM, Keski-Oja J, Moses HL. Proteolytic activation of latent transforming growth factor-beta from fibroblast-conditioned medium. *J Cell Biol*. 1988;106(5):1659-65.
47. Yu Q, Stamenkovic I. Cell surface-localized matrix metalloproteinase-9 proteolytically activates TGF-beta and promotes tumor invasion and angiogenesis. *Genes Dev*. 2000;14(2):163-76.
48. Barcellos-Hoff MH, Dix TA. Redox-mediated activation of latent transforming growth factor-beta 1. *Mol Endocrinol*. 1996;10(9):1077-83.
49. Raugi GJ, Olerud JE, Gown AM. Thrombospondin in early human wound tissue. *J Invest Dermatol*. 1987;89(6):551-4.
50. Wipff PJ, Hinz B. Integrins and the activation of latent transforming growth factor beta1 - an intimate relationship. *Eur J Cell Biol*. 2008;87(8-9):601-15.
51. Verrecchia F, Mauviel A. Transforming growth factor-beta signaling through the Smad pathway: role in extracellular matrix gene expression and regulation. *J Invest Dermatol*. 2002;118(2):211-5.
52. Zhang YE. Non-Smad pathways in TGF-beta signaling. *Cell Res*. 2009;19(1):128-39.
53. Zhang L, Zhou F, ten Dijke P. Signaling interplay between transforming growth factor-beta receptor and PI3K/AKT pathways in cancer. *Trends Biochem Sci*. 2013;38(12):612-20.

54. Xu J, Lamouille S, Derynck R. TGF- β -induced epithelial to mesenchymal transition. *Cell research*. 2009;19(2):156-72.
55. Guerrero PA, McCarty JH. TGF- β activation and signaling in angiogenesis. *Physiologic and Pathologic Angiogenesis-Signaling Mechanisms and Targeted Therapy*. 2017.
56. Lyden D, Young AZ, Zagzag D, Yan W, Gerald W, O'Reilly R, et al. Id1 and Id3 are required for neurogenesis, angiogenesis and vascularization of tumour xenografts. *Nature*. 1999;401(6754):670-7.
57. Liu S, Chen S, Zeng J. TGF β signaling: A complex role in tumorigenesis (Review). *Mol Med Rep*. 2018;17(1):699-704.
58. Finnson KW, Almadani Y, Philip A, editors. Non-canonical (non-SMAD2/3) TGF- β signaling in fibrosis: Mechanisms and targets. *Seminars in cell & developmental biology*; 2020: Elsevier.
59. Zhang YE, Newfeld SJ. Meeting report–TGF- β superfamily: signaling in development and disease. The Company of Biologists Ltd; 2013.
60. Colak S, ten Dijke P. Targeting TGF- β signaling in cancer. *Trends in cancer*. 2017;3(1):56-71.
61. Stylianopoulos T, Jain RK. Combining two strategies to improve perfusion and drug delivery in solid tumors. *Proc Natl Acad Sci U S A*. 2013;110(46):18632-7.
62. Lohr M, Schmidt C, Ringel J, Kluth M, Muller P, Nizze H, et al. Transforming growth factor-beta1 induces desmoplasia in an experimental model of human pancreatic carcinoma. *Cancer Res*. 2001;61(2):550-5.
63. Walker RA. The complexities of breast cancer desmoplasia. *Breast Cancer Res*. 2001;3(3):143-5.
64. Zhou C, Zeldin Y, Baratz ME, Kathju S, Satish L. Investigating the effects of Pirfenidone on TGF- β 1 stimulated non-SMAD signaling pathways in Dupuytren's disease-derived fibroblasts. *BMC musculoskeletal disorders*. 2019;20(1):1-8.
65. Hostettler K, Zhong J, Tamm M, Lardinois D, Roth M. Effect of pirfenidone on TGF- β -induced pro-fibrotic effects in primary human lung cells derived from patients with idiopathic pulmonary fibrosis. *European Respiratory Journal*. 2014;44(Suppl 58).
66. Miura Y, Saito T, Tanaka T, Takoi H, Yatagai Y, Inomata M, et al. Reduced incidence of lung cancer in patients with idiopathic pulmonary fibrosis treated with pirfenidone. *Respiratory Investigation*. 2018;56(1):72-9.
67. Li L, Orner BP, Huang T, Hinck AP, Kiessling LL. Peptide ligands that use a novel binding site to target both TGF- β receptors. *Molecular BioSystems*. 2010;6(12):2392-402.
68. Boswell S, Sharif S, Alisa A, Pereira SP, Williams R, Behboudi S. Induction of latency-associated peptide (transforming growth factor- β 1) expression on CD4+ T cells reduces Toll-like receptor 4 ligand-induced tumour necrosis factor- α production in a transforming growth factor- β -dependent manner. *Immunology*. 2011;133(3):278-87.
69. Boye A, Kan H, Wu C, Jiang Y, Yang X, He S, et al. MAPK inhibitors differently modulate TGF- β /Smad signaling in HepG2 cells. *Tumor Biology*. 2015;36(5):3643-51.

70. Lawrence T. The nuclear factor NF-kappaB pathway in inflammation. *Cold Spring Harb Perspect Biol.* 2009;1(6):a001651.
71. Xia Y, Shen S, Verma IM. NF-kappaB, an active player in human cancers. *Cancer Immunol Res.* 2014;2(9):823-30.
72. Catz SD, Johnson JL. Transcriptional regulation of bcl-2 by nuclear factor κ B and its significance in prostate cancer. *Oncogene.* 2001;20(50):7342-51.
73. Micheau O, Lens S, Gaide O, Alevizopoulos K, Tschopp J. NF-kappaB signals induce the expression of c-FLIP. *Mol Cell Biol.* 2001;21(16):5299-305.
74. Xie TX, Xia Z, Zhang N, Gong W, Huang S. Constitutive NF-kappaB activity regulates the expression of VEGF and IL-8 and tumor angiogenesis of human glioblastoma. *Oncol Rep.* 2010;23(3):725-32.
75. Huber MA, Azoitei N, Baumann B, Grunert S, Sommer A, Pehamberger H, et al. NF-kappaB is essential for epithelial-mesenchymal transition and metastasis in a model of breast cancer progression. *J Clin Invest.* 2004;114(4):569-81.
76. Nan J, Du Y, Chen X, Bai Q, Wang Y, Zhang X, et al. TPCA-1 is a direct dual inhibitor of STAT3 and NF-kappaB and regresses mutant EGFR-associated human non-small cell lung cancers. *Mol Cancer Ther.* 2014;13(3):617-29.
77. Kim BH, Roh E, Lee HY, Lee IJ, Ahn B, Jung SH, et al. Benzoxathiole derivative blocks lipopolysaccharide-induced nuclear factor-kappaB activation and nuclear factor-kappaB-regulated gene transcription through inactivating inhibitory kappaB kinase beta. *Mol Pharmacol.* 2008;73(4):1309-18.
78. Burke JR, Pattoli MA, Gregor KR, Brassil PJ, MacMaster JF, McIntyre KW, et al. BMS-345541 is a highly selective inhibitor of I kappa B kinase that binds at an allosteric site of the enzyme and blocks NF-kappa B-dependent transcription in mice. *J Biol Chem.* 2003;278(3):1450-6.
79. Tanaka A, Konno M, Muto S, Kambe N, Morii E, Nakahata T, et al. A novel NF-kappaB inhibitor, IMD-0354, suppresses neoplastic proliferation of human mast cells with constitutively activated c-kit receptors. *Blood.* 2005;105(6):2324-31.
80. Lee J, Rhee MH, Kim E, Cho JY. BAY 11-7082 is a broad-spectrum inhibitor with anti-inflammatory activity against multiple targets. *Mediators Inflamm.* 2012;2012:416036.
81. Saadane A, Masters S, DiDonato J, Li J, Berger M. Parthenolide inhibits IkappaB kinase, NF-kappaB activation, and inflammatory response in cystic fibrosis cells and mice. *Am J Respir Cell Mol Biol.* 2007;36(6):728-36.
82. Nemeth ZH, Wong HR, Odoms K, Deitch EA, Szabo C, Vizi ES, et al. Proteasome inhibitors induce inhibitory kappa B (I kappa B) kinase activation, I kappa B alpha degradation, and nuclear factor kappa B activation in HT-29 cells. *Mol Pharmacol.* 2004;65(2):342-9.
83. Gao Y, Lecker S, Post MJ, Hietaranta AJ, Li J, Volk R, et al. Inhibition of ubiquitin-proteasome pathway-mediated I kappa B alpha degradation by a naturally occurring antibacterial peptide. *J Clin Invest.* 2000;106(3):439-48.

84. Kisselev AF, Goldberg AL. Proteasome inhibitors: from research tools to drug candidates. *Chem Biol.* 2001;8(8):739-58.
85. Wu Z, Peng H, Du Q, Lin W, Liu Y. GYY4137, a hydrogen sulfide-releasing molecule, inhibits the inflammatory response by suppressing the activation of nuclear factor- κ B and mitogen-activated protein kinases in Coxsackie virus B3-infected rat cardiomyocytes. *Mol Med Rep.* 2015;11(3):1837-44.
86. Chen KM, Spratt TE, Stanley BA, De Cotiis DA, Bewley MC, Flanagan JM, et al. Inhibition of nuclear factor- κ B DNA binding by organoselenocyanates through covalent modification of the p50 subunit. *Cancer Res.* 2007;67(21):10475-83.
87. Aghai ZH, Kumar S, Farhath S, Kumar MA, Saslow J, Nakhla T, et al. Dexamethasone suppresses expression of Nuclear Factor- κ B in the cells of tracheobronchial lavage fluid in premature neonates with respiratory distress. *Pediatric research.* 2006;59(6):811-5.
88. Ying Z, Kampfrath T, Sun Q, Parthasarathy S, Rajagopalan S. Evidence that α -lipoic acid inhibits NF- κ B activation independent of its antioxidant function. *Inflammation research.* 2011;60(3):219-25.
89. Kastrati I, Siklos MI, Calderon-Gierszal EL, El-Shennawy L, Georgieva G, Thayer EN, et al. Dimethyl fumarate inhibits the nuclear factor κ B pathway in breast cancer cells by covalent modification of p65 protein. *Journal of Biological Chemistry.* 2016;291(7):3639-47.
90. Lakshmanan K, Byran G, Bandlamudi S, Krishnamurthy PT. The Role of STAT3 Signaling in Different Types of Cancers: A Comprehensive Review. *Current Enzyme Inhibition.* 2020;16(3):189-98.
91. Lee M, Rhee I. Cytokine Signaling in Tumor Progression. *Immune Netw.* 2017;17(4):214-27.
92. Michalska A, Blaszczyk K, Wesoly J, Bluysen HA. A positive feedback amplifier circuit that regulates interferon (IFN)-stimulated gene expression and controls type I and type II IFN responses. *Frontiers in immunology.* 2018;9:1135.
93. Steen HC, Gamero AM. STAT2 phosphorylation and signaling. *Jak-Stat.* 2013;2(4):e25790.
94. Lee C, Cheung ST. STAT3: an emerging therapeutic target for hepatocellular carcinoma. *Cancers.* 2019;11(11):1646.
95. Dutta P, Sabri N, Li J, Li WX. Role of STAT3 in lung cancer. *Jak-Stat.* 2014;3(4):e999503.
96. Robinson RL, Sharma A, Bai S, Heneidi S, Lee TJ, Kodeboyina SK, et al. Comparative STAT3-regulated gene expression profile in renal cell carcinoma subtypes. *Frontiers in oncology.* 2019;9:72.
97. Liang R, Chen X, Chen L, Wan F, Chen K, Sun Y, et al. STAT3 signaling in ovarian cancer: a potential therapeutic target. *Journal of Cancer.* 2020;11(4):837.

98. Seffens A, Herrera A, Tegla C, Buus TB, Hymes KB, Ødum N, et al. STAT3 dysregulation in mature T and NK cell lymphomas. *Cancers*. 2019;11(11):1711.
99. Ma J-h, Qin L, Li X. Role of STAT3 signaling pathway in breast cancer. *Cell Communication and Signaling*. 2020;18(1):1-13.
100. Yang C, Mai H, Peng J, Zhou B, Hou J, Jiang D. STAT4: an immunoregulator contributing to diverse human diseases. *International Journal of Biological Sciences*. 2020;16(9):1575.
101. Rädler PD, Wehde BL, Wagner K-U. Crosstalk between STAT5 activation and PI3K/AKT functions in normal and transformed mammary epithelial cells. *Molecular and cellular endocrinology*. 2017;451:31-9.
102. Delgoffe GM, Vignali DA. STAT heterodimers in immunity: A mixed message or a unique signal? *Jak-Stat*. 2013;2(1):e23060.
103. Blease K, Schuh JM, Jakubzick C, Lukacs NW, Kunkel SL, Joshi BH, et al. Stat6-deficient mice develop airway hyperresponsiveness and peribronchial fibrosis during chronic fungal asthma. *The American journal of pathology*. 2002;160(2):481-90.
104. Valladao AC, Frevert CW, Koch LK, Campbell DJ, Ziegler SF. STAT6 regulates the development of eosinophilic versus neutrophilic asthma in response to *Alternaria alternata*. *The Journal of Immunology*. 2016;197(12):4541-51.
105. Walford HH, Doherty TA. STAT6 and lung inflammation. *Jak-stat*. 2013;2(4):e25301.
106. Sherman MA. The role of STAT6 in mast cell IL-4 production. *Immunological reviews*. 2001;179(1):48-56.
107. Sadreev II, Chen MZ, Umezawa Y, Biktashev VN, Kemper C, Salakhieva DV, et al. The competitive nature of STAT complex formation drives phenotype switching of T cells. *arXiv preprint arXiv:170105503*. 2017.
108. Song TL, Nairismägi M-L, Laurensia Y, Lim J-Q, Tan J, Li Z-M, et al. Oncogenic activation of the STAT3 pathway drives PD-L1 expression in natural killer/T-cell lymphoma. *Blood, The Journal of the American Society of Hematology*. 2018;132(11):1146-58.
109. Teng TS, Lin B, Manser E, Ng DCH, Cao X. Stat3 promotes directional cell migration by regulating Rac1 activity via its activator β PIX. *Journal of cell science*. 2009;122(22):4150-9.
110. Chen Z, Han ZC. STAT3: a critical transcription activator in angiogenesis. *Medicinal research reviews*. 2008;28(2):185-200.
111. Chen Y, Ji M, Zhang S, Xue N, Xu H, Lin S, et al. Bt354 as a new STAT3 signaling pathway inhibitor against triple negative breast cancer. *Journal of Drug Targeting*. 2018;26(10):920-30.
112. Dai X, Yin C, Zhang Y, Guo G, Zhao C, Wang O, et al. Osthole inhibits triple negative breast cancer cells by suppressing STAT3. *Journal of Experimental & Clinical Cancer Research*. 2018;37(1):1-11.

113. Zhang W, Yu W, Cai G, Zhu J, Zhang C, Li S, et al. A new synthetic derivative of cryptotanshinone KYZ3 as STAT3 inhibitor for triple-negative breast cancer therapy. *Cell death & disease*. 2018;9(11):1-11.
114. Lim EJ, Hong DY, Park JH, Joung YH, Darvin P, Kim SY, et al. Methylsulfonylmethane suppresses breast cancer growth by down-regulating STAT3 and STAT5b pathways. *PloS one*. 2012;7(4):e33361.
115. Turkson J, Zhang S, Palmer J, Kay H, Stanko J, Mora LB, et al. Inhibition of constitutive signal transducer and activator of transcription 3 activation by novel platinum complexes with potent antitumor activity. *Molecular cancer therapeutics*. 2004;3(12):1533-42.
116. Huang W, Dong Z, Chen Y, Wang F, Wang C, Peng H, et al. Small-molecule inhibitors targeting the DNA-binding domain of STAT3 suppress tumor growth, metastasis and STAT3 target gene expression in vivo. *Oncogene*. 2016;35(6):783-92.
117. Kang DY, Sp N, Kim DH, Joung YH, Lee HG, Park YM, et al. Salidroside inhibits migration, invasion and angiogenesis of MDA-MB 231 TNBC cells by regulating EGFR/Jak2/STAT3 signaling via MMP2. *International journal of oncology*. 2018;53(2):877-85.
118. Nakanishi M, Rosenberg DW. Multifaceted roles of PGE2 in inflammation and cancer. *Semin Immunopathol*. 2013;35(2):123-37.
119. Moncada S, Vane J, editors. The role of prostacyclin in vascular tissue. Federation proceedings; 1979.
120. Dorris SL, Peebles RS. PGI2 as a regulator of inflammatory diseases. *Mediators of inflammation*. 2012;2012.
121. Smyth EM. Thromboxane and the thromboxane receptor in cardiovascular disease. *Clinical lipidology*. 2010;5(2):209-19.
122. Schrör K. Thromboxane A2 and platelets as mediators of coronary arterial vasoconstriction in myocardial ischaemia. *European heart journal*. 1990;11(suppl_B):27-34.
123. OHMORI M, KUZUYA T, KODAMA K, NANTO S, KAMADA T, TADA M. Thromboxane A2 as an enhancing factor of coronary vasospasticity in variant angina. *Japanese circulation journal*. 1987;51(5):495-502.
124. Ekambaram P, Lambiv W, Cazzolli R, Ashton AW, Honn KV. The thromboxane synthase and receptor signaling pathway in cancer: an emerging paradigm in cancer progression and metastasis. *Cancer and Metastasis Reviews*. 2011;30(3-4):397-408.
125. Desai SJ, Prickril B, Rasooly A. Mechanisms of phytonutrient modulation of cyclooxygenase-2 (COX-2) and inflammation related to cancer. *Nutrition and cancer*. 2018;70(3):350-75.
126. Parida S, Pal I, Parekh A, Thakur B, Bharti R, Das S, et al. GW627368X inhibits proliferation and induces apoptosis in cervical cancer by interfering with EP4/EGFR interactive signaling. *Cell death & disease*. 2016;7(3):e2154-e.

127. Nakao K, Murase A, Ohshiro H, Okumura T, Taniguchi K, Murata Y, et al. CJ-023,423, a novel, potent and selective prostaglandin EP4 receptor antagonist with antihyperalgesic properties. *Journal of Pharmacology and Experimental Therapeutics*. 2007;322(2):686-94.
128. Brittain R, Boutal L, Carter M, Coleman R, Collington E, Geisow H, et al. AH23848: a thromboxane receptor-blocking drug that can clarify the pathophysiologic role of thromboxane A₂. *Circulation*. 1985;72(6):1208-18.
129. Peskar BM. Role of cyclooxygenase isoforms in gastric mucosal defence. *Journal of Physiology-Paris*. 2001;95(1-6):3-9.
130. Gupta RA, Tejada LV, Tong BJ, Das SK, Morrow JD, Dey SK, et al. Cyclooxygenase-1 is overexpressed and promotes angiogenic growth factor production in ovarian cancer. *Cancer research*. 2003;63(5):906-11.
131. Haakensen VD, Bjørø T, Lüders T, Riis M, Bukholm IK, Kristensen VN, et al. Serum estradiol levels associated with specific gene expression patterns in normal breast tissue and in breast carcinomas. *BMC cancer*. 2011;11(1):332.
132. Sales KJ, Katz AA, Howard B, Soeters RP, Millar RP, Jabbour HN. Cyclooxygenase-1 is up-regulated in cervical carcinomas: autocrine/paracrine regulation of cyclooxygenase-2, prostaglandin e receptors, and angiogenic factors by cyclooxygenase-1. *Cancer Research*. 2002;62(2):424-32.
133. Harris RE, Casto BC, Harris ZM. Cyclooxygenase-2 and the inflammogenesis of breast cancer. *World journal of clinical oncology*. 2014;5(4):677.
134. Kirschenbaum A, Liu X-H, Yao S, Levine AC. The role of cyclooxygenase-2 in prostate cancer. *Urology*. 2001;58(2):127-31.
135. Chen H, Cai W, Chu E, Tang J, Wong C, Wong S, et al. Hepatic cyclooxygenase-2 overexpression induced spontaneous hepatocellular carcinoma formation in mice. *Oncogene*. 2017;36(31):4415-26.
136. Liu B, Qu L, Yan S. Cyclooxygenase-2 promotes tumor growth and suppresses tumor immunity. *Cancer cell international*. 2015;15(1):106.
137. Gately S, Li WW, editors. Multiple roles of COX-2 in tumor angiogenesis: a target for antiangiogenic therapy. *Seminars in Oncology*; 2004: Elsevier.
138. Guo Z, Jiang J-H, Zhang J, Yang H-J, Yang F-Q, Qi Y-P, et al. COX-2 promotes migration and invasion by the side population of cancer stem cell-like hepatocellular carcinoma cells. *Medicine*. 2015;94(44).
139. Puratchikody A, Umamaheswari A, Irfan N, Sinha S, Manju S, Ramanan M, et al. A novel class of tyrosine derivatives as dual 5-LOX and COX-2/mPGES1 inhibitors with PGE₂ mediated anticancer properties. *New Journal of Chemistry*. 2019;43(2):834-46.
140. Henderson WR. The role of leukotrienes in inflammation. *Annals of internal medicine*. 1994;121(9):684-97.

141. Goetzl E, Goldman D, Naccache P, Sha'afi R, Pickett W. Mediation of leukocyte components of inflammatory reactions by lipoxygenase products of arachidonic acid. *Advances in Prostaglandin, Thromboxane, and Leukotriene Research*. 1982;9:273-82.
142. Wisastra R, Dekker FJ. Inflammation, cancer and oxidative lipoxygenase activity are intimately linked. *Cancers*. 2014;6(3):1500-21.
143. Wasilewicz MP, Kołodziej B, Bojułko T, Kaczmarczyk M, Sulżyc-Bielicka V, Bielicki D, et al. Overexpression of 5-lipoxygenase in sporadic colonic adenomas and a possible new aspect of colon carcinogenesis. *International journal of colorectal disease*. 2010;25(9):1079-85.
144. Gao X, Grignon DJ, Chbihi T, Zacharek A, Chen YQ, Sakr W, et al. Elevated 12-lipoxygenase mRNA expression correlates with advanced stage and poor differentiation of human prostate cancer. *Urology*. 1995;46(2):227-37.
145. Nithipatikom K, Isbell MA, See WA, Campbell WB. Elevated 12-and 20-hydroxyeicosatetraenoic acid in urine of patients with prostatic diseases. *Cancer Letters*. 2006;233(2):219-25.
146. Shrimanker R, Borg K, Connolly C, Thulborn S, Cane J, Xue L, et al. Late Breaking Abstract-Effect of timapiprant, a DP2 antagonist, on airway inflammation in severe eosinophilic asthma. *Eur Respiratory Soc*; 2019.
147. Lai Y-J, Pullamsetti SS, Dony E, Weissmann N, Butrous G, Banat G-A, et al. Role of the prostanoid EP4 receptor in iloprost-mediated vasodilatation in pulmonary hypertension. *American journal of respiratory and critical care medicine*. 2008;178(2):188-96.
148. Bateman ED, Guerreros AG, Brockhaus F, Holzhauer B, Pethe A, Kay RA, et al. Fevipiprant, an oral prostaglandin DP2 receptor (CRTh2) antagonist, in allergic asthma uncontrolled on low-dose inhaled corticosteroids. *European Respiratory Journal*. 2017;50(2).
149. Brennan N, Dehabadi MH, Nair S, Quartilho A, Bunce C, Reekie I, et al. Efficacy and safety of bimatoprost in glaucoma and ocular hypertension in non-responder patients. *International Journal of Ophthalmology*. 2017;10(8):1251.
150. Ghlichloo I, Gerriets V. Nonsteroidal Anti-inflammatory Drugs (NSAIDs). 2019.
151. Eliasson O, Densmore MJ, Scherzer HH, DeGraff Jr AC. The effect of sodium meclofenamate in premenstrual asthma: a controlled clinical trial. *Journal of allergy and clinical immunology*. 1987;79(6):909-18.
152. Dahlen B, Nizankowska E, Szczeklik A, Zetterstrom O, Bochenek G, Kumlin M, et al. Benefits from adding the 5-lipoxygenase inhibitor zileuton to conventional therapy in aspirin-intolerant asthmatics. *American journal of respiratory and critical care medicine*. 1998;157(4):1187-94.
153. Sester A, Winand L, Pace S, Hiller W, Werz O, Nett M. Myxochelin-and Pseudochelin-Derived Lipoxygenase Inhibitors from a Genetically Engineered *Myxococcus xanthus* Strain. *Journal of natural products*. 2019;82(9):2544-9.
154. Gryder BE, Sodji QH, Oyelere AK. Targeted cancer therapy: giving histone deacetylase inhibitors all they need to succeed. *Future medicinal chemistry*. 2012;4(4):505-24.

155. Li Y, Seto E. HDACs and HDAC inhibitors in cancer development and therapy. *Cold Spring Harbor perspectives in medicine*. 2016;6(10):a026831.
156. Witt O, Deubzer HE, Milde T, Oehme I. HDAC family: What are the cancer relevant targets? *Cancer letters*. 2009;277(1):8-21.
157. Liu N, He S, Ma L, Ponnusamy M, Tang J, Tolbert E, et al. Blocking the class I histone deacetylase ameliorates renal fibrosis and inhibits renal fibroblast activation via modulating TGF-beta and EGFR signaling. *PloS one*. 2013;8(1):e54001.
158. Zhu H, Shan L, Schiller PW, Mai A, Peng T. Histone deacetylase-3 activation promotes tumor necrosis factor- α (TNF- α) expression in cardiomyocytes during lipopolysaccharide stimulation. *Journal of Biological Chemistry*. 2010;285(13):9429-36.
159. Ziesche E, Kettner-Buhrow D, Weber A, Wittwer T, Jurida L, Soelch J, et al. The coactivator role of histone deacetylase 3 in IL-1-signaling involves deacetylation of p65 NF- κ B. *Nucleic acids research*. 2013;41(1):90-109.
160. Durham BS, Grigg R, Wood IC. Inhibition of histone deacetylase 1 or 2 reduces microglia activation through a gene expression independent mechanism. *bioRxiv*. 2017:107649.
161. Yoon S, Kang G, Eom GH. HDAC inhibitors: therapeutic potential in fibrosis-associated human diseases. *International journal of molecular sciences*. 2019;20(6):1329.
162. Barter MJ, Pybus L, Litherland GJ, Rowan AD, Clark IM, Edwards DR, et al. HDAC-mediated control of ERK-and PI3K-dependent TGF- β -induced extracellular matrix-regulating genes. *Matrix Biology*. 2010;29(7):602-12.
163. Choi JH, Oh SW, Kang MS, Kwon HJ, Oh GT, Kim DY. Trichostatin A attenuates airway inflammation in mouse asthma model. *Clinical & Experimental Allergy*. 2005;35(1):89-96.
164. Cui S-N, Chen Z-Y, Yang X-B, Chen L, Yang Y-Y, Pan S-W, et al. Trichostatin A modulates the macrophage phenotype by enhancing autophagy to reduce inflammation during polymicrobial sepsis. *International Immunopharmacology*. 2019;77:105973.
165. Zhuang S. Regulation of STAT signaling by acetylation. *Cellular signalling*. 2013;25(9):1924-31.
166. Fernández-Álvarez A, Llorente-Izquierdo C, Mayoral R, Agra N, Boscá L, Casado M, et al. Evaluation of epigenetic modulation of cyclooxygenase-2 as a prognostic marker for hepatocellular carcinoma. *Oncogenesis*. 2012;1(7):e23-e.
167. Zhang C, Richon V, Ni X, Talpur R, Duvic M. Selective induction of apoptosis by histone deacetylase inhibitor SAHA in cutaneous T-cell lymphoma cells: relevance to mechanism of therapeutic action. *Journal of Investigative Dermatology*. 2005;125(5):1045-52.
168. Rashidi A, Cashen AF. Belinostat for the treatment of relapsed or refractory peripheral T-cell lymphoma. *Future Oncology*. 2015;11(11):1659-64.
169. Chan TS, Tse E, Kwong Y-L. Chidamide in the treatment of peripheral T-cell lymphoma. *OncoTargets and therapy*. 2017;10:347.

170. Grant C, Rahman F, Piekarz R, Peer C, Frye R, Robey RW, et al. Romidepsin: a new therapy for cutaneous T-cell lymphoma and a potential therapy for solid tumors. *Expert review of anticancer therapy*. 2010;10(7):997-1008.
171. Raedler LA. Farydak (Panobinostat): first HDAC inhibitor approved for patients with relapsed multiple myeloma. *American health & drug benefits*. 2016;9(Spec Feature):84.
172. Zhang L, Zhang J, Jiang Q, Zhang L, Song W. Zinc binding groups for histone deacetylase inhibitors. *Journal of enzyme inhibition and medicinal chemistry*. 2018;33(1):714-21.
173. Ononye SN, VanHeyst MD, Oblak EZ, Zhou W, Ammar M, Anderson AC, et al. Tropolones as lead-like natural products: the development of potent and selective histone deacetylase inhibitors. *ACS medicinal chemistry letters*. 2013;4(8):757-61.
174. Godoy LD, Lucas JE, Bender AJ, Romanick SS, Ferguson BS. Targeting the epigenome: Screening bioactive compounds that regulate histone deacetylase activity. *Molecular nutrition & food research*. 2017;61(4):1600744.
175. Patil V, Sodji QH, Kornacki JR, Mrksich M, Oyelere AK. 3-Hydroxypyridin-2-thione as novel zinc binding group for selective histone deacetylase inhibition. *Journal of medicinal chemistry*. 2013;56(9):3492-506.
176. Sodji QH, Patil V, Kornacki JR, Mrksich M, Oyelere AK. Synthesis and structure–activity relationship of 3-hydroxypyridine-2-thione-based histone deacetylase inhibitors. *Journal of medicinal chemistry*. 2013;56(24):9969-81.
177. Trivedi R, Redente EF, Thakur A, Riches DW, Kompella UB. Local delivery of biodegradable pirfenidone nanoparticles ameliorates bleomycin-induced pulmonary fibrosis in mice. *Nanotechnology*. 2012;23(50):505101.
178. Xu X, Zheng L, Yuan Q, Zhen G, Crane JL, Zhou X, et al. Transforming growth factor- β in stem cells and tissue homeostasis. *Bone research*. 2018;6(1):1-31.
179. Takai E, Tsukimoto M, Kojima S. TGF- β 1 downregulates COX-2 expression leading to decrease of PGE2 production in human lung cancer A549 cells, which is involved in fibrotic response to TGF- β 1. *PLoS One*. 2013;8(10):e76346.
180. Anderton MJ, Mellor HR, Bell A, Sadler C, Pass M, Powell S, et al. Induction of heart valve lesions by small-molecule ALK5 inhibitors. *Toxicologic pathology*. 2011;39(6):916-24.
181. Teixeira AF, Ten Dijke P, Zhu H-J. On-Target Anti-TGF- β Therapies Are Not Succeeding in Clinical Cancer Treatments: What Are Remaining Challenges? *Frontiers in cell and developmental biology*. 2020;8.
182. Hezel AF, Deshpande V, Zimmerman SM, Contino G, Alagesan B, O'Dell MR, et al. TGF- β and α v β 6 integrin act in a common pathway to suppress pancreatic cancer progression. *Cancer research*. 2012;72(18):4840-5.
183. Fisher M, Nathan SD, Hill C, Marshall J, Dejonckheere F, Thuresson P-O, et al. Predicting life expectancy for pirfenidone in idiopathic pulmonary fibrosis. *Journal of managed care & specialty pharmacy*. 2017;23(3-b Suppl):S17-S24.

184. Zeligs KP, Neuman MK, Annunziata CM. Molecular pathways: the balance between cancer and the immune system challenges the therapeutic specificity of targeting nuclear factor- κ B signaling for cancer treatment. *Clinical Cancer Research*. 2016;22(17):4302-8.
185. Shah MA, Power DG, Kindler HL, Holen KD, Kemeny MM, Ilson DH, et al. A multicenter, phase II study of bortezomib (PS-341) in patients with unresectable or metastatic gastric and gastroesophageal junction adenocarcinoma. *Investigational new drugs*. 2011;29(6):1475-81.
186. Hernandez L, Hsu SC, Davidson B, Birrer MJ, Kohn EC, Annunziata CM. Activation of NF- κ B signaling by inhibitor of NF- κ B kinase β increases aggressiveness of ovarian cancer. *Cancer research*. 2010;70(10):4005-14.
187. Wardyn JD, Ponsford AH, Sanderson CM. Dissecting molecular cross-talk between Nrf2 and NF- κ B response pathways. *Biochemical society transactions*. 2015;43(4):621-6.
188. Linker RA, Lee D-H, Ryan S, van Dam AM, Conrad R, Bista P, et al. Fumaric acid esters exert neuroprotective effects in neuroinflammation via activation of the Nrf2 antioxidant pathway. *Brain*. 2011;134(3):678-92.
189. Kobayashi A, Kang M-I, Watai Y, Tong KI, Shibata T, Uchida K, et al. Oxidative and electrophilic stresses activate Nrf2 through inhibition of ubiquitination activity of Keap1. *Molecular and cellular biology*. 2006;26(1):221-9.
190. Saidu NEB, Kaviani N, Leroy K, Jacob C, Nicco C, Batteux F, et al. Dimethyl fumarate, a two-edged drug: current status and future directions. *Medicinal research reviews*. 2019;39(5):1923-52.
191. Choi B-M, Kim S-M, Park T-K, Li G, Hong S-J, Park R, et al. Piperine protects cisplatin-induced apoptosis via heme oxygenase-1 induction in auditory cells. *The Journal of nutritional biochemistry*. 2007;18(9):615-22.
192. Linker RA, Gold R. Dimethyl fumarate for treatment of multiple sclerosis: mechanism of action, effectiveness, and side effects. *Current neurology and neuroscience reports*. 2013;13(11):1-7.
193. Dang CT, Dannenberg AJ, Subbaramaiah K, Dickler MN, Moasser MM, Seidman AD, et al. Phase II study of celecoxib and trastuzumab in metastatic breast cancer patients who have progressed after prior trastuzumab-based treatments. *Clinical cancer research*. 2004;10(12):4062-7.
194. Solomon SD, McMurray JJ, Pfeffer MA, Wittes J, Fowler R, Finn P, et al. Cardiovascular risk associated with celecoxib in a clinical trial for colorectal adenoma prevention. *New England Journal of Medicine*. 2005;352(11):1071-80.
195. Caldwell B, Aldington S, Weatherall M, Shirtcliffe P, Beasley R. Risk of cardiovascular events and celecoxib: a systematic review and meta-analysis. *Journal of the Royal Society of Medicine*. 2006;99(3):132-40.
196. Chavez ML, DeKorte CJ. Valdecoxib: a review. *Clinical therapeutics*. 2003;25(3):817-51.
197. G Perrone M, Scilimati A, Simone L, Vitale P. Selective COX-1 inhibition: A therapeutic target to be reconsidered. *Current medicinal chemistry*. 2010;17(32):3769-805.

198. Brune K. Safety of anti-inflammatory treatment—new ways of thinking. *Rheumatology*. 2004;43(suppl_1):i16-i20.
199. Xiong A, Yang Z, Shen Y, Zhou J, Shen Q. Transcription factor STAT3 as a novel molecular target for cancer prevention. *Cancers*. 2014;6(2):926-57.
200. Perry AS, Watson RWG, Lawler M, Hollywood D. The epigenome as a therapeutic target in prostate cancer. *Nature Reviews Urology*. 2010;7(12):668.
201. Alvarez-Elcoro S, Enzler MJ, editors. The macrolides: erythromycin, clarithromycin, and azithromycin. Mayo Clinic Proceedings; 1999: Elsevier.
202. Miossec-Bartoli C, Pilatre L, Peyron P, N'Diaye E-N, Collart-Dutilleul V, Maridonneau-Parini I, et al. The new ketolide HMR3647 accumulates in the azurophilic granules of human polymorphonuclear cells. *Antimicrobial agents and chemotherapy*. 1999;43(10):2457-62.
203. Bosnar M, Kelnerić Ž, Munić V, Eraković V, Parnham MJ. Cellular uptake and efflux of azithromycin, erythromycin, clarithromycin, telithromycin, and cethromycin. *Antimicrobial agents and chemotherapy*. 2005;49(6):2372-7.
204. LeBel M. Pharmacokinetic properties of clarithromycin: A comparison with erythromycin and azithromycin. *Canadian Journal of Infectious Diseases*. 1993;4.
205. Wildfeuer A, Laufen H, Zimmermann T. Uptake of azithromycin by various cells and its intracellular activity under in vivo conditions. *Antimicrobial agents and chemotherapy*. 1996;40(1):75-9.
206. Hand WL, Hand DL. Characteristics and mechanisms of azithromycin accumulation and efflux in human polymorphonuclear leukocytes. *International journal of antimicrobial agents*. 2001;18(5):419-25.
207. Steel HC, Theron AJ, Cockeran R, Anderson R, Feldman C. Pathogen- and host-directed anti-inflammatory activities of macrolide antibiotics. *Mediators of inflammation*. 2012;2012.
208. Parnham MJ, Haber VE, Giamarellos-Bourboulis EJ, Perletti G, Verleden GM, Vos R. Azithromycin: mechanisms of action and their relevance for clinical applications. *Pharmacology & therapeutics*. 2014;143(2):225-45.
209. Beigelman A, Mikols CL, Gunsten SP, Cannon CL, Brody SL, Walter MJ. Azithromycin attenuates airway inflammation in a mouse model of viral bronchiolitis. *Respiratory research*. 2010;11(1):90.
210. Yamada K, Yanagihara K, Kaku N, Harada Y, Migiyama Y, Nagaoka K, et al. Azithromycin attenuates lung inflammation in a mouse model of ventilator-associated pneumonia by multidrug-resistant *Acinetobacter baumannii*. *Antimicrobial agents and chemotherapy*. 2013;57(8):3883-8.
211. Terao H, Asano K, Kanai K-i, Kyo Y, Watanabe S, Hisamitsu T, et al. Suppressive activity of macrolide antibiotics on nitric oxide production by lipopolysaccharide stimulation in mice. *Mediators of inflammation*. 2003;12(4).

212. Beigelman A, Gunsten S, Mikols CL, Vidavsky I, Cannon CL, Brody SL, et al. Azithromycin attenuates airway inflammation in a noninfectious mouse model of allergic asthma. *Chest*. 2009;136(2):498-506.
213. Geudens N, Timmermans L, Vanhooren H, Vanaudenaerde BM, Vos R, Van De Wauwer C, et al. Azithromycin reduces airway inflammation in a murine model of lung ischaemia reperfusion injury. *Transplant International*. 2008;21(7):688-95.
214. Kohyama T, Yamauchi Y, Takizawa H, Itakura S, Kamitani S, Kato J, et al. Clarithromycin inhibits fibroblast migration. *Respiratory medicine*. 2008;102(12):1769-76.
215. Zimmermann P, Ziesenitz VC, Curtis N, Ritz N. The immunomodulatory effects of macrolides—a systematic review of the underlying mechanisms. *Frontiers in immunology*. 2018;9:302.
216. Stepanic V, Kostrun S, Malnar I, Hlevnjak M, Butkovic K, Caleta I, et al. Modeling cellular pharmacokinetics of 14- and 15-membered macrolides with physicochemical properties. *Journal of medicinal chemistry*. 2011;54(3):719-33.
217. Gladue R, Snider M. Intracellular accumulation of azithromycin by cultured human fibroblasts. *Antimicrobial Agents and Chemotherapy*. 1990;34(6):1056-60.
218. Zarogoulidis P, Papanas N, Kioumis I, Chatzaki E, Maltezos E, Zarogoulidis K. Macrolides: from in vitro anti-inflammatory and immunomodulatory properties to clinical practice in respiratory diseases. *European journal of clinical pharmacology*. 2012;68(5):479-503.
219. Zhang WJ, Wei H, Hagen T, Frei B. Alpha-lipoic acid attenuates LPS-induced inflammatory responses by activating the phosphoinositide 3-kinase/Akt signaling pathway. *Proc Natl Acad Sci U S A*. 2007;104(10):4077-82.
220. Korotchikina LG, Sidhu S, Patel MS. R-lipoic acid inhibits mammalian pyruvate dehydrogenase kinase. *Free Radic Res*. 2004;38(10):1083-92.
221. Xie N, Tan Z, Banerjee S, Cui H, Ge J, Liu R-M, et al. Glycolytic reprogramming in myofibroblast differentiation and lung fibrosis. *American journal of respiratory and critical care medicine*. 2015;192(12):1462-74.
222. Kafara P, Icard P, Guillamin M, Schwartz L, Lincet H. Lipoic acid decreases Mcl-1, Bcl-xL and up regulates Bim on ovarian carcinoma cells leading to cell death. *J Ovarian Res*. 2015;8:36.
223. Na MH, Seo EY, Kim WK. Effects of alpha-lipoic acid on cell proliferation and apoptosis in MDA-MB-231 human breast cells. *Nutr Res Pract*. 2009;3(4):265-71.
224. Ferone R, Roland S. Dihydrofolate reductase: thymidylate synthase, a bifunctional polypeptide from *Crithidia fasciculata*. *Proceedings of the National Academy of Sciences*. 1980;77(10):5802-6.
225. Heppler LN, Walker SR, Attarha S, Page BD, Frank DA. Pyrimethamine inhibits STAT3 transcriptional activity via dihydrofolate reductase. *AACR*; 2019.

226. Cowman AF, Morry MJ, Biggs BA, Cross G, Foote SJ. Amino acid changes linked to pyrimethamine resistance in the dihydrofolate reductase-thymidylate synthase gene of *Plasmodium falciparum*. *Proceedings of the National Academy of Sciences*. 1988;85(23):9109-13.
227. Baek E-J, Nam H-W. Changes in enzyme activity and expression of DHFR of *Toxoplasma gondii* by antifolates. *The Korean journal of parasitology*. 1998;36(3):191.
228. Weiss LM, Perlman DC, Sherman J, Tanowitz H, Wittner M. Isospora belli infection: treatment with pyrimethamine. *Annals of internal medicine*. 1988;109(6):474-5.
229. Mofenson LM, Brady MT, Danner SP, Dominguez KL, Hazra R, Handelsman E, et al. Guidelines for the prevention and treatment of opportunistic infections among HIV-exposed and HIV-infected children: recommendations from CDC, the National Institutes of Health, the HIV Medicine Association of the Infectious Diseases Society of America, the Pediatric Infectious Diseases Society, and the American Academy of Pediatrics. *MMWR Recommendations and reports: Morbidity and mortality weekly report Recommendations and reports/Centers for Disease Control*. 2009;58(RR-11):1.
230. Gryder BE, Akbashev MJ, Rood MK, Raftery ED, Meyers WM, Dillard P, et al. Selectively targeting prostate cancer with antiandrogen equipped histone deacetylase inhibitors. *ACS chemical biology*. 2013;8(11):2550-60.
231. Raji I, Yadudu F, Janeira E, Fathi S, Szymczak L, Kornacki JR, et al. Bifunctional conjugates with potent inhibitory activity towards cyclooxygenase and histone deacetylase. *Bioorganic & medicinal chemistry*. 2017;25(3):1202-18.
232. Guerrant W, Patil V, Canzoneri JC, Oyelere AK. Dual targeting of histone deacetylase and topoisomerase II with novel bifunctional inhibitors. *Journal of medicinal chemistry*. 2012;55(4):1465-77.
233. Oyelere AK, Chen PC, Guerrant W, Mwakwari SC, Hood R, Zhang Y, et al. Non-peptide macrocyclic histone deacetylase inhibitors. *Journal of medicinal chemistry*. 2009;52(2):456-68.
234. Yuan Z-l, Guan Y-j, Chatterjee D, Chin YE. Stat3 dimerization regulated by reversible acetylation of a single lysine residue. *Science*. 2005;307(5707):269-73.
235. Gupta M, Han J, Stenson M, Welik L, Witzig TE. Regulation of STAT3 by histone deacetylase-3 in diffuse large B-cell lymphoma: implications for therapy. *Leukemia*. 2012;26(6):1356-64.
236. Daskalow K, Pfander D, Weichert W, Rohwer N, Thelen A, Neuhaus P, et al. Distinct temporospatial expression patterns of glycolysis-related proteins in human hepatocellular carcinoma. *Histochemistry and cell biology*. 2009;132(1):21-31.
237. Leturque A, Brot-Laroche E, Le Gall M, Stolarczyk E, Tobin V. The role of GLUT2 in dietary sugar handling. *Journal of physiology and biochemistry*. 2005;61(4):529.

CHAPTER 2. MACROLIDE-DERIVED ANTI-FIBROTIC AND ANTI- INFLAMMATORY AGENTS

Bocheng Wu¹, Adegboyega Oyelere^{1,2†}

*School of Chemistry and Biochemistry, School of Biological Sciences, Parker H. Petit Institute
for Bioengineering and Bioscience, Georgia Institute of Technology, Atlanta, GA 30332-0400
USA*

¹School of Chemistry and Biochemistry, Georgia Institute of Technology

²Parker H. Petit Institute for Bioengineering and Bioscience, Georgia Institute of Technology

Correspondence to:

Adegboyega K. Oyelere, **E-mail:** aoyelere@gatech.edu

Key Words: Macrolide, pirfenidone, collagen, extracellular matrix, Idiopathic pulmonary
fibrosis, IPF, tissue-selective, anti-fibrosis, cytokines, TGF- β , MAPK pathway, NF- κ B.

Abstract:

Idiopathic pulmonary fibrosis (IPF) is a chronic and fatal disease that progressively declines the lung function. The FDA approved drugs - pirfenidone (PFD) and nintedanib – are suboptimal in the management of IPF largely due to their toxic side effects, low potency, cost ineffectiveness and minimal beneficial effect on the patients' survival rate. We described herein four classes of macrolide-based anti-fibrotic agents designed, using a structure-based approach, from PFD and azithromycin and clarithromycin as macrolide templates. These agents are designed to exploit the excellent PK and selective lungs and/or liver tissues distribution activities of these macrolide templates to arrive at novel anti-fibrotic agents that may selectively accumulate within these tissues. We synthesized twenty-eight compounds and tested their effects on the viability of four cell lines –MRC-5, A549 Hep-G2 and VERO. We observed that compounds **10c**, **11c**, **11b**, **15c**, **20e** inhibited the proliferation of these cell lines with IC₅₀ range of 2.5-10 μ M. Additionally, these compounds potently inhibit NF- κ B and TGF- β pathways with potency enhancement as high as 1000-fold relative to PFD or the unmodified macrolide templates. Compounds **15c** showed an optimum inhibition and/or downregulation of the fibrosis markers (FN-1, MMP-9, COL1A1, α -SMA) that we investigated at low micromolar IC₅₀. The next best compounds are **10c**, **11c** and **20e**. Collectively, these compounds are excellent candidates for future preclinical studies focused on the evaluation of their potential as tissue-selective anti-fibrotic effects in *in vivo* models of IPF and liver fibrosis.

2.1 Introduction

Pulmonary fibrosis is the thickening and scarring of the connective tissues in the lungs, which can be induced by pulmonary injuries and inflammation caused by exposure to chemicals, environmental pollutants, smoking, age-related dysfunctions, infections, and other risk factors. Idiopathic pulmonary fibrosis (IPF) is the most common interstitial lung disease (ILD).¹ IPF is a chronic and fatal disease which progressively declines the lung function.² The cause of IPF is ambiguous, and the disease affects 50 per 100,000 people worldwide.³ In the US, the prevalent rate of IPF is around 18.2 cases per 100,000 annually, and the incident rate is 5.8 cases per 100,000.⁴ In Europe, IPF prevalent rate is around 1.25 to 23.4 per 100,000, and the incidence IPF is around 0.22 to 7.4 per 100,000.⁵ The prognosis of IPF is the worst among ILD, and its median survival range from 2-5 years.¹ A study has shown the IPF has only 28% 5-year survival rate which is much lower than many types of cancers.^{6,7} In a 2018 study in UK that analyzed data from 2002 to 2012, it was found that IPF incidence rates have increased since 2000 and survival remains poor.⁸

The pathophysiology of IPF has been well studied. IPF is sustained by inflammation caused by chronic injury which promotes inflammatory cytokines release and the accumulation of these cytokines in the bronchial tubes and airways. Consequently, epithelial fibroblasts are stimulated by these cytokines to induce epithelial-mesenchymal transition (EMT),⁹ resulting in the transformation of the fibroblasts to myoblasts overexpressing collagen, actin, fibronectin, MMPs and many other profibrotic extracellular matrix (ECM).¹⁰ TGF- β pathway activation is one of the major initial steps in the progression of fibrosis.¹¹ Studies have shown that TGF- β 1 plays important roles in activating ECM production,¹⁰ EMT,¹² crosslinking to other inflammatory

pathways including MAPK pathway,¹³ NF- κ B pathway,¹⁴ Hippo pathway,¹⁵ STAT3 pathway activation^{16, 17} and many others. Typically, NF- κ B activation is involved in tissue inflammation and necrosis through the transcription of pro-inflammatory cytokines including IL-1, IL-2, IL-6, IL-8, IL-12, TNF- α ; chemokines including CXCL1, CXCL10, and IL-18; proinflammatory gene expression for stimulation of immune cells such as M2 phase polarization of macrophages to cause tissue necrosis.^{18, 19} TGF- β regulated STAT3 activation is essential to IPF via multiple mechanisms as well. Upregulation of p-STAT3/STAT3 ratio is required in TGF- β 1 stimulation to promote EMT transition.²⁰ Inhibition of TGF- β downregulates ECM accumulation, attenuates tissue fibrogenesis, and prevents further tissue necrosis. Thus, TGF- β is an ideal therapeutic target for IPF treatment.

Efforts at developing small molecules for the treatment of IPF have furnished several clinical candidates, targeting several pathways.²¹ However, only pirfenidone (PFD) and Nintedanib have been approved by FDA. PFD is widely used by IPF patients as it improves lung function over long-term treatments.^{22, 23} However, the latest survival data revealed that PFD treatment caused only a limited improvement in 5-yr survival (55.9%) vs placebo (31.5%).²⁴ This pricy drug (avg. 92,000 USD/year) does not completely reverse disease progression; and systemic exposure to PFD causes adverse drug reactions (ADRs), including severe skin burn-like rash, photosensitivity, and gastrointestinal disorders, in treated patients. PFD has a relatively poor pharmacokinetic (PK) properties,²⁵ necessitating 3-9 times daily intake of high dosage (600 mg to 2.4 g) to maintain effective concentration in patient's plasma.²⁶ The adverse effects experienced by patients on PFD therapy and its poor PK properties could be linked to the high rate (28.7%) of therapy discontinuation.²⁷ Efforts have gone into the design of new PFD analogs with improved on-target effects and enhanced half-life.²⁸ However, none of these PFD

analogs has proven superior so far. Therefore, there is an unmet medical need for effective treatment/management modalities for IPF.

Macrolides azithromycin (AZM) and clarithromycin (CLM) are two macrolactone antibiotics that is widely used to treat upper respiratory tract infections. They shared similar mechanism of action with selective target of bacterial protein synthesis by inhibiting the prokaryotic ribosomes activity.²⁹ More than selectivity to bacteria, AZM and CLM also perform outstanding pharmacokinetics (PK) properties and selective distributions to the disease sites, which could be highly effective in treating upper respiratory tract infections. Evidences found that they could selectively accumulate in lung resident macrophages and other immune cells which may overgrow in infectious lung tissue.^{30, 31, 32} AZM and CLM also accumulate in the liver tissues as well. Compare to the bloodstream, the macrolides showed more than 100-fold enrichment in these tissues.³³⁻³⁵ In addition, evidently, AZM and CLM also behave with intrinsic anti-inflammatory activities. For instance, AZM assistants the repair of tissue injury by attenuating the leukocytes activities and the expressions of pro-inflammatory cytokines.³⁶⁻⁴¹ Recently, AZM has been observed to selectively accumulates internally with epithelial cells, fibroblasts, lymphocyte, and hepatocyte.^{31, 42, 43} These evidences make AZM an excellent lung/liver targeting antibiotics with low systematic toxicity. In addition, AZM is well-tolerated by patients as a result of its safe metabolites.³⁶ On the other hand, tissue fibrosis progression could be effectively controlled by CLM with downregulating the cytokines and the fibroblast migration through downregulation of inflammatory product TXA2.^{44, 45} Currently, macrolides have been recognized as potential anti-inflammatory candidates in respiratory disease.⁴⁶ Based on these attributes, AZM and CLM are ideal template molecules for the design of liver- and lung-tissues targeted anti-inflammation and anti-cancer agents.

2.2 Results

2.2.1 Design and molecular docking

We hypothesized that the integration of PFD-like moiety into AZM and CLM templates would afford novel TGF- β inhibiting anti-fibrotic agents that are selectively accumulated in the lungs and/or liver tissues. To test our hypothesis, we designed four classes of macrolide-based PFD-like (macrolide-PFD) compounds with methylene (class I), aryltriazolyl (class II), triazolyl (class III) and alkynyl (class IV) linkers connecting the para-position of PFD's phenyl moiety to the amino group desosamine moieties of AZM and ZLM (Fig. 2.1). Our design is based on molecular docking analysis of the interaction of PFD with its targets – ALK-5 and MAPK p38. We expect that this design approach will furnish macrolide-PFD compounds that optimally present the PFD moiety to the active sites of its targets – MAPK p38 γ and TGF- β receptor ALK-5 – while minimizing potential steric clash that the macrolide moiety might present if it is in the proper distance to the PFD moiety. PFD is known as a pleiotropic small molecule that could inhibit multiple targets of TGF- β 1 pathway. First, PFD is a MAPK p38 γ inhibitor and thus the macrolide-PFD should maintain the property if the linker design is proper. Also, PFD could be the p38 α inhibitor, and the docking of PFD derivatives towards p38 α has been studied in previous study that the PFD moiety of the novel agents interacts with Met-101 and Glu-110.²⁸ In addition, PFD is known to be ALK-5 inhibitor in blocking TGF- β ligand binding. ALK-5 docking of pirfenidone derivatives was also interpreted in previous study that the Pyridone moiety is binding into the hydrophobic region of the active site of ALK-5.⁴⁷

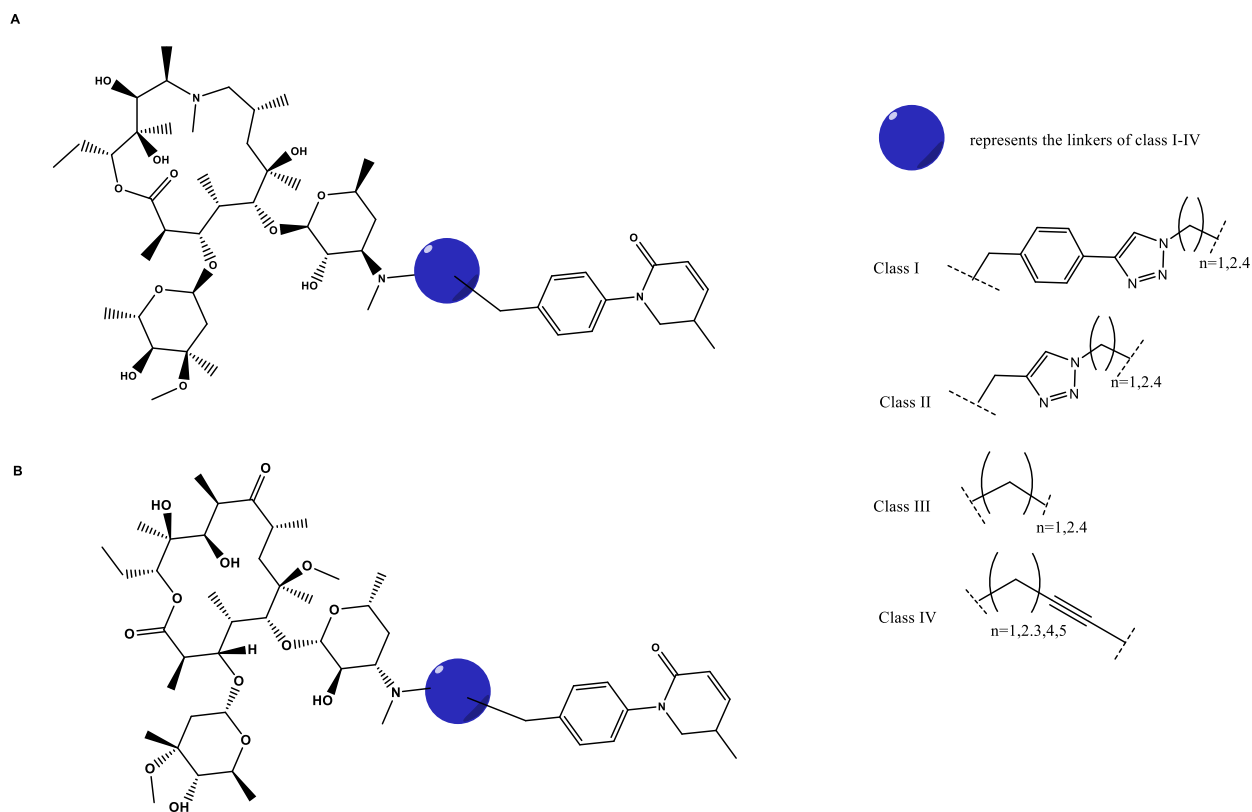


Figure 2.1. Designed macrolide-based PFD-like compounds (a). AZM and (b). CLM with four types of linkers (highlighted in blue).

We used molecular docking to obtain preliminary *in silico* evidence of the accommodation of macrolide-PFD compounds at the p38 and ALK-5 active sites and guide the modification to the linker regions in order to identify candidates with optimal binding affinities. Molecular docking was performed as using Autodock Vina run through PyRx.⁴⁸ PFD, AZM, CLM and the macrolide-PFD compounds (Fig. 2.2) are docked against crystal structures of p-p38 γ (PDB:1CM8), p38 α (PDB: 3HP2), and ALK-5 model (PDB: 5USQ) is gained from Protein Data Base (PDB).⁴⁹ In similar manner to the unmodified PFD, the pyridone moiety of PFD of all compounds maintains invariant binding with the active site hydrophobic pocket of the p-p38 γ interacting with Val-33, Ile-87, Met-109, Phe-111, Met-112, Gly-113, Thr-114, Asp-115, Ala-160, Leu-170; while the linker and macrolide moiety sterically block the Mg from interacting

with any phosphorylated substance (Fig. 2.3a). However, even though all representative candidates' PFD moiety of also binds to the p38 α at the active site interacting with Met-109 and Gly-110 (Fig. 2.3b), the binding affinities are not much enhanced compared to p-p38 γ (Table 2.1). In binding to ALK-5 (Fig. 2.4). Among each class, the key difference is in the orientation of the macrolide moieties that is influenced by the type and the length of the linker groups. Interestingly, we also noticed that these macrolide-PFD compounds bind to p-p38 γ and ALK-5 with significantly increased binding affinities relative to unmodified PFD or AZM/CLM (Table 2.1, Table S2.1 and S2.2). The docking outputs are described herein for a representative member of each class of the macrolide-PFD compounds (**11c**, **13c**, **15c**, **20e**) that optimally interacts with either target based on binding orientation and docking scores.

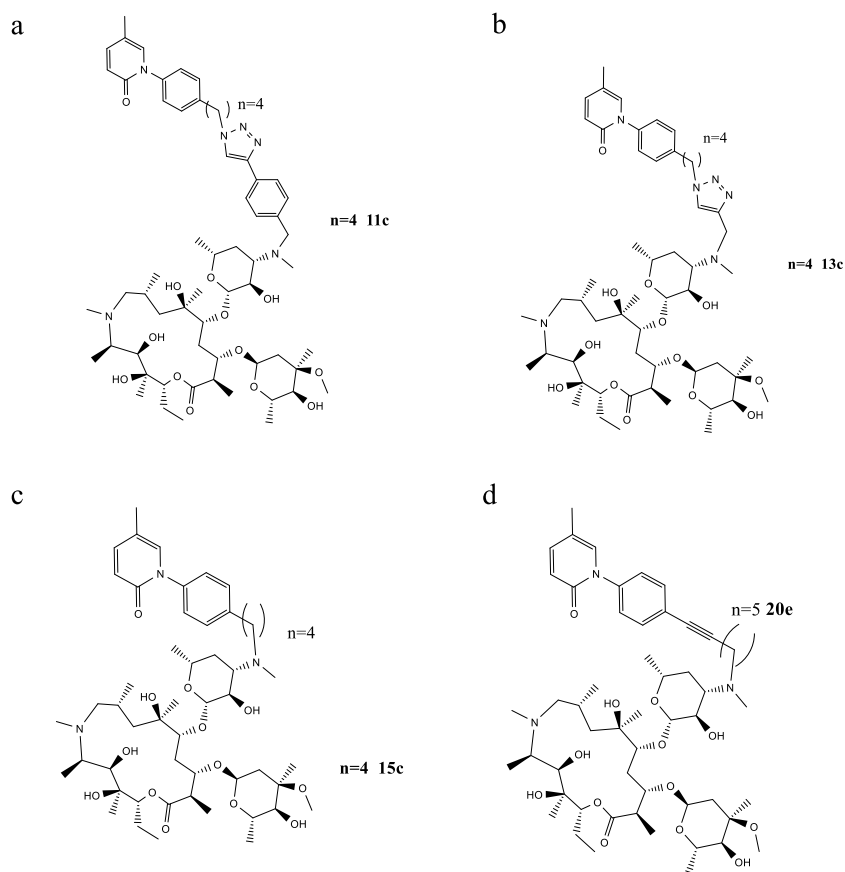
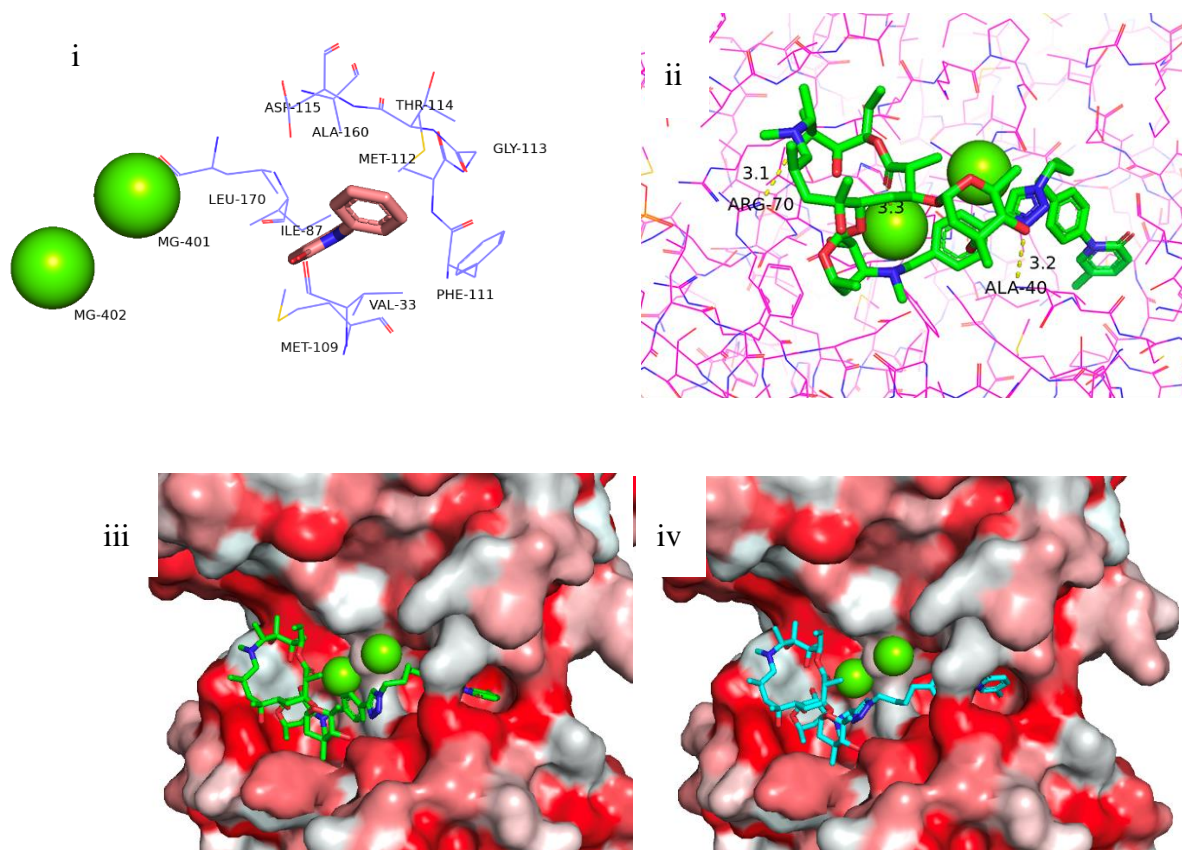
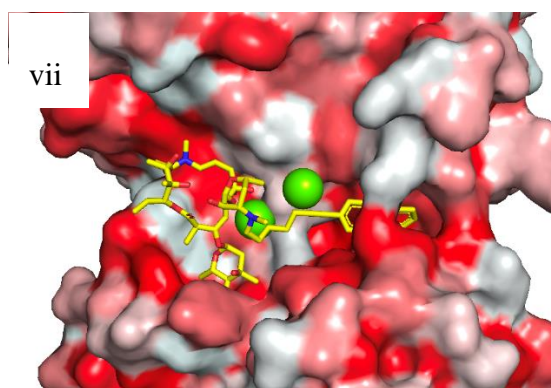
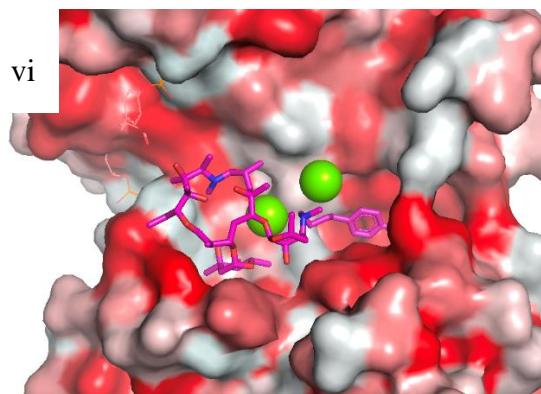
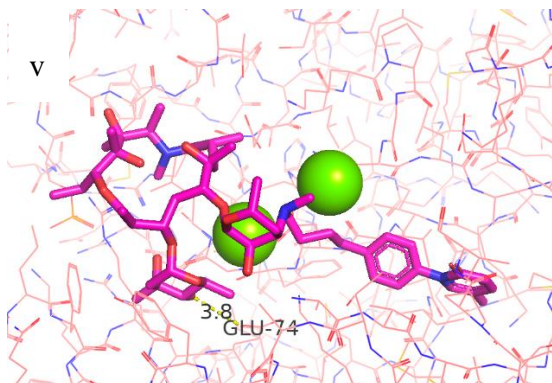


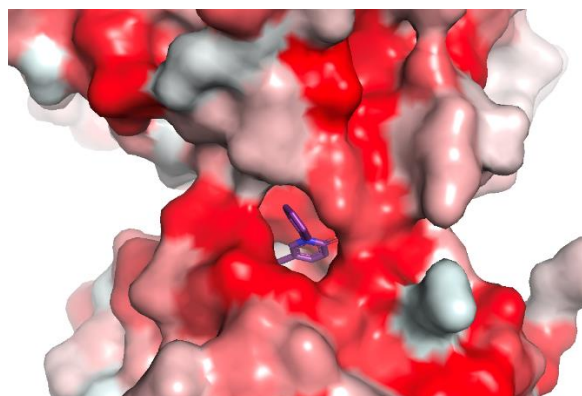
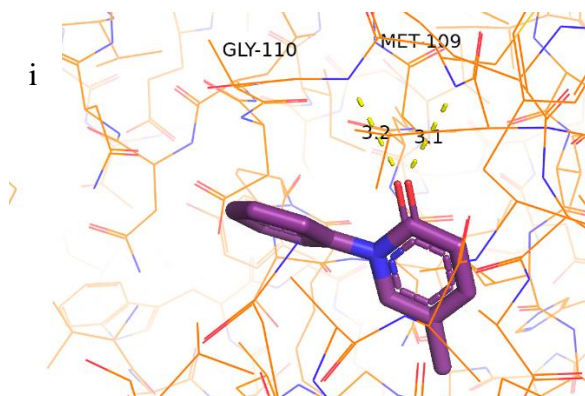
Figure 2.2. AZM representative structures of class I-IV for molecular docking. (a). Structure of **11c**. (a). Structure of **11c**. (b). Structure of **13c**. (c). Structure of **15c**. (d). Structure of **20e**.

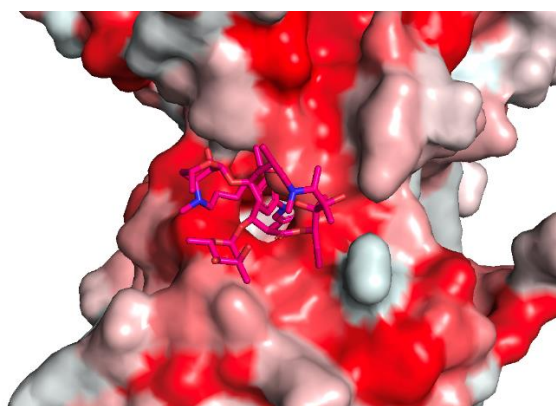
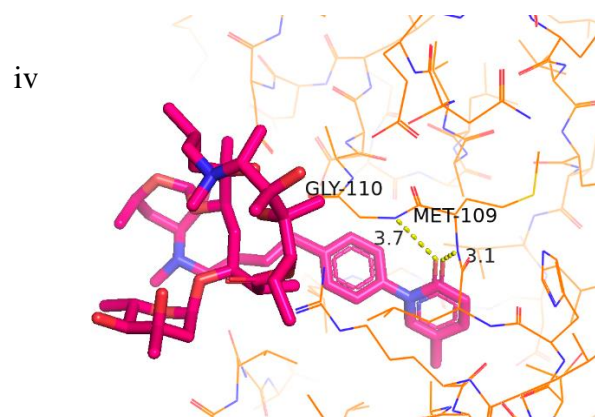
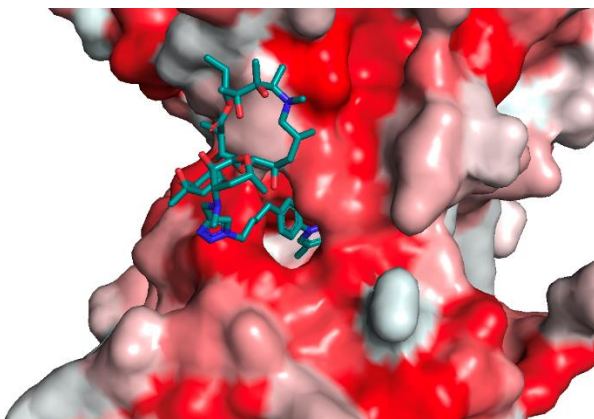
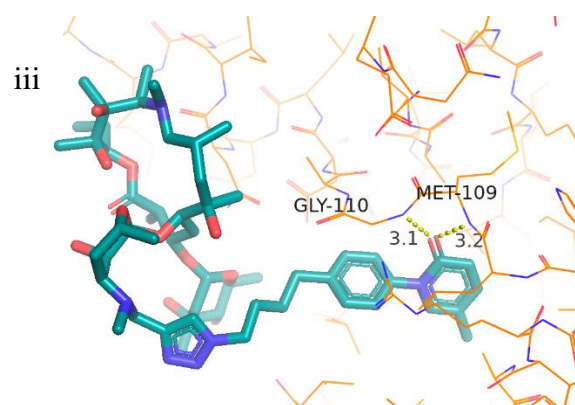
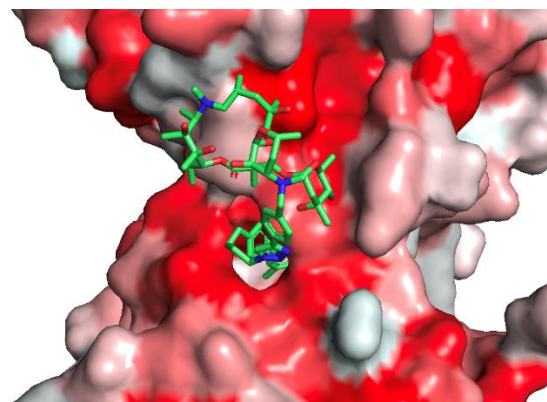
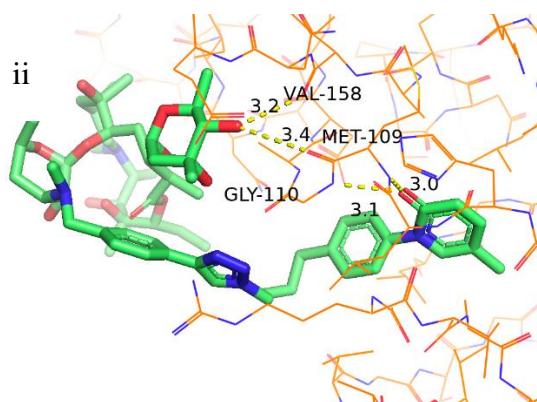
a.





b.





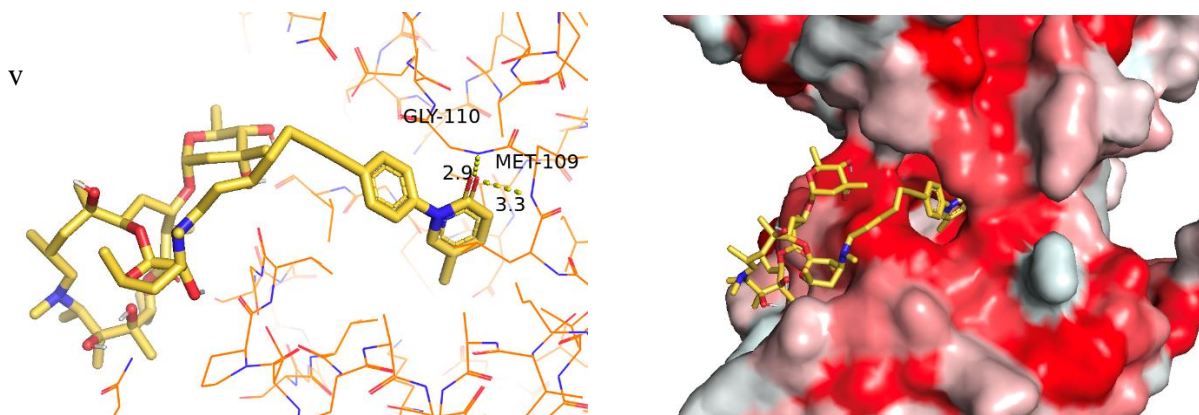
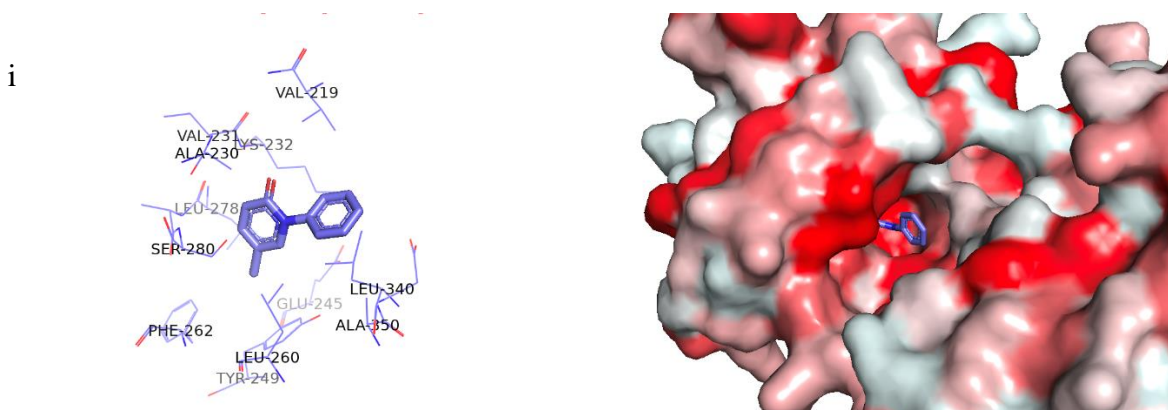
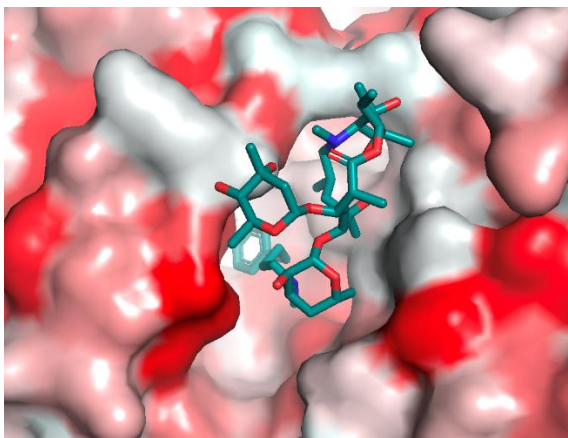
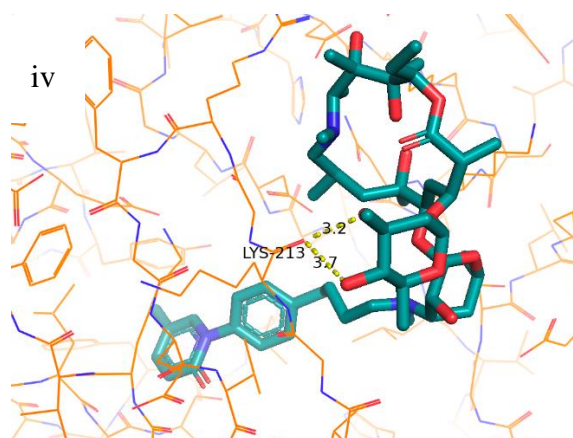
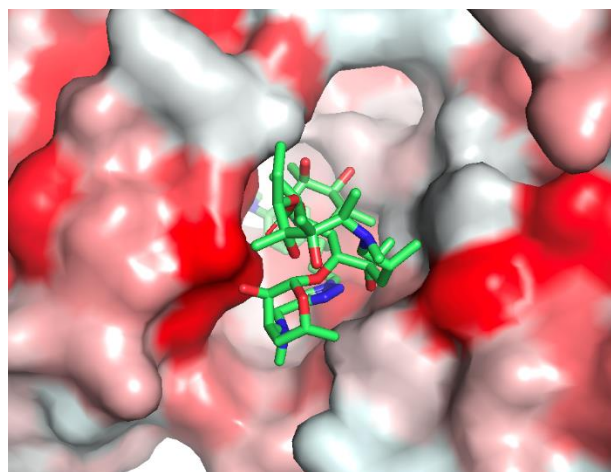
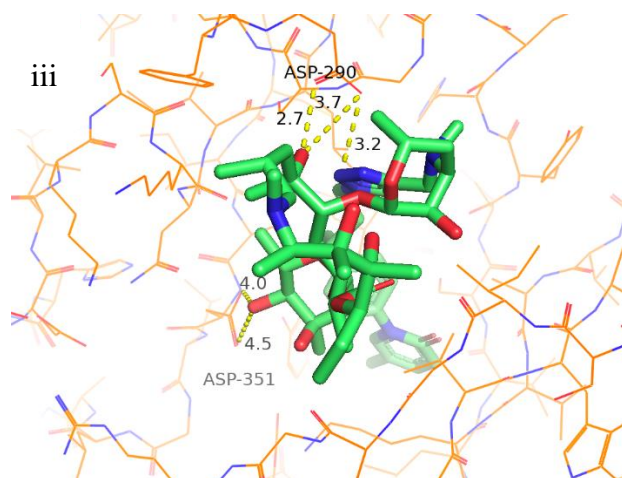
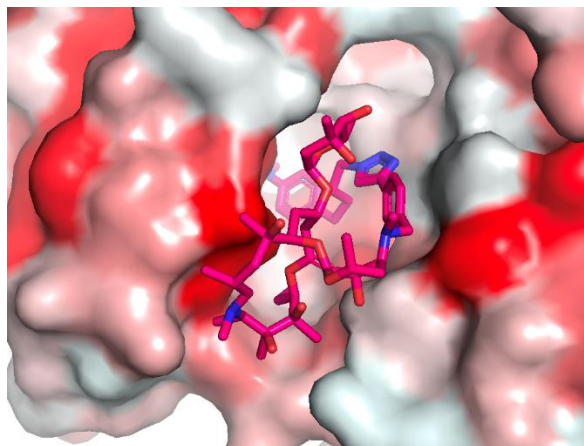
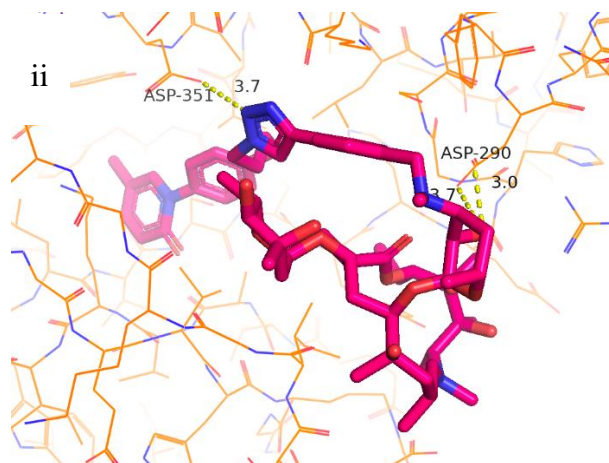
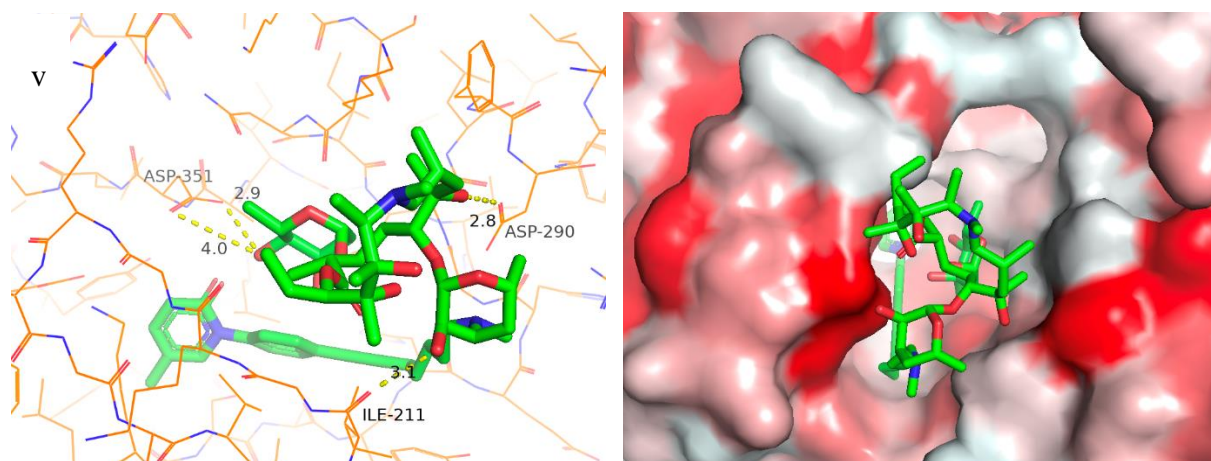


Figure 2.3. Molecular docking analysis of macrolide-PFD compounds at the active site of p-p38 γ (1CM8) and p38 α (3HP2). (a). 1CM8 interacting with PFD and Macrolide-PFD at the Mg site: (i). unmodified PFD trapped into the hydrophobic pocket of the active site. (ii). **11c** binds with the active site of the p-p38 with hydrogen bonding (Ala-40, Arg-70, and Mg-402) with AZM moiety. (iii) and (iv) showed binding orientation of the macrolide-PFD **11c** and **13c** on the surface of p-p38 (red indicates hydrophobicity, white indicates hydrophilicity). (v). with no triazole ring, compound **15c** showed different orientation of binding that the cladinose ring is interacting with Glu-74. (vi) and (vii) **15c** shares the same orientation as **20e** on the binding orientation. (b). PFD and macrolide-PFD binding to p38 α at the active site, where the left is the molecular interaction, and right is the surface presentation reveals hydrophobic character of the active site of p38. (i) PFD is accommodated at p38 active site via crucial H-bonding interaction with MET109 and GLY110; right corner – surface presentation reveals hydrophobic character of the active site of p38. (ii to v). Representatives **11c**, **13c**, **15c**, and **20e** binding to p38.

a.







b.

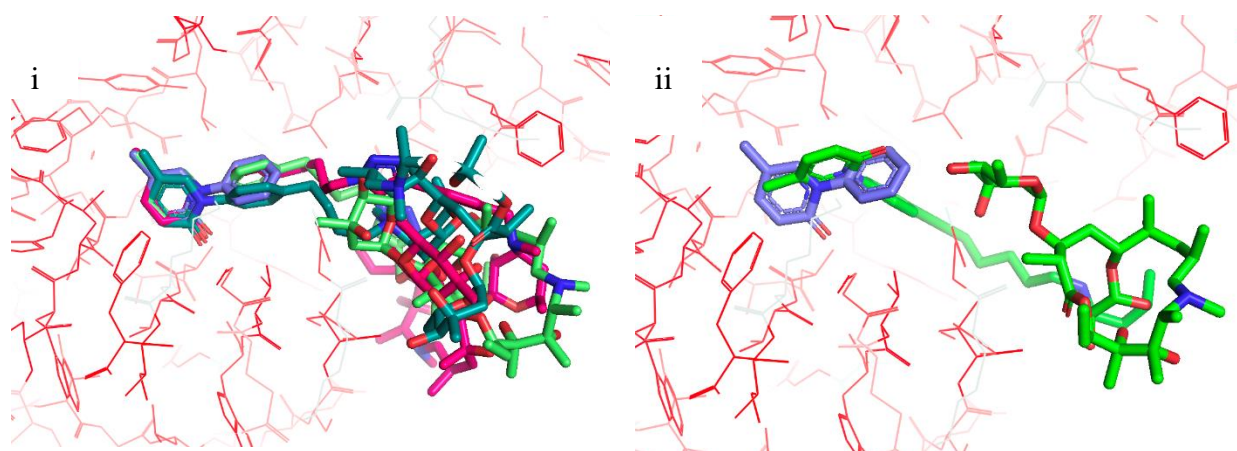


Figure 2.4 Molecular docking analysis of macrolide-PFD compounds at the active site of ALK-5 (5USQ). (a) PFD and Representative macrolide-PFD bind to ALK-5. (i). On the left, unmodified PFD binds to hydrophobic pocket of ALK binding site. (ii) Candidate **11c** interacts with amino acids (Asp-290 and Asp-351) on the surface of the ALK-5 with Hydrogen bonding. (iii). Candidate **13c** interacts with amino acids (Asp-290 and Asp-351) on the surface of the ALK-5 with Hydrogen bonding. (iv). Candidate **15c** interacts with amino acids (Lys-213) on the surface of the ALK-5 with Hydrogen bonding. (v). Candidate **20e** interacts with amino acids (Ile-211, Asp-290, and Asp-351) on the surface of the ALK-5 with Hydrogen bonding. (b). (i) the representatives have the same binding orientation of unmodified PFD except (ii) compound **20e**.

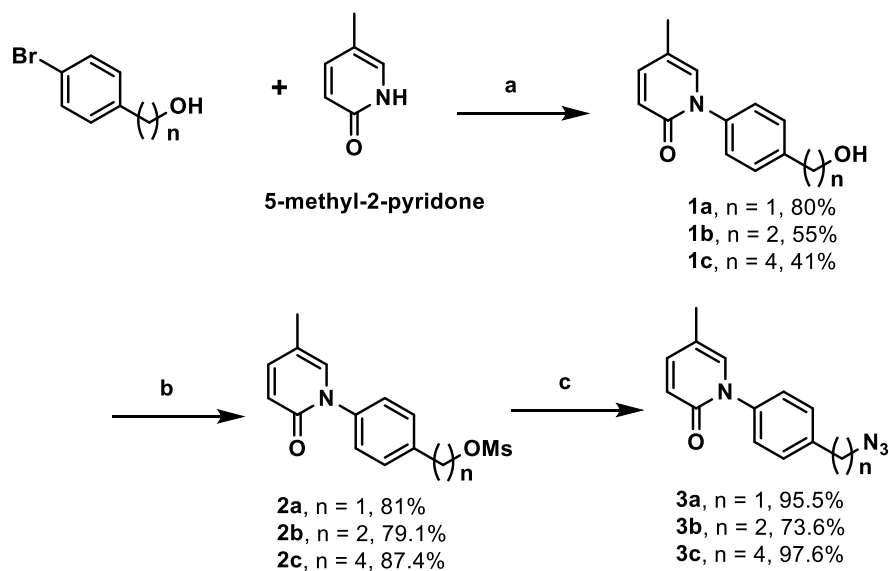
	1CM8 (kcal/mol)	3HP2 (kcal/mol)	5USQ (kcal/mol)
11c	-9.9	-8.8	-9.2
13c	-10.4	-8.3	-9.2
15c	-9.4	-8.0	-8.5
20e	-9.5	-7.9	-8.7
PFD	-7.6	-7.0	7.6
AZM	-7.4	-5.5	-5.9
CLM	-6.5	-5.1	-5.3

Table 2.1. The binding score output of the representatives on 1CM8, 3HP2, and 5USQ.

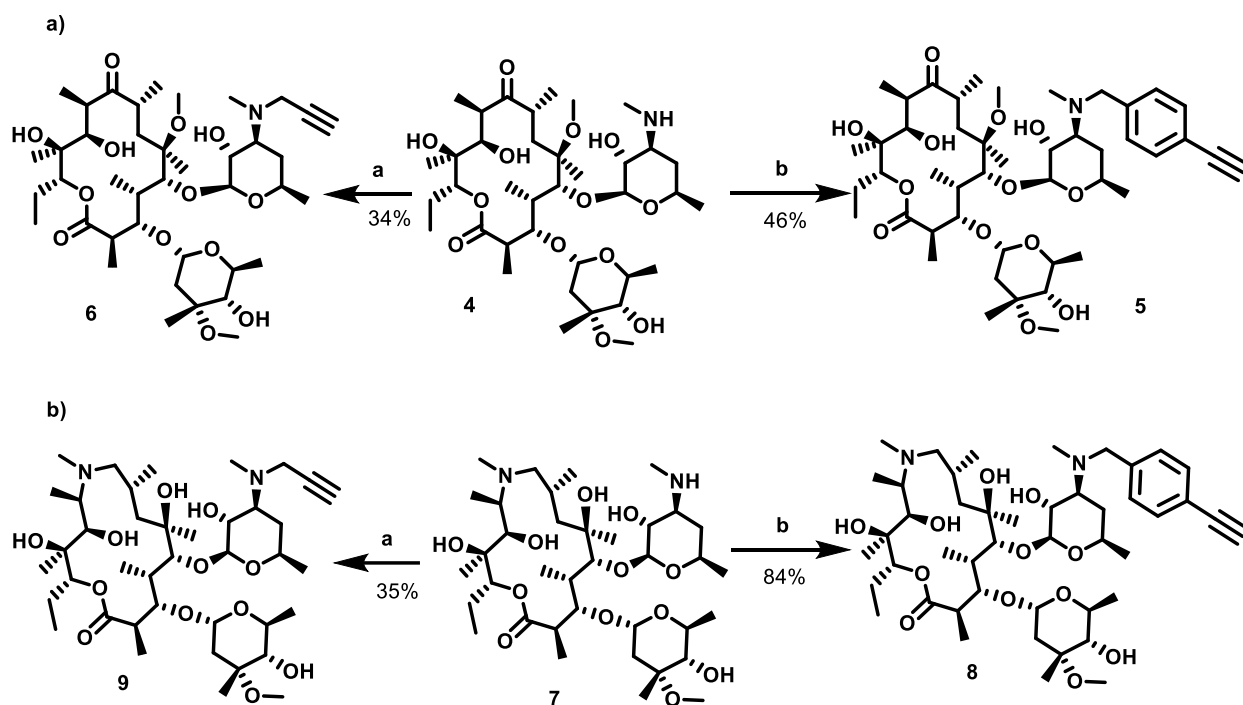
2.2.2 Chemistry:

Compounds **1a-c**, the key intermediates in the synthesis of class I and III compounds were synthesized through Cu(I)-mediated coupling of commercially available 5-methyl-2-pyridine and bromophenyl alcohols. Treatment of **1a-c** with methanesulfonyl chloride afforded mesylated compounds **2a-c**. The reaction of **2a-c** with sodium azide in DMF at elevated temperatures, furnished azide **3a-c** (Scheme 2.1). Desmethylclarithromycin **4** and desmethylazithromycin **7**, the templates for the synthesis of class I compounds was obtained AZM and CLM using published protocol.⁵⁰ The reactions of **4** and **5** with 4-ethynylbenzyl methanesulfonate furnished **5**, **6**, **8** and **9**, the template compounds for the synthesis of class II and III compounds (Scheme 2.2). The copper(I)-catalyzed cycloaddition reaction of azide **3a-c** with template macrolides **5**, **6**, **8** and **9** facilely furnished class I-II compounds **10a-c**, **11a-c**, **12a-c** and **13a-c** (Scheme 2.3a-d).

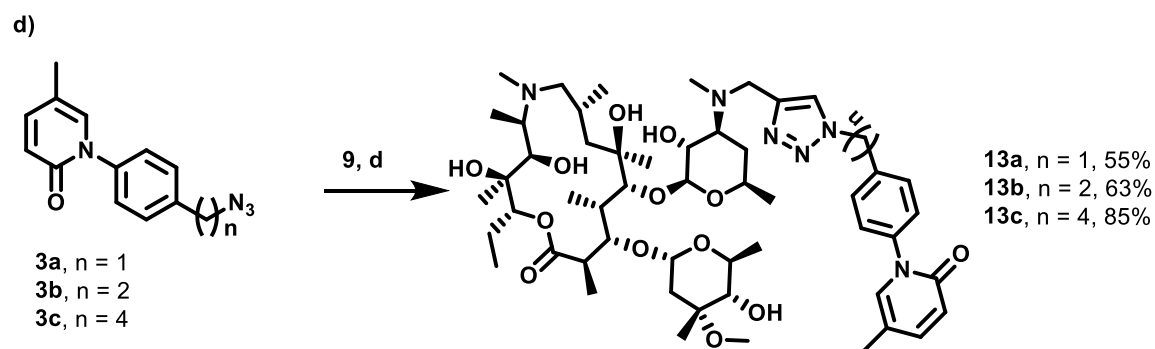
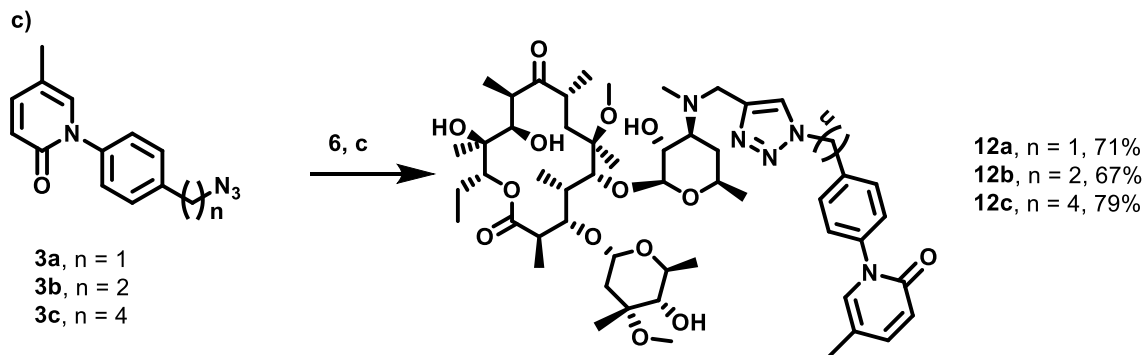
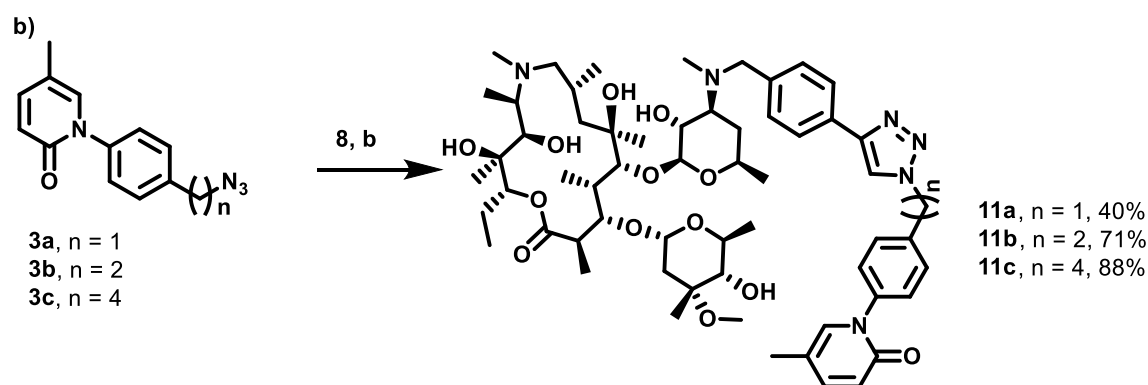
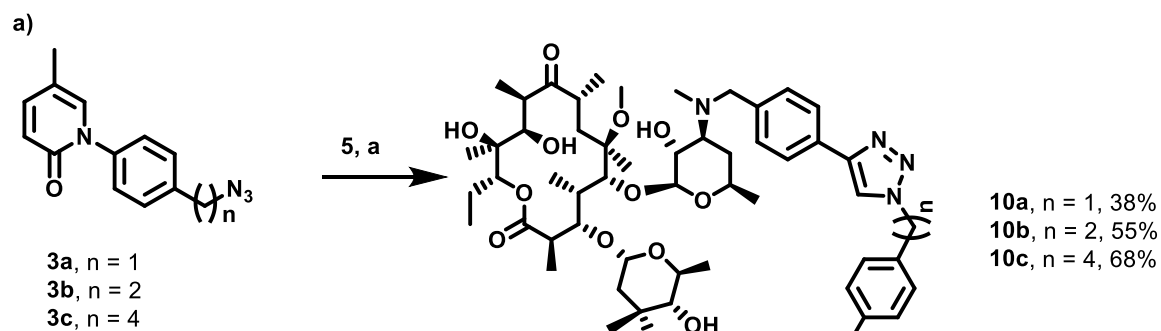
The reactions of **4** and **7** with mesylated compounds **2a-c** in a CH₃CN/DMSO (2:2ml) co-solvent in the presence of Hunig's base at elevated temperatures furnished class III compounds **14a-c** and **15a-c** respectively (Scheme 2.3e-f). To synthesize class IV compound, the 5-methyl-2-pyridone was coupled with 1-iodo-4-methoxybenzene using the same condition as in step a of Scheme 1 to afford compound **16** which was subsequently demethylated with boron tribromide at -30 to 0°C to give compound **17**. Compound **17** was first triflated and then coupled by Sonogashira coupling of this triflyl analog with alkynyl alcohols (n = 1-5) gave alcohols **18a-e**. Mesylation of **18a-e** was achieved by reacting with methanesulfonyl chloride and the reaction of these mesylates with compound **4** and **7** in a CH₃CN/DMSO (2:2ml) co-solvent in the presence of Hunig's base at elevated temperatures furnished class IV compounds **19a-e** and **20a-e** respectively (Scheme 2.4). All compounds were characterized using ¹H NMR, ¹³C NMR, and mass spectroscopy prior to biological testing.

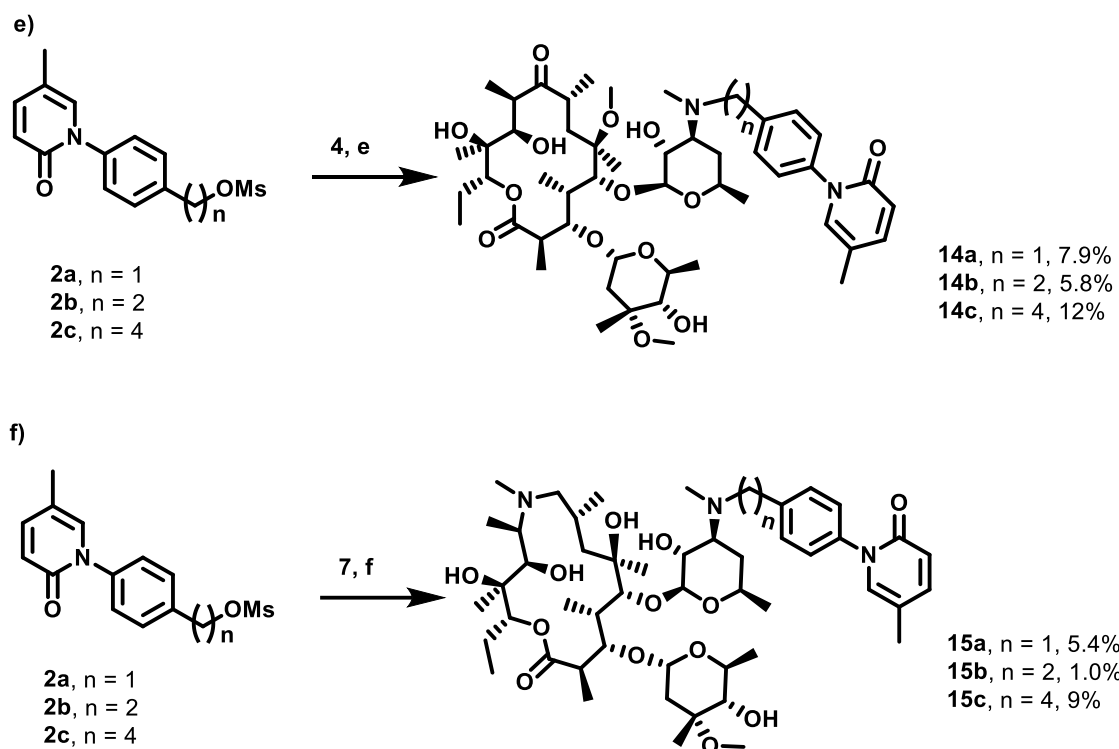


Scheme 2.1. Pirfenidone derivative intermediates synthesis process. (a). CuI, 8-hydroxyquinoline, K₂CO₃, DMSO, 120°C, 24 h. (b). methanesulfonyl chloride, Triethyl amine, DCM, -20°C, 1hr. (c). Sodium azide, DMF, 80°C, overnight.

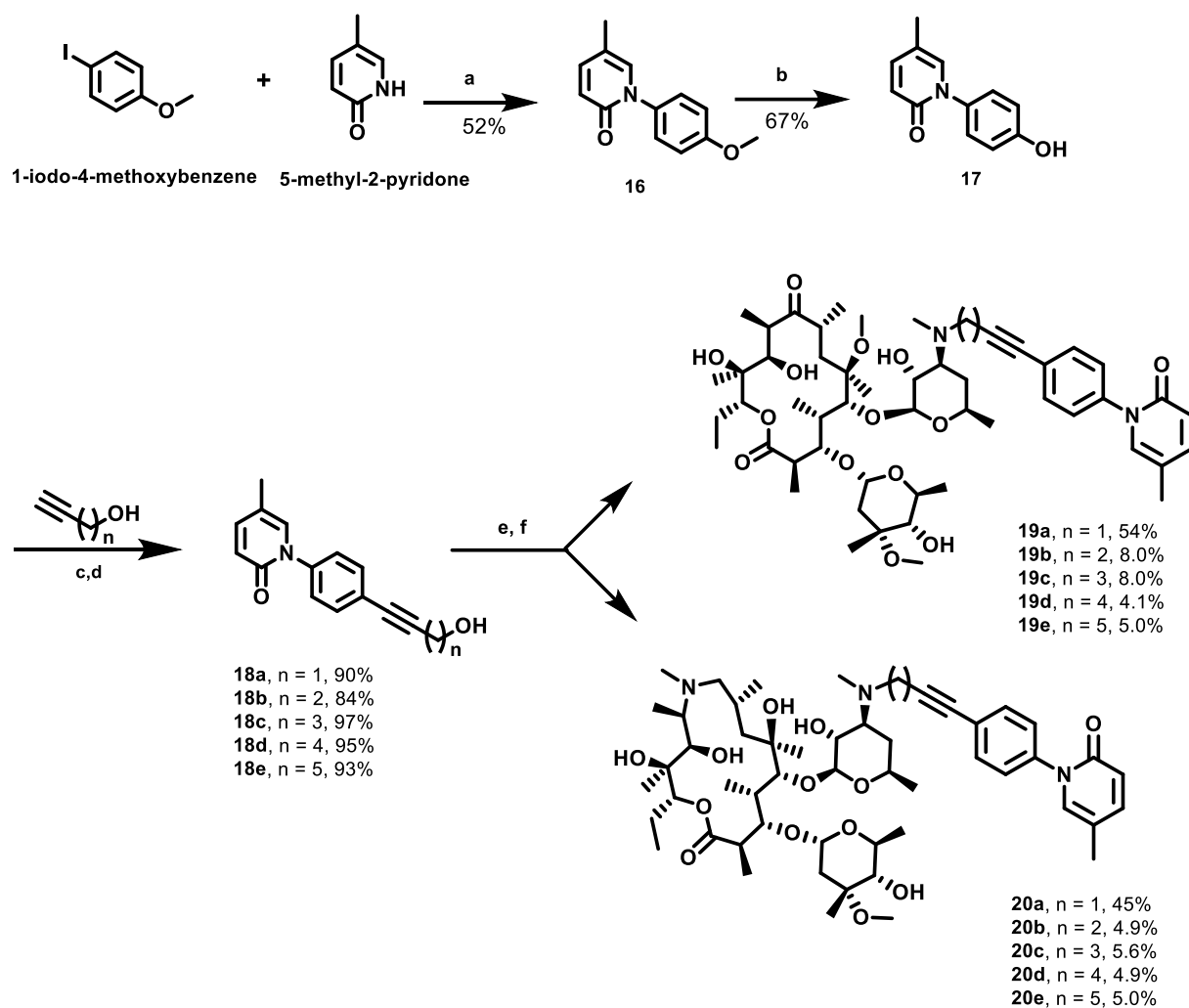


Scheme 2.2. Synthesis of macrolides intermediates. (a) 4-Ethynylbenzyl methanesulfonate, Hunig's base, DMSO, 70°C, 4 h. (b). Prop-2-yn-1-yl methanesulfonate, Hunig's base, DMSO, 70°C, 4 h.





Scheme 2.3. Synthesis of class I-III macrolide-PFD compounds. (a) **5**, CuI, Hunig's base, THF, r.t., overnight. (b) **8**, CuI, Hunig's base, THF, r.t., overnight. (c) **6**, CuI, Hunig's base, THF, r.t., overnight. (d). **9**, CuI, Hunig's base, THF, r.t., overnight. (e) **4**, Hunig's base, CH₃CN/DMSO (2:2ml), 75-80°C, overnight. (f) **7**, Hunig's base, CH₃CN/DMSO (2:2ml), 75-80°C, overnight.



Scheme 2.4. Synthesis of class IV macrolide-PFD compounds. (a) CuI, 8-hydroxyquinoline, K₂CO₃, Toluene, 120°C, 12 h. (b) Boron tribromide, -20°C to r.t., DCM, MeOH. (c) Trifluoromethanesulfonic anhydride, pyridine, DCM, -20°C, 40 min. (d) CuI, Pd[P(C₆H₅)₃]₄, Hunig's base, CH₃CN, 75°C, overnight. (e) Methanesulfonyl chloride, Et₃N, DCM, -20°C, 1 h. (f) **4** or **7**, Hunig's base, CH₃CN/DMSO, 75-80°C, 24 h.

2.2.3 Cell cytotoxicity study

As a cost-effective approach to identify lead compounds for intracellular target validation, we first screened all of the synthesized compounds, PFD (positive control), template macrolides

(AZM and CLM) and combination of PFD and template macrolides against four cell lines: A549, VERO, Hep-G2 and MRC-5 in an MTS assay (Tables 2.1-2.4).

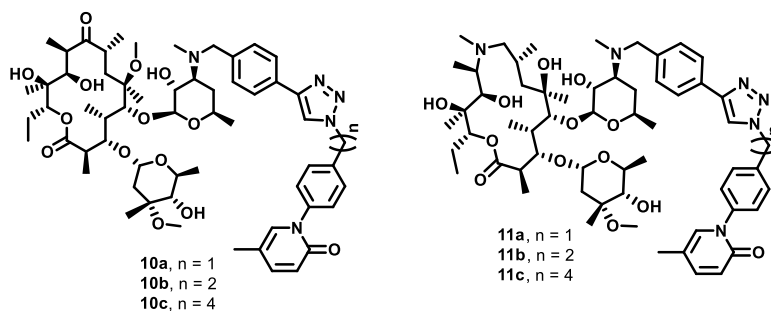


Table 2.1. Effect of class I compounds on cell viability. Structures of class I compounds **10a-c** and **11a-c** are shown atop of the Table.

	MRC-5 (μ M)	VERO (μ M)	A549 (μ M)	Hep-G2 (μ M)
10a	12.3 \pm 1.8	5.1 \pm 0.2	11.1 \pm 2.7	20.3 \pm 1.0
10b	13.1 \pm 1.2	14.2 \pm 0.3	35.3 \pm 1.5	28.1 \pm 1.8
10c	11.6 \pm 0.3	12.4 \pm 0.2	10.9 \pm 0.4	36.4 \pm 6.6
11a	13.4 \pm 0.1	16.2 \pm 2.8	18.4 \pm 4.4	11.1 \pm 0.3
11b	13.3 \pm 0.9	22.6 \pm 4.9	15.8 \pm 3.0	21.8 \pm 0.4
11c	5.7 \pm 0.1	5.9 \pm 0.1	5.0 \pm 0.2	2.6 \pm 0.1

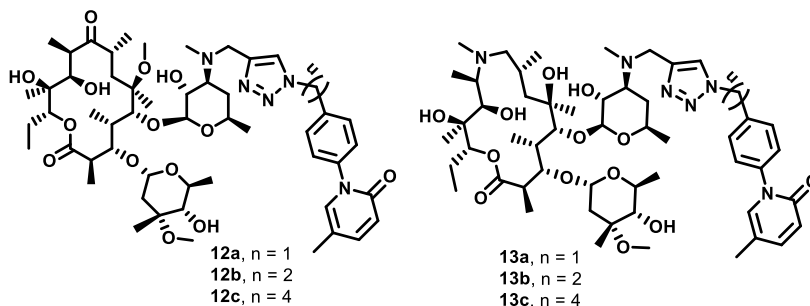


Table 2. 2. Effect of class II compounds on cell viability. Structures of class II compounds **12a-c** and **13a-c** are shown atop of the Table.

	MRC-5 (μM)	VERO (μM)	A549 (μM)	Hep-G2 (μM)
12a	102.6 \pm 0.8	153.2 \pm 19.0	118.3 \pm 28.4	116.5 \pm 16.0
12b	84.0 \pm 4.5	104.5 \pm 20.3	115.9 \pm 4.1	121.7 \pm 3.7
12c	32.8 \pm 5.1	33.3 \pm 1.9	28.7 \pm 3.4	44.8 \pm 3.6
13a	121.0 \pm 14.1	121.6 \pm 19.4	265.1 \pm 4.0	233.6 \pm 31.1
13b	172.1 \pm 26.9	150.6 \pm 30.6	143.5 \pm 24.5	163.4 \pm 1.6
13c	36.1 \pm 6.1	53.2 \pm 0.1	35.2 \pm 5.4	27.7 \pm 3.3

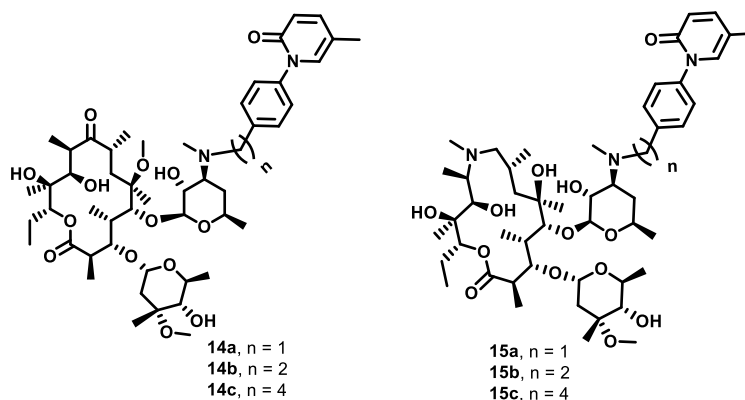


Table 2. 3. Effect of class III compounds on cell viability. Structures of class III compounds **14a-c** and **15a-c** are shown atop of the Table.

	MRC-5 (μM)	VERO (μM)	A549 (μM)	Hep-G2 (μM)
14a	NI	NI	NI	NI
14b	119	NI	NI	NI
14c	15.7 \pm 2.3	19.1 \pm 3.7	16.3 \pm 1.6	30.9 \pm 1.4
15a	55.8 \pm 1.9	47.2 \pm 0.4	47.2 \pm 5.1	33.0 \pm 5.4
15b	36.1 \pm 3.3	30.3 \pm 5.2	40.8 \pm 4.0	27.2 \pm 2.3
15c	5.9 \pm 0.1	23.9 \pm 1.7	43.2 \pm 5.7	52.2 \pm 1.0

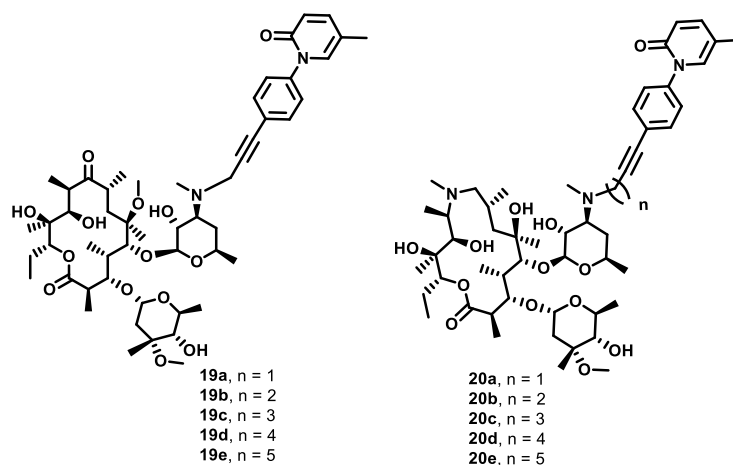


Table 2.4. Effect of class IV compounds and controls (PFD, AZM, CLM, and combinational treatment of PFD+AZM or PFD+CLM) on cell viability. Structures of class IV compounds **19a-e** and **20a-e** are shown atop of the Table 4.

	MRC-5 (μM)	VERO (μM)	A549 (μM)	Hep-G2 (μM)
19a	82.6 \pm 0.3	55.5 \pm 2.6	44.1 \pm 10.8	50.7 \pm 3.0
19b	NI	130.4 \pm 21.2	59.9 \pm 0.8	60.9 \pm 9.0
19c	15.2 \pm 0.1	55.5 \pm 0.4	58.6 \pm 1.4	24.0 \pm 1.2
19d	28.9 \pm 1.9	24.3 \pm 0.1	35.4 \pm 2.1	32.0 \pm 0.1
19e	24.2 \pm 0.6	13.2 \pm 0.7	23.8 \pm 2.1	23.7 \pm 2.0
20a	23.3 \pm 3.3	71.4 \pm 6.3	55.9 \pm 6.4	53.4 \pm 3.3
20b	19.1 \pm 2.6	28.5 \pm 1.8	31.2 \pm 4.8	24.8 \pm 1.7
20c	41.7 \pm 0.1	36.4 \pm 3.8	42.7 \pm 8.4	45.2 \pm 7.4
20d	5.5 \pm 0.2	16.2 \pm 3.1	15.5 \pm 1.1	12.7 \pm 1.3
20e	2.2 \pm 0.1	4.7 \pm 0.3	6.1 \pm 0.3	2.8 \pm 0.0
PFD	5302.0 \pm 177.9	10788 \pm 0.6	5409 \pm 241	10920 \pm 1090
AZM	127.0 \pm 1.0	222.0 \pm 18.1	203.5 \pm 4.5	85.3 \pm 0.9
CLM	138.1 \pm 1.1	NI	NI	130.5 \pm 0
PFD+AZM	54.2 \pm 7.2	136.1 \pm 2.6	136.4 \pm 8.6	102.7 \pm 2.6
PFD+CLM	101.5 \pm 0.5	211.7 \pm 32.5	NI	96.2 \pm 0.0

We investigated MRC-5, a lung fibroblast cell line, because it is the well-used cell line for evaluating *in vitro* anti-fibrotic effects of small molecules as it facilitates ECM production and cytokine release after TGF- β stimulation.⁵¹⁻⁵⁴ Additionally, due to strong linkage between

progression of IPF and liver fibrosis to lung and liver cancers,⁵⁵⁻⁵⁸ we also tested the effects of our compounds against A549 and Hep-G2, lung adenocarcinoma and hepatocellular carcinoma (HCC) cell lines respectively. Non-transformed monkey kidney epithelial cells (VERO) were used as a representative positive control.

Against MRC-5 cells, we found that cytotoxicity of the macrolide-PFD compounds generally increases with increase in the length of the methylene group of the linker moieties for all compound class, with four or five methylene groups being optimum (Tables 2.1-2.4).

Compounds **19b** and **20c** are exceptions to this trend. Comparing the template macrolides, we found that AZM derivatives are relatively more potent than their CLM congeners for class III and IV compounds (Tables 2.3 and 2.4). Relative to PFD, the standard of care for IPF, all of our compounds are 100-2,500-fold more potent. The template macrolides AZM and CLM are also cytotoxic to MRC-5 cells but they are 5 to 50-fold less potent than our potent compounds (compare **14c** vs CLM; and **15c**, **20e** vs AZM). To investigate if simultaneous treatment of PFD and template macrolides has comparable effects as the macrolide-PFD compounds, we treated cells with combination of equal concentrations of PFD+AZM and PFD+CLM. We found that the combinations did not result in significant enhancement of potency relative to AZM and CLM as single agents (Table 2.4). These results suggest that macrolide-PFD compounds are significantly more potent than their template PFD and macrolides as either single agents or combination thereof.

The methylene linker length-dependency largely holds for the effects of these compounds against A549, Hep-G2 and VERO cells. Among the synthesized compounds, we found class III **15c** is 4-9-fold more selective for MRC-5 relative to VERO and the two cancer cell lines tested. This suggest that **15c** could be a lead candidate for target validation and *in vivo* efficacy studies.

2.2.4 *Effect of lead macrolide-PFD compounds on NF- κ B pathway*

NF- κ B pathway plays essential role in tissue fibrosis as it is stimulated by tissue injury-mediated upregulation of pro-inflammatory cytokine TNF- α . The activated NF- κ B contributes to fibroblast-myofibroblast transformation and induces the active mode of ECM production. It has been found that NF- κ B controls the tissue inflammation process and affects the behaviors of immune system. Thus, inhibition of NF- κ B pathway has been found to lead to suppression of tissue inflammation. Specifically, parthenolide, a small molecule NF- κ B inhibitor, was found to be effective in the attenuation of interstitial lung inflammation.^{59, 60} Also, the NF- κ B inhibition activity of PFD has been linked to its effect in decreasing the transcriptional activation of the iNOS gene promoter to suppress the production of pro-inflammatory NO.⁶¹ Thus, it would be of value to investigate and compare the effects of macrolide-PFD compounds relative to PFD on the NF- κ B pathway.

In collaboration with Jia-Dong Li lab at Georgia State University (GSU), we tested the effects of representative compounds (based on cell cytotoxicity) on NF- κ B transcriptional activity using an NF- κ B Luciferase reporter assay (Fig. 2.5). The macrolide-PFD compounds and template macrolides AZM and CLM were screened at 5 μ M while PFD was screened at 5 and 100 μ M in PFD. We noticed that PFD showed no inhibition at 5 μ M, while at 100 μ M it caused a significant inhibition NF- κ B activity. AZM showed significant inhibition in NF- κ B pathway while CLM did not inhibit the pathway at 5 μ M. Among the macrolide-PFD compounds tested, we found that **10b, 10c, 12b, 12c, 13a, 15c, 19a, 19d, 20d** showed significant NF- κ B inhibition at 5 μ M. Based on these findings, we postulated that AZM template may contribute significantly to the strong NF- κ B inhibition activity of the AZM-derived macrolide-PFD compounds. In contrast,

CLM did not contribute to NF- κ B inhibition while its derivatives **10c**, **14c**, **19d** showed significant NF- κ B inhibition. Therefore, for the CLM-derived macrolide-PFD compounds, the PFD moiety may be a significant driver of the NF- κ B inhibition activity. Collectively, compounds **10c**, **15c**, **20e** are highly interesting candidates as they showed anti-fibrotic and anti-cancer activities in addition to inhibiting NF- κ B transcriptional activity.

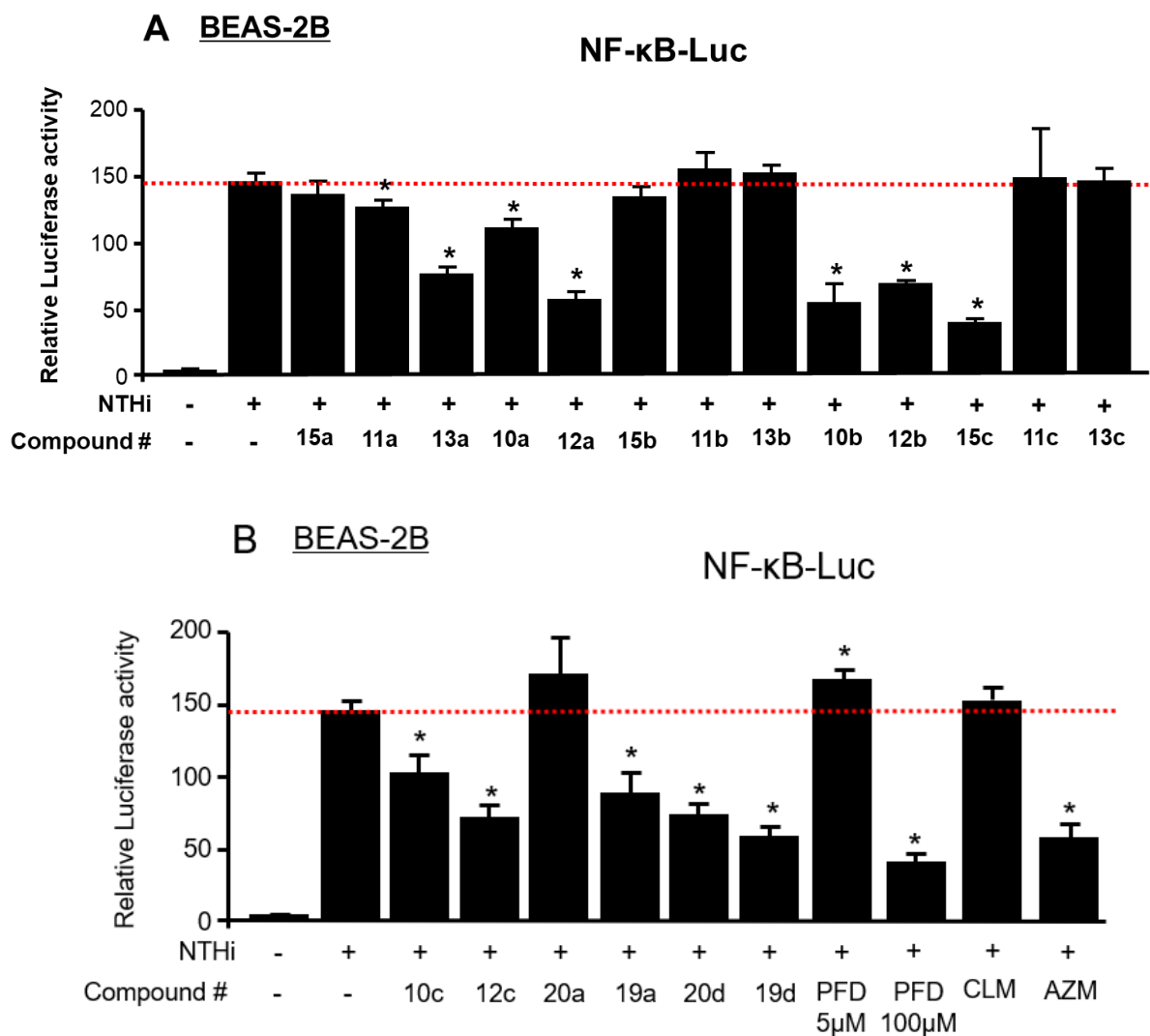


Figure 2.5. Effect of tested agents on NF- κ B transcriptional activity at 5 μ M

2.2.5 *Effect of macrolide-PFD compounds on Pro-COL1A1 expression*

The ECM contains the essential components that contribute to tissue fibrosis and stiffness. Specifically, protein collagen I (COL1A1) is the key protein responsible for fibrosis. In normal tissue under ROS and injury, COL1A1 constructs the tissue with scar healing, while in chronic injury, the collagen expression turned into a continuous expression which induces tissue fibrosis and necrosis. Thus, COL1A1 expression inhibition is one of the direct evidence of tissue fibrosis inhibition. PFD, the standard care for IPF showed significant COL1A1 expression inhibition at IC₅₀ dosage⁶². AZM also caused downregulation of COL1A1 at about 100 μ M range.⁶³ Therefore, we investigated if the macrolide-PFD compounds could inhibit the intracellular expression of COL1A1. We used a pro-COL1A1 expression ELISA assay kit supplied by Abcam (ab210966). Compounds were tested at 1/10th IC₅₀ and IC₅₀, and we observed that they showed concentration-dependent inhibition. Specifically, compounds **10b**, **10c**, **11a**, **12b**, **15c**, **14c**, **19a**, and **20e** showed effects in this assay as they caused 20-55% downregulation of pro-COL1A1 expression at 1/10 IC₅₀ or IC₅₀ concentration after 24 h treatment, whereas PFD to be dosed at 2.5 mM concentration to have similar effect (Fig. 2.6). This data suggests that these macrolide-PFD compounds could suppress ECM production intracellularly.

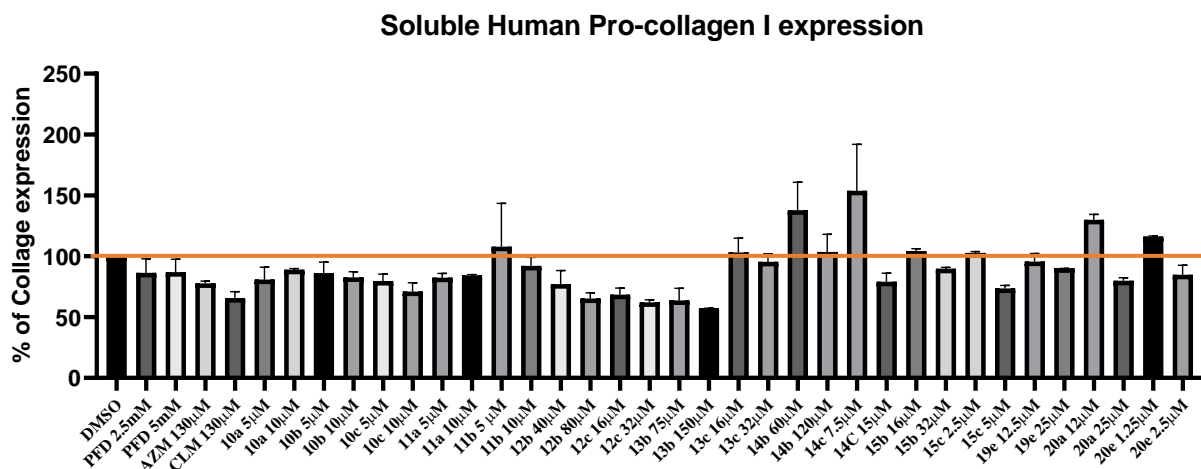


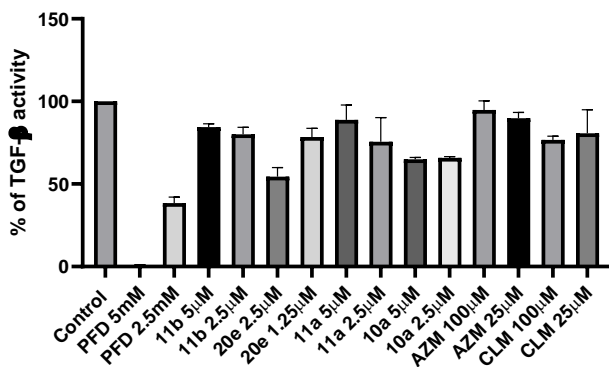
Figure 2.6. Effect of macrolide-PFD compounds on the production of soluble pro-collagen at various concentrations.

2.2.6 Effect of lead macrolide-PFD compounds on TGF- β pathway

As mentioned previously, TGF- β 1 plays a key role in IPF progression. PFD is a TGF- β 1 pathway inhibitor that prevents SMAD2/3-mediated production of ECM and several cytokine mRNAs. Since we used *in silico* tools to design the macrolide-PFD compounds to inhibit TGF- β receptor ALK-5, we expect that these compounds will inhibit TGF- β 1 pathway in analogous manner to the template PFD. So, we used a Promega TGF- β 1 luciferase reporter assay kit (CS2018F03) to examine the effect of our compounds and PFD TGF- β 1 activity. We first scanned the effect of selected compounds (**10a**, **11a-b**, **20e**, **PFD**, AZM and CLM) at two concentrations (1x IC₅₀ and ½ IC₅₀) and found that compound **10a**, **20e** and PFD showed significant TGF- β 1 pathway inhibition at these concentrations while other tested compounds, including AZM and CLM, did not show TGF- β 1 inhibition activity (Fig. 2.6a). Based on this data, we then expand this study to probe the dose-dependent effects of more compounds that

showed both strong cell cytotoxicity and anti-fibrotic and anti-inflammation effects in MRC-5 cell. We found that all selected candidates (**10c**, **11c**, **14c**, **15c**) inhibited the transcriptional activity of TGF- β 1 with IC₅₀s 5-10 μ M, while PFD showed IC₅₀ 1.92 mM (Fig. 2.6b). Through the experiment, we confirmed that the representative macrolide-PFD compounds inhibit TGF- β 1 pathway signaling, key intracellular pro-fibrosis pathway, with 200- to 500-fold enhanced potency relative to PFD. The TGF- β 1 inhibition activity of the macrolide-PFD compounds does not come from the macrolide templates since AZM and CLM are devoid of TGF- β 1 inhibition activity. The TGF- β 1 inhibition activity of the macrolide-PFD compounds is exclusively through their PFD moiety. Therefore, covalent linkage to macrolides (in the context of the macrolide-PFD compounds) facilitates the increased TGF- β 1 pathway inhibition effect of the PFD moiety.

A. Evaluation of the effects of representative compounds on TGF- β activity at $\frac{1}{2}$ IC₅₀ and IC₅₀



B. Dose-dependent effects of representative compounds on TGF- β activity

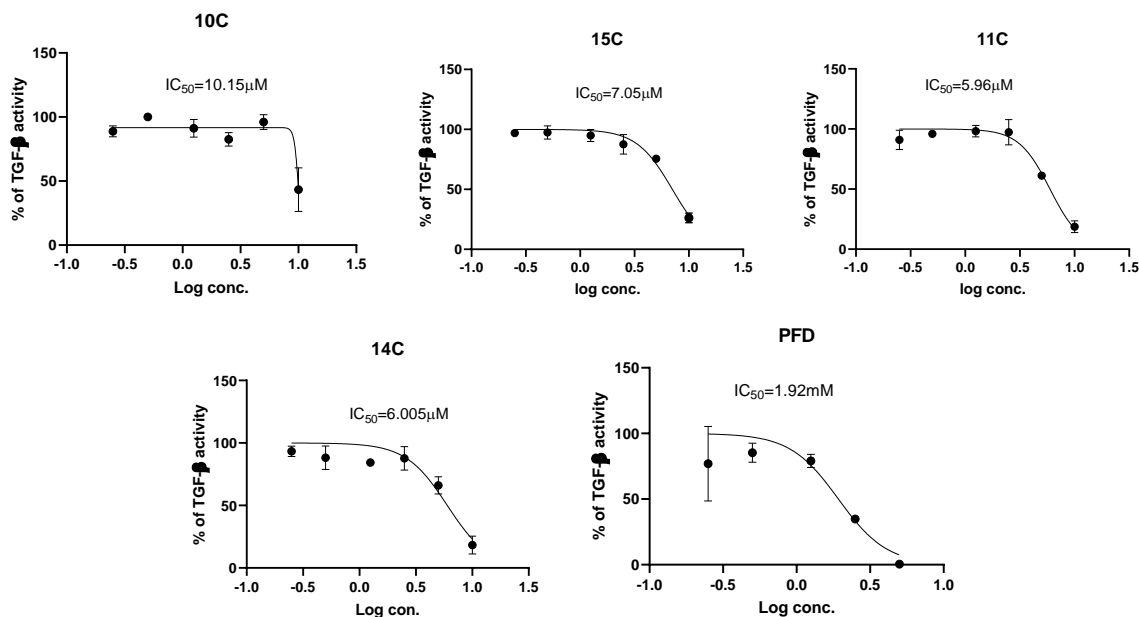


Figure 2.7. Effect of macrolide-PFD compounds on TGF-β activity using Luciferase Gene-reporter assay kit. (A) Evaluation of the effects of representative compounds on TGF-β activity at $\frac{1}{2}$ IC₅₀ and IC₅₀. (B) Dose-dependent effects of representative compounds on TGF-β activity.

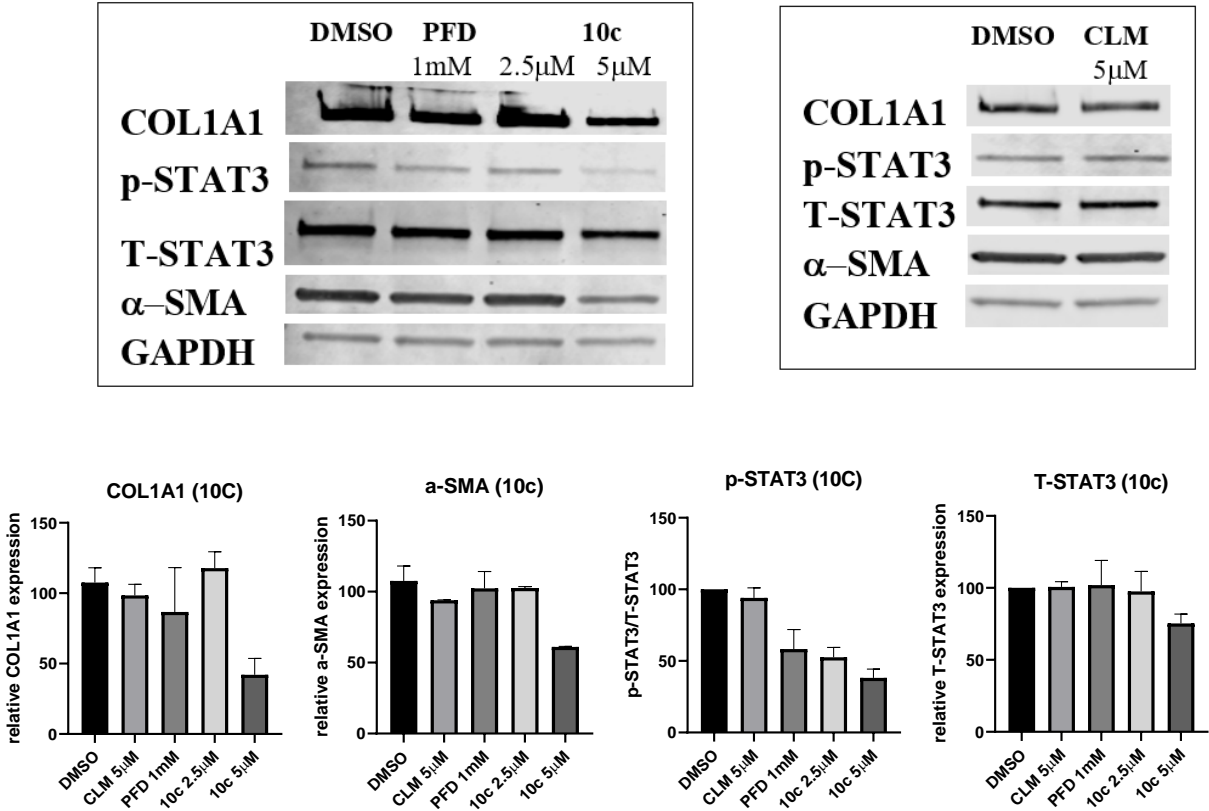
2.2.7 Intracellular target validation study

We used Western blot analysis to test the effects of the macrolide-PFD compounds on the expression status of two main proteins of the ECM components – COL1A1 and α-SMA – in order to confirm the contributions of the targets investigated above on their bioactivity. COL1A1 and α-SMA are proteins essential to the build-up of fibrotic lesion. Previous study on PFD showed that it inhibits the expression of COL1A1 at 2.5-5 mM concentration and only minor inhibition at 1mM.^{64, 65} In addition, the effects of drugs on the levels of p-STAT3 proteins is indicative of effect on fibrosis and proinflammatory markers.⁶⁶⁻⁶⁸ We chose **10c**, **11b**, and **11c** for the first round of Western blot due to their outstanding performance in one or more tests: simulation

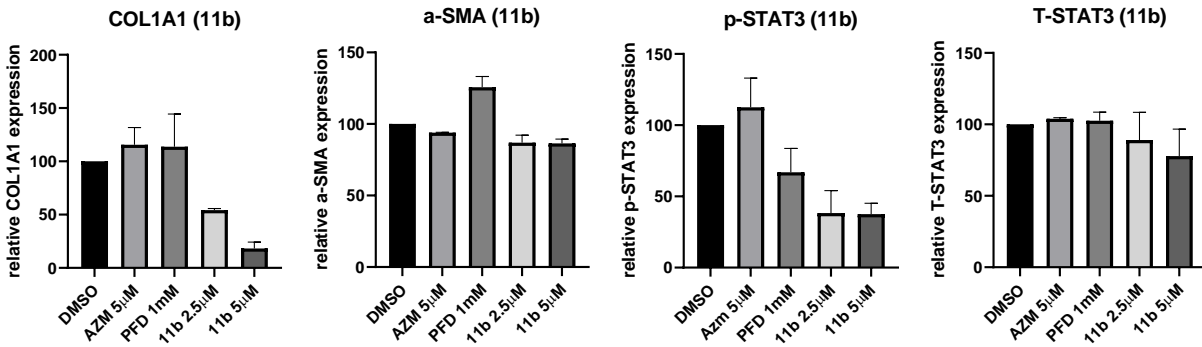
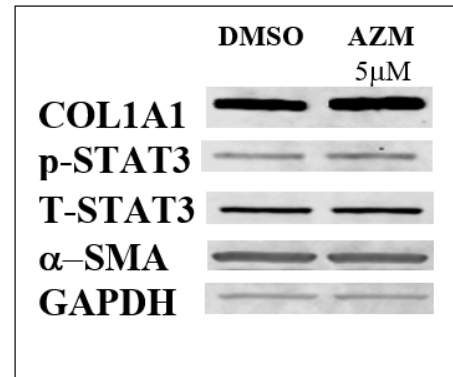
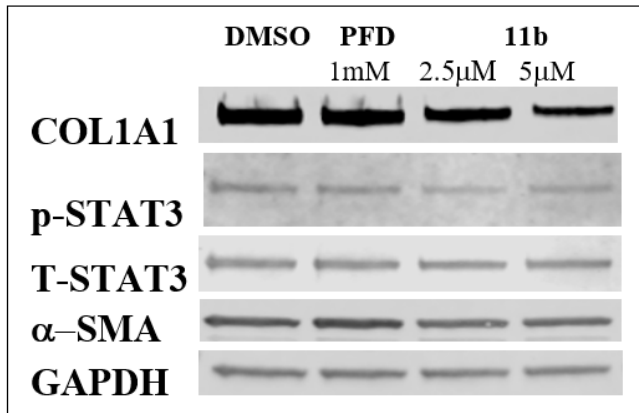
prediction, cytotoxicity, COL1A1 inhibition scanning, and NF-κB inhibition. We used PFD, CLM, and AZM as controls.

A. Effects of representative CLM-PFD **10c** on intracellular markers of fibrosis and inflammation.

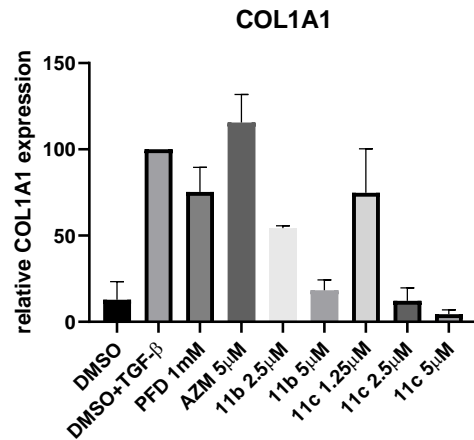
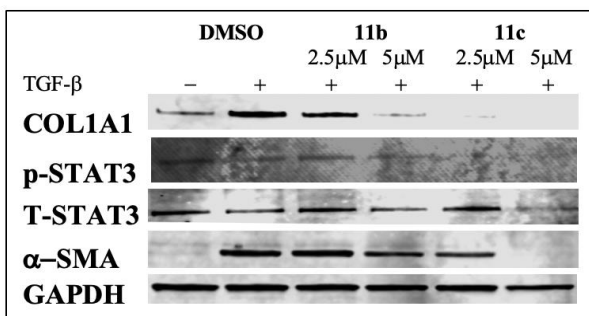
10c:

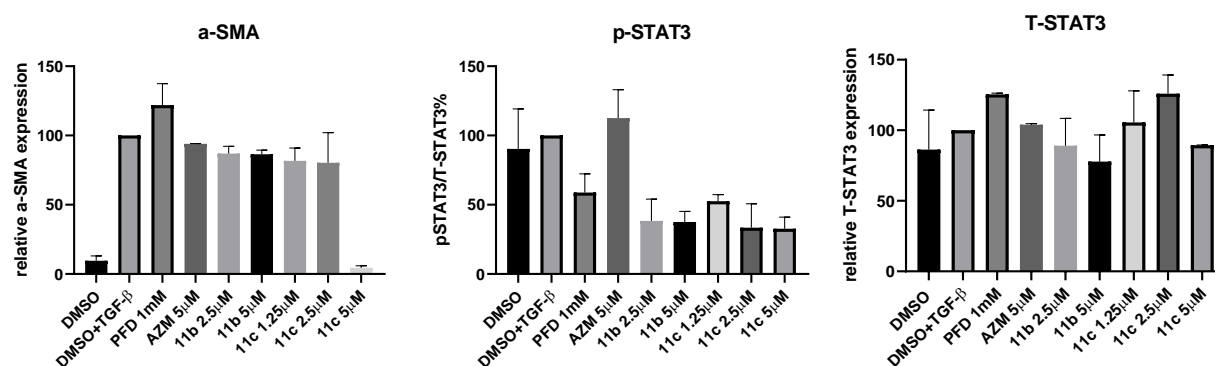


B. Effects of representative AZM-PFD **11b** on intracellular markers of fibrosis and inflammation



c. Effects of representative AZM-PFD **11c** on intracellular markers of fibrosis and inflammation





d. Effects of macrolide-PFD compounds **10c**, **11b** and **11c** on TGF- β expression

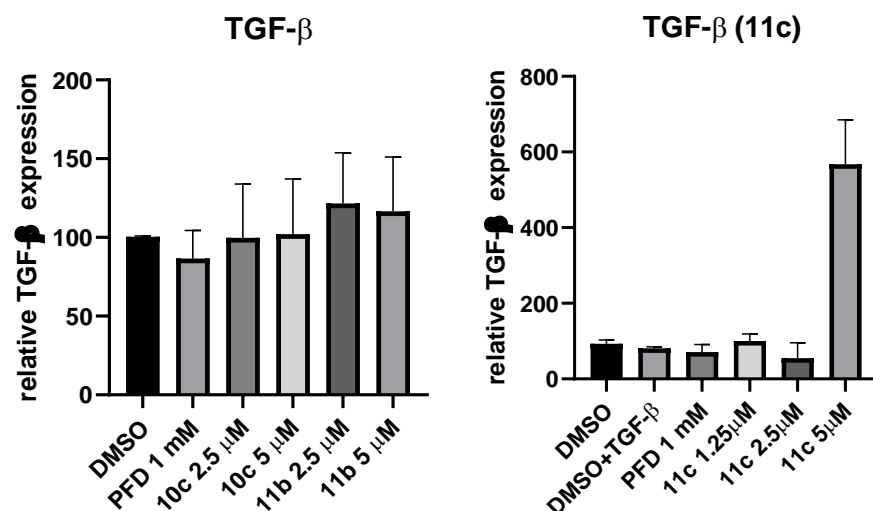
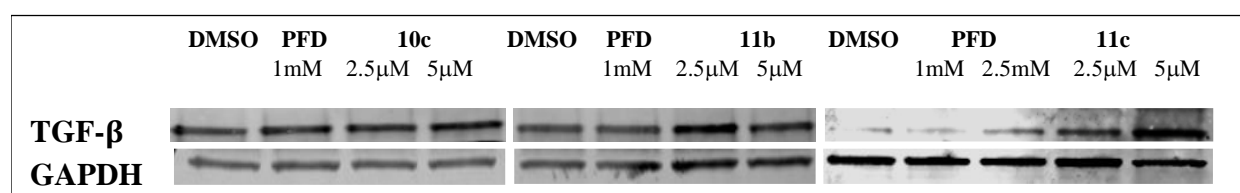
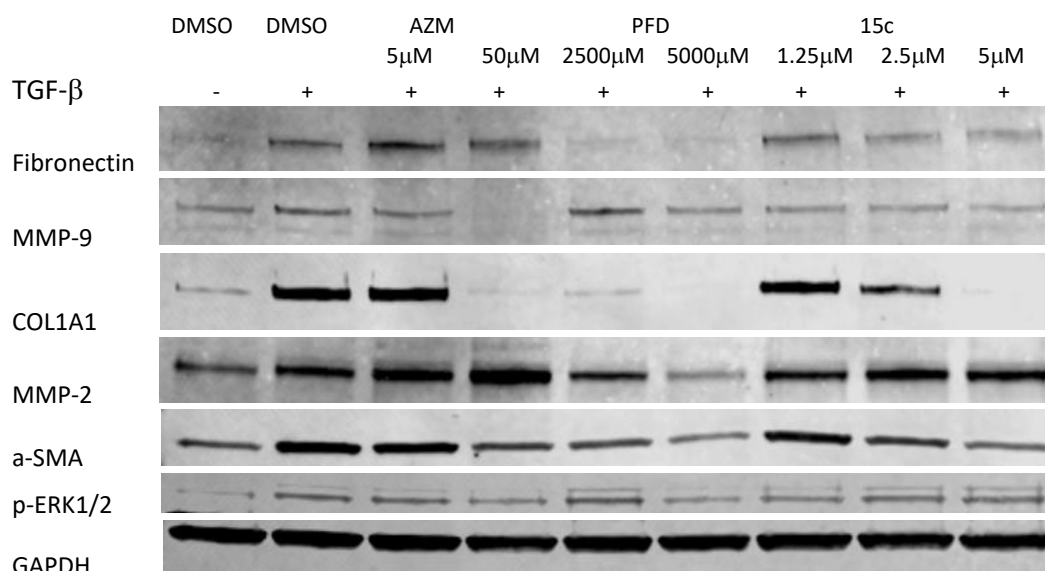


Figure 2.8. Effects of representative macrolide-PFD compounds on the expression status of COL1A1 and α -smooth actin, two main proteins of the ECM components and p-STAT3 in MRC-5 cell after 24 h of treatment. Compounds **10c**, **11b**, and **11c** significantly inhibited the intracellular levels of COL1A1 and α -smooth actin and p-STAT3 with or without TGF- β 1 stimulation (A-C). Compounds **10c** and **11b** have no effect on TGF- β expression, (D) while the **11c** significantly upregulate the TGF- β 1 expression at 5 μ M.

We observed that **10c** and **11b** showed significant downregulation of COL1A1 at 5 μ M (> 50% for **10c** and >80% for **11b**) (Figs. 2.7a-b), while **11c** almost eliminated the COL1A1 expression at the same concentration (Fig. 2.7c). The template macrolides AZM and CLM have no effect on COL1A1 level at 5 μ M and, PFD at 1 mM also did not show any significant downregulation on COL1A1 expression as well. Moreover, **10c** (5 μ M), **11b** (2.5 μ M) and **11c** (2.5 μ M) showed significant p-STAT3 inhibition. It required 1 mM dosage for PFD to achieve comparable p-STAT3 downregulation activities as these macrolide-PFD compounds (Figs 2.7a-c). These data strongly support the potent the anti-fibrotic effects of macrolide-PFD compounds.

We also investigated effects of all compounds on TGF- β level and found that none shows any inhibition of TGF- β 1 expression level (Fig. 2.7d). This result is not unexpected since our compounds are designed to inhibit TGF- β 1 pathway through receptor binding (or SMAD2/3 transcription), instead of direct downregulation of TGF- β 1 expression.



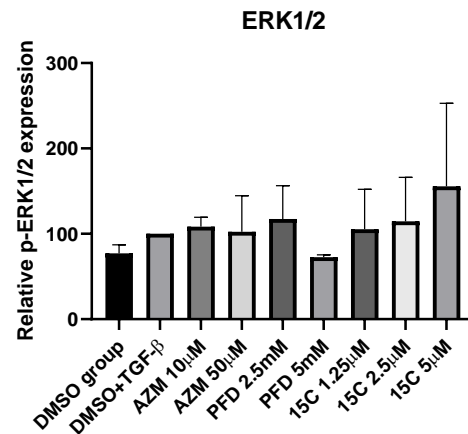
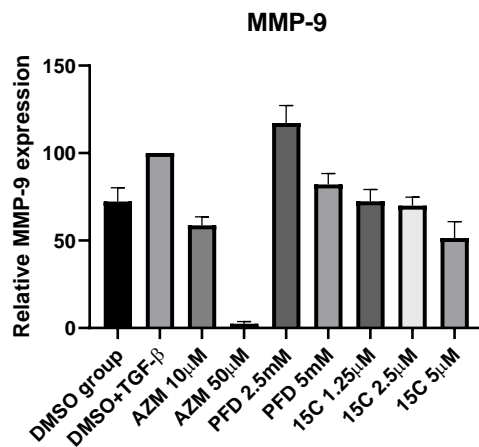
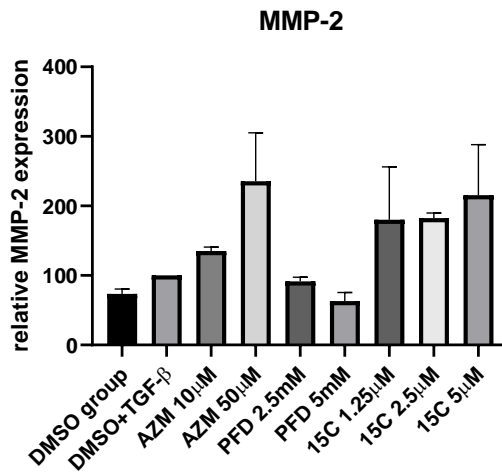
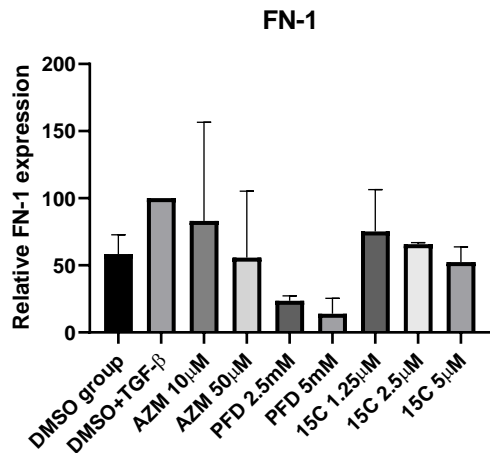
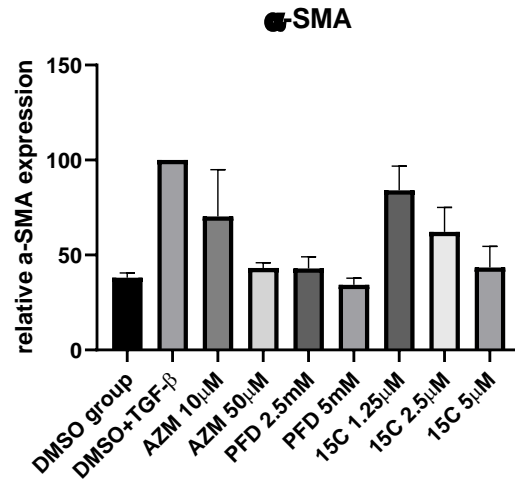
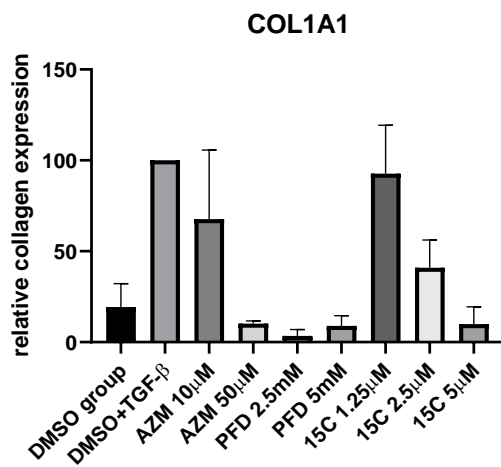


Figure 2.9. Compound **15c** demonstrates strong anti-fibrosis effect in TGF- β stimulated MRC-5 cell line.

We then expanded our investigation intracellular target validation to include **15c**, a lead compound which showed selective toxicity to MRC-5 cells. We used significantly higher concentrations of the control compounds AZM and PFD than the once we used in the experiments described above. We observed that the AZM at 50 μ M demonstrated anti-fibrotic effect with suppression of ECM components COL1A1, α -SMA, and fibronectin (FN-1). Since matrix metalloproteinases (MMPs) contribute to ECM decomposition, and upregulation of MMPs is a biomarker of inflammation and/or fibrosis, we also tested the effects of 15c on MMP-2 and 9 expression levels. We observed that AZM upregulates MMP-2 and phosphorylation of ERK1/2 while it downregulates MMP-9 significantly. In contrast, PFD significantly downregulated MMP-2 at 2.5 or 5 mM, and while it slightly downregulated MMP-9 at 5 mM. Interestingly, **15c** showed a similar pattern as AZM, significantly upregulating MMP-2 and downregulating MMP-9 in a dose-dependent manner (Fig. 2.8). This implies that **15c** derives its anti-fibrotic effects from a unique combination of the mechanism(s) of the anti-fibrotic activities of PFD and AZM. Thus, **15c** represents a novel anti-fibrotic and anti-inflammatory agent.

2.3 Conclusion

Efforts at developing treatment modalities for IPF have focused on three stages of the disease: microinjuries, abnormal wound healing process with immune activation, and fibroblast hyperplasia exaggerated extracellular matrix (ECM, mainly collagens) deposition mediated by transforming growth factor (TGF)- β /Smad signaling.⁶⁹ The potential of the drivers of the later

stage as IPF drug target has been validated with the U.S. Food and Drug Administration (FDA) approval of two drugs – PFD and nintedanib – which inhibit IPF progression via distinct mechanisms. However, neither drug is optimal for IPF therapy due to their adverse side-effects, low potency, cost ineffectiveness (either drug cost over \$94,000 per year) and minimal beneficial effect on the patients' survival rate. We have used herein a structure-based approach, which was validated by *in silico* drug design tool (Autodock Vena), to design 4 classes of macrolide-based anti-fibrotic agents. These agents are designed to exploit the excellent PK and selective lungs and/or liver tissues distribution activities of these macrolide templates to arrive at novel anti-fibrotic agents that may selectively accumulate within these tissues. We designed and synthesized twenty-eight compounds and tested their effects on the viability of four cell lines – MRC-5, A549 Hep-G2 and VERO. We observed that candidate compounds **10c**, **11c**, **11b**, **15c**, **20e** inhibited the proliferation of these cell lines with IC₅₀ range of 2.5-10 μ M. To investigate their cellular targets, we screened selected candidates for their effects on pro-fibrosis and pro-inflammation NF- κ B and TGF- β pathways. We found that these compounds potently inhibit NF- κ B and TGF- β pathways. Relative to PFD or the unmodified macrolide templates, the macrolide-PFD compounds have much effective anti-fibrotic agents with potency enhancement as high as 1000-fold. The enhanced potency of the new macrolide-derived compounds is in agreement with the results from our molecular docking studies which revealed that these compounds could engage in productive interaction with amino acid residues on the outside surface of TGF- β receptor, ALK-5. Among these macrolide-PFD compounds, **15c** showed an optimum inhibition and/or downregulation of the fibrosis markers (FN-1, MMP-9, COL1A1, α -SMA) that we investigated at low micromolar IC₅₀. The next best compounds are **10c**, **11c** and **20e**. These

compounds are excellent candidates for future preclinical studies focused on the evaluation of their PK, tissue distribution and anti-fibrotic effects in in vivo models of IPF and liver fibrosis.

2.4 Materials and Methods

2.4.1 Materials

Analtech silica gel plates (60 F254) were used for analytical TLC while Analtech preparative TLC plates (UV 254, 2000 μm) or silica gel (400 Mesh) was used for compound purification. NMR spectra were taken on Varian-Gemini 400 MHz and Bruke 700 MHz magnetic resonance spectrometer. ^1H NMR spectra were recorded in parts per million (ppm) relative to the residual peaks of CHCl_3 (7.24 ppm) in CDCl_3 . ^{13}C spectra were recorded relative to the central peak of the CDCl_3 triplet (81.5 ppm) were recorded with complete hetero-decoupling. Multiplicities are described using the abbreviation: s, singlet; d, doublet, t, triplet; q, quartet; p, pentet; dd: doublet of doublet; dt: doublet of triplet; dq: doublet of quartets, m, multiplet; and app, apparent. High-resolution mass spectra were recorded at the Georgia Institute of Technology mass spectrometry facility in Atlanta.

2.4.2 Synthesis

Compound 1a.⁶⁹ 2-Hydroxy-5-methyl pyridine (1.32 g, 12.1 mmol) was added to potassium carbonate (1.67 g, 12.1 mmol), 8-hydroxyquinoline (348 mg, 2.4 mmol) and (4-bromophenyl) methanol (4 mL, 4.17 g, 22.02 mmol) in a 100ml round bottom flask with reflux condenser. Dimethyl sulfoxide (DMSO) (25 mL) was added into the mixture and purged with argon for 30

min. Then, copper(I) iodide (696 mg, 3.66 mmol) was added into the solution. The pressure tube was capped after another 15 min of argon purge. The reaction was covered with aluminum foil and heated to 120°C with reflux for 24 h. The reaction was cooled to room temperature and the resulting green mixture was worked up with DCM (100 mL x 3) with water (150 mL). The combined DCM layer was washed with HCl solution (1M, 100 mL) and the green color turned back to pale yellow. The aqueous layer also turned yellow. So, more DCM (50 mL x 5) was used to extract product in the aqueous layer. The combined DCM layer was dried over Na₂SO₄, evaporated *in vacuo* to give the crude product as yellow power. The crude was purified using silica gel chromatography (EtOAc: methanol=10:0.7) to furnish **1a** as pale yellow solid (2.08 g, 80%). ¹H NMR (400 MHz, CDCl₃) δ 7.52 – 7.41 (d, 2H), 7.34 (d, *J* = 8.4 Hz, 2H), 7.27 (d, *J* = 9.7 Hz, 1H), 7.15 – 7.05 (m, 1H), 6.61 (d, *J* = 9.3 Hz, 1H), 4.71 (d, *J* = 5.8 Hz, 2H), 2.20 (t, *J* = 6.0 Hz, 1H), 2.10 (d, *J* = 1.1 Hz, 3H).

Compound 1b.⁶⁹ The reaction of 2-hydroxy-5-methyl pyridine (0.2 g, 1.83 mmol), potassium carbonate (0.5 g, 3.6 mmol), 8-hydroxyquinoline (60 mg, 0.423 mmol) and 2-(4-bromophenyl) ethanol (0.36 mL, 0.37g, 1.84 mmol) in DMSO, as described for the synthesis of **1a**, furnished **1b** as pale yellow solid (125 mg, 55%). ¹H NMR (400 MHz, cdcl₃) δ 7.33 (d, *J* = 4.5 Hz, 3H), 7.28 – 7.27 (d, *J* = 2.5 Hz, 1H), 7.25 (d, *J* = 2.5 Hz, 1H), 7.11 (d, *J* = 2.5 Hz, 1H), 6.60 (d, *J* = 9.3 Hz, 1H), 3.88 (q, *J* = 6.4 Hz, 2H), 2.91 (t, *J* = 6.5 Hz, 2H), 2.10 (d, *J* = 1.1 Hz, 3H).

Compound 1c.⁶⁹ The reaction of 2-hydroxy-5-methyl pyridine (0.35 mg, 3.21 mmol), potassium carbonate (0.500 g, 3.6 mmol), 8-hydroxyquinoline (38 mg, 0.26 mmol) and 4-(4-bromophenyl) butanol (0.3mL, 1.37mmol) in DMSO (8 mL), as described for the synthesis of **1a**, furnished **1c**

as yellow oil (145mg, 41%). ^1H NMR (400 MHz, CDCl_3) δ 7.45 (d, $J = 7.2$ Hz, 5H), 7.28 (dt, $J = 2.7, 1.0$ Hz, 1H), 6.78 (d, $J = 9.3$ Hz, 1H), 3.85 (t, $J = 6.6$ Hz, 2H), 2.86 (t, $J = 7.5$ Hz, 2H), 2.27 (d, $J = 1.1$ Hz, 3H), 1.94 – 1.86 (m, 2H), 1.79 (t, $J = 3.1$ Hz, 2H).

Compound 2a. The **1a** (2.7 g, 12.6 mmol) was added into anhydrous DCM (50 mL). Triethylamine (4 mL, 30.88 mmol) was added and the mixture was purged with argon at -15°C . 15 min later, methanesulfonyl chloride (2 g, 20.4 mmol) was added into the solution. The reaction ran for 1-2 h until all starting materials have reacted. The solution was worked up by adding saturated NaHCO_3 solution (30 mL) and the two layers separated. The aqueous layer was extracted with (30 mL x 3). The combined DCM layer was washed with brine (30 mL), and dried over Na_2SO_4 . The mixture was evaporated off resulting in compound **2a** (2.7 g, 10.1 mmol, 81%) as yellow liquid. The crude product was used for the next step reaction without purification.

Compound 2b. The reaction of **1b** (0.154 g, 0.67 mmol) with methanesulfonyl chloride (0.147 g, 1.2 mmol) in anhydrous DCM (20 mL) and triethylamine (0.17 mL, 1.2 mmol) mixture, as described for **2a**, furnished **2b** (150 mg, 0.53 mmol, 79.1%) as yellow liquid. The crude product was used for the next step reaction without purification.

Compound 2c. The reaction of **1c** (2 g, 7.8 mmol) with methanesulfonyl chloride (1.75 g, 16.8 mmol) in anhydrous DCM solution (30 mL) and triethylamine (2 mL, 15.44 mmol) mixture, as described for **2a**, furnished **2C** (2.1 g, 6.81 mmol, 87.4%) as yellow liquid. The crude product was used for the next step reaction without purification.

Compound 3a. Compound **2a** (600 mg, 2.23 mmol) was dissolved in to DMF (10 mL), NaN₃ (200 mg, 3.08 mmol) was added and the mixture was heated to 80°C for 24 h. The reaction was allowed to cool down to room temperature, partitioned between DCM (50 mL) and water (100 mL) and the two layers separated. The aqueous layer was extracted with DCM (50 mL x 3). The combined DCM layer was washed again with water (100 mL x 2), dried over Na₂SO₄ and evaporated off to give **3a** (503 mg, 2.13mmol, 95.5% as yellow liquid. ¹H NMR (400 MHz, CDCl₃) δ 7.49 – 7.38 (m, 4H), 7.29 (d, *J* = 2.6 Hz, 1H), 7.16 – 7.08 (m, 1H), 6.62 (d, *J* = 9.3 Hz, 1H), 4.40 (s, 2H), 2.11 (d, *J* = 1.1 Hz, 3H).

Compound 3b. The reaction of **2b** (680 mg, 2.2 mmol) with NaN₃ (175 mg, 2.69 mmol) in DMF (10 mL), as described for the synthesis of **3a**, furnished **3b** (405 mg, 1.62mmol, 73.6%) as yellow liquid. ¹H NMR (400 MHz, CDCl₃) δ 7.24 – 7.10 (m, 5H), 7.04 – 6.94 (m, 1H), 6.45 (d, *J* = 9.3 Hz, 1H), 3.42 (t, *J* = 7.2 Hz, 2H), 2.80 (d, *J* = 7.2 Hz, 2H), 1.97 (d, *J* = 1.3 Hz, 3H).

Compound 3c. The reaction of **2c** (2.5 g, 6.08 mmol) with NaN₃ (700 mg, 10.8 mmol)) in DMF (10 mL), as described for the synthesis of **3a**, furnished **3c** (1.65 g, 5.9mmol, 97.6%) as yellow liquid. ¹H NMR (400 MHz, CDCl₃) δ 7.27 (m, 5H), 7.10 (m, 1H), 6.60 (d, *J* = 9.3 Hz, 1H), 3.56 (t, *J* = 6.2 Hz, 2H), 2.73 – 2.64 (m, 2H), 2.09 (d, *J* = 1.1 Hz, 3H), 1.89 – 1.74 (m, 4H).

Compound 4: Clarithromycin (15.00 g, 20.04 mmol) was added to 500 mL round bottom flask (RBF). Sodium acetate (14.04g, 171mmol) was added. Then 250 mL methanol with 10mL chloroform solvent was added to completely dissolve CLM. The mixture was heated to 80°C with addition of water to dissolve NaOAc. The solution was cooled to 60°C and iodine (5.24 g, 20.60 mmol) was added to the solution in three aliquots in 3 min to ensure no sticky gels formed.

The solution turned from cloudy white to dark yellow in 10 min. Sodium hydroxide (1 M, 10 mL) was added into the solution in the first 10 min. Then the solution was stirred for 30 min. Another 2 aliquots of sodium hydroxide (1 M, 10 mL) were added into the solution. The solution turned clear and stirred for another 2 h at 60°C. Cool to room temperature, water (500 mL) and NH₄OH (10 M, 15 mL) were added. Extraction was done using DCM (150 mL X 4). The combined DCM solution was washed with ammonium hydroxide (1 M, 200 mL). The aqueous layer is extracted with DCM (100 mL x 2). The combined DCM solution was evaporated and the product was recrystallized using acetone:NH₄OH (15:1, 20 mL) to give **4** (12.5 g, 85%) as white powder.

Compound 5. Compound **4** (1 g, 1.3 mmol) and 4-ethynylbenzyl methanesulfonate (280 mg, 1.33 mmol) were dissolved in DMSO (10 mL). Hunig's base (0.6mL, 3.25mmol) was added and the mixture was heated to 75°C for 4 h. The reaction was partitioned between DCM (50 mL) and water (100 mL) and the two layers were separated. The aqueous layer was extracted with DCM (50 mL x 3). The combined DCM layer was dried over Na₂SO₄ and evaporated off. The crude was purified using column chromatography eluting with ethyl acetate: hexanes (4:6) to give compound **5** (512 mg, 46 %) as pale yellow solid.

Synthesis of 6. The reaction of compound **4** (2 g, 2.6 mmol) with propargyl bromide (376.8mg, 2.6mmol) in DMSO (10 mL) and Hunig's base (1.2 mL, 6.5 mmol) at 50°C (note: over 50°C will generate multiple byproducts) for 4 h, followed by work up as described for the synthesis of **5**, furnished a crude product. The crude purified using column chromatography eluting with CHCl₃: MeOH: NH₄OH=20: 1: 0.1 to furnish **6** (650 mg, 34%) as pale yellow solid. ¹H NMR (400 MHz, cdcl₃) δ 7.26 (s, 3H), 5.05 (dd, *J* = 11.0, 2.5 Hz, 1H), 4.93 (d, *J* = 4.8 Hz, 1H), 4.46 (d, *J* = 7.1

Hz, 1H), 3.98 (s, 2H), 3.80 – 3.73 (m, 2H), 3.66 (d, $J = 7.5$ Hz, 1H), 3.53 – 3.45 (m, 1H), 3.40 (dd, $J = 3.9, 2.5$ Hz, 2H), 3.33 (d, $J = 1.1$ Hz, 4H), 3.24 (d, $J = 7.4$ Hz, 1H), 3.21 (d, $J = 2.9$ Hz, 1H), 3.18 (s, 1H), 3.07 – 2.94 (m, 6H), 2.94 – 2.82 (m, 1H), 2.74 – 2.54 (m, 2H), 2.40 – 2.31 (m, 5H), 2.29 – 2.21 (m, 1H), 2.19 (d, $J = 10.3$ Hz, 1H), 1.95 – 1.85 (m, 2H), 1.85 – 1.77 (m, 2H), 1.74 – 1.65 (m, 1H), 1.62 – 1.53 (m, 4H), 1.53 – 1.40 (m, 3H), 1.37 – 1.17 (m, 19H), 1.15 – 1.05 (m, 16H), 0.84 (t, $J = 7.5$ Hz, 4H).

Compound 7. Azithromycin (15.00 g, 20.05 mmol) was added to 500 mL round bottom flask. Sodium acetate (14.04 g, 171 mmol) and 120 mL 80%:20% V/V% methanol:H₂O were added. The mixture was heated to 50°C. Iodine (5.24 g, 20.60 mmol) was added to the solution in three aliquots within 3 min. The solution turned from cloudy white to clear yellow in 10 min. Sodium hydroxide (1 M, 10 mL) was added into the solution in the first 10 min. Then the solution was stirred for 30 min and another 2 aliquots of sodium hydroxide solution (1 M, 10 mL) were added into the reaction. The solution turned clear and was stirred for another 2 h at 50°C. Cool to room temperature, the reaction was poured into water (500 mL) and NH₄OH (10 M, 15mL) and extracted with DCM (150 mL x 4). The combined DCM layer was washed with ammonium hydroxide (1 M, 200 mL). The combined DCM layer was dried over Na₂SO₄ and evaporated. The crude solid was in acetone:NH₄OH (15:1, 20 mL) to yield 7 as white powder (10.8 g, 73%).

Compound 8. Compound 7 (1 g, 1.3 mmol) and 4-ethynylbenzyl methanesulfonate (280 mg, 1.33mmol) were dissolved in DMSO (10 mL) and Hunig's base (0.6 mL, 3.25 mmol). The reaction mixture was heated to 75°C for 4 h, cooled to room temperature, partitioned between DCM (50 mL) and water (100 mL) and the two layers were separated. The aqueous layer was

extracted by DCM (500 mL x 3), the combined DCM layer was dried over Na₂SO₄ and evaporated off. The crude was purified using column chromatography eluting with DCM: MeOH: NH₄OH=15: 1: 0.1. to give **8** (512 mg, 0.60mmol, 46.3% as pale yellow solid.

Synthesis of 9. The reaction of compound **7** (2 g, 2.6 mmol) and propargyl bromide (376.8 mg, 2.6mmol) in DMSO (10 mL) and Hunig's base (1.2 mL, 6.5 mmol) at 50°C (note: over 50°C will generate multiple byproducts) for 2 h, followed by work up 10% methanol in DCM as described for the synthesis of **8**, furnished a crude product. The crude purified using column chromatography eluting with CHCl₃: MeOH: NH₄OH=10: 1: 0.1 to furnish **9** (710 mg, 34.6%) as pale yellow solid. ¹H NMR (400 MHz, cdcl₃) δ 7.30 – 7.23 (m, 2H), 5.12 (d, J = 7.6 Hz, 1H), 4.75 (s, 1H), 4.46 (d, J = 7.1 Hz, 1H), 4.26 (s, 1H), 4.05 (d, J = 6.8 Hz, 1H), 3.77 – 3.69 (m, 0H), 3.63 (d, J = 6.8 Hz, 1H), 3.54 (s, 2H), 3.40 (s, 2H), 3.34 (d, J = 2.3 Hz, 3H), 3.25 (t, J = 8.6 Hz, 1H), 3.04 (t, J = 9.7 Hz, 1H), 2.73 (s, 1H), 2.24 (s, 1H), 2.15 (d, J = 10.5 Hz, 1H), 1.95 – 1.87 (m, 3H), 1.79 (t, J = 14.2 Hz, 2H), 1.59 (dd, J = 15.0, 4.6 Hz, 1H), 1.46 (dd, J = 15.8, 8.1 Hz, 1H), 1.39 – 1.30 (m, 4H), 1.25 (s, 8H), 1.33 – 1.18 (m, 5H), 1.18 (s, 1H), 1.13 – 1.08 (m, 2H), 1.04 (d, J = 7.8 Hz, 3H), 0.95 (s, 1H), 0.91 (d, J = 7.0 Hz, 2H), 0.87 (d, J = 8.2 Hz, 1H).

Compound 10a. Compounds **3a** (60 mg, 0.25 mmol) and **5** (150 mg, 0.178 mmol) were dissolved in THF (2 mL) and DMSO (1 mL). Hunig's base (0.3 mL, 1.77 mmol) was added and the mixture was purged with argon for 20 min. CuI (5 mg, 0.03 mmol) was added and the reaction mixture was at room temperature overnight. The reaction was partitioned between DCM (30 mL) and water (50 mL) and the two layers separated. The aqueous layer was extracted with DCM (50 mL); the combined DCM was dried by Na₂SO₄ and evaporated off. The crude

was purified in preparative TLC, eluting DCM:methanol=15:1 to furnish **10a** (74 mg, 38%) as white powder. ¹H NMR (400 MHz, CDCl₃) δ 7.79 – 7.74 (m, 2H), 7.73 (s, 1H), 7.33 (d, *J* = 8.0 Hz, 2H), 7.30 – 7.23 (m, 4H), 7.11 – 7.04 (m, 2H), 6.59 (dd, *J* = 9.3, 1.5 Hz, 2H), 5.03 (dt, *J* = 11.1, 2.3 Hz, 2H), 4.89 (t, *J* = 6.2 Hz, 2H), 4.41 (d, *J* = 7.2 Hz, 2H), 4.34 (t, *J* = 7.1 Hz, 1H), 4.00 – 3.93 (m, 2H), 3.81 – 3.68 (m, 4H), 3.63 (dd, *J* = 11.6, 7.0 Hz, 2H), 3.45 (dd, *J* = 18.1, 10.4 Hz, 3H), 3.36 – 3.25 (m, 1H), 3.23 (s, 2H), 3.14 (d, *J* = 27.8 Hz, 5H), 3.02 (d, *J* = 3.8 Hz, 5H), 2.88 – 2.79 (m, 2H), 2.68 (t, *J* = 7.5 Hz, 1H), 2.55 (d, *J* = 10.3 Hz, 3H), 2.29 (dd, *J* = 13.6, 5.1 Hz, 1H), 2.09 (d, *J* = 1.3 Hz, 6H), 1.96 – 1.78 (m, 5H), 1.74 – 1.59 (m, 2H), 1.56 – 1.44 (m, 2H), 1.39 (d, *J* = 2.5 Hz, 5H), 1.31 – 1.13 (m, 8H), 1.13 – 1.03 (m, 17H), 0.82 (td, *J* = 7.5, 1.6 Hz, 6H). ¹³C NMR (101 MHz, CDCl₃) δ 220.1, 174.8, 160.8, 160.6, 147.1, 141.8, 140.4, 133.9, 128.2, 127.8, 126.4, 125.5, 124.8, 120.5, 118.6, 114.2, 113.9, 101.7, 94.9, 79.9, 77.3, 73.2, 71.5, 68.0, 67.6, 64.6, 62.9, 56.5, 52.6, 49.6, 48.4, 44.2, 44.0, 38.1, 36.2, 35.9, 33.7, 28.7, 20.5, 20.3, 18.8, 17.6, 17.0, 16.0, 15.0, 14.9, 11.3, 9.6, 8.1. HRMS (ESI) *m/z* Calcd. for C₅₄H₈₆O₁₆N₇ [M+H⁺]: 1088.6126, found 1088.6149.

Compound 10b. The reaction of **3b** (200 mg, 0.75 mmol), **5** (500 mg, 0.59 mmol), CuI (20 mg, 0.11 mmol) in THF (2mL), DMSO (1mL) and Hunig's base (0.3 mL, 1.77 mmol), as described for the synthesis of **10a**. The product was furnished by column chromatography using solvent DCM:MeOH=15:1 to yield **10b** (359 mg, 55%) as white powder. ¹H NMR (400 MHz, CDCl₃) δ 7.73 (d, *J* = 7.8 Hz, 2H), 7.64 (s, 1H), 7.36 – 7.18 (m, 8H), 7.05 (d, *J* = 2.5 Hz, 1H), 6.56 (d, *J* = 9.3 Hz, 1H), 5.28 (s, 2H), 5.01 (dd, *J* = 11.0, 2.3 Hz, 1H), 4.86 (d, *J* = 4.9 Hz, 1H), 4.61 (t, *J* = 7.3 Hz, 2H), 4.39 (d, *J* = 7.1 Hz, 1H), 3.97 – 3.88 (m, 2H), 3.79 – 3.67 (m, 3H), 3.60 (d, *J* = 7.1 Hz, 1H), 3.50 – 3.37 (m, 2H), 3.28 (q, *J* = 7.1, 5.8 Hz, 3H), 3.17 (s, 1H), 3.09 (s, 3H), 3.01 – 2.89 (m, 5H), 2.84 (t, *J* = 8.2 Hz, 1H), 2.55 (d, *J* = 21.1 Hz, 3H), 2.27 (d, *J* = 15.2 Hz, 1H), 2.21

(s, 3H), 2.13 (d, $J = 9.9$ Hz, 1H), 2.06 (s, 3H), 1.93 – 1.79 (m, 2H), 1.71 (dt, $J = 21.9, 13.4$ Hz, 2H), 1.53 – 1.42 (m, 1H), 1.37 (s, 3H), 1.32 – 1.18 (m, 8H), 1.18 – 1.01 (m, 17H), 0.81 (q, $J = 8.4, 7.4$ Hz, 6H). ^{13}C NMR (101 MHz, CDCl_3) δ 221.1, 175.8, 161.8, 147.4, 142.8, 140.0, 137.3, 135.1, 129.6, 127.0, 125.8, 121.4, 119.9, 115.2, 102.7, 95.9, 80.9, 78.3, 77.9, 74.3, 72.5, 70.7, 69.1, 68.6, 65.6, 63.9, 57.6, 51.4, 50.6, 49.4, 45.2, 45.0, 39.2, 39.1, 37.2, 36.9, 36.3, 34.8, 29.7, 21.5, 21.3, 21.0, 19.8, 18.6, 18.0, 17.0, 15.9, 12.3, 10.6, 9.1. HRMS (ESI) m/z Calcd. for $\text{C}_{60}\text{H}_{88}\text{O}_{14}\text{N}_5$ $[\text{M}+\text{H}^+]$: 1102.6322, found 1102.6310.

Compound 10c. The reaction of **3c** (200 mg, 0.79 mmol), **5** (500 mg, 0.59 mmol), CuI (20 mg, 0.11 mmol) in THF (2 mL), DMSO (1 mL) and Hunig's base (0.3 mL, 1.77 mmol), as described for the synthesis of **10a**. The product was furnished by column chromatography using solvent DCM:MeOH=15:1 to yield **10c** (453 mg, 68%) as pale-yellow powder. ^1H NMR (400 MHz, CDCl_3) δ 7.82 – 7.75 (m, 2H), 7.73 (s, 1H), 7.33 (d, $J = 7.9$ Hz, 2H), 7.30 – 7.20 (m, 5H), 7.11 – 7.05 (m, 1H), 6.58 (d, $J = 9.3$ Hz, 1H), 5.28 (s, 1H), 5.03 (dd, $J = 11.0, 2.2$ Hz, 1H), 4.88 (d, $J = 4.8$ Hz, 1H), 3.94 (d, $J = 20.0$ Hz, 1H), 3.81 – 3.69 (m, 3H), 3.61 (d, $J = 7.1$ Hz, 1H), 3.50 – 3.39 (m, 2H), 3.30 (dd, $J = 10.2, 7.1$ Hz, 1H), 3.17 (s, 1H), 3.11 (s, 3H), 3.03 – 2.91 (m, 5H), 2.86 (dd, $J = 9.2, 7.0$ Hz, 1H), 2.69 (t, $J = 7.5$ Hz, 2H), 2.62 – 2.52 (m, 2H), 2.32 – 2.24 (m, 4H), 2.08 (d, $J = 1.1$ Hz, 3H), 1.98 (q, $J = 7.5$ Hz, 1H), 1.92 – 1.84 (m, 1H), 1.84 – 1.74 (m, 1H), 1.74 – 1.63 (m, 3H), 1.55 – 1.41 (m, 1H), 1.39 (s, 3H), 1.24 (dd, $J = 13.2, 6.2$ Hz, 6H), 1.16 (d, $J = 7.2$ Hz, 2H), 1.11 (dd, $J = 6.1, 2.0$ Hz, 15H), 1.06 (d, $J = 7.5$ Hz, 2H), 0.82 (t, $J = 7.4$ Hz, 3H). ^{13}C NMR (101 MHz, CDCl_3) δ 175.8, 161.8, 147.5, 142.6, 141.6, 139.1, 135.4, 129.2, 126.5, 125.7, 121.3, 119.4, 114.9, 102.7, 95.9, 80.9, 78.3, 75.4, 72.5, 70.7, 69.0, 68.9, 65.6, 50.6, 50.2, 49.4, 45.6, 45.3, 45.0, 40.4, 39.3, 36.8, 34.8, 31.5, 29.8, 28.0, 21.5, 21.3, 21.0, 19.8, 18.6, 18.3, 18.0,

16.8, 16.0, 15.9, 12.3, 10.6. HRMS (ESI) m/z Calcd. for $C_{62}H_{92}O_{14}N_5$ $[M+H]^+$: 1130.6635, found 1130.6625.

Compound 11a. Compounds **3a** (60 mg, 0.25 mmol) and **8** (150 mg, 0.18 mmol) were dissolved in THF (2 mL) and DMSO (1 mL). Hunig's base (0.3 mL, 1.77 mmol) was added and the mixture was purged with argon for 20 min. CuI (5 mg, 0.03 mmol) was added and the reaction was stirred at room temperature overnight. The reaction was partitioned between DCM (30 mL) and water (50 mL) and the two layers separated. The aqueous layer was extracted with DCM (50 mL); the combined DCM was dried by Na_2SO_4 and evaporated off. The crude was purified in preparative TLC, eluting with DCM: methanol=15:1 to furnish **11a** (80 mg, 40%) as white powder. 1H NMR (400 MHz, $CDCl_3$) δ 7.71 (d, J = 7.8 Hz, 2H), 7.64 (s, 1H), 7.34 – 7.23 (m, 4H), 7.21 (d, J = 8.2 Hz, 2H), 7.04 (s, 1H), 6.55 (d, J = 9.3 Hz, 1H), 5.27 (s, 2H), 5.12 (d, J = 4.8 Hz, 1H), 4.71 – 4.55 (m, 3H), 4.38 (d, J = 7.2 Hz, 1H), 4.19 (t, J = 2.6 Hz, 1H), 4.02 (dq, J = 12.6, 6.4 Hz, 1H), 3.75 (d, J = 13.1 Hz, 1H), 3.62 (s, 1H), 3.55 (d, J = 7.3 Hz, 1H), 3.44 (q, J = 13.3, 12.0 Hz, 3H), 3.36 – 3.22 (m, 3H), 3.13 (d, J = 24.8 Hz, 3H), 2.97 (t, J = 9.7 Hz, 1H), 2.72 – 2.60 (m, 2H), 2.53 (dd, J = 20.6, 8.7 Hz, 2H), 2.26 (d, J = 6.9 Hz, 4H), 2.21 (s, 3H), 2.12 (d, J = 10.3 Hz, 1H), 2.05 (s, 2H), 1.99 (q, J = 6.9 Hz, 1H), 1.73 (dd, J = 14.6, 4.9 Hz, 2H), 1.28 (t, J = 3.2 Hz, 6H), 1.20 (d, J = 6.2 Hz, 3H), 1.12 (d, J = 7.7 Hz, 5H), 1.09 – 1.01 (m, 5H), 0.99 (d, J = 7.5 Hz, 2H), 0.85 (q, J = 7.4, 6.8 Hz, 6H). ^{13}C NMR (176 MHz, $CDCl_3$) δ 179.1, 161.7, 148.2, 142.9, 141.4, 139.1, 134.9, 129.3, 128.9, 127.4, 125.8, 121.5, 119.6, 115.4, 102.9, 94.4, 83.5, 78.1, 77.7, 74.1, 73.7, 73.3, 72.8, 70.6, 70.1, 68.7, 65.6, 64.3, 62.6, 57.7, 53.6, 49.4, 45.5, 42.7, 42.1, 36.9, 36.1, 34.6, 29.6, 27.7, 26.8, 18.1, 17.0, 16.3, 14.5, 11.2, 8.9, 7.1. HRMS (ESI) m/z Calcd. for $C_{59}H_{89}O_{13}N_6$ $[M+H]^+$: 1089.6482, found 1089.6474.

Compound 11b. The reaction of compounds **3b** (65 mg, 0.28 mmol), **8** (150 mg, 0.19 mmol), CuI (20 mg, 0.11 mmol) in THF (2 mL), DMSO (1 mL) and Hunig's base (0.2 mL, 0.49 mmol), as described for the synthesis of **11a**, followed by prep TLC eluting with DCM:methanol: NH₄OH=10:1:0.2, furnished **11b** (150 mg, 71%) as white powder. ¹H NMR (400 MHz, CDCl₃) δ 7.77 – 7.70 (m, 2H), 7.64 (s, 1H), 7.36 – 7.19 (m, 7H), 7.05 (dd, *J* = 2.5, 1.3 Hz, 1H), 6.56 (d, *J* = 9.3 Hz, 1H), 5.27 (s, 2H), 5.11 (d, *J* = 4.8 Hz, 1H), 4.71 – 4.58 (m, 3H), 4.40 (d, *J* = 7.3 Hz, 1H), 4.21 (dd, *J* = 3.9, 2.0 Hz, 1H), 4.14 – 3.96 (m, 1H), 3.77 (d, *J* = 13.1 Hz, 1H), 3.66 (s, 1H), 3.57 (d, *J* = 7.2 Hz, 1H), 3.48 – 3.43 (m, 2H), 3.40 – 3.17 (m, 3H), 3.09 (d, *J* = 18.3 Hz, 4H), 2.97 (t, *J* = 9.8 Hz, 1H), 2.70 (dd, *J* = 7.5, 3.6 Hz, 2H), 2.62 – 2.50 (m, 2H), 2.34 – 2.20 (m, 7H), 2.13 – 2.05 (m, 4H), 2.01 (s, 1H), 1.97 – 1.81 (m, 1H), 1.75 (d, *J* = 14.8 Hz, 2H), 1.55 – 1.39 (m, 2H), 1.35 (t, *J* = 7.3 Hz, 1H), 1.28 (d, *J* = 6.2 Hz, 2H), 1.19 – 1.05 (m, 11H), 1.00 (d, *J* = 7.5 Hz, 3H), 0.92 – 0.81 (m, 6H). ¹³C NMR (101 MHz, CDCl₃) δ 161.7, 147.4, 142.8, 140.1, 137.3, 135.1, 129.6, 129.3, 127.0, 125.8, 121.4, 119.8, 115.1, 102.9, 94.4, 83.5, 78.1, 74.2, 73.7, 72.8, 70.6, 69.9, 68.7, 65.6, 64.3, 57.7, 51.4, 49.3, 45.4, 42.5, 36.9, 36.3, 34.6, 31.6, 29.7, 27.5, 26.7, 22.6, 22.0, 21.5, 21.4, 18.1, 17.0, 16.3, 14.6, 14.1, 11.2, 9.0, 7.3. HRMS (ESI) *m/z* Calcd. for C₆₀H₉₁O₁₃N₆ [M+H⁺]: 1103.6639, found 1103.6634.

Compound 11c. The reaction of compounds **3c** (200 mg, 0.70 mmol), **8** (150 mg, 0.18 mmol), CuI (32 mg, 0.17 mmol) in THF (2 mL) and DMSO (2 mL) and Hunig's base (0.5 mL, 2.86 mmol), as described for the synthesis of **11a**, furnished **11c** (170 mg, 88%) as white powder. ¹H NMR (400 MHz, CDCl₃) δ 7.76 (d, *J* = 7.8 Hz, 2H), 7.72 (s, 1H), 7.32 (d, *J* = 7.8 Hz, 2H), 7.24 (p, *J* = 4.5, 3.9 Hz, 5H), 7.07 (s, 1H), 6.57 (d, *J* = 9.3 Hz, 1H), 5.27 (s, 2H), 5.06 (d, *J* = 4.8 Hz,

1H), 4.66 (d, $J = 9.5$ Hz, 2H), 4.44 – 4.35 (m, 3H), 4.22 (d, $J = 4.4$ Hz, 1H), 4.00 (dq, $J = 12.4$, 6.4 Hz, 1H), 3.77 (d, $J = 13.0$ Hz, 1H), 3.68 – 3.56 (m, 2H), 3.47 (q, $J = 15.1$, 11.4 Hz, 3H), 3.38 – 3.29 (m, 1H), 3.11 (s, 3H), 3.01 – 2.87 (m, 2H), 2.77 – 2.64 (m, 4H), 2.61 – 2.47 (m, 2H), 2.33 – 2.20 (m, 8H), 2.12 – 2.02 (m, 4H), 1.96 (q, $J = 7.6$ Hz, 3H), 1.81 – 1.62 (m, 3H), 1.54 – 1.40 (m, 2H), 1.36 – 1.25 (m, 8H), 1.22 (d, $J = 6.1$ Hz, 4H), 1.08 (d, $J = 18.8$ Hz, 7H), 1.01 (d, $J = 7.4$ Hz, 2H), 0.87 (q, $J = 7.5$, 6.5 Hz, 7H). ^{13}C NMR (101 MHz, CDCl_3) δ 179.1, 161.8, 147.5, 142.7, 141.7, 139.1, 135.4, 129.7, 129.3, 126.5, 125.7, 121.3, 119.5, 115.0, 102.9, 94.4, 83.4, 78.0, 77.7, 74.1, 73.7, 73.2, 72.8, 70.6, 70.0, 68.7, 65.6, 64.2, 62.7, 57.7, 50.2, 49.3, 45.5, 42.6, 29.7, 28.0, 27.6, 26.7, 22.0, 21.4, 21.4, 18.1, 17.0, 16.3, 14.5, 11.2, 8.9, 7.1. HRMS (ESI) m/z Calcd. for $\text{C}_{62}\text{H}_{95}\text{O}_{13}\text{N}_6$ $[\text{M}+\text{H}^+]$: 1131.6952, found 1131.6942.

Synthesis of 12a. Compound **3a** (105 mg, 0.20 mmol) and **6** (150 mg, 0.2 mmol) were dissolved in THF (1 mL). Hunig's base (0.1 mL, 0.25 mmol) was added and the mixture was purged with argon for 20 min. CuI (10 mg, 0.53 mmol) was added and the reaction was stirred at room temperature overnight. The reaction was partitioned between DCM (30 mL) and water (50 mL) and the two layers separated. The aqueous layer was extracted with DCM (50 mL); the combined DCM was dried by Na_2SO_4 and evaporated off. The crude was purified in preparative TLC, eluting with ethyl acetate:hexanes:MeOH=16:1:1 to furnish **12a** (145 mg, 71%) as pale-yellow powder. ^1H NMR (400 MHz, CDCl_3) δ 7.45 (s, 1H), 7.39 – 7.29 (m, 4H), 7.26 (s, 2H), 7.23 (s, 0H), 7.05 (s, 1H), 6.56 (d, $J = 9.3$ Hz, 1H), 5.52 (d, $J = 1.6$ Hz, 2H), 5.01 (dd, $J = 11.1$, 2.3 Hz, 1H), 4.87 (d, $J = 4.8$ Hz, 1H), 4.38 (d, $J = 7.2$ Hz, 1H), 3.96 (d, $J = 8.2$ Hz, 2H), 3.80 (d, $J = 14.0$ Hz, 1H), 3.74 – 3.59 (m, 4H), 3.52 – 3.43 (m, 1H), 3.28 – 3.15 (m, 5H), 2.99 (s, 4H), 2.87 – 2.77 (m, 1H), 2.56 (dtd, $J = 22.5$, 10.4, 7.7, 4.7 Hz, 2H), 2.36 – 2.19 (m, 5H), 2.07 (s, 3H), 1.94 – 1.61

(m, 5H), 1.53 (dd, $J = 15.2, 5.0$ Hz, 1H), 1.36 (s, 3H), 1.31 – 1.12 (m, 12H), 1.11 – 1.00 (m, 11H), 0.80 (t, $J = 7.3$ Hz, 3H). ^{13}C NMR (101 MHz, CDCl_3) δ 220.9, 175.8, 161.6, 146.5, 142.9, 141.3, 134.8, 128.9, 127.3, 122.4, 121.4, 115.3, 102.8, 96.1, 81.0, 78.3, 77.9, 77.3, 76.6, 74.2, 72.7, 71.0, 69.0, 68.6, 65.7, 64.1, 53.5, 50.6, 49.3, 48.9, 45.2, 45.0, 39.3, 38.2, 37.2, 36.8, 34.9, 30.0, 21.4, 21.4, 21.0, 19.7, 18.7, 18.0, 17.0, 15.9, 12.3, 10.6, 9.1. HRMS (ESI) m/z Calcd. for $\text{C}_{53}\text{H}_{82}\text{O}_{14}\text{N}_5$ $[\text{M}+\text{H}^+]$: 1012.5853, found 1012.5822.

Synthesis of 12b. The reaction of compounds **3b** (65 mg, 0.26 mmol), **6** (150 mg, 0.2 mmol) and CuI (10 mg, 0.53 mmol) in THF (1 mL) and Hunig's base (0.1 mL, 0.25 mmol), as described for the synthesis of **12a**, followed by prep TLC eluting with DCM:MeOH:

$\text{NH}_4\text{OH}=10:1:0.2$ furnished **12b** (135 mg, 67%) as white powder. ^1H NMR (400 MHz, CDCl_3) δ 7.32 – 7.21 (m, 3H), 7.19 (d, $J = 8.1$ Hz, 2H), 7.06 (s, 1H), 6.56 (d, $J = 9.3$ Hz, 1H), 5.06 – 4.99 (m, 1H), 4.88 (d, $J = 4.8$ Hz, 1H), 4.56 (t, $J = 7.3$ Hz, 2H), 4.39 (d, $J = 7.2$ Hz, 1H), 3.96 (d, $J = 9.7$ Hz, 2H), 3.72 (d, $J = 8.9$ Hz, 2H), 3.63 (d, $J = 7.2$ Hz, 1H), 3.48 (s, 1H), 3.22 (d, $J = 4.6$ Hz, 5H), 2.99 (d, $J = 11.3$ Hz, 6H), 2.59 (d, $J = 0.8$ Hz, 30H), 2.36 – 2.27 (m, 1H), 2.25 (s, 4H), 2.14 (d, $J = 0.8$ Hz, 1H), 2.08 (s, 3H), 1.92 – 1.75 (m, 2H), 1.67 (d, $J = 14.5$ Hz, 1H), 1.54 (dd, $J = 15.1, 5.1$ Hz, 1H), 1.37 (s, 3H), 1.22 (td, $J = 15.2, 13.5, 6.9$ Hz, 13H), 1.12 – 1.01 (m, 13H), 0.81 (t, $J = 7.3$ Hz, 3H). ^{13}C NMR (101 MHz, CDCl_3) δ 221.1, 175.8, 161.8, 142.8, 140.0, 137.3, 135.2, 129.6, 127.0, 121.4, 115.2, 102.83, 96.1, 81.1, 78.4, 78.0, 77.2, 76.6, 74.3, 72.7, 70.9, 69.0, 68.6, 65.7, 63.7, 51.4, 50.7, 49.4, 49.0, 45.2, 45.0, 40.9, 39.3, 39.1, 37.2, 36.6, 36.4, 34.9, 29.9, 21.5, 21.4, 21.0, 19.7, 18.7, 18.0, 17.0, 16.0, 12.3, 10.6, 9.1. HRMS (ESI) m/z Calcd. for $\text{C}_{54}\text{H}_{84}\text{O}_{14}\text{N}_5$ $[\text{M}+\text{H}^+]$: 1026.6009, found 1026.5978.

Synthesis of 12c. The reaction of compounds **3c** (150 mg, 0.53 mmol), **6** (80 mg, 0.10 mmol) and CuI (9 mg, 0.05 mmol) in THF (2 mL) DMSO (2 mL) and Hunig's base (0.4 mL, 2.2 mmol), as described for the synthesis of **12a**, followed by prep TLC eluting with DCM:MeOH: NH₄OH=10:1:0.2 furnished **12c** (85 mg, 79%) as white powder. ¹H NMR (400 MHz, CDCl₃) δ 7.43 (s, 1H), 7.32 – 7.15 (m, 5H), 7.08 (td, *J* = 1.8, 1.1 Hz, 1H), 6.57 (d, *J* = 9.3 Hz, 1H), 5.02 (dd, *J* = 11.1, 2.2 Hz, 1H), 4.89 (d, *J* = 4.8 Hz, 1H), 4.40 (d, *J* = 7.1 Hz, 1H), 4.32 (td, *J* = 7.0, 1.7 Hz, 2H), 3.96 (s, 1H), 3.83 (d, *J* = 14.0 Hz, 1H), 3.76 – 3.59 (m, 4H), 3.48 (dd, *J* = 10.6, 5.7 Hz, 1H), 3.30 – 3.12 (m, 5H), 3.00 (s, 4H), 2.88 – 2.82 (m, 1H), 2.66 (t, *J* = 7.5 Hz, 2H), 2.62 – 2.51 (m, 1H), 2.35 – 2.29 (m, 1H), 2.26 (s, 3H), 2.14 (d, *J* = 0.8 Hz, 7H), 2.12 – 1.99 (m, 3H), 1.90 (tt, *J* = 14.7, 7.0 Hz, 4H), 1.72 – 1.59 (m, 3H), 1.54 (dd, *J* = 15.1, 5.0 Hz, 1H), 1.38 (s, 3H), 1.26 (d, *J* = 6.2 Hz, 3H), 1.23 – 1.14 (m, 8H), 1.11 – 1.02 (m, 12H), 0.81 (t, *J* = 7.3 Hz, 3H). ¹³C NMR (101 MHz, CDCl₃) δ 221.0, 175.8, 161.8, 142.6, 141.6, 139.1, 135.4, 129.2, 126.5, 121.3, 114.8, 102.7, 96.0, 80.9, 78.3, 78.3, 77.9, 76.5, 74.2, 72.7, 70.9, 69.0, 68.6, 65.7, 64.1, 50.6, 50.1, 49.3, 45.2, 45.0, 39.3, 39.1, 34.9, 34.7, 30.9, 29.7, 28.0, 21.4, 21.0, 19.7, 18.7, 18.0, 17.0, 15.9, 12.3, 10.6, 9.1. HRMS (ESI) *m/z* Calcd. for C₅₆ H₉₁ O₁₃ N₆ [M+H⁺]: 1055.6639, found 1055.6623.

Synthesis of 13a. The reaction of compounds **3a** (65 mg, 0.27 mmol), **9** (150 mg, 0.2 mmol) and CuI (10 mg, 0.53 mmol) in THF (1 mL) and Hunig's base (0.1 mL, 0.25 mmol), as described for the synthesis of **12a**, followed by prep TLC eluting with ethyl acetate:hexane:MeOH=16:1:1 furnished **13a** (110 mg, 55%) as pale-yellow powder. ¹H NMR (400 MHz, CDCl₃) δ 7.47 (s, 1H), 7.41 – 7.31 (m, 4H), 7.30 – 7.23 (m, 1H), 7.07 (dt, *J* = 2.1, 1.0 Hz, 1H), 6.59 (d, *J* = 9.3 Hz, 1H), 5.28 (s, 1H), 5.15 (d, *J* = 4.7 Hz, 1H), 4.68 (dd, *J* = 9.8, 2.6 Hz, 1H), 4.39 (d, *J* = 7.3 Hz,

2H), 4.22 (dd, $J = 3.7, 2.0$ Hz, 1H), 4.12 – 4.00 (m, 1H), 3.85 (d, $J = 13.9$ Hz, 1H), 3.72 – 3.62 (m, 2H), 3.59 (d, $J = 7.2$ Hz, 1H), 3.55 – 3.46 (m, 1H), 3.35 – 3.26 (m, 1H), 3.24 (s, 3H), 3.02 (d, $J = 9.4$ Hz, 1H), 2.73 – 2.65 (m, 2H), 2.61 (d, $J = 5.8$ Hz, 1H), 2.55 (d, $J = 10.4$ Hz, 1H), 2.30 (d, $J = 15.8$ Hz, 7H), 2.16 (d, $J = 2.6$ Hz, 1H), 2.11 – 2.01 (m, 5H), 1.99 – 1.83 (m, 1H), 1.79 – 1.71 (m, 2H), 1.56 (dd, $J = 15.2, 5.0$ Hz, 1H), 1.50 – 1.39 (m, 1H), 1.31 (d, $J = 5.5$ Hz, 6H), 1.25 – 1.19 (m, 10H), 1.15 (d, $J = 7.5$ Hz, 3H), 1.08 (t, $J = 3.4$ Hz, 6H), 0.99 (d, $J = 7.5$ Hz, 3H), 0.87 (q, $J = 7.4, 6.8$ Hz, 6H). ^{13}C NMR (176 MHz, CDCl_3) δ 178.7, 161.6, 142.9, 141.4, 134.9, 128.9, 127.5, 127.4, 121.5, 115.3, 102.9, 94.6, 83.6, 78.1, 77.8, 74.2, 73.7, 73.5, 73.0, 70.8, 67.0, 69.5, 68.7, 65.6, 64.5, 53.8, 53.5, 49.4, 49.1, 45.3, 42.2, 36.9, 36.3, 34.7, 31.8, 29.7, 29.3, 27.5, 26.7, 22.0, 21.6, 21.3, 18.2, 17.1, 16.3, 14.7, 14.1, 11.3, 9.1, 7.4. HRMS (ESI) m/z Calcd. for $\text{C}_{53}\text{H}_{85}\text{O}_{13}\text{N}_6$ $[\text{M}+\text{H}^+]$: 1013.6169, found 1013.6157.

Synthesis of 13b. The reaction of compounds **3b** (65 mg, 0.24 mmol), **9** (150 mg, 0.2 mmol) and CuI (10 mg, 0.53 mmol) in THF (1 mL) and Hunig's base (0.1 mL, 0.25 mmol), as described for the synthesis of **12a**, followed by prep TLC eluting with DCM:MeOH: NH_4OH =10:1:0.2 furnished **13b** (127 mg, 63%) as white powder. ^1H NMR (400 MHz, CDCl_3) δ 7.33 (s, 1H), 7.31 – 7.24 (m, 3H), 7.19 (d, $J = 8.1$ Hz, 2H), 7.06 (d, $J = 2.5$ Hz, 1H), 6.56 (d, $J = 9.3$ Hz, 1H), 5.12 (d, $J = 4.8$ Hz, 1H), 5.02 (s, 1H), 4.66 (dd, $J = 9.8, 2.6$ Hz, 1H), 4.56 (t, $J = 7.3$ Hz, 2H), 4.38 (d, $J = 7.2$ Hz, 1H), 4.27 – 4.21 (m, 1H), 4.04 (dt, $J = 12.4, 6.2$ Hz, 1H), 3.81 (d, $J = 14.0$ Hz, 1H), 2.76 – 2.62 (m, 1H), 2.59 (d, $J = 1.1$ Hz, 2H), 2.51 (d, $J = 10.3$ Hz, 1H), 2.31 (d, $J = 15.6$ Hz, 4H), 2.24 (s, 3H), 2.08 (s, 3H), 1.99 (dd, $J = 25.6, 8.9$ Hz, 2H), 1.80 – 1.69 (m, 2H), 1.54 (dd, $J = 15.2, 5.0$ Hz, 1H), 1.43 (ddt, $J = 16.8, 14.3, 7.3$ Hz, 1H), 1.28 (d, $J = 5.7$ Hz, 8H), 1.26 – 1.18 (m, 7H), 1.15 (d, $J = 7.4$ Hz, 3H), 1.12 – 0.96 (m, 10H), 0.94 – 0.82 (m, 6H). ^{13}C NMR (101 MHz, cdcl_3) δ 161.7, 142.7, 140.0, 137.2, 135.1, 129.5, 126.9, 121.4, 115.0, 102.9, 78.1, 77.7, 77.4,

77.1, 76.7, 74.2, 73.6, 73.0, 70.8, 68.6, 65.5, 64.0, 51.3, 49.3, 49.1, 45.2, 42.2, 41.0, 36.7, 36.3, 36.2, 34.7, 27.5, 26.7, 22.0, 21.6, 21.3, 18.2, 17.0, 16.2, 14.6, 11.2, 9.0. HRMS (ESI) m/z Calcd. for $C_{54}H_{87}O_{13}N_6$ $[M+H]^+$: 1027.6326, found 1027.6318.

Synthesis of 13c. The reaction of compounds **3c** (100 mg, 0.35 mmol), **9** (50 mg, 0.07 mmol) and CuI (10 mg, 0.53 mmol) in THF (1 mL), DMSO (1 mL) and Hunig's base (0.1 mL, 0.57 mmol), as described for the synthesis of **12a**, followed by prep TLC eluting with DCM:MeOH: $NH_4OH=10:1:0.2$ furnished **13c** (58 mg, 85%) as white powder. 1H NMR (400 MHz, $CDCl_3$) δ 7.45 (s, 1H), 7.32 – 7.20 (m, 7H), 7.11 – 7.07 (m, 1H), 6.59 (d, $J = 9.3$ Hz, 1H), 5.15 (d, $J = 4.8$ Hz, 1H), 4.69 (dd, $J = 9.8, 2.7$ Hz, 1H), 4.40 (d, $J = 7.3$ Hz, 1H), 4.34 (td, $J = 7.0, 1.2$ Hz, 2H), 4.26 (dd, $J = 4.0, 2.0$ Hz, 1H), 4.14 – 4.02 (m, 1H), 3.86 (d, $J = 13.9$ Hz, 1H), 3.75 – 3.58 (m, 3H), 3.51 (dt, $J = 13.8, 6.9$ Hz, 1H), 3.33 (dd, $J = 10.2, 7.2$ Hz, 2H), 3.25 (s, 3H), 3.01 (d, $J = 8.8$ Hz, 2H), 2.70 (ddd, $J = 19.3, 8.5, 5.7$ Hz, 4H), 2.53 (d, $J = 9.8$ Hz, 1H), 2.30 (d, $J = 8.8$ Hz, 7H), 2.18 (d, $J = 5.8$ Hz, 0H), 2.09 (d, $J = 1.1$ Hz, 3H), 2.04 – 1.84 (m, 3H), 1.77 (t, $J = 11.3$ Hz, 2H), 1.71 – 1.53 (m, 3H), 1.45 (ddd, $J = 14.1, 9.7, 7.1$ Hz, 1H), 1.31 (t, $J = 3.2$ Hz, 6H), 1.27 – 1.20 (m, 8H), 1.17 (d, $J = 7.4$ Hz, 3H), 1.08 (t, $J = 3.4$ Hz, 6H), 1.02 (d, $J = 7.5$ Hz, 3H), 0.89 (td, $J = 7.4, 6.8, 2.6$ Hz, 7H). ^{13}C NMR (176 MHz, $CDCl_3$) δ 161.9, 161.8, 149.7, 142.6, 141.7, 139.2, 135.4, 129.2, 126.6, 121.4, 114.9, 102.9, 94.5, 83.5, 78.2, 77.6, 77.5, 74.2, 73.7, 73.0, 70.9, 68.7, 65.6, 64.3, 50.1, 49.3, 45.3, 42.4, 36.9, 36.2, 34.8, 30.1, 29.7, 28.0, 27.6, 26.8, 22.0, 21.6, 21.3, 18.2, 17.0, 16.2, 14.6, 11.3, 9.0, 7.3. HRMS (ESI) m/z Calcd. for $C_{56}H_{91}O_{13}N_6$ $[M+H]^+$: 1055.6639, found 1055.6629.

Synthesis of 14a. Compounds **2a** (60 mg, 0.20 mmol) and **4** (150 mg, 0.20 mmol) were dissolved in CH₃CN (0.5 mL), DMSO (0.5 mL) and Hunig's base (0.07 mL, 0.39 mmol). The mixture was purged with argon for 20 min, KI (5 mg, 0.03 mmol) was added and the reaction was heat to 75°C overnight covered with aluminum foil. The reaction was quenched with Na₂S₂O₃ (10 mL) and DCM (30 mL). The two layers were separated and the DCM layer was washed with water (50 mL). The aqueous layer was back extracted with DCM (50 mL) and the combined DCM layer was dried with Na₂SO₄ and evaporated off. The crude was purified using preparative TLC eluting with DCM:MeOH:NH₄OH=10:1:0.2 to furnish **14a** (15 mg, 7.9%) as white powder. ¹H NMR (400 MHz, CDCl₃) δ 7.47 – 7.38 (m, 1H), 7.36 – 7.31 (m, 1H), 7.30 – 7.24 (m, 1H), 7.11 (d, *J* = 1.9 Hz, 1H), 6.61 (d, *J* = 9.3 Hz, 1H), 5.06 (dd, *J* = 11.1, 2.3 Hz, 1H), 4.93 (d, *J* = 4.8 Hz, 1H), 4.48 (d, *J* = 7.1 Hz, 1H), 4.06 – 3.91 (m, 2H), 3.79 – 3.74 (m, 2H), 3.68 (d, *J* = 7.4 Hz, 1H), 3.57 – 3.43 (m, 1H), 3.40 – 3.30 (m, 1H), 3.27 (s, 2H), 3.20 (s, 1H), 3.07 – 2.97 (m, 5H), 2.94 – 2.80 (m, 1H), 2.67 – 2.55 (m, 2H), 2.36 (d, *J* = 15.2 Hz, 1H), 2.25 (s, 2H), 2.18 (s, 1H), 2.16 – 2.04 (m, 3H), 1.92 (ddd, *J* = 14.5, 7.4, 2.1 Hz, 1H), 1.87 – 1.68 (m, 1H), 1.66 – 1.46 (m, 1H), 1.42 (s, 3H), 1.31 (d, *J* = 6.2 Hz, 2H), 1.28 – 1.17 (m, 10H), 1.18 – 1.08 (m, 10H), 0.85 (dd, *J* = 9.6, 5.0 Hz, 3H). ¹³C NMR (101 MHz, CDCl₃) δ 175.9, 161.8, 142.7, 135.3, 130.0, 129.5, 126.6, 121.4, 115.0, 102.7, 96.1, 80.9, 78.4, 77.9, 74.3, 72.7, 71.0, 69.1, 68.7, 65.7, 57.2, 50.6, 49.5, 45.2, 45.1, 39.2, 37.2, 37.0, 34.9, 30.1, 29.7, 21.5, 21.0, 19.8, 18.7, 18.0, 17.0, 16.0, 12.3, 10.6, 9.1. HRMS (ESI) *m/z* Calcd. for C₅₀ H₇₉ O₁₄ N₂ [M+H⁺]: 931.5526, found 931.5506.

Synthesis of 14b. The reaction of compounds **2b** (60 mg, 0.20 mmol), **4** (150 mg, 0.20 mmol) and KI (5 mg, 0.03 mmol) dissolved in CH₃CN (0.5 mL), DMSO (0.5 mL) and Hunig's base (0.07 mL, 0.39 mmol), as described for the synthesis of **14a**, followed by prep TLC eluting with

DCM:MeOH:NH₄OH=10:1:0.2 furnished **14b** (11 mg, 5.8%) as white powder. ¹H NMR (400 MHz, CDCl₃) δ 7.27 (d, *J* = 10.8 Hz, 6H), 7.07 (s, 1H), 6.59 (d, *J* = 9.3 Hz, 1H), 5.08 – 5.00 (m, 1H), 4.91 (d, *J* = 4.8 Hz, 1H), 4.43 (d, *J* = 7.2 Hz, 1H), 3.97 (d, *J* = 6.5 Hz, 2H), 3.75 (t, *J* = 4.9 Hz, 2H), 3.65 (d, *J* = 7.2 Hz, 1H), 3.48 (s, 1H), 3.31 (s, 3H), 3.18 (s, 1H), 3.02 (s, 5H), 2.87 (t, *J* = 8.1 Hz, 2H), 2.58 (dt, *J* = 12.1, 6.4 Hz, 1H), 2.35 (d, *J* = 15.1 Hz, 3H), 2.19 (d, *J* = 10.5 Hz, 1H), 2.09 (s, 3H), 1.93 – 1.78 (m, 3H), 1.68 (d, *J* = 14.7 Hz, 1H), 1.58 (dd, *J* = 15.1, 4.8 Hz, 1H), 1.39 (s, 3H), 1.34 – 1.16 (m, 14H), 1.15 – 1.04 (m, 12H), 0.83 (t, *J* = 7.3 Hz, 4H). ¹³C NMR (176 MHz, CDCl₃) δ 174.8, 160.8, 141.6, 138.3, 134.2, 128.5, 125.5, 120.4, 113.8, 101.7, 95.1, 79.7, 77.4, 77.0, 73.3, 71.7, 69.8, 68.0, 67.7, 64.9, 54.3, 49.6, 48.5, 44.3, 44.0, 38.3, 38.2, 36.2, 35.7, 33.9, 28.7, 20.5, 20.0, 18.7, 17.7, 17.0, 16.0, 14.9, 11.3, 9.6, 8.1. HRMS (ESI) *m/z* Calcd. for C₄₆H₈₁O₁₆N₄ [M+H⁺]: 945.5642, found 945.5667.

Synthesis of 14c. The reaction of compounds **2c** (60 mg, 0.16 mmol), **4** (120 mg, 0.17 mmol) and KI (5 mg, 0.03 mmol) dissolved in CH₃CN (0.5 mL), DMSO (0.5 mL) and Hunig's base (0.1 mL, 0.5.8 mmol), as described for the synthesis of **14a**, followed by prep TLC eluting with DCM:MeOH:NH₄OH=10:1:0.2 furnished **14c** (19 mg, 12%) as white powder. ¹H NMR (400 MHz, CDCl₃) δ 7.27 – 7.23 (m, 6H), 7.09 (d, *J* = 2.6 Hz, 1H), 6.58 (d, *J* = 9.3 Hz, 1H), 5.02 (d, *J* = 16.4, 5.2 Hz, 1H), 4.90 (d, *J* = 4.9 Hz, 1H), 4.42 (d, *J* = 7.2 Hz, 1H), 4.04 – 3.93 (m, 4H), 3.77 – 3.70 (m, 3H), 3.64 (d, *J* = 7.4 Hz, 1H), 3.49 – 3.44 (m, 1H), 3.30 (s, 4H), 3.18 (q, *J* = 6.3, 5.6 Hz, 2H), 3.05 – 2.91 (m, 8H), 2.86 (dd, *J* = 9.2, 7.1 Hz, 1H), 2.72 – 2.48 (m, 6H), 2.35 (d, *J* = 15.2 Hz, 1H), 2.21 (d, *J* = 4.7 Hz, 5H), 2.08 (d, *J* = 1.1 Hz, 3H), 1.94 – 1.78 (m, 3H), 1.72 – 1.52 (m, 4H), 1.38 (s, 2H), 1.28 (d, *J* = 6.2 Hz, 2H), 1.24 – 1.13 (m, 8H), 1.13 – 1.00 (m, 12H), 0.82 (t, *J* = 7.4 Hz, 2H). ¹³C NMR (101 MHz, CDCl₃) δ 175.9, 161.9, 142.6, 138.9, 135.5, 129.2,

126.4, 121.3, 114.9, 102.8, 96.1, 80.7, 78.4, 74.3, 72.7, 70.7, 69.0, 68.8, 65.7, 52.9, 50.6, 49.5, 45.3, 45.0, 39.2, 37.0, 35.4, 34.9, 29.5, 28.8, 27.9, 21.5, 21.0, 19.8, 18.7, 18.0, 17.0, 15.9, 12.3, 10.6, 9.0. HRMS (ESI) m/z Calcd. for $C_{53}H_{85}O_{14}N_2$ $[M+H]^+$: 973.5995, found 973.5978.

Synthesis of 15a. The reaction of compounds **2a** (60 mg, 0.20 mmol), **7** (150 mg, 0.20 mmol) and KI (5 mg, 0.03 mmol) dissolved in CH_3CN (2 mL), DMSO (2 mL) and Hunig's base (0.07 mL, 0.42 mmol), as described for the synthesis of **14a**, followed by prep TLC eluting with DCM:MeOH:NH₄OH=10:1:0.2 furnished **15a** (10.5 mg, 5.4%) as pale-yellow powder. ¹H NMR (400 MHz, $CDCl_3$) δ 7.40 – 7.13 (m, 5H), 7.03 (s, 1H), 6.53 (d, J = 9.3 Hz, 1H), 5.12 (d, J = 4.8 Hz, 1H), 4.63 (d, J = 9.7 Hz, 1H), 4.40 (d, J = 7.4 Hz, 1H), 4.20 (s, 1H), 4.06 – 3.97 (m, 1H), 3.74 (d, J = 13.4 Hz, 1H), 3.61 (s, 1H), 3.56 (d, J = 7.4 Hz, 1H), 3.44 (t, J = 13.8 Hz, 1H), 3.31 (dd, J = 17.2, 8.7 Hz, 1H), 3.21 (s, 2H), 3.08 – 3.03 (m, 1H), 2.97 (s, 1H), 2.70 – 2.56 (m, 1H), 2.55 (s, 3H), 2.48 (d, J = 9.7 Hz, 1H), 2.33 – 2.20 (m, 5H), 2.18 (s, 2H), 2.04 (d, J = 10.4 Hz, 4H), 1.72 (d, J = 13.9 Hz, 1H), 1.44 (dd, J = 55.6, 15.0, 6.3 Hz, 1H), 1.27 (d, J = 6.4 Hz, 5H), 1.17 (d, J = 4.4 Hz, 5H), 1.12 (d, J = 7.4 Hz, 2H), 1.06 – 0.91 (m, 7H), 0.82 (q, J = 7.5, 6.4 Hz, 6H). ¹³C NMR (176 MHz, $CDCl_3$) δ 161.8, 142.6, 140.1, 139.4, 135.3, 129.4, 126.5, 121.5, 114.9, 102.9, 94.5, 83.5, 78.2, 74.2, 73.7, 73.00 71.0, 70.0, 68.7, 65.6, 62.5, 57.43, 49.5, 45.3, 42.3, 41.0, 37.1, 36.2, 34.7, 30.3, 29.7, 27.6, 26.8, 22.0, 21.7, 21.4, 18.2, 17.0, 16.2, 14.6, 11.3, 9.0, 7.3. HRMS (ESI) m/z Calcd. for $C_{50}H_{82}O_{13}N_3$ $[M+H]^+$: 932.5842, found 932.5824.

Synthesis of 15b. The reaction of compounds **2b** (500 mg, 1.4 mmol), **7** (200.5 mg, 0.28 mmol) and KI (40 mg, 0.24 mmol), dissolved in CH_3CN (2 mL), DMSO (2 mL) and Hunig's base (0.5 mL, 2.92 mmol), as described for the synthesis of **14a**, followed by prep TLC eluting with DCM: MeOH: NH₄OH=10:1:0.2 furnished **15b** (12 mg, 1%) as pale-yellow powder. ¹H NMR (400

MHz, CDCl₃) δ 7.37 – 7.13 (m, 5H), 7.07 (d, J = 6.4 Hz, 1H), 6.57 (d, J = 9.3 Hz, 1H), 5.27 (s, 1H), 5.02 (d, J = 4.8 Hz, 1H), 4.65 (d, J = 9.9 Hz, 1H), 4.42 (d, J = 7.2 Hz, 1H), 4.25 (d, J = 5.2 Hz, 1H), 4.04 (dq, J = 12.6, 6.3 Hz, 1H), 3.84 (t, J = 6.9 Hz, 0H), 3.68 – 3.59 (m, 2H), 3.47 (dq, J = 16.5, 9.1, 7.5 Hz, 1H), 3.30 (s, 2H), 3.21 (dd, J = 10.3, 7.4 Hz, 0H), 3.00 (t, J = 9.8 Hz, 1H), 2.81 (tq, J = 20.7, 7.0 Hz, 3H), 2.75 – 2.56 (m, 1H), 2.47 (d, J = 11.2 Hz, 1H), 2.39 – 2.15 (m, 6H), 2.07 (s, 5H), 1.89 – 1.72 (m, 1H), 1.72 – 1.40 (m, 2H), 1.28 (d, J = 6.9 Hz, 5H), 1.25 – 1.12 (m, 9H), 1.12 – 0.95 (m, 7H), 0.95 – 0.71 (m, 5H). ¹³C NMR (101 MHz, CDCl₃) δ 161.8, 142.5, 139.2, 135.4, 129.9, 129.5, 126.4, 121.4, 114.8, 102.8, 95.0, 83.7, 78.4, 78.1, 74.3, 73.6, 72.9, 70.7, 68.7, 65.8, 65.5, 55.3, 53.5, 49.5, 45.1, 42.4, 41.7, 38.6, 36.8, 36.5, 34.9, 29.7, 26.7, 22.0, 21.6, 21.4, 18.3, 17.0, 16.3, 15.2, 11.3, 9.2. HRMS (ESI) m/z Calcd. for C₅₁ H₈₄ O₁₃ N₃ [M+H⁺]: 946.5999, found 946.5982.

Synthesis of 15c. The reaction of compounds **2c** (300 mg, 0.95 mmol), **7** (700 mg, 0.95 mmol) and KI (40 mg, 0.24 mmol) dissolved in CH₃CN (2 mL), DMSO (2 mL) and Hunig's base (0.4 mL, 1.4 mmol), as described for the synthesis of **14a**, followed by prep TLC eluting with DCM:MeOH:NH₄OH=10:1:0.2 furnished **15c** (75.8 mg, 9%) as pale-yellow powder. ¹H NMR (400 MHz, CDCl₃) δ 7.31 – 7.23 (m, 6H), 7.12 (s, 1H), 6.60 (d, J = 9.3 Hz, 1H), 5.33 – 5.28 (m, 1H), 5.05 (d, J = 4.7 Hz, 1H), 4.71 – 4.64 (m, 1H), 4.47 (d, J = 7.2 Hz, 1H), 4.32 – 4.26 (m, 1H), 4.07 (dt, J = 12.6, 6.3 Hz, 1H), 3.71 – 3.63 (m, 2H), 3.52 (s, 1H), 3.34 (s, 3H), 3.26 (t, J = 8.9 Hz, 1H), 3.04 (t, J = 9.7 Hz, 1H), 2.85 – 2.77 (m, 2H), 2.62 (s, 7H), 2.50 (d, J = 11.2 Hz, 1H), 2.34 (s, 3H), 2.23 (d, J = 15.2 Hz, 3H), 2.10 (s, 3H), 2.00 (t, J = 7.2 Hz, 1H), 1.93 – 1.77 (m, 1H), 1.61 (ddd, J = 30.4, 15.1, 6.6 Hz, 3H), 1.32 (d, J = 6.4 Hz, 6H), 1.26 (s, 4H), 1.12 – 1.03 (m, 8H), 1.00 – 0.81 (m, 7H). ¹³C NMR (101 MHz, CDCl₃) δ 161.3, 142.0, 138.3, 128.7, 125.8,

120.8, 114.2, 102.4, 94.5, 83.3, 77.9, 77.6, 73.8, 73.0, 72.4, 70.1, 68.2, 65.0, 53.0, 48.9, 44.5, 40.4, 36.0, 34.9, 34.4, 31.1, 29.2, 28.4, 26.2, 22.1, 21.5, 21.1, 20.9, 20.6, 17.8, 16.5, 15.7, 14.7, 13.6, 10.8, 8.7, 7.2. HRMS (ESI) m/z Calcd. for $C_{53}H_{88}O_{13}N_3$ $[M+H]^+$: 974.6312, found 974.6288.

Compound 16⁶⁹. 2-Hydroxy-5-methyl pyridine (500 mg, 4.58 mmol) was added to potassium carbonate (900 mg, 6.42 mmol), 8-hydroxyquinoline (220mg, 1.49 mmol) and 4-iodoanisole (700 mg, 2.97 mmol) in a round bottom flask. Dimethyl sulfoxide (DMSO) (30 mL) was added to the mixture and the mixture was purged with argon for 15 min. Then, copper(I) iodide (250 mg, 1.49 mmol) was added to the mixture. The pressure tube was capped after another 15 min of argon purge. The reaction was covered with aluminum foil and heated to 120°C for 12 h. The reaction was cooled to room temperature and the resulting green mixture was worked up as described for the synthesis of **1a**. The crude was purified using silica gel chromatography eluting with EtOAc:methanol=10:0.7 to furnish **16** (510 mg, 52%) as pale-yellow solid. ¹H NMR (400 MHz, CDCl₃) δ 7.30 – 7.22 (m, 3H), 7.09 (ddd, J = 2.6, 1.2, 0.7 Hz, 1H), 7.01 – 6.95 (m, 2H), 6.60 (d, J = 9.6 Hz, 1H), 3.84 (s, 3H), 2.10 (s, 3H).

Compound 17. Compound **16** (500 mg, 2.37 mmol) was dissolved in DCM (10 mL) and the solution was purged with argon gas for 15 min and cooled to -30°C. BBr₃ (2 mL) was added to the solution dropwisely and stirring continued at -30 °C for 1 h. The reaction temperature was raised to 0°C (ice bath) and stirring continued overnight. MeOH (20 mL) was added dropwisely, followed by NaHCO₃ to adjust pH to 8-9 and precipitate resulted. The suspension was filtered through vacuum and the filtrate was extracted by DCM:MeOH=10:1 (100 mL x 5). The combined DCM layer was dried over Na₂SO₄ and evaporated off to furnish **17** (320 mg, 67%).

^1H NMR (400 MHz, CDCl_3) δ 7.35 (ddd, $J = 9.2, 2.6, 0.4$ Hz, 1H), 7.16 – 7.11 (m, 1H), 7.04 – 6.95 (m, 2H), 6.65 (t, $J = 9.0$ Hz, 3H), 2.12 (d, $J = 1.0$ Hz, 3H).

Compound 18a. Compound **17** (300 mg, 1.49 mmol) was dissolved in DCM (5 mL) and cooled to -10 to -20°C . Pyridine (0.7 mL, 8.6 mmol) was added to the solution and triflic anhydride (0.4 mL, 2.38 mmol) was added dropwisely. The reaction was complete within 30 min and 1M HCl solution (5 mL) was added to the solution to quench the reaction. Then DCM (30 mL) and water (50 mL) were added and the two layers separated. The DCM layer was washed water (30 mL), dried over Na_2SO_4 and evaporated off. The crude product (dark yellow solid) was purified using column chromatography eluting with neat EtOAc to furnish the triflate intermediate product as pale-yellow solid (320 mg, 51%). The intermediate triflate compound (300 mg, 0.9 mmol) was treated with prop-2-yn-1-ol (100.1 mg, 1.8 mmol), Tetrakis(triphenylphosphine)palladium (520 mg, 0.45 mmol) and CuI (85.5 mg, 0.45 mmol) in CH_3CN (7 mL). The mixture was purged with argon for 5 min and after the addition of Hunig's base (0.7 mL, 4 mmol), heated to 75°C and kept stirring overnight. The mixture was filtered through celite bed and the filtrate was evaporated off. The crude compound was purified using column chromatography, eluting with EtOAc:MeOH=13:1 to furnish **18a** (323 mg, 90%) as yellow oil. ^1H NMR (400 MHz, CDCl_3) δ 7.57 – 7.51 (m, 2H), 7.41 – 7.30 (m, 2H), 7.30 – 7.23 (m, 1H), 7.09 (ddd, $J = 2.6, 1.2, 0.8$ Hz, 1H), 6.64 – 6.57 (m, 1H), 4.51 (d, $J = 6.2$ Hz, 2H), 2.11 (d, $J = 1.1$ Hz, 4H), 1.88 (t, $J = 6.2$ Hz, 1H).

Compound 18b. The triflate intermediate (400 mg, 1.2 mmol) was prepared as described for the synthesis of **18a**. The triflate intermediate was treated with 3-butyne-1-ol (500 mg, 6.84 mmol),

Tetrakis(triphenylphosphine)palladium (200 mg, 0.17 mmol) and CuI (33 mg, 0.17 mmol) in CH₃CN (10 mL). The mixture was purged with argon for 5 min and after the addition of Hunig's base (1 mL, 10 v/v%), heated to 65°C and kept stirring overnight. The mixture was filtered through celite bed and the filtrate was evaporated off. The crude compound was purified using column chromatography, eluting with neat EtOAc to furnish **18b** (370 mg, 84%) as yellow oil. ¹H NMR (400 MHz, CDCl₃) δ 7.57 – 7.43 (d, *J* = 8.3 Hz, 2H), 7.40 – 7.29 (d, *J* = 8.3 Hz, 2H), 7.26 (d, *J* = 0.6 Hz, 1H), 7.09 (d, *J* = 2.3 Hz, 1H), 6.60 (d, *J* = 9.4 Hz, 1H), 3.83 (q, *J* = 6.3 Hz, 2H), 2.71 (t, *J* = 6.3 Hz, 2H), 2.11 (d, *J* = 1.1 Hz, 3H), 1.83 (t, *J* = 6.3 Hz, 1H).

Compound 18c. The triflate intermediate (200 mg, 0.58 mmol) was prepared as described for the synthesis of **18a**. The triflate intermediate was treated with pent-4-yn-1-ol (0.135 g, 1.6 mmol), Tetrakis(triphenylphosphine)palladium (320 mg, 0.25 mmol) and CuI (68 mg, 0.25 mmol) in CH₃CN (10 mL). The mixture was purged with argon for 5 min and after the addition of Hunig's base (0.8 mL, 8 v/v%), heated to 65°C and kept stirring overnight. The mixture was filtered through celite bed and the filtrate was evaporated off. The crude compound was purified using column chromatography, eluting with neat EtOAc to furnish **18c** (150 mg, 97%) as yellow oil. ¹H NMR (400 MHz, CDCl₃) δ 7.52 – 7.44 (d, *J* = 8.3 Hz, 2H), 7.34 – 7.28 (d, *J* = 8.3 Hz, 2H), 7.26 (m, 1H), 7.08 (dt, *J* = 2.7, 1.0 Hz, 1H), 6.60 (d, *J* = 9.3 Hz, 1H), 3.83 (q, *J* = 6.0 Hz, 2H), 2.56 (t, *J* = 7.0 Hz, 2H), 2.10 (s, *J* = 1.1 Hz, 3H), 1.87 (tt, *J* = 7.0, 6.2 Hz, 2H), 1.51 (t, *J* = 5.4 Hz, 1H).

Compound 18d. The triflate intermediate (500 mg, 1.5 mmol) was prepared as described for the synthesis of **18a**. The triflate intermediate was treated with hex-5-yn-1-ol (294 mg, 3 mmol),

Tetrakis(triphenylphosphine)palladium (433 mg, 0.375 mmol) and CuI (71mg, 0.375mmol) in CH₃CN (8 mL). The mixture was purged with argon for 5 min and after the addition of Hunig's base (0.8 mL, 8 v/v%), heated to 65°C and kept stirring overnight. The mixture was filtered through celite bed and the filtrate was evaporated off. The crude compound was purified using column chromatography, eluting with neat EtOAc to furnish **18d** (400 mg, 95%) as yellow oil. ¹H NMR (400 MHz, CDCl₃) δ 7.48 (d, *J* = 8.6 Hz, 2H), 7.32 – 7.28 (d, *J* = 8.6 Hz, 2H), 7.29 – 7.24 (m, 1H), 7.09 – 7.05 (m, 1H), 6.60 (d, *J* = 9.3 Hz, 1H), 3.73 (s, 2H), 2.48 (t, *J* = 6.6 Hz, 2H), 2.14 – 2.03 (m, 3H), 1.80 – 1.65 (m, 2H), 1.28 (d, *J* = 18.0 Hz, 3H).

Compound 18e. The triflate intermediate (200 mg, 0.58 mmol) was prepared as described for the synthesis of **18a**. The triflate intermediate was treated with hex-5-yn-1-ol (180 mg, 1.6 mmol), Tetrakis(triphenylphosphine)palladium (320 mg, 0.25 mmol) and CuI (68 mg, 0.25 mmol) in CH₃CN (10 mL). The mixture was purged with argon for 5 min and after the addition of Hunig's base (0.8 mL, 8 v/v%), heated to 65°C and kept stirring overnight. The mixture was filtered through celite bed and the filtrate was evaporated off. The crude compound was purified using column chromatography, eluting with neat EtOAc to furnish **18e** (160 mg, 0.54 mmol, 93.2%) as yellow oil. ¹H NMR (400 MHz, CDCl₃) δ 7.48 (d, *J* = 8.6 Hz, 2H), 7.33 – 7.28 (d, *J* = 8.6 Hz, 1H), 7.27 – 7.24 (m, 1H), 7.10 – 7.05 (m, 1H), 6.60 (d, *J* = 9.4 Hz, 1H), 3.69 (q, *J* = 6.0 Hz, 2H), 2.44 (t, *J* = 6.9 Hz, 2H), 2.10 (d, *J* = 1.1 Hz, 3H), 1.65 (h, *J* = 6.9 Hz, 4H), 1.69 – 1.51 (m, 4H).

Compound 19a. Compound **18a** (170 mg, 0.7 mmol) was dissolved in DCM (15 mL) and triethylamine (360 mg, 3.5 mmol) and stirred at -20°C. Methanesulfonyl chloride (0.20 g, 3.0

mmol) was added slowly to the solution under argon; the reaction was kept stirring for 45-60 min and quenched with NaHCO₃ (1 mL). The reaction was partitioned between DCM (50 mL) and water (50mL) and the two layers separated. The organic layer was washed with water (30 mL), dried over Na₂SO₄ and evaporated off to give a crude mesylated intermediate that was used without purification. The mesylated intermediate (85 mg, 0.27 mmol) was dissolved in THF/DMSO solution (1:1 mL); and compound **4** (170 mg, 0.26 mmol) and Hunig's base (0.68 mL, 4 mmol) were added to the solution. The mixture was heated to 50°C for 2 h during which the starting materials were consumed. The solution was worked up with water (50 mL) and chloroform (30 mL x 3). The organic layer was dried over Na₂SO₄ and the solvent was evaporated off. The crude product was purified using preparative TLC plate eluting with EtOAc:MeOH=15:1 to furnish **19a** as pale-yellow solid (135 mg, 54%). ¹H NMR (400 MHz, CDCl₃) δ 7.52 – 7.44 (m, 2H), 7.35 – 7.28 (m, 2H), 7.27 – 7.22 (m, 1H), 7.07 (d, *J* = 7.1 Hz, 1H), 6.58 (d, *J* = 9.4 Hz, 1H), 5.04 (dd, *J* = 11.2, 2.3 Hz, 1H), 4.91 (d, *J* = 4.9 Hz, 1H), 4.47 (d, *J* = 7.2 Hz, 1H), 3.98 (d, *J* = 11.4 Hz, 2H), 3.74 (q, *J* = 6.4, 5.3 Hz, 2H), 3.57 – 3.45 (m, 1H), 3.26 (s, 3H), 3.17 (s, 1H), 3.01 (d, *J* = 10.6 Hz, 4H), 2.93 – 2.81 (m, 1H), 2.81 – 2.67 (m, 1H), 2.57 (dt, *J* = 7.7, 4.1 Hz, 1H), 2.40 (s, 2H), 2.34 (d, *J* = 15.2 Hz, 1H), 2.19 (d, *J* = 10.0 Hz, 1H), 2.10 (d, *J* = 6.0 Hz, 3H), 1.97 – 1.78 (m, 3H), 1.74 – 1.62 (m, 1H), 1.60 – 1.42 (m, 1H), 1.42 (s, 0H), 1.38 – 1.32 (m, 1H), 1.29 (d, *J* = 6.1 Hz, 3H), 1.25 – 1.16 (m, 8H), 1.16 – 1.00 (m, 10H), 0.83 (t, *J* = 7.3 Hz, 3H). ¹³C NMR (101 MHz, CDCl₃) δ 175.8, 161.5, 142.7, 140.7, 134.7, 132.4, 126.8, 126.6, 123.2, 121.5, 115.1, 102.7, 96.0, 87.2, 83.9, 80.8, 78.4, 77.9, 74.2, 72.6, 71.1, 69.0, 68.6, 65.7, 64.3, 50.6, 49.5, 45.2, 45.0, 44.5, 39.3, 37.2, 35.9, 21.5, 21.0, 19.8, 18.7, 18.0, 17.0, 16.0, 12.3, 10.6, 9.1. HRMS (ESI) *m/z* Calcd. for C₅₂ H₇₉ O₁₄ N₂ [M+H⁺]: 955.5526, found 955.5505.

Compound 19b. The preparation of mesylated intermediate was as described for synthesis of mesylated intermediate to **19a**. The prepared intermediate (100mg, 0.32 mmol) was reacted with compound **4** (200 mg, 0.28 mmol) in THF/DMSO (1ml:1ml) and Hunig's base (0.7mL, 7 V/V%) at 75-80°C overnight. The work-up procedure was described in synthesis procedure of **19a**. The crude product was dried and purified through preparative TLC eluting with EtOAc:MeOH=20:1 to furnish **19b** as yellow solid (22 mg, 8%). ¹H NMR (400 MHz, CDCl₃) δ 7.54 – 7.47 (d, *J* = 6.8, 2H), 7.35 – 7.22 (m, 2H), 7.26 (m, 1H), 7.07 (s, 1H), 6.60 (d, *J* = 9.4 Hz, 1H), 5.04 (d, *J* = 9.3 Hz, 1H), 4.92 (d, *J* = 4.8 Hz, 1H), 4.48 (d, *J* = 7.1 Hz, 1H), 3.98 (d, *J* = 7.4 Hz, 2H), 3.87 – 3.74 (m, 2H), 3.75 (d, *J* = 4.7 Hz, 1H), 3.66 (d, *J* = 7.1 Hz, 1H), 3.31 (s, 3H), 3.25 (s, 1H), 3.19 (d, *J* = 2.4 Hz, 1H), 3.03 (s, 4H), 2.90 – 2.80 (m, 2H), 2.71 (t, *J* = 6.3 Hz, 1H), 2.60 (s, 6H), 2.36 (d, *J* = 15.3 Hz, 1H), 2.33 (s, 4H), 2.10 (d, *J* = 1.2 Hz, 4H), 1.86 (dd, *J* = 26.5, 11.6 Hz, 4H), 1.58 (dd, *J* = 15.0, 4.9 Hz, 1H), 1.40 (s, 3H), 1.30 (d, *J* = 6.2 Hz, 3H), 1.25 (s, 8H), 1.26 – 1.16 (m, 8H), 1.15 – 1.08 (m, 12H), 0.84 (q, *J* = 7.6 Hz, 3H). ¹³C NMR (176 MHz, CDCl₃) δ 220.7, 188.0, 175.4, 164.3, 161.6, 142.7, 140.0, 135.1, 128.7, 127.3, 121.4, 115.1, 102.5, 96.1, 81.9, 78.3, 78.1, 77.6, 76.7, 74.2, 73.1, 71.8, 69.1, 67.9, 66.2, 58.8, 50.6, 49.6, 45.1, 45.0, 39.1, 38.6, 37.3, 35.0, 21.5, 20.9, 19.7, 18.7, 18.0, 17.0, 16.1, 12.3, 10.6, 9.9. HRMS (ESI) *m/z* Calcd. for C₅₃ H₈₁ O₁₄ N₂ [M+H⁺]: 969.5682, found 969.5662.

Compound 19c. The preparation of mesylated intermediate was as described for synthesis of mesylated intermediate to **19a**. The prepared intermediate (75 mg, 0.23 mmol) was reacted with compound **4** (200 mg, 0.27 mmol) in THF/DMSO (5:2 mL) and Hunig's base (0.8mL, 8 V/V%) at 75-80°C overnight. The work-up procedure was described in synthesis procedure of **19a**. The crude product was dried and purified through preparative TLC eluting with EtOAc:MeOH=20:1

to furnish **19c** as yellow solid (19 mg, 8%). ¹H NMR (400 MHz, CDCl₃) δ 7.48 (d, *J* = 8.7, 2.6 Hz, 2H), 7.32 – 7.21 (m, 3H), 7.06 (s, 1H), 6.59 (d, *J* = 9.4 Hz, 1H), 5.04 (d, *J* = 11.1, 2.3 Hz, 1H), 4.91 (d, *J* = 4.8 Hz, 1H), 4.46 (d, *J* = 7.2 Hz, 1H), 4.11 (q, *J* = 7.1 Hz, 1H), 3.99 (s, 1H), 3.97 (s, 1H), 3.79 – 3.72 (m, 2H), 3.66 (d, *J* = 7.2 Hz, 1H), 3.49 (s, 1H), 3.28 (s, 2H), 3.17 (s, 1H), 3.01 (d, *J* = 14.2 Hz, 5H), 2.93 – 2.83 (m, 1H), 2.55 (d, *J* = 9.1 Hz, 2H), 2.48 (d, *J* = 7.5 Hz, 2H), 2.35 (d, *J* = 15.2 Hz, 1H), 2.29 (s, 2H), 2.15 (s, 1H), 2.06 (d, *J* = 22.8 Hz, 4H), 1.95 – 1.82 (m, 2H), 1.81 (s, 1H), 1.69 (d, *J* = 15.7 Hz, 2H), 1.57 (dd, *J* = 15.2, 4.9 Hz, 1H), 1.39 (s, 3H), 1.26 (s, 3H), 1.32 – 1.15 (m, 13H), 1.14 – 1.07 (m, 10H), 0.84 (dd, *J* = 14.8, 7.3 Hz, 6H), ¹³C NMR (101 MHz, CDCl₃) δ 221.0, 175.8, 161.7, 142.8, 134.0, 137.3, 135.2, 129.6, 127.0, 121.3, 115.2, 102.8, 96.1, 81.0, 78.3, 78.0, 76.6, 74.2, 72.7, 70.9, 69.0, 68.5, 65.7, 63.7, 51.4, 50.6, 49.3, 49.0, 45.2, 45.0, 39.3, 39.1, 37.2, 36.5, 36.3, 34.9, 29.7, 21.4, 21.0, 19.7, 18.7, 18.0, 17.0, 16.0, 12.3, 10.6, 9.1. HRMS (ESI) *m/z* Calcd. for C₅₄ H₈₃ O₁₄ N₂ [M+H⁺]: 983.5839, found 983.5817.

Compound 19d. The preparation of mesylated intermediate was as described for synthesis of mesylated intermediate to **19a**. The prepared intermediate (170mg, 0.54mmol) was reacted with compound **4** (370 mg, 0.52mmol) in THF/DMSO (5:1 mL) and Hunig's base (0.6mL, 8 V/V%) at 75-80°C overnight. The work-up procedure was described in synthesis procedure of **19a**. The crude product was dried and purified through preparative TLC eluting with EtOAc:MeOH=20:1 to furnish **19d** as yellow solid (21mg, 4.1%). ¹H NMR (400 MHz, CDCl₃) δ 7.47 (d, *J* = 8.5 Hz, 2H), 7.30 (d, *J* = 8.5 Hz, 2H), 7.25 (d, *J* = 5.0 Hz, 1H), 7.09 – 7.05 (m, 1H), 6.60 (d, *J* = 9.3 Hz, 1H), 5.04 (dd, *J* = 11.1, 2.2 Hz, 1H), 4.92 (d, *J* = 5.0 Hz, 2H), 4.47 (d, *J* = 7.2 Hz, 2H), 3.99 (q, *J* = 5.5, 5.1 Hz, 3H), 3.79 – 3.70 (m, 4H), 3.66 (d, *J* = 7.3 Hz, 1H), 3.50 (s, 2H), 3.31 (d, *J* = 4.3 Hz, 6H), 3.02 (d, *J* = 5.4 Hz, 9H), 2.88 (dd, *J* = 9.3, 7.1 Hz, 2H), 2.64 – 2.53 (m, 2H), 2.48 –

2.25 (m, 9H), 2.11 – 2.05 (m, 5H), 1.94 – 1.79 (m, 4H), 1.74 – 1.48 (m, 2H), 1.39 (s, 3H), 1.33 – 1.16 (m, 13H), 1.15 – 1.05 (m, 10H), 0.93 – 0.75 (m, 6H). ^{13}C NMR (101 MHz, CDCl_3) δ 221.04, 175.8, 161.6, 142.7, 140.1, 134.9, 132.4, 126.4, 124.1, 121.5, 115.1, 96.1, 78.3, 77.9, 77.3, 77.0, 76.7, 74.3, 72.7, 70.7, 69.1, 50.6, 49.5, 45.3, 45.0, 39.3, 37.2, 34.9, 31.9, 29.7, 29.4, 26.1, 22.7, 21.5, 21.4, 21.0, 19.8, 19.3, 18.7, 18.0, 17.0, 16.0, 14.1, 12.3, 10.6, 9.1. HRMS (ESI) m/z Calcd. for $\text{C}_{55}\text{H}_{85}\text{O}_{14}\text{N}_2$ $[\text{M}+\text{H}^+]$: 997.5995, found 997.5977.

Compound 19e. The preparation of mesylated intermediate was as described for synthesis of mesylated intermediate to **19a**. The prepared intermediate (85mg, 0.236mmol) was reacted with compound **4** (230 mg, 0.31 mmol) in THF/DMSO (5:5mL) and Hunig's base (0.8 mL, 8 V/V%) at 75-80°C overnight. The work-up procedure was described in synthesis procedure of **19a**. The crude product was dried and purified through preparative TLC eluting with EtOAc:MeOH=20:1 to furnish **19e** as yellow solid (11 mg, 5%). ^1H NMR (400 MHz, CDCl_3) δ 7.46 (d, J = 8.5 Hz, 2H), 7.28 (d, J = 8.5 Hz, 2H), 7.26 – 7.22 (m, 1H), 7.06 (dt, J = 2.3, 1.1 Hz, 1H), 6.57 (d, J = 9.3 Hz, 1H), 5.03 (dd, J = 11.1, 2.3 Hz, 1H), 4.90 (d, J = 4.8 Hz, 1H), 4.43 (d, J = 7.2 Hz, 1H), 4.04 – 3.93 (m, 3H), 3.78 – 3.71 (m, 2H), 3.64 (d, J = 7.3 Hz, 1H), 3.52 – 3.42 (m, 1H), 3.31 (s, 4H), 3.24 – 3.16 (m, 2H), 3.02 – 2.93 (m, 6H), 2.62 – 2.51 (m, 2H), 2.40 (t, J = 7.0 Hz, 2H), 2.35 (d, J = 15.2 Hz, 1H), 2.25 (s, 3H), 2.08 (d, J = 1.1 Hz, 3H), 1.94 – 1.78 (m, 4H), 1.73 – 1.43 (m, 5H), 1.38 (s, 3H), 1.28 (d, J = 6.1 Hz, 3H), 1.26 – 1.15 (m, 12H), 1.09 (dt, J = 7.6, 4.0 Hz, 13H), 0.88 – 0.78 (m, 6H). ^{13}C NMR (101 MHz, CDCl_3) δ 175.8, 161.6, 142.7, 140.0, 134.9, 132.3, 126.4, 124.2, 121.5, 115.0, 102.7, 96.0, 91.4, 80.7, 80.1, 78.3, 77.9, 74.2, 72.7, 70.7, 69.0, 65.7, 50.6, 49.5, 45.3, 45.0, 39.2, 36.9, 34.9, 31.6, 29.7, 28.5, 26.4, 22.6, 21.5, 21.0, 19.8, 19.4, 18.7, 18.0, 17.0, 15.9, 14.1, 12.3, 10.6, 9.0. HRMS (ESI) m/z Calcd. for $\text{C}_{56}\text{H}_{87}\text{O}_{14}\text{N}_2$ $[\text{M}+\text{H}^+]$: 1011.6152, found 1011.6123.

Compound 20a. The preparation of mesylated intermediate was as described for synthesis of mesylated intermediate to **19a**. Subsequently, the mesylated intermediate (85 mg, 0.27 mmol) reacted with compound **7** (170 mg, 0.27 mmol) in THF/DMSO (5:5mL) and Hunig's base (0.68 mL, 4 mmol) at 50°C for 2 h. The reaction was worked up with water (50 mL) and chloroform (30 mL x 3). The crude product was purified through preparative TLC eluting with EtOAc:MeOH=15:1 to furnish **20a** as pale-yellow solid (115 mg, 45%). ¹H NMR (400 MHz, CDCl₃) δ 7.52 – 7.46 (m, 2H), 7.36 – 7.29 (m, 2H), 7.25 (d, *J* = 9.8 Hz, 1H), 7.06 (d, *J* = 2.6 Hz, 1H), 6.59 (d, *J* = 9.3 Hz, 1H), 5.12 (d, *J* = 4.8 Hz, 1H), 4.82 (s, 1H), 4.68 (dd, *J* = 9.9, 2.6 Hz, 1H), 4.47 (d, *J* = 7.2 Hz, 1H), 4.27 (dd, *J* = 4.4, 2.0 Hz, 1H), 4.06 (dt, *J* = 12.5, 6.4 Hz, 1H), 3.68 (s, 1H), 3.55 (dt, *J* = 11.0, 7.5 Hz, 1H), 3.28 (s, 4H), 3.21 (s, 1H), 3.02 (t, *J* = 9.9 Hz, 1H), 2.92 (s, 1H), 2.81 – 2.63 (m, 3H), 2.53 (d, *J* = 10.5 Hz, 1H), 2.41 (s, 3H), 2.31 (s, 4H), 2.18 – 2.14 (m, 3H), 2.09 (s, 3H), 2.08 – 1.95 (m, 2H), 1.87 (ddd, *J* = 15.6, 9.2, 4.1 Hz, 2H), 1.79 (d, *J* = 14.6 Hz, 1H), 1.56 (dd, *J* = 15.2, 5.0 Hz, 1H), 1.50 – 1.35 (m, 1H), 1.32 (t, *J* = 3.1 Hz, 6H), 1.26 – 1.14 (m, 8H), 1.13 – 1.00 (m, 8H), 0.89 (q, *J* = 7.4, 6.6 Hz, 6H). ¹³C NMR (101 MHz, CDCl₃) δ 178.9, 161.7, 142.8, 140.8, 134.9, 132.5, 126.7, 123.4, 121.7, 115.2, 103.0, 94.7, 87.7, 83.7, 78.3, 77.9, 77.4, 74.4, 73.8, 73.1, 71.1, 70.2, 68.8, 65.7, 64.6, 62.5, 49.6, 45.4, 44.7, 42.5, 42.2, 36.4, 36.3, 34.9, 31.2, 31.1, 27.7, 26.9, 22.1, 21.7, 21.5, 18.4, 17.2, 16.3, 14.9, 11.4, 9.3, 7.6. HRMS (ESI) *m/z* Calcd. for C₅₂ H₈₂ O₁₃ N₃ [M+H⁺]: 956.5842, found 956.5822.

Compound 20b. The preparation of mesylated intermediate was as described for synthesis of mesylated intermediate to **19a**. Subsequently, the mesylated intermediate (100 mg, 0.32 mmol) reacted with compound **7** (200 mg, 0.27 mmol) in THF/DMSO (5:5mL) and Hunig's base (0.7

mL, 4 mmol) at 50°C overnight. The reaction was worked up as described for **19a**. The crude product was purified through preparative TLC eluting with EtOAc:MeOH=15:1 to furnish **20b** as pale-yellow solid (13mg, 0.0134mmol, 4.9%). ¹H NMR (400 MHz, CDCl₃) δ 7.52 (d, *J* = 8.4 Hz, 2H), 7.30 (dd, *J* = 8.6, 2.0 Hz, 2H), 7.26 (d, *J* = 2.6 Hz, 1H), 7.08 (d, *J* = 2.5 Hz, 1H), 6.61 (d, *J* = 9.4 Hz, 1H), 5.12 (d, *J* = 4.9 Hz 1H), 5.04 (s, 1H), 4.70 (d, *J* = 9.8 Hz, 1H), 4.52 (dd, *J* = 15.7, 7.3 Hz, 2H), 4.30 (d, *J* = 4.7 Hz, 1H), 4.23 (d, *J* = 6.6 Hz, 1H), 4.08 (d, *J* = 6.6 Hz, 2H), 3.83 (s, 1H), 3.74 – 3.58 (m, 4H), 3.55 (s, 2H), 3.44 – 3.22 (m, 8H), 3.17 – 2.98 (m, 2H), 2.96 (s, 2H), 2.86 (d, *J* = 6.5 Hz, 4H), 2.80 (s, 3H), 2.72 (d, *J* = 7.5 Hz, 2H), 2.65 – 2.46 (m, 6H), 2.35 (d, *J* = 3.8 Hz, 13H), 2.23 – 1.96 (m, 2H), 1.94 – 1.83 (m, 4H), 1.82 – 1.43 (m, 10H), 1.41 – 1.03 (m, 10H), 1.02 – 0.69 (m, 6H). ¹³C NMR (176 MHz, CDCl₃) δ 188.1, 164.3, 161.6, 142.7, 140.2, 135.1, 132.5, 128.8, 127.2, 126.4, 123.9, 121.5, 113.8, 103.2, 95.1, 80.8, 78.2, 77.8, 74.3, 73.3, 73.0, 68.2, 65.9, 65.6, 52.6, 49.5, 45.1, 41.0, 36.7, 35.9, 34.9, 31.9, 29.7, 27.1, 26.7, 21.6, 18.3, 17.0, 11.3, 7.7. HRMS (ESI) *m/z* Calcd. for C₅₃ H₈₄ O₁₃ N₃ [M+H⁺]: 970.4432, found 970.4513.

Compound 20c. The preparation of mesylated intermediate was as described for synthesis of mesylated intermediate to **19a**. Subsequently, the mesylated intermediate (100 mg, 0.30 mmol) reacted with compound **7** (170 mg, 0.23 mmol) in THF/DMSO (5:5mL) and Hunig's base (0.7 mL, 4.1 mmol) at 70°C overnight. The reaction was worked up as described for **19a**. The crude product was purified through preparative TLC eluting with EtOAc:MeOH=15:1 to furnish **20c** as pale-yellow solid (15mg, 0.0152mmol, 5.58%). ¹H NMR (400 MHz, CDCl₃) δ 7.48 (d, *J* = 8.2 Hz, 2H), 7.32 – 7.22 (m, 3H), 7.07 (s, 1H), 6.59 (d, *J* = 9.4 Hz, 1H), 5.10 (s, 2H), 4.68 (s, 1H), 4.50 – 4.39 (m, 1H), 4.25 (s, 1H), 4.07 (s, 2H), 3.64 (d, *J* = 7.3 Hz, 3H), 3.53 (s, 1H), 3.36 – 3.28 (m, 4H), 2.74 (s, 2H), 2.54 (s, 2H), 2.47 (s, 1H), 2.34 (d, *J* = 13.6 Hz, 6H), 2.29 (s, 2H), 2.14 –

2.07 (m, 3H), 2.00 (s, 3H), 1.77 – 1.65 (m, 3H), 1.59 (s, 2H), 1.33 (s, 10H), 1.31 – 1.10 (m, 13H), 1.08 (d, $J = 1.8$ Hz, 3H), 1.04 (dd, $J = 17.7, 8.5$ Hz, 2H), 0.98 – 0.80 (m, 10H). ^{13}C NMR (176 MHz, CDCl_3) δ 161.6, 142.7, 140.2, 134.9, 132.4, 126.4, 121.5, 115.1, 102.9, 94.6, 78.2, 74.3, 73.0, 70.6, 65.6, 49.5, 45.3, 42.2, 36.3, 34.7, 31.9, 29.4, 26.7, 22.7, 22.0, 21.6, 21.4, 18.2, 17.1, 16.3, 14.6, 14.1, 11.3, 9.1, 7.4. HRMS (ESI) m/z Calcd. for $\text{C}_{54}\text{H}_{86}\text{O}_{13}\text{N}_3$ $[\text{M}+\text{H}^+]$: 984.5712, found 984.5863.

Compound 20d. The preparation of mesylated intermediate was as described for synthesis of mesylated intermediate to **19a**. Subsequently, the mesylated intermediate (100 mg, 0.32 mmol) reacted with compound **7** (170 mg, 0.23 mmol) in THF/DMSO (5:5mL) and Hunig's base (0.7 mL, 4.1 mmol) at 50°C overnight. The reaction was worked up as described for **19a**. The crude product was purified through preparative TLC eluting with EtOAc:MeOH=15:1 to furnish **20d** as pale-yellow solid (13mg, 0.0134mmol, 4.9%). ^1H NMR (400 MHz, CDCl_3) δ 7.47 (d, $J = 8.5$ Hz, 1H), 7.29 (d, $J = 8.5$ Hz, 1H), 7.26 (s, 4H), 7.07 (q, $J = 1.5, 1.0$ Hz, 1H), 6.59 (d, $J = 9.3$ Hz, 1H), 5.10 (d, $J = 4.8$ Hz, 2H), 4.68 (dd, $J = 9.9, 2.6$ Hz, 2H), 4.45 (d, $J = 7.2$ Hz, 2H), 4.29 – 4.26 (m, 1H), 4.12 – 4.01 (m, 2H), 3.69 (d, $J = 1.6$ Hz, 2H), 3.67 – 3.62 (m, 3H), 3.47 (q, $J = 7.0$ Hz, 2H), 3.32 (d, $J = 8.1$ Hz, 6H), 3.29 – 3.22 (m, 1H), 3.04 (d, $J = 8.4$ Hz, 2H), 2.77 (dd, $J = 7.5, 4.8$ Hz, 1H), 2.70 (d, $J = 6.9$ Hz, 1H), 2.51 (d, $J = 10.9$ Hz, 2H), 2.43 (s, 1H), 2.37 (s, 1H), 2.32 (s, 8H), 2.25 (d, $J = 6.1$ Hz, 4H), 2.17 (s, 0H), 2.09 (d, $J = 1.1$ Hz, 3H), 2.07 – 1.93 (m, 4H), 1.93 – 1.84 (m, 1H), 1.80 (d, $J = 14.6$ Hz, 1H), 1.70 – 1.53 (m, 6H), 1.46 (ddd, $J = 14.4, 10.0, 7.3$ Hz, 1H), 1.32 (t, $J = 3.1$ Hz, 8H), 1.28 – 1.15 (m, 13H), 1.13 – 1.01 (m, 10H), 0.89 (td, $J = 7.4, 7.0, 2.0$ Hz, 10H). ^{13}C NMR (176 MHz, CDCl_3) δ 179.1, 161.8, 142.8, 140.2, 135.1, 132.5, 126.6, 124.4, 121.6, 115.2, 103.1, 94.6, 91.3, 83.5, 80.2, 78.3, 77.8, 77.6, 74.4, 73.8, 73.6, 73.2, 70.7,

70.2, 69.0, 66.2, 65.7, 62.7, 49.6, 45.5, 42.6, 42.4, 36.4, 34.8, 32.1, 29.8, 27.7, 26.9, 26.4, 22.1, 21.8, 21.5, 19.5, 18.3, 17.2, 16.4, 14.7, 11.4, 9.1, 7.4. HRMS (ESI) m/z Calcd. for $C_{55}H_{88}O_{13}N_3$ $[M+H^+]$: 998.6312, found 998.6296.

Compound 20e. The preparation of mesylated intermediate was as described for synthesis of mesylated intermediate to **19a**. [Subsequently, the mesylated intermediate (85 mg, 0.24 mmol) reacted with compound **7** (170 mg, 0.23 mmol) in THF/DMSO (5:5mL) and Hunig's base (0.8 mL, 4.65 mmol) at 70°C overnight. The reaction was worked up as described for **19a**. The crude product was purified through preparative TLC eluting with EtOAc:MeOH=15:1 to furnish **20e** as pale-yellow solid (13 mg, 5%). 1H NMR (400 MHz, $CDCl_3$) δ 7.48 (d, J = 8.6 Hz, 2H), 7.30 (d, J = 8.6 Hz, 2H), 7.26 (m, 1H), 7.07 (d, J = 2.4 Hz, 1H), 6.60 (d, J = 9.5 Hz, 1H), 5.13 (s, 1H), 4.68 (d, J = 10.5 Hz, 2H), 4.45 (d, J = 7.0 Hz, 1H), 4.29 (s, 1H), 4.07 (s, 1H), 3.70 – 3.61 (m, 2H), 3.52 (s, 2H), 3.34 (s, 3H), 3.25 (s, 1H), 3.04 (t, J = 9.9 Hz, 1H), 2.86 (s, 1H), 2.81 – 2.64 (m, 1H), 2.52 (d, J = 10.6 Hz, 1H), 2.41 (t, J = 7.0 Hz, 2H), 2.32 (s, 4H), 2.25 (s, 3H), 2.17 (d, J = 0.6 Hz, 4H), 2.10 (d, J = 1.1 Hz, 3H), 1.83 (s, 12H), 1.69 – 1.42 (m, 8H), 1.32 (d, J = 5.4 Hz, 6H), 1.28 – 1.15 (m, 7H), 1.07 (q, J = 7.7, 7.2 Hz, 9H), 0.93 – 0.83 (m, 8H). ^{13}C NMR (176 MHz, $CDCl_3$) δ 161.7, 142.8, 140.2, 135.1, 132.5, 126.6, 124.4, 121.7, 115.2, 103.1, 94.6, 91.5, 83.5, 80.1, 78.3, 77.8, 74.4, 73.8, 73.2, 70.7, 65.7, 62.6, 53.4, 49.6, 45.4, 42.4, 36.4, 34.8, 29.8, 28.7, 27.7, 26.9, 22.2, 21.8, 21.5, 19.5, 18.4, 17.2, 16.4, 14.8, 11.4, 9.1, 7.5. HRMS (ESI) m/z Calcd. for $C_{56}H_{90}O_{13}N_3$ $[M+H^+]$: 1012.6468, found 1012.6451.

2.4.3 Cell culture

Cell culture and viability assays protocol were described in our previous work. In brief, VERO, and A549 cell lines were maintained in Dulbecco's Modified Eagle Medium (DMEM) (Corning, 10-017-CV), supplemented with 10% fetal bovine serum (FBS) (Corning, 35-010-CV). MRC-5 and Hep-G2 cells were cultured in phenol red free Minimum Essential Medium (MEM) (Corning, 17-305-CV), supplemented with 10% fetal bovine serum (FBS).

2.4.4 *MTS assay*

Cells were seeded into a 96-well plate (2000 counts/100uL) for 24 h prior to treatment and then treated with various drug concentrations for 72 h. All drugs were dissolved in medium via DMSO solution with DMSO concentration maintained at 1%. The effect of compounds on cell viability was measured using the MTS assay (CellTiter 96 Aqueous One Solution and CellTiter 96 Non-Radioactive Cell Proliferation Assays, Promega, Madison, WI) as described by the manufacturer. IC₅₀s were calculated using Prism GraphPad 8.

2.4.5 *Anti-inflammatory activity assay (NF- κ B inhibition assay)*

NF- κ B activity was measured by luciferase assay. BEAS-2B cells were transfected with NF- κ B luciferase reporter construct in pGL3 basic vector 40 h after transfection, the cells were treated with drugs for 1 h followed by stimulation with NTHi for 5 h. Then cells were lysed with cell lysis buffer (250 mM Tris-HCl (pH 7.5), 0.1% Triton-X, 1 mM DTT) and luciferase activity was measured by luciferase assay system (Promega). Relative luciferase activity (RLA) was determined using the following equation; $RLA = \frac{\text{luciferase unit of the cells treated with NTHi}}{\text{and drug/ luciferase unit of the cells treated with mock}}$.

2.4.6 Human Pro-collagen ELISA kit

Human pro-collagen ELISA kit was supplied by Abcam (ab210966). Cells were trypsinized and seeded to 24-well plates with 5×10^5 cell/well for 2-3 days until confluence reach to 80%. Fresh drug solutions at IC_{50} and $1/10 IC_{50}$ concentrations were used to treat cells for 24 h. The assays were run in duplicate following the manufacturer's protocol. In brief, the conditioned medium was extracted from the cell plate to the COL1A1 antibody precoated plate with Human Pro-collagen I alpha 1 capture antibody. After 3 times of wash, a Human Pro-collagen I alpha 1 detector antibody was incubated into the precoated plate for 2 h. After the addition of the developing reagents, the absorbance was read at 450 nm. MTS assay was used to determine cell proliferation in order to normalize the collagen expression with cell number.

2.4.7 Western blot

Cells were cultured in 6-well plate with 1×10^6 cells/well. After 24 h, cells were incubated with serum-free MEM 24 h prior to treatment. Then the cells were treated with 50 ng/mL TGF- β with or without treatment. PFD, AZM, CLM, and selected compounds **10c**, **11b**, **11c** and **15c** were independently incubated with the cells for 24 h prior to lysis. Then cells were washed by 1x cold PBS and lysed with RIPA buffer containing phosphatase and protease inhibitors under 4°C. The lysates were collected, and the concentrations were normalized using BCA protein quantification assay (Biovision, CA, USA). The lysates were mixed with 10% mercaptoethanol Laemmi buffer and denatured by heating to 100°C. The lysates were loaded on to 4-20% Criterion TGX Precast Gel and electrophoresed running at 150V for 66 minutes; and transferred to PVDF membrane.

The membrane was blocked with 5% BSA in TBST buffer for 1 h. Then the membrane was incubated with primary antibody overnight at 4°C. The Anti-CollA1(84336), anti-p-STAT3 (9145), anti-MMP-2 (40994s), anti-Fibronectin (26836s) were purchased from Cell Signal Technology®; Anti- α -SMA (ab5694) were from Abcam®; anti-GAPDH (sc-47724) were purchased from Santa Cruz®; The membrane is washed with 1x TBST 3 times before secondary antibody incubation. The secondary antibody were rabbit IgG 800 and mouse IgG 680 from IRDye. After washing again 3 times with TBST, the membrane fluorescence was read using Odyssey CLx Imagine System.

2.4.8 Bioassay (*TGF- β pathway inhibition*)

The assay kit containing A549 cell engineered with Luciferase reporter gene was provided by Promega. The cells were cultured with the provided medium and 10% FBS. Followed manufacturer's instruction, we seeded the cells into two 96 well plates and followed by treatment with 1% DMSO or 1% DMSO solution of candidates. We investigated multiple dosages of selected candidates (**10c**, **11b**, **14c**, **15c**, and PFD) and scanned the other potential candidates by treating for 6 h with TGF- β stimulation (50 ng/mL). The cell medium were transferred to a white OptiPlate™ 96-well plate (VWR, 25382-208) and incubated at room temperature with 1 mM Luciferin. After 1 min incubation, luminescence was read and data was processed by Prism GraphPad 8.

2.5 References:

1. Raghu, G.; Collard, H. R.; Egan, J. J.; Martinez, F. J.; Behr, J.; Brown, K. K.; Colby, T. V.; Cordier, J. F.; Flaherty, K. R.; Lasky, J. A.; Lynch, D. A.; Ryu, J. H.; Swigris, J. J.; Wells, A. U.; Ancochea, J.; Bouros, D.; Carvalho, C.; Costabel, U.; Ebina, M.; Hansell, D. M.; Johkoh, T.; Kim, D. S.; King, T. E., Jr.; Kondoh, Y.; Myers, J.; Muller, N. L.; Nicholson, A. G.; Richeldi, L.; Selman, M.; Dudden, R. F.; Griss, B. S.; Protzko, S. L.; Schunemann, H. J.; Fibrosis, A. E. J. A. C. o. I. P., An official ATS/ERS/JRS/ALAT statement: idiopathic pulmonary fibrosis: evidence-based guidelines for diagnosis and management. *Am J Respir Crit Care Med* **2011**, *183* (6), 788-824.
2. Raghu, G.; Weycker, D.; Edelsberg, J.; Bradford, W. Z.; Oster, G., Incidence and prevalence of idiopathic pulmonary fibrosis. *Am J Respir Crit Care Med* **2006**, *174* (7), 810-6.
3. Hutchinson, J.; Fogarty, A.; Hubbard, R.; McKeever, T., Global incidence and mortality of idiopathic pulmonary fibrosis: a systematic review. *Eur Respir J* **2015**, *46* (3), 795-806.
4. Raghu, G.; Chen, S. Y.; Hou, Q.; Yeh, W. S.; Collard, H. R., Incidence and prevalence of idiopathic pulmonary fibrosis in US adults 18-64 years old. *Eur Respir J* **2016**, *48* (1), 179-86.
5. Nalysnyk, L.; Cid-Ruzafa, J.; Rotella, P.; Esser, D., Incidence and prevalence of idiopathic pulmonary fibrosis: review of the literature. *Eur Respir Rev* **2012**, *21* (126), 355-61.

6. Cancer Facts & Figures 2018. *American Cancer Society*.
7. M du Bois, R., *An earlier and more confident diagnosis of idiopathic pulmonary fibrosis*. 2012; Vol. 21, p 141-6.
8. Strongman, H.; Kausar, I.; Maher, T. M., Incidence, Prevalence, and Survival of Patients with Idiopathic Pulmonary Fibrosis in the UK. *Adv Ther* **2018**, 35 (5), 724-736.
9. Willis, B. C.; Borok, Z., TGF- β -induced EMT: mechanisms and implications for fibrotic lung disease. *American Journal of Physiology-Lung Cellular and Molecular Physiology* **2007**, 293 (3), L525-L534.
10. Upagupta, C.; Shimbori, C.; Alsilmi, R.; Kolb, M., Matrix abnormalities in pulmonary fibrosis. *European Respiratory Review* **2018**, 27 (148).
11. Broekelmann, T. J.; Limper, A. H.; Colby, T. V.; McDonald, J. A., Transforming growth factor beta 1 is present at sites of extracellular matrix gene expression in human pulmonary fibrosis. *Proceedings of the National Academy of Sciences* **1991**, 88 (15), 6642-6646.
12. Yun, S.-M.; Kim, S.-H.; Kim, E.-H., The molecular mechanism of transforming growth factor- β signaling for intestinal fibrosis: a mini-review. *Frontiers in pharmacology* **2019**, 10, 162.
13. Kolosova, I.; Nethery, D.; Kern, J. A., Role of Smad2/3 and p38 MAP kinase in TGF- β 1-induced epithelial-mesenchymal transition of pulmonary epithelial cells. *Journal of cellular physiology* **2011**, 226 (5), 1248-1254.
14. Wright, J. G.; Christman, J. W., The role of nuclear factor kappa B in the pathogenesis of pulmonary diseases: implications for therapy. *American Journal of Respiratory Medicine* **2003**, 2 (3), 211-219.
15. Noguchi, S.; Saito, A.; Nagase, T., YAP/TAZ signaling as a molecular link between fibrosis and cancer. *International journal of molecular sciences* **2018**, 19 (11), 3674.
16. Itoh, Y.; Saitoh, M.; Miyazawa, K., Smad3-STAT3 crosstalk in pathophysiological contexts. *Acta biochimica et biophysica Sinica* **2018**, 50 (1), 82-90.
17. Tang, L.-Y.; Heller, M.; Meng, Z.; Yu, L.-R.; Tang, Y.; Zhou, M.; Zhang, Y. E., Transforming growth factor- β (TGF- β) directly activates the JAK1-STAT3 axis to induce hepatic fibrosis in coordination with the SMAD pathway. *Journal of Biological Chemistry* **2017**, 292 (10), 4302-4312.
18. Liu, T.; Zhang, L.; Joo, D.; Sun, S.-C., NF- κ B signaling in inflammation. *Signal transduction and targeted therapy* **2017**, 2 (1), 1-9.
19. Zhang, F.; Wang, H.; Wang, X.; Jiang, G.; Liu, H.; Zhang, G.; Wang, H.; Fang, R.; Bu, X.; Cai, S., TGF- β induces M2-like macrophage polarization via SNAIL-mediated suppression of a pro-inflammatory phenotype. *Oncotarget* **2016**, 7 (32), 52294.
20. Liu, R.-Y.; Zeng, Y.; Lei, Z.; Wang, L.; Yang, H.; Liu, Z.; Zhao, J.; Zhang, H.-T., JAK/STAT3 signaling is required for TGF- β -induced epithelial-mesenchymal transition in lung cancer cells. *International Journal of Oncology* **2014**, 44 (5), 1643-1651.

21. Liu, Y. M.; Nepali, K.; Liou, J. P., Idiopathic Pulmonary Fibrosis: Current Status, Recent Progress, and Emerging Targets. *J Med Chem* **2017**, *60* (2), 527-553.
22. King, T. E., Jr.; Bradford, W. Z.; Castro-Bernardini, S.; Fagan, E. A.; Glaspole, I.; Glassberg, M. K.; Gorina, E.; Hopkins, P. M.; Kardatzke, D.; Lancaster, L.; Lederer, D. J.; Nathan, S. D.; Pereira, C. A.; Sahn, S. A.; Sussman, R.; Swigris, J. J.; Noble, P. W.; Group, A. S., A phase 3 trial of pirfenidone in patients with idiopathic pulmonary fibrosis. *N Engl J Med* **2014**, *370* (22), 2083-92.
23. Cottin, V., Changing the idiopathic pulmonary fibrosis treatment approach and improving patient outcomes. *Eur Respir Rev* **2012**, *21* (124), 161-7.
24. Zurkova, M.; Kriegova, E.; Kolek, V.; Lostakova, V.; Sterclova, M.; Bartos, V.; Doubkova, M.; Binkova, I.; Svoboda, M.; Strenkova, J., Effect of pirfenidone on lung function decline and survival: 5-yr experience from a real-life IPF cohort from the Czech EMPIRE registry. *Respiratory research* **2019**, *20* (1), 1-11.
25. FDA Approved Drug Products: Esbriet (pirfenidone) for oral use.
26. Agrawal, N.; Vaidya, P. J.; Chavhan, V. B.; Lele, T. T.; Leuppi-Taegtmeyer, A.; Leuppi, J. D.; Chhajed, P. N., Best tolerated dose of Pirfenidone in patients with idiopathic pulmonary fibrosis. *Eur Respiratory Soc*: 2019.
27. Cottin, V.; Koschel, D.; Günther, A.; Albero, C.; Azuma, A.; Sköld, C. M.; Tomassetti, S.; Hormel, P.; Stauffer, J. L.; Strombom, I., Long-term safety of pirfenidone: results of the prospective, observational PASSPORT study. *ERJ open research* **2018**, *4* (4).
28. Ma, Z.; Pan, Y.; Huang, W.; Yang, Y.; Wang, Z.; Li, Q.; Zhao, Y.; Zhang, X.; Shen, Z., Synthesis and biological evaluation of the pirfenidone derivatives as antifibrotic agents. *Bioorg Med Chem Lett* **2014**, *24* (1), 220-3.
29. Alvarez-Elcoro, S.; Enzler, M. J. In *The macrolides: erythromycin, clarithromycin, and azithromycin*, Mayo Clinic Proceedings, Elsevier: 1999; pp 613-634.
30. Miossec-Bartoli, C.; Pilatre, L.; Peyron, P.; N'Diaye, E.-N.; Collart-Dutilleul, V.; Maridonneau-Parini, I.; Diu-Hercend, A., The new ketolide HMR3647 accumulates in the azurophil granules of human polymorphonuclear cells. *Antimicrobial agents and chemotherapy* **1999**, *43* (10), 2457-2462.
31. Bosnar, M.; Kelnerić, Ž.; Munić, V.; Eraković, V.; Parnham, M. J., Cellular uptake and efflux of azithromycin, erythromycin, clarithromycin, telithromycin, and cethromycin. *Antimicrobial agents and chemotherapy* **2005**, *49* (6), 2372-2377.
32. LeBel, M., Pharmacokinetic properties of clarithromycin: A comparison with erythromycin and azithromycin. *Canadian Journal of Infectious Diseases* **1993**, *4*.
33. Wildfeuer, A.; Laufen, H.; Zimmermann, T., Uptake of azithromycin by various cells and its intracellular activity under in vivo conditions. *Antimicrobial agents and chemotherapy* **1996**, *40* (1), 75-79.
34. Hand, W. L.; Hand, D. L., Characteristics and mechanisms of azithromycin accumulation and efflux in human polymorphonuclear leukocytes. *International journal of antimicrobial agents* **2001**, *18* (5), 419-425.

35. Steel, H. C.; Theron, A. J.; Cockeran, R.; Anderson, R.; Feldman, C., Pathogen-and host-directed anti-inflammatory activities of macrolide antibiotics. *Mediators of inflammation* **2012**, 2012.
36. Parnham, M. J.; Haber, V. E.; Giamarellos-Bourboulis, E. J.; Perletti, G.; Verleden, G. M.; Vos, R., Azithromycin: mechanisms of action and their relevance for clinical applications. *Pharmacology & therapeutics* **2014**, 143 (2), 225-245.
37. Beigelman, A.; Mikols, C. L.; Gunsten, S. P.; Cannon, C. L.; Brody, S. L.; Walter, M. J., Azithromycin attenuates airway inflammation in a mouse model of viral bronchiolitis. *Respiratory research* **2010**, 11 (1), 90.
38. Yamada, K.; Yanagihara, K.; Kaku, N.; Harada, Y.; Migiyama, Y.; Nagaoka, K.; Morinaga, Y.; Nakamura, S.; Imamura, Y.; Miyazaki, T., Azithromycin attenuates lung inflammation in a mouse model of ventilator-associated pneumonia by multidrug-resistant *Acinetobacter baumannii*. *Antimicrobial agents and chemotherapy* **2013**, 57 (8), 3883-3888.
39. Terao, H.; Asano, K.; Kanai, K.-i.; Kyo, Y.; Watanabe, S.; Hisamitsu, T.; Suzaki, H., Suppressive activity of macrolide antibiotics on nitric oxide production by lipopolysaccharide stimulation in mice. *Mediators of inflammation* **2003**, 12 (4).
40. Beigelman, A.; Gunsten, S.; Mikols, C. L.; Vidavsky, I.; Cannon, C. L.; Brody, S. L.; Walter, M. J., Azithromycin attenuates airway inflammation in a noninfectious mouse model of allergic asthma. *Chest* **2009**, 136 (2), 498-506.
41. Geudens, N.; Timmermans, L.; Vanhooren, H.; Vanaudenaerde, B. M.; Vos, R.; Van De Wauwer, C.; Verleden, G. M.; Verbeken, E.; Lerut, T.; Van Raemdonck, D. E., Azithromycin reduces airway inflammation in a murine model of lung ischaemia reperfusion injury. *Transplant International* **2008**, 21 (7), 688-695.
42. Stepanic, V.; Kostrun, S.; Malnar, I.; Hlevnjak, M.; Butkovic, K.; Caleta, I.; Dukši, M.; Kragol, G.; Makaruha-Stegic, O.; Mikac, L., Modeling cellular pharmacokinetics of 14-and 15-membered macrolides with physicochemical properties. *Journal of medicinal chemistry* **2011**, 54 (3), 719-733.
43. Gladue, R.; Snider, M., Intracellular accumulation of azithromycin by cultured human fibroblasts. *Antimicrobial Agents and Chemotherapy* **1990**, 34 (6), 1056-1060.
44. Kohyama, T.; Yamauchi, Y.; Takizawa, H.; Itakura, S.; Kamitani, S.; Kato, J.; Nagase, T., Clarithromycin inhibits fibroblast migration. *Respiratory medicine* **2008**, 102 (12), 1769-1776.
45. Zimmermann, P.; Ziesenitz, V. C.; Curtis, N.; Ritz, N., The immunomodulatory effects of macrolides—a systematic review of the underlying mechanisms. *Frontiers in immunology* **2018**, 9, 302.
46. Zarogoulidis, P.; Papanas, N.; Kioumis, I.; Chatzaki, E.; Maltezos, E.; Zarogoulidis, K., Macrolides: from in vitro anti-inflammatory and immunomodulatory properties to clinical practice in respiratory diseases. *European journal of clinical pharmacology* **2012**, 68 (5), 479-503.

47. Li, W.; Liu, X.; Muhammad, S.; Shi, J.; Meng, Y.; Wang, J., Computational investigation of TGF- β receptor inhibitors for treatment of idiopathic pulmonary fibrosis: Field-based QSAR model and molecular dynamics simulation. *Computational biology and chemistry* **2018**, 76, 139-150.
48. Trott, O.; Olson, A. J., AutoDock Vina: improving the speed and accuracy of docking with a new scoring function, efficient optimization, and multithreading. *Journal of computational chemistry* **2010**, 31 (2), 455-461.
49. Li, W.; Liu, X.; Muhammad, S.; Shi, J.; Meng, Y.; Wang, J., Computational investigation of TGF-beta receptor inhibitors for treatment of idiopathic pulmonary fibrosis: Field-based QSAR model and molecular dynamics simulation. *Comput Biol Chem* **2018**, 76, 139-150.
50. Oyelere, A. K.; Chen, P. C.; Guerrant, W.; Mwakwari, S. C.; Hood, R.; Zhang, Y.; Fan, Y., Non-peptide macrocyclic histone deacetylase inhibitors. *Journal of medicinal chemistry* **2009**, 52 (2), 456-468.
51. Conte, E.; Gili, E.; Fagone, E.; Fruciano, M.; Iemmolo, M.; Vancheri, C., Effect of pirfenidone on proliferation, TGF- β -induced myofibroblast differentiation and fibrogenic activity of primary human lung fibroblasts. *European Journal of Pharmaceutical Sciences* **2014**, 58, 13-19.
52. Ueki, N.; Taguchi, T.; Takahashi, M.; Adachi, M.; Ohkawa, T.; Amuro, Y.; Hada, T.; Higashino, K., Inhibition of hyaluronan synthesis by vesnarinone in cultured human myofibroblasts. *Biochimica et Biophysica Acta (BBA)-Molecular Cell Research* **2000**, 1495 (2), 160-167.
53. Yoshihara, T.; Nanri, Y.; Nunomura, S.; Yamaguchi, Y.; Feghali-Bostwick, C.; Ajito, K.; Murakami, S.; Mawatari, M.; Izuhara, K., Periostin plays a critical role in the cell cycle in lung fibroblasts. *Respiratory research* **2020**, 21 (1), 1-12.
54. Choe, J.-Y.; Jung, H.-J.; Park, K.-Y.; Kum, Y.-S.; Song, G. G.; Hyun, D.-S.; Park, S.-H.; Kim, S.-K., Anti-fibrotic effect of thalidomide through inhibiting TGF- β -induced ERK1/2 pathways in bleomycin-induced lung fibrosis in mice. *Inflammation research* **2010**, 59 (3), 177-188.
55. Multhoff, G.; Molls, M.; Radons, J., Chronic inflammation in cancer development. *Frontiers in immunology* **2012**, 2, 98.
56. Park, J.; Kim, D.; Shim, T.; Lim, C.; Koh, Y.; Lee, S.; Kim, W.; Kim, W.; Lee, J.; Song, K., Lung cancer in patients with idiopathic pulmonary fibrosis. *European Respiratory Journal* **2001**, 17 (6), 1216-1219.
57. Pietras, E. M., Inflammation: a key regulator of hematopoietic stem cell fate in health and disease. *Blood, The Journal of the American Society of Hematology* **2017**, 130 (15), 1693-1698.
58. Arrese, M.; Hernandez, A.; Astete, L.; Estrada, L.; Cabello-Verrugio, C.; Cabrera, D., TGF- β and hepatocellular carcinoma: when a friend becomes an enemy. *Current Protein and Peptide Science* **2018**, 19 (12), 1172-1179.

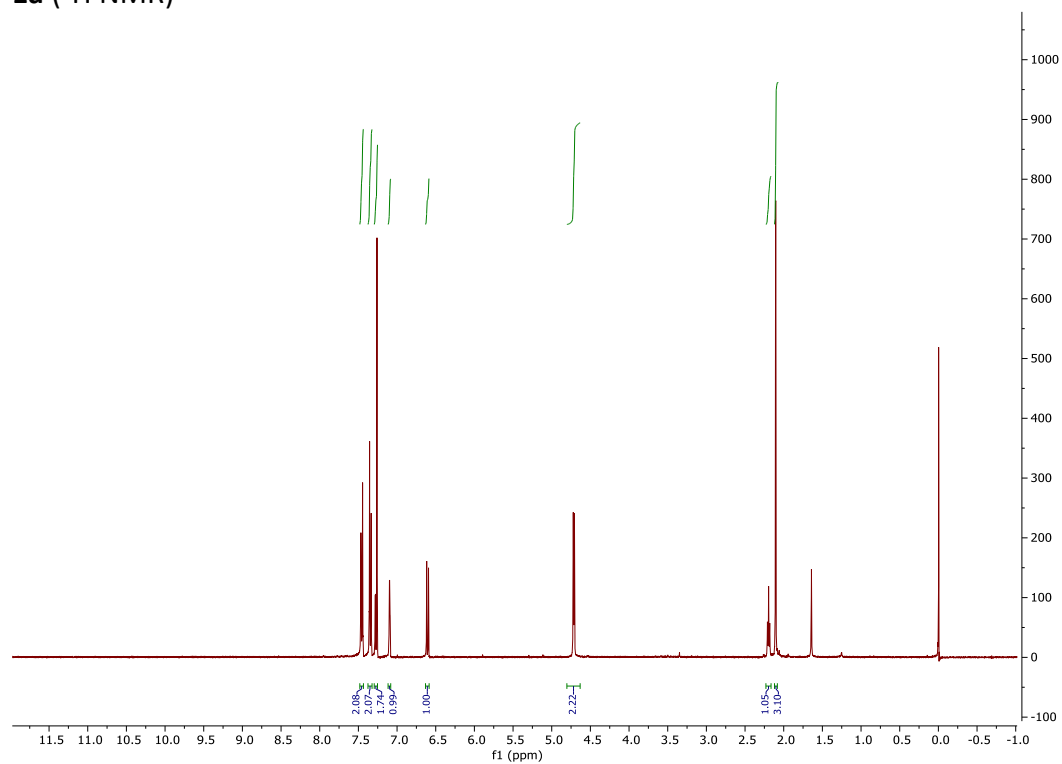
59. Li, X.-h.; Xiao, T.; Yang, J.-h.; Qin, Y.; Gao, J.-j.; Liu, H.-j.; Zhou, H.-g., Parthenolide attenuated bleomycin-induced pulmonary fibrosis via the NF- κ B/Snail signaling pathway. *Respiratory research* **2018**, *19* (1), 1-12.
60. Saadane, A.; Masters, S.; DiDonato, J.; Li, J.; Berger, M., Parthenolide inhibits I κ B kinase, NF- κ B activation, and inflammatory response in cystic fibrosis cells and mice. *American journal of respiratory cell and molecular biology* **2007**, *36* (6), 728-736.
61. Nakanishi, H.; Kaibori, M.; Teshima, S.; Yoshida, H.; Kwon, A. H.; Kamiyama, Y.; Nishizawa, M.; Ito, S.; Okumura, T., Pirfenidone inhibits the induction of iNOS stimulated by interleukin-1 β at a step of NF- κ B DNA binding in hepatocytes. *Journal of Hepatology* **2004**, *41* (5), 730-736.
62. Cui, Y.; Zhang, M.; Leng, C.; Blokzijl, T.; Jansen, B. H.; Dijkstra, G.; Faber, K. N., Pirfenidone inhibits cell proliferation and collagen I production of primary human intestinal fibroblasts. *Cells* **2020**, *9* (3), 775.
63. Tsubouchi, K.; Araya, J.; Minagawa, S.; Hara, H.; Ichikawa, A.; Saito, N.; Kadota, T.; Sato, N.; Yoshida, M.; Kurita, Y.; Kobayashi, K.; Ito, S.; Fujita, Y.; Utsumi, H.; Yanagisawa, H.; Hashimoto, M.; Wakui, H.; Yoshii, Y.; Ishikawa, T.; Numata, T.; Kaneko, Y.; Asano, H.; Yamashita, M.; Odaka, M.; Morikawa, T.; Nakayama, K.; Nakanishi, Y.; Kuwano, K., Azithromycin attenuates myofibroblast differentiation and lung fibrosis development through proteasomal degradation of NOX4. *Autophagy* **2017**, *13* (8), 1420-1434.
64. Molina-Molina, M.; Machahua-Huamani, C.; Vicens-Zygmunt, V.; Llatjós, R.; Escobar, I.; Sala-Llinas, E.; Luburich-Hernaiz, P.; Dorca, J.; Montes-Worboys, A., Anti-fibrotic effects of pirfenidone and rapamycin in primary IPF fibroblasts and human alveolar epithelial cells. *BMC pulmonary medicine* **2018**, *18* (1), 1-13.
65. Stahnke, T.; Kowtharapu, B. S.; Stachs, O.; Schmitz, K.-P.; Wurm, J.; Wree, A.; Guthoff, R. F.; Hovakimyan, M., Suppression of TGF- β pathway by pirfenidone decreases extracellular matrix deposition in ocular fibroblasts in vitro. *PLoS One* **2017**, *12* (2), e0172592.
66. Pechkovsky, D. V.; Prêle, C. M.; Wong, J.; Hogaboam, C. M.; McAnulty, R. J.; Laurent, G. J.; Zhang, S. S.-M.; Selman, M.; Mutsaers, S. E.; Knight, D. A., STAT3-mediated signaling dysregulates lung fibroblast-myofibroblast activation and differentiation in UIP/IPF. *The American journal of pathology* **2012**, *180* (4), 1398-1412.
67. Milara, J.; Hernandez, G.; Ballester, B.; Morell, A.; Roger, I.; Montero, P.; Escrivá, J.; Lloris, J. M.; Molina-Molina, M.; Morcillo, E., The JAK2 pathway is activated in idiopathic pulmonary fibrosis. *Respiratory research* **2018**, *19* (1), 1-12.
68. Yu, H.; Pardoll, D.; Jove, R., STATs in cancer inflammation and immunity: a leading role for STAT3. *Nature reviews cancer* **2009**, *9* (11), 798-809.
69. Sibinska, Z.; Tian, X.; Korfei, M.; Kojonazarov, B.; Kolb, J. S.; Klepetko, W.; Kosanovic, D.; Wygrecka, M.; Ghofrani, H. A.; Weissmann, N., Amplified canonical transforming growth factor- β signalling via heat shock protein 90 in pulmonary fibrosis. *European Respiratory Journal* **2017**, *49* (2).

70. Doerner-Ciossek, C.; Eickmeier, C.; Fiegen, D.; Fox, T.; Fuchs, K.; Giovannini, R.; Heine, N.; Rosenbrock, H.; Schaenzle, G., WO2009 121919-A1. AU2009232017-A1: 2009.

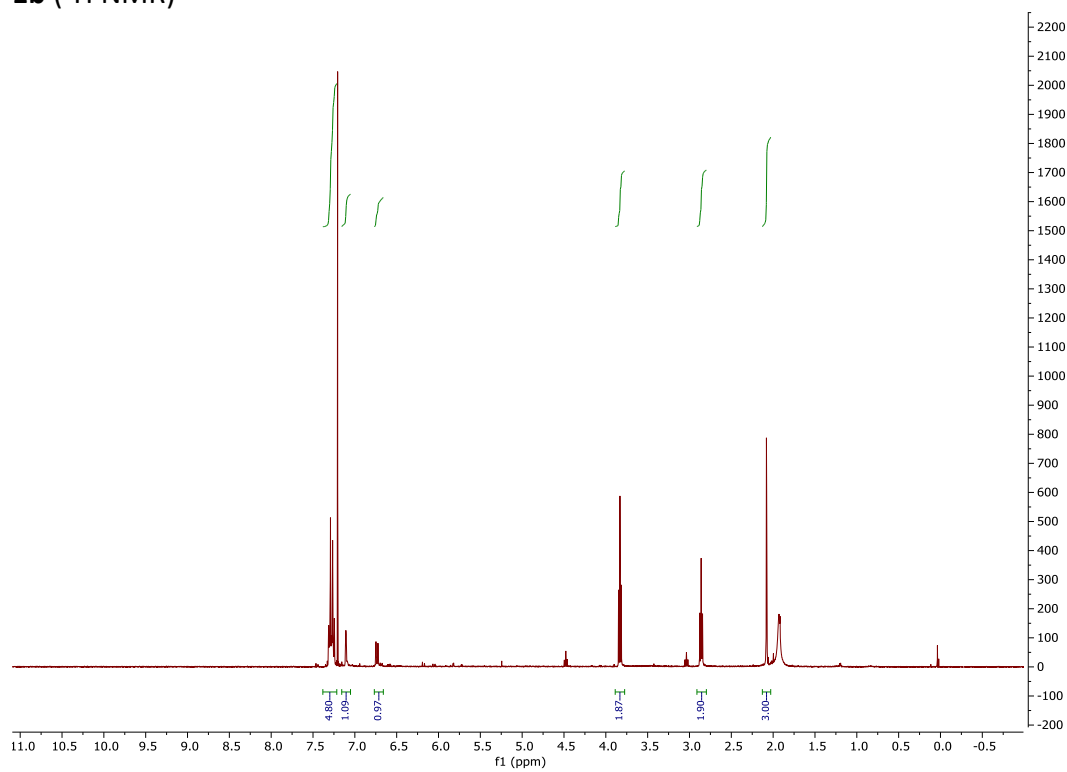
2.6 Supporting Information

NMRs

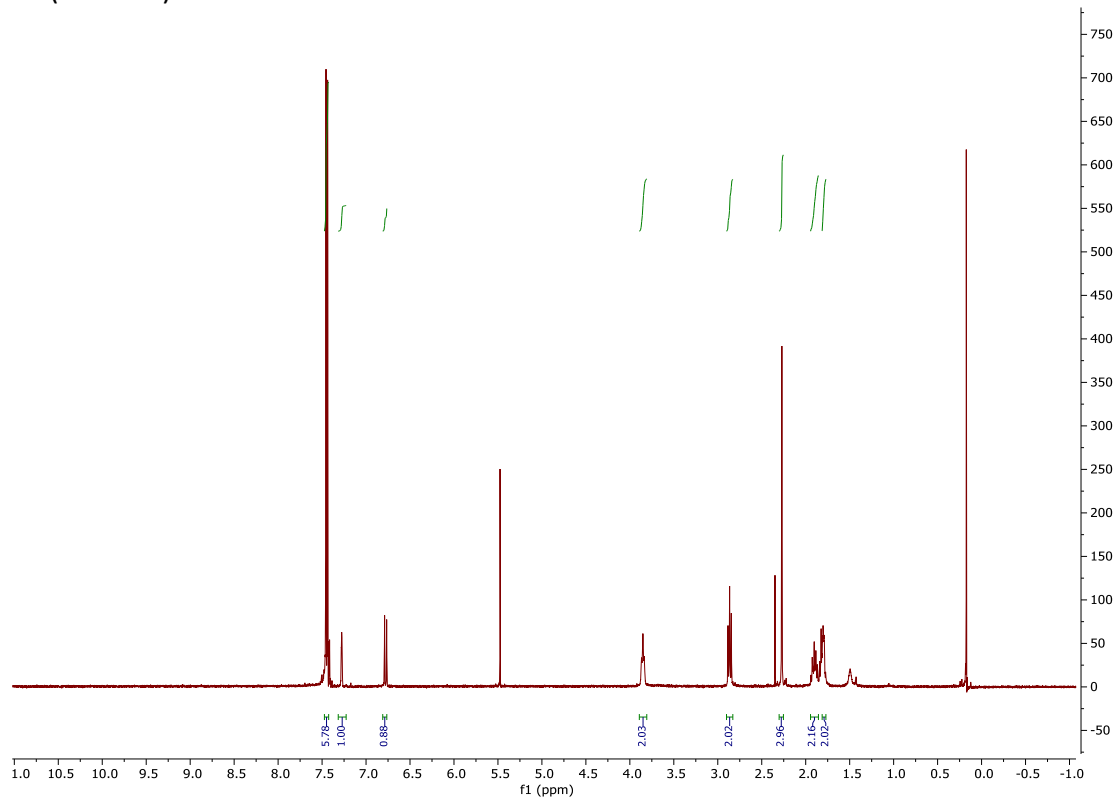
1a (^1H NMR)



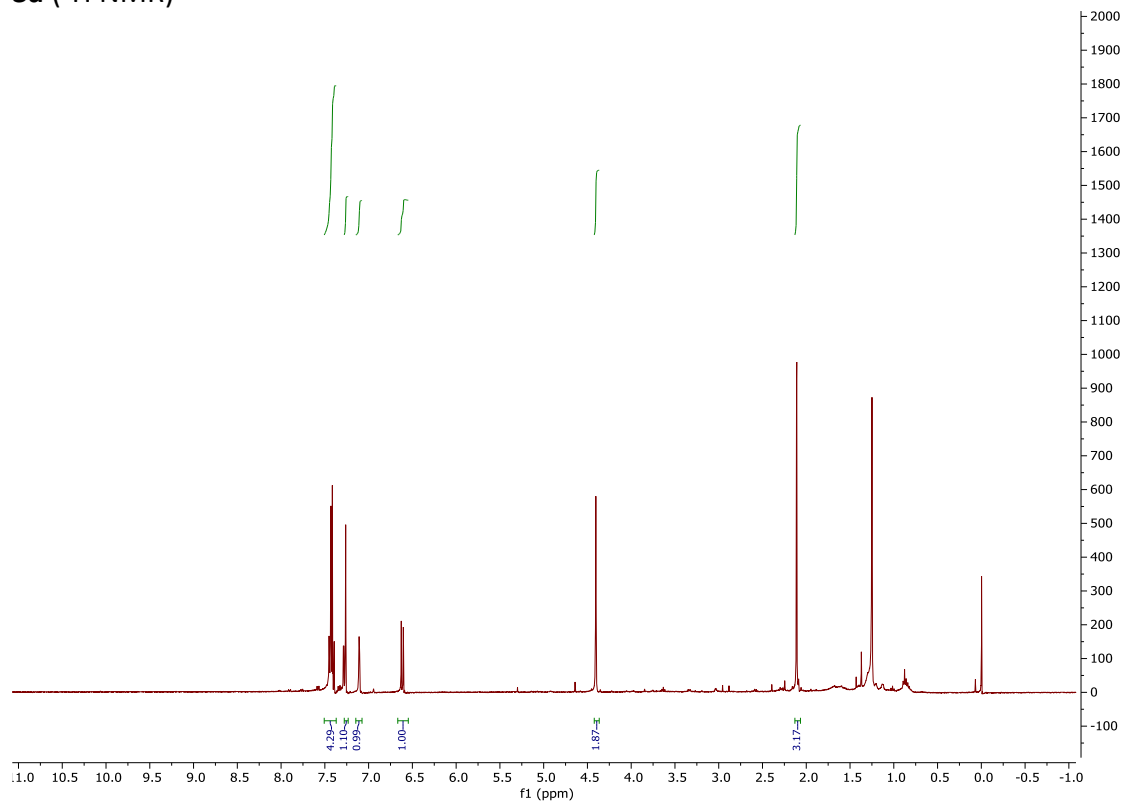
1b (^1H NMR)



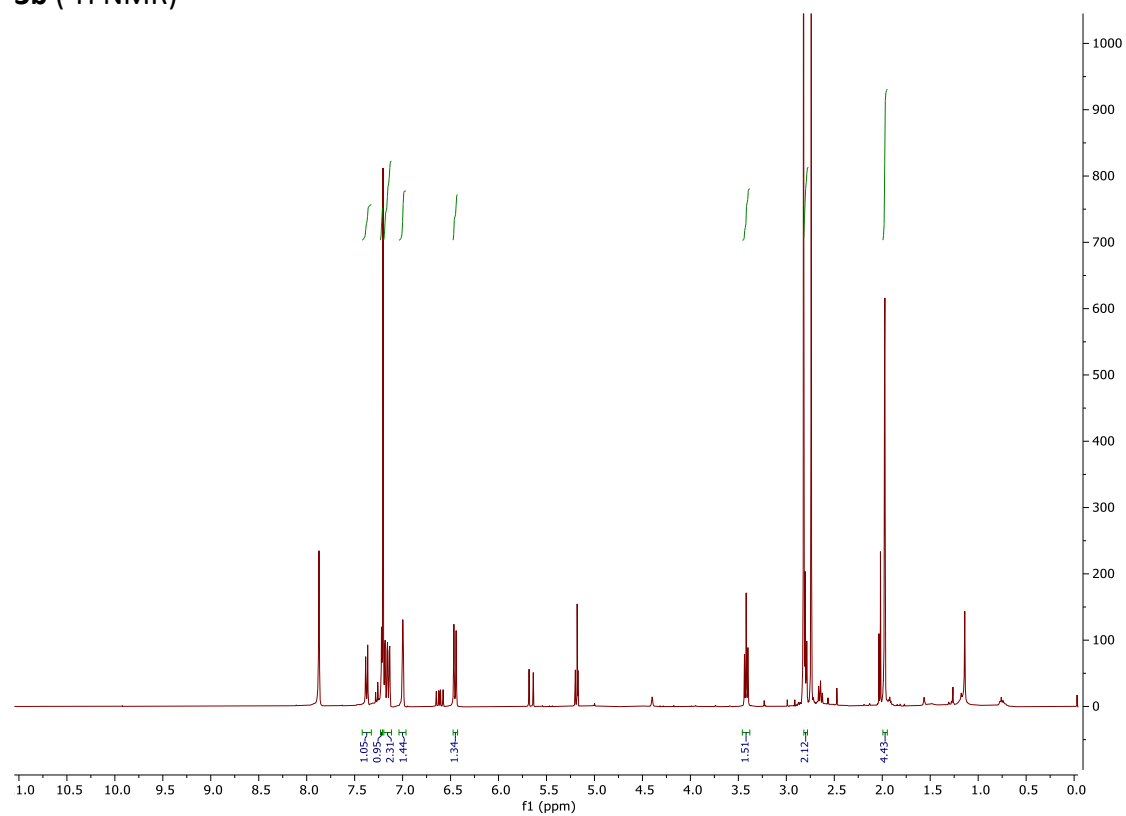
1c (^1H NMR)



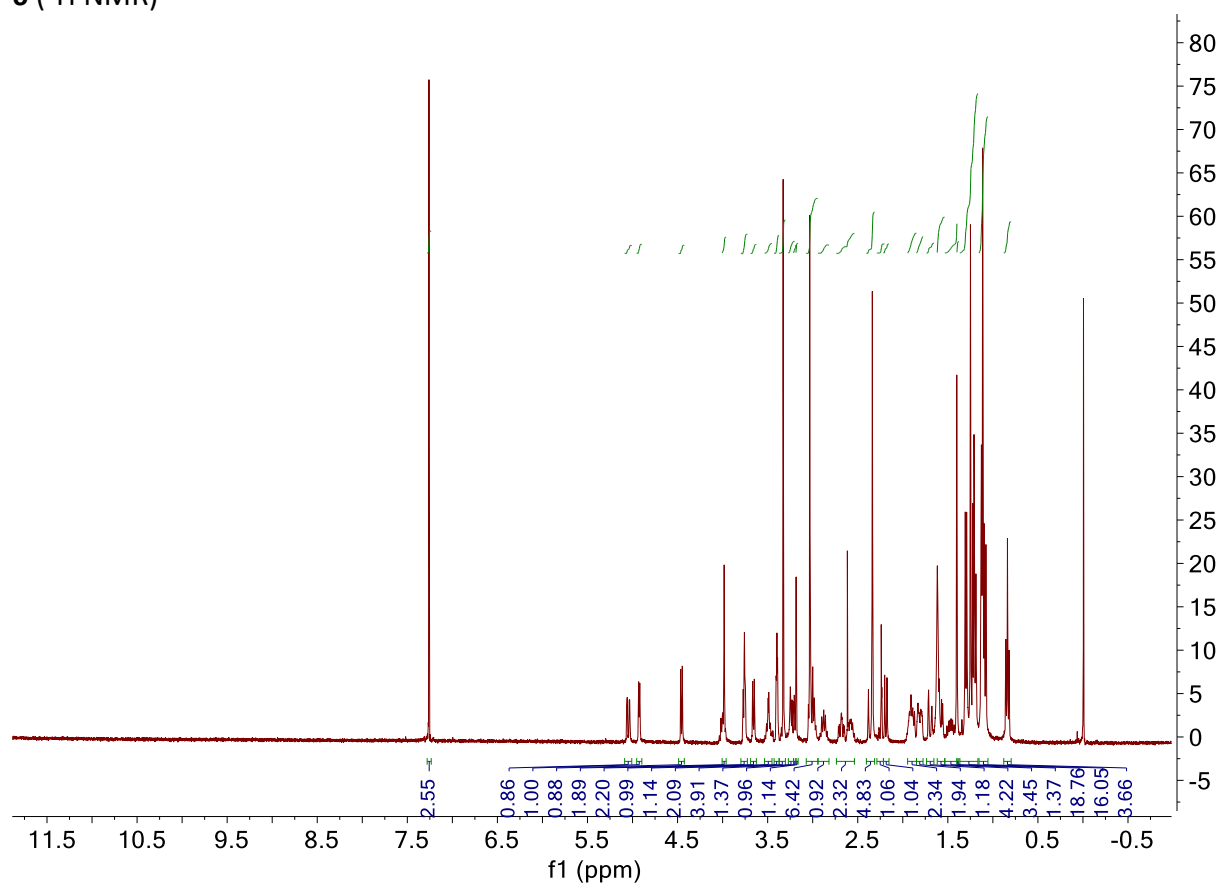
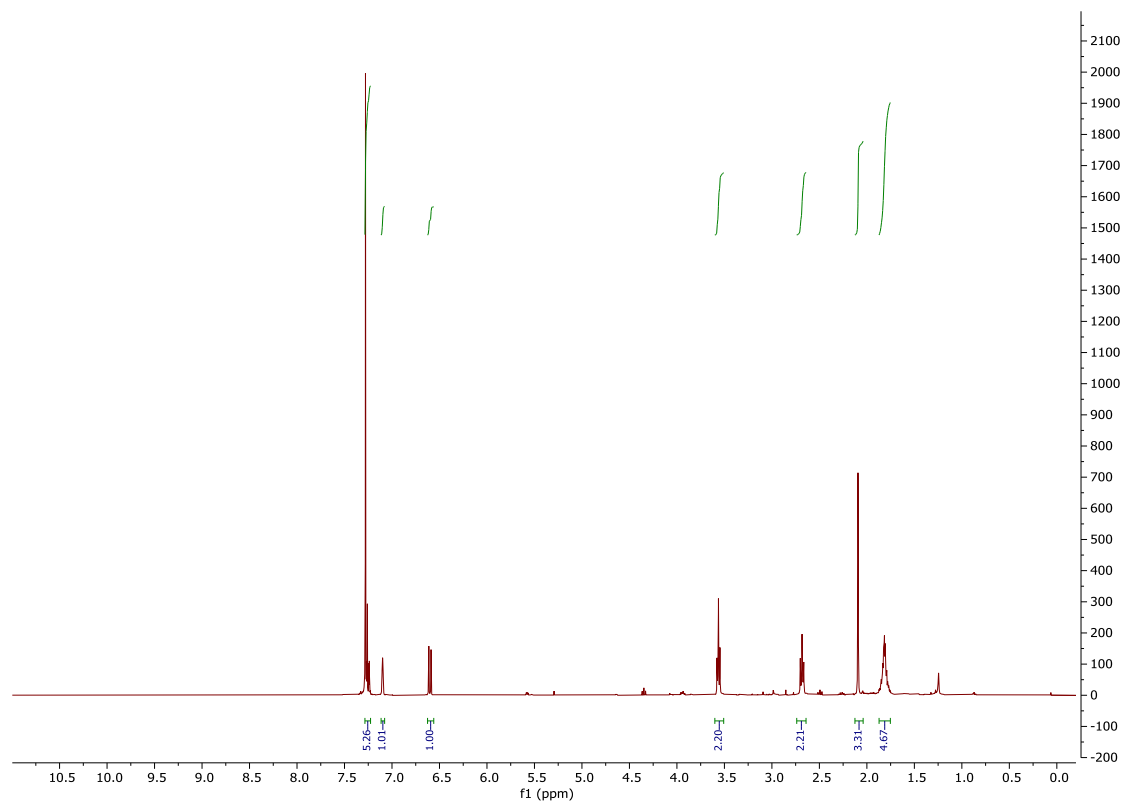
3a (^1H NMR)



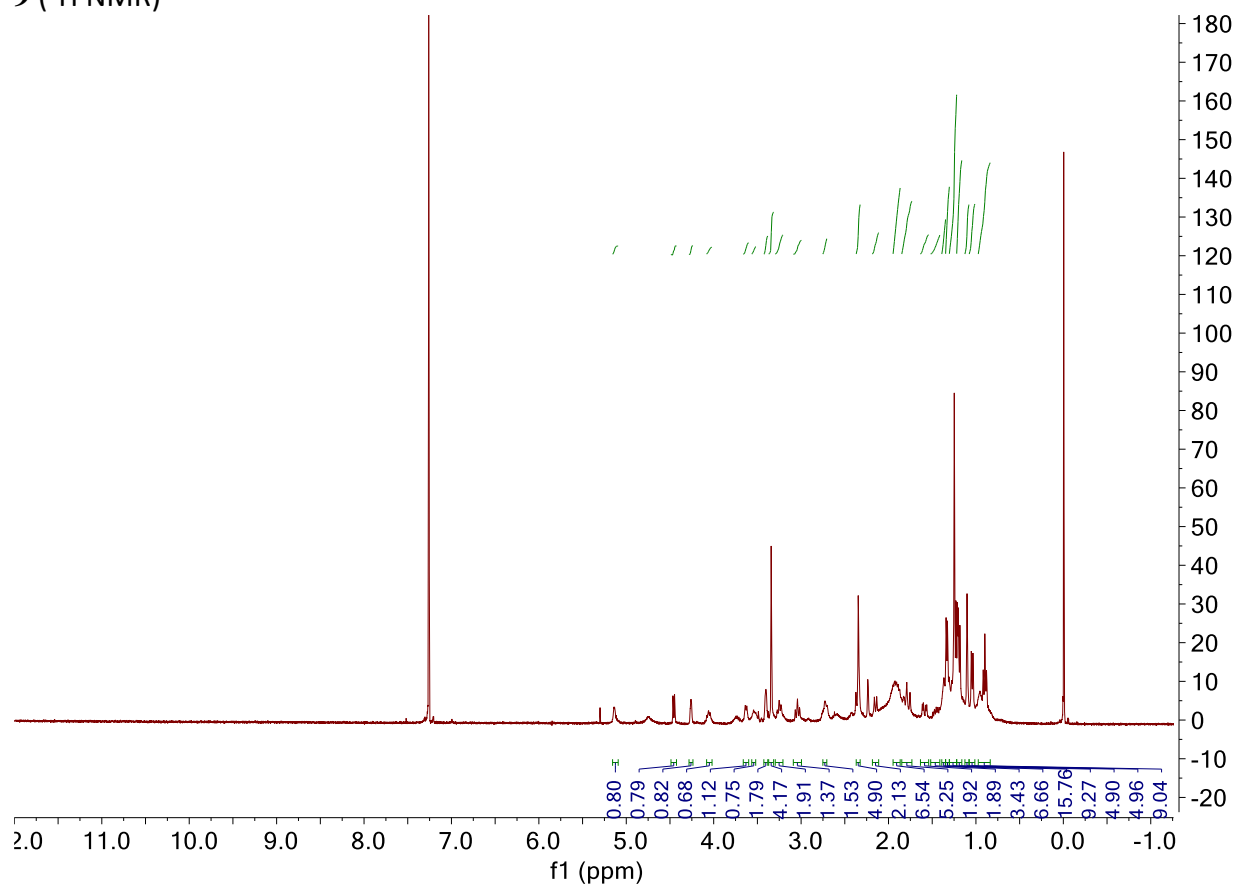
3b (^1H NMR)



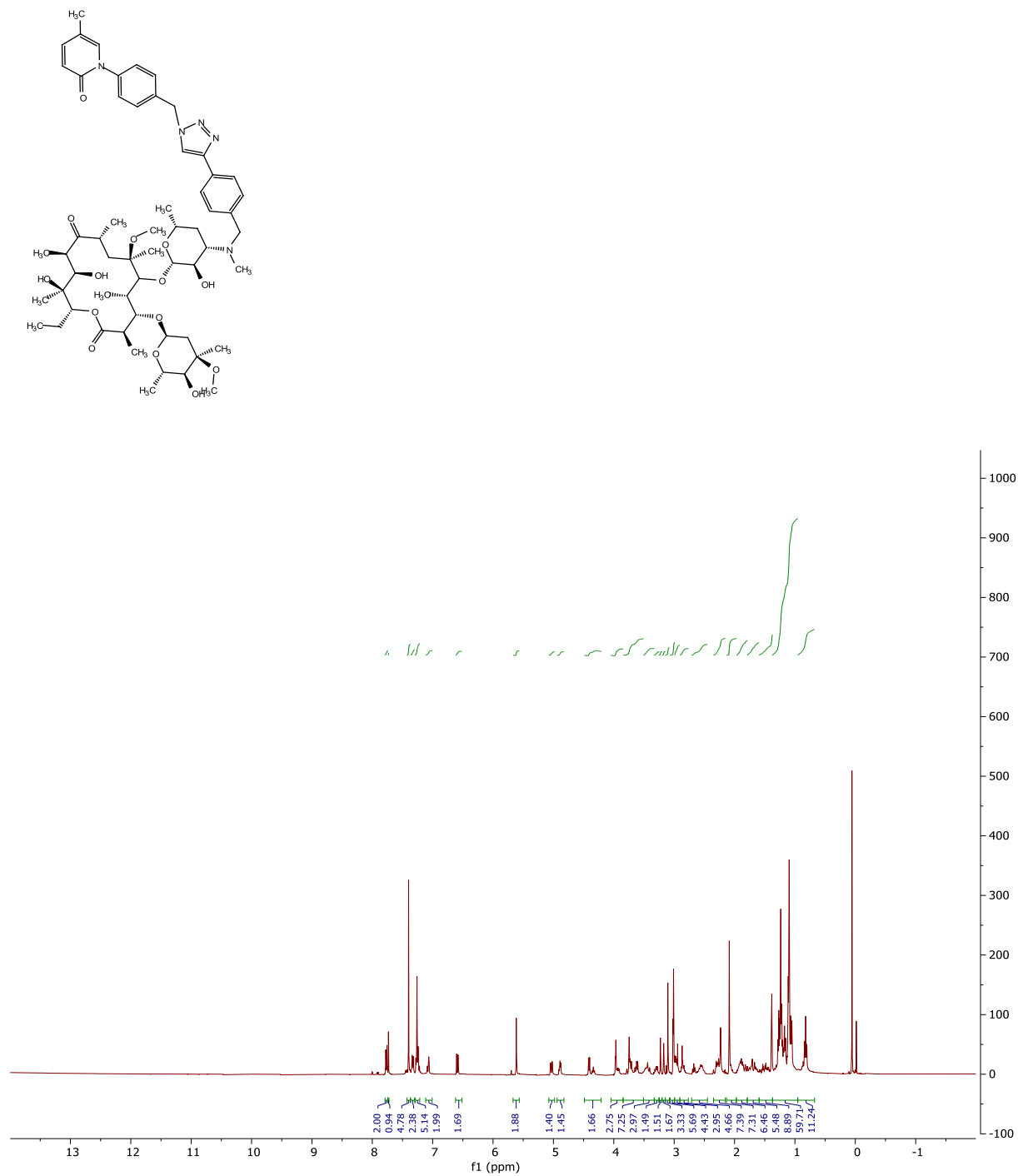
3c (^1H NMR)



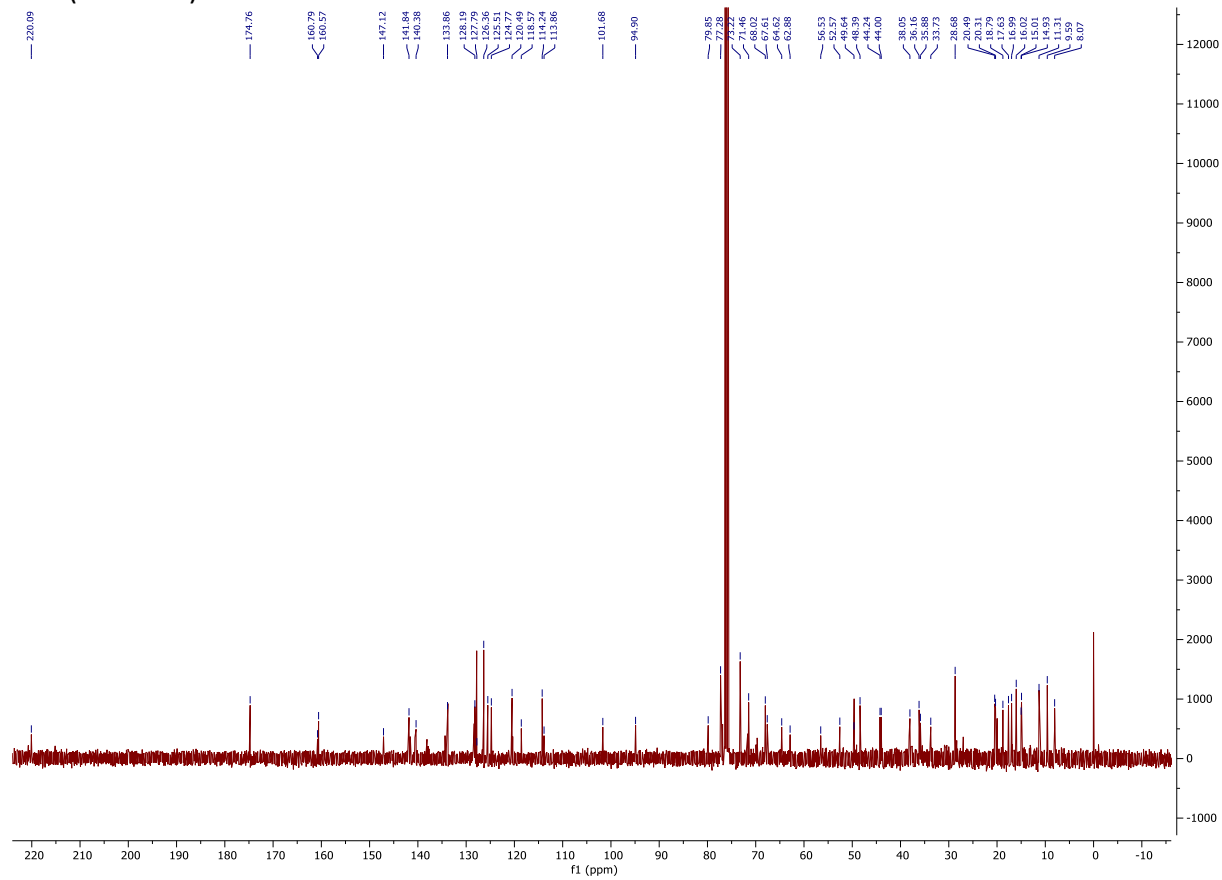
9 (^1H NMR)



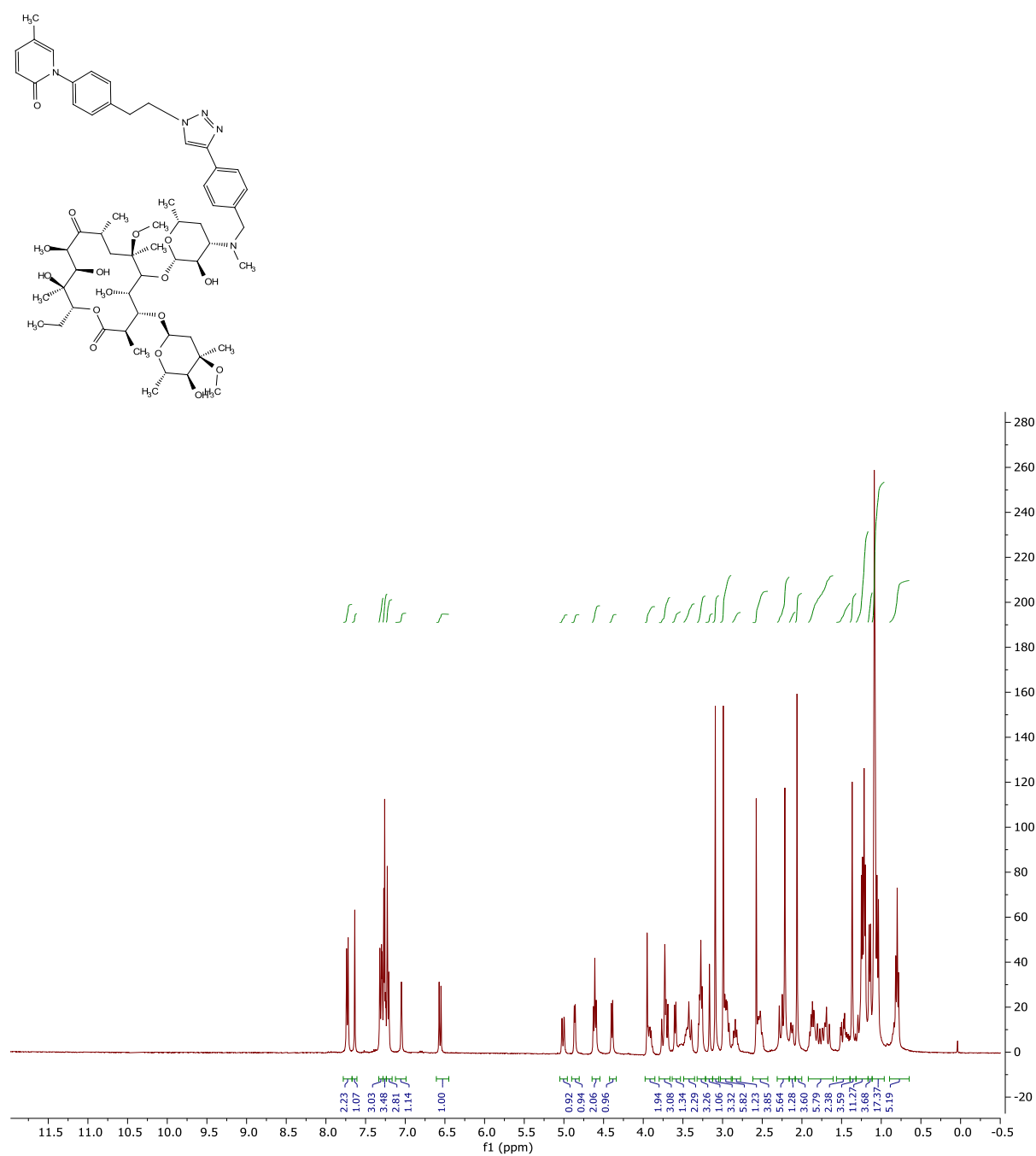
10a (¹H NMR)



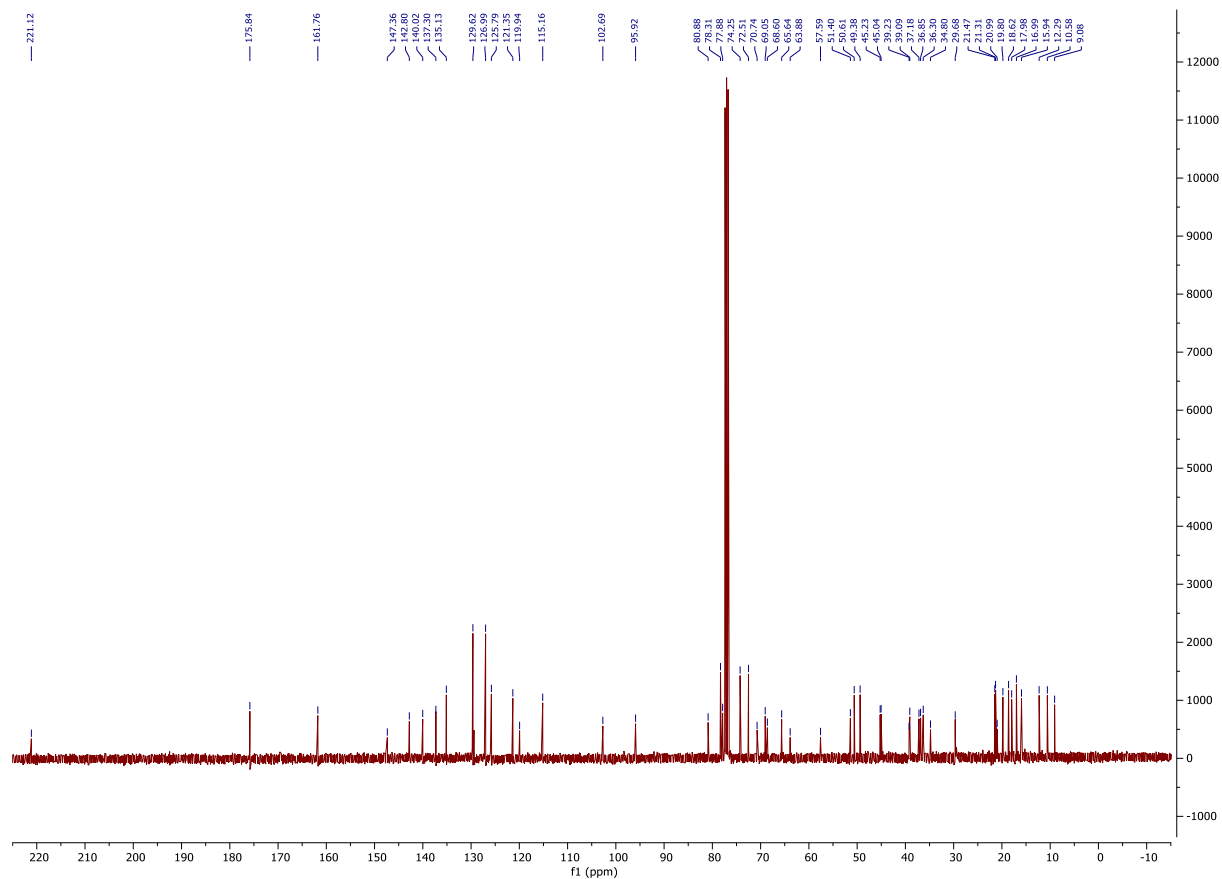
10a (¹³C NMR)



10b (^1H NMR)

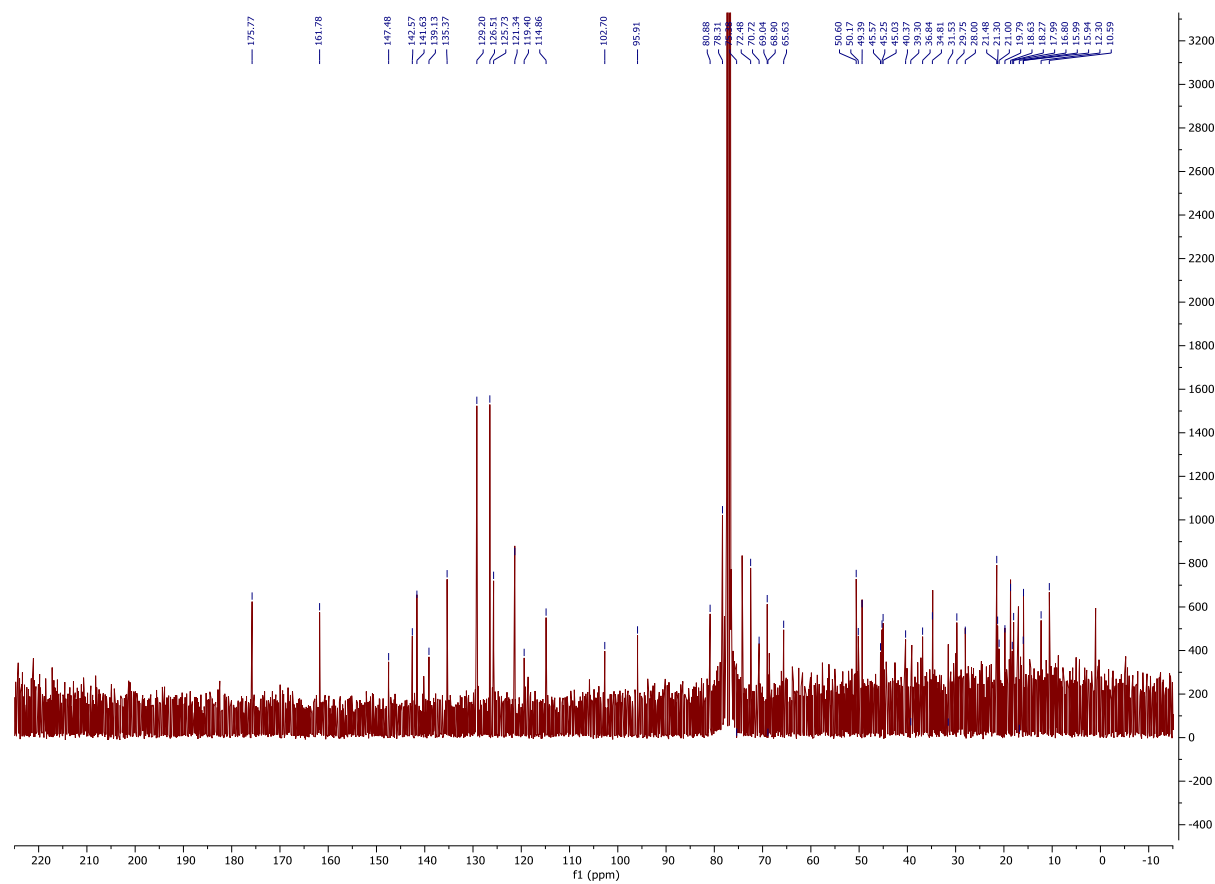


10b (¹³C NMR)

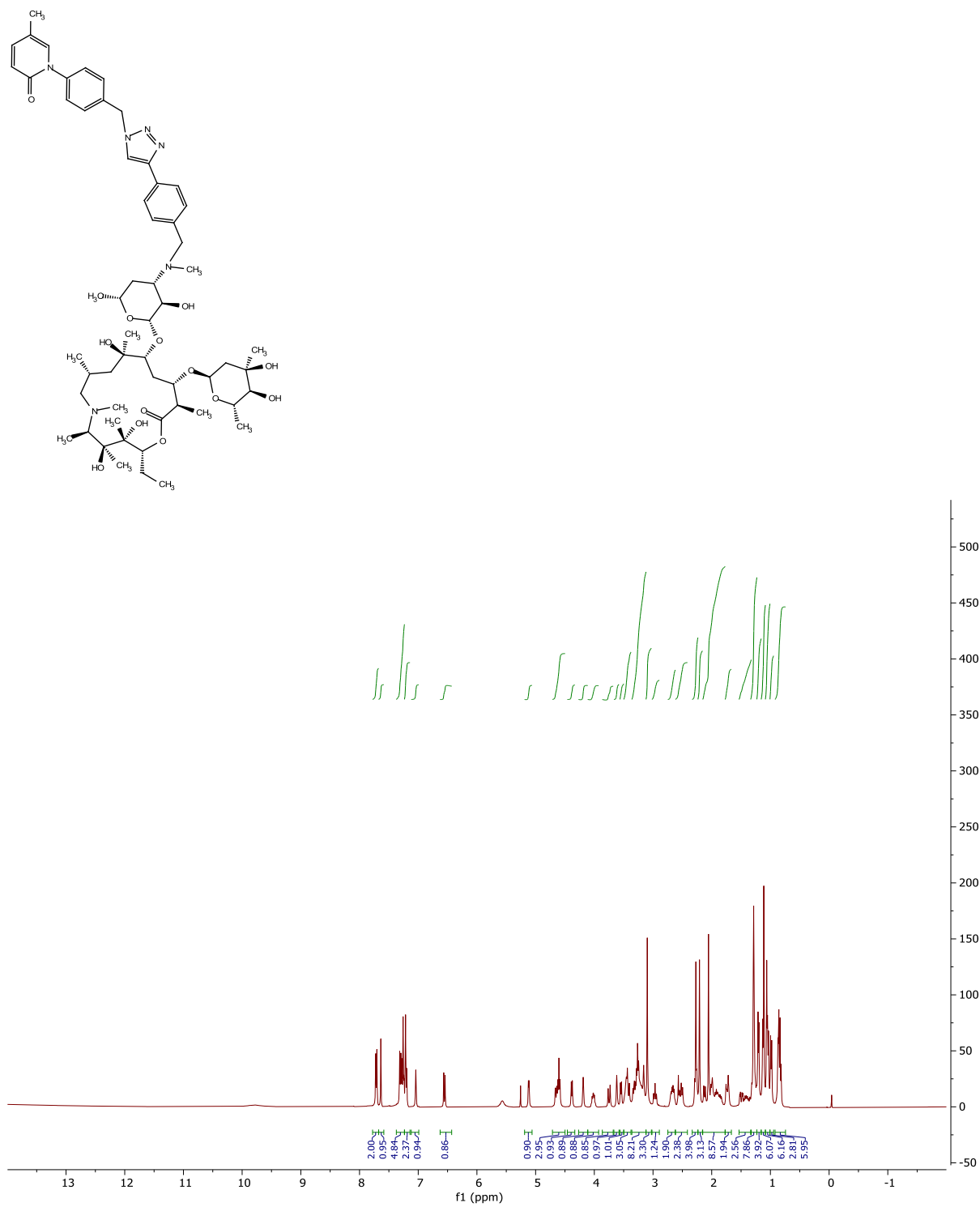


Cc1cc(C2=CC=C(C=C2)N3C(=O)C=CC=C3C4=CC=CC=C4CCCCCN5C=NC(=C5)C6=CC=CC=C6CN7C=C(C)OC7)C=C1

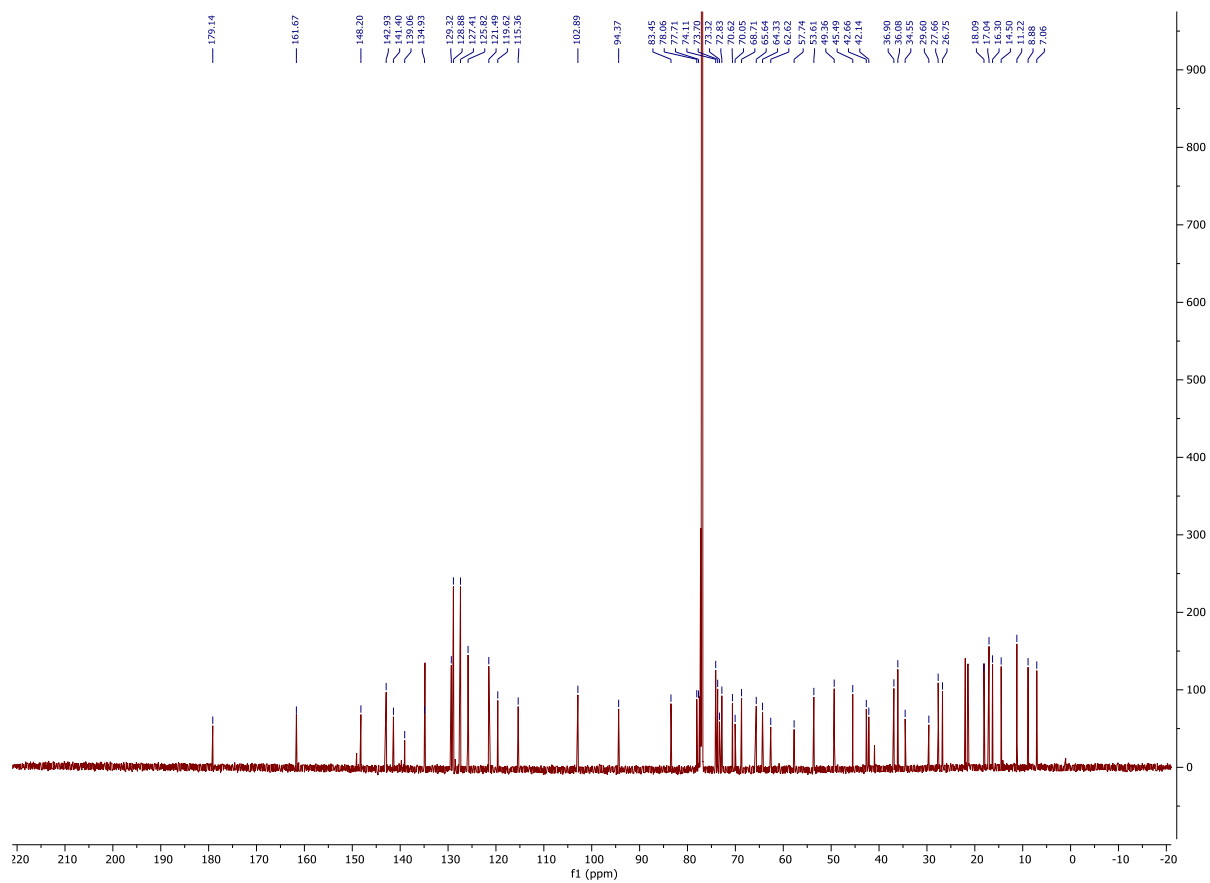
10c (^{13}C NMR)



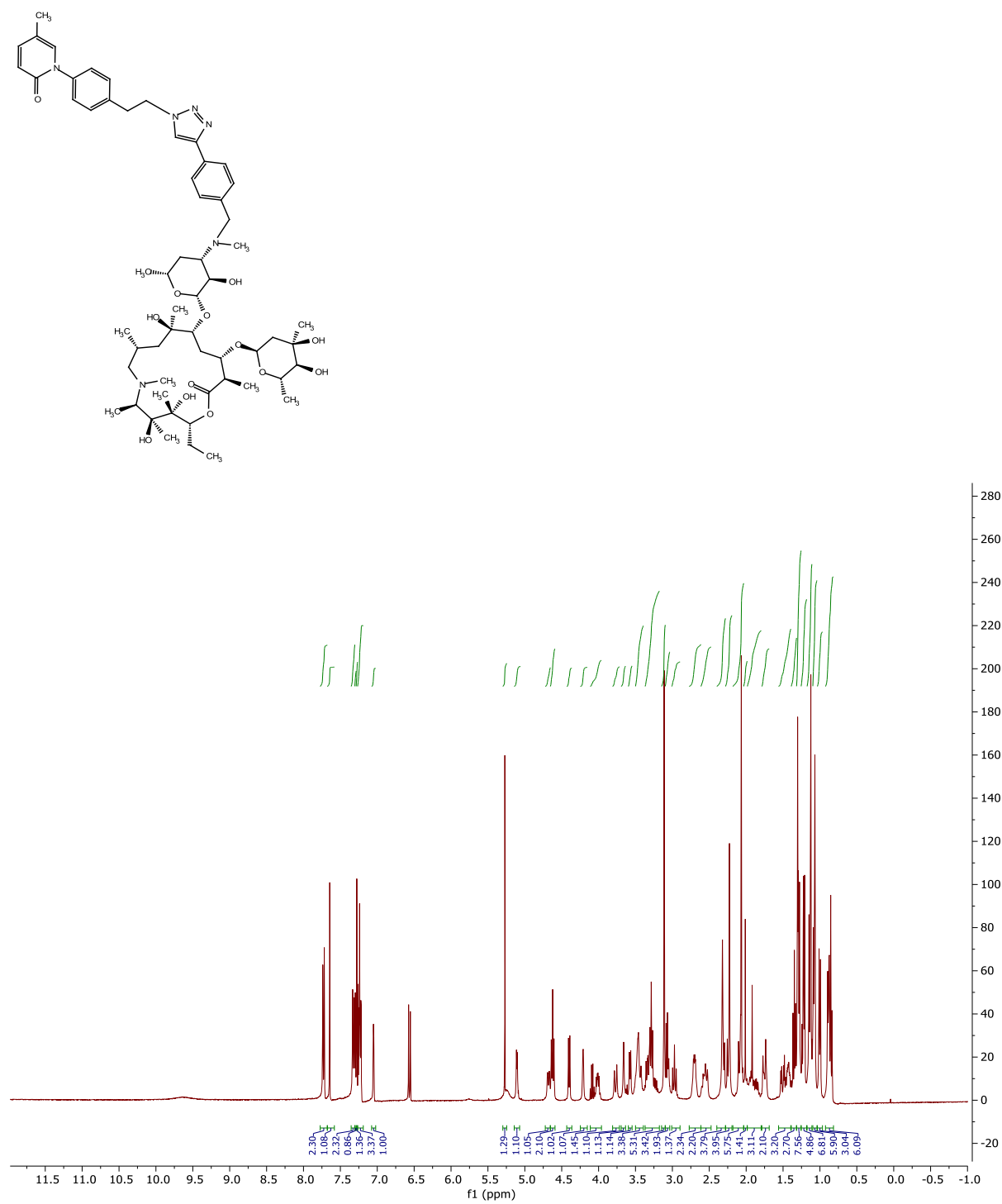
11a (^1H NMR)



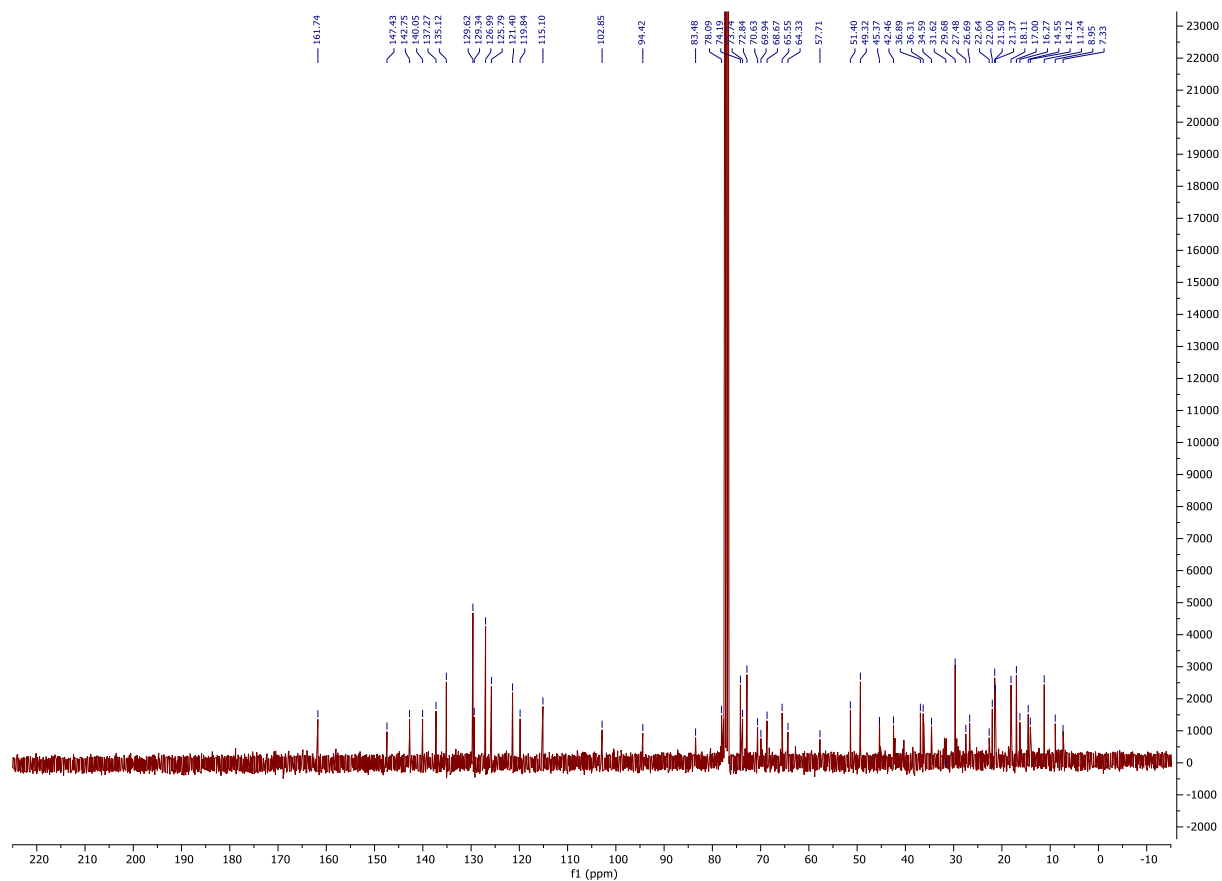
11a (^{13}C NMR)



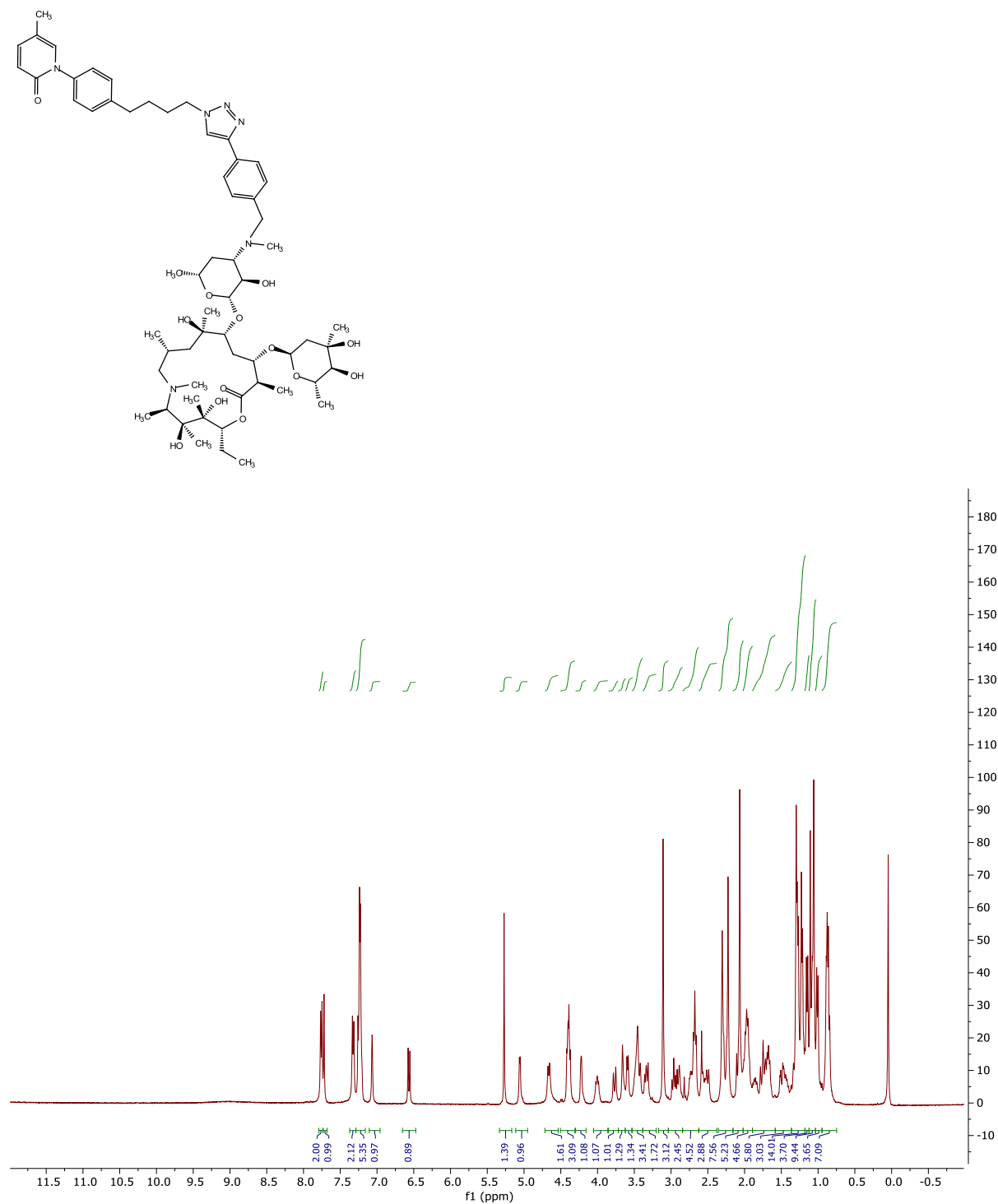
11b (^1H NMR)



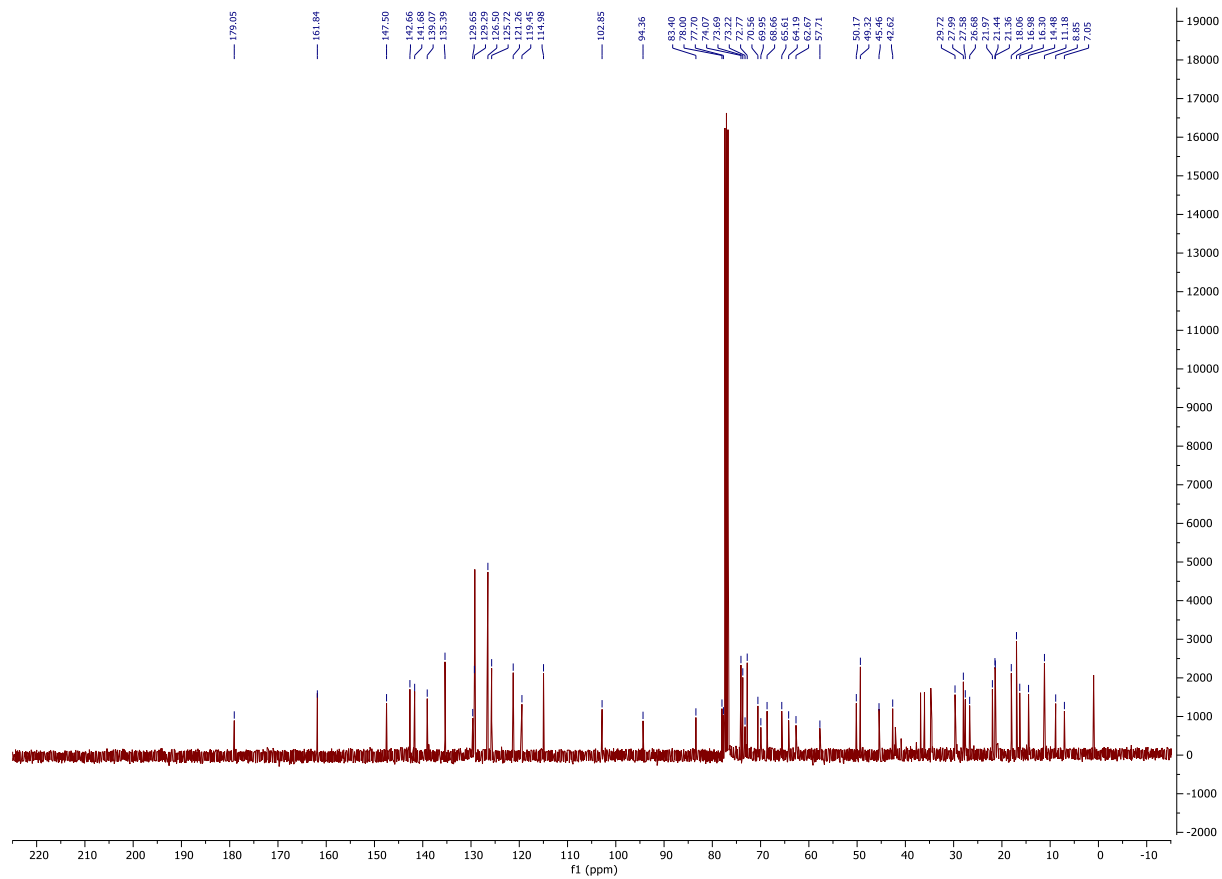
11b (^{13}C NMR)



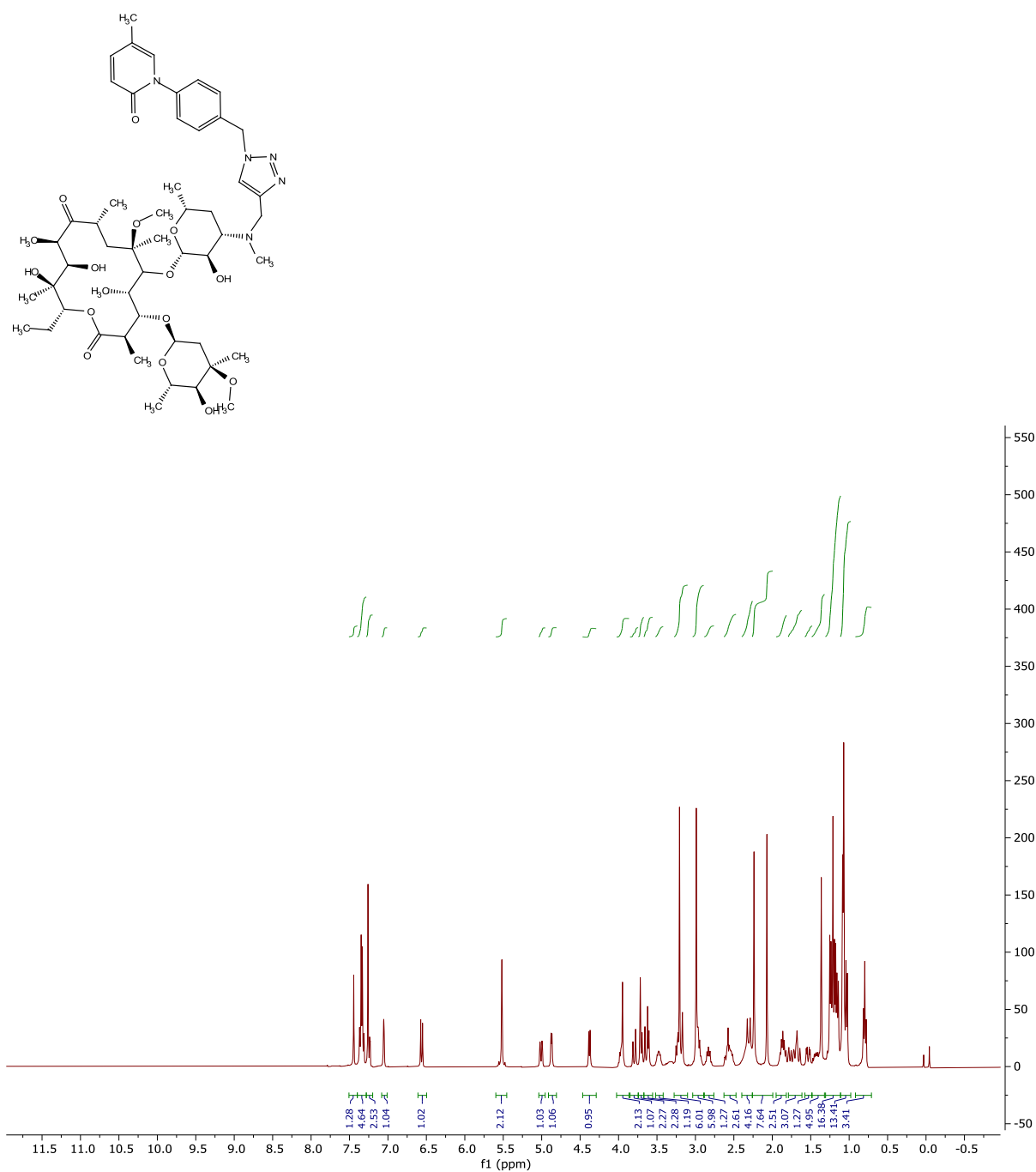
11c (^1H NMR)



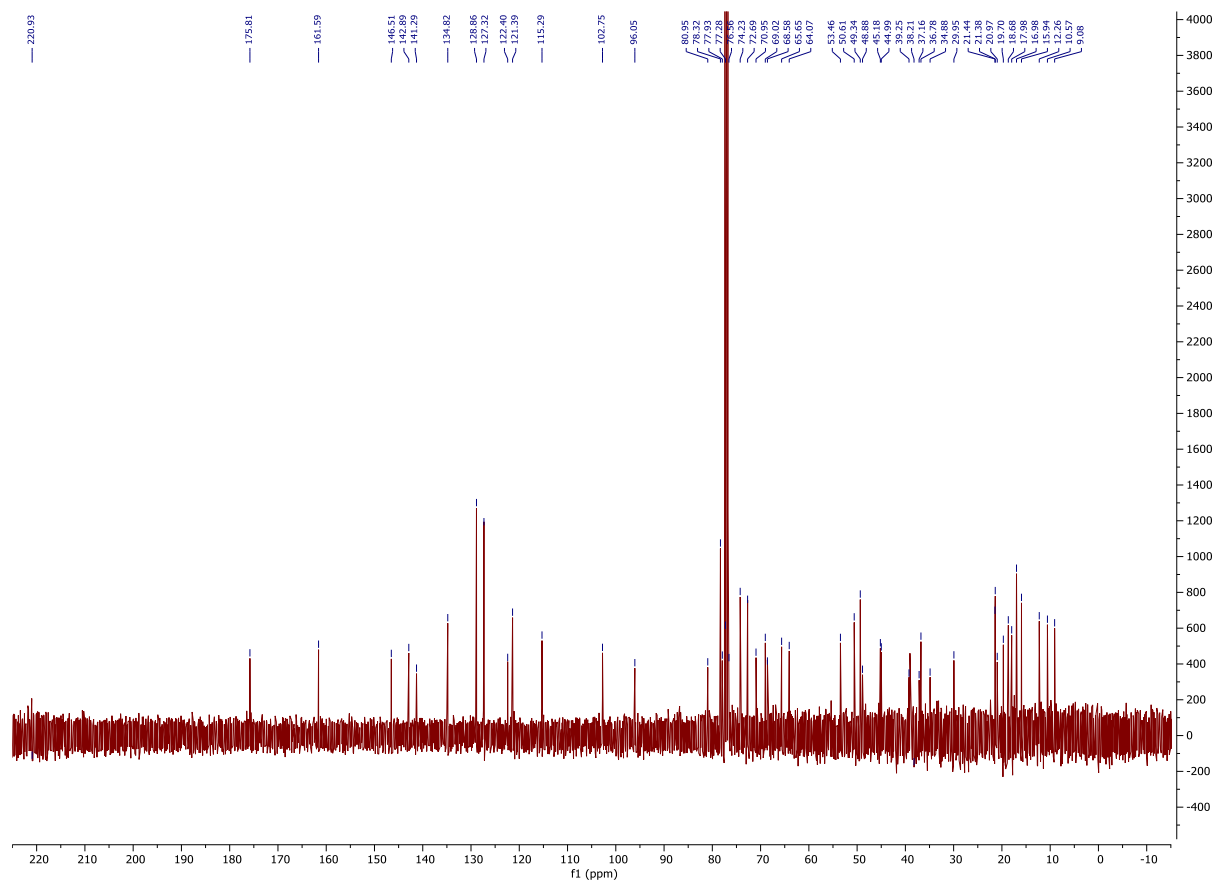
11c (^{13}C NMR)



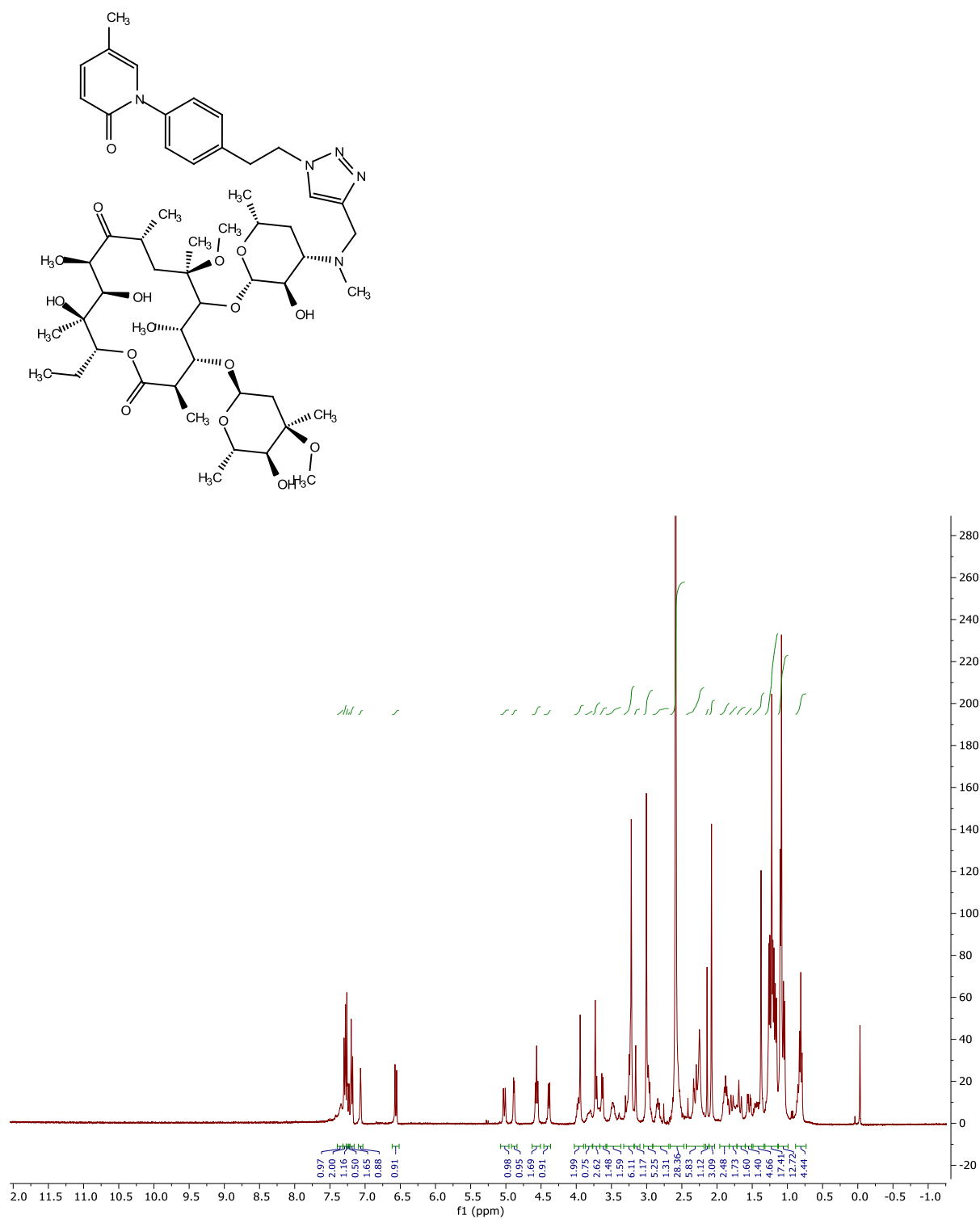
12a (^1H NMR)



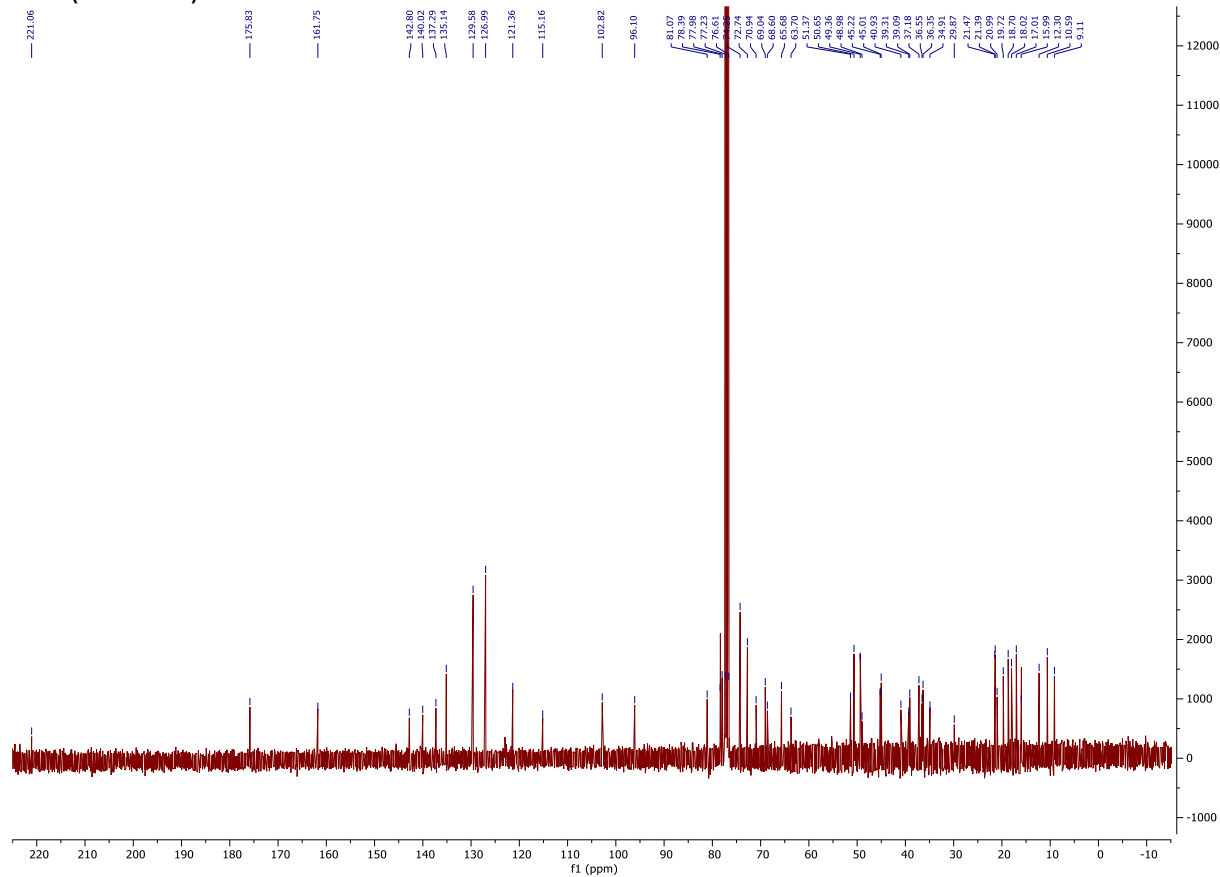
12a (¹³C NMR)



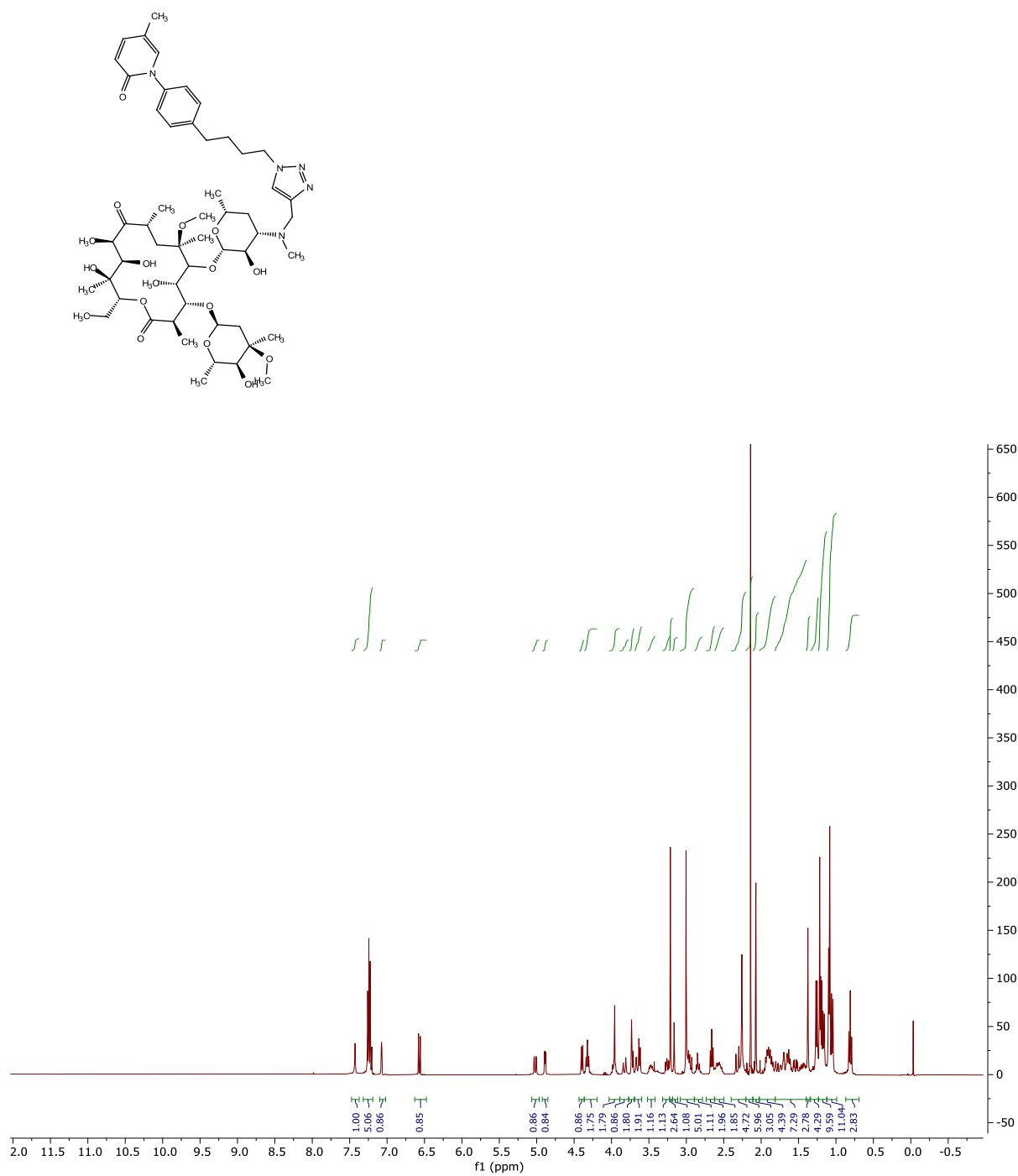
12b (^1H NMR)



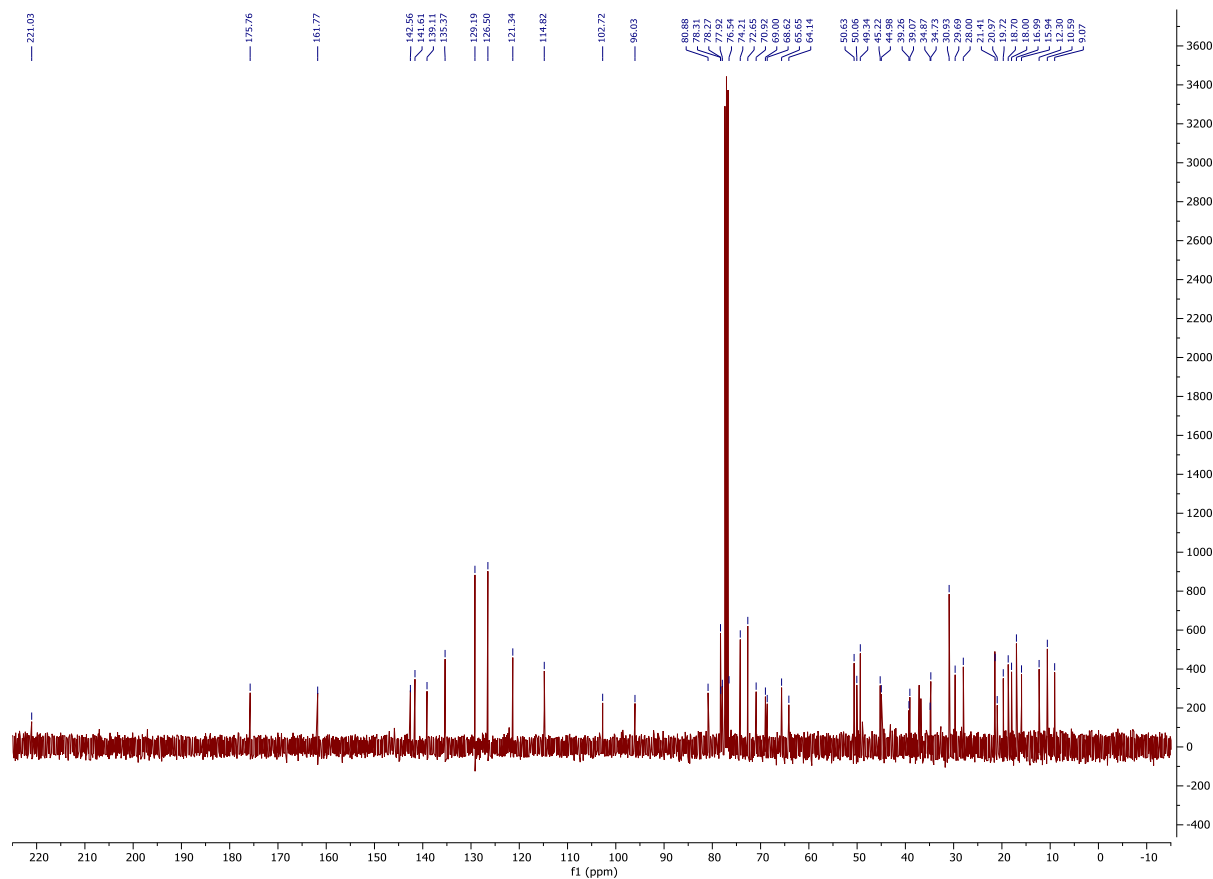
12b (^{13}C NMR)



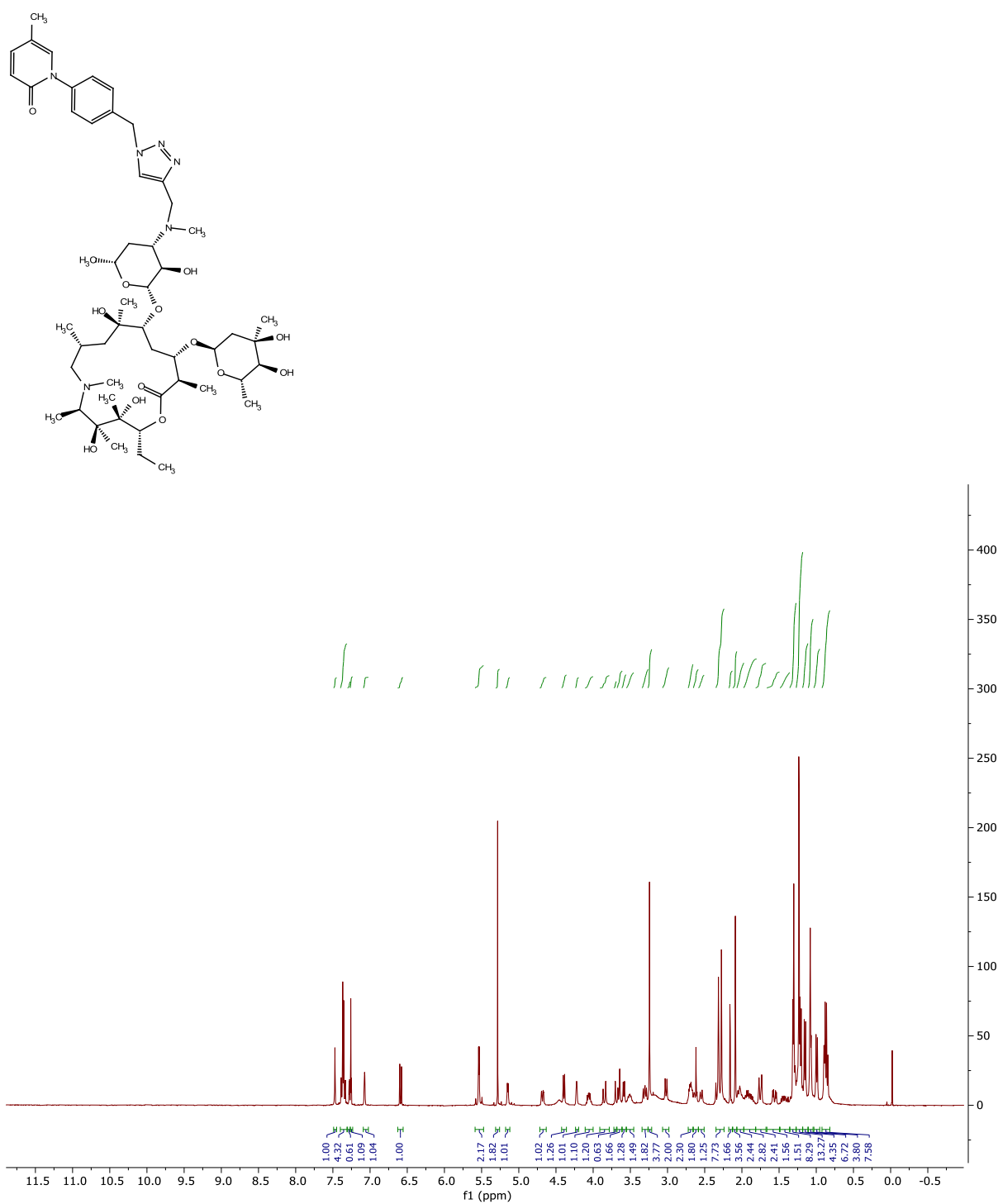
12c (^1H NMR)



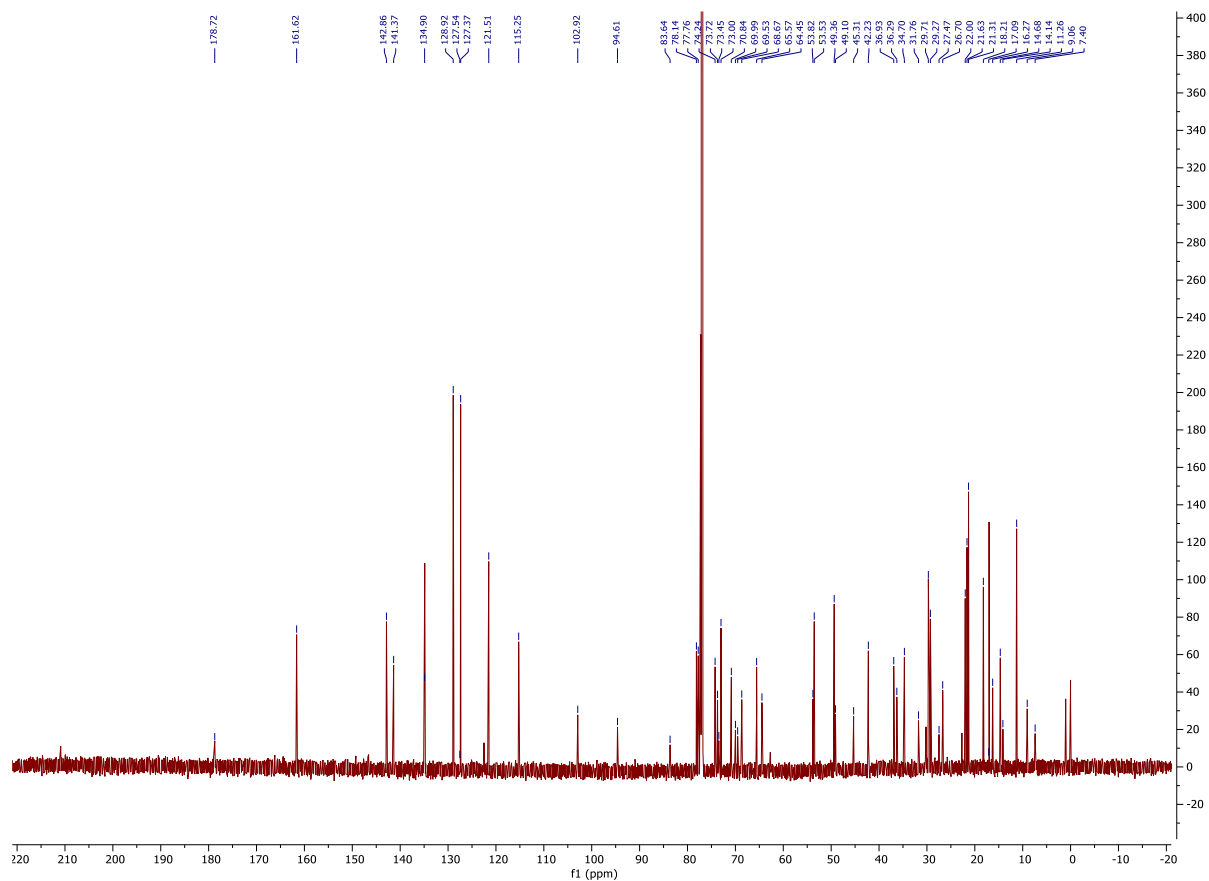
12c (¹³C NMR)



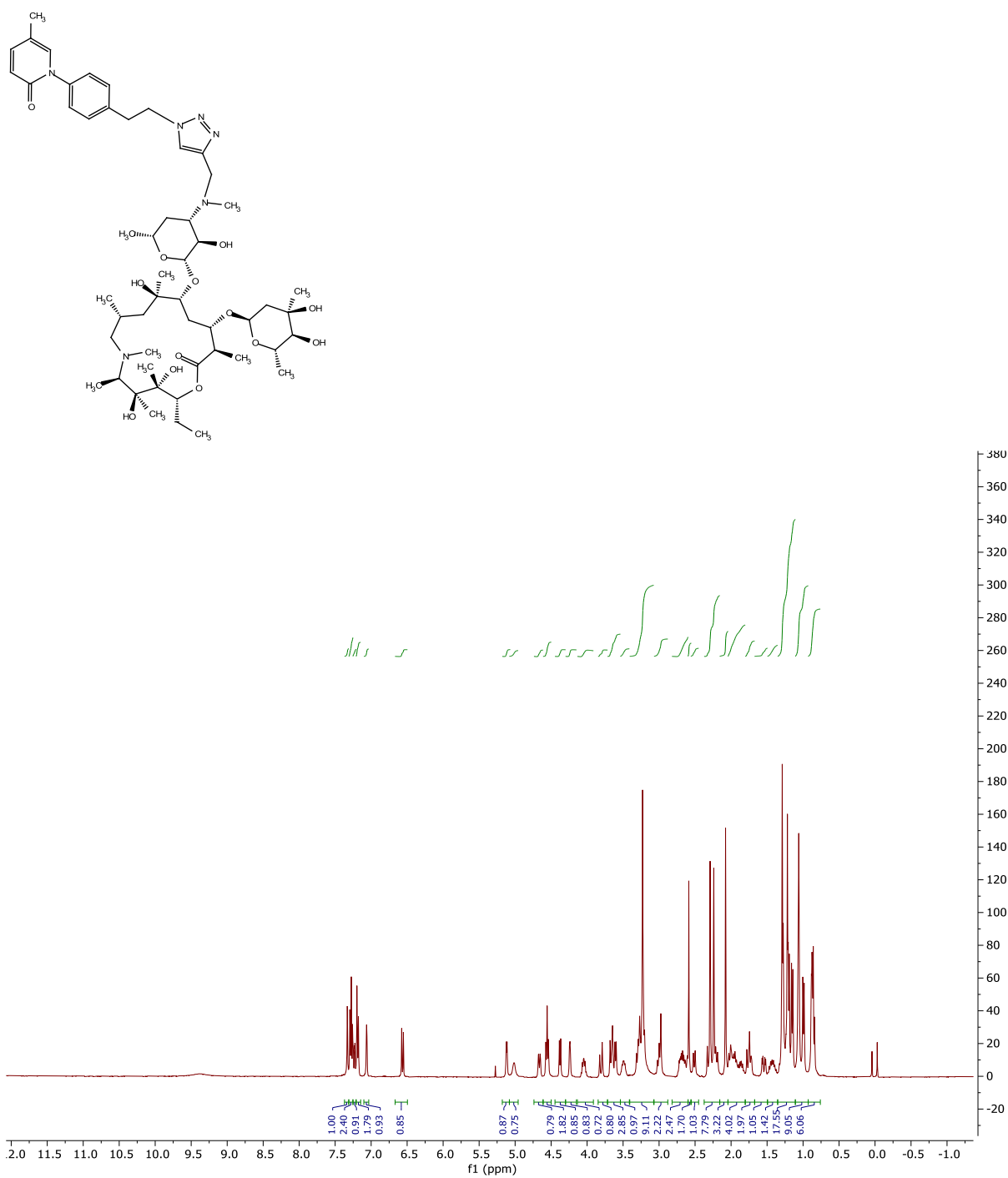
13a (^1H NMR)



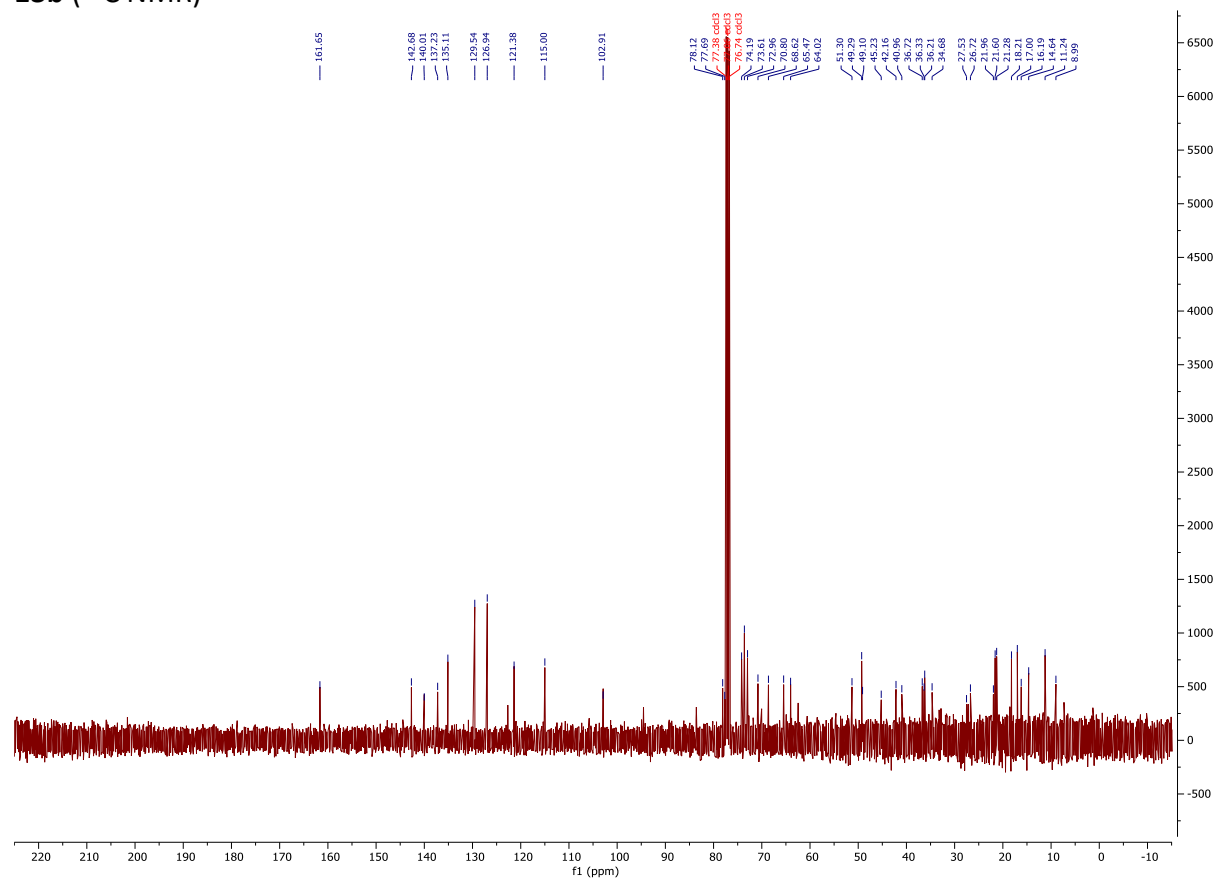
13a (^{13}C NMR)



13b (^1H NMR)

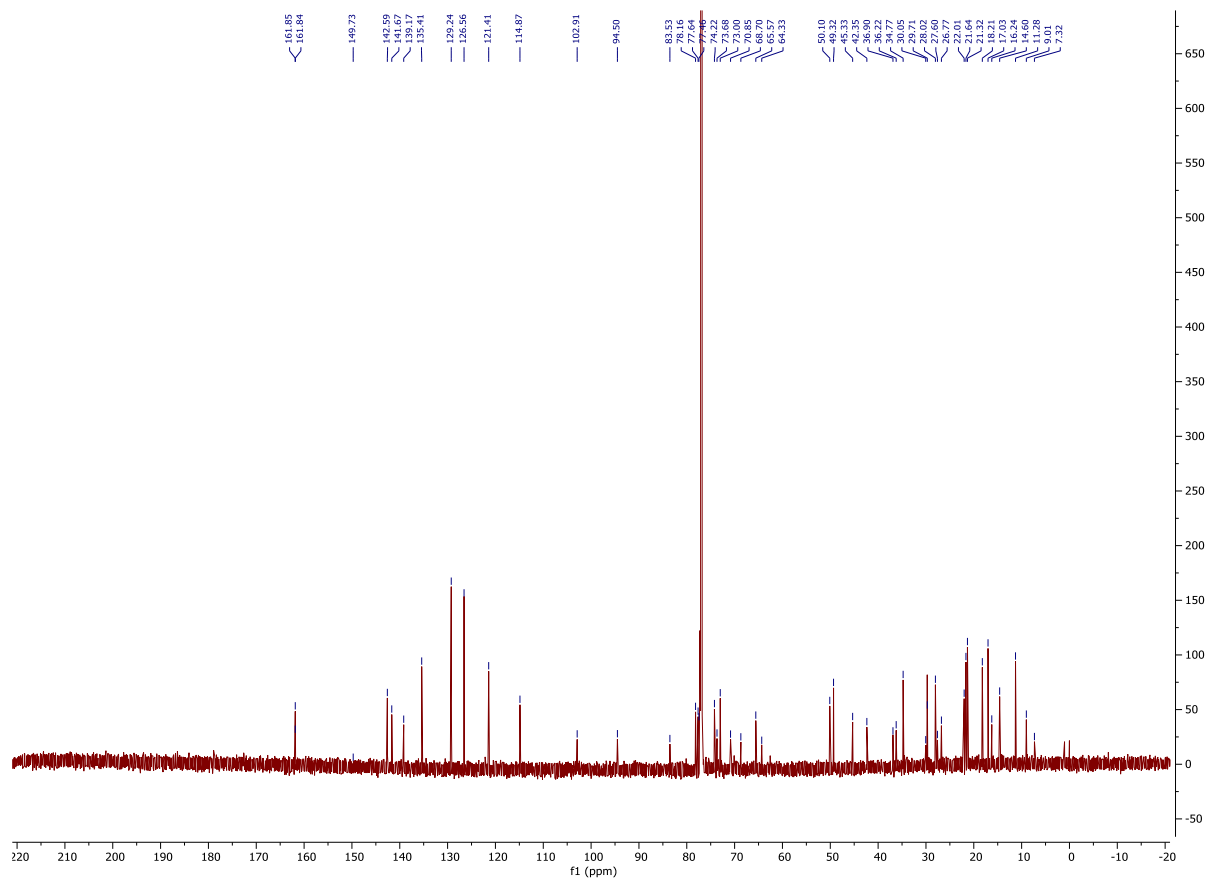


13b (^{13}C NMR)

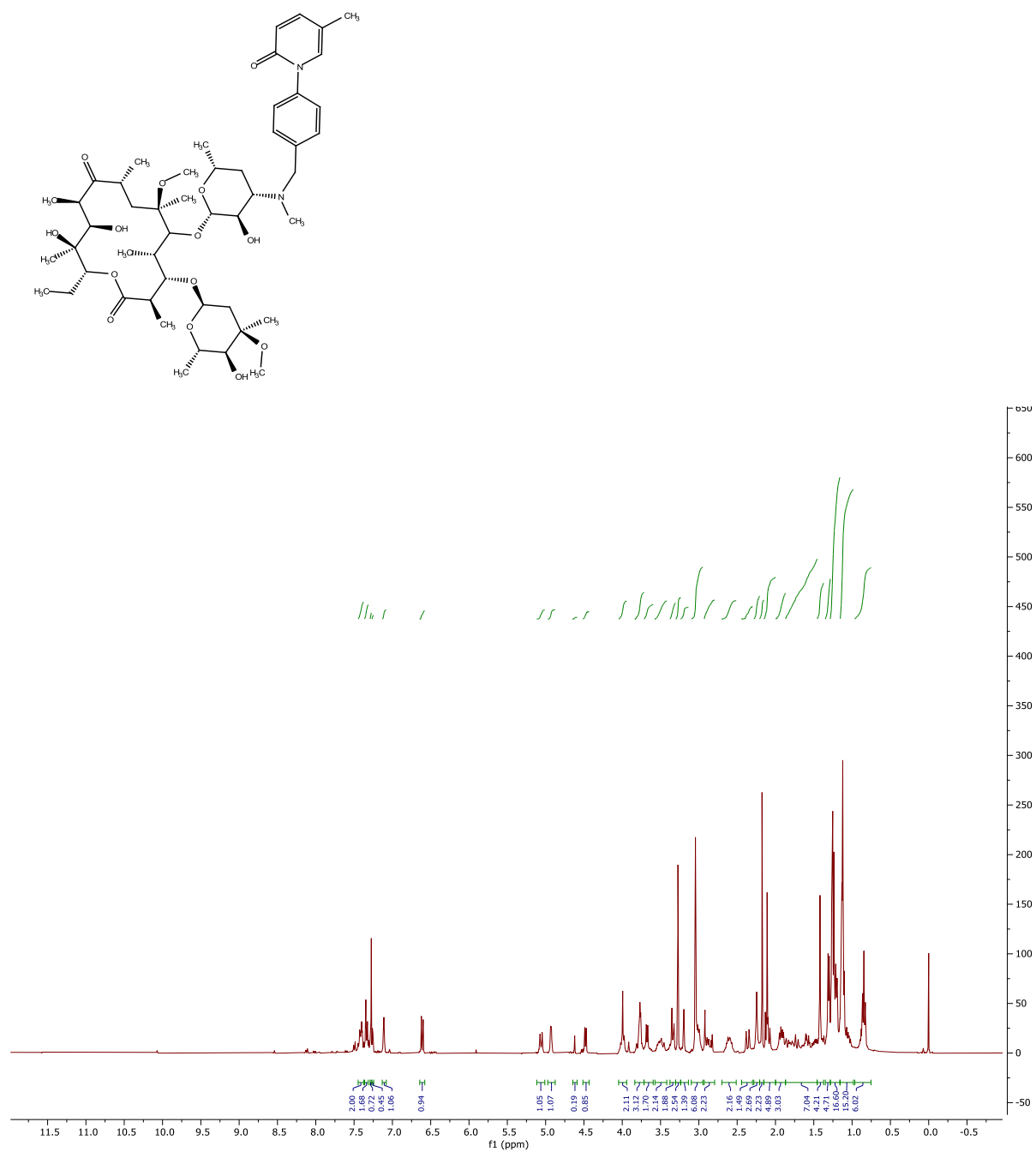




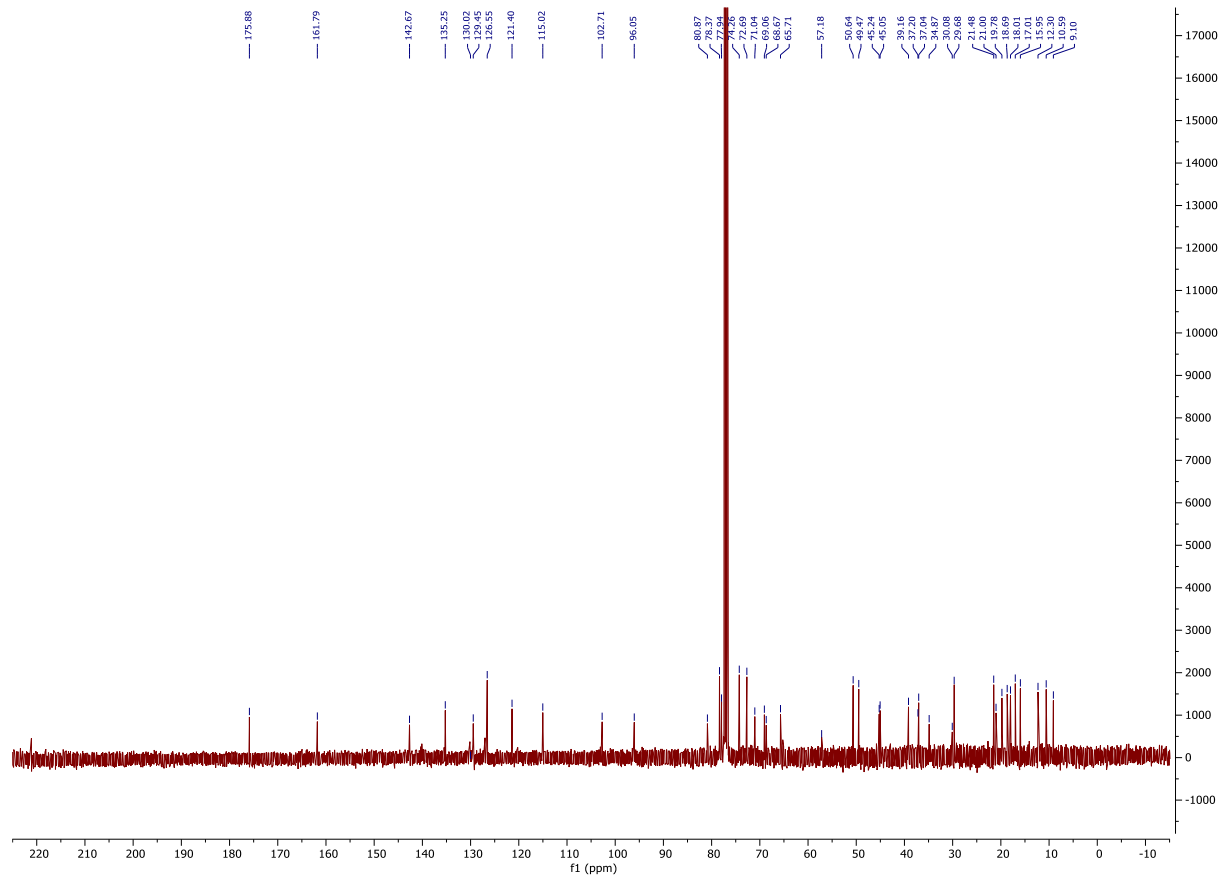
13c (¹³C NMR)



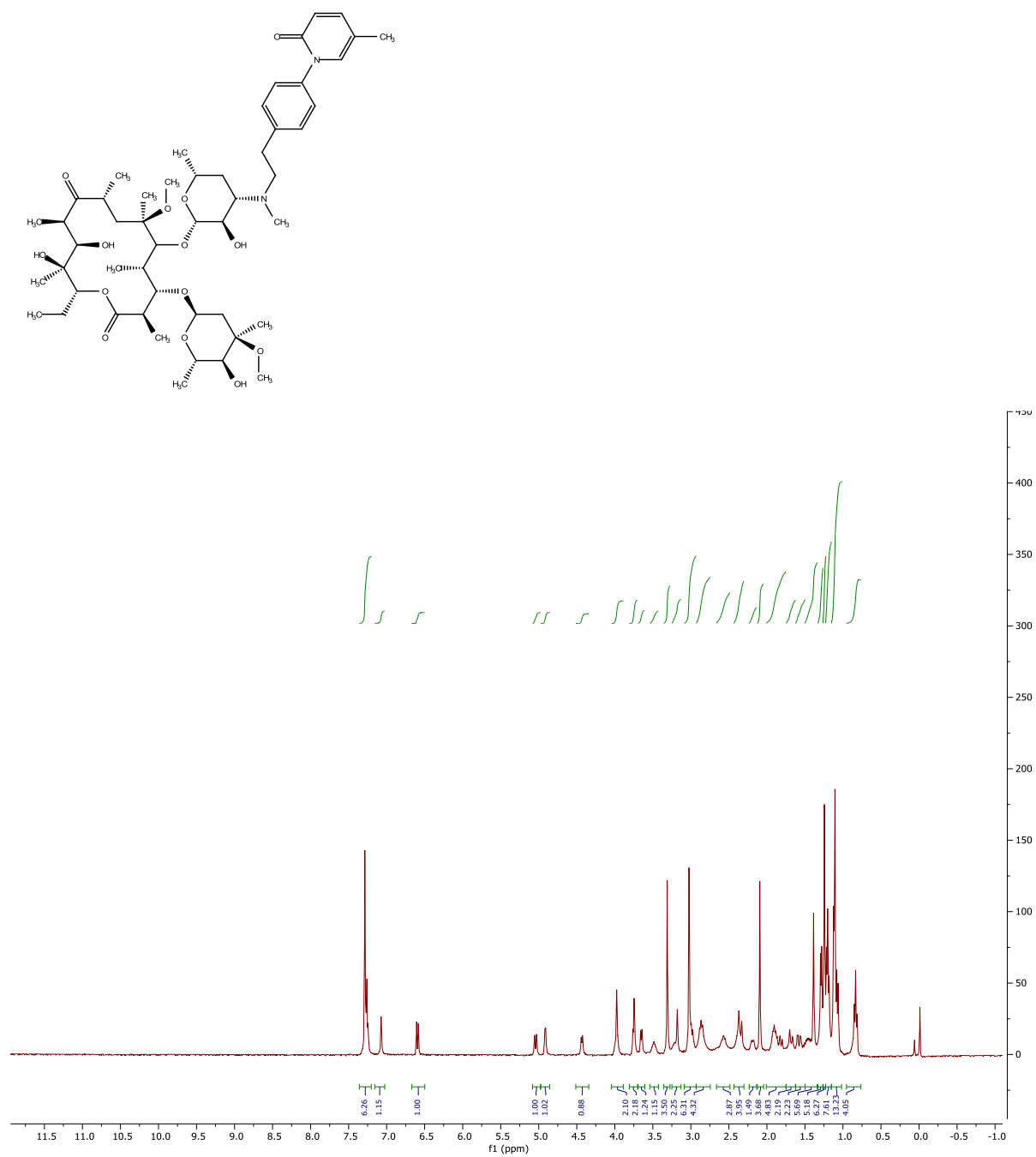
14a (¹H NMR)



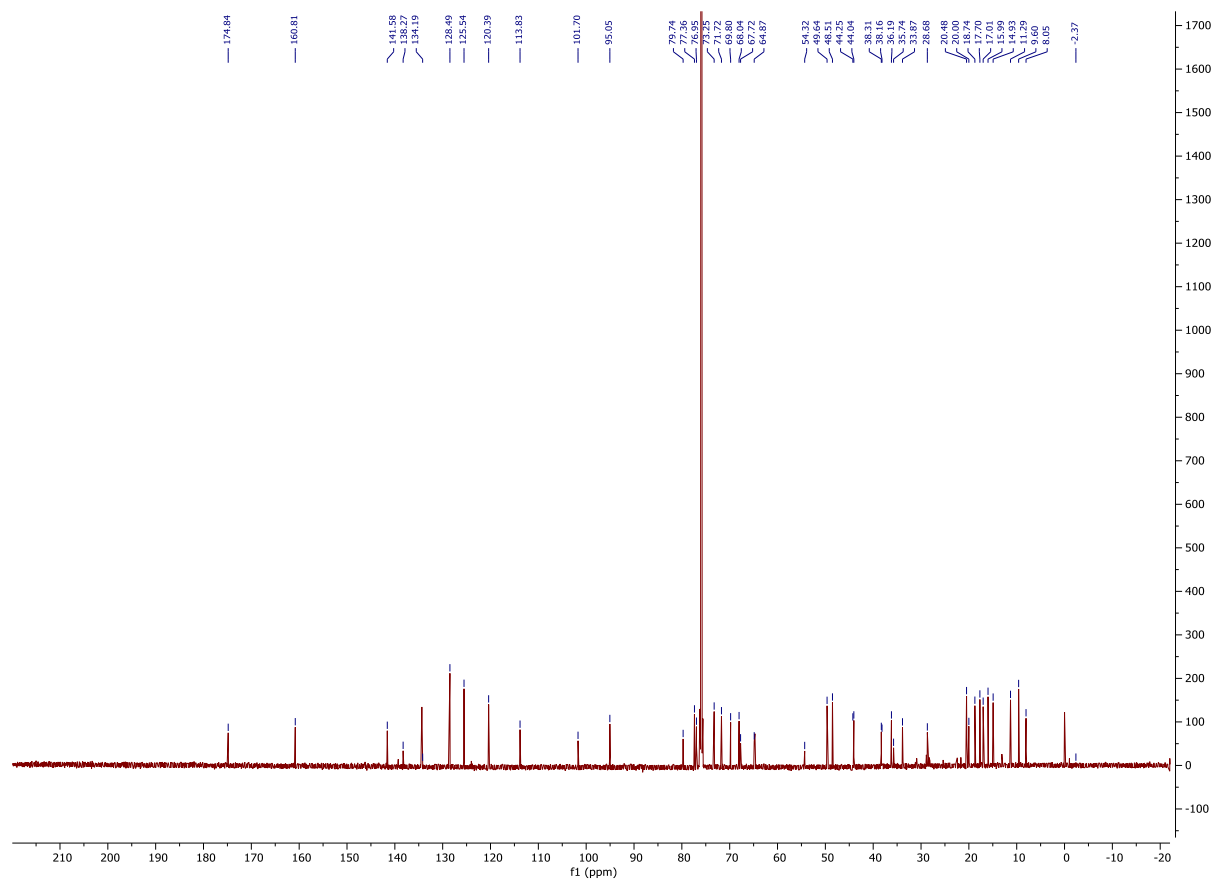
14a (^{13}C NMR)



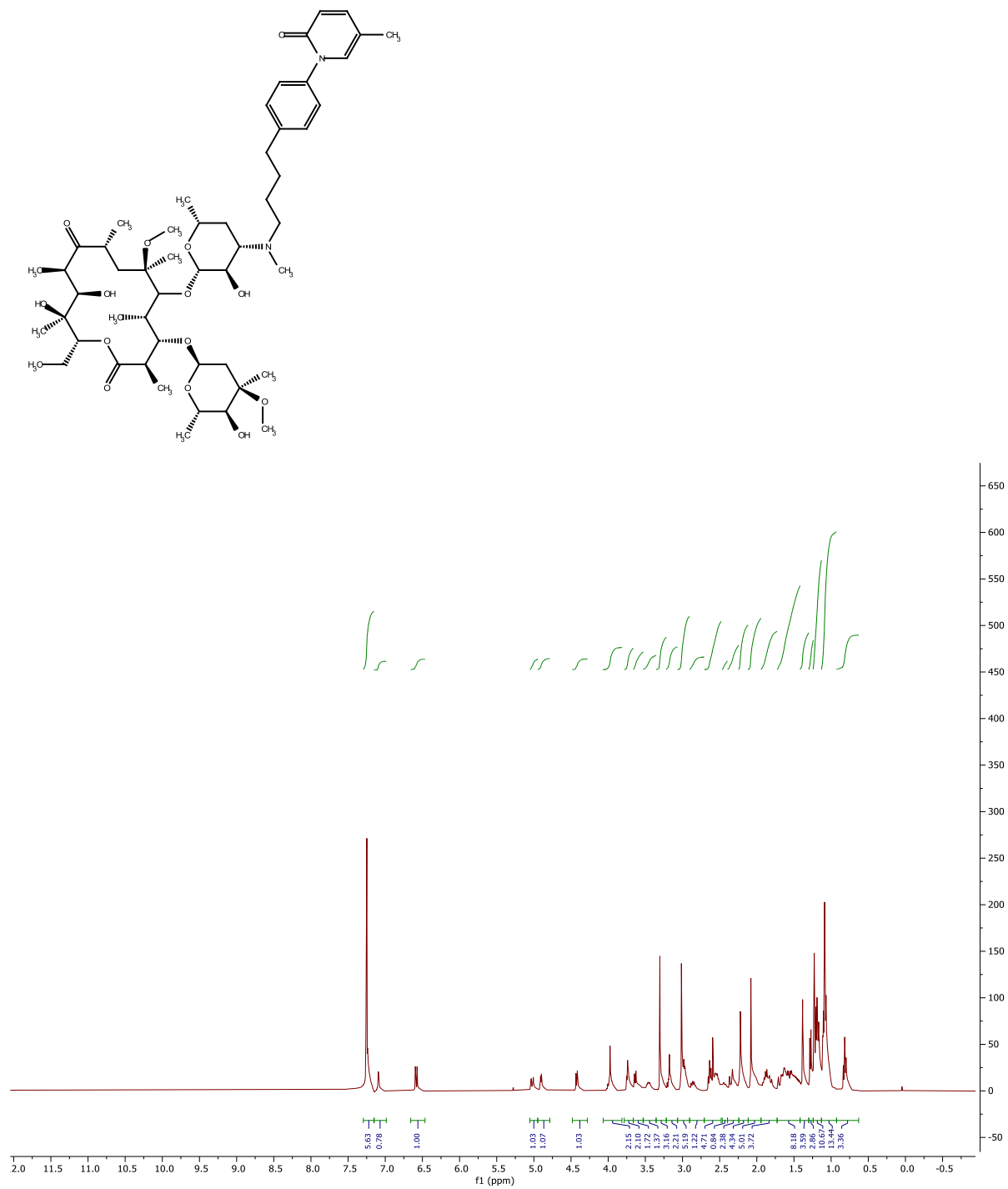
14b (^1H NMR)



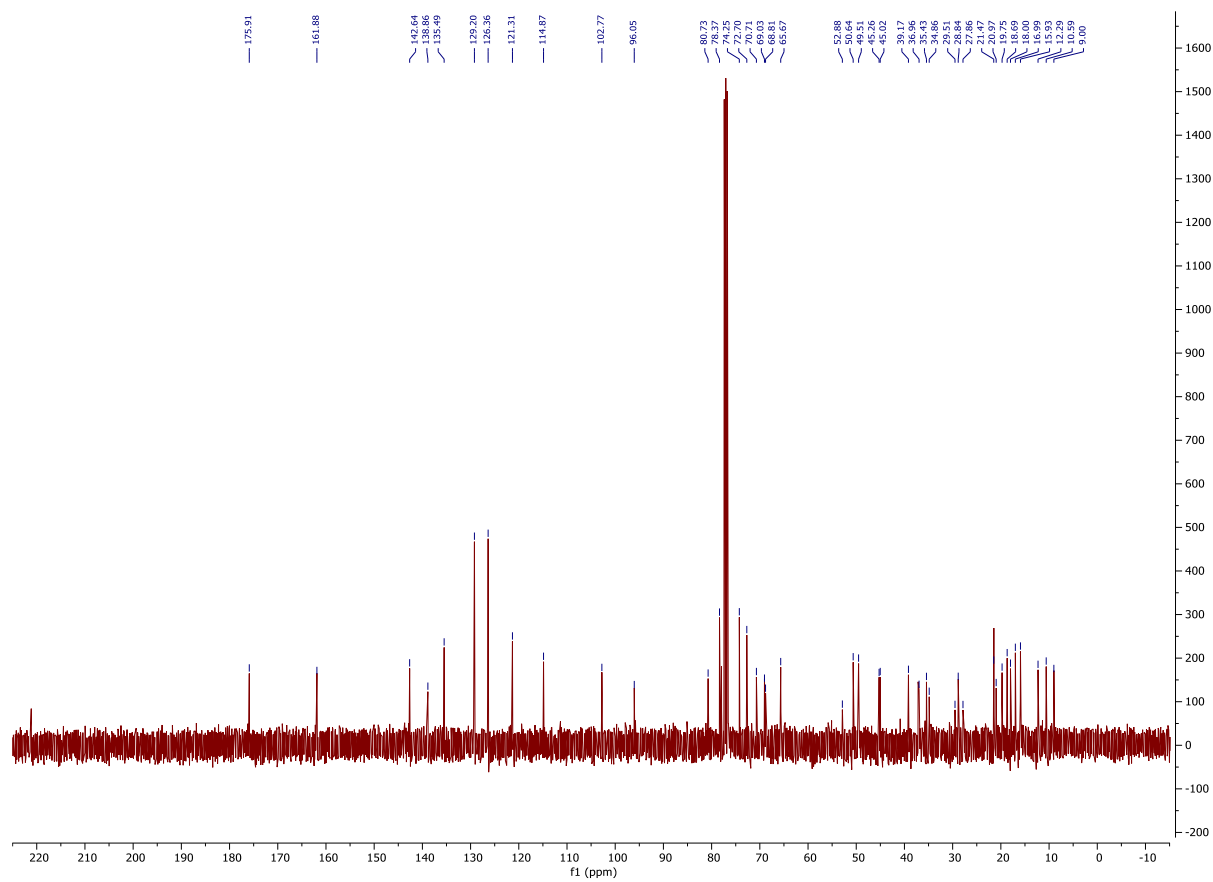
14b (^{13}C NMR)



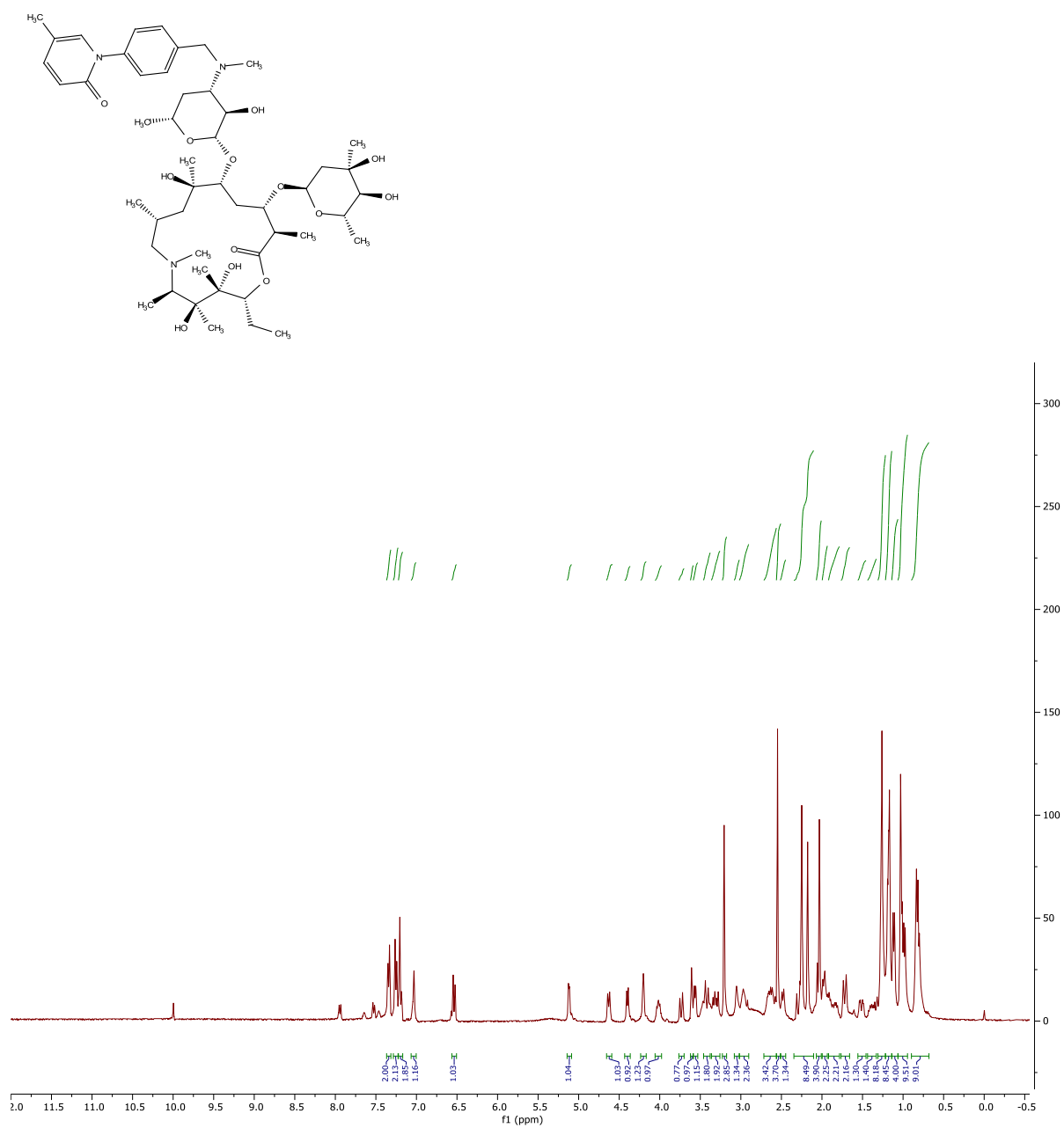
14c (¹H NMR)



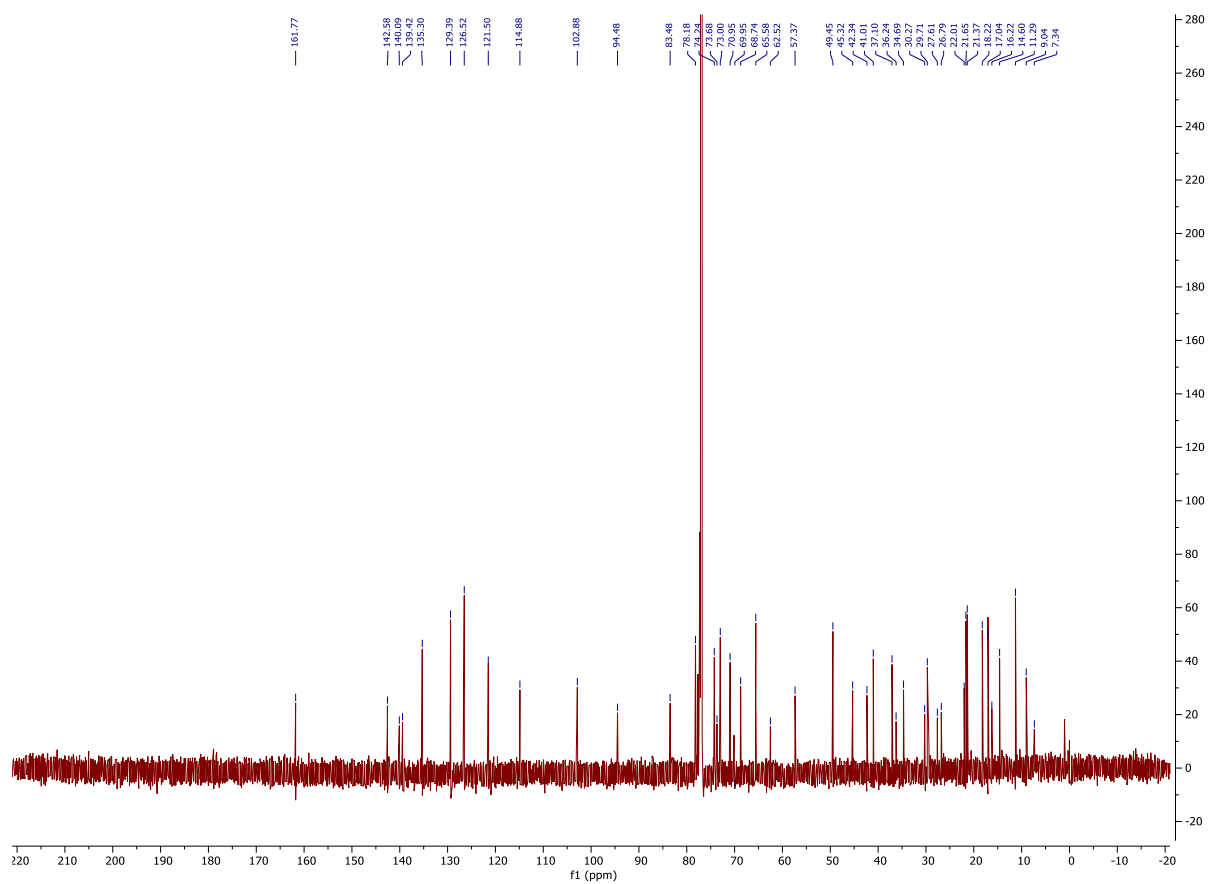
14c (^{13}C NMR)



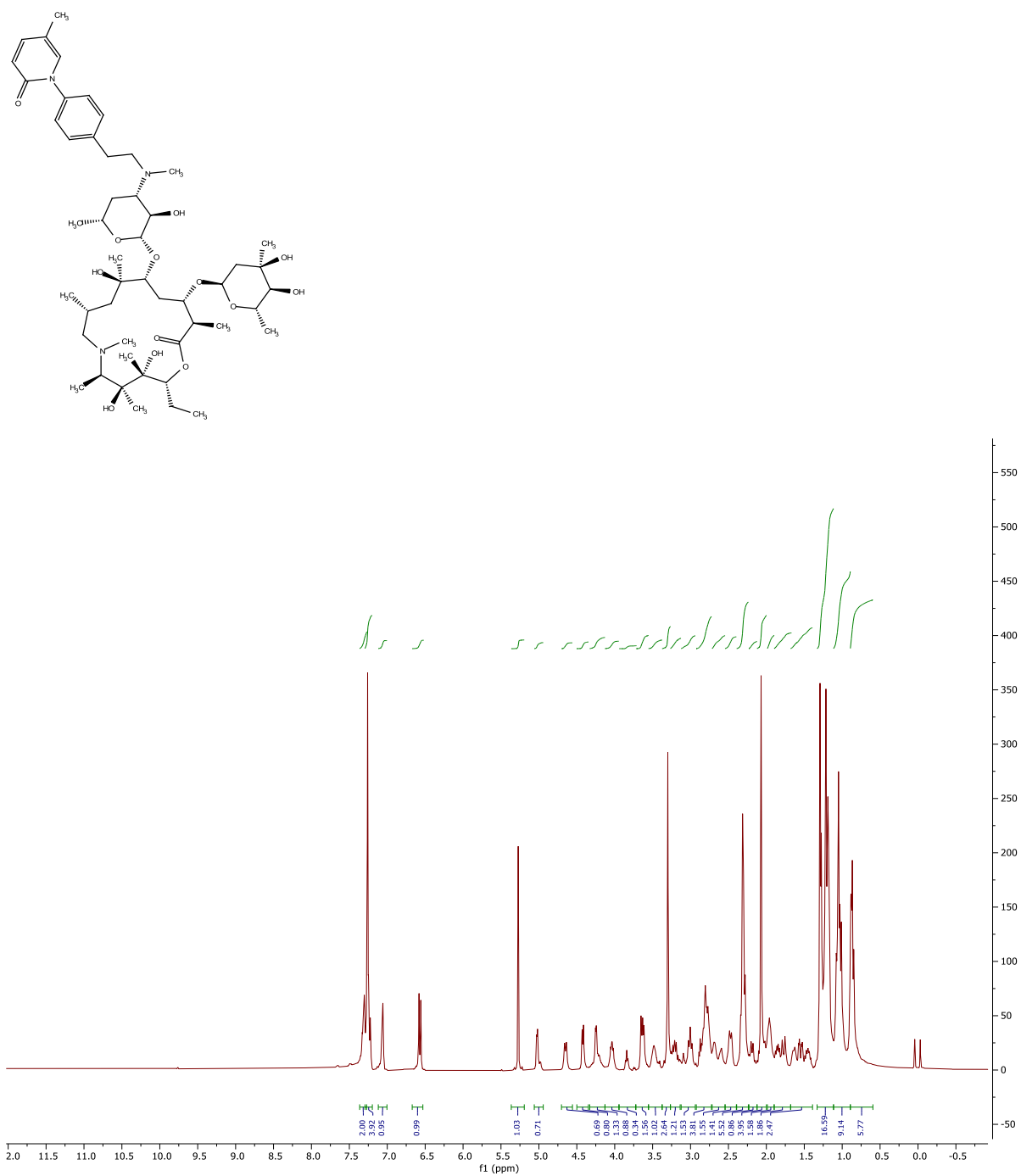
15a (^1H NMR)



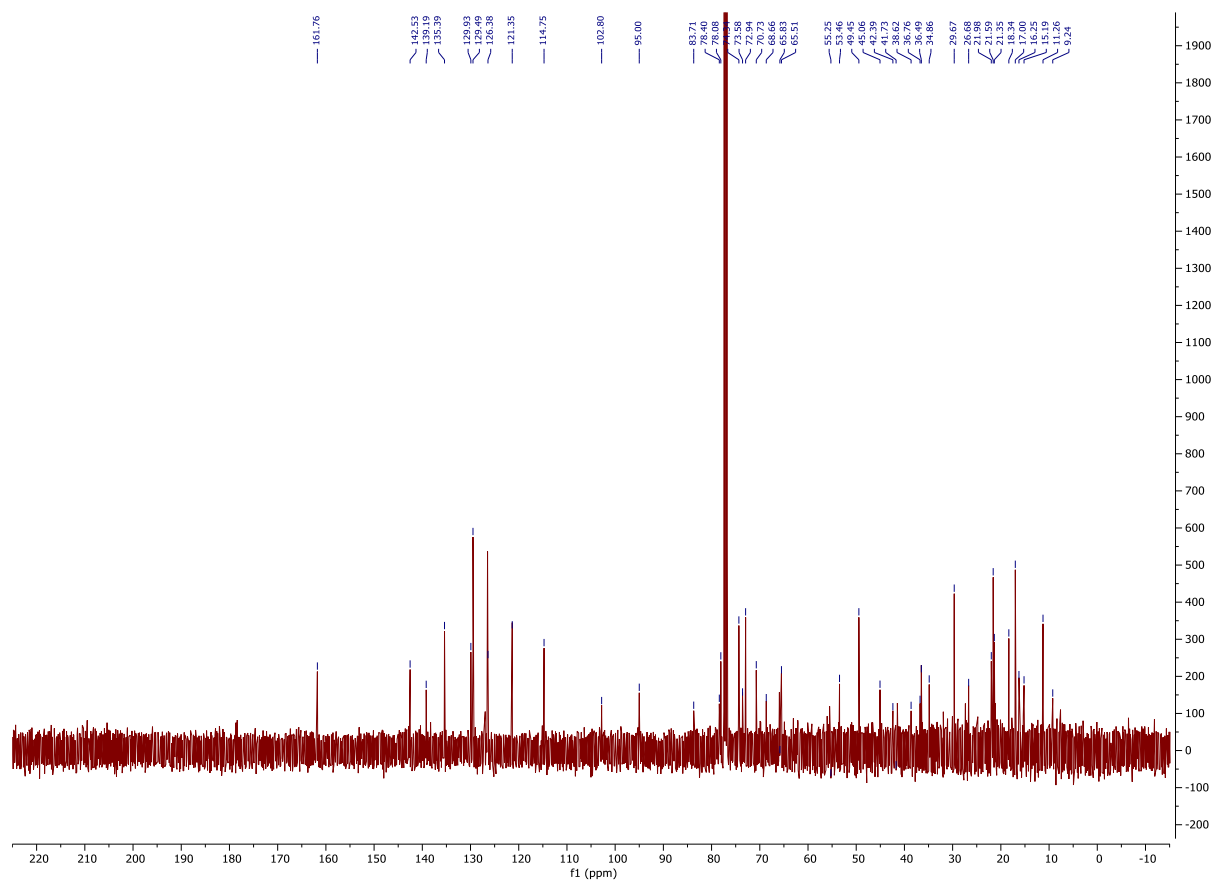
15a (^{13}C NMR)



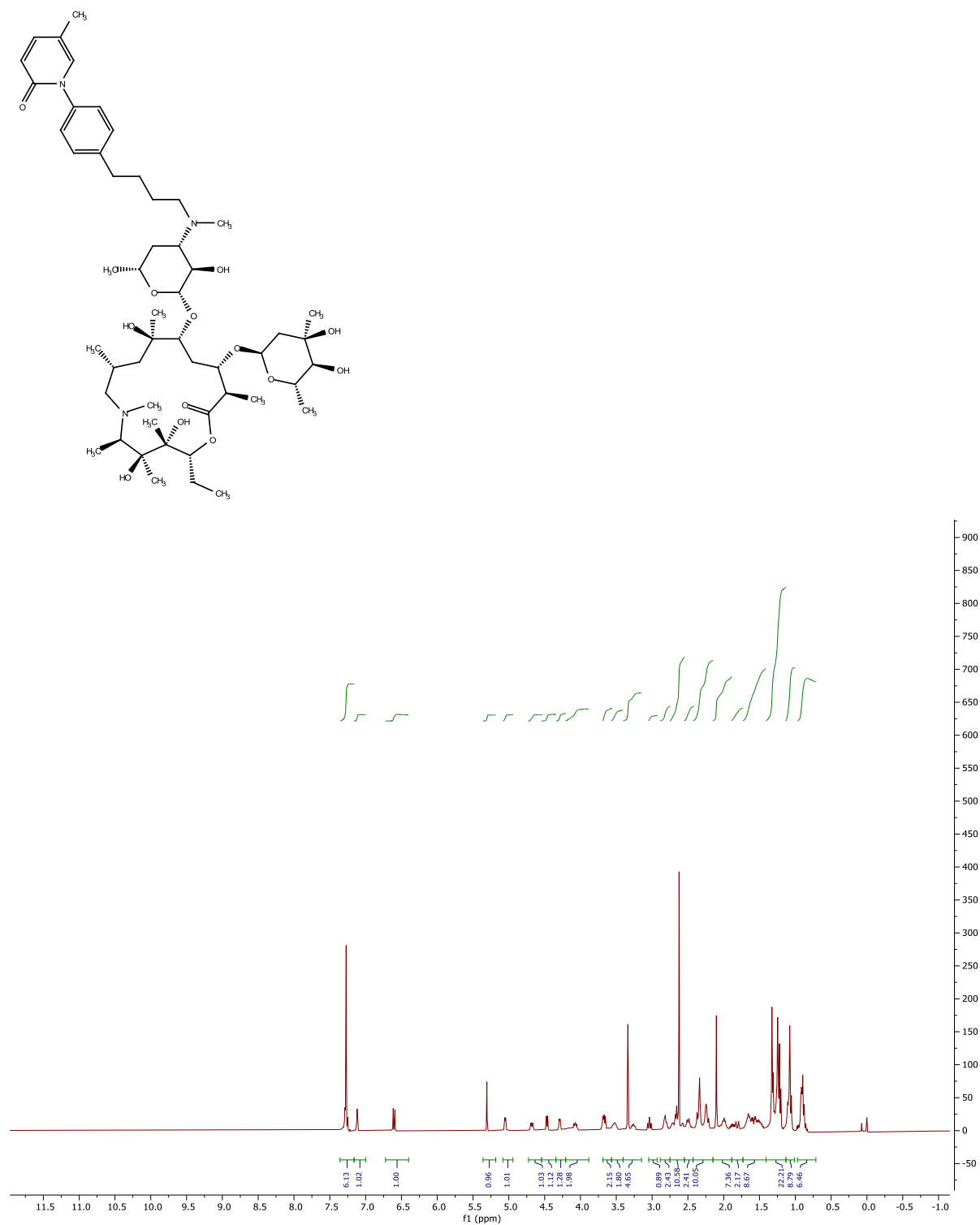
15b (^1H NMR)



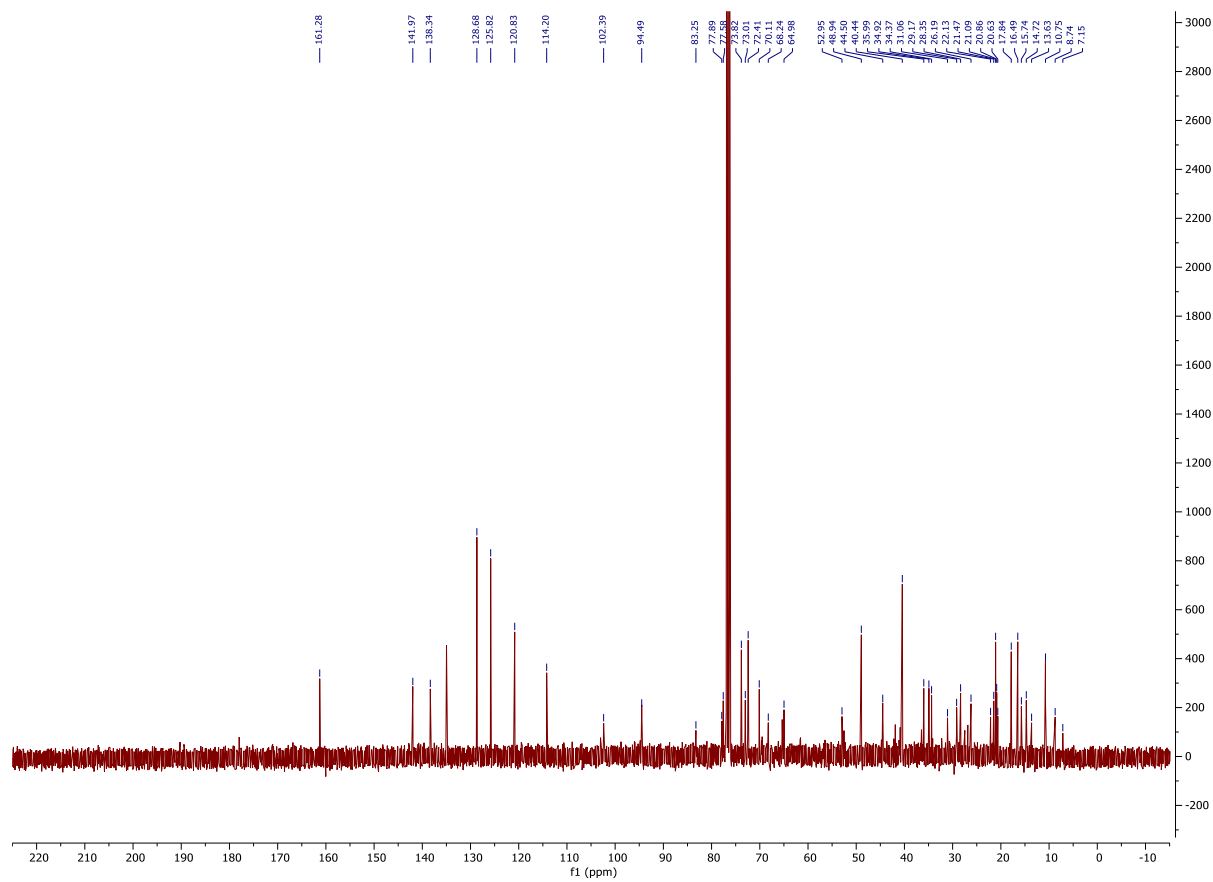
15b (^{13}C NMR)



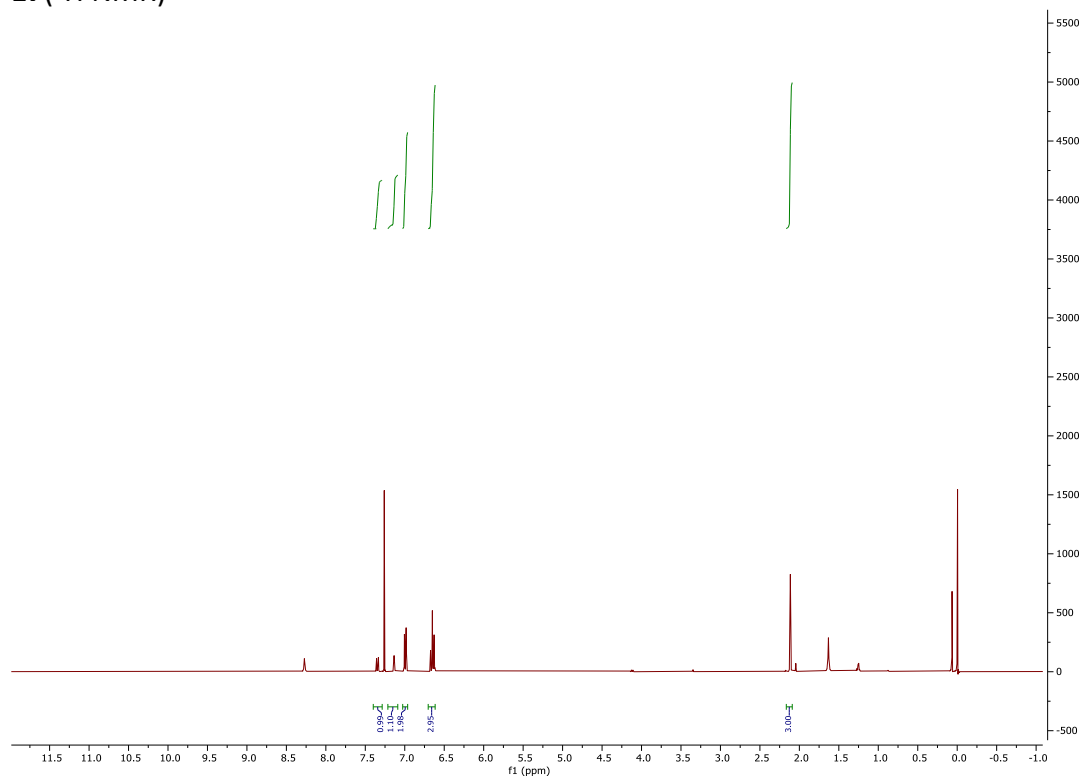
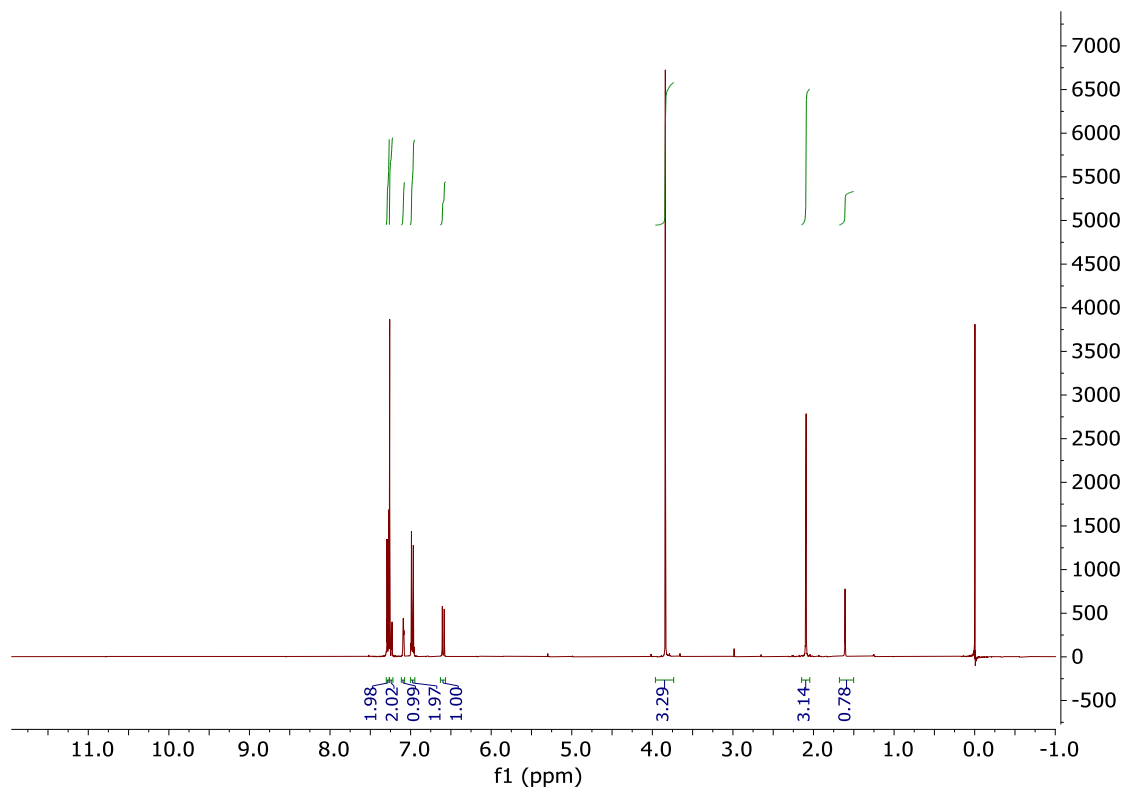
15c (^1H NMR)

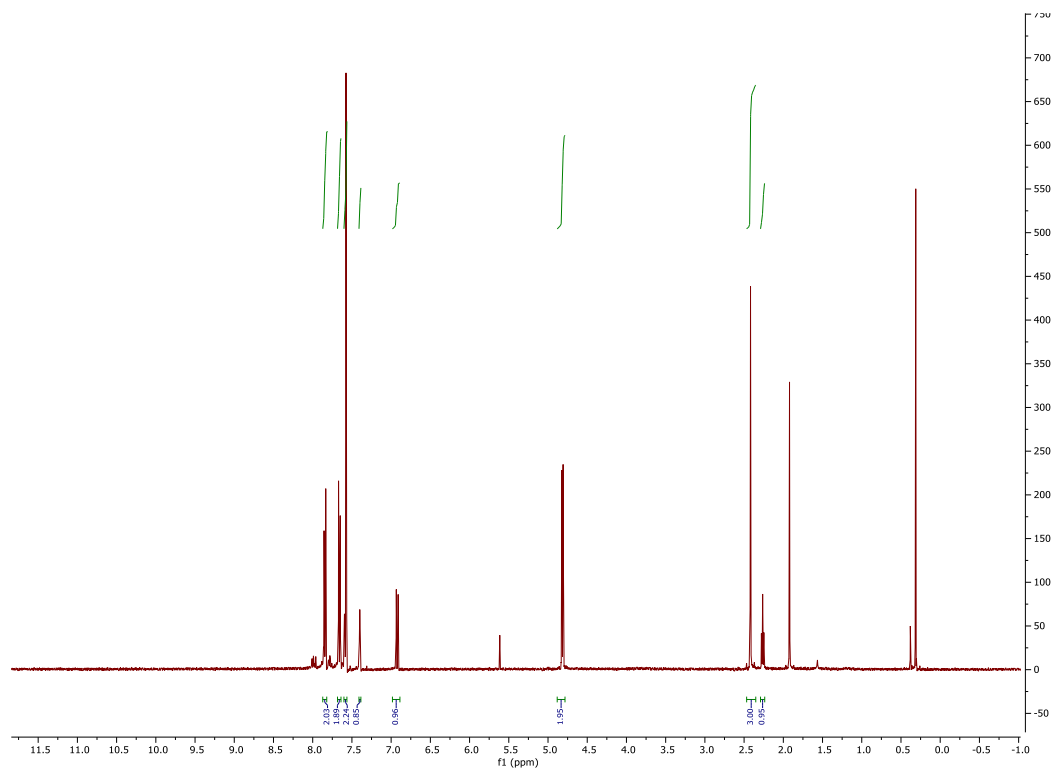


15c (^{13}C NMR)

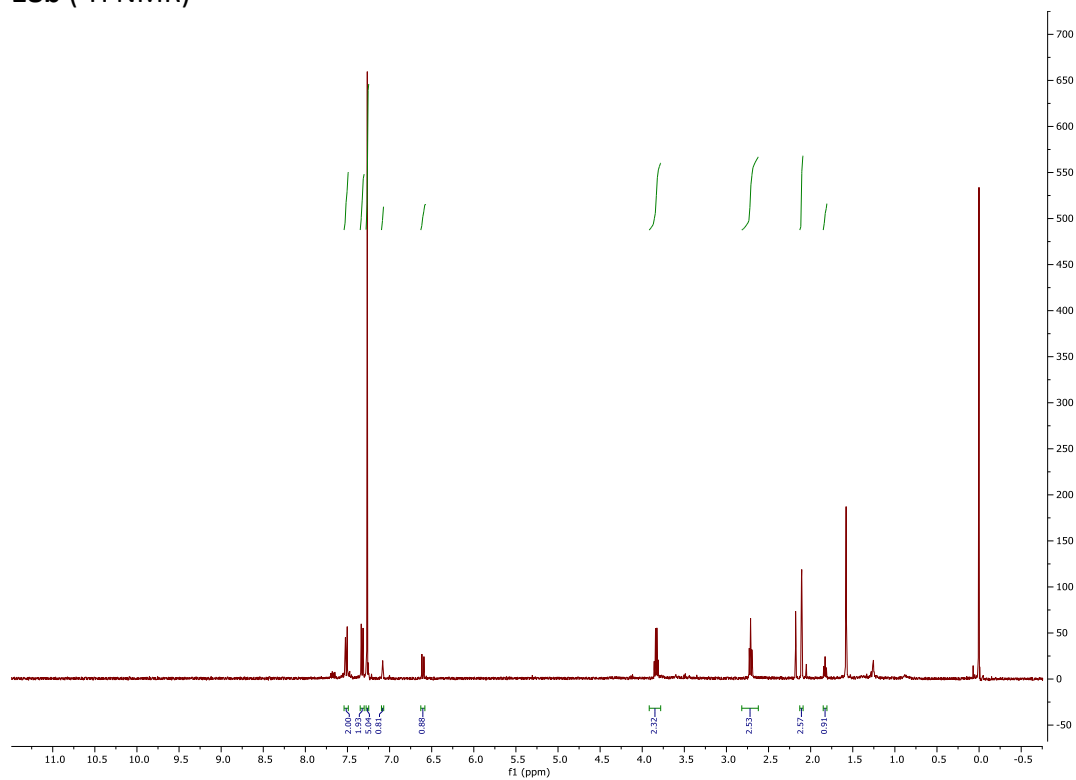


16 (^1H NMR)

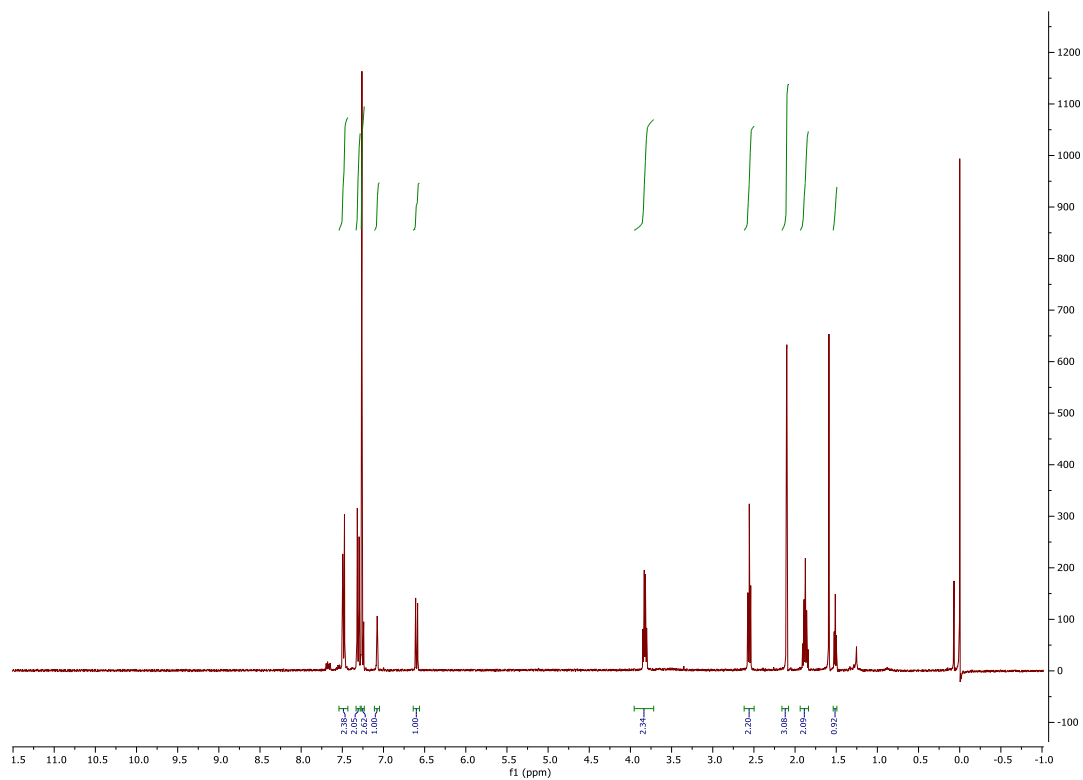




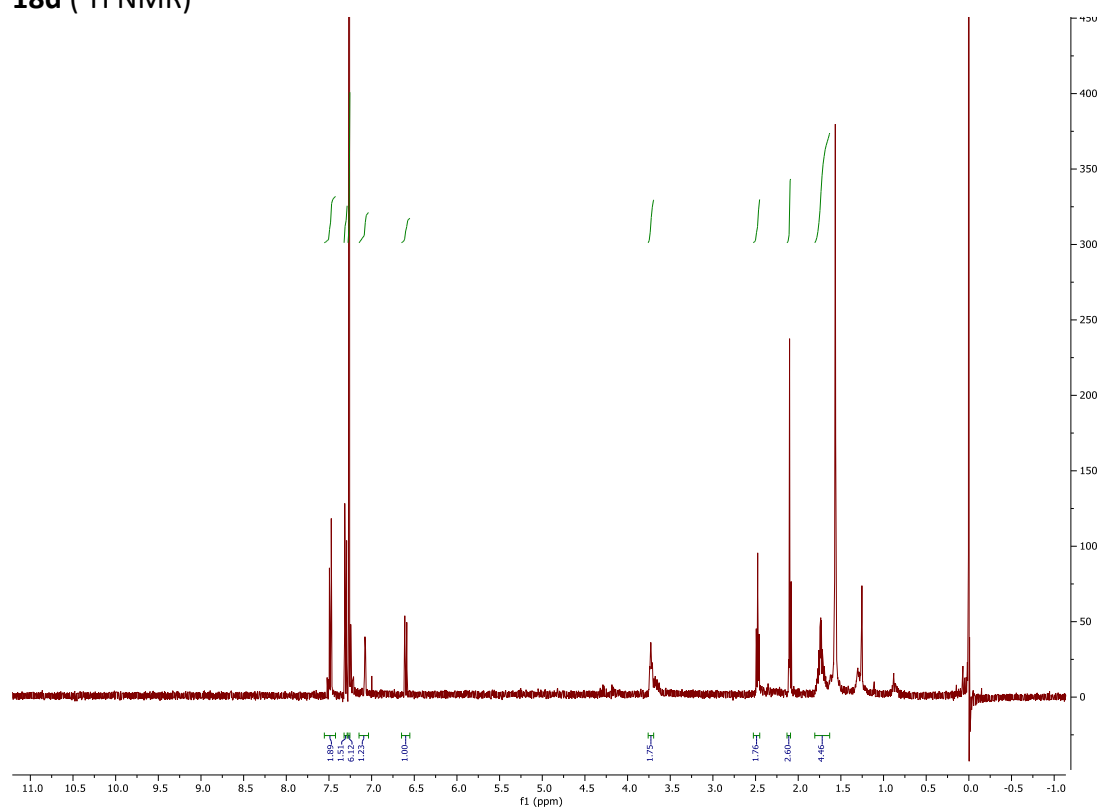
18b (^1H NMR)



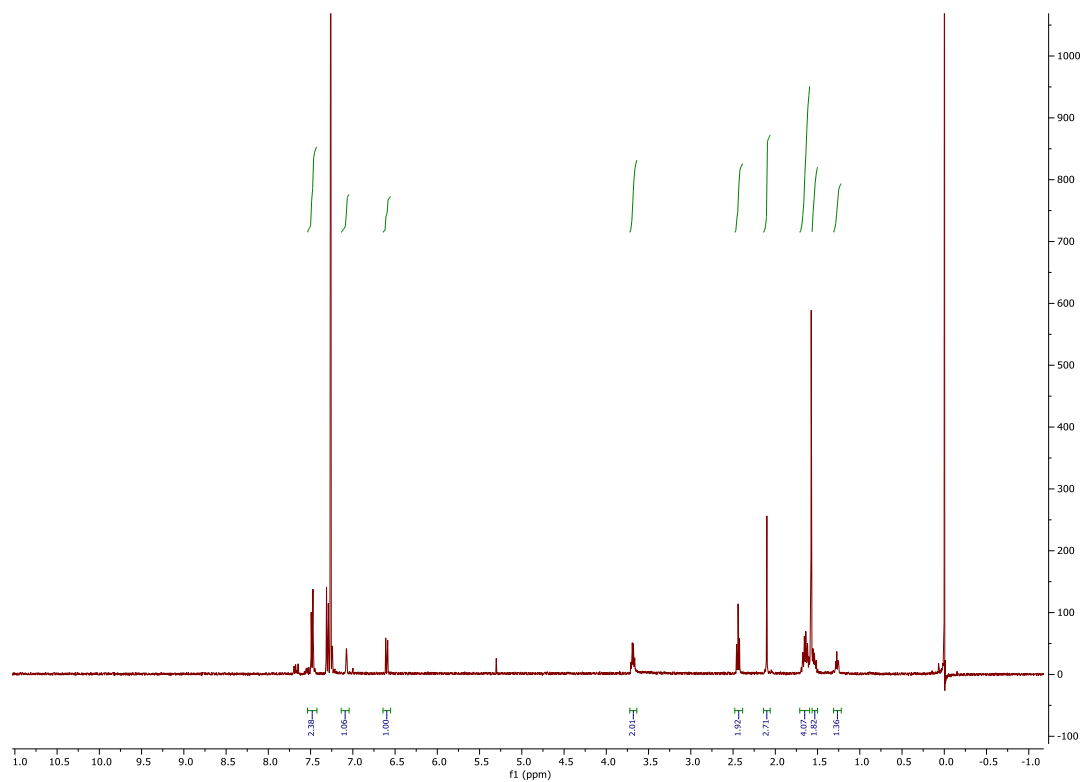
18c (^1H NMR)



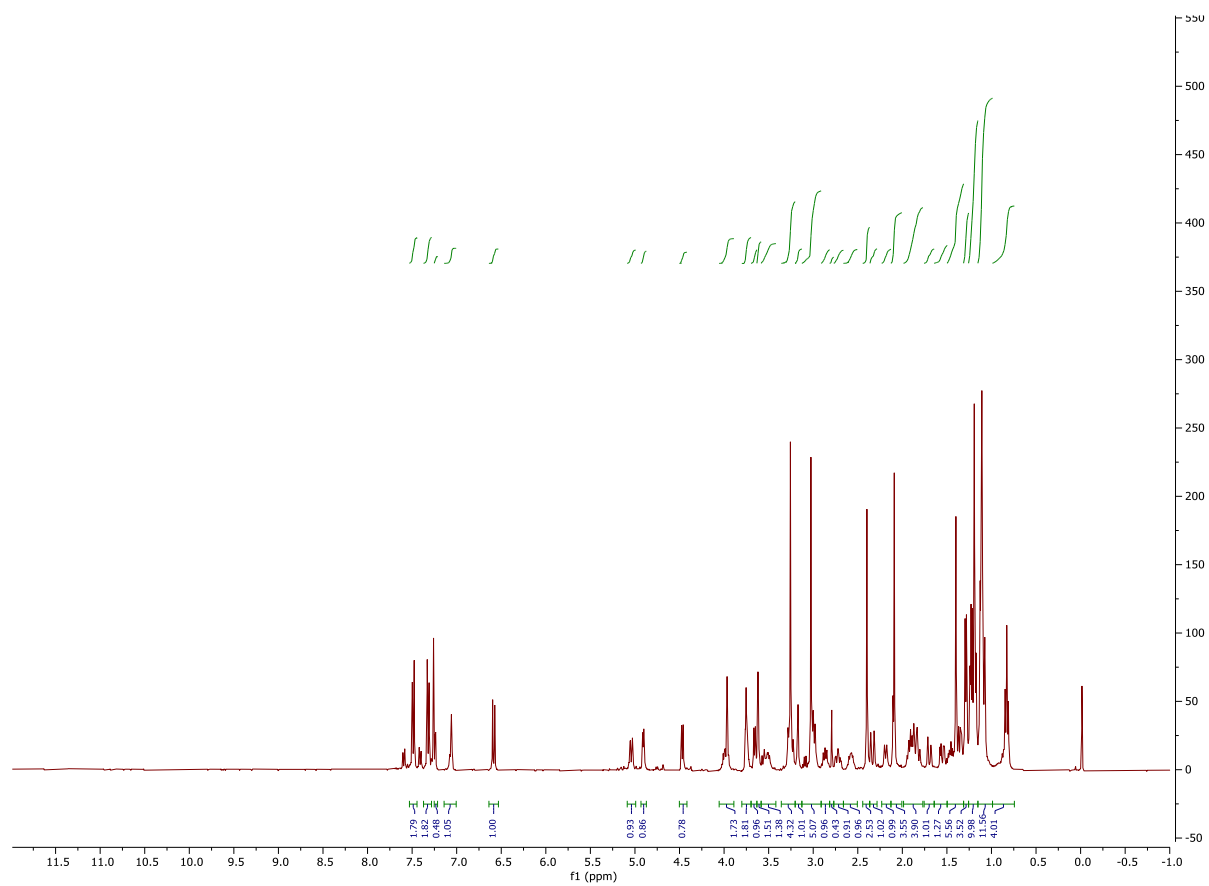
18d (^1H NMR)



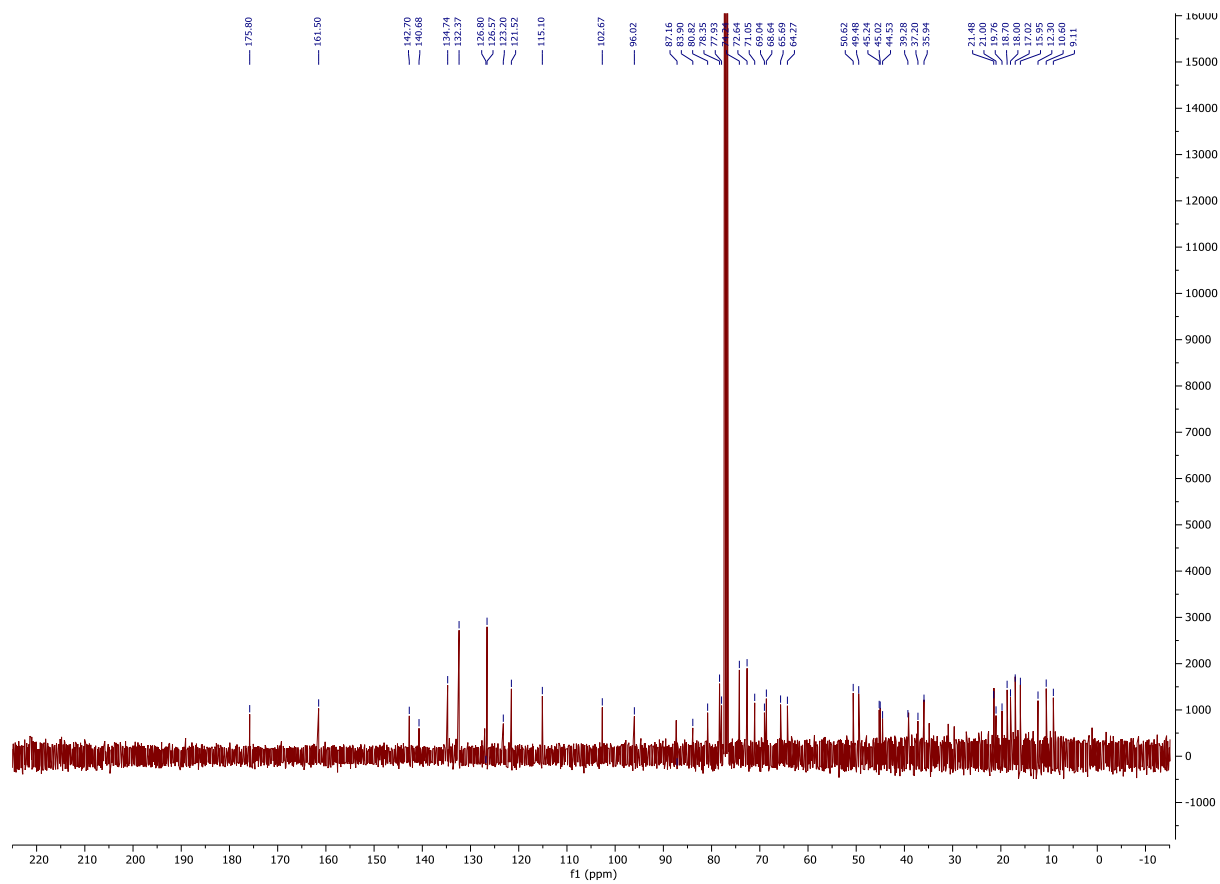
18e (^1H NMR)



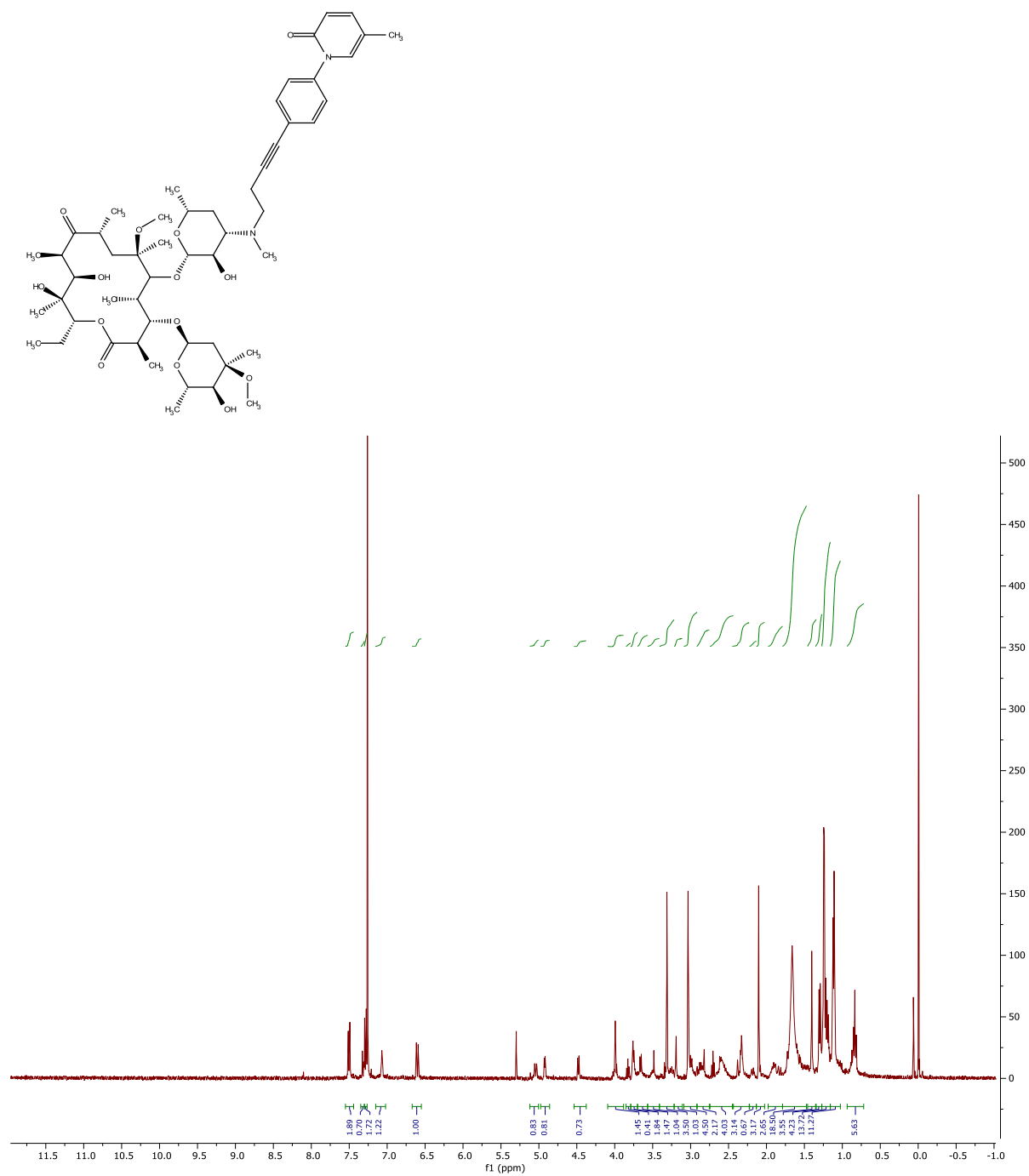
19a (¹H NMR)



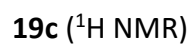
206

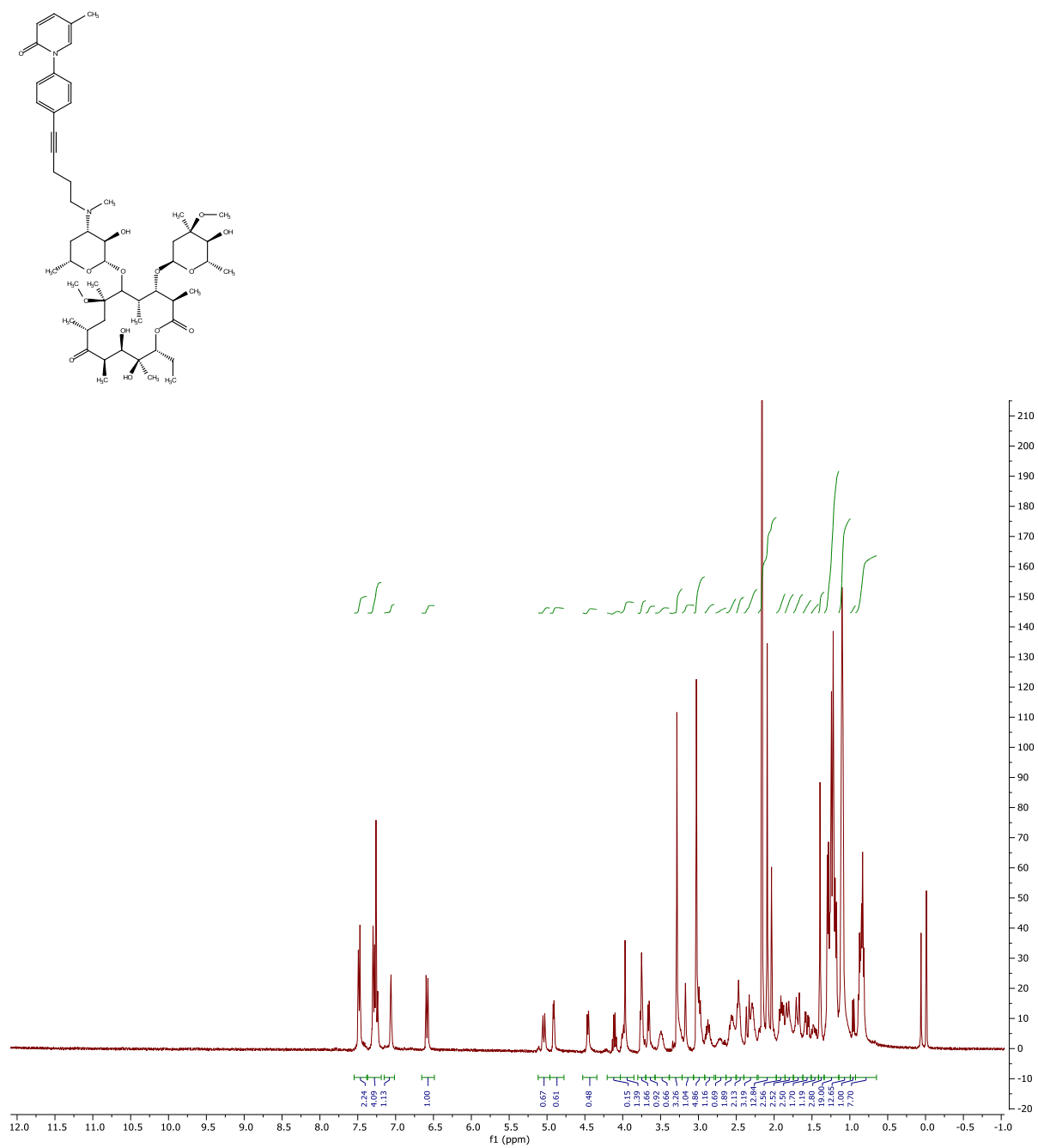


19b (^1H NMR)

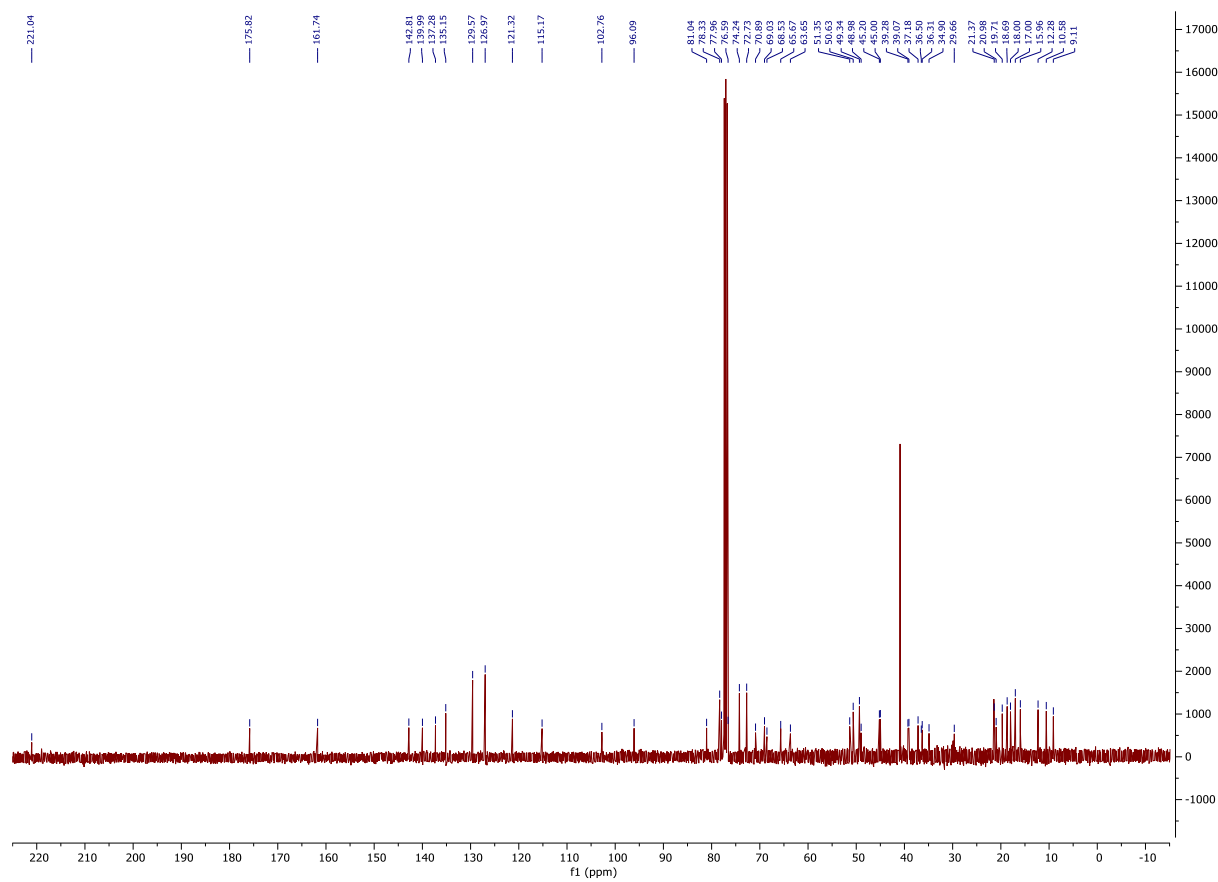


19b (^{13}C NMR)

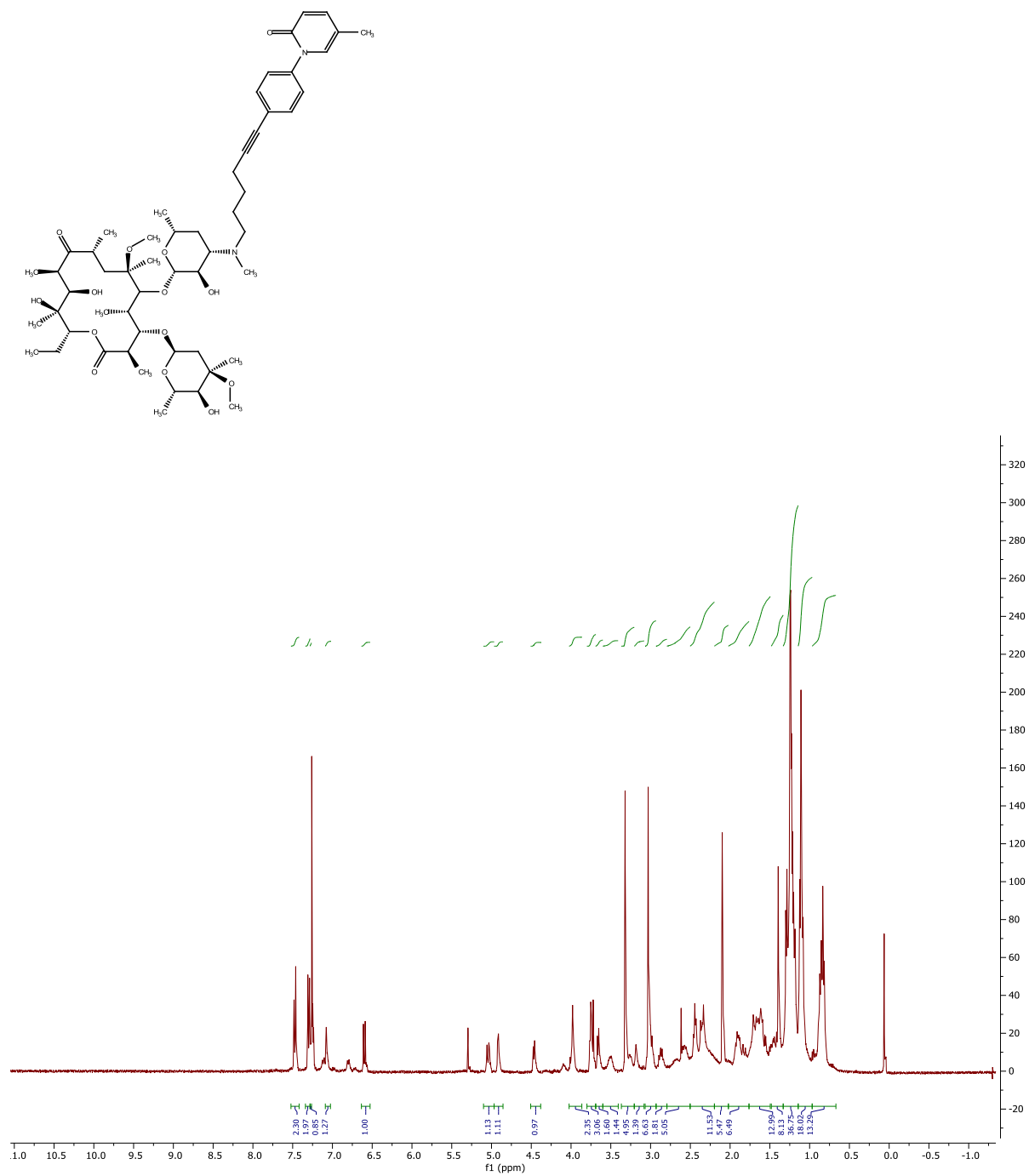




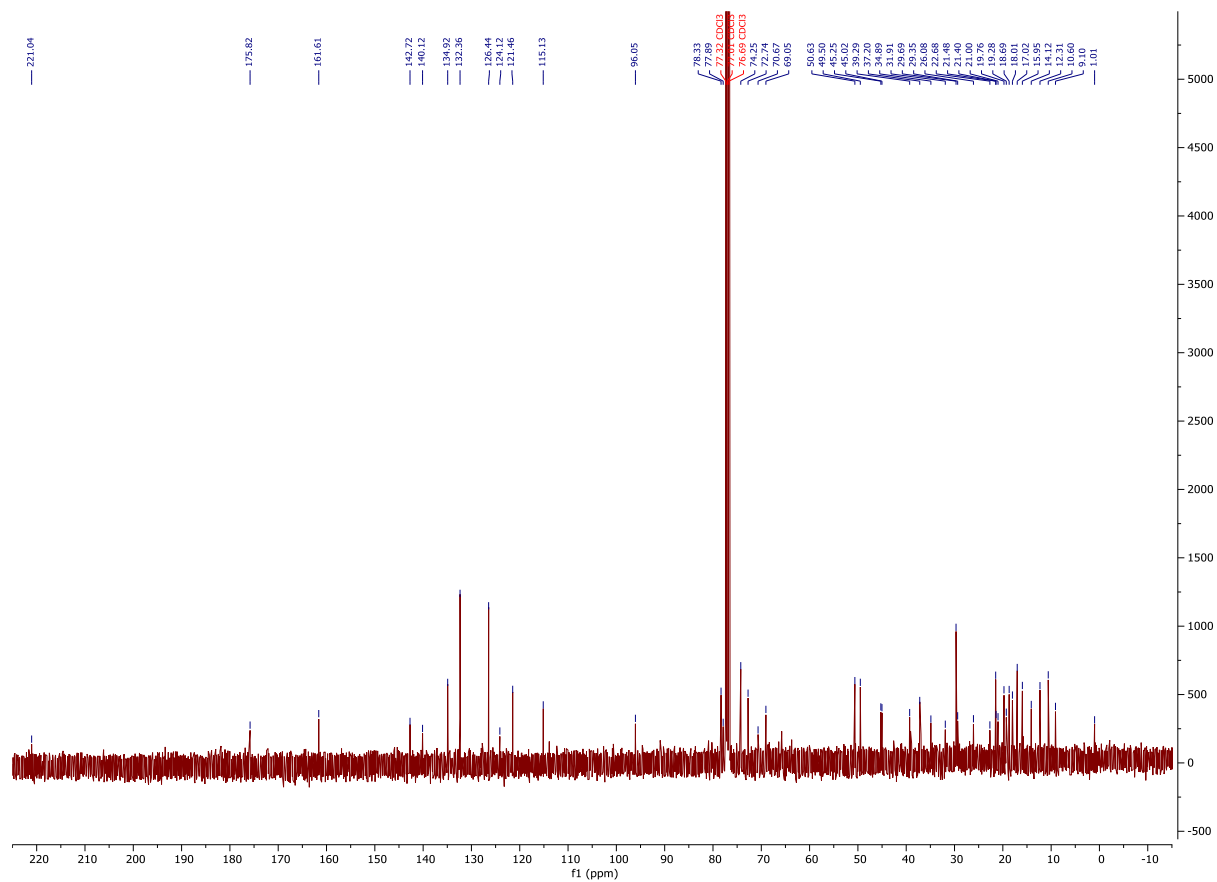
19c (¹³C NMR)



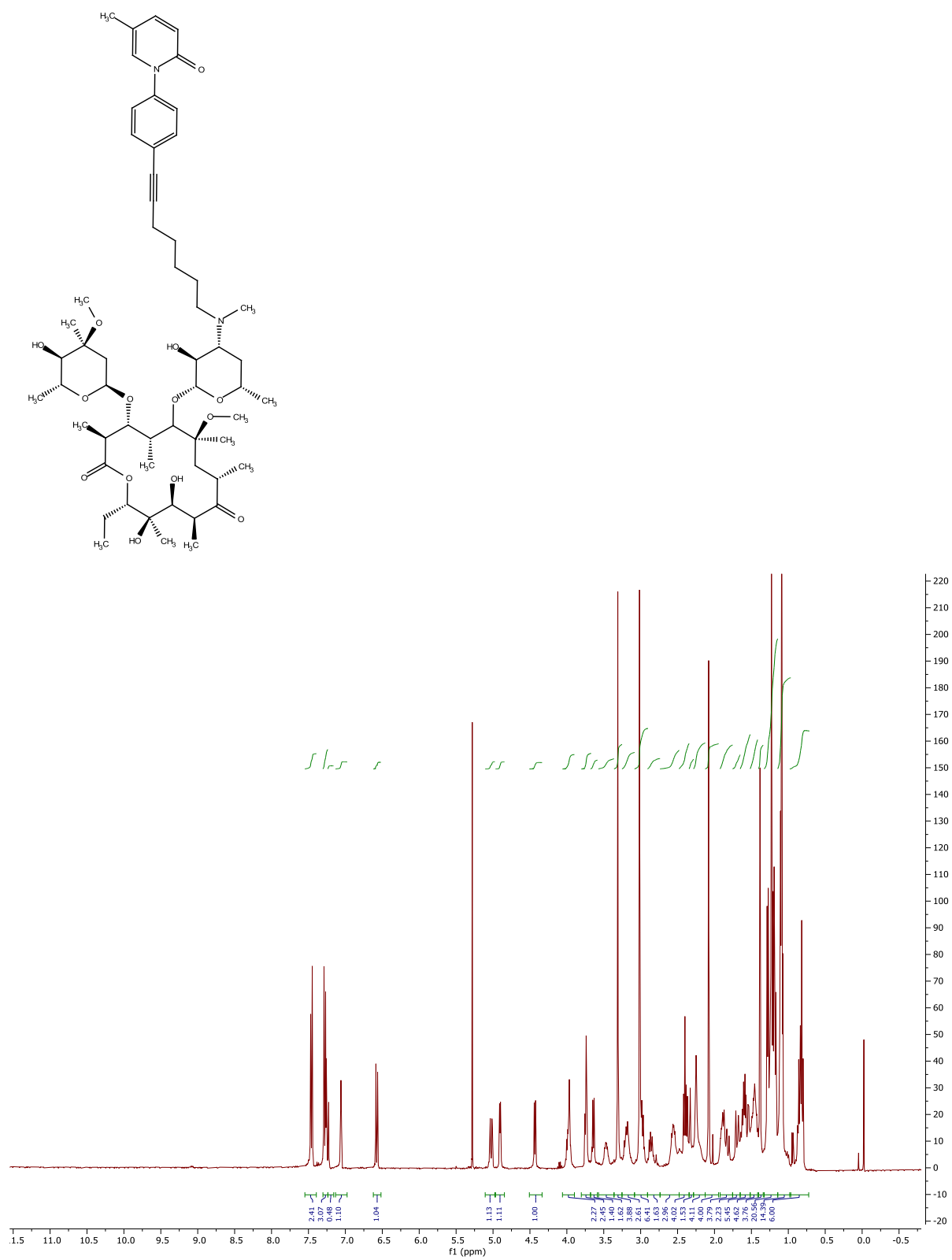
19d (¹H NMR)



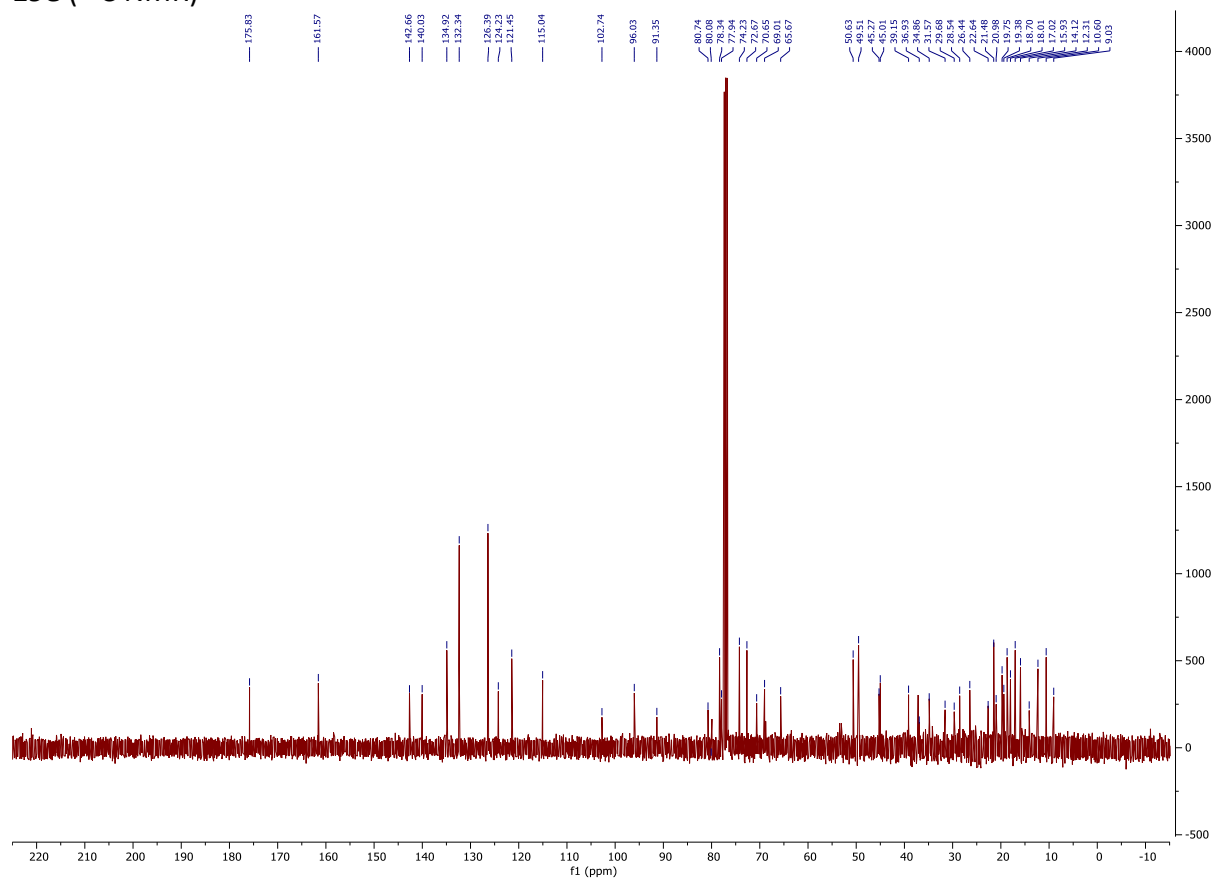
19d (^{13}C NMR)



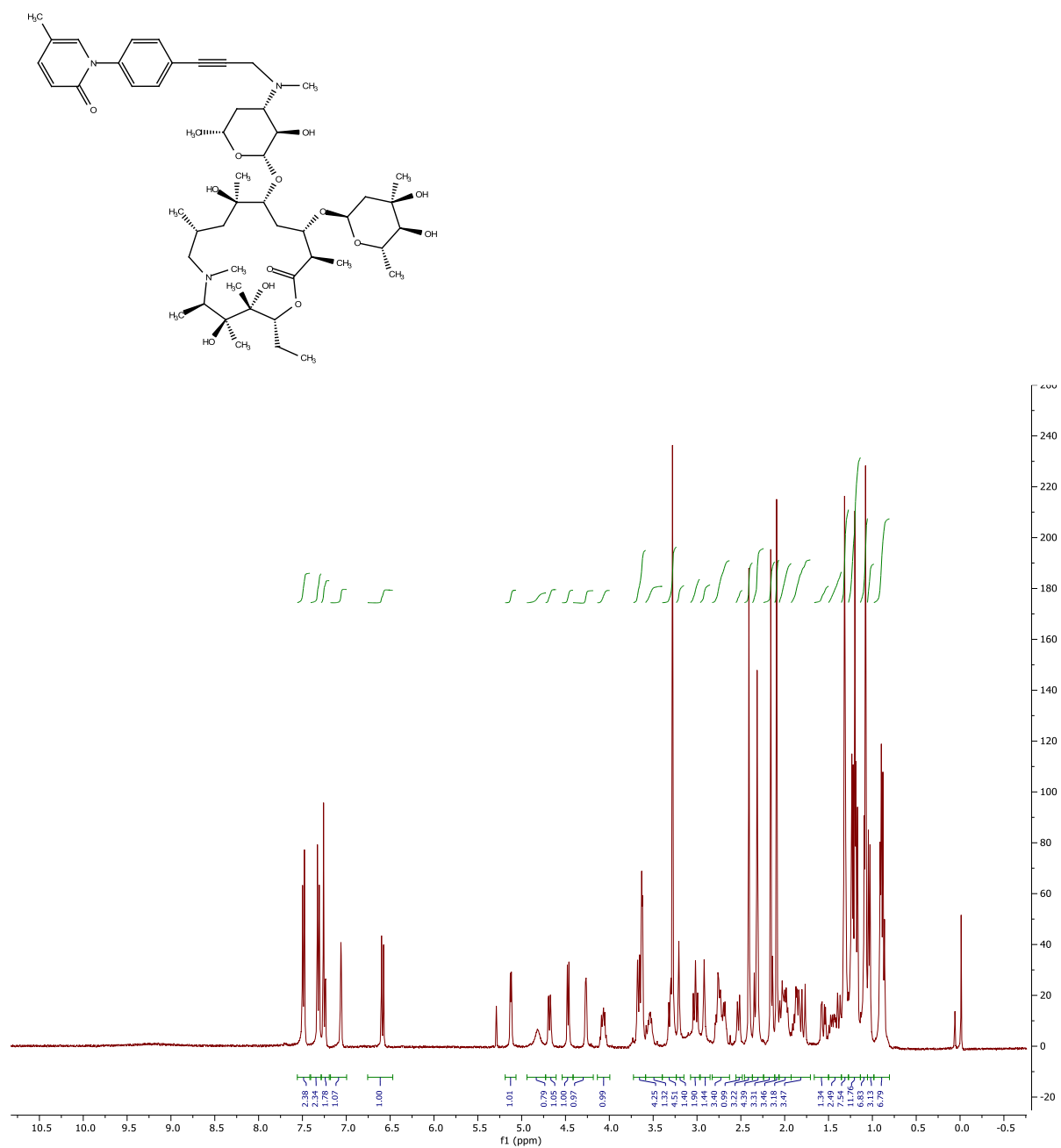
19e (^1H NMR)



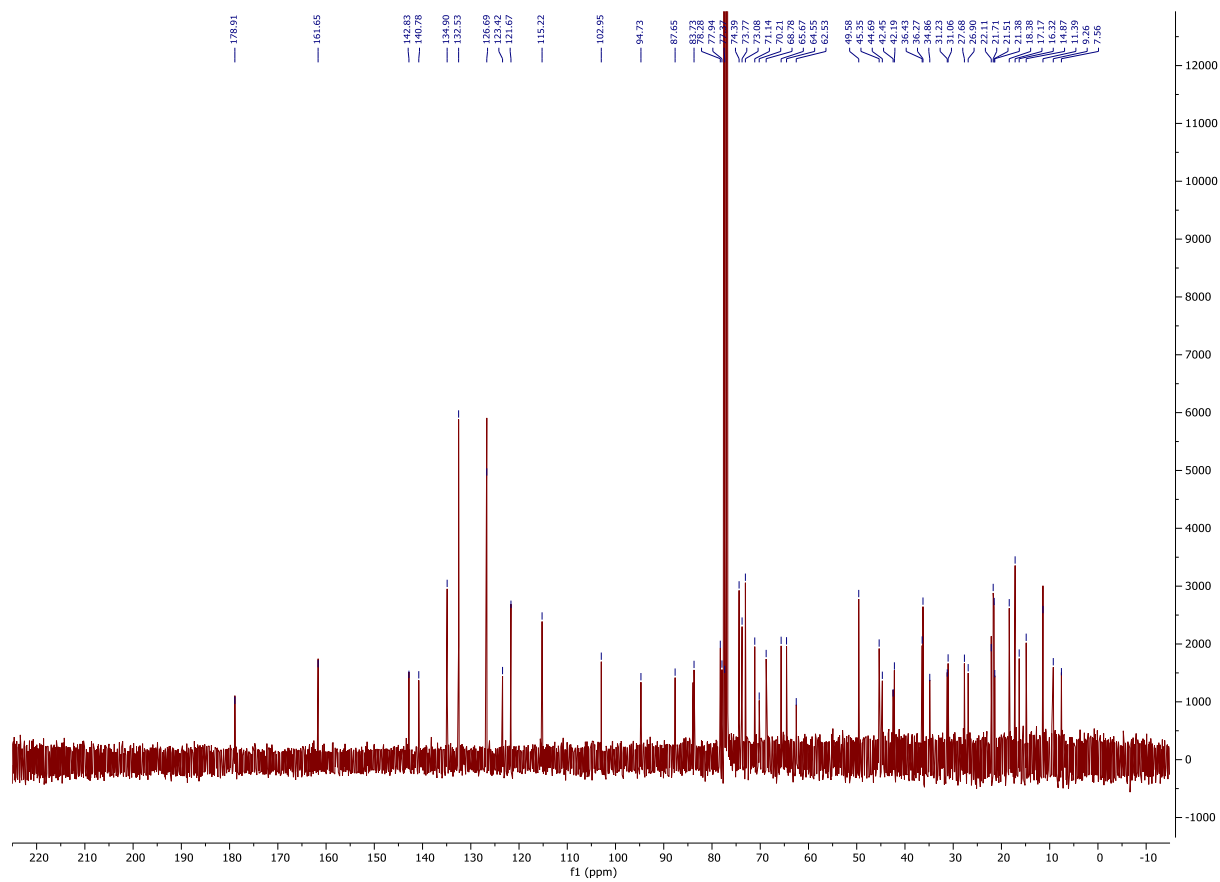
19e (^{13}C NMR)



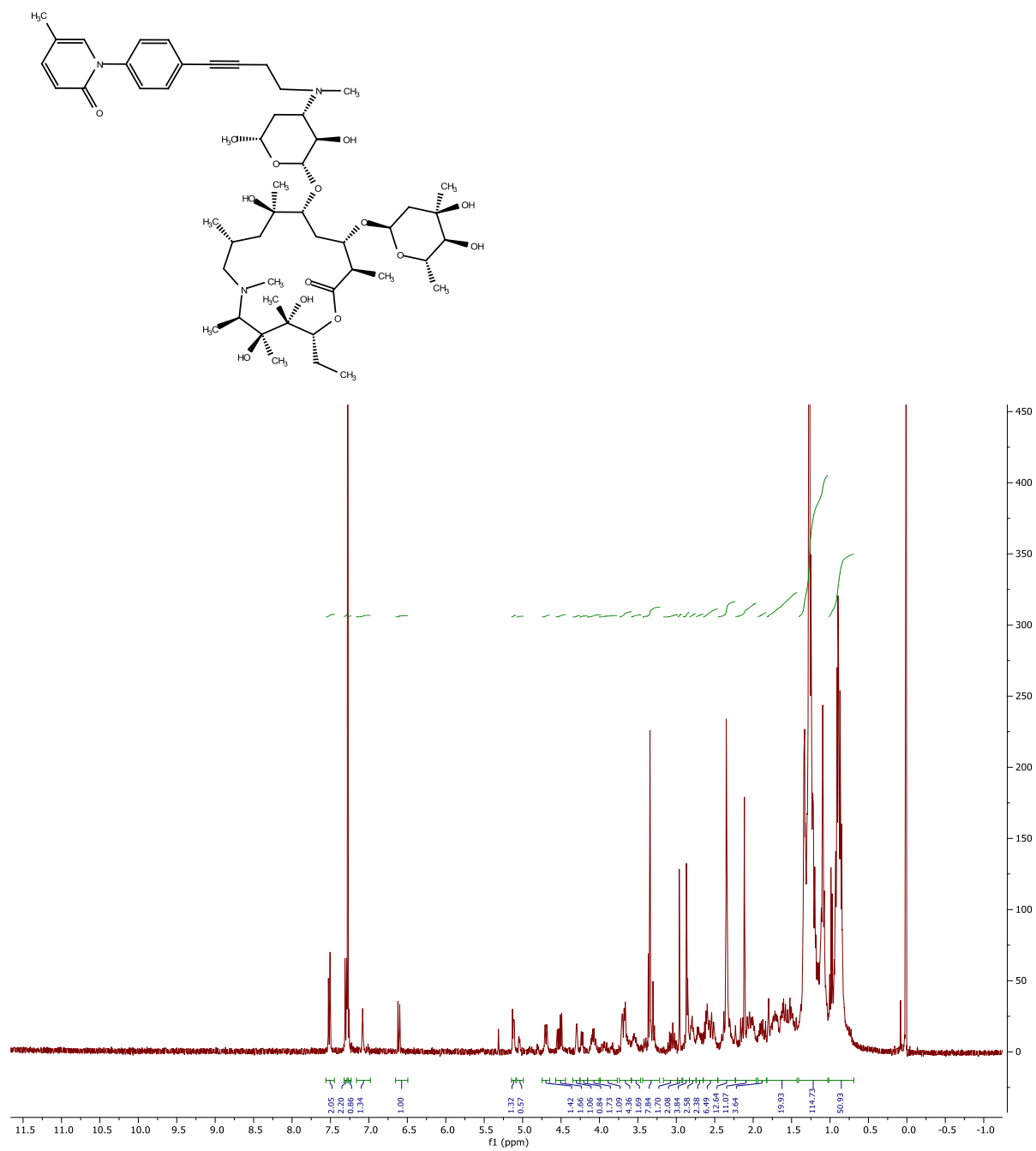
20a (^1H NMR)



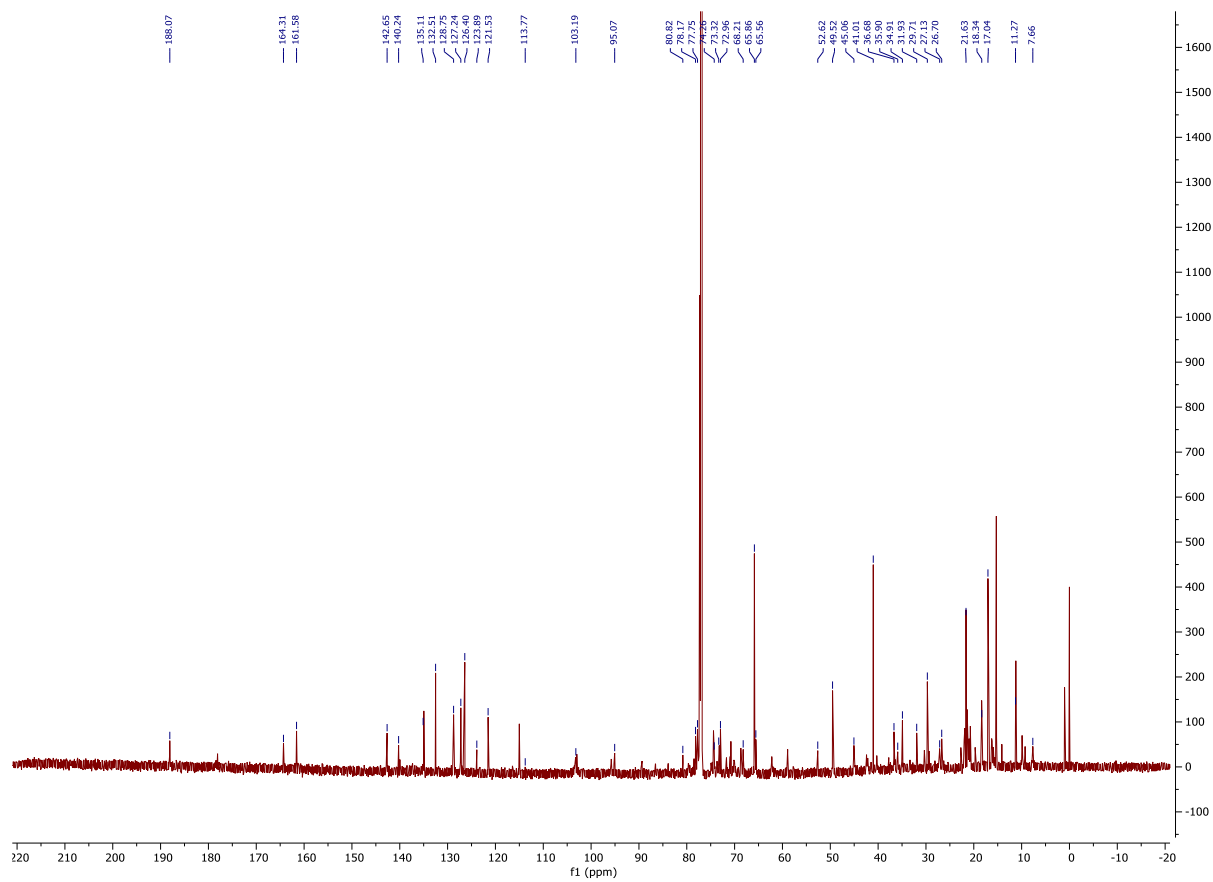
20a (^{13}C NMR)



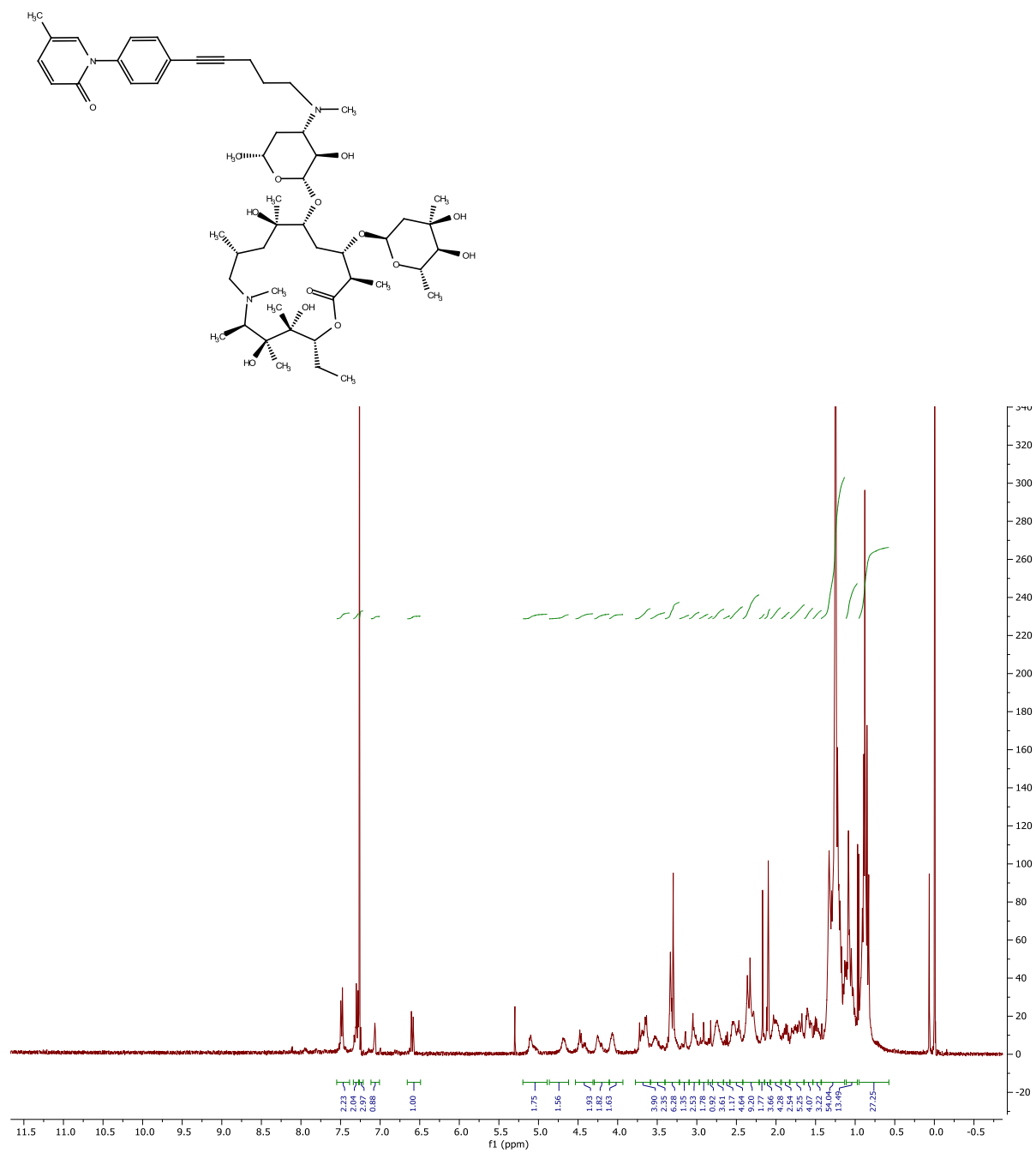
20b (^1H NMR)



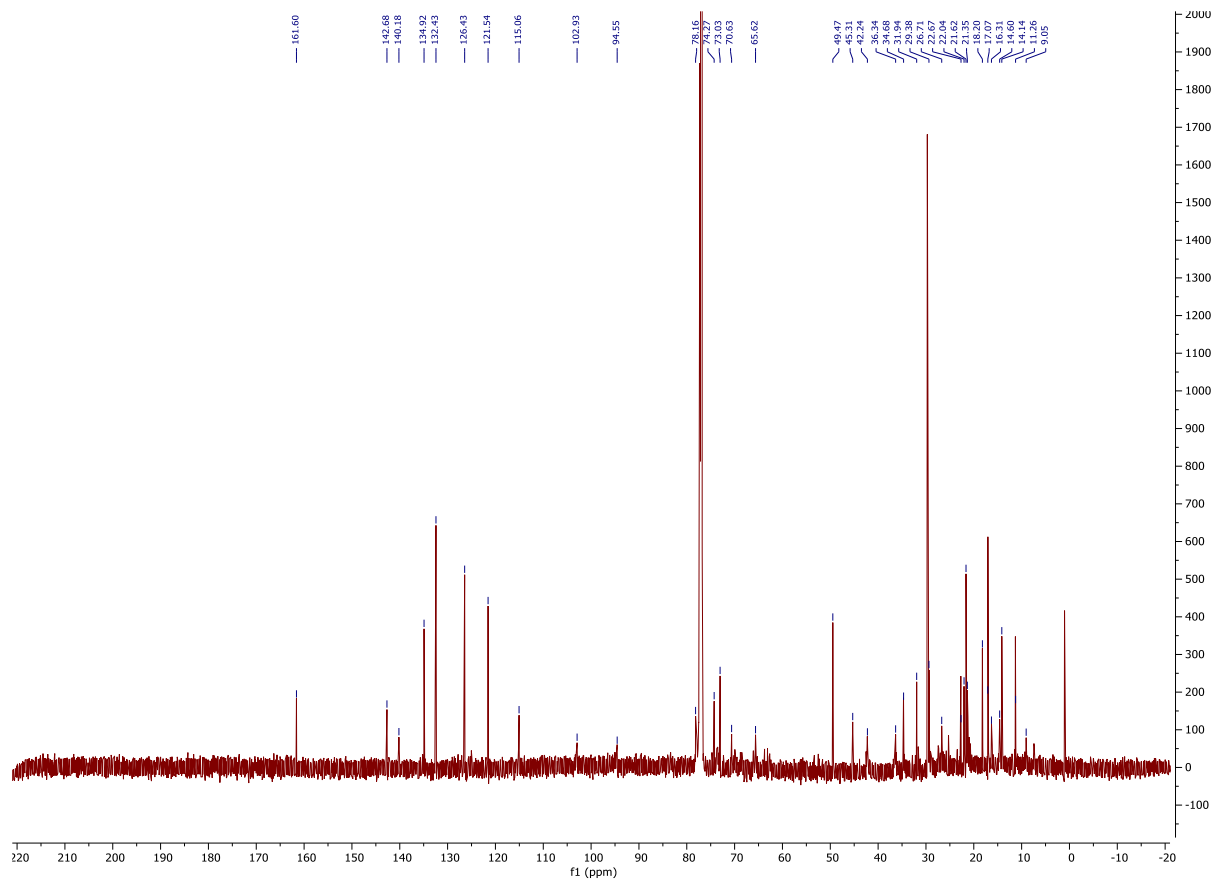
20b (^{13}C NMR)



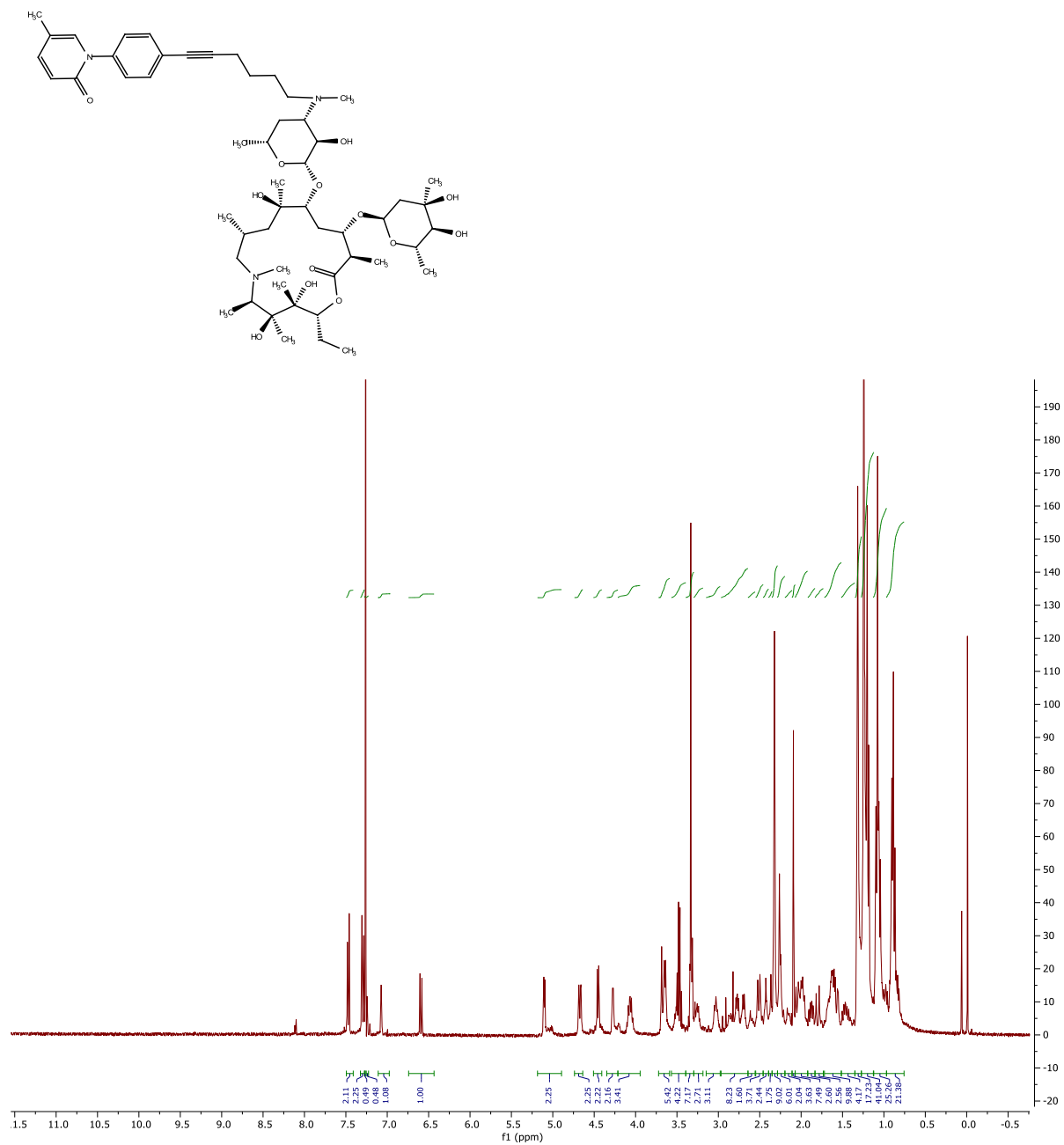
20c (^1H NMR)



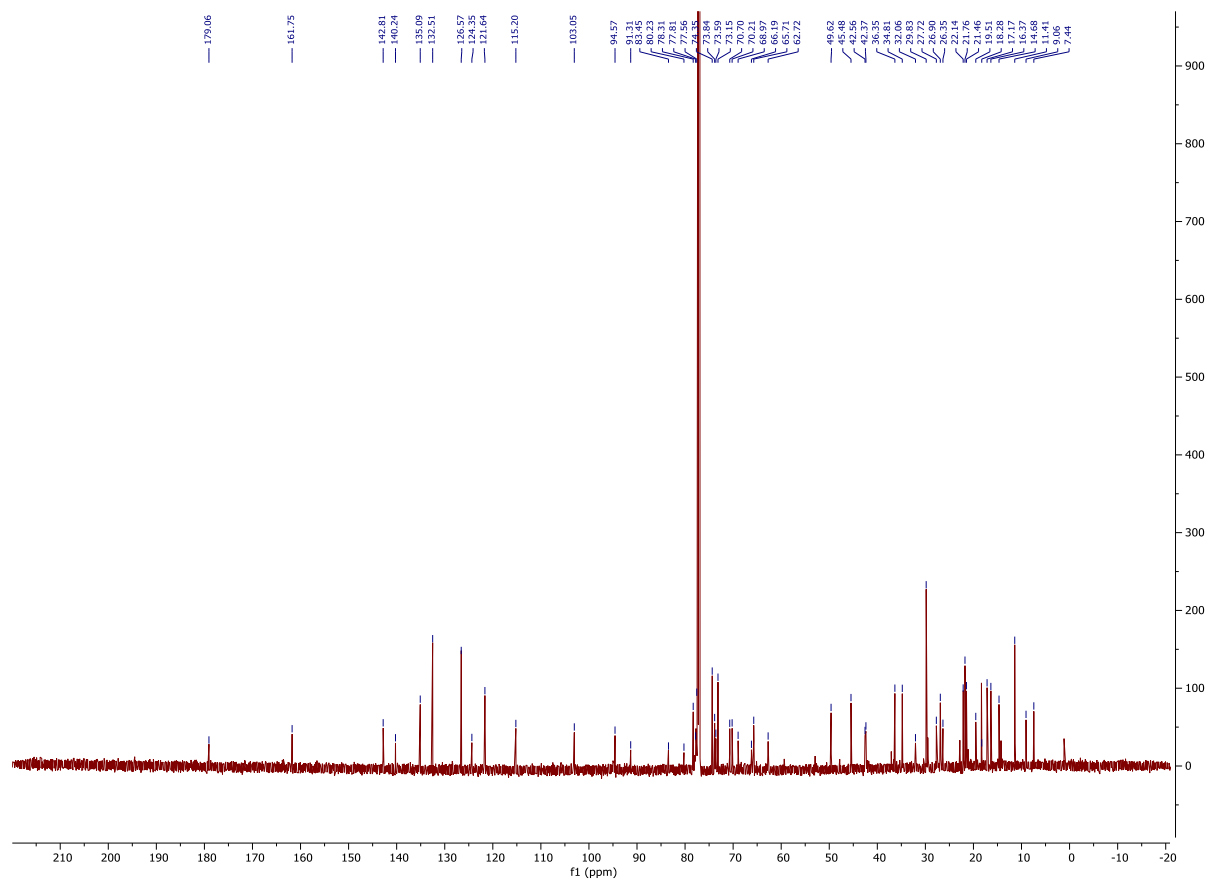
20c (^{13}C NMR)



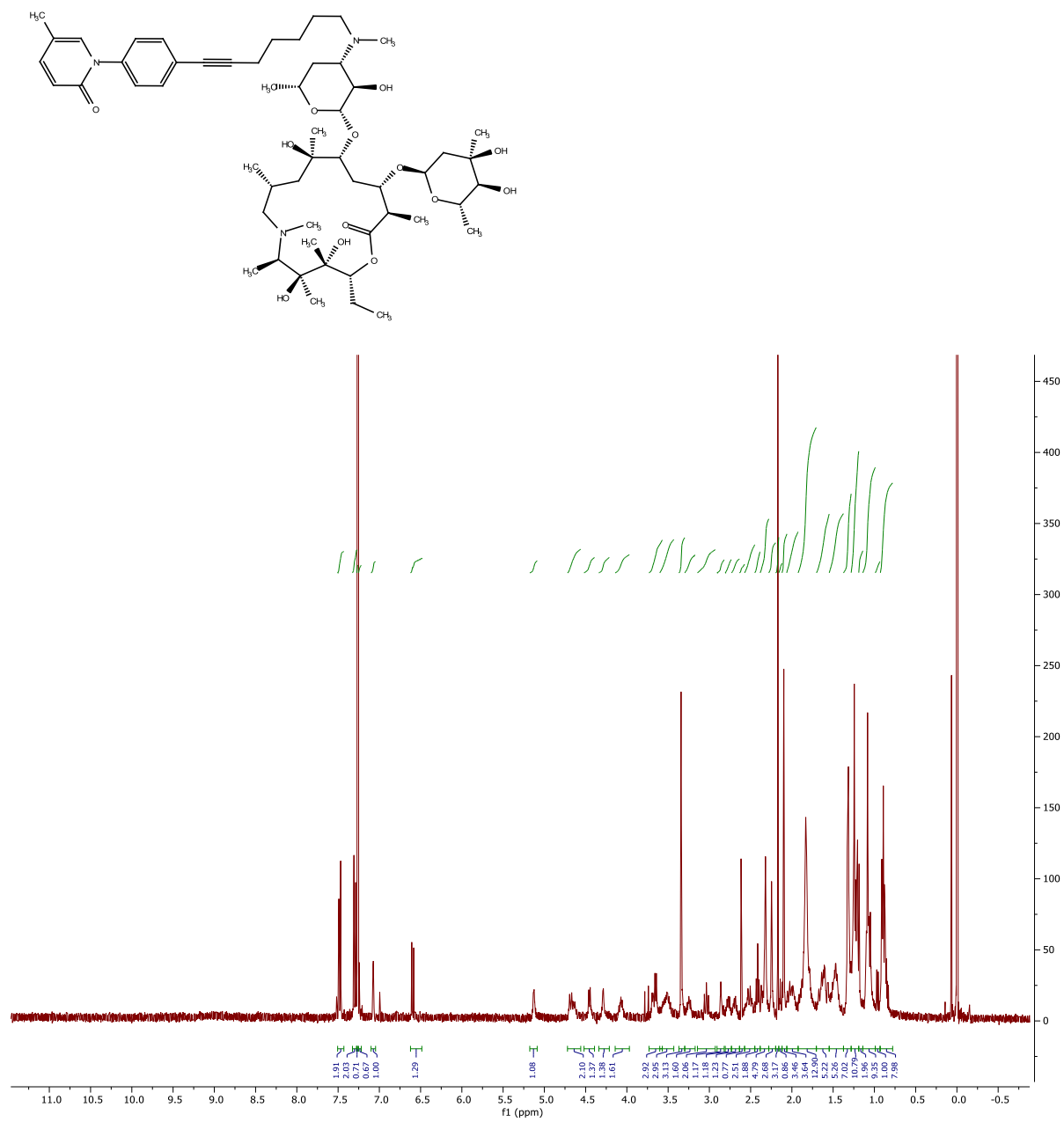
20d (¹H NMR)



20d (^{13}C NMR)



20e (^1H NMR)



20e (^{13}C NMR)

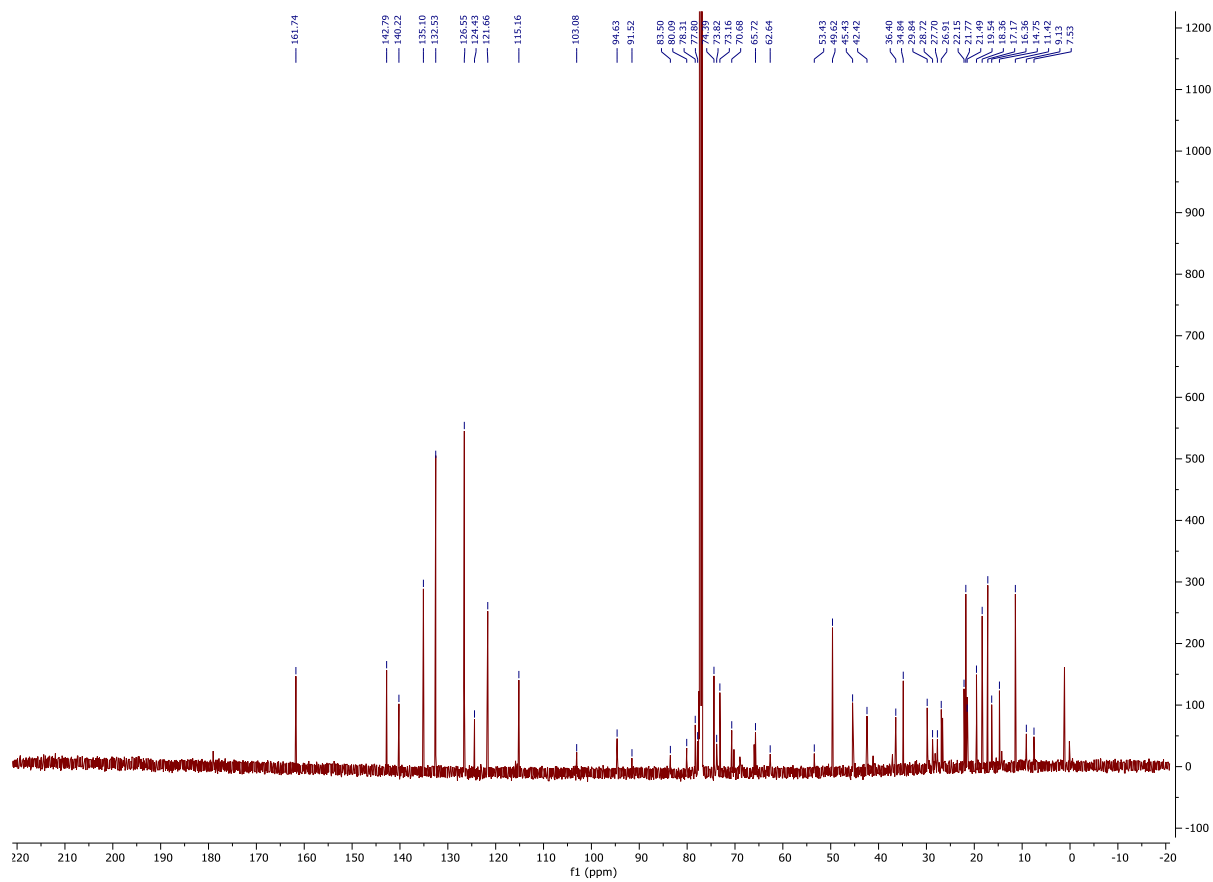


Table 2S.1. Docking scores of all candidates on ALK-5 (PDB:5USQ). All candidates showed highly enhanced binding affinity on interaction with ALK-5.

Compound	Cal. Binding affinity (kcal/mol)	Compound	Cal. Binding affinity (kcal/mol)
10a (n=1)	-9.5	19a	-8.1
10b (n=2)	-9.6	19b	-9.2
10c (n=4)	-9.9	19c	-8.7
11a (n=1)	-9.8	19d	-8.5
11b (n=2)	-10.2	19e	-8.4
11c (n=4)	-9.2	20a	-9.2
12a (n=1)	-9.2	20b	-8.6
12b (n=2)	-9.1	20c	-7.7
12c (n=4)	-9.5	20d	-8.2
13a (n=1)	-10.2	20e	-8.7
13b (n=2)	-9.6	PFD	-7.6
13c (n=4)	-9.2	CLM	-5.3
14a (n=1)	-8.4	AZM	-5.9
14b (n=2)	-8.5		
14c (n=4)	-9.1		
15a (n=1)	-7.9		
15b (n=2)	-8.3		
15c (n=4)	-8.5		

Table 2S.2. Docking scores of all candidates on p-P38 γ (PDB:1CM8). All candidates showed highly enhanced binding affinity on interaction with p-P38 γ relative to PFD or macrolides.

Compound	Cal. Binding affinity (kcal/mol)	Compound	Cal. Binding affinity (kcal/mol)
10a (n=1)	-8.9	19a	-8.3
10b (n=2)	-10.5	19b	-9.0
10c (n=4)	-10.2	19c	-9.2
11a (n=1)	-10.5	19d	-9.1
11b (n=2)	-10.4	19e	-9.5
11c (n=4)	-9.9	20a	-10.0
12a (n=1)	-10.2	20b	-9.3
12b (n=2)	-9.4	20c	-9.0
12c (n=4)	-10.3	20d	-9.3
13a (n=1)	-11.1	20e	-9.5
13b (n=2)	-10.2	PFD	-7.6
13c (n=4)	-10.4	CLM	-6.5
14a (n=1)	-7.5	AZM	-7.4
14b (n=2)	-8.8		
14c (n=4)	-9.3		

Table 2S.2 Continued.

15a (n=1)	-9.6		
15b (n=2)	-8.9		
15c (n=4)	-9.4		

CHAPTER 3. STRUCTURAL MODIFICATION OF ANTIOXIDANTS WITH MACROLIDE CONJUGATION ENHANCED ANTI-CANCER AND ANTI-FIBROSIS EFFECT.

Bocheng Wu¹, Adegboyega K. Oyelere^{1,2}

*School of Chemistry and Biochemistry, School of Biological Sciences, Parker H. Petit Institute
for Bioengineering and Bioscience, Georgia Institute of Technology, Atlanta, GA 30332-0400
USA*

¹School of Chemistry and Biochemistry, Georgia Institute of Technology

²Parker H. Petit Institute for Bioengineering and Bioscience, Georgia Institute of Technology

Correspondence to:

Adegboyega K. Oyelere, **E-mail:** aoyelere@gatech.edu

Keywords: Antioxidant, α -Lipoic acid, piperic acid, piperine, dimethyl fumarate, monomethyl fumarate, macrolide, azithromycin, clarithromycin, anti-fibrosis, anti-cancer, ROS, lung tissue targeting, liver tissue targeting, STAT3, HO-1, Nrf-2.

Abstract:

Antioxidants are widely used as supplements for chronic inflammation and cancer treatment, as they were proved to fight against Reactive Oxidation species (ROS) and attenuate tissue inflammation progression. α -Lipoic acid (ALA) is regarded as an ideal antioxidant which demonstrated promising antioxidation effects with high bioavailability and high dose tolerance. The electrophilic antioxidants dimethyl fumarate (DMF) and piperine (PIPE) are also strong antioxidants that showed promising progression in cancer treatment by Nrf-2 activation. Through the activation, anti-ROS proteins could be induced and prevent ROS-related inflammation in cancer and fibrosis. However, none of them was used as a standalone medicine for cancer or fibrosis treatment because they lack tumor penetration and tissue accumulation activities. To largely enhance the efficacy of the antioxidants, we conjugated them with the macrolides azithromycin (AZM) and clarithromycin (CLM) as the lung/liver tissue targeting template. By methods of conjugation, we successfully made derivatives on each antioxidant and observed significant enhancement in cytotoxicity (from 10 to 100-fold) against cancer cell lines and fibroblast. Also, in each antioxidant derivatives, there are selected candidates with strong extracellular matrix (ECM) expression inhibition by attenuating the TGF- β stimulation in MRC-5 cell line. On the side of antioxidation effect, ALA, ACC0NL and APC2NL of the ALA derivative revealed STAT3 pathway inhibition. The piperic acid (PPA) derivatives WBC-04-16, WBC-04-14, and WBC-04-11 showed upregulation of HO-1 expression, an indicator of Nrf-2 activation. In addition, the fumarate derivatives ST-01-95 and AO-02-112 also showed similar HO-1 upregulation effect as PPA derivatives. Collectively, the macrolide-antioxidants with strong anticancer and anti-inflammation effect might be potential cancer therapy agents with potential tissue targeting effect.

3.1 Introduction

Decades of research has shown strong connection between tumor, tissue injury and inflammatory microenvironment. Reactive oxygen species (ROS), which play a key role in cancer and chronic inflammatory diseases, strongly promotes the expression of pro-inflammatory cytokines and cause tissue fibrosis and tumorigenesis. ROS could also induce the activation of pro-tumor pathways including Ras, NF- κ B, TGF- β , MAPK etc.¹ Studies of anti-inflammation and anti-oxidant drugs in cancer treatments have demonstrated promising results. Antioxidants are substances that protect human tissues and cells from damages from ROS. The most famous anti-oxidant, Vitamin C, has been proven to be protective and/or demonstrate promising efficacious effects against cancers and other tissue inflammation by neutralizing the free radicals and strengthen the immune system.^{2, 3} Anti-oxidants could also elicit anti-fibrotic effect due to their attenuation of the expression of inflammatory cytokines and inhibition of cell proliferation and invasion.⁴ For example, Alpha R-Lipoic acid (ALA) has shown adjuvant effect when co-administered with Non-steroid Anti-inflammation drugs (NSAIDs) or anti-cancer drugs as it could strengthen the anti-inflammation effect while protecting the gastrointestinal tract.⁵⁻⁷ The anti-ROS agents Dimethyl fumarate (DMF) and Piperine (PIPE) could also be adjuvant of anti-cancer agents as they could regulate cytokine production and prevent immune system damage that is caused by chemotherapy.

ALA is an essential component of several metabolic pathways, including glycolysis. It is widely used as a supplement in managing several diseases. In cancer treatment, ALA has shown potential, regulating inflammatory mechanism through controlling cytokine signaling pathways such as prevention of NF- κ B activation⁸ and quenching reactive oxygen species.⁹ It also showed STAT3 pathway (p-STAT3, Bcl-2, Bcl-xL) down-regulation by inhibiting IL-8 expression.¹⁰ ALA also inhibits hepatic PAI-1 expression in TGF- β pathway, in which it mitigates tissue fibrosis in tumor

environment and TGF- β -induced cancer inflammation.¹¹ Due to its inhibitory effect on STAT3 and TGF- β , ALA also showed strong anti-fibrotic effect, reducing the expression of ECM protein fibronectin and p-ERK back to unstimulated level from TGF- β stimulation.¹²

Electrophilic anti-ROS agents, including Dimethyl fumarate (DMF) and piperine (PIPE), are Nrf-2 activators that could induce Nrf-2 gene expression and attenuate ROS by stimulating the expression of anti-ROS enzymes. Specifically, DMF and PIPE could induce the expression of Heme oxygenase-1 (HO-1) via activation of Nrf-2 gene transcription. HO-1 could degrade Heme that is in ‘free’ form (no protein bound) which could cause oxidative stress in cells and tissues.¹³ In addition, HO-1 could also attenuate intracellular inflammation that can be caused by stimulation of LPS, IL-6, COX-2, TNF- α and other pro-inflammatory cytokines.¹⁴ In many inflammation-linked cancers such as gastric cancer related to Inflammatory bowel disease (IBD), HO-1 could protect the intestine with anti-inflammation activity and prevent the tumorigenesis.¹⁵ Clinical trials evaluating the anti-inflammation potential of HO-1 are ongoing.¹⁵ Beside Nrf-2 activation, both DMF and PIPE showed pleotropic anti-cancer effects. More specifically, PIPE could induce cancer cell apoptosis through PI3K/Akt pathway inhibition or inducing ER stress proteins.¹⁶ While DMF could target the NF- κ B pathway and mitigate cell migration and tumor growth of cutaneous T-cell lymphoma (CTCL).¹⁷ In fact, DMF has been tested in clinic trials for multiple diseases including multiple sclerosis, CTCL, Glioblastoma Multiforme, etc.¹⁸ Collectively, these literature observations suggest that DMF and PIPE could be potential anti-cancer and anti-inflammation agents.

However, antioxidants, such as ALA, DMF and PIPE, have low potency and they have not been approved as standalone agents in cancer therapy. To enhance potency, Structural-Activity Relationship studies have been performed on these antioxidants. For example, ALA conjugated

with alloxanthoxyletin showed enhanced cell cytotoxicity on A549 cells, causing downregulation of IL-6 expression.¹⁹ In another study, forty-six ALA derivatives were designed and synthesized for optimized COX-2-selective inhibition.^{20, 21} In contrast, though DMF and PIPE have been well-studied for their mechanisms of actions in cancers, not many SAR studies have done. In order to increase their cell exposure and tissue-targeting effects, which could result in improved anti-inflammatory effects, we introduce in this paper macrolide conjugated forms of antioxidants (ALA, PIPE, and fumarate).

Inspired by our previous study on macrolide derivatives of pirfenidone, we designed and synthesized azithromycin (AZM) and clarithromycin (CLM) conjugates of ALA, fumarate and PIPE. We investigated their cytotoxicity in cancer cells, normal kidney cell line, and fibroblast cell line. We observed that most of novel compounds showed significant enhancement in cytotoxicity relative to their unconjugated antioxidant. In addition, selected novel candidates from every antioxidant agent showed improved anti-fibrotic effects in TGF- β stimulated fibroblast cells. Also, these compounds perturb different cellular target to elicit their bioactivities. ALA derivatives showed STAT3 pathway inhibition in triple negative breast cancer (TNBC) cell line. Fumarate and PIPE derivatives showed significant HO-1 up-regulation.

3.2 Results

3.2.1 Conjugates Design

3.2.1.1 Macrolide-ALA Conjugates:

We synthesized ten derivatives which link ALA to the macrolide templates through with different covalent bonds. We used three different covalent linkage to achieve this conjugation: direct linkage to the desosamine OH group via ester bond (Fig. 3.1a), direct linkage to desmethyl-desosamine via amide bond (Fig. 3.1b), linkage to desmethyl-desosamine via aryl triazolyl group that contains 2 or 3 methylene group (Fig. 3.1c). As macrolide templates, AZM and CLM were used. We also synthesized analogs lacking the cladinose sugar (Fig. 3.1d) in order to evaluate the consequence of this change on the bioactivity of these macrolide-ALA conjugates.

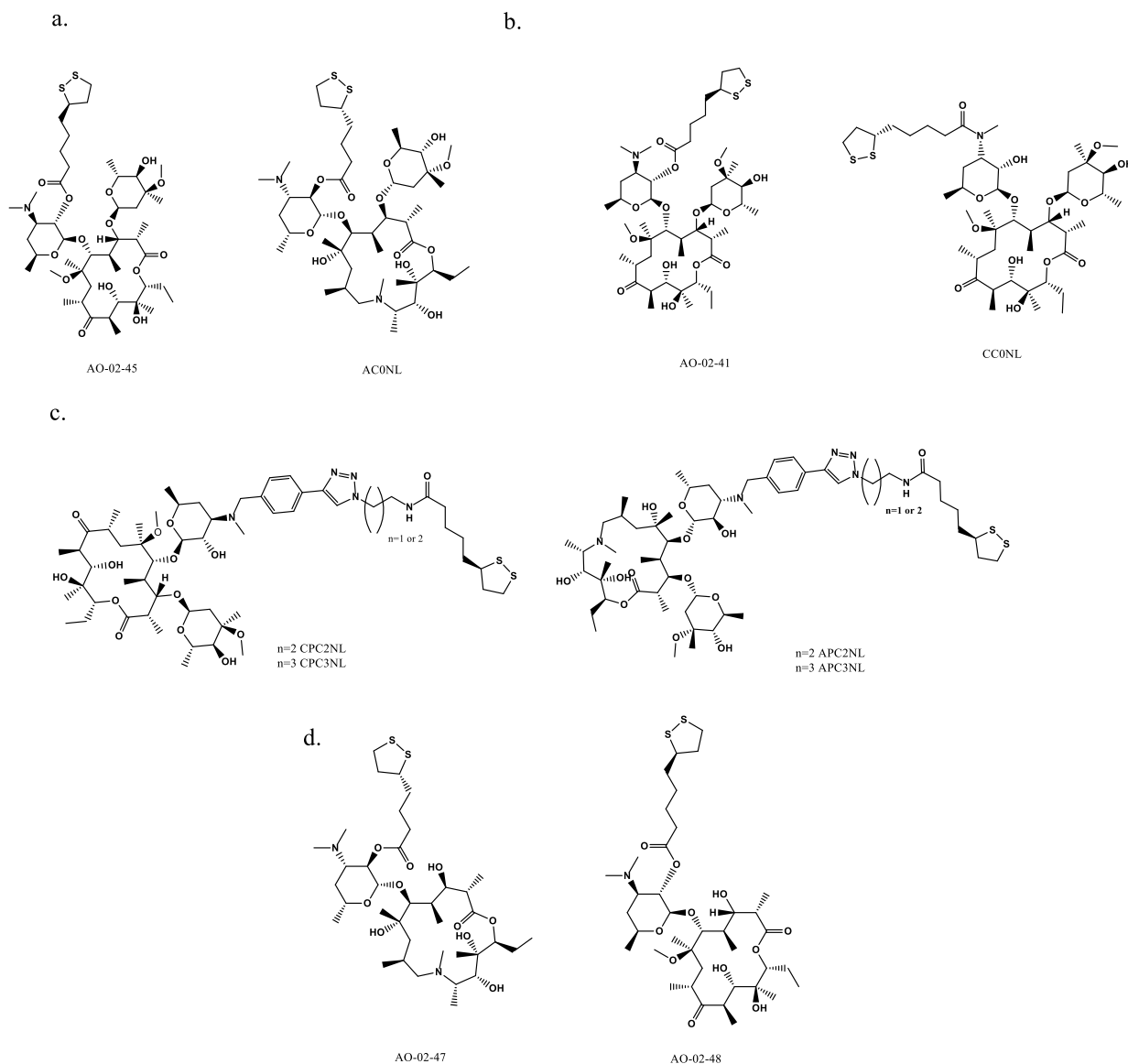
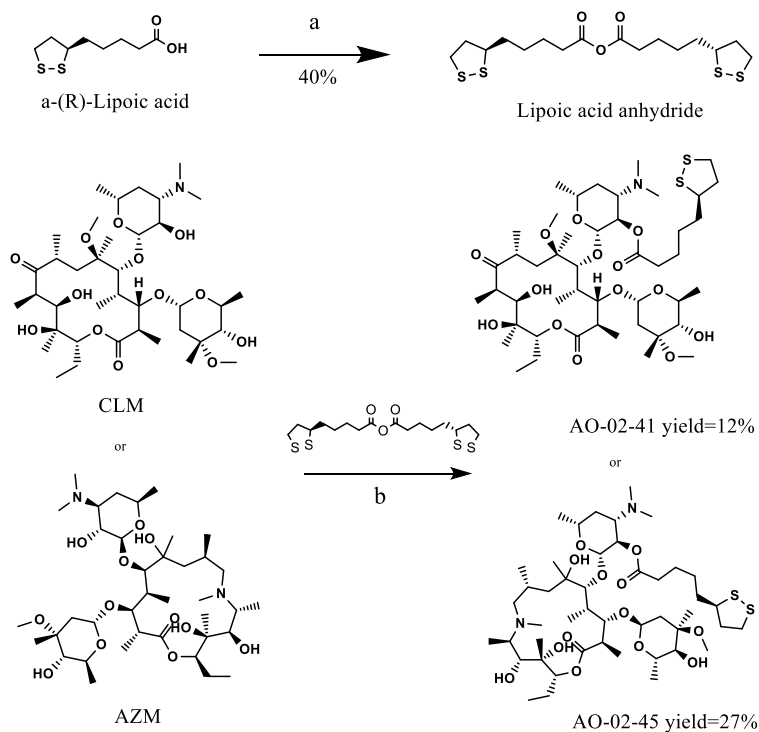
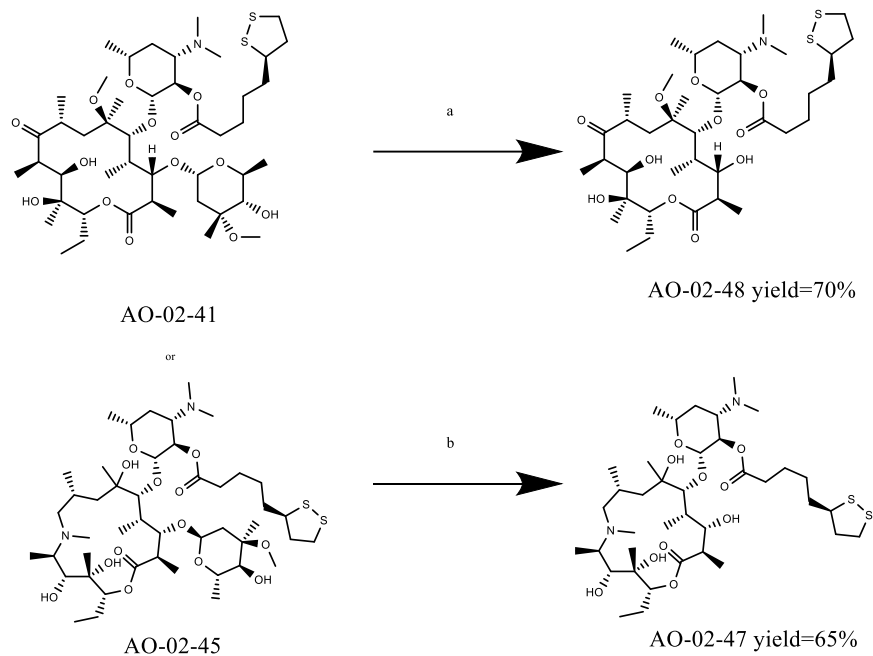


Figure 3.1 The designed macrolide-ALA conjugates. (a) Direct linkage of ALA to dimethyl-desosamine via amide bond. (b) Direct linkage of ALA to desmethyl-desosamine via amide bond. (c) Linkage to desmethyl-desosamine via aryl triazolyl group that contains 2 or 3 methylene group. (d) Macrolide-ALA conjugates lacking cladinose sugar - derivatives of ester AO-02-45 and AO-02-41.

To synthesize the target macrolide-ALA conjugates; we first prepared lipoic acid anhydride by reacting lipoic acid and EDCI in DCM solution, overnight. The anhydride was then reacted with AZM or CLM in DCM, overnight at room temperature to furnish AO-02-41 or AO-02-45 (Scheme 1).

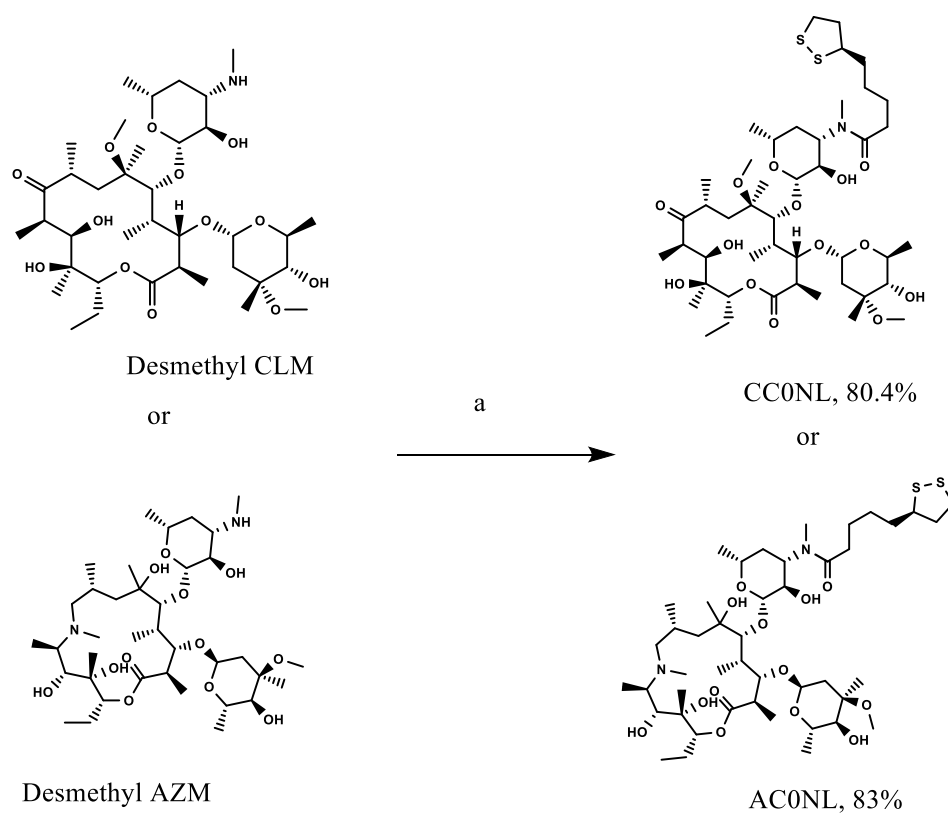


Scheme 1. The synthesis of ester-linked macrolide-ALA conjugates. (1) ALA, EDCI, DCM, rt, overnight, 40%. (2) Lipoic anhydride, AZM or CLM, DCM, 48-72h, rt., 12% for AO-02-41, 27% for AO-02-45.



Scheme 2. Synthesis of macrolide-ALA conjugates lacking cladinose sugar. (a) 0.25M HCl water solution stir for 6h, 70%. (b) 1M HCl stir for overnight. 65%.

Mild acid treatment of AO-02-41 and AO-02-45 afforded the macrolide-ALA conjugates lacking cladinose AO-02-48 and AO-02-47 respectively (Scheme 2).



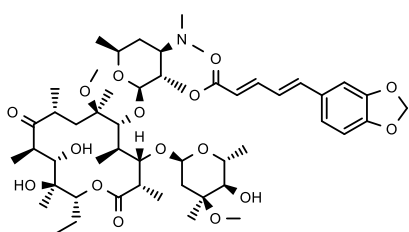
Scheme 3. The synthesis of macrolide-ALA conjugates linked to desmethyl-desosamine via amide bond. (a) Desmethyl AZM or desmethyl CLM, ALA, EDCI, DMAP, Hunig's base, DCM, rt, overnight. 80.4% for CC0NL, 83% for AC0NL.

The synthesis of macrolide-ALA conjugates linked to desmethyl-desosamine (AC0NL and CC0NL) was accomplished by reacting desmethyl AZM or desmethyl CLM with ALA and EDCI in Hunig's base (10 v/v%)/DCM mixture in the presence of 0.1 eq (Scheme 3).

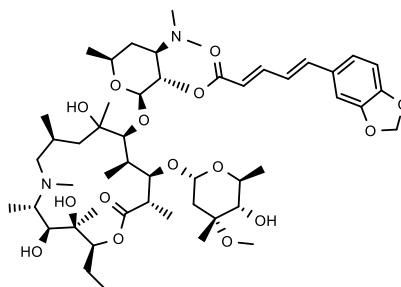
reaction between C2NL or C3NL and PCC or PCA, following literature protocol,²² furnished the target macrolide-ALA compounds CPC2NL, CPC3NL, APC2NL and APC3NL (Scheme 4).

3.2.1.2 macrolide-PIPE Conjugates:

a

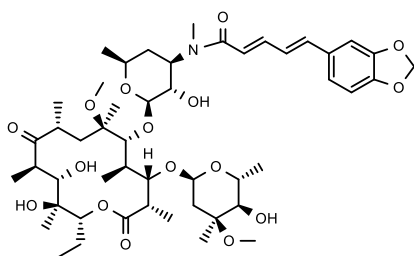


WBC-04-14

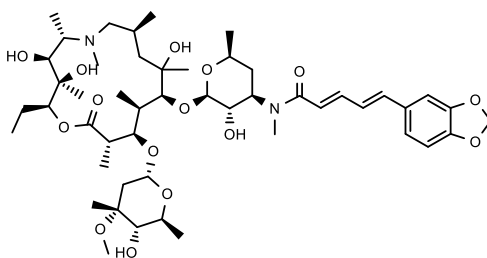


WBC-04-11

b



WBC-04-15

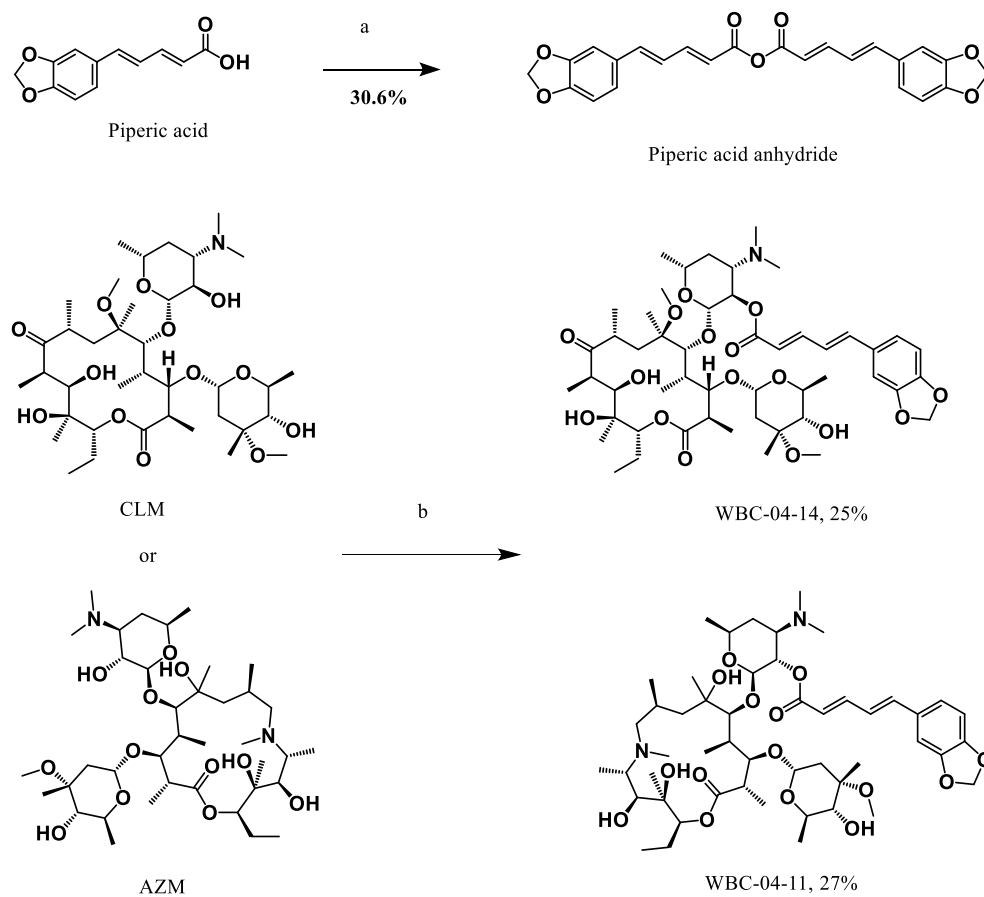


WBC-04-16

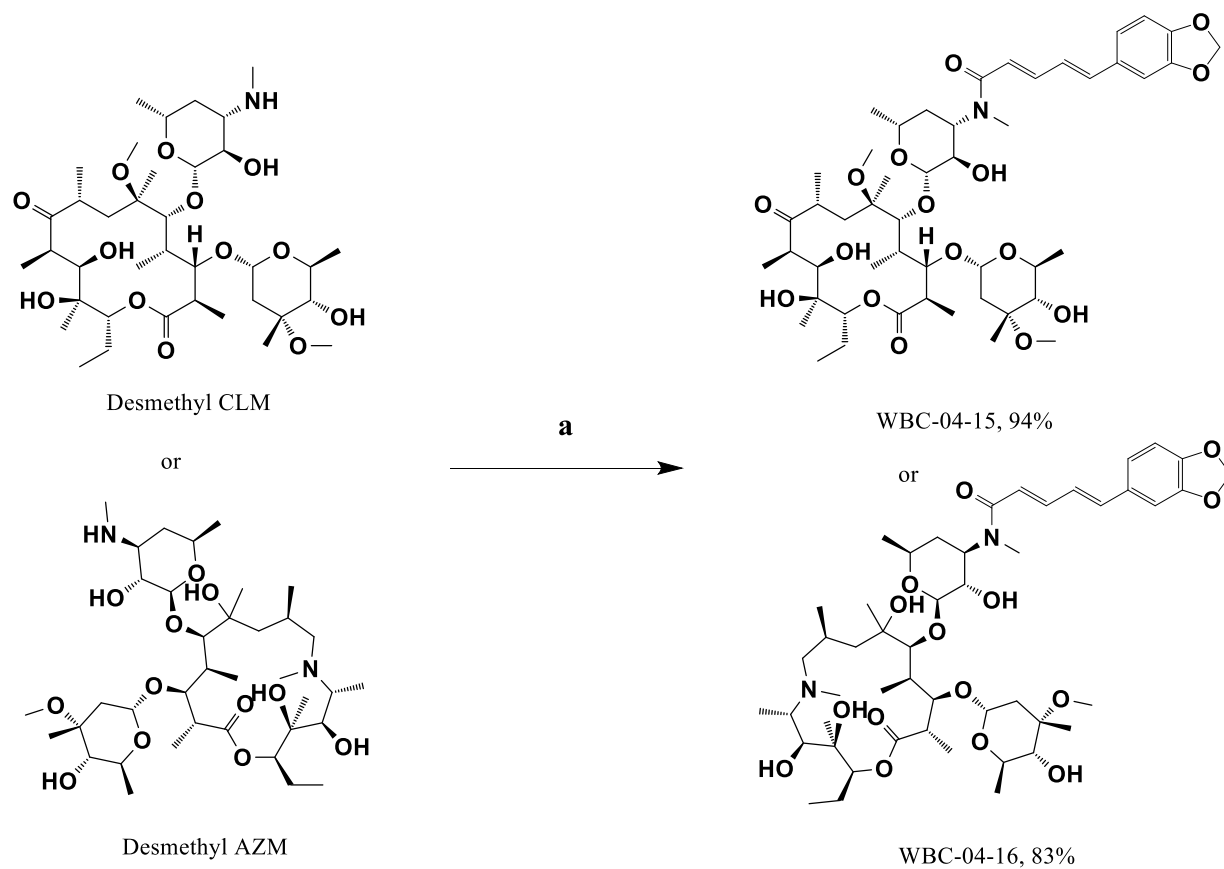
Figure 3.2. Designed macrolide-PIPE conjugates. (a) Ester-linked macrolide-PIPE conjugates. (b). Amide-linked macrolide-PIPE conjugates.

The ester-linked macrolide-PIPE conjugates WBC-04-11 and WBC-04-14 were synthesized from piperic acid anhydride as described for the analogous macrolide-ALA conjugates (Scheme 5).

Similarly, the amide-linked macrolide-PIPE conjugates WBC-04-15 and WBC-04-16 were synthesized from EDCI mediated coupling of Des-CLM or Des-AZM to piperic acid as described the macrolide-ALA congeners (Scheme 6).



Scheme 5. The synthesis of ester-linked macrolide-PIPE conjugates. (a) Piperic acid, EDCI, DCM, rt, overnight, 30.6%. (b) AZM or CLM, piperic acid anhydride, DCM, rt, 24 h to 48 h. 25% for WBC-04-14, 27% for WBC-04-11.



Scheme 6. The synthesis of amide-linked macrolide-PIPE conjugates. (a) Desmethyl CLM or Desmethyl AZM, piperic acid, EDCI, DMAP, Hunig's base, DCM, rt, 6 h to overnight. 94% for WBC-04-15, 83% for WBC-04-16.

3.2.1.3 Fumarate derivatives

In the same conjugation method as ALA and PPA, fumarate derivatives also conjugate in amide or ester bond linking with desosamine ring in macrolides. However, due to the cell accessibility issue of the methyl fumarate, we also introduce a butyl fumarate derivative to enhance the lipophilicity. Thus, we have synthesized eight macrolide derivatives listed in figure 3.3.

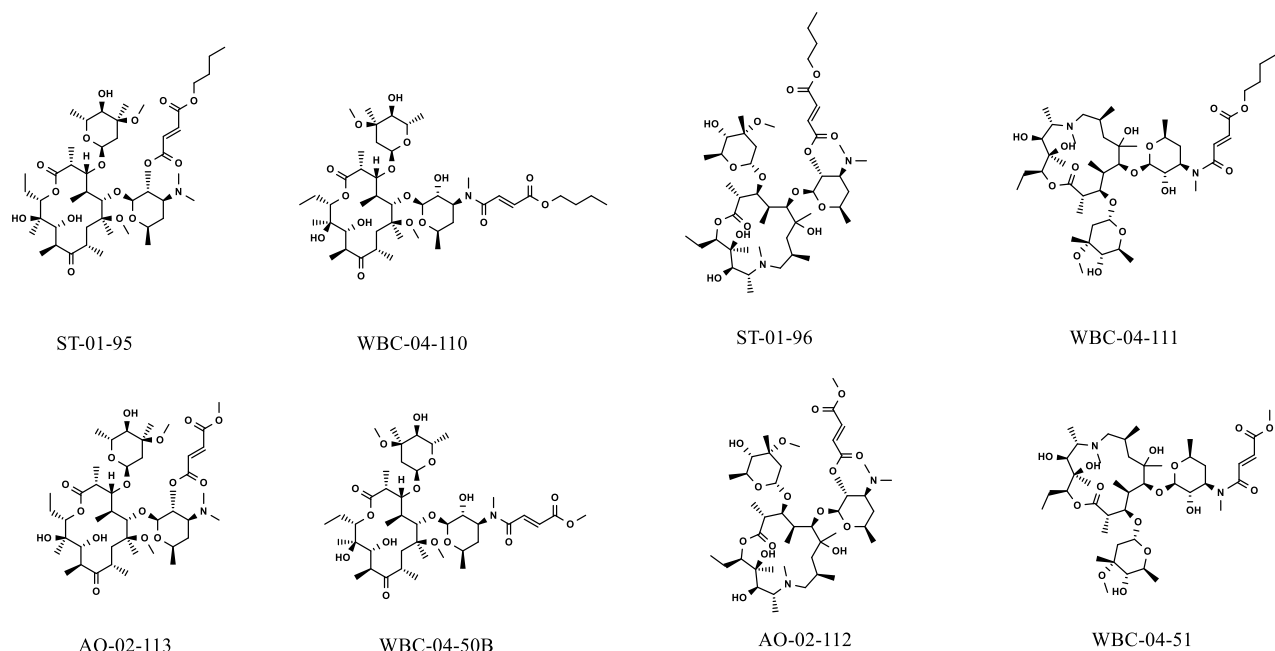
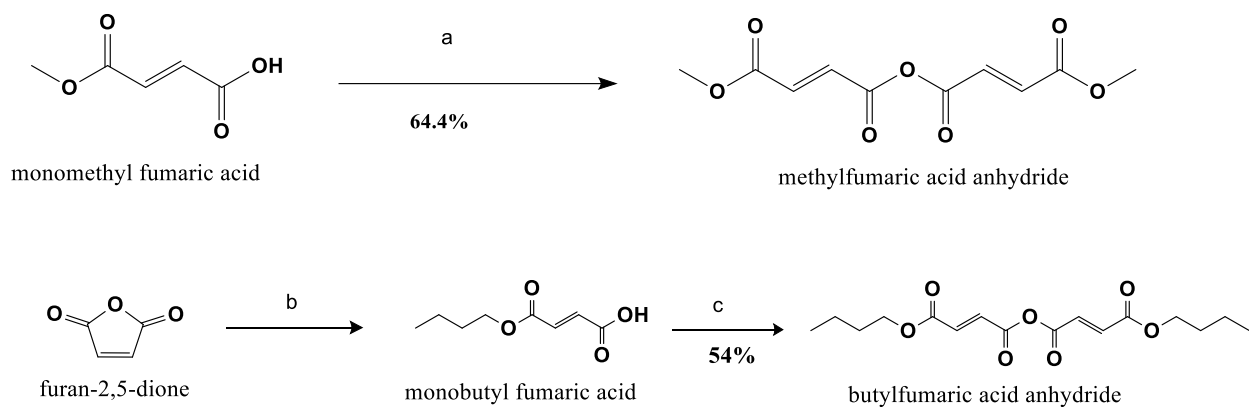
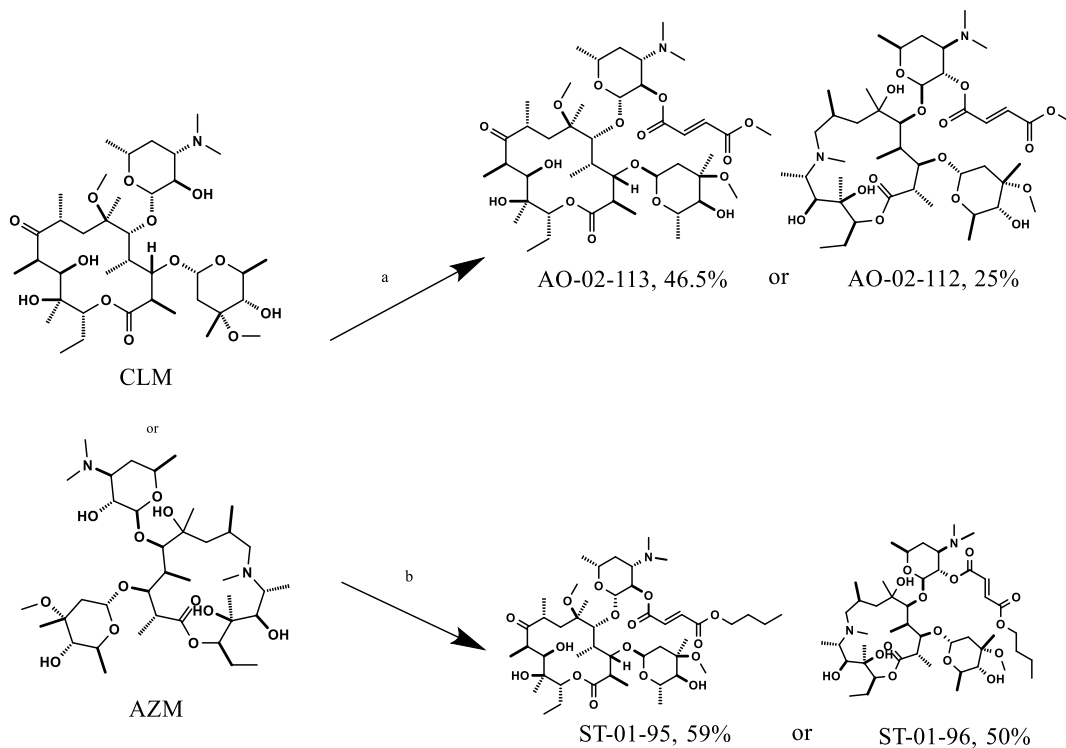


Figure 3.3. Designed macrolide-fumarate conjugates.

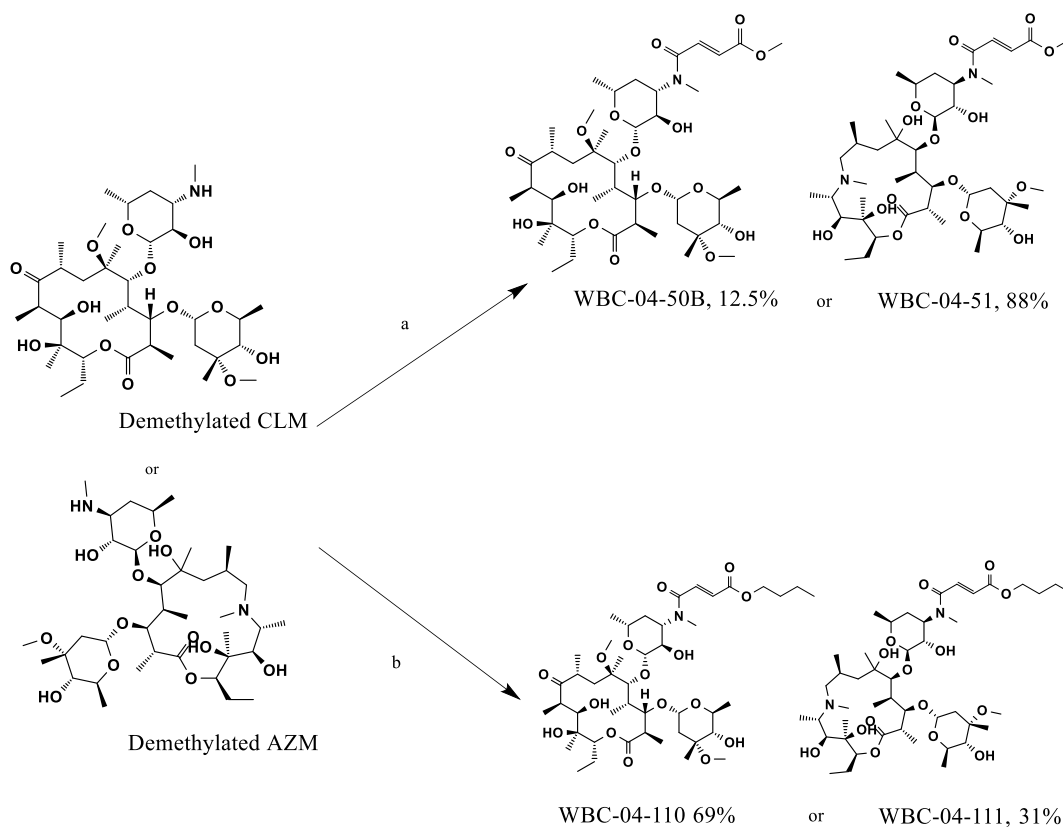
To synthesize the macrolide-fumarate conjugates, we require monomethyl fumarate and monobutyl fumarate. The monomethyl fumarate was obtained from commercial source while we synthesized the monobutyl fumarate from furan-2,5-dione (maleic anhydride) following a patent protocol (Scheme 7).²³ All of the macrolide-fumarate conjugates were synthesized by following the same protocol used in making the ALA and PIPE conjugates (Schemes 7-9).



Scheme 7. Synthesis of fumarate anhydrides. (a) Monomethyl fumaric acid, EDCI, DCM, 64.4%. (b) (i) furan-2,5-dione, butanol, toluene, 70°C, 24 h; (ii) AcCl, toluene, 70°C, 48 h. (c) Monobutyl fumaric acid, EDCI, DCM, 54%.



Scheme 8. The synthesis of ester-linked macrolide-fumarate conjugates. (a) AZM or CLM, monomethyl fumarate anhydride, DCM, rt, overnight. 46.5% for AO-02-113, 25% for AO-02-112. (b) AZM or CLM, monobutyl fumarate anhydride, DCM, rt, overnight, 59% for ST-01-95, 50% for ST-01-96.



Scheme 9. The synthesis of amide-linked macrolide-Fumarate conjugates. (a) Desmethyl CLM or desmethyl AZM, monomethyl fumarate, EDCI, DMAP, Hunig's base, DCM; 12.5% for WBC-04-50B, 88% for WBC-04-51. (b) Desmethyl CLM or desmethyl AZM, monobutyl fumarate, EDCI, DMAP, Hunig's base, DCM, 69% for WBC-04-110, 31% for WBC-04-111.

3.2.2 *Cell cytotoxicity*

After synthesis, we tested the effects of our Macrolide-antioxidants conjugates on the proliferation of MRC-5 (pulmonary fibroblast cell line) and representative cancer cell lines (), using normal monkey kidney fibroblast-like cell (VERO) as a control. We used the MTS assay evaluate the effects of compounds on cell proliferation.

3.2.2.1 Effects of macrolide-ALA conjugates on cell proliferation

The macrolide-ALA conjugates, unconjugated ALA and the macrolide templates (AZM and CLM) were screened in MTS assay to assess their effects on cell proliferation. All drugs were dissolved in 1% DMSO solution and incubated with VERO (monkey kidney fibroblast-like cell), Hep-G2 (hepatic carcinoma), A549 (pulmonary epithelial carcinoma), MRC-5 (pulmonary fibroblast cell line), MDA-MB-231 (triple negative breast cancer cell line), and MCF-7 (ER+ breast cancer cell line) at varying doses. The results from these experiments are shown in Table 3.1.

Table 3.1. The effects of macrolide-ALA conjugates on cell proliferation. IC₅₀s are given in μ M concentration. NI: no inhibition up to 500 μ M. All data are from two independent experiments. NT: not tested.

	Hep-G2	A549	MDA-MB-231	MCF-7	VERO	MRC-5
	(μ M)	(μ M)	(μ M)	(μ M)	(μ M)	(μ M)
AO-02-41	NI	NI	65 \pm 0.9	256.6 \pm 34.7	NI	44.8 \pm 7.1
AO-02-45	29.5 \pm 4.4	23.0 \pm 0.5	45.0 \pm 1.3	38.2 \pm 0.8	55.8 \pm 2.2	13.4 \pm 0.3
AO-02-47	221.8 \pm 5.3	NI	414.4 \pm 1.7	477.3 \pm 3.4	NI	262.5 \pm 0.2
AO-02-48	224.7 \pm 12.8	281.8 \pm 14.2	400.3 \pm 32.4	496.65 \pm 10.1	273.1 \pm 26.9	143.1 \pm 17
AC0NL	13.6 \pm 0.06	18.8 \pm 4.1	11.9 \pm 1.7	17.04	24.4 \pm 2.4	20.3 \pm 3.4
CC0NL	NI	NI	NI	NI	NI	NI
APC2NL	8.5 \pm 1.0	10.3 \pm 0.9	16.6 \pm 2.3	17.4 \pm 2.8	16.9 \pm 0.4	6.1 \pm 0.3
CPC2NL	14.4 \pm 0.5	26.9 \pm 0.2	22.4 \pm 0.8	45.8	40.3 \pm 4.9	24.5 \pm 2.6
DC-APC2NL	57.3 \pm 1.2	58.6 \pm 0	61.2 \pm 3.0	59.7 \pm 6.9	65.0 \pm 12.2	56.1 \pm 1.2
APC3NL	49.2 \pm 1.4	56.9 \pm 0.8	52.5 \pm 2.8	95.7	68.1 \pm 12.6	51.6 \pm 5.0
CPC3NL	14.8 \pm 2.1	27.4 \pm 0.4	291.3	285.9	47.7 \pm 6.2	17.9 \pm 0.5
DC-APC3NL	137.0 \pm 8.9	92.9 \pm 13.3	133.4	165.8	168.3 \pm 19.7	144.8 \pm 3.5
ALA	NI	NI	NI	NI	NI	NI
AZM	85.3 \pm 0.9	203.5 \pm 4.5	128.4 \pm 27.5	271.9 \pm 32.1	222.0 \pm 18.1	127 \pm 1
CLM	130.5 \pm 0.2	NI	156.9 \pm 6.2	197.7 \pm 14.7	NI	138.1 \pm 1.1

From the data of Table 3.1, CLM-based ester linked compound AO-02-41 shows selective toxicity to MRC-5 and MDA-MB-231, while the corresponding AZM-based compound AO-02-45 does not have such selective toxicity. In general, however, the AZM-based compounds are more cytotoxic than the CLM-based compounds. For example, AO-02-41 is less toxic than AO-02-45, and APC2NL is more potent than CPC2NL. AC0NL is also widely toxic to all cell lines including cancers and fibroblast, while CC0NL is non-toxic to all cells. Analogs lacking the cladinose sugar are also significantly less toxic to the cells in both ester- and aryl triazolyl-linked compounds. In contrast, the aryl triazolyl-linked compounds are highly cytotoxic to the cells. AZM derivative APC2NL has the highest cell cytotoxicity among these compounds, while APC3NL is 5-6 times weaker in potency. The length of the methylene linkers also influence potency as we noticed that the C2 linked compounds are more potent than C3 linked compounds. Relative to these macrolide-ALA conjugates, the template CLM and AZM, and the unconjugated ALA elicit weak cell cytotoxicity. Collectively, covalent linkage of ALA to AZM and CLM resulted in conjugates having significantly increased cytotoxic effects against the tested cell lines.

3.2.2.2 Effects of Macrolide-PIPE conjugates on cell proliferation

The macrolide-PIPE conjugates, unconjugated piperic acid, piperine and the macrolide templates (AZM and CLM) were similarly screened in MTS assay to assess their effects on the proliferation of VERO, Hep-G2, A549, MRC-5 cell lines. The results from these experiments are shown in Table 3.2.

Table 3.2. The effects of macrolide-PIPE conjugates on cell proliferation. IC₅₀s are given in μ M concentration. NI=no inhibition IC₅₀ up to 500 μ M. All data are from two independent experiments.

Compound	MRC-5	A549	Hep-G2	VERO
	(μ M)	(μ M)	(μ M)	(μ M)
WBC-04-11	3.78 \pm 0.8	15.63 \pm 2.6	5.0 \pm 0.5	13.19 \pm 1.5
WBC-04-14	7.82 \pm 0.7	16.89 \pm 0.7	5.59 \pm 0.1	20.99 \pm 2.3
WBC-04-15	NI	NI	NI	NI
WBC-04-16	11.38 \pm 0.4	19.56 \pm 1.8	10.19 \pm 1.9	12.92
Piperic Acid	NI	NI	NI	NI
Piperine	NI	NI	NI	NI

As shown in Table 3.2, piperine and piperic acid are not cytotoxic to any of the tested cell lines. Interestingly, WBC-04-11, an AZM derivative, potently inhibits the proliferation of MRC-5 (IC₅₀=3.78 μ M) against fibroblast and Hep-G2 (IC₅₀=5.0 μ M). The CLM derivative, WBC-04-14, has comparable potency as WBC-04-11. The potency enhancement displayed by WBC-04-11 and WBC-04-14 is more than 125-fold relative to piperine and piperic acid. Similar to the corresponding ALA derivative, the amide-linked CLM-PIPE conjugate WBC-04-15 is non-cytotoxic to all tested lines up to 500 μ M. In contrast, the amide-linked AZM-PIPE conjugate WBC-04-16 inhibits the proliferation of all tested cell lines with 10-20 μ M IC₅₀ range.

3.2.2.3 Effects of macrolide-fumarate conjugates on cell proliferation

The macrolide-Fumarate conjugates and monomethyl fumarate were similarly tested in MTS assay to assess their effects on the proliferation of VERO, Hep-G2, A549, MRC-5, MDA-MB-231 and MCF-7 cell lines.

Table 3.3. The effects of macrolide-fumarate conjugates on cell proliferation. IC₅₀s are given in μ M concentration. NI=no IC₅₀ at 500 μ M. NT=not tested. All data are from two independent experiments.

	MRC-5 (μ M)	A549 (μ M)	Hep-G2 (μ M)	VERO (μ M)	MDA-MB-231 (μ M)	MCF-7 (μ M)
AO-02-112	68.27	284.5	117.7	238.3 \pm 29.1	117.9	278
AO-02-113	88.41	278.5	133.2	219.4 \pm 45.8	139.9	127.5 \pm 16.5
WBC-04-51	NT	214	126.5	211.5	NT	NT
WBC-04-50B	NT	NI	NI	NI	NT	NT
ST-01-95	NI	NI	NI	NI	NI	NI
ST-01-96	43.60 \pm 8.5	140.9 \pm 4.3	63.56 \pm 7.7	126.2 \pm 2.4	29.6 \pm 3.0	50.00 \pm 1.5
WBC-04-110	44.92 \pm 0.6	NI	208.9 \pm 11.2	68.26 \pm 16.8	28.37 \pm 3.9	72.26 \pm 5.2
WBC-04-111	78.9 \pm 2.6	111.1 \pm 4.6	64.9 \pm 2.4	97.2 \pm 15.5	34.76 \pm 2.8	39.27 \pm 7.1
Monomethyl Fumarate	258.9	NT	NT	844	NT	NT

We found that for either macrolide template, the methyl fumarate derivatives are generally less potent than the butyl fumarate (Table 3.3). Specifically, the monomethyl fumarate compound AO-02-112 is less toxic than butyl fumarate derivative ST-01-96. This could possibly be to the increased the cell penetration and/or increased target-binding affinity afforded by the butyl group. As we observed for the ALA and PIPE conjugates, the amide-linked CLM-methyl fumarate

conjugate WBC-04-50B is not cytotoxic to the tested cell lines up to 500 μ M. Interestingly, unlike WBC-04-50B, we found that the amide-linked CLM-butyl fumarate conjugate WBC-04-111 is cytotoxic to all tested cell lines. Lastly, we found that monomethyl fumarate shows no inhibition against the tested cell lines up to 500 μ M except for MRC-5 against which it elicits growth inhibition at $IC_{50}=258.9$ μ M. This data suggests that AZM and CLM conjugation augments the anti-proliferative activities of piperine/piperic acid.

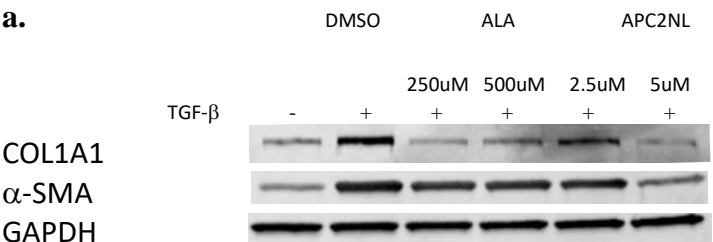
3.2.3 Anti-fibrotic effects macrolide-antioxidant conjugates

Tissue fibrosis is usually closely linked with inflammation and tumorigenesis. Typically, TGF- β stimulation could strongly induce ROS progression intracellularly. The cell stress induced by the upregulated levels of ROS could increase the expression of the components of the extracellular matrix (ECM), cause cytokine storm and immune response. Antioxidants, such as ALA and electrophilic anti-ROS agents PIPE and DMF could effectively attenuate TGF- β -induced tissue inflammation in fibrosis and cancer.^{11, 24-27} In the introduction and chapter 2 of this thesis, I showed that macrolides possessed intrinsic anti-fibrotic and anti-inflammation activities. It is likely that the macrolide-antioxidant conjugates described herein would retain the anti-fibrotic and anti-inflammation activities of the template macrolide.

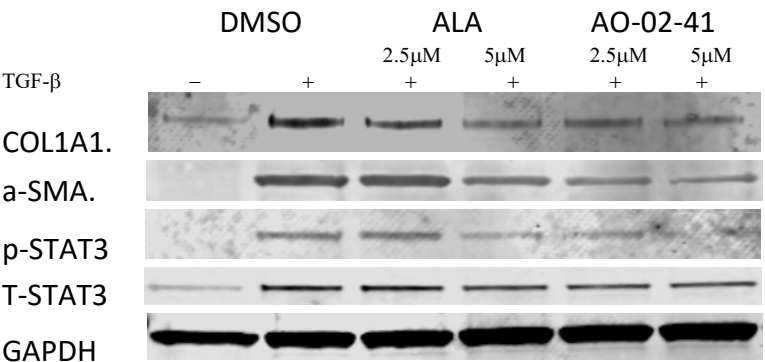
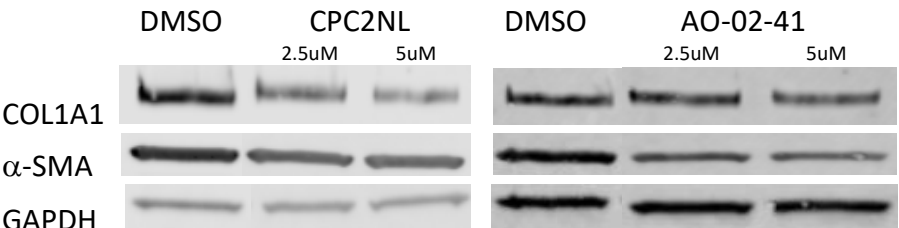
To investigate the anti-fibrotic activities of these Macrolide-antioxidant conjugates, we probed their effect on the expression of major components of ECM (COL1A1 and α -SMA) in TGF- β stimulated MRC-5 cells. Also, we tested for their effects on p-STAT3 levels as another biomarker of TGF- β stimulation.

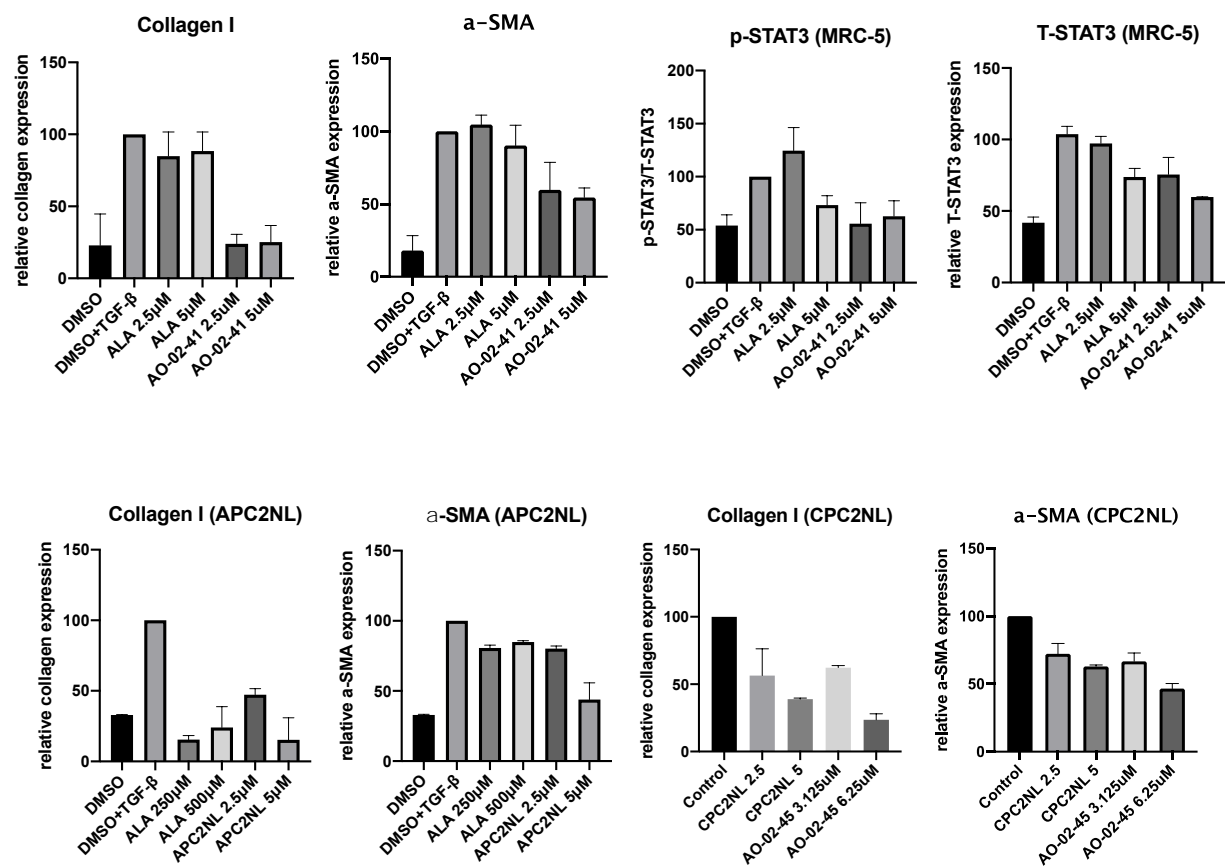
3.2.3.1 Macrolide-ALA conjugates showed strong anti-fibrotic effects.

APC2NL Western blot data

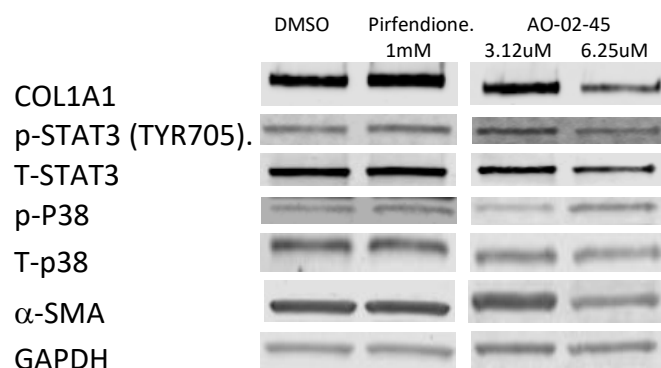


CPC2NL & AO-02-41 Western blot data





b. AO-02-45 Western blot data



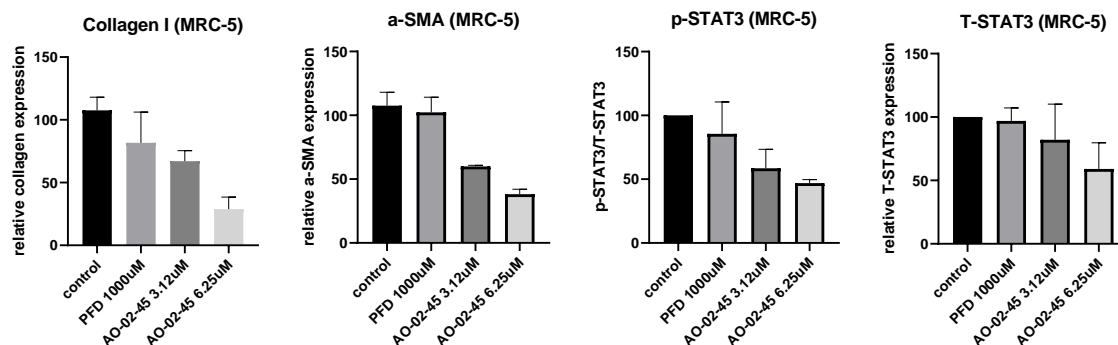


Figure 3.4. Anti-fibrotic effects of Macrolide-ALA conjugates. MRC-5 cells (1×10^6 cells/well) were stimulated by TGF- β after 24 h serum starvation in FBS-free medium. The cells were treated with 0.1% of DMSO or DMSO solution of selected candidates for 24 h. The MRC-5 cells were lysed and lysates analyzed by electrophoresis. (a) Gels showing ALA, AO-02-41, APC2NL, and CPC2NL. (b) Gels showing pirfenidone and AO-02-45. Quantification of the Western blots data probing for the effects of compounds on the ECM expression and STAT3 pathway in MRC-5 cells is shown below each gel.

APC2NL, CPC2NL, and AO-02-41 (Fig. 3.4a), and AO-02-45 (Fig. 3.4b) showed strong inhibition of COL1A1 and α -SMA at 5 μ M, suggesting that these compounds could attenuate tissue fibrosis at low concentration. AO-02-41 and AO-02-45 also showed p-STAT3 inhibition and suppression of the expression of total STAT3. In later experiment, we also found that these ALA derivatives could suppress the expression of STAT3 downstream proteins in a TNBC cell line (See section 2.4). These data indicate that these ALA derivative could be STAT3 pathway inhibitors for cancer therapy. In contrast, ALA at 2.5 and 5 μ M did not inhibit ECM production, although at 5 μ M it suppressed STAT3 phosphorylation. ALA only suppressed ECM components production at 250 and 500 μ M. This indicates that our compounds have improved anti-fibrotic and anti-inflammation effects relative to ALA.

3.2.3.2 Macrolide-PIPE conjugates showed strong anti-fibrotic effects.

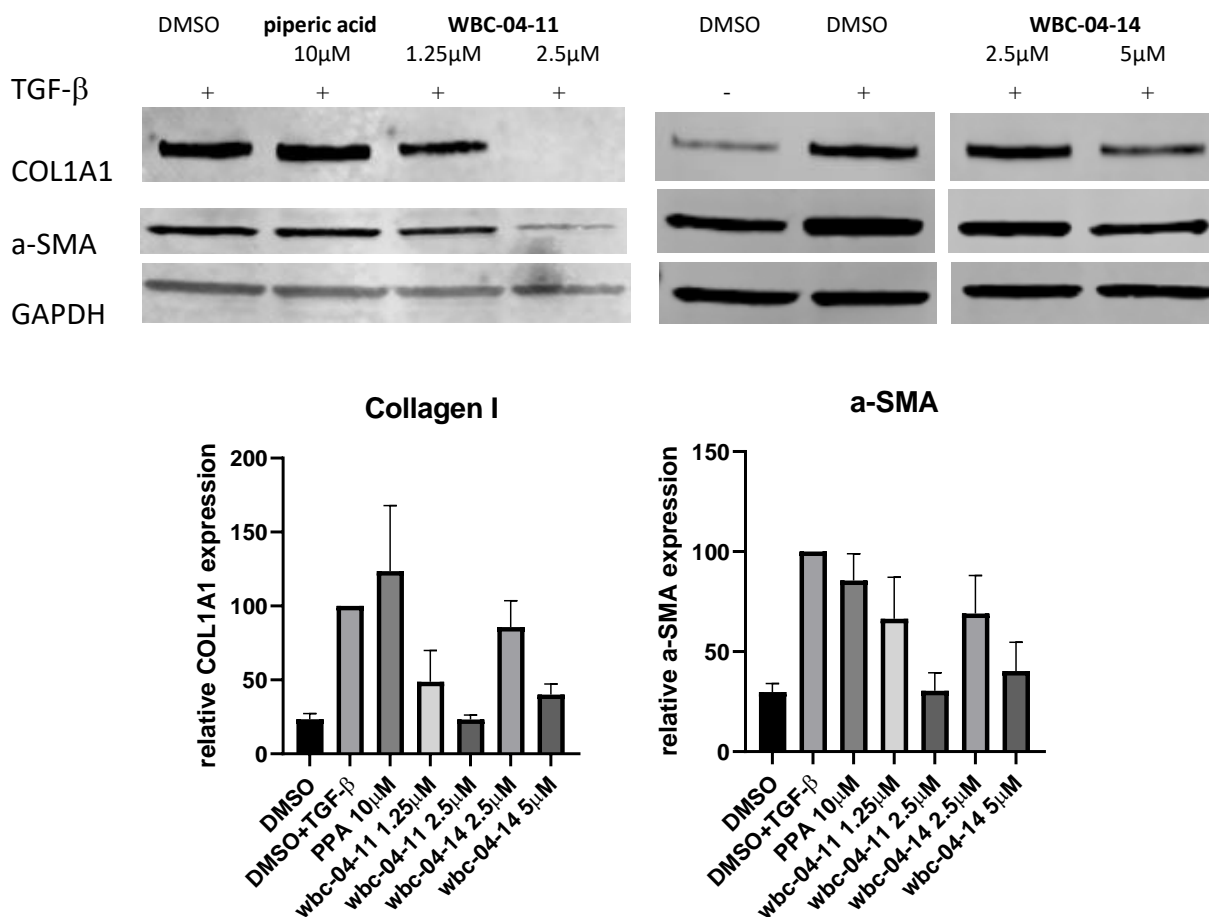


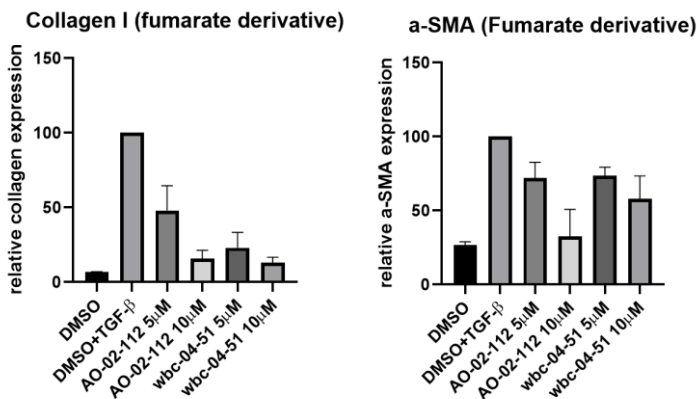
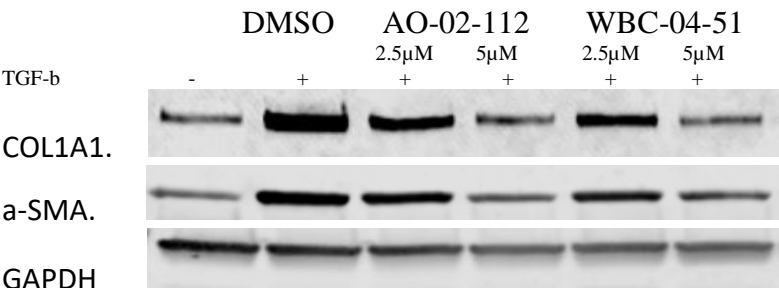
Figure 3.5. Anti-fibrotic effects of Macrolide-PIPE conjugates. MRC-5 cells (1×10^6 cells/well) were stimulated by TGF- β after 24 h serum starvation in FBS-free medium. The cells were treated with 0.1% of DMSO or DMSO solution of selected candidates for 24 h. The MRC-5 cells were lysed and lysates analyzed by electrophoresis. Piperic acid, WBC-04-11 and WBC-04-14 were tested. Quantification of the Western blots data probing for the effects of compounds on the ECM components expression in MRC-5 cells is shown below the gel.

We found that, at low micromolar concentrations, WBC-04-11 strongly inhibited COL1A1 and α -SMA expression in MRC-5 cell while WBC-04-14 did not inhibit the ECM production as strongly (Fig. 3.5). Although WBC-04-14 was not as potent as WBC-04-11, it is much improved relative

to piperic acid which at 10 μ M did not show any inhibition in ECM production. Therefore, the conjugation piperic acid to AZM and CLM enhanced the anti-fibrotic effect of the template macrolides and piperic acid significantly.

3.2.3.3 macrolide-fumarate conjugates showed strong anti-fibrotic effects.

a.



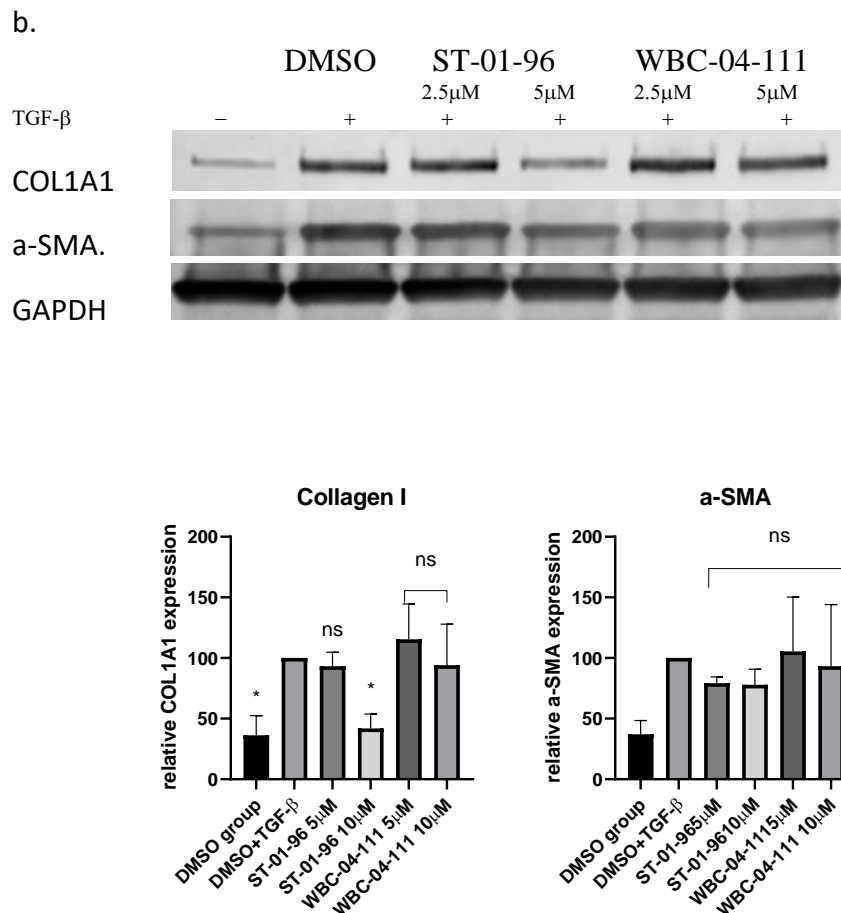


Figure 3.6. Anti-fibrotic effects of macrolide-fumarate conjugates. MRC-5 cells (1×10^6 cells/well) were stimulated by TGF- β after 24 h serum starvation in FBS-free medium. The cells were treated with 0.1% of DMSO or DMSO solution of selected candidates for 24 h. The MRC-5 cells were lysed and lysate analyzed by electrophoresis. (a) Gels showing methyl fumarate derivatives AO-02-112, WBC-04-51. (b) Gels showing the butyl fumarate derivatives ST-01-96 and WBC-04-111. Quantification of the Western blots data probing for the effects of candidates on the ECM expression in MRC-5 cells is shown below the gel.

We observed that both the ester and amide forms of the methyl fumarate compounds – AO-02-112 and WBC-04-51 – significantly inhibited the ECM production (Fig. 3.6). However, the butyl fumarates did not have the same pattern. While the ester analog, ST-01-96, showed significant COL1A1 downregulation, the amide compound WBC-04-111 showed no inhibition of ECM

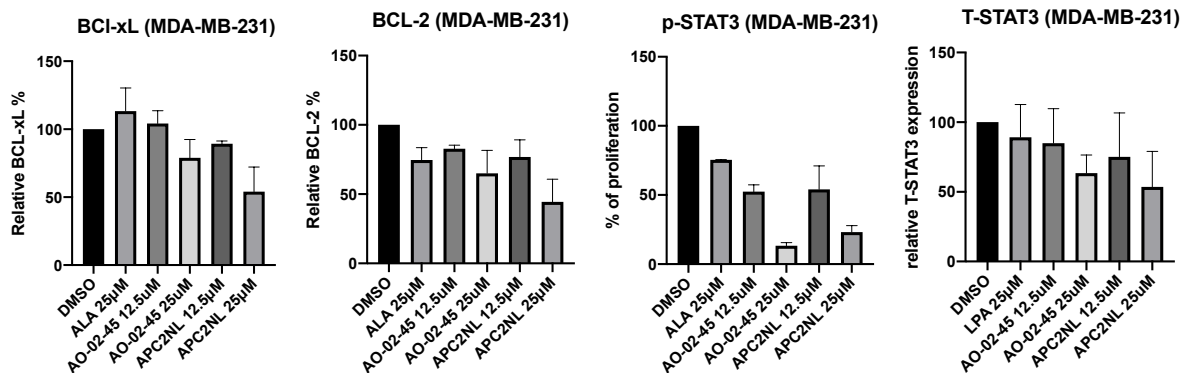
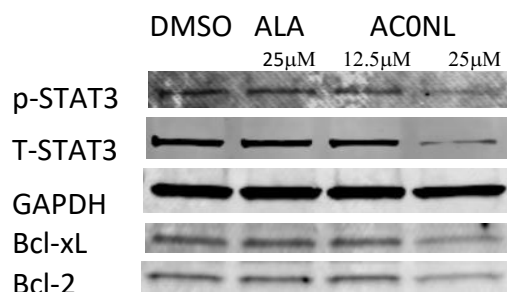
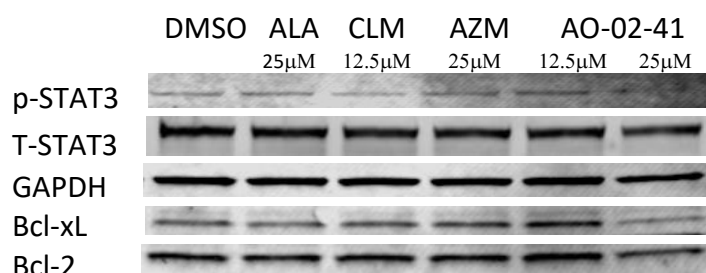
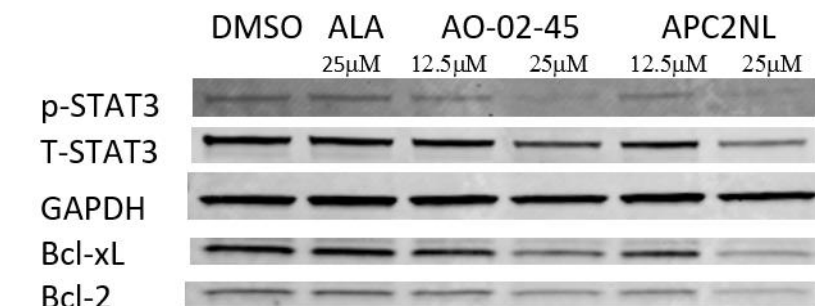
production. This data indicates that the mode of conjugation could significantly influence the anti-fibrotic and cytotoxic properties of the fumarate derivatives.

In summary, the macrolide-conjugated derivatives of ALA, PIPE and fumarate showed significantly enhanced anti-fibrotic effects, as they potently attenuate the TGF- β -induced cellular expression of ECM components. Additionally, the ALA derivatives also inhibit the STAT3 pathway at very low concentration range (2.5-5 μ M). These compounds are good candidates for future evaluation in *in vivo* models of tissue fibrosis and chronic inflammation.

3.2.4 *Investigation of the mechanisms of the antiproliferative effects of macrolide-antioxidant conjugates.*

To effectively investigate the new agents' eligibility in cancer therapy, we performed mechanistic studies to probe their potency in anti-cancer activities. In this chapter, we tested STAT3 pathway inhibition studies on MDA-MB-231 cell line with ALA derivatives, as previous studies imply a STAT3 pathway inhibition, and TNBC MDA-MB-231 is a STAT3-dependent cell line that may be sensitive to STAT3 inhibition. On the other hand, we tested HO-1 regulation studies in electrophilic agents fumarate and PIPE derivative, as they were known as Nrf-2 activators to attenuate ROS in cancer cells and fibroblast to prevent tissue inflammation.

3.2.4.1 ALA derivatives showed STAT3 pathway inhibition



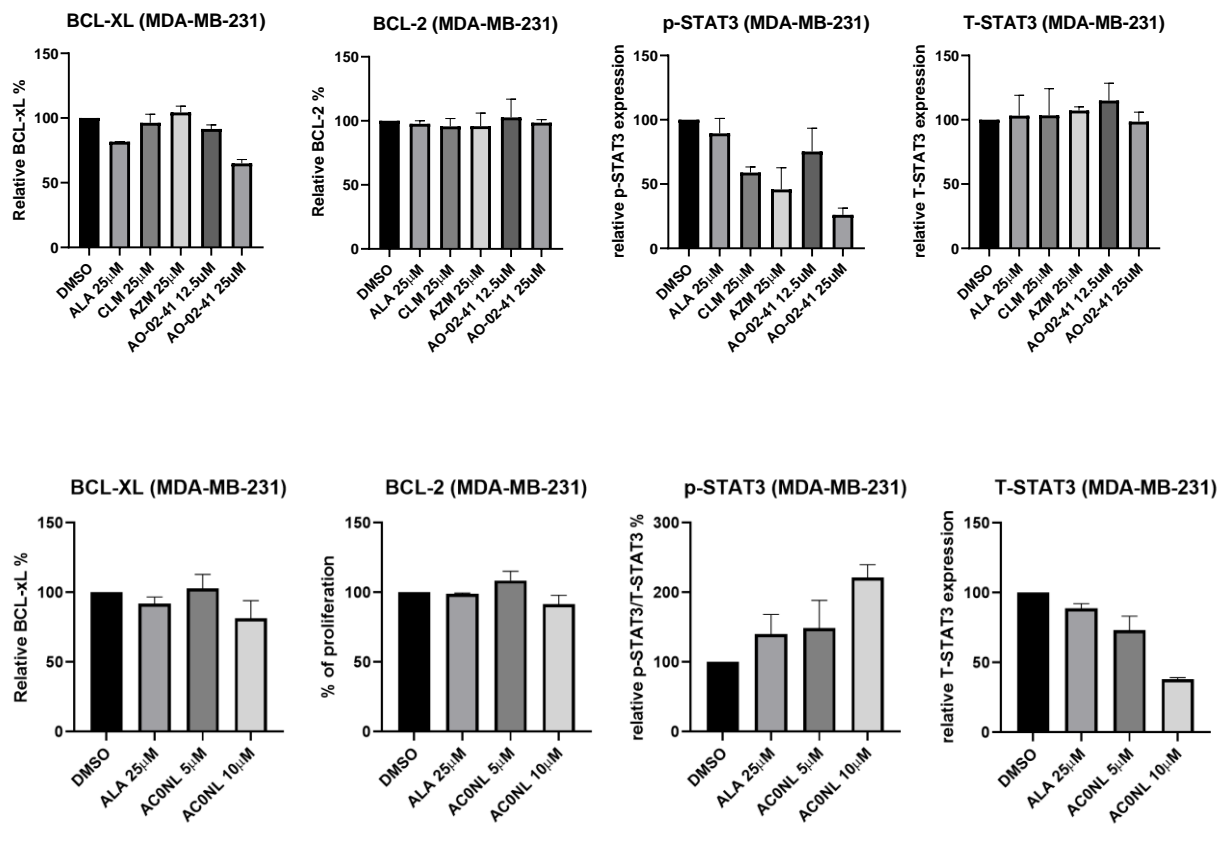


Figure 3.7. Anti-cancer effects of ALA and its derivatives towards MDA-MB-231. MDA-MB-231 cell line (1×10^6 cells/well) was incubated in DMEM until 80% confluency. The cells were serum starved for 24 h prior to drug treatment. In day 2, MDA-MB-231 were treated by 0.1% DMSO or DMSO solution of ALA, AO-02-45, APC2NL, AO-02-41, AC0NL, CLM, and AZM.

From the Western blot data for MRC-5, we noticed that the models can reduce p-STAT3 and T-STAT3 expression significantly. As we know the TNBC, MDA-MB-231 cell line, is highly dependent on STAT3 pathway for its proliferation and survival. Therefore, the Western blot has studied on MDA-MB-231 expression on p-STAT3, T-STAT3, Bcl-2, and Bcl-xL with treatment on selected candidates. We selected **AO-02-45**, **APC2NL**, **AC0NL**, **AO-02-41** as our candidates, as **AO-02-41** is selective to MRC-5 and MDA-MB-231 in MTS assay, and compound **AO-02-45** and **APC2NL** is critically effective on MRC-5 anti-fibrosis effect. We also tested AC0NL because

the amide conjugate may stabilize the conjugate more than ester. In this study, we found that the ALA at 25 μ M does not show significant p-STAT3, T-STAT3, Bcl-xL, and Bcl-2 down-regulation in MDA-MB-231. However, the **AO-02-41** shows significant Bcl-xL and p-STAT3 down-regulation at 25 μ M, but it does not show any effect on Bcl-2 and T-STAT3 regulation. Nonetheless, compound **AO-02-45** and **APC2NL** show significant down regulation on both Bcl-2 and Bcl-xL. As we expected, compound **AO-02-45** and **APC2NL** are both very outstanding in inhibition of p-STAT3 and T-STAT3 in both MDA-MB-231. This may cause the cell death eventually. Last, AC0NL is an interesting candidate that it showed no significant downregulation on Bcl-xl and Bcl-2, while it upregulates the p-STAT3 and down regulate the T-STAT3 with a dose-dependent manner. This unexpected result may indicate that the amide linker of ALA shares difference in mechanism of action.

3.2.4.2 PPA and Fumarate derivatives showed HO-1 upregulation

Since PPA and Fumarate have been recorded as Nrf-2 activator and upregulate the HO-1 expression in cells to attenuate the ROS stress in cancer and fibrosis, we investigated the novel macrolide derivatives of PPA and Fumarate against HO-1 regulation by immunoblotting. In brief, we used the MRC-5 cell as the source of HO-1 in western blot, as lung fibroblasts EMT are responsible for fibrosis and tissue inflammation in response of ROS. To perform the unbiased experimental data, we chose not to stimulate the cells with cytokines because cells could response in upregulation of HO-1 to against cytokine storm, which may falsely affect our results. Therefore, MRC-5 was starved with serum-free medium for overnight prior to the drug treatment. In figure 3.8, we observed that PPA, and AZM at 10 μ M slightly upregulated the HO-1, but not statistically

significant. CLM, on the contrary, did not upregulate the HO-1 at all. As expected, WBC-04-16, WBC-04-14, and WBC-04-11, the novel derivatives of PPA, induced significant HO-1 upregulation after 6 h treatment. We also observed a HO-1 restoration after 24 h treatment (data not shown). All these indicate that both AZM or CLM conjugated derivatives of PPA could upregulate the HO-1 at 5 μ M or 2.5 μ M, which implies a strong enhancement in Nrf-2 activation.

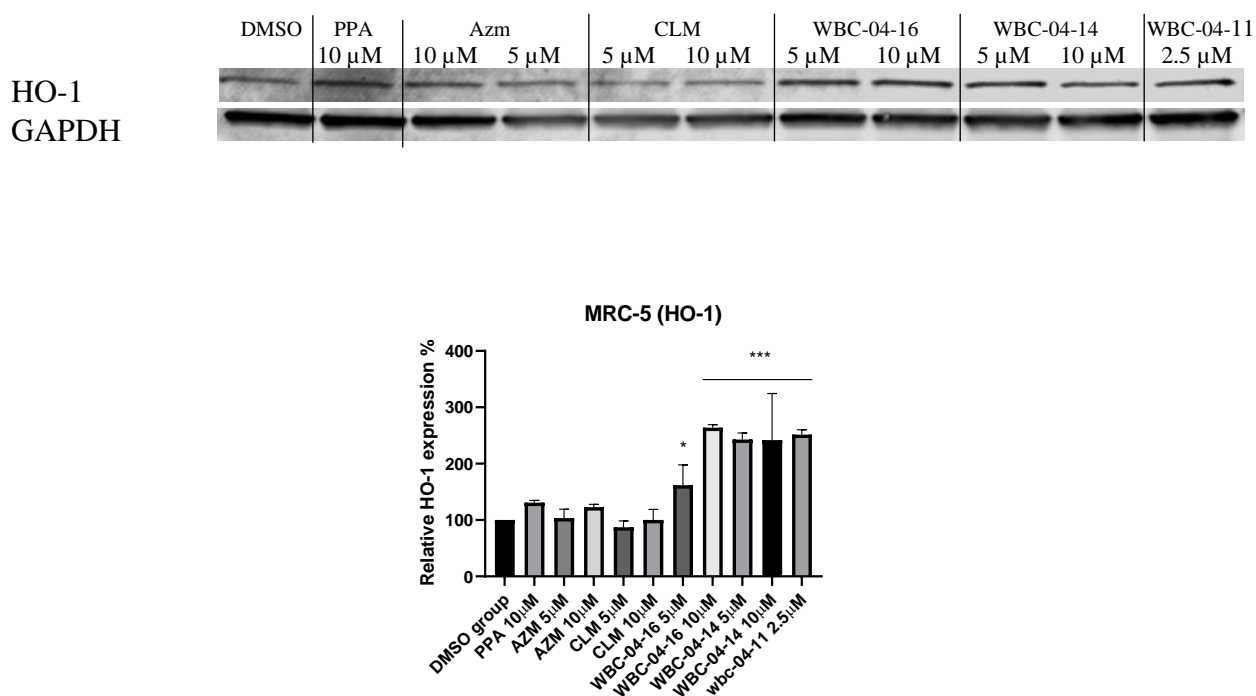
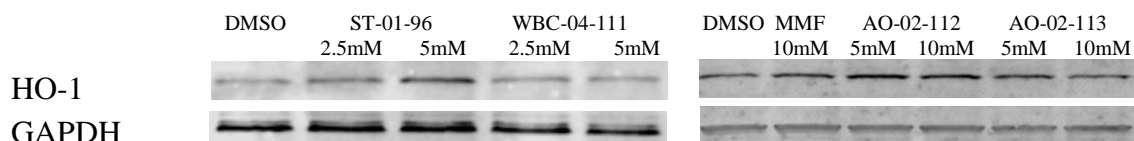


Figure 3.8. The HO-1 is upregulated by the macrolide derivatives of PPA, but not Macrolide alone or PPA alone. MRC-5 cells (1×10^6 cells/well) were starved by 24 h with FBS-free medium. The cells were treated with 0.1% of DMSO or DMSO solution of selected candidates or antioxidant PPA and group of Macrolides for 24 h. The MRC-5 cells were lysed and loaded for electrophoresis. The immunoblots were shown with anti-body detection. (a). cropped bands of HO-1 and GAPDH after treatment of PPA (10 μ M), AZM and CLM (5 and 10 μ M), WBC-04-16 (5 and 10 μ M), WBC-04-14 (5 and 10 μ M), and WBC-04-11 (2.5 μ M). (b) Quantification of the Western blots data probing for the effects of candidates on the ECM expression in MRC-5 cells.

a.



b.

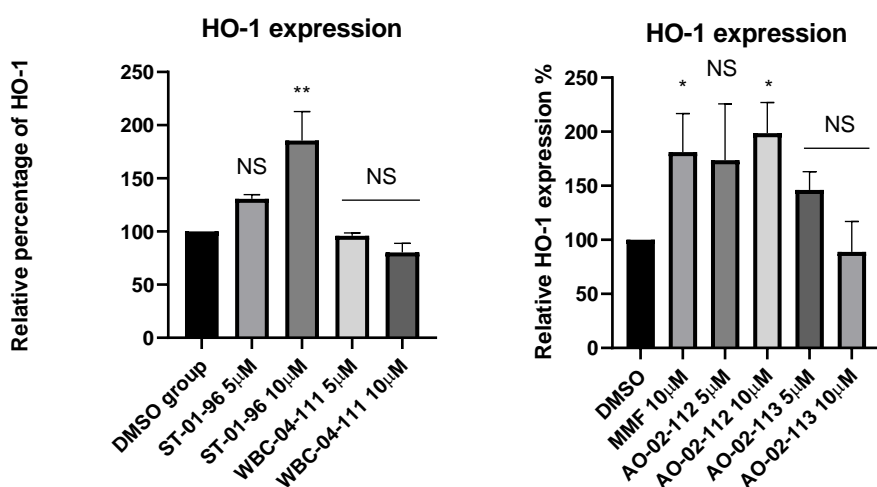


Figure 3.9. (a). Cropped bands for treatment with DMSO or 0.1% DMSO solution of ST-01-96, WBC-04-111, AO-02-112, AO-02-113. (b). Quantification of the Western blots data probing for the effects of candidates on the HO-1 upregulation in MRC-5 cells.

On the other hand, Fumarate derivatives also showed significant HO-1 upregulation with treatment towards MRC-5. First of all, monomethyl fumaric acid (MMF) at 10μM significantly up-regulate the HO-1 expression. ST-01-96 and AO-02-112, the ester conjugated AZM derivatives of methyl or butyl fumarate, also showed similar upregulation pattern as MMF. The HO-1 expression was up-regulated by ST-01-96, and AO-02-112 after 6 h treatment. However, surprisingly, WBC-04-

111, the butyl fumarate amide conjugation of CLM did not upregulate HO-1 at all. Interestingly, the AO-02-113, which is monomethyl fumarate ester conjugation of CLM, showed restoration effect in 10 μ M with 6 h treatment. This indicates that the CLM might not be the ideal template for fumarate conjugation on sustaining the HO-1 upregulation. Collectively, both fumarate and PPA demonstrated significant HO-1 upregulation after conjugating with macrolides on the desosamine region, which remains or enhances the electrophilic anti-oxidants Nrf-2 activation activity.

3.3 Conclusion:

Anti-oxidants Lipoic acid, and electrophilic anti-ROS agents Piperine and Dimethyl fumarate are proved to have effective therapeutic output to tissue inflammation and fibrosis. Due to the understanding of the linkage between tissue inflammation and cancer, studies of anti-cancer activities on these antioxidants were elucidated. ALA have been found to have strong anti-cancer effects on regulation of oncogenic STAT3 pathway and tumor metabolism. DMF and PIPE also regulates Nrf-2 activation against cancer inflammation. Therefore, they were considered as potential anti-cancer drugs. However, due to their low potency and off-target biodistribution, these anti-oxidants were not broadly use as standalone therapy for any certain types of cancer. In this chapter, by the inspiration of Macrolide-PFD model in chapter 2, we conjugate the macrolides to these antioxidants in desosamine ring. After design and synthesis, we tested cytotoxicity against Hep-G2, A549, MDA-MB-231, MCF-7, VERO, and MRC-5 cell lines, and observed that many candidates are more than 100-fold enhanced in cytotoxicity on cancer cells. Later, we found that all three types of Macrolide-antioxidants are showing strong anti-fibrosis effect on downregulation of ECM components COL1A1 and α -SMA. Subsequently, we investigated the target validation on

the antioxidant derivatives. Typically, ALA candidates showed outstanding STAT3 pathway inhibition in downregulating p-STAT3, T-STAT3, Bcl-xL and Bcl-2 against MDA-MB-231 cell line. The HO-1 downregulation was induced by piperic acid derivatives and fumarate derivatives, which implies that the compounds remains Nrf-2 activation activity as PPA and DMF. Collectively, the conjugated novel agents of antioxidants strongly improved in their cytotoxicity and maintained the functions of the antioxidant moiety in anti-inflammatory, anti-fibrosis, and anti-cancer activity.

3.4 Materials and methodology

3.4.1 Materials:

Analtech silica gel plates (60 F254) were used for analytical TLC while Analtech preparative TLC plates (UV 254, 2000 μm) or silica gel (400 Mesh) was used for compound purification. NMR spectra were taken on Varian-Gemini 400 MHz and Bruke 700 MHz magnetic resonance spectrometer. ^1H NMR spectra were recorded in parts per million (ppm) relative to the residual peaks of CHCl_3 (7.24 ppm) in CDCl_3 . ^{13}C spectra were recorded relative to the central peak of the CDCl_3 triplet (81.5 ppm) were recorded with complete hetero-decoupling. Multiplicities are described using the abbreviation: s, singlet; d, doublet, t, triplet; q, quartet; p, pentet; dd: doublet of doublet; ddd, doublet of doublet of doublet; dt: doublet of triplet; dq: doublet of quartets, m, multiplet; and app, apparent. High-resolution mass spectra were recorded at the Georgia Institute of Technology mass spectrometry facility in Atlanta.

3.4.2 Synthesis:

3.4.2.1 ALA derivatives:

Lipoic acid anhydride:

Lipoic acid (400mg, 1.94mmol) was dissolved into DCM (10 mL) with EDCI (1.2g, 7.74mmol). The solution was stirred for overnight with Ar protection. The solution was washed by water (30 mL) and extracted by DCM (20 mL) for four times so that remaining EDCI could be removed. The extracted organic solution was evaporated by vacuum and the crude product was yielded in yellow oil (160mg, 0.78mmol, 40.0%). This product is ready to use for next reaction without purification.

AO-02-41

Azithromycin (400mg, 0.54mmol) was mixed with the Lipoic acid anhydride (100mg, 0.26mmol) in DCM. The solution was stirred for overnight under Ar protection. The solution was washed by water (50 mL) and extracted by DCM (30 mL) twice. The organic solution was collected and evaporated to dryness by vacuum. The crude product was purified through Preparative TLC plate with solvent system DCM:MeOH=15:1. The final product was yielded as pale-yellow solid (60mg, 0.063mmol, 11.8%). ¹H NMR (400 MHz, cdcl₃) δ 4.99 (d, *J* = 10.9 Hz, 1H), 4.87 (d, *J* = 4.9 Hz, 1H), 4.67 (dd, *J* = 10.4, 7.5 Hz, 1H), 4.52 (d, *J* = 7.4 Hz, 1H), 3.98 – 3.83 (m, 2H), 3.69 (d, *J* = 8.1 Hz, 2H), 3.51 (dt, *J* = 20.9, 7.1 Hz, 2H), 3.42 (dd, *J* = 11.1, 6.0 Hz, 1H), 3.31 (s, 4H), 3.23 – 3.02 (m, 3H), 3.02 – 2.85 (m, 6H), 2.79 (p, *J* = 7.8 Hz, 1H), 2.50 (t, *J* = 9.8 Hz, 2H), 2.45 – 2.36 (m, 1H), 2.36 – 2.07 (m, 12H), 1.84 (ddt, *J* = 21.2, 14.3, 6.9 Hz, 4H), 1.72 – 1.49 (m, 10H), 1.43 (h, *J*

= 8.3, 7.6 Hz, 3H), 1.32 (s, 4H), 1.28 – 0.95 (m, 27H), 0.94 – 0.68 (m, 7H). ¹³C NMR (101 MHz, cdcl₃) δ 175.6, 172.2, 100.4, 95.8, 80.4, 78.3, 78.0, 76.5, 74.1, 72.8, 71.5, 69.0, 68.2, 65.8, 63.7, 56.5, 50.4, 49.4, 45.2, 40.6, 40.3, 38.9, 38.4, 37.2, 34.7, 34.4, 28.6, 24.7, 21.5, 19.8, 18.6, 17.9, 16.1, 12.3, 10.6, 9.0. HRMS (ESI) m/z Calcd. C₄₆ H₈₂ O₁₄ N S₂ [M+H⁺]: 936.5171, found 936.5149.

AO-02-45

Azithromycin (400mg, 0.54mmol) was mixed with the Lipoic acid anhydride (100mg, 0.26mmol) in DCM. The solution was stirred for overnight under Ar protection. The solution was washed by water (50 mL) and extracted by DCM (20 mL) twice. The organic solution was collected and evaporated to dryness by vacuum. The crude product was purified through Preparative TLC plate with solvent system DCM: MeOH=10:1. The final product was yielded as pale-yellow solid (62mg, 0.061mmol, 26.6%). ¹H NMR (400 MHz, cdcl₃) δ 5.10 (d, *J* = 4.8 Hz, 1H), 4.72 (dd, *J* = 10.6, 7.5 Hz, 1H), 4.64 (dd, *J* = 9.9, 2.7 Hz, 1H), 4.49 (d, *J* = 7.6 Hz, 1H), 4.19 (dd, *J* = 4.2, 2.0 Hz, 1H), 4.12 – 3.89 (m, 1H), 3.66 – 3.57 (m, 1H), 3.57 – 3.40 (m, 3H), 3.33 (s, 2H), 3.23 – 3.03 (m, 2H), 2.99 (d, *J* = 8.0 Hz, 1H), 2.74 – 2.60 (m, 2H), 2.60 – 2.35 (m, 3H), 2.36 – 2.07 (m, 10H), 2.04 – 1.92 (m, 2H), 1.93 – 1.75 (m, 3H), 1.62 (dd, *J* = 28.4, 20.5, 13.7, 5.1 Hz, 6H), 1.43 (tdd, *J* = 15.8, 9.3, 6.1 Hz, 3H), 1.36 – 1.09 (m, 14H), 1.04 (d, *J* = 7.1 Hz, 4H), 0.96 – 0.66 (m, 6H). ¹³C NMR (101 MHz, cdcl₃) δ 178.7, 172.2, 100.6, 94.4, 82.9, 78.1, 74.2, 73.6, 73.0, 71.5, 70.0, 68.2, 65.5, 63.9, 62.4, 56.5, 49.4, 45.2, 42.0, 40.7, 40.2, 38.5, 36.2, 34.7, 30.1, 28.6, 27.5, 26.6, 24.6, 21.9, 21.6, 21.2, 18.2, 16.2, 14.6, 11.2, 8.9, 7.3. HRMS (ESI) m/z Calcd. C₄₆H₈₅O₁₃N₂S₂ [M+H⁺]: 937.5488, found 937.5445.

AO-02-47

AO-02-41 (25mg, 0.026mmol) was dissolved into the 1N HCl (15 mL) and stir for 20 h under room temperature. The solution was washed by water and use DCM (25 mL) to extract the cladinoses. The aqueous layer was basified to pH=8-9 by sat. NaHCO₃ and then use DCM to extract the final product. The organic layer was collected and evaporated to dryness. To purify the product, the preparative TLC plate was used with condition DCM:MeOH=12:1 and the pure product was yielded as white solid (13mg, 0.017mmol, 65.3%). ¹H NMR (400 MHz, cdcl₃) δ 5.12 (dd, *J* = 11.2, 2.4 Hz, 1H), 4.99 – 4.85 (m, 1H), 4.82 (d, *J* = 7.4 Hz, 1H), 3.90 (s, 1H), 3.83 – 3.66 (m, 4H), 3.58 – 3.49 (m, 1H), 3.44 – 3.28 (m, 2H), 3.22 (d, *J* = 8.3 Hz, 2H), 3.20 – 3.03 (m, 3H), 3.03 – 2.93 (m, 2H), 2.90 (s, 4H), 2.75 (s, 8H), 2.63 (dq, *J* = 10.3, 6.6 Hz, 2H), 2.55 – 2.39 (m, 3H), 2.39 – 2.24 (m, 2H), 2.19 (dt, *J* = 12.9, 4.9 Hz, 2H), 2.14 – 1.98 (m, 1H), 1.98 – 1.82 (m, 3H), 1.67 (dddd, *J* = 18.5, 16.1, 13.9, 9.2 Hz, 6H), 1.59 – 1.36 (m, 6H), 1.36 – 1.24 (m, 7H), 1.24 – 0.97 (m, 19H), 0.88 (d, *J* = 7.4 Hz, 3H), 0.79 (t, *J* = 7.3 Hz, 3H). ¹³C NMR (101 MHz, cdcl₃) δ 174.9, 173.0, 98.4, 81.5, 74.1, 69.7, 68.9, 67.6, 63.2, 56.5, 49.7, 45.5, 44.1, 40.3, 38.5, 37.4, 35.6, 34.7, 28.9, 24.0, 20.8, 19.3, 17.9, 16.3, 15.5, 12.6, 10.4, 8.4. HRMS (ESI) *m/z* Calcd. C₃₈ H₆₈ O₁₁ N S₂ [M+H⁺]: 778.4228, found 778.4193.

AO-02-48

AO-02-45 (50mg, 0.053mmol) was dissolved into the 0.25 N HCl (10 mL) and stir for 20 h under room temperature. The solution was washed by water and use DCM (25 mL) to extract the

cladinose. The aqueous layer was basified to pH=8-9 by NaOH and then use DCM to extract the final product. The organic layer was collected and evaporated to dryness. With the TLC and staining, we observe that a new lower spot showed up as the final product. The pure product was yielded as white solid (29mg, 0.037mmol, 70.4%). ^1H NMR (400 MHz, cdcl_3) δ 4.75 – 4.54 (m, 1H), 3.78 – 3.58 (m, 2H), 3.54 (dd, J = 19.5, 13.2 Hz, 2H), 3.30 – 2.95 (m, 2H), 2.82 – 2.55 (m, 2H), 2.46 (dq, J = 12.3, 6.3 Hz, 1H), 2.30 (d, J = 48.4 Hz, 6H), 2.00 (d, J = 38.8 Hz, 1H), 1.90 (dt, J = 13.8, 6.9 Hz, 2H), 1.79 – 1.33 (m, 14H), 1.33 – 1.17 (m, 7H), 1.17 – 0.99 (m, 4H), 0.99 – 0.73 (m, 6H). ^{13}C NMR (101 MHz, cdcl_3) δ 177.4, 172.2, 99.9, 86.2, 78.4, 77.8, 74.2, 73.1, 71.6, 68.9, 63.5, 62.4, 56.5, 43.9, 41.3, 40.7, 38.5, 36.9, 35.9, 34.7, 34.3, 30.5, 28.7, 26.1, 24.7, 21.3, 21.1, 20.8, 16.1, 11.0, 7.6. HRMS (ESI) m/z Calcd. $\text{C}_{38}\text{H}_{71}\text{O}_{10}\text{N}_2\text{S}_2$ $[\text{M}+\text{H}^+]$: 779.4545, found 779.4516.

AC0NL

Des-AZM (180mg, 0.245mmol) was mixed with Hunig's base (0.5 mL) in 5 mL DCM solution with stirring. ALA (100mg, 0.485mmol) was mixed with EDCI (200mg, 1.29mmol) in another 5 mL DCM solution. After 5 minutes stirring with Argon, the ALA solution was added to the Des-AZM solution dropwisely with stirring, and DMAP (10mg, 0.082mmol) was added afterwards. The reaction was stirred for 24 h at room temperature with protection of Argon gas. The solution was washed by 100 mL water and extracted by DCM (30 mL). Then, the organic layer was washed again by water (100 mL) and extracted with 50 mL DCM. The organic layer was combined and evaporated by vacuum. The crude product was purified by Prep TLC with solvent condition as

EtOAc: MeOH=13:1. The final product was yielded in yellow foam (166mg, 0.203mmol, 83%). ¹H NMR (700 MHz, CDCl₃) δ 5.11 (d, *J* = 3.1 Hz, 1H), 4.78 – 4.74 (m, 1H), 4.72 – 4.66 (m, 1H), 4.49 (dd, *J* = 15.9, 7.3 Hz, 1H), 4.19 (dt, *J* = 6.6, 3.3 Hz, 1H), 4.07 (td, *J* = 9.8, 4.9 Hz, 1H), 3.68 (s, 1H), 3.62 – 3.55 (m, 2H), 3.38 (s, 2H), 3.34 (s, 1H), 3.17 (tdd, *J* = 7.9, 5.3, 2.7 Hz, 1H), 3.14 – 3.02 (m, 3H), 2.91 (s, 2H), 2.83 (s, 1H), 2.74 – 2.67 (m, 1H), 2.58 – 2.51 (m, 1H), 2.51 – 2.42 (m, 3H), 2.41 – 2.29 (m, 2H), 1.97 – 1.86 (m, 2H), 1.77 – 1.56 (m, 5H), 1.47 (dd, *J* = 19.4, 12.9, 9.9, 6.3, 2.6 Hz, 3H), 1.37 (s, 2H), 1.34 (d, *J* = 6.3 Hz, 3H), 1.27 – 1.14 (m, 8H), 1.11 (d, *J* = 7.9 Hz, 3H), 1.04 – 0.94 (m, 5H), 0.88 (t, *J* = 7.4 Hz, 3H). ¹³C NMR (176 MHz, CDCl₃) δ 174.3, 103.5, 94.9, 84.2, 78.0, 78.0, 77.3, 76.90, 74.5, 74.2, 73.9, 73.1, 71.6, 70.9, 69.3, 69.1, 68.4, 65.9, 62.3, 62.0, 57.5, 56.6, 53.9, 49.5, 42.3, 40.3, 38.5, 36.6, 36.4, 35.8, 34.8, 34.1, 33.8, 33.2, 31.9, 31.7, 29.7, 29.40, 29.10, 26.9, 26.4, 25.3, 25.0, 24.8, 24.7, 22.6, 22.6, 22.1, 21.6, 21.6, 21.4, 21.3, 21.0, 20.9, 20.7, 18.1, 16.5, 14.7, 14.1, 11.2, 9.4, 7.5. HRMS (ESI) *m/z* Calcd. C₄₅ H₈₂ O₁₃ N₂ S₂ [M+H⁺]: 923.5331, found 923.5334.

CC0NL

Des-CLM (180mg, 0.245mmol) was mixed with Hunig's base (0.5 mL) in 5 mL DCM solution with stirring. ALA (100mg, 0.485mmol) was mixed with EDCI (200mg, 1.29mmol) in another 5 mL DCM solution. After 5 minutes stirring, the ALA solution was added to the Des-CLM solution dropwisely with stirring, and DMAP (10mg, 0.082mmol) was added afterwards. The reaction was stirred for 24 h at room temperature with protection of Argon gas. The solution was washed by 100 mL water and extracted by DCM (30 mL). Then, the organic layer was washed again by water (100 mL) and extracted with 50 mL DCM. The organic layer was combined and evaporated by

vacuum. The crude product was purified by Prep TLC with solvent condition as EtOAc: hexane=8:2. The final product was yielded in yellow foam (186mg, 0.197mmol, 80.4%). ¹H NMR (700 MHz, CDCl₃) δ 5.03 (dd, *J* = 11.4, 3.9 Hz, 1H), 4.90 (dt, *J* = 8.4, 3.9 Hz, 1H), 4.68 – 4.61 (m, 1H), 4.49 (dd, *J* = 7.4, 2.5 Hz, 1H), 4.00 (q, *J* = 7.4 Hz, 1H), 3.95 (d, *J* = 4.9 Hz, 1H), 3.74 – 3.69 (m, 2H), 3.68 – 3.61 (m, 2H), 3.55 (q, *J* = 7.0 Hz, 1H), 3.34 – 3.27 (m, 3H), 3.19 (d, *J* = 6.0 Hz, 1H), 3.15 (dt, *J* = 11.7, 6.4 Hz, 0H), 3.09 (ddd, *J* = 11.1, 7.1, 3.6 Hz, 1H), 3.00 (d, *J* = 3.4 Hz, 3H), 2.96 (d, *J* = 7.1 Hz, 1H), 2.88 (d, *J* = 2.8 Hz, 2H), 2.84 (h, *J* = 8.1, 7.5 Hz, 1H), 2.80 (d, *J* = 3.2 Hz, 1H), 2.59 – 2.52 (m, 2H), 2.44 (dp, *J* = 12.5, 6.4, 4.7 Hz, 1H), 2.36 – 2.17 (m, 4H), 1.89 (qd, *J* = 17.3, 13.9, 5.3 Hz, 1H), 1.79 – 1.51 (m, 0H), 1.50 – 1.41 (m, 2H), 1.39 (d, *J* = 3.2 Hz, 2H), 1.28 (d, *J* = 5.7 Hz, 2H), 1.25 – 1.13 (m, 3H), 1.14 – 1.08 (m, 8H), 1.05 – 0.98 (m, 3H), 0.81 (dt, *J* = 10.6, 5.2 Hz, 3H). ¹³C NMR (176 MHz, CDCl₃) δ 220.8, 175.6, 174.3, 103.5, 96.2, 82.1, 76.6, 74.2, 72.8, 71.8, 69.0, 68.3, 65.7, 56.4, 53.7, 50.6, 49.4, 45, 40.2, 39.2, 38.8, 37.2, 35.7, 34.7, 33.8, 29.5, 29, 24.7, 21.4, 21, 19.6, 18.5, 17.9, 16, 12.3, 10.5, 9.5. HRMS (ESI) *m/z* Calcd. C₄₅H₇₉O₁₄NNaS₂ [M+Na⁺]: 944.4834, found 944.4843.

C2NL

2-bromoethan-1-aminium bromide (500mg, 2.44mmol) mixed with NaN₃ (400mg, 5.88mmol) in DMF (20 mL). The solution was heated to 80°C for overnight. The solution was not washed because water could be miscible to the product. DMF was evaporated with high temperature water bath and vacuum. The remained DMF solution of intermediate was used directly to couple with ALA so the final product C2NL could be formed. In brief, ALA (200mg, 2.32mmol) dissolved with DCM (20 mL) with EDCI (400mg, 2.11mmol) and DMAP (50mg, 0.41mmol). The solution

stirred for 30 minutes and the DMF solution of intermediate was added to the reaction. The solution stirred in room temperature for 1 hour and the product was made as C2NL linker. The crude product was washed by water (50 mL) and extracted by DCM (30 mL) for 3 times. Then, the product was purified by EtOAc to gain pure C2NL as liquid (188mg, 0.681mmol, 29%). ^1H NMR (400 MHz, cdCl_3) δ 4.12 – 4.02 (m, 1H), 3.69 – 3.55 (m, 2H), 3.48 (s, 3H), 3.42 (d, $J = 0.5$ Hz, 3H), 2.94 (dtd, $J = 13.1, 6.6, 5.4$ Hz, 1H), 2.80 (t, $J = 7.5$ Hz, 2H), 2.39 (dq, $J = 12.7, 6.9$ Hz, 1H), 2.24 – 2.03 (m, 6H), 1.97 (ddd, $J = 13.5, 8.7, 5.4, 2.6$ Hz, 2H).

C3NL

3-bromopropan-1-aminium bromide (400mg, 1.83mmol) mixed with NaN_3 (200mg, 3.07mmol) in DMF (10 mL). The solution was heated to 80°C for overnight. The solution was not washed because water could be miscible to the product. DMF was evaporated with high temperature water bath and vacuum. The remained DMF solution of intermediate was used directly to couple with ALA so the final product C2NL could be formed. In brief, ALA (400mg, 1.94mmol) dissolved with DCM (20 mL) with EDCI (1g, 5.26mmol) and DMAP (60mg, 0.49mmol). The solution stirred for 30 minutes and the DMF solution of intermediate was added to the reaction. The solution stirred in room temperature for 1 hour and the product was made as C3NL linker. The crude product was washed by water (50 mL) and extracted by DCM (30 mL) for 3 times. Then, the product was purified by EtOAc to gain pure C3NL as liquid (450mg, 1.65mmol, 85%). ^1H NMR (400 MHz, cdCl_3) δ 3.59 (dq, $J = 8.5, 6.4$ Hz, 1H), 3.44 – 3.36 (m, 2H), 3.23 – 3.08 (m, 3H), 3.01 (s, 3H), 2.94 (s, 3H), 2.47 (dtd, $J = 13.0, 6.6, 5.4$ Hz, 1H), 2.33 (t, $J = 7.5$ Hz, 2H), 1.99 – 1.80 (m, 2H), 1.77 – 1.61 (m, 3H), 1.49 (ddd, $J = 8.8, 7.6, 5.6, 2.8$ Hz, 2H).

CPC2NL

The PCC (50mg, 0.06mmol) mixed with C2NL linker (50mg, 0.18mmol) and dissolved in THF/DMSO solution (1:1 mL). The CuI (10mg, 0.05mmol) was added to the solution. The solution was purged with Argon and stirred for 5 minutes. Hunig's base (0.2 mL) was added to the solution. Then, the solution was stirred for overnight to complete the reaction. To remove Copper, the NH_4OH (1M, 30 mL) was poured to the DCM mixture of reaction solution. After 2 extractions, the DCM layer was collected and evaporated to dryness. The crude product was purified by DCM: MeOH=15:1 in Preparative TLC. The final product is yellow solid (60mg, 0.053mmol, 90%). ^1H NMR (700 MHz, CDCl_3) δ 7.71 (t, J = 4.1 Hz, 2H), 7.30 (d, J = 8.1 Hz, 2H), 4.98 (dd, J = 11.0, 2.3 Hz, 1H), 4.84 (d, J = 4.6 Hz, 1H), 4.50 – 4.45 (m, 2H), 4.37 (d, J = 7.2 Hz, 1H), 3.92 – 3.85 (m, 2H), 3.79 – 3.75 (m, 2H), 3.75 – 3.68 (m, 2H), 3.68 (dd, J = 9.4, 1.4 Hz, 1H), 3.60 – 3.54 (m, 1H), 3.48 – 3.36 (m, 2H), 3.28 – 3.23 (m, 1H), 3.13 – 3.06 (m, 5H), 3.02 (dt, J = 11.1, 6.9 Hz, 1H), 2.96 (s, 2H), 2.95 – 2.90 (m, 1H), 2.83 – 2.78 (m, 1H), 2.54 – 2.48 (m, 1H), 2.36 (dtd, J = 13.1, 6.7, 5.3 Hz, 1H), 2.30 – 2.22 (m, 1H), 2.19 (s, 2H), 2.11 (td, J = 7.3, 1.3 Hz, 2H), 1.88 – 1.74 (m, 5H), 1.66 – 1.50 (m, 7H), 1.47 – 1.34 (m, 2H), 1.34 (s, 3H), 1.21 (d, J = 6.1 Hz, 4H), 1.18 (d, J = 5.9 Hz, 10H), 1.12 (d, J = 7.3 Hz, 3H), 1.08 – 1.03 (m, 11H), 1.02 (d, J = 7.6 Hz, 3H), 0.84 – 0.79 (m, 3H), 0.81 – 0.75 (m, 6H). ^{13}C NMR (176 MHz, CDCl_3) δ 174.8, 172.3, 146.6, 128.4, 124.8, 119.4, 101.7, 94.9, 79.9, 77.3, 76.9, 75.6, 73.2, 71.5, 69.8, 68.0, 64.7, 63.2, 56.5, 55.3, 49.6, 48.6, 48.4, 44.2, 39.2, 38.2, 37.4, 36.2, 35.9, 35.2, 33.5, 30.9, 30.6, 28.7, 27.8, 24.2, 21.7, 20.5, 20.0, 18.8, 17.6, 17.0, 15.0, 14.9, 13.1, 11.3, 9.6, 8.1. HRMS (ESI) m/z Calcd. $\text{C}_{56}\text{H}_{92}\text{O}_{14}\text{N}_5\text{S}_2$ $[\text{M}+\text{H}^+]$: 1122.6077, found 1122.6064.

APC2NL

The PCA (50mg, 0.06mmol) mixed with C2NL linker (50mg, 0.18mmol) and dissolved in THF/DMSO solution (2:2 mL). The CuI (10mg, 0.05mmol) was added to the solution. The solution was purged with Argon and stirred for 5 minutes. Hunig's base (0.4ml) was added to the solution. Then, the solution was stirred for overnight to complete the reaction. To remove Copper, the NH_4OH (1M, 30ml) was poured to the DCM mixture of reaction solution. After 2 extractions, the DCM layer was collected and evaporated to dryness. The crude product was purified by DCM: MeOH=9:1 in Preparative TLC. The final product is pale-yellow solid (46mg, 0.041mmol, 80%). ^1H NMR (700 MHz, CDCl_3) δ 8.03 (s, 1H), 7.83 – 7.73 (m, 3H), 7.38 (d, J = 7.8 Hz, 2H), 6.09 (t, J = 6.0 Hz, 1H), 5.12 (d, J = 5.0 Hz, 1H), 4.75 – 4.64 (m, 2H), 4.61 – 4.52 (m, 2H), 4.45 (d, J = 7.3 Hz, 1H), 4.27 (dd, J = 4.4, 2.0 Hz, 1H), 4.11 – 4.03 (m, 1H), 3.91 – 3.77 (m, 3H), 3.77 – 3.59 (m, 3H), 3.59 – 3.45 (m, 4H), 3.45 – 3.32 (m, 2H), 3.26 (d, J = 14.9 Hz, 1H), 3.24 – 3.13 (m, 4H), 3.10 (dt, J = 11.1, 6.9 Hz, 1H), 3.02 (t, J = 9.7 Hz, 1H), 3.00 – 2.83 (m, 6H), 2.83 – 2.66 (m, 3H), 2.62 (ddd, J = 13.6, 10.3, 3.8 Hz, 1H), 2.55 (d, J = 11.7 Hz, 2H), 2.44 (dtd, J = 13.1, 6.6, 5.3 Hz, 1H), 2.34 (d, J = 6.9 Hz, 4H), 2.29 (d, J = 26.8 Hz, 4H), 2.19 (td, J = 7.4, 1.4 Hz, 2H), 2.16 – 1.96 (m, 5H), 1.96 – 1.85 (m, 3H), 1.85 – 1.73 (m, 3H), 1.73 – 1.60 (m, 5H), 1.56 (dd, J = 15.3, 5.1 Hz, 2H), 1.52 – 1.37 (m, 5H), 1.37 – 1.30 (m, 8H), 1.30 – 1.22 (m, 8H), 1.22 – 1.13 (m, 7H), 1.11 (d, J = 8.8 Hz, 6H), 1.05 (d, J = 7.5 Hz, 4H), 1.01 – 0.78 (m, 9H). ^{13}C NMR (176 MHz, CDCl_3) δ 178.8, 173.4, 162.5, 147.7, 139.3, 129.3, 129.3, 125.7, 120.4, 102.9, 94.6, 83.7, 78.1, 77.9, 77.2, 77.0, 76.9, 74.3, 73.7, 72.9, 70.8, 68.7, 65.5, 64.6, 57.7, 56.4, 49.6, 49.4, 45.2, 42.3, 42.1, 40.2, 39.2, 38.5, 37.0, 36.5, 36.3, 36.2, 34.7, 34.6, 31.4, 29.8,

29.7, 29.7, 29.4, 28.8, 27.5, 26.8, 25.3, 22.7, 22.0, 21.5, 21.4, 21.3, 18.2, 16.2, 14.8, 11.3, 9.1, 7.5. HRMS (ESI) m/z Calcd. $C_{56}H_{95}O_{13}N_6S_2$ $[M+H^+]$: 1123.6393, found 1123.6383.

CPC3NL

The PCC (50mg, 0.06mmol) mixed with C3NL linker (100mg, 0.35mmol) and dissolved in THF/DMSO solution (2:1 mL). The CuI (20mg, 0.05mmol) was added to the solution. The solution was purged with Argon and stirred for 5 minutes. Hunig's base (0.3 mL) was added to the solution. Then, the solution was stirred for overnight to complete the reaction. To remove Copper, the NH_4OH (1M, 30 mL) was poured to the DCM mixture of reaction solution. After 2 extractions, the DCM layer was collected and evaporated to dryness. The crude product was purified by DCM: MeOH=15:1 in Preparative TLC. The final product is yellow solid (40mg, 0.035mmol, 58.9%). 1H NMR (700 MHz, $CDCl_3$) δ 8.23 (s, 1H), 8.05 – 7.68 (m, 3H), 7.38 (d, J = 7.7 Hz, 2H), 6.05 (t, J = 6.6 Hz, 1H), 5.06 (d, J = 11.0 Hz, 1H), 4.92 (d, J = 5.1 Hz, 1H), 4.70 – 4.34 (m, 3H), 4.08 – 3.87 (m, 2H), 3.87 – 3.67 (m, 3H), 3.65 (d, J = 7.3 Hz, 1H), 3.48 (dd, J = 18.1, 9.5 Hz, 2H), 3.41 – 3.25 (m, 3H), 3.25 – 2.81 (m, 12H), 2.59 (dq, J = 19.1, 11.4, 9.0 Hz, 2H), 2.50 – 2.06 (m, 8H), 2.06 – 1.62 (m, 12H), 1.56 – 1.33 (m, 7H), 1.33 – 1.01 (m, 29H), 0.87 (dt, J = 27.8, 7.1 Hz, 5H). ^{13}C NMR (176 MHz, $CDCl_3$) δ 175.8, 161.6, 147.8, 129.4, 125.8, 120.0, 102.8, 96.0, 80.9, 78.3, 78.3, 77.9, 77.2, 77.0, 76.9, 74.3, 72.5, 70.8, 69.1, 68.7, 65.7, 64.0, 57.6, 50.6, 49.4, 47.6, 45.3, 45.1, 39.3, 39.1, 37.2, 36.9, 35.1, 34.8, 30.1, 29.7, 29.5, 21.5, 21.3, 21.0, 19.8, 18.7, 18.0, 16.0, 14.1, 12.3, 10.6, 9.1. HRMS (ESI) m/z Calcd. $C_{57}H_{94}O_{14}N_5S_2$ $[M+H^+]$: 1136.6233, found 1136.6259.

APC3NL

The PCA (50mg, 0.06mmol) mixed with C3NL linker (100mg, 0.35mmol) and dissolved in THF/DMSO solution (2:1 mL). The CuI (20mg, 0.05mmol) was added to the solution. The solution was purged with Argon and stirred for 5 minutes. Hunig's base (0.3 mL) was added to the solution. Then, the solution was stirred for overnight to complete the reaction. To remove Copper, the NH_4OH (1M, 30 mL) was poured to the DCM mixture of reaction solution. After 2 extractions, the DCM layer was collected and evaporated to dryness. The crude product was purified by DCM: MeOH=10:1 in Preparative TLC. The final product is yellow solid (33mg, 0.028mmol, 48.6%). ^1H NMR (700 MHz, CDCl_3) δ 8.25 (d, J = 1.6 Hz, 1H), 7.97 – 7.68 (m, 3H), 7.38 (d, J = 7.9 Hz, 2H), 6.07 (t, J = 6.2 Hz, 1H), 5.32 (s, 1H), 5.15 (d, J = 4.9 Hz, 2H), 4.71 (dd, J = 9.9, 2.7 Hz, 1H), 4.60 – 4.36 (m, 3H), 4.26 (dd, J = 3.9, 2.0 Hz, 1H), 4.06 (dq, J = 8.9, 6.2 Hz, 2H), 3.82 (d, J = 13.0 Hz, 1H), 3.77 – 3.58 (m, 3H), 3.58 – 3.43 (m, 4H), 3.41 – 3.25 (m, 4H), 3.25 – 2.86 (m, 7H), 2.84 – 2.47 (m, 7H), 2.47 – 2.16 (m, 14H), 2.16 – 1.87 (m, 7H), 1.87 – 1.59 (m, 4H), 1.59 – 1.41 (m, 3H), 1.41 – 0.99 (m, 17H), 0.99 – 0.79 (m, 9H). ^{13}C NMR (176 MHz, CDCl_3) δ 178.9, 161.8, 147.8, 139.1, 129.4, 129.3, 125.8, 120.0, 102.9, 94.5, 83.6, 78.1, 77.7, 77.2, 77.0, 76.8, 74.2, 73.7, 73.6, 72.9, 70.7, 70.1, 68.7, 65.9, 65.6, 64.4, 62.5, 57.7, 49.3, 47.6, 45.3, 42.3, 42.3, 40.3, 36.9, 36.2, 35.1, 34.6, 31.9, 30.1, 29.7, 29.7, 27.6, 26.8, 22.7, 22.0, 21.5, 21.4, 21.3, 18.2, 16.2, 15.3, 14.8, 14.6, 14.1, 11.3, 9.0, 7.3. HRMS (ESI) m/z Calcd. $\text{C}_{57}\text{H}_{97}\text{O}_{13}\text{N}_6\text{S}_2$ $[\text{M}+\text{H}^+]$: 1137.6550, found 1137.6565.

3.4.2.2 Piperic acid derivatives:

Piperic acid anhydride

Piperic acid (400mg, 1.83mmol) was dissolved into DCM (10 mL) with EDCI (1137mg, 7.34mmol). The solution was stirred for overnight with Ar protection. The solution was washed by water (30 mL) and extracted by DCM (20 mL) for four times to ensure all EDCI could be removed. The extracted organic solution was evaporated by vacuum and the crude product was yielded in yellow solid (235mg, 0.562mmol, 30.6%). This product is ready to use for next reaction without purification.

WBC-04-11

Azithromycin (170mg, 0.23mmol) was mixed with the piperic acid anhydride (235mg, 0.56mmol) in DCM. The solution was stirred for overnight under Ar protection. The solution was washed by water (50 mL) and extracted by DCM (20 mL) twice. The organic solution was collected and evaporated to dryness by vacuum. The crude product was purified through Preparative TLC plate with solvent system DCM:MeOH=10:1. The final product was yielded as pale-yellow solid (58mg, 0.061mmol, 26.6%). ¹H NMR (700 MHz, CDCl₃) δ 7.41 (dd, *J* = 15.2, 10.8 Hz, 1H), 7.01 (d, *J* = 1.6 Hz, 1H), 6.93 (d, *J* = 8.0 Hz, 1H), 6.87 – 6.77 (m, 2H), 6.72 (dd, *J* = 15.5, 10.9 Hz, 1H), 6.01 (s, 2H), 5.95 (d, *J* = 15.2 Hz, 1H), 5.09 (d, *J* = 4.8 Hz, 1H), 4.92 (q, *J* = 10.0, 9.5 Hz, 1H), 4.69 (d, *J* = 9.6 Hz, 1H), 4.63 (d, *J* = 7.5 Hz, 1H), 4.25 (d, *J* = 5.2 Hz, 1H), 4.07 (dt, *J* = 12.2, 6.1 Hz, 1H), 3.68 (s, 1H), 3.62 (d, *J* = 7.1 Hz, 1H), 3.57 (t, *J* = 9.6 Hz, 1H), 3.50 (q, *J* = 7.0 Hz, 2H), 3.43 (s, 3H), 3.40 – 3.33 (m, 1H), 3.08 (t, *J* = 8.3 Hz, 1H), 2.77 – 2.69 (m, 3H), 2.52 (d, *J* = 11.9 Hz, 1H), 2.38 (d, *J* = 15.0 Hz, 4H), 2.34 (s, 4H), 2.18 (d, *J* = 10.2 Hz, 1H), 1.94 – 1.85 (m, 2H), 1.71 (d, *J* = 14.6 Hz, 1H), 1.62 (dd, *J* = 15.2, 5.3 Hz, 2H), 1.45 (tdd, *J* = 13.8, 8.2, 4.9 Hz, 2H), 1.42 – 1.36

(m, 2H), 1.36 – 1.32 (m, 6H), 1.31 – 1.26 (m, 9H), 1.26 (s, 2H), 1.25 – 1.18 (m, 8H), 1.12 (tq, $J = 15.2, 6.8$ Hz, 4H), 1.05 (s, 4H), 0.95 (d, $J = 6.8$ Hz, 3H), 0.94 – 0.82 (m, 9H). ^{13}C NMR (176 MHz, CDCl_3) δ 178.4, 166.0, 148.6, 148.3, 139.9, 130.6, 124.7, 123.6, 122.9, 109.2, 105.8, 101.4, 101.3, 100.8, 94.8, 83.3, 78.1, 77.2, 77.0, 76.8, 74.3, 73.8, 73.1, 71.6, 70.1, 68.2, 65.9, 65.7, 63.8, 49.4, 45.1, 42.0, 41.6, 40.8, 36.5, 34.9, 31.9, 31.2, 29.7, 29.4, 27.3, 26.6, 22.7, 22.0, 21.7, 21.6, 21.2, 18.3, 18.3, 16.2, 15.3, 15.1, 14.1, 11.3, 9.3, 7.6. HRMS (ESI) m/z Calcd. $\text{C}_{50}\text{H}_{81}\text{O}_{15}\text{N}_2$ $[\text{M}+\text{H}^+]$: 949.5631, found 949.5605.

WBC-04-14

Clarithromycin (100mg, 0.13mmol) was mixed with the piperic acid anhydride (200mg, 0.48mmol) in DCM. The solution was stirred for overnight under Ar protection. The solution was washed by water (50 mL) and extracted by DCM (20 mL) twice. The organic solution was collected and evaporated to dryness by vacuum. The crude product was purified through Preparative TLC plate with solvent system DCM:MeOH=10:1. The final product was yielded as pale-yellow solid (30mg, 0.032mmol, 24.6%). ^1H NMR (700 MHz, CDCl_3) δ 7.41 (dd, $J = 15.2, 10.8$ Hz, 1H), 7.01 (d, $J = 1.7$ Hz, 1H), 6.93 (dd, $J = 8.0, 1.8$ Hz, 1H), 6.85 – 6.77 (m, 2H), 6.72 (dd, $J = 15.6, 10.8$ Hz, 1H), 6.01 (s, 2H), 5.93 (d, $J = 15.2$ Hz, 1H), 5.31 (s, 1H), 5.04 (dd, $J = 11.0, 2.4$ Hz, 1H), 4.94 (d, $J = 4.9$ Hz, 1H), 4.88 (dd, $J = 10.6, 7.5$ Hz, 1H), 4.64 (d, $J = 7.4$ Hz, 1H), 4.02 (dq, $J = 8.8, 6.2$ Hz, 1H), 3.98 (s, 1H), 3.78 – 3.74 (m, 1H), 3.74 (d, $J = 1.7$ Hz, 1H), 3.63 (d, $J = 6.9$ Hz, 1H), 3.53 (ddd, $J = 10.8, 6.2, 1.9$ Hz, 1H), 3.44 (s, 3H), 3.20 (s, 1H), 3.07 (d, $J = 9.0$ Hz, 1H), 3.02 (s, 3H), 2.97 (tt, $J = 7.0, 3.9$ Hz, 1H), 2.87 – 2.80 (m, 1H), 2.70 (d, $J = 12.4$ Hz, 1H), 2.58 (dtd, $J = 13.6, 7.0, 2.1$ Hz, 1H), 2.41 – 2.36 (m, 1H), 2.30 (s, 6H), 2.24 – 2.18 (m, 1H), 1.94

– 1.86 (m, 1H), 1.86 – 1.80 (m, 1H), 1.79 – 1.74 (m, 1H), 1.69 (dd, $J = 14.8, 11.7$ Hz, 1H), 1.62 (ddd, $J = 14.8, 6.3, 3.7$ Hz, 2H), 1.44 (dtd, $J = 14.2, 7.2, 4.3$ Hz, 2H), 1.38 – 1.32 (m, 3H), 1.31 (d, $J = 8.3$ Hz, 5H), 1.26 (dd, $J = 12.6, 4.9$ Hz, 6H), 1.21 (dd, $J = 7.3, 3.9$ Hz, 4H), 1.15 (d, $J = 7.0$ Hz, 3H), 1.14 – 1.08 (m, 7H), 0.88 (d, $J = 7.5$ Hz, 3H), 0.83 (t, $J = 7.4$ Hz, 3H). ^{13}C NMR (176 MHz, CDCl_3) δ 175.7, 166.0, 148.6, 148.33, 144.7, 134.0, 130.5, 124.6, 122.9, 120.9, 108.6, 105.8, 101.4, 100.8, 95.8, 95.8, 80.6, 78.4, 78.1, 77.9, 77.2, 77.0, 76.6, 74.2, 72.9, 72.8, 71.6, 69.1, 68.2, 65.9, 65.8, 63.6, 53.4, 50.4, 49.5, 49.3, 45.2, 45.0, 40.8, 39.1, 38.7, 37.3, 34.9, 31.0, 29.7, 21.6, 21.3, 21.0, 19.9, 18.7, 17.9, 16.0, 12.3, 10.6, 9.2. HRMS (ESI) m/z Calcd. $\text{C}_{50}\text{H}_{78}\text{O}_{16}\text{N}$ $[\text{M}+\text{H}^+]$: 948.5315, found 948.5293.

WBC-04-15

Des-CLM (200mg, 0.273mmol) was mixed with Hunig's base in 5 mL DCM solution with stirring. Piperic acid (75mg, 0.34mmol) was mixed with EDCI (210mg, 1.35mmol) in another 5 mL DCM solution. After 5 minutes stirring, the piperic acid solution was added to the Des-CLM solution dropwisely with stirring, and DMAP (10mg, 0.082mmol) was added afterwards. The reaction was stirred for 24 h at room temperature with protection of Argon gas. The solution was washed by 100ml water and extracted by DCM (30 mL). Then, the organic layer was washed again by water (100 mL) and extracted with 50ml DCM. The organic layer was combined and evaporated by vacuum. The crude product was purified by Prep TLC with solvent condition as EtOAc: MeOH=20:1. The final product was yielded in yellow foam (240mg, 0.257mmol, 94%). ^1H NMR (700 MHz, CDCl_3) δ 7.46 (dd, $J = 14.5, 10.1$ Hz, 1H), 7.01 (s, 1H), 6.92 (d, $J = 8.0$ Hz, 1H), 6.82 – 6.79 (m, 2H), 6.77 (d, $J = 10.4$ Hz, 1H), 6.41 (d, $J = 14.6$ Hz, 1H), 6.00 (s, 2H), 5.32 (d, $J = 1.8$

Hz, 1H), 5.08 (d, $J = 10.8$ Hz, 1H), 4.95 (d, $J = 5.1$ Hz, 1H), 4.76 (td, $J = 11.9, 4.1$ Hz, 1H), 4.56 (d, $J = 7.1$ Hz, 1H), 4.05 (q, $J = 7.1, 6.6$ Hz, 1H), 3.99 (s, 1H), 3.77 (d, $J = 8.6$ Hz, 2H), 3.73 – 3.69 (m, 1H), 3.69 (s, 1H), 3.39 (d, $J = 11.0$ Hz, 4H), 3.21 (s, 1H), 3.06 (s, 4H), 3.04 – 2.98 (m, 4H), 2.95 (s, 1H), 2.89 (q, $J = 7.7$ Hz, 1H), 2.73 (d, $J = 4.6$ Hz, 1H), 2.61 (dq, $J = 13.9, 7.5, 6.6$ Hz, 2H), 2.39 (d, $J = 15.1$ Hz, 1H), 2.01 – 1.94 (m, 1H), 1.94 – 1.89 (m, 1H), 1.81 (t, $J = 13.4$ Hz, 1H), 1.72 (d, $J = 18.3$ Hz, 2H), 1.69 – 1.59 (m, 3H), 1.56 – 1.45 (m, 2H), 1.44 (s, 3H), 1.34 (d, $J = 6.1$ Hz, 3H), 1.30 – 1.21 (m, 10H), 1.19 – 1.13 (m, 9H), 1.08 (dd, $J = 22.7, 7.6$ Hz, 3H), 0.86 (t, $J = 7.4$ Hz, 3H). ^{13}C NMR (176 MHz, CDCl_3) δ 220.9, 175.7, 168.6, 148.3, 148.2, 143.8, 139.3, 130.8, 125.0, 122.8, 119.9, 108.5, 105.7, 103.7, 101.3, 96.2, 82.1, 78.5, 78.3, 78.0, 77.2, 74.2, 72.8, 72.1, 69.1, 68.4, 65.8, 54.4, 53.4, 50.7, 49.5, 45.2, 45.0, 39.2, 38.9, 37.3, 35.8, 35.01, 29.8, 21.6, 21.1, 21.0, 19.7, 18.7, 18.0, 16.0, 12.3, 10.6, 9.5. HRMS (ESI) m/z Calcd. $\text{C}_{49}\text{H}_{75}\text{O}_{16}\text{N Na}$ $[\text{M}+\text{Na}^+]$: 956.4978, found 956.4958.

WBC-04-16

Des-AZM (180mg, 0.245mmol) was mixed with Hunig's base (0.5 mL) in 5 ml DCM solution with stirring. Piperic acid (85mg, 0.39mmol) was mixed with EDCI (200mg, 1.29mmol) in another 5 ml DCM solution. After 5 minutes stirring, the Piperic acid solution was added to the Des-CLM solution dropwisely with stirring, and DMAP (10mg, 0.082mmol) was added afterwards. The reaction was stirred for 24 h at room temperature with protection of Argon gas. The solution was washed by 100ml water and extracted by DCM (30 mL). Then, the organic layer was washed again by water (100 mL) and extracted with 50ml DCM. The organic layer was combined and evaporated by vacuum. The crude product was purified by Prep TLC with solvent condition as EtOAc:

MeOH=13:1. The final product was yielded in yellow foam (190mg, 0.203mmol, 83%). ^1H NMR (700 MHz, CDCl_3) δ 7.46 (dd, $J = 14.6, 9.4$ Hz, 1H), 7.00 (d, $J = 12.1$ Hz, 1H), 6.92 (d, $J = 8.2$ Hz, 1H), 6.82 – 6.77 (m, 2H), 6.77 – 6.73 (m, 1H), 6.42 (d, $J = 14.6$ Hz, 1H), 6.00 (s, 2H), 5.32 (d, $J = 1.7$ Hz, 1H), 5.05 (dd, $J = 18.2, 4.7$ Hz, 1H), 4.79 (td, $J = 11.6, 4.1$ Hz, 1H), 4.69 (d, $J = 10.2$ Hz, 1H), 4.56 (dd, $J = 25.0, 7.3$ Hz, 1H), 4.25 (d, $J = 5.7$ Hz, 1H), 4.14 – 4.08 (m, 1H), 3.72 – 3.67 (m, 2H), 3.52 – 3.48 (m, 2H), 3.41 (s, 2H), 3.37 (s, 1H), 3.08 (q, $J = 9.9$ Hz, 1H), 3.03 (s, 2H), 2.95 (s, 1H), 2.80 (d, $J = 14.2$ Hz, 2H), 2.73 (t, $J = 6.8$ Hz, 1H), 2.68 – 2.65 (m, 1H), 2.55 (t, $J = 10.5$ Hz, 2H), 2.36 (d, $J = 3.7$ Hz, 3H), 2.08 (t, $J = 11.8$ Hz, 1H), 2.05 – 2.00 (m, 2H), 1.90 (dq, $J = 15.0, 7.6$ Hz, 1H), 1.81 – 1.67 (m, 3H), 1.61 (dd, $J = 15.1, 5.4$ Hz, 1H), 1.58 – 1.47 (m, 2H), 1.38 – 1.34 (m, 6H), 1.32 – 1.20 (m, 13H), 1.12 (d, $J = 6.7$ Hz, 3H), 1.09 (s, 3H), 1.04 (d, $J = 7.3$ Hz, 2H), 1.01 (d, $J = 7.8$ Hz, 1H), 0.93 (dt, $J = 24.4, 7.3$ Hz, 6H). ^{13}C NMR (176 MHz, CDCl_3) δ 178.5, 168.3, 148.3, 148.2, 143.5, 139.0, 130.9, 125.2, 122.7, 120.2, 108.5, 105.7, 103.7, 101.3, 95.3, 85.2, 78.7, 78.1, 77.2, 77.0, 76.9, 74.5, 74.3, 73.5, 73.0, 71.8, 70.1, 68.4, 65.9, 65.8, 62.2, 54.5, 53.4, 49.5, 45.0, 42.3, 41.1, 35.8, 35.0, 29.8, 27.3, 26.7, 22.0, 21.7, 21.1, 18.3, 16.2, 15.3, 15.3, 11.2, 9.6, 7.6. HRMS (ESI) m/z Calcd. $\text{C}_{49}\text{H}_{79}\text{O}_{15}\text{N}_2$ $[\text{M}+\text{H}^+]$: 935.5475, found 935.5466.

3.4.2.3 Fumarate derivatives:

Methyl fumarate anhydride:

Monomethyl fumaric acid (929mg, 5.47mmol) was dissolved into DCM (25 mL) with EDCI (630mg, 3.28mmol). The solution was stirred for overnight with Ar protection. The solution was washed by water (30 mL) and extracted by DCM (25 mL) for four times to ensure all EDCI could

be removed. The extracted organic solution was evaporated by vacuum and the crude product was yielded in yellow solid (458mg, 3.52mmol, 64.4%). This product is ready to use for next reaction without purification.

Butyl fumarate anhydride²³

Furan-2,5-dione (1.5g, 15.3mmol) was mixed with butanol (7.5 mL) and dissolved in Toluene (7.5 mL). The solution was heated to 70°C for 24 h. Then, the intermediate product was gained after evaporation of toluene. The crude product was purified by Column chromatography to gain 2.26g. The intermediate (1.57g) was dissolved into Toluene (7.5 mL) with addition of Acetyl chloride (100μL, 0.28mmol) and heated to 70°C again for 48 h. The product was gained and worked up with EtOAc (25 mL) and water (50 mL). The organic layer was separated and washed by water (30 mL) again. The organic layer was collected and dried by Na₂SO₄ and vacuum evaporation. The crude product was purified by column with solvent condition of EtOAc:hexane:MeOH=4:1:0.5. The final product was yield as white solid (1.40g, 8.23mmol, 53.8%)

AO-02-112

Azithromycin (500mg, 0.67mmol) was mixed with the fumaric anhydride (10 mL, 1.05mmol) in DCM (5 mL). The solution was stirred for overnight under Ar protection. The solution was washed by water (50 mL) and extracted by DCM (30 mL) twice. The organic solution was collected and evaporated to dryness by vacuum. The crude product was purified through Preparative TLC plate with solvent system DCM:MeOH=14:1. The final product was yielded as

pale-yellow solid (147mg, 0.017mmol, 25%). ^1H NMR (700 MHz, CDCl_3) δ 6.86 – 6.78 (m, 2H), 5.29 (s, 1H), 4.96 (s, 1H), 4.84 (dd, $J = 10.7, 7.5$ Hz, 1H), 4.67 – 4.64 (m, 1H), 4.61 (d, $J = 7.5$ Hz, 1H), 4.18 (d, $J = 5.6$ Hz, 1H), 4.03 – 3.98 (m, 1H), 3.79 (s, 4H), 3.67 (s, 2H), 3.67 – 3.62 (m, 1H), 3.63 (s, 1H), 3.61 – 3.57 (m, 1H), 3.53 (s, 1H), 3.34 (s, 3H), 3.03 (t, $J = 9.3$ Hz, 1H), 2.75 (s, 3H), 2.68 (d, $J = 12.6$ Hz, 1H), 2.48 – 2.45 (m, 2H), 2.35 – 2.25 (m, 1H), 2.23 (s, 6H), 1.95 (s, 1H), 1.89 (s, 1H), 1.85 (ddd, $J = 14.1, 7.4, 2.3$ Hz, 1H), 1.76 – 1.71 (m, 1H), 1.66 (d, $J = 14.7$ Hz, 1H), 1.58 (dd, $J = 15.1, 5.1$ Hz, 1H), 1.45 (ddt, $J = 17.2, 14.4, 7.2$ Hz, 1H), 1.33 (dd, $J = 12.8, 11.1$ Hz, 1H), 1.32 – 1.26 (m, 6H), 1.25 (s, 3H), 1.23 (s, 2H), 1.23 – 1.18 (m, 5H), 1.11 (s, 3H), 1.09 (d, $J = 8.0$ Hz, 0H), 1.02 (s, 3H), 0.92 (d, $J = 7.1$ Hz, 3H), 0.87 (t, $J = 7.5$ Hz, 3H), 0.79 (d, $J = 7.6$ Hz, 3H). ^{13}C NMR (176 MHz, CDCl_3) δ 178.1, 165.6, 165.3, 163.9, 134.5, 133.4, 132.8, 100.4, 95.2, 83.7, 78.7, 78.0, 77.4, 77.3, 77.1, 76.9, 74.4, 73.6, 73.0, 72.8, 70.5, 68.3, 65.6, 63.6, 53.5, 52.3, 52.3, 49.4, 44.8, 42.0, 40.7, 36.6, 35.0, 30.3, 27.1, 26.5, 22.0, 21.6, 21.6, 21.2, 18.4, 18.3, 16.3, 15.5, 11.2, 9.6. HRMS (ESI) m/z Calcd. $\text{C}_{43}\text{H}_{76}\text{O}_{15}\text{N}_2$ $[\text{M}+2\text{H}^+]$: 431.2695, found 431.2696.

AO-02-113

Clarithromycin (500mg, 0.67mmol) was mixed with the fumaric anhydride (10 mL, 1.05mmol) in DCM (5 mL). The solution was stirred for overnight under Ar protection. The solution was washed by water (50 mL) and extracted by DCM (30 mL) twice. The organic solution was washed one more time with brine (30ml) and collected and evaporated to dryness by vacuum. The crude product was purified through Preparative TLC plate with solvent system DCM:MeOH=16:1. The final product was yielded as pale-yellow solid (273mg, 0.31mmol,

46.5%). ^1H NMR (700 MHz, CDCl_3) δ 6.79 (s, 2H), 5.26 (s, 1H), 4.98 (dd, $J = 11.1, 2.4$ Hz, 1H), 4.88 – 4.85 (m, 1H), 4.78 (dd, $J = 10.7, 7.4$ Hz, 1H), 4.58 (d, $J = 7.4$ Hz, 1H), 3.96 – 3.90 (m, 1H), 3.91 (s, 1H), 3.77 (s, 3H), 3.70 – 3.65 (m, 2H), 3.57 (d, $J = 6.8$ Hz, 1H), 3.49 (dq, $J = 12.1, 5.9, 1.9$ Hz, 1H), 3.33 (s, 3H), 3.17 (s, 1H), 3.00 (t, $J = 9.1$ Hz, 1H), 2.95 (s, 3H), 2.91 (tt, $J = 6.9, 3.3$ Hz, 1H), 2.76 (dq, $J = 9.4, 7.3$ Hz, 1H), 2.68 – 2.62 (m, 1H), 2.54 – 2.47 (m, 1H), 2.33 – 2.26 (m, 2H), 1.85 (dq, $J = 15.1, 7.5, 2.2$ Hz, 1H), 1.80 – 1.70 (m, 2H), 1.64 – 1.53 (m, 2H), 1.51 (dd, $J = 14.8, 2.1$ Hz, 1H), 1.40 (ddq, $J = 14.4, 11.1, 7.2$ Hz, 1H), 1.32 (s, 3H), 1.31 – 1.25 (m, 1H), 1.26 – 1.22 (m, 6H), 1.19 (d, $J = 6.1$ Hz, 3H), 1.14 (d, $J = 7.4$ Hz, 3H), 1.06 (dd, $J = 17.2, 7.1$ Hz, 6H), 1.05 (s, 3H), 0.77 (t, $J = 7.3$ Hz, 6H). ^{13}C NMR (176 MHz, CDCl_3) δ 175.7, 165.5, 163.9, 134.1, 133.0, 100.2, 95.8, 80.5, 78.2, 78.0, 77.8, 77.3, 77.1, 76.9, 76.6, 74.1, 72.8, 72.6, 69.1, 68.1, 65.8, 63.4, 53.5, 52.3, 50.4, 49.5, 45.1, 44.9, 40.6, 38.9, 38.6, 37.2, 34.9, 30.3, 21.4, 21.2, 21.0, 19.8, 18.6, 17.8, 16.1, 15.9, 12.2, 10.5, 9.3. HRMS (ESI) m/z Calcd. $\text{C}_{43}\text{H}_{73}\text{O}_{16}\text{N}$ $[\text{M}+\text{H}^+]$: 860.5002, found 860.5005.

ST-01-95

CLM (235mg, 0.321mmol) was mixed with butyl fumarate anhydride (182mg, 0.977mmol) and dissolved in DCM (10 mL) at room temperature for 24 h. The reaction was stopped by adding sat. NaHCO_3 (30ml) and extracted by DCM (40 mL). Then, the organic layer was washed 2 more times with sat. NaHCO_3 (30 mL). Subsequently, the organic layer was washed again with brine (25 mL) and dried by Na_2SO_4 and vacuum evaporation. The product was purified by column with gradient of solvent system DCM: MeOH=20:1 to 16:1. The product was yielded in white foam (170mg, 0.188mmol, 58.7%). ^1H NMR (700 MHz, CDCl_3) δ 6.80 (s, 2H), 5.00 (dd, $J = 11.0, 2.5$ Hz, 1H),

4.88 (d, $J = 5.2$ Hz, 1H), 4.79 (dd, $J = 10.8, 7.4$ Hz, 1H), 4.59 (d, $J = 7.5$ Hz, 1H), 4.18 (td, $J = 6.7, 2.6$ Hz, 2H), 3.98 – 3.92 (m, 2H), 3.72 – 3.68 (m, 2H), 3.59 (d, $J = 6.9$ Hz, 1H), 3.49 (ddt, $J = 12.2, 8.0, 3.8$ Hz, 1H), 3.34 (s, 3H), 3.04 – 2.99 (m, 1H), 2.97 (s, 3H), 2.94 (d, $J = 7.3$ Hz, 1H), 2.81 – 2.74 (m, 1H), 2.63 (td, $J = 11.5, 4.2$ Hz, 1H), 2.53 (ddt, $J = 14.1, 8.9, 4.5$ Hz, 1H), 2.33 (d, $J = 15.1$ Hz, 1H), 2.26 (dd, $J = 7.7, 4.2$ Hz, 1H), 2.21 (s, 6H), 1.87 (dq, $J = 15.1, 7.5, 2.4$ Hz, 1H), 1.79 (q, $J = 7.5$ Hz, 1H), 1.74 – 1.69 (m, 1H), 1.63 (dt, $J = 17.3, 8.8$ Hz, 3H), 1.60 – 1.51 (m, 2H), 1.46 – 1.39 (m, 2H), 1.39 – 1.36 (m, 2H), 1.28 – 1.21 (m, 8H), 1.20 (d, $J = 6.1$ Hz, 3H), 1.16 (d, $J = 7.3$ Hz, 3H), 1.12 – 1.08 (m, 5H), 1.07 (s, 5H), 0.93 (t, $J = 7.5$ Hz, 3H), 0.79 (dt, $J = 7.6, 3.7$ Hz, 6H). ^{13}C NMR (176 MHz, CDCl_3) δ 175.7, 165.2, 164.0, 133.9, 133.5, 100.3, 95.9, 80.5, 78.3, 78.1, 77.8, 77.3, 77.1, 76.9, 76.6, 74.1, 72.8, 72.7, 69.1, 68.2, 65.8, 65.2, 50.4, 49.5, 45.1, 45.0, 40.6, 39.0, 38.7, 37.2, 34.9, 30.1, 19.8, 19.1, 18.7, 17.9, 16.1, 15.9, 13.6, 13.4, 12.3, 10.6, 9.3. HRMS (ESI) m/z Calcd. $\text{C}_{46}\text{H}_{79}\text{O}_{16}\text{N}$ $[\text{M}+\text{H}^+]$: 902.5472, found 902.5475.

ST-01-96

AZM (240mg, 0.321mmol) was mixed with butyl fumarate anhydride (182mg, 0.977mmol) and dissolved in DCM (6 mL) at room temperature for 24 h. The reaction was stopped by adding sat. NaHCO_3 (30 mL) and extracted by DCM (40 mL). Then, the organic layer was washed 2 more times with sat. NaHCO_3 (30 mL). Subsequently, the organic layer was washed again with brine (25 mL) and dried by Na_2SO_4 and vacuum evaporation. The product was purified by column with gradient of solvent system DCM: MeOH=10:1 to 8:1. The product was yielded in white foam (145mg, 0.16mmol, 49.8%). ^1H NMR (700 MHz, CDCl_3) δ 6.83 (d, $J = 2.3$ Hz, 2H), 5.24 (td, $J = 6.0, 3.0$ Hz, 1H), 5.15 (d, $J = 4.9$ Hz, 1H), 4.89 – 4.82 (m, 1H), 4.68 (dd, $J = 9.9, 2.8$ Hz,

1H), 4.58 (d, $J = 7.5$ Hz, 1H), 4.28 (ddd, $J = 13.7, 6.7, 4.4$ Hz, 1H), 4.21 (dd, $J = 5.9, 3.4$ Hz, 2H), 4.20 – 4.17 (m, 1H), 4.15 (ddd, $J = 12.0, 6.0, 3.4$ Hz, 1H), 4.06 (dq, $J = 9.5, 6.2$ Hz, 1H), 3.63 (d, $J = 1.3$ Hz, 1H), 3.57 (d, $J = 7.3$ Hz, 1H), 3.53 (qd, $J = 6.1, 1.9$ Hz, 1H), 3.38 (s, 3H), 3.05 (t, $J = 9.3$ Hz, 2H), 2.67 (qd, $J = 7.5, 4.2$ Hz, 3H), 2.53 (dd, $J = 11.8, 2.2$ Hz, 1H), 2.39 – 2.33 (m, 1H), 2.33 – 2.30 (m, 3H), 2.24 (s, 5H), 2.17 (dd, $J = 10.8, 3.9$ Hz, 1H), 2.09 – 2.05 (m, 2H), 2.05 – 1.95 (m, 3H), 1.89 (dtd, $J = 15.2, 7.6, 4.9$ Hz, 2H), 1.76 (ddd, $J = 13.0, 4.4, 2.0$ Hz, 1H), 1.70 – 1.63 (m, 3H), 1.60 (dd, $J = 10.7, 4.6$ Hz, 2H), 1.49 (d, $J = 2.7$ Hz, 1H), 1.44 – 1.38 (m, 3H), 1.33 (d, $J = 6.2$ Hz, 4H), 1.32 – 1.20 (m, 20H), 1.17 (t, $J = 8.3$ Hz, 5H), 1.10 – 1.01 (m, 6H), 0.95 (t, $J = 7.4$ Hz, 4H), 0.92 – 0.85 (m, 8H), 0.80 (d, $J = 7.6$ Hz, 3H). ^{13}C NMR (176 MHz, CDCl_3) δ 178.80, 172.9, 170.5, 170.5, 170.1, 165.3, 164.0, 134.1, 133.4, 100.5, 94.4, 83.0, 78.1, 77.4, 76.9, 74.4, 73.1, 72.7, 70.1, 69.1, 68.3, 65.2, 63.6, 62.0, 52.3, 49.5, 45.2, 42.2, 41.9, 40.7, 36.2, 34.1, 34.0, 31.7, 30.3, 29.2, 27.5, 26.6, 25.3, 24.8, 22.6, 20.9, 19.1, 18.2, 16.2, 14.6, 13.7, 11.2, 9.11, 7.2. HRMS (ESI) m/z Calcd. $\text{C}_{46}\text{H}_{82}\text{O}_{15}\text{N}_2$ $[\text{M}+\text{H}^+]$: 903.5788, found 903.5798.

WBC-04-50B

Monomethyl fumaric acid (100mg, 0.77mmol) was dissolved in DCM (10 mL) with EDCI (250mg, 1.3mmol). The solution was stirred for 5-10 minutes with Argon protection. Then, Des-CLM was added to the solution and stirred at room temperature for overnight. The solution was washed by water (50 mL) with two times extraction of DCM (15 mL). The organic layer was combined and evaporated to dryness. The crude product was purified by Preparative TLC with solvent condition EtOAc:MeOH=20:1.5. The final product was yielded as yellow solid (81mg, 0.096mmol, 12.5%). ^1H NMR (700 MHz, CDCl_3) δ 7.47 (dd, $J = 65.4, 15.4$ Hz, 1H), 6.77 (dd, J

= 68.4, 15.4 Hz, 1H), 5.08 (dd, $J = 11.2, 8.6$ Hz, 1H), 4.94 (t, $J = 6.1$ Hz, 1H), 4.59 – 4.54 (m, 1H), 4.02 (dt, $J = 8.9, 5.4$ Hz, 1H), 3.98 (s, 1H), 3.90 – 3.74 (m, 6H), 3.73 – 3.66 (m, 2H), 3.42 (ddd, $J = 17.0, 10.3, 7.2$ Hz, 1H), 3.35 (d, $J = 16.8$ Hz, 3H), 3.21 (d, $J = 5.8$ Hz, 1H), 3.10 – 3.06 (m, 1H), 3.05 (s, 5H), 3.03 – 2.97 (m, 1H), 2.95 (s, 1H), 2.92 – 2.85 (m, 1H), 2.64 – 2.60 (m, 1H), 2.60 – 2.55 (m, 1H), 2.39 – 2.32 (m, 2H), 2.01 – 1.89 (m, 2H), 1.83 – 1.78 (m, 1H), 1.78 – 1.74 (m, 1H), 1.69 – 1.62 (m, 2H), 1.62 – 1.58 (m, 1H), 1.56 – 1.45 (m, 2H), 1.42 (d, $J = 10.9$ Hz, 3H), 1.32 (dd, $J = 11.2, 6.3$ Hz, 3H), 1.28 (d, $J = 10.1$ Hz, 3H), 1.27 – 1.24 (m, 4H), 1.22 (dt, $J = 5.7, 4.2$ Hz, 4H), 1.20 – 1.17 (m, 1H), 1.15 (dd, $J = 8.0, 6.4$ Hz, 9H), 1.05 (dd, $J = 17.7, 7.6$ Hz, 3H), 1.01 – 0.96 (m, 2H), 0.90 (d, $J = 6.8$ Hz, 1H), 0.88 – 0.82 (m, 3H). ^{13}C NMR (176 MHz, CDCl_3) δ 220.8, 175.6, 166.2, 135.7, 134.4, 131.9, 131.3, 129.8, 120.7, 103.4, 102.6, 96.2, 82.2, 81.8, 79.5, 78.5, 78.2, 77.9, 77.0, 74.3, 74.2, 72.9, 71.1, 69.8, 69.1, 68.4, 68.0, 66.1, 65.9, 58.2, 54.5, 52.2, 52.1, 50.7, 50.6, 49.5, 49.3, 48.6, 45.1, 45.0, 39.1, 38.8, 38.6, 37.3, 36.5, 35.5, 35.0, 34.4, 34.1, 30.1, 29.7, 28.3, 27.3, 23.1, 21.6, 21.3, 21.1, 19.7, 18.6, 18.0, 17.8, 16.1, 16.0, 16.0, 12.4, 10.6, 9.9. HRMS (ESI) m/z Calcd. $\text{C}_{42}\text{H}_{71}\text{O}_{16}\text{N Na}$ $[\text{M}+\text{H}^+]$: 868.4665, found 868.4637.

WBC-04-51

Monomethyl fumaric acid (30mg, 0.23mmol) was dissolved in DCM (4 mL) with EDCI (200mg, 1.04mmol). The solution was stirred for 5-10 minutes with Argon protection. Then, Des-AZM (200mg, 0.272mmol) was added to the solution and stirred at room temperature for overnight. The solution was washed by water (50 mL) with two times extraction of DCM (15 mL). The organic layer was combined and evaporated to dryness. The crude product was purified by Preparative TLC with solvent condition EtOAc:MeOH=20:1.5. The final product was yielded as yellow solid

(170mg, 0.20mmol, 87.7%). ^1H NMR (700 MHz, CDCl_3) δ 7.46 (dd, $J = 67.1, 15.4$ Hz, 1H), 6.74 (dd, $J = 72.7, 15.4$ Hz, 1H), 5.01 (s, 1H), 4.74 – 4.66 (m, 2H), 4.56 (t, $J = 7.7$ Hz, 1H), 4.18 (dt, $J = 27.1, 6.3$ Hz, 2H), 4.06 (td, $J = 8.9, 6.3$ Hz, 1H), 3.89 – 3.81 (m, 1H), 3.80 (s, 2H), 3.78 (s, 2H), 3.75 – 3.68 (m, 2H), 3.68 – 3.60 (m, 7H), 3.45 (dq, $J = 13.2, 7.0$ Hz, 1H), 3.36 (s, 2H), 3.32 (s, 1H), 3.07 (dd, $J = 15.2, 6.6$ Hz, 1H), 3.03 (s, 2H), 2.94 (s, 2H), 2.78 (td, $J = 6.9, 2.9$ Hz, 1H), 2.63 – 2.52 (m, 2H), 2.36 (s, 2H), 2.35 – 2.29 (m, 2H), 2.13 – 1.97 (m, 5H), 1.88 (tdq, $J = 10.3, 7.3, 3.4, 2.7$ Hz, 1H), 1.76 – 1.64 (m, 3H), 1.59 (tt, $J = 10.1, 4.7$ Hz, 2H), 1.54 – 1.44 (m, 3H), 1.32 (dd, $J = 11.4, 7.3$ Hz, 7H), 1.30 – 1.17 (m, 22H), 1.17 (s, 1H), 1.14 – 1.10 (m, 3H), 1.07 (d, $J = 3.1$ Hz, 3H), 1.02 – 0.92 (m, 9H), 0.89 (h, $J = 4.2, 3.7$ Hz, 7H). ^{13}C NMR (176 MHz, CDCl_3) δ 177.0, 176.6, 173.3, 171.0, 170.5, 170.1, 166.2, 166.1, 165.7, 135.8, 134.6, 131.1, 130.9, 129.7, 129.5, 103.5, 102.9, 95.4, 85.5, 79.5, 78.9, 77.8, 74.3, 73.4, 71.4, 71.0, 70.0, 68.4, 66.1, 62.3, 62.3, 62.0, 58.4, 54.64, 52.2, 52.0, 49.4, 45.1, 42.3, 40.9, 38.9, 36.5, 35.5, 34.9, 34.1, 31.9, 29.7, 28.3, 27.1, 26.1, 25.3, 24.8, 22.6, 21.3, 20.7, 19.7, 18.9, 18.2, 17.8, 16.2, 15.3, 14.1, 14.1, 13.7, 11.2, 9.9, 9.7, 7.6. HRMS (ESI) m/z Calcd. $\text{C}_{42}\text{H}_{75}\text{O}_{15}\text{N}_2$ $[\text{M}+\text{H}^+]$: 847.5162, found 847.5139.

WBC-04-110

Monobutyl fumaric acid (100mg, 0.58mmol) was dissolved in DCM (5ml) with EDCI (400mg, 2.1mmol). The solution was stirred for 5-10 minutes with Argon protection. Then, Des-CLM (180mg, 0.24mmol) was added to the solution and stirred at room temperature for overnight. The solution was washed by water (100 mL) with two times extraction of DCM (50 mL). The organic layer was combined and evaporated to dryness. The crude product was purified by Preparative TLC with solvent condition EtOAc:hexane=7:3. The final product was yielded as white solid (140mg, 0.167mmol, 69.3%). ^1H NMR (700 MHz, CDCl_3) δ 7.44 (dd, $J = 71.3, 15.4$ Hz, 1H),

6.75 (dd, $J = 65.1, 15.4$ Hz, 1H), 5.07 (ddd, $J = 11.2, 5.9, 2.4$ Hz, 1H), 4.93 (t, $J = 4.6$ Hz, 1H), 4.69 (ddd, $J = 12.5, 10.8, 4.4$ Hz, 1H), 4.55 (dd, $J = 9.9, 7.2$ Hz, 1H), 4.19 (dt, $J = 19.1, 6.7$ Hz, 2H), 4.01 (dt, $J = 8.9, 5.7$ Hz, 1H), 3.96 (s, 1H), 3.77 – 3.73 (m, 2H), 3.73 – 3.64 (m, 2H), 3.41 (dddd, $J = 15.0, 11.2, 7.4, 4.6$ Hz, 1H), 3.35 (s, 2H), 3.32 (s, 1H), 3.19 (d, $J = 5.5$ Hz, 1H), 3.10 – 3.00 (m, 5H), 2.99 (s, 1H), 2.94 (s, 1H), 2.87 (pd, $J = 7.2, 3.5$ Hz, 1H), 2.63 – 2.54 (m, 1H), 2.44 – 2.40 (m, 1H), 2.38 – 2.29 (m, 1H), 2.00 – 1.88 (m, 2H), 1.82 – 1.75 (m, 1H), 1.75 – 1.68 (m, 2H), 1.68 – 1.63 (m, 3H), 1.60 (ddd, $J = 15.1, 4.8, 1.9$ Hz, 2H), 1.55 – 1.44 (m, 2H), 1.41 (d, $J = 11.4$ Hz, 4H), 1.34 – 1.19 (m, 12H), 1.17 – 1.11 (m, 7H), 1.04 (dd, $J = 18.5, 7.5$ Hz, 3H), 0.95 (td, $J = 7.4, 3.9$ Hz, 3H), 0.84 (td, $J = 7.4, 1.7$ Hz, 3H). ^{13}C NMR (176 MHz, CDCl_3) δ 220.7, 175.6, 166.2, 165.8, 135.5, 134.1, 131.8, 130.3, 103.5, 102.6, 96.0, 82.2, 81.8, 78.5, 78.1, 76.7, 74.2, 72.9, 71.7, 71.2, 69.1, 68.4, 68.0, 66.0, 65.0, 58.2, 54.5, 50.6, 49.4, 45.0, 39.2, 38.6, 37.3, 36.5, 35.5, 35.0, 30.6, 30.1, 21.5, 21.0, 19.8, 19.1, 18.6, 18.6, 18.0, 16.0, 13.7, 12.4, 10.6, 9.9, 9.6. HRMS (ESI) m/z Calcd. $\text{C}_{45}\text{H}_{77}\text{O}_{16}\text{N}$ [$\text{M}+\text{H}^+$]: 888.5315, found 888.5337.

WBC-04-111

Monobutyl fumaric acid (100mg, 0.58mmol) was dissolved in DCM (5 mL) with EDCI (400mg, 2.1mmol). The solution was stirred for 5-10 minutes with Argon protection. Then, Des-AZM (180mg, 0.24mmol) and DMAP (45mg, 0.36mmol) was added to the solution and stirred at room temperature for overnight. The solution was washed by water (100 mL) with two times extraction of DCM (50 mL). The organic layer was combined and evaporated to dryness. The crude product was purified by Preparative TLC with solvent condition EtOAc:MeOH=10:1. The final product was yielded as white solid (65mg, 0.075mmol, 31.3%). ^1H NMR (700 MHz, CDCl_3) δ 7.45 (dd,

$J = 78.0, 15.4$ Hz, 1H), 6.74 (dd, $J = 74.1, 15.4$ Hz, 1H), 5.26 (dp, $J = 10.1, 5.2$ Hz, 1H), 5.13 (t, $J = 5.4$ Hz, 1H), 4.85 (p, $J = 6.3$ Hz, 1H), 4.72 (td, $J = 11.9, 4.5$ Hz, 1H), 4.29 (td, $J = 6.9, 4.6$ Hz, 1H), 4.23 – 4.13 (m, 4H), 4.07 (ddd, $J = 13.3, 9.4, 6.4$ Hz, 1H), 3.68 (s, 1H), 3.64 (t, $J = 6.1$ Hz, 1H), 3.45 (tt, $J = 12.6, 6.5$ Hz, 1H), 3.39 (s, 1H), 3.34 (s, 1H), 3.07 (t, $J = 8.9$ Hz, 1H), 3.03 (s, 2H), 2.94 (s, 1H), 2.77 – 2.69 (m, 2H), 2.59 (d, $J = 13.3$ Hz, 1H), 2.39 – 2.26 (m, 5H), 2.10 – 2.05 (m, 4H), 2.04 (s, 2H), 1.99 (p, $J = 8.3$ Hz, 1H), 1.90 (dt, $J = 11.9, 7.6, 3.9$ Hz, 1H), 1.74 – 1.63 (m, 4H), 1.60 (td, $J = 9.6, 9.0, 4.5$ Hz, 2H), 1.51 (q, $J = 8.0, 6.8$ Hz, 3H), 1.40 (tt, $J = 7.5, 3.9$ Hz, 2H), 1.36 – 1.33 (m, 5H), 1.26 (d, $J = 7.5$ Hz, 13H), 1.20 (d, $J = 7.5$ Hz, 3H), 1.13 (d, $J = 7.1$ Hz, 2H), 1.09 (s, 2H), 1.01 – 0.92 (m, 8H), 0.88 (q, $J = 7.4$ Hz, 5H). ^{13}C NMR (176 MHz, CDCl_3) δ 173.35, 173.0, 170.5, 170.1, 166.3, 165.8, 135.8, 134.3, 131.6, 130.2, 103.2, 102.7, 94.8, 84.5, 77.9, 77.5, 77.2, 76.9, 74.5, 74.2, 73.6, 73.1, 71.3, 70.9, 69.1, 68.7, 68.4, 68.1, 65.9, 64.9, 62.30, 62.0, 58.4, 54.6, 49.5, 45.3, 41.9, 36.3, 35.5, 34.7, 34.0, 31.7, 30.6, 29.5, 29.0, 27.3, 26.6, 25.3, 22.6, 22.1, 21.6, 21.3, 20.7, 18.9, 18.1, 16.3, 14.7, 14.1, 13.7, 11.2, 9.7, 9.5. HRMS (ESI) m/z Calcd. $\text{C}_{45}\text{H}_{80}\text{N}_2\text{O}_{15}$ $[\text{M}+\text{H}^+]$: 889.5631, found 889.5624.

3.4.3 Cell culture

The cell culture and viability assay protocol were described in our previous work. In brief, VERO, A549, MDA-MB-231 cell lines were maintained in Dulbecco's Modified Eagle Medium (DMEM) (Corning, 10-017-CV), supplemented with 10% fetal bovine serum (FBS) (Corning, 35-010-CV). MCF-7 cell line was maintained in Dulbecco's Modified Eagle Medium (DMEM) (Quality Biological, 112-132-101). MRC-5 and Hep-G2 cells were cultured in phenol red free Minimum

Essential Medium (MEM) (Corning, 17-305-CV), supplemented with 10% fetal bovine serum (FBS).

3.4.4 *MTS assay*

Cells were seeded into a 96-well plate (2000 counts/100uL) for 24 h prior to treatment and then treated with various drug concentrations for 72 h. All drugs were dissolved in medium via DMSO solution with DMSO concentration maintained at 1%. The effect of compounds on cell viability was measured using the MTS assay (CellTiter 96 Aqueous One Solution and CellTiter 96 Non-Radioactive Cell Proliferation Assays, Promega, Madison, WI) as described by the manufacturer. IC₅₀s were determined using Prism GraphPad 8.

3.4.5 *Western blot*

The Western blot protocol was described in our previous work.²⁸ In brief, MRC-5 cells were seeded into 6-well plate at 1×10^6 /well in MEM for 24 h after which the cells were starved in serum-free MEM for another 24 h. For STAT3 experiment, MDA-MB-231 cells (1×10^6 /well) were seeded to the 6-well plate in DMEM with 24 h starvation. Various concentrations of selected candidates solutions in DMSO were added to the cell culture such that the final DMSO level is 0.1%. For anti-fibrosis experiment, the cells were stimulated with 50ng/well of TGF- β cytokine in MEM (VWR 10208-658). Cells were treated for 24 h, washed with cold PBS, and lysed with RIPA buffer (120 μ L) (VWR, VWRVN653-100ML) buffer containing phosphatase inhibitor (Fisher Thermo, A32957) and protease inhibitor (Fisher Thermo, A32955). The cell lysates were scraped, collected,

and vortexed for 15s followed by sonication for 60s. The lysate was then centrifuged at 14000x rpm for 10 min and the supernatants were collected. The total protein concentration was determined using a BCA protein assay kit (BioVision, K813-2500). Based on the results from the BSA assay, the lysates were diluted to make equal protein concentration and 20-40 µg of each lysate was loaded to each well of the TGX MIDI 4-20% gel (Biorad, cat. 5671093) and ran at 150V for 70 min. The gel was then transferred on to the Turbo PDVF membrane (Biorad, 1704273) and after blocking with 5% BSA for 1-2 h, the membrane was incubated overnight with primary antibodies Anti-Col1A1(84336), anti-p-STAT3 (9145), anti-T-STAT3 (79D7), anti-HO-1 (5853S) were purchased from Cell Signal Technology®; Anti-α-SMA (ab5694) were from Abcam®; anti-GAPDH (sc-47724), Bcl-2 (sc-7382), Bcl-xL (sc-8392) were purchased from Santa Cruz®. The second day, the membrane was washed with TBST for 3x5 min; secondary antibody (LiCOR) was added, and the membrane was incubated with agitation for 1 h. After washing with TBS-T 3x5 mins, bands were quantified using Odyssey CLx Image system. Quantification was evaluated by using Prism GraphPad 8.

3.5 References:

1. Liou, G.-Y.; Storz, P., Reactive oxygen species in cancer. *Free radical research* **2010**, *44* (5), 479-496.
2. Patterson, R. E.; White, E.; Kristal, A. R.; Neuhausser, M. L.; Potter, J. D., Vitamin supplements and cancer risk: the epidemiologic evidence. *Cancer Causes & Control* **1997**, *8* (5), 786-802.
3. Yun, J.; Mullarky, E.; Lu, C.; Bosch, K. N.; Kavalier, A.; Rivera, K.; Roper, J.; Chio, I. I. C.; Giannopoulou, E. G.; Rago, C., Vitamin C selectively kills KRAS and BRAF mutant colorectal cancer cells by targeting GAPDH. *Science* **2015**, *350* (6266), 1391-1396.
4. Mut-Salud, N.; Álvarez, P. J.; Garrido, J. M.; Carrasco, E.; Aránega, A.; Rodríguez-Serrano, F., Antioxidant intake and antitumor therapy: toward nutritional

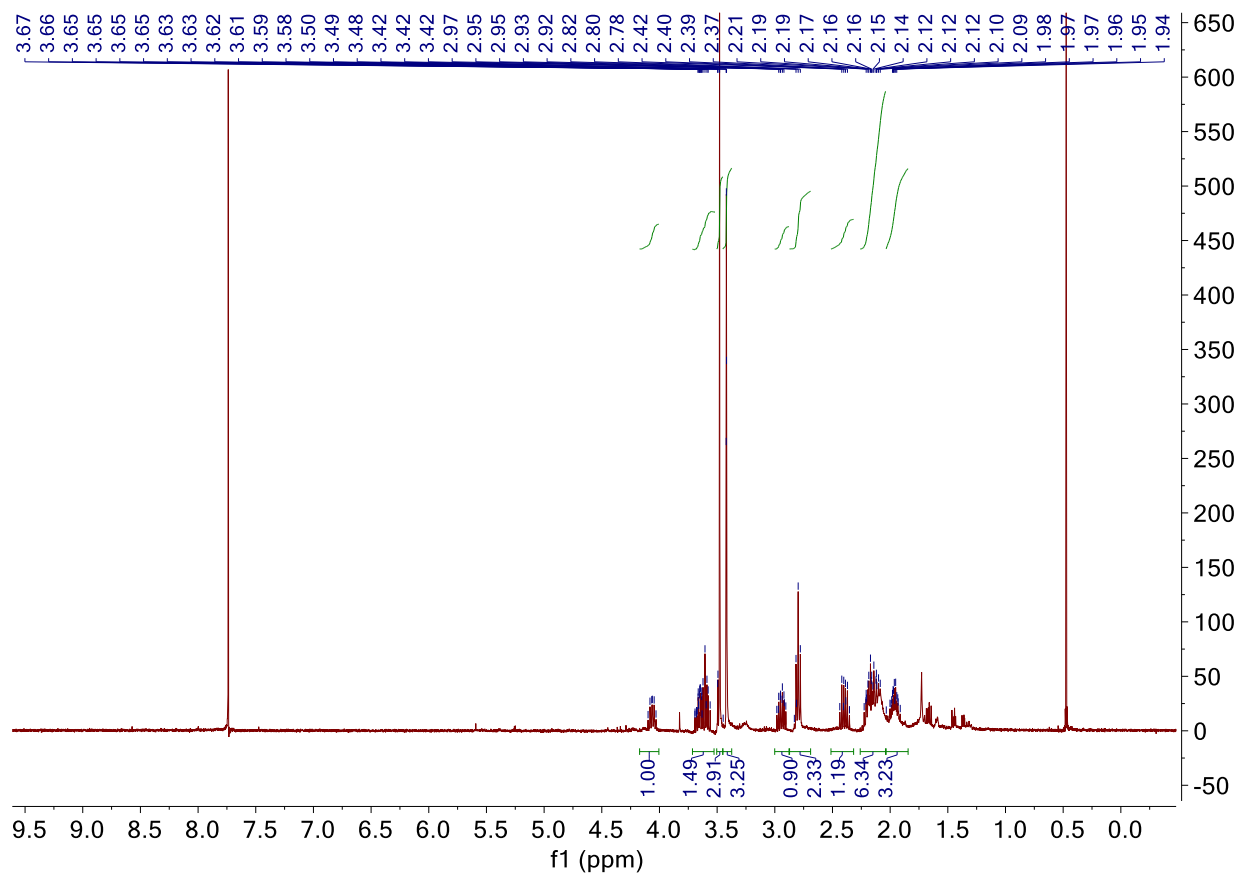
- recommendations for optimal results. *Oxidative medicine and cellular longevity* **2016**, 2016.
5. Barut, E. N.; Engin, S.; Saygın, İ.; Kaya-Yasar, Y.; Arici, S.; Sezen, S. F., Alpha-lipoic acid: A promising adjuvant for nonsteroidal anti-inflammatory drugs therapy with improved efficacy and gastroprotection. *Drug Development Research* **2021**.
 6. Jeon, M. J.; Kim, W. G.; Lim, S.; Choi, H.-J.; Sim, S.; Kim, T. Y.; Shong, Y. K.; Kim, W. B., Alpha lipoic acid inhibits proliferation and epithelial mesenchymal transition of thyroid cancer cells. *Molecular and cellular endocrinology* **2016**, 419, 113-123.
 7. Farhat, D.; Léon, S.; Ghayad, S. E.; Gadot, N.; Icard, P.; Le Romancer, M.; Hussein, N.; Lincet, H., Lipoic acid decreases breast cancer cell proliferation by inhibiting IGF-1R via furin downregulation. *British journal of cancer* **2020**, 122 (6), 885-894.
 8. Ying, Z.; Kampfrath, T.; Sun, Q.; Parthasarathy, S.; Rajagopalan, S., Evidence that α -lipoic acid inhibits NF- κ B activation independent of its antioxidant function. *Inflammation research* **2011**, 60 (3), 219-225.
 9. Suzuki, Y. J.; Tsuchiya, M.; Packer, L., Thiocetic acid and dihydrolipoic acid are novel antioxidants which interact with reactive oxygen species. *Free radical research communications* **1991**, 15 (5), 255-263.
 10. Choi, J. H.; Cho, S. O.; Kim, H., α -Lipoic acid inhibits expression of IL-8 by suppressing activation of MAPK, Jak/Stat, and NF- κ B in H. pylori-infected gastric epithelial AGS cells. *Yonsei medical journal* **2016**, 57 (1), 260.
 11. Min, A.-K.; Kim, M.-K.; Seo, H.-Y.; Kim, H.-S.; Jang, B. K.; Hwang, J. S.; Choi, H.-S.; Lee, K.-U.; Park, K.-G.; Lee, I.-K., Alpha-lipoic acid inhibits hepatic PAI-1 expression and fibrosis by inhibiting the TGF- β signaling pathway. *Biochemical and biophysical research communications* **2010**, 393 (3), 536-541.
 12. Foo, N.-P.; Lin, S.-H.; Lee, Y.-H.; Wu, M.-J.; Wang, Y.-J., α -Lipoic acid inhibits liver fibrosis through the attenuation of ROS-triggered signaling in hepatic stellate cells activated by PDGF and TGF- β . *Toxicology* **2011**, 282 (1-2), 39-46.
 13. Vijayan, V.; Mueller, S.; Baumgart-Vogt, E.; Immenschuh, S., Heme oxygenase-1 as a therapeutic target in inflammatory disorders of the gastrointestinal tract. *World journal of gastroenterology: WJG* **2010**, 16 (25), 3112.
 14. Soares, M. P.; Marguti, I.; Cunha, A.; Larsen, R., Immunoregulatory effects of HO-1: how does it work? *Current opinion in pharmacology* **2009**, 9 (4), 482-489.
 15. Puentes-Pardo, J. D.; Moreno-SanJuan, S.; Carazo, Á.; León, J., Heme Oxygenase-1 in Gastrointestinal Tract Health and Disease. *Antioxidants* **2020**, 9 (12), 1214.
 16. Saidu, N. E. B.; Bretagne, M.; Mansuet, A. L.; Just, P.-A.; Leroy, K.; Cerles, O.; Chouzenoux, S.; Nicco, C.; Damotte, D.; Alifano, M., Dimethyl fumarate is highly cytotoxic in KRAS mutated cancer cells but spares non-tumorigenic cells. *Oncotarget* **2018**, 9 (10), 9088.
 17. Nicolay, J. P.; Müller-Decker, K.; Schroeder, A.; Brechmann, M.; Möbs, M.; Géraud, C.; Assaf, C.; Goerdt, S.; Krammer, P. H.; Gülow, K., Dimethyl fumarate restores

- apoptosis sensitivity and inhibits tumor growth and metastasis in CTCL by targeting NF- κ B. *Blood, The Journal of the American Society of Hematology* **2016**, 128 (6), 805-815.
18. Kourakis, S.; Timpani, C. A.; de Haan, J. B.; Gueven, N.; Fischer, D.; Rybalka, E., Dimethyl fumarate and its esters: A drug with broad clinical utility? *Pharmaceuticals* **2020**, 13 (10), 306.
 19. Olejarz, W.; Wrzosek, M.; Józwiak, M.; Grosicka-Maciąg, E.; Roszkowski, P.; Filipek, A.; Cychol, A.; Nowicka, G.; Struga, M., Synthesis and anticancer effects of α -lipoic ester of alloxanthoxyletin. *Medicinal Chemistry Research* **2019**, 28 (5), 788-796.
 20. Scholz, M.; Blobaum, A. L.; Marnett, L. J.; Hey-Hawkins, E., Ortho-carbaborane derivatives of indomethacin as cyclooxygenase (COX)-2 selective inhibitors. *Bioorganic & medicinal chemistry* **2012**, 20 (15), 4830-4837.
 21. Wey, S.-J.; Augustyniak, M. E.; Cochran, E. D.; Ellis, J. L.; Fang, X.; Garvey, D. S.; Janero, D. R.; Letts, L. G.; Martino, A. M.; Melim, T. L., Structure-based design, synthesis, and biological evaluation of indomethacin derivatives as cyclooxygenase-2 inhibiting nitric oxide donors. *Journal of medicinal chemistry* **2007**, 50 (25), 6367-6382.
 22. Oyelere, A. K.; Chen, P. C.; Guerrant, W.; Mwakwari, S. C.; Hood, R.; Zhang, Y.; Fan, Y., Non-peptide macrocyclic histone deacetylase inhibitors. *Journal of medicinal chemistry* **2009**, 52 (2), 456-468.
 23. Raillard, S. P.; Scheuerman, R. A.; Manthati, S. K., Method of making monomethyl fumarate. Google Patents: 2016.
 24. Welge-Lussen, U.; Birke, K.; Kopsachilis, N.; Kruse, F.; Yu, A., Alpha Lipoic Acid Inhibits Tgf- β and Oxidative Stress Induced Poag Like Changes in Human Astrocytes by Inhibition of P38MAPK Pathway. *Investigative Ophthalmology & Visual Science* **2010**, 51 (13), 6099-6099.
 25. Marques da Fonseca, L.; Jacques da Silva, L. R.; Santos dos Reis, J.; Rodrigues da Costa Santos, M. A.; de Sousa Chaves, V.; Monteiro da Costa, K.; Sa-Diniz, J. d. N.; Freire de Lima, C. G.; Morrot, A.; Nunes Franklim, T., Piperine Inhibits TGF- β Signaling Pathways and Disrupts EMT-Related Events in Human Lung Adenocarcinoma Cells. *Medicines* **2020**, 7 (4), 19.
 26. Oh, C. J.; Kim, J.-Y.; Choi, Y.-K.; Kim, H.-J.; Jeong, J.-Y.; Bae, K.-H.; Park, K.-G.; Lee, I.-K., Dimethylfumarate attenuates renal fibrosis via NF-E2-related factor 2-mediated inhibition of transforming growth factor- β /Smad signaling. *PloS one* **2012**, 7 (10), e45870.
 27. Timpani, C. A.; Rybalka, E., Calming the (Cytokine) Storm: Dimethyl Fumarate as a Therapeutic Candidate for COVID-19. *Pharmaceuticals* **2021**, 14 (1), 15.
 28. Wu, B.; Fathi, S.; Mortley, S.; Mohiuddin, M.; Jang, Y. C.; Oyelere, A. K., Pyrimethamine conjugated histone deacetylase inhibitors: Design, synthesis and evidence for triple negative breast cancer selective cytotoxicity. *Bioorg Med Chem* **2020**, 28 (6), 115345.

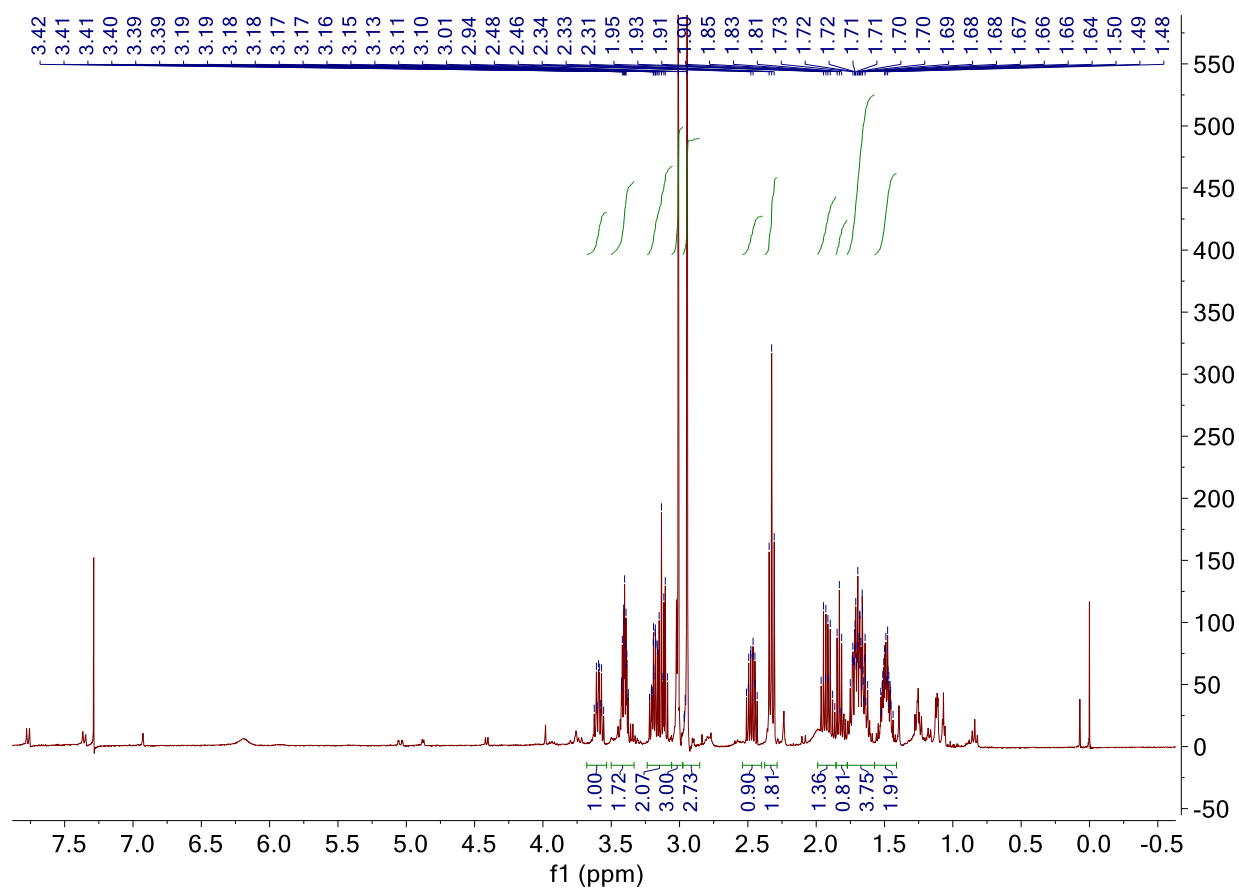
3.6 Supporting information

NMRs

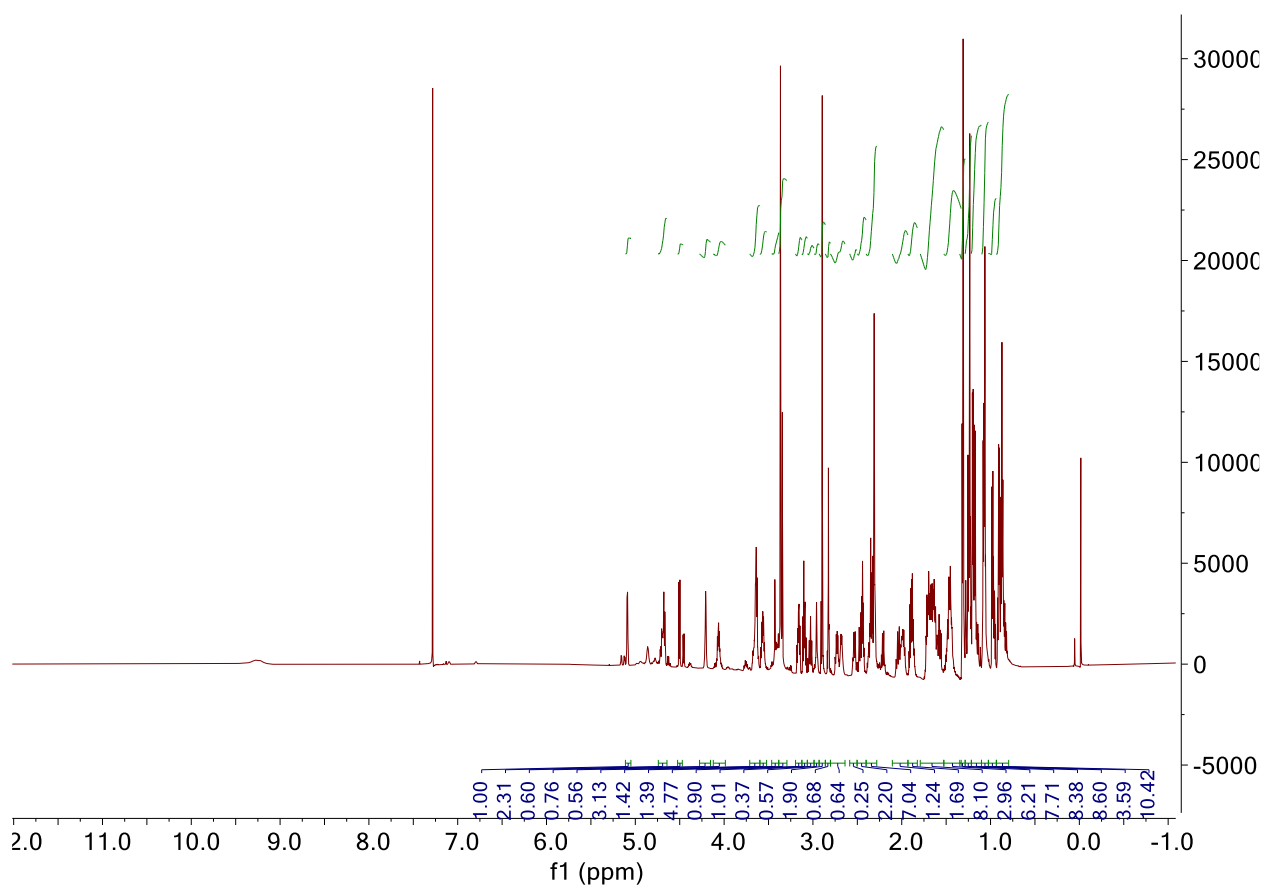
C2NL (^1H NMR)



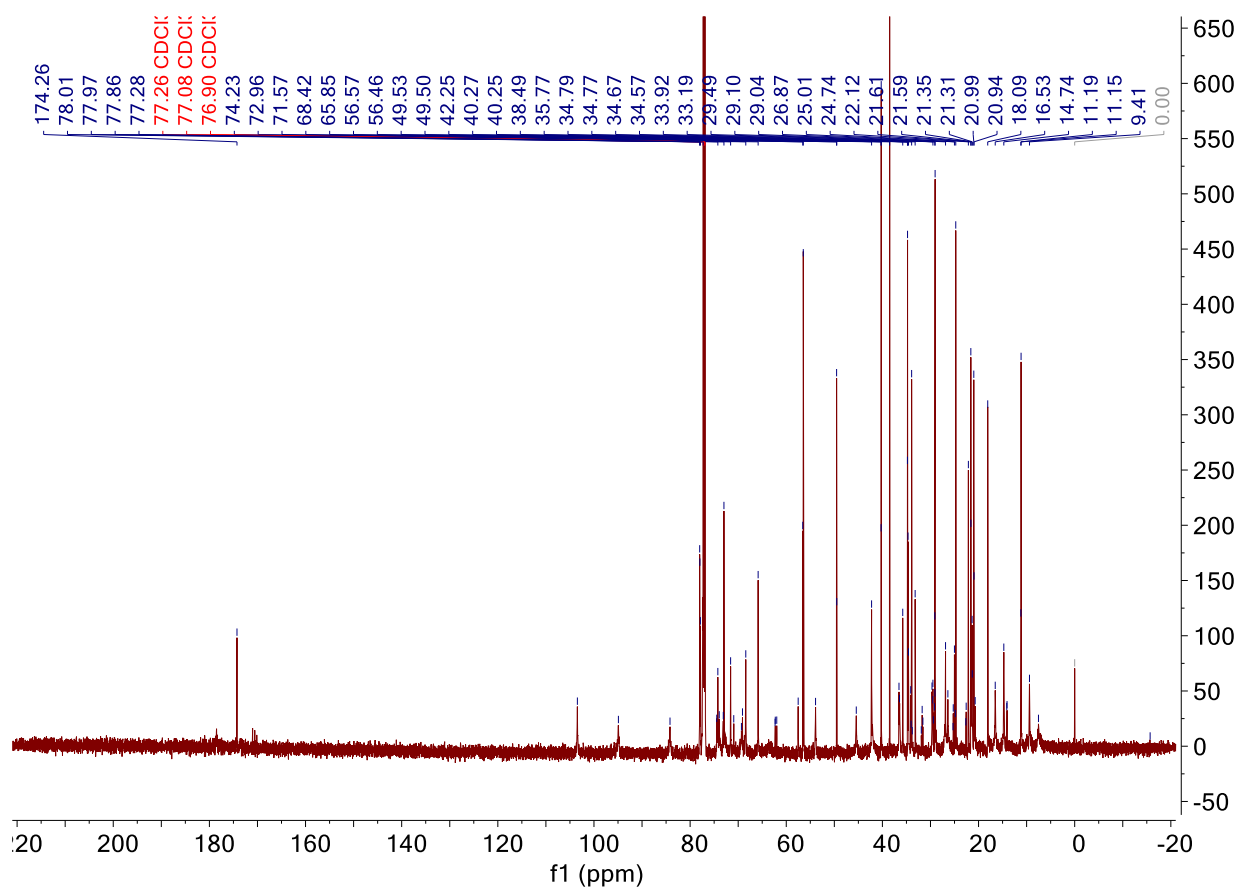
C3NL (^1H NMR)



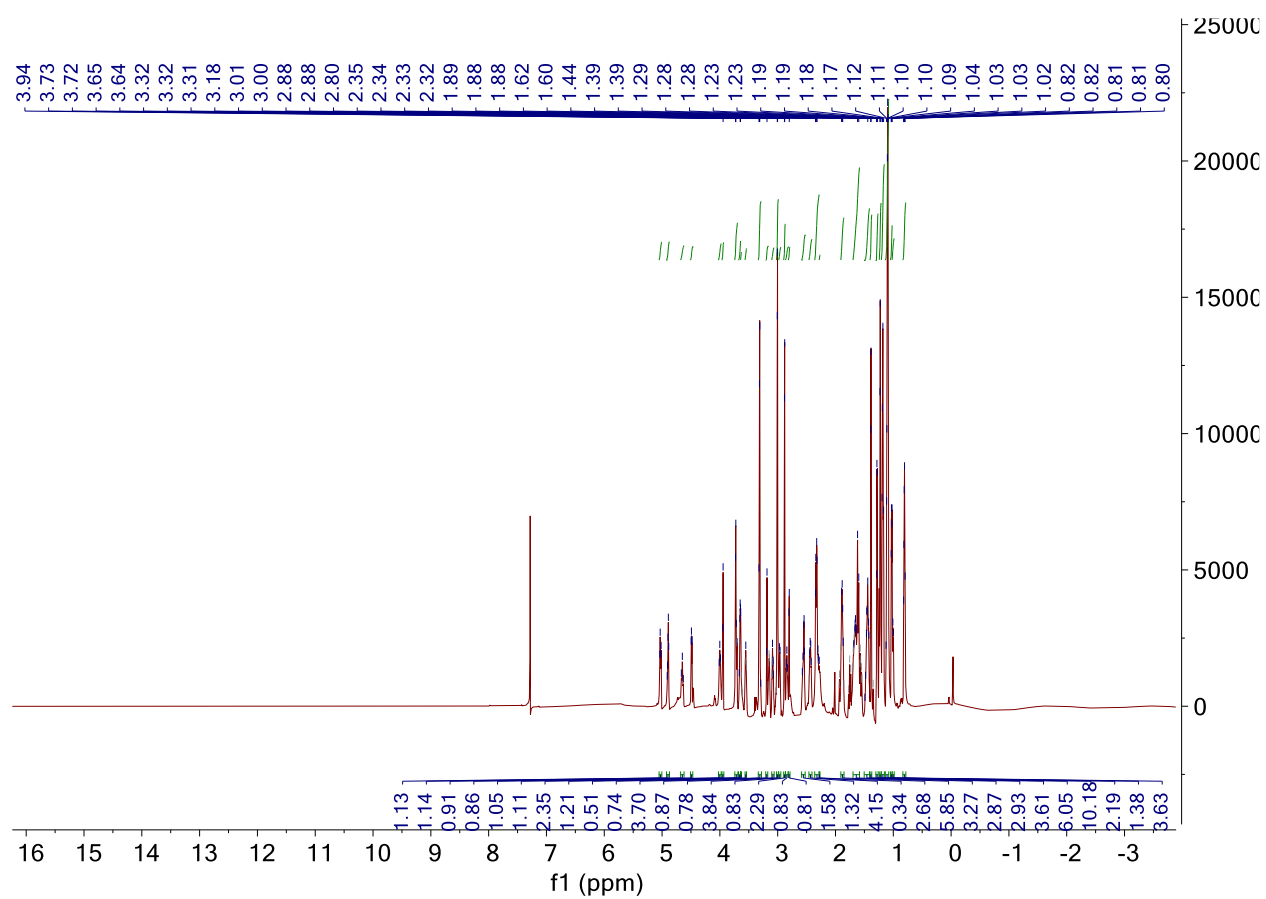
ACONL (^1H NMR)



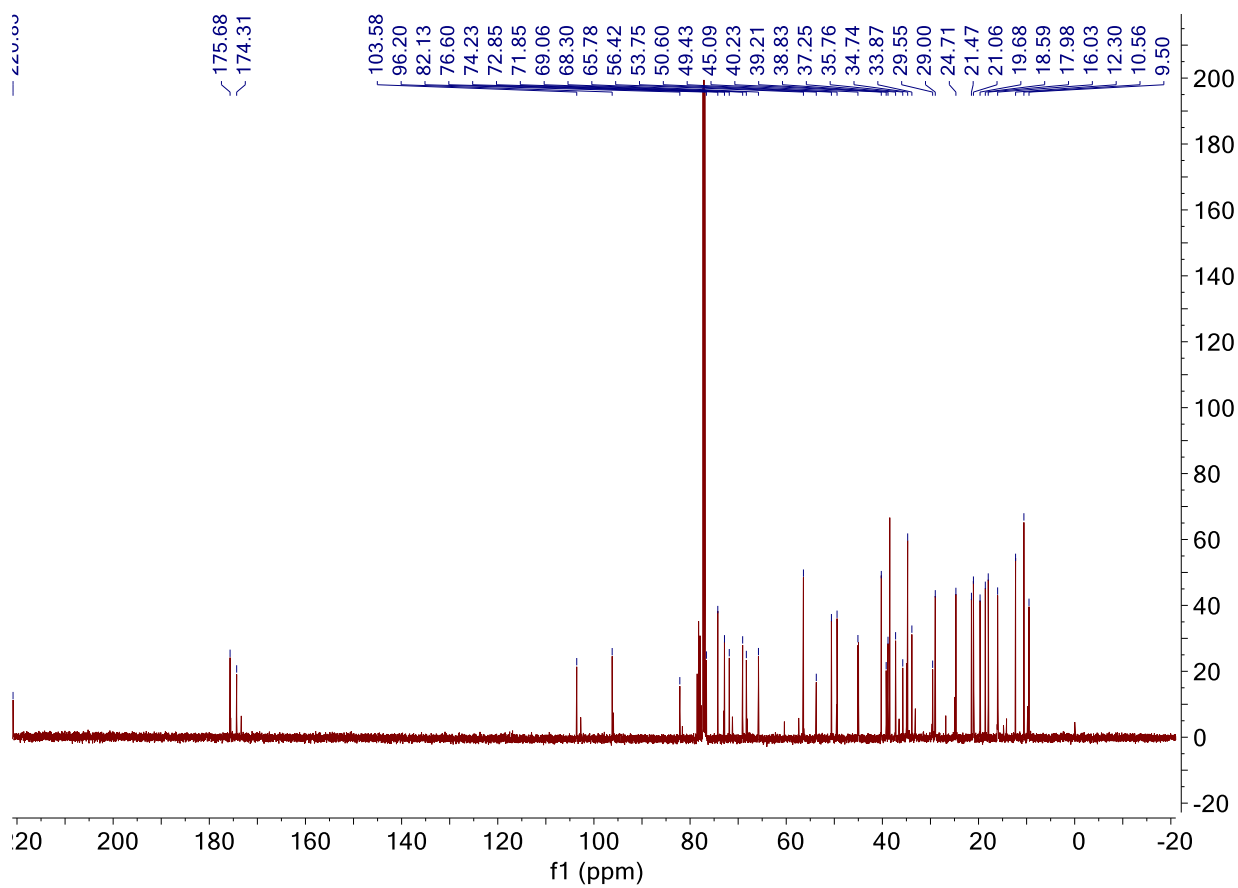
AC0NL (^{13}C NMR)



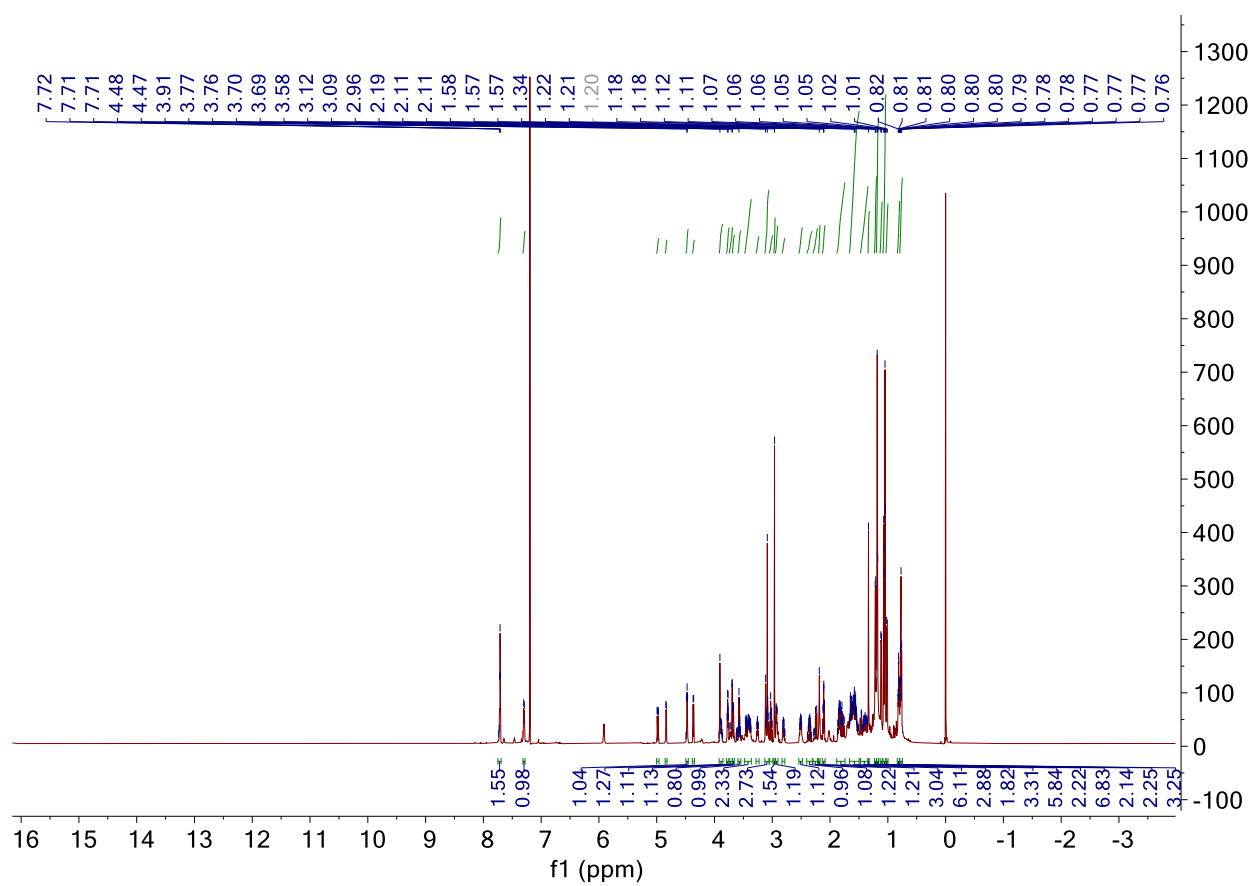
CC0NL(¹H NMR)



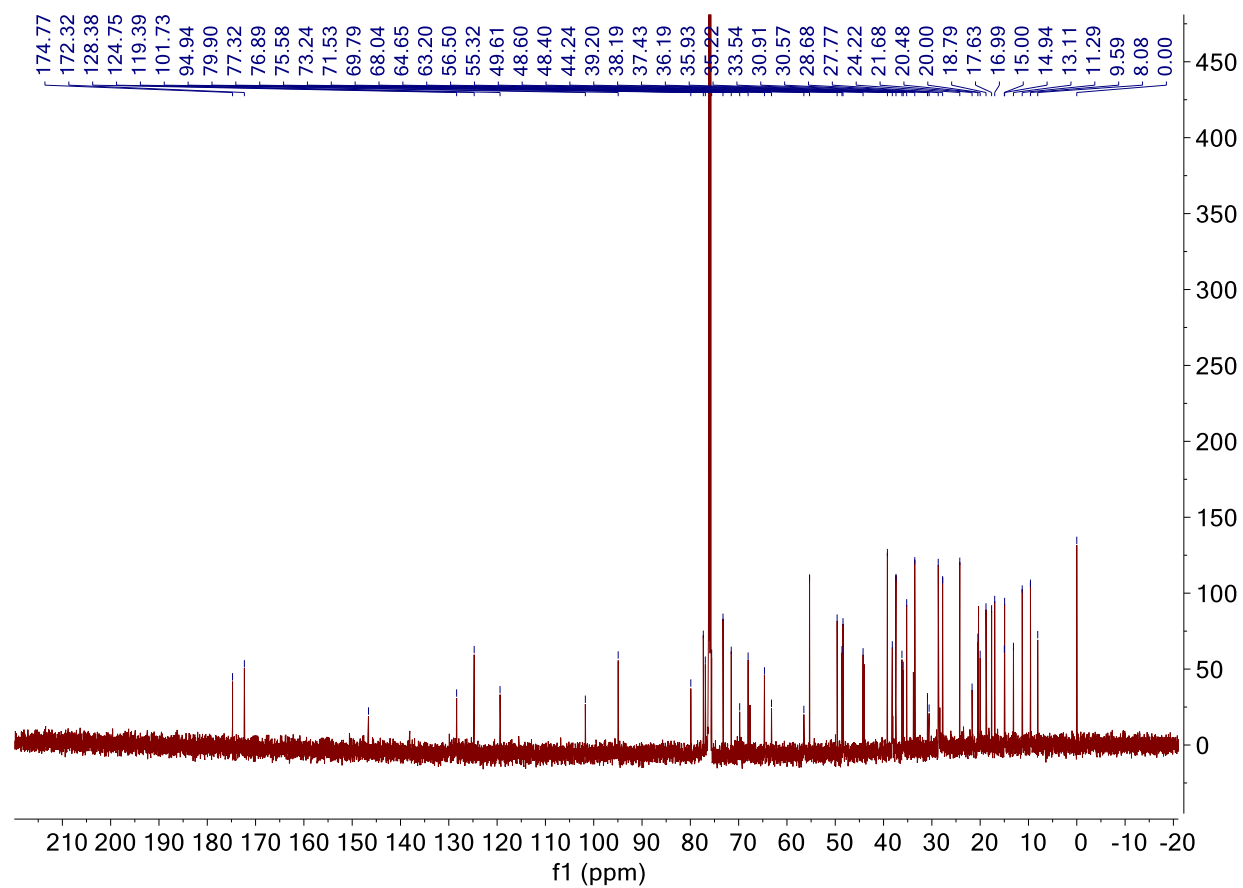
CC0NL (¹³C NMR)



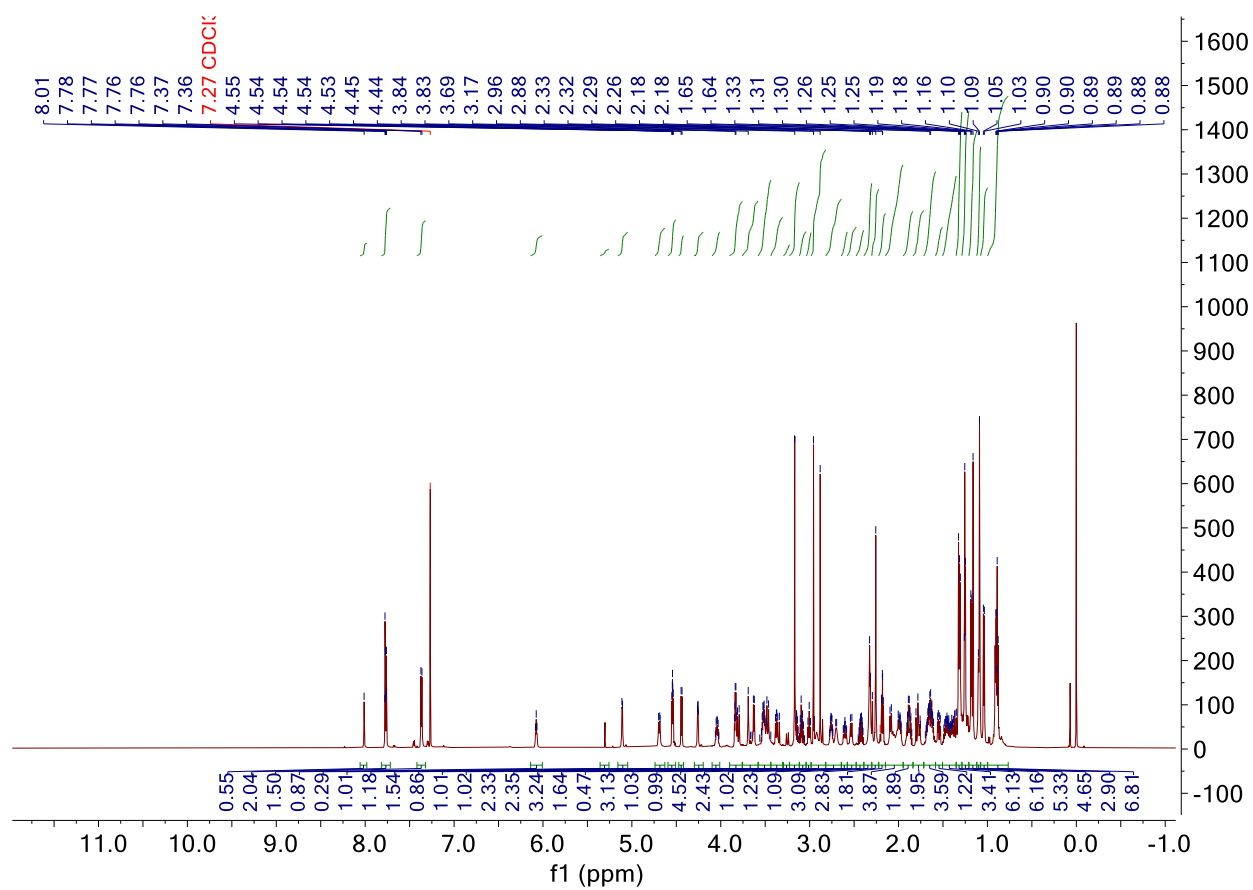
CPC2NL (¹H NMR)



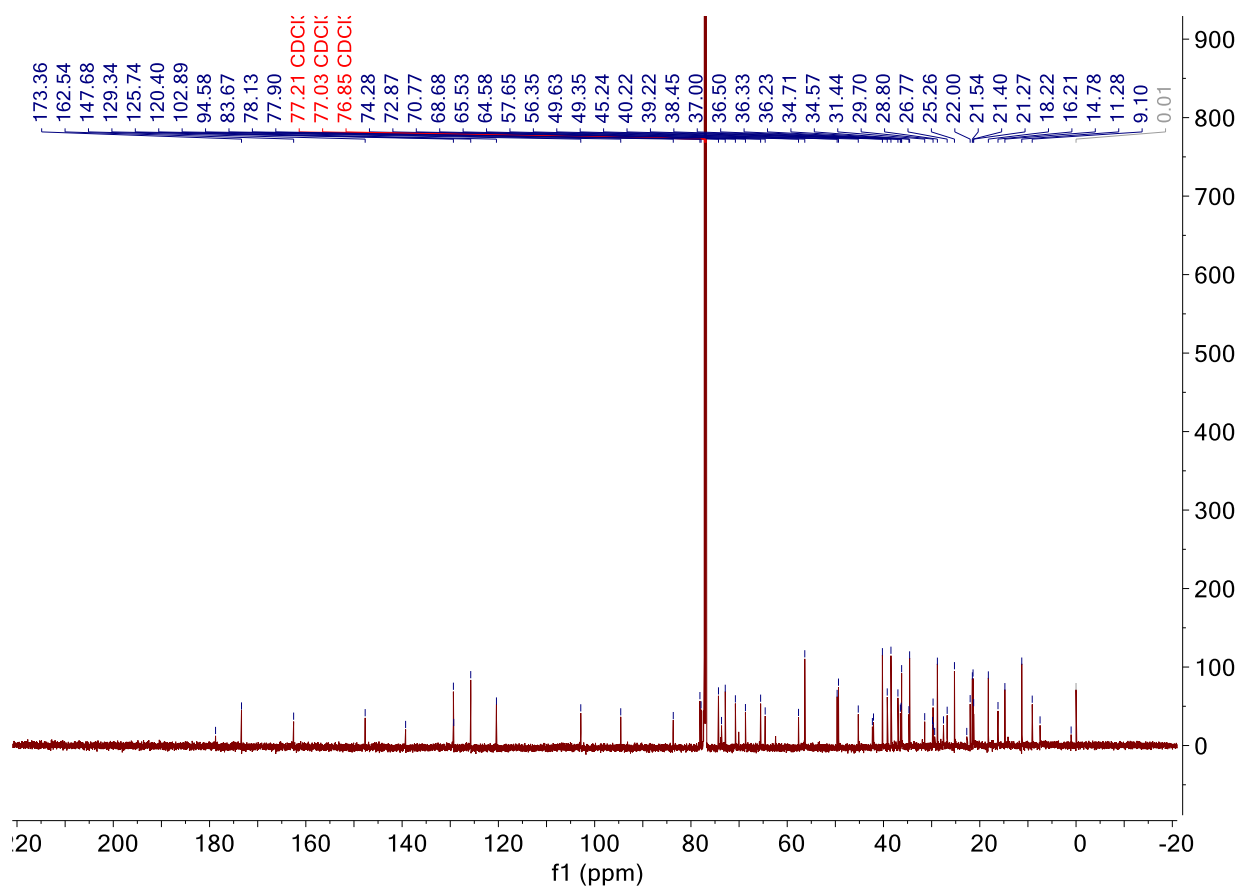
CPC2NL (^{13}C NMR)



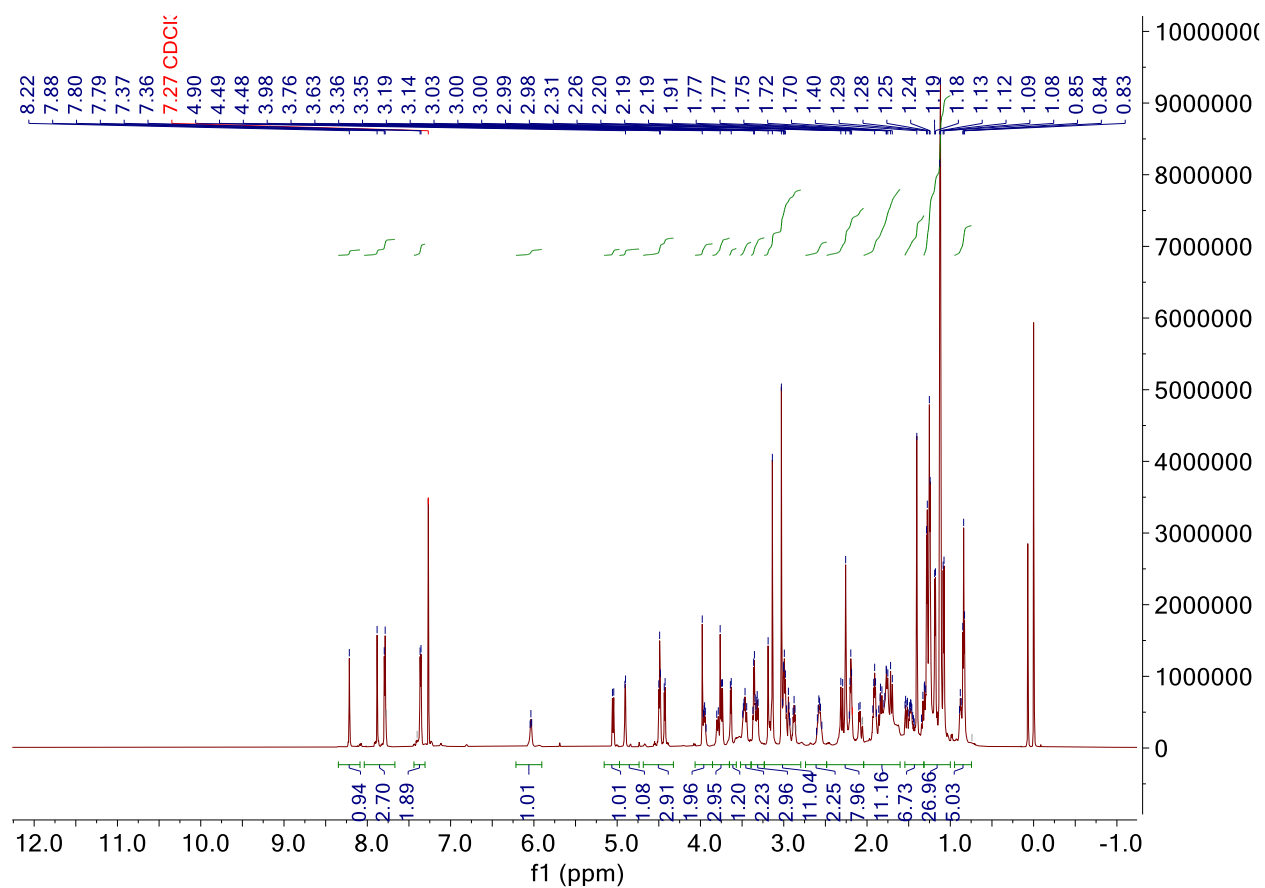
APC2NL (¹H NMR)



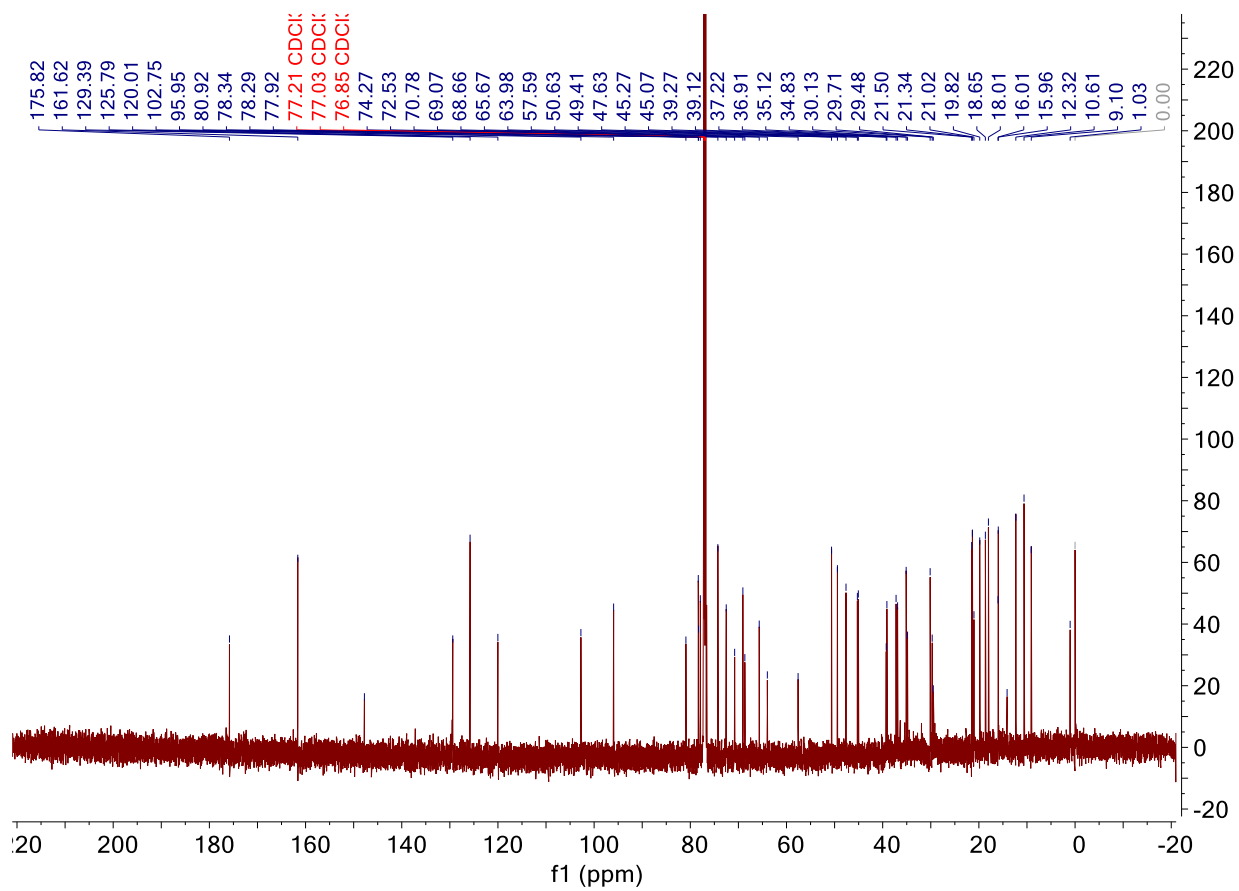
APC2NL (¹³C NMR)



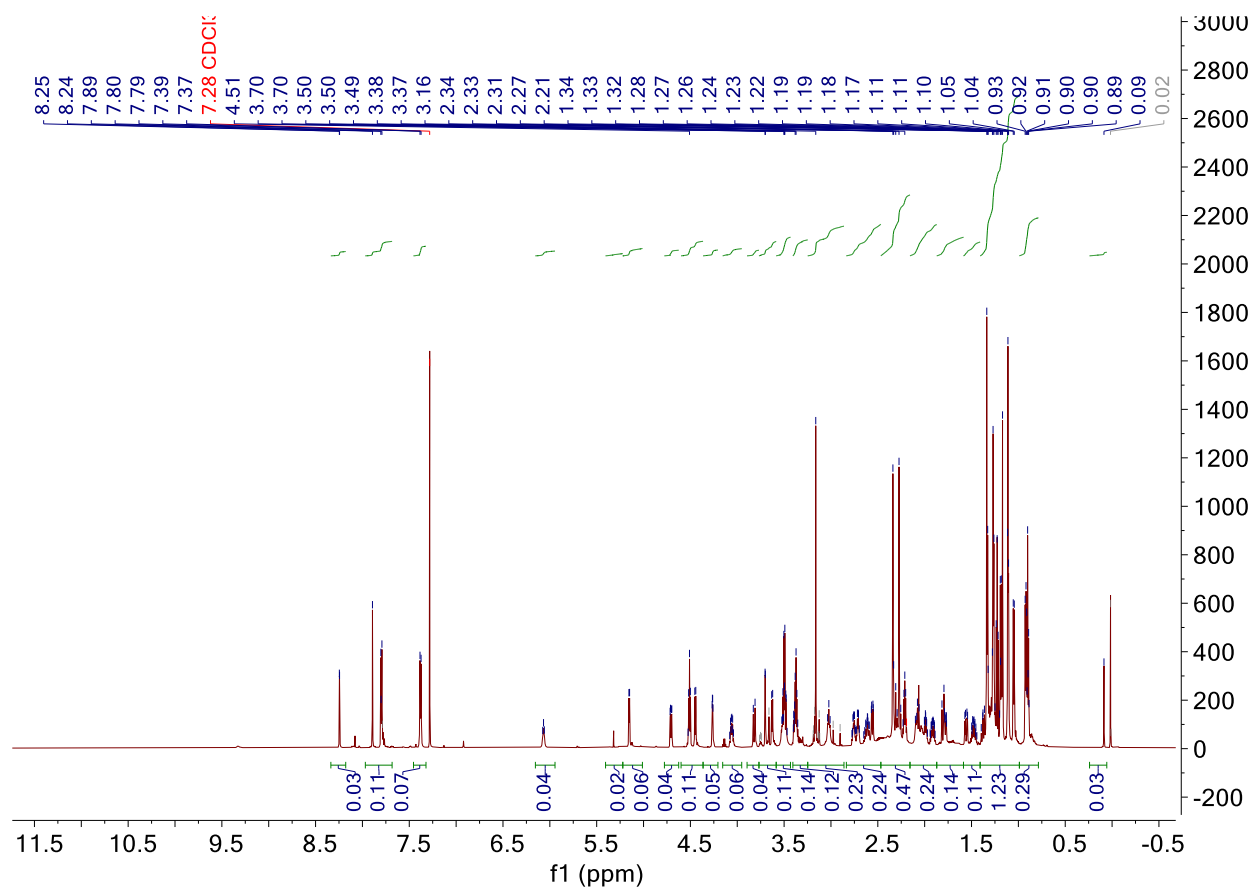
CPC3NL (^1H NMR)



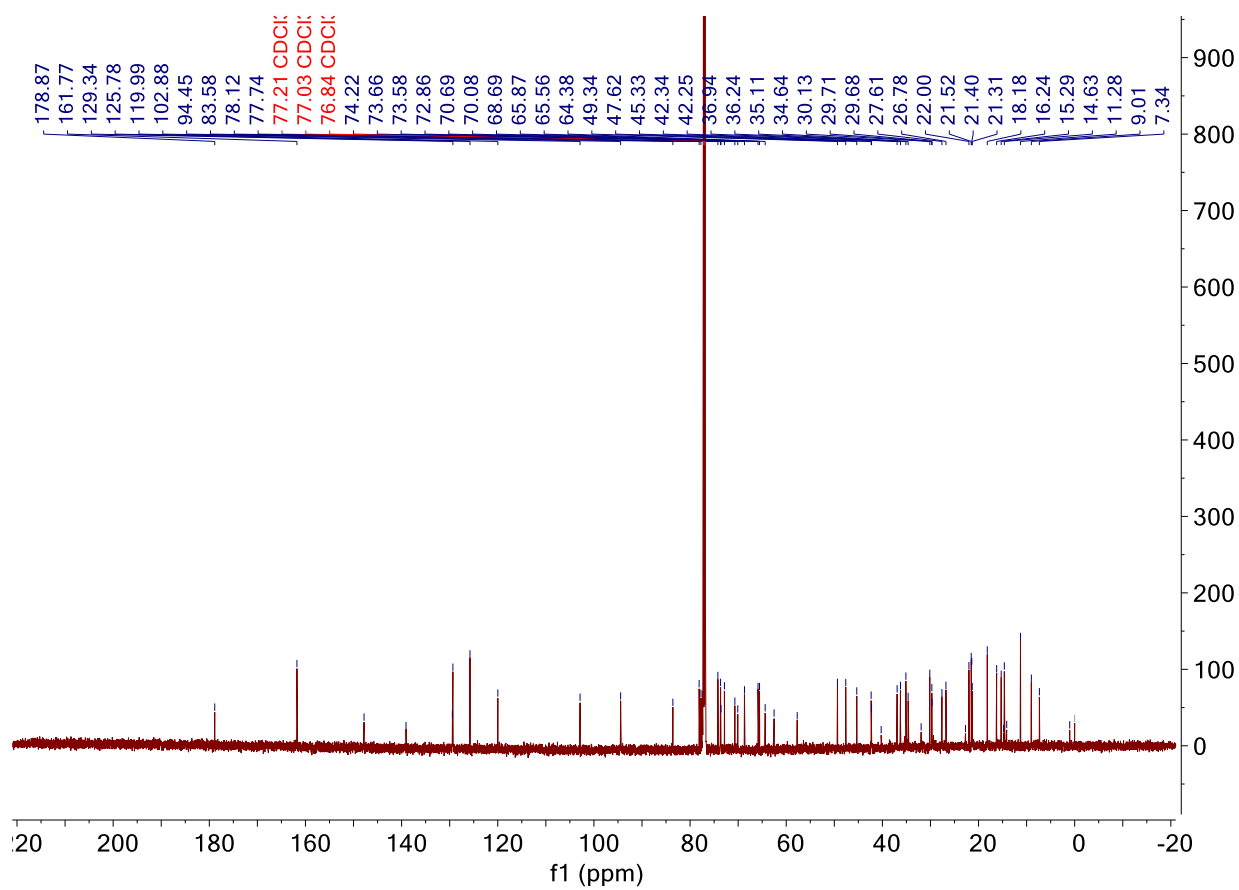
CPC3NL (^{13}C NMR)



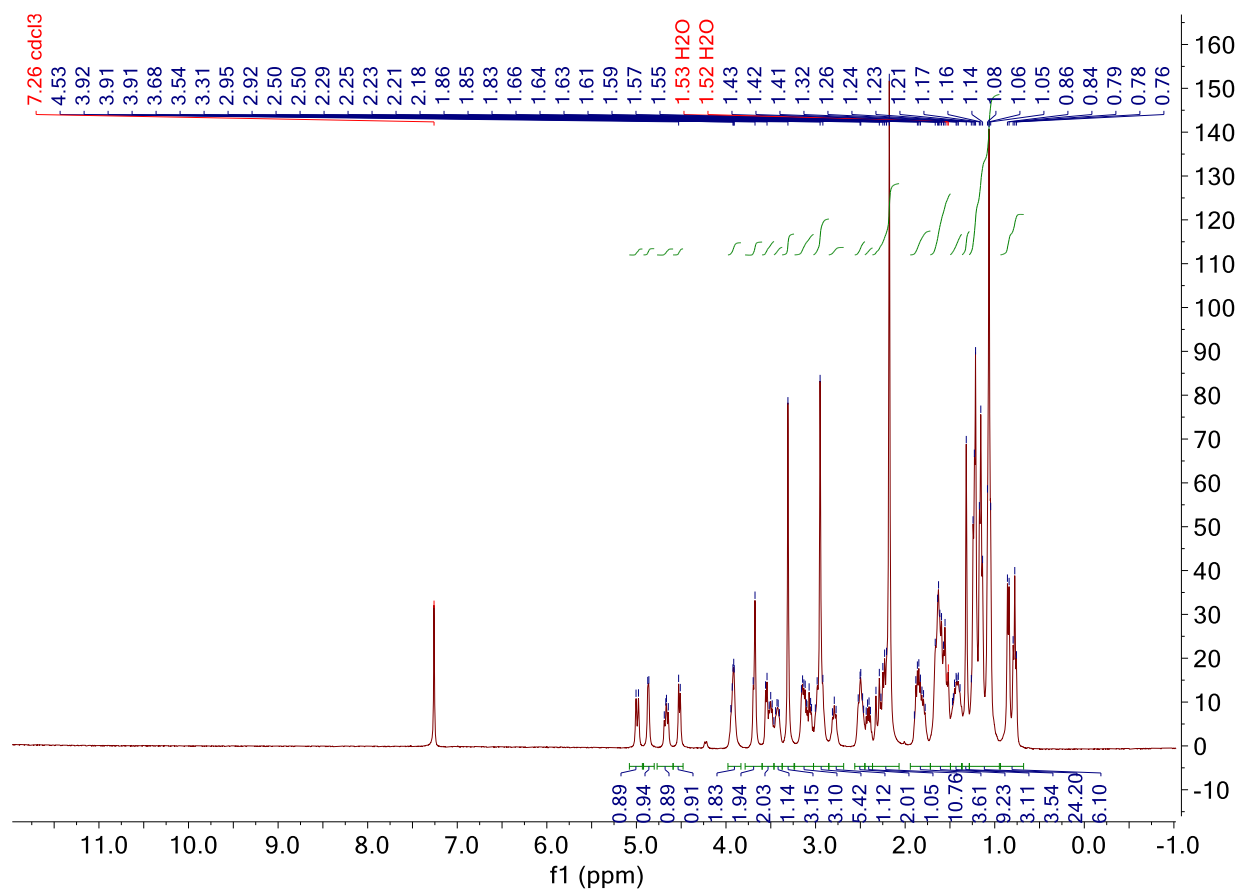
APC3NL (¹H NMR)



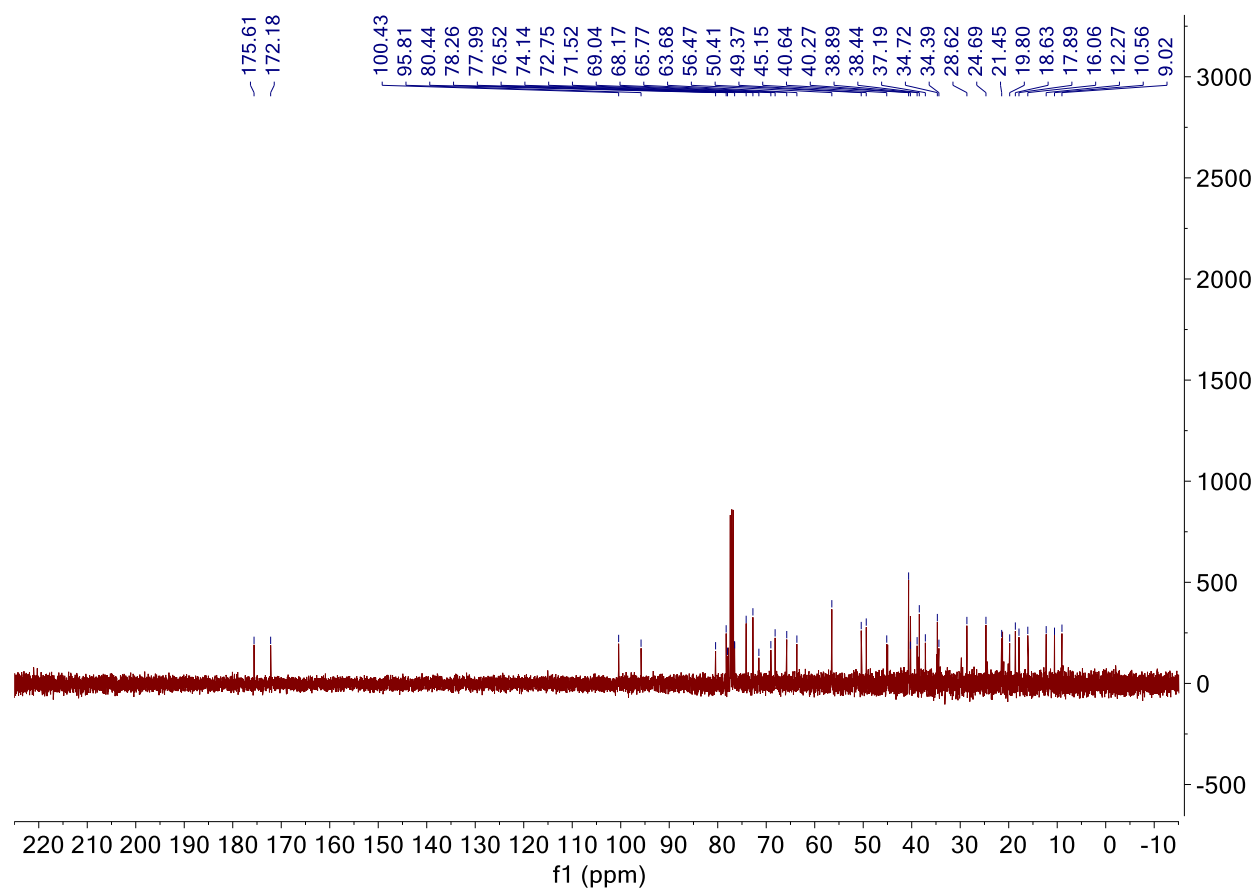
APC3NL (¹³C NMR)



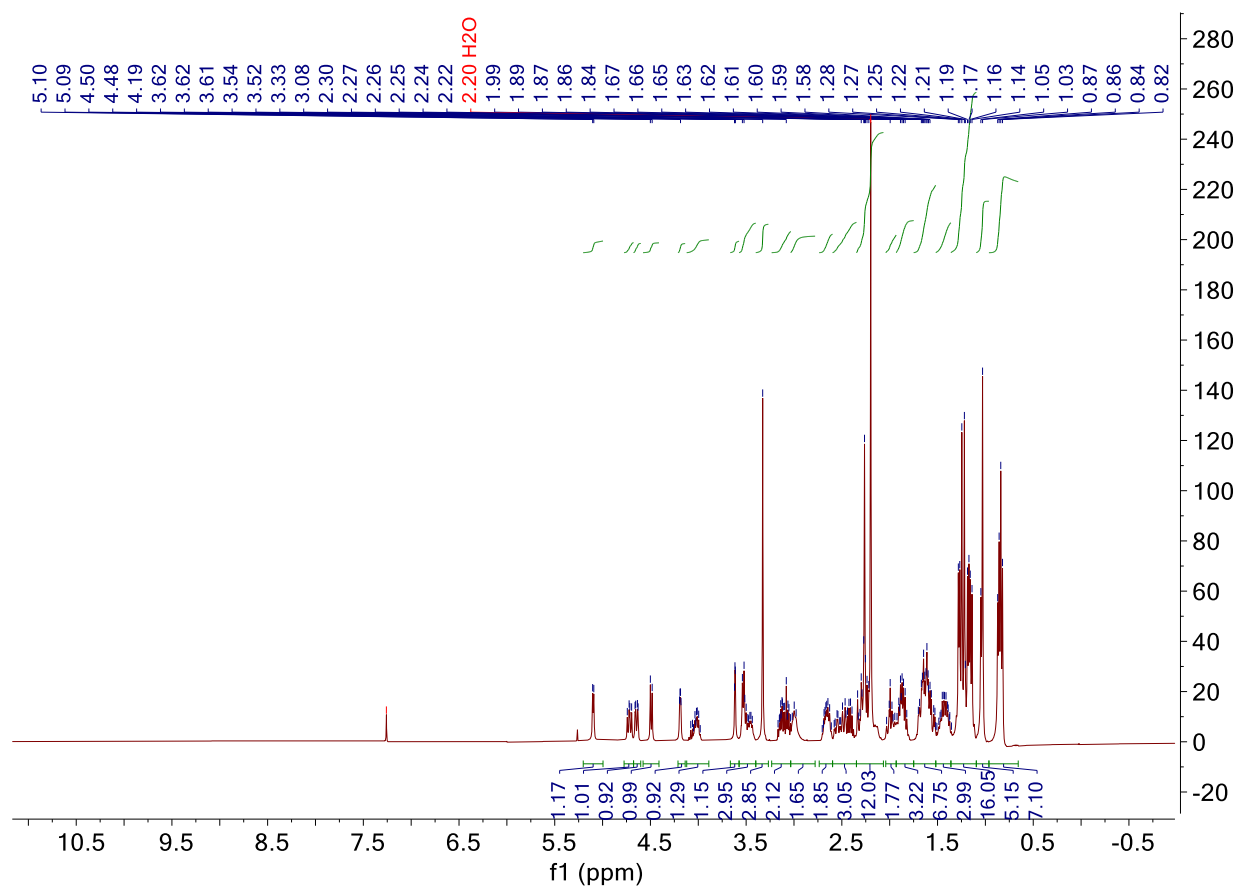
AO-02-41 (¹H NMR)



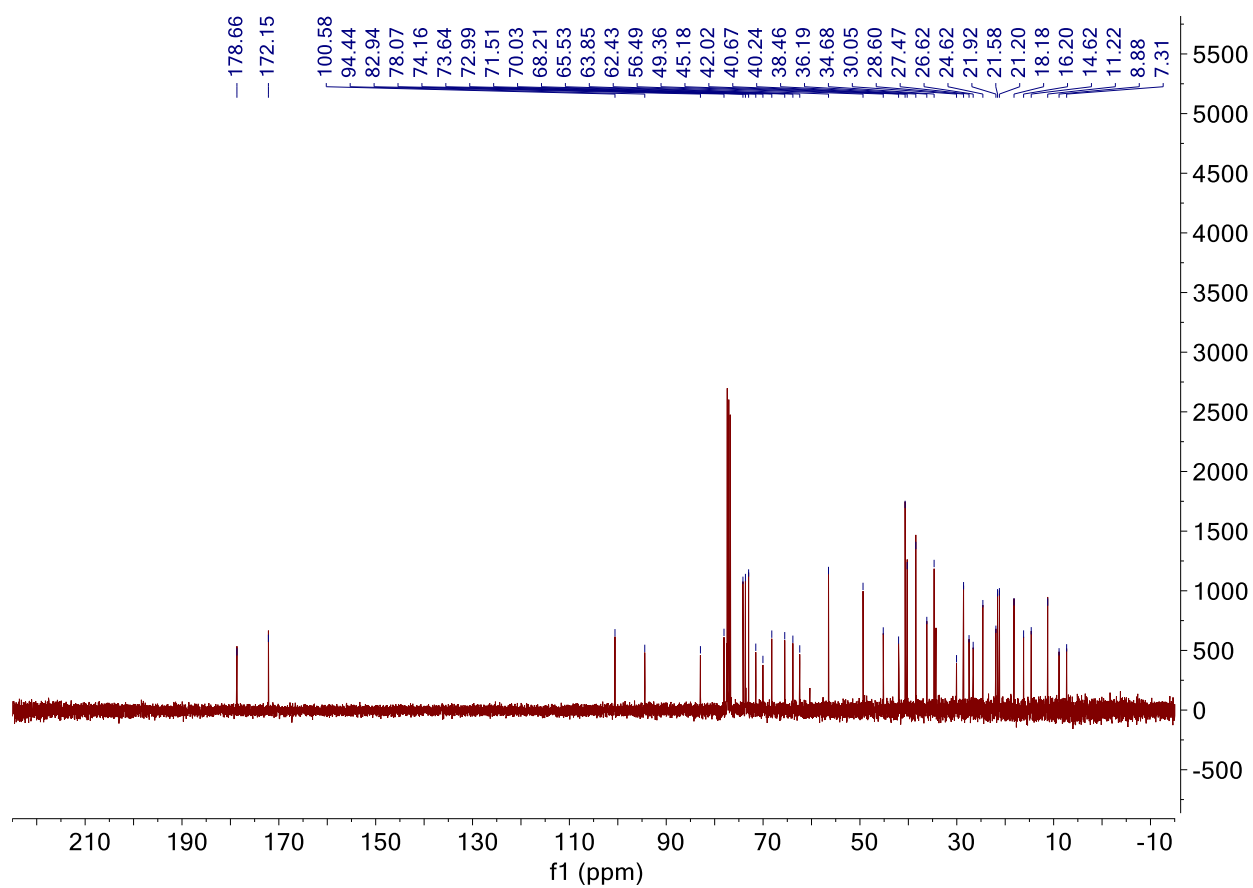
AO-02-41 (^{13}C NMR)



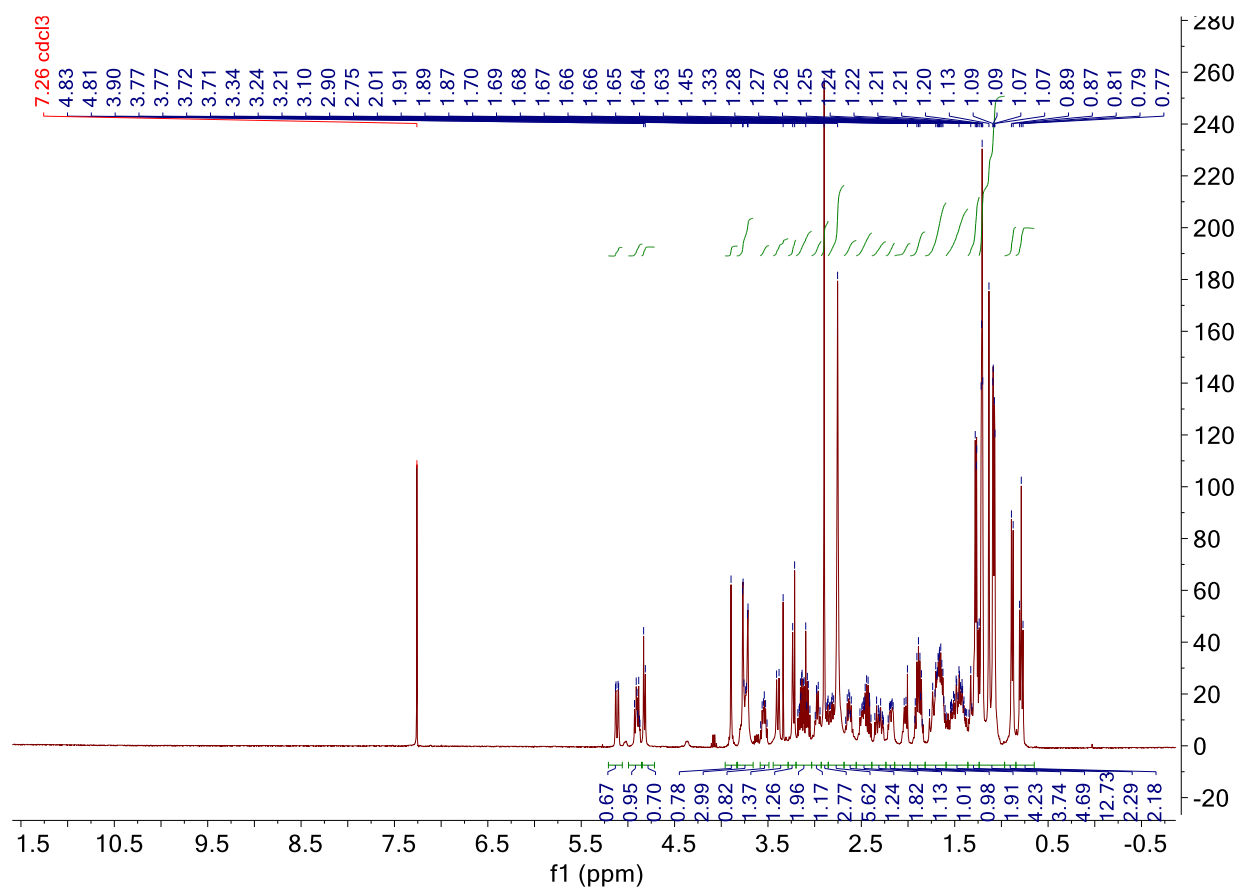
AO-02-45 (^1H NMR)



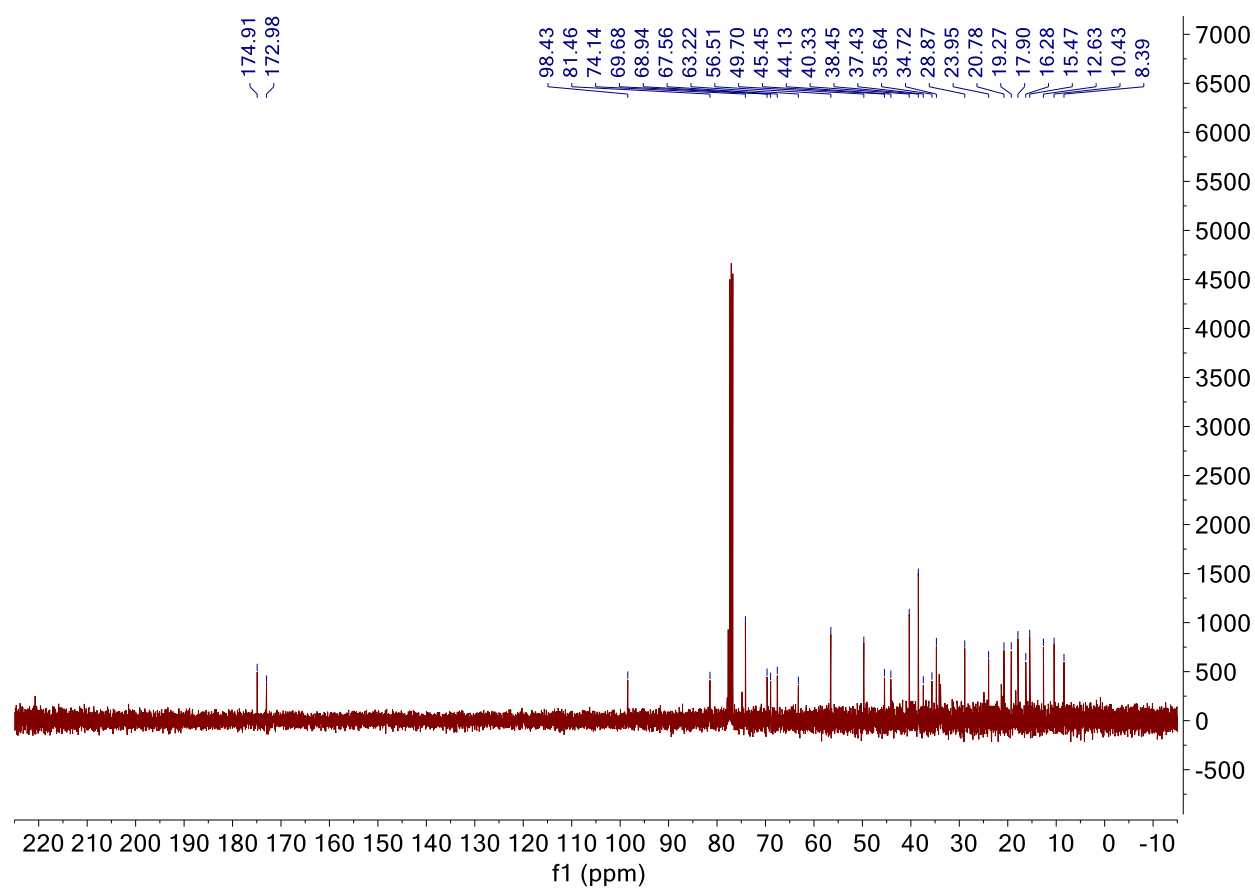
AO-02-45 (¹³C NMR)



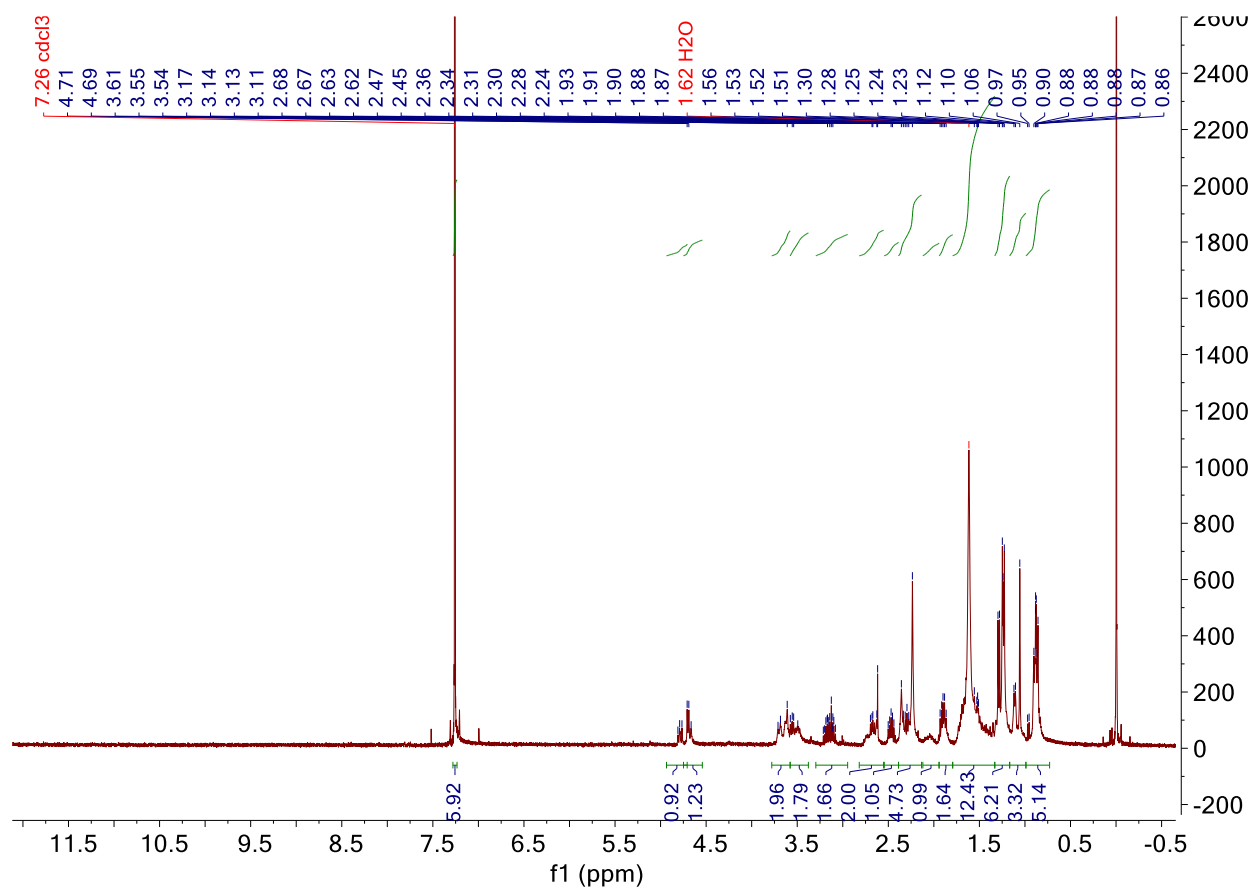
AO-02-47 (¹H NMR)



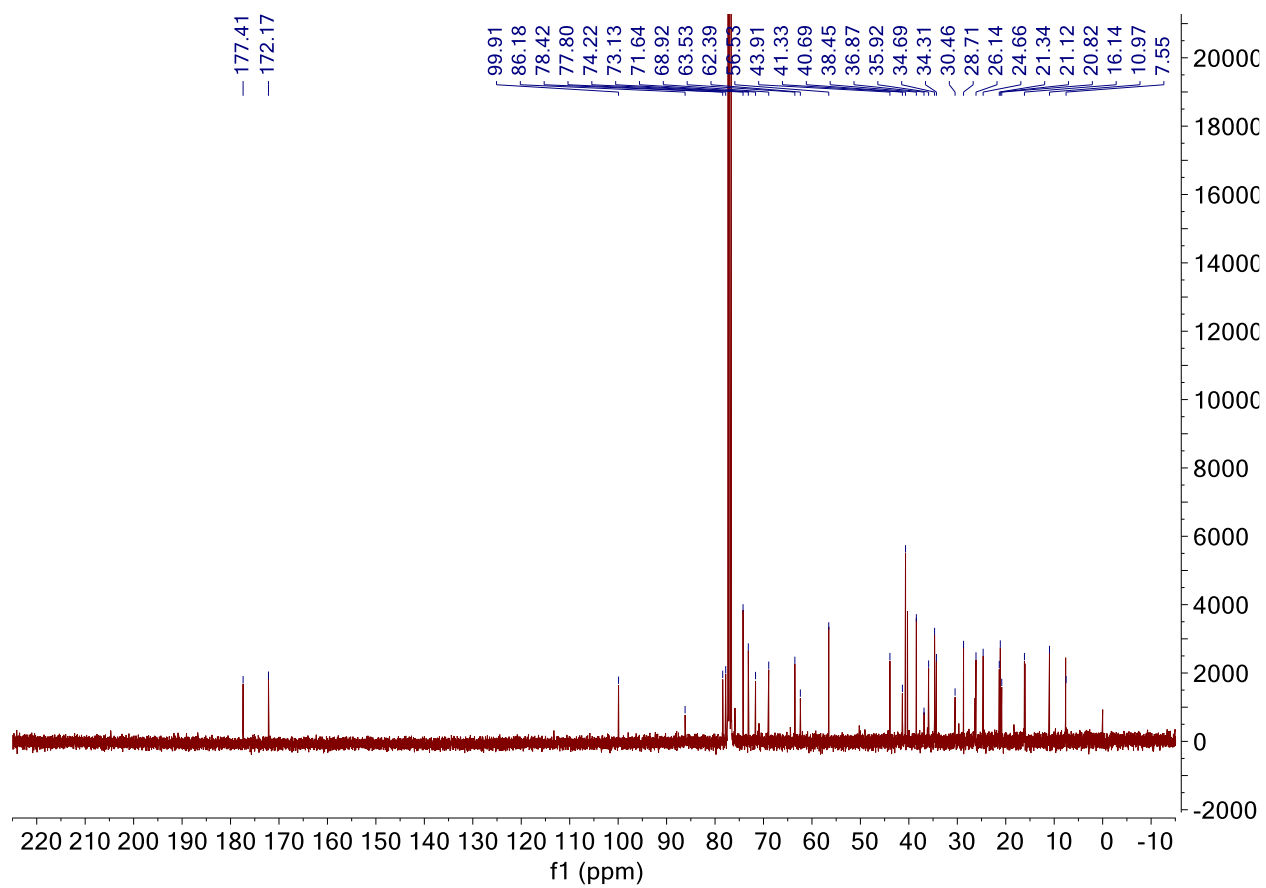
AO-02-47 (^{13}C NMR)



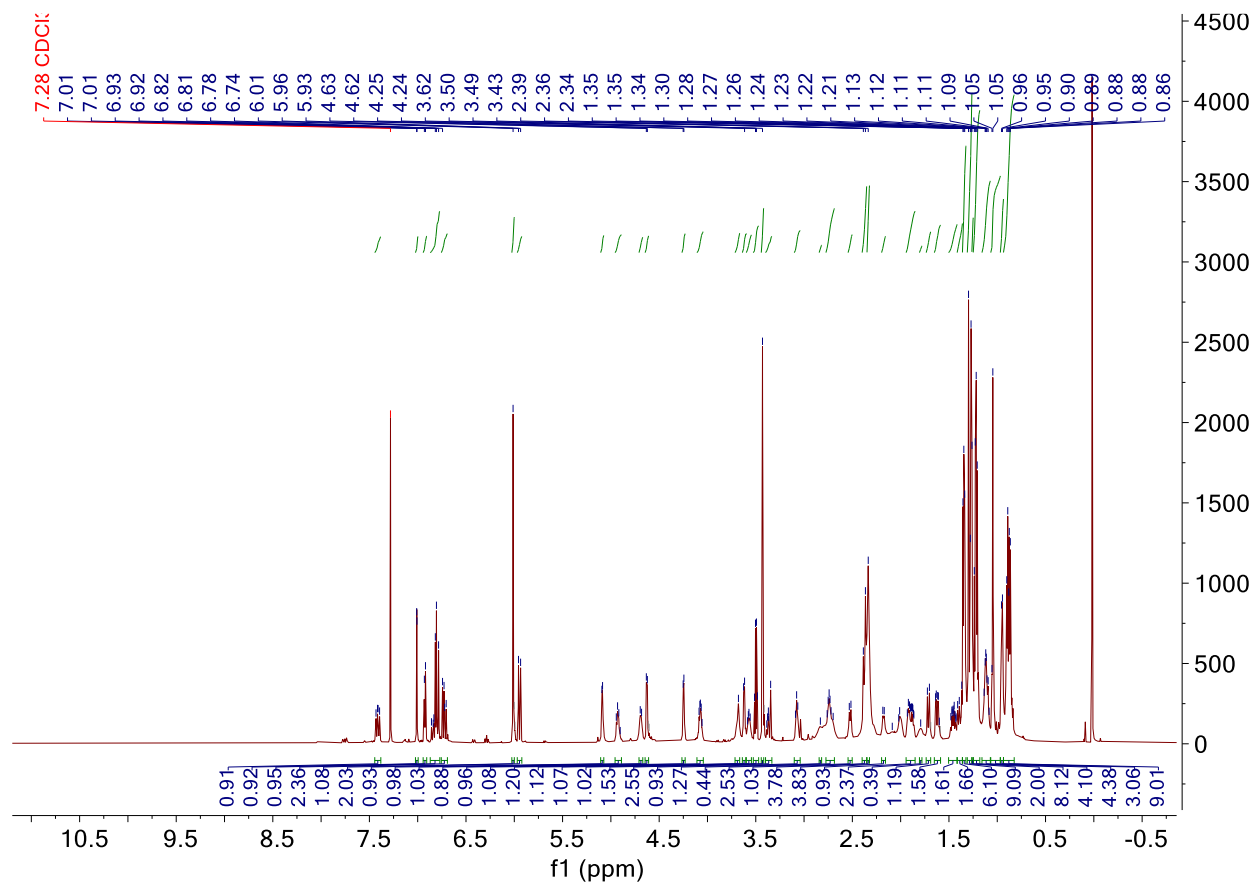
AO-02-48 (^1H NMR)



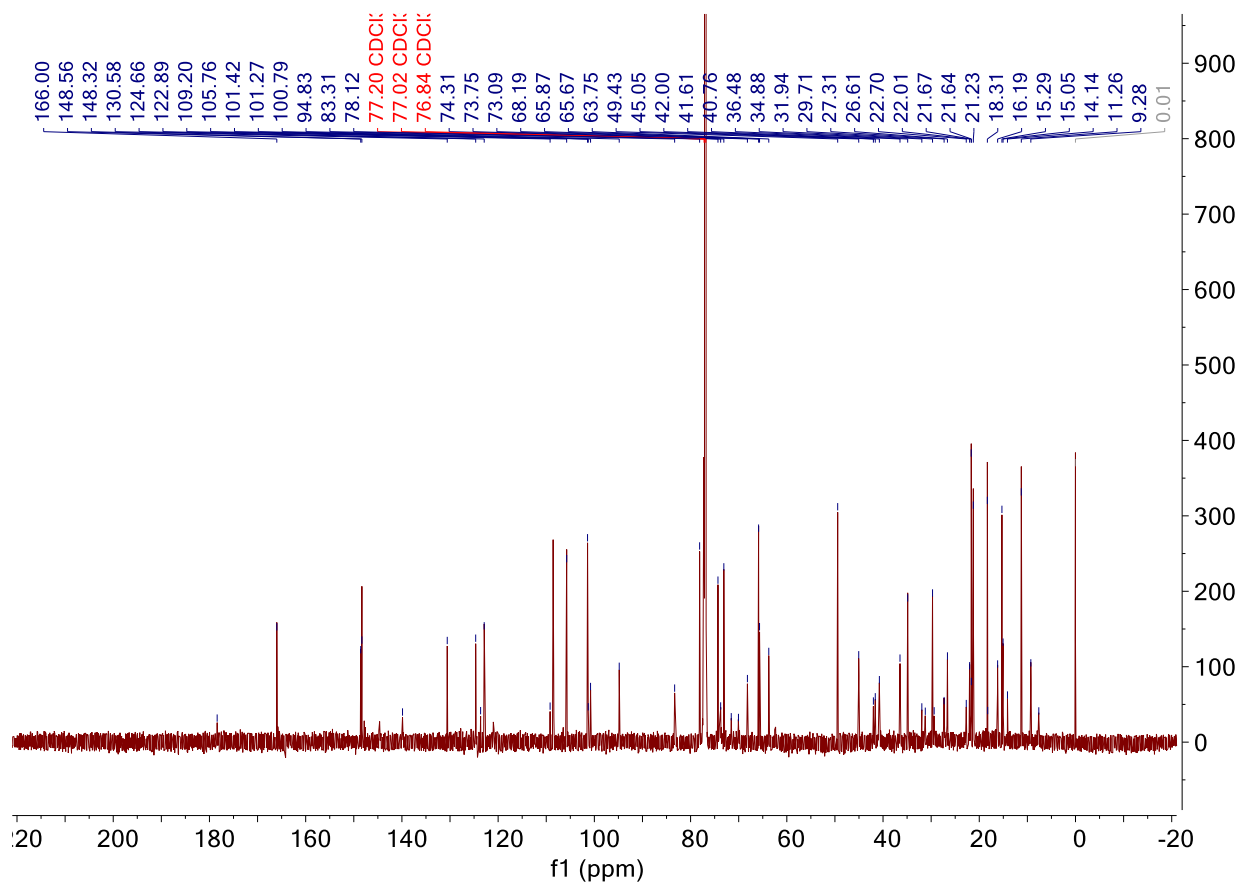
AO-02-48 (^{13}C NMR)



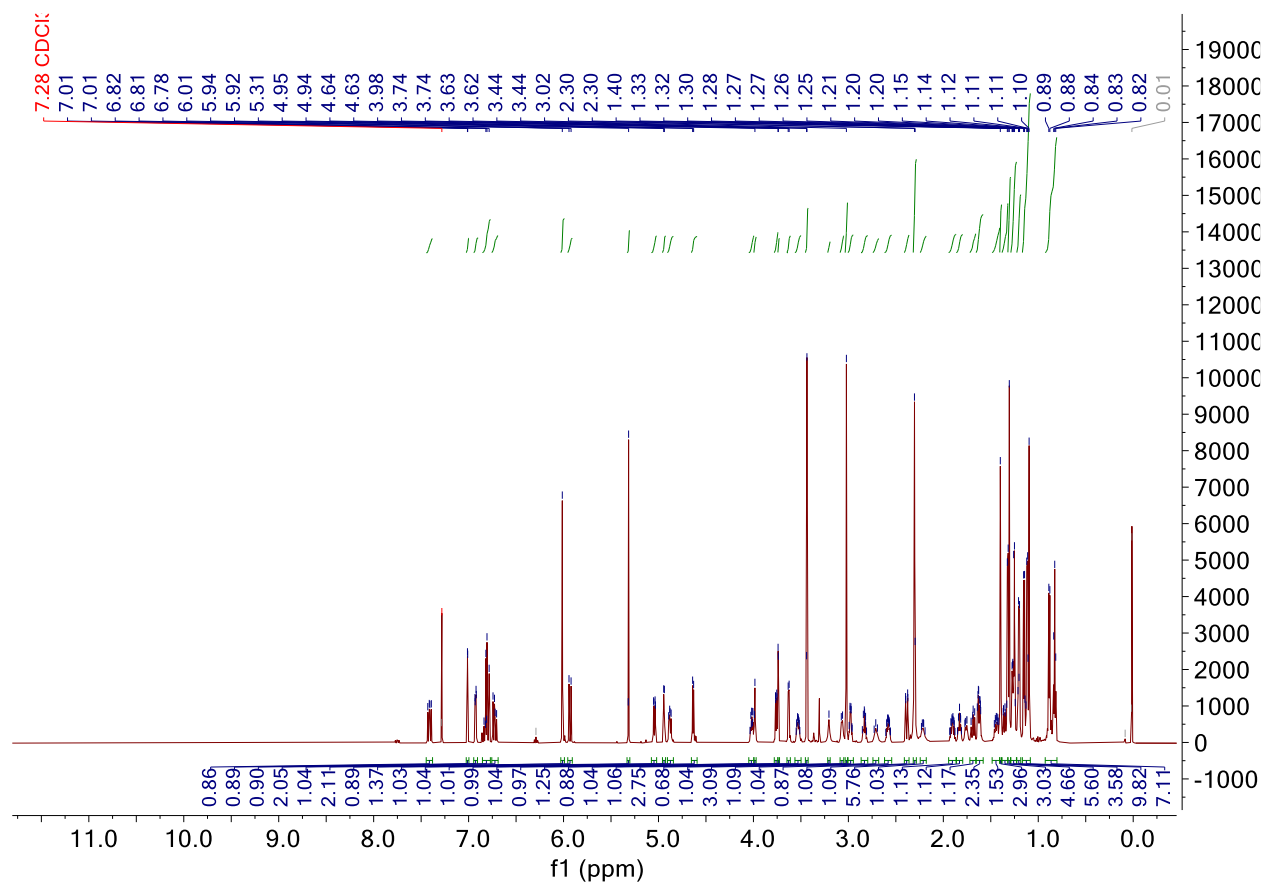
AO-02-11 (^1H NMR)



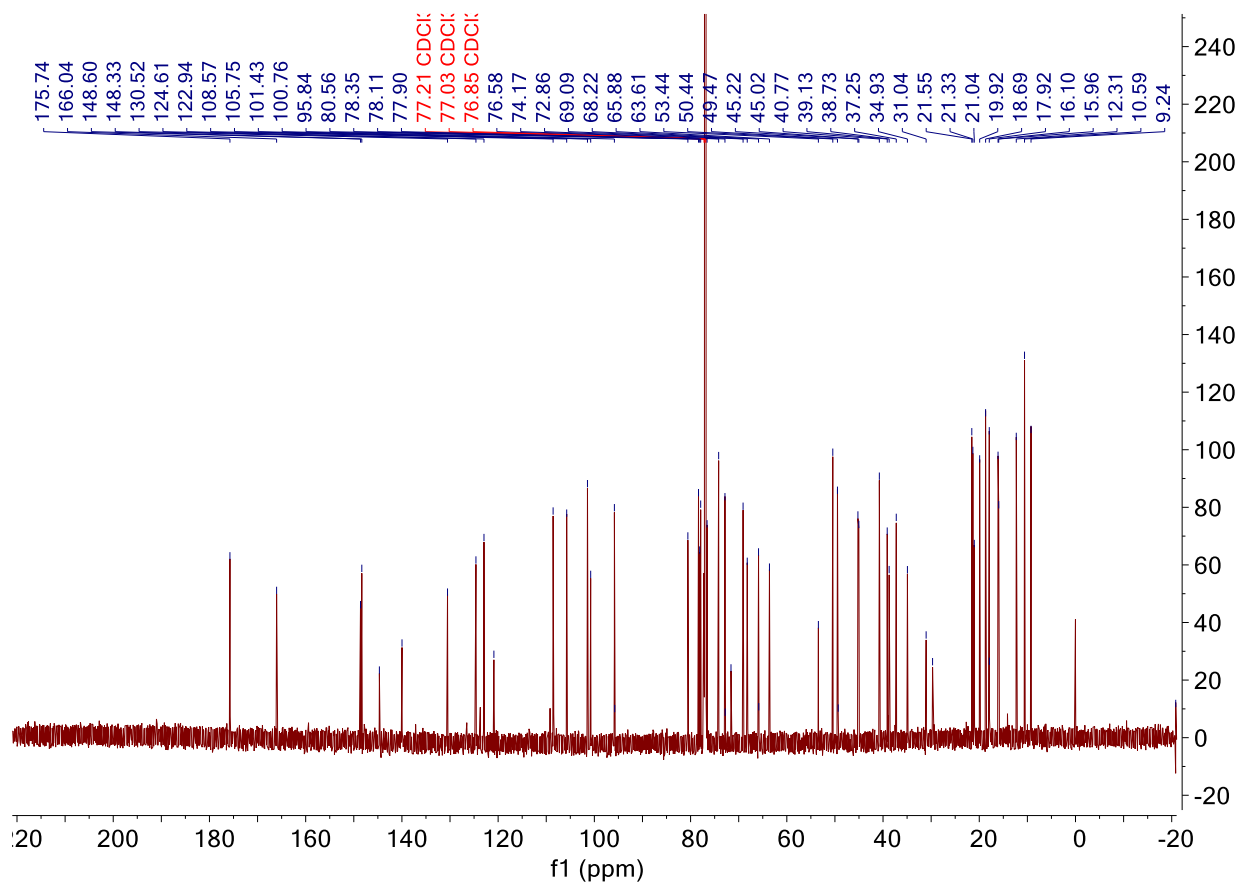
AO-02-11 (^{13}C NMR)



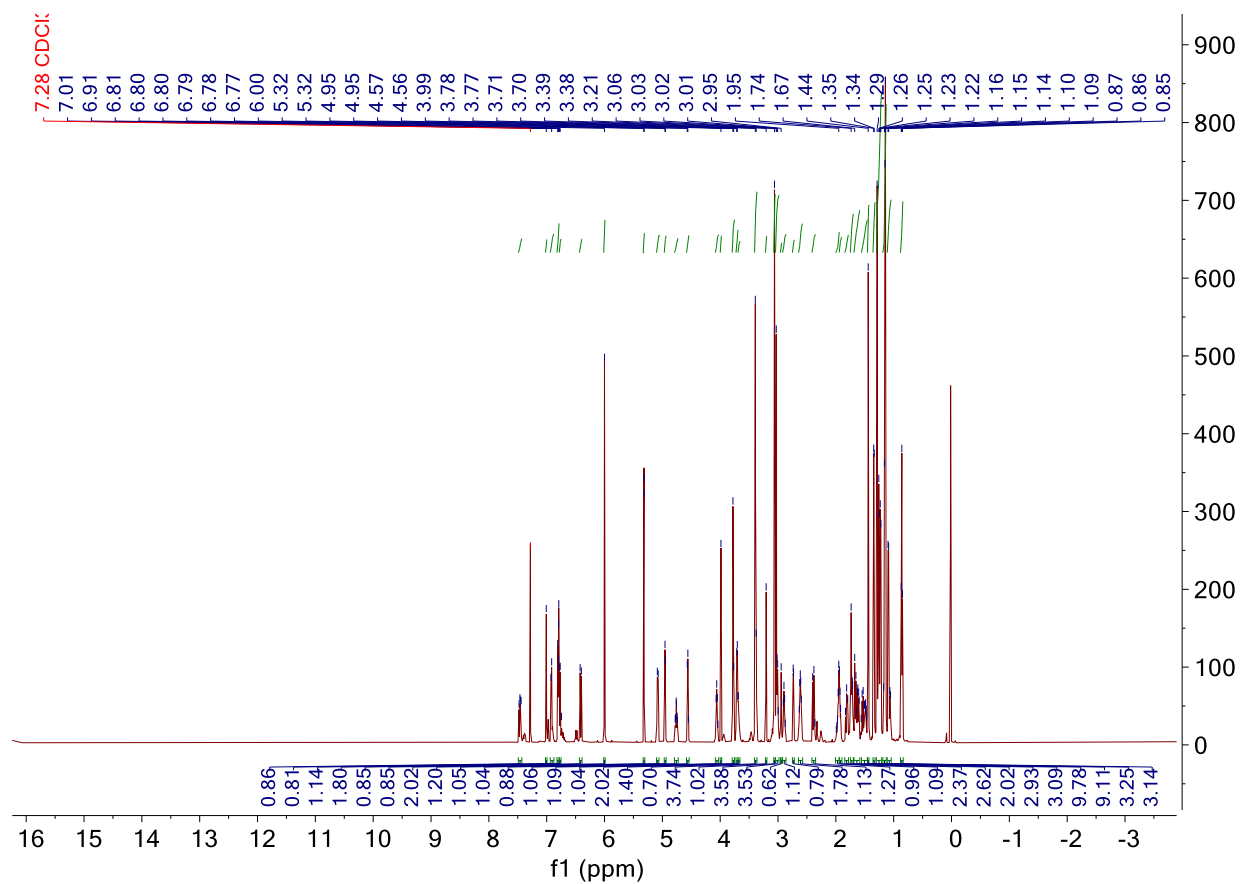
WBC-04-14 (^1H NMR)



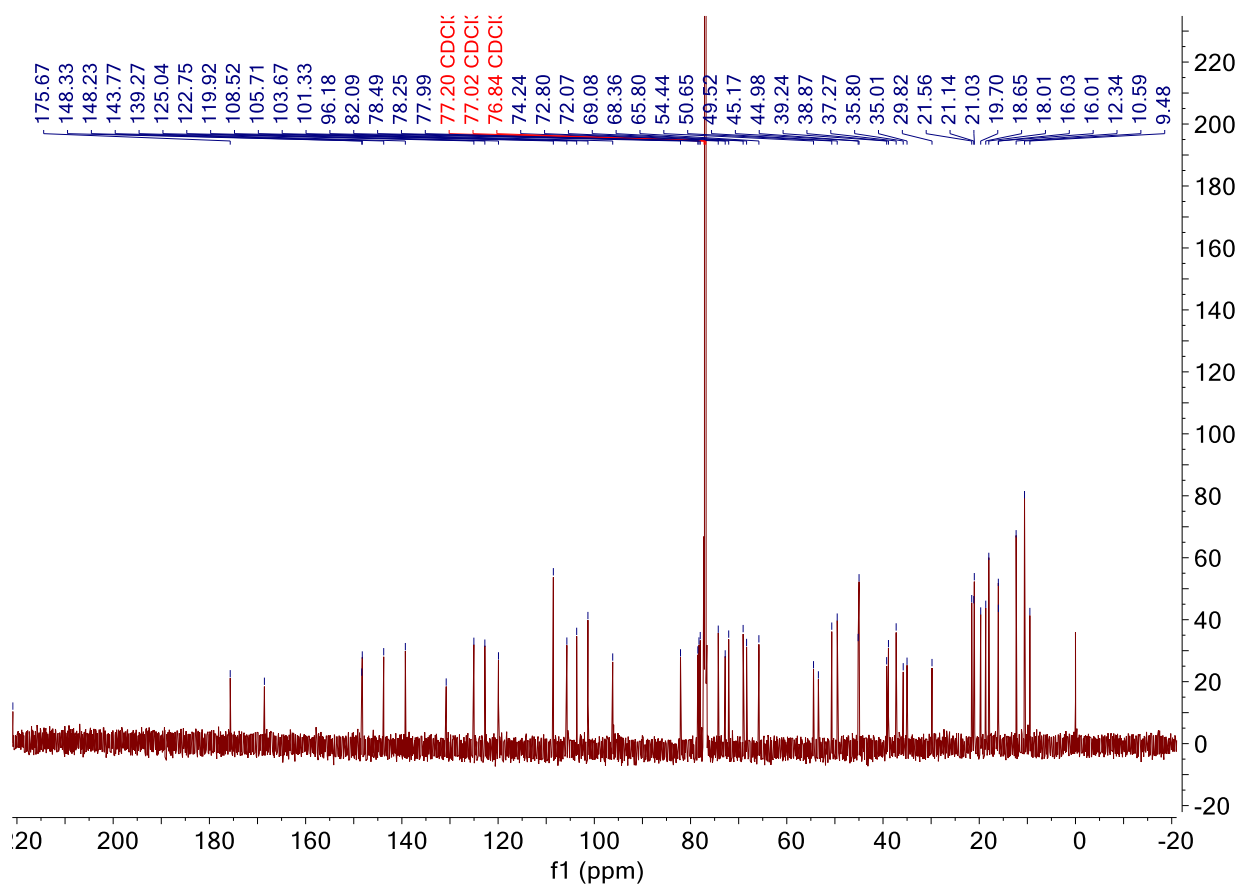
WBC-04-14 (^{13}C NMR)



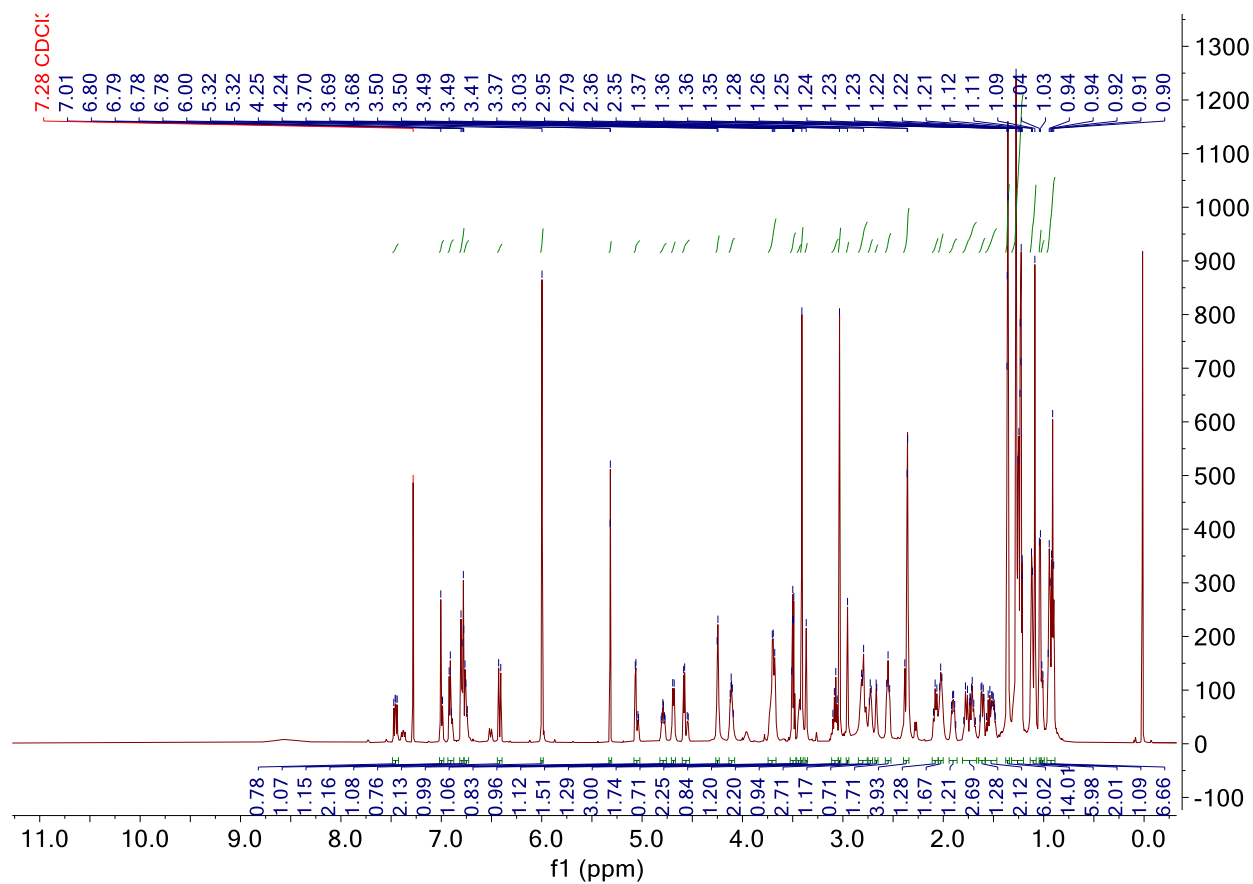
WBC-04-15 (¹H NMR)



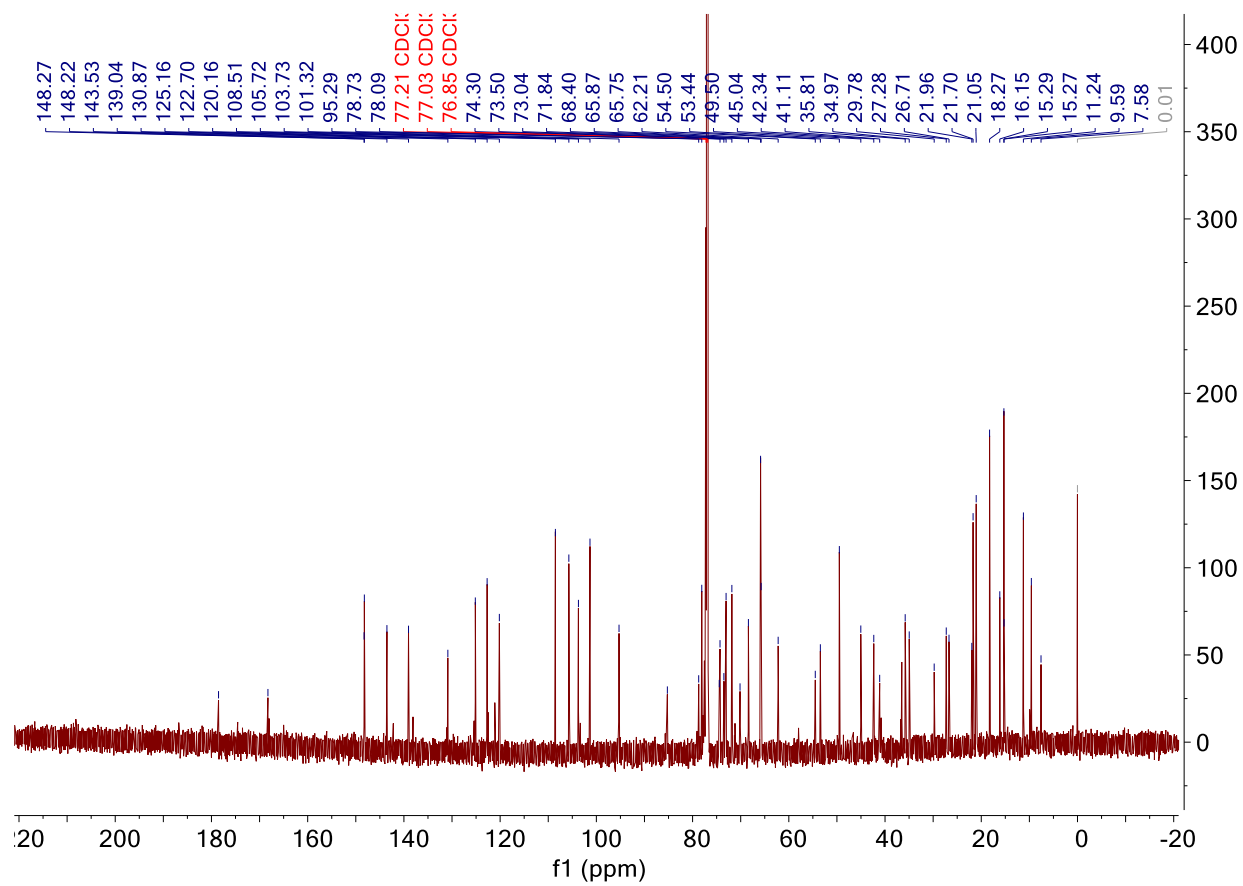
WBC-04-15 (^{13}C NMR)



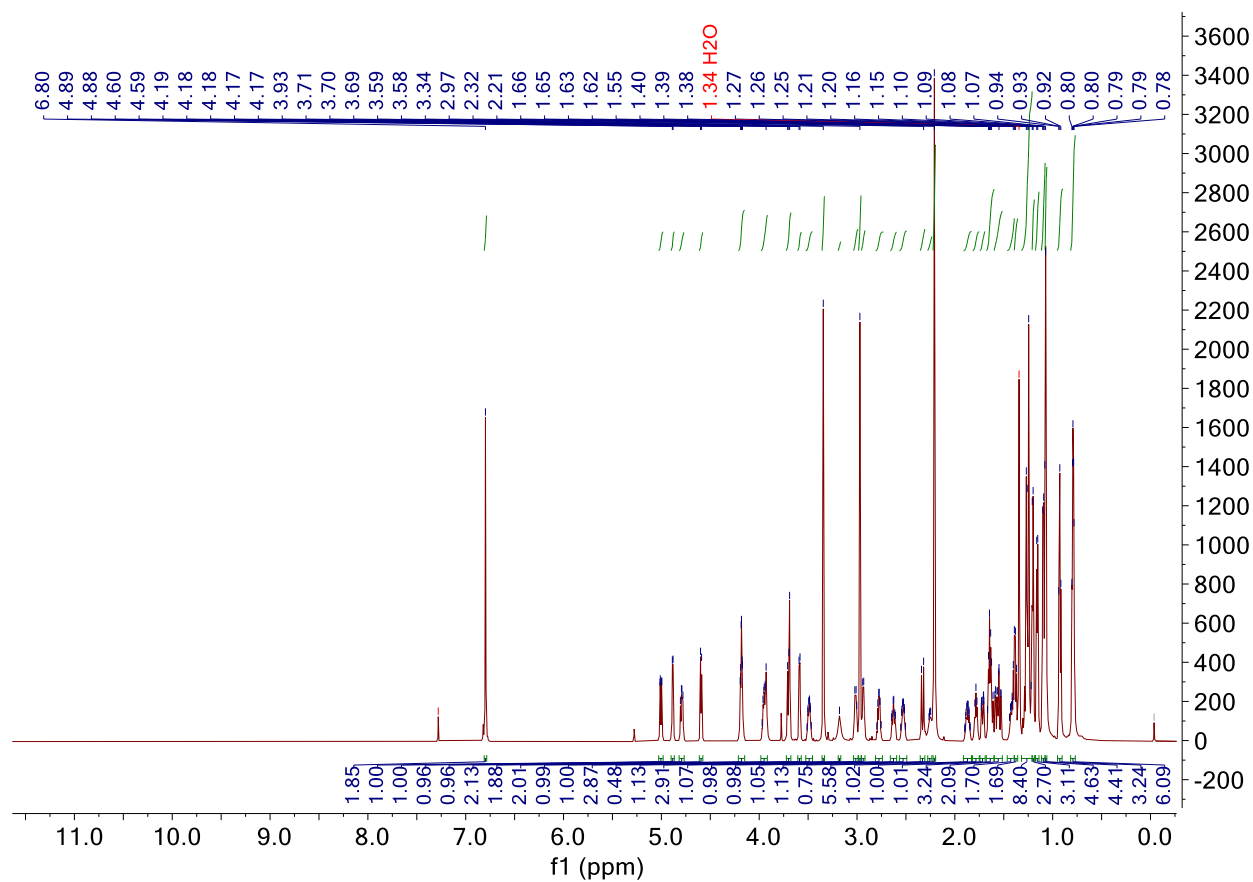
WBC-04-16 (¹H NMR)



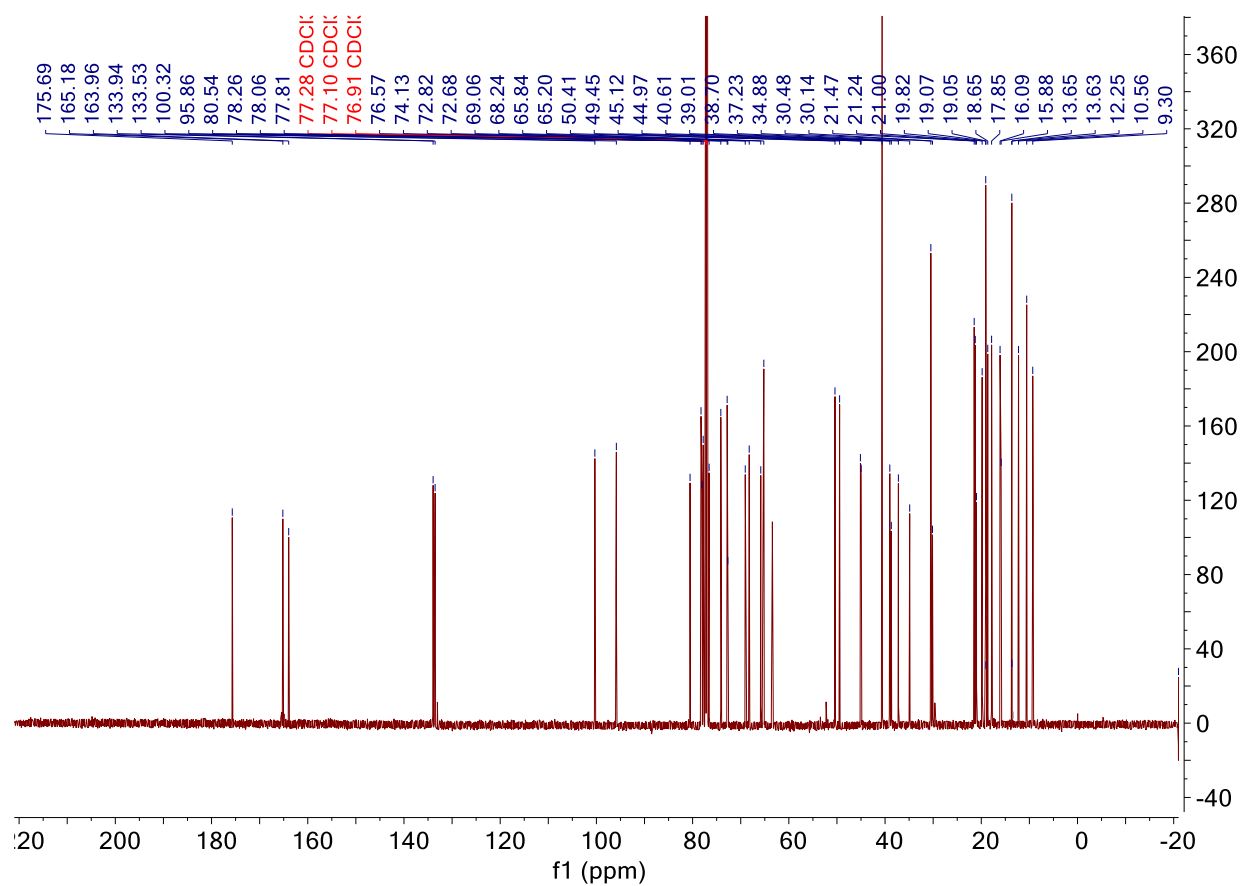
WBC-04-16 (^{13}C NMR)



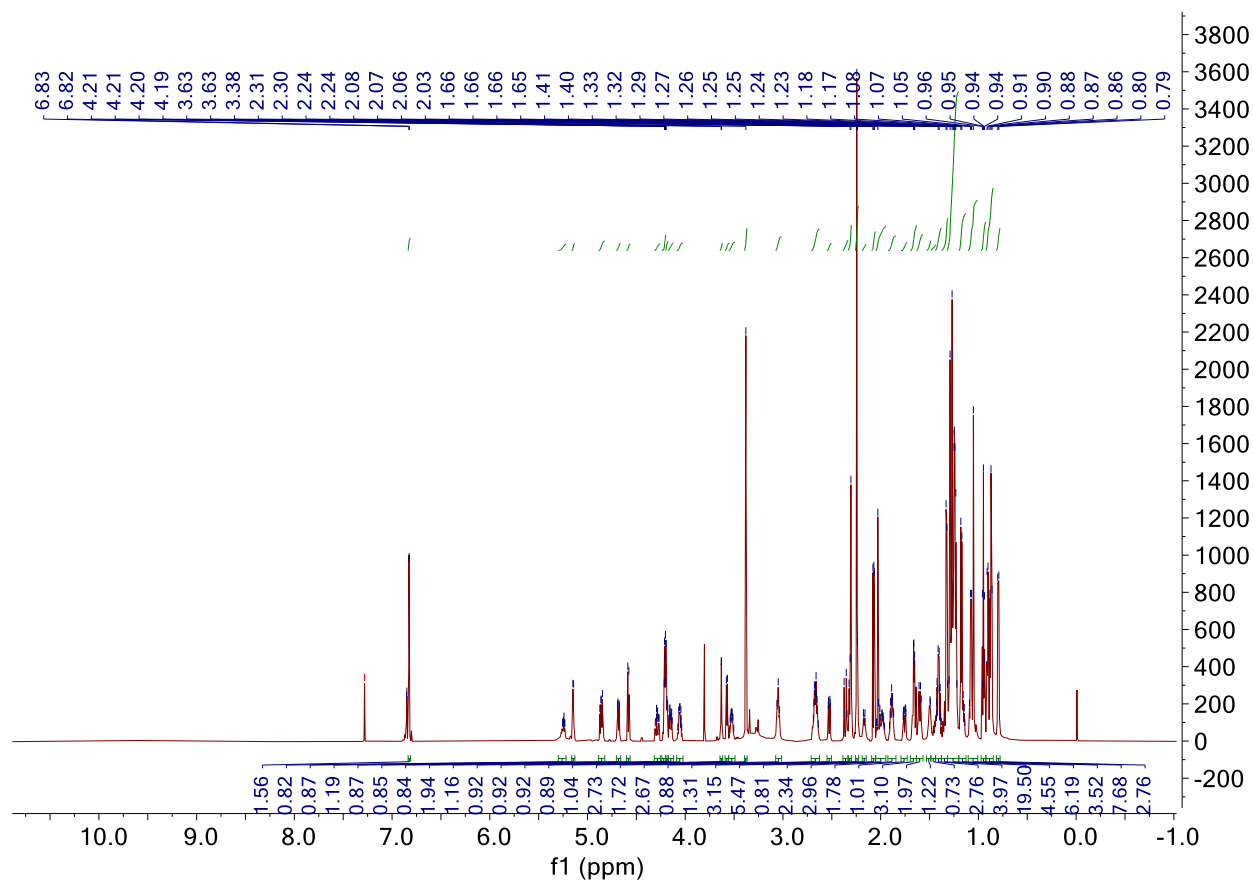
ST-01-95 (^1H NMR)



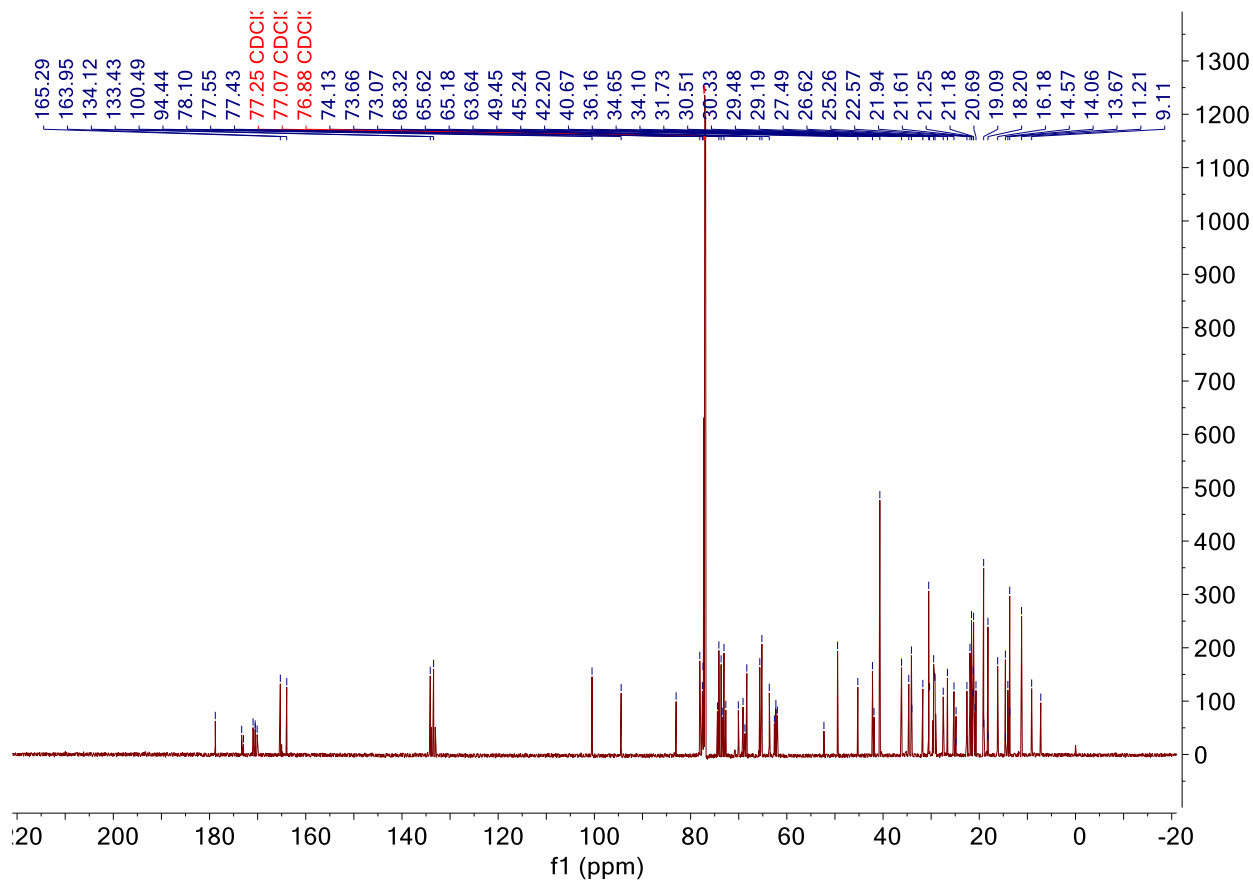
ST-01-95 (^{13}C NMR)



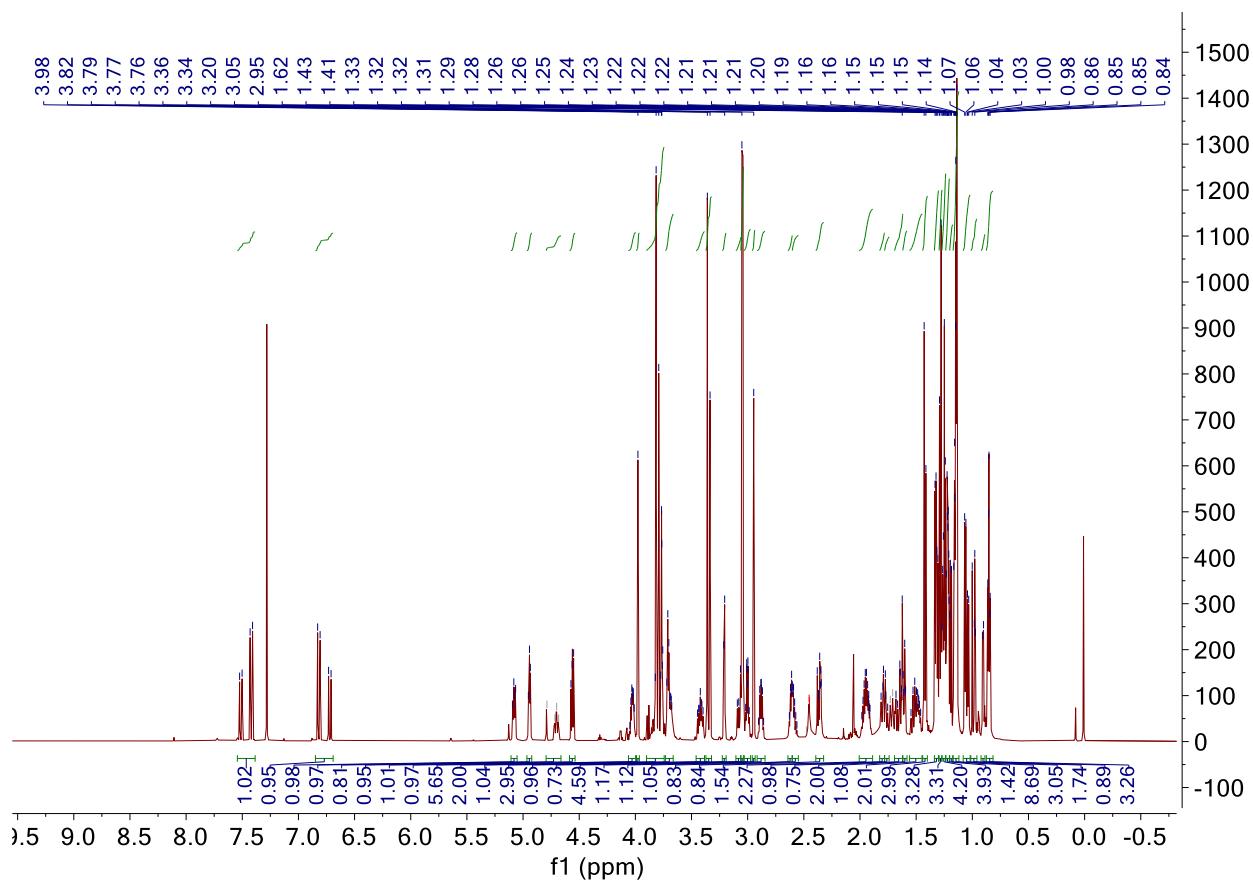
ST-01-96 (¹H NMR)



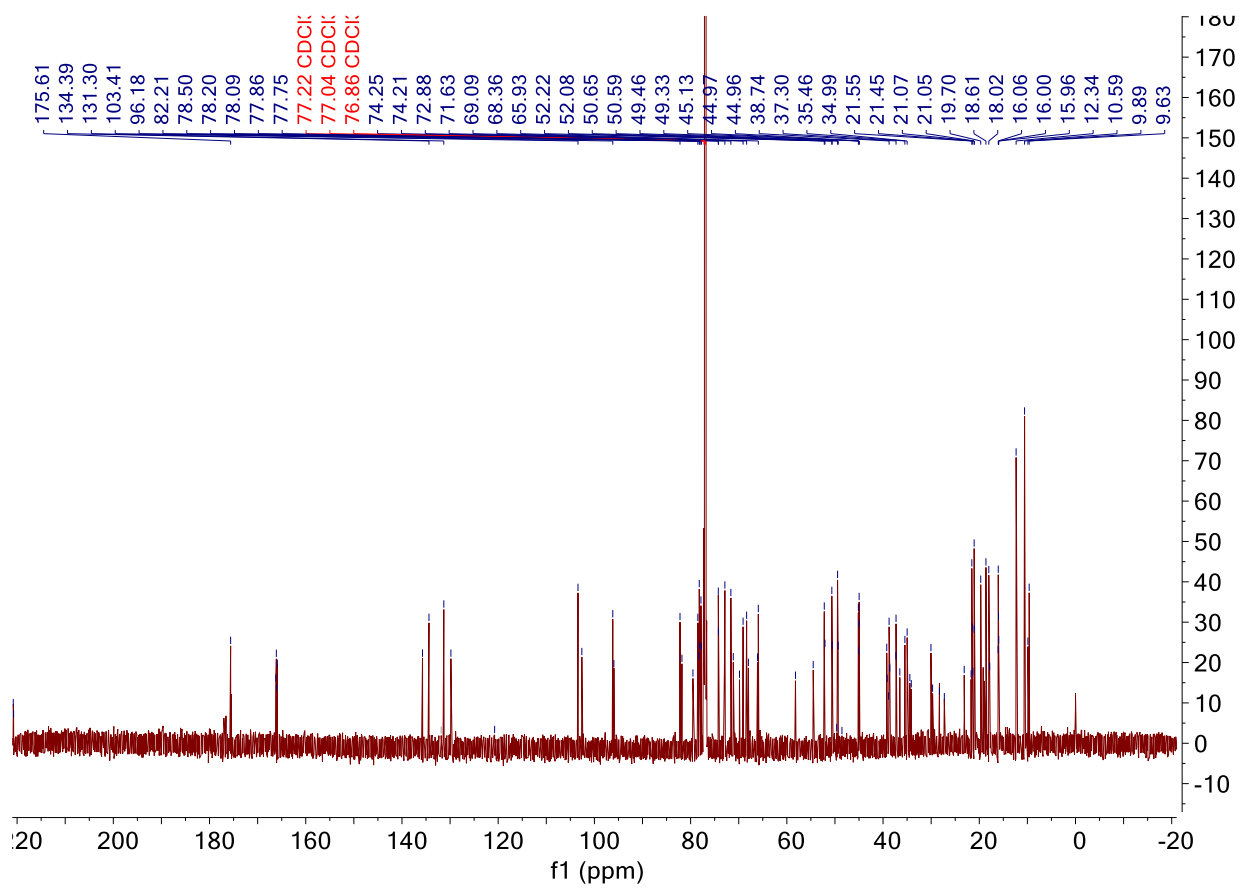
ST-01-96 (^{13}C NMR)



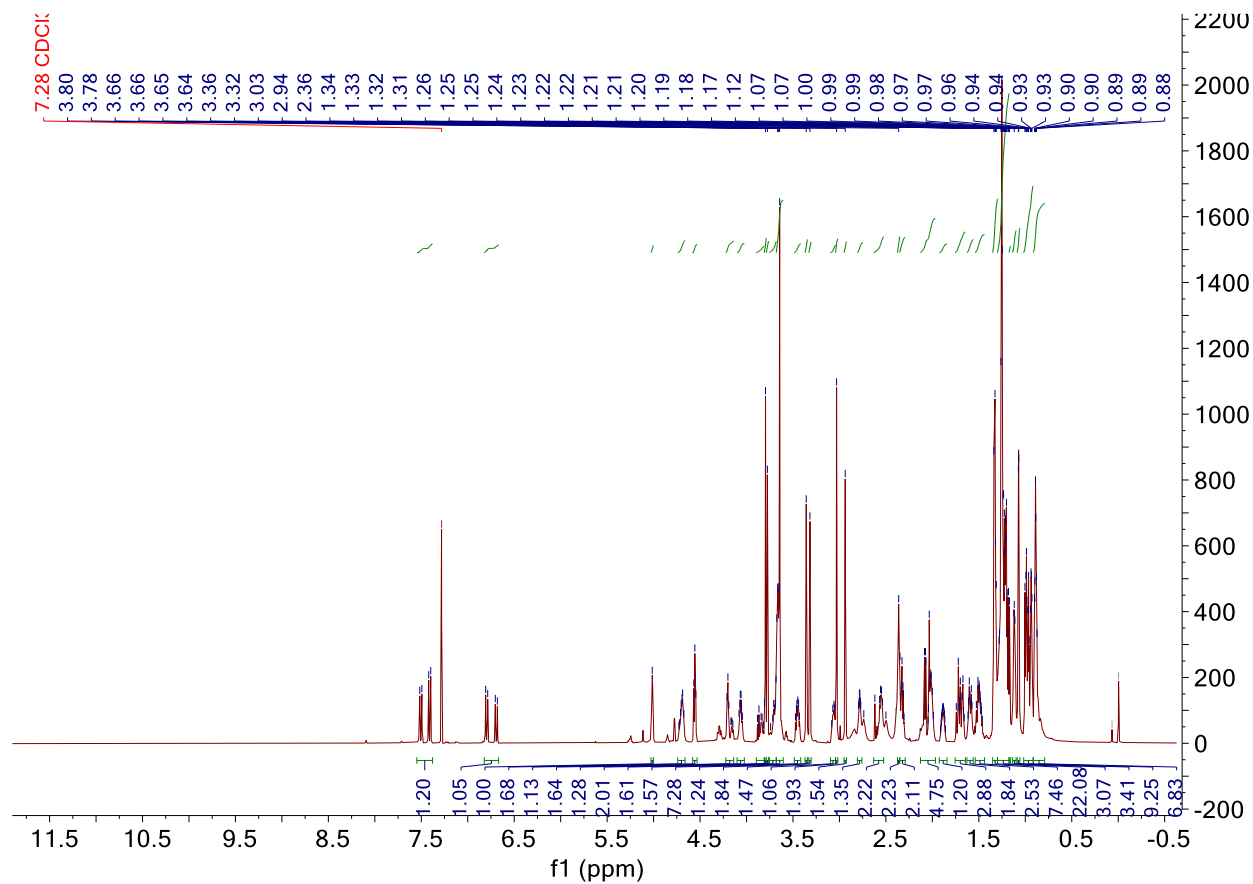
WBC-04-50B (^1H NMR)



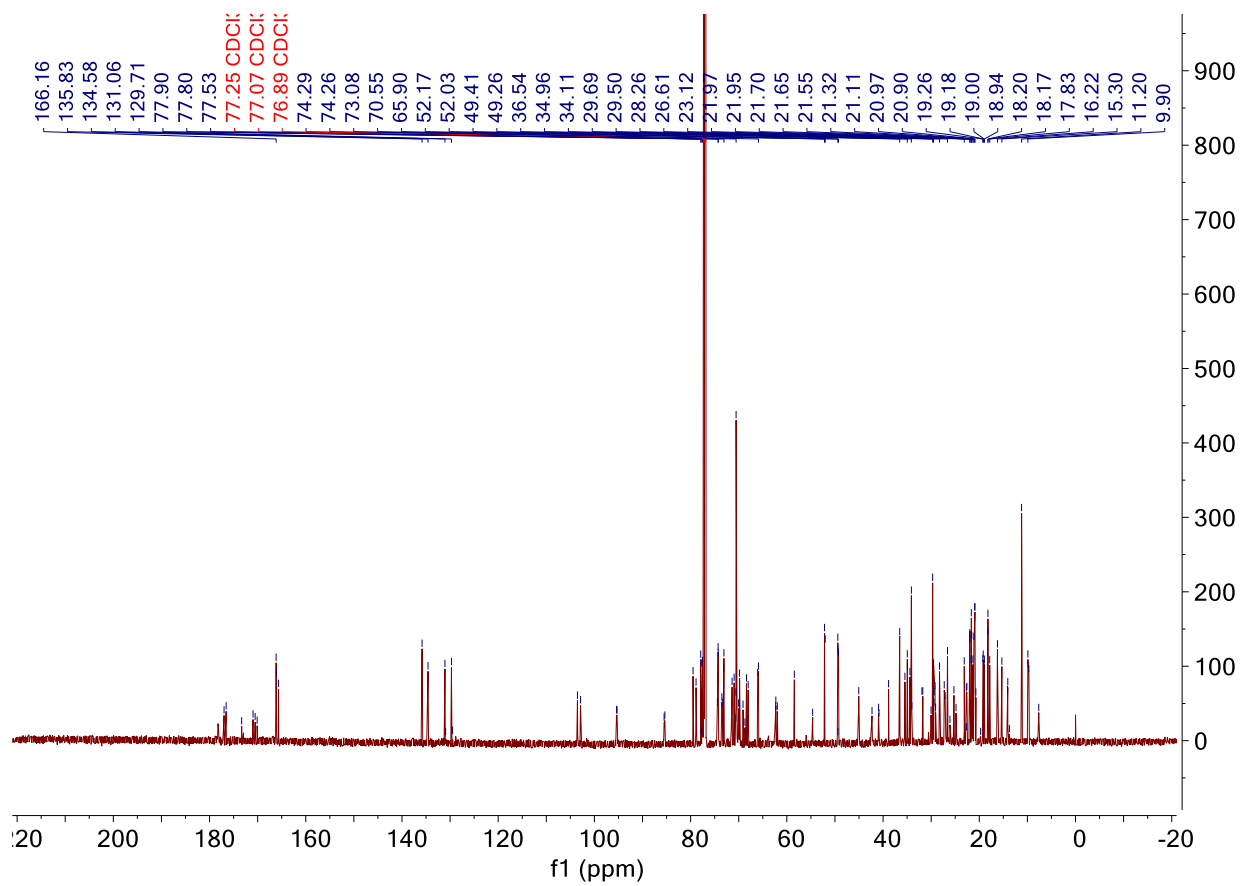
WBC-04-50B (^{13}C NMR)



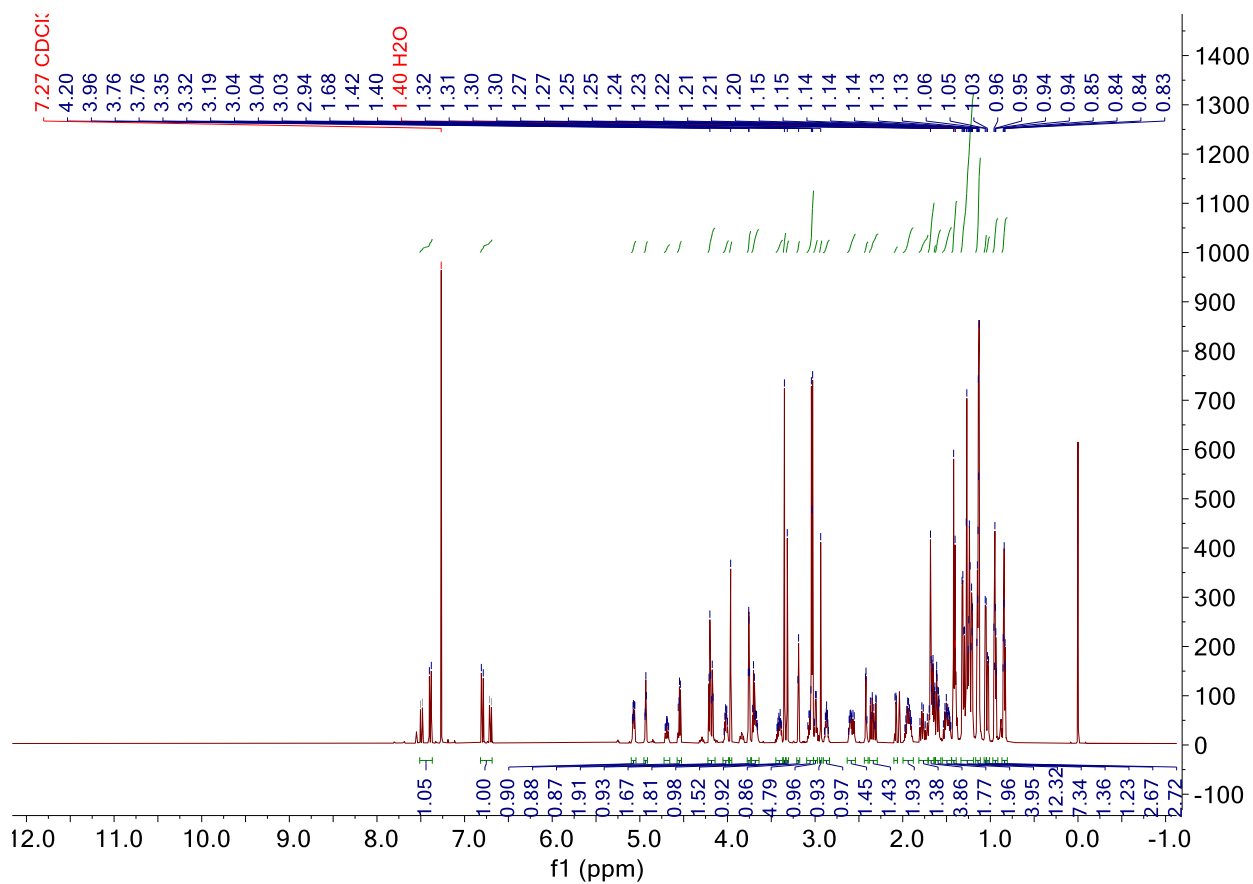
WBC-04-51 (^1H NMR)



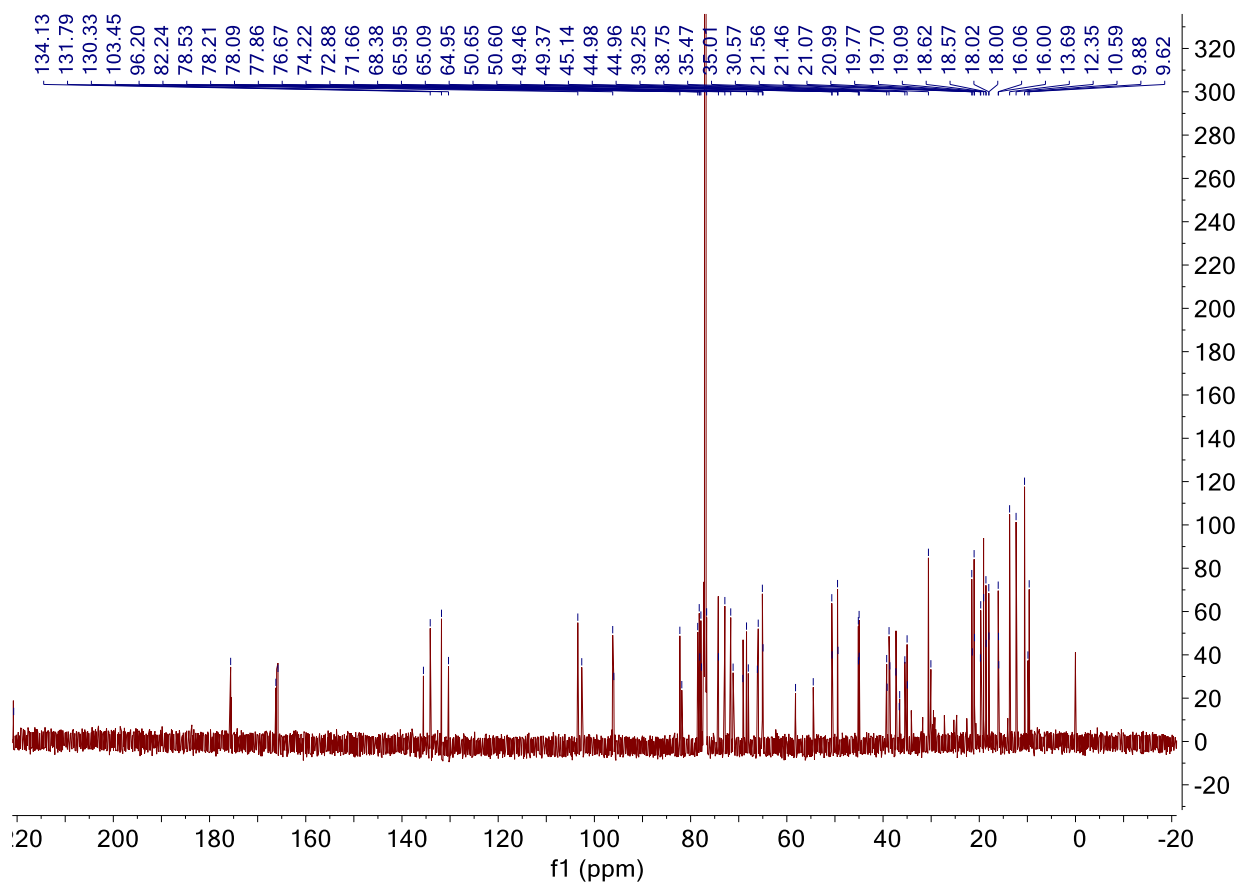
WBC-04-51 (^{13}C NMR)



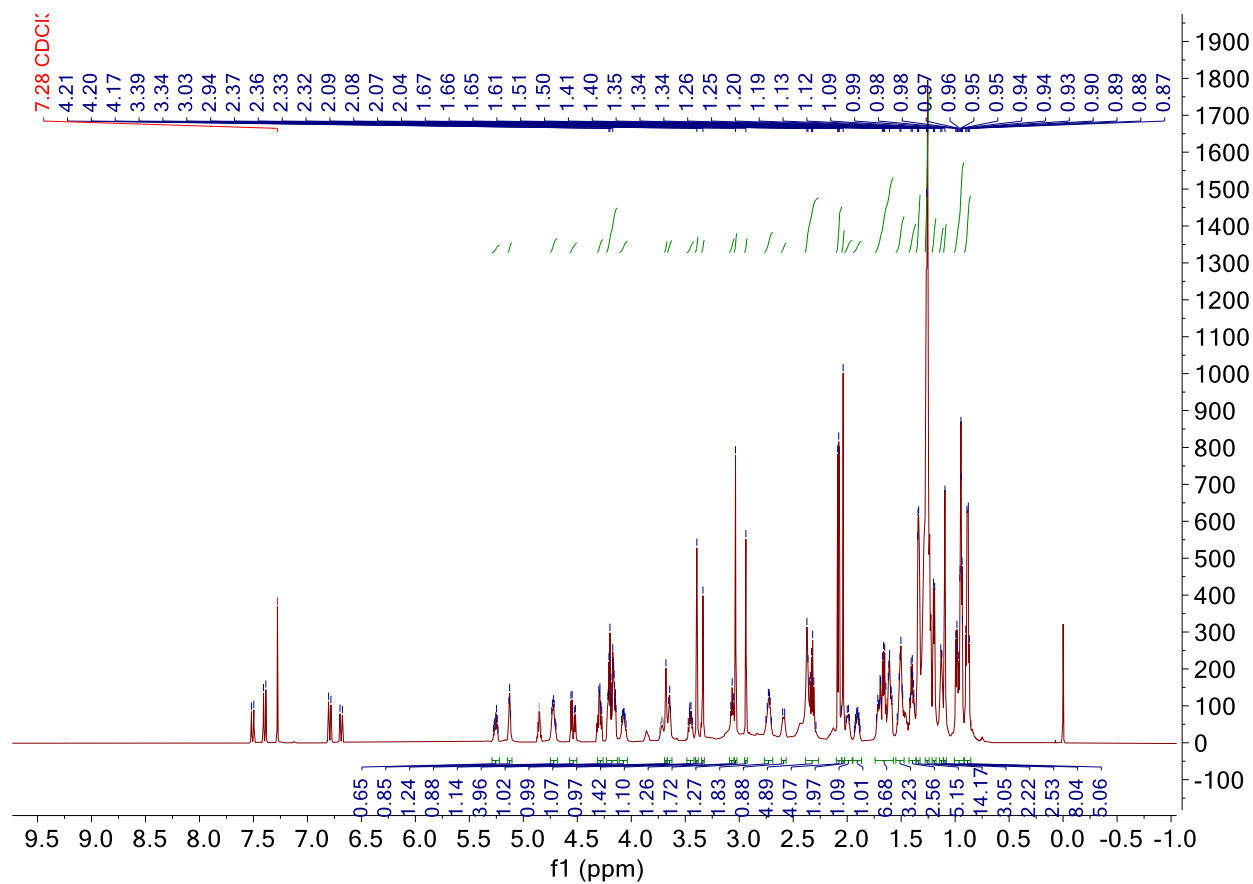
WBC-04-110 (^1H NMR)



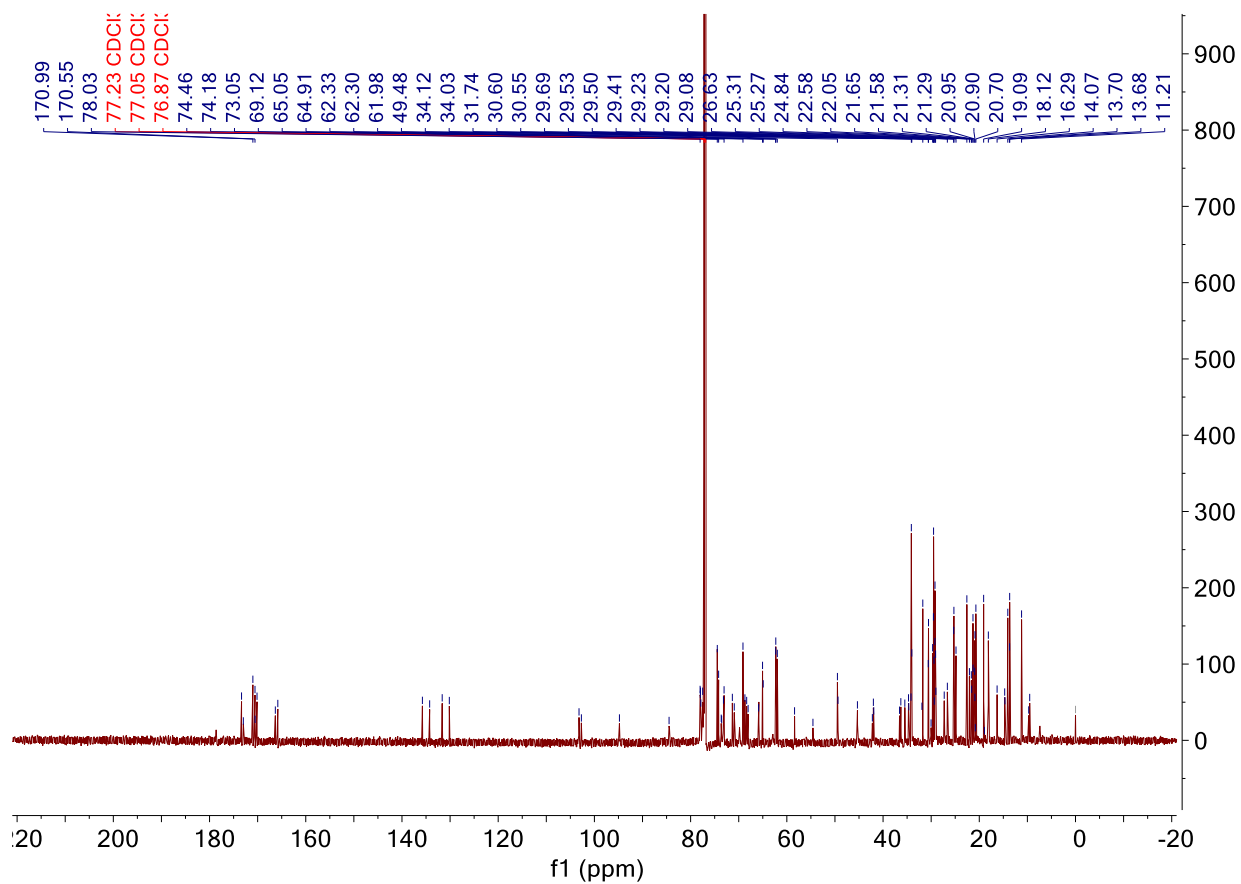
WBC-04-110 (^{13}C NMR)



WBC-04-111 (^1H NMR)



WBC-04-111 (^{13}C NMR)



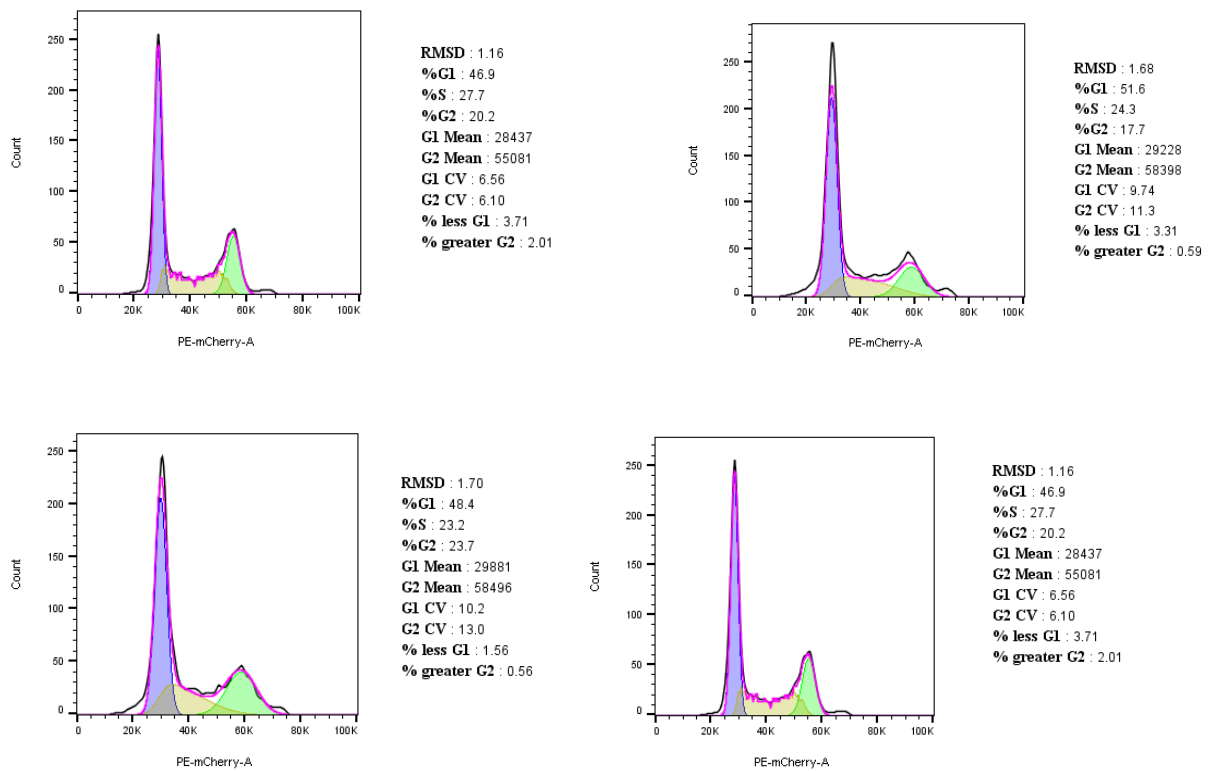


Figure 3S.1. Both ALA and AO-02-41 do not change Cell cycle progression. The cells were treated with DMSO or drugs for 24h before cell cycle analysis. (A). The DMSO group; (B). The ALA 60μM; (C) AO-02-41 40μM; (D). AO-02-41 60μM.

CHAPTER 4. DISCOVERY OF A NOVEL CLARITHROMYCIN DERIVATIVE WITH EUKARYOTIC RIBOSOME INHIBITION AND ANTI-CANCER ACTIVITY

Bocheng Wu^{1,2†}, Adegboyega Oyelere^{1, 2}

*School of Chemistry and Biochemistry, School of Biological Sciences, Parker H. Petit Institute
for Bioengineering and Bioscience, Georgia Institute of Technology, Atlanta, GA 30332-0400
USA*

¹School of Chemistry and Biochemistry, Georgia Institute of Technology

²Parker H. Petit Institute for Bioengineering and Bioscience, Georgia Institute of Technology

Correspondence to:

Adegboyega K. Oyelere, **E-mail:** aoyelere@gatech.edu

Keywords: eukaryotic ribosome, ribosomal proteins, clarithromycin, anti-cancer, translation inhibition, X-ray crystallography, conjugation ring formation, dehydration reagent.

Abstract:

Clarithromycin (CLM) is an antibiotic in clinical use for the treatment of respiratory tract bacterial infections. CLM derives its antibacterial effects from selective inhibition of prokaryotic ribosome. We have discovered that CLM undergoes tandem dehydration- cyclization-dehydration reactions, involving C-11 and C-12 hydroxyl groups and the C-9 keto moiety, to furnish a dihydrofuranyl macrolide AO-02-63. We elucidated the structure of AO-02-63 using mass spectroscopy, NMR, and X-ray crystallography. Using a combination cell free protein translation and pull-down assays, we found that this novel macrolide inhibits the activities of prokaryotic and eukaryotic ribosomes and possibly disrupts the activity of hnRNPs. We observed that AO-02-63 inhibits the proliferation of all cell lines in the NCI-60 panel with low micromolar IC₅₀s. The broad anti-cancer activity of AO-02-63 could be due to its inhibition of protein synthesis and mRNA processing, two processes that are vital for the survival of cells. Furthermore, AO-02-63 elicits anti-inflammatory activity similar to CLM, although with a 10-fold potency enhancement. This work unveils yet another layer of the rich biological activities of macrolide antibiotics.

4.1 Introduction:

Clarithromycin is a synthetic erythromycin derivative with broad antibacterial activities. Erythromycin (ERM), azithromycin (AZM) and clarithromycin (CLM) are a class of macrolide antibiotics (Fig. 4.1) which have been in use for several years for the treatment of respiratory tract infections. Macrolides derive their antibacterial activities from the inhibition of prokaryotic translation by blocking the nascent peptide exit tunnel.¹⁻³ Over the past 20 years, macrolides have also been shown to have other non-antibiotic properties.^{4,5} For example, they have demonstrated anti-inflammatory and immunomodulatory effects that make them promising candidates for the management of diseases of chronic airway inflammation.⁴ AZM and CLM have shown improved pulmonary function, and decrease morbidity and mortality in patients with diffuse panbronchiolitis (DPB).⁵

CLM, like AZM and ERM, consists of a highly hydroxylated macrolactone ring and two monosaccharide (desosamine and cladinose) moieties. The contribution of these moieties to the overall prokaryotic ribosome selectivity has been extensively investigated using biochemical and structural biology tools. Prior X-ray structures have revealed few insights that may explain the contributions of each of these moieties to the preferential binding of macrolides to the prokaryotic ribosomes exit tunnel. What is clear so far is that a narrow variation in the size of the macrolactone ring and removal of the cladinose ring, followed by esterification or the oxidation of the unmasked secondary hydroxyl group to ketone, are compatible with selective prokaryotic translation inhibition.^{6,7} However, the desosamine moiety is less tolerant of most modifications. Prior structural studies have revealed that the 2'-OH of desosamine invariantly forms H-bond with N1 of A2058 (E.coli numbering).^{1,2,8} A recent study has revealed new insights about the role of water-mediated H-bond in the crucial interactions of the desosamine moiety with A2058 and the

phosphate backbone of G2505.⁹ Given the indispensability of the desosamine group to binding, most efforts at optimization of macrolides have been on the macrolactone moiety of macrolides. These have resulted in clinically useful synthetic macrolides with improved pharmacokinetic profiles (CLM, AZM, Roxithromycin and Dirithromycin), broader spectrum ketolides showing enhanced potency against some macrolide-resistant bacteria (Telithromycin) and other more potent macrolides in preclinical investigations.¹⁰⁻¹⁷

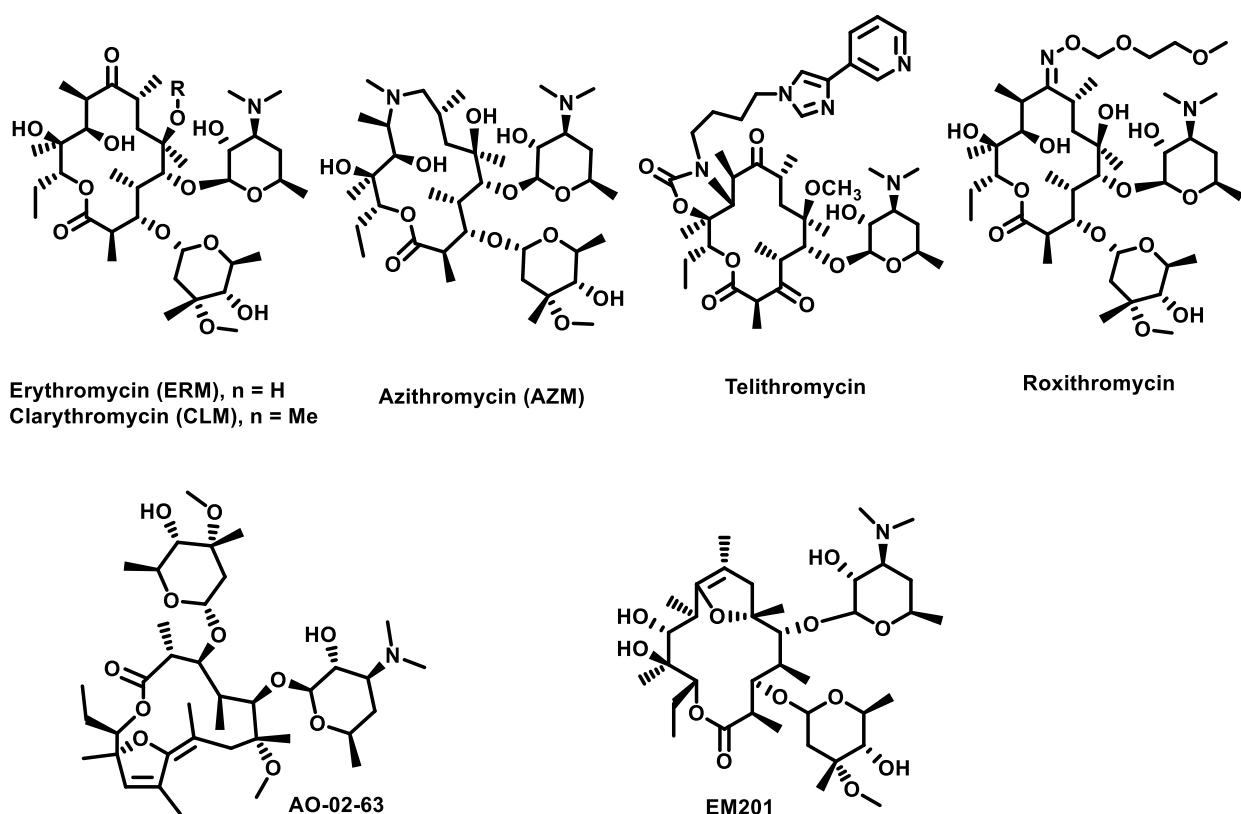


Figure 4.1. Structures of representative clinically useful macrolide antibiotics, new macrolide (AO-02-63) and EM201.

CLM was inspired by the need to improve the acid stability of ERM. Under mild acid conditions, ERM undergoes degradation reactions due to the reactivity of its C-6 and C-12 hydroxyl groups.

One of the well-characterized products of CLM acid instability is EM201, a dihydrofuran compound that results from a dehydrative-condensation reaction between its C-6 hydroxyl and the C-9 keto groups.^{18, 19} Despite the fact that the desosamine moiety is unaffected, EM201 is devoid of antibacterial activity.¹⁸ Methylation of the C-6 hydroxyl precluded EM201 formation from ERM and also attenuated the reactivity of C-12 hydroxyl group, as the resulting CLM is significantly more acid stable. It is not clear why the C-12 hydroxyl group of CLM is not as reactive under the conditions that caused ERM degradation. However, it is known that several functional groups on macrolides display unique reactivity, largely due to the steric effect of their macrolactone moiety. We have discovered that CLM undergoes dehydrative cyclization, mediated by its C-12 hydroxyl group, when treated with isoniazid under mildly acidic condition, leading to a dihydrofuranyl compound AO-02-63 (Fig. 4.1). We found that, unlike EM201, AO-02-63 retained the prokaryotic translation inhibition activity of ERM/CLM. Interestingly, AO-02-63 inhibits eukaryotic ribosome translation with micromolar IC_{50} (28 μ M) while CLM lacks eukaryotic translation inhibitory activities at concentrations $>250 \mu$ M. More importantly, AO-02-63 inhibits the proliferation of all cell lines in the NCI-60 panel with low micromolar IC_{50} . CLM also has anti-inflammatory anti-fibrosis effects.^{20,21, 22} We observed that the anti-inflammatory effect AO-02-63 is enhanced 10-fold relative to CLM. Collectively, this data suggests that AO-02-63 is a promising anti-cancer, anti-inflammatory agent that may partly derive its bioactivity from the inhibition of eukaryotic ribosome translation.

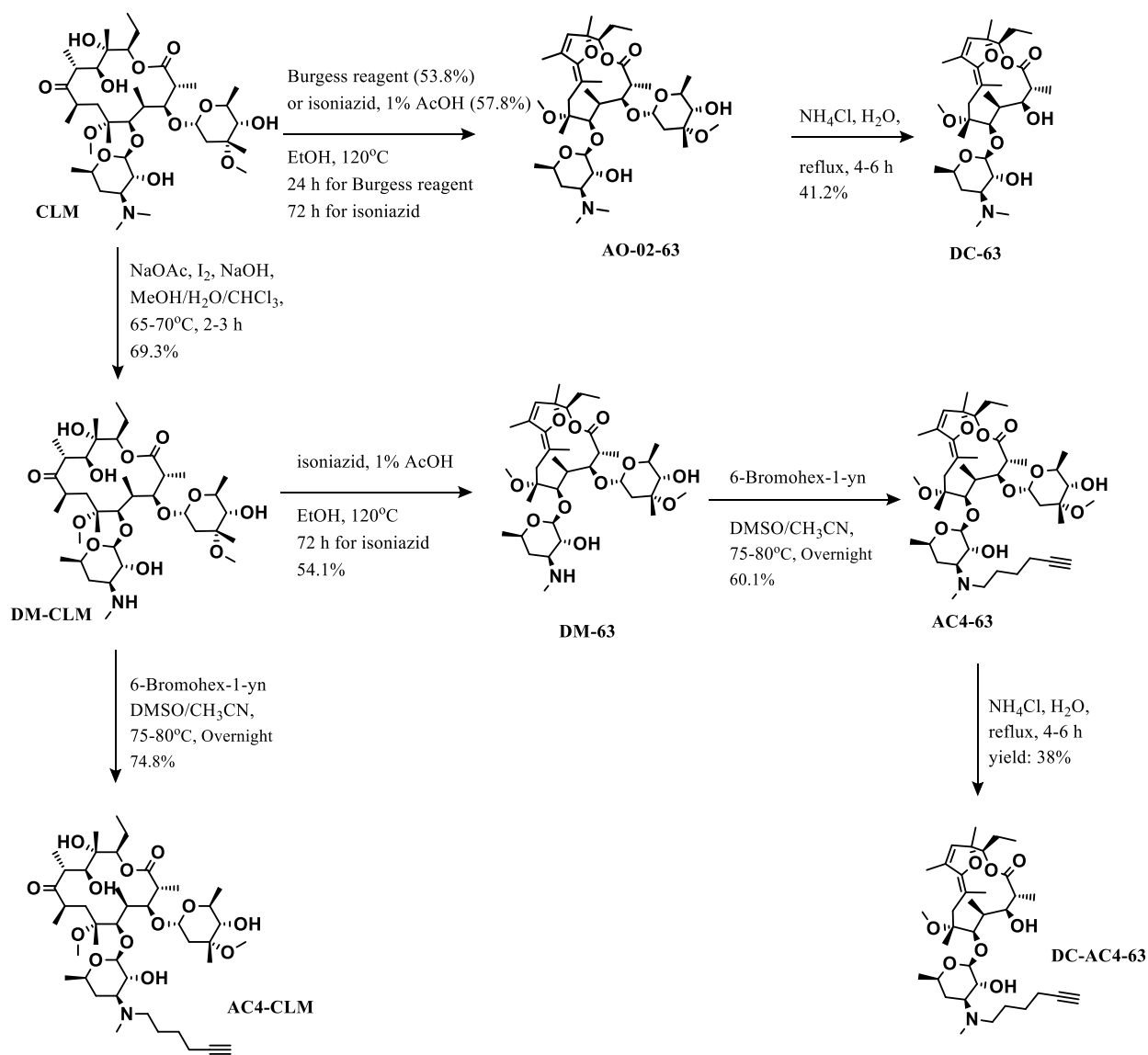
4.2 Result and Discussion:

4.2.1 Chemistry

EM201 is easily formed from ERM exposure to glacial acetic acid under ambient conditions.²³ However, we found that CLM is recalcitrant to ethanolic acetic acid even under refluxing condition for an extended period. We exposed CLM to basic conditions – ethanolic solution of pyridine or ethanolic solution of isonicotinic acid hydrazide (isoniazid) – and found it to be stable to these reagents. As a result, none of these conditions could convert CLM into new compounds. However, interestingly, we found that co-treatment of isoniazid and acetic acid in DMF or ethanol at 100-120°C for 72 h resulted in a new UV active product (Scheme 1) which was isolated by column chromatography. The structure of the new product was determined, by selective cladinose hydrolysis reaction to furnish DC-63 (scheme 4.1), ¹H- and ¹³C-NMR, and high-resolution mass spectrometry, to be that of dihydrofuranyl compound AO-02-63 (Scheme 4.1). We also found that N-desmethyl CLM (DM-CLM) could be similarly converted to the desmethyl analog of AO-02-63 (DM-63). Subsequently, the identity of AO-02-63 was confirmed using single crystal X-ray diffraction analysis (Figure 4.2). Evidently, CLM undergoes tandem dehydration- cyclization- dehydration reactions similar to those proposed in Figure 4.3 to furnish AO-02-63. The first dehydration reaction will be facilitated by base deprotonation of the alpha proton at C10 which result in the acid catalyzed loss of the C-11 hydroxyl group as water. The nucleophilic attack of the C-12 hydroxyl at C-9 keto group should result in a hemiketal that undergoes the second dehydration, leading to AO-02-63.

If the mechanism we proposed in Figure 4.3 holds, we postulated that CLM should similarly react with reagents that promote dehydration of secondary alcohols. We observed that Burgess reagent, a strong dehydration reagent; more facilely facilitate the conversion of CLM to AO-02-63 in similar yield with a shorter time.

Subsequently, we synthesized alkyne analog of AO-02-63 (AC4-63) and the corresponding CLM analog (AC4-CLM) for pulldown experiment in our subsequent target validation studies (described later).



Scheme 4.1. Synthesis of AO-02-63 and its analogs.

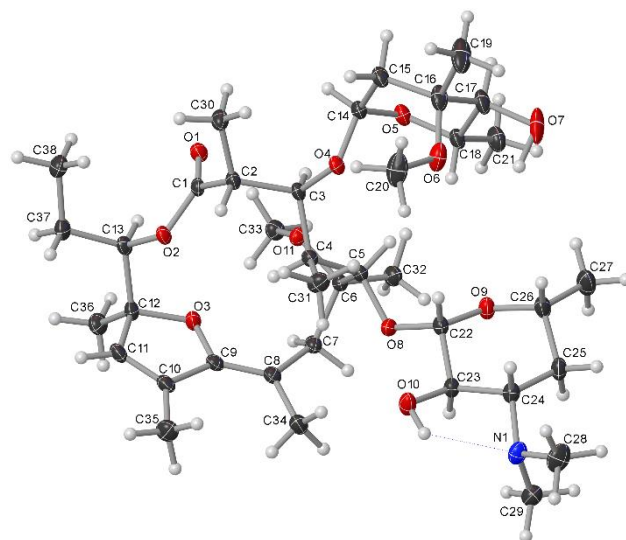


Figure 4.2. X-ray structure of the AO-02-63

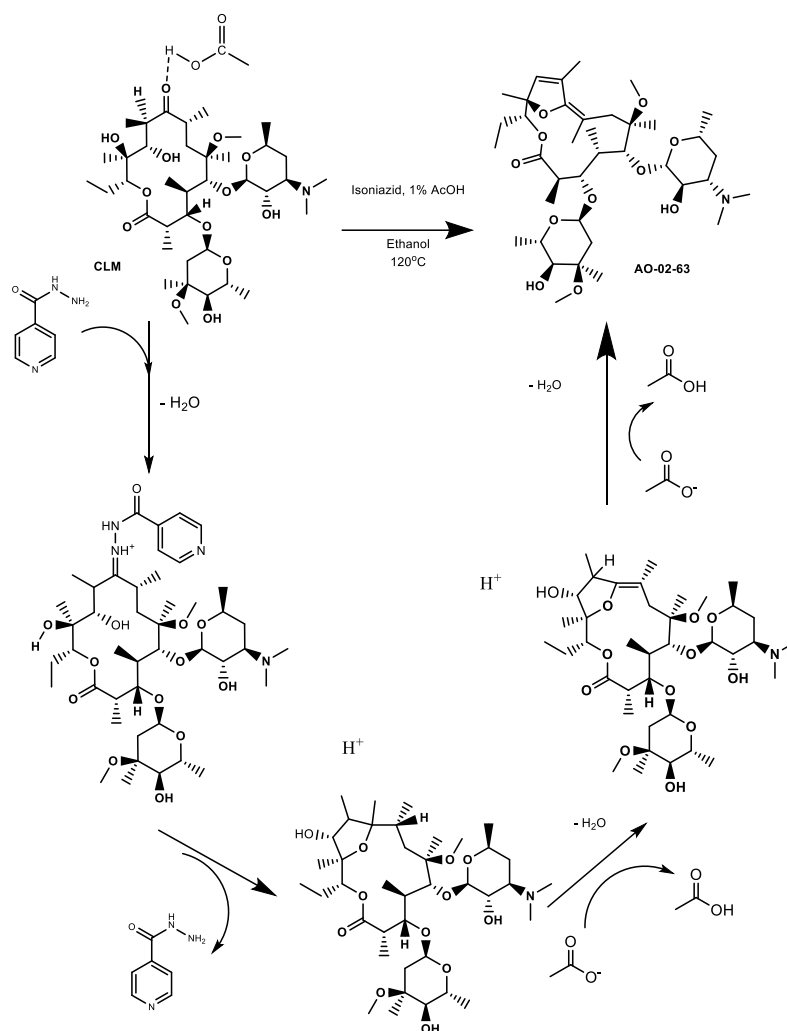
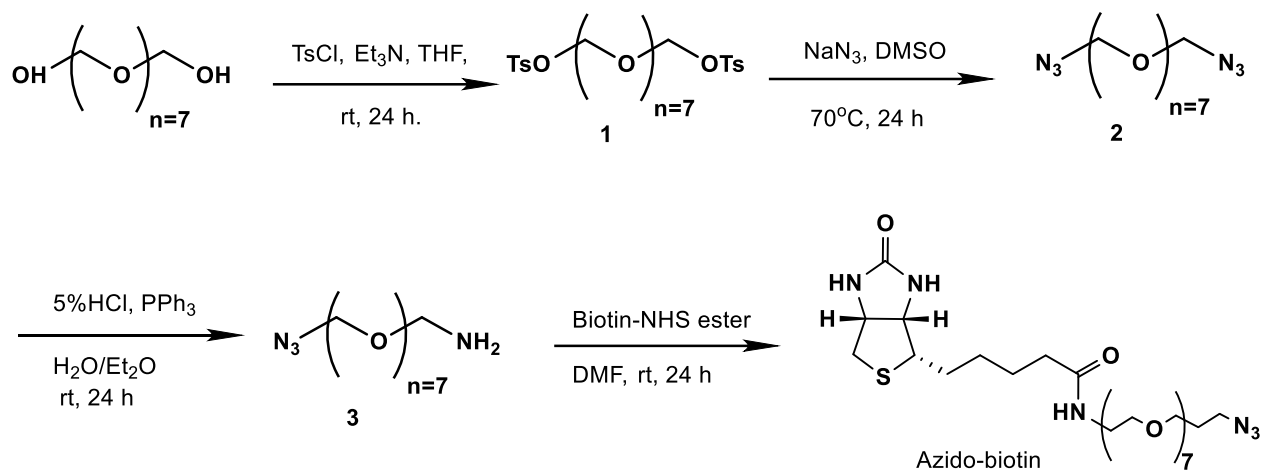
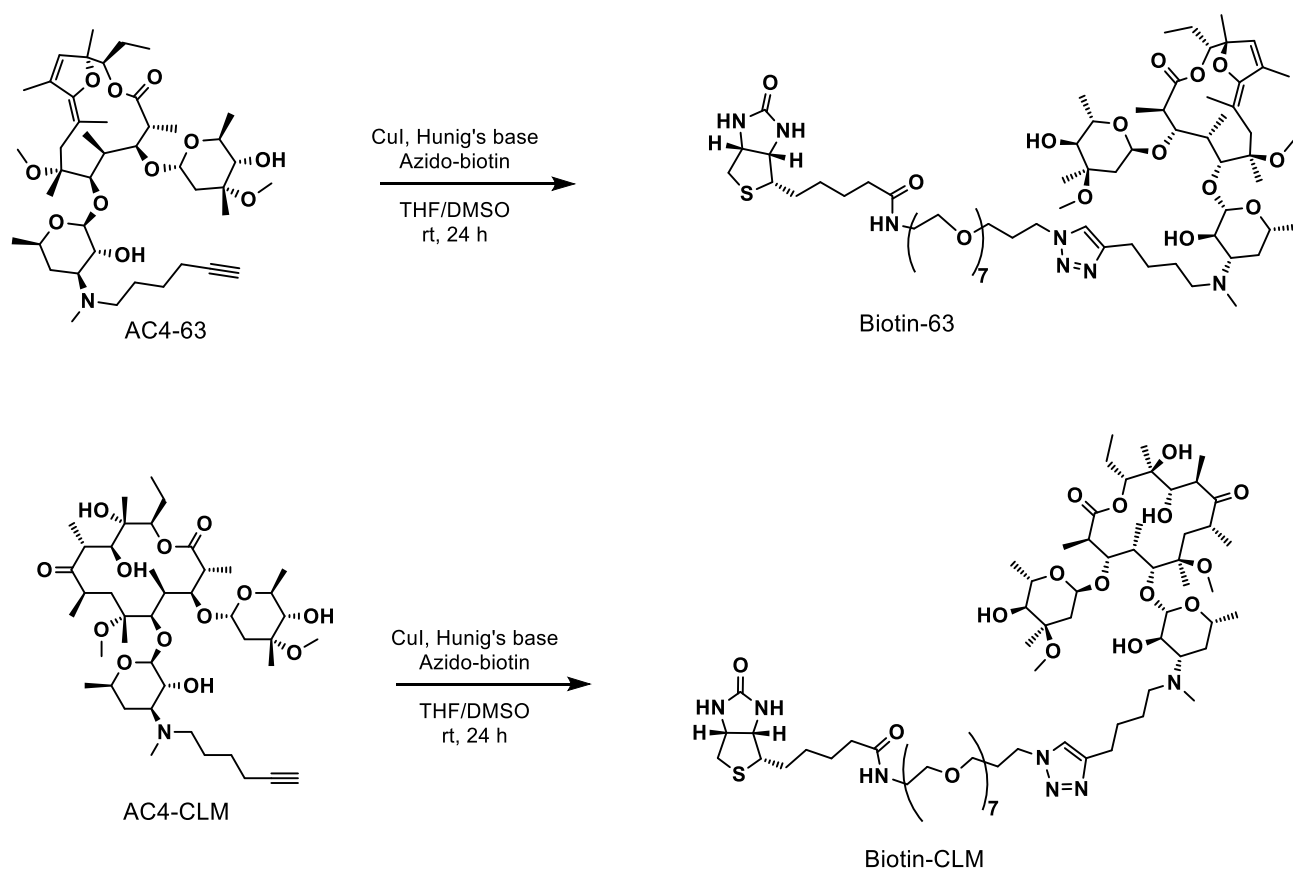


Figure 4.3. Proposed mechanism of the conversion of CLM to AO-02-63 by Isoniazid with 1V/V% Acetic acid.

For the pulldown experiments, we synthesized a Pegylated-azido biotin (Azido-biotin) through EDCI coupling biotin and 1-azido-PEG (n=7)-amine as described in Scheme 4.2. The Azido-biotin was clicked with AC4-63 or AC4-CLM, via Cu(I) promoted Huisgen cyclization reaction to furnish the biotinylated derivatives of AO-02-63 and CLM (Scheme 4.3) then we subsequently used for the pulldown experiments.



Scheme 4.1. Synthesis of Azido-biotin.



Scheme 4.2. Synthesis of biotinylated derivatives of AO-02-63 and CLM.

4.2.2 *Effects of AO-02-63 on the prokaryotic and eukaryotic protein translation*

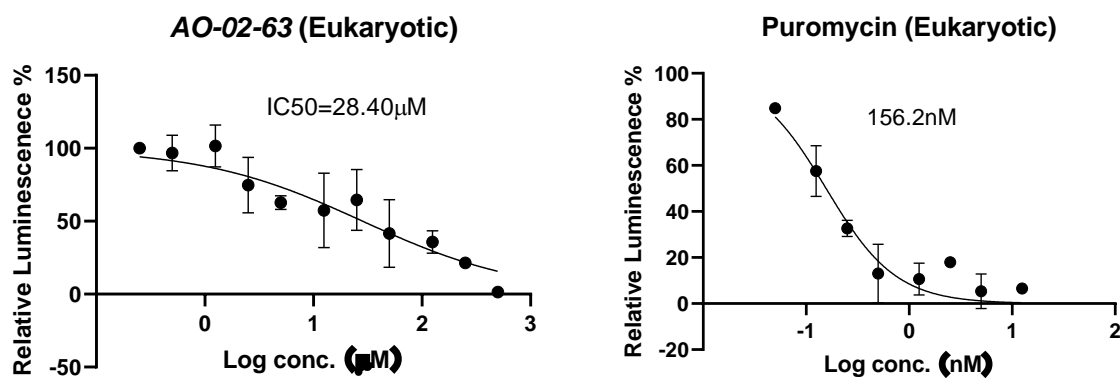
The dehydrative-condensation reaction between its C-6 hydroxyl and the C-9 keto groups of CLM, which resulted in EM201, abolished the antibacterial activity. To investigate if AO-02-63 will be befallen with a similar fate, we investigated its effects on the translation activities of prokaryotic and eukaryotic ribosomes. We used CLM and Puromycin, which inhibits the prokaryotic and eukaryotic ribosomes, as positive controls. We observed that AO-02-63 potently inhibits the prokaryotic ribosome activity with $IC_{50}=2.87\text{ }\mu\text{M}$ which is about 4-fold weaker than that of CLM ($IC_{50}=0.74\text{ }\mu\text{M}$) (Fig. 4.4). This suggests that AO-02-63, unlike EM201, could retain the antibacterial activity of the parent CLM. We confirmed that AO-02-63 has antibacterial activity against *B. subtilis*, a non-lethal bacterial strain that is susceptible to CLM as well (Fig. 4.5).

Interestingly, AO-02-63 also inhibits the eukaryotic ribosome activity with $IC_{50}=28.4\text{ }\mu\text{M}$, quite in contrast to CLM, which lacks eukaryotic translation inhibitory activities at concentrations $>500\text{ }\mu\text{M}$. The control compound Puromycin inhibits eukaryotic ribosome activity with nanomolar IC_{50} (Fig. 4.4A). This result suggests that AO-02-63 could inhibit the proliferation of transformed eukaryotic cells, akin to other eukaryotic ribosome inhibitors, including the control compound Puromycin (discussed later).

To elucidate the potential intracellular targets of AO-02-63, we used Biotin-63 and Biotin-CLM for pulldown experiments on Hep-G2 cell lysate. In brief, Hep-G2 cells were lysed using ultrasonic probe and incubated with DMSO, Biotin-63, or Biotin-CLM with or without competition with AO-

02-63 or CLM, respectively. The mixture was incubated with Avidin magnetic beads and the pulled beads were washed by TBS buffer, and eluted by the elution buffer (Thermo Scientific 21028). The eluate proteins were neutralized by NaOH and denatured by RIPA buffer (VWR 97063-270), ran through gel electrophoresis and silver stained before mass spectroscopy analysis. Silver staining revealed that the protein bands pulled-out by Biotin-63 and Biotin-CLM are similar but not identical in size (Figure S4.1). The background signals are different from the bands from the experiments with Biotin-63 and Biotin-CLM. Moreover, the competition experiments with unmodified AO-02-63 and CLM eliminated almost all bands. Collectively, these data suggest that most of the pulled proteins are unlikely due to non-selective adsorption to the Avidin beads.

A



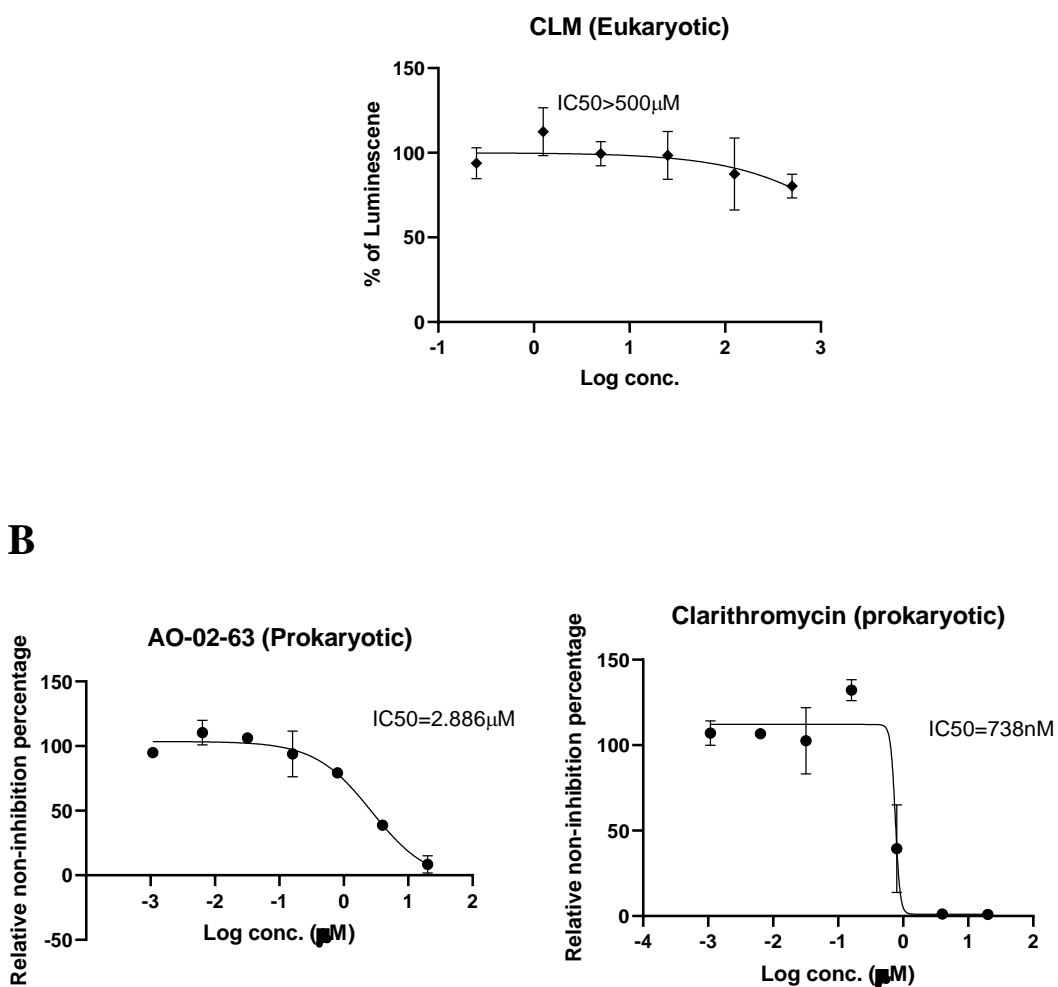


Figure 4.4. Translation inhibition of AO-02-63 and control inhibitors. (A). Eukaryotic translation inhibition of AO-02-63, Puromycin, and CLM. (B) Prokaryotic translation inhibition on CLM and AO-02-63. Inhibition was calculated through luminescence. Quantifications and % of luminescence were obtained from independent duplicate experimental data.

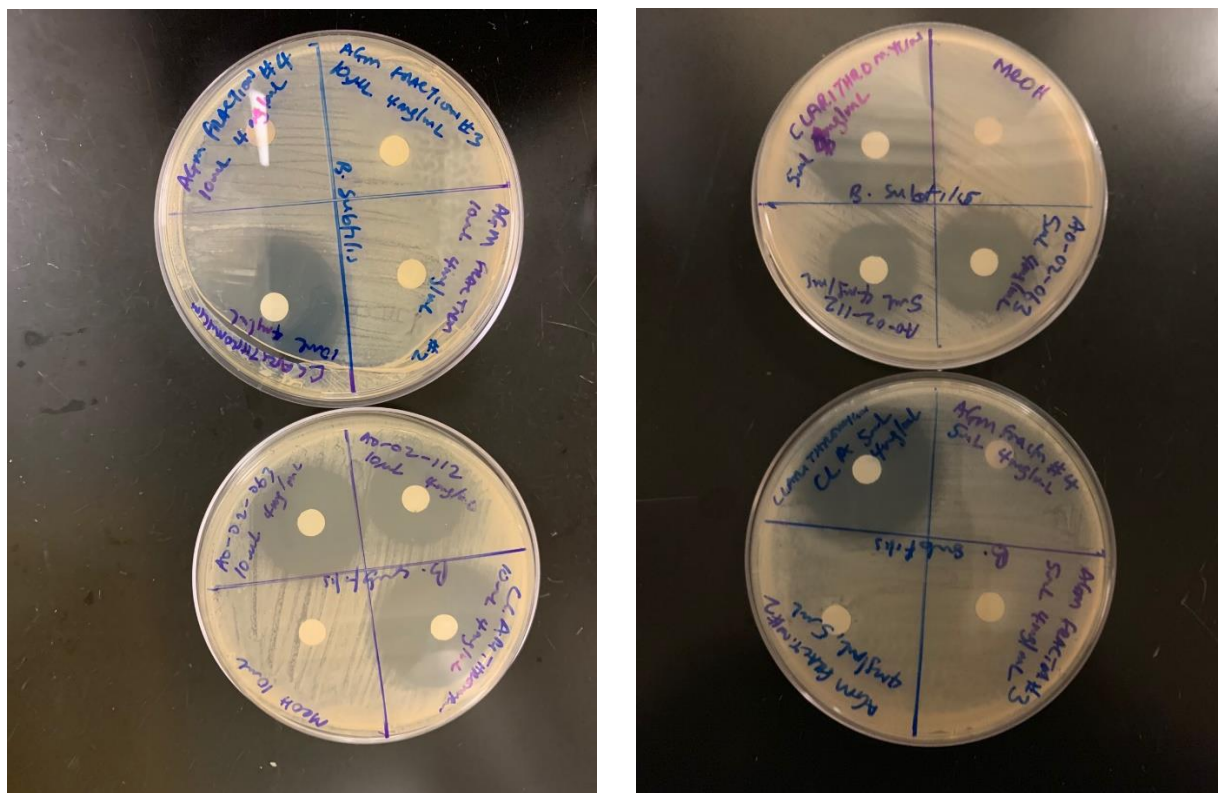


Figure 4.5. AO-02-63 inhibits the growth of *B. subtilis* in disk diffusion test (disk diffusion assay).

Subsequently, using mass spectrometry on the pulled proteins and fragmentation data analysis based on Peptide Spectral Matches (PSMs) with human protein database, we found that AO-02-63 pulled-down several eukaryotic ribosomal proteins (40s and 60s ribosomal proteins) that are unique compare to Biotin-CLM group and Biotin only group (Table 4.1). We set the lower boundary of PSM score as 20 because it would be more informative to compare proteins in higher PSM score. In Table 4.2, we listed all the of ribosomal proteins that Biotin-63 group pulled down with their PSM scores and sequence. The other major translational protein pulled down by AO-02-63 is the heterogeneous nuclear ribonucleoproteins (hnRNP), a series of RNA-binding protein which plays critical roles in RNA metabolism including RNA splicing, transcription, mRNA

stability and translation initiation.²⁴ The expression of hnRNPs are upregulated in several cancers such as A2/B1 and knockdown of hnRNPs in MDA-MB-231 cells decreases cell viability.^{25, 26} Additionally, disruption of the hnRNP U-actin complex, by a noncoding RNA H19, results in the inhibition of RNA Pol II-mediated transcription.²⁷ The inhibition of the eukaryotic ribosome activity and the possibility of the disruption of the function of hnRNPs strongly suggests that AO-02-63 could have broad anticancer activity.

Table 4.1. Major proteins pulled down by Biotin-63, Biotin-CLM, and Biotin only ranked by mass spectroscopy and human protein database analysis. Note that the unrelated pollution including keratin, actin, tubulin, myosin or cellular skeletal proteins were removed in all groups in the table. Also, the common proteins that appeared in both Biotin-63 group and Biotin-CLM group were also removed. The ranking is listed from the highest PSM score to 20.

PSM #	Biotin-63	PSM #	Biotin-CLM	PSM #	Biotin only
110	40S ribosomal protein S3	202	Alpha-1,4 glucan phosphorylase	23	Protein S100-A8
58	Trifunctional enzyme subunit beta, mitochondrial	172	MYH11 protein	22	Protein S100-A9
51	Nucleolin	131	Filamin-A		
51	Phosphoenolpyruvate carboxykinase [GTP], mitochondrial	122	Nebulin		
42	40S ribosomal protein S18	120	Tropomyosin alpha-1 chain		
39	60 kDa heat shock protein, mitochondrial	116	Creatine kinase M-type		
39	Elongation factor Tu, mitochondrial	116	Filamin C		
36	Heterogeneous nuclear ribonucleoproteins C1/C2	110	Glyceraldehyde-3-phosphate dehydrogenase		
35	Aldehyde dehydrogenase X, mitochondrial	107	Sarcoplasmic/endoplasmic reticulum calcium ATPase 1		
35	40S ribosomal protein S19	94	Tropomyosin 1 (Alpha), isoform CRA_f		
29	40S ribosomal protein S3a	91	Beta-enolase		
28	60S ribosomal protein L23a	84	Desmin		
28	40S ribosomal protein S25	83	Fructose-bisphosphate aldolase		
25	T-complex protein 1 subunit eta	77	Tropomyosin beta chain		

Table 4.1 continued

25	40S ribosomal protein S4	69	MYBPC1 protein		
24	Heterogeneous nuclear ribonucleoprotein U	69	Nebulin		
24	60S ribosomal protein L7a	69	Pyruvate kinase PKM		
23	Galectin-3-binding protein	62	ATP-dependent 6-phosphofructokinase		
23	40S ribosomal protein S10	56	Tropomyosin alpha-3 chain		
23	60S ribosomal protein L13	55	Alpha-enolase		
22	60S ribosomal protein L36	55	Fructose-bisphosphate aldolase A		
		54	Troponin T3, fast skeletal type		
		53	Pyruvate kinase		
		51	Glycogen phosphorylase, brain form		
		50	Glucose-6-phosphate isomerase		
		50	Serum albumin		
		48	Phosphoglucomutase-1		
		47	Heat shock cognate 71 kDa protein		
		42	Phosphoglycerate kinase 1		
		42	Calcium-transporting ATPase		
		39	POTE ankyrin domain family member I		
		38	Transgelin		
		36	Myoglobin		
		32	Calsequestrin		
		32	Calponin-1		
		32	Alpha-crystallin B chain		
		32	Troponin I2, fast skeletal type		
		32	L-lactate dehydrogenase A chain		
		31	Carbonic anhydrase 3		
		30	Gamma-enolase		
		29	Triosephosphate isomerase 1		
		28	Malate dehydrogenase, mitochondrial		
		28	Heat shock 70 kDa protein 1B		

Table 4.1 Continued

		27	Talin-1		
		27	Myomesin-1		
		27	Phosphoglycerate mutase		
		26	Vimentin		
		26	Hemoglobin subunit beta		
		24	Plectin		
		24	Heat shock protein beta-1		
		23	Creatine kinase S-type, mitochondrial		
		23	Hemoglobin subunit alpha		
		22	Cysteine and glycine-rich protein 1		
		21	Aconitate hydratase, mitochondrial		
		21	Creatine kinase B-type		
		21	14-3-3 protein zeta/delta		
		20	14-3-3 protein epsilon		
		20	Glyceraldehyde-3- phosphate dehydrogenase, testis-specific		

Table 4. 2 All ribosomal proteins pulled down by Biotin-63 based on mass spectroscopy and human protein database analysis. The first ranking is 40s ribosomal proteins, the second ranking is 60s ribosomal proteins, and the third ranking is hnRNPs.

PSM #	Biotin-63	Protein Accession code	Peptide sequence hit
40s Ribosomal proteins			
110	40S ribosomal protein S3	Q3T169	ELAEDGYSGVEVR
42	40S ribosomal protein S18	Q3T0R1	AGELTEDEVER
35	40S ribosomal protein S19	P39019	ALAAFLK
29	40S ribosomal protein S3a	P61247	NCLTNFHGMDLTR
28	40S ribosomal protein S25	P62851	LNNLVLFDK
25	40S ribosomal protein S4	F1MJH2	VNDTIQIDLETGK
23	40S ribosomal protein S10	F6U211	DYLHLPPEIVPATLR
20	40S ribosomal protein S13	Q56JX8	GLTPSQIGVILR
17	40S ribosomal protein S8	Q5E958	LTPEEEEILNK
17	40S ribosomal protein S11	P62280	ILSGVVTK
15	40S ribosomal protein S5	Q5E988	WSTDDVQINDISLQDYIAVK
13	40S ribosomal protein S6	E1BG13	DIPGLTDTTVPR
12	40S ribosomal protein S24	E7ETK0	TPPDVIFVFGFR
11	40S ribosomal protein S7	P62081	VETFSGVYK

Table 4.2 continued

10	Ubiquitin-40S ribosomal protein S27a	P62979	ECPSDECGAGVFMASHFDR
9	40S ribosomal protein S20	Q3ZBH8	VCADLIR
9	40S ribosomal protein S27	H0YMV8	LVQSPNSYFMDVK
8	40S ribosomal protein S16	Q3T0X6	GPLQSVQVFGR
8	40S ribosomal protein S30	A0A3Q1LRQ8	IIAVSFPSTANEENFR
5	40S ribosomal protein S9	B5MCT8	LFEGNALLR
5	40S ribosomal protein S29	A0A087WTT6	YGLNMCRC
4	40S ribosomal protein S15	K7EM56	EAPPMKPEVVK
2	40S ribosomal protein S26	F1MB60	NIVEAAAVR
60s Ribosomal proteins			
28	60S ribosomal protein L23a	J3KTJ3	ECADLWPR
24	60S ribosomal protein L7a	Q2TBQ5	AGVNTVTTLVENK
23	60S ribosomal protein L13	F1MK30	VATWFNQPAR
22	60S ribosomal protein L36	J3QSB5	YPMVAVGLNK
19	60S ribosomal protein L3	P39872	HGSLGFLPR
18	60S ribosomal protein L24	C9JXB8	VELCSFSGYK
18	60S ribosomal protein L27	P61353	VYNYNHLMPTR
18	60S ribosomal protein L27a	E1BE42	TGAAPIIDVVR
17	60S ribosomal protein L6	Q58DQ3	VLATVTKPVGGDK
12	60S ribosomal protein L18a	M0R117	DLTTAGAVTQCYR
11	60S ribosomal protein L4	P36578	QPYAVSELAGHQTSAESWGTGR
11	60S ribosomal protein L13a	P40429	YQAVTATLEEK
11	60S ribosomal protein L12	P30050	IGPLGLSPK
11	60S ribosomal protein L26	P61257	HFNAPSHIR
10	60S ribosomal protein L11	P62913	YDGIILPGK
9	60S ribosomal protein L23	P62829	NLYIISVK
8	60S ribosomal protein L14	E7EPB3	LVAIVDVIDQNR
7	60S ribosomal protein L28	H0YMF4	NCSSFLIK
7	60S ribosomal protein L19	P84098	LLADQAEAR
6	60S ribosomal protein L9	P32969	KFLDGIYVSEK
6	60S ribosomal protein L35a	P18077	DETEFYLGK
6	60S ribosomal protein L7	P18124	IALTDNALIAR
6	60S ribosomal protein L21	P46778	KGDIVDIK
5	60S ribosomal protein L29	P47914	LAYIAHPK
5	60S ribosomal protein L34	P49207	IVYLYTK
5	60S ribosomal protein L36a	Q3SZ59	HFELGGDK
4	60S ribosomal protein L10	F8W7C6	GAFGKPQGTVAR
4	60S ribosomal protein L32	F8W727	GQILMPNIGYGSNK
4	60S ribosomal protein L30	Q3T0D5	VCTLAIDPGDSDIIR
4	60S ribosomal protein L37a	Q3MIC0	TVAGGAWTYNTTSAVTVK
3	60S ribosomal protein L35	Q56JY1	DETEFYLGK
2	60S ribosomal protein L38	J3QL01	YLYTLVITDK
Heterogeneous nuclear ribonucleoproteins			
36	Heterogeneous nuclear ribonucleoproteins C1/C2	G3V4M8	SDVEAIFSK
24	Heterogeneous nuclear ribonucleoprotein U	Q00839	FIEIAAR
19	Heterogeneous nuclear ribonucleoprotein A0	F6RSR1	LFVGGGLK
15	Heterogeneous nuclear ribonucleoproteins A2/B1	P22626	LFVGGIK
1	Heterogeneous nuclear ribonucleoproteins K	Q3T0D0	IITITGTQDQIQNAQYLLQNSVK
1	Heterogeneous nuclear ribonucleoproteins M	P52272	AAGVEAAAEEVAATEIK

4.2.3 *Anti-cancer effects of AO-02-63*

Encouraged by the eukaryotic ribosome inhibition and the possibility of the disruption of the function of hnRNPs by AO-02-63, we tested its effects and those of its analogs on the growth of selected cancer cell lines: breast (MCF-7 and MDA-MB-231), lung (A549), and liver (Hep-G2). cancer cell lines. Healthy monkey kidney epithelial cell line (VERO) was used as a control. Excitingly, we observed that AO-02-63 and its desmethyl analog (DM-63) potently inhibit the proliferation of all the cell lines tested. Further alteration to AO-02-63, including alkylation on the desosamine sugar (AC4-63) and cladinose sugar removal (DC-63 and DC-AC4-63), severely attenuated cell cytotoxicity (Table 4.2). As expected, CLM is minimally toxic to all tested cell lines.

To obtain further information about the broadness of the cytotoxic activity of AO-02-63, we screened it in the NCI-60 panel. In a 5-dose IC_{50} study, we observed that AO-02-63 inhibits the proliferation of all cell lines in the NCI-60 panel with low micromolar IC_{50} (Fig. 4.5). The broad anti-cancer activity of AO-02-63 could be due to its inhibition of protein synthesis and mRNA processing, two processes that are vital for the survival of cells.

Table 4. 3. Cell growth inhibitory activity (IC₅₀ in μ M) of AO-02-63 in selected cancer and healthy cell lines. NI: No inhibition up to 500 μ M. NT: not tested.

	Hep-G2	A549	MDA-MB-231	MCF-7	VERO
	(μ M)	(μ M)	(μ M)	(μ M)	(μ M)
AO-02-63	3.93 \pm 0.08	7.64 \pm 0.26	4.29 \pm 0.22	6.83 \pm 0.86	4.03 \pm 0.73
DM-63	3.25 \pm 0.75	5.75 \pm 0.96	4.28 \pm 0.72	4.24 \pm 0.35	4.74 \pm 1.01
DC-63	47.59 \pm 2.43	55.68 \pm 0.38	57.58 \pm 6.08	70.42 \pm 5.18	47.79 \pm 3.04
AC4-63	11.64 \pm 1.54	27.11 \pm 8.09	13.39 \pm 1.17	13.25 \pm 0.5	16.26 \pm 3.36
DC-AC4-63	64.10 \pm 9.61	56.77 \pm 7.76	NT	93.58 \pm 3.73	38.3 \pm 5.2
CLM	130.5 \pm 0.56	NI	150.7 \pm 0.51	177.50 \pm 5.4	NI

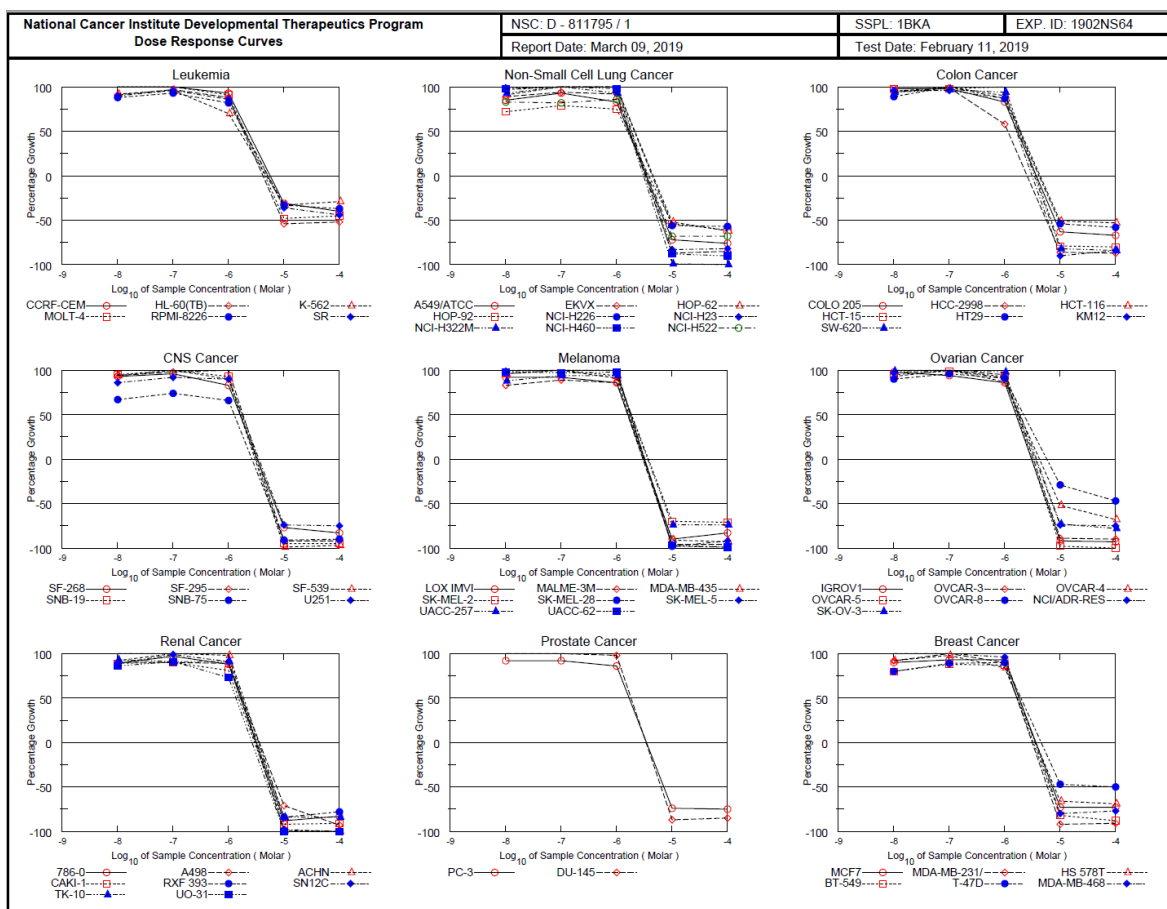
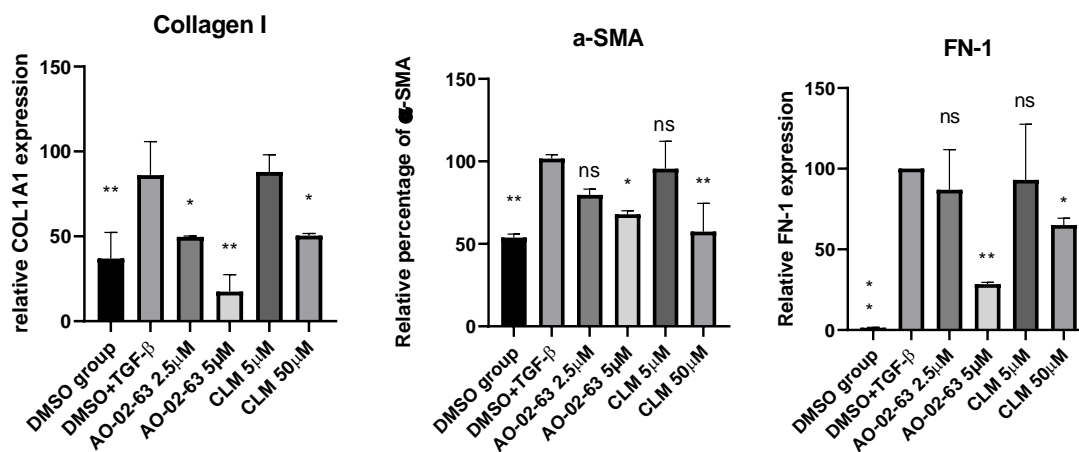
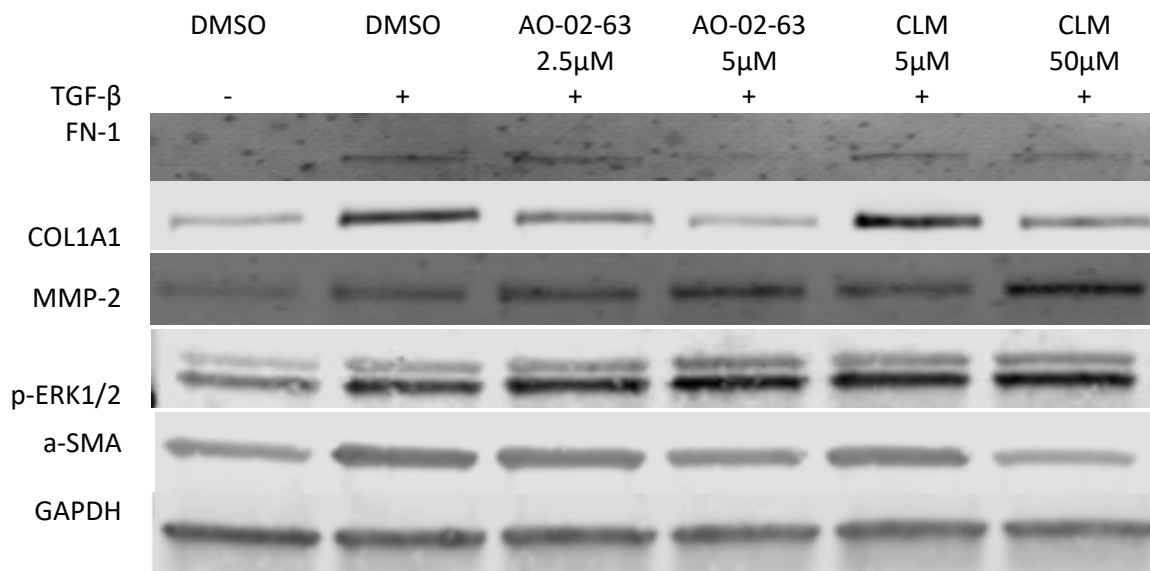


Figure 4. 6. Cell growth inhibitory activity (GI_{50} in μM) of AO-02-63 in NCI-60 panel. (a). Graphs of GI_{50} Data presented for the 5-dose GI_{50} study. (b). The detail growth inhibition curves of each cell type were presented.

4.2.4 Anti-inflammation effect of AO-02-63

A non-antibiotic property of CLM is its attenuation of ECM production and inflammation. To investigate if AO-02-63 retains the anti-inflammatory effects of CLM, we probed its effects on several markers of inflammation in TGF- β stimulated fibroblast cell line MRC-5 and lung cancer cell A549. We noticed that CLM significantly downregulates the fibronectin 1 (FN-1), collagen 1 (COL1A1) and alpha smooth muscle actin (α -SMA) at 50 μM . Interestingly, AO-02-63 induced a

similar effect at 5 μ M (Fig. 4.7), suggesting that AO-02-63 could be about 10-fold more potent than CLM. We also found that both CLM and AO-02-63 upregulated the expression of MMP-2 in dose-dependent manner. CLM has been shown to induce a similar effect in a previous study.²⁸ Both compounds have no significant effect on p-ERK1/2 levels (Fig. 4.7). This data is in agreement with the previous observation on CLM.²⁹ Collectively, this data indicates that AO-02-63 acts similarly as CLM, although 10-fold more potent, to attenuate inflammation and could suggest that they share the same or common mechanisms of action



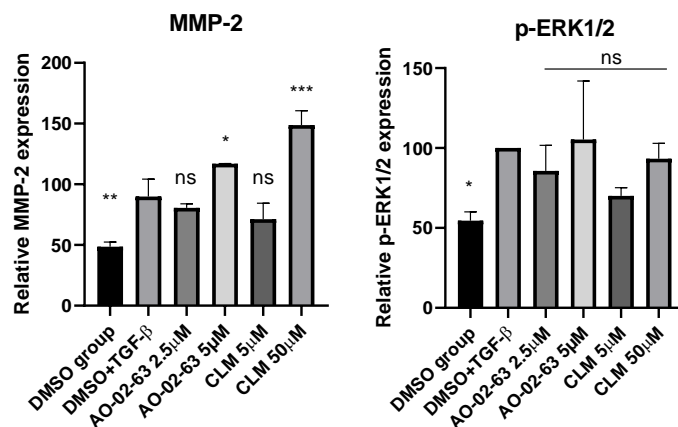


Figure 4.7. Anti-inflammation effect of AO-02-63 based on inhibition of ECM components production. MRC-5 cells were starved for 24 h before treatment of 0.1% DMSO, solutions of CLM and AO-02-63 in DMSO. TGF- β cytokine was added after 5 mins incubation. (a) Cropped gels indicating the levels of target proteins. (b) Quantification of target proteins expression. (Bars show mean plus standard deviation; statistic was performed via Ordinary One-way ANOVA compare with control group, * $P < 0.0332$; ** $P < 0.0021$; *** $P < 0.0002$; **** $P < 0.0001$).

A less explored mechanism of anti-inflammatory activity of CLM is its upregulation of HDAC 2 activity, which has been suggested to overcome the inflammation-induced NF- κ B activation.^{30, 31} Additionally, HDAC2 upregulation suppresses the expression of inflammatory genes.³¹⁻³³ We used immunoblotting on A549 cell lysates to investigate the effects of AO-02-63 and CLM on the levels of Ac-H4, a marker of the intracellular activity of class I HDAC such as HDAC 2. We used the levels of acetylated α -tubulin (Ac- α -tubulin), a marker of class IIb HDAC activity, to obtain an indication of selectivity. We observed that the HDAC6-regulated α -tubulin was not affected by the treatment of cells with AO-02-63 or CLM. However, the level of Ac-H4 was attenuated when cells were treated with low concentrations of AO-02-63 (7.5 μ M) and CLM (75 μ M). This data implies that AO-02-63 and CLM upregulate HDAC 2 activity, resulting in hypoacetylated H4. Surprisingly however, we noticed an upregulation of Ac-H4 levels when the cells were treated with higher concentrations of AO-02-63 (15 μ M) and CLM (150 μ M). The reason for the

compensatory effect of higher drug concentrations is not clear to us. It is important to emphasize that even at these higher concentrations, the level of Ac-H4 is significantly lower (>70%) relative to the DMSO control (Fig. 4.8).

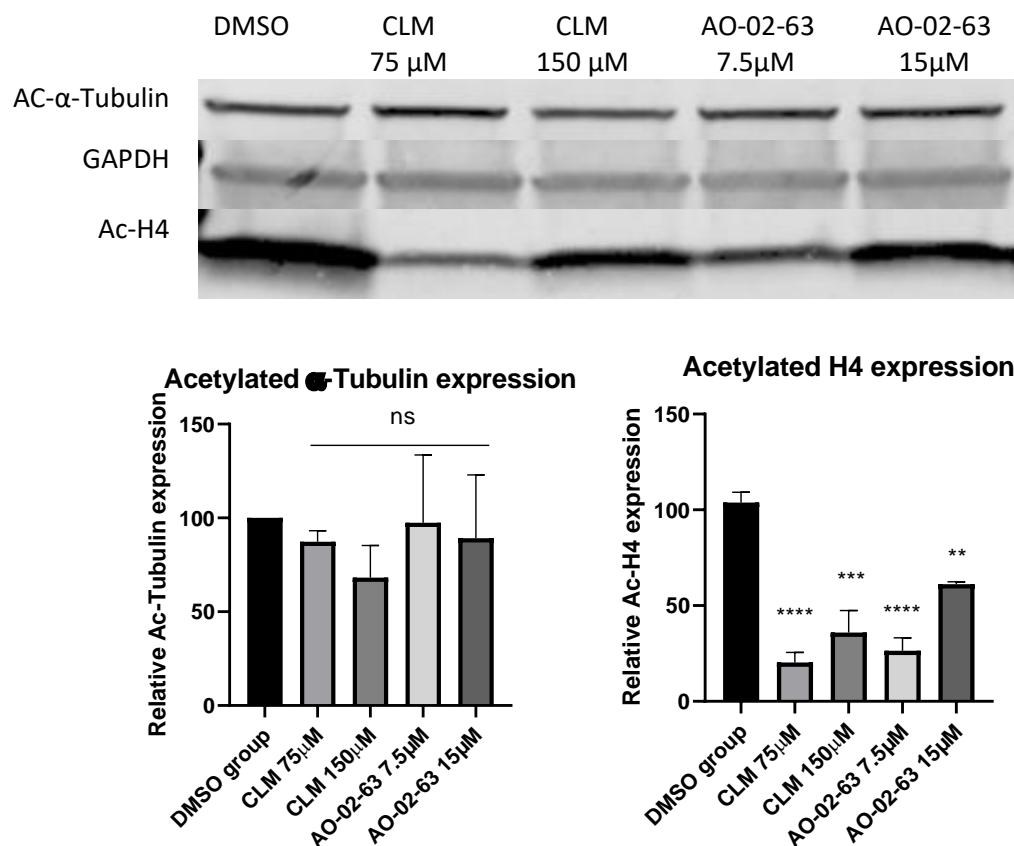


Figure 4. 8. Effects of AO-02-63 and CLM on intracellular HDAC2 activity. A549 cells were treated with 0.1% DMSO, DMSO solutions of AO-02-63 (7.5 and 15 μM) and CLM (75 and 150 μM). (a) Cropped gels indicating the levels of target proteins. (b) Quantification of target proteins expression. (Bars show mean plus standard deviation; statistic was performed via Ordinary One-way ANOVA compare with control group, * $P < 0.0332$; ** $P < 0.0021$; *** $P < 0.0002$; **** $P < 0.0001$).

4.3 Conclusion:

We have discovered that CLM undergoes tandem dehydration- cyclization-dehydration reactions, involving C-11 and C-12 hydroxyl groups and the C-9 keto moiety, to furnish a dihydrofuranyl

compound AO-02-63. The structure of AO-02-63 was confirmed by mass spectroscopy, NMR, and X-ray crystallography. This novel macrolide inhibits the activities of prokaryotic and eukaryotic ribosomes and possibly disrupts the activity of hnRNPs. These attributes may significantly contribute to the broad cytotoxic effects of AO-02-63 against cancer cell lines in the NCI-60 panel. Furthermore, AO-02-63 elicits anti-inflammatory activity like CLM, with 10-fold enhancement. This work unveils yet another layer of the rich biological activities of macrolide antibiotics. The potential of AO-02-63 as anti-cancer and an anti-inflammation agent and its mechanism(s) of action merits additional studies in the future.

4.4 Material and Methods

4.4.1 Synthesis:

AO-02-63: Clarithromycin (1.00g, 1.34mmol) mixed with isonicotinic acid hydrazide (550mg, 3.64mmol) and dissolved in 15 mL ethanol in a 50 mL pressure tube. The mixture was stirred and heated up to 120°C with Argon protection. Subsequently, 1V/V% acetic acid (0.45 mL) were added drop-wisely. The milky solution turned into clear followed by capping. The reaction processed for 72 h and the solution turned into yellowish. The reaction was terminated by cooling down and partitioned with sat. NaHCO₃ (50 mL) and DCM (50 mL). The DCM layer is separated and collected. Then, the DCM (50 mL x2) were added to extract the crude product from the aqueous layer and combined. NaSO₄ was added to the organic extraction followed by the vacuum evaporation. A yellow foam of crude product was gained and furnished by column chromatography with gradient solvent system: ethyl acetate: hexane: TEA=10:2:0.5 to 10:1:1. The pure product gained in white foam (550mg, 0.77mmol), with yield of 57.80%.

Alternatively, Clarithromycin (250mg, 0.34mol) mixed with Burgess reagent (160mg, 0.67mmol) and dissolve in 8 mL ethanol in a pressure tube. The mixture stirred and heated up to 120°C. Argon was purged and 1V/V% acetic acid (0.1 mL, 1.7mmol) were added. The milky solution turned into clear followed by capping. The reaction processed for 24 h and the solution turned into yellowish. The reaction was terminated by cooling down and partitioned with sat. NaHCO₃ (50 mL) and DCM (50 mL). The DCM layer is separated and collected. Then, the DCM (50 mLx2) were added to extract the crude product from the aqueous layer and combined. NaSO₄ was added to the organic extraction followed by the vacuum evaporation. A yellow foam of crude product was furnished by column chromatography with gradient solvent system: ethyl acetate: hexane: TEA=10:2:0.5 to 10:1:1. The pure product gained in white foam (130mg, 0.183mmol), with yield of 53.82%.

¹H NMR (400 MHz, cdcl₃) δ 5.69 (s, 1H), 5.01 (dd, *J* = 10.6, 2.9 Hz, 1H), 4.85 (d, *J* = 4.6 Hz, 1H), 4.39 (d, *J* = 7.2 Hz, 1H), 4.11 (d, *J* = 10.0 Hz, 1H), 3.98 (dd, *J* = 9.4, 6.2 Hz, 1H), 3.47 (d, *J* = 8.7 Hz, 1H), 3.29 (s, 3H), 3.15 (s, 3H), 3.05 – 2.95 (m, 2H), 2.79 – 2.53 (m, 1H), 2.55 – 2.42 (m, 1H), 2.37 – 2.23 (m, 8H), 2.06 (s, 5H), 1.64 (s, 4H), 1.54 – 1.47 (m, 1H), 1.44 – 1.36 (m, 1H), 1.32 (s, 3H), 1.30 – 1.26 (m, 6H), 1.22 (t, *J* = 3.0 Hz, 6H), 1.12 (d, *J* = 7.1 Hz, 3H), 0.99 (d, *J* = 7.5 Hz, 3H), 0.88 (t, *J* = 7.4 Hz, 3H). ¹³C NMR (101 MHz, cdcl₃) δ 175.6 154.3, 135.6, 129.8, 103.8, 96.0, 87.7, 84.3, 81.3, 80.5, 78.1, 72.5, 71.2, 68.8, 65.4, 65.0, 49.4, 47.4, 45.5, 40.5, 39.2, 36.9, 34.9, 29.0, 25.8, 24.6, 24.1, 21.6, 21.4, 19.5, 18.4, 16.7, 15.7, 10.6, 9.0. HRMS (ESI) Calcd for C₃₈H₆₆O₁₁N [M⁺H⁺] 712.4630, found 712.4624.

DC-63: AO-02-63 (100mg, 0.148mmol) added into a NH₄Cl aqueous solution (10 mL) with pH=5. The solution was stirred with reflux for 4-6 h and all solids dissolved into the aqueous solution.

By check the TLC plate, we confirmed the de-cladinose reaction is complete. The crude product was extracted by DCM (30 mL) with sat. NaHCO_3 (20 mL). The organic layer were washed one more time with brine (10 mL) and followed by drying with NaSO_4 . The organic extraction was evaporated and purified through column chromatography with solvent system: DCM: MeOH=15:1. The product is white solid (33.6mg, 0.061mmol, 41.2%). ^1H NMR (400 MHz, cdCl_3) δ 5.80 (d, J = 1.7 Hz, 1H), 5.10 (dd, J = 11.3, 2.4 Hz, 1H), 4.42 (d, J = 7.6 Hz, 1H), 3.99 – 3.81 (m, 1H), 3.68 (d, J = 2.2 Hz, 1H), 3.54 (ddd, J = 10.9, 6.2, 2.0 Hz, 1H), 3.29 – 3.19 (m, 1H), 3.16 (s, 3H), 2.77 (d, J = 14.2 Hz, 1H), 2.50 (ddt, J = 13.6, 10.9, 5.4 Hz, 2H), 2.25 (s, 6H), 2.03 (d, J = 1.5 Hz, 3H), 1.97 (d, J = 14.2 Hz, 1H), 1.90 (d, J = 1.1 Hz, 3H), 1.81 (td, J = 7.4, 6.9, 1.6 Hz, 1H), 1.75 – 1.56 (m, 2H), 1.53 – 1.45 (m, 1H), 1.42 (s, 3H), 1.33 – 1.28 (m, 2H), 1.28 – 1.23 (m, 7H), 1.20 (d, J = 6.8 Hz, 3H), 0.95 (d, J = 6.6 Hz, 1H), 0.93 – 0.79 (m, 11H). HRMS (ESI) Calcd for $\text{C}_{30}\text{H}_{52}\text{O}_8\text{N}$ $[\text{M}+\text{H}^+]$ 554.3687, found 554.3670.

DM-CLM: Clarithromycin (10.00g, 13.4mmol) dissolved in 150 mL methanol with 10 mL chloroform. Sodium Acetate (8.8g, 107.3mmol) were added into a mixture of methanol: water=50:10 mL in another beaker and stirred until complete dissolve. Then two solutions combined and stir in 60°C oil bath until the mixture turned clear. Then, 3 aliquots of Iodine were added with increment of 5 min. The solution turned dark red. After 10 min reaction, 30 mL of 1M NaOH were prepared, and 10 mL was injected into the solution. The solution turned less dark, and another injection of 10 mL is followed. After 30 min, the third injection of NaOH was processed and the solution turned clear. The solution continues to react in the next 1-3 h until TLC indicated the completion. Then let the solution cooled to room temperature and followed with one injection of sat. NH_4OH to quench the reaction. The solution was washed with sat. $\text{Na}_2\text{S}_2\text{O}_3$ solution (100

mL) and extracted by DCM (150 mL x2). The organic layer was washed again with water and brine, dried by NaSO₄ and vacuum evaporation. The crude product is yellow oil. To purify the product, a solution of Acetone: NH₄OH= 40:1 mL solvent system added to the oil and stirred in ice bath. The white product crushed out in 10 minutes. Then, with vacuum filtration, the white pure product DM-CLM was yield (6.8g, 9.29mmol, 69.32%).

DM-63: procedure identical to the synthesis process of *AO-02-63* on the top. DM-CLM (1.00g, 1.37mmol) mixed with isonicotinic acid hydrazide (550mg, 3.64mmol) and dissolve in 15 mL ethanol in a pressure tube. The mixture stirred and heated up to 120°C. Argon was purged and 3% acetic acid (0.45 mL) were added. The milky solution turned into clear followed by capping. The reaction processed for 72 h and the solution turned into yellowish. The reaction was terminated by cooling down and washed with sat. NaHCO₃. The DCM (100 mL x2) were added to extract the crude product and NaSO₄ was added to dry up the organic extraction. The vacuum evaporation gave us a yellow foam of crude product. To purify the compound, column chromatography was applied with gradient solvent system: ethyl acetate: TEA=10:0.5 to 10:1. The pure product gained in white foam (515mg, 0.74mmol), with yield of 54.01%. ¹H NMR (700 MHz, CDCl₃) δ 5.71 (d, *J* = 1.8 Hz, 1H), 5.02 (dd, *J* = 10.7, 2.9 Hz, 1H), 4.86 (d, *J* = 4.7 Hz, 1H), 4.42 – 4.37 (m, 1H), 4.06 (d, *J* = 10.2 Hz, 1H), 4.00 – 3.97 (m, 1H), 3.54 (ddd, *J* = 11.4, 6.2, 2.0 Hz, 1H), 3.47 (d, *J* = 8.3 Hz, 1H), 3.28 (d, *J* = 1.0 Hz, 3H), 3.15 (d, *J* = 1.0 Hz, 3H), 3.08 – 2.89 (m, 2H), 2.78 – 2.70 (m, 1H), 2.65 – 2.54 (m, 1H), 2.45 (s, 3H), 2.32 (d, *J* = 15.2 Hz, 1H), 2.15 – 2.01 (m, 3H), 1.99 (s, 3H), 1.74 – 1.66 (m, 1H), 1.58 – 1.45 (m, 2H), 1.45 – 1.38 (m, 1H), 1.32 (s, 3H), 1.28 (dt, *J* = 4.2, 1.9 Hz, 6H), 1.25 – 1.21 (m, 6H), 1.12 (d, *J* = 7.1 Hz, 3H), 0.96 – 0.92 (m, 3H), 0.92 – 0.86 (m, 3H). HRMS (ESI) Calcd for C₃₇ H₆₄ O₁₁ N [M+H⁺] 698.4474, found 698.4460.

AC4-CLM: DM-CLM (80mg, 0.115mmol) dissolved in DMSO (5 mL) with a mixture of hex-5-yn-1-yl 4-methylbenzenesulfonate (200mg, 0.79mmol). Hunig's base (0.5 mL, 10V/V% of solvent) were added into the solution and heated to 75°C for overnight. By checking TLC plate with Anisaldehyde staining, a new spot showed in a higher R_f. The reaction was quenched by cooling down to room temperature and washed with water (100ml) and extraction by DCM (50 mL). The solution was dried by NaSO₄. The vacuum evaporation gave out a yellow oil of crude product. To purify the compound, column chromatography was applied with gradient solvent system: ethyl acetate: hexane=8:2. The pure product gained in white foam (70mg, 0.086mmol, with yield of 74.8%). ¹H NMR (400 MHz, cdcl₃) δ 5.09 – 5.00 (d, 1H), 4.92 (d, *J* = 4.8 Hz, 1H), 4.44 (d, *J* = 6.8 Hz, 1H), 3.99 (s, 2H), 3.79 – 3.73 (m, 2H), 3.68 – 3.62 (m, 6H), 3.52 – 3.41 (m, 1H), 3.32 (s, 4H), 3.25-3.16 (m, 2H), 3.05-2.81 (m, 7H), 2.87 (d, *J* = 9.1 Hz, 2H), 2.62 (s, 4H), 2.60-2.56 (m, 2H), 2.36 (d, *J* = 15.2 Hz, 2H), 2.21 (m, 6H), 1.97 – 1.81 (m, 5H), 1.70 (d, *J* = 13.5 Hz, 2H), 1.62 – 1.52 (m, 6H), 1.50 – 1.43 (m, 2H), 1.40 (s, 4H), 1.30 (d, *J* = 6.2 Hz, 4H), 1.25 (s, 6H), 1.21 (dd, *J* = 8.7, 6.6 Hz, 8H), 1.15 – 1.06 (m, 13H), 0.84 (t, *J* = 7.3 Hz, 3H).

AC4-63: DM-63 (80mg, 0.115mmol) dissolved in DMSO (5 mL) with hex-5-yn-1-yl 4-methylbenzenesulfonate (400mg, 1.58mmol). Hunig's base (0.5 mL, 10V/V% of solvent) were added into the solution and heated to 75°C for overnight. The reaction was quenched by cooling down to room temperature and washed with water (100 mL) and extraction by DCM (50 mL). The solution was dried by NaSO₄. The vacuum evaporation gave out a yellow oil of crude product. To purify the compound, column chromatography was applied with gradient solvent system: DCM:

MeOH=10:1 The pure product gained in white foam (55mg, 0.069mmol), with yield of 60.1%. ^1H NMR (700 MHz, CDCl_3) δ 5.69 (s, 1H), 5.00 (ddd, $J = 10.6, 3.0, 1.2$ Hz, 1H), 4.85 (d, $J = 4.7$ Hz, 1H), 4.40 (dd, $J = 7.2, 1.2$ Hz, 1H), 4.12 (d, $J = 10.0$ Hz, 1H), 3.98 (dt, $J = 12.3, 6.3$ Hz, 1H), 3.46 (dd, $J = 14.3, 7.4$ Hz, 2H), 3.31 – 3.24 (m, 4H), 3.15 (d, $J = 1.2$ Hz, 3H), 3.00 (d, $J = 14.6$ Hz, 1H), 2.68 (t, $J = 7.9$ Hz, 1H), 2.62 (tt, $J = 9.2, 6.6$ Hz, 1H), 2.55 (dd, $J = 12.6, 7.0$ Hz, 1H), 2.48 (s, 1H), 2.38 (dd, $J = 12.5, 7.3$ Hz, 1H), 2.35 – 2.31 (m, 2H), 2.25 – 2.18 (m, 5H), 2.07 – 2.02 (m, 6H), 1.78 – 1.40 (m, 22H), 1.31 (s, 3H), 1.29 – 1.24 (m, 9H), 1.24 – 1.19 (m, 7H), 1.11 (d, $J = 7.2$ Hz, 4H), 1.00 (dd, $J = 7.5, 1.3$ Hz, 3H), 0.88 (td, $J = 7.4, 1.2$ Hz, 4H). HRMS (ESI) Calcd for $\text{C}_{43} \text{H}_{72} \text{O}_{11} \text{N}$ $[\text{M}+\text{H}^+]$ 778.5100, found 778.5072

DC-AC4-63

Compound 1: Octaethylene Glycol (200mg, 0.54mmol) mixed with Tosyl Chloride (400mg, 2.1mmol) and Triethylamine (375mg, 3.71mmol) in 10 mL DCM. The reaction was stirred at room temperature for overnight. The solution was dried via vacuum evaporation and obtained a yellow oil of crude product. Subsequently, Column chromatography was applied with gradient solvent system: ethyl acetate: MeOH=10:1 to furnish the final product in clear oil (305mg, 0.46mmol), with yield of 85.2%. The intermediate has been used directly to the next step.

Compound 2: The compound **2** (300mg, 0.45mmol) was mixed with sodium azide (400mg, 6.15mmol) and dissolved in 10 mL DMF. The solution was heated to 70 C° for overnight. In the second day, the solution was dried by vacuum evaporation and obtained a yellow oil of crude product. The crude product was used directly for the next step.

Compound 3: all the Compound **3** (180mg, 0.43mmol) was dissolved in ether (10 mL) and mixed with triphenyl phosphine (106mg, 0.405mmol). The solution was stirred at room temperature with argon protection for 5 minutes. A 5% (V/V%) HCl solution (10 mL) was added into the solution and kept stirring for overnight. The next day, aqueous layer was separated from the solution and basified by ammonia chloride (1M, 5 mL). The basic aqueous solution was extracted by DCM:MeOH (10:1) solution three times. The organic layers combined and evaporated to dryness and yielded yellow oil of crude product (145mg, 0.37mmol, 91.4%). This crude product is used directly to the next reaction.

Azido-Biotin: Biotin (240mg, 0.98mmol) were mixed with dicyclohexylcarbodiimide (200mg, 0.97mmol) for 10 minutes, then N-chlorosuccinimide (130mg, 1.02mmol) were added to the solution. The solution was protected by argon and stirred for overnight. The solution became cloudy with accumulation of white precipitates. The solution added with ether and filtered. The filtrate solution was dried by vacuum evaporation and obtained a yellow solid of crude product (320mg, 0.95mmol). The crude product (135mg, 0.4mmol) was mixed with Compound **4** (145mg, 0.37mmol) in 5 mL DMF and stirred for overnight. The gained Compound **5** was dried by vacuum evaporation and obtained a white solid. The solid was washed by ether (10 mL) for 5 times. The solid was filtered and gained with 92mg (0.15mmol, 40%). ¹H NMR (400 MHz, cdcl₃) δ 4.56 – 4.48 (m, 2H), 4.32 (ddd, *J* = 8.5, 6.4, 3.6 Hz, 2H), 4.10 (s, 9H), 3.75 – 3.59 (m, 15H), 3.50 – 3.33 (m, 4H), 3.26 – 3.12 (m, 2H), 3.02 – 2.89 (m, 2H), 2.93 – 2.81 (m, 4H), 2.79 – 2.71 (m, 2H), 2.72 (s, 2H), 2.66 (td, *J* = 7.1, 4.2 Hz, 2H), 1.92 – 1.82 (m, 2H), 1.85 – 1.67 (m,

4H), 1.70 – 1.63 (m, 2H), 1.67 – 1.55 (m, 2H), 1.58 – 1.41 (m, 2H), 1.44 – 1.23 (m, 2H), 1.22 – 1.02 (m, 2H).

Biotin-63: Compound **5** (30mg, 0.48mmol) add to THF:DMSO (1ml:1ml) solution with AC4-63 (28mg, 0.35mmol) and CuI (5mg, 0.026mmol) was added before purged with Ar. The solution temperature went down as evaporation processes. Then 10V/V% Hunig's base was added and the color of the solution turned into dark green. The reaction was capped and stirred for overnight. In TLC plate in new spot in lower R_f generated which indicates the triazole formation. The reaction was quenched by adding NH₄OH (1M, 20ml) solution. The solution was extracted by 50ml DCM. The solution was dried by NaSO₄ and vacuum evaporation. A yellow oil of crude product was gained. To purify the compound, column chromatography was applied with gradient solvent system: DCM: MeOH: NH₄OH=8:1:0.1. The pure product gained in clear oil (8.2mg, 0.0058mmol) with yield of 14.1%. ¹H NMR (400 MHz, cdcl₃) δ 7.53 (s, 0H), 5.71 (d, *J* = 16.5 Hz, 1H), 5.00 (dd, *J* = 10.7, 2.8 Hz, 1H), 4.84 (d, *J* = 4.5 Hz, 1H), 4.55 – 4.40 (m, 2H), 3.90 – 3.82 (m, 1H), 3.67 – 3.52 (m, 15H), 3.50 – 3.32 (m, 2H), 3.27 (d, *J* = 3.0 Hz, 2H), 3.14 (s, 2H), 2.81 – 2.70 (m, 2H), 2.62 (d, *J* = 0.4 Hz, 21H), 2.08 – 2.00 (m, 4H), 1.67 (td, *J* = 14.0, 13.4, 6.7 Hz, 4H), 1.49 – 1.40 (m, 1H), 1.40 – 1.19 (m, 12H), 1.11 (d, *J* = 7.1 Hz, 2H), 0.97 (d, *J* = 7.7 Hz, 1H), 0.87 (t, *J* = 7.3 Hz, 2H). HRMS (ESI) Calcd for C₆₉ H₁₁₉ N₇ O₂₀ S [M+2H]²⁺ 699.4575, found 699.9193.

Biotin-CLM: Compound **5** (10mg, 0.0161mmol) add to THF: DMSO (1ml:1ml) solution with AC4-CLM (37mg, 0.474mmol) and CuI (5mg, 0.026mmol) was added before purged with Ar. The solution temperature went down as evaporation processes. Then 10V/V% Hunig's base was added and the color of the solution turned into dark green. The reaction was capped and stirred for overnight. In TLC plate in new spot in lower R_f generated which indicates the triazole formation. The reaction was quenched by adding NH₄OH (1M, 20ml) solution. The solution was extracted by 50ml DCM. The solution was dried by NaSO₄ and vacuum evaporation. A yellow oil of crude product was gained. To purify the compound, column chromatography was applied with gradient solvent system: DCM: MeOH: NH₄OH=8:1:0.1. The pure product gained in white solid (3.6mg, 0.0025mmol) with yield of 15.6%. ¹H NMR (400 MHz, cdcl₃) δ 7.65 (s, 0H), 5.05 (d, *J* = 10.9 Hz, 1H), 4.91 (d, *J* = 4.1 Hz, 1H), 4.52 (t, *J* = 4.9 Hz, 2H), 4.35 – 4.23 (m, 1H), 4.15 (ddd, *J* = 12.1, 6.1, 2.1 Hz, 1H), 3.95 (s, 1H), 3.86 (t, *J* = 5.3 Hz, 2H), 3.77 – 3.72 (m, 2H), 3.66 – 3.59 (m, 22H), 3.55 (t, *J* = 5.1 Hz, 2H), 3.47 (q, *J* = 7.0 Hz, 6H), 3.31 (s, 2H), 3.02 (s, 4H), 2.80 (d, *J* = 12.2 Hz, 4H), 2.32 (td, *J* = 7.7, 4.9 Hz, 2H), 2.23 (t, *J* = 7.2 Hz, 2H), 2.09 – 2.04 (m, 3H), 2.04 (d, *J* = 3.5 Hz, 2H), 1.91 (dd, *J* = 12.3, 7.8 Hz, 3H), 1.74 (s, 4H), 1.67 (q, *J* = 7.8 Hz, 3H), 1.59 (dd, *J* = 11.8, 7.0 Hz, 4H), 1.56 – 1.40 (m, 8H), 1.37 (s, 4H), 1.30 – 1.15 (m, 15H), 1.12 (d, *J* = 5.5 Hz, 6H), 1.04 (d, *J* = 7.6 Hz, 2H), 0.92 – 0.81 (m, 7H). HRMS (ESI) Calcd for C₆₉H₁₂₃N₇O₂₂S [M+H]⁺ 1434.8515, found 1434.8495

4.4.2 Cell culture and viability assay.

MDA-MB-231, VERO, and A549 cell lines were maintained in Dulbecco's Modified Eagle Medium (DMEM) (Corning, 10-017-CV), supplemented with 10% fetal bovine serum (FBS) (Corning, 35-010-CV). MCF-7 cells were cultured in phenol red free Minimum Essential Medium

(MEM) (Corning, 17-305-CV), supplemented with 10% fetal bovine serum (FBS). Cells were seeded into a 96-well plate (2000 counts/100uL) for 24 h prior to treatment and then treated with various drug concentrations for 72 h. All drugs were dissolved in DMEM/DMSO with DMSO concentration maintained at 1%. Every drug was tested repeatedly with 8 dosage in triplicate. The effect of compounds on cell viability was measured using the MTS assay (CellTiter 96 Aqueous One Solution and CellTiter 96 Non-Radioactive Cell Proliferation Assays, Promega, Madison, WI) as described by the manufacturer. IC₅₀s were determined using Prism GraphPad 8.

4.4.3 *X-ray crystallography:*

Single colorless block crystals of *AO-02-63* were chosen from the sample as supplied. A suitable crystal with dimensions $0.56 \times 0.44 \times 0.38$ mm³ was selected and mounted on a loop with paratone oil on a XtaLAB Synergy-S diffractometer. The crystal was kept at a steady T = 105(8) K during data collection. The structure was solved with the ShelXT³⁴ solution program using dual methods and by using Olex2³⁵ as the graphical interface. The model was refined with ShelXL 2018/3³⁴ using full matrix least squares minimisation on F².

4.4.4 *Translation Inhibition Assay:*

Rabbit reticulocyte lysate system (Promega L4960). The assay was performed by following the manual instruction. In brief, lysate mixed with a self-prepared amino acid master mix with RNAsin and aliquots 12.5μL to 12x4 0.2ml centrifuge tubes. Compound *AO-02-63* were prepared into 11 concentration (13, 6.5, 3.25, 1.625, 0.8125, 0.406, 0.205, 0.103, 0.0508, 0.0254, 0.0127mM) points

with DMSO while puromycin was prepared into 8 points starting from 325 to 1.3 μ M with 2-fold dilution increment. 0.5 μ L DMSO solution of drug was added to the aliquots so that the final concentration of AO-02-63 diluted to 500 to 0.05 μ M and puromycin to (12.5 to 0.05 μ M). 2 aliquots were treated with only DMSO as a negative control. The solutions incubate in 37°C for 2 h and cool to ice bath to quench the reaction. A pre-made 1M potassium luciferin substrate solution was aliquoted 70 μ L to 12x4 wells of the luminescence white 96-well plate. Then the 10 μ L lysate were added to the wells. Plate was shaken in room temperature for 1 minute to 5 minutes prior to screen. The Luminescence signal were detected and the data analyzed by Prism GraphPad 8.

E. coli S30 Extract System for Circular DNA (Promega L1020). The assay was performed by following the manual instruction. In brief, S30 extract, S30 premix, amino acids, and pBESTluc circular DNA were thawed on ice. Master Mix (MM) was created by combining 180 μ L S30 premix, 135 μ L S30 extract, 95 μ L nanopure water, and 40 μ L amino acid mix for a total volume of 450 μ L. One tube of MM was sufficient for each compound run at 10 concentration points with 3 vehicle controls. CLM and AO-02-63 were serially diluted in DMSO so that the 8 concentration points ranged from 520 μ M to 00208 μ M by 5-fold dilution. The pBESTluc provided in the kit was dilutes from 10 μ L to 54.4 μ L with 1x TE buffer. 12.5 μ L of MM were aliquoted to a 0.2 mL centrifuge tubes, followed by 0.5 μ L compound addition, which made final concentrations as 20 μ M to 1.08nM. The tubes were then mixed gently by pipetting. The tubes were held at room temperature for 20 minutes after which 0.4 μ L pBESTluc was added. After brief mixing, the tubes were incubated at 37° C for 60 min. The tubes were put on ice for a 5-minute inactivation period. After gentle mixing by pipette, 10 μ L were aliquoted to a white half-volume 96-well plate (supplied by Greiner). 70 μ L 1mM luciferin solution was added to each well, and the plate was

read for luminescence after a 1-5 minutes shaking period. Luminescence was normalized to DMSO controls. Data was processed with Graphpad Prism 8.

4.4.5 *Pull-down assay and Mass spectroscopy:*

Hep-G2 cells (1×10^6 cell/plate) with 3 plates were washed by 1X cold PBS, scratched, and collected into a 1.5ml centrifuge tube with 1ml of 1X PBS stored in -80°C . After one freeze thaw, the cells were sonicated with a probe sonicator. The lysate was gained and aliquoted to 10 test tubes with 100 μL on each. Every five tubes are distributed to control group, Biotin-63 group, Biotin-63 with AO-02-63 competition, Biotin-CLM, and Biotin-CLM with CLM competition. Each tube added 1 μL of DMSO or DMSO solution of compounds. For Biotin-63 and Biotin-CLM, the final concentrations are 500 μM , and for the competition group, a 1 μL DMSO solution of a mixture of 500 μM Biotinylated compound and 500 μM competitor was added. The compounds incubated in the lysate for 1 h prior to the pull-down. Streptavidin Bead (Thermo Fisher; cat. 88817) were washed by 1x PBS 3 times prior to use. A magnetic stand is applied to immobilize the beads. After drug incubation, the lysates were added into the beads and incubated in a centrifuge tube rotator at room temperature for another 2 h. The lysates were removed from the beads from magnetic stands. The beads were washed gently by adding 1X PBS 3 times. Then, an elution process is performed by adding 50 μL pH=2 elution buffer (Thermo Fisher. 21028) on each tube and pipetting thoroughly for 5-10 minutes. The eluents were removed from beads and the pH will be adjusted to 7.5 by adding appropriate amount of 5M NaOH determined by pH paper. The pull-down proteins were denatured followed by Western blot process: added 50 μL 2x Laemmli buffer and heated to 100°C for 5 minutes, each lysate was loaded to each well of the TGX MIDI

4-20% gel (Biorad, cat. 5671093) and ran at 150V for 70 mins. The gel was collected, washed by water, and deactivated by 10% alcohol. Then, followed by instruction of Pierce™ Silver Stain for Mass Spectrometry kit (Thermo Fisher 24600), we gained the proteins bands. On the other hand, whole cell lysate, pull-down lysates and background lysates were sent to the Mass spectroscopy core and analyzed by Dr. David Smalley and Hyojung Kim in Georgia Institution of Technology.

4.5 References:

1. Hansen JL, Ippolito JA, Ban N, Nissen P, Moore PB, Steitz TA. The structures of four macrolide antibiotics bound to the large ribosomal subunit. *Molecular cell*. 2002;10(1):117-28.
2. Bulkley D, Innis CA, Blaha G, Steitz TA. Revisiting the structures of several antibiotics bound to the bacterial ribosome. *Proceedings of the National Academy of Sciences*. 2010;107(40):17158-63.
3. Kannan K, Mankin AS. Macrolide antibiotics in the ribosome exit tunnel: species-specific binding and action. *Annals of the New York Academy of Sciences*. 2011;1241(1):33-47.
4. Tsai WC, Standiford TJ. Immunomodulatory effects of macrolides in the lung: lessons from in-vitro and in-vivo models. *Current pharmaceutical design*. 2004;10(25):3081-93.
5. Yanagihara K, Kadoto J, Kohno S. Diffuse panbronchiolitis—pathophysiology and treatment mechanisms. *International journal of antimicrobial agents*. 2001;18:83-7.
6. Pestka S, Lemahieu RA. Effect of erythromycin analogues on binding of [14C] erythromycin to Escherichia coli ribosomes. *Antimicrobial agents and chemotherapy*. 1974;6(4):479-88.
7. LeTourneau N, Vimal P, Klepacki D, Mankin A, Melman A. Synthesis and antibacterial activity of desosamine-modified macrolide derivatives. *Bioorganic & medicinal chemistry letters*. 2012;22(14):4575-8.
8. Washington AZ, Benicewicz DB, Canzoneri JC, Fagan CE, Mwakwari SC, Maehigashi T, et al. Macrolide-peptide conjugates as probes of the path of travel of the nascent peptides through the ribosome. *ACS chemical biology*. 2014;9(11):2621-31.

9. Svetlov MS, Syroegin EA, Aleksandrova EV, Atkinson GC, Gregory ST, Mankin AS, et al. Structure of Erm-modified 70S ribosome reveals the mechanism of macrolide resistance. *Nature Chemical Biology*. 2021;1-9.
10. Klein LL, Freiberg LA, Kurath P, Henry RF. Synthesis of (9R)-9-dihydro-6,9-anhydroerythromycin A. *The Journal of Organic Chemistry*. 1993;58(11):3209-12.
11. Agouridas C, Bonnefoy A, Chantot JF. Antibacterial activity of RU 64004 (HMR 3004), a novel ketolide derivative active against respiratory pathogens. *Antimicrobial Agents and Chemotherapy*. 1997;41(10):2149-58.
12. Puri SK, Lassman HB. Roxithromycin: a pharmacokinetic review of a macrolide. *Journal of Antimicrobial Chemotherapy*. 1987;20(suppl_B):89-100.
13. Fernandes P, Hardy D. Comparative in vitro potencies of nine new macrolides. *Drugs under experimental and clinical research*. 1988;14(7):445-51.
14. WATANABE Y, MORIMOTO S, ADACHI T, KASHIMURA M, ASAKA T. CHEMICAL MODIFICATION OF ERYTHROMYCINS. IX. 1) SELECTIVE METHYLATION AT THE C-6 HYDROXYL GROUP OF ERYTHROMYCIN A OXIME DERIVATIVES AND PREPARATION OF CLARITHROMYCIN. *The Journal of antibiotics*. 1993;46(4):647-60.
15. Washington AZ, Tapadar S, George A, Oyelere AK. Exploiting translational stalling peptides in an effort to extend azithromycin interaction within the prokaryotic ribosome nascent peptide exit tunnel. *Bioorganic & medicinal chemistry*. 2015;23(16):5198-209.
16. Jelić D, Antolović R. From erythromycin to azithromycin and new potential ribosome-binding antimicrobials. *Antibiotics*. 2016;5(3):29.
17. Liang JH, Li XL, Wang H, An K, Wang YY, Xu YC, et al. Structure-activity relationships of novel alkylides: 3-O-arylalkyl clarithromycin derivatives with improved antibacterial activities. *Eur J Med Chem*. 2012;49:289-303.
18. Yoshida K, Sunazuka T, Nagai K, Sugawara A, Cho A, Nagamitsu T, et al. Macrolides with promotive activity of monocyte to macrophage differentiation. *J Antibiot (Tokyo)*. 2005;58(1):79-81.
19. Dunlap N, Huryn DM. Medicinal chemistry. New York , NY: Garland Science, Taylor & Francis Group, LLC; 2018. pages cm p.
20. LeBel M. Pharmacokinetic properties of clarithromycin: A comparison with erythromycin and azithromycin. *Canadian Journal of Infectious Diseases*. 1993;4.
21. Kohyama T, Yamauchi Y, Takizawa H, Itakura S, Kamitani S, Kato J, et al. Clarithromycin inhibits fibroblast migration. *Respiratory medicine*. 2008;102(12):1769-76.

22. Zimmermann P, Ziesenitz VC, Curtis N, Ritz N. The immunomodulatory effects of macrolides—a systematic review of the underlying mechanisms. *Frontiers in immunology*. 2018;9:302.
23. Kurath P, Jones PH, Egan RS, Perun TJ. Acid degradation of erythromycin A and erythromycin B. *Experientia*. 1971;27(4):362-.
24. Liu, Y., Li, H., Liu, F., Gao, L. B., Han, R., Chen, C., Ding, X., Li, S., Lu, K., Yang, L., Tian, H. M., Chen, B. B., Li, X., Xu, D. H., Deng, X. L., & Shi, S. L. (2020). Heterogeneous nuclear ribonucleoprotein A2/B1 is a negative regulator of human breast cancer metastasis by maintaining the balance of multiple genes and pathways. *EBioMedicine*, 51, 102583. <https://doi.org/10.1016/j.ebiom.2019.11.044>
25. Xing S, Li Z, Ma W, He X, Shen S, Wei H, et al. DIS3L2 promotes progression of hepatocellular carcinoma via hnRNP U-mediated alternative splicing. *Cancer research*. 2019;79(19):4923-36.
26. Liu X, Zhou Y, Lou Y, Zhong H. Knockdown of HNRNPA1 inhibits lung adenocarcinoma cell proliferation through cell cycle arrest at G0/G1 phase. *Gene*. 2016;576(2):791-7.
27. Bi H-s, Yang X-y, Yuan J-h, Yang F, Xu D, Guo Y-j, et al. H19 inhibits RNA polymerase II-mediated transcription by disrupting the hnRNP U–actin complex. *Biochimica et Biophysica Acta (BBA)-General Subjects*. 2013;1830(10):4899-906.
28. Amado-Rodríguez L, González-López A, López-Alonso I, Aguirre A, Astudillo A, Batalla-Solís E, et al. Anti-inflammatory effects of clarithromycin in ventilator-induced lung injury. *Respiratory research*. 2013;14(1):1-9.
29. Shinkai M, Foster GH, Rubin BK. Macrolide antibiotics modulate ERK phosphorylation and IL-8 and GM-CSF production by human bronchial epithelial cells. *American Journal of Physiology-Lung Cellular and Molecular Physiology*. 2006;290(1):L75-L85.
30. Hao M, Lin J, Shu J, Zhang X, Luo Q, Pan L, et al. Clarithromycin might attenuate the airway inflammation of smoke-exposed asthmatic mice via affecting HDAC2. *Journal of thoracic disease*. 2015;7(7):1189.
31. Ashburner BP, Westerheide SD, Baldwin AS. The p65 (RelA) subunit of NF- κ B interacts with the histone deacetylase (HDAC) corepressors HDAC1 and HDAC2 to negatively regulate gene expression. *Molecular and cellular biology*. 2001;21(20):7065-77.
32. Tan C, Xuan L, Cao S, Yu G, Hou Q, Wang H. Decreased histone deacetylase 2 (HDAC2) in peripheral blood monocytes (PBMCs) of COPD patients. *PLoS One*. 2016;11(1):e0147380.
33. Barnes PJ. Theophylline. *American journal of respiratory and critical care medicine*. 2013;188(8):901-6.

34. Sheldrick GM. SHELXT—Integrated space-group and crystal-structure determination. *Acta Crystallographica Section A: Foundations and Advances*. 2015;71(1):3-8.
35. Dolomanov OV, Bourhis LJ, Gildea RJ, Howard JA, Puschmann H. OLEX2: a complete structure solution, refinement and analysis program. *Journal of applied crystallography*. 2009;42(2):339-41.

4.6 Supporting Information

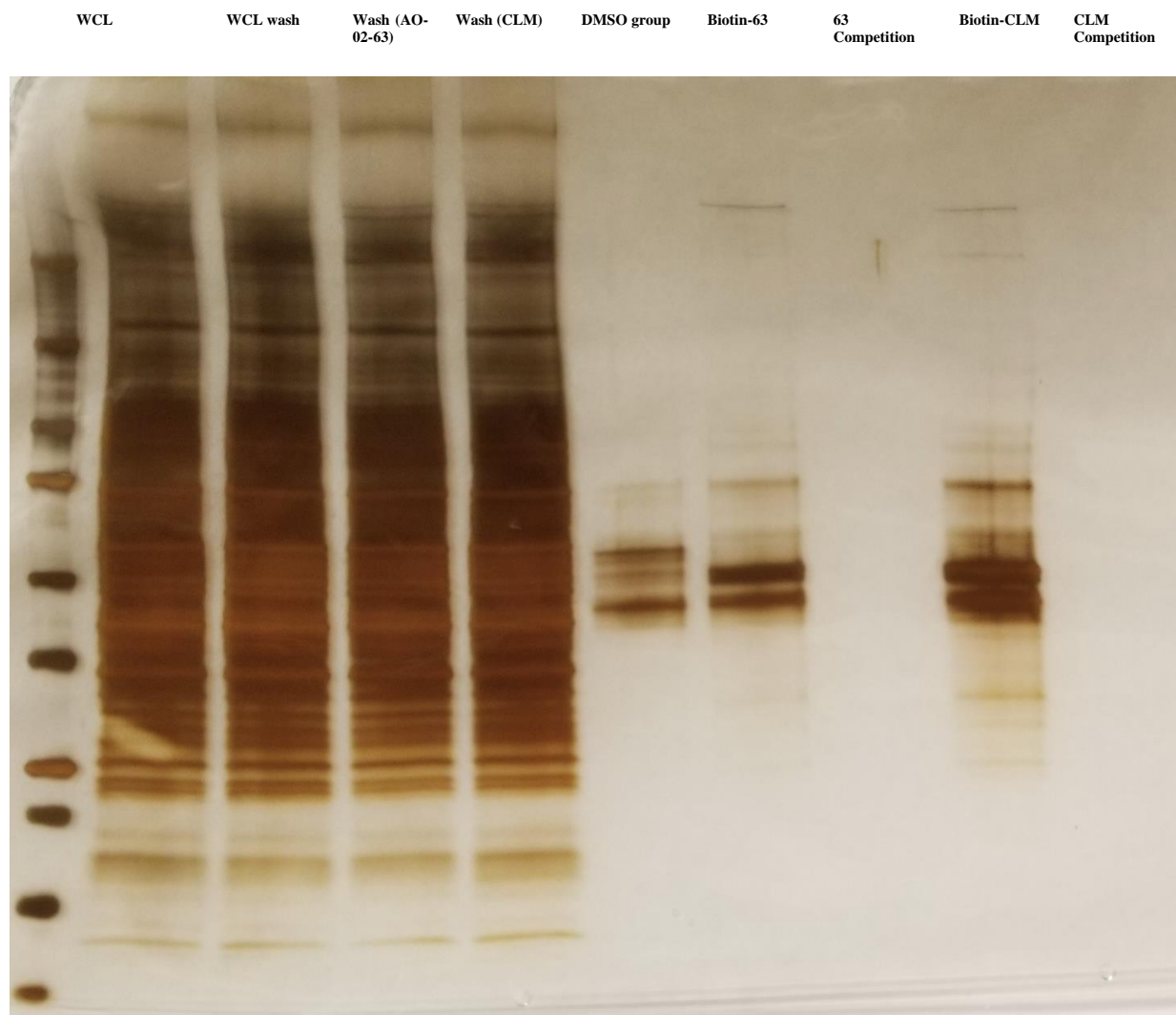
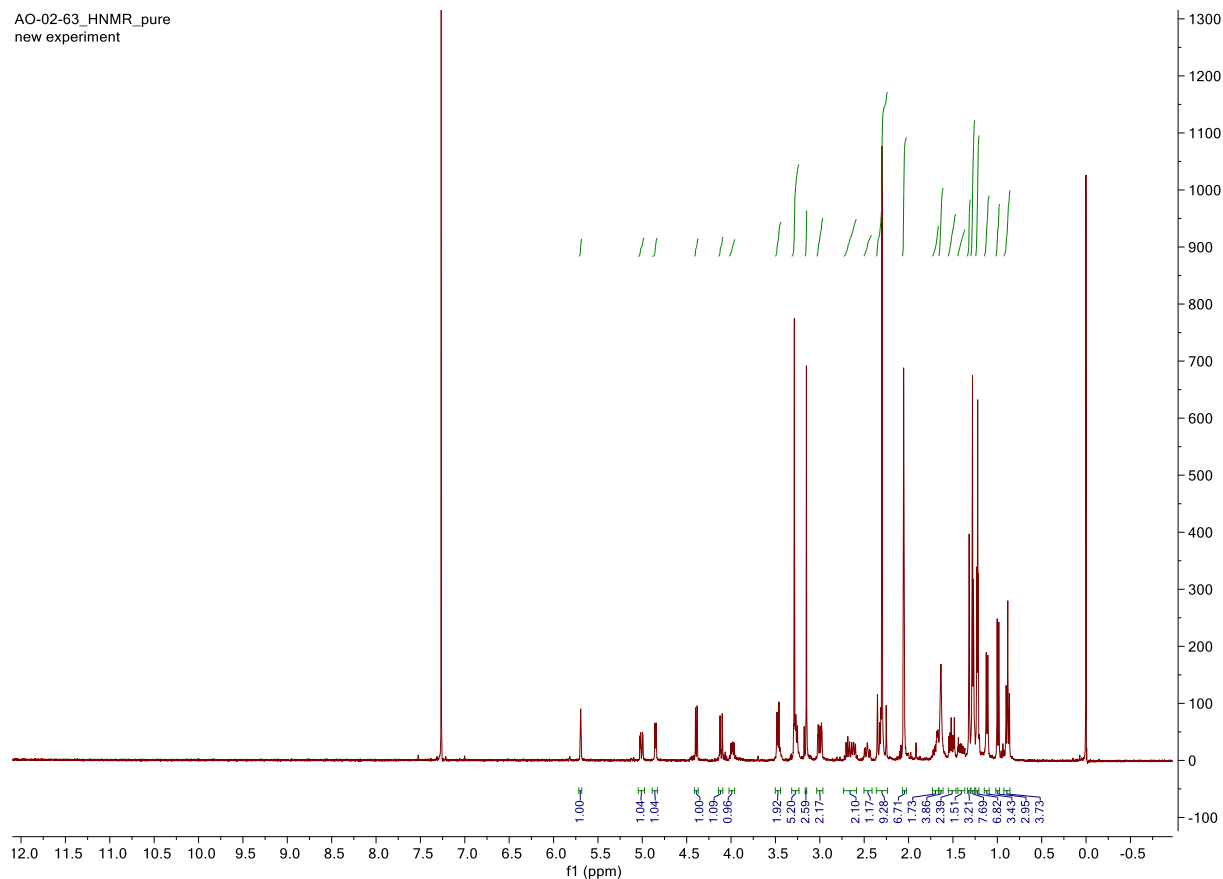


Figure S4. 1. Gel with silver staining after pulldown assay. WCL: The Whole cell lysate group; WCL wash: Unbounded protein group of DMSO treated group; Wash (AO-02-63): Unbounded protein group of 1% DMSO solution of AO-02-63 incubated with Streptavidin bead in WCL; Wash (CLM) unbounded protein group of 1% DMSO solution of CLM incubated with Streptavidin in WCL; DMSO group: The bounded proteins of streptavidin beads in DMSO treated group; Biotin-63 group: bounded proteins of streptavidin beads in 1% DMSO solution of Biotin-63 treated group; 63 Competition group: bounded protein group of AO-02-63 co-incubated with Biotin-63 in WCL and streptavidin group; Biotin-CLM group: bounded proteins of streptavidin beads in 1% DMSO solution of Biotin-CLM treated group; CLM Competition group: bounded protein group of CLM co-incubated with Biotin-CLM in WCL and streptavidin group;

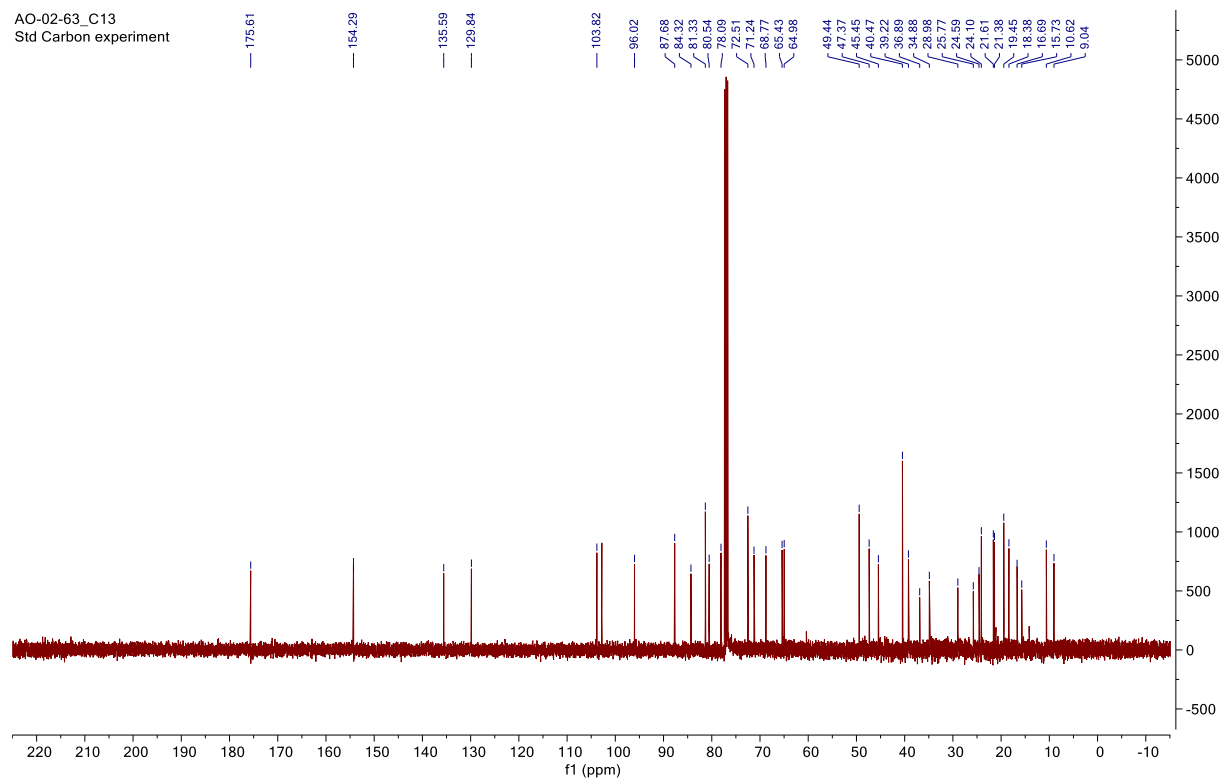
Table S4. 1. Compare of PSM scores on top ribosomal proteins pulled down by Biotin-CLM and Biotin-63.

Protein name	Sequence	Biotin-CLM (PSM#)	Biotin-63 (PSM#)
40S ribosomal protein S3	ELAEDGYSGVEVR	11	110
40S ribosomal protein S18	AGELTEDEVER	5	42
40S ribosomal protein S19	ALAAFLK	6	35
40S ribosomal protein S3a	NCLTNFHGMDLTR	2	29
40S ribosomal protein S25	LNNLVLFDK	2	28
40S ribosomal protein S4	VNDTIQIDLETGK	9	25
60S ribosomal protein L23a	ECADLWPR	6	28
60S ribosomal protein L7a	AGVNTVTTLVENK	10	24
60S ribosomal protein L13	VATWFNQPAR	5	23
60S ribosomal protein L36	YPMAGVLNK	7	22

AO-02-63

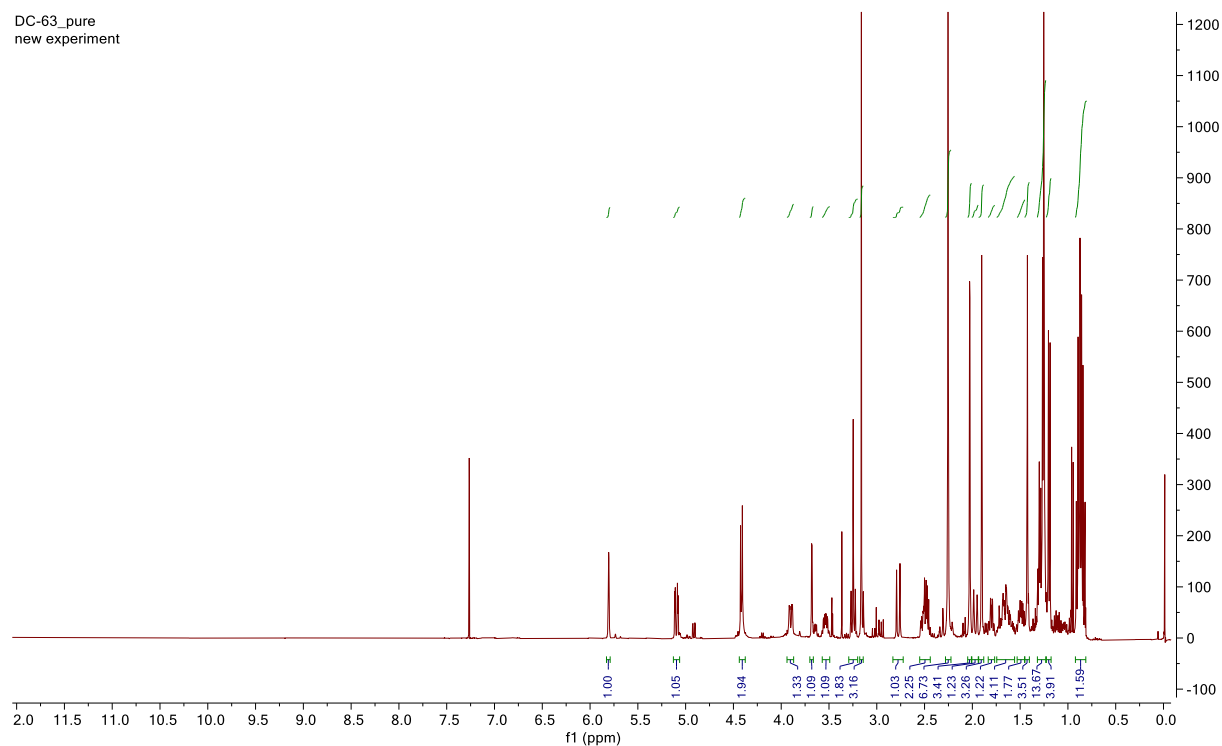


AO-02-63 (¹³C NMR)



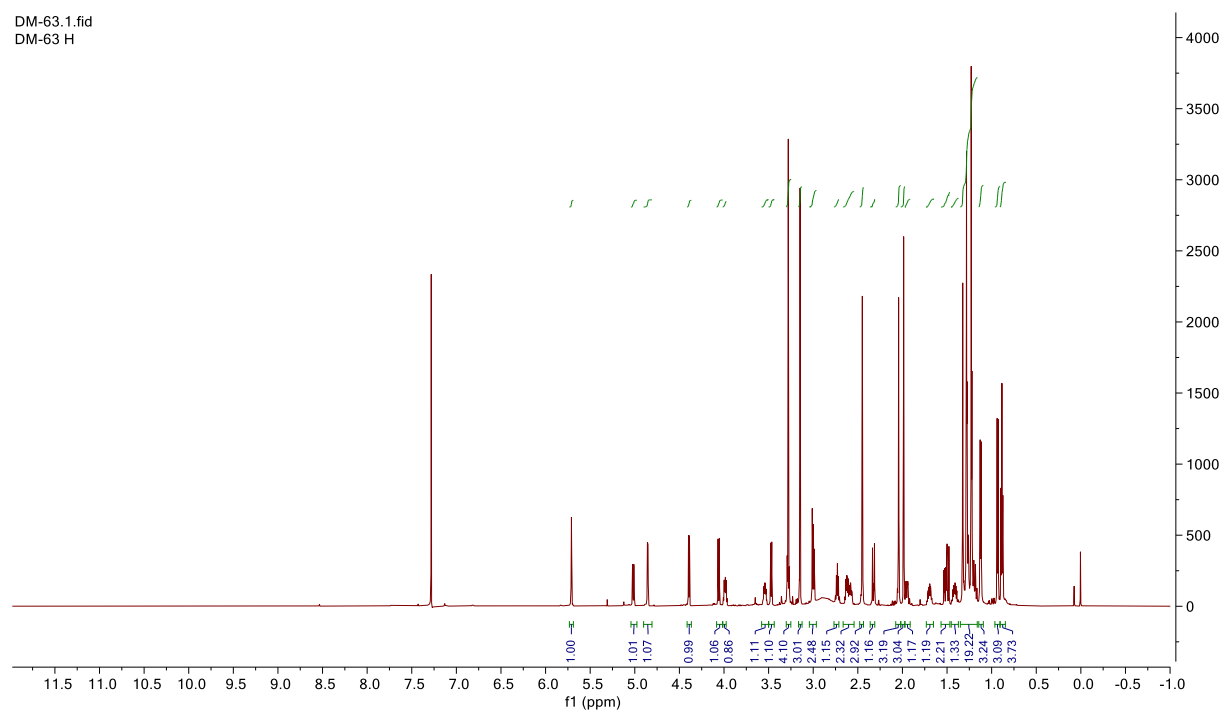
DC-63

DC-63_pure
new experiment



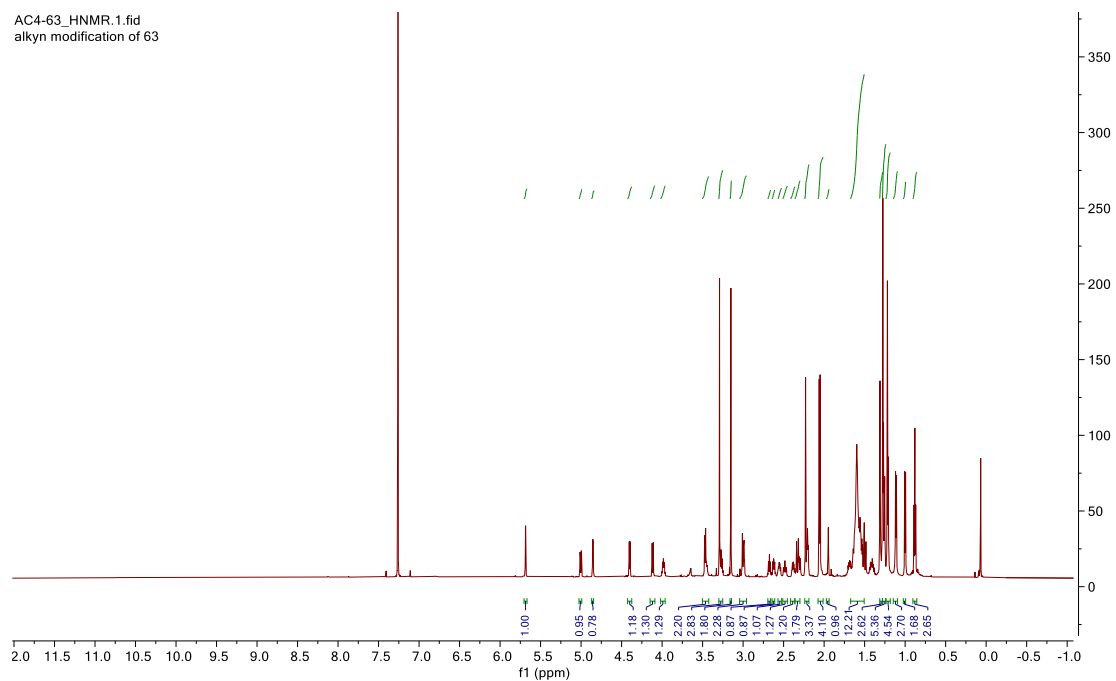
DM-63

DM-63.1.fid
DM-63 H

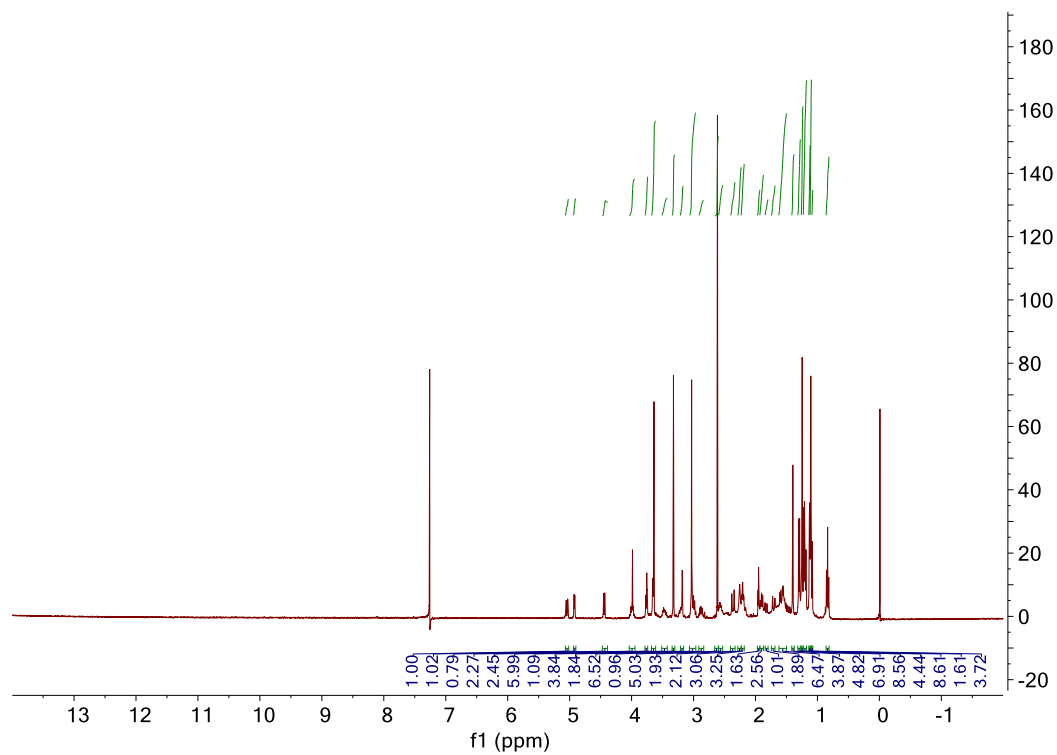


AC4-63

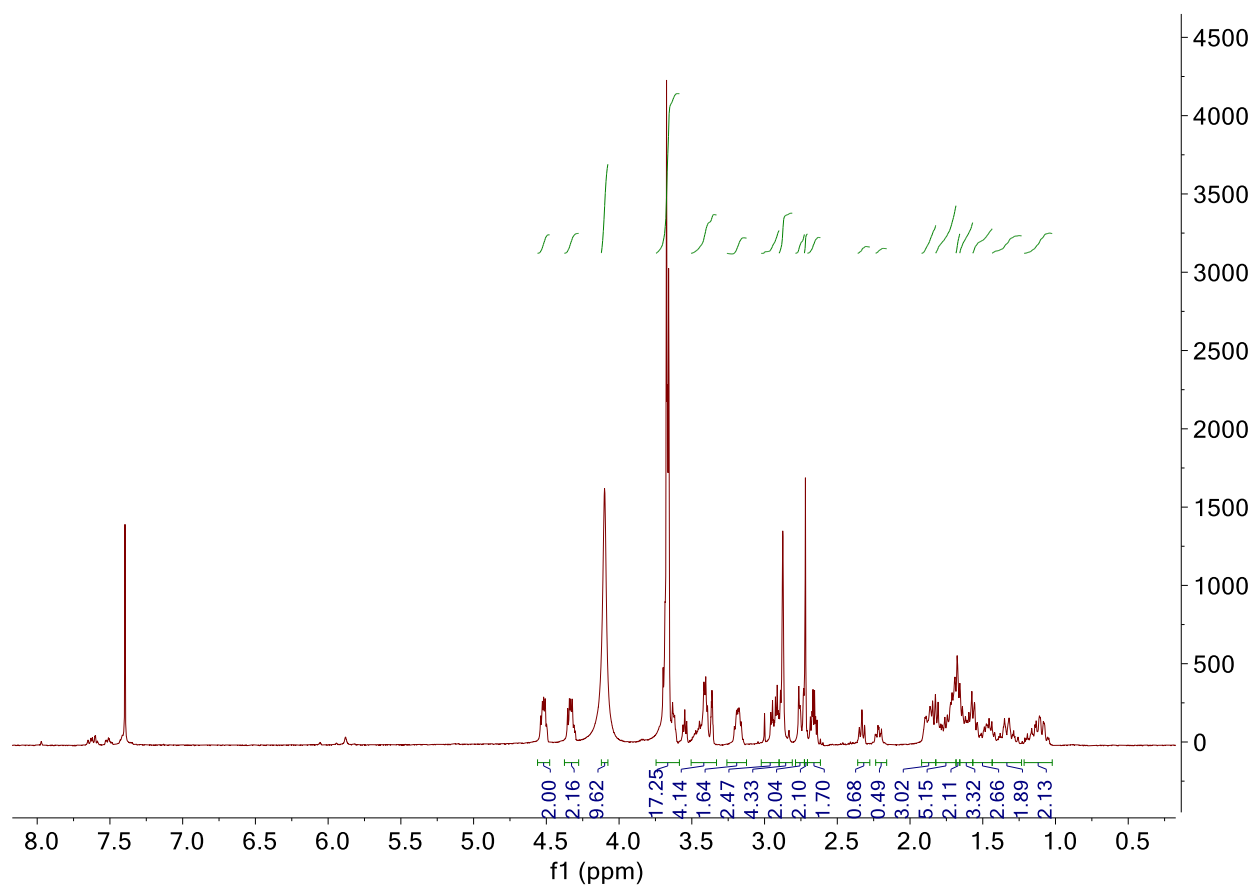
AC4-63_HNMR.1.fid
alkyn modification of 63



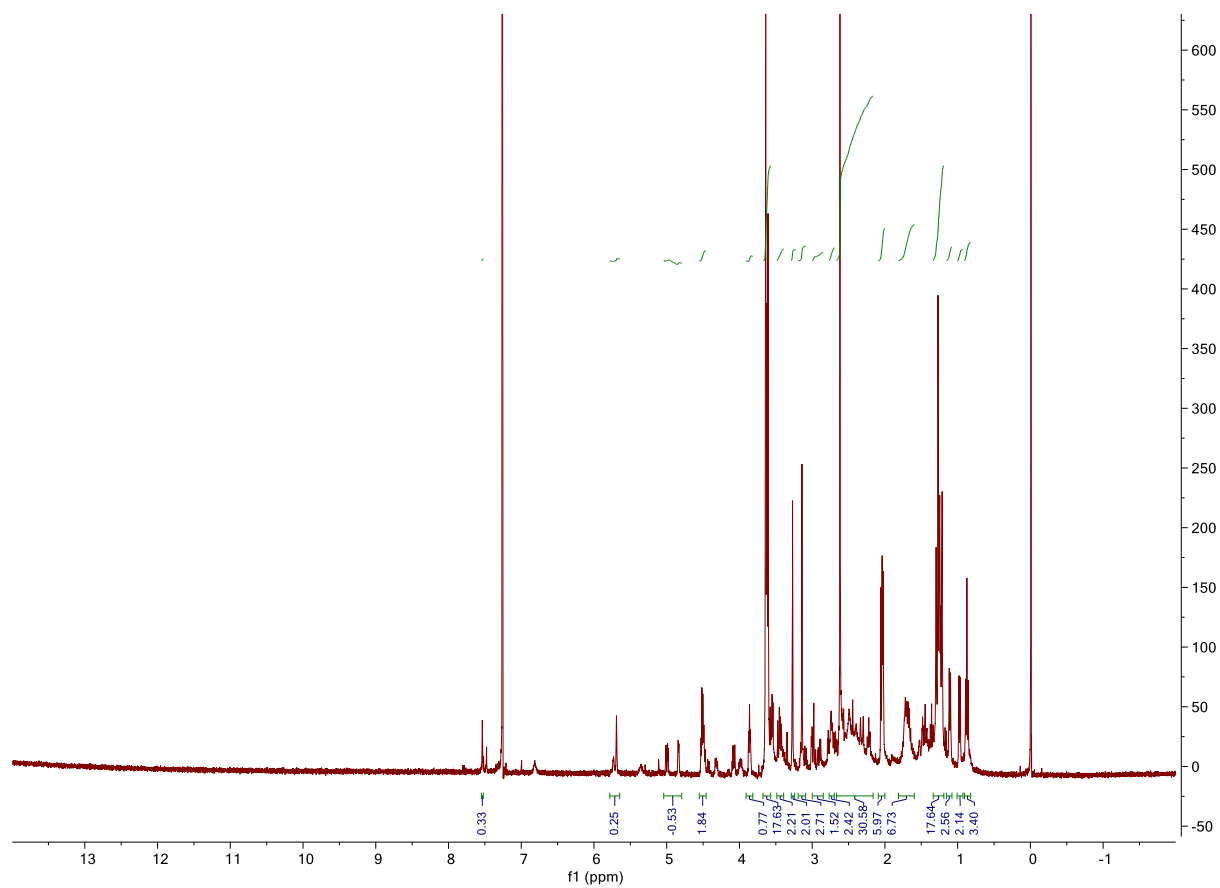
AC4-CLM



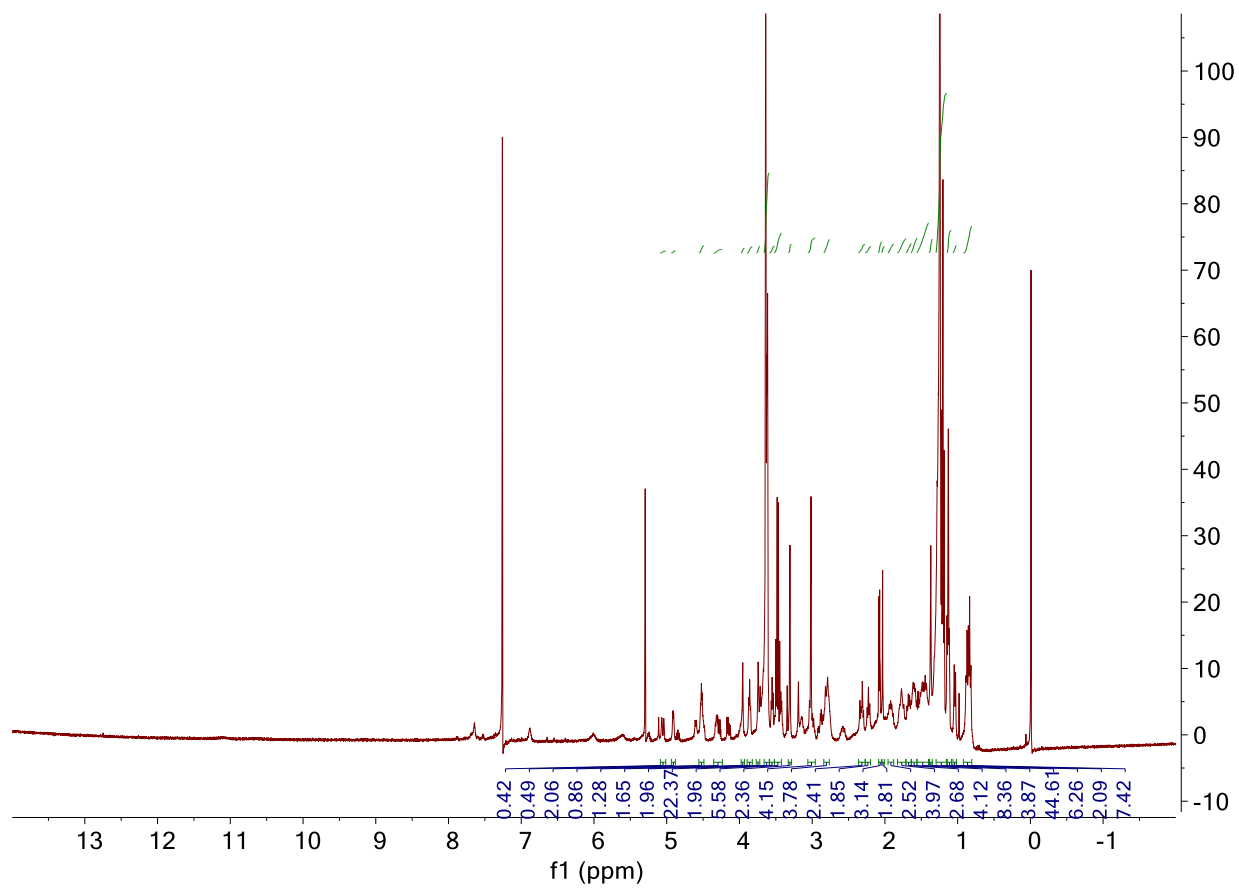
Azido biotin



Biotin-63



Biotin-CLM



Pyrimethamine derivatives as Novel Anti-cancer agents

In this thesis, we discovered two types of pyrimethamine (PYM) derivatives. PYM is a pleiotropic and polypharmacophore small molecule that revealed strong STAT3 pathway inhibition. As mentioned in the introduction section 1.6.2 and 1.6.3a, we designed the type I STAT3 inhibitor as PYM-HDACi and type II as novel pyrimethamine derivatives based on Structure-Activity Relationship (SAR) study. On purpose of detailed explanation, we divided type I and II into two separate topics Chapter 5 and 6. In these two chapters, we will fully demonstrate the rationale of design, procedures in synthesis, and biological activities of these STAT3 inhibition small molecules.

**CHAPTER 5. PYRIMETHAMINE CONJUGATED HISTONE
DEACETYLASE INHIBITORS: DESIGN, SYNTHESIS AND
EVIDENCE FOR TRIPLE NEGATIVE BREAST CANCER
SELECTIVE CYTOTOXICITY.**

Bocheng Wu^{1†}, Shaghayegh Fathi^{1, 2†}, Shanee Mortley¹, Mahir Mohiuddin^{4, 5}, Young C. Jang^{3, 4, 5}, Adegboyega Oyelere^{1, 4*}

*School of Chemistry and Biochemistry, School of Biological Sciences, Parker H. Petit Institute
for Bioengineering and Bioscience, Georgia Institute of Technology, Atlanta, GA 30332-0400*

USA

¹School of Chemistry and Biochemistry, Georgia Institute of Technology

²Current Address: University of Chicago

³School of Biological Sciences, Georgia Institute of Technology

⁴Parker H. Petit Institute for Bioengineering and Bioscience, Georgia Institute of Technology

⁵Wallace H. Coulter Department of Biomedical Engineering, Georgia Institute of Technology

[†]These Authors contributed equally to the manuscript

Correspondence to:

Adegboyega K. Oyelere, **E-mail:** aoyelere@gatech.edu

Keywords: Pyrimethamine, STAT proteins, STAT3, histone deacetylases, histone deacetylase inhibitors, triple negative breast cancer, molecular docking

Abstract:

Signal transducer and activator of transcription 3 (STAT3) is an oncogenic transcription factor which has been recognized as a promising cancer therapeutic target. Small molecule pyrimethamine (PYM) is a known direct inhibitor of activated STAT3 and it is currently under clinical trial. Also, histone deacetylase (HDAC) inhibition has been shown to indirectly attenuate STAT3 signaling through inhibition of STAT3 activation. Herein we described the design and biological profiling of two classes of PYM-conjugated HDAC inhibitors (HDACi). We observed that the class I PYM-HDACi compounds **12a-c** potently inhibited HDACs 1 and 6 in cell free assays while a lead class II PYM-HDACi compound **23** showed a strong HDAC 6 selective inhibition. In a cell-based assay, **12a-c** are preferentially cytotoxic to MDA-MB-231, a TNBC cell line that is highly STAT3-dependent, while **23** showed no such selective toxicity. Subsequent target validation studies revealed that a representative class I PYM-HDACi compound **12c** elicited a signature of HDAC and STAT3 pathway inhibition intracellularly. Collectively, these data suggest that PYM-HDACi compounds are promising leads to develop targeted therapy for TNBC.

Key words: Triple Negative Breast Cancer, Pyrimethamine, HDAC inhibitor, STAT3 pathway

5.1 Introduction:

Pyrimethamine (PYM) (Figure 5.1) is an FDA approved drug which, due to its perturbation of the functions of several intracellular targets, has found use for the management of various human diseases including toxoplasmosis and malaria.^{1,2} PYM has also been used in chemotherapy along with other drugs such as proguanil for few decades.³ PYM's anti-parasitic activity originates from its ability to specifically bind and inhibit dihydrofolate reductase (DHFR, 5,6,7,8-tetrahydrofolate: NADP⁺ oxidoreductase, EC 1.5.1.3) in *Plasmodium falciparum* and other protozoa.⁴ DHFR is critical for folate metabolism and has been a drug target for fungal, protozoal and bacterial infections and cancer. DHFR facilitates an NADPH-dependent reduction of dihydrofolate to tetrahydrofolate, a cofactor necessary for the biosynthesis of thymidylate, purine nucleotides, and many other essential amino acids required for protein, RNA, and DNA synthesis.⁵ DHFR inhibition by antifolate compounds interferes with these pathways, resulting in cell cycle arrest and cell death.⁶

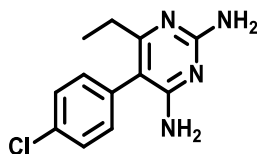


Figure 5. 1. Structure of pyrimethamine.

PYM is also an inhibitor of STAT3 (Signal transducer and activator of transcription 3) transcriptional function.⁷ STAT3 is a member of STAT proteins comprising of seven sub-family members (STAT1, 2, 3, 4, 5a, 5b, 6).⁸ STAT3, an oncogenic transcription factor with critical role in the signaling of a number of cytokines and growth factors, confers resistance to apoptosis in various cell types⁹ and is activated in many cancers including triple-negative breast cancer

(TNBC), acute myeloid leukemia (AML), chronic lymphocytic leukemia (CLL) and small lymphocytic lymphoma (SLL).^{10,11}

STAT3 activation through its tyrosine phosphorylation by JAK (Janus kinase) or IL-6 signaling cascade¹² enhances its dimerization and translocation from cytoplasm to nucleus where it can bind to certain DNA sequences and regulate genes expression involved in various cellular processes.

Tyrosine phosphorylation is not the only way to activate STAT3. It can be activated through other processes such as serine phosphorylation, acetylation, methylation, and glutathionylation.^{13,14}

Once STAT3 is activated, it enhances various cell processes such as cell proliferation, differentiation, survival, and angiogenesis that contribute to malignant transformation and progression in many cancers such as breast, ovary, and prostate.¹⁵ Although STAT3 also has non-transcriptional responsibilities, such as regulation of mitochondrial function, most of its oncogenic activities are related to its gene regulation in the nucleus.¹⁶

Activation of STAT3 is tightly regulated in normal conditions; however, in cancer, it is highly activated and leads to malignant cancer cells phenotype.¹⁷ Therefore, inhibiting STAT3 activation is a promising strategy for cancer therapy, as several cancer types depend on activated STAT3 for their survival. In fact, PYM is currently in phase I/II clinical trials as a standalone agent for the treatment of relapsed CLL and SLL (ClinicalTrials.gov Identifier: NCT01066663). Interestingly, however, it has been observed that STAT3 inhibitors exhibit a synergistic effect with other therapeutic agents in inhibiting tumor stem cells, leading to improved therapeutic indices for these agents.¹⁸

Histone deacetylase (HDAC) enzymes are a class of proteins that play an important role in regulating STAT3 activation.¹⁹ HDACs, along with histone acetyltransferase (HAT), control gene expression, chromatin condensation and play an essential role in transcriptional activation by

regulating acetylation state of histone proteins.²⁰ In addition to histones, the expression levels and acetylation status of several non-histone proteins, including transcription factors (E2F, STAT3, P53, NF- κ B), estrogen receptor (ER α), androgen receptor (AR), α -tubulin, and chaperons (HSP90), are regulated by HDAC and HAT activity.²¹ Due to their critical roles in regulating a wide range of cellular pathways, HDACs are considered as promising drug discovery targets, and their inhibition has emerged as a potential strategy in treating various diseases including neurological diseases, malaria, leishmania and cancer.²² To date, there are four US FDA approved HDAC inhibitors (HDACi), namely, SAHA (suberoylanilide hydroxamic acid, vorinostat) approved in 2006 for relapsed and refractory cutaneous T-cell lymphoma (CTCL),²³ romidepsin (FK228) approved in 2009 for relapsed/refractory peripheral T-cell lymphoma,²⁴ belinostat (PXD101) approved in 2014 for relapsed/refractory peripheral T-cell lymphoma,²⁵ and panobinostat (LBH589) approved in 2015 for treating acute myeloma (Figure 5.2).²⁶ Chidamide (CS055) is another HDACi which is approved in China for treating relapsed/ refractory peripheral T-cell lymphoma. Chidamide is in phase II clinical trials in the US.²⁷ Inhibition and knockdown of class I HDACs have been shown to result in inhibition of STAT3 activation, through upregulation STAT3 Lys685 acetylation and attenuation of STAT3 Tyr705 phosphorylation, resulting in the inhibition of the survival of p-STAT3-positive lymphoma (DLBCL) cells.²⁸ Therefore, targeting STAT3-positive cancer cells with HDACi is another potentially viable therapeutic option for managing these tumors. Inhibition of STAT3 pathway has been mediated by HDACi SAHA through the acetylation on bromodomain protein 4 (BRD4) to down-regulate Leukemia Inhibitory Factor Receptor (LIFR).²⁹

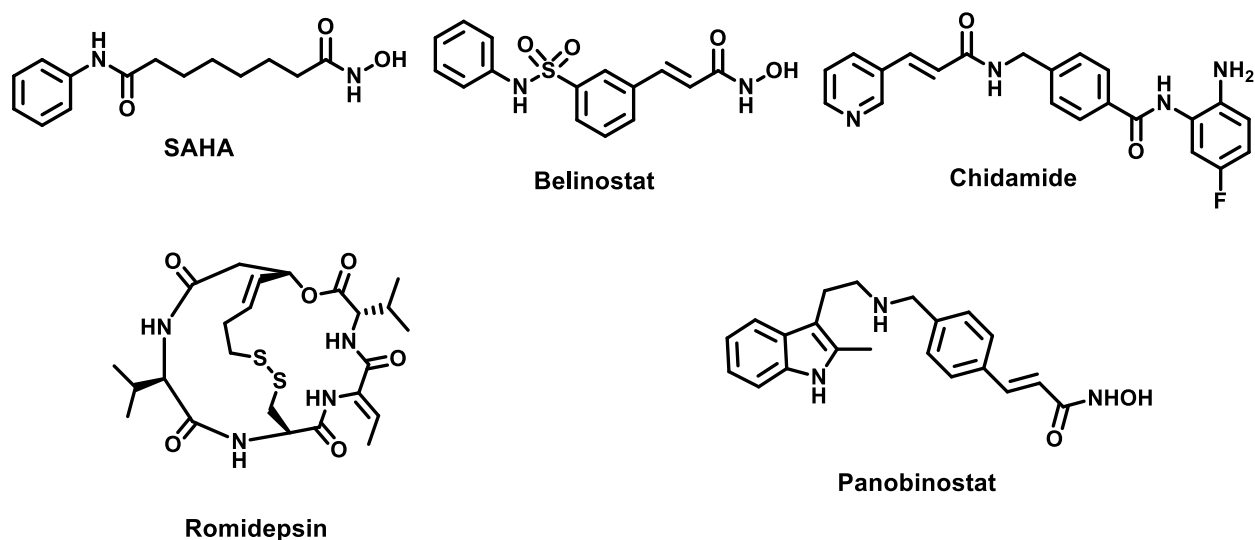


Figure 5.2 Structures of approved HDACi.

We hypothesized that designed multiple ligands comprising PYM and HDAC inhibition chemotype would integrate direct STAT3- and HDAC-inhibition within a single molecular template. These PYM-HDACi compounds are anticipated to be efficient inhibitors of proliferation of tumors which are exquisitely dependent on STAT3 signaling pathway. Herein we demonstrate that PYM-HDACi compounds inhibit representative HDACs, downregulate the expression of selected STAT3 target proteins and are selectively cytotoxic to MDA-MB-231, a triple-negative breast cancer (TNBC) cell that is highly dependent on STAT3 Pathway for its proliferation and metastasis.

5.2 Results and discussion

5.2.1 Design of PYM-HDACi compounds

The three-motif HDACi pharmacophoric model consists of a recognition cap group, linker group, and zinc-binding group (ZBG) (Figure 5.3).³⁰ PYM structure closely resembles the HDACi aryl-derived cap group. Our molecular docking analysis (discussed below) suggested that the PYM halogen group could be replaced by the HDACi linker and ZBG groups without significantly impacting STAT3 binding. Interestingly, the substitution of the PYM halogen group with alkyl, aryl, and ring systems have been shown to be compatible with its biological activities.³¹ Based on these observations, we designed two classes of PYM-HDACi compounds using PYM as a surrogate for HDACi cap group. The restriction on the length of the linker group of class I compounds is based on our previous study which revealed that five and six methylenes are an ideal length for linker group for aryl triazolyl HDACi which inspired the design of this class of compounds.²² Relatedly, the linker group of class II compounds is based on a similar moiety in the approved HDACi belinostat and panobinostat.

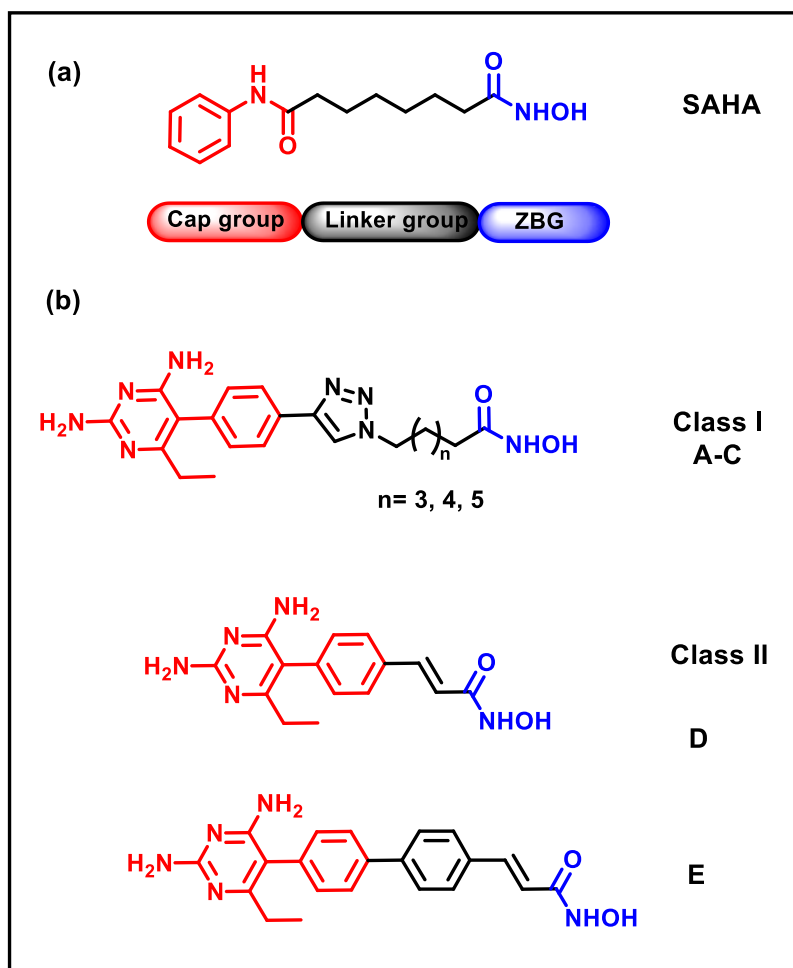
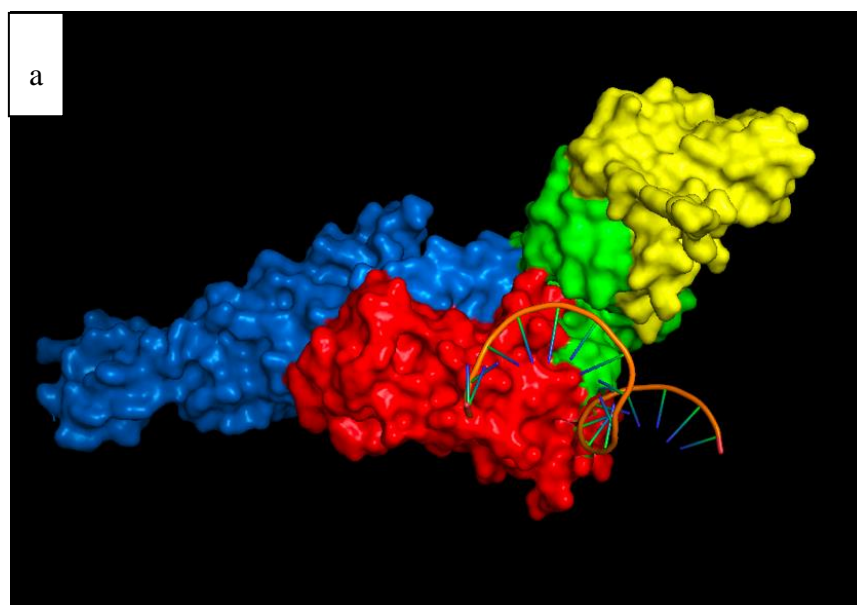


Figure 5.3. (a) Pharmacophoric model of HDACi using SAHA as a prototypical HDACi. (b) Structures of the designed two classes of PYM-HDACi compounds.

5.2.2 Molecular docking study

We first performed an unbiased molecular docking, using AutoDock Vina,³² to determine the potential docking poses of PYM on the structure of STAT3 (PDB ID: 1BG1). The docking outputs revealed that PYM binds to two pockets (P1 and P2) within the DNA binding domain (DBD) and one solvent-exposed, shallow pocket (P3) between the connector (a part of DBD) and the SH2 domains of STAT3 (Figure 5.4). Although PYM is accommodated through stabilizing H-bonding and hydrophobic interactions with key residues within P1, P2 and P3, the binding energies of PYM

at the three sites revealed a strong preference for P2. In P1 and P2, the halogen moiety of PYM is oriented in regions adjoining solvent-accessible grooves/sub-pockets which could potentially accommodate the substitution of the halogen by the HDACi linker and ZBG groups of the designed PYM-HDACi compounds (Figure 5.3). Conversely, in P3, the halogen moiety of PYM is tucked into a shallow pocket, an orientation which may necessitate an extensive change in the binding orientation for the PYM-HDACi to be accommodated at this location. Subsequent docking of a representative class I PYM-HDACi compound **B** revealed that it adopts similar docking poses as PYM at P1 and P2. At P3, however, the phenylpyrimidinediamine end of **B** is forced out into the protein surface to accommodate its HDAC inhibition moiety. Interestingly, **B** binds to P1 and P2 with enhanced binding affinities relative to PYM (Figure 5.4). This observation strongly suggests that the replacement of the PYM halogen group by the designed HDAC inhibiting moieties is compatible with the STAT3 binding attributes of PYM at P1 and P2.



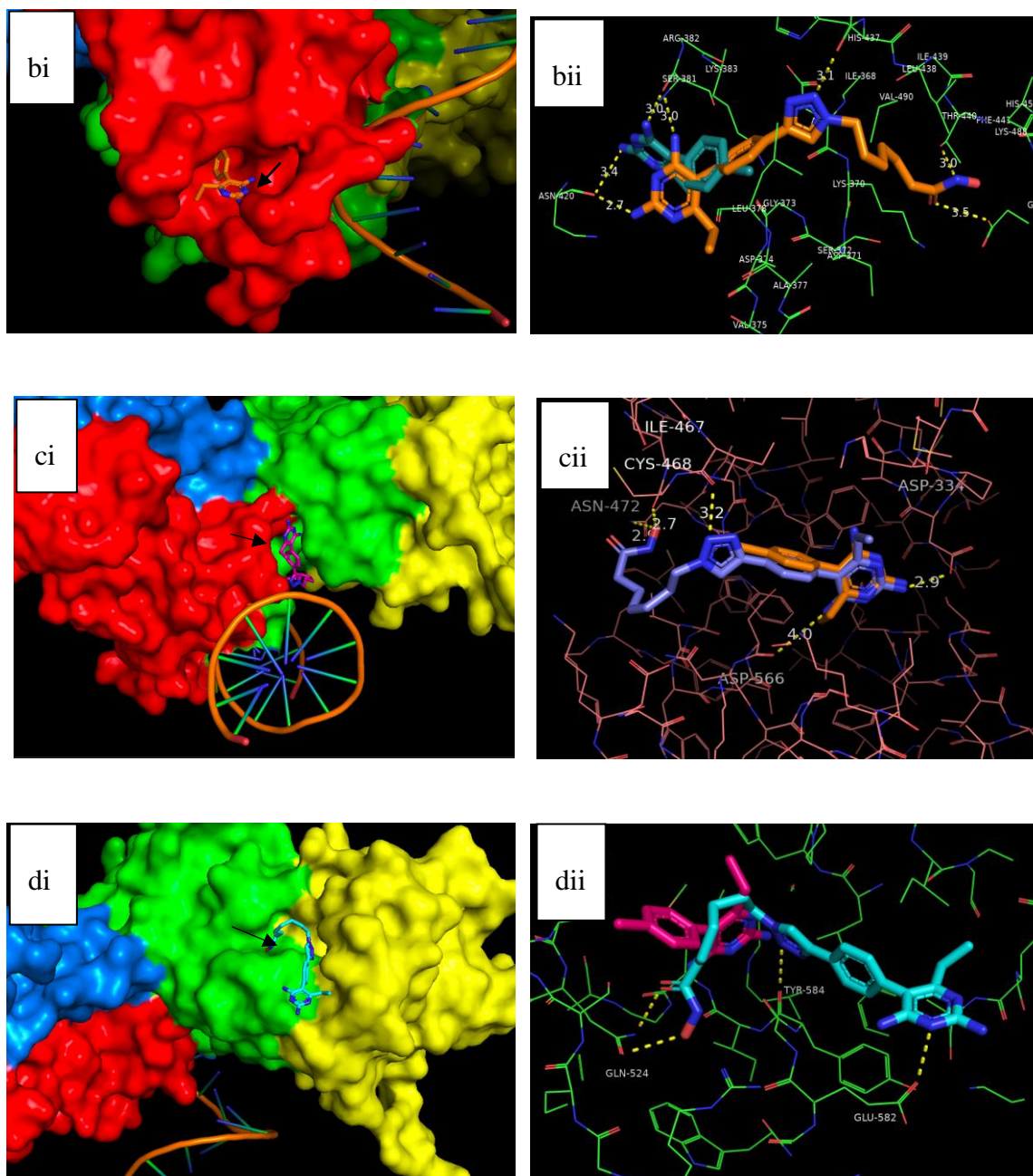
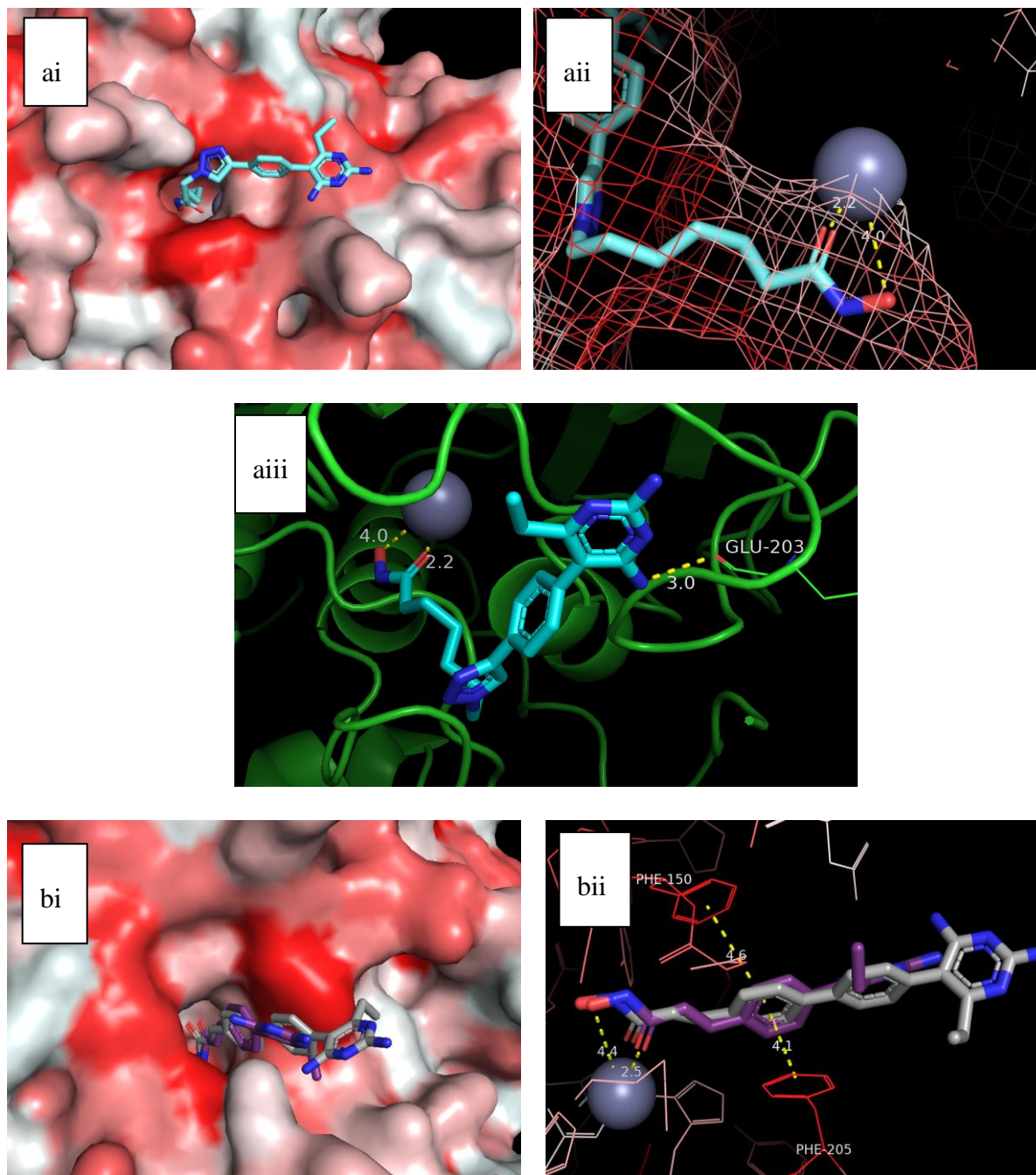


Figure 5.4. Molecular docking of PYM and class I PYM-HDACi compound **B** to STAT3 (PDB:1BG1). (a) The 4 domains of the STAT3 – 4-Helix bundle (blue), β -barrel (red), connector (green) and SH2 (yellow) domains. Docked poses of PYM and class I compound **B** at P1 (bi-ii), P2 (ci-ii) and P3 (di-ii). The binding energies of PYM at P1, P2 and P3 are -5.6kcal/mol, -6.4kcal/mol and -6.0kcal/mol respectively, while **B** bound to P1, P2 and P3 with binding energies of -9.2kcal/mol, -9.3kcal/mol and -7.3kcal/mol, respectively. Note that the binding of compound **B** to P1 could be potentially stabilized by H-bonding interactions with Ser-381, Asn-420, His-437, Thr-440, and Glu-455. In P2, compound **B** could form stabilizing H-bonding interactions with

Asp-334, Ile-467, Cys-468, Asn-472 and Asp-566. In P3, compound **B** could form H-bonding interactions with Gln-524, Glu-582 and Tyr-584.

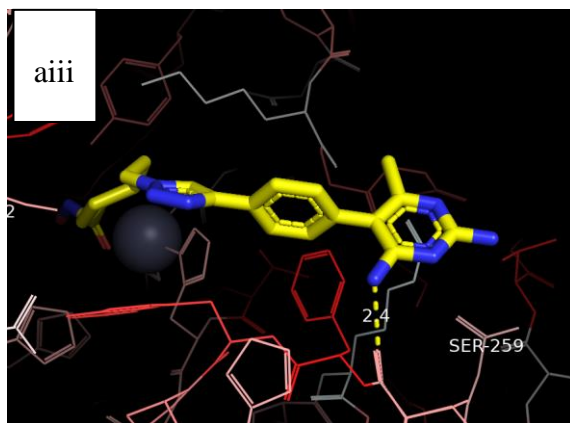
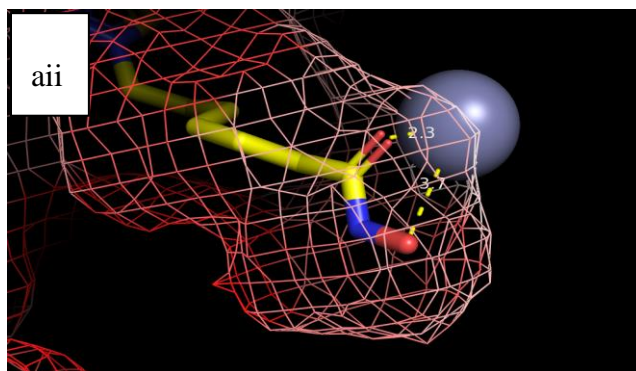
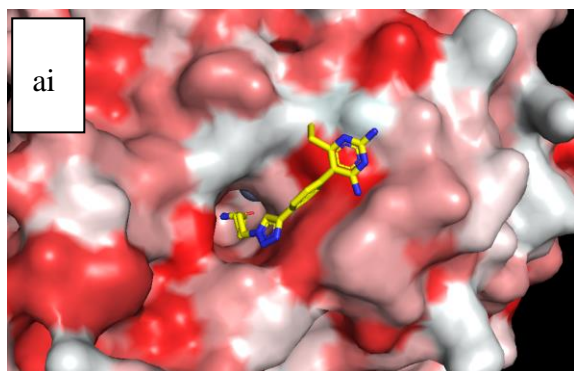
To confirm that the PYM could act as a surrogate for HDACi cap group, we performed molecular docking analyses to interrogate the interaction between the designed PYM-HDACi and selected HDAC isoforms. We observed that, in addition to engaging in stabilizing H-bonding interaction with enzymes' outer rim residues, class I compounds **B** and **C** adopt poses that may allow effective chelation of zinc ion in the active sites of HDAC 1 and HDAC 6 (Figures 5.5 and 5.6). In both HDAC 1 and HDAC 6, class I compound **B** shows strong evidence of zinc ion chelation in the pocket. Presumably due to its flexible linker, class I compound **B** is able to facilely access the pockets of both enzymes, allowing efficient chelation of the active site zinc ion which is a key driver of HDAC 1 binding by both classes of compounds. Relative to class II compounds **D** and **E**, the hydroxamate group of **B** seems to be positioned to allow a more efficient zinc ion chelation at HDAC 1 active site. The somewhat less optimal zinc ion chelation by **D** and **E** could be partially compensated by the possibility of formation of π - π interaction with rings of Phe-155 and Phe-210 (Figure 5.5). Nevertheless, the rigidity of **D** and **E** constrained their phenylpyrimidinediamine moiety to be presented on HDAC 1 surface where there is no obvious prospect for stabilizing interactions. In contrast, the flexibility of the alkyl linker of **B** allows its phenylpyrimidinediamine moiety to be tucked into a hydrophobic patch on HDAC 1 surface where it is further stabilized by a hydrogen bonding interaction with Glu-203. This *in silico* observation suggests that compound **B** could be better accommodated at HDAC 1 active site than **D** and **E**. Interestingly, the extra benzene ring of class II compound **E** is able to overcome the deficiency of class II compound **D** as it enables better zinc ion chelation and optimal binding within hydrophobic regions at outer rims guarding the active sites of HDAC 6. Specifically, compound **E** could potentially form two

π - π interactions with Phe-202 and Trp-261 while compound **D** docked poses could only support one π - π interaction with Phe-202. Also, compound **B** could form H-bonding with the amide backbone of Ser-259 at the enzyme rim. The extra interactions displayed by **B** and **E** could confer on them better binding affinities for HDAC 6 relative to compound **D**.



*Note that the red portion of the protein surface indicates hydrophobic and white area indicates the hydrophilic areas.

Figure 5.5. Docked poses of PYM-HDACi at the active sites of HDAC 1 (PDB:5ICN). Grey sphere represents zinc ion in the active site of HDAC isoform. (ai-iii) Docked pose of class I compound **B** on HDAC 1. (bi-ii) Overlay of the docked poses of class II compounds **D** (in purple) and **E** (in grey) on HDAC 1. The compounds are accommodated at enzyme's active site through a combination of zinc chelation, H-bonding and hydrophobic interactions.



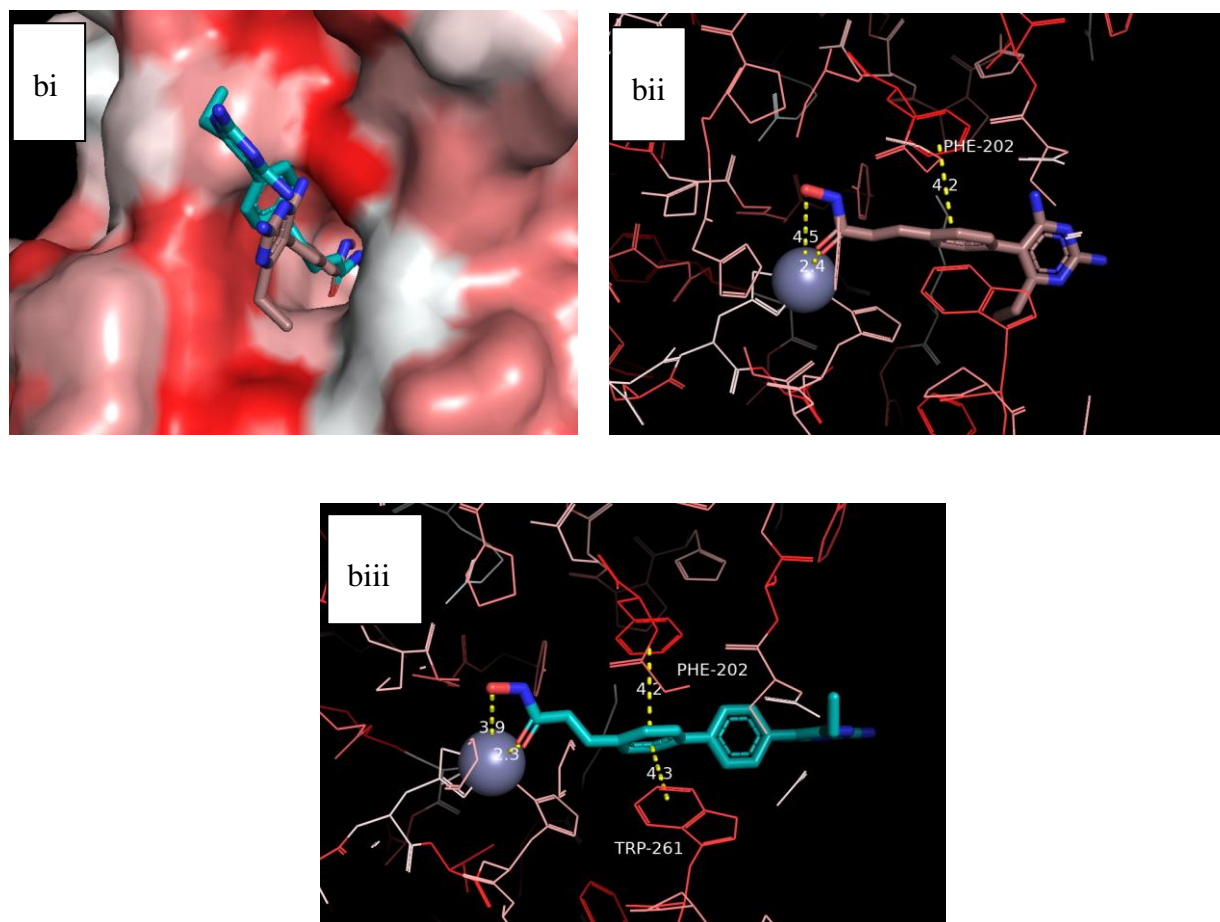


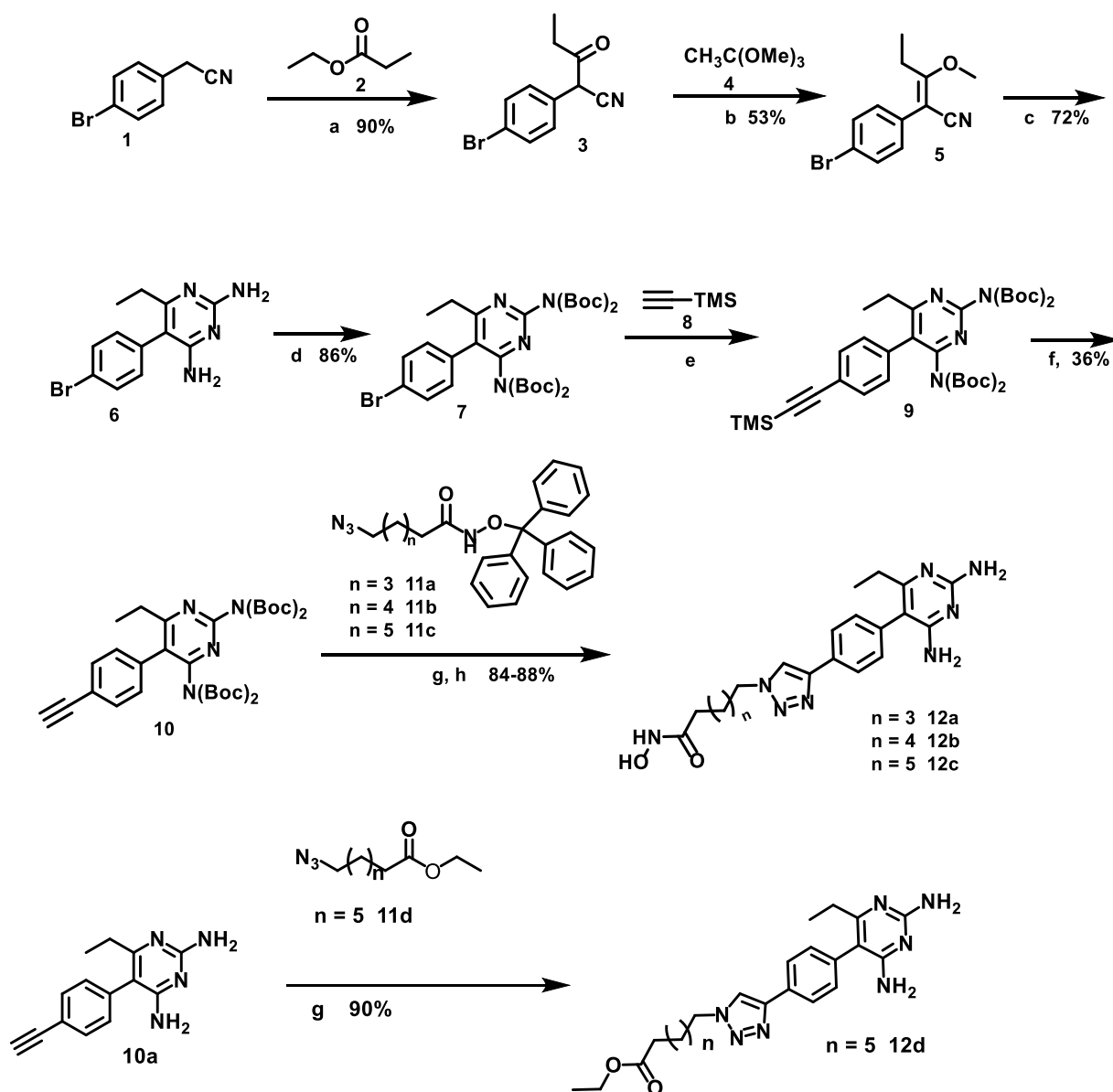
Figure 5.6. Docked poses of PYM-HDACi at the active sites of HDAC 6 (PDB:5G0G). Grey sphere represents zinc ion in the active site of HDAC isoform. (ai-iii) Docked pose of class I compound **B** on HDAC 6. (bi-iii) Overlay of the docked poses of class II compounds **A** (color in light pink) and **B** (color in cyan) on HDAC 6. The compounds are accommodated at enzyme's active site through a combination of zinc chelation, H-bonding and hydrophobic interactions. *Dotted lines indicate interatomic distance for H-bonding and stacking interaction.

Based on evidence from the previous molecular docking analysis on human DHFR (hDHFR),³³ it seemed that the replacement of the halogen group of PYM may not be compatible with DHFR binding. Nevertheless, we docked these compounds against the structure of hDHFR (PDB code 1U72). We observed that the PYM moiety of the PYM-HDACi compounds bind hDHFR with similar orientation as PYM (Figure 5.S1). However, the PYM-HDACi compounds'

pyrimidinediamine head does not gain access into the hDHFR binding pocket as efficiently as PYM, largely due to the interruption caused by their HDACi moiety. This result suggests that the docked poses of PYM-HDACi may not be favorable thus making DHFR inhibition a less likely attribute of the PYM-HDACi compounds.

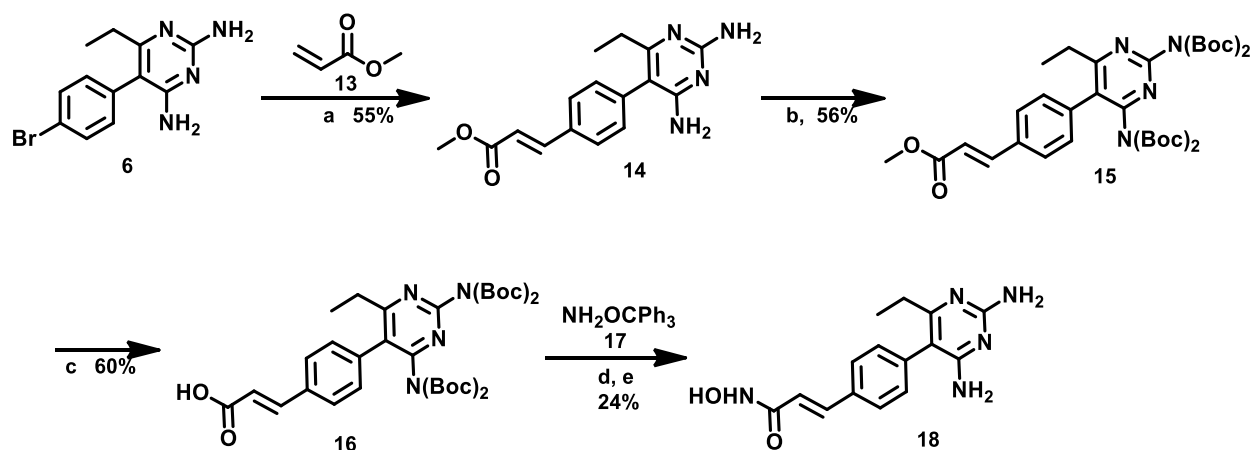
5.2.3 Chemistry

To synthesize the class I PYM-HDACi compounds, 4-bromophenyl acetonitrile **1** was reacted with ethyl propanoate **2** under basic condition to yield β -ketonitrile³⁴ **3** which was then converted to the methoxyphenol **5** using trimethyl orthoformate **4**.³⁵ Pyrimidine ring was formed through cyclization reaction of **5** with guanidine hydrochloride to afford compound **6**.³¹ Boc protection of amine^{36,37} groups of **6**, to give **7**, followed by sonogashira reaction with trimethylsilylacetylene **8** resulted in compound **9**.³⁸ Trimethylsilyl group was removed using potassium carbonate to afford alkyne **10**. Subsequently, copper (I) catalyzed azide-alkyne-cycloaddition (AAC)³⁹ reaction between alkyne **10** and compounds **11a-c**,⁴⁰ followed by removal of trityl- protecting group resulted in the final class I compounds **12a-c**. Control compound **12d** was similarly synthesized from Boc deprotected compound **10a** and azido ester **11d** (Scheme 5.1).



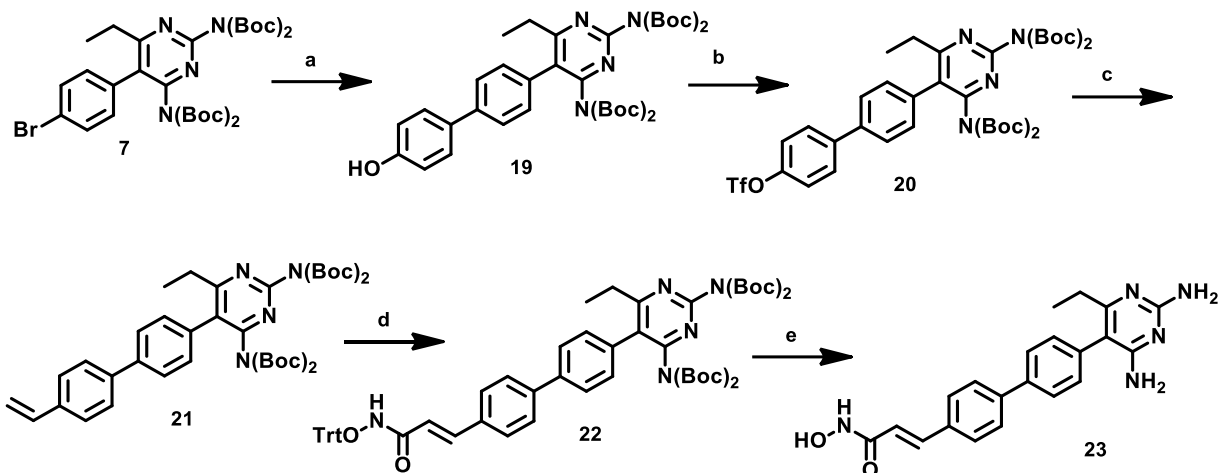
Scheme 5.1. (a) Potassium tert-pentylate 25% in toluene, THF, rt, 20 min, 90%; (b) 6 h, neat reaction 120 °C, 53%; (c) Guanidine hydrochloride, NaHCO₃, DMSO, 100 °C, 6 h, 72%; (d) Boc₂O, THF, DMAP, 45 °C, THF, 86%; (e) Hunig's base, Pd(PPh₃)₄, acetonitrile, CuI, 75 °C, overnight; (f) K₂CO₃, MeOH, 0 °C, 2 h, 36% (e and f); (g) CuI, Hunig's base, rt, overnight; (h) TFA, DCM, rt, 2 h, 84-88% (g and h).

To synthesize the monophenyl class II PYM-HDACi compound, a Heck reaction was performed on intermediate **6** with methyl acrylate **13**.⁴¹ After the Boc protection to give intermediate ester **15** which was subsequently converted to carboxylic acid **16** using sodium hydroxide.⁴² The desired hydroxamic acid compound **18** was synthesized through the coupling of carboxylic acid **16** and *O*-trityl hydroxylamine **17** followed by trityl deprotection (Scheme 2).⁴⁰



Scheme 5.2 . (a) Tri-*O*-tolyl phosphine, Pd(OAc)₂, TEA, DMF, 120 °C, overnight, 55%; (b) Boc₂O, THF, DMAP, 45 °C, THF, 56%; (c) NaOH, H₂O, Dioxane, 20 °C, 12 h, 60%; (d) EDCI, HOBT, DCM, rt, 6 h; (e) TFA, DCM, rt, 2 h, 24% (d and e).

To synthesize the biphenyl class II PYM-HDACi compound, a Suzuki coupling reaction of Boc protected intermediate **7** with 4-hydroxyphenyl boronic acid furnished compound **19** which was converted to triflate compound **20** using standard protocol. Suzuki coupling between compound **20** and potassium vinyl trifluoroborate furnished aryl vinyl compound **21**. Cross metathesis reaction of **21** with *N*-(trityloxy)acrylamide using Hoveyda-Grubbs 2nd generation catalyst⁴³ afforded compound **22** which upon treatment with TFA and TIPS furnished the desired class II compound **23** (Scheme 3).



Scheme 5.3. (a) 4-hydroxyphenyl boronic acid, $\text{Pd(PPh}_3)_4$, Cs_2CO_3 , 80 °C, 4 h, 81%; (b) Trifluoromethanesulfonic anhydride, pyridine, -20 °C, 1 h, 77%; (c) $\text{Pd(PPh}_3)_4$, Potassium vinyl trifluoroborate, Cs_2CO_3 , DMF, 80 °C, 4 h, 90%; (d) Hoveyda-Grubbs 2nd generation catalyst, N-[Tris(hydroxymethyl)-methyl]acrylamide, DCM, 33°C, overnight, 33%; (e) TFA, TIPS, rt, 2 h, 80%.

5.2.4 HDAC inhibition study

PYM-HDACi compounds were tested against HDAC isoforms 1, 6 and 8. These compounds inhibited the HDAC isoforms tested with IC_{50} s ranging from low nanomolar to micromolar. Specifically, class I compounds **12a-c** broadly inhibited HDACs 1 and 6 but are less potent against HDAC 8 (Table 5.1). Within this class, there is a linker length dependency in HDAC 1 and 6 inhibition potency which optimal for compound **12b**. The monophenyl class II compound **18** is a relatively weaker HDACi which displayed the strongest inhibitory effect towards HDAC 6. The inclusion of an additional phenyl ring, however, broadened and enhanced potency as the biphenyl class II compound **23** inhibited both HDAC 6 (Table 5.1). This HDAC inhibition pattern is in agreement with the predictions from the *in silico* docking study shown in Figures 5.5 and 5.6.

Table 5.1: HDAC inhibition activities of PYM-HDACi compounds (IC₅₀ in μM).^a

Compound	HDAC1 (μM)	HDAC6 (μM)	HDAC8 (μM)
12a	0.26	0.046 \square	2.8 \square
12b	0.045 \square	0.017 \square	0.78 \square
12c	0.21	0.021	NT ^b
18	2.2 \square	0.40 \square	1.8 \square
23	3.7	0.073	NT
SAHA	0.042 \square	0.034 \square	2.8 \square

^aPerformed through contractual agreement with BPS Bioscience. ^bNT: Not Tested.

5.2.5 Anti-proliferative activity

The PYM-HDACi compounds were tested against three transformed and one normal cell lines with SAHA, an FDA approved HDACi, as a positive control. The chosen transformed cell lines were lung (A549), ER-positive (MCF-7) and TNBC (MDA-MB-231) breast cancer cell lines, while monkey kidney epithelial cell (VERO) was selected as the nontransformed cell line. Our choice of the transformed cell lines is informed by the STAT3 pathway dependency of these cell lines. TNBCs, which account for 20% of all breast cancer incidence, lack Estrogen Receptor (ER), Human Epidermal Growth Factor receptor 2 (HER2), and Progesterone Receptor (PR).⁴⁴ TNBCs are characterized by high metastasis, chemo-resistance, and poor prognosis with a lower five-year survival rate relative to all the other non-TNBCs.⁴⁵ Currently, there are no efficient targeted

treatment options for TNBC. Therefore, identification of new drug candidates for TNBC is urgently warranted.

STAT3 plays a critical role in TNBCs, as it regulates several genes vital to cell survival, metastasis, and invasiveness.⁴⁶ Constitutive activation of STAT3 in MDA-MB-231 cells promotes cell survival by regulating the expression of Bcl-2, Bcl-xL, Survivin, cyclin D1, c-Myc, and Mcl-1.⁴⁷ Conversely, A549 and MCF-7 cell lines have very low levels of constitutively active STAT3.⁴⁸⁻⁵³ Due to their combined effect on inhibition of STAT3 pathway, PYM-HDACi compounds are expected to be more cytotoxic to STAT3-dependent cells such as MDA-MB-231 while somewhat less toxic to cell lines, such as A549 and MCF-7, with low levels of constitutively active STAT3.

We observed that the two classes of the PYM-HDACi compounds have distinct effects on the viability of the cell lines tested. Class I compounds **12a-c** showed preferential cytotoxicity to the STAT3-dependent MDA-MB-231 cells with linker-length-dependent potency that also closely tracks with their HDAC inhibition potency. Specifically, compound **12a** is only cytotoxic to MDA-MB-231 with an IC₅₀ of 38.38 ± 1.0 µM. In addition to being more potent than **12a** against MDA-MB-231, compounds **12b** and **12c** are also cytotoxic toward A549 and MCF-7 cells. However, **12b** and **12c** displayed >3-5-fold selectivity for MDA-MB-231 relative to the other tested cell lines (Table 5.2). By testing the intermediate ester **12d**, we subsequently confirmed that the modification that we introduced did not abolish the independent antiproliferative effect of PYM. In fact, compound **12d** is 2.5-4.6-fold more potent than PYM against the two cell lines for which PYM IC₅₀s were measurable within the concentration range we used (Table 5.2).

Presumably, due to its poor HDAC inhibitory activity and/or high hydrophilicity (CLogP = 0.877) which may negatively impact cell penetration, compound **18** did not show anti-proliferative activity towards all the cell lines tested. The additional phenyl ring in compound **23**, which resulted in the enhancement of its HDAC6 inhibition activity relative to **18** and higher hydrophobicity

(CLogP = 2.765), also results in it having broad antiproliferative activities against the tested cell lines. However, **23** displayed little or no cell line selectivity (Table 5.2) which suggests that its antiproliferative activity may be largely due to HDAC inhibition. Although all the PYM-HDACi compounds are less potent relative to SAHA, the control HDACi, the selectivity of the class I compounds **12a-c** toward STAT3-dependent MDA-MB-231 suggest the contribution of the inhibition of STAT3 pathway to the anti-proliferative activities of these compounds since most non-targeted HDACi are incapable of tumor cells selectivity, a cause of their off-target toxic effects.²⁰ Interestingly, a combination therapy experiment whereby we used fixed concentration of of PYM (100 μ M, approx $\frac{1}{2}$ IC₅₀ against MDA-MB-231 cells) and varying the concentrations of SAHA showed only slight to moderate improvements in the potency, relative to SAHA as a standalone agent, against all cell lines tested, including the non-transformed Vero cells. This combination did not result in MDA-MB-231 cell-selectivity that we noticed in the designed multiple ligands PYM-HDACi **12b** and **12c**.

Table 5. 2. Anti-proliferative activity of PYM-HDACi compounds (IC₅₀ in μ M).

Compound	A549 (μ M)	MCF-7 (μ M)	MDA-MB-231 (μ M)	VERO (μ M)
12a	NI	NI	38.4 \pm 1.0	ND
12b	65.5 \pm 4.6	57.3 \pm 3.4	12.2 \pm 2.2	40.3 \pm 3.6
12c	88.4 \pm 10.5	83.3 \pm 15.5	21.4 \pm 3.7	NI
12d	113.8 \pm 4.0	96.6 \pm 6.9	94.9 \pm 9.7	112.7 \pm 8.2
18	NI	NI	NI	ND
23	10.0 \pm 1.9	9.3 \pm 1.6	5.4 \pm 1.2	6.9 \pm 0.4
PYM	NI	453	238	NI
SAHA	15.7 \pm 1.0	3.5 \pm 0.05	3.4 \pm 0.2	4.5 \pm 0.7
PYM + SAHA	10.2 \pm 0.9	2.3 \pm 0.46	1.9 \pm 0.5	1.3 \pm 0.1

*Each value is obtained from a duplicate of three simultaneous experiments. NI: No Inhibition. ND: Not Determined at a maximum concentration of 100 μ M. Comb. means SAHA with variable concentration combined with 100 μ M PYM

5.2.6 Intracellular target validation

To determine the contributions of HDAC and STAT3 pathway inhibition to the antiproliferative activities of PYM-HDACi compounds, we used immunoblotting to investigate the MDA-MB-231 cells response to one of the lead compounds **12c** using SAHA and PYM as positive controls for HDAC and STAT3 inhibition respectively. For HDAC inhibition, we monitored histone 4 (H4) and tubulin acetylation states as markers for HDACs 1 and 6 intracellular inhibition activities, respectively.^{54,55} GAPDH expression was used as a protein loading control. When exposed to the cells at $\frac{1}{2}$ -IC₅₀, IC₅₀ and 2x-IC₅₀, **12c** induced accumulation of acetylated H4 and acetylated tubulin. Similarly, SAHA at 1.5 μ M induced H4 and tubulin hyperacetylation (Figure 5.7). PYM has no effect on the acetylation status of tubulin and H4. This result strongly suggests that the PYM-HDACi **12c** inhibits these HDACs intracellularly, an attribute which contributes to their antiproliferative activity.

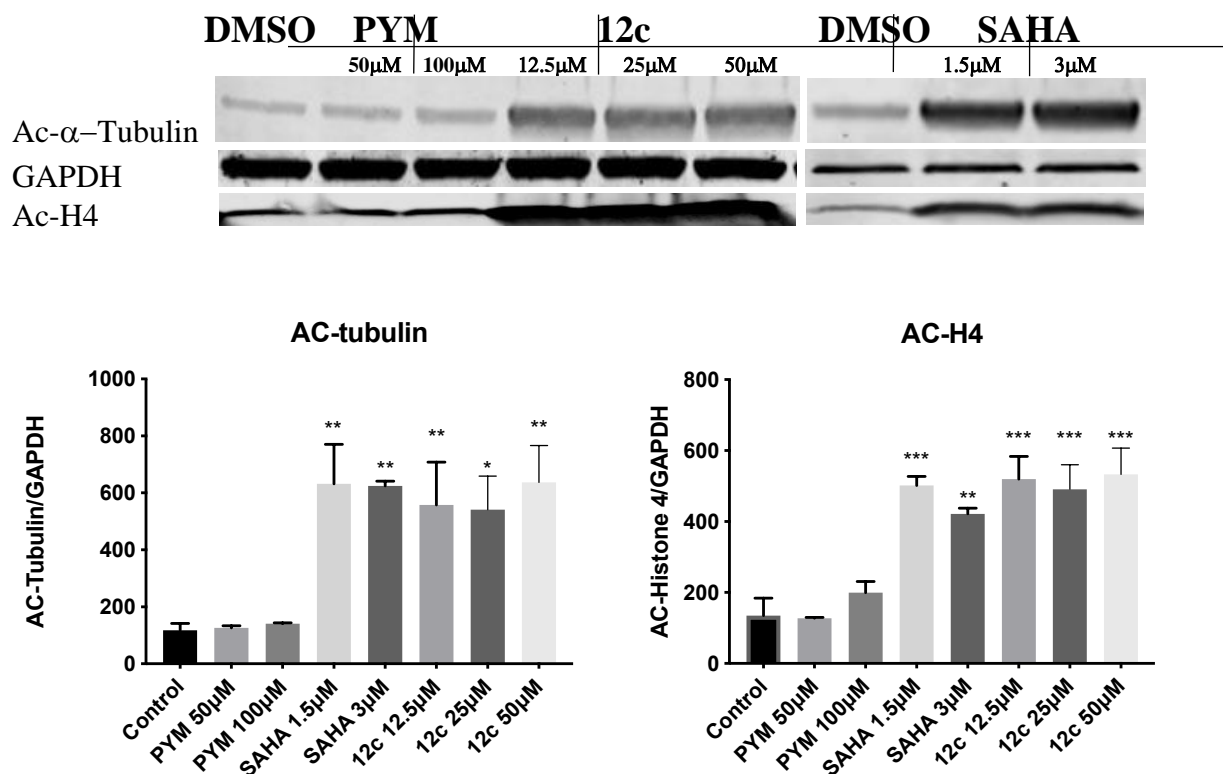


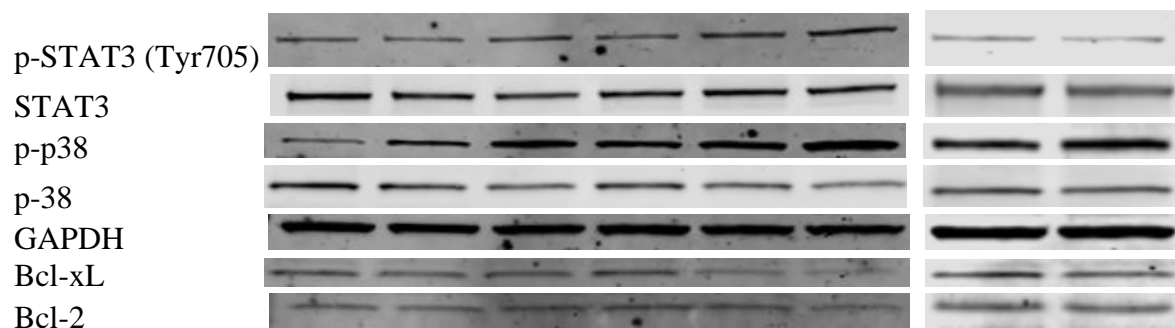
Figure 5. 7. The Western blot analysis. (a) Immunoblotting of the acetylation status of tubulin and H4 of MDA-MB-231 treated with DMSO, PYM, SAHA, and **12c** for 4 h. Cells were serum-starved 24 h prior to the treatment. Acetylated α -tubulin and acetylated H4 are upregulated by SAHA and **12c** but not PYM. (b) Quantification of acetylated α -tubulin and acetylated H4 obtained by averaging data from two independent experiments. (Bars show mean plus standard deviation; * $P < 0.05$; ** $P < 0.0021$; *** $P < 0.0002$)

To elucidate the effect of the PYM-HDACi compounds on the STAT3 pathway, we probed the effects of **12c**, SAHA and PYM on the intracellular expression of STAT3, p-STAT3, p38, p-p38, Bcl-2, and Bcl-xL. Bcl-2 and Bcl-xL are anti-apoptotic genes whose expressions are upregulated by constitutive activation of STAT3.⁵⁶⁻⁵⁸ Conversely, inhibition of STAT3 upregulates the intracellular level of p-p38.⁵⁹⁻⁶¹ As stated earlier, HDACi inhibits STAT3 pathway through direct downregulation of p-STAT3. The exact mechanism of the inhibition of

the STAT3 pathway by PYM has not been fully elucidated. However, it has been recently shown that PYM is a direct inhibitor of STAT3 transcriptional activity as PYM could upregulate p-STAT3 cellular levels while downregulating the expression of p-STAT3 target genes, including Bcl-2 and Bcl-xL, in TNBC cell lines.⁶² We observed that **12c** (at 1/4th-, 1/2- and 1x-IC₅₀) and SAHA (at 1/4th- and 1/2-IC₅₀) caused concentration-dependent upregulation of p-p38 and downregulation of Bcl-xL in MDA-MB-231 cells. Within this concentration range, **12c** slightly downregulates Bcl-2 levels while SAHA caused no statistically relevant changes to the intracellular levels of Bcl-2. PYM (at 50 μM and 100 μM) has a similar effect as SAHA, causing concentration-dependent upregulation of p-p38 and Bcl-xL and no effect on Bcl-2 levels (Figures 5.8a and 5.8b). Interestingly, the effects of **12c** and PYM on p-STAT3 levels are closely aligned as they both caused upregulation of p-STAT3 while SAHA cause a slight downregulation of p-STAT3. The observed PYM-induced upregulation of p-STAT3 is in agreement with a previous observation.⁶² To further confirm this effect on STAT3 pathway, we investigated the effects of **12c**, SAHA and PYM on the intracellular levels of the cyclin D1, a downstream protein of STAT3 pathway.⁴⁷ We observed that cyclin D1 is significantly downregulated with **12c**, SAHA and PYM at approx. 1/2 - and 1x-IC₅₀ concentration (Figures 5.9a and 5.9b). Collectively, this data suggests that the intracellular inhibitions of HDACs and the STAT3 pathway contribute to the anti-proliferative activity of the PYM-HDACi compounds **12c**. However, the mechanism of STAT3 pathway inhibition of **12c** is distinct from that of prototypical HDACi and very similar to that of STAT3 inhibitor template PYM. This distinction could be the basis for the TNBC cell selectivity of the PYM-HDACi.

a.

DMSO	PYM		12c			SAHA	
	50μM	100μM	5μM	12.5μM	25μM	0.8μM	1.6μM



b.

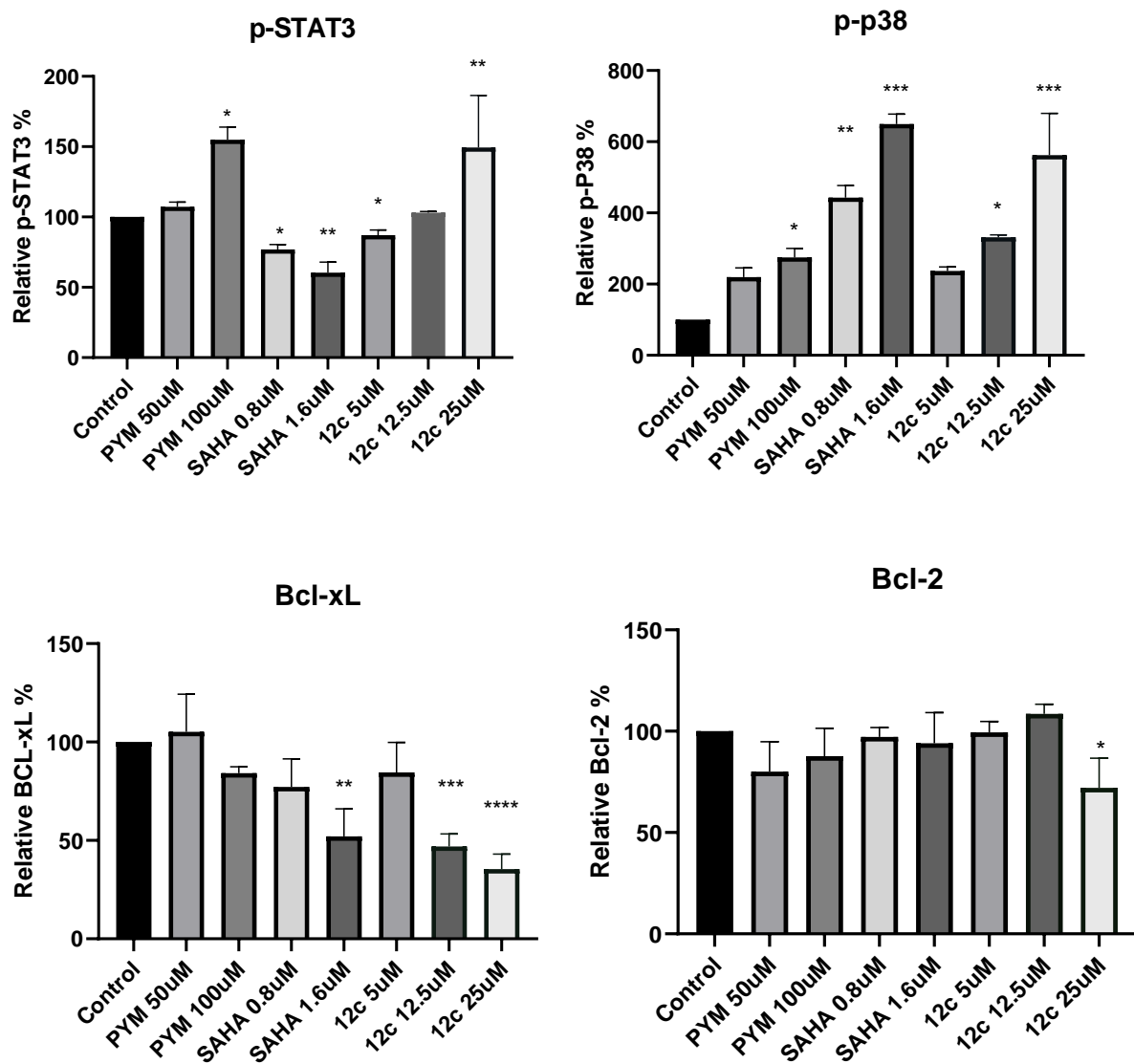
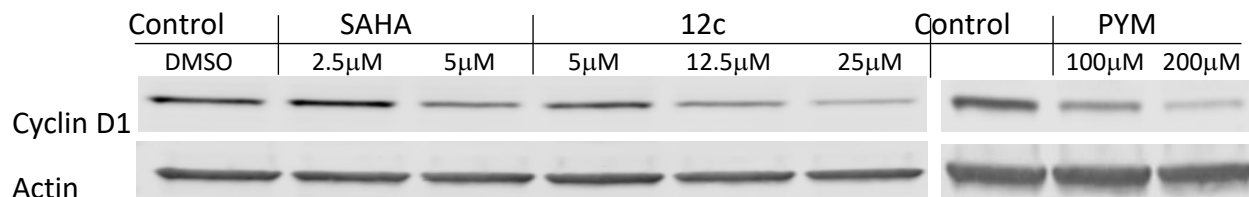


Figure 5.8. (a) Western blot analysis of the effects of compounds on the STAT3 pathway in MDA-MB-231 cells. Cells were serum-starved for 24 h prior to treatment with the tested agents such that

the final DMSO content in the media is 0.1%. Cells were treated with the tested agents for 24 h. Images show the effects of DMSO, PYM, **12c** and SAHA on the intracellular levels of selected STAT3 pathway markers. (b) Quantification of the Western blots data probing for the effects of PYM, SAHA, and **12c** on the STAT3 pathway in MDA-MB-231 cells. (Bars show mean plus standard deviation; * $P < 0.05$; ** $P < 0.0021$; *** $P < 0.0002$).

a.



b.

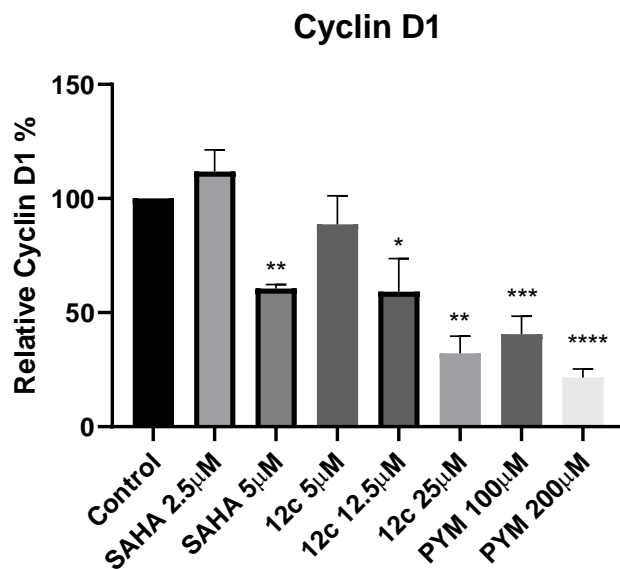
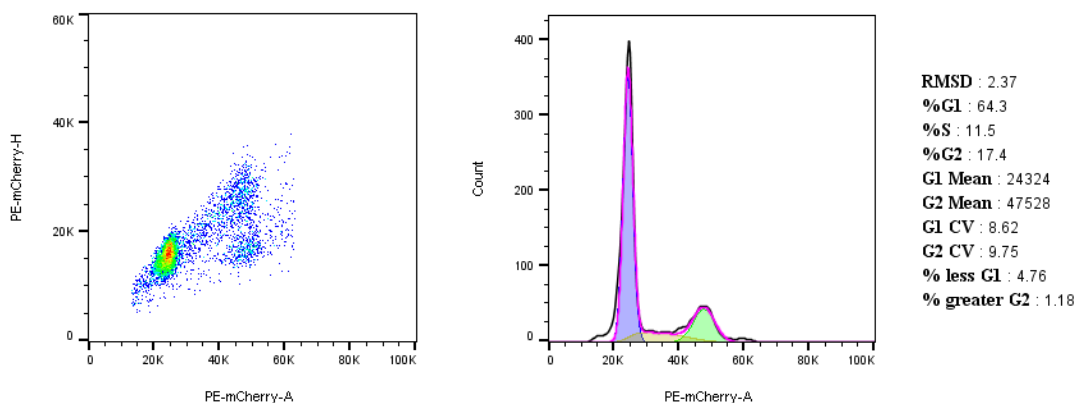


Figure 5.9. Western blot analysis of Cyclin D1 expression level after treatments. (a) Crops of bands of Actin and Cyclin D1, and (b) quantification of the Western blots data revealed the effects of **12c** on the cyclin D1 expression MDA-MB-231 cells. Experimental conditions are the same for the data shown in Figure 5.8. (Bars show mean plus standard deviation; * $P < 0.05$; ** $P < 0.0021$; *** $P < 0.0002$; **** $P < 0.00001$).

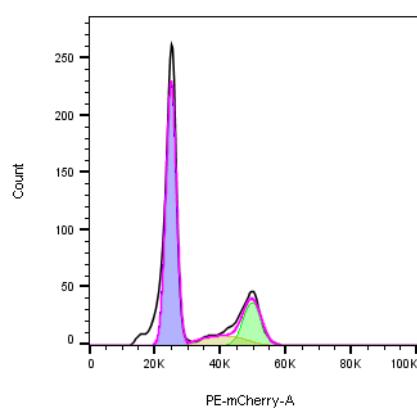
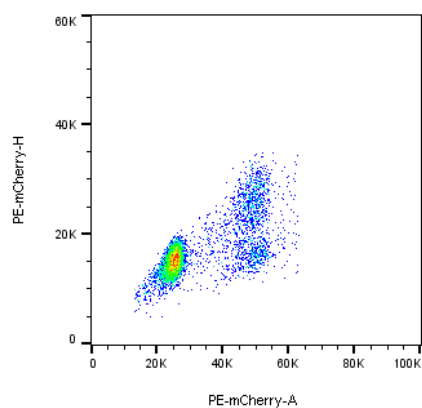
5.2.7 Flow Cytometry for Cell Cycle Analysis.

We then performed cell cycle analysis to determine the effects of PYM-HDACi **12c**, **12b** and SAHA on MDA-MB-231 cell cycle distribution. We observed that the effects of **12c** (12.5 and 25 μ M), **12b** (15 μ M) and SAHA (5 μ M) on cell cycle are very similar as they induced significant G2 phase arrest (Figure 5.10 and Figure 5S.2). Previous studies have shown that SAHA caused G2 arrest when exposed to breast cancer cells at concentrations above 3.0 μ M⁶³. The G2 cell cycle arrest induced by these compounds suggests that in addition to their cytotoxicity effects, they also induce MDA-MB-231 cell apoptosis.

A.

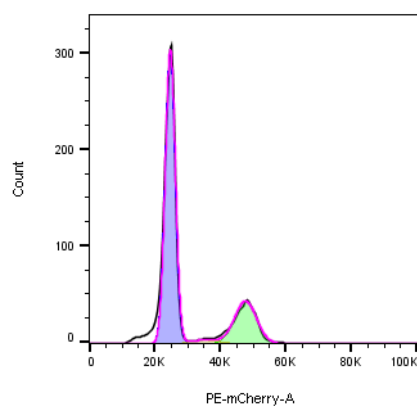
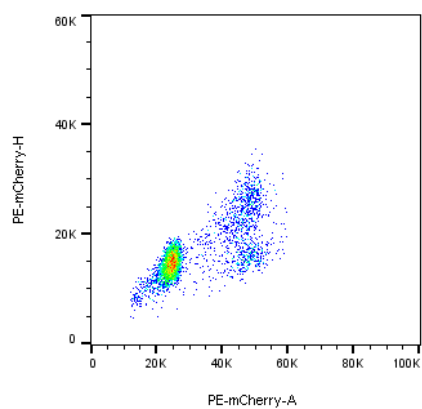


B.



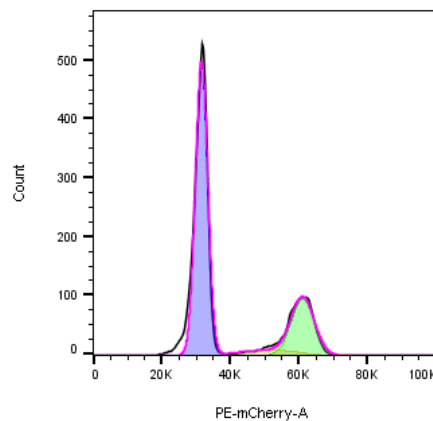
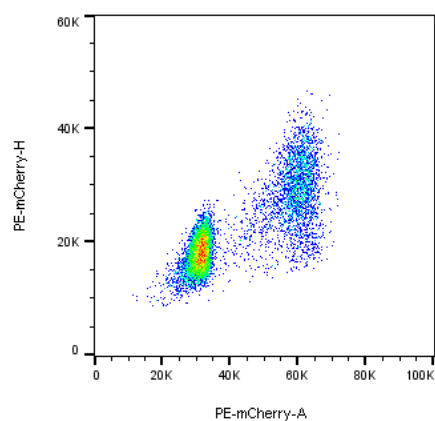
RMSD : 1.78
 %G1 : 65.1
 %S : 8.97
 %G2 : 18.2
 G1 Mean : 24902
 G2 Mean : 49482
 G1 CV : 9.00
 G2 CV : 7.80
 % less G1 : 7.77
 % greater G2 : -0.47

C.



RMSD : 1.54
 %G1 : 70.6
 %S : 1.63
 %G2 : 22.1
 G1 Mean : 24574
 G2 Mean : 47461
 G1 CV : 8.70
 G2 CV : 9.79
 % less G1 : 5.44
 % greater G2 : 0.54

D.



RMSD : 2.99
 %G1 : 66.8
 %S : 5.17
 %G2 : 24.0
 G1 Mean : 31449
 G2 Mean : 60839
 G1 CV : 7.92
 G2 CV : 7.71
 % less G1 : 4.11
 % greater G2 : -0.49

Figure 5.10. Effect of (a) DMSO control, (b) **12c** (12.5 μ M), (c) **12c** (25 μ M), and (d) SAHA (5 μ M) on MDA-MB-231 cell cycle progression.

5.3 Conclusion

We disclosed in this study two classes of dual-acting compounds designed to inhibit HDACs and the STAT3 pathway. We observed that the class I PYM-HDACi compounds **12a-c** potently inhibit HDACs 1 and 6 in cell-free assays and are preferentially cytotoxic to MDA-MB-231, a TNBC cell line that is highly STAT3-dependent. Moreover, target validation studies revealed that a representative compound **12c** elicited a signature of HDAC and STAT3 pathway inhibition intracellularly. In addition, **12b** and **12c** show significant selective cell cytotoxicity to TNBC. Overall, these compounds show promise as leads to develop targeted therapy for TNBC.

5.4 Experimental section

5.4.1 Materials and methods

4-Bromophenyl acetonitrile, ethyl propionate, O-tritylhydroxylamine, methyl acrylate, were purchased from Sigma-Aldrich. Trimethylsilylacetylene was purchased from Alfa Aesar. All commercially available starting materials were used without purification. Reaction solvents were high performance liquid chromatography (HPLC) grade or American Chemical Society (ACS) grade and used without purification. Analtech silica gel plates (60 F254) were used for analytical TLC, and Analtech preparative TLC plates (UV 254, 2000 μ m) were used for purification. UV light and anisaldehyde/iodine stain were used to visualize the spots. 200-400 Mesh silica gel was used in column chromatography. Nuclear magnetic resonance (NMR) spectra were recorded on a

Varian-Gemini 400 MHz, Bruker 500 MHz or 700 MHz magnetic resonance spectrometer. ^1H NMR Spectra were recorded in parts per million (ppm) relative to the residual peaks of CHCl_3 (7.24 ppm) in CDCl_3 or CHD_2OD (4.78 ppm) in CD_3OD or $\text{DMSO-}d_5$ (2.49 ppm) in $\text{DMSO-}d_6$. ^{13}C spectra were recorded relative to the central peak of the CDCl_3 triplet (77.0 ppm) or CD_3OD septet (49.3 ppm) or $\text{DMSO-}d_6$ septet (39.7 ppm) and were recorded with complete hetero-decoupling. Original 'fid' files were processed using MestReNova LITE (version 5.2.5-5780) program. High-resolution mass spectra were recorded at the Georgia Institute of Technology mass spectrometry facility in Atlanta.

2-(4-Bromophenyl)-3-oxopentanenitrile (**3**). To a solution of 4-bromophenyl acetonitrile **1** (1.4 g, 7 mmol) in THF (10 mL), potassium tert-pentylate **2** (25% in toluene) (12.2 mL, 21 mmol) was added dropwise, followed by addition of ethyl propionate. The reaction mixture was stirred for 20 min, and then neutralized (approx. pH=7) with 1N HCl to. Water (5 mL) and EtOAc (10 mL) were added and the two layers separated. The organic layer was washed with water (10 mL) and brine (10 mL) and dried over Na_2SO_4 . The crude was purified by column chromatography on silica gel, eluting with hexane: EtOAc 4:1, to furnish compound **3** (1.6 g, 90%) as yellow oil. ^1H NMR (400 MHz, CD_3OD) δ 7.62 – 7.53 (m, 2H), 7.49 – 7.41 (m, 2H), 2.71 – 2.55 (m, 2H), 1.31 – 1.23 (m, 3H). ^{13}C NMR (101 MHz, CD_3OD) δ 173.5, 132.1, 131.9, 130.9, 130.0, 129.0, 120.0, 119.4, 85.6, 28.8, 11.2. HRMS (ESI) m/z Calcd. for $\text{C}_{11}\text{H}_{10}\text{NO Br}$ $[\text{M}+\text{H}^+]$: 250.9946, found 250.9946.

2-(4-Bromophenyl)-3-methoxypent-2-enenitrile (**5**). A mixture of compound **3** (3.1 g, 12.5 mmol) and trimethyl orthoacetate **4** (12.3 mL, 96.5 mmol) was heated at 107 °C for 6 h.

Dichloromethane (DCM) (15mL) was added and the mixture was washed with water (15 mL), NaHCO₃ (15 mL), and brine (15 mL). The organic layer was dried over Na₂SO₄ and the crude was purified by column chromatography on silica gel, eluting with hexanes:EtOAc 3:1, to furnish compound **5** (1.1 g, 33%) as yellow oil. ¹H NMR (400 MHz, CDCl₃) δ 7.57 – 7.35 (m, 4H), 2.77 (q, *J* = 7.6 Hz, 2H), 1.32 – 1.26 (m, 3H). ¹³C NMR (101 MHz, CDCl₃) δ 173.1, 131.4, 130.8, 129.8, 120.7, 119.7, 91.5, 56.4, 24.1, 12.8. HRMS (ESI) *m/z* Calcd. for C₁₂H₁₂NO Br [M+H⁺]: 265.0102, found 265.0103.

5-(4-Bromophenyl)-6-ethylpyrimidine-2,4-diamine (**6**). A mixture of compound **5** (846 mg, 3.2 mmol), sodium hydrogen carbonate (588 mg, 7mmol) and guanidine hydrochloride (668 mg, 7 mmol) in dry DMSO (10 mL) was heated at 100 °C for 5 h. To the reaction was added 10% MeOH in DCM (30 mL) and the mixture was washed with water (3× 15 mL) and brine (15 mL). The organic layer was dried over Na₂SO₄, concentrated and the concentrate was purified by precipitation with EtOAc to furnish compound **6** (670 mg, 72%) as a white powder. ¹H NMR (400 MHz, CD₃OD) δ 7.62 (d, *J* = 8.5 Hz, 2H), 7.16 (d, *J* = 8.5 Hz, 2H), 2.22 (q, *J* = 7.6 Hz, 2H), 1.03 (t, *J* = 7.6 Hz, 3H). ¹³C NMR (126 MHz, DMSO-*d*₆) δ 166.8, 162.6, 162.4, 135.9, 133.4, 132.3, 121.0, 105.9, 49.1, 27.9, 13.7. HRMS (ESI) *m/z* Calcd. for C₁₂H₁₄N₄Br [M+H⁺]: 293.0396, found for 293.0399.

Di-*tert*-butyl (5-(4-bromophenyl)-6-ethylpyrimidine-2,4-diyl)bis((*tert*-butoxycarbonyl) carbamate) (**7**). Compound **6** (104.4 mg, 0.3 mmol) and DMAP (4.3 mg, 0.03 mmol) were dissolved in THF (5 mL) and flushed with argon. Boc₂O (622.7 mg, 2.8 mmol) was added to the solution and thereaction was stirred overnight at 40 °C. The mixture was partitioned between

water (15 mL) and DCM (25 mL), the organic layer was separated, washed with brine (15 mL) and dried over Na₂SO₄. The crude was purified on preparative TLC eluting with hexanes:EtOAc 4:1 to yield compound **7** (204 mg, 86% conversion) as a yellow oil. ¹H NMR (400 MHz, CDCl₃) δ 7.56 – 7.48 (m, 2H), 7.14 – 7.03 (m, 2H), 2.59 (q, *J* = 7.5 Hz, 2H), 1.42 (s, 18H), 1.31 (s, 18H), 1.13 (t, *J* = 7.5 Hz, 3H). ¹³C NMR (101 MHz, CDCl₃) δ 173.9, 158.6, 157.4, 150.3, 149.8, 132.0, 131.7, 130.8, 128.3, 122.6, 83.5, 83.1, 28.4, 27.9, 13.0. HRMS (ESI) *m/z* Calcd. for C₃₂H₄₆O₈N₄Br [M+H⁺]: 693.2494, found 693.2493.

Di-*tert*-butyl (6-ethyl-5-(4-((trimethylsilyl)ethynyl)phenyl)pyrimidine-2,4-diyl)bis((*tert*-butoxycarbonyl)carbamate) (**9**). Compound **7** (315 mg, 0.4 mmol), Pd(PPh₃)₄ (26 mg, 0.02 mmol), and CuI (8.6 mg, 0.04 mmol) were dissolved in acetonitrile (5 mL) under argon. Trimethylsilylacetylene **8** (0.1 mL, 0.9 mmol) was added, followed by Hunig's base (0.2 mL, 0.9 mmol). The reaction mixture was heated at 75 °C overnight. The mixture was partitioned between water (15 mL) and DCM (25 mL). The organic layer was separated, washed with brine (5 mL) and dried over Na₂SO₄. Crude product **9** was used in the next step without purification.

Di-*tert*-butyl (6-ethyl-5-(4-ethynylphenyl)pyrimidine-2,4-diyl)bis((*tert*-butoxycarbonyl)carbamate) (**10**). Potassium carbonate (74 mg, 0.5 mmol) was added to a solution of crude compound **9** (190 mg) in methanol (3 mL). The reaction mixture stirred for 2 h at room temperature. The mixture was partitioned between water (10 mL) and DCM (20 mL). The organic layer was separated, washed with brine (10 mL), and dried over Na₂SO₄. The crude was purified on preparative TLC eluting with hexanes:EtOAc:Ether 8:1:1 to furnish compound **10** (93 mg, 36% overall yield two steps starting from **7**) as a white powder. ¹H NMR (400 MHz,

CDCl_3) δ 7.57 – 7.49 (m, 2H), 7.25 – 7.18 (m, 2H), 3.14 (s, 1H), 2.61 (dt, $J = 7.5, 6.0$ Hz, 2H), 1.45 (s, 18H), 1.34 (s, 18H), 1.17 (q, $J = 7.6$ Hz, 3H). ^{13}C NMR (101 MHz, CDCl_3) δ 173.8, 158.7, 157.1, 150.9, 150.0, 134.0, 132.3, 129.5, 128.8, 122.4, 83.8, 83.5, 83.1, 78.4, 28.5, 27.7, 13.0. HRMS (ESI) m/z Calcd. for $\text{C}_{34}\text{H}_{47}\text{O}_8\text{N}_4$ $[\text{M}+\text{H}^+]$: 639.3388, found 639.3382.

6-ethyl-5-(4-ethynylphenyl)pyrimidine-2,4-diamine (**10a**). Potassium carbonate (37 mg, 0.25 mmol) was added to a solution of crude compound **9** (95 mg, 0.13mmol) in methanol (3 mL). The reaction mixture stirred for 2 h at room temperature. The mixture was partitioned between water (10 mL) and DCM (20 mL). The organic layer was separated, washed with brine (10 mL), and dried over Na_2SO_4 . The crude was purified on preparative TLC eluting with hexanes:EtOAc:Ether 8:1:1 to furnish compound **10** (63 mg, 0.098mmol, 75%) as a white powder. The product was added to TFA (2 mL) for a neat deprotection of the Boc group at ambient temperature for 4-8h. The TFA solution was neutralized with sodium bicarbonate and the mixture partitioned between water (30 mL) and DCM (50 mL). The two layers were separated, the organic layer was dried over Na_2SO_4 and the solvent evaporated off. The crude product was purified by column or prep-TLC, eluting with DCM: MeOH=10:1, to give **10a** as solid, 19 mg (0.08mmol, yield 81%). ^1H NMR (400 MHz, $\text{DMSO}-d_6$) δ 7.51 (d, $J=8.3$ Hz, 2H), 7.19 (d, $J=8.3$ Hz, 2H), 4.22 (d, $J = 0.8$ Hz, 1H), 2.09 (q, $J = 7.5$ Hz, 2H), 1.17 – 0.73 (t, $J=7.6$ Hz 3H). HRMS (ESI) m/z Calcd. for $\text{C}_{14}\text{H}_{14}\text{N}_4$ $[\text{M}+\text{H}^+]$: 239.1287, found 239.1291

6-(4-(4-(2,4-Diamino-6-ethylpyrimidin-5-yl)phenyl)-1H-1,2,3-triazol-1-yl)-N-hydroxyhexanamide (**12a**). Compound **10** (41 mg, 0.06 mmol) and 4-azido-N-

(trityloxy)hexanamide **11a** (32 mg, 0.08 mmol) were dissolved in anhydrous THF (5 mL) and purged with argon for 15 min. Copper (I) iodide (6 mg, 0.03 mmol) and Hunig's base (0.02 mL, 0.1 mmol) were added, the mixture was purged with argon for additional 15 min and stirring continued for approx. 12 h. The reaction was partitioned between DCM (20 mL) and sat. NH₄Cl/ conc. NH₄OH (4:1) (15 mL) and the two layers separated. The organic layer was washed with sat. NH₄Cl/ conc. NH₄OH (4:1) (2 x 15 mL), sat. brine (15 mL), dried over Na₂SO₄ and the solvent was evaporated off. The crude was then dissolved in DCM: TFA (1: 0.2 mL) and triisopropyl silane was added dropwise until the color transformed from dark yellow to pale yellow. TLC indicated the complete consumption of the starting material after 1 h. Solvent was evaporated off and the crude product was purified by precipitation in EtOAc to give the title compound (23 mg, 88%) as a pale yellow solid. ¹H NMR (500 MHz, CD₃OD) δ 8.46 (s, 1H), 8.02 (d, *J* = 7.7 Hz, 2H), 7.40 (dd, *J* = 15.1, 8.0 Hz, 2H), 4.50 (d, *J* = 6.2 Hz, 2H), 2.42 (q, *J* = 7.2 Hz, 2H), 2.21 – 2.04 (m, 2H), 2.02 (s, 2H), 1.71 (s, 2H), 1.41 (s, 2H), 1.21 – 1.12 (m, 3H). ¹³C NMR (126 MHz, CD₃OD) δ 165.2, 155.5, 154.6, 146.9, 131.6, 130.9, 126.7, 121.4, 108.8, 71.2, 50.1, 29.8, 29.2, 25.6, 24.6, 23.9, 17.3, 11.8. HRMS (ESI) *m/z* Calcd. for C₂₀H₂₇O₂N₈ [M+H⁺]: 411.2251, found 411.2246.

7-(4-(4-(2,4-Diamino-6-ethylpyrimidin-5-yl)phenyl)-1H-1,2,3-triazol-1-yl)-N-hydroxyheptanamide (**12b**). The reaction of compound **10** (40 mg, 0.06 mmol), 4-azido-N-(trityloxy)heptanamide **11b** (32 mg, 0.08 mmol), copper (I) iodide (6 mg, 0.03 mmol) and Hunig's base (0.02 mL, 0.1 mmol) in anhydrous THF (5 mL) as described for the synthesis **12a** furnished the title compound **12b**. ¹H NMR (400 MHz, CD₃OD) δ 8.43 (s, 1H), 7.99 (d, *J* = 6.4

Hz, 2H), 7.37 (s, 2H), 4.47 (s, 2H), 2.39 (s, 2H), 2.19 (d, $J = 31.3$ Hz, 2H), 1.99 (d, $J = 11.8$ Hz, 2H), 1.60 (s, 2H), 1.38 (s, 4H), 1.14 (d, $J = 6.1$ Hz, 3H). ^{13}C NMR (126 MHz, CD_3OD) δ 164.9, 155.4, 154.8, 146.7, 131.4, 130.9, 130.6, 126.5, 121.4, 108.8, 50.1, 29.8, 29.4, 28.1, 26.1, 25.0, 23.7, 23.0, 11.8. HRMS (ESI) m/z Calcd. for $\text{C}_{21}\text{H}_{29}\text{O}_2\text{N}_8$ $[\text{M}+\text{H}^+]$: 425.2408, found 425.2402.

8-(4-(4-(2,4-Diamino-6-ethylpyrimidin-5-yl)phenyl)-1H-1,2,3-triazol-1-yl)-N-hydroxyoctanamide (**12c**). The reaction of compound **10** (110 mg, 0.16 mmol), 4-azido-N-(trityloxy)heptanamide **11c** (100 mg, 0.22 mmol), copper (I) iodide (20 mg, 0.1 mmol) and Hunig's base (0.2 mL, 1.17 mmol) in anhydrous THF (5 mL) as described for the synthesis **12a** furnished the title compound **12c**. ^1H NMR (700 MHz, $\text{DMSO}-d_6$) δ 12.40 (s, 1H), 10.31 (s, 1H), 8.66 (s, 1H), 8.14 (s, 1H), 7.95 (d, $J = 8.0$ Hz, 2H), 7.61 (s, 2H), 7.33 (d, $J = 7.9$ Hz, 2H), 6.87 (s, 1H), 2.25 (q, $J = 7.6$ Hz, 2H), 1.88 (dt, $J = 24.4, 7.2$ Hz, 4H), 1.45 (t, $J = 7.5$ Hz, 2H), 1.24 (d, $J = 17.7$ Hz, 6H), 1.13 – 0.75 (m, 5H). ^{13}C NMR (176 MHz, DMSO) δ 169.5, 164.6, 155.2, 154.7, 146.3, 131.5, 130.9, 126.5, 122.1, 108.5, 65.4, 50.0, 32.6, 30.1, 28.9, 28.5, 26.2, 25.5, 24.1, 18.3, 15.6, 13.1. HRMS (ESI) m/z Calcd. for $\text{C}_{21}\text{H}_{29}\text{O}_2\text{N}_8$ $[\text{M}+\text{H}^+]$: 439.2564, found 439.2558.

Ethyl 8-(4-(4-(2,4-diamino-6-ethylpyrimidin-5-yl)phenyl)-1H-1,2,3-triazol-1-yl)octanoate (**12d**). A mixture of compound **10a** (20 mg, 0.084 mmol), ethyl 8-azidoctanoate **11d** (50 mg, 0.11 mmol), copper (I) iodide (5 mg, 0.026 mmol) and Hunig's base (0.2 mL, 1.17 mmol) in anhydrous THF (3 mL) was purged with argon for 15 min and the reaction was kept stirring for approx. 12 h. The reaction was partitioned between DCM (20 mL) and sat. NH_4Cl / conc.

NH₄OH (4:1) (15 mL) and the two layers separated. The organic layer was washed with sat. NH₄Cl/conc. NH₄OH (4:1) (2 x 15 mL), sat. brine (15 mL), dried over Na₂SO₄ and the solvent was evaporated off. The product was purified by prep-TLC plate with EtOAc:MeOH=9:1. ¹H NMR (700 MHz, chloroform-*d*) δ 7.92 (d, *J* = 8.2 Hz, 2H), 7.81 (s, 1H), 7.32 (d, *J* = 8.2 Hz, 2H), 5.00 (s, 2H), 4.65 (s, 2H), 4.43 (t, *J* = 7.2 Hz, 2H), 4.13 (q, *J* = 7.1 Hz, 2H), 2.34 (q, *J* = 7.6 Hz, 2H), 2.29 (t, *J* = 7.5 Hz, 2H), 2.11 – 2.06 (m, 1H), 2.05 (s, 1H), 1.98 (t, *J* = 7.2 Hz, 2H), 1.63 (p, *J* = 7.4 Hz, 3H), 1.38 (q, *J* = 3.8 Hz, 4H), 1.34 (td, *J* = 6.5, 2.4 Hz, 1H), 1.31 – 1.22 (m, 7H), 1.09 (t, *J* = 7.5 Hz, 3H). ¹³C NMR (176 MHz, CDCl₃) δ 173.7, 162.3, 147.2, 131.1, 130.3, 126.5, 119.5, 107.9, 76.9, 60.2, 50.4, 34.2, 30.3, 28.8, 28.7, 28.0, 26.3, 24.8, 14.3, 13.4. HRMS (ESI) *m/z* Calcd. for C₂₁H₂₉O₂N₈ [M+H⁺]: 452.2768, found 452.2758.

(E)-Methyl 3-(4-(2,4-diamino-6-ethylpyrimidin-5-yl)phenyl)acrylate (**14**). Compound **6** (90 mg, 0.3 mmol), methyl acrylate **13** (0.09 mL, 0.9 mmol), TEA (0.1 mL, 0.8 mmol), and tri-*O*-tolylphosphine (28 mg, 0.09 mmol) were dissolved in DMF (3 mL). The reaction mixture was purged with argon for 15 min, then Pd (OAc)₂ (10.3 mg, 0.05 mmol) was added, and the mixture was heated at 120 °C overnight. The reaction was partitioned between water (10 mL) and DCM (10 mL). The organic layer was separated, washed with brine (5 mL), and dried over Na₂SO₄. Solvent was evaporated off and the crude was purified on preparative TLC eluting with EtOAc:hexanes:NEt₃ 10:1:0.5 to yield compound **14** (50 mg, 55%) as a pale yellow powder. ¹H NMR (400 MHz, CD₃OD) δ 7.74 (d, *J* = 8.2 Hz, 3H), 7.32 (d, *J* = 7.7 Hz, 2H), 6.60 (d, *J* = 16.2 Hz, 1H), 2.38 – 2.21 (m, 2H), 1.10 (t, *J* = 7.4 Hz, 3H). ¹³C NMR (126 MHz, CD₃OD) δ 167.4,

164.1, 157.7, 144.1, 134.6, 134.2, 130.9, 128.7, 118.6, 107.9, 70.3, 51.1, 31.8, 29.2, 25.4, 12.0.

HRMS (ESI) m/z Calcd. $C_{16}H_{19}O_2N_4$ $[M+H^+]$: 299.1503, found 299.1503.

(E)-Methyl 3-(4-(2,4-bis(bis(tert-butoxycarbonyl)amino)-6-ethylpyrimidin-5-yl)phenyl)acrylate (**15**). Compound **14** (27 mg, 0.09 mmol) and DMAP (1.1 mg, 0.009 mmol) were dissolved in THF (3 mL) and flushed with argon. Boc_2O was added to the solution and the mixture was stirred overnight at 40 °C. The reaction was partitioned between water (10 mL) and DCM (20 mL) and the organic layer was separated, washed with brine (10 mL), and dried over Na_2SO_4 . Solvent was evaporated off and the crude was purified on preparative TLC eluting with hexanes:EtOAc 3:1 to yield compound **15** (35 mg, 56%) as a white solid. 1H NMR (400 MHz, CD_3OD) δ 7.77 (s, 1H), 7.74 (d, J = 7.0 Hz, 2H), 7.34 (dd, J = 17.5, 8.2 Hz, 2H), 6.63 (dd, J = 16.1, 10.6 Hz, 1H), 3.80 (s, 3H), 2.80 – 2.57 (m, 2H), 1.48 (s, 18H), 1.35 (d, J = 4.3 Hz, 18H), 1.19 (t, J = 7.5 Hz, 3H). ^{13}C NMR (101 MHz, $CDCl_3$) δ 173.8, 167.3, 158.6, 157.4, 150.9, 149.8, 143.8, 135.3, 134.5, 129.8, 128.0, 118.7, 82.2, 81.3, 70.4, 51.9, 51.8, 29.7, 29.0, 28.6, 28.2, 28.0, 27.9, 27.8, 27.7, 13.2, 12.9. HRMS (ESI) m/z Calcd. $C_{36}H_{51}O_{10}N_4$ $[M+H^+]$: 699.3600, found 699.3595.

(E)-3-(4-(2,4-Bis(bis(tert-butoxycarbonyl)amino)-6-ethylpyrimidin-5-yl)phenyl)acrylic acid (**16**). Compound **15** (60 mg, 0.08 mmol) was dissolved in 1,4-dioxane (3 mL) and added dropwise to an aqueous solution (3 mL) containing hydroxylamine (6 mg, 0.2 mmol) and sodium hydroxide (10.2 mg, 0.2 mmol) at room temperature and stirred for 12 h. The mixture was concentrated under vacuum to remove organic solvent. The aqueous solution was adjusted to pH=1 with 1N HCl. The resulting precipitate was collected by filtration and dried to give

compound **16** (35 mg, 60%) as a pale yellow solid. ^1H NMR (400 MHz, CDCl_3) δ 7.70 (s, 1H), 7.60 – 7.52 (m, 2H), 7.27 (d, J = 5.2 Hz, 1H), 7.22 (d, J = 8.1 Hz, 1H), 6.54 (s, 1H), 2.62 (dq, J = 15.2, 7.5 Hz, 2H), 1.51 (d, J = 15.4 Hz, 6H), 1.50 – 1.44 (m, 12H), 1.32 (s, 18H), 1.24 (d, J = 3.9 Hz, 3H). ^{13}C NMR (101 MHz, CDCl_3) δ 174.3, 158.9, 158.2, 157.6, 156.7, 150.7, 150.5, 150.0, 130.0, 129.5, 128.8, 128.1, 125.5, 81.5, 29.7, 29.0, 28.6, 28.3, 28.0, 27.8, 27.7, 13.1, 12.9. HRMS (ESI) m/z Calcd. $\text{C}_{35}\text{H}_{49}\text{O}_{10}\text{N}_4$ $[\text{M}+\text{H}^+]$: 685.3443, found 685.3434.

(*E*)-3-(4-(2,4-Diamino-6-ethylpyrimidin-5-yl)phenyl)-*N*-hydroxyacrylamide (**18**). Compound **16** (35 mg, 0.05 mmol), EDCI (9.5 mg, 0.05 mmol) and HOBT (6.9 mg, 0.05 mmol) were dissolved in DCM (3 mL) at 0 °C. After stirring at 0 °C for 15 min, *O*-tritylhydroxylamine (20.6 mg, 0.07 mmol) and Hunig's base (0.03 mL, 0.15 mmol) were added, and the mixture stirred for 12 h at room temperature. The reaction was partitioned between water (10 mL) and DCM (20 mL) and the organic layer was separated, washed with brine, and dried over Na_2SO_4 . Solvent was evaporated off, the crude was dissolved in DCM: TFA (1: 0.2 mL) and triisopropyl silane was added dropwise until the color transformed from dark yellow to pale yellow. TLC indicated a complete consumption of the starting material after 1 h. Solvent was evaporated off and the crude product was purified by precipitation with EtOAc to give the title compound (3.6 mg, 24%) as a pale yellow solid. ^1H NMR (500 MHz, CD_3OD) δ 7.75 (d, J = 7.4 Hz, 2H), 7.66 (d, J = 15.6 Hz, 1H), 7.37 (d, J = 6.9 Hz, 2H), 6.59 (d, J = 15.3 Hz, 1H), 2.38 (d, J = 7.4 Hz, 2H), 1.15 (t, J = 7.3 Hz, 3H). ^{13}C NMR (126 MHz, CD_3OD) δ 171.8, 165.2, 158.0, 155.3, 144.8, 135.7, 130.7, 128.7, 120.4, 29.6, 27.2, 23.9, 12.0. HRMS (ESI) m/z Calcd. $\text{C}_{15}\text{H}_{18}\text{O}_2\text{N}_5$ $[\text{M}+\text{H}^+]$: 300.1455, found 300.1451.

Di-tert-butyl (6-ethyl-5-(4'-hydroxy-[1,1'-biphenyl]-4-yl)pyrimidine-2,4-diyl)bis(tert-butoxycarbonylcarbamate) (**19**). Compound **7** (500 mg, 0.72 mmol) was mixed with iodo phenol (200 mg, 0.91 mmol), copper (I) iodide (20 mg, 0.105 mmol), and Tetrakis(triphenylphosphine) palladium (0) (83 mg, 0.072 mmol) in a pressure tube. Acetonitrile (5 mL) was added to dissolve the solids; the reaction tube was filled with argon and heated to 75°C for 10 min. Hunig's base (0.5 mL, 2.92 mmol) was added and the reaction was stirred at 75°C overnight. Solvent was evaporated off and the crude was purified on silica gel eluting with EtOAc:hexanes 1:1 to furnish compound **19** (401 mg, 77.7%) as a pale yellow solid. ¹H NMR (400 MHz, CDCl₃) δ 7.69 (d, *J* = 8.5 Hz, 2H), 7.62 (d, *J* = 8.7 Hz, 2H), 7.41 (d, *J* = 8.5 Hz, 2H), 7.04 (d, *J* = 8.7 Hz, 2H), 2.82 (q, *J* = 7.9 Hz, 2H), 1.67 (s, 8H), 1.59 (s, 14H), 1.46 (s, 14H), 1.32 (t, *J* = 7.5 Hz, 3H).

4'-(2,4-Bis(bis(tert-butoxycarbonyl)amino)-6-ethylpyrimidin-5-yl)-[1,1'-biphenyl]-4-yl trifluoromethanesulfonate (**20**).

Compound **19** (200 mg, 0.28 mmol) was dissolved into DCM (10 mL). To the solution was added pyridine (0.7 mL, 8.66 mmol) and the mixture cooled to -20°C for 10 min with stirring under Argon. Trifluoromethanesulfonic anhydride (0.3 mL, 1.78 mmol) was added dropwise to the mixture with stirring which continued for 30 min. The reaction was quenched with water (100 mL) and DCM (30 mL) was added. The two layers were separated, the organic layer was dried over Na₂SO₄ and solvent was evaporated off to furnish compound **20** (211 mg, 0.252 mmol) as yellow solid. Compound **20** was analytically pure and used for the next reaction without purification. ¹H NMR (400 MHz, CDCl₃) δ 7.62 (d, *J* = 3.2 Hz, 2H), 7.59 (d, *J* = 2.9 Hz, 2H), 7.33 (d, *J* = 8.4 Hz, 2H), 7.28 (d, *J* = 8.8 Hz, 2H), 2.70 (q, *J* = 7.9 Hz, 2H), 1.59 (s, 8H), 1.48 (s, 14H), 1.35 (s, 14H), 1.20 (t, *J* = 7.5 Hz, 3H).

Di-tert-butyl (6-ethyl-5-(4'-vinyl-[1,1'-biphenyl]-4-yl)pyrimidine-2,4-diyl)bis(tert-butoxycarbonylcarbamate) (**21**). Compound **20** (200 mg, 0.24 mmol) and potassium vinyltrifluoroborate (130mg, 0.97mmol) were dissolved in DMF (20 mL). Tetrakis(triphenylphosphine) palladium (0) (80 mg, 0.07 mmol) and Cesium carbonate (315 mg, 0.96 mmol) were added to the mixture and the reaction heated to 80°C for 5 min. Subsequently, water (1 mL) was added dropwise into the mixture with stirring until the solution turned clear. Stirring continued at 80°C and the reaction was complete after 3 h. The solution was cooled down and partitioned between water (100 mL) and DCM (30 mL). The two layers were separated and the aqueous layer was extracted with DCM (30mL). The combined organic layers was washed with water (100 mL), dried over Na₂SO₄ and solvent was evaporated of *in vacuo*. The mixture was purified with column chromatography with ethyl acetate: hexane=2:3. The furnish compound **21** was gained (120mg, 70 %) as yellow liquid. ¹H NMR (400 MHz, CDCl₃) δ 7.66 (d, *J* = 8.4 Hz, 2H), 7.61 (d, *J* = 8.3 Hz, 2H), 7.53 (d, *J* = 8.3 Hz, 2H), 7.34 (d, *J* = 8.4 Hz, 2H), 6.79 (dd, *J* = 17.6, 10.9 Hz, 1H), 5.83 (d, *J* = 17.6 Hz, 1H), 5.32 (d, *J* = 11.6 Hz, 1H), 2.74 (t, *J* = 7.9 Hz, 2H), 1.51 (s, 18H), 1.37 (s, 18H), 1.23 (t, *J* = 7.5 Hz, 3H).

(E)-Di-tert-butyl (6-ethyl-5-(4'-(3-oxo-3-((trityloxy)amino)prop-1-en-1-yl)-[1,1'-biphenyl]-4-yl)pyrimidine-2,4-diyl)bis(tert-butoxycarbonylcarbamate) (**22**). Compound **21** (100 mg, 0.14 mmol), N-[Tris(hydroxymethyl)methyl]acrylamide (56 mg, 0.17 mmol) and Hoveyda-Grubbs 2nd generation catalyst (10 mg, 0.016 mmol) was added to the reaction flask and the mixture was dissolved in DCM (10 mL). The reaction mixture was heated under Argon atmosphere at 33°C overnight. The solution was evaporated and the crude was purified by preparative TLC eluting

with EtOAc:hexane 1:1 to furnish compound **22** (35mg, 23 %) as white solid. ¹H NMR (400 MHz, CDCl₃) δ 7.79 (d, *J* = 8.8 Hz, 2H), 7.73 (d, *J* = 8.3 Hz, 2H), 7.63 – 7.25 (m, 21H), 2.80 (q, *J* = 7.9 Hz, 2H), 1.60 (s, 18H), 1.47 (s, 18H), 1.35 (t, *J* = 7.5 Hz, 3H).

(E)-3-(4'-(2,4-Diamino-6-ethylpyrimidin-5-yl)-[1,1'-biphenyl]-4-yl)-N-hydroxyacrylamide (**23**).

Compound **22** (35 mg, 0.032 mmol) was cooled to 0°C and mixed with TFA (2 mL) as a neat reaction. The solution was stirred at room, triisopropylsilane (0.3-0.5 mL) was added until the bright yellow color vanished and stirring continued for 2 h. The solvent was evaporated by Rotovap and the residue was dried using high vacuum. The dried residue was washed by titrated with diethyl ether and a brown solid which crashed out was filtered to furnish compound **23** (8.8 mg, 72 %). ¹H NMR (400 MHz, DMSO-*d*₆) δ 10.81 (s, 1H), 9.09 (s, 1H), 8.32 (s, 1H), 7.84 (d, *J* = 22.8 Hz, 3H), 7.69 (s, 1H), 7.52 (d, *J* = 15.8 Hz, 1H), 6.52 (d, *J* = 15.8 Hz, 1H), 2.25 (q, *J* = 7.7 Hz, 2H), 1.07 (t, *J* = 7.5 Hz, 3H). ¹³C NMR (176 MHz, DMSO-*d*₆) δ 163.1, 158.4, 158.2, 140.6, 139.8, 138.2, 134.7, 131.6, 128.7, 127.9, 127.5, 119.7, 118.7, 108.3, 79.6, 24.2, 13.1. HRMS (ESI) *m/z* Calcd. C₂₁H₂₂O₂N₅ [M+H⁺]: 376.1751, found 376.1768.

5.4.2 Cell culture and viability assay

MDA-MB-231, VERO, and A549 cell lines were maintained in Dulbecco's Modified Eagle Medium (DMEM) (Corning, 10-017-CV), supplemented with 10% fetal bovine serum (FBS) (Corning, 35-010-CV). MCF-7 cells were cultured in phenol red free Minimum Essential Medium (MEM) (Corning, 17-305-CV), supplemented with 10% fetal bovine serum (FBS). Cells were seeded into a 96-well plate (2000 cells/100uL) for 24 h prior to treatment and then treated with various drug concentrations for 72 h. All drugs were dissolved in DMSO/DMEM

with DMSO concentration maintained at 1%. The effect of compounds on cell viability was measured using the MTS assay (CellTiter 96 Aqueous One Solution and CellTiter 96 Non-Radioactive Cell Proliferation Assays, Promega, Madison, WI) as described by the manufacturer. IC₅₀s were determined using Prism GraphPad 8.

5.4.3 In vitro HDAC inhibition assay.

In vitro HDAC inhibition assay was performed through contractual agreement with BPS Bioscience.

5.4.4 Western blots analysis.

MDA-MB-231 cells were seeded into 6-well plate at 1×10^6 /well in DMEM for 24 h after which the cells were starved in serum-free DMEM for another 24 h. Various concentrations of SAHA, PYM and **12c** solutions in DMSO were added to the cell culture media such that the final DMSO level is 0.1%. Cells were treated for 24 h, washed with cold PBS, and lysed with RIPA buffer (110 μ l) (VWR, VWRVN653-100ML) buffer containing phosphatase inhibitor (Fisher Thermo, A32957) and protease inhibitor (Fisher Thermo, A32955). The cells were scraped and the lysate was collected and vortexed for 15s followed by sonication for 60s. The lysate was then centrifuged at 14000 rpm for 10 min and the supernatants were collected. The total protein concentration was determined using a BCA protein assay kit (BioVision, K813-2500). Based on the results from the BSA assay, the lysates were diluted to make equal protein concentration and 20-40 μ g of each lysate was loaded to each well of the TGX MIDI 4-20% gel (Biorad, cat. 5671093) and ran at 150V for 70 mins. Subsequently, the gel was transferred on to the Turbo

PDVF membrane (Biorad, 1704273) and after blocking with 5% BSA for 1-2 h, the membrane was incubated overnight with Ac-Tubulin (Santa Cruz, sc-23950), Ac-H4 (Santa cruz, sc-515319), Bcl-2 (Santa Cruz, sc-7382), Bcl-xL (Santa Cruz, sc-8392), and p-STAT3/STAT3 (Cellsignal, D3A7/D1B2J) antibodies. The second day, the membrane was washed with TBST for 3x5 min. Secondary antibody (Immunoreagents, part. IR2173) was added and the membrane was incubated with agitation for 1 h. Bands were quantified using Odyssey CLx Image system.

5.4.5 Flow cytometry

MDA-MB-231 cells (5×10^6) were seeded to 10 cm plate with DMEM for 24 h prior to drug treatment. Cells were treated with DMSO (control) and DMSO solutions of SAHA (5 μ M) and **12b** (15 μ M), such that the final DMSO level is 0.1%, for another 48 h. Cells were trypsinized and washed with cold 1X PBS solution twice. Subsequently, cells were collected using 1x PBS buffer and fixed overnight at -20°C using 70% ethanol. Cells were then washed, centrifuged and re-suspended in 1X PBS; and the suspension was treated with 200ug/mL RNase for 30 min. Then cells were treated with 50ug/mL PI staining at room temperature for 30 mins. The cell cycle was analyzed with BD FACS Aria Illu analyzer and the data was processed using FlowJo.

Acknowledgments

This work was supported by the Georgia Institute of Technology and by the Vasser-Woolley Fellowship (A.K.O.).

5.5 References :

1. Cowman AF, Morry MJ, Biggs BA, Cross GA, Foote SJ. Amino acid changes linked to pyrimethamine resistance in the dihydrofolate reductase-thymidylate synthase gene of *Plasmodium falciparum*. *Proc Natl Acad Sci U S A*. 1988;85(23):9109-13.
2. Curd FH, Davey DG, Rose FL. Studies on synthetic antimalarial drugs; some biguanide derivatives as new types of antimalarial substances with both therapeutic and causal prophylactic activity. *Ann Trop Med Parasitol*. 1945;39:208-16.
3. James, Fraction, Deborah, Elissa, Joseph, Lisa, et al. Molecular Markers for Failure of Sulfadoxine-Pyrimethamine and Chlorproguanil-Dapsone Treatment of *Plasmodium falciparum* Malaria. *The Journal of Infectious Diseases*. 2002;185(3):380-8.
4. Ferone R, Roland S. Dihydrofolate reductase: thymidylate synthase, a bifunctional polypeptide from *Crithidia fasciculata*. *Proc Natl Acad Sci U S A*. 1980;77(10):5802-6.
5. Kompis IM, Islam K, Then RL. DNA and RNA synthesis: antifolates. *Chem Rev*. 2005;105(2):593-620.
6. Li R, Sirawaraporn R, Chitnumsub P, Sirawaraporn W, Wooden J, Athappilly F, et al. Three-dimensional structure of *M. tuberculosis* dihydrofolate reductase reveals opportunities for the design of novel tuberculosis drugs. *J Mol Biol*. 2000;295(2):307-23.
7. Sharma A, Jyotsana N, Lai CK, Chaturvedi A, Görlich K, Murphy C, et al. High-throughput drug screening identifies pyrimethamine as a potent and selective inhibitor of acute myeloid leukemia. *Am Soc Hematology*; 2014.
8. Shuai K, Ziemiecki A, Wilks AF, Harpur AG, Sadowski HB, Gilman MZ, et al. Polypeptide signalling to the nucleus through tyrosine phosphorylation of Jak and Stat proteins. *Nature*. 1993;366(6455):580.
9. Weimbs T, Talbot JJ. STAT3 Signaling in Polycystic Kidney Disease. *Drug Discov Today Dis Mech*. 2013;10(3-4):e113-e8.
10. Miklossy G, Hilliard TS, Turkson J. Therapeutic modulators of STAT signalling for human diseases. *Nat Rev Drug Discov*. 2013;12(8):611-29.
11. Chaudhari S, Desai JS, Adam A, Mishra P. JAK/STAT as a novel target for treatment of leukemia. *Int J Pharm Pharm Sci*. 2014;6(1):1-7.
12. Spitzner M, Ebner R, Wolff HA, Ghadimi BM, Wienands J, Grade M. STAT3: A Novel Molecular Mediator of Resistance to Chemoradiotherapy. *Cancers (Basel)*. 2014;6(4):1986-2011.
13. Kim E, Kim M, Woo DH, Shin Y, Shin J, Chang N, et al. Phosphorylation of EZH2 activates STAT3 signaling via STAT3 methylation and promotes tumorigenicity of glioblastoma stem-like cells. *Cancer Cell*. 2013;23(6):839-52.

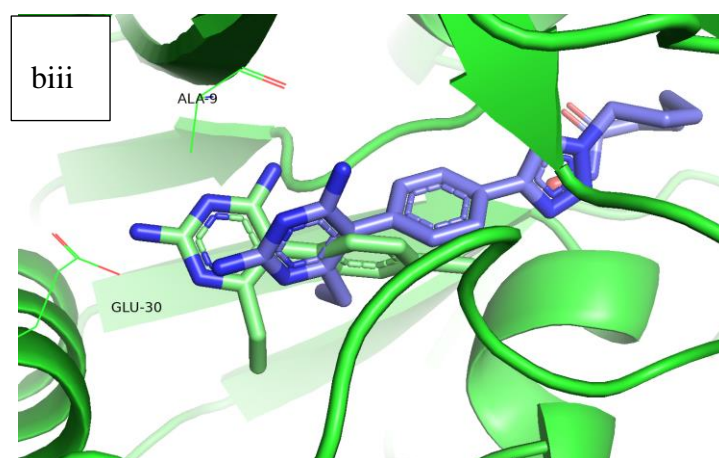
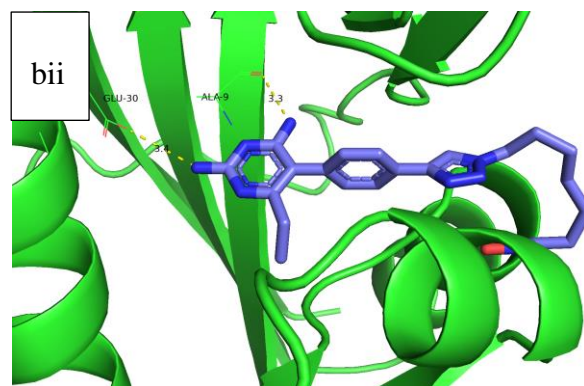
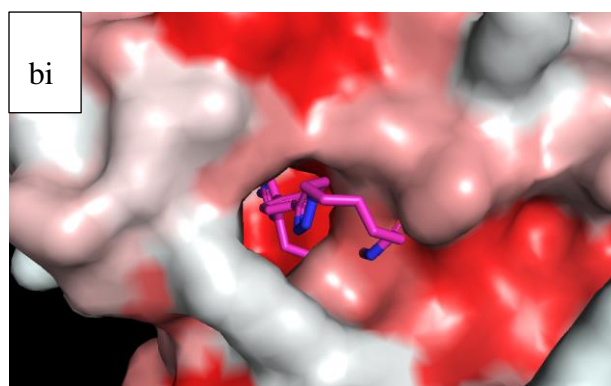
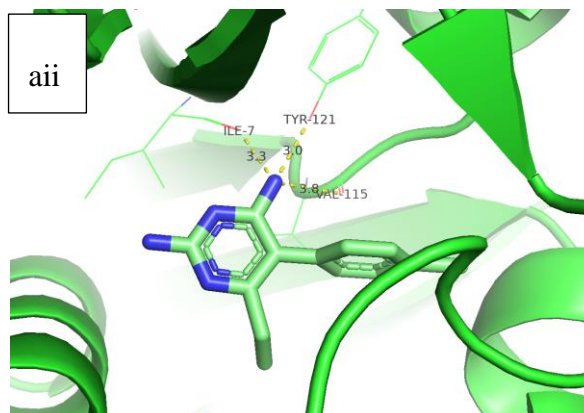
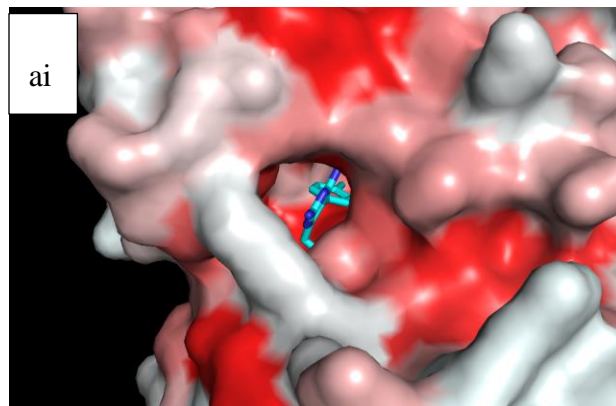
14. Lee H, Zhang P, Herrmann A, Yang C, Xin H, Wang Z, et al. Acetylated STAT3 is crucial for methylation of tumor-suppressor gene promoters and inhibition by resveratrol results in demethylation. *Proceedings of the National Academy of Sciences*. 2012;109(20):7765-9.
15. Alvarez JV, Febbo PG, Ramaswamy S, Loda M, Richardson A, Frank DA. Identification of a genetic signature of activated signal transducer and activator of transcription 3 in human tumors. *Cancer research*. 2005;65(12):5054-62.
16. Yeh JE, Frank DA. STAT3-Interacting Proteins as Modulators of Transcription Factor Function: Implications to Targeted Cancer Therapy. *ChemMedChem*. 2016;11(8):795-801.
17. Nelson EA, Sharma SV, Settleman J, Frank DA. A chemical biology approach to developing STAT inhibitors: molecular strategies for accelerating clinical translation. *Oncotarget*. 2011;2(6):518.
18. Chang C-H, Liu W-T, Hung H-C, Gean C-Y, Tsai H-M, Su C-L, et al. Synergistic inhibition of tumor growth by combination treatment with drugs against different subpopulations of glioblastoma cells. *BMC cancer*. 2017;17(1):905.
19. Kabra DG, Pfuhlmann K, García-Cáceres C, Schriever SC, García VC, Kebede AF, et al. Hypothalamic leptin action is mediated by histone deacetylase 5. *Nature Communications*. 2016;7:10782.
20. Gryder BE, Sodji QH, Oyeler AK. Targeted cancer therapy: giving histone deacetylase inhibitors all they need to succeed. *Future medicinal chemistry*. 2012;4(4):505-24.
21. Mottamal M, Zheng S, Huang T, Wang G. Histone deacetylase inhibitors in clinical studies as templates for new anticancer agents. *Molecules*. 2015;20(3):3898-941.
22. Tapadar S, Fathi S, Raji I, Omesiete W, Kornacki JR, Mwakwari SC, et al. A structure–activity relationship of non-peptide macrocyclic histone deacetylase inhibitors and their anti-proliferative and anti-inflammatory activities. *Bioorganic & medicinal chemistry*. 2015;23(24):7543-64.
23. Mann BS, Johnson JR, Cohen MH, Justice R, Pazdur R. FDA approval summary: vorinostat for treatment of advanced primary cutaneous T-cell lymphoma. *The oncologist*. 2007;12(10):1247-52.
24. Coiffier B, Pro B, Prince HM, Foss F, Sokol L, Greenwood M, et al. Romidepsin for the treatment of relapsed/refractory peripheral T-cell lymphoma: pivotal study update demonstrates durable responses. *Journal of hematology & oncology*. 2014;7(1):11.
25. Plumb JA, Finn PW, Williams RJ, Bandara MJ, Romero MR, Watkins CJ, et al. Pharmacodynamic response and inhibition of growth of human tumor xenografts by the novel histone deacetylase inhibitor PXD101. *Molecular cancer therapeutics*. 2003;2(8):721-8.

26. Laubach JP, Moreau P, San-Miguel JF, Richardson PG. Panobinostat for the treatment of multiple myeloma. *Clinical cancer research*. 2015;21(21):4767-73.
27. Ning Z-Q, Li Z-B, Newman MJ, Shan S, Wang X-H, Pan D-S, et al. Chidamide (CS055/HBI-8000): a new histone deacetylase inhibitor of the benzamide class with antitumor activity and the ability to enhance immune cell-mediated tumor cell cytotoxicity. *Cancer chemotherapy and pharmacology*. 2012;69(4):901-9.
28. Gupta K, Gulen F, Sun L, Aguilera R, Chakrabarti A, Kiselar J, et al. GSK3 is a regulator of RAR-mediated differentiation. *Leukemia*. 2012;26(6):1277.
29. Zeng H, Qu J, Jin N, Xu J, Lin C, Chen Y, et al. Feedback Activation of Leukemia Inhibitory Factor Receptor Limits Response to Histone Deacetylase Inhibitors in Breast Cancer. *Cancer Cell*. 2016;30(3):459-73.
30. Mwakwari SC, Guerrant W, Patil V, Khan SI, Tekwani BL, Gurard-Levin ZA, et al. Non-peptide macrocyclic histone deacetylase inhibitors derived from tricyclic ketolide skeleton. *Journal of medicinal chemistry*. 2010;53(16):6100-11.
31. Tropak MB, Zhang J, Yonekawa S, Rigat BA, Aulakh VS, Smith MR, et al. Pyrimethamine derivatives: insight into binding mechanism and improved enhancement of mutant β -N-acetylhexosaminidase activity. *Journal of medicinal chemistry*. 2015;58(11):4483-93.
32. Trott O, Olson AJ. AutoDock Vina: improving the speed and accuracy of docking with a new scoring function, efficient optimization, and multithreading. *J Comput Chem*. 2010;31(2):455-61.
33. Liu H, Qin Y, Zhai D, Zhang Q, Gu J, Tang Y, et al. Antimalarial Drug Pyrimethamine Plays a Dual Role in Antitumor Proliferation and Metastasis through Targeting DHFR and TP. *Molecular cancer therapeutics*. 2019;18(3):541-55.
34. Ji Y, Trenkle WC, Vowles JV. A high-yielding preparation of β -ketonitriles. *Organic letters*. 2006;8(6):1161-3.
35. Kuroyanagi J-i, Kanai K, Sugimoto Y, Fujisawa T, Morita C, Suzuki T, et al. Novel antifungal agents: Triazolopyridines as inhibitors of β -1, 6-glucan synthesis. *Bioorganic & medicinal chemistry*. 2010;18(16):5845-54.
36. Chan DC, Fu H, Forsch RA, Queener SF, Rosowsky A. Design, synthesis, and antifolate activity of new analogues of piritrexim and other diaminopyrimidine dihydrofolate reductase inhibitors with ω -carboxyalkoxy or ω -carboxy-1-alkynyl substitution in the side chain. *Journal of medicinal chemistry*. 2005;48(13):4420-31.
37. Porcheddu A, Giacomelli G, Piredda I, Carta M, Nieddu G. A practical and efficient approach to PNA monomers compatible with Fmoc-mediated solid-phase synthesis protocols. *European Journal of Organic Chemistry*. 2008;2008(34):5786-97.

38. Dhokale B, Jadhav T, Mobin SM, Misra R. Meso alkynylated tetraphenylethylene (TPE) and 2, 3, 3-triphenylacrylonitrile (TPAN) substituted BODIPYs. *The Journal of organic chemistry*. 2015;80(16):8018-25.
39. Rostovtsev VV, Green LG, Fokin VV, Sharpless KB. A stepwise huisgen cycloaddition process: copper (I)-catalyzed regioselective “ligation” of azides and terminal alkynes. *Angewandte Chemie International Edition*. 2002;41(14):2596-9.
40. Gryder BE, Akbashev MJ, Rood MK, Raftery ED, Meyers WM, Dillard P, et al. Selectively targeting prostate cancer with antiandrogen equipped histone deacetylase inhibitors. *ACS chemical biology*. 2013;8(11):2550-60.
41. De Savi C, Bradbury RH, Rabow AA, Norman RA, de Almeida C, Andrews DM, et al. Optimization of a Novel Binding Motif to (E)-3-(3, 5-Difluoro-4-((1 R, 3 R)-2-(2-fluoro-2-methylpropyl)-3-methyl-2, 3, 4, 9-tetrahydro-1 H-pyrido [3, 4-b] indol-1-yl) phenyl) acrylic Acid (AZD9496), a Potent and Orally Bioavailable Selective Estrogen Receptor Downregulator and Antagonist. *Journal of medicinal chemistry*. 2015;58(20):8128-40.
42. Liu W, Lau F, Liu K, Wood HB, Zhou G, Chen Y, et al. Benzimidazolones: A new class of selective peroxisome proliferator-activated receptor γ (PPAR γ) modulators. *Journal of medicinal chemistry*. 2011;54(24):8541-54.
43. Garber SB, Kingsbury JS, Gray BL, Hoveyda AH. Efficient and recyclable monomeric and dendritic Ru-based metathesis catalysts. *Journal of the American Chemical Society*. 2000;122(34):8168-79.
44. Bramati A, Girelli S, Torri V, Farina G, Galfrascoli E, Piva S, et al. Efficacy of biological agents in metastatic triple-negative breast cancer. *Cancer Treat Rev*. 2014;40(5):605-13.
45. Podo F, Santoro F, Di Leo G, Manoukian S, de Giacomi C, Corcione S, et al. Triple-Negative versus Non-Triple-Negative Breast Cancers in High-Risk Women: Phenotype Features and Survival from the HIBCRIT-1 MRI-Including Screening Study. *Clin Cancer Res*. 2016;22(4):895-904.
46. Aryappalli P, Al-Qubaisi SS, Attoub S, George JA, Arafat K, Ramadi KB, et al. The IL-6/STAT3 Signaling Pathway Is an Early Target of Manuka Honey-Induced Suppression of Human Breast Cancer Cells. *Front Oncol*. 2017;7:167.
47. Banerjee K, Resat H. Constitutive activation of STAT3 in breast cancer cells: A review. *Int J Cancer*. 2016;138(11):2570-8.
48. Schütz A, Röser K, Klitzsch J, Lieder F, Aberger F, Gruber W, et al. Lung adenocarcinomas and lung cancer cell lines show association of MMP-1 expression with STAT3 activation. *Translational oncology*. 2015;8(2):97-105.
49. Yu X, He L, Cao P, Yu Q. Eriocalyxin B inhibits STAT3 signaling by covalently targeting STAT3 and blocking phosphorylation and activation of STAT3. *PLoS One*. 2015;10(5):e0128406.

50. Berishaj M, Gao SP, Ahmed S, Leslie K, Al-Ahmadie H, Gerald WL, et al. Stat3 is tyrosine-phosphorylated through the interleukin-6/glycoprotein 130/Janus kinase pathway in breast cancer. *Breast Cancer Research*. 2007;9(3):R32.
51. Aldinucci D, Colombatti A. The inflammatory chemokine CCL5 and cancer progression. *Mediators of inflammation*. 2014;2014.
52. Li L, Shaw PE. Autocrine-mediated activation of STAT3 correlates with cell proliferation in breast carcinoma lines. *Journal of Biological Chemistry*. 2002;277(20):17397-405.
53. Garcia R, Bowman TL, Niu G, Yu H, Minton S, Muro-Cacho CA, et al. Constitutive activation of Stat3 by the Src and JAK tyrosine kinases participates in growth regulation of human breast carcinoma cells. *Oncogene*. 2001;20(20):2499.
54. Sodji QH, Kornacki JR, McDonald JF, Mrksich M, Oyelere AK. Design and structure activity relationship of tumor-homing histone deacetylase inhibitors conjugated to folic and pteronic acids. *European journal of medicinal chemistry*. 2015;96:340-59.
55. Bantscheff M, Hopf C, Savitski MM, Dittmann A, Grandi P, Michon A-M, et al. Chemoproteomics profiling of HDAC inhibitors reveals selective targeting of HDAC complexes. *Nature biotechnology*. 2011;29(3):255.
56. Epling-Burnette PK, Liu JH, Catlett-Falcone R, Turkson J, Oshiro M, Kothapalli R, et al. Inhibition of STAT3 signaling leads to apoptosis of leukemic large granular lymphocytes and decreased Mcl-1 expression. *Journal of Clinical Investigation*. 2001;107(3):351-62.
57. Xiong A, Yang Z, Shen Y, Zhou J, Shen Q. Transcription Factor STAT3 as a Novel Molecular Target for Cancer Prevention. 2014;6(2):926-57.
58. Hata AN, Engelman JA, Faber AC. The BCL2 family: key mediators of the apoptotic response to targeted anticancer therapeutics. *Cancer discovery*. 2015;5(5):475-87.
59. Lin L, Hutzen B, Zuo M, Ball S, Deangelis S, Foust E, et al. Novel STAT3 phosphorylation inhibitors exhibit potent growth-suppressive activity in pancreatic and breast cancer cells. *Cancer research*. 2010;70(6):2445-54.
60. Cheng X, Peuckert C, Wolfl S. Essential role of mitochondrial Stat3 in p38(MAPK) mediated apoptosis under oxidative stress. *Sci Rep*. 2017;7(1):15388.
61. Liu J, Qu X, Shao L, Hu Y, Yu X, Lan P, et al. Pim-3 enhances melanoma cell migration and invasion by promoting STAT3 phosphorylation. *Cancer Biol Ther*. 2018;19(3):160-8.
62. Yeh JE. Molecular Modulators of the Oncogenic Transcription Factor STAT3. Doctoral dissertation, Harvard University, Graduate School of Arts & Sciences. 2015.
63. Huang L, Pardee AB. Suberoylanilide hydroxamic acid as a potential therapeutic agent for human breast cancer treatment. *Mol Med*. 2000;6(10):849-66.

5.6 Supporting Information



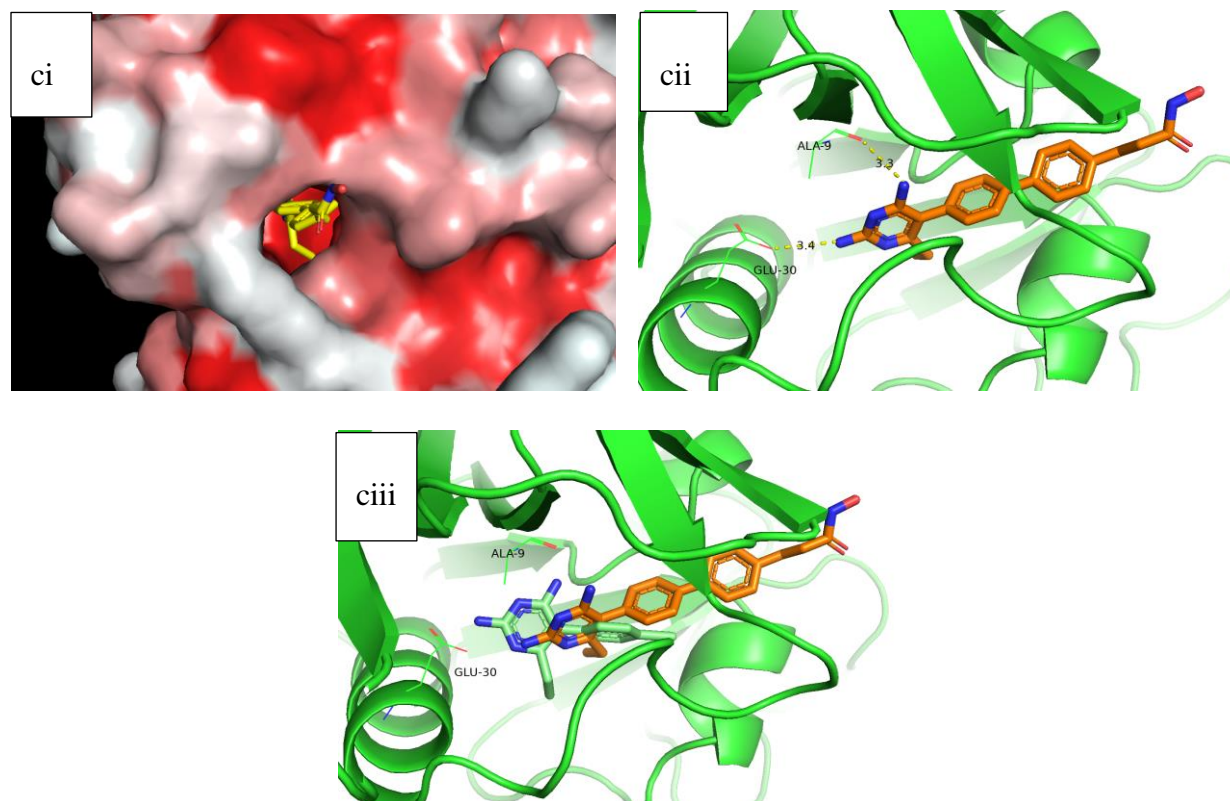


Figure 5S.1. Docking outputs of PYM and class I compound **B** and class II compound **E** on hDHFR (PDB:1U72). Docked pose of PYM (ai-aii) on hDHFR shows that PYM could potentially form H-bonding interactions with ILE-7, VAL-115, and TYR-121 (3.3Å, 3.8Å, 3.0Å, respectively). Class I compound **B** (bi-biii) adopts docked orientation which potentially enables its pyrimidinediamine head to engage in H-bonding interactions with ALA-9 and GLU-30 (3.3Å, 3.4Å, respectively) while its hydroxamate moiety forms H-bonding with THR-56, GLY117, and SER-119. Similarly, class II compound **E** (ci-ciii) adopts docked orientation which potentially enables its pyrimidinediamine head to engage in H-bonding interactions with ALA-9 and GLU-30 (3.3Å, 3.4Å, respectively). The pyrimidinediamine head of both PYM-HDACi compounds does not gain access into the hDHFR binding pocket as efficiently as PYM (biii and ciii).

Docking on 12d

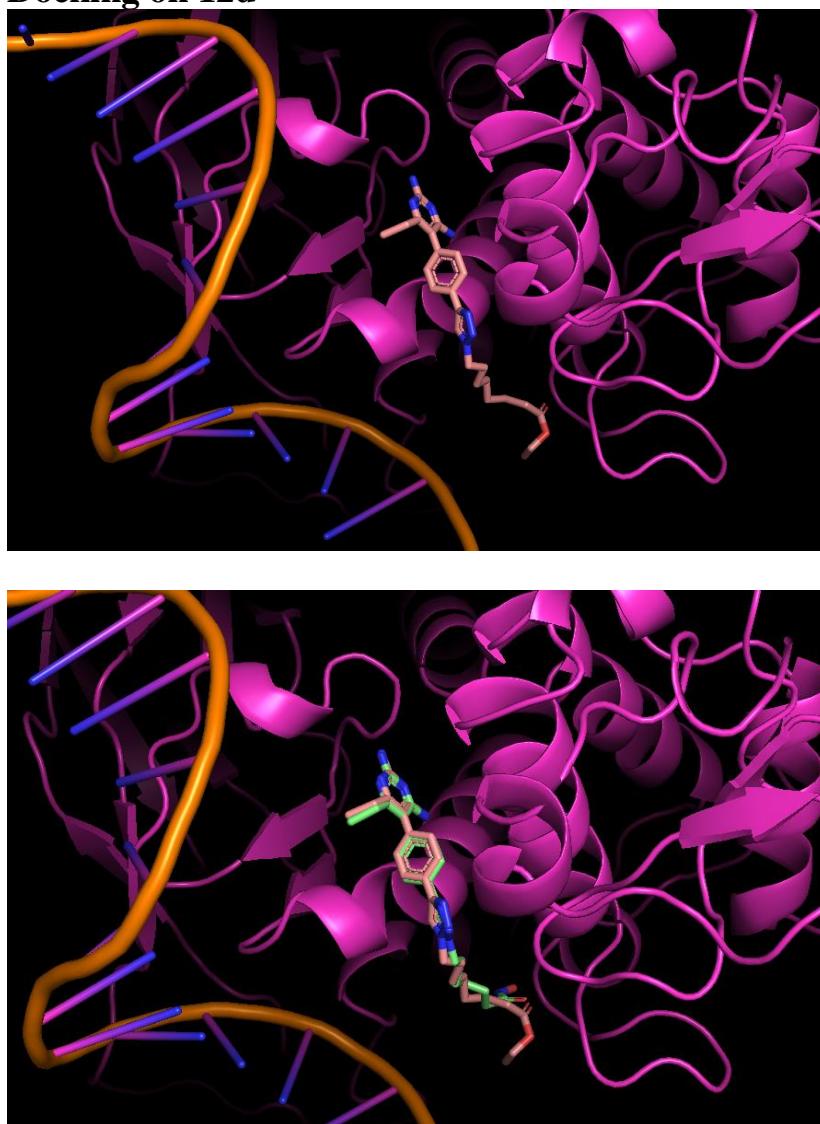


Figure 5S.2. The docking of **12d** on the DBD region of STAT3 protein. (a). The pink chemical is the **12d** interacting in the DBD region with Binding affinity -7.5kcal/mol. (b). The green chemical is the **12b** overlapping with the **12d** compound in the same region.

12b Flow Cytometry for cell cycle arrestment.

We performed cell cycle analysis to determine the effects of PYM-HDACi **12b** and SAHA on MDA-MB-231 cell cycle distribution. We observed the effects of **12b** (15 μ M) and SAHA (5 μ M) on cell cycle.

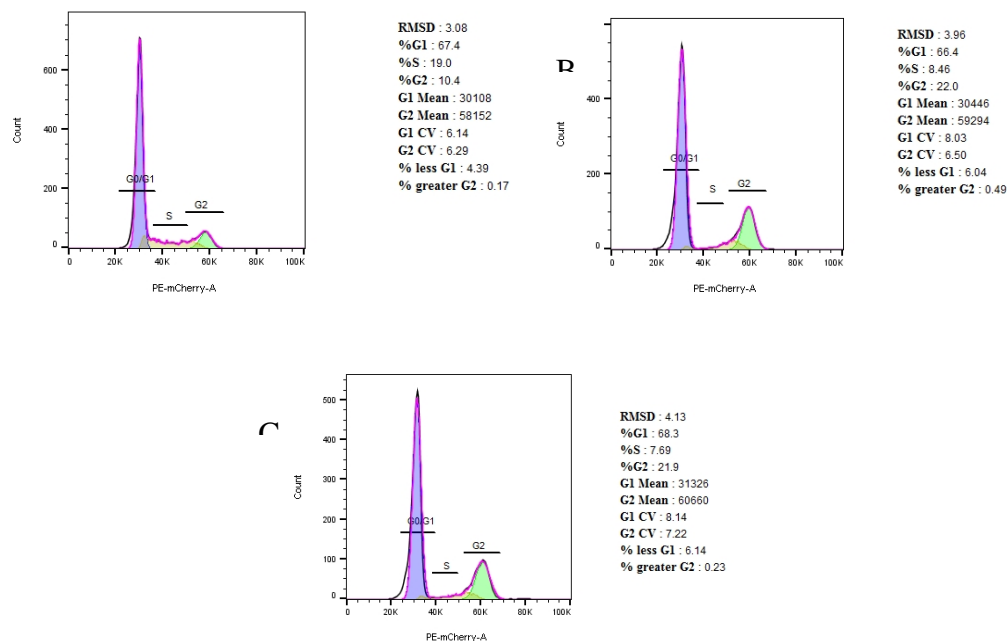
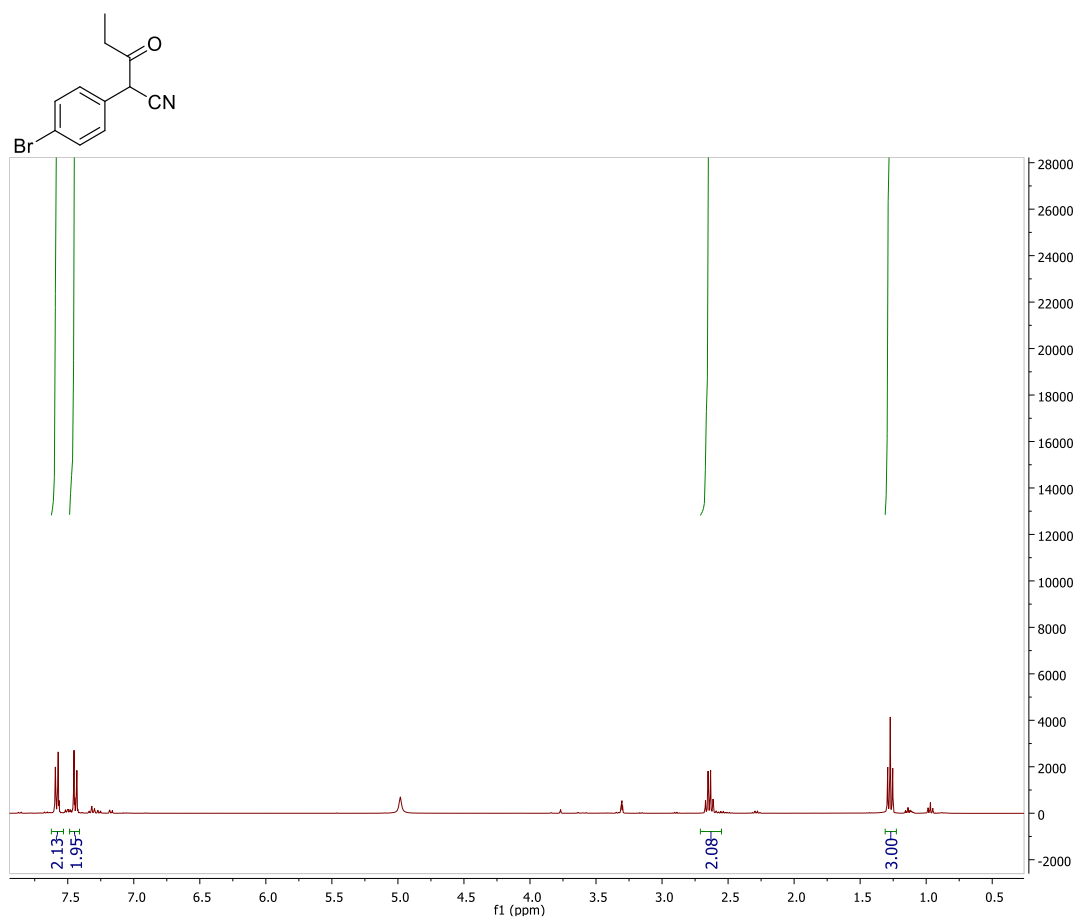


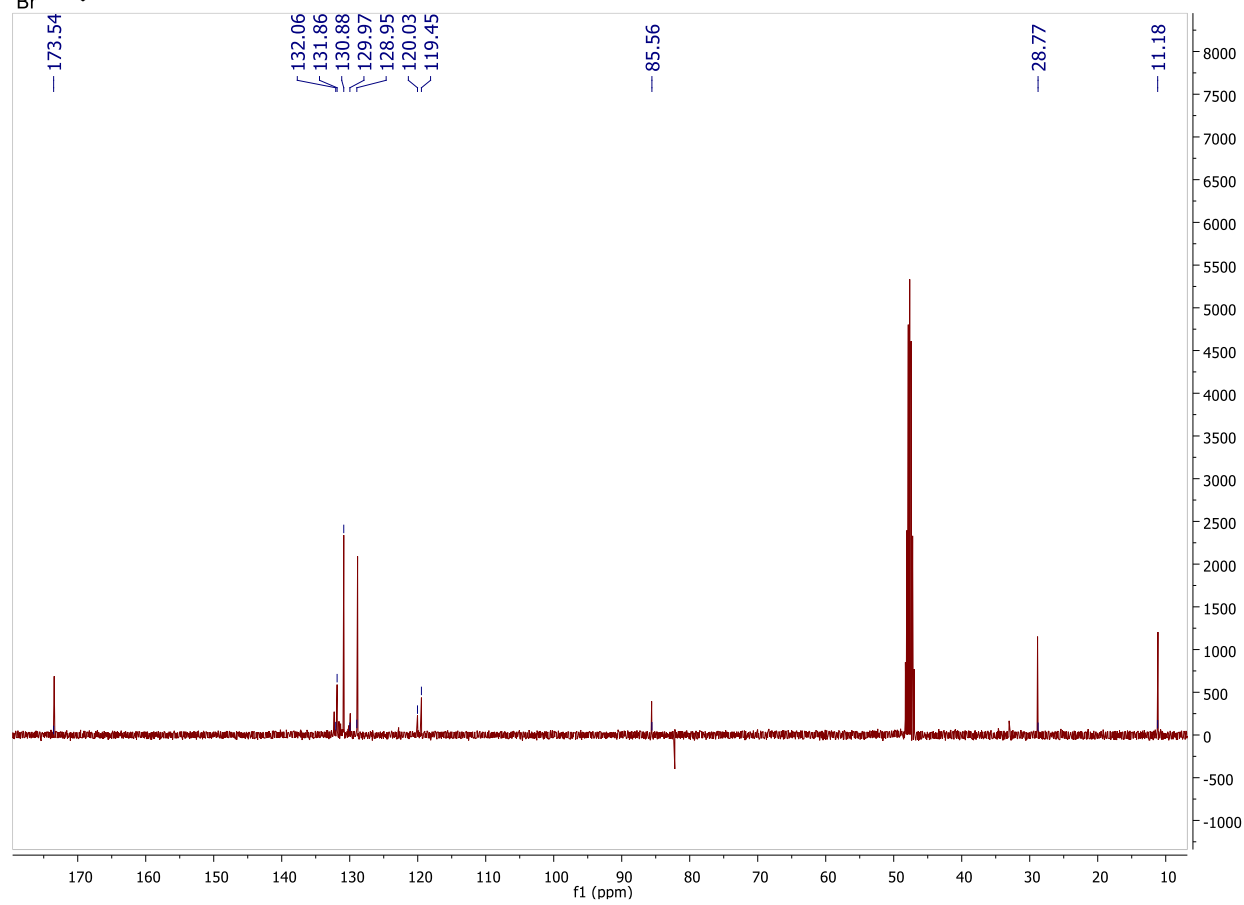
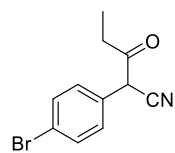
Figure 5S.3. Effect of (a) DMSO control, (b) SAHA and (c) **12b** on MDA-MB-231 cell cycle progression.

^1H NMR and ^{13}C NMR

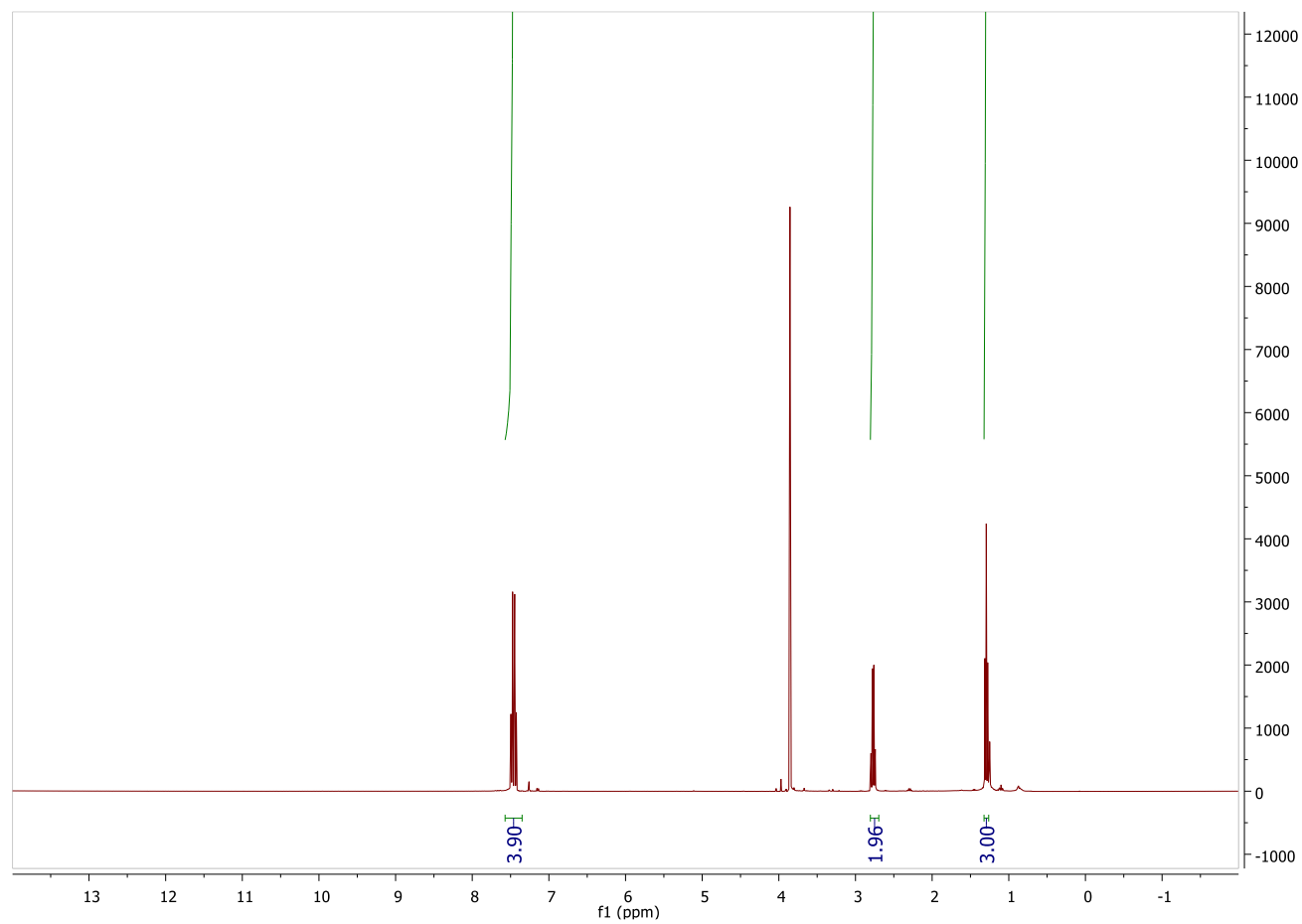
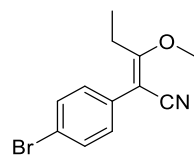
3 ^1H NMR



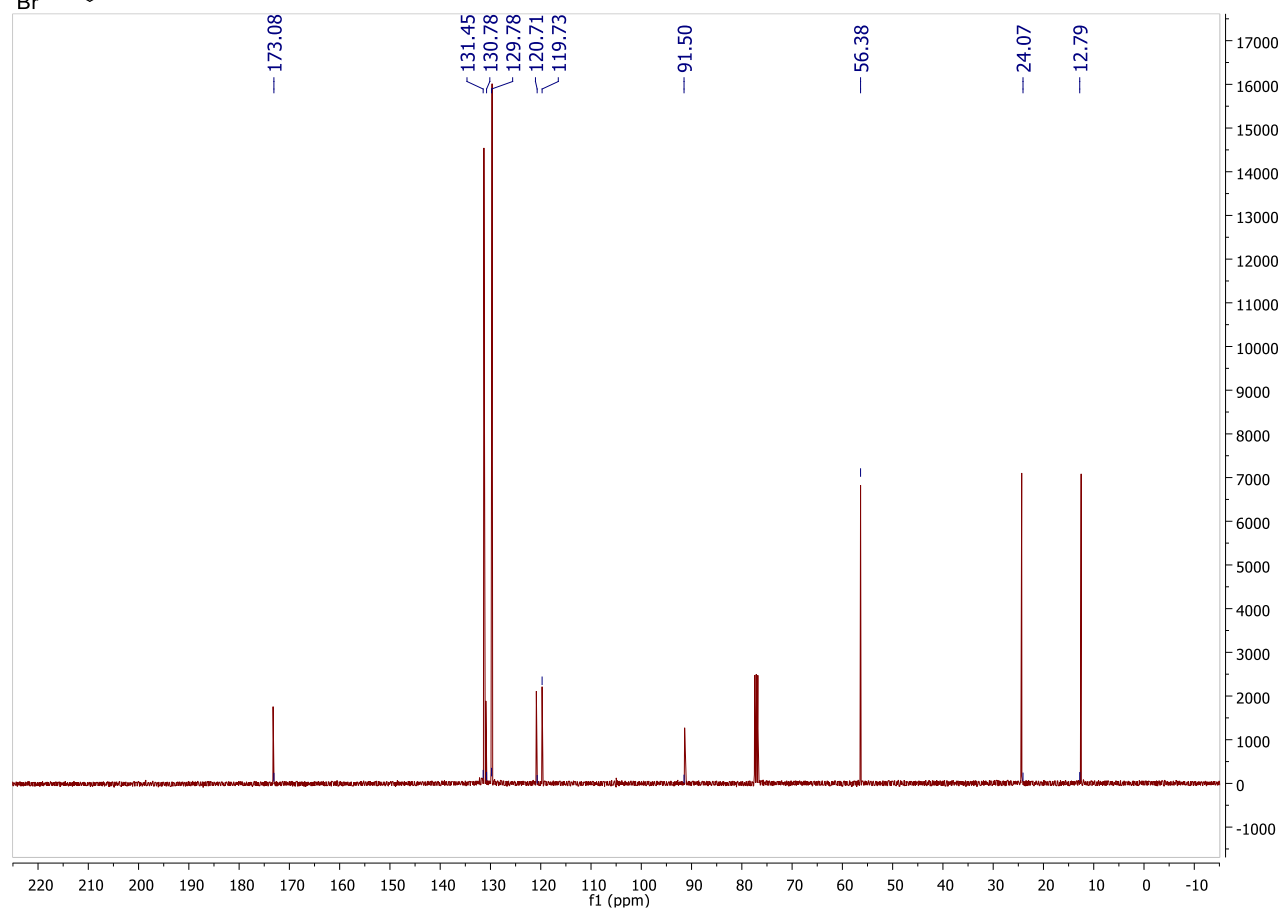
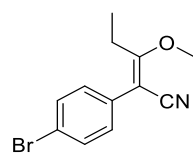
3 ^{13}C NMR



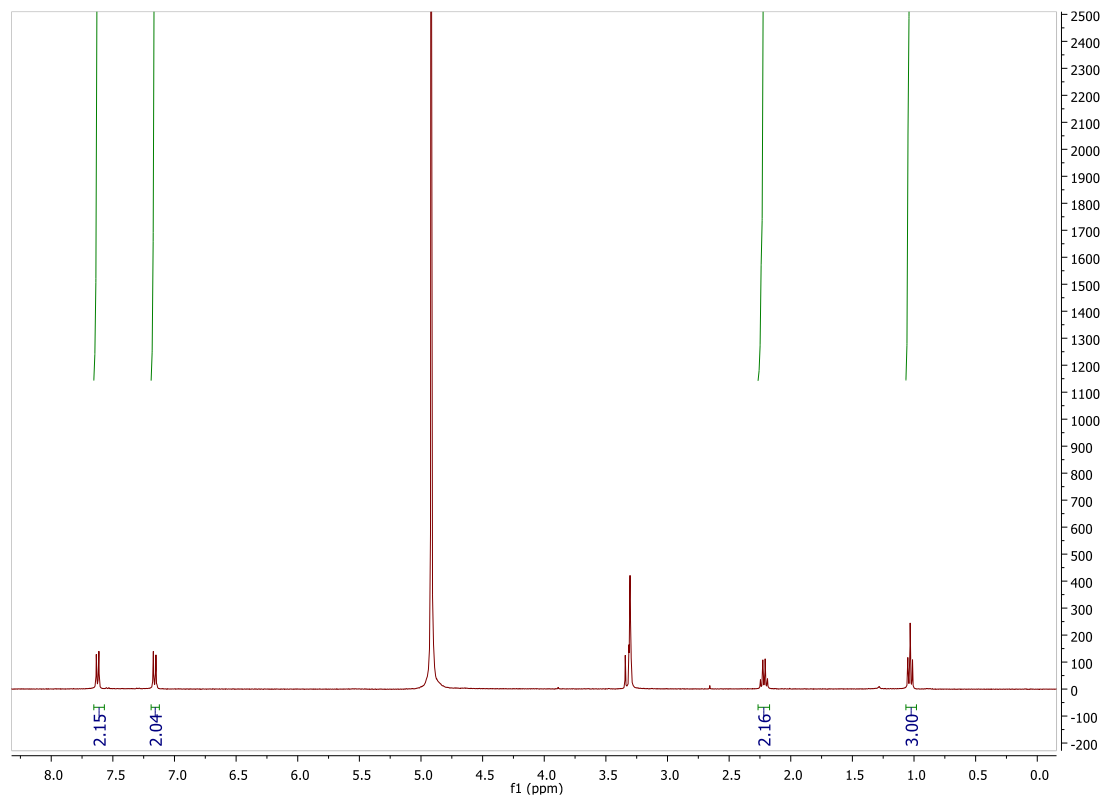
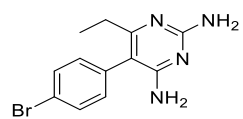
5 ^1H NMR



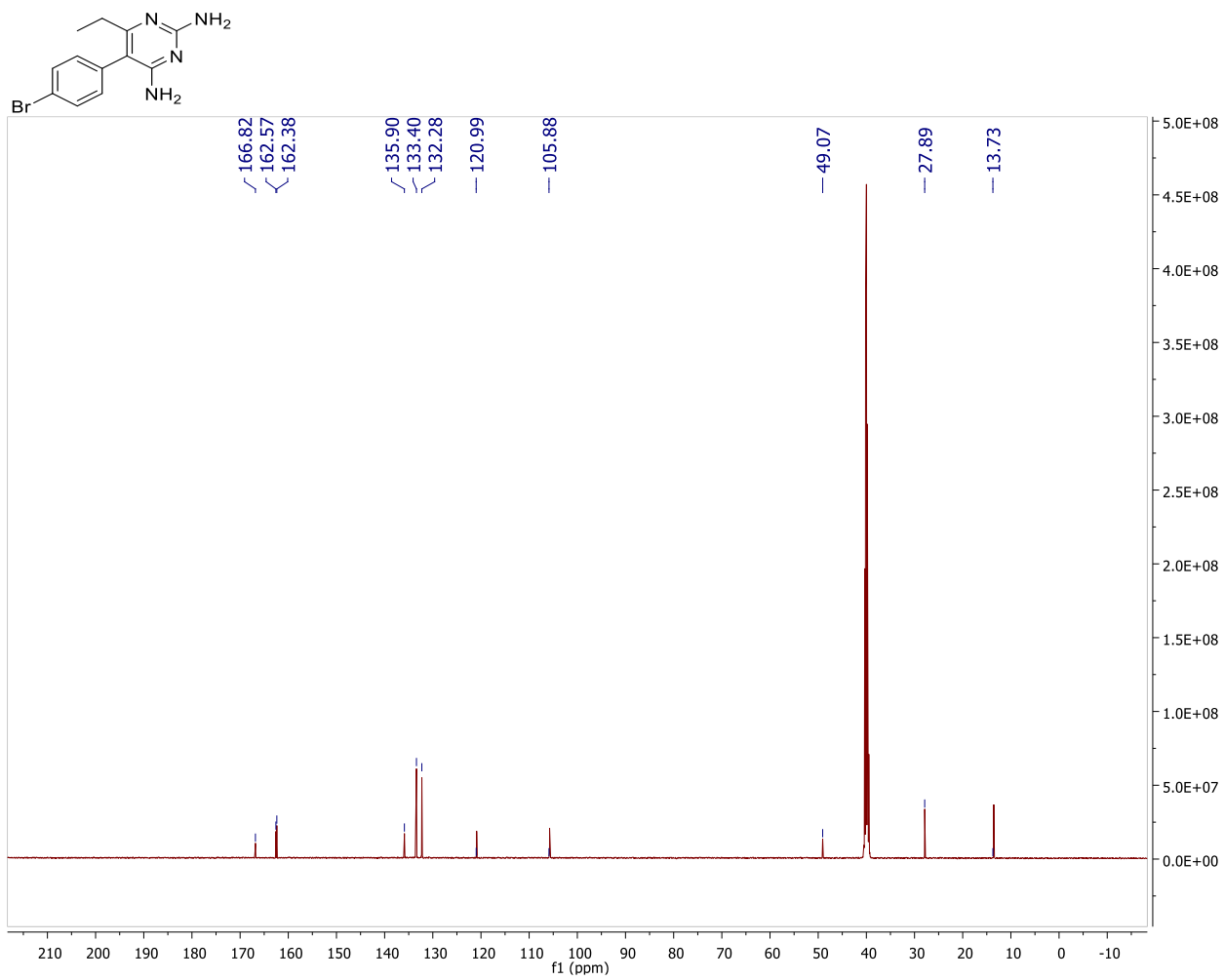
5 ¹³C NMR



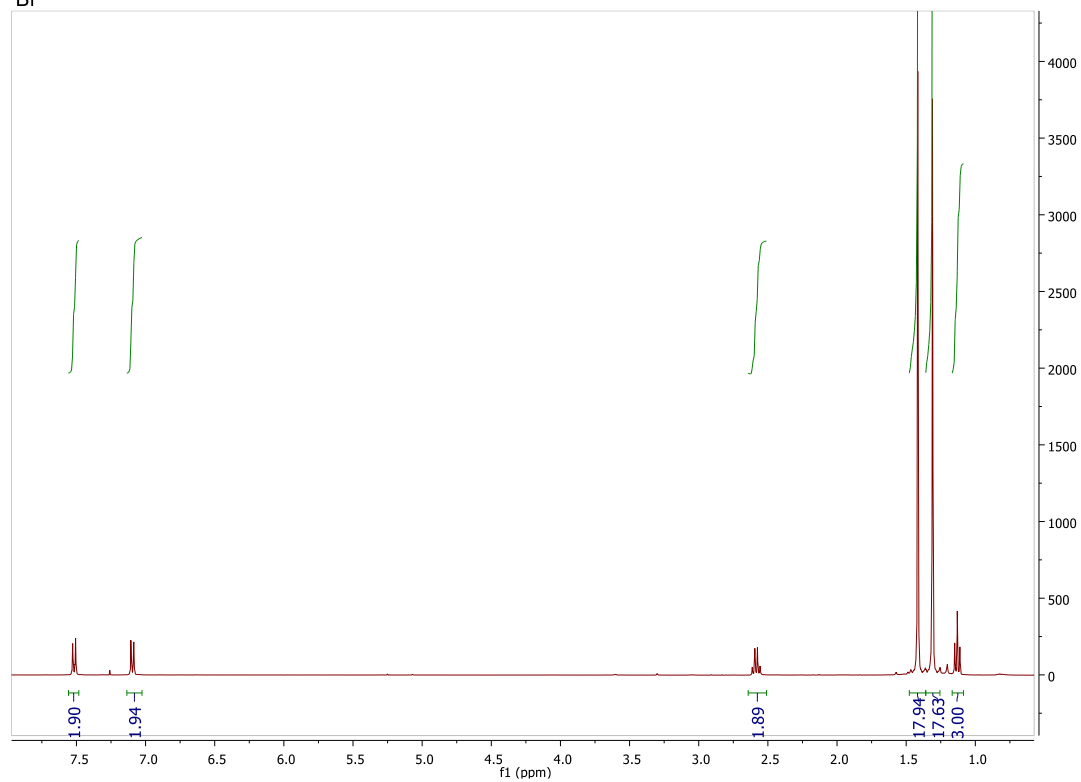
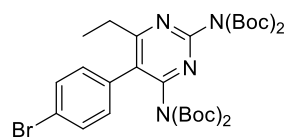
6 ^1H NMR



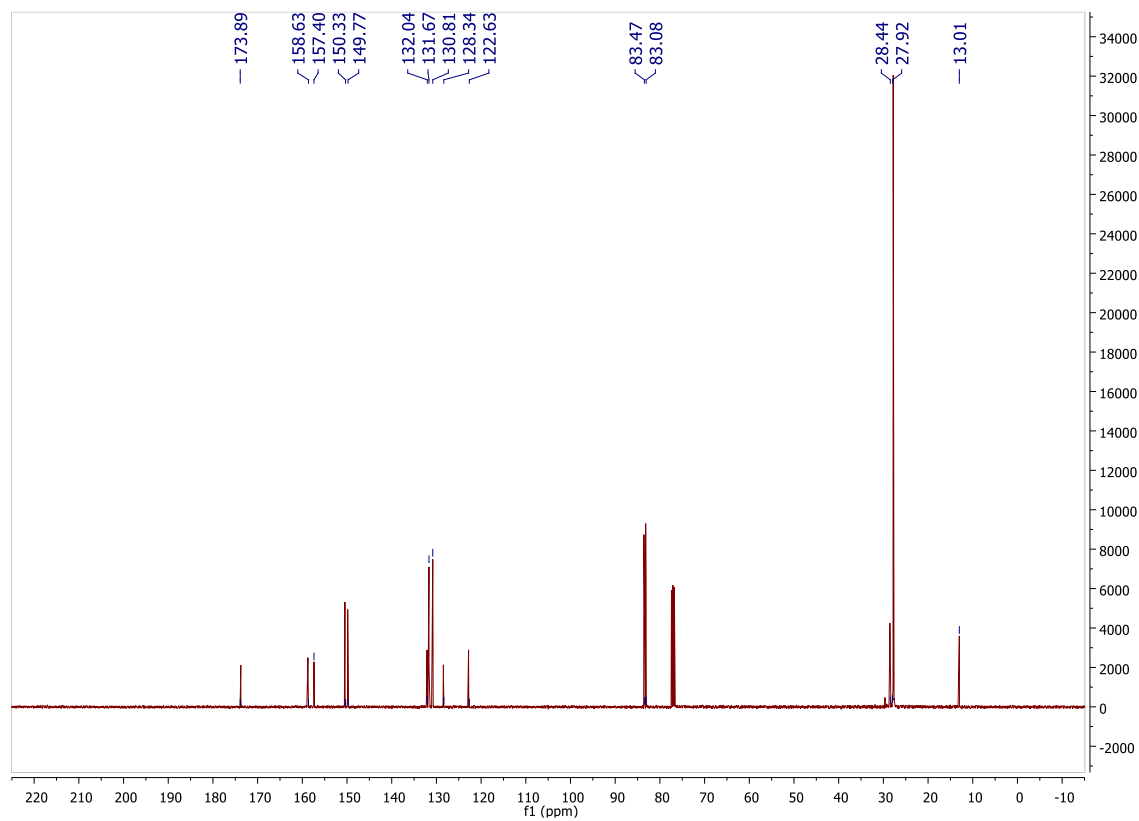
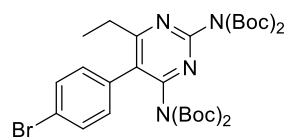
6 ¹³C NMR



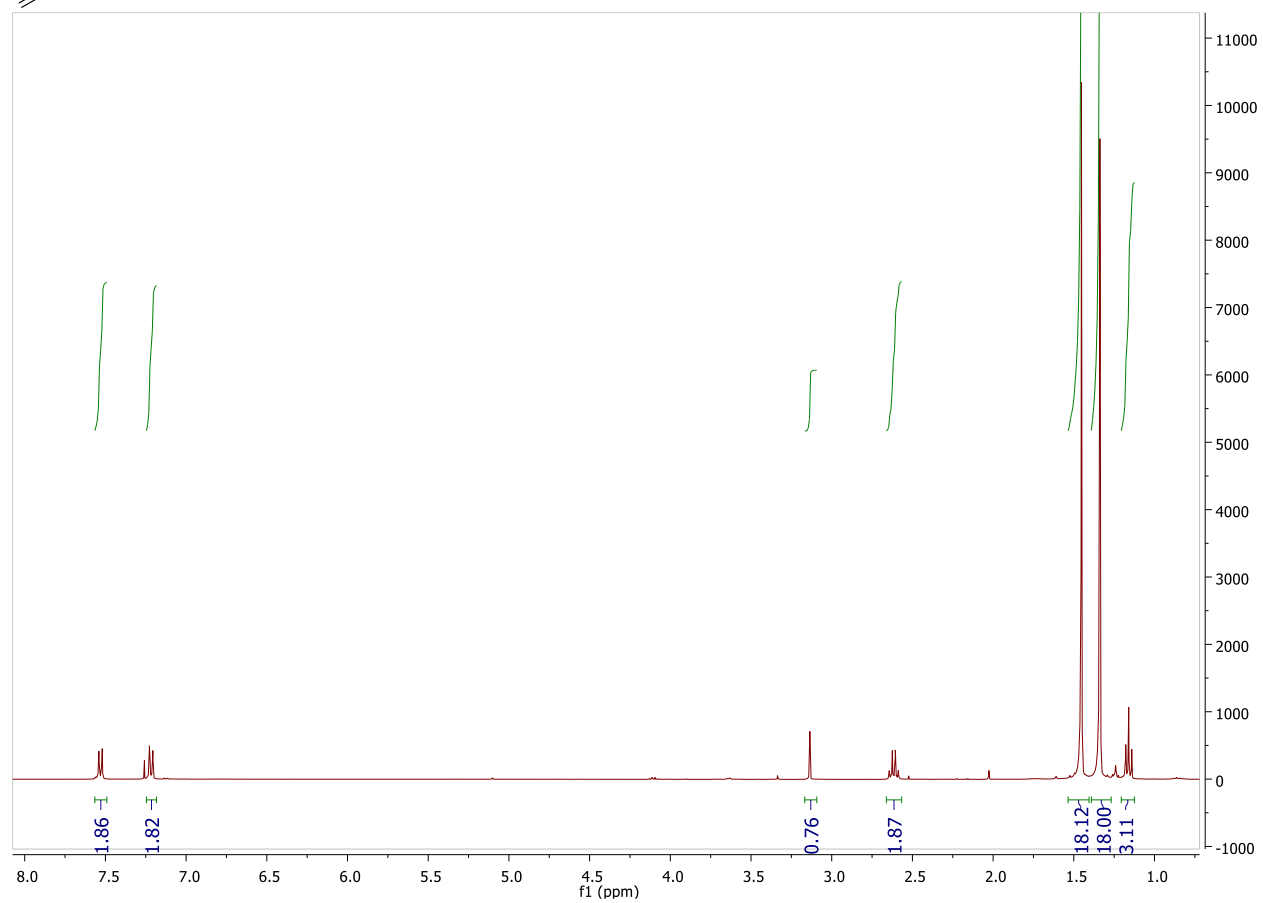
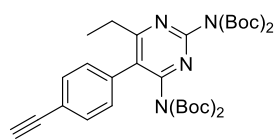
7 ¹H NMR



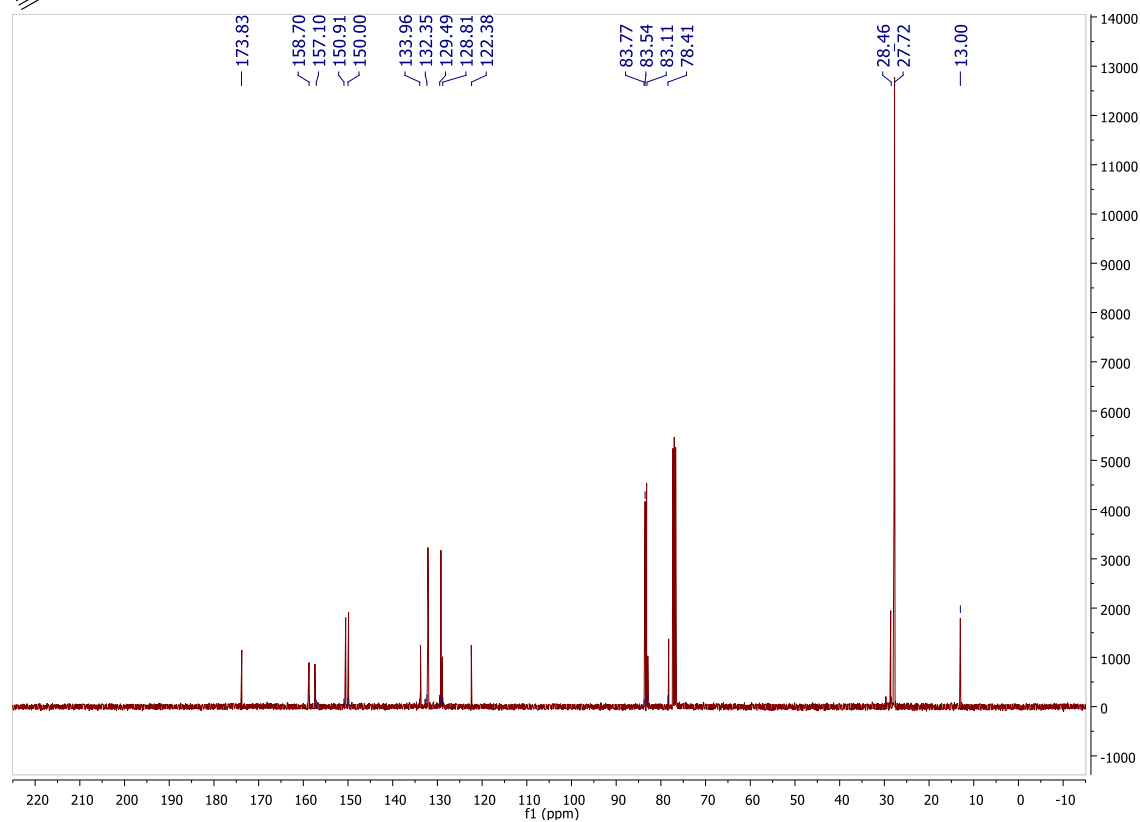
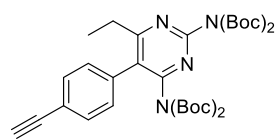
7 ¹³C NMR



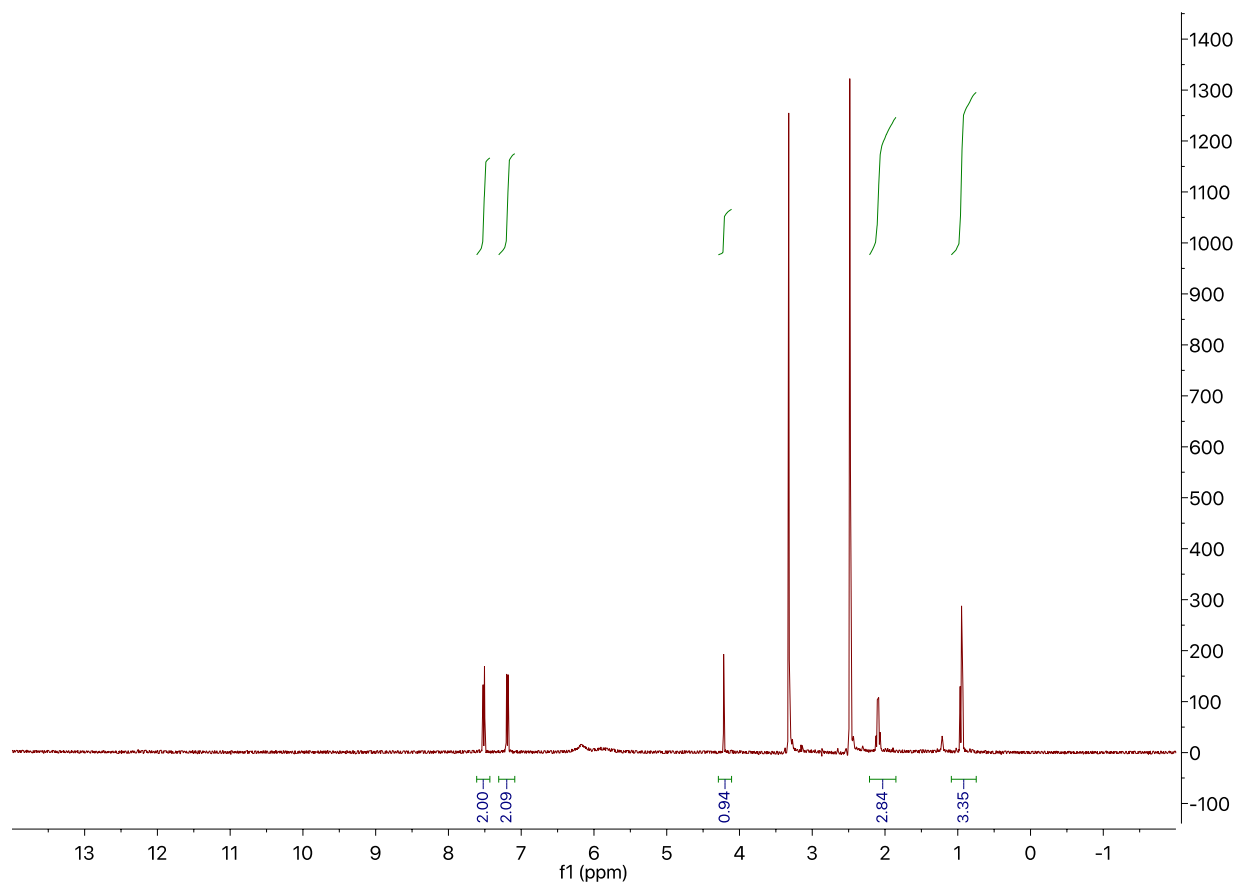
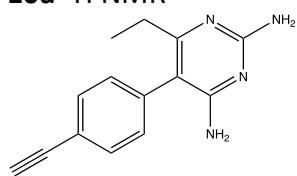
10 ^1H NMR



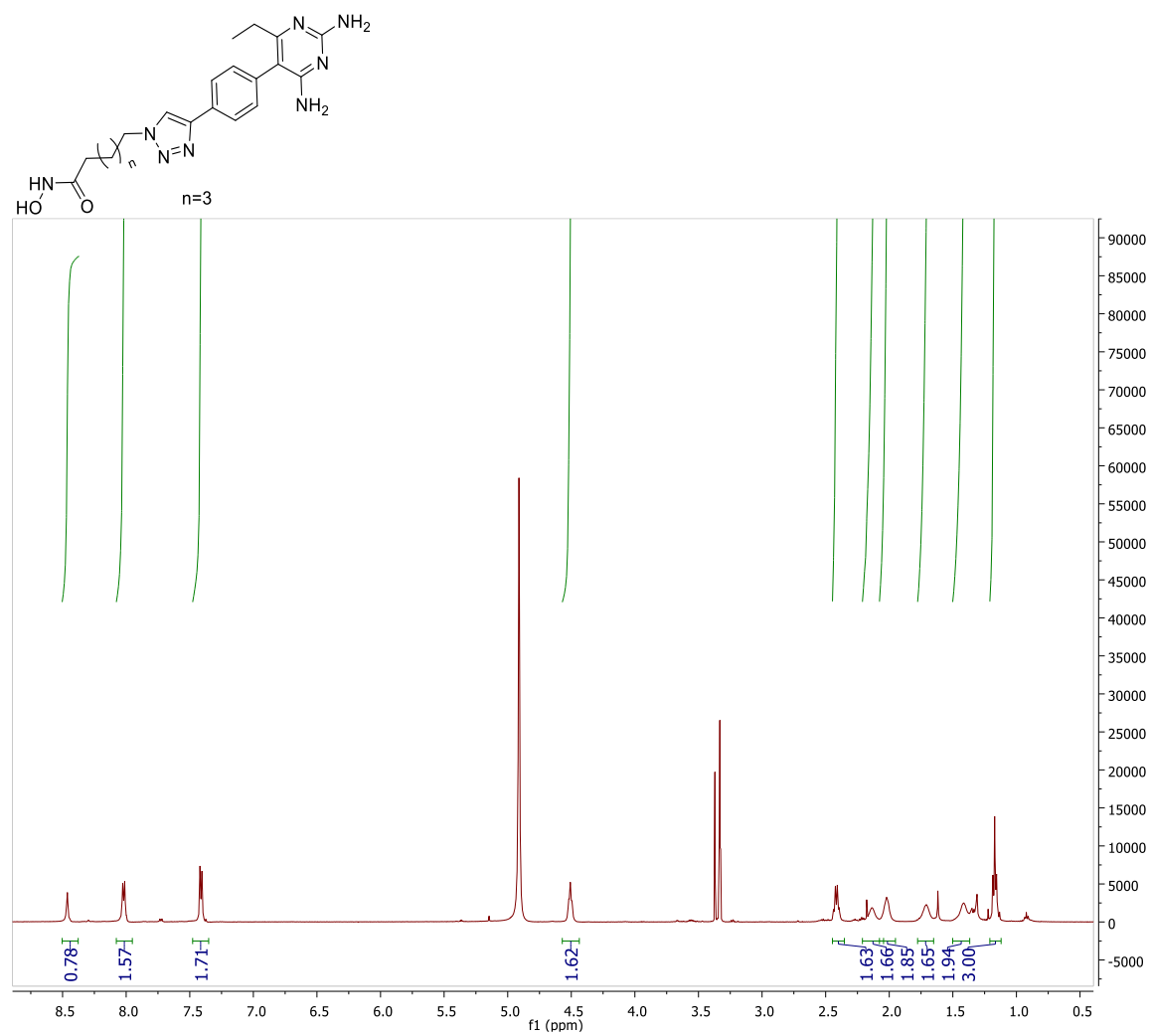
10 ^{13}C NMR



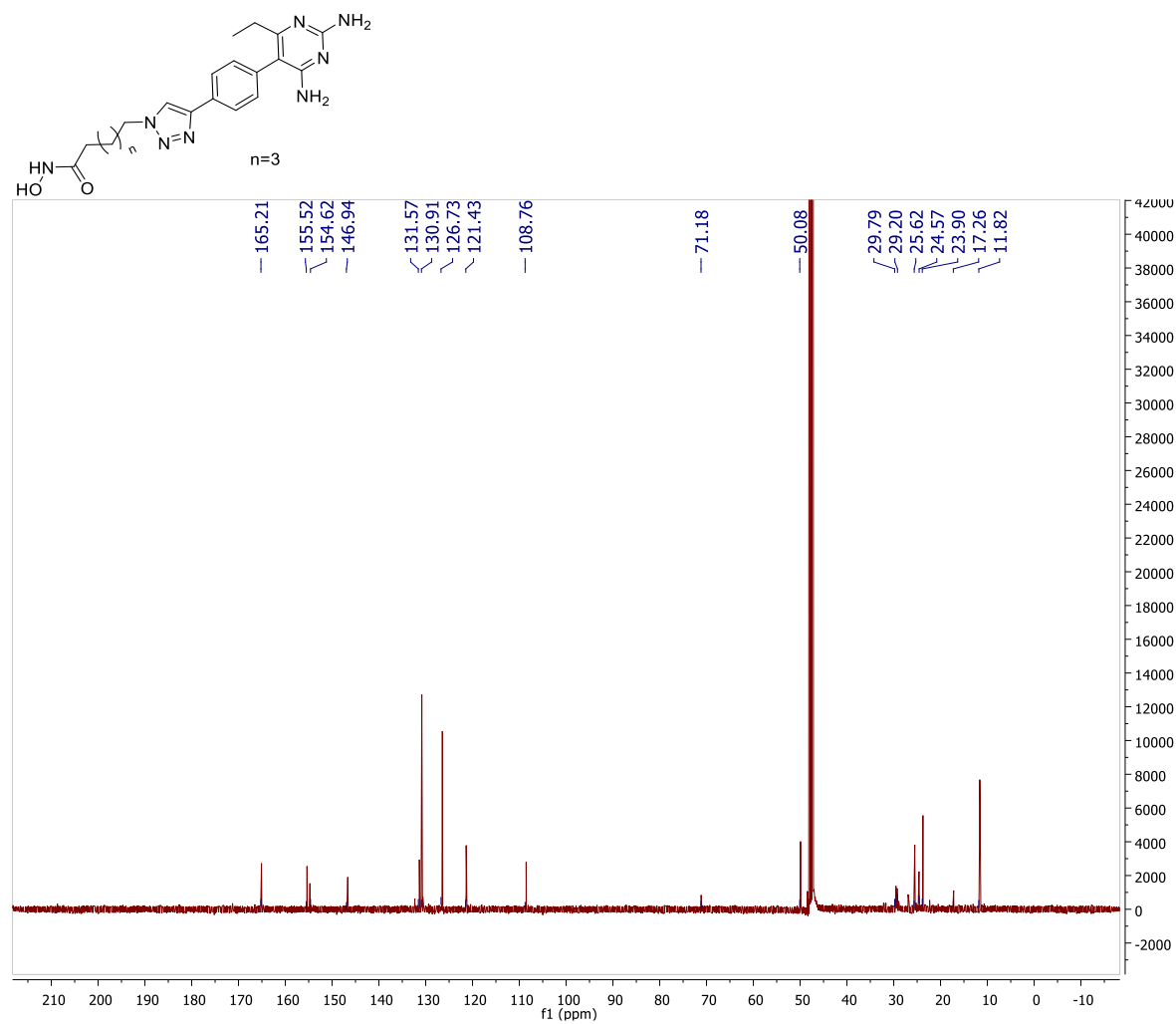
10a ^1H NMR



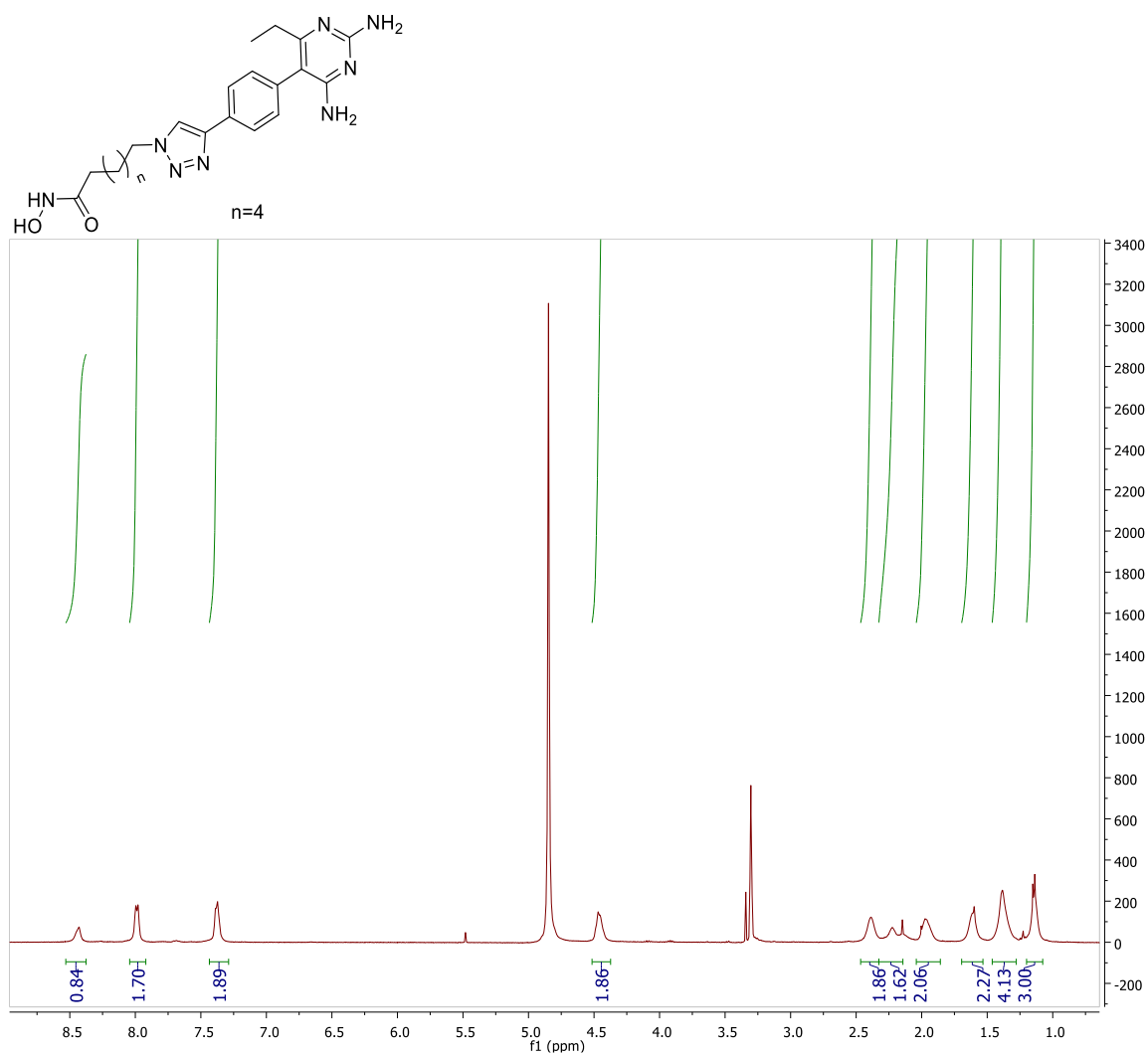
12a ^1H NMR



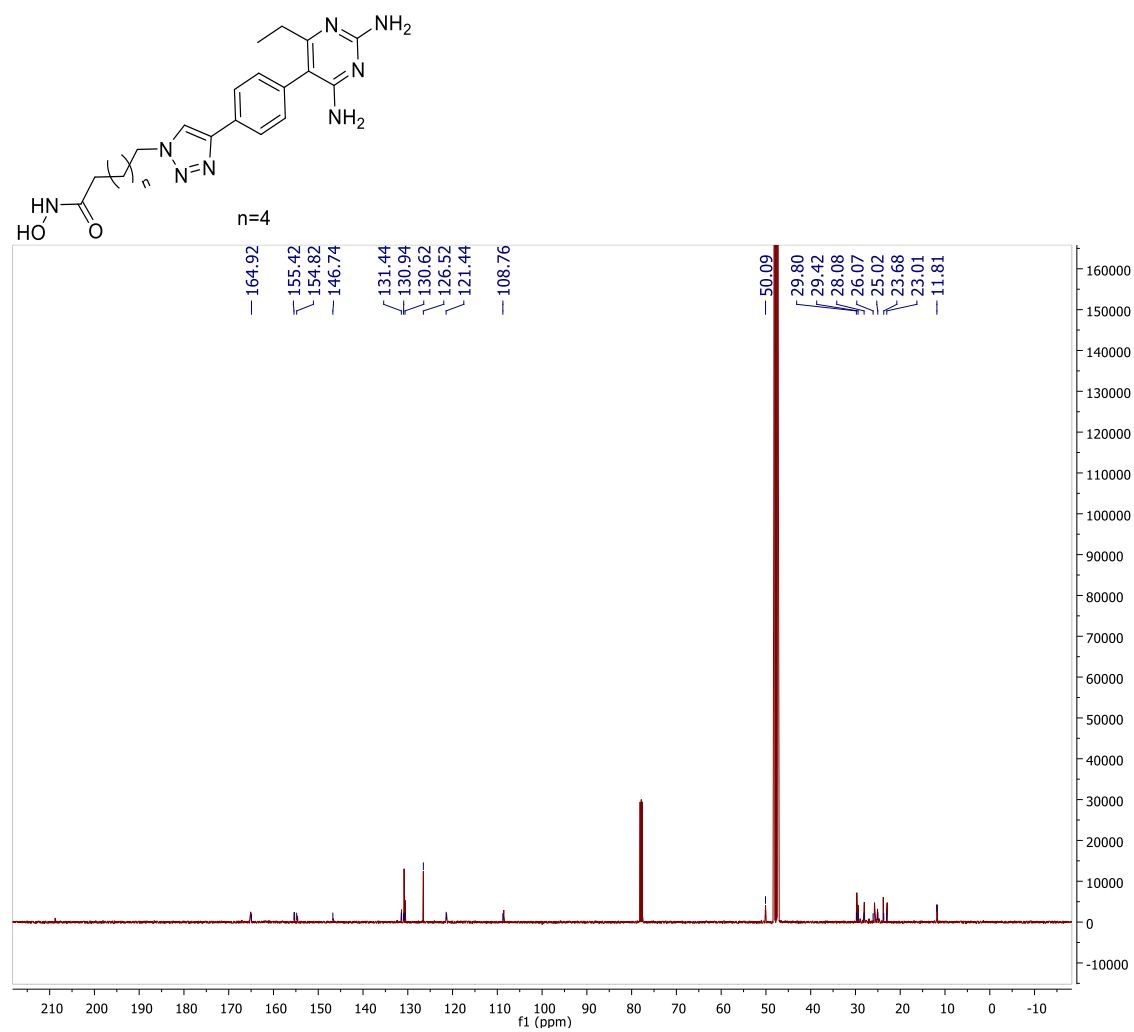
12a ^{13}C NMR



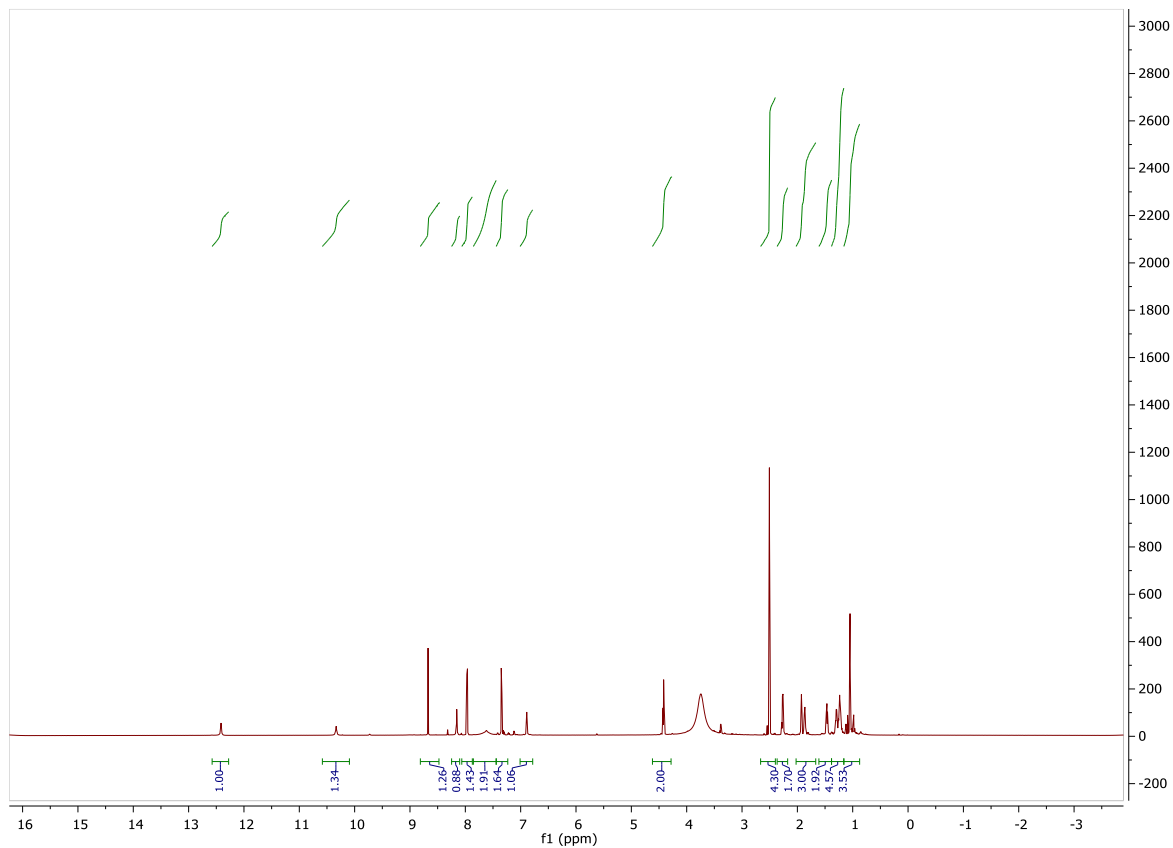
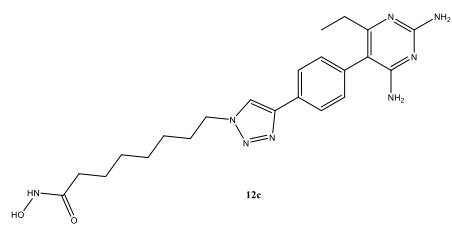
12b ^1H NMR



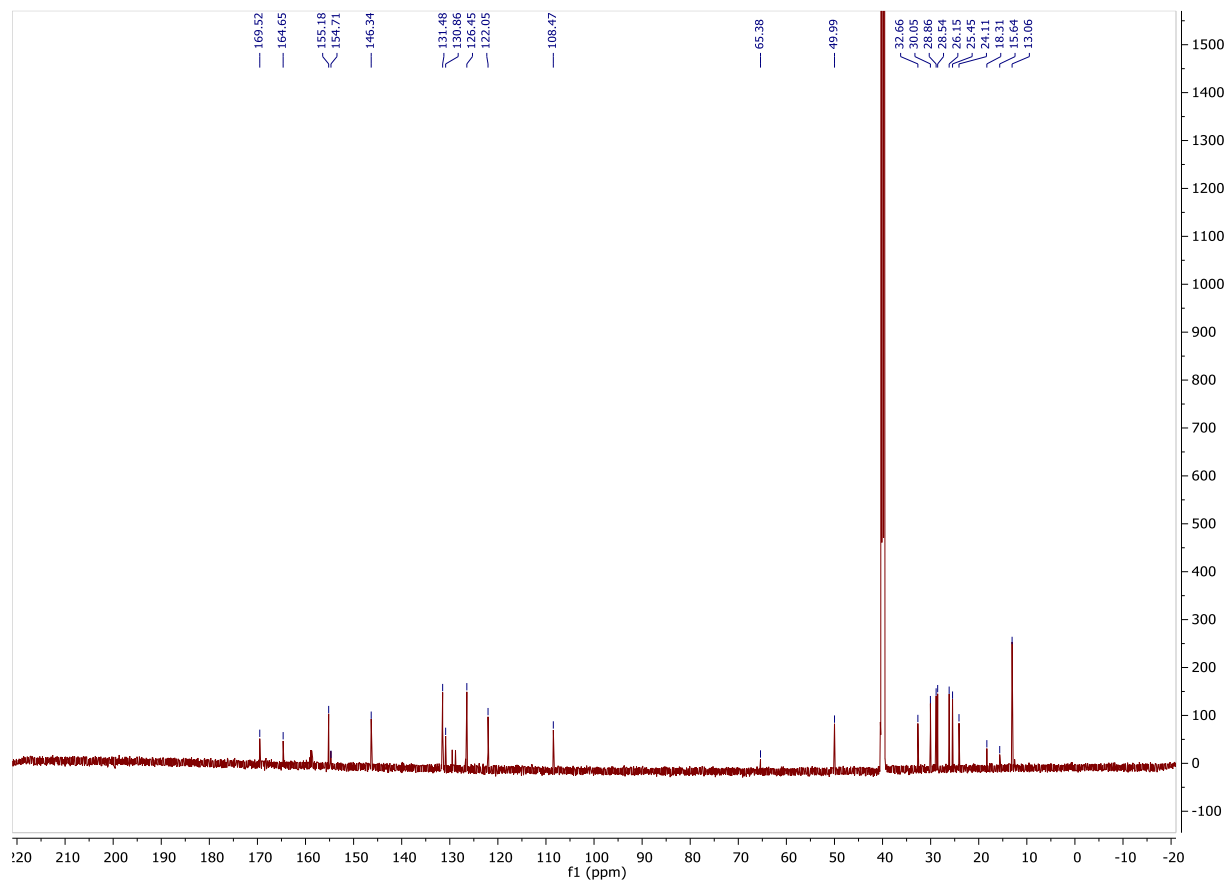
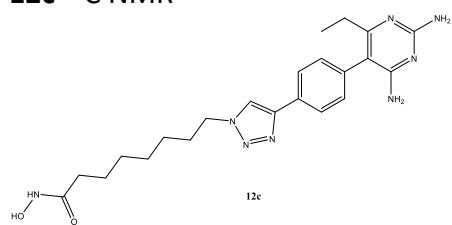
12b ^{13}C NMR



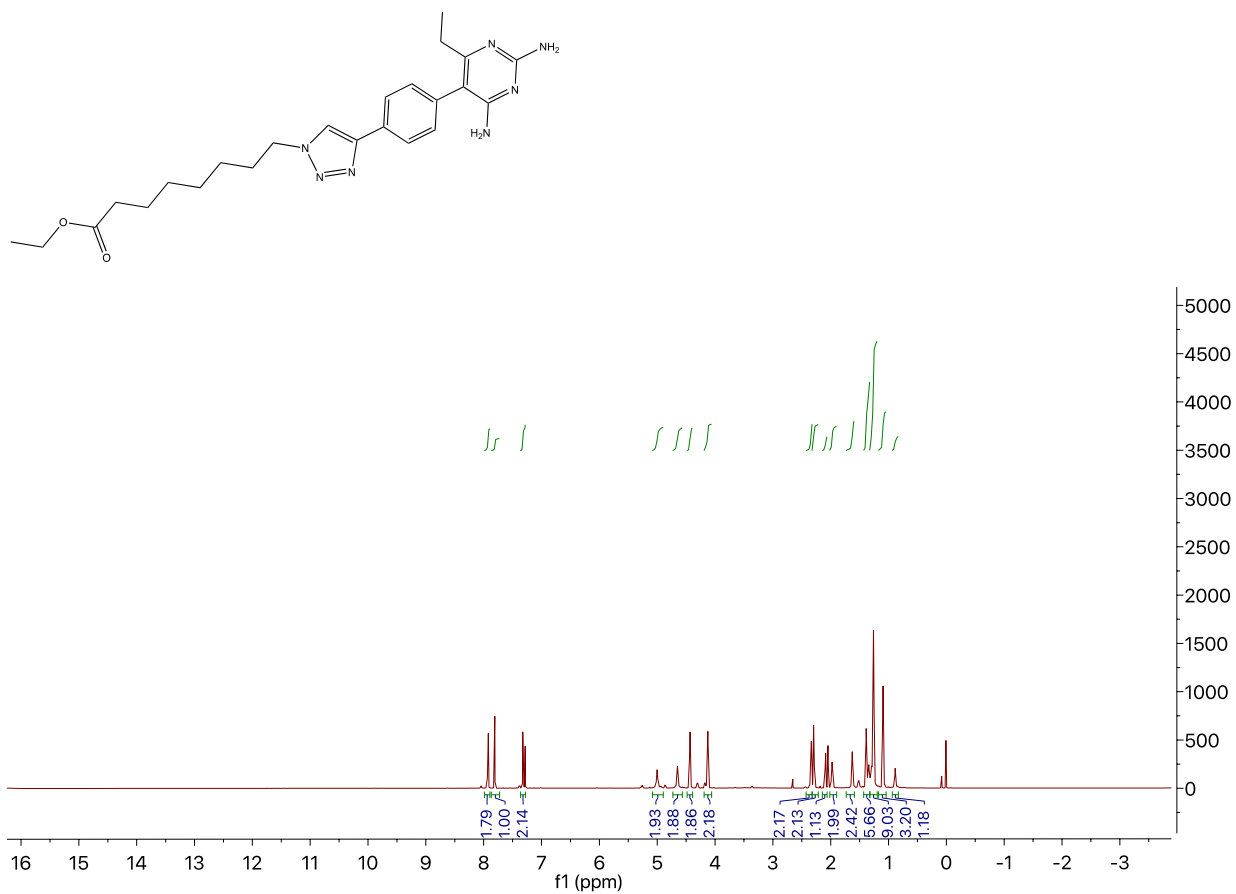
12c ^1H NMR



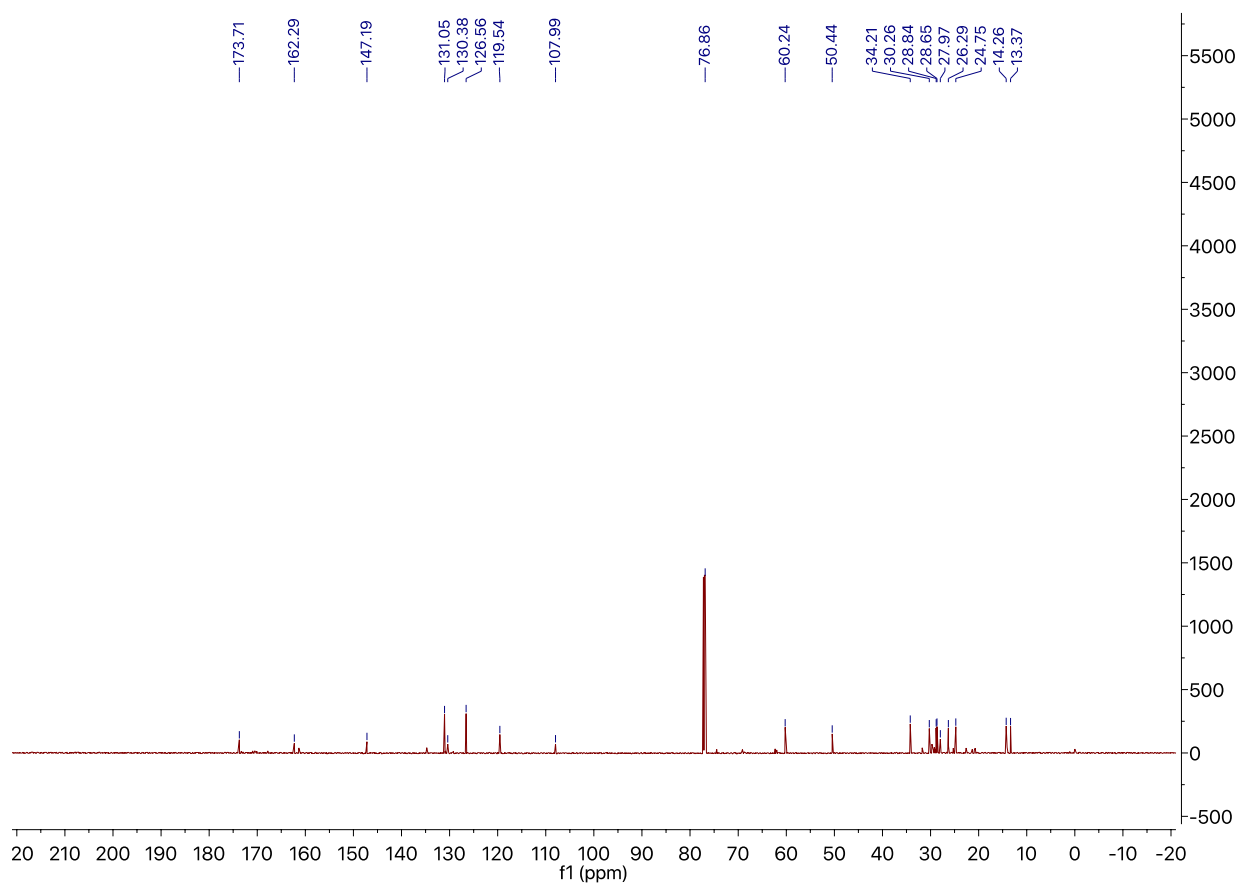
12c ^{13}C NMR



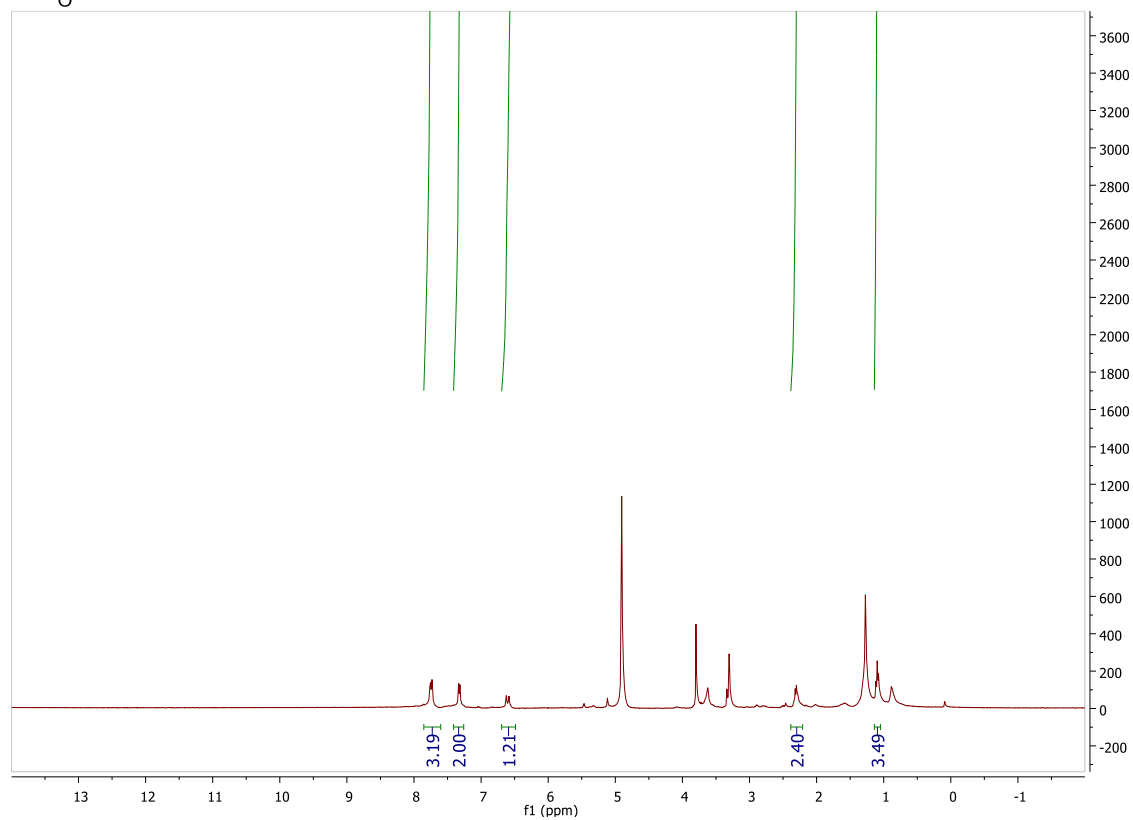
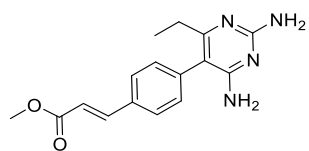
12d. ^1H NMR



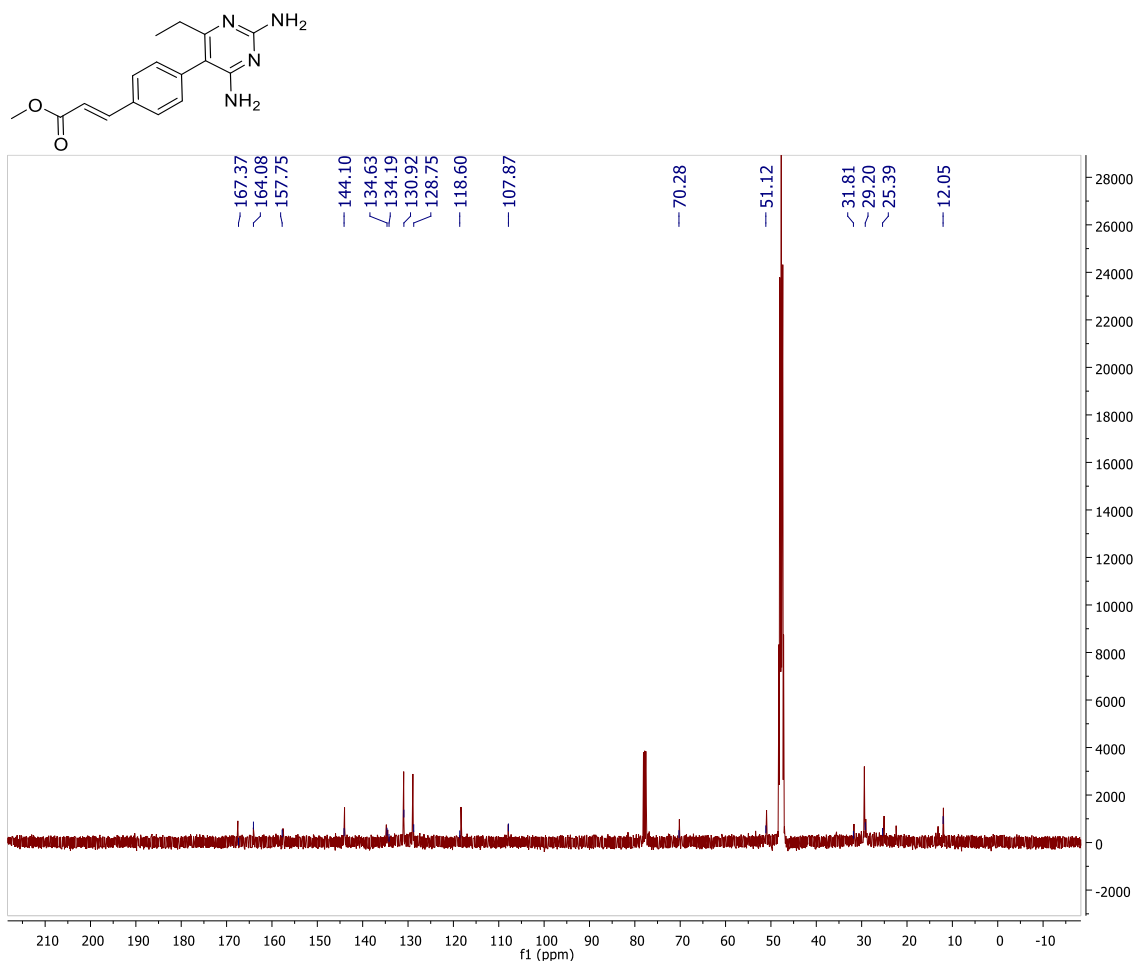
12d ^{13}C NMR



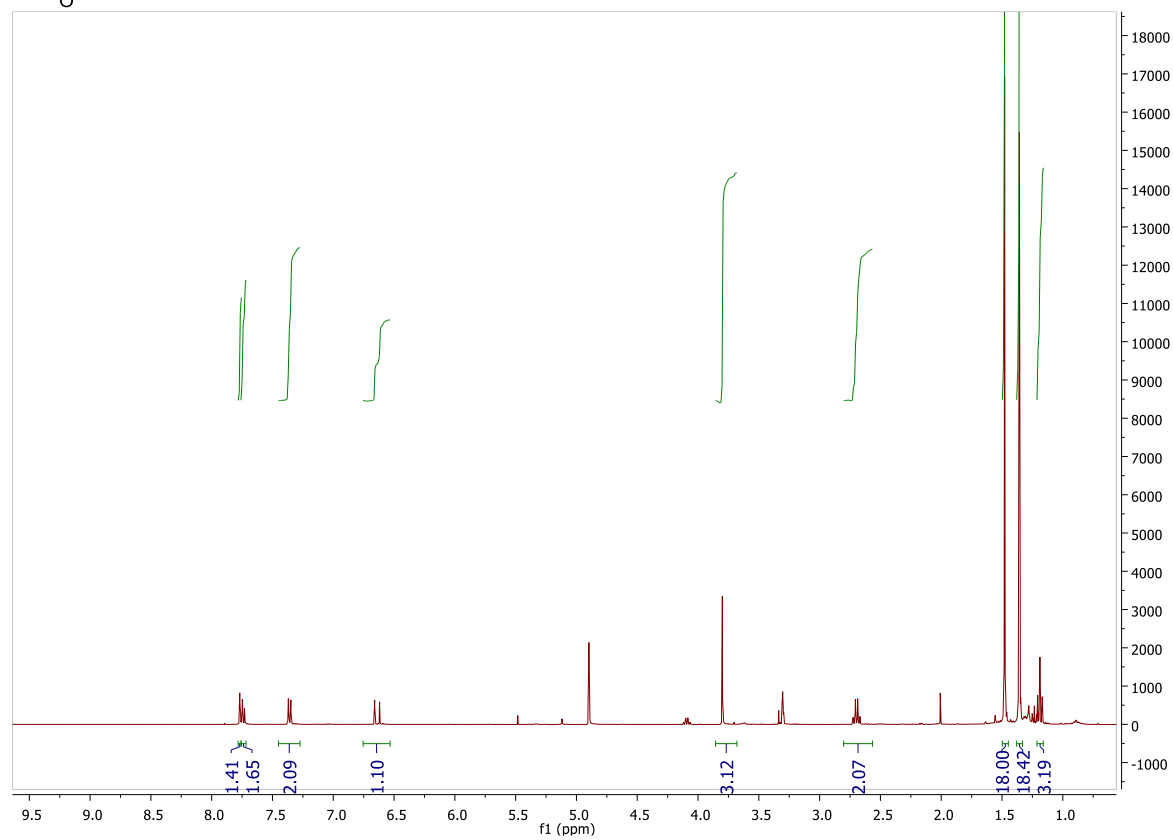
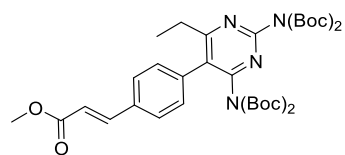
14 ¹H NMR



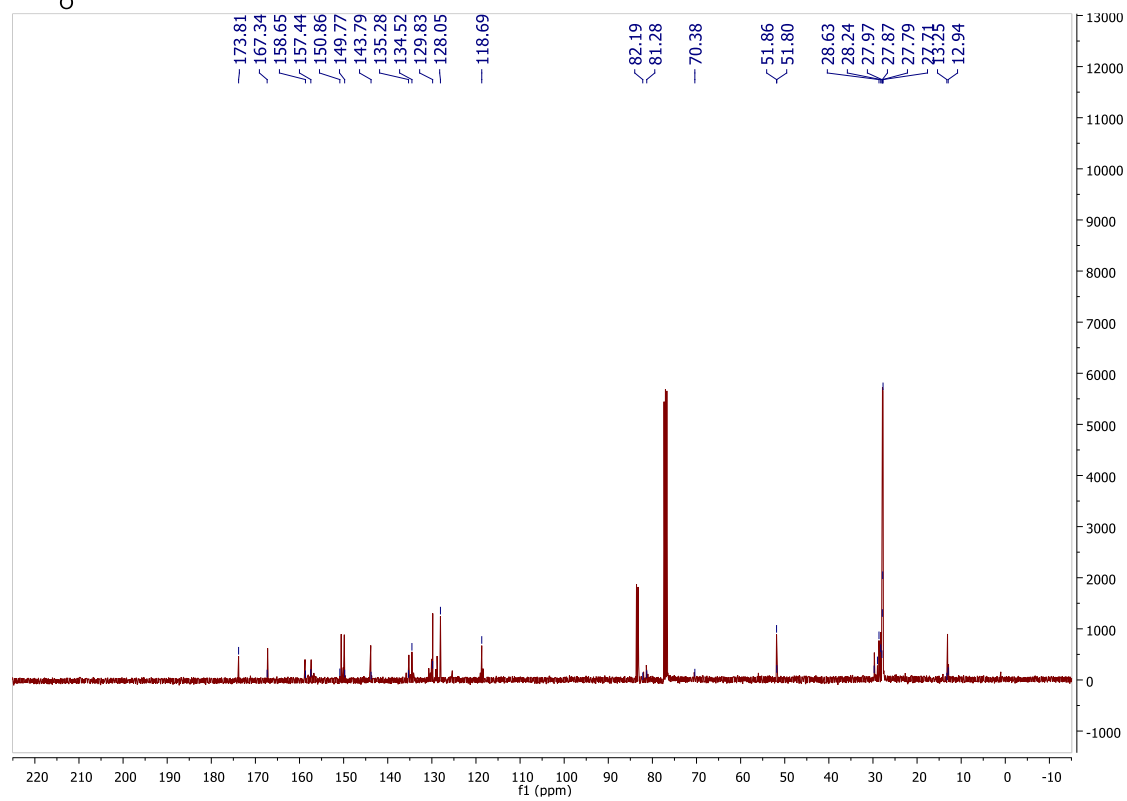
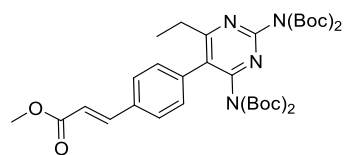
14 ¹³C NMR



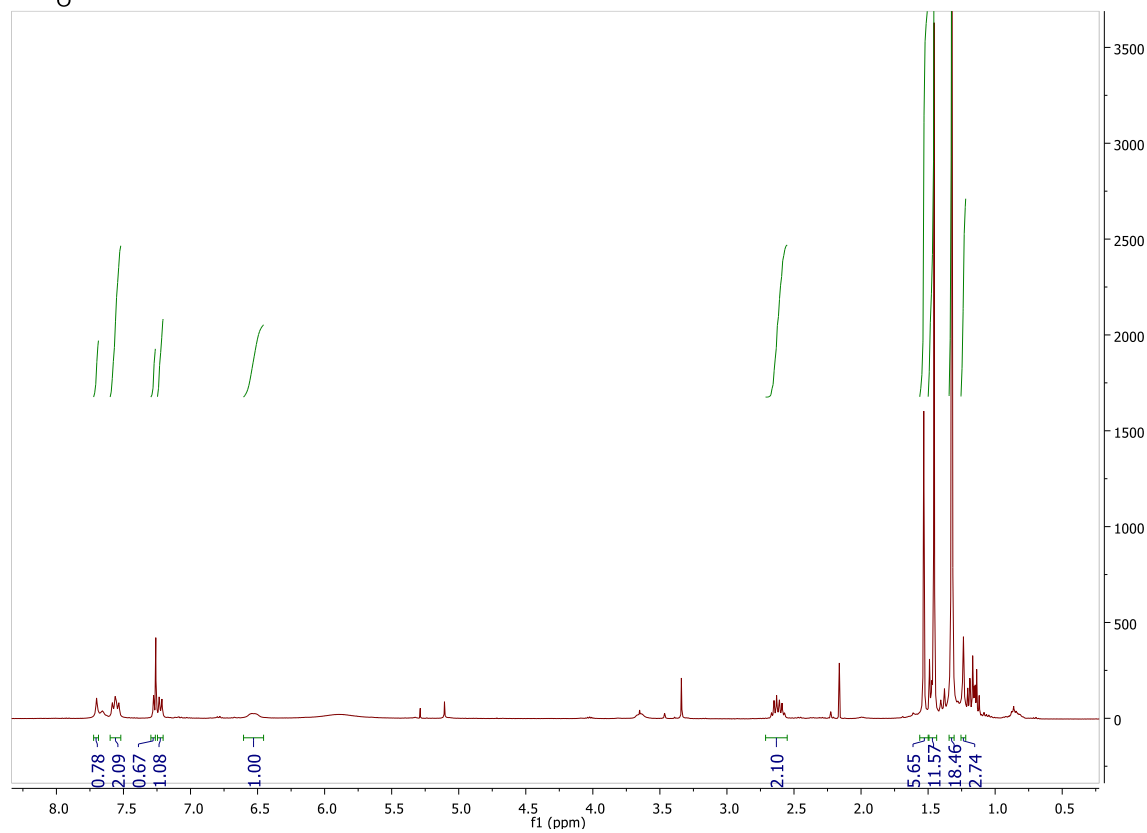
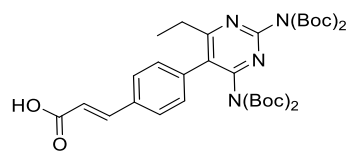
15 ¹H NMR



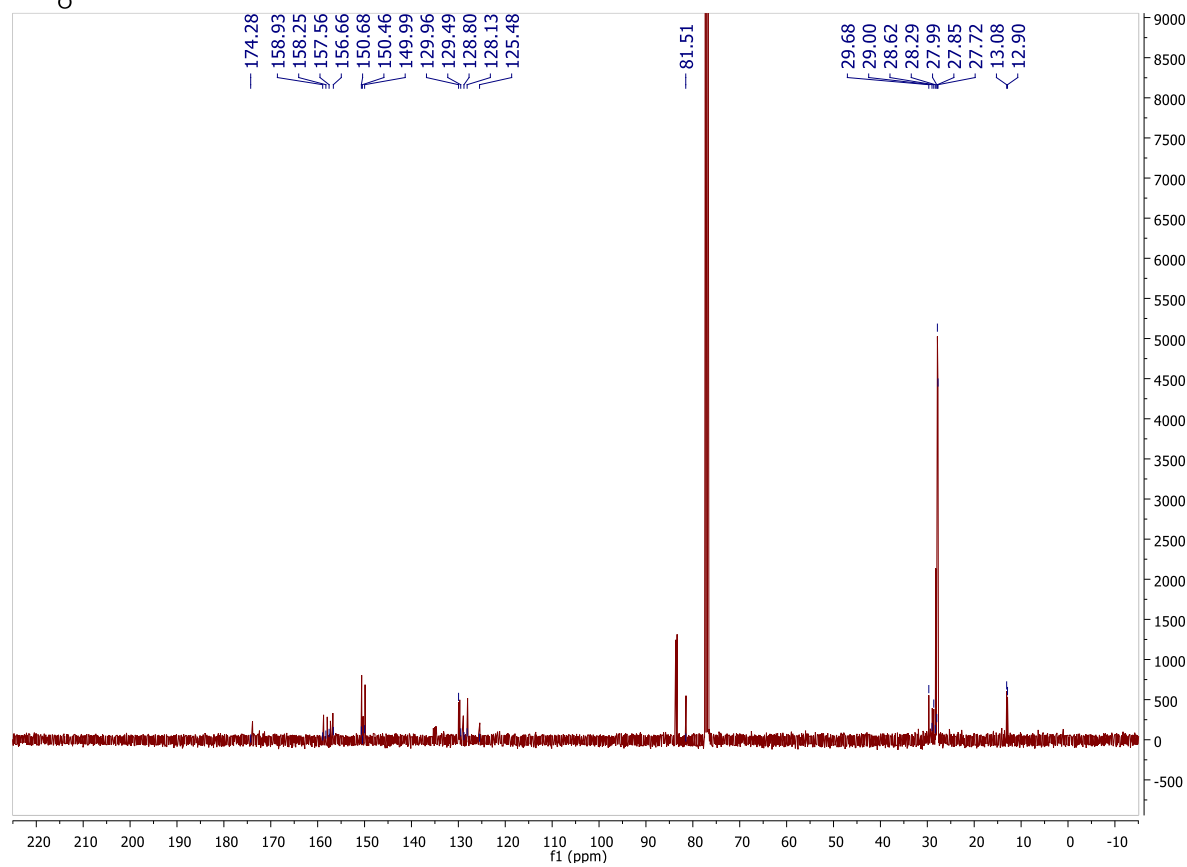
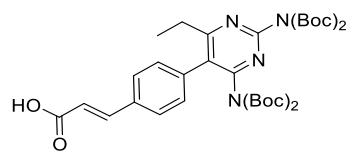
15 ¹³C NMR



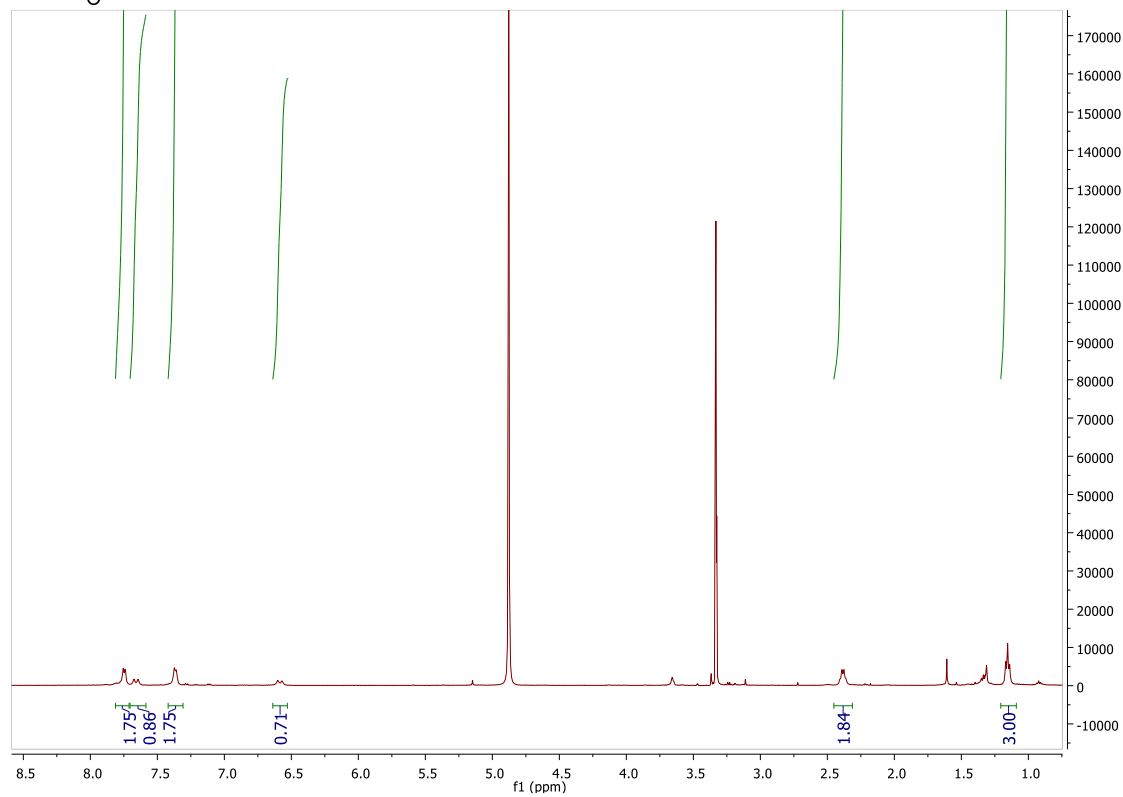
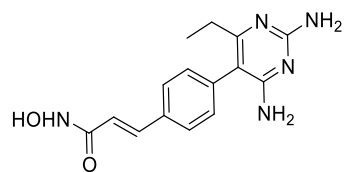
16 ^1H NMR



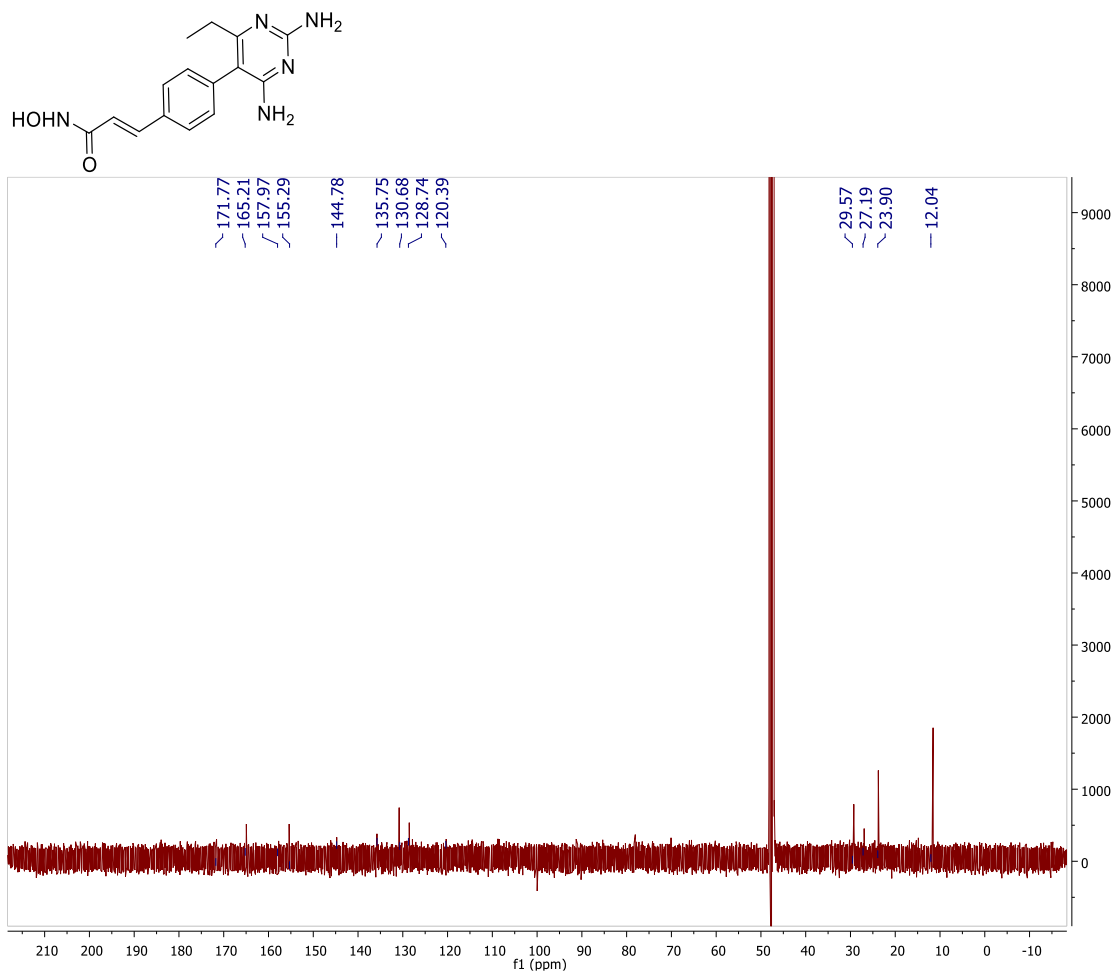
16 ^{13}C NMR



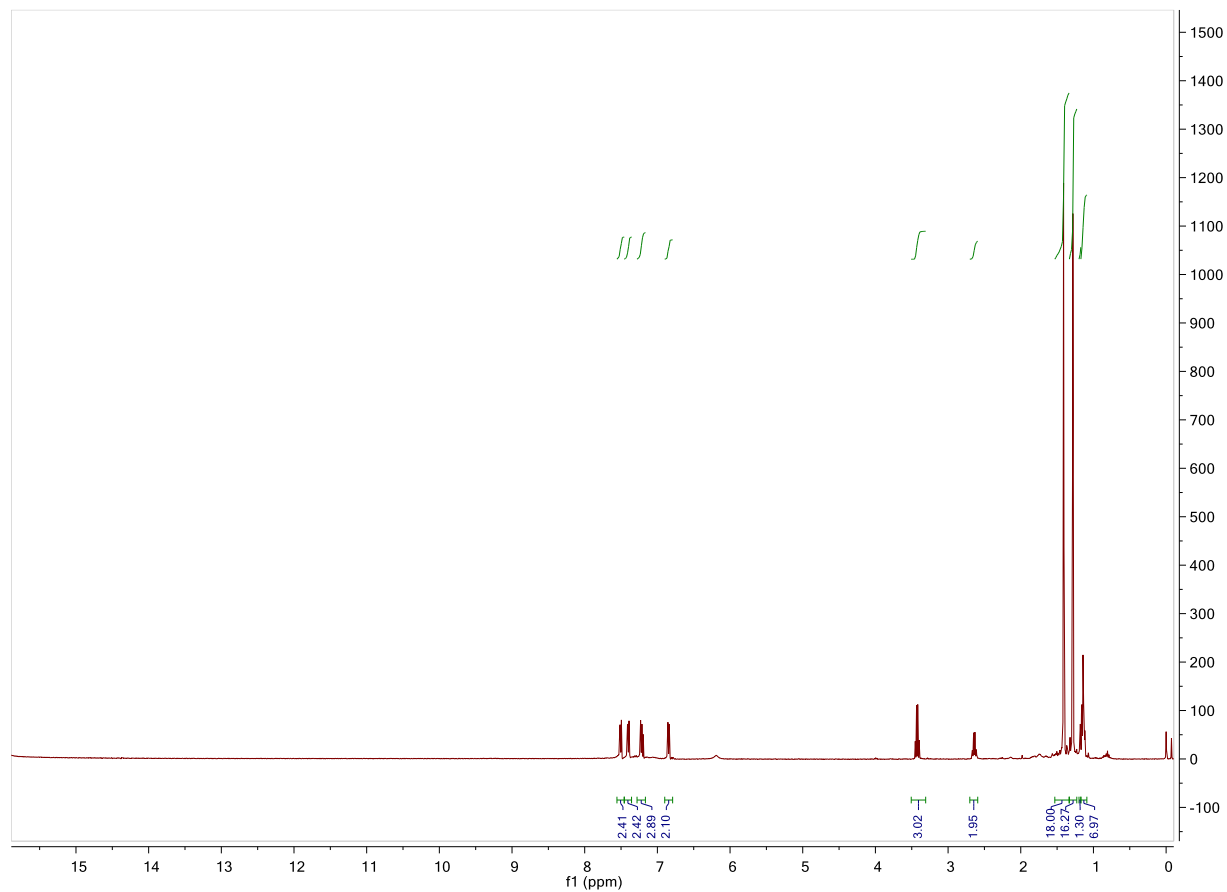
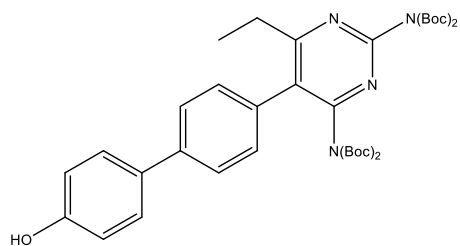
18 ^1H NMR



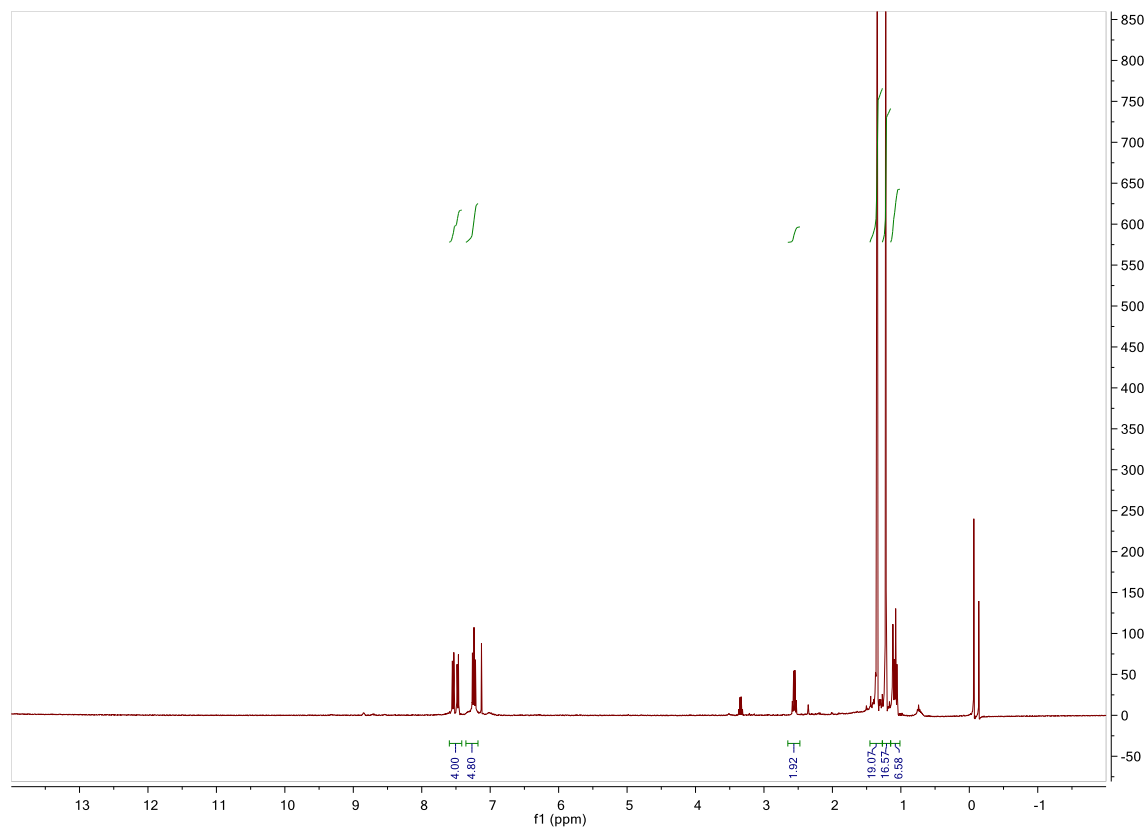
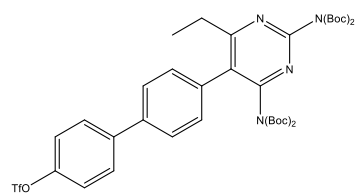
18 ^{13}C NMR



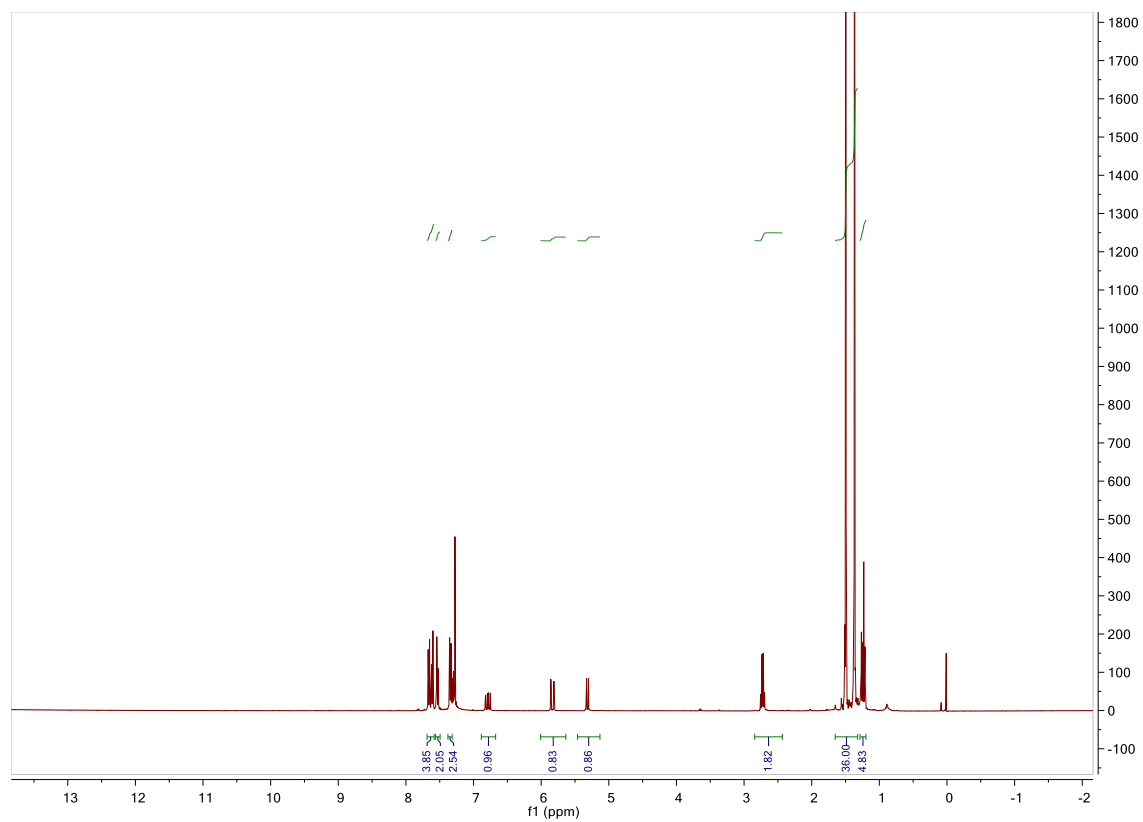
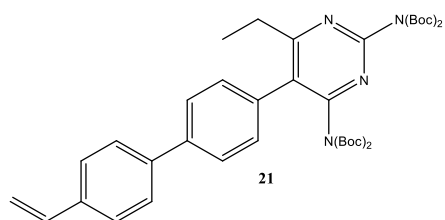
19 ¹H NMR



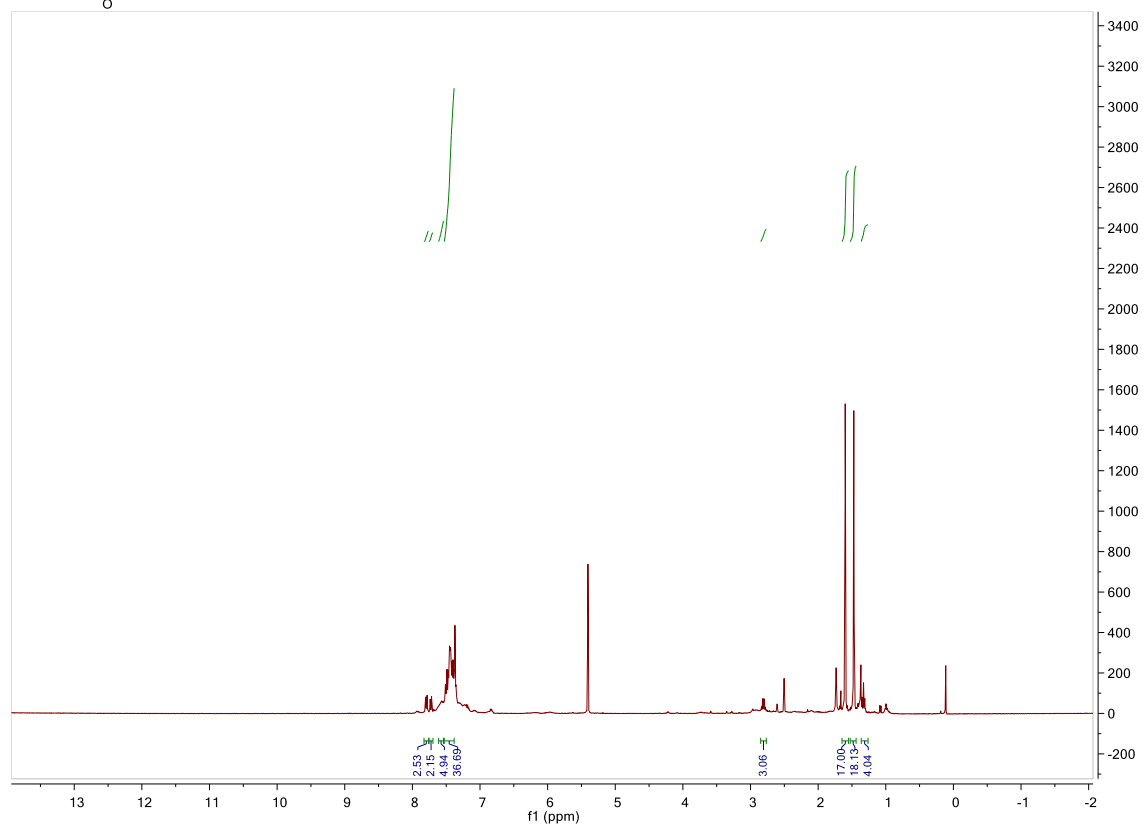
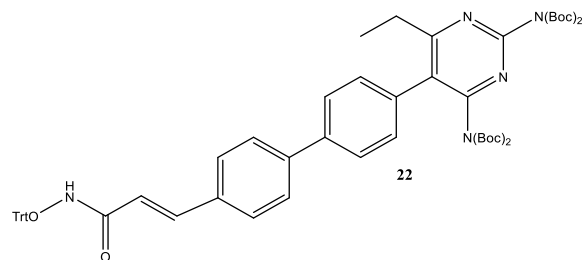
20 ^1H NMR



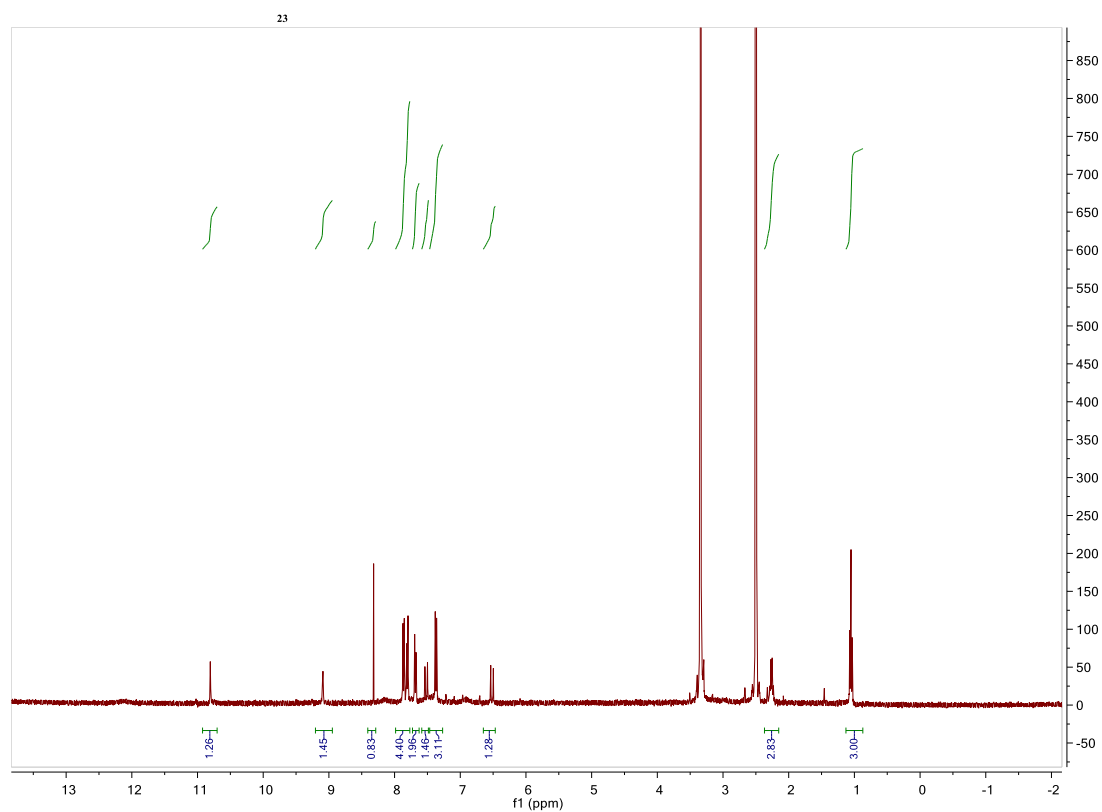
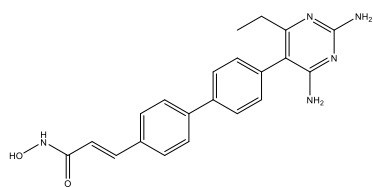
21 ^1H NMR



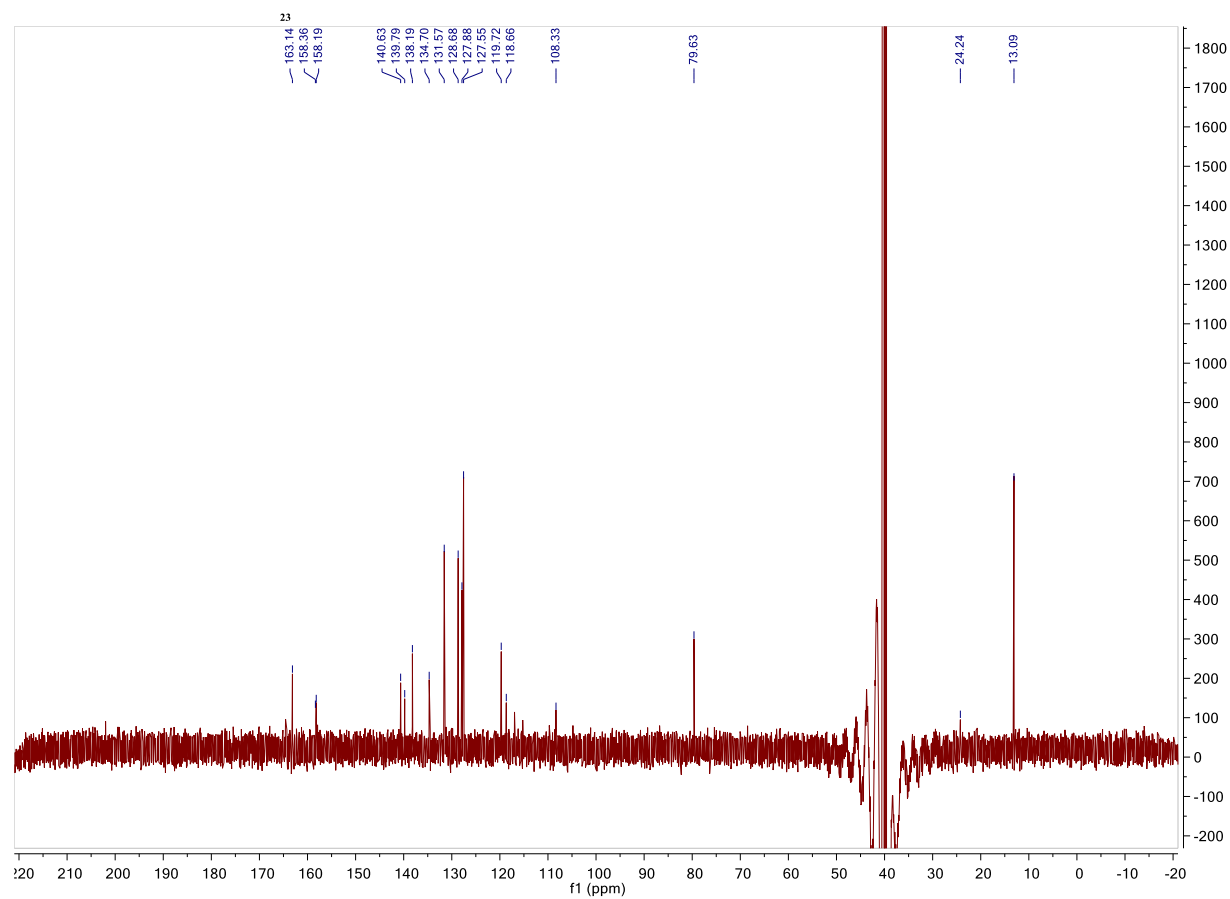
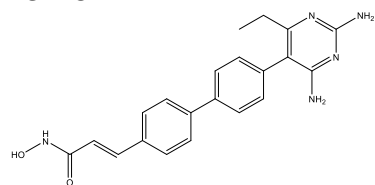
22 ¹H NMR



23 ¹H NMR



23 ¹³C NMR



CHAPTER 6. DISCOVERY OF NOVEL STAT3 DNA BINDING DOMAIN INHIBITORS.

Bocheng Wu¹, Benny Payero¹, Sydney Taylor¹, Adegboyega K. Oyelere^{1, 2*}

*School of Chemistry and Biochemistry, School of Biological Sciences, Parker H. Petit Institute
for Bioengineering and Bioscience, Georgia Institute of Technology, Atlanta, GA 30332-0400
USA*

¹School of Chemistry and Biochemistry, Georgia Institute of Technology

²Parker H. Petit Institute for Bioengineering and Bioscience, Georgia Institute of Technology

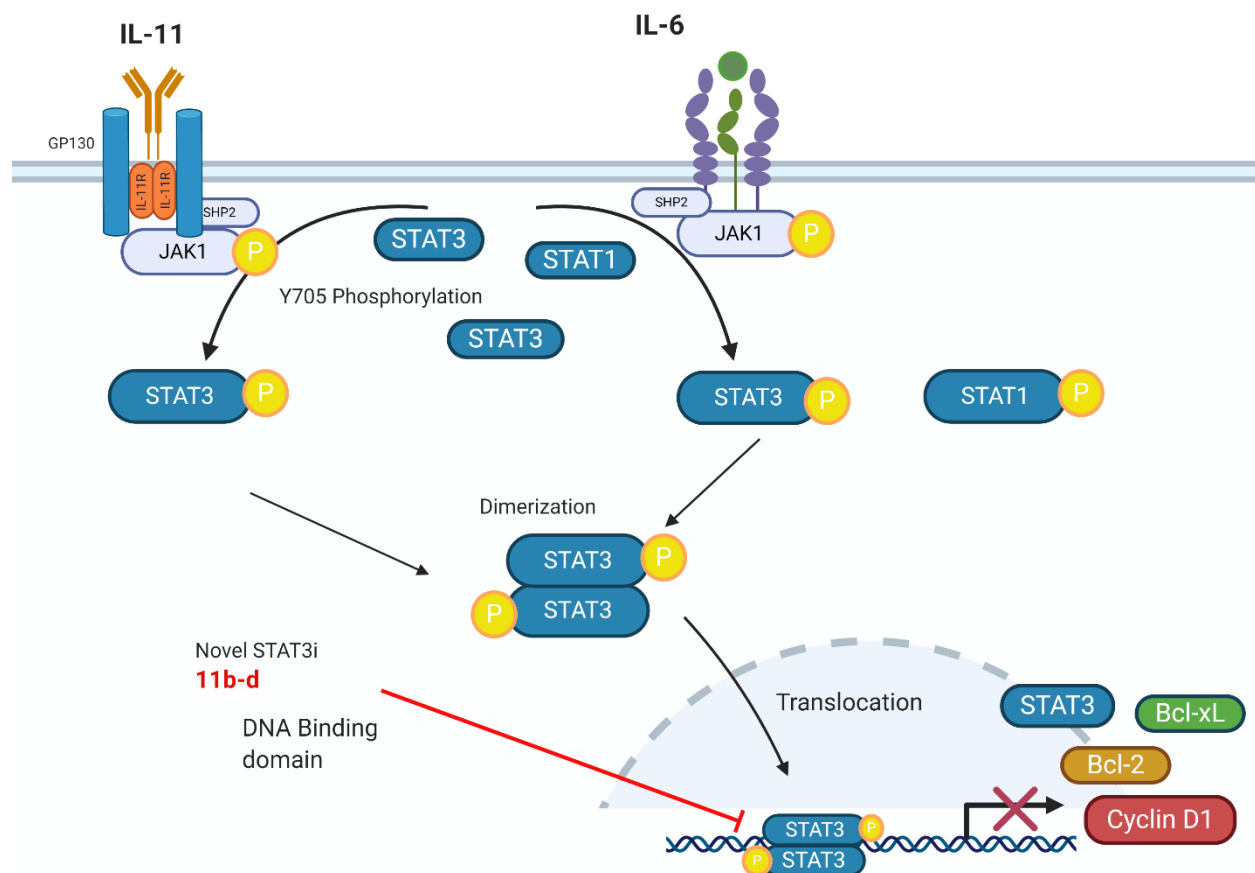
Correspondence to:

Adegboyega K. Oyelere, **E-mail:** aoyelere@gatech.edu

Abstract:

Signal transducer and activator of transcription 3 (STAT3) is a transcription factor that promotes the expression of oncogenes essential for tumor survival. Pyrimethamine (PYM) is a known STAT3 inhibitor that suppresses the proliferation of some cancer cells through downregulation of the expression of STAT3 downstream proteins. In this paper, we have used structure-based tools to design three classes of novel PYM-based compounds. Relative to PYM, several of these compounds more potently inhibited the proliferation of the tested cancer cell lines (A549, Hep-G2, MCF-7, MDA-MB-231) with VERO as a non-transformed control cell line. Representative compounds are able to distinguish between cancer cell lines that are highly dependent on STAT3 signaling (MDA-MB-231 and Hep-G2) relative to those with low levels of constitutively active STAT3 (A549 and MCF-7). Intracellular target validation studies revealed that a cohort of these compounds down-regulate the STAT3 downstream proteins Cyclin D1, Bcl-2 and Bcl-xL. Additionally, further mechanistic studies strongly suggest that the inhibition of STAT3 binding to its DNA target is a key contributor to the anti-cancer activities of these PYM-based compounds. Specifically, compounds **11b** and **11d** more strongly inhibited the interaction of p-STAT3 to its target DNA relative to PYM. Collectively, these data showed that **11b** and **11d** are promising lead STAT3 DBD inhibitors for further preclinical evaluation as therapeutic agents for STAT3-dependent cancers.

Graphical Abstract



Keywords: STAT3 protein, DNA binding domain, pyrimethamine, molecular docking, STAT3 pathway downstream proteins, cancer therapy, SAR, novel STAT3 inhibitors, transcription factor.

6.1 Introduction

Signal Transducer and Activator of Transcription 3 (STAT3) is a transcriptional factor that plays important role in cancer cell proliferation, survival, migration, angiogenesis, invasiveness, and anti-apoptosis. As part of normal biology, the activity of STAT3 is tightly regulated. However, dysfunction in STAT3 regulation results in its persistent upregulation in many cancers, including breast, ovary, and prostate cancers. The constitutive activation sustains the oncogenic activities¹⁻³ of STAT3 in several of these cancers although others have reported tumor suppressor roles for STAT3 in other cancer as well.⁴

Cytosolic STAT 3 is activated through phosphorylation by cell-surface associated Janus Kinases (JAKs) in response to stimuli by oncogenic cytokines.^{3, 5} The phosphorylated STAT 3 undergoes dimerization at the SH-2 domain⁶ and translocates to the nucleus and becomes a part of complex of transcription factor promoting the expression of oncogenes essential for tumor survival⁷. Due to a better understanding of its molecular mechanism, efforts at targeting STAT3 pathway for therapy development include inhibition of JAK1/2, SH2 domain and nuclear translocation of STAT3. These efforts have furnished several lead candidates some of which are currently in clinical trials.^{3, 8, 9} Specifically, JAK1/2 inhibitor AZD1480, shown to inhibit the proliferation and immunity of the Hodgkin Lymphoma in preclinical characterization, has gone through Phase I clinical trial (NCT01112397) and discontinued for further development due to severe adverse effects with unclear dose-limiting toxicity.^{10, 11} Also, OPB-51602 and OPB-31121 are two small molecules SH2 domain inhibitors in early stage of clinical trials.¹² However, excessive toxicity, off-target effects and poor pharmacokinetics profiles are major barriers to the clinical progression

of these compounds.¹³ Other STAT3 inhibitors have been or currently being investigated in various preclinical and clinical settings.^{3, 14, 15} However, none has received FDA approval due to their limited efficacy and toxic side effects.^{9, 16}

Although the STAT3 DNA binding domain (DBD) is considered an undruggable target due its less pronounced 3-dimensional architecture, inhibition of STAT3 by targeting its DBD could be another option for regulating STAT3 pathway. In this regard, it has been shown that platinum (IV) compounds CPA-1, CPA-7, and platinum tetrachloride significantly disrupt the DNA binding activity of STAT3 and inhibit the growth of STAT3-dependent tumor cells.¹⁷ Unfortunately, these platinum (IV) compounds have very poor STAT3 selectivity and have not been considered for further development.¹⁸ More recently, other groups have reported structurally distinct small molecules that could target STAT3 DBD.^{19, 20} Using virtual screening tools, Huang *et al* identified inS3-54 as STAT3 DBD inhibitor showing good STAT3 selectivity and promising anticancer activities *in vitro* and *in vivo*.¹⁹ Additionally, Lim *et al* found that at high milimolar concentrations, methylsulfonyl-methane (MSM) is able to suppress the growth MDA-MD-231 cells *in vitro* and *in vivo* by attenuating the STAT3 and STAT5b pathways. MSM acts through the inhibition of the binding of STAT3 and STAT5b to the promoter regions of VEGFR and IGF-1R respectively.²¹

Pyrimethamine (PYM) is an FDA approved polypharmacology drug which intracellular targets include STAT3. Its STAT3 inhibition activity is the basis for the evaluation of PYM in clinical trials for the treatment of relapsed CLL and SLL (ClinicalTrials.gov Identifier: NCT01066663). We recently disclosed PYM conjugated histone deacetylase inhibitors (HDACi) which, relative to PYM, more potently inhibited STAT3 pathway and proliferation of representative STAT3-dependent cancer cells.²² Despite their inhibition of the expression of intracellular markers of STAT3 pathway, these PYM-HDACi did not suppress STAT3 activation, suggesting that they

may act as direct inhibitors of activated STAT3 (p-STAT3). Through the molecular docking analyses, we have found that these PYM-HDACi could potentially bind to two possible locations within STAT3 DBD. Inspired by this work, we designed three classes of PYM compounds to further investigate the structure activity relationship (SAR) of PYM-STAT3 DBD interaction. We disclosed herein the identification of a cohort of novel PYM-based compounds that, relative to PYM, more potently inhibited STAT3 signaling and the growth of STAT3-dependent MDA-MB-231 and Hep-G2 cells. We provided evidence which strongly suggest that the inhibition of STAT3 binding to its DNA target is a key contributor to the anti-cancer activities of these PYM-based compounds.

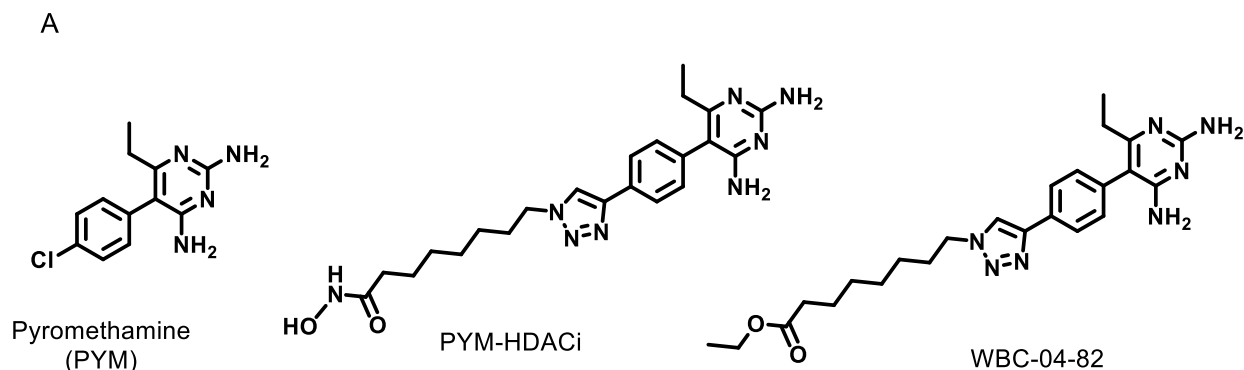
6.2 Results and Discussion

6.2.1 Design of PYM-based Novel STAT3 inhibitors and Molecular docking

In our previous work, we conducted an unbiased docking analyses on STAT3 protein (PDB:1BG1) with Autodock Vina²³ and noticed that PYM and representatives PYM-HDACi bound to 3 locations (*P1-P3*) within STAT3, where *P1* and *P2* are in the DBD domain. Specifically, PYM, PYM-HDACi and WBC-04-82, an analog of PYM-HDACi lacking the HDAC inhibition moiety (Fig. 6.1A), showed preferential binding towards the DBD area (*P1* and *P2*) of STAT3²². In *P1*, the docked poses are stabilized by H-bonding between the pyrimidine moiety of PYM and Gly-419, and the triazole group and Asn-420 of STAT3. In *P2*, PYM interacts through H-bonding with His-332 and Lys-573, while the triazole ring with Leu-467. Each position also has tunnel lined by hydrophobic residues that allows additional stabilizing hydrophobic interactions. Hydrophobic residues at *P1* are Val-375, Ala-376, Ala-377, Leu-378, Val-490 and Leu-438; while Met-470, Pro-471 and Ile-467 contributed to the hydrophobicity at *P2*. However, the tunnel in *P1* is

somewhat less hydrophobic as it has hydrophilic residue (Lys-488) guarding its solvent exposed end.

Using this observed pattern, we designed three classes of new PYM compounds (I-III) in order to gain in-depth insights into the SAR of their interaction at these two positions within the STAT3 DBD (Fig. 6.1B). In class I compounds, PYM moiety is connected to a methylene linker with a terminal 1-methyl piperazine moiety. With this design, we envisioned that the methylene group could fit the hydrophobic tunnel, projecting the piperazine moiety out into the solvent exposed region at the end of the tunnel. To design class II compounds, we replaced the methylene moiety in class I compounds with 4,4'-Oxybis phenyl group capped with various moieties having varying degree of hydrophilic/hydrophobic properties. We envisioned that, relative to the flexible methylene moiety, the more rigid 4,4'-Oxybis phenyl group could better fit the hydrophobic channels in the DBD. To design class III compounds, the methylene moiety in class I compounds is substituted with a benzyl group functionalized at the para position with an ureido group. We expect the ureido group to provide additional stabilizing interaction with the tunnels residue without unduly perturbing the overall hydrophobic character of the linker group.



B

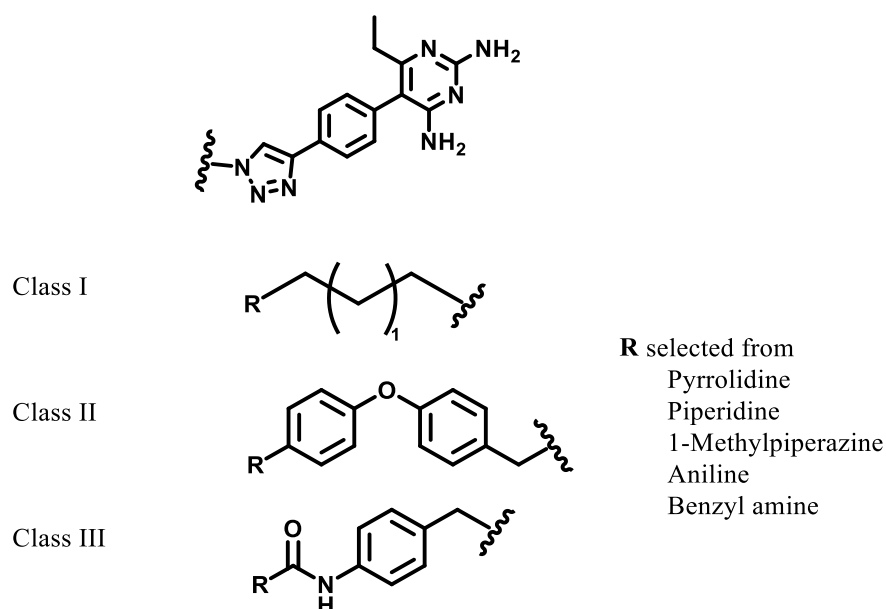
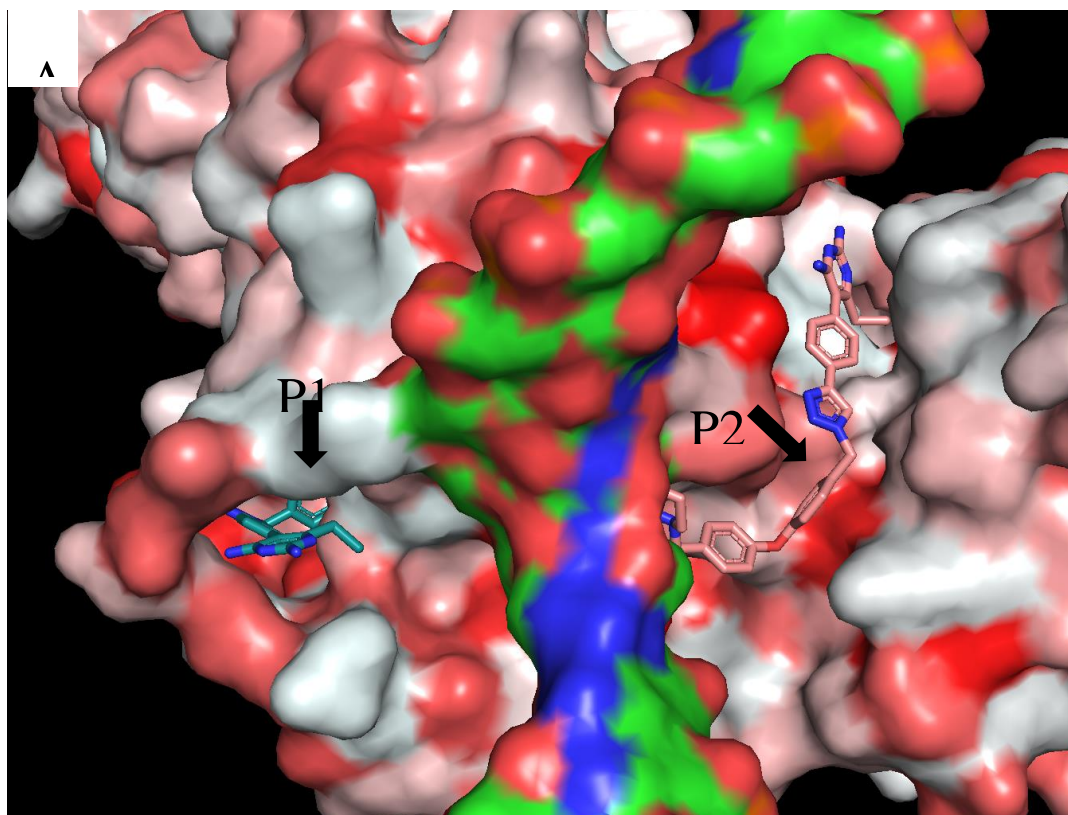


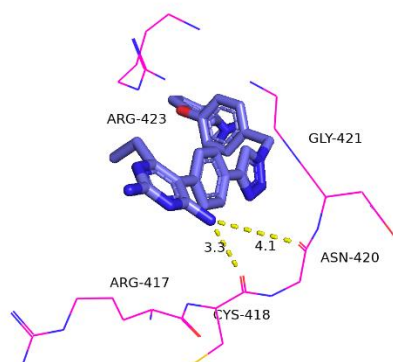
Figure 6.1. (a) Structures of pyrimethamine (PYM), representative PYM-HDACi and WBC-04-82. (b) General structures of the designed three classes of STAT3 DBD inhibitors based on PYM moiety.

Subsequently, molecular docking analysis gave credence to our design. Specifically, a representative compound **11b**, binds to *P1* and *P2* and have improved docking scores relative to PYM and WBC-04-82 (Figs. 6.2A-C, Table 6.S1). Specifically, in *P1*, the pyrimidine moiety of **11b** is bound within a basic hydrophilic pocket (lined by Arg-417 and Arg-423) where it is engaged in hydrogen bonding interaction with Cys-418 and Asn-420. The oxybis phenyl group of **11b** is encased in hydrophobic tunnel formed by Ile-368, Ala-376, Ala-377, Leu-378, Lys-383, Leu-438, and Val-490. The pyrrolidine moiety of **11b** is oriented into a pocket comprising of both hydrophilic (Lys-370, Thr-440 and Lys-488) and hydrophobic (Leu-438) residues (Figs. 6.2A and 2B1-2). At *P2*, the pyrimidine moiety of **11b** forms hydrogen bonding with Asp-566 within a hydrophilic binding pocket that also contains His-332, Arg-335 and Lys-573 (Fig. 6.2C1). The oxybis phenyl group of **11b** is accommodated within a tunnel through a combination of

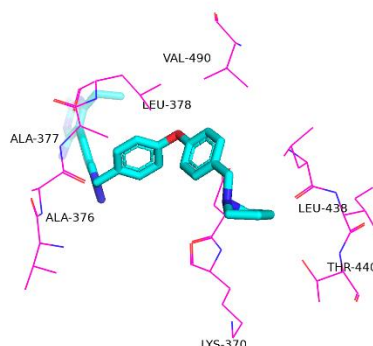
hydrophobic interaction with Cys-468, Pro-471 and Val-563, and possibly hydrogen bonding between its ether moiety and Asn-472 and Lys-615 (Fig.6.2C2). The pyrrolidine moiety is buried in a partially hydrophobic/hydrophilic pocket formed by Ile-431, Val-432 and Thr-433. However, **11b** seems to slightly prefer binding pocket *P1*. This inference is supported by the fact that the docking scores of **11b** at *P1* and *P2* are -10.6 kcal/mol and -9.1 kcal/mol, respectively. Regardless, both positions may provide ideal binding pockets for **11b** and other agents disclosed herein.



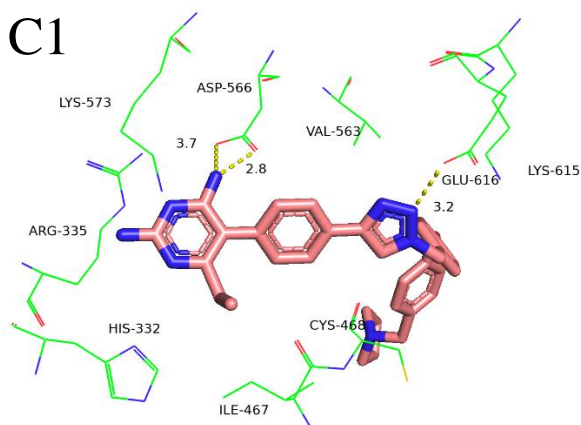
B1



B2



C1



C2

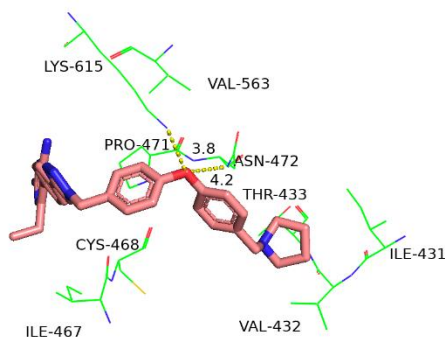


Figure 6.2. *In silico* interrogation of the interaction of **11b** with the STAT3 DBD (PDB:1BG1): (a) Docked poses of **11b** within the *P1* and *P2* binding pockets of STAT3 DBD. The docking scores of **11b** at *P1* and *P2* are -10.6 kcal/mol and -9.1 kcal/mol, respectively. Binding orientations and interactions of the pyrimidine (b1) and oxybis phenyl (b2) moieties of **11b** within in *P1*. Binding orientations and interactions of the pyrimidine (c1) and oxybis phenyl (c2) moieties of **11b** within in *P2*.

6.2.2 Chemistry.

The syntheses of class I-III compounds followed the reaction routes shown in schemes 1-4. Alkynyl-PYM (compound **A**) (Fig. 6.3), a key intermediate in each scheme, was synthesized as we described in our previous work.²² The azido acids **2a-c** were synthesized from **1a-c** following

published procedures.^{24, 25} EDCI coupling between **2a-c** and methylpiperazine furnished azido methylpiperazine amides **3a-c**. Copper(I)-catalyzed cycloaddition reaction²⁶ between azides **3a-c** terminal alkyne compound **A** furnished the target class I compounds **4-c** (Scheme 6.1).

To synthesize alcohol- and amine-based class II, 4,4'-Oxybis benzoic acid **5** was reduced to alcohol **6** using NaBH₄ and BF₃ etherate in THF. Monotosylation to give **7** was accomplished using tosyl chloride and trimethylamine (TEA) in dichloromethane (DCM) solution. Treatment of **7** with NaN₃ in DMF resulted in compound **8** which was subsequently converted to the mesylate **9** by reaction with mesyl chloride and TEA in DCM at -20°C. The reaction of compound **9** with pyrrolidine, piperidine, and 1-methylpiperazine resulted in azido-amine **10a-c** respectively. Copper(I)-catalyzed cycloaddition reaction between azides **8** or **10a-c** and terminal alkyne compound **A** furnished the target alcohol- and amine-based class II compounds **11a-d** (Scheme 6.2). To synthesize the amide-based class II, azide **8** was subjected to mild oxidation using Burgess Reagent and DMSO²⁷ to give aldehyde **12**. Pinnick oxidation²⁸ of **12** using sodium chlorite, sodium phosphate monobasic, 2-methyl-2-butene in tert-butanol furnished the corresponding carboxylic acid **13**. EDCI coupling between **13** and pyrrolidine, piperidine, and 1-methylpiperazine resulted in azido amide **14a-c**. Copper(I)-catalyzed cycloaddition reaction between **14a-c** and terminal alkyne compound **A** furnished the target amide-based class II compounds **15a-c** (scheme 6.3).

The synthesis of class III compounds started with p-nitrobenzyl alcohol which was subjected to catalytic hydrogenation to give aniline **16**. Reaction of **16** with diphenylphosphoryl azide (DPPA), DBU in THF followed by NaN₃ gave azido compound **17**. Treatment of **17** with carbonyldiimidazole (CDI) in followed by the addition of piperidine, aniline, benzyl amine resulted in urea **18a-c**. Copper(I)-catalyzed cycloaddition reaction between **18a-c** and terminal alkyne compound **A** furnished the target class III compounds **19a-c** (scheme 6.4).

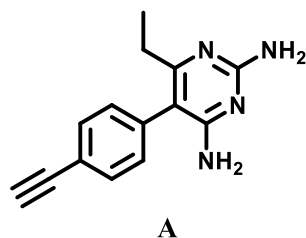
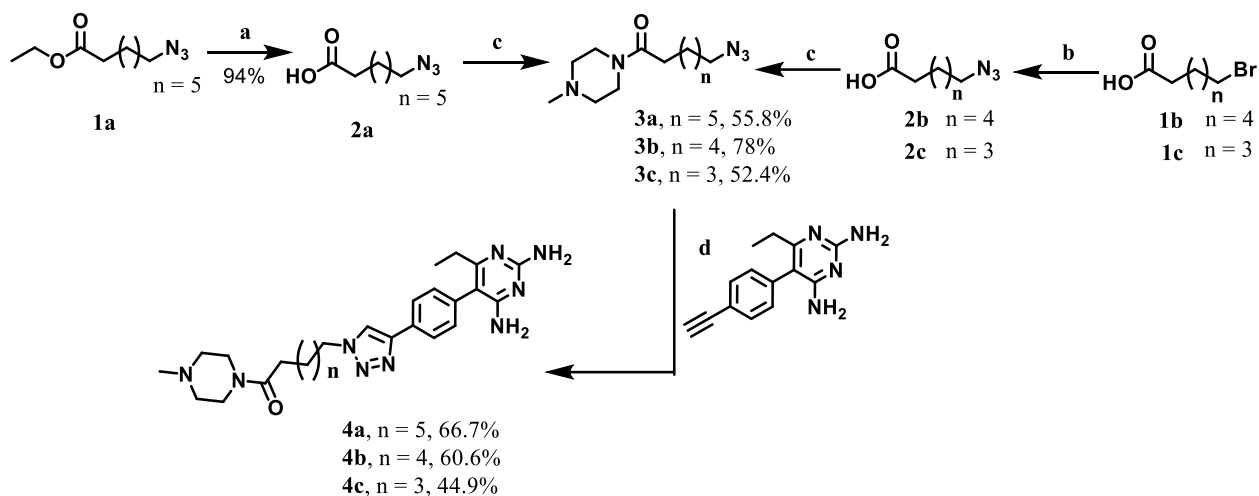
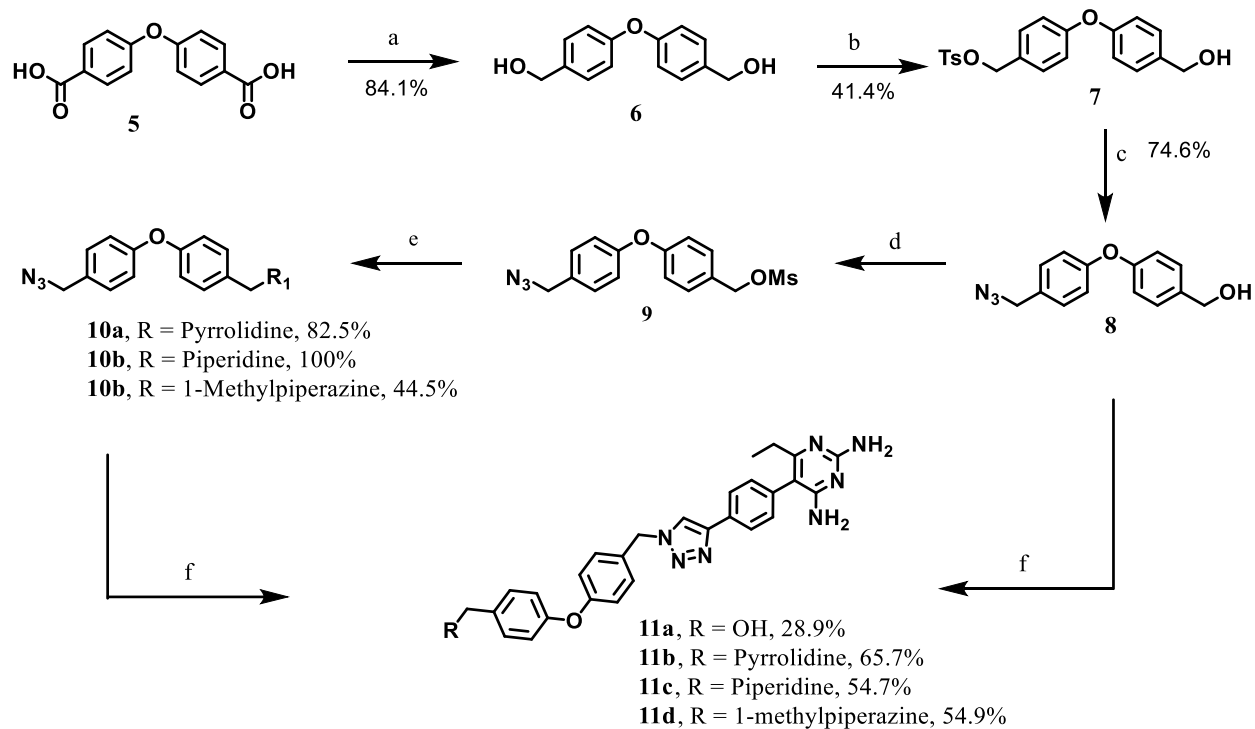


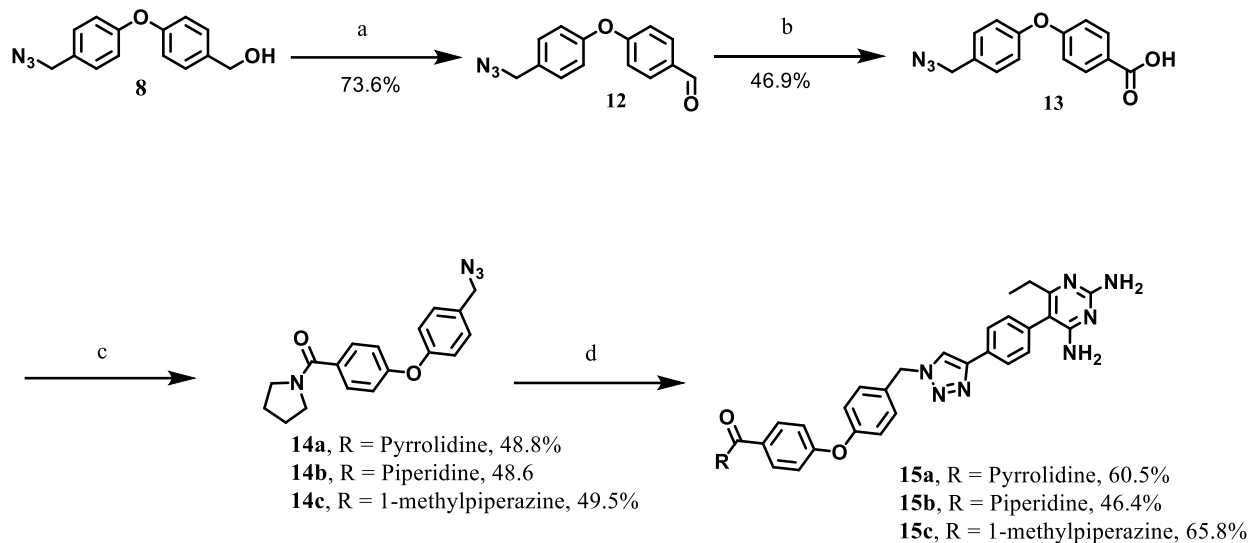
Fig. 6.3. Structure of compound **A**.



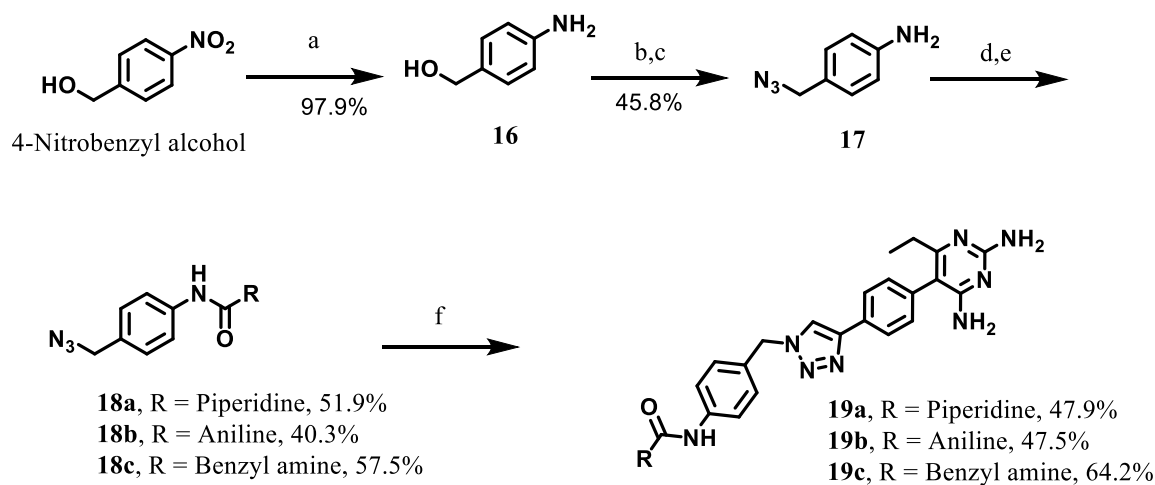
Scheme 6.1: Synthesis of class I compounds **4a-b**. (a) KOH, THF, r.t., overnight; 94% (b) NaN_3 , DMF, 90°C , overnight; (c) EDCI, HOBt, DCM, Hunig's base, 1-methylpiperazine, r.t., overnight; yields listed above. (d) Compound **A**, CuI, Hunig's base, DMSO and THF, Argon, r.t., overnight. Yields listed above.



Scheme 6.2: Synthesis of class II compounds **11a-d**. (a) NaBH₄, BF₃ etherate, THF, overnight; 84.1% (b) TsCl, TEA, THF, DCM, r.t., overnight; 41.4% (c) NaN₃, DMF, 120°C, overnight; 74.6% (d) Mesyl chloride, Hunig's base, 0°C to r.t. 2-3 h; (e) Pyrrolidine or piperidine or 1-methylpiperazine, DMSO, r.t., overnight; yields of products listed above. (f) Compound A, CuI, Hunig's base, THF, DMSO, Argon, r.t., overnight. Yields listed above.



Scheme 6.3: Synthesis of class II compounds **15a-c**. (a) Burgess reagent, DMSO, r.t. overnight; 73.6% (b) NaClO₂, t-BuOH, NaH₂PO₄, 2-Methyl-2-butene, r.t., 4h; 46.9%. (c) EDCI, DMAP, Hunig's base, pyrrolidine or piperidine or 1-methylpiperazine, r.t., overnight; yields listed above. (d) Compound **A**, CuI, Hunig's base, THF, Argon, 35 °C, 6 h. Yields listed above.



Scheme 6.4: Synthesis of class III compounds **19a-c**. (a) Pd/C, H₂, ethyl acetate, r.t.; 24 h; 97.9% (b) DPPA, THF, r.t., overnight; (c) NaN₃, DMF, 80°C, overnight; 45.8% (d) CDI, DCM, Argon,

24 h; (e) Dropwise addition of amines (piperidine, aniline or benzyl amine), r.t., 24 h; yields listed above (f) Compound **A**, CuI, Hunig's base, THF, Argon, 35°C, 6 h. Yields listed above.

6.2.3 Cell Cytotoxicity

As a cost-effective approach to identify lead compounds for intracellular target validation, we first screened all of the synthesized compounds against five cell lines: A549 (lung adenocarcinoma), VERO (kidney epithelial cell), Hep-G2 (hepatocellular carcinoma), MDA-MB-231 (triple negative breast adenocarcinoma), and MCF-7 (ER+ breast adenocarcinoma) (Table 6.1). We used PYM and WBC-04-82 as controls. We observed that class I compound **4a**, which has improved docking scores relative to PYM and WBC-04-82 (Table 6.S1), has slightly enhanced cytotoxicity against all cell lines except A549. Also, **4a**, analog with a longer linker (C8) is more potent than the shorter linker (C6) compound **4c**, suggesting a better fit of the C8 to the hydrophobic tunnel of the STAT3 DBD.

The class-II compounds **11a-d** and **15a-c** are more cytotoxic than the class I compounds against all tested cell lines. The enhanced potency of class II compounds is in overall agreement with the docking scores (Table 6.S1) for these compounds and could be due to the entropic advantage of a more rigid linker that is also better accommodated with the DBD tunnel. Within this group however, amine-based compounds **11b-d** are 3-12-fold more potent than the alcohol compound **11a** while the introduction of amide moiety in **15a-c** has deleterious effects on potency. The attenuation of the potency of **15a-c** relative to **11b-d**, despite their comparable docking scores, could be due to the negative impact of the loss of basic functional group in **15a-c** on cell penetration. Compounds **11c-d** are the most potent among class II compounds and are 1.5 to 4-

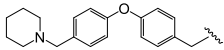
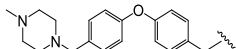
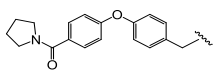
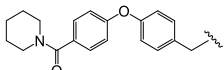
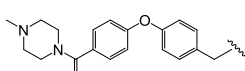
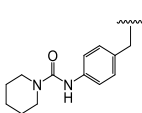
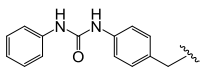
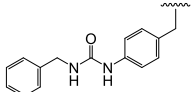
fold more cytotoxic to STAT3-dependent MDA-MB-231 and Hep-G2 compare to A549 cells that are less reliant of the STAT3 signaling.

The class III compounds showed limited cytotoxicity against the tested cell lines except for **19a** which is only slightly more potent than class I compounds. The poor cell activity of these compounds is unexpected given that their docking scores are identical to those of class II. We do not have experimental data that may explain this disparity; it may however be connected with the reduction in cell permeability potentially caused by the ureido moiety of these compounds.²⁹

Table 6. 1. Cytotoxicity of the Novel PYM-derivatives.

ID	Structures of R group	Cytotoxicity IC ₅₀ s (μM)				
		Hep-G2	MDA-MB-231	MCF-7	A549	VERO
Wbc-04-82		NT	95.5±9.3	96.6±6.8	113.8±4.0	112.7±8.2
4a		48.8±7.4	63.8±9.3	90.1±6.3	327.0±23.0	87.1±1.9
4b		85.5±3.3	75.8±2.4	95.6±4.4	NI	NI
4c		NI	NI	NI	NI	NI
11a		14.8±1.4	17.3±0.9	19.5±4.3	86.4±9.6	76.4±13.0
11b		4.5±0.4	2.83±0.9	4.8±0.1	14.9±2.0	8.2±1.0

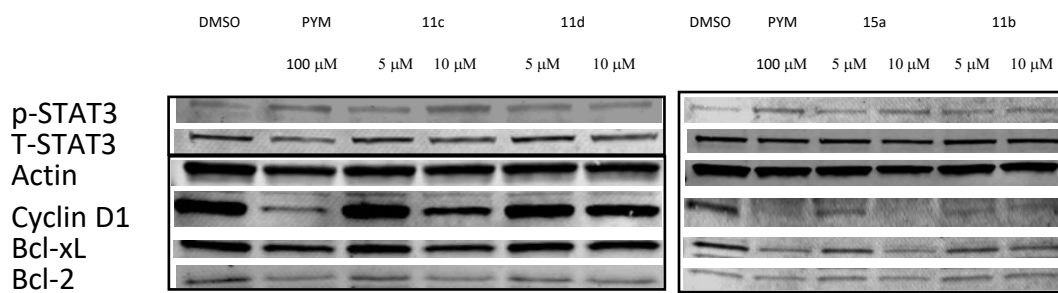
Table 6.1 continued.

11c		1.9±0.5	2.0±0.2	3.2±0.8	8.0±1.0	6.5±0.8
11d		2.0±0.4	2.5 ±0.1	3.3±0.8	9.0±1.8	6.4±1.3
15a		11.3±0.8	9.9±0.6	7.5±0.4	29.3±3.9	NI
15b		15.0±0.1	15.1 ±1.7	8.7±0.6	35.5±0.3	35.6±8.3
15c		14.0±0.1	38.8±0.1	28.5±3.2	NI	NI
19a		25.4±0.3	35.4±2.4	20.2±1.1	NI	37.3±1.6
19b		NI	NI	NI	NI	NI
19c		NI	NI	NI	NI	NI
PYM		NT	238	453	>500	>500

6.2.4 Intracellular target validation

Based on the cell growth inhibition data described above, we selected **11b-d** and **15a** for further mechanistic study aimed at determining the contribution of the contribution of STAT3 pathway inhibition to the anti-proliferative activities. We used immunoblotting method to investigate the effects of these compounds on the expression status of Bcl-xL, Bcl-2, p-STAT3/T-STAT3 and Cyclin D1, key down-stream proteins of STAT3 pathway. Actin was used to control for protein loading in this experiment. One of the mechanisms of STAT3 activation is by phosphorylation of

a critical tyrosine residue (Tyr 705), resulting in the dimerization of p-STAT3 to form a transcriptionally active complex at the promoter regions of STAT3 target genes. We observed upregulated levels of p-STAT3 and increase in p-STAT/T-STAT3 ratios in cells treated with PYM and our compounds. Conversely, **11b-d** and **15a** (5 μ M and 10 μ M) showed concentration-dependent down regulation of the STAT3 down-stream proteins Bcl-xL, Bcl-2, and Cyclin D1. PYM at 100 μ M caused the down-regulation of these STAT3 target proteins as well (Fig. 6.3). These observations matched our previous results on PYM and PYM-HDACi²² and they suggest that the anti-proliferative activities of PYM and compounds **11b-d** and **15a** are not due to the inhibition of STAT3 activation. It is plausible that these compounds are direct inhibitors of p-STAT3, which function by blocking the STAT3 DBD as suggested by our *in silico* docking analyses, thereby preventing the binding of p-STAT3 to its target DNA.



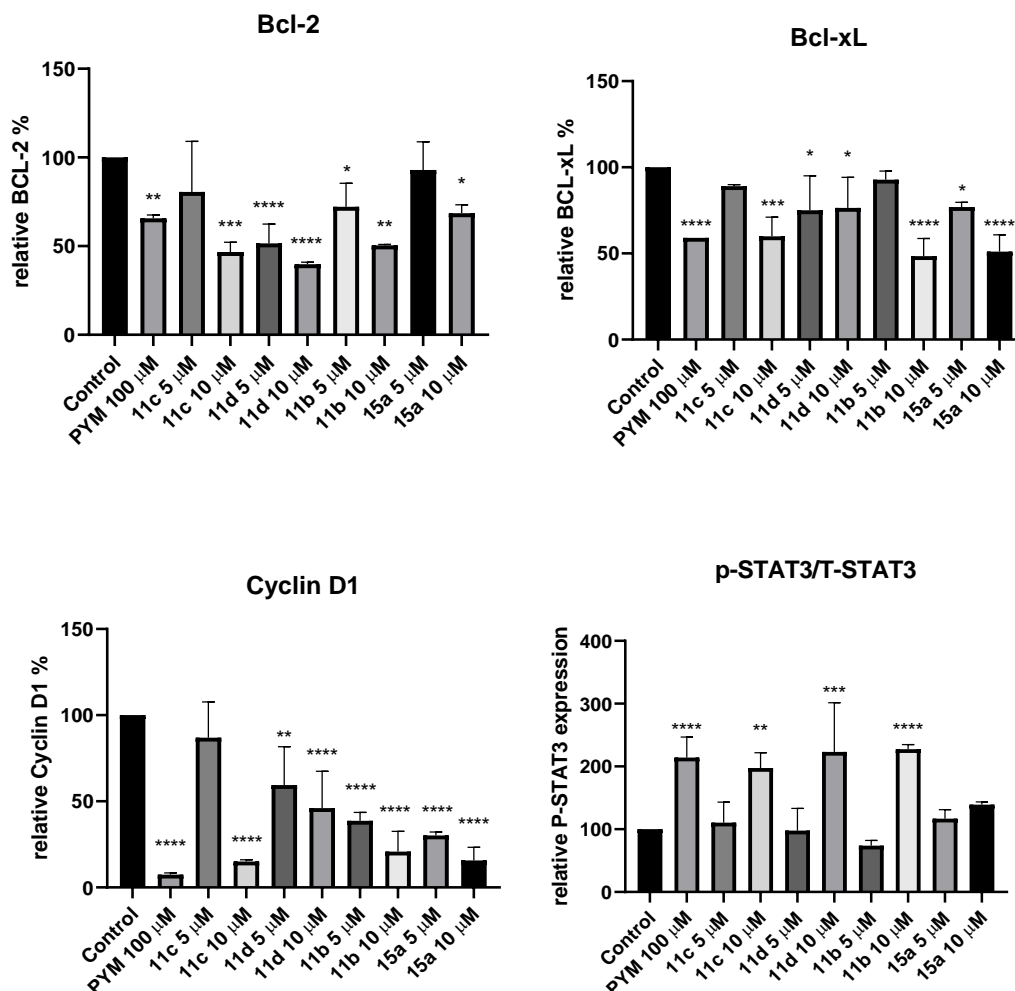


Figure 6.3. Western blot data of the effect of selected compounds on STAT3 signaling. MDA-MB-231 cell line was seeded to the 6-well plates and serum starved for 24 h when confluency is around 80%. The cells were treated with 0.1% DMSO as control, PYM 100 μ M, **11b**, **11c**, **11d** and **15a** at 5 μ M and 10 μ M for 24 h. The cells were harvested and lysed before blotting. (Bars show mean plus standard deviation; Statistic Calculation was performed via Ordinary One-way ANOVA compare with control group, * $P < 0.0332$; ** $P < 0.0021$; *** $P < 0.0002$; **** $P < 0.0001$).

6.2.5 STAT3 DNA binding inhibition

To obtain experimental indication of the binding of our compounds to p-STAT3, we performed p-STAT3 DNA binding assay using kit supplied by AVIVA (cat. OAKG00467) on PYM and

representative compounds **11b-d** and **15a**. In brief, we lysed MDA-MB-231 cell line and collected the nuclear supernatant which was incubated with compound PYM (dosed at 50, 125, 250, 312.5, and 625 μ M; and compounds **11b-d** and **15a** (dosed at 0.313, 1.25, 5, 12.5 and 25 μ M) for 1.5 h in a 96-well plate pre-coated with p-STAT3 oligonucleotide ligand. We also added 1/10, 1/20, and 1/40 dilution of the positive control which was provided in the kit to prove the eligibility of the kit. The buffer was removed, and each well was washed with a washing buffer. Subsequently, the residual p-STAT3 bound to the oligonucleotide in each well was determined by adding primary and secondary antibodies along with developing buffer to generate colorimetric signal at 490 nm as recommended by the supplier.

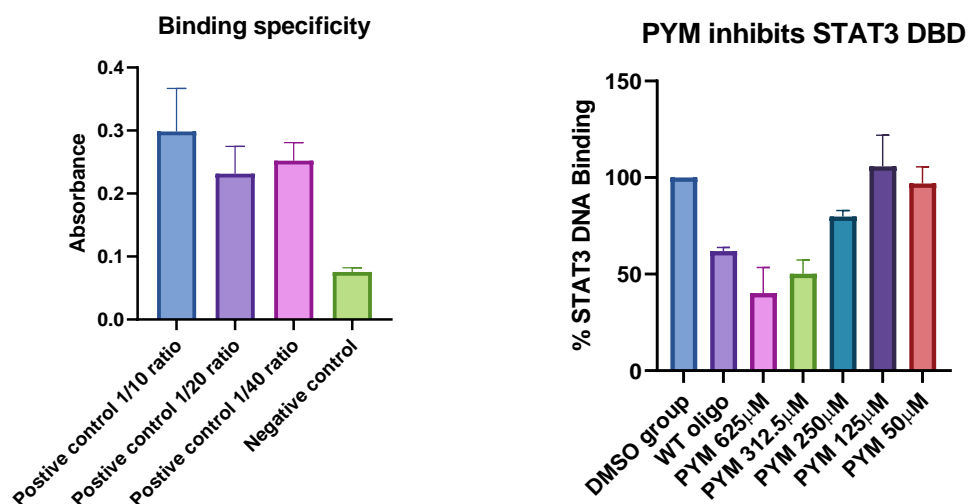


Figure 6.4. DNA binding of p-STAT3 was inhibited by the novel STAT3i. (i) Positive and negative controls revealed evidence of binding specificity. (ii) Control STAT3 inhibitor PYM inhibits STAT3-oligonucleotide interaction. MDA-MB-231 cell nuclear fraction was used as a source of p-STAT3. DMSO lane shows 1% DMSO treatment with no inhibitor to the well. The attenuation of DNA binding in the presence of wild-type oligo indicates competition between the immobilized and free p-STAT3 oligos.

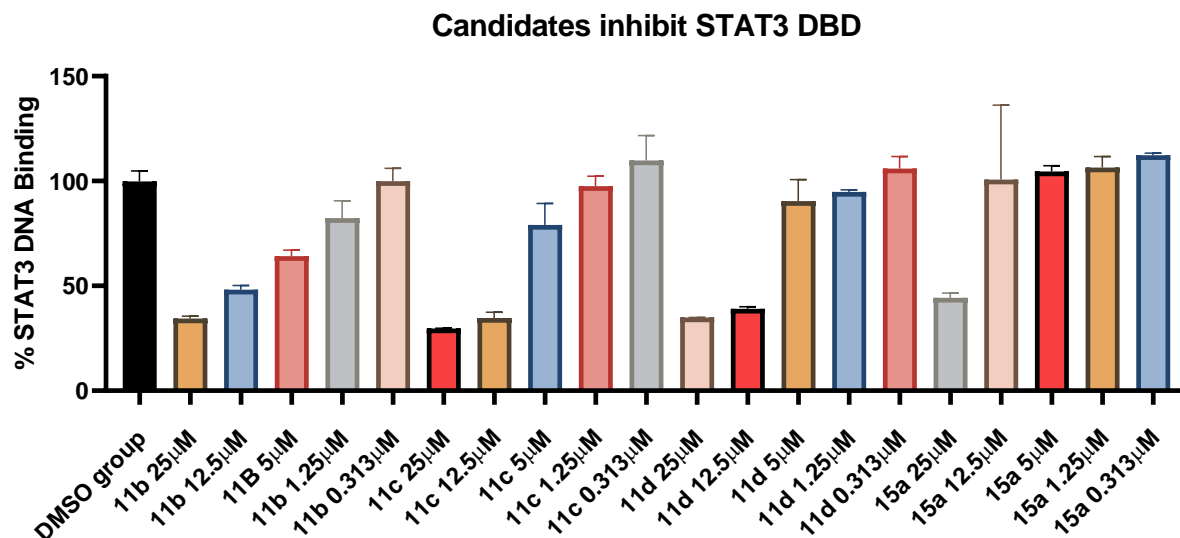


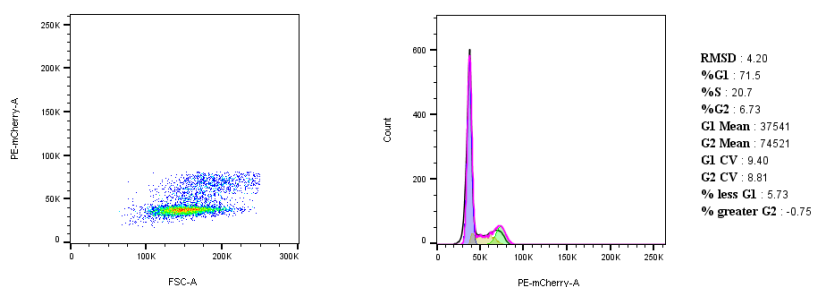
Fig. 6.6. Evidence for direct interaction of DMSO, PYM, **11b-d** and **15a** with dimerized p-STAT3. MDA-MB-231 cell nuclear fraction was used as a source of p-STAT3. Data for the quantification of % of STAT3 binding rate were obtained by replicated data from two independent experiments.

We first confirmed the specificity of the immobilized DNA oligo for p-STAT3 using serial dilution of MDA-MB-231 cell nuclear fraction that revealed p-STAT3 binding to the immobilized oligo (Fig. 6.5 (i)). Further, specificity was further confirmed from a competition which revealed that free p-STAT3 oligo effectively competes with the immobilized oligo for p-STAT3 binding (Fig 6.5 (ii)). Subsequently, we observed that PYM at 312.5-625 μ M caused about 50% reduction in the levels of bound p-STAT3, while at 125 μ M and 50 μ M, PYM has no effects on bound p-STAT3. Lead compounds **11b-d** and **15a** displayed dose-dependent inhibition of p-STAT3 DNA binding that is 10-25 more potent than that of PYM based on concentration range tested. This data strongly suggests that PYM and our compounds **11b-d** and **15a** could inhibit the STAT3 pathway through direct binding to the p-STAT3 DBD domain with our compound **11b-d** and **15a** showing improved

DBD inhibition activity. The stronger inhibition of p-STAT3 direct DNA interaction by **11b-d** and **15a** most likely contributes to their enhanced anti-proliferative effects.

6.2.6 Cell cycle analysis by flow cytometry

We used flow cytometry analysis to determine the effects of PYM and representative lead compound **11c** on the cell cycle progression of MDA-MB-231 cells. Prior to the analysis, cells were treated with DMSO (control group), PYM (100 μ M) and **11c** (at IC₅₀ (2.5 μ M) and 2X IC₅₀ (5 μ M)) for 48 h. Relative to the DMSO control, we observed that PYM and **11c** induced significant S-phase cell cycle arrest (Fig. 6.6). This data matches prior observation by others about the effect of PYM on adrenal gland carcinoma cell NCI-H295R.³⁰ The S-phase arrest caused by PYM and **11c** indicates the transcription was inhibited and thus initiating cell apoptosis. A similar effect on cell cycle has been observed for other STAT3 inhibitor exposed to MDA-MB-231 cell line, in which the S-phase arrest caused downregulation of mRNA of STAT3 down-stream proteins including cyclin D1.³¹



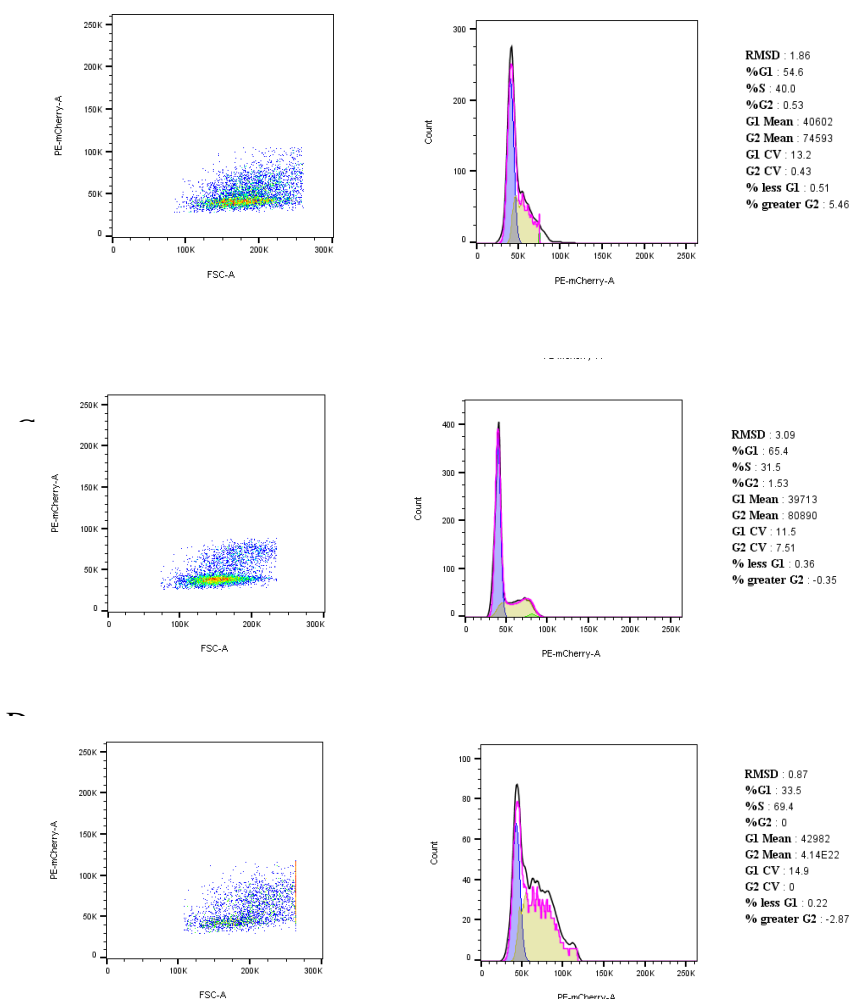


Figure 6.5. Cell Cycle arrest analysis. MDA-MB-231 were treated with (a) 0.1% DMSO or 0.1% of DMSO solution of (b) Pym (100 μ M), (c) **11c** (2.5 μ M) and (d) **11c** (5 μ M) for 48 h.

6.3 Conclusion

We have identified a class of novel PYM-based STAT3 inhibiting compounds that, relative to PYM, more potently inhibited the proliferation of the tested cancer cell lines. Representative compounds are able to distinguish between cancer cell lines that are highly dependent on STAT3 signaling (MDA-MB-231 and Hep-G2) relative to those low levels of constitutively active STAT3 (A549 and MCF-7). Intracellular target validation studies strongly suggest that the inhibition of

STAT3 binding to its DNA target is a key contributor to the anti-cancer activities of these PYM-based compounds. Specifically, compounds **11b-d** and **15a** potently down-regulate the STAT3 downstream proteins Cyclin D1, Bcl-2 and Bcl-xL and strongly inhibited the interaction of p-STAT3 to its target DNA relative to PYM. Because the human dihydrofolate reductase (hDHFR) is another potential of PYM, we probed for the effects of **11b-d** and **15a** on hDHFR activity and found that, up to 10x IC₅₀ concentrations, **11b-d** and **15a** did not elicit any DHFR inhibition effect (Fig. 6.S3 and 6.S4). This data further suggest that STAT3 DBD inhibition could be the leading cause of cell cytotoxicity. Collectively, **11b-d** and **15a** are promising lead STAT3 DBD inhibitors for further preclinical evaluation as therapeutic agents for STAT3-dependent cancers.

6.4 Material and Methods

6.4.1 Materials:

Analtech silica gel plates (60 F254) were used for analytical TLC while Analtech preparative TLC plates (UV 254, 2000 μ m) or silica gel (400 Mesh) was used for compound purification. NMR spectra were taken on Varian-Gemini 400 MHz and Bruke 700 MHz magnetic resonance spectrometer. ¹H NMR spectra were recorded in parts per million (ppm) relative to the residual peaks of CHCl₃ (7.24 ppm) in CDCl₃ or CHD₂OD (4.78 ppm) in CD₃OD or DMSO-*d*₅ (2.49 ppm) in DMSO-*d*₆ or HOD (3.63 ppm) in D₂O. ¹³C spectra were recorded relative to the central peak of the CDCl₃ triplet (81.5 ppm), CD₃OD (52.4 ppm), or the DMSO-*d*₆ septet (39.7 ppm) and were recorded with complete hetero-decoupling. Multiplicities are described using the abbreviation: s, singlet; d, doublet; t, triplet; q, quartet; p, pentet; dd: doublet of doublet; dt: doublet of triplet; dq: doublet of quartets, m, multiplet; and app, apparent. High-resolution mass spectra were recorded

at the Georgia Institute of Technology mass spectrometry facility in Atlanta. The purity of all tested compounds was established by HPLC to be >95%. HPLC analyses were performed on a Beckman Coulter instrument using a Luna[®] 5 μ m C-18 column 100 Å (100 mm \times 4.6 mm), eluting with solvent A (0.1% formic acid–water) and solvent B (0.1% formic acid–acetonitrile) at a gradient of 5–100% over 24 min, with detection at 254 nm and a flow rate of 0.5 mL/min. Sample concentrations were 250 μ M – 1 mM, injecting 20 μ L. Compounds **4a-c**, **11b-d**, **15c** were acidified using 5-10% formic acid before running the solution of each sample by HPLC. Intermediates **2b-c** were synthesized as previously reported.^{32, 33}

Cell lines including Hep-G2, A549, MDA-MB-231, MCF-7, and VERO were purchased from ATCC (Manassas, VA). MDA-MB-231, VERO, and A549 cell lines were maintained in Dulbecco's Modified Eagle Medium (DMEM) (Corning, 10-017-CV), supplemented with 10% fetal bovine serum (FBS) (Corning, 35-010-CV). MCF-7 cells were cultured in phenol red free Minimum Essential Medium (MEM) (Corning, 17-305-CV), supplemented with 10% fetal bovine serum (FBS). For Western blot, Bcl-2 (sc-7382) and Bcl-xL (sc-8392) anti-bodies were purchased from Santa Cruz; p-STAT3/STAT3 anti-bodies were purchased from Cellsignaling (D3A7/D1B2J), Cyclin D1 anti-body was purchased from Cell Signaling (92G2), Actin was purchased from Sigma-Aldrich (A2066-100UL). Secondary antibodies – anti-mouse conjugated to IRDye680, and goat anti-rabbit conjugated to IRDye800 – were obtained from LI-COR Biosciences, Lincoln, NE. CellTiter 96 Aqueous One Solution Cell Proliferation assay (MTS) kit was purchased from Promega (G3581). The STAT3 assay kit (OKAG00467) was purchased from AVIVA while Propidium Iodide (P4170-25MG) was from Sigma-Aldrich.

6.4.2 Synthesis

8-Azido-octanoic acid (2a). Compound **1a** (100 mg, 0.46 mmol) dissolved into ethanol (10 mL). Crushed KOH (85 mg, 1.52 mmol) was added to the solution and the mixture was stirred at 55°C for 2-4 h during which TLC using ethyl acetate showed complete of reaction. The reaction was acidified with 1N HCl (30 mL) and extracted with dichloromethane (DCM) (2x50 mL). The organic layer was washed with brine (50 mL) and dried with Na₂SO₄. Solvent was evaporated to furnish **2a** as liquid, 80 mg (yield 94.0%). ¹H NMR (400 MHz, CDCl₃) δ 3.25 (t, *J* = 6.9 Hz, 2H), 2.35 (t, *J* = 7.5 Hz, 2H), 1.75-1.50 (m, 4H), 1.51 – 1.13 (m, 6H).

8-Azido-1-(4-methylpiperazin-1-yl)octan-1-one (3a). **2a** (80 mg, 0.43 mmol) dissolved in anhydrous DCM (3 mL) to which EDCI (150 mg, 0.78 mmol) and HOBt (120 mg, 0.78 mmol) were added. In another flask, 4-methylpiperazine (100 μL, 0.9 mmol) was dissolved in DCM (5 mL) and Hunig's base (0.3 mL). Both solutions were stirred at room temperature (rt) for about 5 min and then combined. The reaction was stirred overnight at rt over argon atmosphere during which TLC (DCM: MeOH=10:1) indicated complete consumption of **2a**. The reaction was poured into saturated NaHCO₃ (30 mL) and extracted with DCM (2x30 mL). The organic layer was extracted with saturated brine (50 mL), dried with Na₂SO₄ and the solvent evaporated off. The crude was purified by column chromatography, eluting with DCM: MeOH=10:1 to give **3a** as yellow liquid, 65 mg (yield 55.8%). ¹H NMR (400 MHz, CDCl₃) δ 3.61 (dd, *J* = 6.2, 4.1 Hz, 2H), 3.52 – 3.38 (m, 2H), 3.22 (t, *J* = 6.9 Hz, 2H), 2.36 (dt, *J* = 10.1, 5.1 Hz, 4H), 2.28 (s, 5H), 1.66-1.51 (m, 4H), 1.41 – 1.28 (m, 6H).

7-Azido-1-(4-methylpiperazin-1-yl)heptan-1-one (3b). To a solution of compound **2b** (130 mg, 0.82 mmol) in DCM (3 mL) was added EDCI (300 mg, 1.57 mmol) and HOBt (270 mg, 2 mmol). In another flask, 4-methylpiperazine (200 μ L, 1.80 mmol) was dissolved in DCM (3 mL) and Hunig's base (0.3 mL). Both solutions were stirred at rt for about 5 min and then combined. The reaction was stirred overnight at rt over argon atmosphere. The reaction was worked-up as described above for **3a** and the crude product was purified by column chromatography, eluting with ethyl acetate: hexanes 3:7 to give **3b** as yellow liquid, 162 mg (yield 78%). ^1H NMR (400 MHz, CDCl_3) δ 3.63 (t, $J = 5.2$ Hz, 2H), 3.47 (t, $J = 5.1$ Hz, 2H), 3.28 (dd, $J = 7.4, 6.3$ Hz, 2H), 2.45 – 2.28 (m, 9H), 1.72 – 1.57 (m, 4H), 1.50 – 1.36 (m, 2H).

6-Azido-1-(4-methylpiperazin-1-yl)hexan-1-one (3c). To a solution of compound **2c** (100 mg, 0.63 mmol) in DCM (3 mL) was added EDCI (170 mg, 0.89 mmol) and HOBt (150 mg, 1.11 mmol). In another flask, 4-methylpiperazine (100 μ L, 0.90 mmol) was dissolved in DCM (3 mL) and Hunig's base (0.5 mL). Both solutions were stirred at rt for about 5 min and then combined. The reaction was stirred overnight at rt over argon atmosphere. The reaction was worked-up as described above for **3a** and the crude product was purified by column chromatography, eluting with ethyl acetate: hexanes 3:7 to give **3c** as yellow liquid, 80 mg (yield 52.4%). ^1H NMR (400 MHz, CDCl_3) δ 3.63 (t, $J = 5.2$ Hz, 2H), 3.47 (t, $J = 5.1$ Hz, 2H), 3.28 (dd, $J = 7.4, 6.3$ Hz, 2H), 2.45 – 2.28 (m, 9H), 1.72 – 1.57 (m, 4H), 1.50 – 1.36 (m, 2H).

8-(4-(4-(2,4-Diamino-6-ethylpyrimidin-5-yl)phenyl)-1H-1,2,3-triazol-1-yl)-1-(4-methylpiperazin-1-yl)octan-1-one (4a). Compound **A** (25 mg, 0.10 mmol), **3a** (30 mg, 0.11 mmol) and CuI (10 mg,

0.05 mmol) were dissolved in THF (3 mL) and DMSO (2 mL). The mixture was stirred at rt under argon for 10 min, Hunig's base (0.5 mL, 2.90 mmol) was added and the reaction was stirred overnight. The reaction was quenched with 5% aqueous NH_4OH (0.1 mL) and poured into sat. NH_4Cl and 10% NH_4OH (50 mL) and extracted with DCM (2x30 mL). The two layers were separated, the organic layer was washed with saturated brine (30 mL) and dried with Na_2SO_4 . Solvent was evaporated off and the crude was purified using preparative TLC, eluting with ethyl acetate: MeOH 9:1 to furnish **4a** as pale yellow solid, 35 mg (yield 66.7%). ^1H NMR (700 MHz, $\text{DMSO}-d_6 + \text{D}_2\text{O}$) δ 8.56 (s, 1H), 7.88 (d, $J = 8.2$ Hz, 2H), 7.24 (d, $J = 8.2$ Hz, 2H), 4.39 (t, $J = 6.9$ Hz, 2H), 3.38 (td, $J = 6.2, 5.4, 2.8$ Hz, 4H), 2.27 – 2.22 (m, 4H), 2.20 (t, $J = 5.2$ Hz, 2H), 2.13 (d, $J = 3.8$ Hz, 5H), 1.85 (p, $J = 7.1$ Hz, 2H), 1.43 (p, $J = 7.5$ Hz, 2H), 1.28 (q, $J = 7.4$ Hz, 2H), 1.26 – 1.18 (m, 5H), 0.96 (t, $J = 7.5$ Hz, 3H). ^{13}C NMR (176 MHz, $\text{DMSO}-d_6 + \text{D}_2\text{O}$) δ 171.4, 167.0, 162.4, 162.2, 146.6, 135.7, 131.6, 130.0, 126.2, 121.7, 106.7, 55.2, 54.7, 50.0, 46.0, 45.3, 41.3, 32.6, 29.9, 28.9, 28.5, 27.9, 26.1, 25.1, 13.6. HRMS (ESI) Calcd for $\text{C}_{27}\text{H}_{40}\text{N}_9\text{O}$ $[\text{M}+\text{H}^+]$: 506.3350, found 506.3335. HPLC retention time: 2.9 min.

7-(4-(4-(2,4-Diamino-6-ethylpyrimidin-5-yl)phenyl)-1H-1,2,3-triazol-1-yl)-1-(4-methylpiperazin-1-yl)heptan-1-one (4b). The reaction of compound **A** (20 mg, 0.08 mmol), **3b** (80 mg, 0.32 mmol) and CuI (10 mg, 0.05 mmol) in THF (2 mL), DMSO (1 mL) and Hunig's base (0.5 mL, 2.90 mmol), followed by purification as described for the synthesis of **4a**, furnished **4b** as pale yellow solid, 25 mg (yield 60.6%). ^1H NMR (700 MHz, DMSO) δ 8.55 (s, 1H), 7.89 (d, $J = 8.2$ Hz, 2H), 7.24 (d, $J = 8.1$ Hz, 2H), 4.39 (t, $J = 6.9$ Hz, 2H), 4.01 (q, $J = 7.1$ Hz, 1H), 3.39 (dt, $J = 10.5, 5.5$ Hz, 4H), 2.28 – 2.23 (m, 4H), 2.21 (t, $J = 5.2$ Hz, 2H), 2.18 – 2.12 (m, 5H), 1.91 – 1.81 (m, 2H), 1.48 – 1.41 (m, 2H), 1.29 (dd, $J = 11.2, 4.3$ Hz, 2H), 1.26 – 1.19 (m, 2H), 1.16 (t, $J = 7.1$ Hz, 2H),

0.95 (t, $J = 7.5$ Hz, 3H). ^{13}C NMR (176 MHz, DMSO- d_6 + D $_2$ O) δ 171.5, 162.5, 158.6, 146.6, 138.1, 131.6, 130.0, 126.2, 121.8, 106.8, 55.2, 54.6, 50.0, 45.9, 45.2, 41.2, 32.5, 29.9, 28.4, 27.8, 25.9, 25.0, 13.6. HRMS (ESI) Calcd for C $_{26}$ H $_{37}$ N $_9$ O [M+H $^+$]: 492.3193, found 492.3179. HPLC retention time: 2.8 min.

6-(4-(4-(2,4-Diamino-6-ethylpyrimidin-5-yl)phenyl)-1H-1,2,3-triazol-1-yl)-1-(4-methylpiperazin-1-yl)hexan-1-one (4c). The reaction of compound **A** (50 mg, 0.21 mmol), **3c** (150 mg, 0.67 mmol) and CuI (10 mg, 0.05 mmol) in THF (3 mL), DMSO (2 mL) and Hunig's base (0.5 mL, 2.90 mmol), followed by purification using preparative TLC (CHCl $_3$:MeOH 9:1) as described for the synthesis of **4a**, furnished **4c** as pale yellow solid, 45 mg (yield 44.9%). ^1H NMR (700 MHz, DMSO- d_6 + D $_2$ O) δ 8.56 (s, 1H), 7.88 (d, $J = 8.2$ Hz, 2H), 7.24 (d, $J = 8.2$ Hz, 2H), 4.39 (t, $J = 6.9$ Hz, 2H), 3.39 (t, $J = 4.5$ Hz, 4H), 2.31 – 2.20 (m, 4H), 2.19 (t, $J = 5.2$ Hz, 2H), 2.13 (d, $J = 7.5$ Hz, 5H), 1.86 (p, $J = 7.1$ Hz, 2H), 1.50 (p, $J = 7.6$ Hz, 2H), 1.30 – 1.19 (m, 2H), 0.95 (t, $J = 7.5$ Hz, 4H). ^{13}C NMR (176 MHz, DMSO- d_6 + D $_2$ O) δ 171.3, 167.1, 162.2, 146.6, 135.7, 131.6, 130.0, 126.2, 122.2, 106.7, 55.2, 54.7, 49.9, 45.9, 45.2, 41.3, 32.5, 29.8, 27.9, 25.9, 24.6, 13.6. HRMS (ESI) Calcd for C $_{25}$ H $_{36}$ N $_9$ O [M+H $^+$]: 478.3021, found 478.3037. HPLC retention time 2.3 min.

4,4'-Oxybis benzyl alcohol (6). To a solution of 4,4'-Oxybis(benzoic acid) (2 g, 7.75 mmol) in THF (25 mL) was added boron trifluoride etherate (4 mL, 32.3 mmol) and the resulting mixture was stirred for 5 min. NaBH $_4$ (1.18 g, 32 mmol) was added in 4 aliquots to avoid excessive bubbling and the reaction was stirred at rt overnight. The reaction was quenched with CH $_3$ OH (10 mL) and 5% NaHCO $_3$ (100 mL) was added. The mixture was extracted with DCM (2x50 mL) and

the DCM extract was washed with saturated brine (50 mL) and dried over Na₂SO₄. Solvent was evaporated off to furnish **6** come as white solid, 1.50 g (yield 84.1%). ¹H NMR (400 MHz, CDCl₃) δ 7.28 (d, *J*=6.0Hz, 4*H*), 6.93 (d, *J*=8Hz, 4*H*), 4.61 (d, *J* = 5.5 Hz, 4*H*), 1.57 (t, *J* = 5.9 Hz, 2*H*).

4-(4-(Azidomethyl)phenoxy)phenyl)methanol (8). To a stirring solution of compound **6** (1.5 g, 6.52 mmol) in DCM (20 mL) and triethylamine (1.0 mL, 7.77 mmol) was added tosyl chloride (2.3 g, 12.20 mmol) and the resulting mixture was stirred at rt overnight. The reaction was partitioned between water (80 mL) and DCM (2x50 mL) and the two layers separated. The organic layer was washed with saturated brine (50 mL) and dried with Na₂SO₄. Solvent was evaporated off and the crude purified by column chromatography, eluting with ethyl acetate: hexanes 1:2 to give the mono-tosylated compound **7** as white paste, 1.03 g (yield 41.1%). Compound **7** (1 g, 2.68 mmol) was dissolved into DMF (10 mL), NaN₃ (1 g, 15.6 mmol) was added into the solution and the mixture was stirred overnight at 80°C. The reaction was poured into water (100 mL) and extracted with DCM (50 mL). The organic layer was extracted with water (4x50 mL) and dried over Na₂SO₄. Solvent was evaporated to furnish **8** as yellow liquid, 510 mg (yield 74.6%). ¹H NMR (400 MHz, CDCl₃) δ 7.29 (d, *J*=16Hz 4*H*), 7.21 (dd, *J*=8.8Hz 4*H*), 6.94 (dd, *J*=4.6 Hz, 4*H*), 4.62 (d, *J* = 4.6 Hz, 2*H*), 4.25 (s, 2*H*).

4-(4-(Azidomethyl)phenoxy)benzyl methanesulfonate (9). Compound **8** (510 mg, 2 mmol) was dissolved in DCM (5 mL) and Hunig's base (1 mL, 5.74 mmol) was added. The solution was cooled to -20°C on dry-ice bath with ethylene glycol and purged with argon. Mesyl chloride (500 mg, 5.1 mmol) was added drop wisely, the solution was allowed to warm to rt and stirred for 2-3

h. The reaction was quenched with 5% NaHCO₃ (1 mL). Water (30 mL) was added, the mixture was extracted with DCM (2x50 mL) and the organic layer was dried with Na₂SO₄. Solvent was evaporated off to give **9** which was used for the next reaction without further purification.

1-(4-(4-(Azidomethyl)phenoxy)benzyl)pyrrolidine (10a). Compound **9** (133 mg, 0.40 mmol) was dissolved in DMSO (5 mL) and pyrrolidine (1 mL, 12.2 mmol) was added and stirring continued overnight. The reaction was partitioned between water (20 mL) and DCM (40 mL) and the two layers separated. The organic layer was washed with saturated brine (50 mL) and dried with Na₂SO₄. Solvent was evaporated and the crude was purified by column chromatography, eluting with CHCl₃: MeOH 15:1 to furnish **10a** as yellow solid, 100 mg (yield 82.5%). ¹H NMR (400 MHz, CDCl₃) δ 7.68 – 7.40 (d, *J* = 8.6, 2H), 7.34 – 7.14 (d, *J* = 8.5, 2H), 6.94 (td, *J* = 8.8, 1.7 Hz, 4H), 4.27 (d, *J* = 1.5 Hz, 2H), 4.08 (d, *J* = 1.5 Hz, 2H), 3.09 (d, *J* = 6.5 Hz, 4H), 2.12 – 1.81 (m, 4H).

1-(4-(4-(Azidomethyl)phenoxy)benzyl)piperidine (10b). The reaction of **9** (133 mg, 0.40 mmol) with piperidine (1 mL, 11.7 mmol) in DMSO (5 mL), followed by purification as described for the synthesis of **10a**, furnished **10b** as yellow solid, 130 mg (yield 100%). ¹H NMR (400 MHz, CDCl₃) δ 7.41 (d, *J* = 8.5 Hz, 2H), 7.28 – 7.23 (m, 2H), 6.96 (ddd, *J* = 13.3, 8.6, 0.9 Hz, 4H), 4.28 (s, 2H), 3.76 (s, 2H), 2.68 (s, 4H), 1.76 (p, *J* = 5.7 Hz, 4H), 1.49 (p, *J* = 7.0, 6.2 Hz, 2H).

1-(4-(4-(Azidomethyl)phenoxy)benzyl) 4-methyl piperazine (10c). The reaction of **9** (133 mg, 0.40 mmol) with 4-methyl piperazine (1 mL, 8.46 mmol) in DMSO (5 mL), followed by purification as described for the synthesis of **10a**, furnished **10c** as dark yellow oil, 60mg (yield 44.5%). ¹H NMR (400 MHz, CDCl₃) δ 7.26 (ddt, *J* = 8.0, 5.1, 2.4 Hz, 4H), 7.12 – 6.82 (m, 4H), 4.29 (s, 2H), 3.51 (s, 2H), 2.60 (s, 8H), 2.41 (s, 3H).

(4-(4-((4-(4-(2,4-Diamino-6-ethylpyrimidin-5-yl)phenyl)-1H-1,2,3-triazol-1-yl)methyl)phenoxy)phenyl)methanol (11a). Compound **A** (45 mg, 0.19 mmol), **8** (70 mg, 0.22 mmol) and CuI (20 mg, 0.11 mmol) were dissolved in THF (3 mL) and DMSO (2 mL). The mixture was stirred at rt under argon for 10 min, Hunig's base (0.5 mL, 2.90 mmol) was added and the reaction was stirred overnight. The reaction was quenched with 5% aqueous NH₄OH (0.1 mL) and poured into sat. NH₄Cl and 10% NH₄OH (30 mL) and extracted by DCM (2x50 mL). The two layers were separated, the organic layer was washed with saturated brine (50 mL) and dried with Na₂SO₄. Solvent was evaporated off and the crude was purified using preparative TLC, eluting with CHCl₃: MeOH 8:1 to furnish **11a** as yellow solid, 30 mg (yield 28.9%). ¹H NMR (700 MHz, CDCl₃ + CD₃OD) δ 8.03 (s, 1H), 7.90 (d, *J* = 7.7 Hz, 2H), 7.34 (d, *J* = 2.6 Hz, 4H), 7.31 (d, *J* = 7.6 Hz, 2H), 7.00 (dt, *J* = 8.1, 3.9 Hz, 4H), 5.60 (s, 2H), 4.61 (s, 2H), 2.30 (t, *J* = 7.6 Hz, 2H), 1.07 (t, *J* = 7.5 Hz, 3H). ¹³C NMR (176 MHz, CDCl₃) δ 170.6, 166.6, 159.6, 151.5, 140.9, 138.4, 134.0, 133.6, 133.1, 132.5, 130.5, 123.1, 122.6, 67.6, 57.6, 33.4, 31.3, 16.8. HRMS (ESI) Calcd. for C₂₈H₂₈N₇O₂ [M+H]⁺ 494.2299, found 494.2287. HPLC retention time: 13.8 min.

6-Ethyl-5-(4-(1-(4-(4-(pyrrolidin-1-ylmethyl)phenoxy)benzyl)-1H-1,2,3-triazol-4-

yl)phenyl)pyrimidine-2,4-diamine (11b). The reaction of compound **A** (45 mg, 0.19 mmol), **10a** (70 mg, 0.22 mmol) and CuI (20 mg, 0.11 mmol) in THF (3 mL), DMSO (2 mL) and Hunig's base (0.5 mL, 2.90 mmol), followed by purification using preparative TLC (CHCl₃:MeOH 9:1) as described for the synthesis of **11a**, furnished **11b** as pale yellow solid, 70 mg (yield 65.7%). ¹H NMR (700 MHz, CDCl₃ + CD₃OD) δ 8.05 (dd, *J* = 18.2, 10.0 Hz, 1H), 7.93 – 7.87 (m, 2H), 7.53 (dd, *J* = 18.4, 9.9 Hz, 2H), 7.40-7.25 (m, 4H), 7.06-6.93 (m, 4H), 5.61 (s, *J* = 18.5, 9.9 Hz, 2H), 3.79 (s, 2H), 2.77 – 2.61 (m, 4H), 2.29 (q, *J* = 17.2, 7.0 Hz, 2H), 1.88 (dt, *J* = 16.7, 8.3 Hz, 4H), 1.06 (dt, *J* = 17.0, 7.5 Hz, 3H). ¹³C NMR (176 MHz, CDCl₃ + CD₃OD) δ 171.0, 166.5, 165.0, 161.7, 160.2, 151.5, 138.5, 135.0, 133.9, 133.7, 133.4, 130.4, 124.4, 122.9, 111.6, 63.3, 57.6, 33.4, 31.5, 26.9, 16.9. HRMS (ESI) Calcd for C₃₂H₃₅N₈O [M+H⁺]: 547.2928, found 547.914. HPLC retention time: 2.9 min.

6-ethyl-5-(4-(1-(4-(4-(piperidin-1-ylmethyl)phenoxy)benzyl)-1H-1,2,3-triazol-4-

yl)phenyl)pyrimidine-2,4-diamine (11c). The reaction of compound **A** (45 mg, 0.19 mmol), **10b** (70 mg, 0.22 mmol) and CuI (20 mg, 0.11 mmol) in THF (3 mL), DMSO (2 mL) and Hunig's base (0.5 mL, 2.90 mmol), followed by purification using preparative TLC (CHCl₃:MeOH 9:1) as described for the synthesis of **11a**, furnished **11c** as pale yellow solid, 60 mg (yield 54.7%). ¹H NMR (700 MHz, CDCl₃ + CD₃OD) δ 8.00 (s, *J* = 2.5 Hz, 1H), 7.90 (dd, *J* = 8.1, 1.9 Hz, 2H), 7.44 – 7.23 (m, 6H), 7.01 (ddt, *J* = 26.9, 8.5, 2.0 Hz, 4H), 5.60 (s, 2H), 3.60 (s, 2H), 2.54 (s, 4H), 2.30 (t, *J* = 7.5 Hz, 2H), 1.66 (p, *J* = 5.6 Hz, 4H), 1.50 (q, *J* = 6.0 Hz, 2H), 1.07 (t, *J* = 7.2 Hz, 3H). ¹³C NMR (176 MHz, CDCl₃) δ 170.9, 166.5, 164.9, 161.7, 160.2, 151.5, 138.4, 135.4, 135.0, 134.0,

133.7, 133.3, 130.5, 123.0, 122.8, 66.4, 57.8, 33.4, 31.4, 28.8, 27.5, 16.8. HRMS (ESI) Calcd for $C_{33}H_{37}N_8O$ $[M+H^+]$: 561.3085, found 561.3065. HPLC retention time: 2.9 min.

6-Ethyl-5-(4-(1-(4-(4-((4-methylpiperazin-1-yl)methyl)phenoxy)benzyl)-1H-1,2,3-triazol-4-yl)phenyl)pyrimidine-2,4-diamine (11d). The reaction of compound **A** (45 mg, 0.19 mmol), **10c** (74 mg, 0.22 mmol) and CuI (20 mg, 0.11 mmol) in THF (3 mL), DMSO (2 mL) and Hunig's base (0.5 mL, 2.90 mmol), followed by purification using preparative TLC ($CHCl_3$:MeOH 9:1) as described for the synthesis of **11a**, furnished **11d** as pale yellow solid, 60 mg (yield 54.9%). 1H NMR (700 MHz, $DMSO-d_6 + D_2O$) δ 8.64 (s, 1H), 7.89 (d, $J = 8.2$ Hz, 2H), 7.38 (d, $J = 8.7$ Hz, 2H), 7.28 (d, $J = 8.5$ Hz, 2H), 7.24 (d, $J = 8.2$ Hz, 2H), 7.00 (d, $J = 8.7$ Hz, 2H), 6.94 (d, $J = 8.5$ Hz, 2H), 5.62 (s, 2H), 3.40 (s, 2H), 2.32 (s, 8H), 2.17 – 2.05 (m, 5H), 0.95 (t, $J = 7.5$ Hz, 3H). ^{13}C NMR (176 MHz, $DMSO-d_6 + D_2O$) δ 162.3, 157.3, 155.6, 147.1, 135.8, 134.0, 131.6, 131.3, 131.0, 130.3, 129.8, 126.2, 122.0, 119.1, 108.4, 106.6, 61.8, 55.0, 52.8, 46.1, 27.9, 13.6. HRMS (ESI) Calcd for $C_{33}H_{38}N_9O$ $[M+H^+]$: 576.3194, found 576.3175. HPLC retention time: 2.8 min.

4-(4-(Azidomethyl)phenoxy)benzaldehyde (12). A mixture of compound **8** (26 mg, 0.10 mmol) and Burgess reagent (48.5 mg, 0.20 mmol) in DMSO (0.5 mL) was stirred at rt overnight during which TLC (ethyl acetate: hexanes 1:2) showed a complete consumption of **8**. The reaction was partitioned between water (3x30 mL) and DCM (3x25 mL) and the two layers were separated. The organic layer was dried with Na_2SO_4 , solvent was evaporated off to give **12** as yellow liquid (19 mg, 0.074 mmol, yield 73.6%). 1H NMR (400 MHz, $CDCl_3$) δ 9.93 (s, 1H), 7.86 (d, $J = 8.8$ Hz, 2H), 7.37 (d, $J = 8.4$ Hz, 2H), 7.09 (dd, $J = 10.5, 8.4$ Hz, 4H), 4.37 (s, 2H).

4-(4-(Azidomethyl)phenoxy)benzoic acid (13). A solution of NaClO₂ (22.2 mg, 0.25 mmol) and NaH₂PO₄·H₂O (36.8 mg, 0.31 mmol) in water (1.9 mL) was added drop-wisely at rt into a stirring mixture of **12** (19 mg, 0.08 mmol) and 2-methyl-2-butene (0.45 mL) dissolved in tert-butanol (0.9 mL). The reaction was stirred for at rt for 1 h after which more water (0.9 mL) was added. Stirring continued at rt for another hour. The reaction was partitioned between water (2x30 mL) and ethyl acetate (2x30 mL) and the two layers were separated. The organic layer was dried with Na₂SO₄, solvent was evaporated off to give **13** (9.5mg, 0.035mmol, 47%) which was used without further purification. ¹H NMR (400 MHz, CD₃OD) δ 8.01 (d, *J* = 8.9 Hz, 2H), 7.40 (d, *J* = 8.5 Hz, 2H), 7.04 (dd, *J* = 31.7, 8.7 Hz, 4H), 4.92 (s, 2H).

(4-(4-(Azidomethyl)phenoxy)phenyl)(pyrrolidin-1-yl)methanone (14a). To a solution of compound **13** (20 mg, 0.07 mmol) in anhydrous DCM (3 mL) was added EDCI (70 mg, 0.37 mmol) and DMAP (20 mg, 0.16 mmol) and stirring continued for about 5 min. To this mixture was added a solution of pyrrolidine (50 µL, 0.61 mmol) in anhydrous DCM (2 mL) and Hunig's base (0.5 mL) and stirring continued overnight during which TLC (ethyl acetate:hexanes 7:3) indicated a complete consumption of **13**. The reaction was partitioned between saturated NaHCO₃ (20 mL) and DCM (30 mL) and the two layers were separated. The organic layer was dried with Na₂SO₄ and solvent evaporated off. The crude was purified by column chromatography eluting with ethyl acetate:hexanes 1:1 to furnish **14a** as white solid, 11 mg (yield 48.8 %). ¹H NMR (400 MHz, CDCl₃) δ 7.51 – 7.36 (d, 4H), 7.30 (d, *J* = 8.4 Hz, 2H), 7.19 – 7.10 (m, 2H), 7.07 – 6.83 (m, 4H), 4.62 (s, 2H), 3.58 (t, *J* = 6.9 Hz, 2H), 3.41 (t, *J* = 6.6 Hz, 2H), 1.96-1.73 (m, 4H).

(4-(4-(Azidomethyl)phenoxy)phenyl)(piperidin-1-yl)methanone (14b). The reaction of **13** (20 mg, 0.07 mmol), piperidine (50 μ L, 0.51 mmol), EDCI (70 mg, 0.37 mmol), DMAP (20 mg, 0.16 mmol), Hunig's base (0.5 mL) in DCM (5 mL), as described for the synthesis of **14a**, furnished compound **14b** as white solid, 13 mg (48.6%). ^1H NMR (400 MHz, CD_3OD) δ 7.45 – 7.38 (m, 4H), 7.10 – 7.02 (m, 4H), 4.37 (s, 2H), 3.67 (m, 4H), 1.88 – 1.65 (m, 6H).

(4-(4-(azidomethyl)phenoxy)phenyl)(4-methylpiperazin-1-yl)methanone (14c). The reaction of **13** (65 mg, 0.22 mmol), 1-methyl piperazine (100 μ L, 0.9 mmol), EDCI (140 mg, 0.73 mmol), DMAP (20 mg, 0.16 mmol), Hunig's base (0.5 mL) in DCM (5 mL), as described for the synthesis of **14a**, furnished compound **14b** as white solid, 43 mg (49.5 %). ^1H NMR (400 MHz, CDCl_3) δ 7.41 (d, J = 8.7 Hz, 2H), 7.31 (d, J = 8.5 Hz, 2H), 7.14 – 6.91 (m, 4H), 4.33 (s, 2H), 3.52 (m, 4H), 2.33 (m, 7H).

(4-(4-((4-(4-(2,4-Diamino-6-ethylpyrimidin-5-yl)phenyl)-1H-1,2,3-triazol-1-yl) methyl) phenoxy) phenyl) (pyrrolidin-1-yl) methanone (15a). Compound **A** (10 mg, 0.04 mmol), **14a** (20 mg, 0.06 mmol) and CuI (5 mg, 0.03 mmol) were dissolved in THF (1 mL) and DMSO (1 mL). The mixture was stirred at rt under argon for 10 min, Hunig's base (0.2 mL, 1.16 mmol) was added and the reaction was stirred overnight. The reaction was quenched with 1M aqueous NH_4OH (0.1 mL), poured into sat. NH_4Cl and 10% NH_4OH (30 mL), and extracted by DCM (2x50 mL). The organic layer was washed with saturated brine (30 mL) and dried with Na_2SO_4 . Solvent was evaporated

off and the crude was purified using preparative TLC, eluting with CHCl₃: MeOH 9:1 to furnish **15a** as pale yellowish solid, 15 mg (yield 60.5%). ¹H NMR (700 MHz, DMSO-*d*₆ + D₂O) δ 8.67 (s, 1H), 7.95 (d, *J* = 8.2 Hz, 2H), 7.53 (d, *J* = 8.7 Hz, 2H), 7.42 (d, *J* = 8.6 Hz, 2H), 7.32 (d, *J* = 8.2 Hz, 2H), 7.08 (d, *J* = 8.6 Hz, 2H), 6.99 (d, *J* = 8.6 Hz, 2H), 5.65 (s, 2H), 3.40 (dt, *J* = 31.4, 6.8 Hz, 4H), 2.23 (q, *J* = 7.6 Hz, 2H), 1.81 (dq, *J* = 37.3, 6.8 Hz, 4H), 1.01 (t, *J* = 7.6 Hz, 3H). ¹³C NMR (176 MHz, DMSO-*d*₆ + D₂O) δ 168.3, 158.2, 156.2, 146.8, 132.3, 132.0, 131.5, 130.5, 129.8, 129.4, 128.7, 126.6, 125.8, 122.3, 120.0, 118.1, 53.0, 49.6, 46.6, 26.4, 24.3, 13.0. HRMS (ESI) Calcd for C₃₃H₃₇N₈O [M+H⁺]: 561.2703, found 561.2721. HPLC retention time: 14.2 min.

(4-(4-((4-(4-(2,4-Diamino-6-ethylpyrimidin-5-yl)phenyl)-1H-1,2,3-triazol-1-yl)methyl)phenoxy)phenyl) (piperidin-1-yl) methanone (**15b**). The reaction of compound **A** (10 mg, 0.04 mmol), **14b** (10 mg, 0.03 mmol) and CuI (5 mg, 0.03 mmol) in THF (1 mL), DMSO (1 mL) and Hunig's base (0.2 mL, 1.16 mmol), followed by purification as described for the synthesis of **15a**, furnished **15b** as pale yellow solid, 8 mg (yield 46.4%). ¹H NMR (700 MHz, DMSO-*d*₆ + D₂O) δ 8.57 (s, 1H), 7.87 (d, *J* = 7.3 Hz, 2H), 7.41 (d, *J* = 7.2 Hz, 2H), 7.34 (d, *J* = 8.6, 2H), 7.24 (d, *J* = 7.3 Hz, 2H), 7.04 (d, *J* = 8.5, 2H), 6.99 (d, *J* = 8.5, 2H), 5.60 (s, 2H), 3.64 – 3.23 (m, 4H), 2.11 (q, *J* = 7.6 Hz, 2H), 1.56 (q, *J* = 5.8 Hz, 2H), 1.53 – 1.37 (m, 4H), 0.91 (t, *J* = 7.6, 3H). ¹³C NMR (176 MHz, DMSO-*d*₆ + D₂O) δ 169.5, 162.5, 157.8, 156.3, 147.1, 131.8, 131.6, 131.4, 130.5, 129.7, 129.3, 126.4, 122.1, 119.9, 118.6, 107.1, 53.1, 48.9, 43.2, 27.9, 25.6, 13.6. HRMS (ESI) Calcd for C₃₂H₃₃N₈O₂ [M+H⁺]: 575.2855, found 575.2877. HPLC retention time: 14.6 min.

(4-(4-((4-(4-(2,4-Diamino-6-ethylpyrimidin-5-yl)phenyl)-1H-1,2,3-triazol-1-yl)methyl)phenoxy)phenyl) (4-methylpiperazin-1-yl)methanone (**15c**). The reaction of compound **A** (15 mg, 0.065 mmol), **14c** (64 mg, 0.18 mmol) and CuI (10 mg, 0.052 mmol) in THF (1 mL), DMSO (1 mL) and Hunig's base (0.2 mL, 1.16 mmol), followed by purification as described for the synthesis of **15a**, furnished **15c** as pale yellow solid, 25 mg (yield 65.8%). ¹H NMR (700 MHz, CDCl₃ + CD₃OD) δ 8.23 (s, 1H), 7.92 (d, *J* = 7.9 Hz, 2H), 7.43 (dd, *J* = 11.1, 8.4 Hz, 4H), 7.33 (d, *J* = 7.9 Hz, 2H), 7.07 (dd, *J* = 21.9, 8.2 Hz, 4H), 5.65 (s, 2H), 3.95 – 3.46 (m, 4H), 2.50 (d, *J* = 69.5 Hz, 4H), 2.35 (s, 3H), 2.30 (q, *J* = 7.6 Hz, 2H), 1.07 (t, *J* = 7.6 Hz, 3H). ¹³C NMR (176 MHz, CDCl₃ + CD₃OD) δ 174.5, 166.8, 164.3, 162.6, 160.6, 159.3, 151.5, 135.1, 135.0, 134.6, 134.0, 133.9, 133.8, 133.7, 133.0, 130.4, 123.7, 122.2, 111.6, 64.4, 57.4, 49.1, 33.4, 31.1, 16.8. HRMS (ESI) Calcd for C₃₃H₃₆N₉O₂ [M+H⁺]: 590.2967, found 590.2986. HPLC retention time: 2.9 min.

4-Aminophenyl ethanol (**16**). A mixture of 4-nitrobenzyl alcohol (470 mg, 3.07 mmol) and Palladium on activated carbon (5%) (100 mg) was charged with hydrogen gas at 1 atmosphere. The mixture was stirred at rt for 24 h and filtered over celite bed. The filtrate was evaporated off to give **16** as yellow solid, 370 mg (yield 97.9%). ¹H NMR (400 MHz, CDCl₃) δ 7.22 – 7.08 (m, 2H), 6.68 (dd, *J* = 8.4, 2.0 Hz, 2H), 4.55 (d, *J* = 1.8 Hz, 2H).

4-Azidopmethyl aniline (**17**). Compound **16** (180 mg, 1.46 mmol) was mixed with diphenyl phosphine azide (400 mg, 1.46 mmol) and DBU (220 mg, 1.46 mmol) in anhydrous THF (10 mL). The mixture was cloudy at the beginning and turned clear gradually. The solution was stirred overnight at rt during which TLC revealed a complete consumption of **16**. The reaction was poured

into saturated NaHCO₃ (30 mL) and extracted with ethyl acetate (2x50 mL). The organic layer was dried with Na₂SO₄ and solvent was evaporated off. The crude product obtained was dissolved in DMF (10 mL), NaN₃ (200 mg, 3.07 mmol) was added and the mixture was heated at 80°C overnight. The reaction was poured into water (200 mL) and extracted with DCM (3x50 mL). The organic layer was dried with Na₂SO₄ and solvent was evaporated off. The crude was purified by column chromatography eluting with ethyl acetate: hexanes (gradient of 3:7 to 5:5) to furnish **17** as reddish liquid, 100 mg (yield 45.8%). ¹H NMR (700 MHz, CDCl₃) δ 7.13 (d, *J* = 8.4 Hz, 2H), 6.70 (d, *J* = 8.4 Hz, 2H), 4.23 (s, 2H).

N-(4-(Azidomethyl)phenyl)piperidine-1-carboxamide (**18a**). To a solution of compound **17** (33 mg, 0.223 mmol) in anhydrous DCM (5 mL) was added carbonyldiimidazole (44 mg, 0.26 mmol) and the mixture was stirred at rt overnight. To this mixture was added piperidine (63 mg, 0.51 mmol) and stirring continued for another 24 h. To the reaction was added 1N HCl (50 mL) and the mixture was extracted with DCM (2x50 mL). The organic layer was dried with Na₂SO₄ and solvent evaporated off. The crude was purified by column chromatography eluting with ethyl acetate:hexanes (gradient of 3:5 to 5:5) to furnish **18a** as white solid, 30 mg (yield 51.9%). ¹H NMR (400 MHz, CDCl₃) δ 7.38 (d, *J* = 8.5 Hz, 2H), 7.25 – 7.21 (m, 2H), 4.27 (s, 2H), 3.45 (t, *J* = 5.2 Hz, 4H), 1.67 – 1.61 (m, 6H).

N-(4-(Azidomethyl)phenyl)-3-phenylurea (**18b**). The reaction of **17** (33 mg, 0.22 mmol), carbonyldiimidazole (44 mg, 0.26 mmol), and aniline (52 mg, 0.51 mmol), followed by purification, as described for the synthesis of **18a**, furnished compound **18b** as white solid, 24 mg

(yield 40.3%). ^1H NMR (400 MHz, CDCl_3) δ 7.40 (d, $J=6.8\text{Hz}$, 2H), 7.38 (s, 1H), 7.36 (d, $J = 1.8$ Hz, 2H), 7.36 – 7.33 (m, 2H), 7.29 (d, $J = 1.2$ Hz, 1H), 4.30 (s, 2H).

1-(4-(Azidomethyl)phenyl)-3-benzylurea (**18c**). The reaction of **17** (33 mg, 0.22 mmol), carbonlydiimidazole (44 mg, 0.26 mmol), and benzyl amine (49 mg, 0.42 mmol), followed by purification, as described for the synthesis of **18a**, furnished compound **18c** as white solid, 36 mg (yield 57.5 %). ^1H NMR (400 MHz, CDCl_3) δ 7.33 – 7.27 (m, 1H), 7.26 (d, $J = 5.4$ Hz, 5H), 7.18 (d, $J = 8.2$ Hz, 2H), 6.99 (d, $J = 85.4$ Hz, 1H), 4.37 (d, $J = 5.8$ Hz, 2H), 4.25 (s, 2H).

N-(4-((4-(4-(2,4-Diamino-6-ethylpyrimidin-5-yl)phenyl)-1H-1,2,3-triazol-1-yl)methyl)phenyl)piperidine-1-carboxamide (**19a**). Compound **A** (20 mg, 0.08 mmol), **18a** (30 mg, 0.12 mmol) and CuI (10 mg, 0.05 mmol) were dissolved in THF (3 mL) and DMSO (2 mL). The mixture was stirred at rt under argon for 10 min, Hunig's base (0.5 mL, 2.90 mmol) was added and the reaction was stirred at 35-40°C overnight. The reaction was quenched with 5% aqueous NH_4OH (0.1 mL), poured into sat. NH_4Cl and 10% NH_4OH (30 mL), and extracted with DCM (2x50 mL). The organic layer was washed with saturated brine (50 mL) and dried with Na_2SO_4 . Solvent was evaporated off and the crude was purified using preparative TLC, eluting with CHCl_3 : MeOH 9:1 to furnish **19a** as pale yellow solid, 20 mg (yield 47.9%). ^1H NMR (700 MHz, $\text{DMSO}-d_6 + \text{D}_2\text{O}$) δ 8.59 (s, 1H), 7.90 (d, $J = 8.2$ Hz, 2H), 7.43 – 7.40 (m, 2H), 7.24 (dd, $J = 17.8, 8.5$ Hz, 4H), 5.54 (s, 2H), 3.44 – 3.31 (m, 4H), 2.16 (q, $J = 7.5$ Hz, 2H), 1.54 (q, $J = 6.4$ Hz, 2H), 1.49 – 1.42 (m, 4H), 0.96 (t, $J = 7.6$ Hz, 3H). ^{13}C NMR (176 MHz, $\text{DMSO}-d_6 + \text{D}_2\text{O}$) δ 207.9, 163.0, 155.4, 146.9, 141.1, 131.5, 130.3, 129.3, 128.6, 126.3, 121.9, 120.1, 107.2, 53.3, 45.1, 31.1, 25.9,

24.4, 13.4. HRMS (ESI) Calcd for $C_{27}H_{32}N_9O$ $[M+H^+]$: 498.2705, found 498.2724. HPLC retention time: 13.4 min.

1-(4-((4-(4-(2,4-Diamino-6-ethylpyrimidin-5-yl)phenyl)-1H-1,2,3-triazol-1-yl)methyl)phenyl)-3-phenylurea (19b). The reaction of compound **A** (20 mg, 0.08 mmol), **18b** (30 mg, 0.11 mmol) and CuI (10 mg, 0.05 mmol) in THF (3 mL), DMSO (2 mL) and Hunig's base (0.5 mL, 2.90 mmol), followed by purification using preparatory TLC ($CHCl_3$:MeOH: NH_4OH 9:1:0.05) as described for the synthesis of **19a**, furnished **19b** as yellow powder, 24 mg (yield 47.5%). 1H NMR (700 MHz, $DMSO-d_6 + D_2O$) δ 8.58 (s, 1H), 7.88 (d, $J = 8.2$ Hz, 2H), 7.43 (d, $J = 8.5$ Hz, 2H), 7.39 (d, $J = 7.6$ Hz, 2H), 7.32 – 7.22 (m, 7H), 6.97 (t, $J = 5.6$ Hz, 1H), 5.55 (s, 2H), 2.13 (q, $J = 7.5$ Hz, 2H), 0.94 (t, $J = 7.5$ Hz, 3H). ^{13}C NMR (176 MHz, $DMSO-d_6 + D_2O$) δ 152.8, 147.0, 131.6, 129.5, 129.2, 126.3, 122.6, 121.9, 118.9, 118.8, 53.2, 29.3, 13.6. HRMS (ESI) Calcd for $C_{28}H_{28}N_9O$ $[M+H^+]$: 506.2387, found 506.2411. HPLC retention time: 14.1 min.

1-Benzyl-3-(4-((4-(4-(2,4-diamino-6-ethylpyrimidin-5-yl)phenyl)-1H-1,2,3-triazol-1-yl)methyl)phenyl)urea (19c). The reaction of compound **A** (20 mg, 0.08 mmol), **18c** (30 mg, 0.12 mmol) and CuI (10 mg, 0.05 mmol) in THF (3 mL), DMSO (2 mL) and Hunig's base (0.5 mL, 2.90 mmol), followed by purification using preparatory TLC as described for the synthesis of **19a**, furnished **19c** as yellow solid, 28 mg (yield 64.2%). 1H NMR (700 MHz, $DMSO-d_6 + D_2O$) δ 8.67 (d, $J = 1.5$ Hz, 1H), 8.60 (s, 1H), 7.90 (d, $J = 8.1$ Hz, 2H), 7.40 (d, $J = 8.6$ Hz, 2H), 7.33 – 7.20 (m, 5H), 6.63 (t, $J = 5.6$ Hz, 1H), 5.54 (s, 2H), 4.27 (s, 2H), 2.16 (q, $J = 7.5$ Hz, 2H), 0.97 (t, $J = 7.6$ Hz, 3H). ^{13}C NMR (176 MHz, $DMSO-d_6 + D_2O$) δ 155.6, 146.9, 140.8, 140.6, 131.5, 129.1,

128.9, 128.8, 127.5, 127.2, 126.3, 121.9, 118.3, 118.6, 53.6, 48.9, 43.0, 13.5. HRMS (ESI) Calcd for $C_{29}H_{30}N_9O$ $[M+H]^+$: 520.2548, found 520.2568. HPLC retention time: 13.8 min.

6.4.3 *Cell culture and viability assay*

The cell culture and viability assay protocol was as described in our previous work.²² In brief, MDA-MB-231, VERO, and A549 cell lines were maintained in Dulbecco's Modified Eagle Medium (DMEM) (Corning, 10-017-CV), supplemented with 10% fetal bovine serum (FBS) (Corning, 35-010-CV). MCF-7 cells were cultured in phenol red free Minimum Essential Medium (MEM) (Corning, 17-305-CV), supplemented with 10% fetal bovine serum (FBS). Cells were seeded into a 96-well plate (2000 counts/100uL) for 24 h prior to treatment and then treated with various drug concentrations for 72 h. All drugs were dissolved in DMEM/DMSO with DMSO concentration maintained at 1%. The effect of compounds on cell viability was measured using the MTS assay (CellTiter 96 Aqueous One Solution and CellTiter 96 Non-Radioactive Cell Proliferation Assays, Promega, Madison, WI) as described by the manufacturer. IC_{50} s were determined using Prism GraphPad 8.

6.4.4 *Western blots analysis*

The Western blot protocol was as described in our previous work²². In brief, MDA-MB-231 cells were seeded into 6-well plate at 1×10^6 /well in DMEM for 24 h after which the cells were starved in serum-free DMEM for another 24 h. Various concentrations of PYM, **11b-d** and **15a** solutions in DMSO were added to the cell culture such that the final DMSO level is 0.1%. Cells were treated

for 24 h, washed with cold PBS, and lysed with RIPA buffer (120 μ L) (VWR, VWRVN653-100ML) buffer containing phosphatase inhibitor (Fisher Thermo, A32957) and protease inhibitor (Fisher Thermo, A32955). The cell lysates were scraped, collected, and vortexed for 15s followed by sonication for 60s. The lysate was then centrifuged at 14000x rpm for 10 min and the supernatants were collected. The total protein concentration was determined using a BCA protein assay kit (BioVision, K813-2500). Based on the results from the BSA assay, the lysates were diluted to make equal protein concentration and 20-40 μ g of each lysate was loaded to each well of the TGX MIDI 4-20% gel (Biorad, cat. 5671093) and ran at 150V for 70 min. The gel was then transferred on to the Turbo PDVF membrane (Biorad, 1704273) and after blocking with 5% BSA for 1-2 h, the membrane was incubated overnight with Bcl-2 (Santa Cruz, sc-7382), Bcl-xL (Santa Cruz, sc-8392), p-STAT3/STAT3 (Cellsignaling, D3A7/D1B2J), Cyclin D1 (Cellsignaling, 92G2), Actin (A2066-100UL, Sigma-Aldrich) antibodies. The second day, the membrane was washed with TBST for 3x5 min; secondary antibody (LiCOR) was added, and the membrane was incubated with agitation for 1 h. After washing with TBS-T 3x5 mins, bands were quantified using Odyssey CLx Image system.

6.4.5 STAT3 DNA-Binding ELISA Assay

MDA-MB-231 cells were incubated in 3x10 cm diameter Petri dish with 10% FBS DMEM until more than 80% confluency before overnight starvation with serum-free DMEM. Cells were washed with cold 1X PBS and lysed using nuclear extraction buffer that came with the kit. Following supplier's instruction, we obtained nuclear lysate and stored at -80 °C overnight. In the 2nd day, the lysate was defrosted in ice and diluted 5X the original lysate with the nuclear extraction

buffer again to obtain the sufficient volume for assay. Then, 20 μ L aliquot was taken from the lysate and diluted with 80 μ L water for each well and mixed with 100 μ L 2X binding buffer. The total volume for each well is 200 μ L. These prepared aliquots were treated with positive control nuclear lysate provided from the kit, DMSO, and various concentrations of PYM, **11b-d**, and **15a** at room temperature for 15-20 min. Then, each mixture was added into designated DNA-coated well. Subsequently, binding buffer (100 μ L) was added to each well with gentle mixing using multichannel pipet. The plate was incubated in room temperature for 1 h. Then, the solutions were removed by gentle suction and the wells washed with a wash buffer supplied with the kit. The primary antibody was added and followed by incubation for another 2 h at room temperature in a plate shaker. The secondary antibody was then added after another wash and the plate was incubated for another 2 h in plate shaker. After washing with the wash buffer, TMB substrate was added and the plate was incubated for another 30 min to allow color development. Stop solution was added and the plate was read in microplate spectrophotometer reader at 490 nm.

6.4.6 Flow cytometry

The Flow cytometry protocol was as described in our previous work²². In brief, MDA-MB-231 cells (5×10^6) were seeded to 10 cm plate with DMEM for 24 h prior to drug treatment. Cells were treated with DMSO (control) and DMSO solutions of Pym (100 μ M) and **11c** (2.5 μ M and 5 μ M), such that the final DMSO level is 0.1%, for another 48 h. Cells were washed with cold 1X PBS solution twice then trypsinized. Subsequently, cells were collected using 1X PBS buffer and fixed overnight at -20°C using 70% ethanol. Cells were then washed, centrifuged and re-suspended in 1X PBS buffer solution of 200 μ g/mL RNase A for 30 min. Then cells were treated with 100

ug/mL PI staining at room temperature for 30 min. Cell cycle progression was analyzed with BD FACS Aria Illu analyzer and the data was processed using FlowJo.

Acknowledgements. This work was financially supported by the Vasser-Woolley Fellowship (AKO) and by the Georgia Institute of Technology (A.K.O.).

Author Contributions: B.W.: designed, synthesized and performed cell work and mechanistic validation on of all the reported compounds. B.P. and S.T.: conducted synthesis of key intermediates and representative reported compounds. A.K.O. and B.W: developed the concept, analyzed the results and wrote the manuscript.

Additional Information: Supplementary data associated with this article, including ^1H NMR and ^{13}C NMR spectral information; HPLC data and molecular docking scores, can be found, in the online version, at <http://www.nature.com/scientificreports>

Competing interests: The authors declare no competing financial and non-financial interests.

6.5 References :

1. Alvarez JV, Febbo PG, Ramaswamy S, Loda M, Richardson A, Frank DA. Identification of a genetic signature of activated signal transducer and activator of transcription 3 in human tumors. *Cancer Res.* 2005;65(12):5054-62.
2. Nelson EA, Sharma SV, Settleman J, Frank DA. A chemical biology approach to developing STAT inhibitors: molecular strategies for accelerating clinical translation. *Oncotarget.* 2011;2(6):518-24.
3. Qin JJ, Yan L, Zhang J, Zhang WD. STAT3 as a potential therapeutic target in triple negative breast cancer: a systematic review. *J Exp Clin Cancer Res.* 2019;38(1):195.
4. Zhang HF, Lai R. STAT3 in Cancer-Friend or Foe? *Cancers (Basel).* 2014;6(3):1408-40.
5. Spitzner M, Ebner R, Wolff H, Ghadimi B, Wienands J, Grade M. STAT3: A Novel Molecular Mediator of Resistance to Chemoradiotherapy. 2014;6(4):1986-2011.
6. Haan S, Hemmann U, Hassiepen U, Schaper F, Schneider-Mergener J, Wollmer A, et al. Characterization and binding specificity of the monomeric STAT3-SH2 domain. *J Biol Chem.* 1999;274(3):1342-8.
7. Becker S, Groner B, Muller CW. Three-dimensional structure of the Stat3beta homodimer bound to DNA. *Nature.* 1998;394(6689):145-51.
8. Yue P, Turkson J. Targeting STAT3 in cancer: how successful are we? *Expert Opin Investig Drugs.* 2009;18(1):45-56.
9. Arshad S, Naveed M, Ullia M, Javed K, Butt A, Khawar M, et al. Targeting STAT-3 signaling pathway in cancer for development of novel drugs: Advancements and challenges. *Genet Mol Biol.* 2020;43(1):e20180160.
10. Derenzini E, Lemoine M, Buglio D, Katayama H, Ji Y, Davis RE, et al. The JAK inhibitor AZD1480 regulates proliferation and immunity in Hodgkin lymphoma. *Blood Cancer J.* 2011;1(12):e46.
11. Plimack ER, Lorusso PM, McCoon P, Tang W, Krebs AD, Curt G, et al. AZD1480: a phase I study of a novel JAK2 inhibitor in solid tumors. *Oncologist.* 2013;18(7):819-20.
12. Genini D, Brambilla L, Laurini E, Merulla J, Civenni G, Pandit S, et al. Mitochondrial dysfunction induced by a SH2 domain-targeting STAT3 inhibitor leads to metabolic synthetic lethality in cancer cells. *Proc Natl Acad Sci U S A.* 2017;114(25):E4924-E33.
13. Wong AL, Soo RA, Tan DS, Lee SC, Lim JS, Marban PC, et al. Phase I and biomarker study of OPB-51602, a novel signal transducer and activator of transcription (STAT) 3 inhibitor, in patients with refractory solid malignancies. *Ann Oncol.* 2015;26(5):998-1005.
14. Chen Y, Ji M, Zhang S, Xue N, Xu H, Lin S, et al. Bt354 as a new STAT3 signaling pathway inhibitor against triple negative breast cancer. *J Drug Target.* 2018;26(10):920-30.
15. Zhang X, Yue P, Fletcher S, Zhao W, Gunning PT, Turkson J. A novel small-molecule disrupts Stat3 SH2 domain-phosphotyrosine interactions and Stat3-dependent tumor processes. *Biochem Pharmacol.* 2010;79(10):1398-409.

16. Thilakasiri PS, Dmello RS, Nero TL, Parker MW, Ernst M, Chand AL. Repurposing of drugs as STAT3 inhibitors for cancer therapy. *Semin Cancer Biol.* 2019.
17. Turkson J, Zhang S, Palmer J, Kay H, Stanko J, Mora LB, et al. Inhibition of constitutive signal transducer and activator of transcription 3 activation by novel platinum complexes with potent antitumor activity. *Mol Cancer Ther.* 2004;3(12):1533-42.
18. Wong ALA, Hirpara JL, Pervaiz S, Eu JQ, Sethi G, Goh BC. Do STAT3 inhibitors have potential in the future for cancer therapy? *Expert Opin Investig Drugs.* 2017;26(8):883-7.
19. Huang W, Dong Z, Wang F, Peng H, Liu JY, Zhang JT. A small molecule compound targeting STAT3 DNA-binding domain inhibits cancer cell proliferation, migration, and invasion. *ACS Chem Biol.* 2014;9(5):1188-96.
20. Huang W, Dong Z, Chen Y, Wang F, Wang CJ, Peng H, et al. Small-molecule inhibitors targeting the DNA-binding domain of STAT3 suppress tumor growth, metastasis and STAT3 target gene expression in vivo. *Oncogene.* 2016;35(6):783-92.
21. Lim EJ, Hong DY, Park JH, Joung YH, Darvin P, Kim SY, et al. Methylsulfonylmethane suppresses breast cancer growth by down-regulating STAT3 and STAT5b pathways. *PLoS One.* 2012;7(4):e33361.
22. Wu B, Fathi S, Mortley S, Mohiuddin M, Jang YC, Oyelere AK. Pyrimethamine conjugated histone deacetylase inhibitors: Design, synthesis and evidence for triple negative breast cancer selective cytotoxicity. *Bioorg Med Chem.* 2020;28(6):115345.
23. Trott O, Olson AJ. AutoDock Vina: improving the speed and accuracy of docking with a new scoring function, efficient optimization, and multithreading. *J Comput Chem.* 2010;31(2):455-61.
24. Raji I, Yadudu F, Janeira E, Fathi S, Szymczak L, Kornacki JR, et al. Bifunctional conjugates with potent inhibitory activity towards cyclooxygenase and histone deacetylase. *Bioorg Med Chem.* 2017;25(3):1202-18.
25. El Aissi R, Liu J, Besse S, Canitrot D, Chavignon O, Chezal JM, et al. Synthesis and Biological Evaluation of New Quinoxaline Derivatives of ICF01012 as Melanoma-Targeting Probes. *ACS Med Chem Lett.* 2014;5(5):468-73.
26. Rostovtsev VV, Green LG, Fokin VV, Sharpless KB. A stepwise Huisgen cycloaddition process: copper(I)-catalyzed regioselective "ligation" of azides and terminal alkynes. *Angew Chem Int Ed Engl.* 2002;41(14):2596-9.
27. Sultane PR, Bielawski CW. Burgess Reagent Facilitated Alcohol Oxidations in DMSO. *J Org Chem.* 2017;82(2):1046-52.
28. Bal B, Childers W, Pinnick H. Tetra-hedron, 1981, vol. 37. doi 10.1016/S0040-4020 (01) 97963-3.
29. Yang NJ, Hinner MJ. Getting across the cell membrane: an overview for small molecules, peptides, and proteins. Site-specific protein labeling: Springer; 2015. p. 29-53.

30. Nilubol N, Zhang L, Shen M, Zhang YQ, He M, Austin CP, et al. Four clinically utilized drugs were identified and validated for treatment of adrenocortical cancer using quantitative high-throughput screening. *J Transl Med.* 2012;10:198.
31. Liu Z, Ge X, Gu Y, Huang Y, Liu H, Yu M, et al. Small molecule STAT3 inhibitor, 6Br-6a suppresses breast cancer growth in vitro and in vivo. *Biomed Pharmacother.* 2020;121:109502.
32. Chen PC, Patil V, Guerrant W, Green P, Oyelere AK. Synthesis and structure-activity relationship of histone deacetylase (HDAC) inhibitors with triazole-linked cap group. *Bioorg Med Chem.* 2008;16(9):4839-53.
33. Oyelere AK, Chen PC, Guerrant W, Mwakwari SC, Hood R, Zhang Y, et al. Non-peptide macrocyclic histone deacetylase inhibitors. *J Med Chem.* 2009;52(2):456-68.

Highlights

Structure-based design furnished three classes of novel pyrimethamine-based STAT3 DNA binding domain Inhibitors

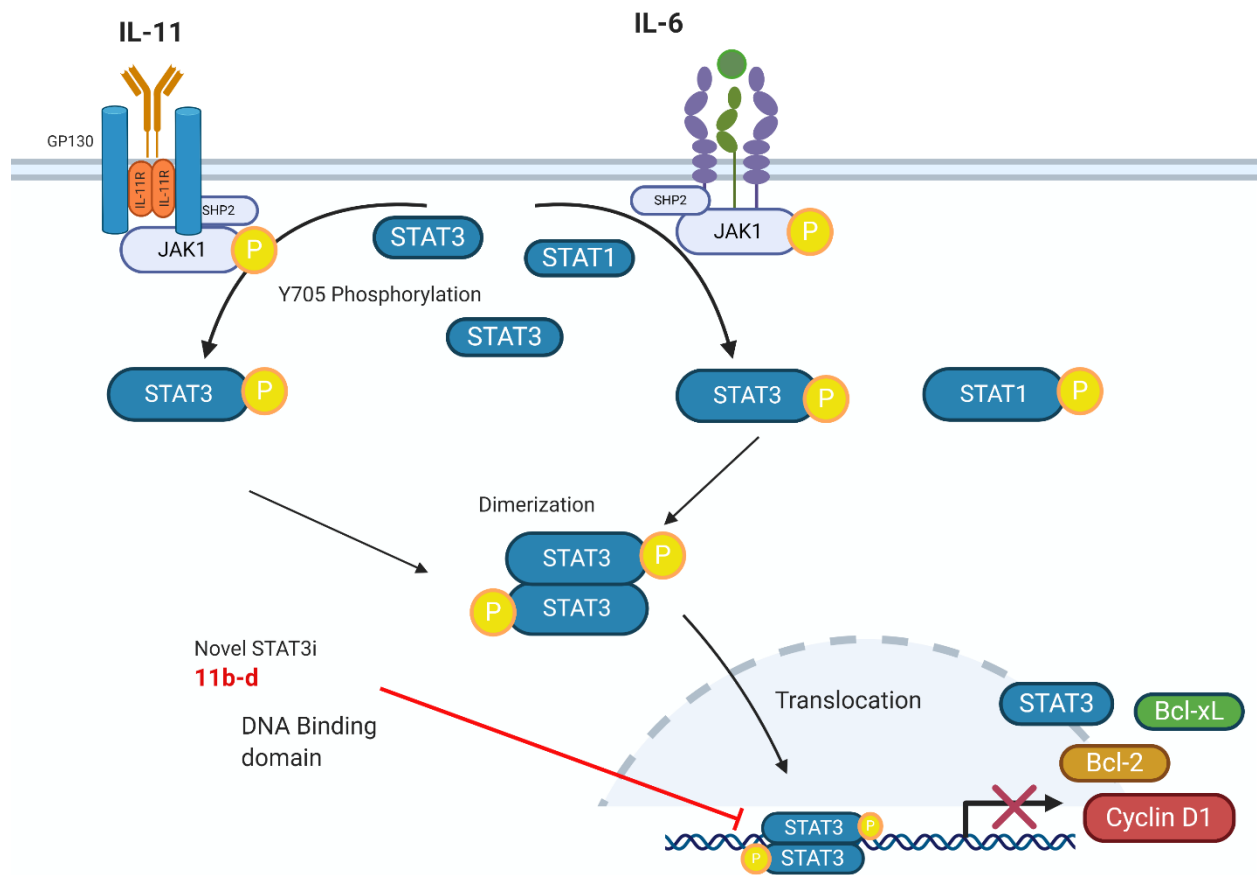
Representative compounds down-regulate the STAT3 downstream proteins Cyclin D1, Bcl-2 and Bcl-xL

Representative compounds are able to distinguish between cancer cell lines

Representative compound and pyrimethamine induced significant S-phase cell cycle arrest

Compounds **11b** and **11d** more strongly inhibited the interaction of p-STAT3 to its target DNA

Graphical Abstract

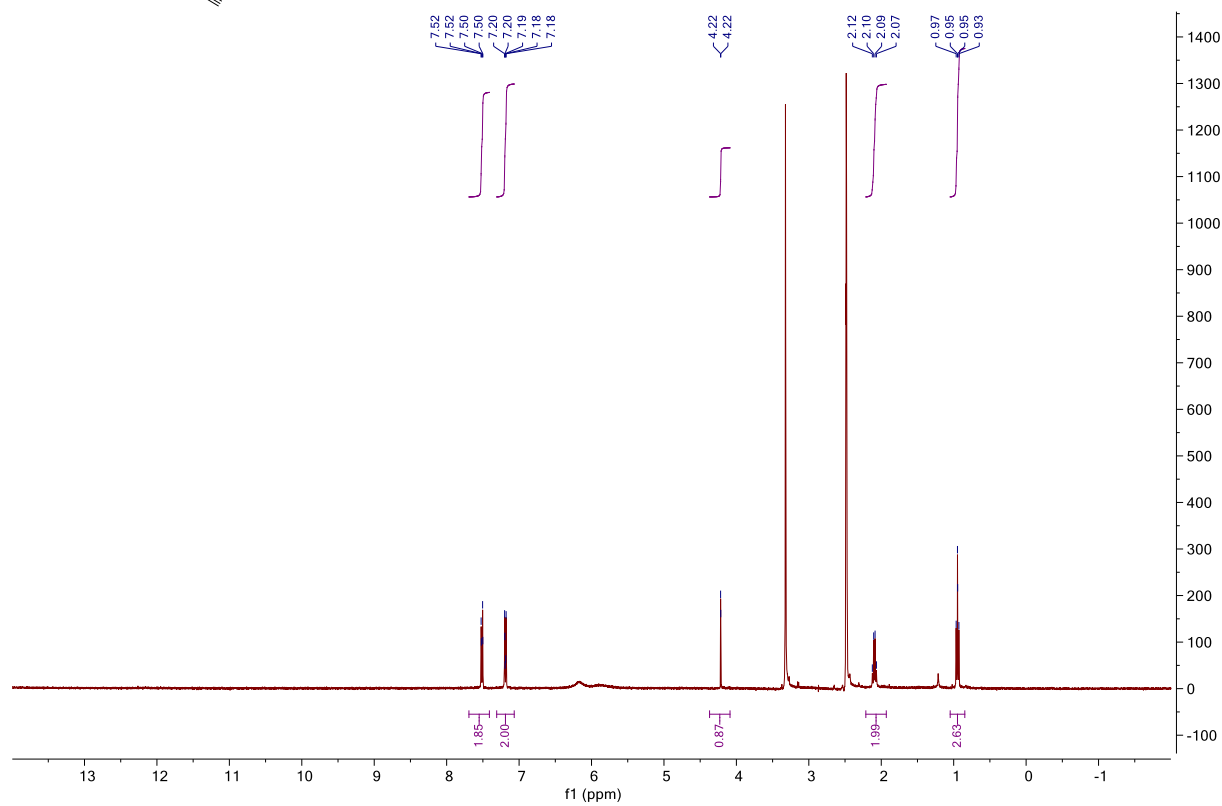
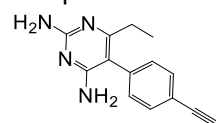


6.6 Supporting Information

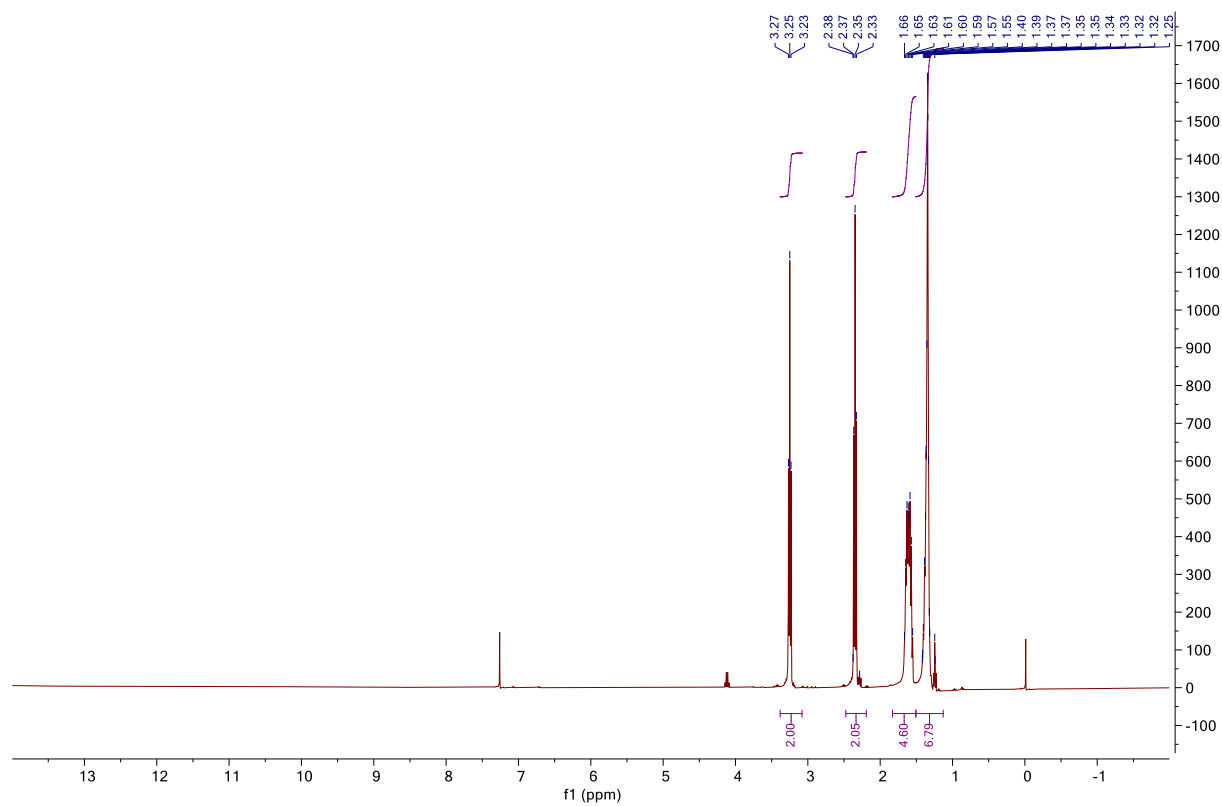
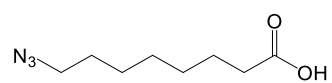
Table 6S.1. Docking score of 11b and controls on P1 and P2 postions of DBD domain.

Compounds	P1 Docking score (kcal/mol)	P2 Docking score (kcal/mol)
PYM	-6.4	-5.8
Wbc-04-82	-8.5	-7.5
11b	-10.6	-9.1

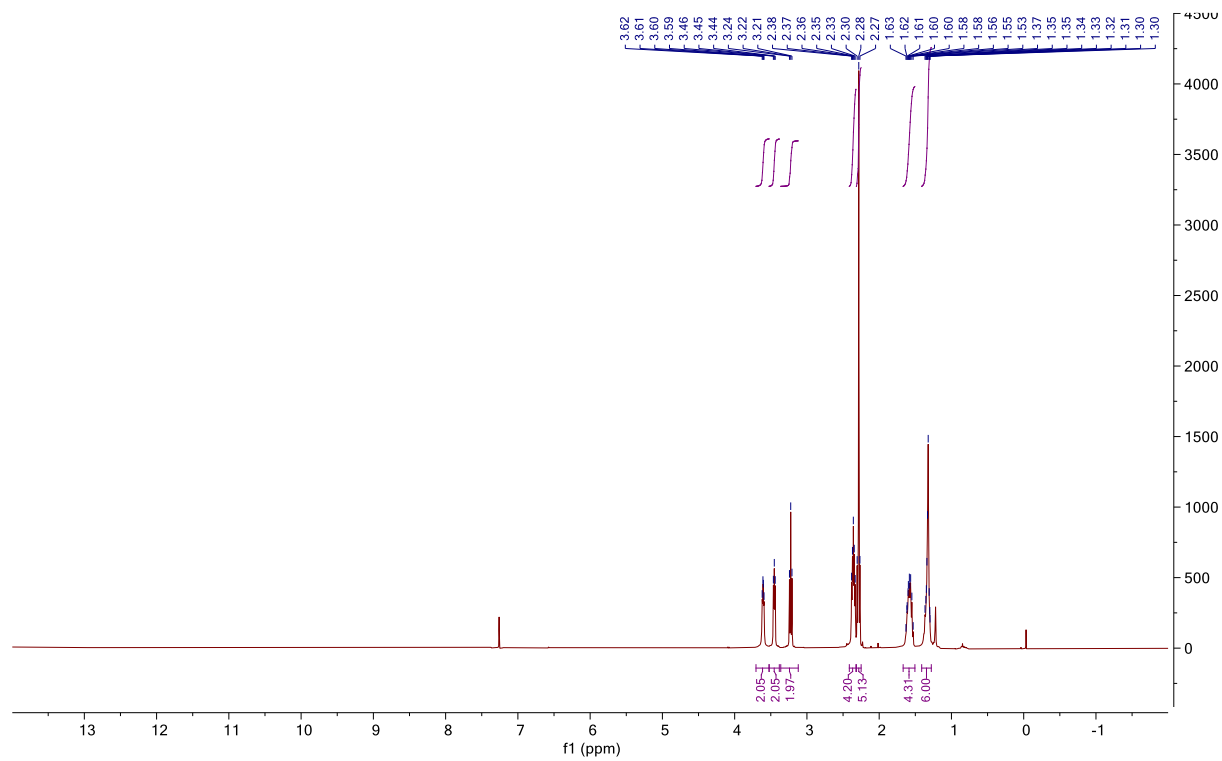
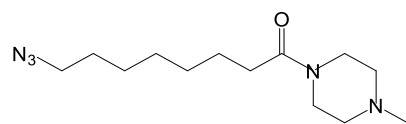
Compound A



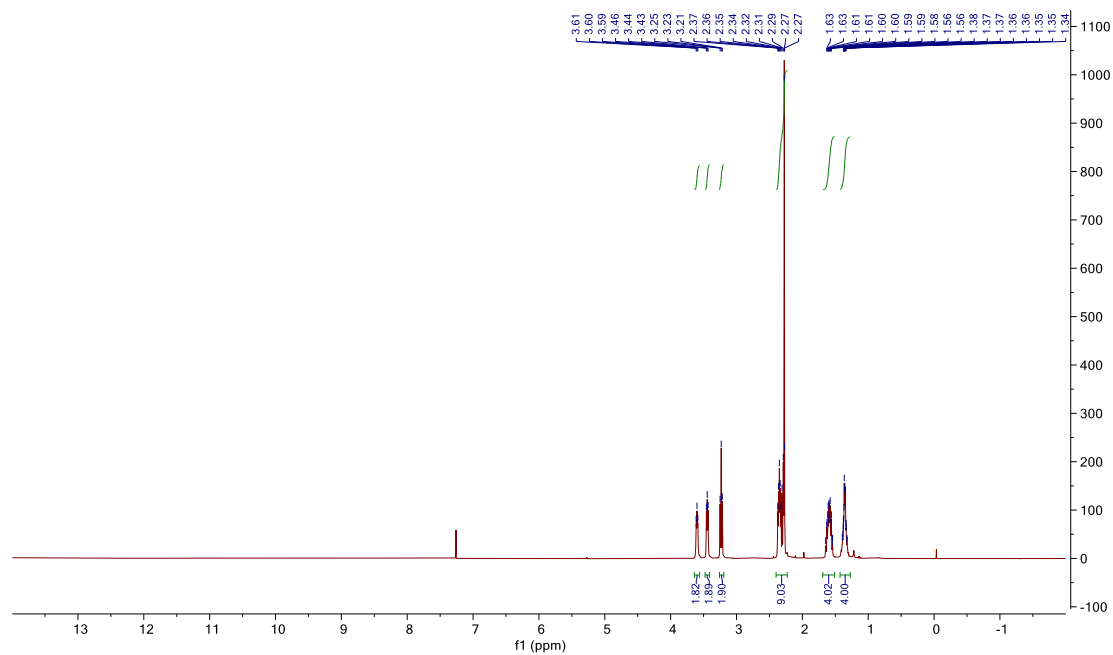
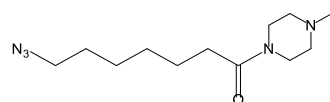
Compound 2



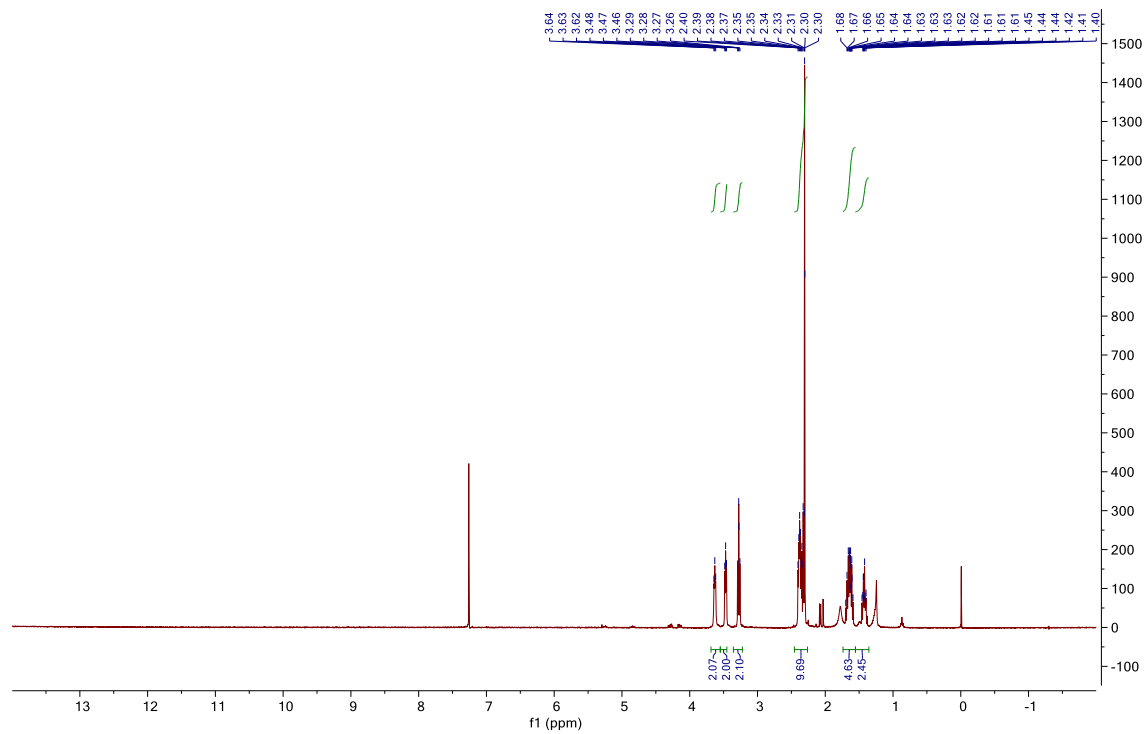
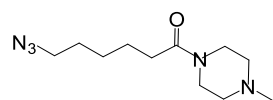
Compound 3a



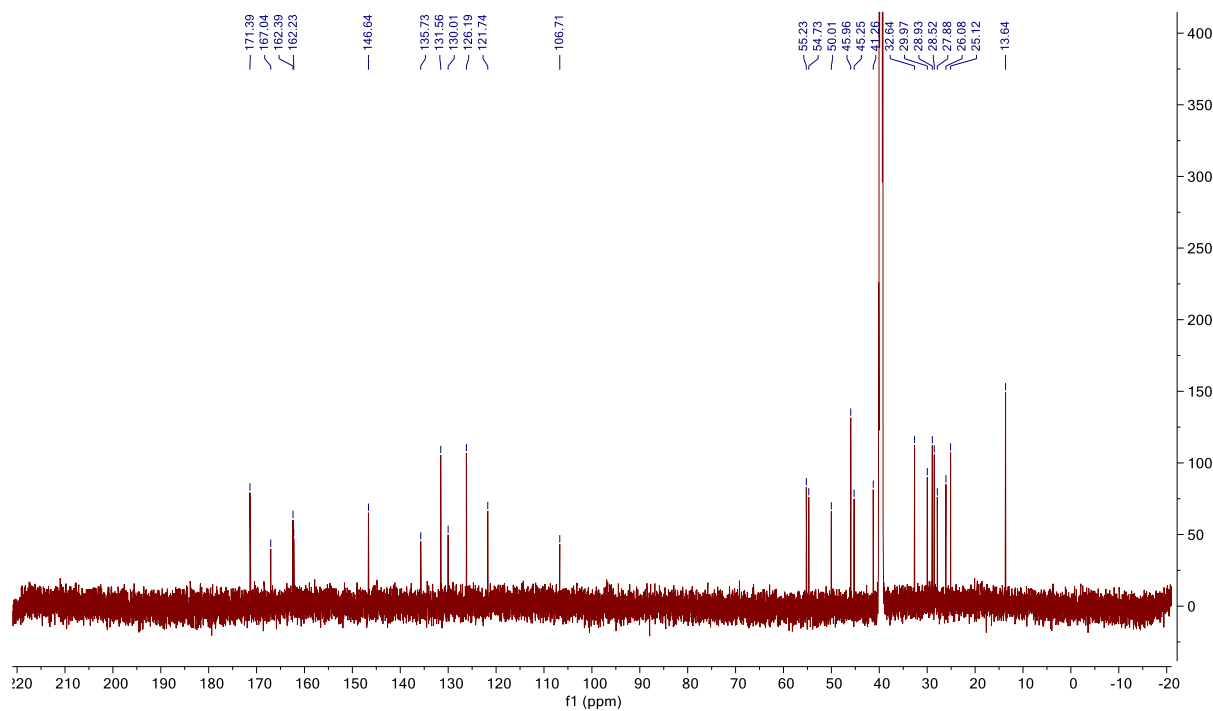
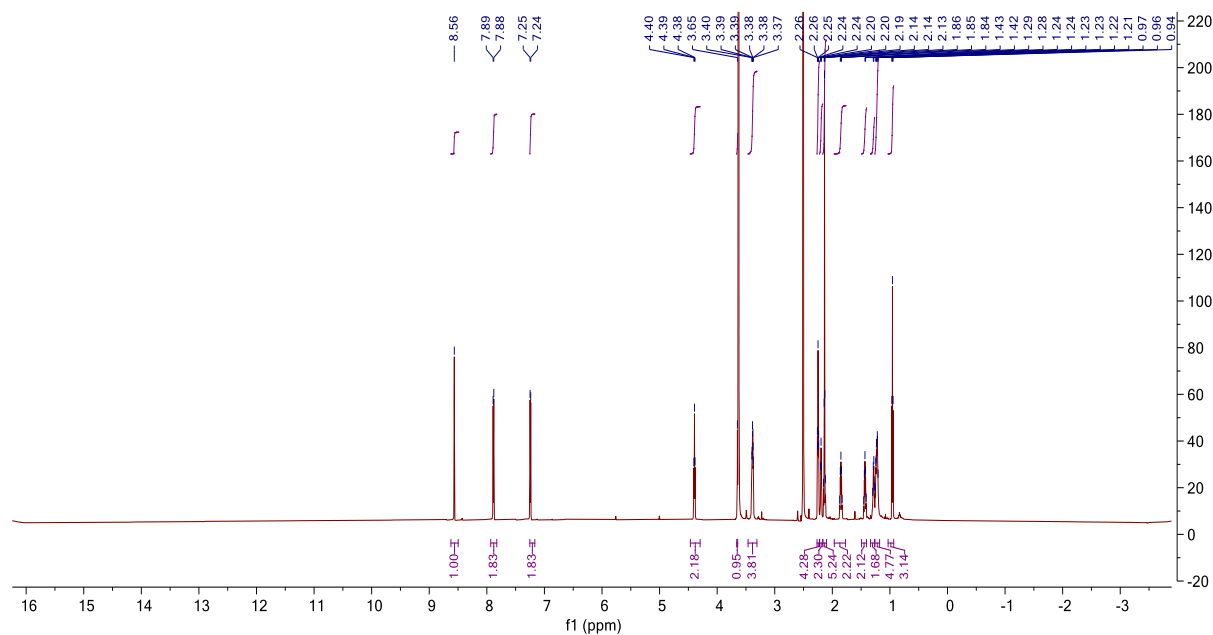
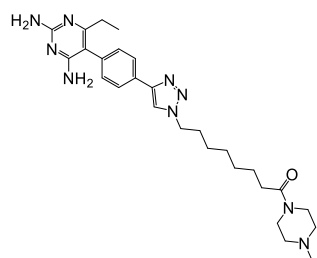
Compound 3b



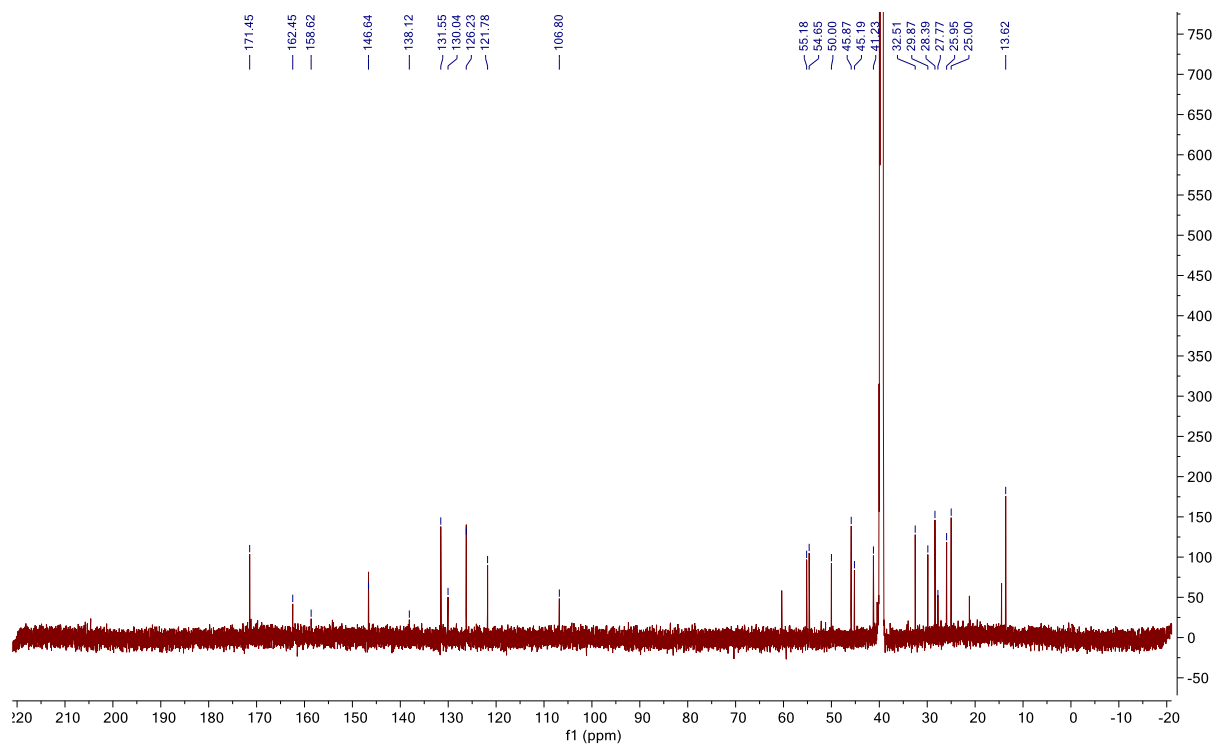
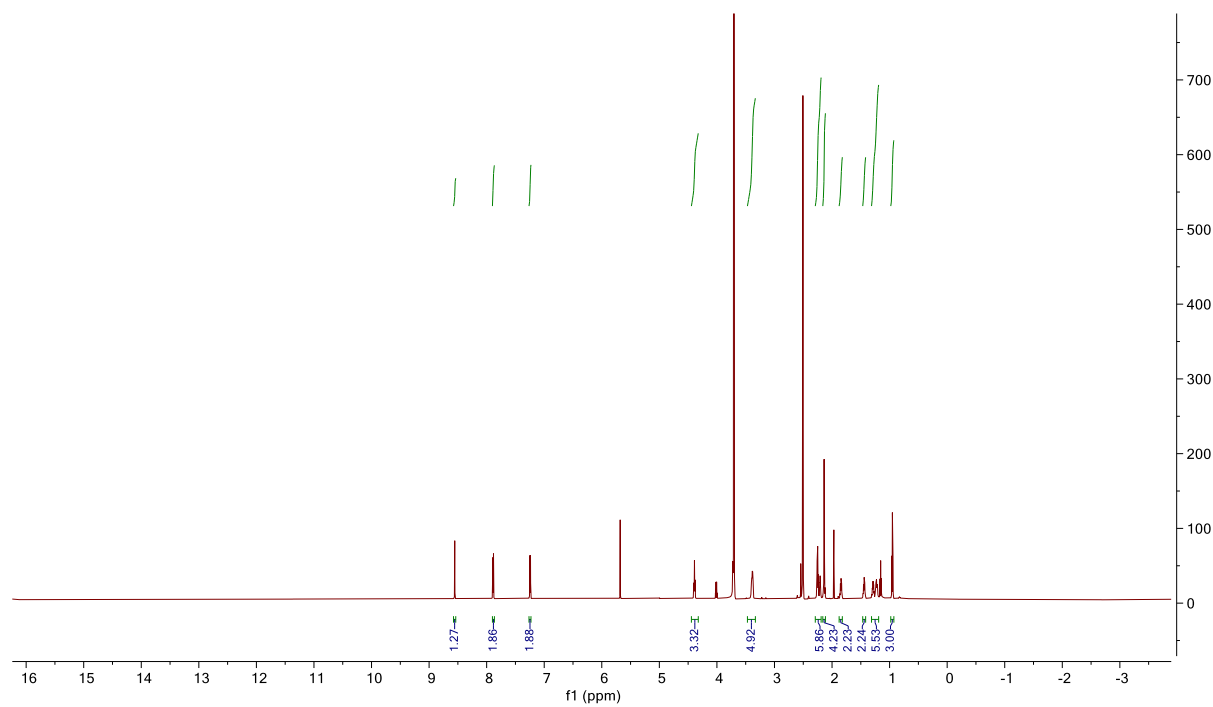
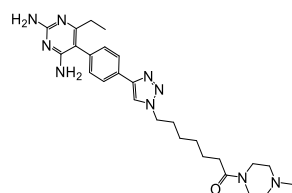
Compound 3c



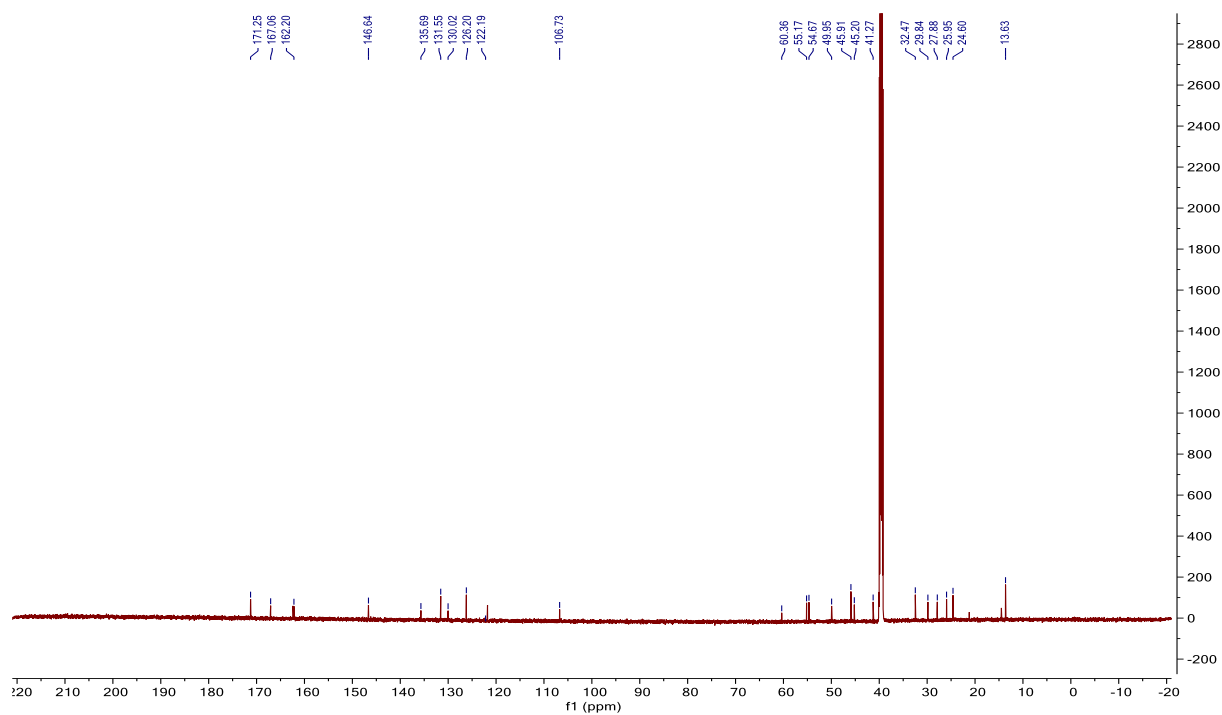
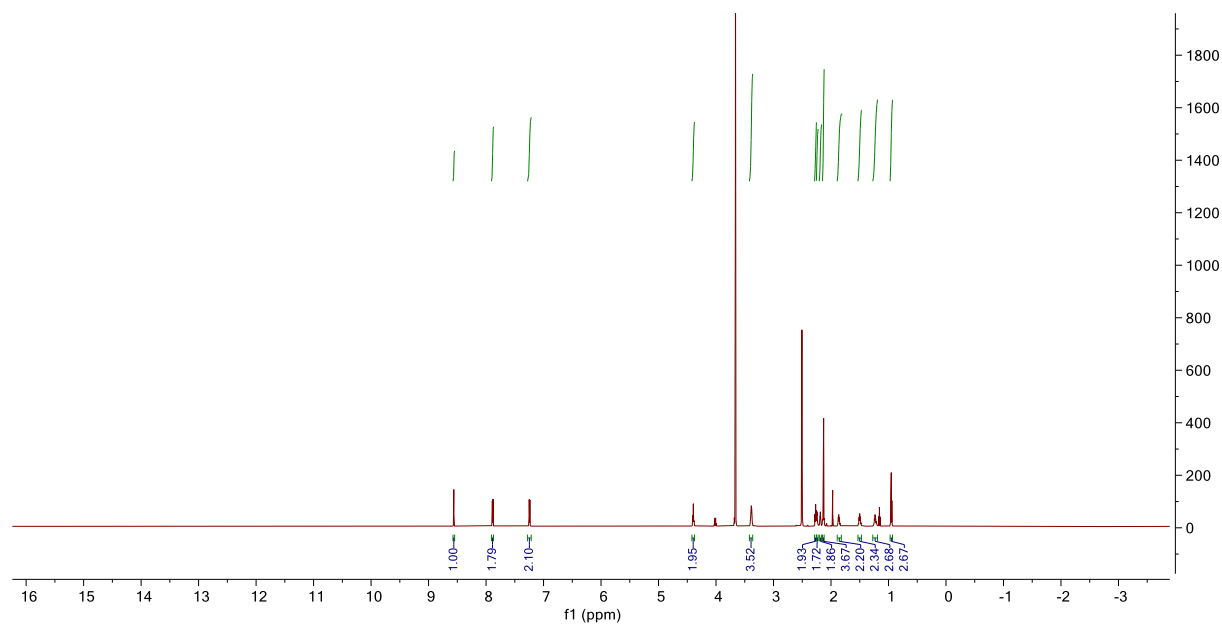
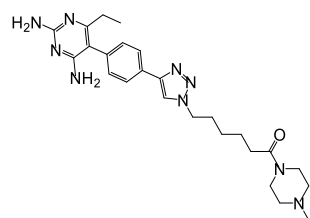
Compound 4a



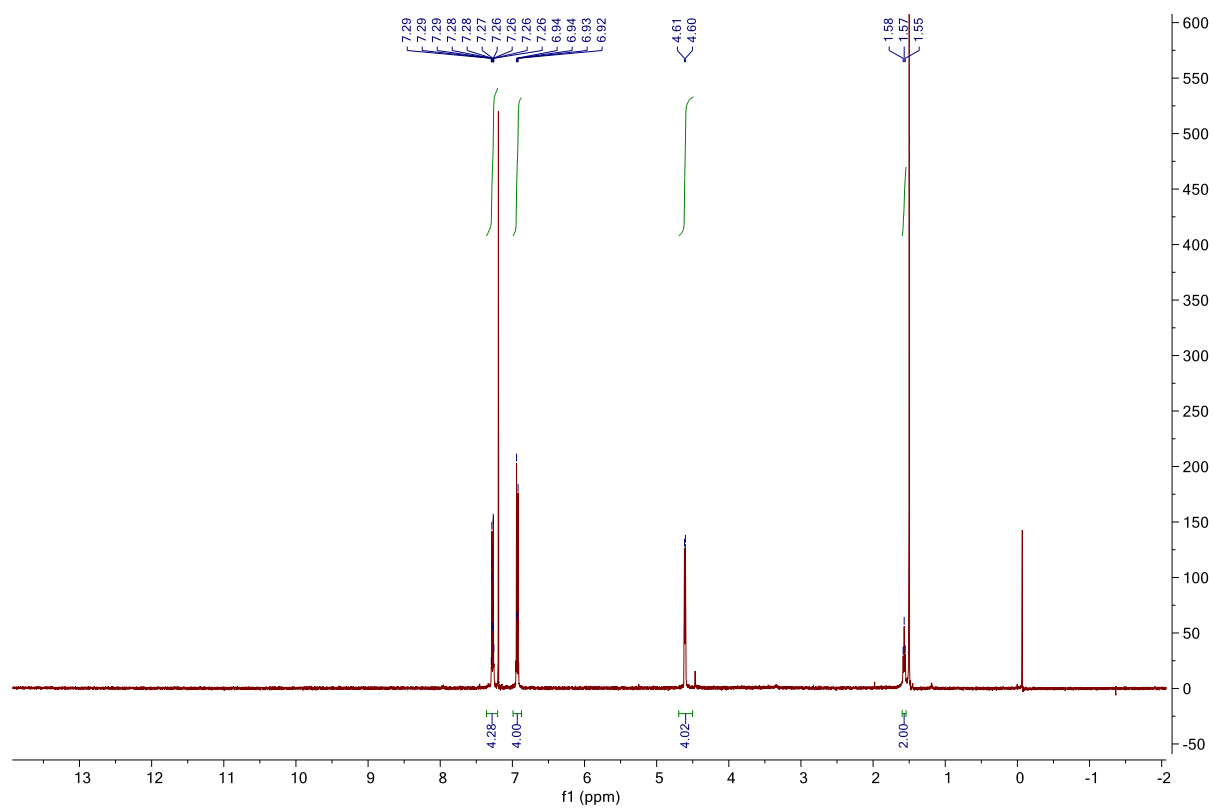
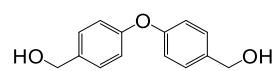
Compound 4b



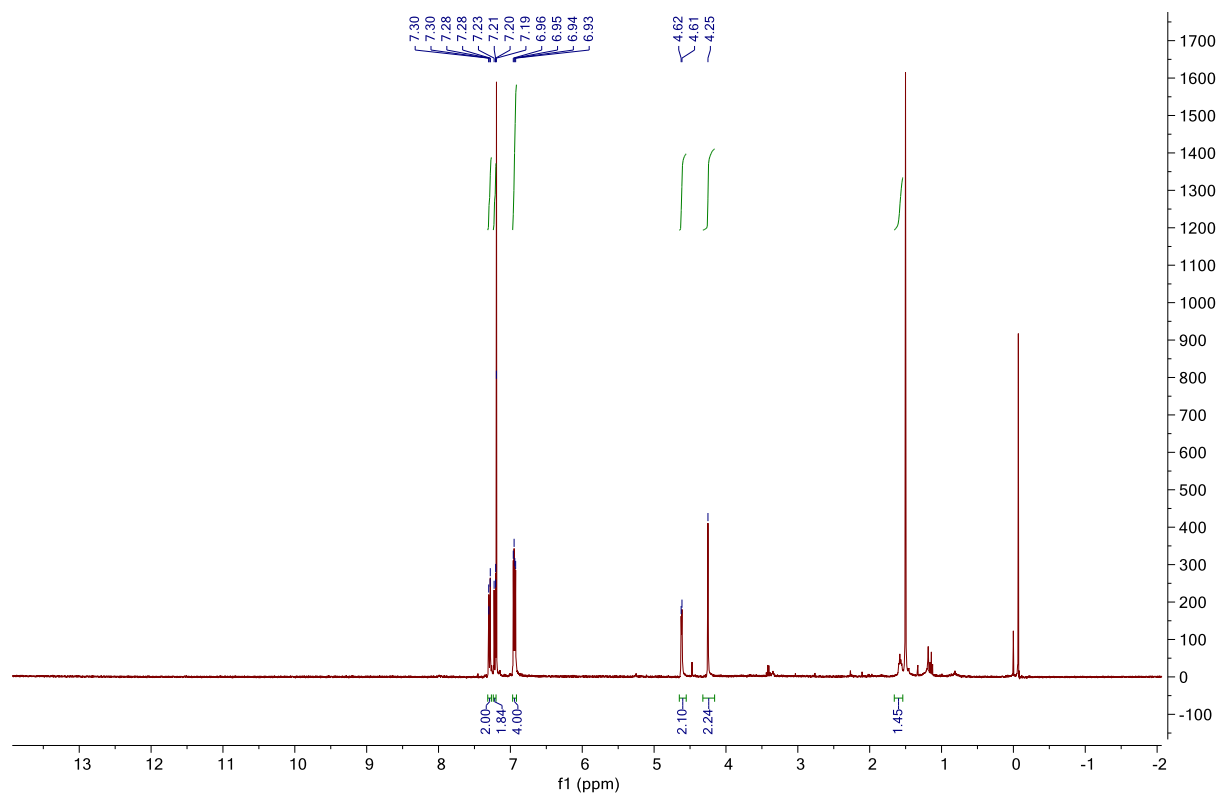
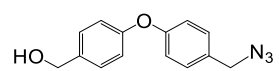
Compound 4c



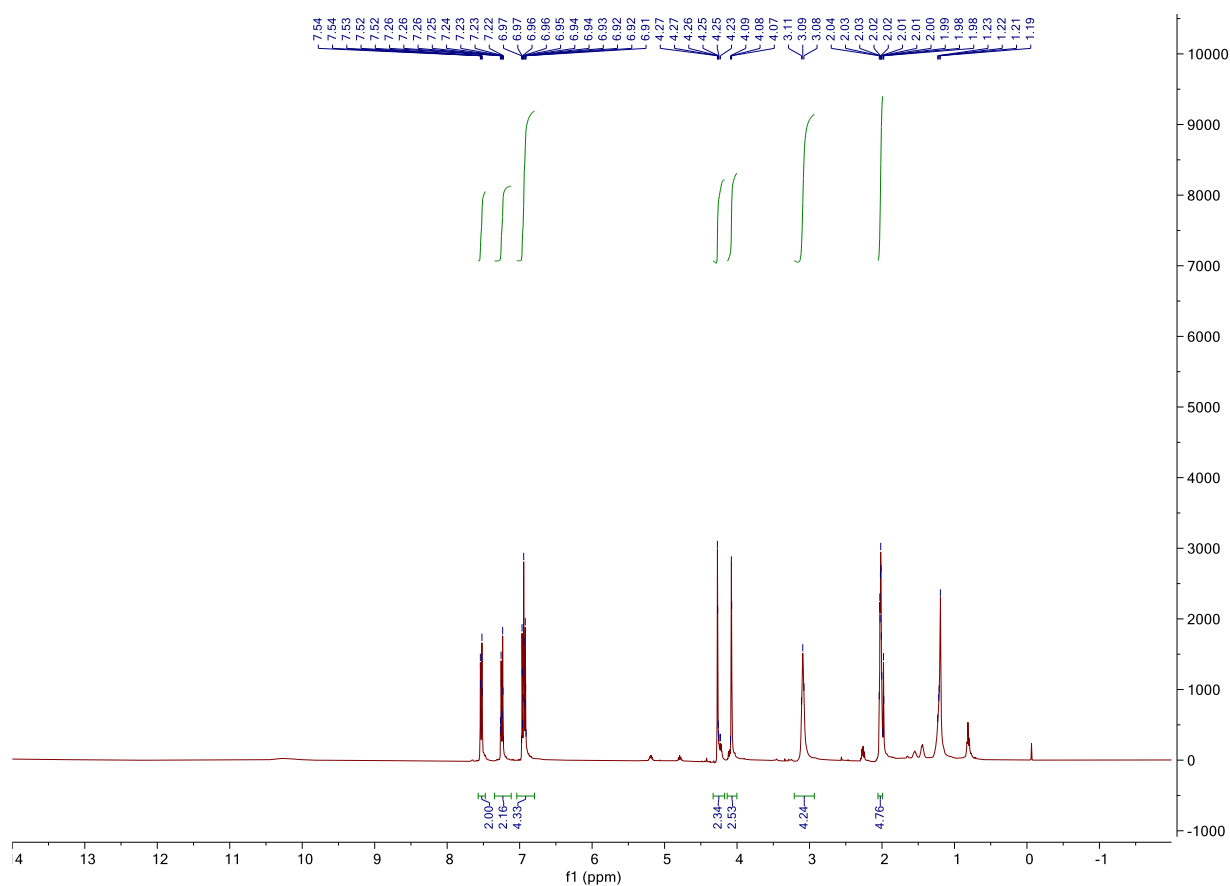
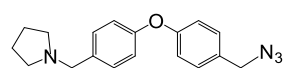
Compound 6



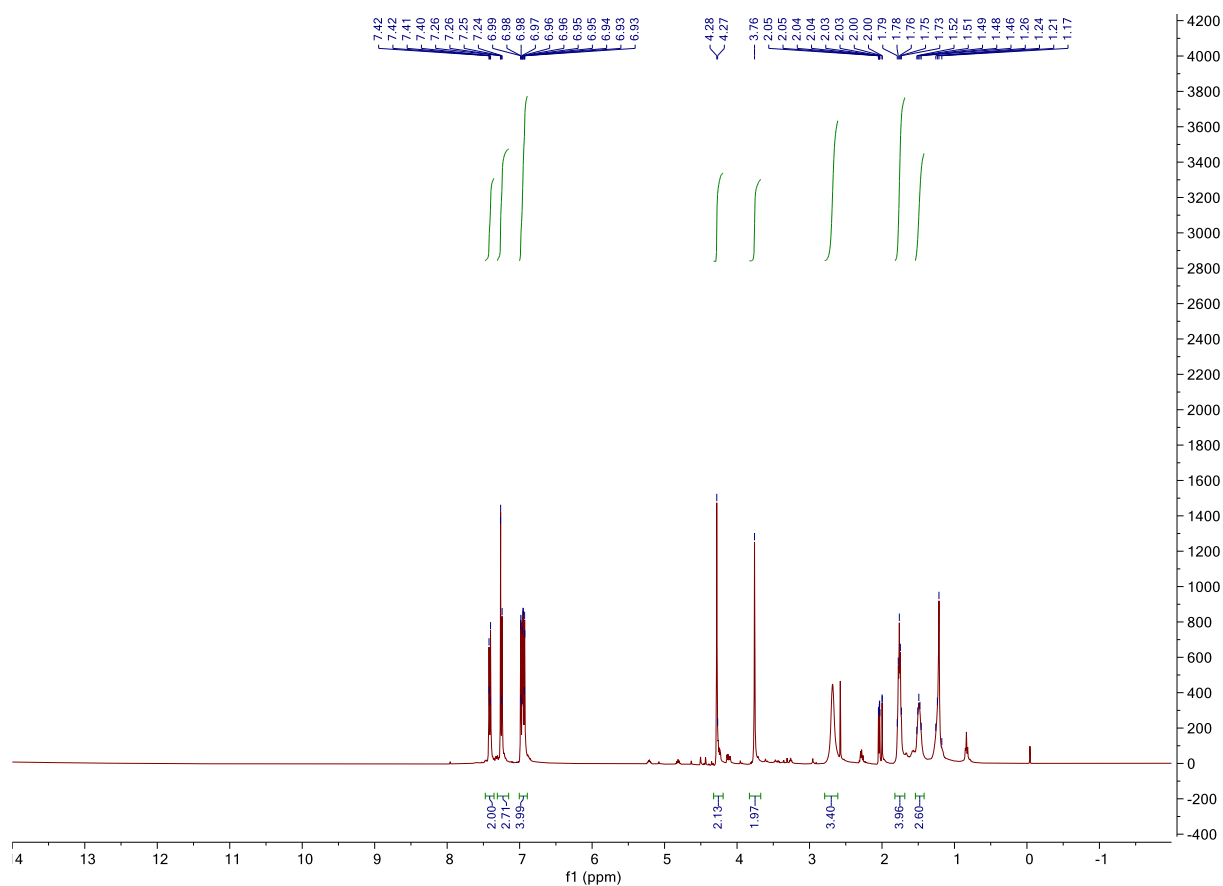
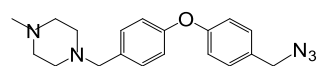
Compound 8



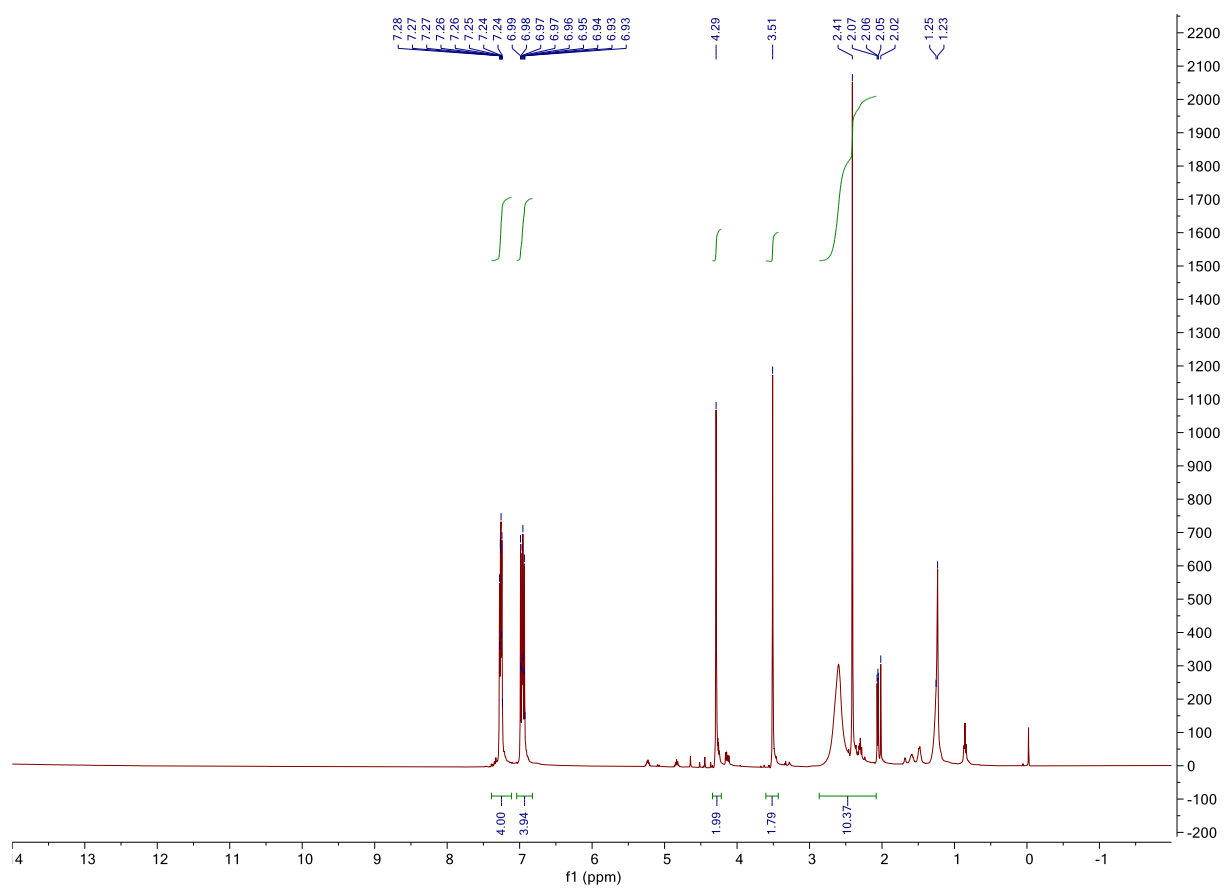
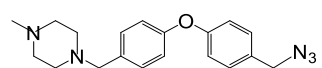
Compound 10a



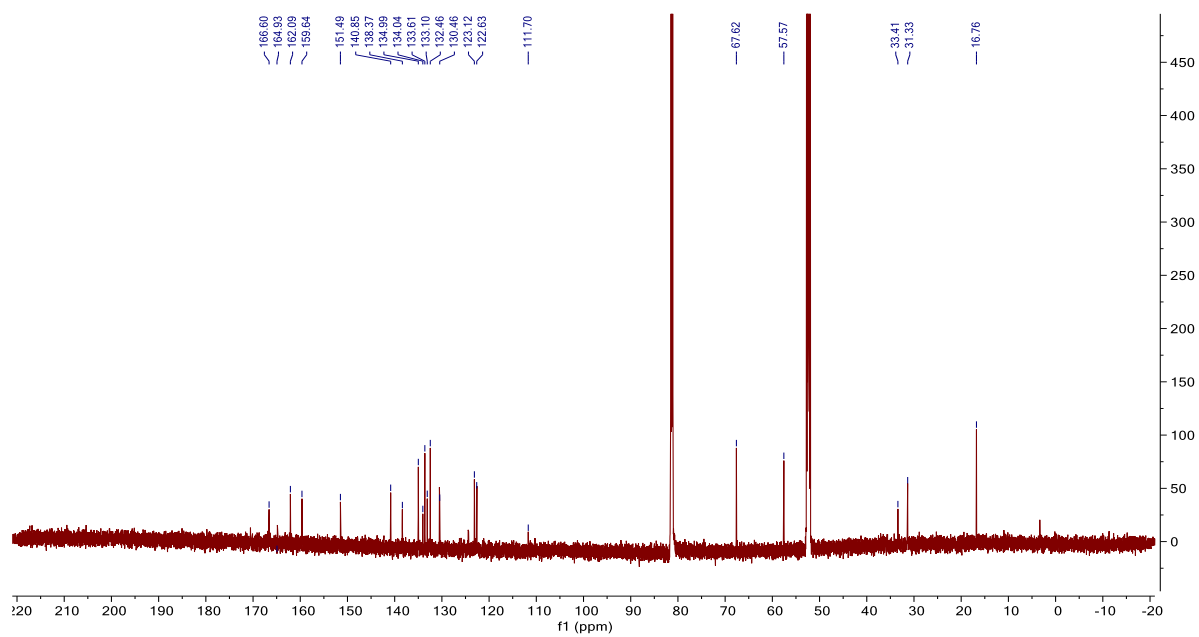
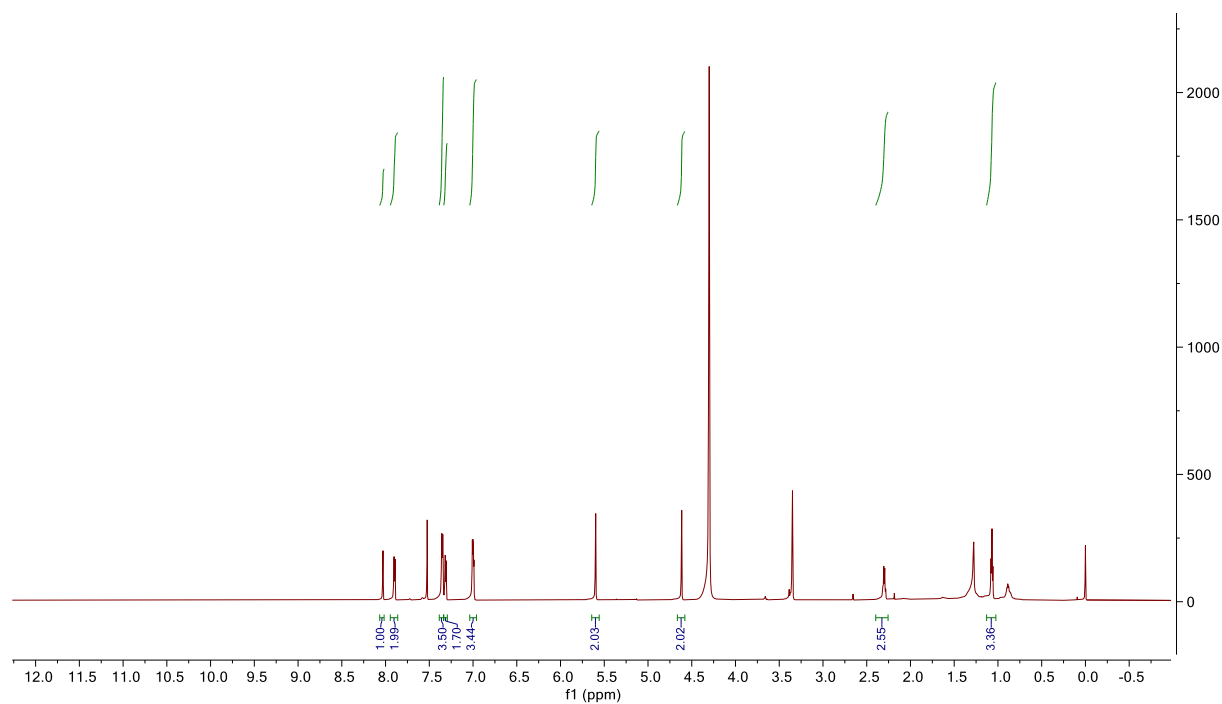
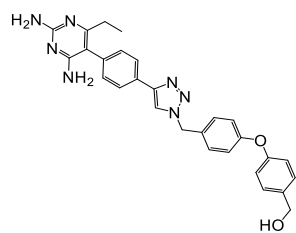
Compound 10b



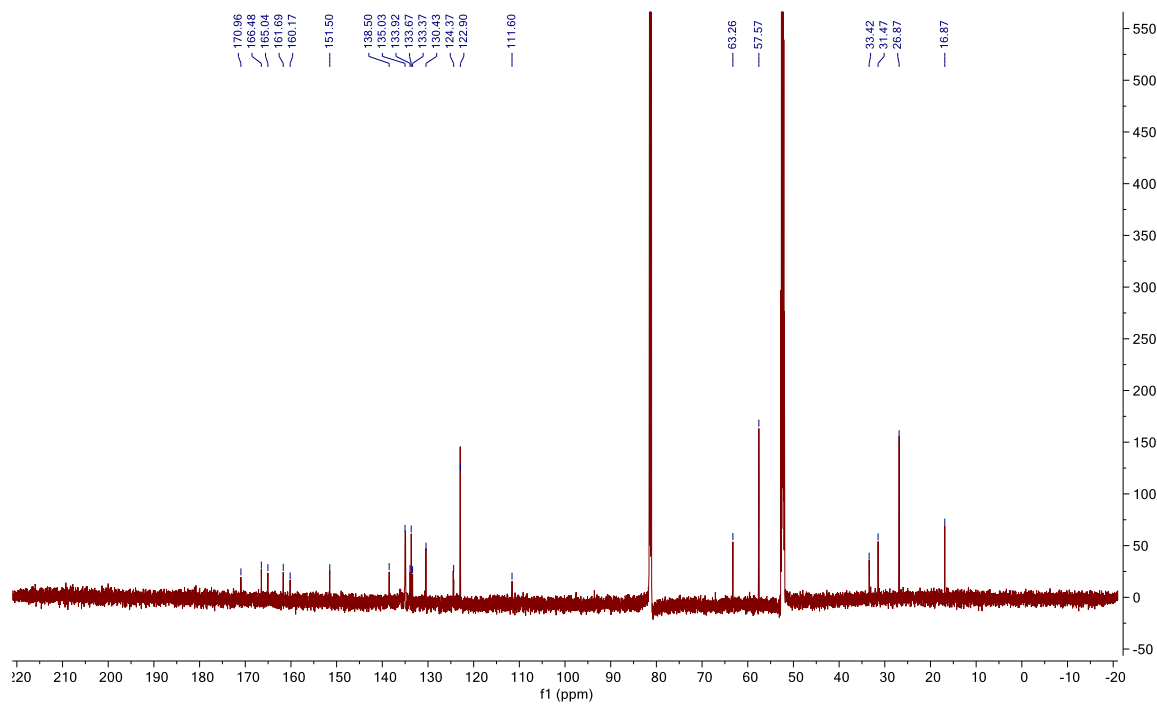
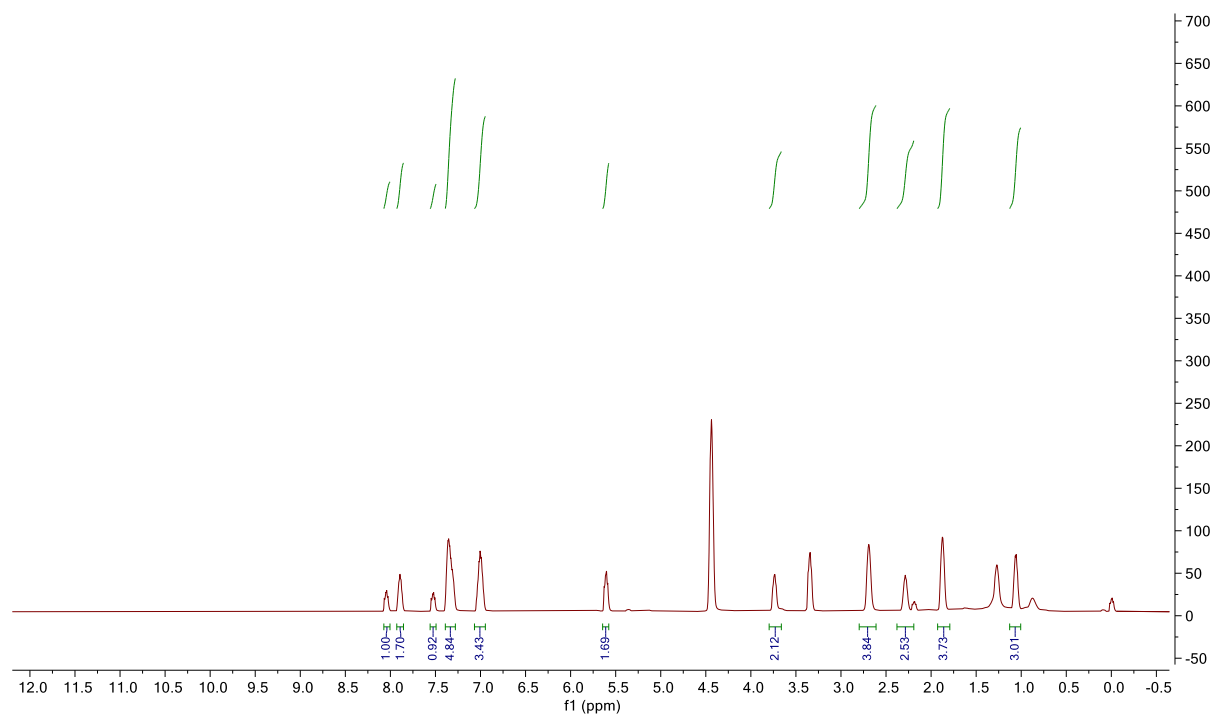
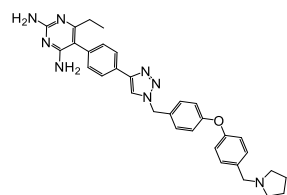
Compound 10c



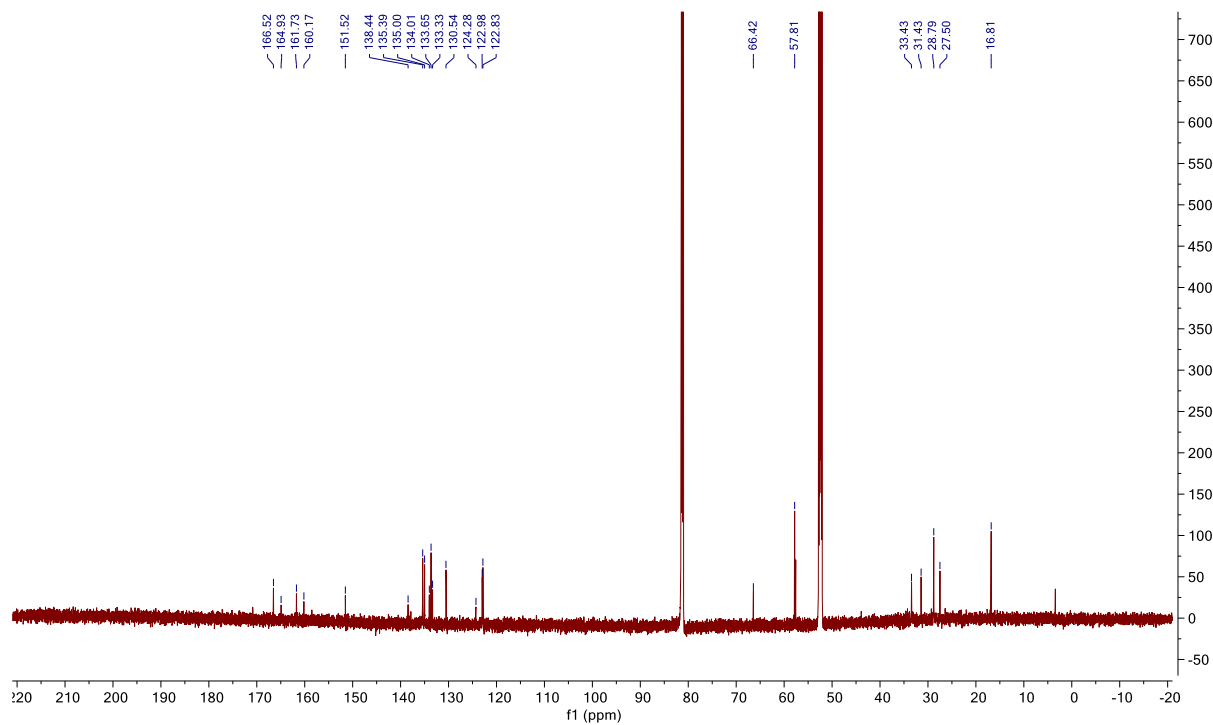
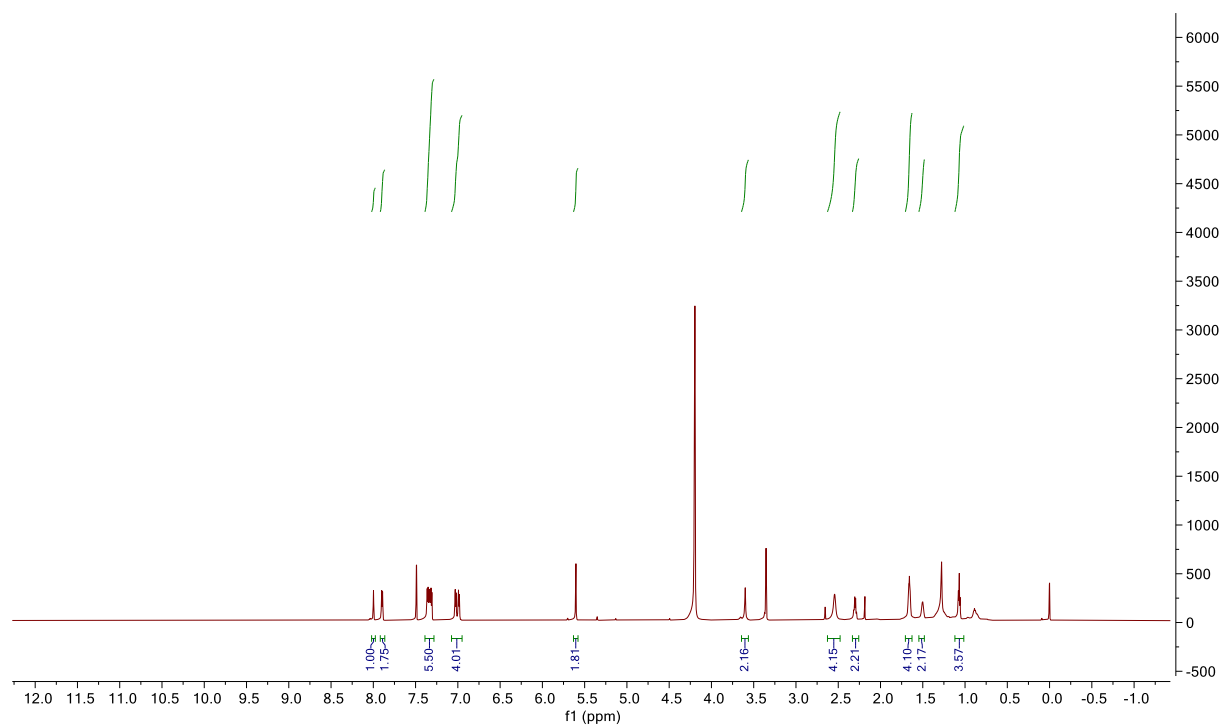
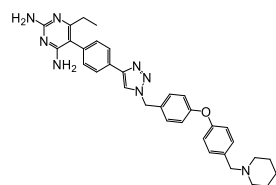
Compound 11a



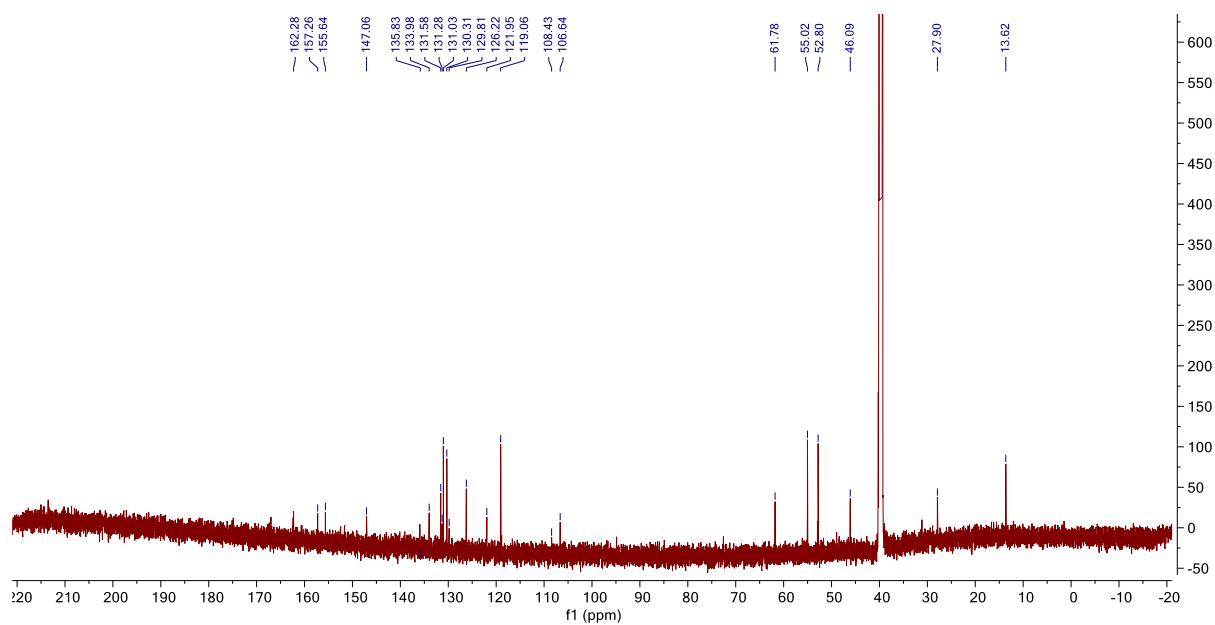
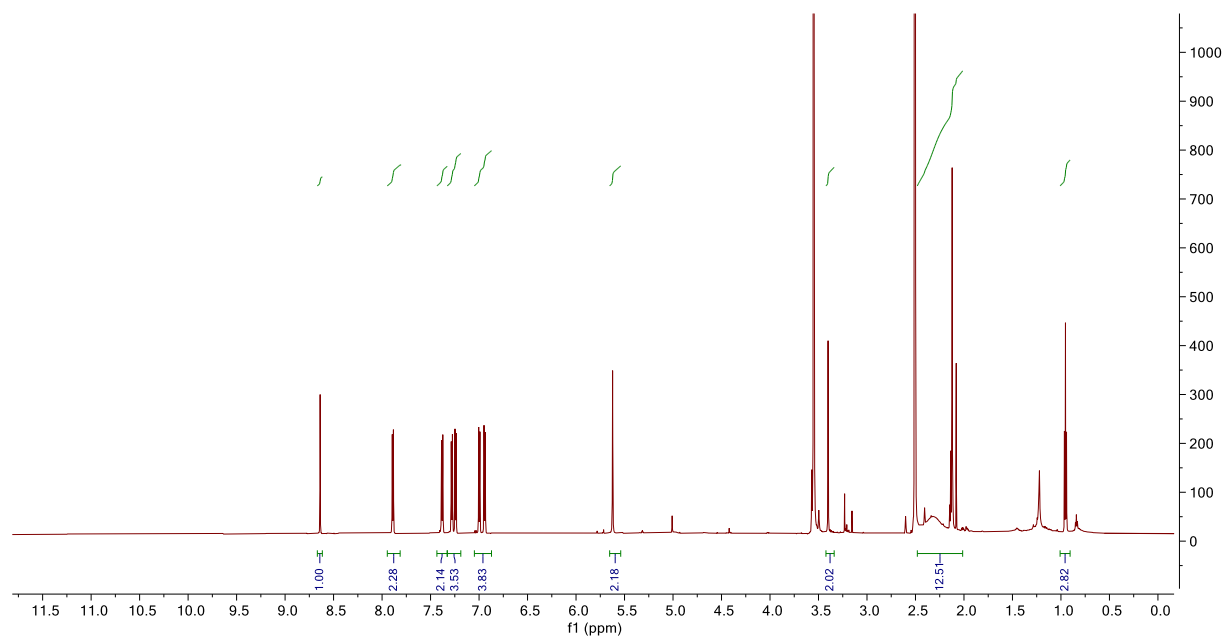
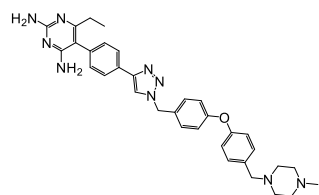
Compound 11b



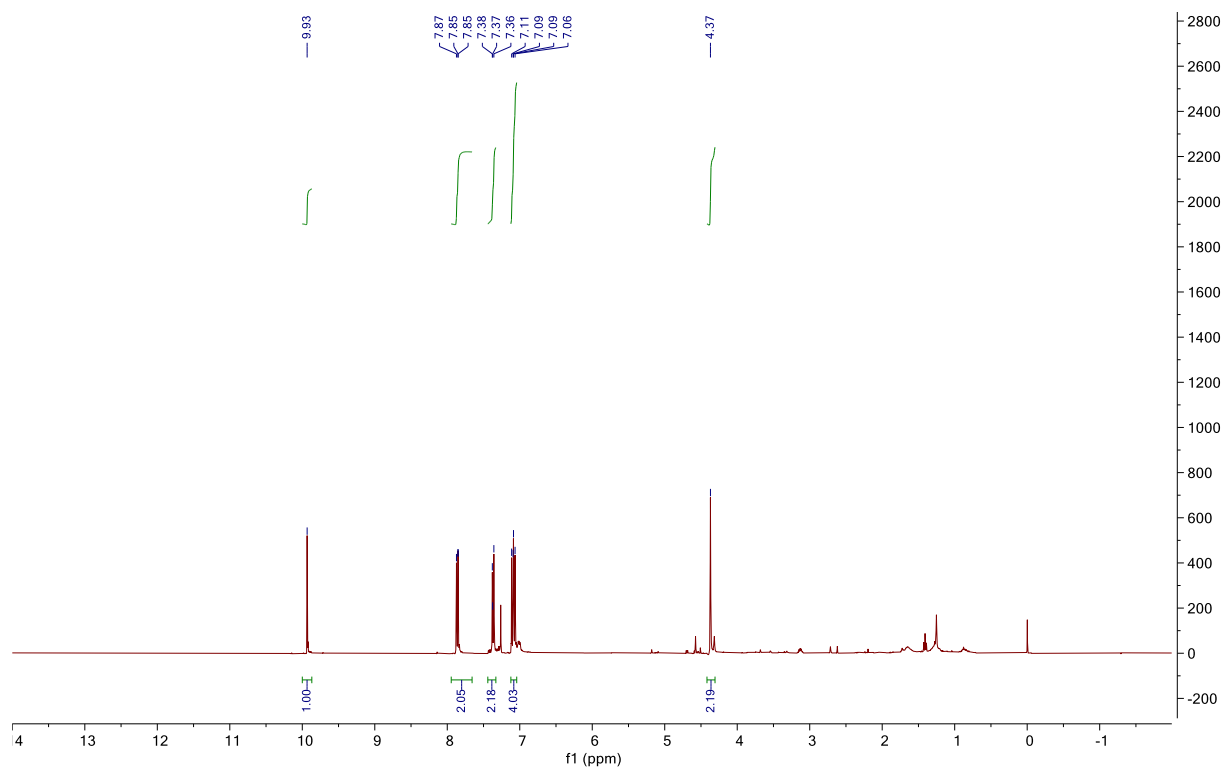
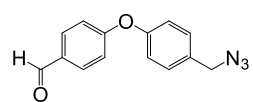
Compound 11c



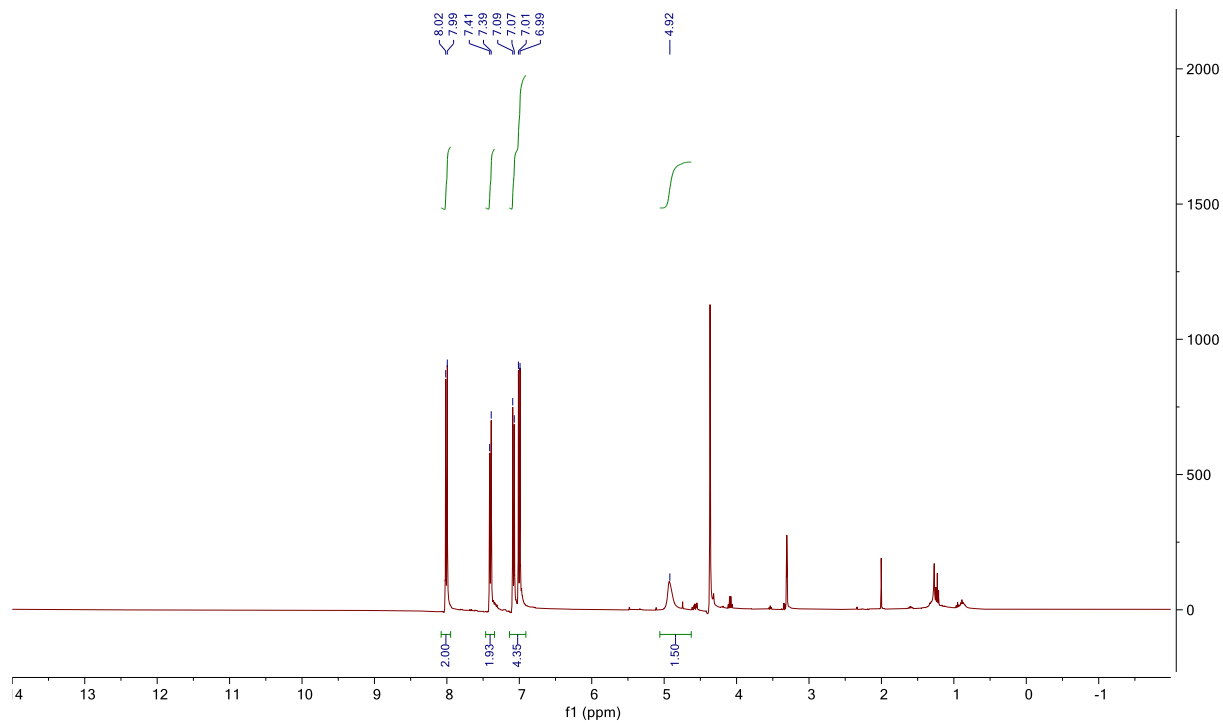
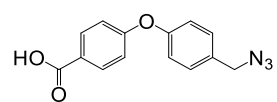
Compound 11d



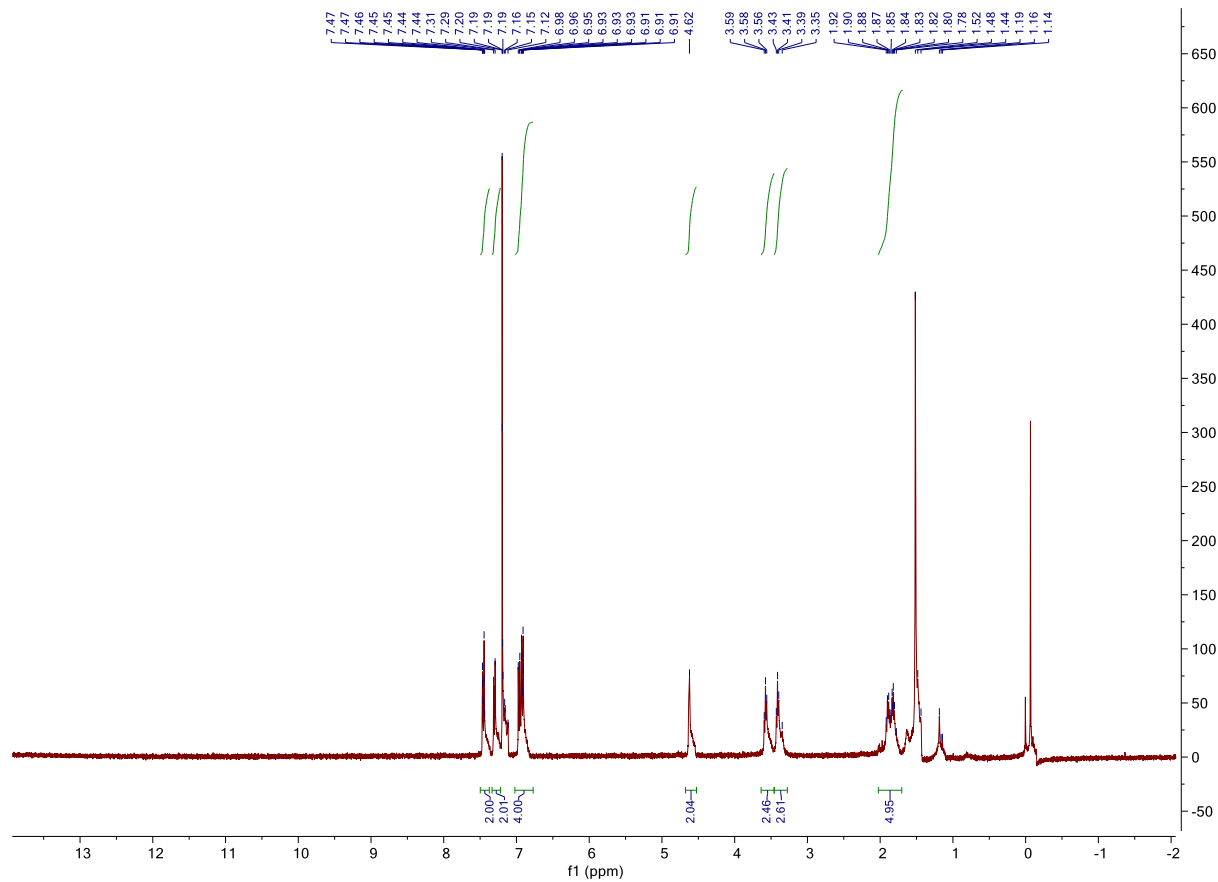
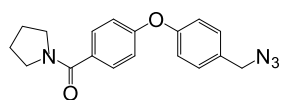
Compound 12



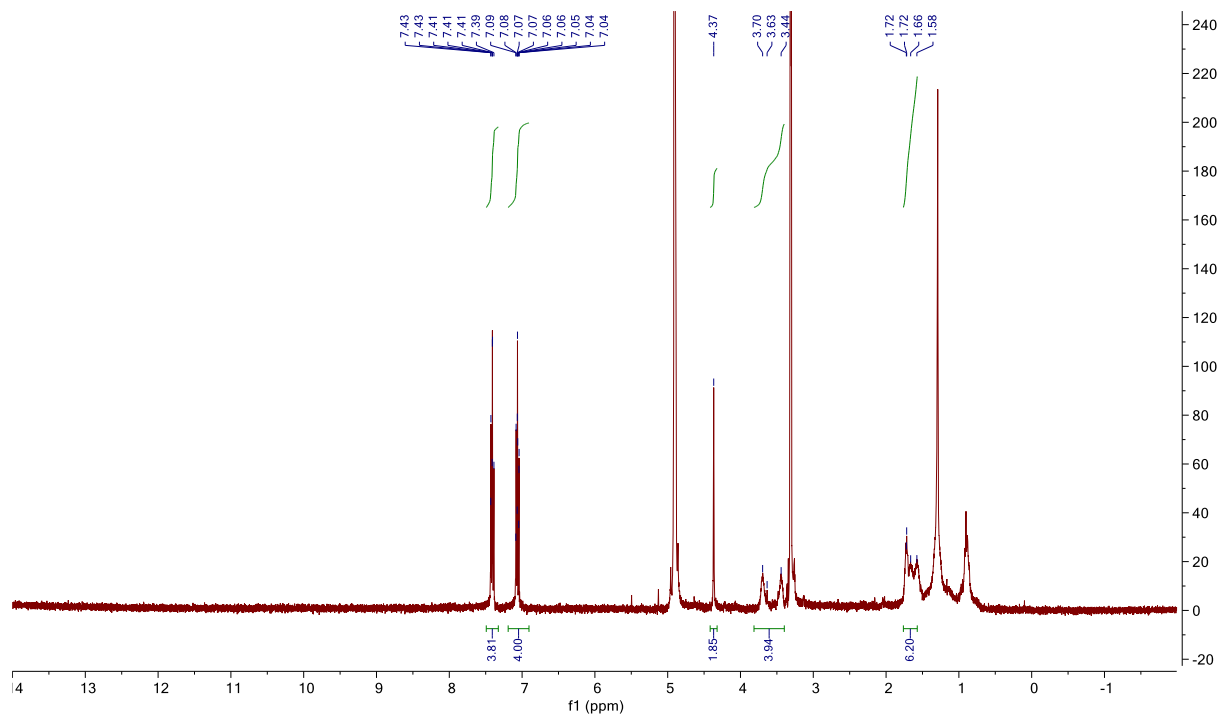
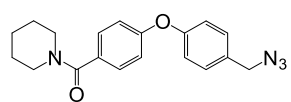
Compound 13



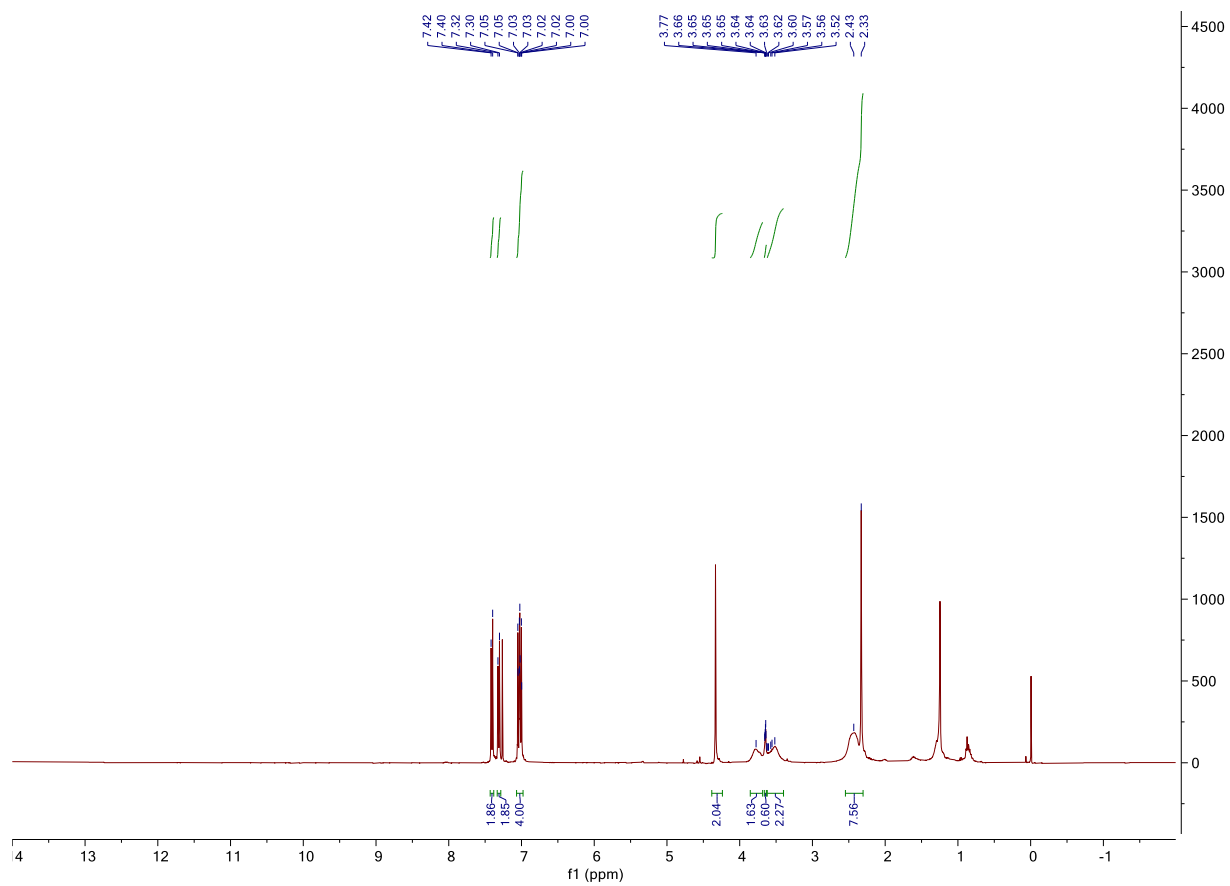
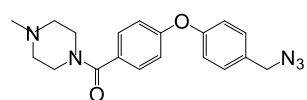
Compound 14a

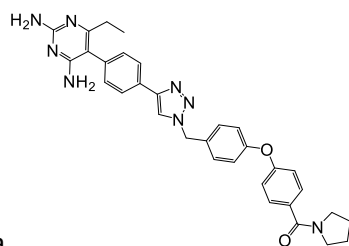


Compound 14b

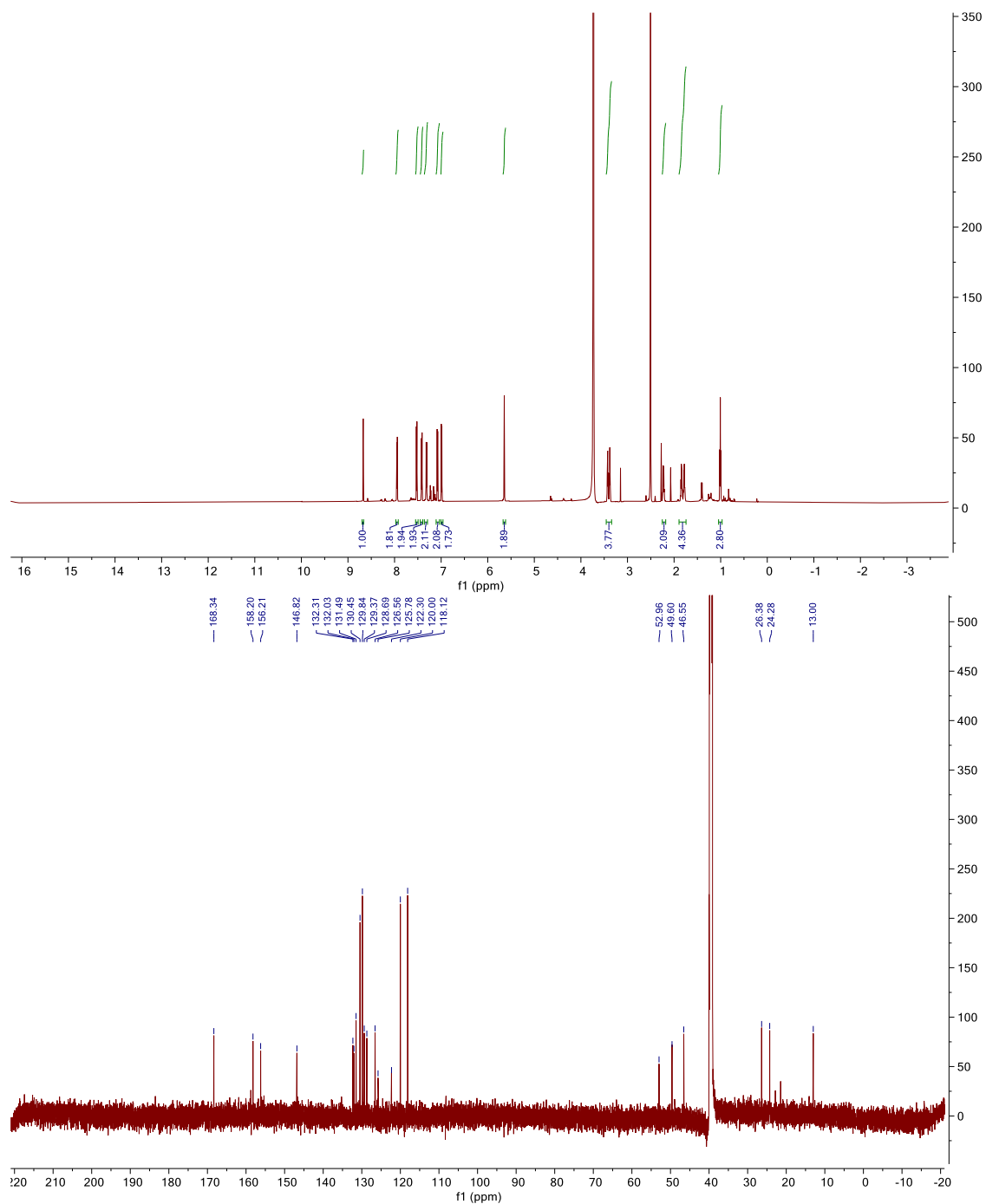


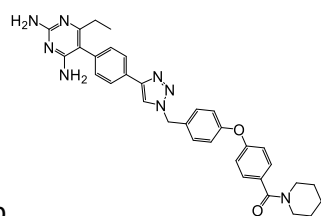
Compound 14c



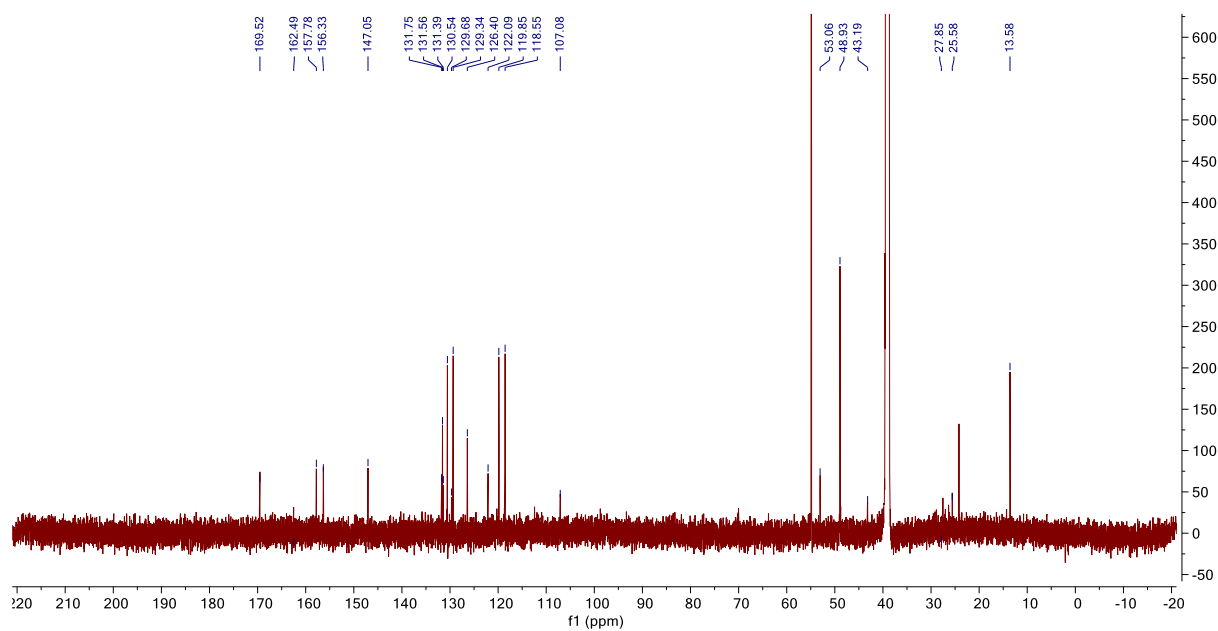
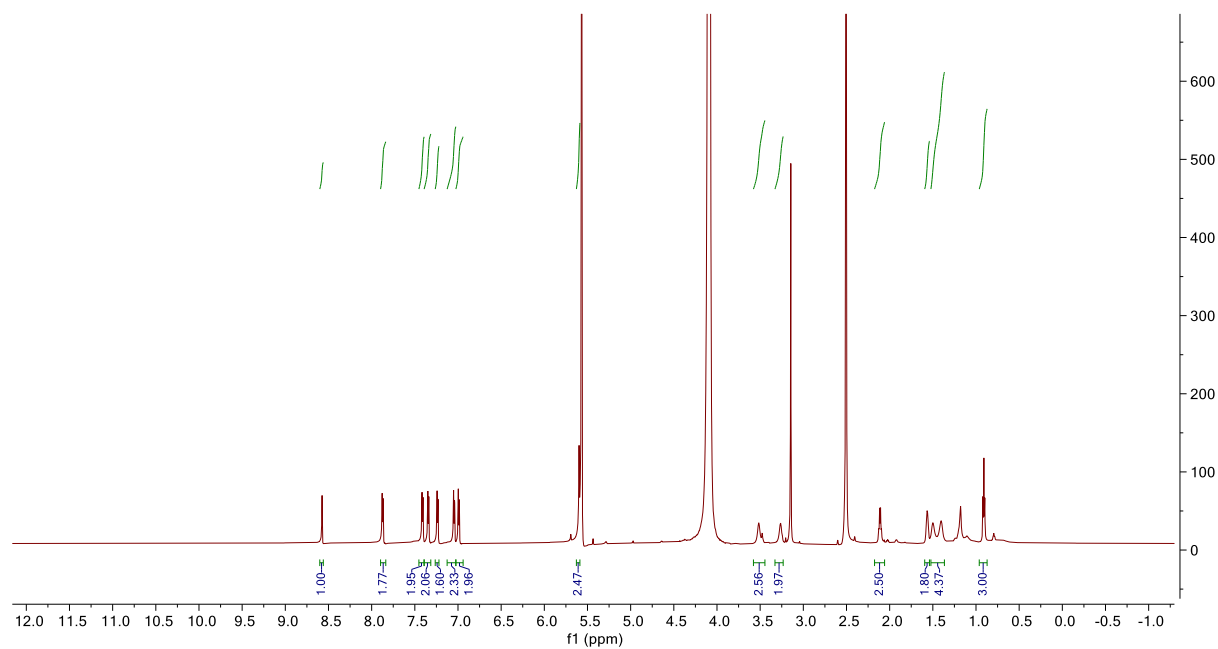


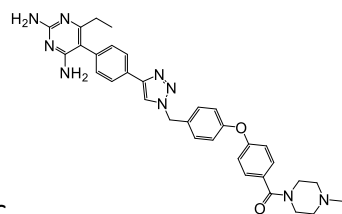
Compound 15a



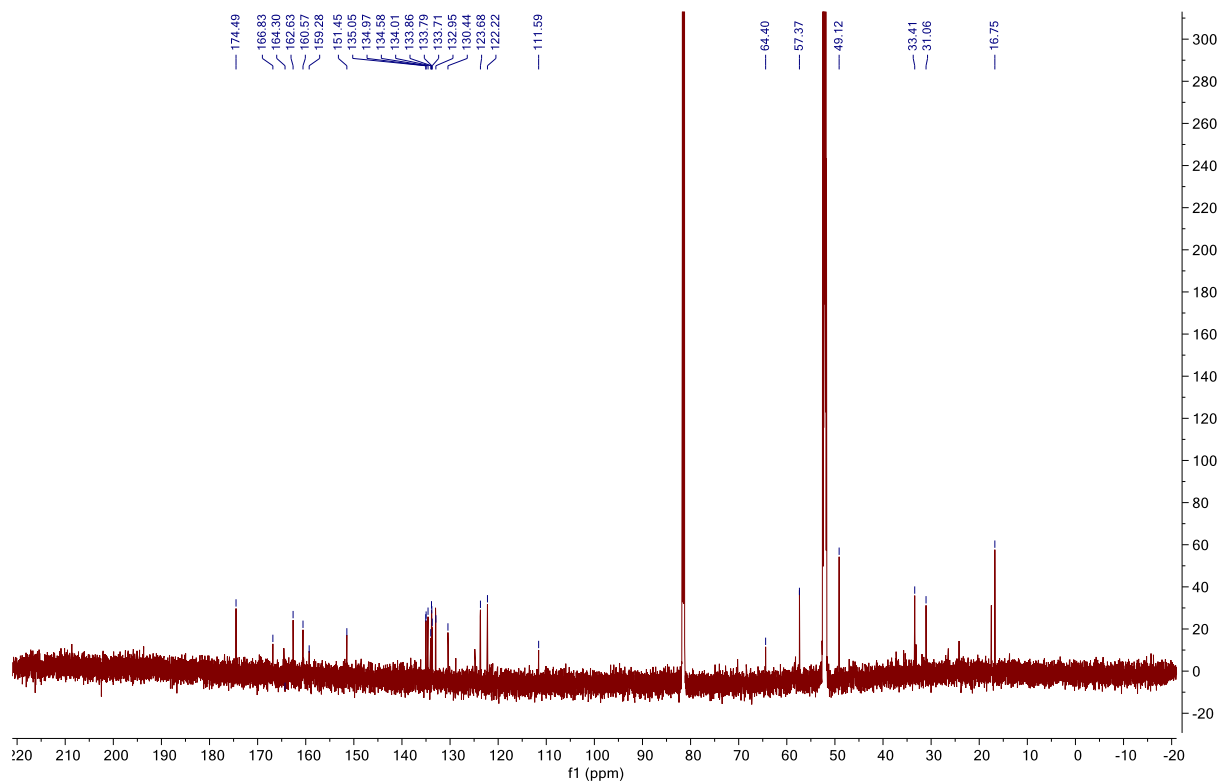
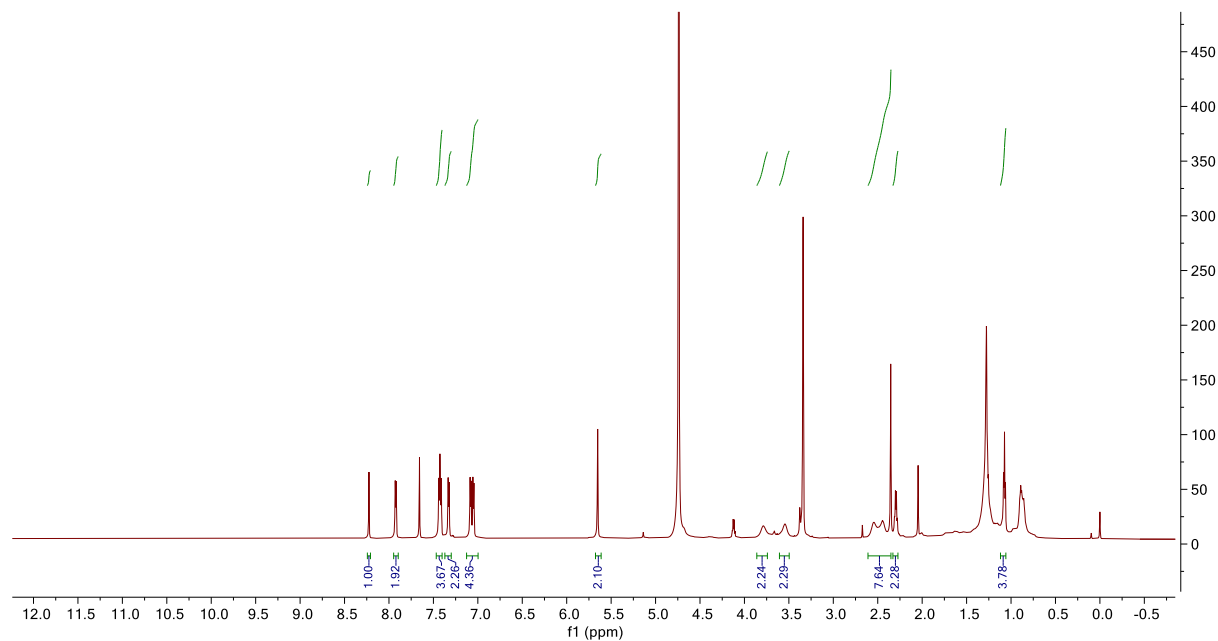


Compound 15b

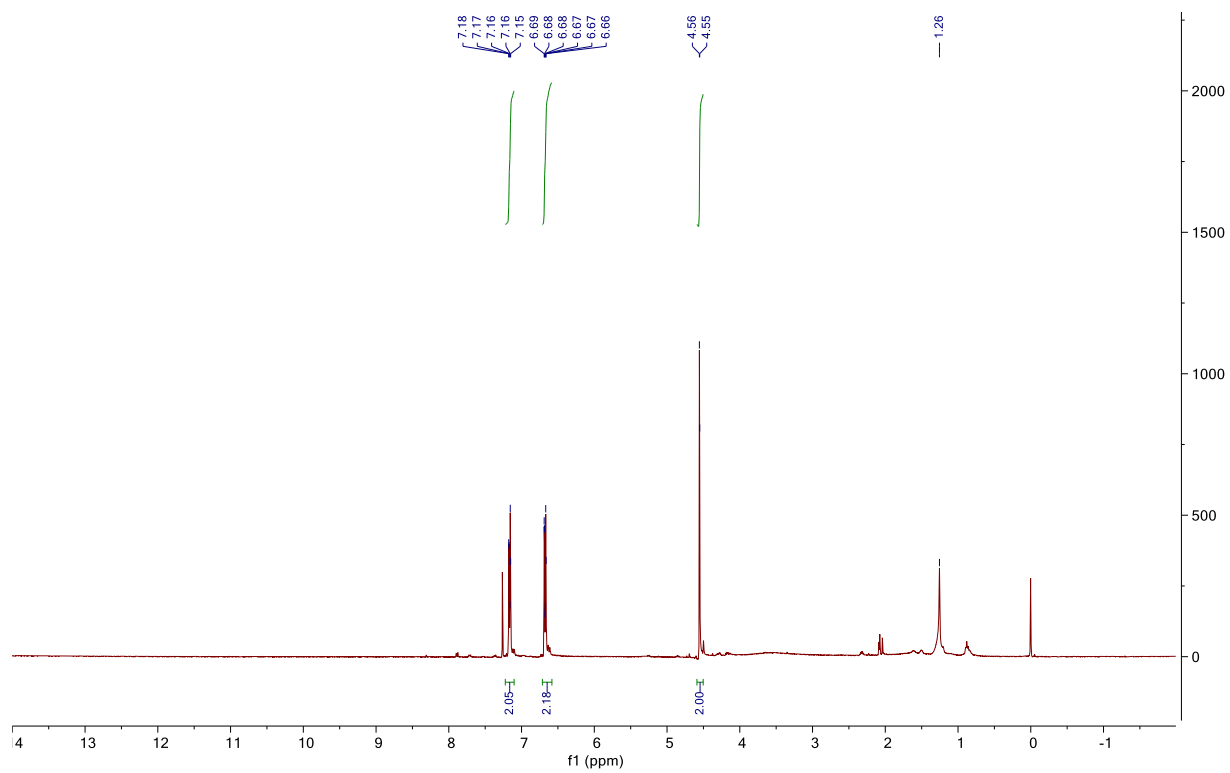
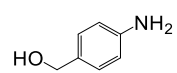




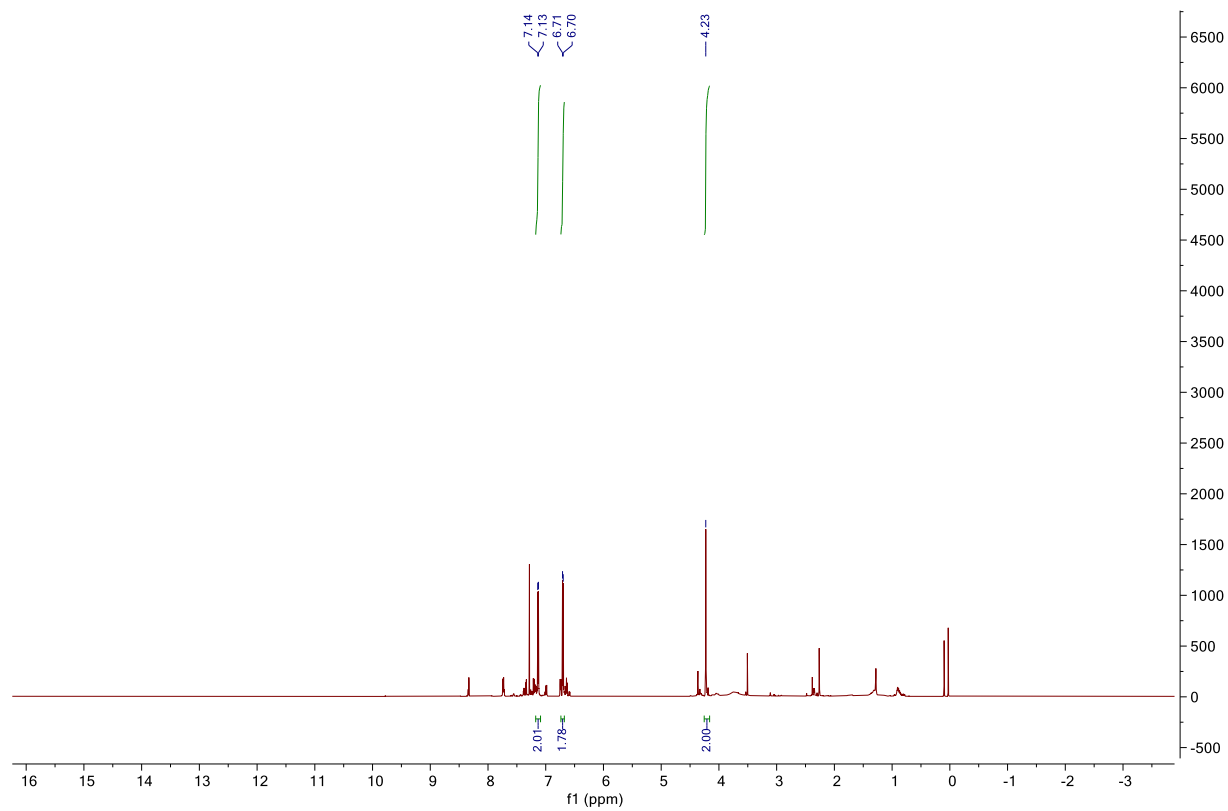
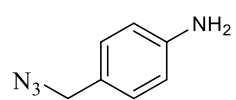
Compound 15c



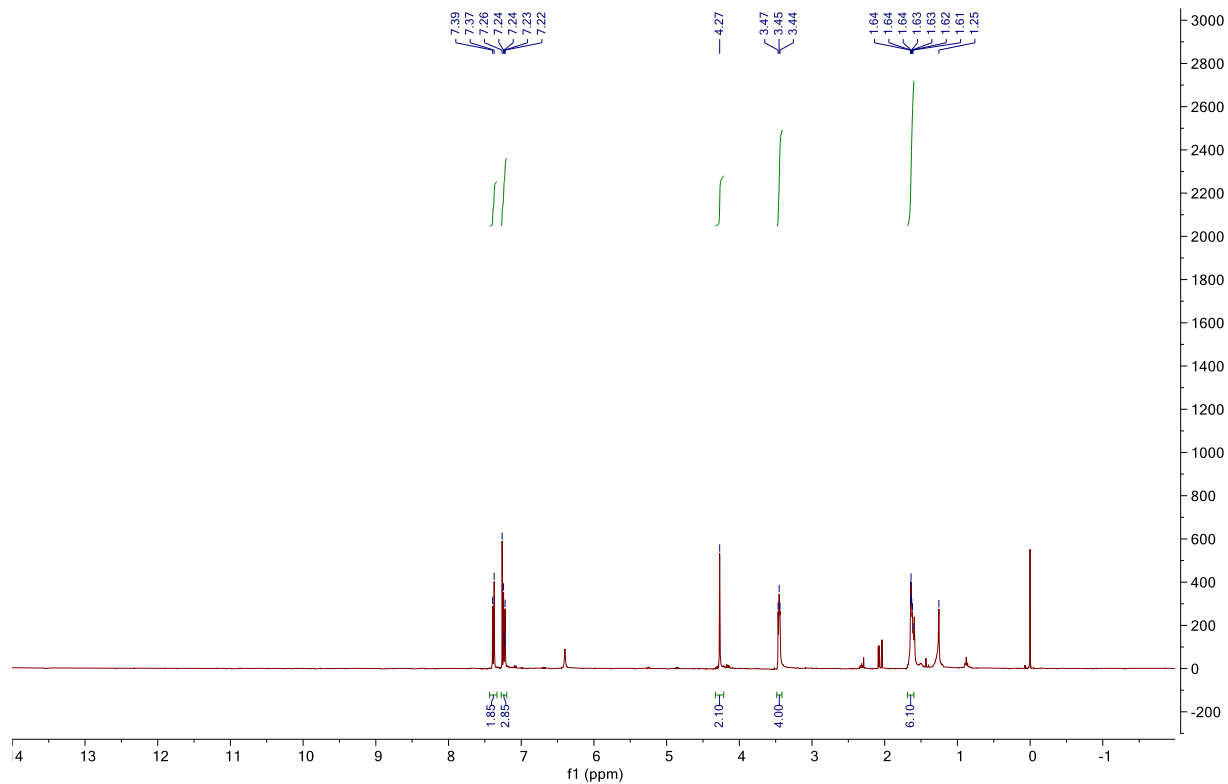
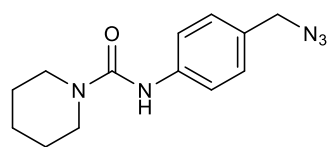
Compound 16



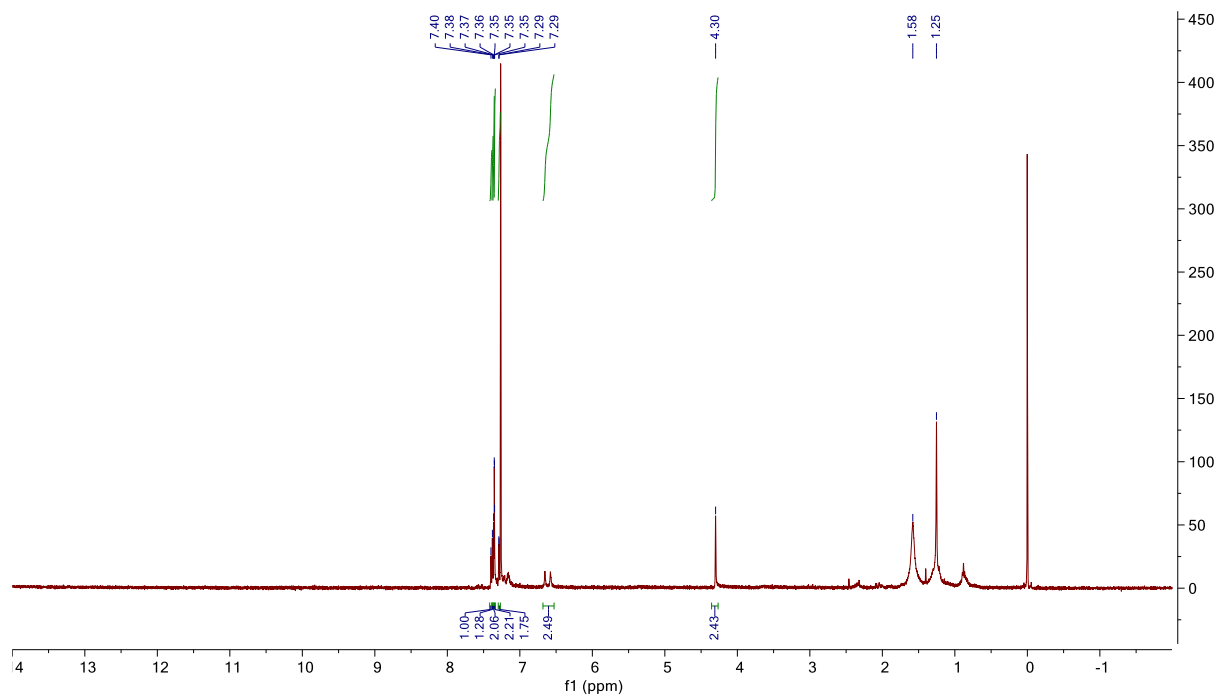
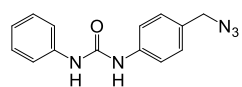
Compound 17



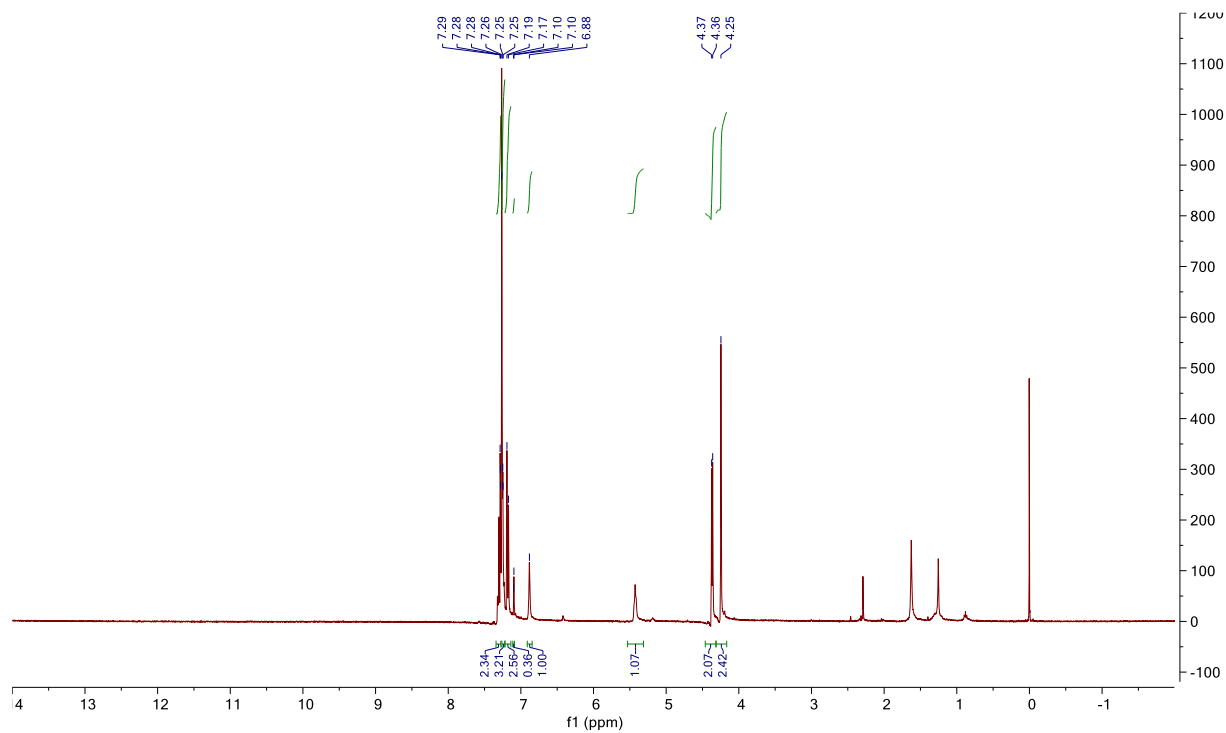
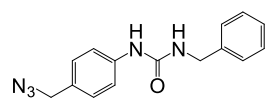
Compound 18a

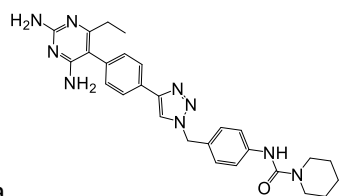


Compound 18b

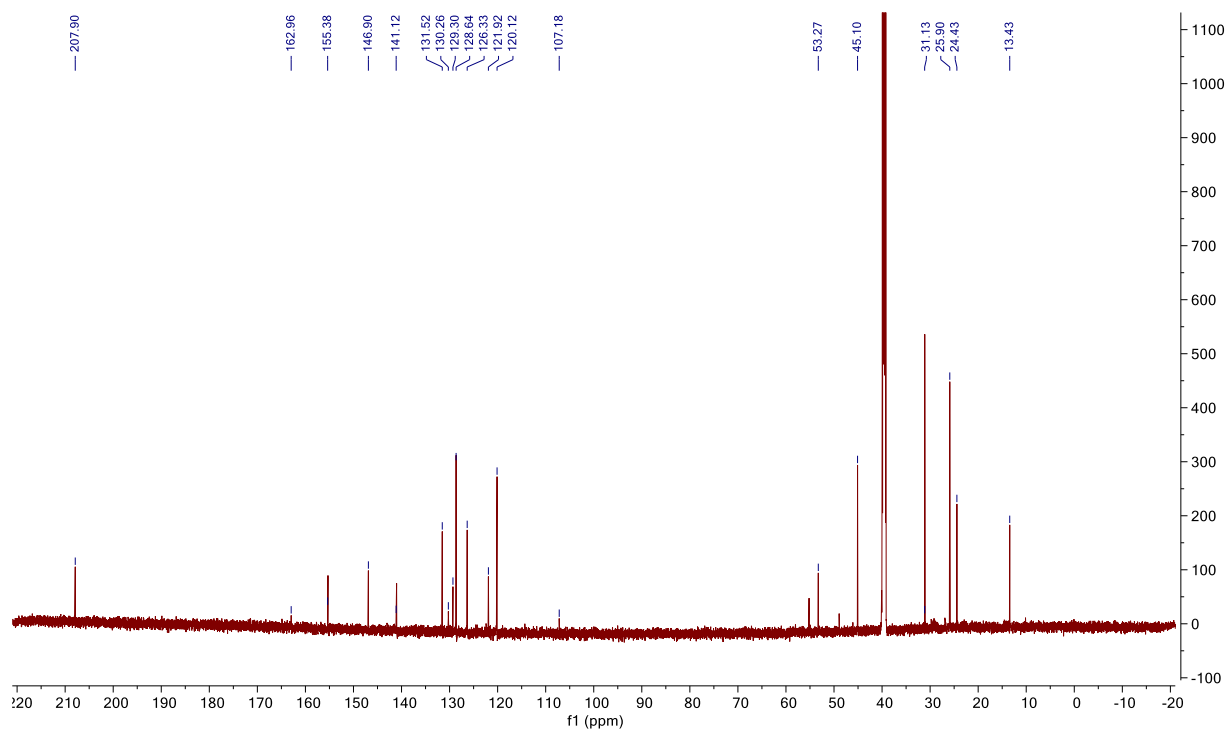
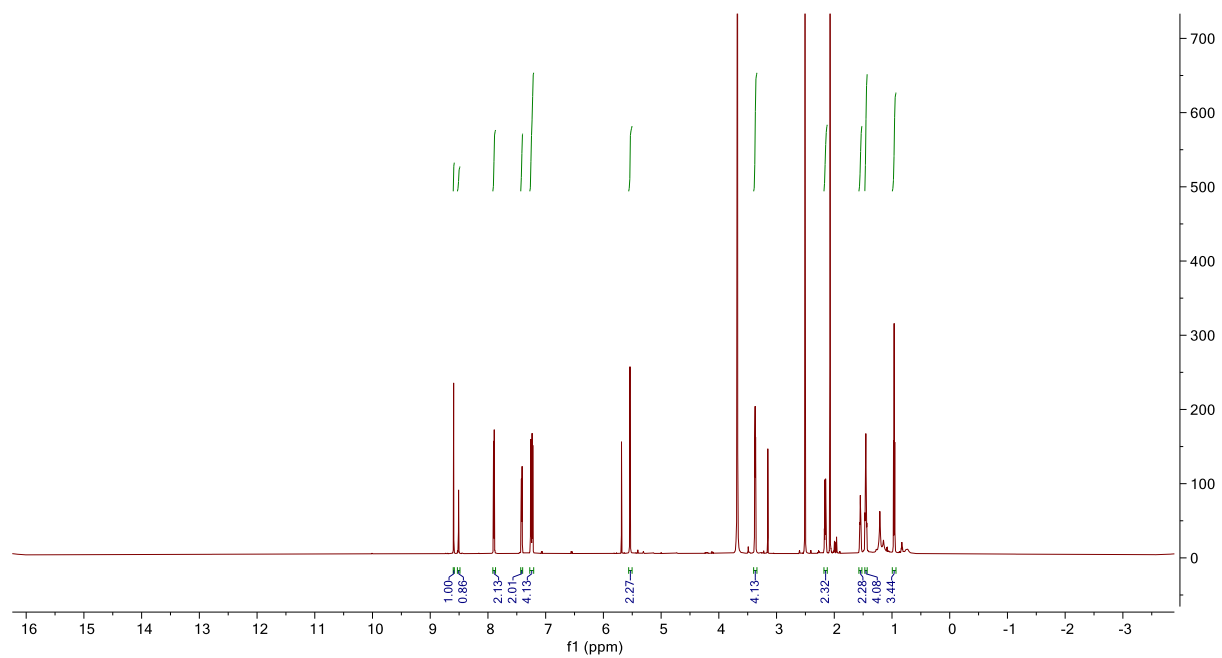


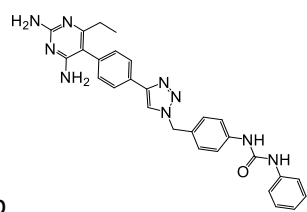
Compound 18c



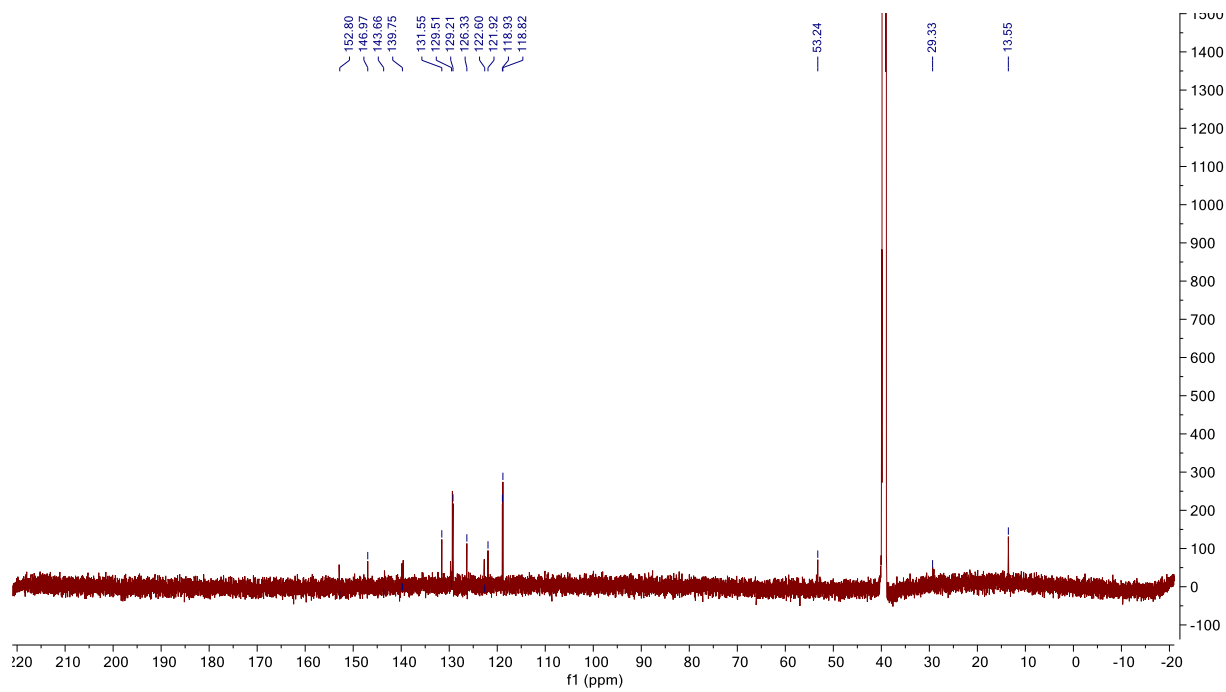
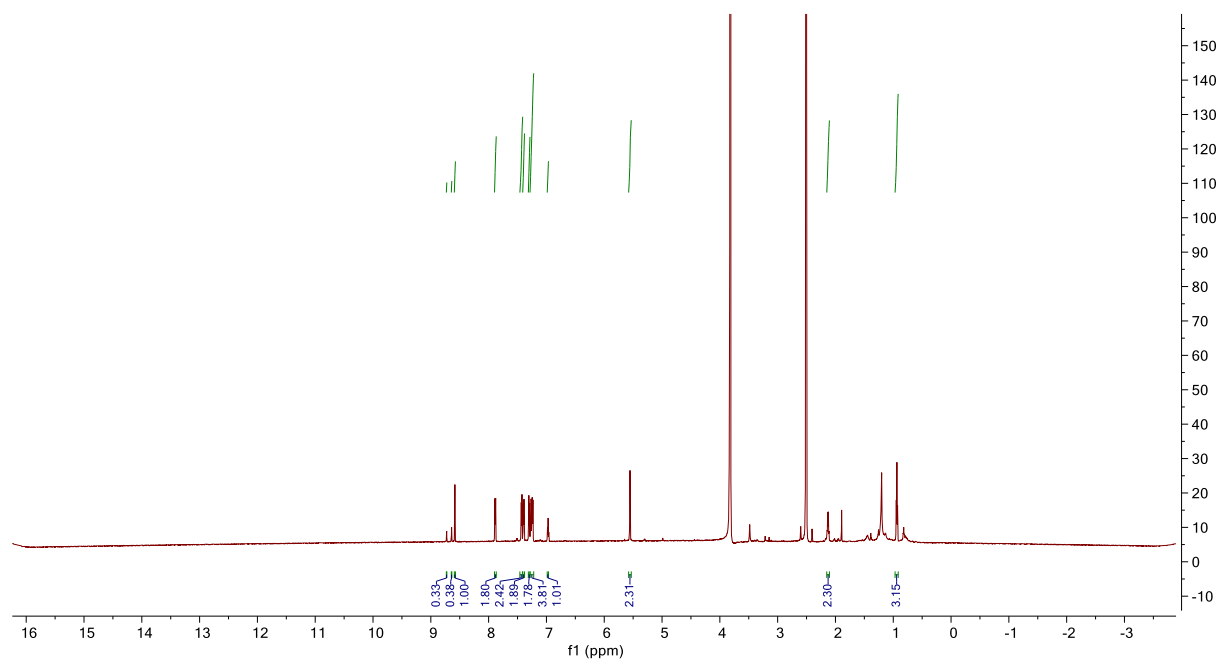


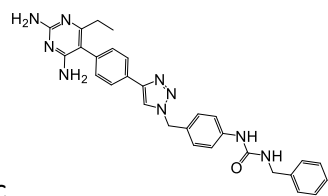
Compound 19a



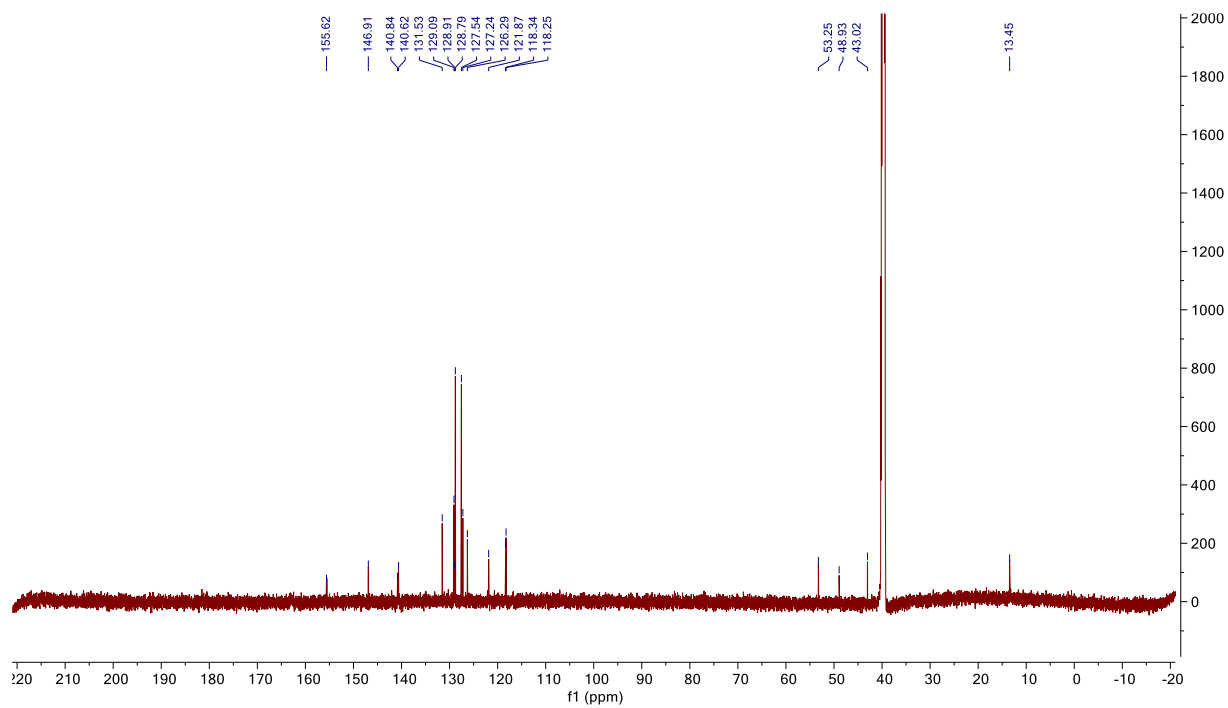
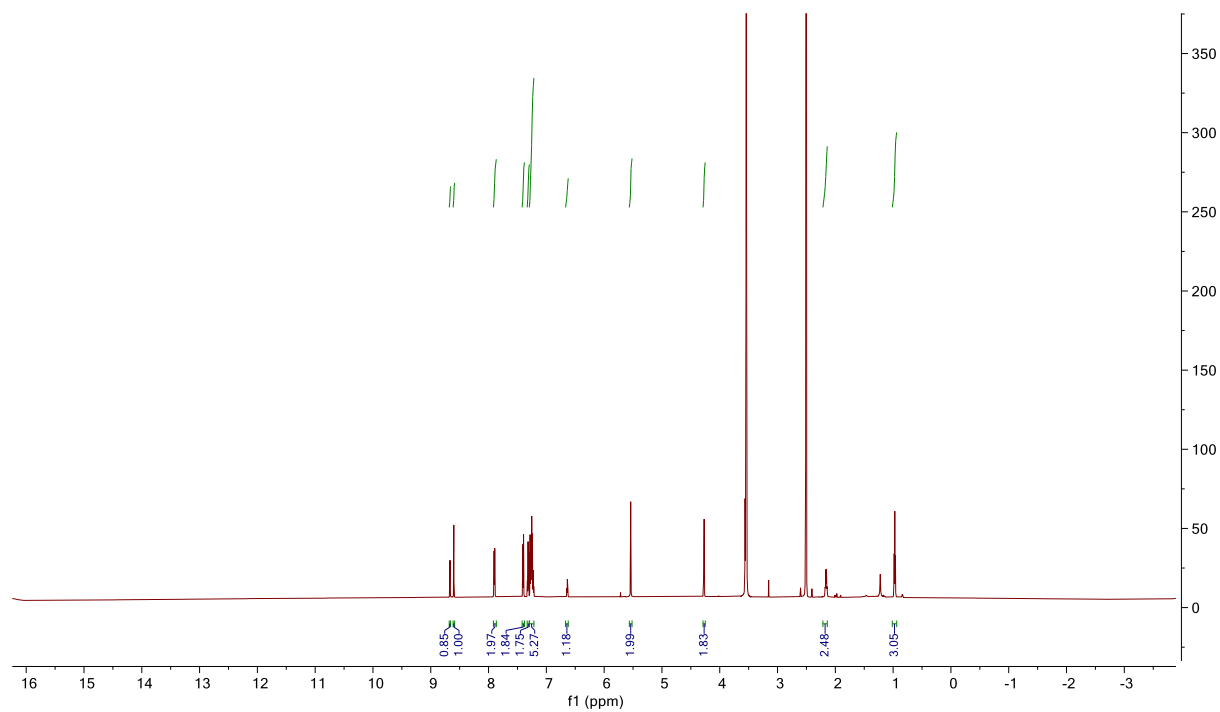


Compound 19b



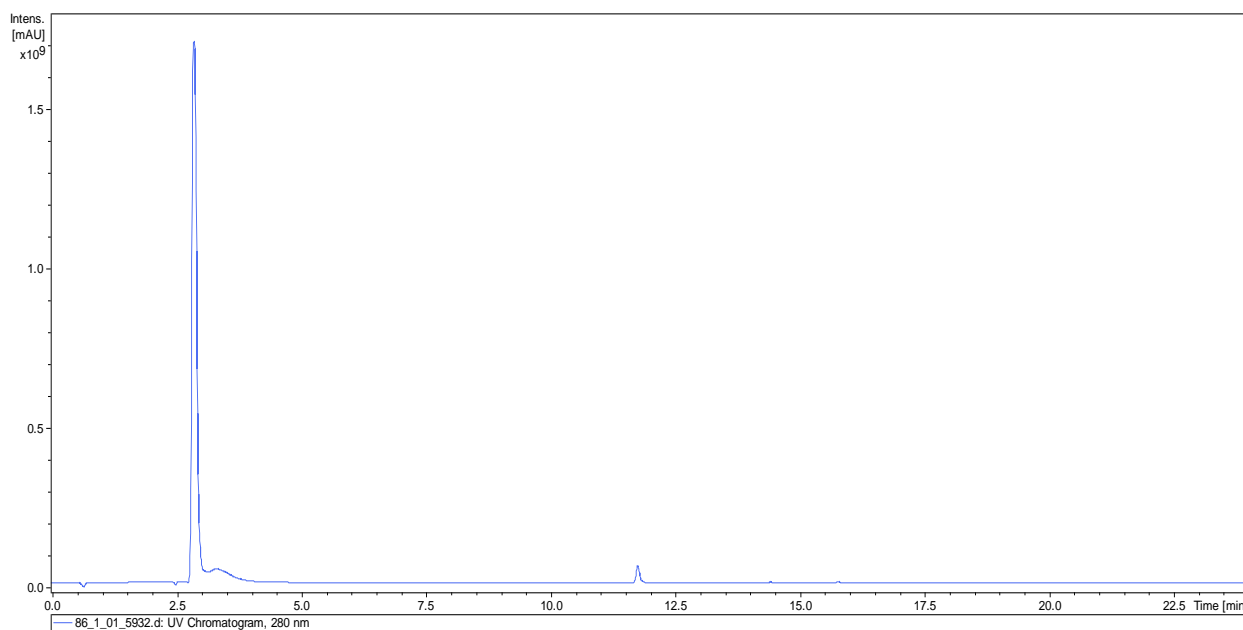


Compound 19c

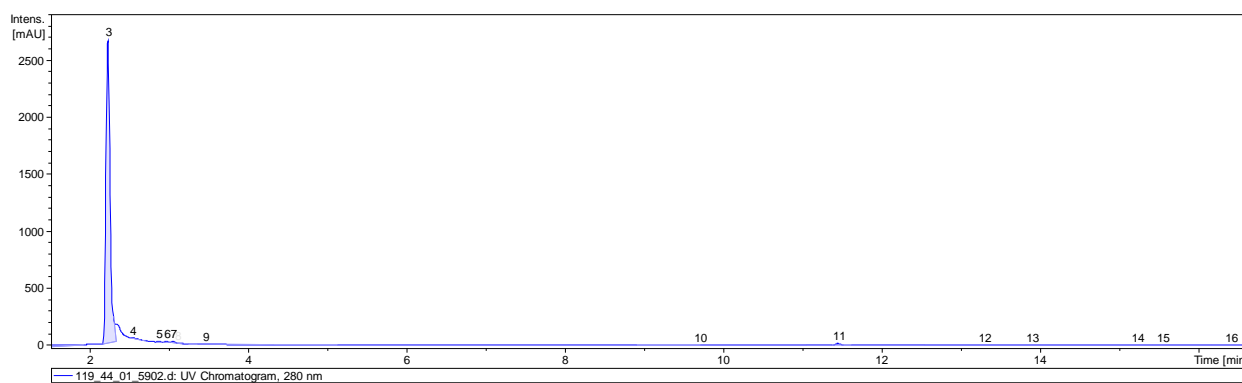


LC-MS data

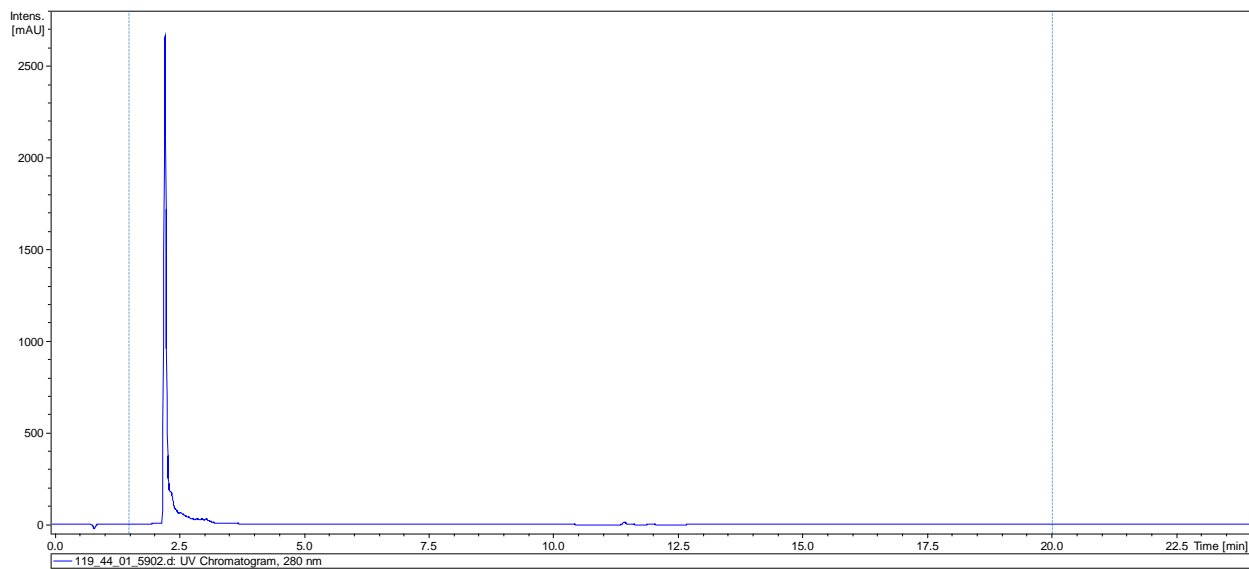
Compound 4a



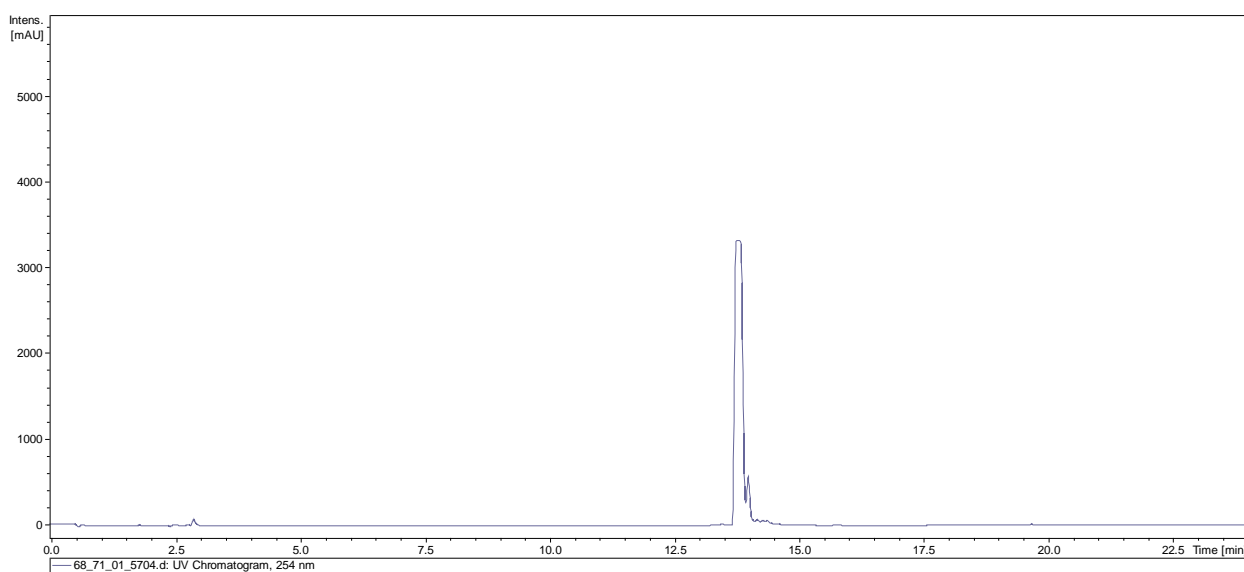
Compound 4b



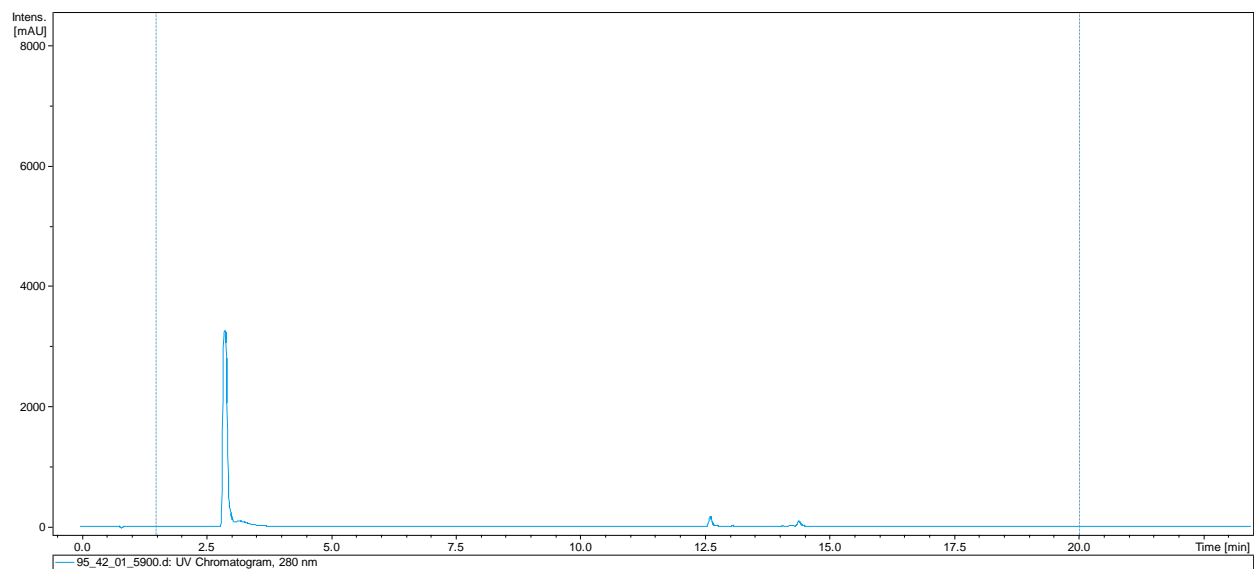
Compound 4c



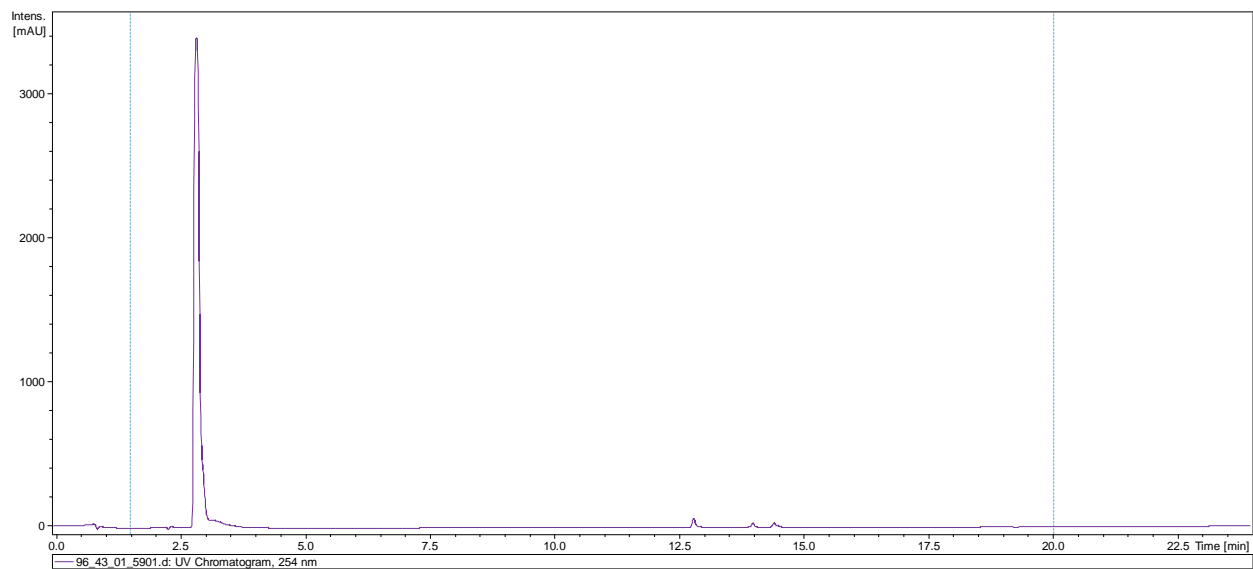
Compound 11a



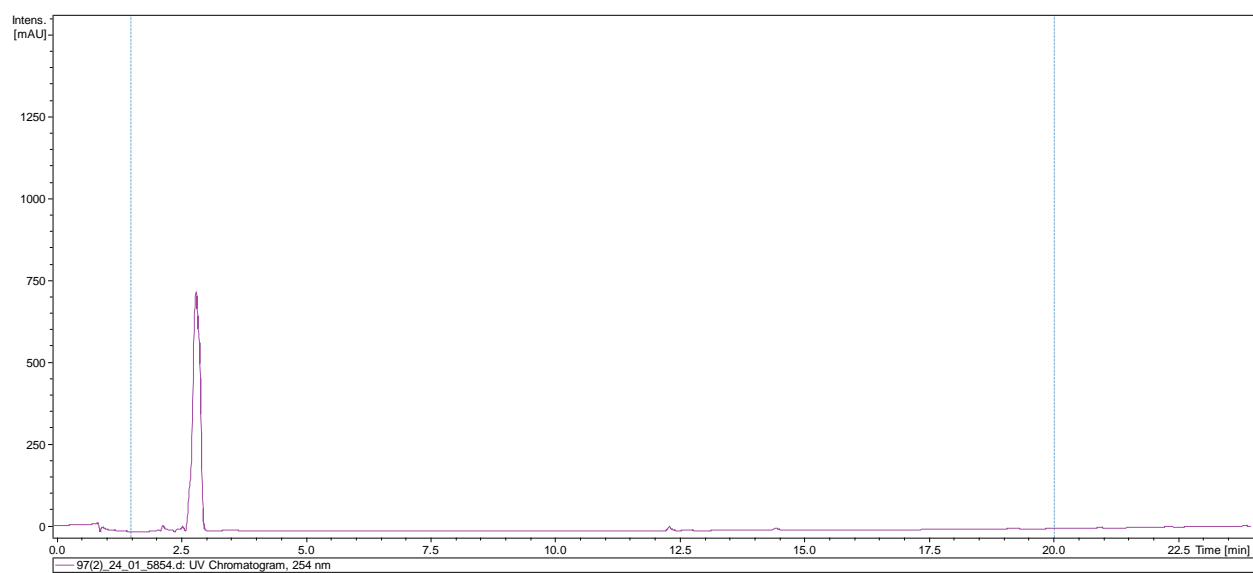
Compound 11b



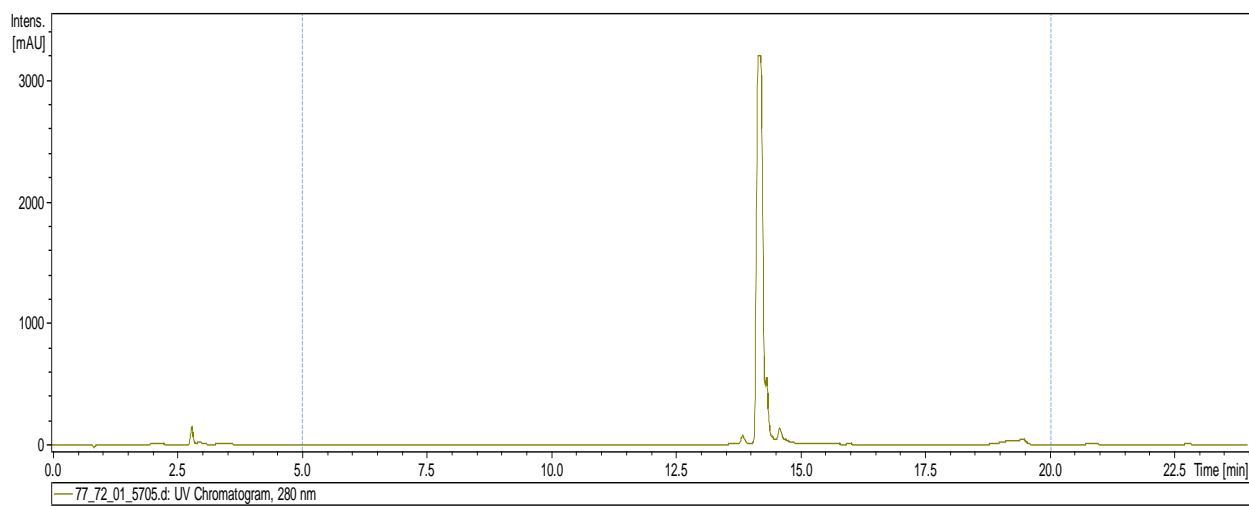
Compound 11c



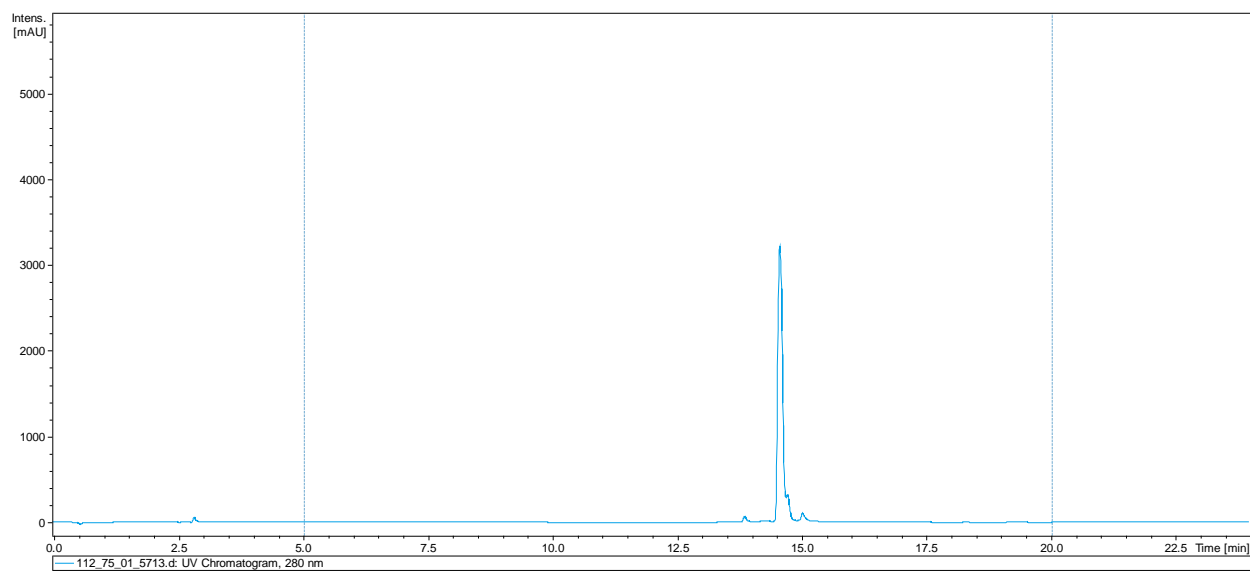
Compound 11d



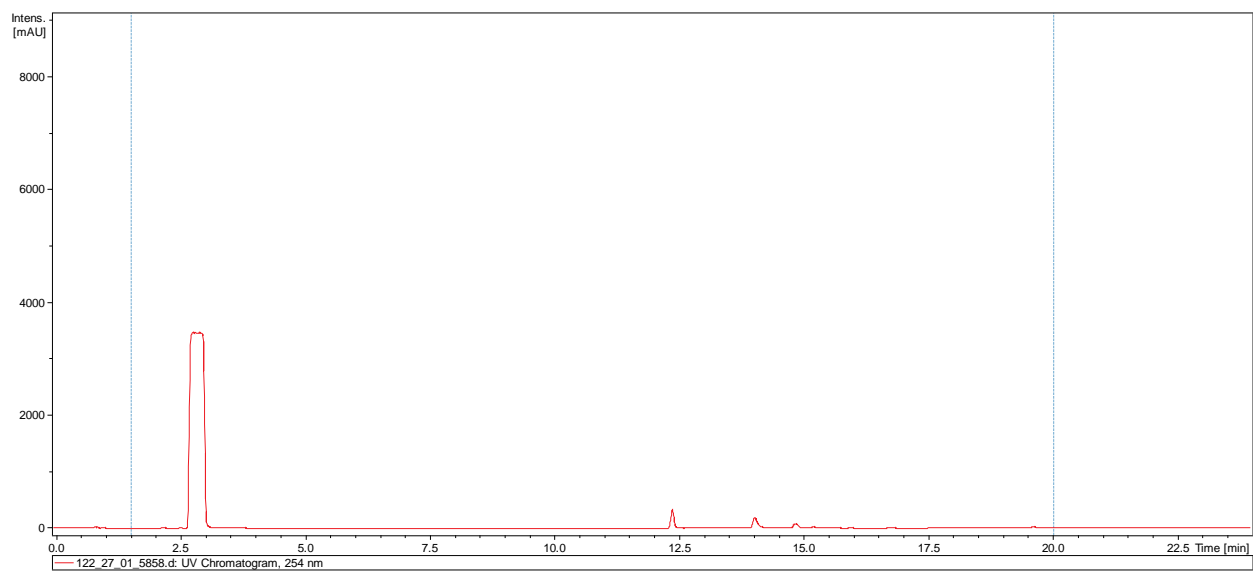
Compound 15a



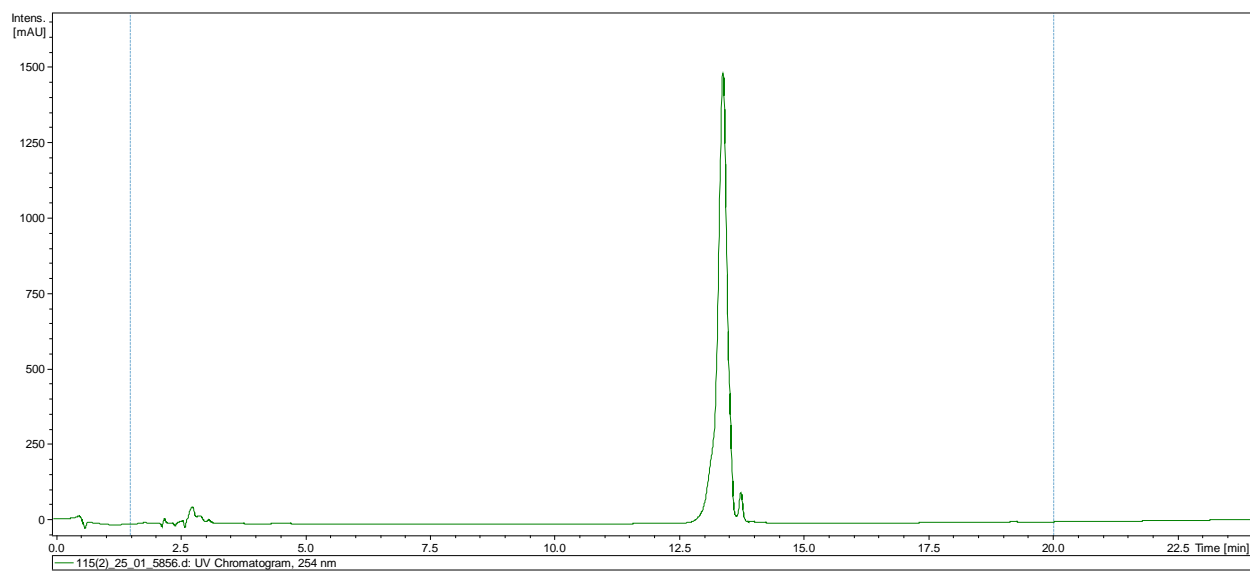
Compound 15b



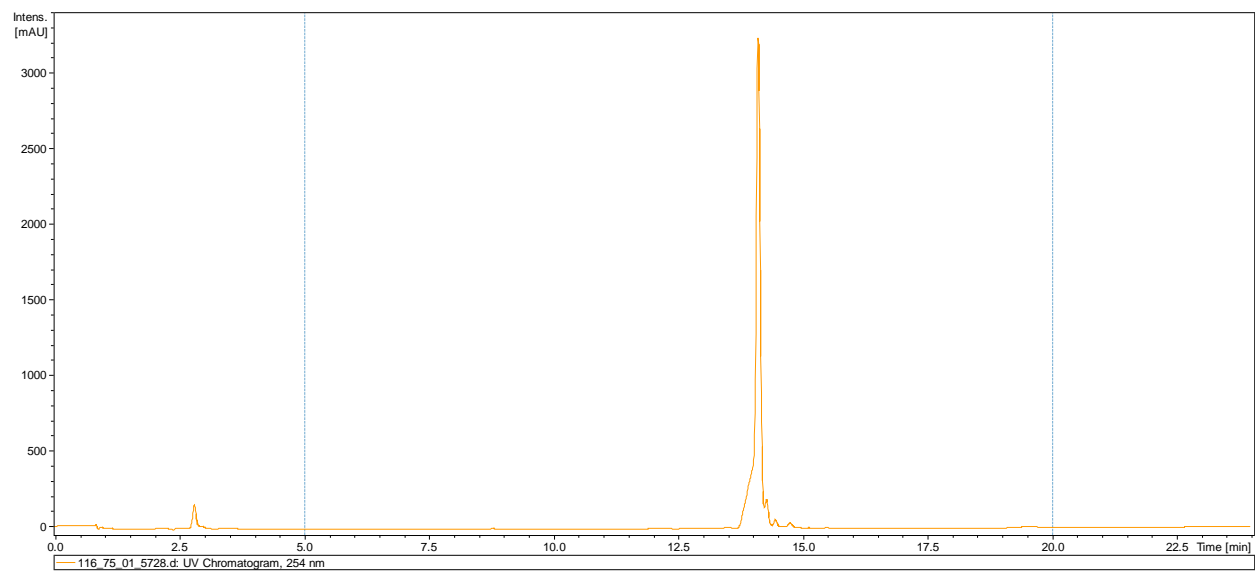
Compound 15c



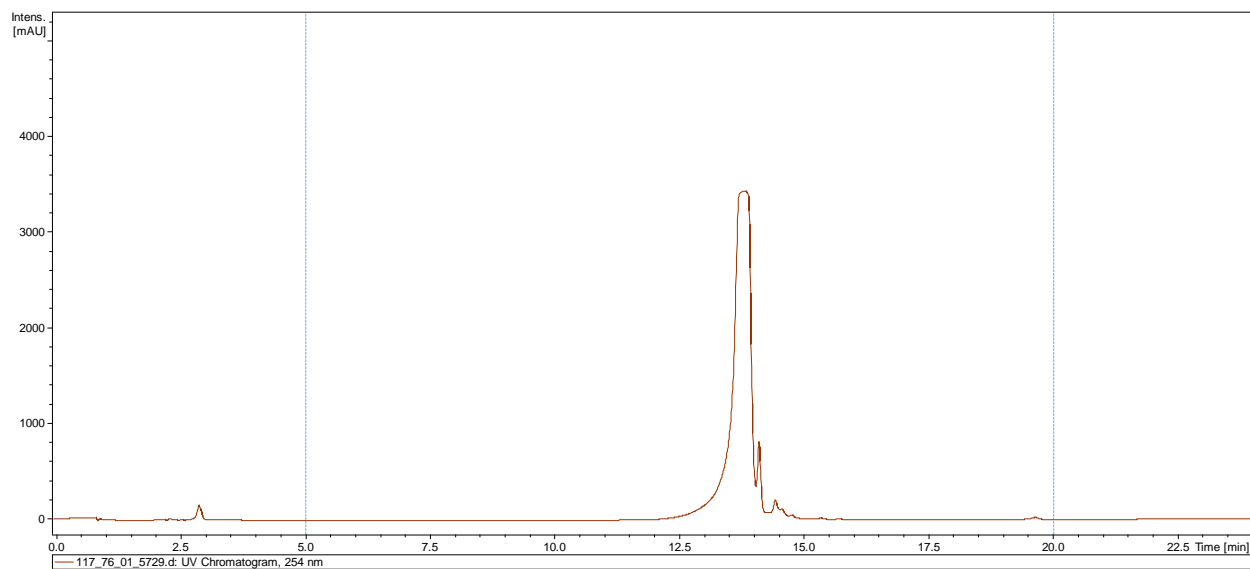
Compound 19a



Compound 19b

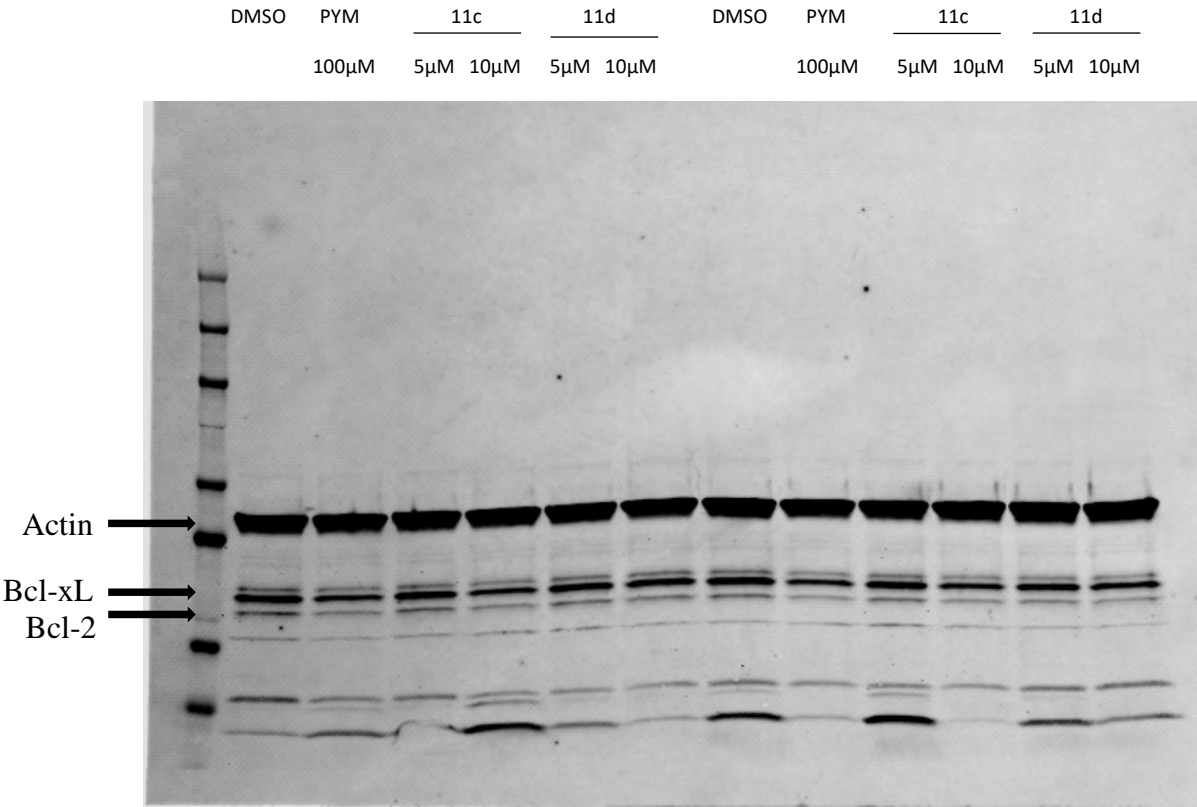


Compound 19c

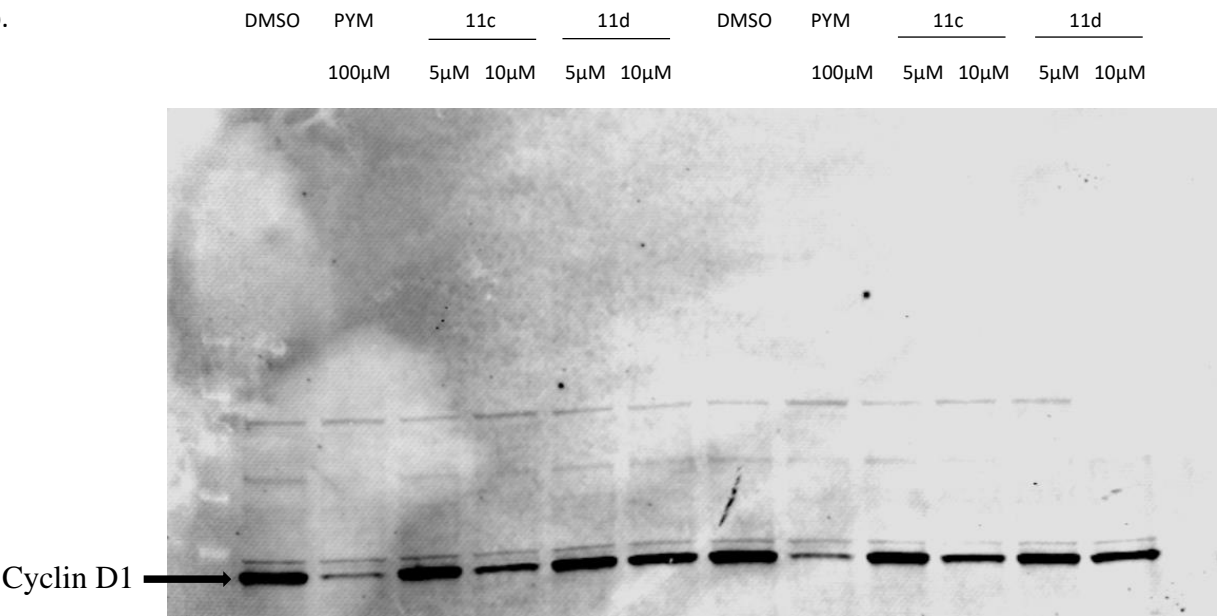


Full Gels

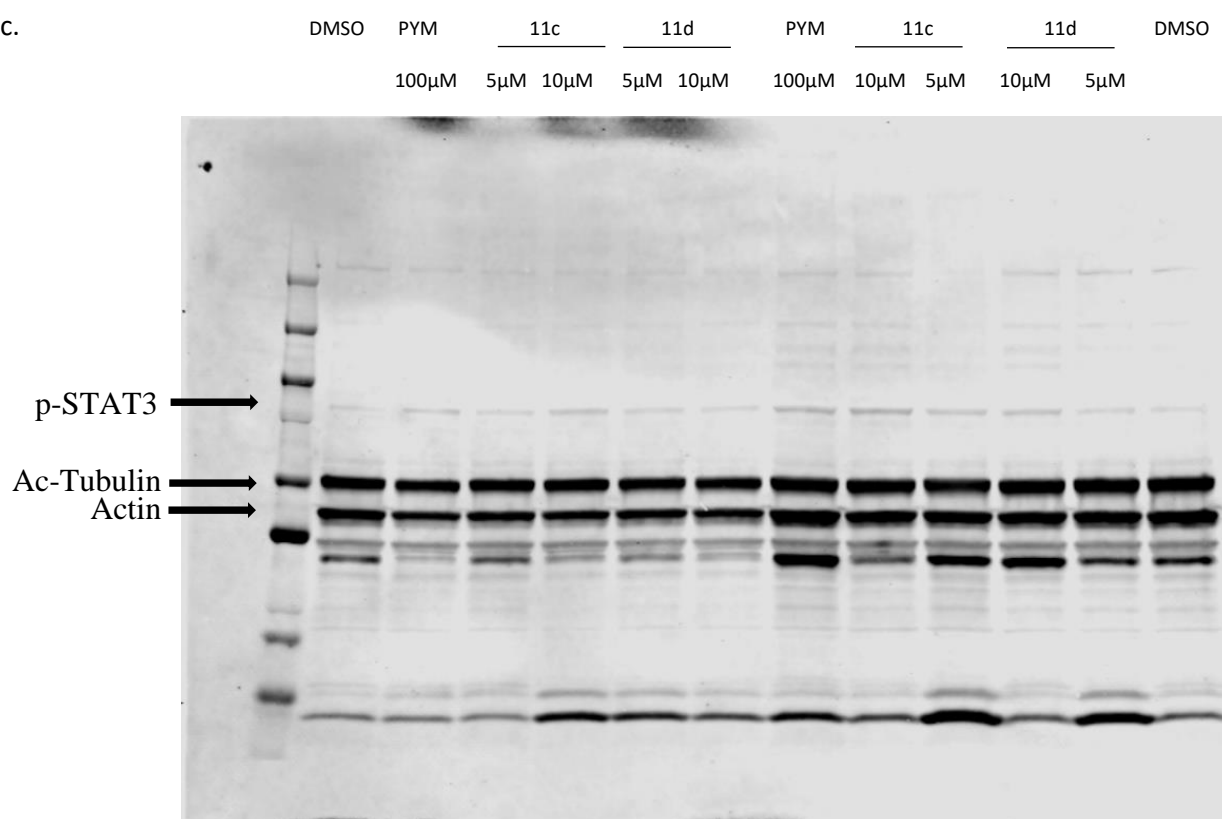
1a.



1b.



1c.



1d.

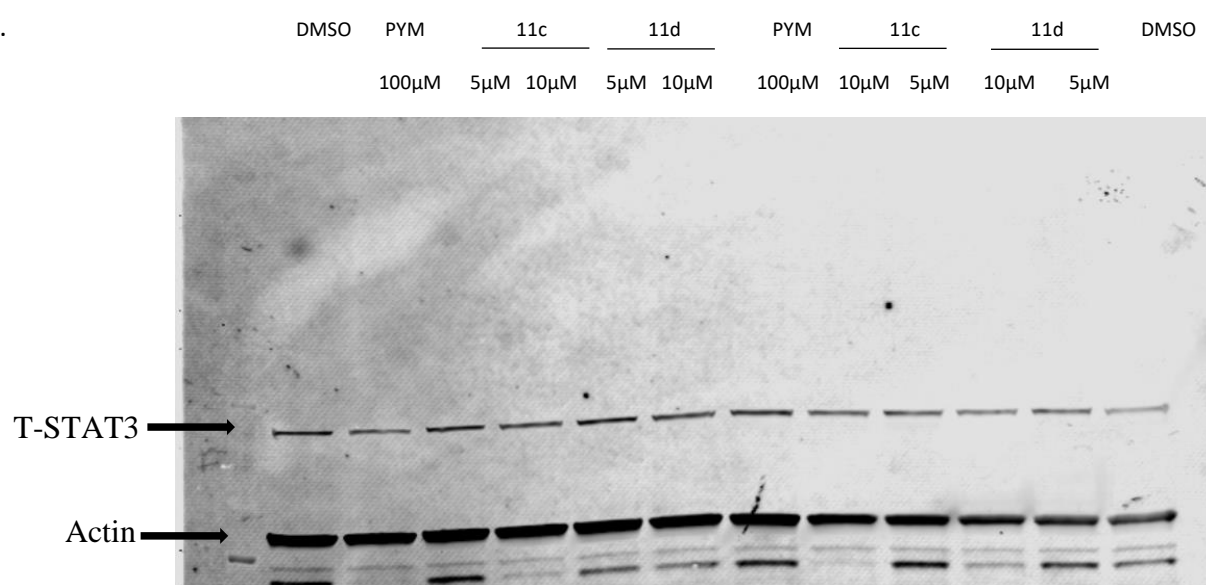
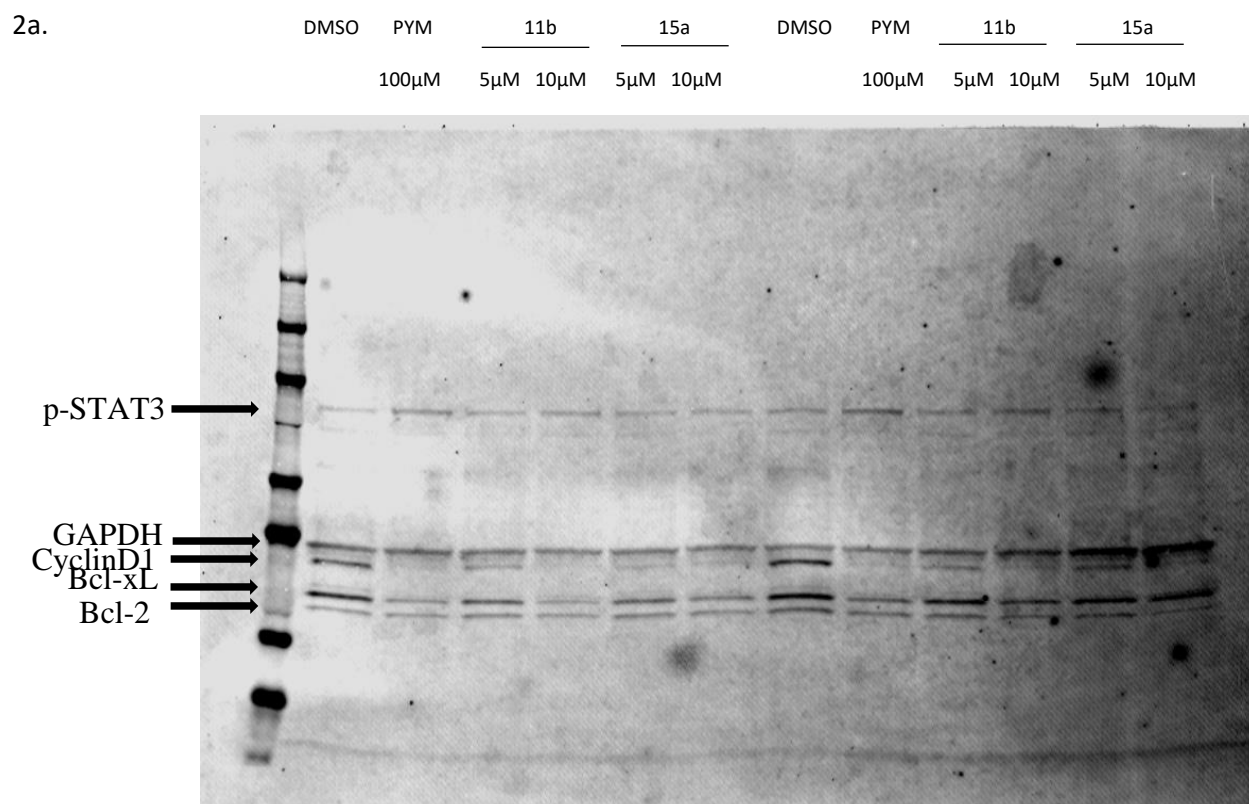


Figure 6S.1. Western blot gel for Compound **11c** and **11d**. MDA-MB-231 cell line treated by DMSO (0.1%), PYM 100 μ M, 11c (5 μ M and 10 μ M), 11d (5 μ M and 10 μ M) for 24 h. (a) gel of Actin, Bcl-2, and Bcl-xL. (b) Gel of Cyclin D1. (c) Gel for p-STAT3 and Actin. (d) Gel of T-STAT3 and Actin.



2b.

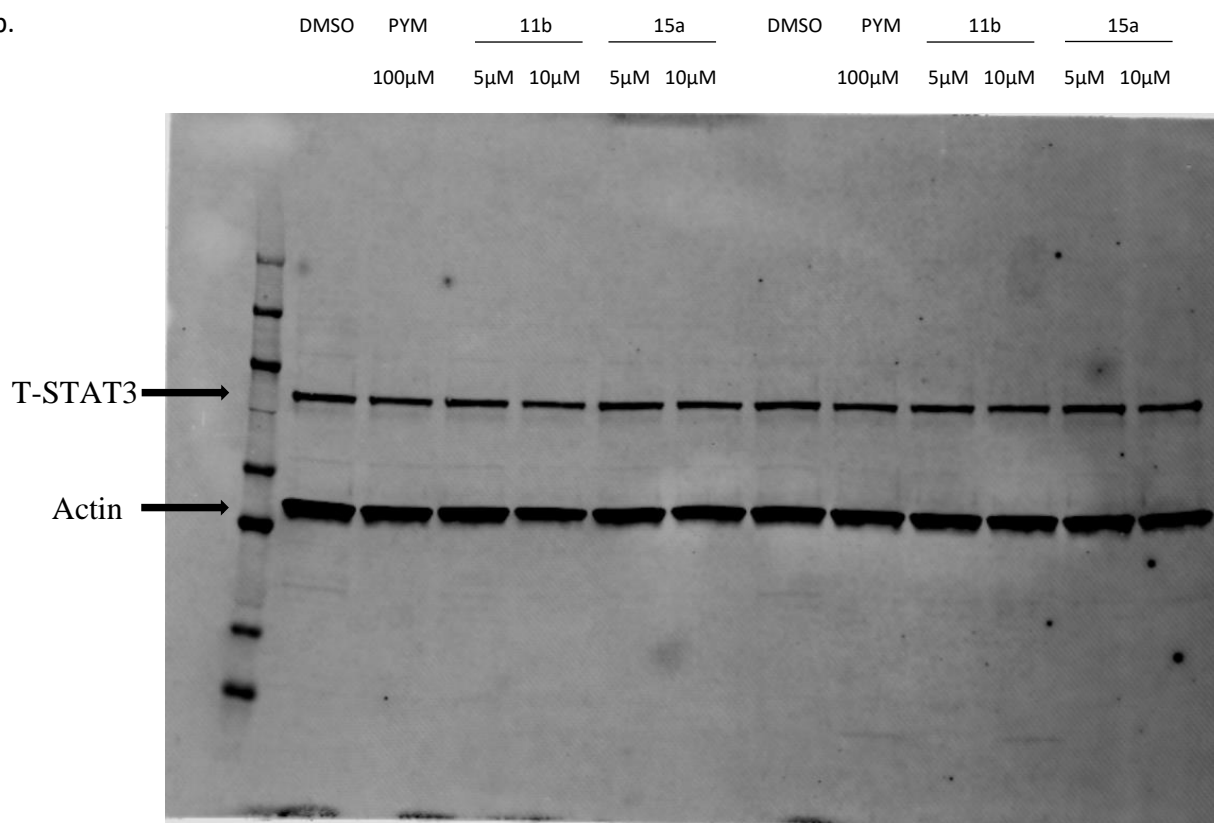


Figure 6S.2. Western blot gel for Compound **11b** and **15a**. MDA-MB-231 cell line treated by DMSO (0.1%), PYM 100μM, **11b** (5 μM and 10 μM), **15a** (5 μM and 10 μM) in two separate experiments for 24 h. (a). gel of p-STAT3, GAPDH, Cyclin D1, Bcl-2, and Bcl-xL. (b). Gel of T-STAT3 and Actin.

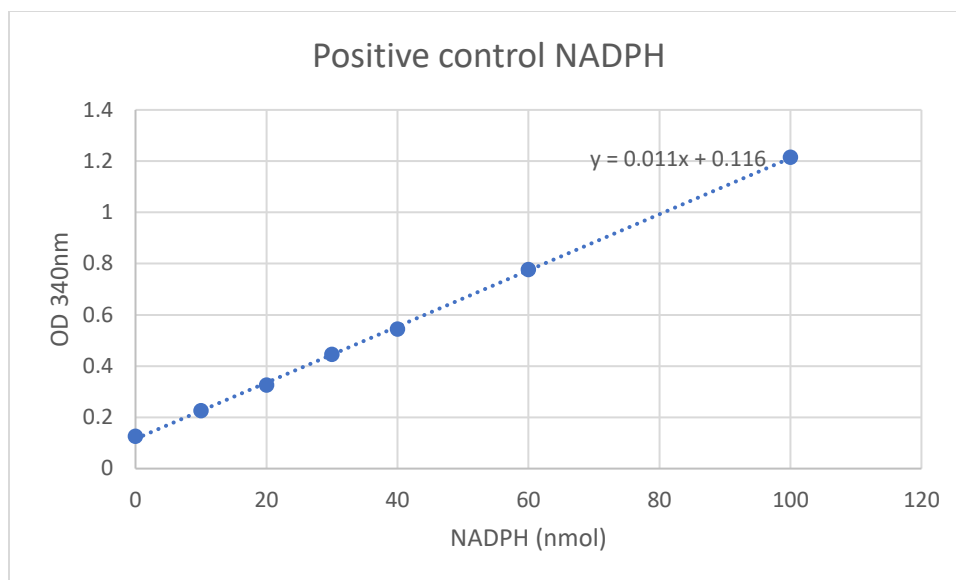


Figure 6S.3. Absorbance of NADPH without DHFR reduction.

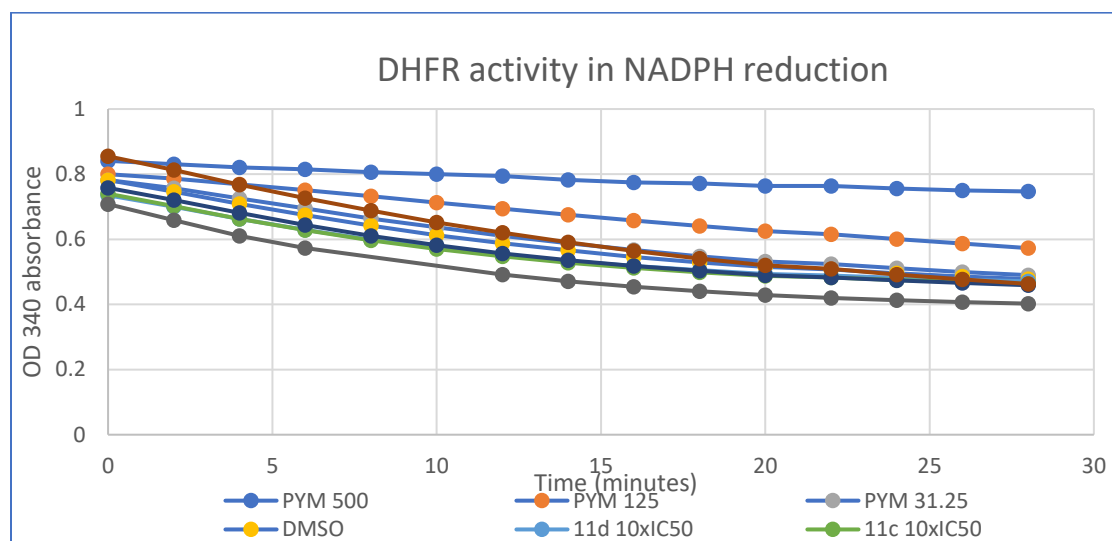


Figure 6S.4. Novel STAT3 inhibitor candidates do not inhibit DHFR activities. DHFR activity assay was performed with 1% provided hDHFR incubating with NADPH and DHFR substrate as the positive control. The treatment group was treated with 1% DMSO, or DMSO solution of Pym 500 μ M (2x IC₅₀), 125 μ M, 31.25 μ M, **11b-d** (10x IC₅₀) and **15a** (1x IC₅₀) along with provided hDHFR, NADPH and DHFR substrate. DHFR activity was read at OD 340nm for NADPH absorbance with kinetic scanning (2-minute intervals from 0 to 28 minutes). The experiment was performed in duplicate data.

CHAPTER 7. NOVEL GLYCOSYLATED HISTONE DEACETYLASE INHIBITORS FOR TARGETED TREATMENT OF HEPATOCELLULAR CARCINOMA

Bocheng Wu¹, Subhasish Tapadar^{1,2,3}, Adegboyega K. Oyelere^{1,2,3†}

*School of Chemistry and Biochemistry, School of Biological Sciences, Parker H. Petit Institute
for Bioengineering and Bioscience, Georgia Institute of Technology, Atlanta, GA 30332-0400*

USA

¹School of Chemistry and Biochemistry, Georgia Institute of Technology

²Parker H. Petit Institute for Bioengineering and Bioscience, Georgia Institute of Technology

³Sophia Bioscience, Inc. 311 Ferst Drive NW, Ste. L1325A, Atlanta, GA 30332, USA.

Correspondence to:

Adegboyega K. Oyelere, **E-mail:** aoyelere@gatech.edu

Keywords : HDAC inhibition, hepatocellular carcinoma, GLUT-2 transporter, tumor suppression, glycosylation, liver cancer, tissue-selective, HCC, cell-type selective, cell apoptosis.

Abstract

Hepatocellular cancer (HCC) is a heterogeneous cancer sustained by gene-silencing chromatin histone hypoacetylation due to dysfunctions in the activities of histone deacetylases (HDACs). HCC is also highly dependent on Warburg effect, an altered state of metabolism in which cancer cells depend on anaerobic glycolysis for energy source. We report herein that the integration of glycoside moieties into the prototypical HDAC inhibitors (HDACi) surface recognition group afforded glycosylated HDACi that are selectively cytotoxic to Hep-G2 cells. A cohort of these compounds demonstrated intracellular on-target effect and selectively induced in Hep-G2 cells. Lead compound **STR-V-53** displayed exquisite HCC cell line selectivity, as it is none toxic to cells in the NCI-60 panel and derived a significant part of its Hep-G2 cell penetration through GLUT-2-mediated transport. Furthermore, **STR-V-53** is relatively non-toxic to mice and robustly suppressed tumor growths in an orthotopic model of HCC as standalone agent. **STR-V-53** also enhanced the potency of SORA in a combination therapy experiment. Collectively, our data suggests that **STR-V-53** is a novel HDACi whose potential as targeted anti-HCC agent merits further evaluation in additional preclinical studies.

7.1 Introduction

Liver cancer is among the leading causes of global cancer deaths.¹ Hepatocellular carcinoma (HCC) is the most common of liver cancer types. HCC is responsible for over 80% of all liver cancer cases, and occurring in >90% of cases in patients with liver damage.² The prognosis of HCC is very grim, with an estimated 10-12% 5-year survival.³ The common risk factors for HCC are ethnicity, gender, chronic viral hepatitis, cirrhosis, alcohol addiction, inherited metabolic diseases, obesity, tobacco use, and type-2 diabetes.⁴⁻⁷ There is a strong link between chronic inflammation and several cancer types. This relationship is stronger in HCC as it is initiated in inflamed liver tissues.^{8,9}

Surgical resection is a treatment option for HCC. However, surgery is limited to patients with the early stage of the disease and good liver function. Only a small proportion of HCC patients are eligible for surgery and the post-surgery relapse rate (50-80 %) is very high.^{10, 11} Liver transplantation is another treatment option for early-stage but shortage of organs and late stage diagnosis of the disease have significantly limited this option.^{12, 13} Systemic chemotherapy became a mainstay treatment option for unresectable HCC with the FDA approval of sorafenib, an inhibitor of multiple protein kinases including Raf serine/threonine kinases and receptor tyrosine kinases.¹⁴ The subsequent approval of other multikinase angiogenesis inhibitors such as lenvatinib, regorafenib, and cabozantinib have added more pharmacological tools for HCC treatment.¹⁵ However, none of these drugs could extend advanced HCC patients survival beyond 3 months.¹⁶ More recently, immunotherapy strategy, involving blockade of immune checkpoints (PD-1 alone or with CTLA-4), has shown promising therapeutic effects in the clinic, however, the vast majority of patients (>70%) do not positively respond to immunotherapy either as standalone treatment or

when combined with antiangiogenic drugs.¹⁷ Therefore, there is a significant unmet need for more efficacious treatment modalities for HCC.

Histone deacetylase (HDAC) inhibition is a clinically validated epigenetic-based strategy for cancer treatment. HDACs, through their lysine deacetylase activities, play important roles in epigenetically moderating gene expression at the chromatin level. Dysregulation of HDACs expression has been linked to the proliferation, survival, and invasiveness of HCC.¹⁸ Specifically, the overexpression of class I HDACs (HDACs 1 and 2) and class IIa HDACs (HDACs 4, 7 and 9) in HCC cells and patient samples strongly correlates with reduced patient survival.¹⁸ To date, five HDAC inhibitors (HDACi) – Vorinostat, Belinostat, Chidamide, Romidepsin and Panobinostat – have been approved to treat hematological malignancies.¹⁹ The potential of Belinostat as anti-HCC agents has been studied in clinical trial (NCT00321594).²⁰ However, the results from the trial revealed that Belinostat caused median progression-free survival (PFS) and overall survival (OS) of 2.64 and 6.60 months, respectively.²⁰ While this result indicates the potential of HDAC inhibition as treatment strategy for HCC, improvement of the efficacy is a key challenge that must be overcome for the future use of HDACi in the treatment of HCC.

In previous studies, we have found that bio-inspired alterations to the HDACi surface recognition cap group could furnish HDACi with cell-type and tissue selectivity.¹⁶⁻¹⁸ More specific to HCC, we have found that selective-liver tissue accumulation is a viable approach to improving the anti-HCC efficacy of HDACi. We have discovered that the integration of macrolide azithromycin into the surface recognition group of sub-class I HDAC isoform selective HDACi resulted in macrolide-based HDACi, which preferentially accumulated in the liver tissue and robustly suppressed HCC tumor growths in an orthotopic model.²² In this study, we explored targeting the Warburg effect as a strategy to selectively target HDACi to cancer cells. Warburg effect is an

altered state of metabolism in which cancer cells depend on anaerobic glycolysis for energy source even in the presence of oxygen. To sustain this altered metabolism and proliferation,²³ cancer cells upregulate the expressions of several glucose transporters (GLUT) to facilitate enhanced sugar uptake. Overexpressed on several cancers cells surfaces are GLUT-1, GLUT-2, GLUT-3, and GLUT-4.^{24, 25} Unlike several other cancers, HCC is known to overexpress GLUT-2 which could effectively promote the uptake glucose and mannose in order to support Warburg effect.²⁶ GLUT-2 is a major facilitator of sugar transport in the hepatocytes, having higher capacity and lower binding affinity to glucose.²⁵ In addition, GLUT-2 could promote the cell uptake of fructose and several glycosylated small molecules. This unique property makes GLUT-2 the preferred sugar transporter relative to the other GLUTs,^{25, 27}

Based on this understanding, we designed and synthesized four classes of novel glycosylated HDACi having glycoside moieties (D-glucose, D-mannose, and desosamine sugar) integrated into the prototypical HDACi surface recognition cap group.²⁸ We evaluated the HDAC inhibition activities of the glycosylated HDACi against representative class I and class II HDACs and screened then against representative cancer (A549 and Hep-G2) and normal (VERO) cell lines.

We found that these compounds demonstrated potent HDAC inhibition activities and a cohort of (**STR-V-53**, **STR-I-195**, and **STR-V-114**) are 8- to 10-fold selectively cytotoxic to HCC cell line. Also, we found that the HCC cell line (Hep-G2) largely uptakes the glycosylated HDACi through GLUT-2 transporter. In addition, these HDACi caused cell-line dependent apoptosis through caspase 3 cleavage and p21 upregulations. We also found that a selected candidate compound **STR-V-53** efficiently suppressed HCC tumor growth over 21-day treatment with no significant toxicity. Subsequently, we screened **STR-V-53** in the NCI-60 panel. Although the NCI-60 panel is lacking liver cancer cell lines, we performed this experiment to obtain further information about

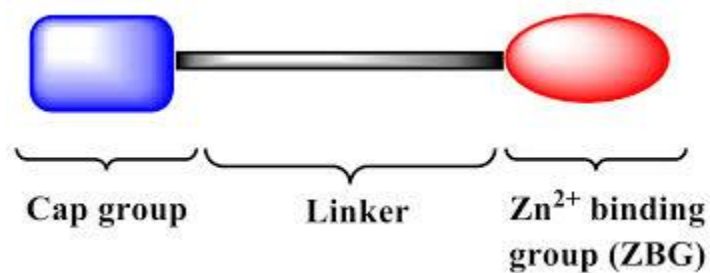
the cancer cell-type selectivity of **STR-V-53**. We observed that, in a one-dose experiment (10 μ M), **STR-V-53** has negligible effect on proliferation showing a mean cell growth of 99.6%. Our cell activity data on **STR-V-53** and the lack of growth inhibition effect of **STR-V-53** in the NCI-60 panel strongly support of our conclusion of HCC cell-selectivity attribute of **STR-V-53**. Overall, the compounds disclosed herein have high translational potential as new agents for HCC treatment.

7.2 Result

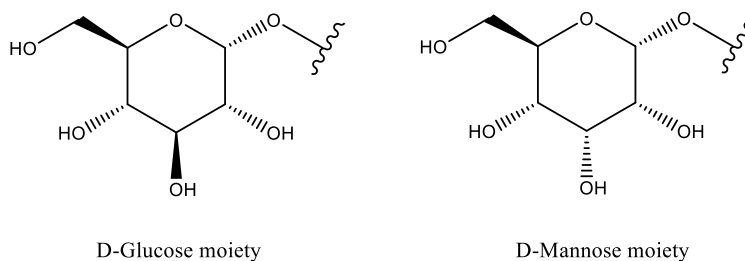
7.2.1 Chemistry (*The synthesis described in this section was performed by Dr. Subhasish Tapadar*)

Prototypical HDACi are based on three pharmacophoric model – surface recognition cap-linker moiety-zinc binding group (ZBG) (Fig. 7.1a). In designing the disclosed compounds, we individually integrated three different glycosides D-glucose, D-mannose, or desosamine – into the standard HDACi surface recognition cap group while we adopted the linker moieties that have afforded optimum HDC inhibition effect based on our previous studies and those by others.²¹ As ZBGs, we used hydroxamate and N-(2-amino-phenyl)acylamide (NAPA), two moieties that afford pan-selective and HDAC class-selective inhibition respectively. This design furnished four classes of linkers shown below in Figure 7.1b-c. In addition to these glycosylated HDACi, we also synthesized and tested compounds **STR-V-46**, **STR-V-48** and **STR-V-183** (Fig. 7.1d) as controls to decipher the contributions of the glycoside moieties to the bioactivity of these compounds.

a.



b.



c.

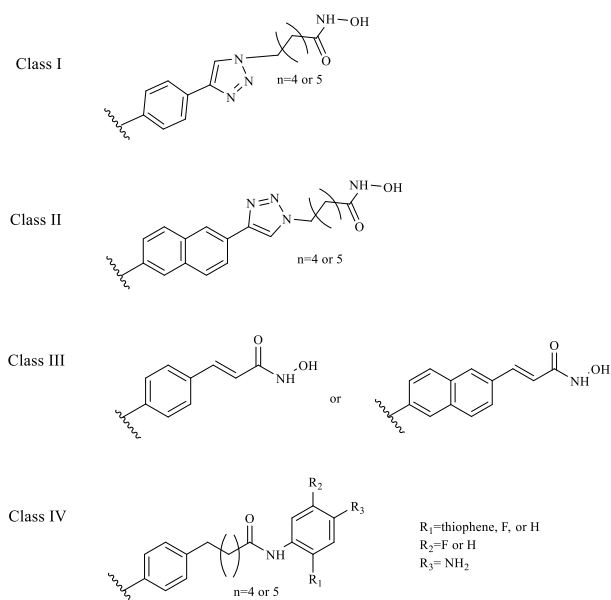
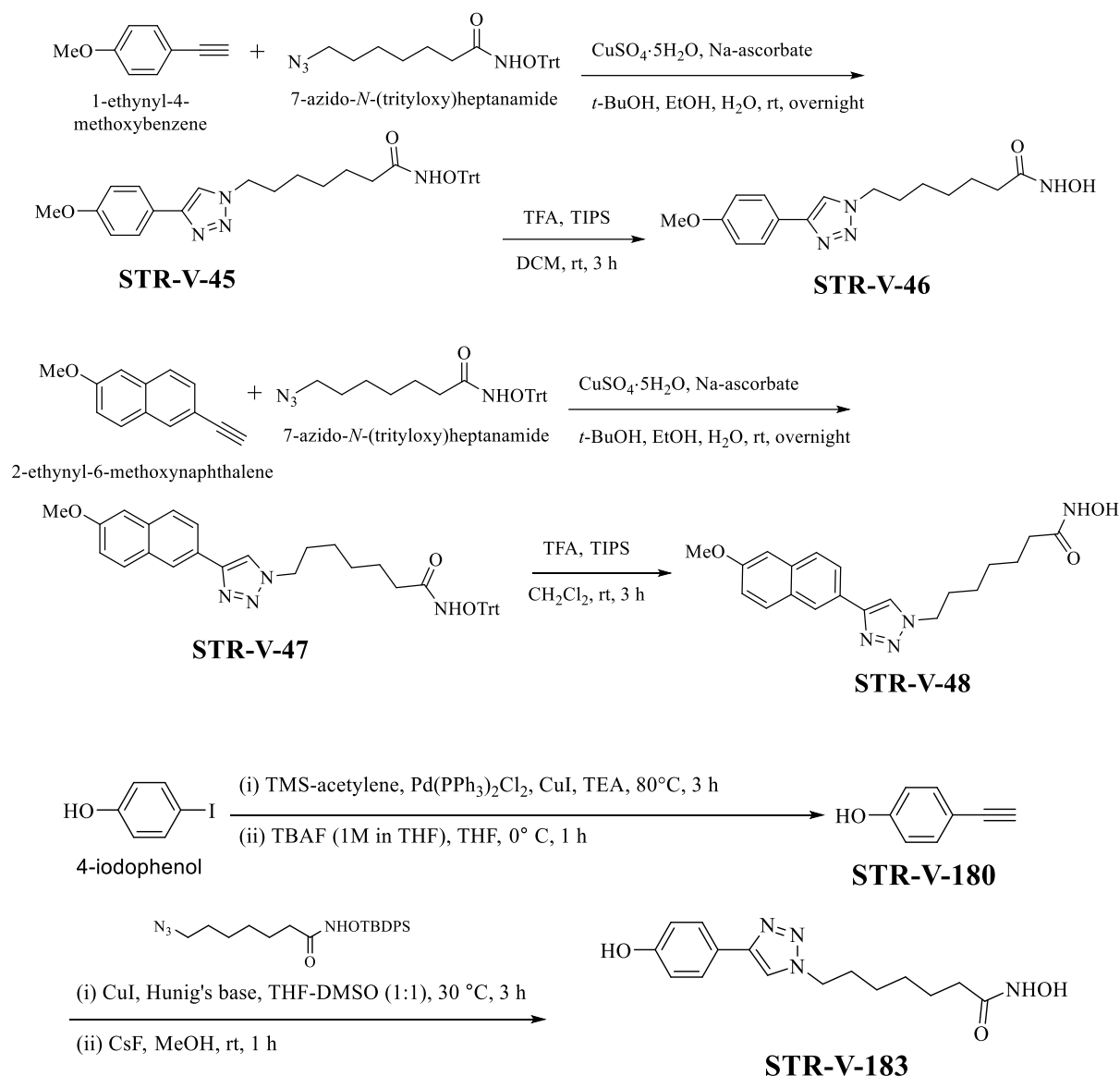
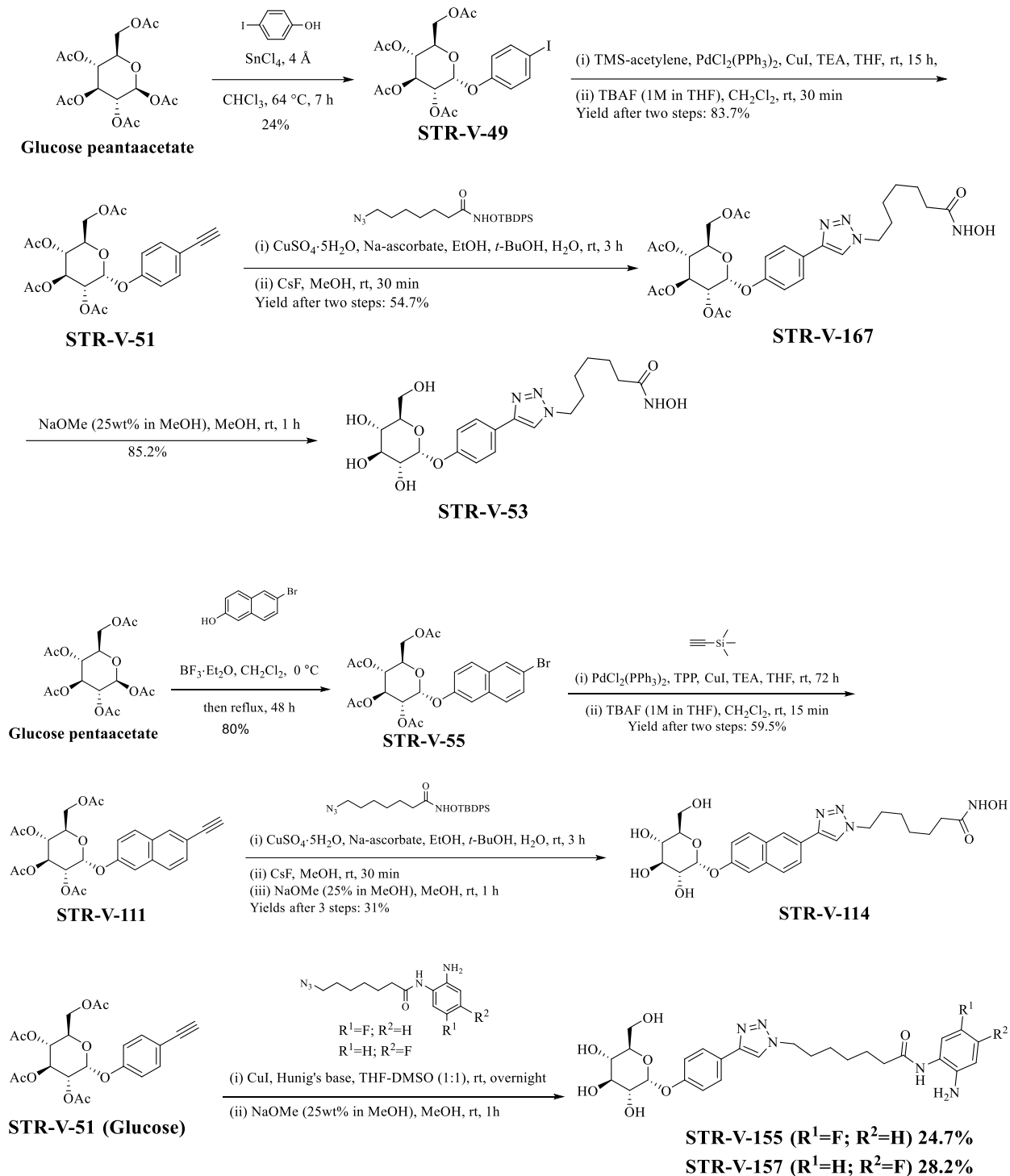


Figure 7.1. Models and designs of the glycosylated HDACi. (a) The three pharmacophoric model of HDACi. (b) The aglycone moieties of the designed HDACi. (c) The glycoside moieties of the designed HDACi. (d) Structures of control compounds **STR-V-46**, **STR-V-48** and **STR-V-183**.



Scheme 7.1. Synthesis of control compounds **STR-V-46**, **STR-V-48**, and **STR-V-183**.

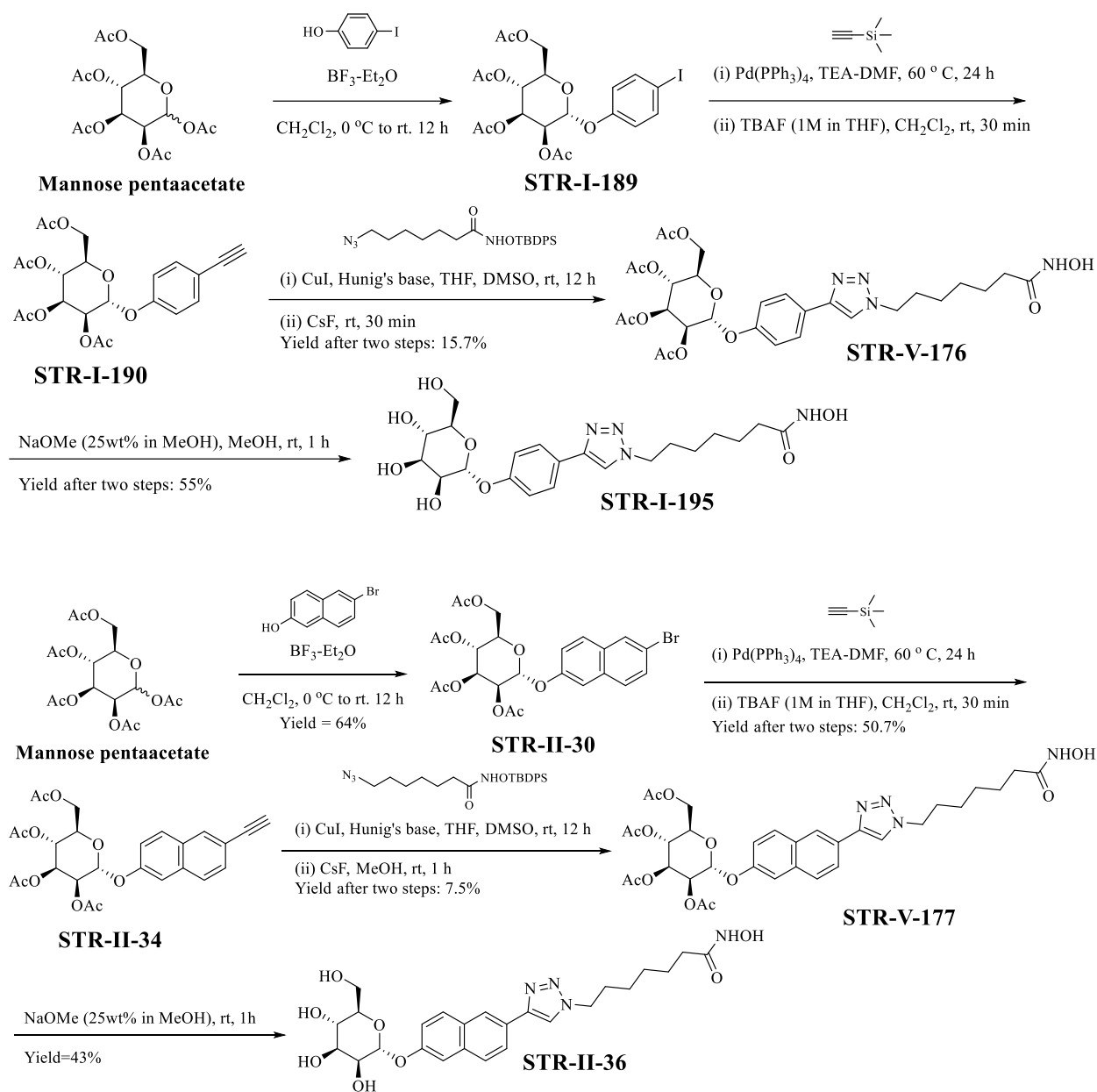
The synthesis of the control compounds **STR-V-46**, **STR-V-48**, and **STR-V-183** was accomplished via Cu(I) promoted Huisgen cyclization²⁹ between appropriate terminal alkynes and azide intermediates,^{30, 31, 32} followed by functional group deprotection adapting our published protocol (Scheme 7.1).³³



Scheme 7.2. Synthesis of the glucosylated HDACi .

Toward the glucosylated HDACi, glucose penta-acetate was coupled with the 4-iodophenol in the presence of Lewis acid Tin (IV) chloride in chloroform to yield **STR-V-49**.³⁴ The TMS group of **STR-V-49** was removed by treatment TBAF to furnish **STR-V-51** which was clicked with the TBDPS protect azido azidohydroxamates and the resulting protected product treated with cesium fluoride to yield **STR-V-166**. The acetyl groups of **STR-V-166** was hydrolyzed by treatment with sodium methoxide in methanol to furnish the target class I compounds **STR-V-53** (Scheme 7.2).

To synthesize the class II glucosylated HDACi, 6-bromonaphthalen-2-ol was coupled to the glucose penta-acetate using Lewis acid boron trifluoride etherate in DCM under refluxing condition to form **STR-V-55**.³⁵ The Sonogashira coupling of the bromo naphthalene **STR-V-55** and TMS-acetylene using catalysts copper iodide, Bis(triphenylphosphine)palladium(II) dichloride, TPP in THF, followed by deprotection of the TMS moiety of the resulting product using TBAF, resulted in **STR-V-111**. Subsequently, **STR-V-111** was clicked to the TBDPS protect azido azidohydroxamates, followed by Cesium fluoride deprotection and acetyl group removal; furnished target class II compounds **STR-V-115** (Scheme 7.2). We synthesized the class IV compounds **STR-V-155** and **STR-V-157**, which has the class I selective NAPA as ZBG,³⁶ using a variant of the Cu(I) promoted Huisgen cyclization (Scheme 7.2).³⁷

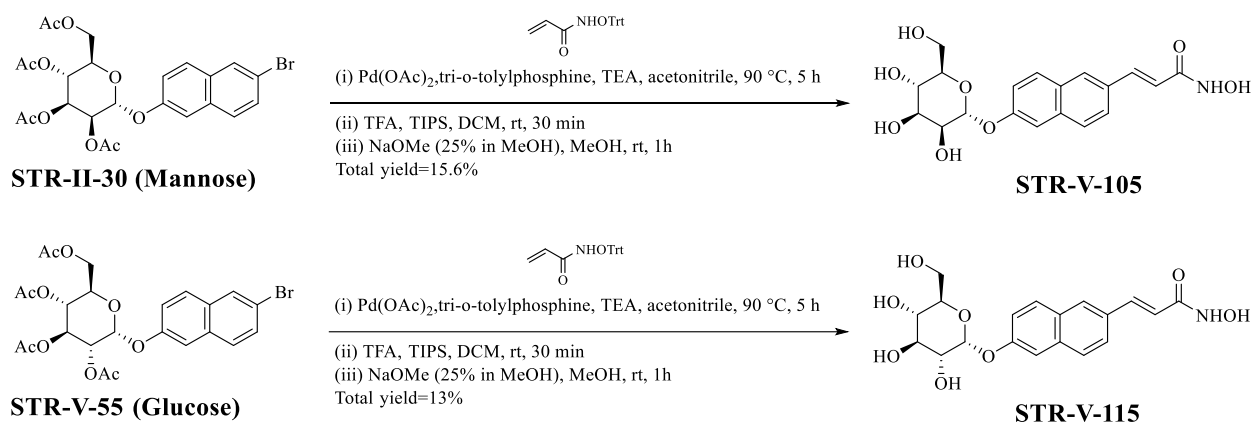


Scheme 7.3. Synthesis of mannosylated HDACi

To synthesize the mannose derivatives, mannose penta-acetate was coupled with 4-iodophenol using boron trifluoride etherate in DCM. The product **STR-I-189** was coupled with TMS-acetylene using the same condition for the synthesis of **STR-V-51**. The resulting acetylated compound **STR-I-190** was clicked with TBDPS protect azido azidohydroxamates using the same

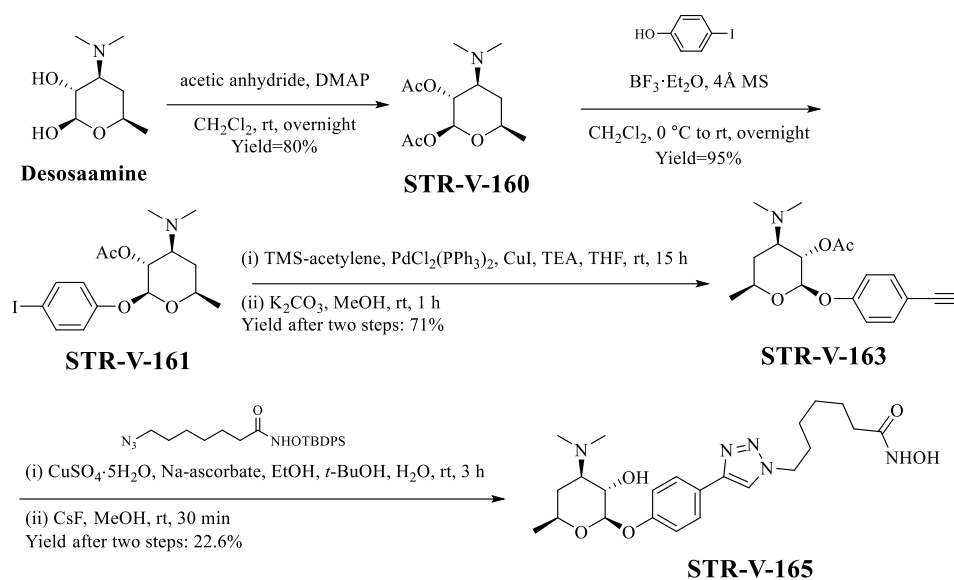
condition as in the synthesis of **STR-V-167** to furnish **STR-V-176**. Subsequent hydrolysis of the acetyl groups yielded the target class I mannose compounds **STR-I-195**.

In order to form the mannosylated class II, we coupled the mannose penta-acetate with 6-bromonaphthalen-2-ol using boron trifluoride etherate under the same condition for the synthesis of **STR-V-55** to furnish **STR-II-30**. The transformation of **STR-II-30** to the target mannosylated class II compounds **STR-II-36** (Scheme 7.3), followed similar reaction steps used to synthesize analogous glucose compounds.



Scheme 7.4. Synthesis of glucosylated or mannosylated hydroxamate HDACi.

Toward the class III glucosylated compounds, the Heck coupling of mannose derivative **STR-II-30** with *O*-trityl acrylamide followed by the deprotection of the *O*-trityl group with TFA/TIPS in DCM and the acetyl group with sodium methoxide furnished the final product **STR-V-105**. The glucosylated compound **STR-V-105** was similarly made from **STR-V-55** and *O*-trityl acrylamide (Scheme 7.4).



Scheme 7.5. Synthesis of desosaminylated hydroxamate HDACi.

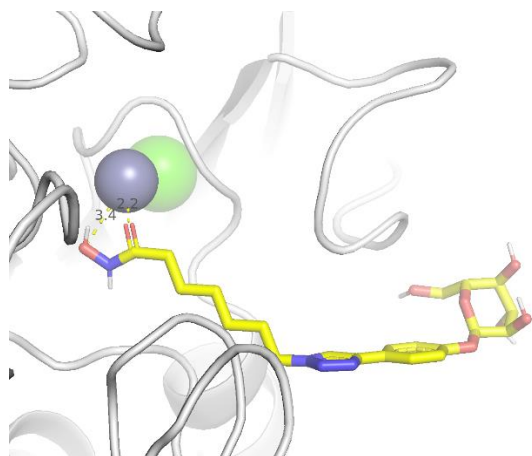
Lastly, we synthesized the desosaminylated compounds from diacetyl desosamine **STR-V-160** which was synthesized via acetylation of desosamine (Scheme 7.5). The coupling of **STR-V-160** with 4-iodophenol, using the same method described for the synthesis of **STR-I-189**, resulted in **STR-V-161**, which was converted to **STR-V-163** using the same condition as in the synthesis of **STR-V-51**. Subsequently, the **STR-V-163** clicked with TBDPS protect azido azidohydroxamate; and the TBDPS and acetyl groups deprotected to form **STR-V-165** in analogous manner to the synthesis of **STR-V-53**.

7.2.2 Molecular Docking

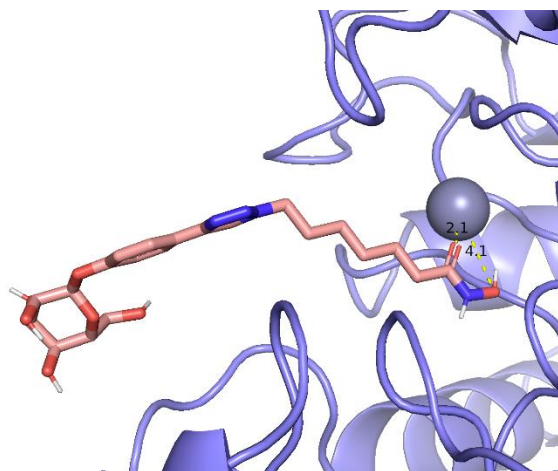
To gain insight into the prospect of productive interaction between these glucosylated HDACi and HDACs and GLUT transporter, we used the *in silico* molecular docking analysis (Autodock Vina)³⁸ to interrogate the binding orientations and the docking scores of a selected compound

STR-V-53 against HDAC2 (PDB: 4LXZ), HDAC6 (5G0G) and, GLUT-1 (4PYP) which shared 55% sequence similarity of GLUT-2. We used GLUT-1 for this analysis due to the absence of GLUT-2 structure in the PDB.

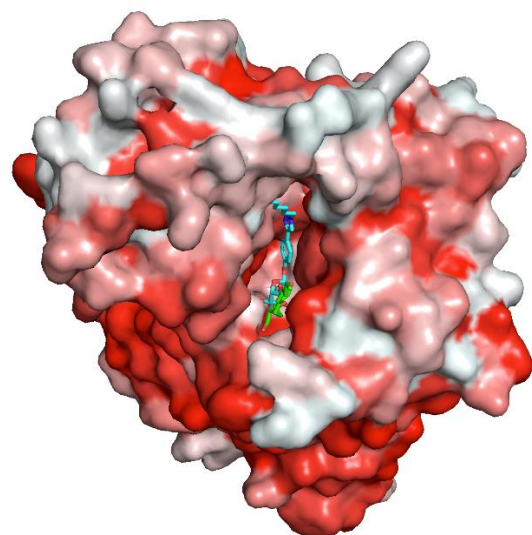
a.



b.



C1.



C2

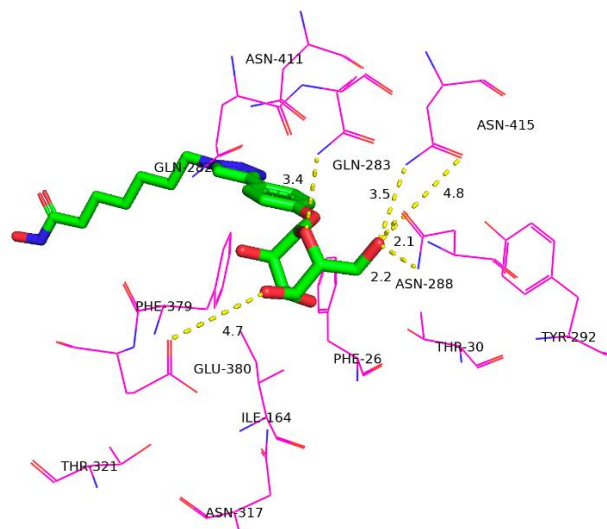


Figure 7.2. Molecular docking on (a) HDAC2 (PDB:4LXZ) and (b) HDAC6(5G0G) revealed efficient zinc chelation, and (c1) hydrophobicity presentation of GLUT-1(4PYP) with overlay of

STR-V-53 and nonyl beta-D-glucopyranoside. (c2) Putative hydrogen bonding interactions between glucose moiety of **STR-V-53** and amino acids side chains at the binding pocket of GLUT-1.(d1 and d2) showed STR-V-176 (Desosamine moiety) overlay with Nonyl-beta-D-glucopyranoside and the intermolecular interaction was demonstrated.

Molecular docking analyses were performed as we described before.^{39,40} We observed that, **STR-V-53** efficiently chelate the Zn^{+2} ion at the active sites of HDAC2 and HDAC6 (Fig 7.2a-b), an interaction that is crucial to effective HDAC inhibition. The docking scores of the binding poses of **STR-V-53** which have most plausible interactions within HDACs 2 and 6 active sites are 9.3kcal/mol and 10.3 kcal/mol respectively. Both binding affinities are relatively high for protein-ligand interaction, which strongly suggest that they could be potent HDACi.

Against GLUT-1, we found that the glucose moiety of **STR-V-53** optimally interacts within the region where the sugar analog nonyl beta-D-glucopyranoside seats (figure 7.2c). More specifically, the glucose moiety of **STR-V-53** forms H-bonds with Asn-288, Gln-283, Glu-380, Asn-415 (Fig. 7.2d). This docking also results in -12.2 kcal/mol binding affinity, a much strongly binding affinity relative to unmodified glucose (-6.4kcal/mol) and nonyl beta-D-glucopyranoside (-9.5kcal/mol). Based on this *in silico* prediction, we postulate that glucosylated compound **STR-V-53** will be preferentially transported by GLUT-1, and possibly GLUT-2. STR-V-176 as the desosamine derivative HDACi showed less H-bonding in the GLUT-1 binding pocket than STR-V-53 as it has less hydroxyl group around, which lowers its binding affinity to -10.2kcal/mol. These indicates that STR-V-176 may not be as selective as STR-V-53 in cellular uptake to GLUT-1- or GLUT-2-enriched cell lines.

7.2.3 Anti-proliferation activity.

As a cost-effective approach to identify lead compounds for intracellular target validation, we first screened all of the synthesized compounds for their effects on the viability of three cell lines: A549 (lung adenocarcinoma), VERO (kidney epithelial cell), and Hep-G2 (hepatocellular carcinoma). We observed that the control compounds **STR-V-46** and **STR-V-48** showed strong cytotoxicity against all three cell lines while there is no selectivity between VERO and Hep-G2. In contrast, class I glucose candidate **STR-V-53** showed relatively high cytotoxicity and cell-type selectivity against Hep-G2 over other cell lines. However, the mannose derivative STR-I-195 showed some selectivity but it is not as strong as **STR-V-53**. In the class II, **STR-V-114** (glucose compound) still showed 7- to 10-fold selectivity in Hep-G2 with a lower IC₅₀, while the mannose class II candidate **STR-II-36** is not as selective as **STR-V-114**. For the cinnamic derivatives in class III, we observed that the **STR-V-105**, **STR-V-115** and **STR-V-121** showed Hep-G2 selectivity, whereas the cytotoxicity is not ideal (>45 μ M). HDAC class I selectivity of these compounds may contribute to their Hep-G2 selectivity. Thus, we examined the class IV against all three cell lines, and we found that none of them could induce significant cytotoxicity on Hep-G2. The reason of the failure could be due to the structural-activity relationship (SAR) that the conjugation of sugar may not compatible with the NAPA ZBG in HDAC inhibition. Finally, we were interested in activities of desosamine derivatives **STR-V-165**. Interestingly, the desosamine candidate also showed 7-fold selectivity on Hep-G2 over VERO. This may not unexpected as GLUT-2 could facilitate the transport of several sugars, desosamine included based on this data.

Table 7.1. IC₅₀ of anti-proliferation effects of glycosylated HDACi. *NI=no inhibition up to 100 μ M. *NT= not tested

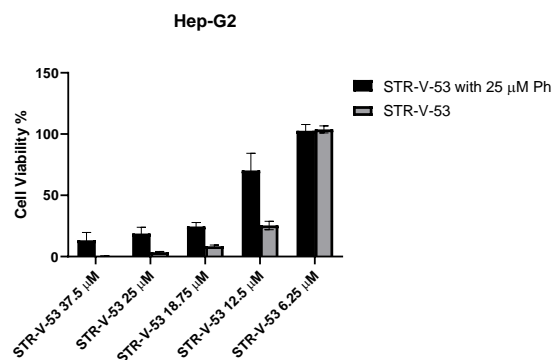
Compound name	A549 (μM)	Hep-G2 (μM)	VERO (μM)
STR-V-46	2.8 \pm 0.2	0.3 \pm 0.05	0.3 \pm 0.08
STR-V-48	1.4 \pm 0.2	0.4 \pm 0.04	0.2 \pm 0.05
STR-V-183	83.1 \pm 6.6	11.8 \pm 4.8	41.8 \pm 6.1
STR-V-53	NI*	10.4 \pm 0.6	NI
STR-V-114	77.2 \pm 4.3	6.7 \pm 1.6	34.1 \pm 3.0
STR-V-176	64.7 \pm 7.0	8.0 \pm 0.9	77.4 \pm 5.6
STR-I-195	NI	22.3 \pm 2.0	65.5 \pm 8.3
STR-V-177	39.6 \pm 0.6	7.4 \pm 0.9	19.2 \pm 0.9
STR-II-36	20.1 \pm 1.1	7.5 \pm 0.8	33.6 \pm 5.5
STR-V-105	NI	78.5 \pm 11.6	NI
STR-V-115	NI	66.1 \pm 10.3	82.1
STR-V-165	33.7 \pm 1.8	9.6 \pm 3.4	76.4
STR-V-155	59.9 \pm 1.3	NT*	NI
STR-V-157	NI	NI	NI
Sorafenib	18.1 \pm 2.9	3.7 \pm 0.4	12.2 \pm 0.1
SAHA	15.7 \pm 0.99	5.6 \pm 1.7	4.5 \pm 0.68

Relative to SAHA, a prototypical HDACi, and Sorafenib, a clinically approved anti-HCC agent, our compounds **STR-V-53**, **STR-V-114**, **STR-I-195**, and **STR-V-165** could be lead candidates cell-type selectivity anti-HCC agents (Table 7.1). As expected, though the Desosamine STR-V-176 showed potency in HCC, the selectivity over VERO or A549 is around 10-fold, while the STR-V-53 is more than 10-fold because it does not induce any cytotoxicity up to 100 μM .

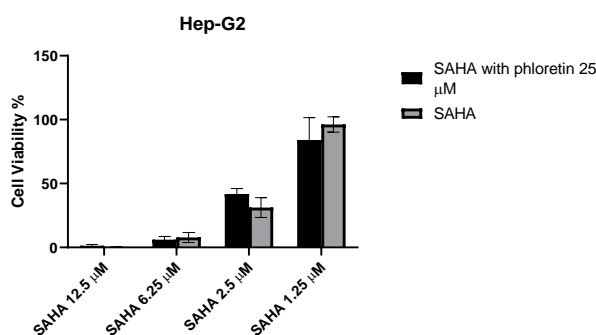
To further investigate the cancer cell-type selectivity of our compounds, we screened **STR-V-53** (10 μ M) in the NCI 60 panel. We found that **STR-V-53** has negligible effect on proliferation of all cancer cells in NCI panel, which is lacking HCC cell lines, showing a mean cell growth of 99.6%. Our cell activity data on **STR-V-53** and the lack of growth inhibition effect of **STR-V-53** in the NCI-60 panel (Fig. S7.1) strongly support of our conclusion of HCC cell-selectivity attribute of **STR-V-53** and possibly other lead glycosylated HDACi disclosed herein.

7.2.4 Hep-G2 cell line uptake glycosylated HDACi via GLUT-2

a.



b.



c.

d.

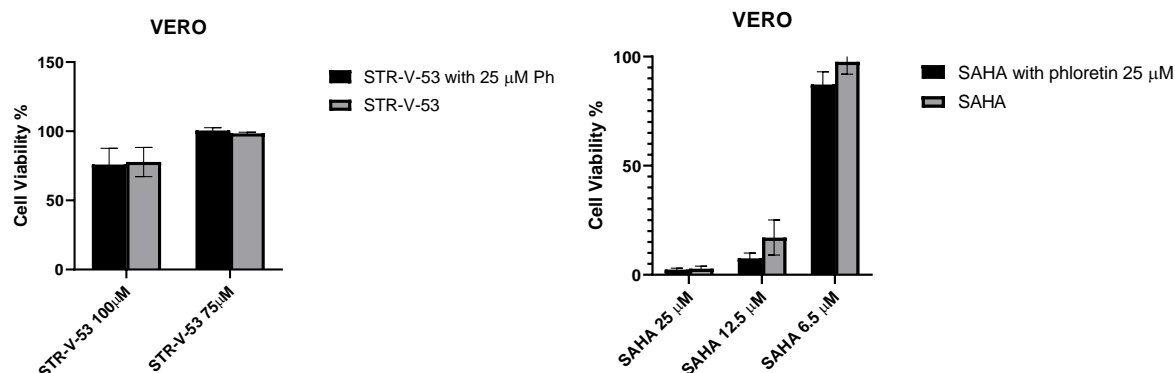


Figure 7.3. Blockage of GLUT-2 attenuates the cytotoxicity of **STR-V-53** against Hep-G2. Hep-G2 and VERO were treated with Phloretin (Ph) for 24 h prior to incubation with **STR-V-53** or SAHA. (a) Hep-G2 treated by **STR-V-53** with or without Ph. (b) Hep-G2 treated by SAHA with or without Ph. (c) VERO treated by **STR-V-53** with or without Ph. (d) VERO treated with SAHA with or without Ph.

To investigate the role of GLUT-2 in the uptake of **STR-V-53** by Hep-G2, we pharmacologically blocked GLUT-2 with an inhibitor, phloretin (Ph) and assess the effect of this blockage on cell cytotoxicity using MTS assay. We observed that Ph selectively mitigated the cytotoxicity of **STR-V-53** against Hep-G2 cell line with no apparent effect on the cytotoxicity of SAHA (Fig. 7.3a-b). Against VERO cell line, we did not observe any significant change in the effects of **STR-V-53** or SAHA in the presence of Ph (Fig. 7.3c-d). This matches our expectation because VERO has limited expression of GLUT-2. Collectively, this data suggests that the glycosylated compound **STR-V-53** derives a significant part of its Hep-G2 cell penetration through GLUT-2-mediated transport and much less from passive diffusion.

7.2.5 Glycosylated HDACi showed intracellular HDAC inhibition

a.

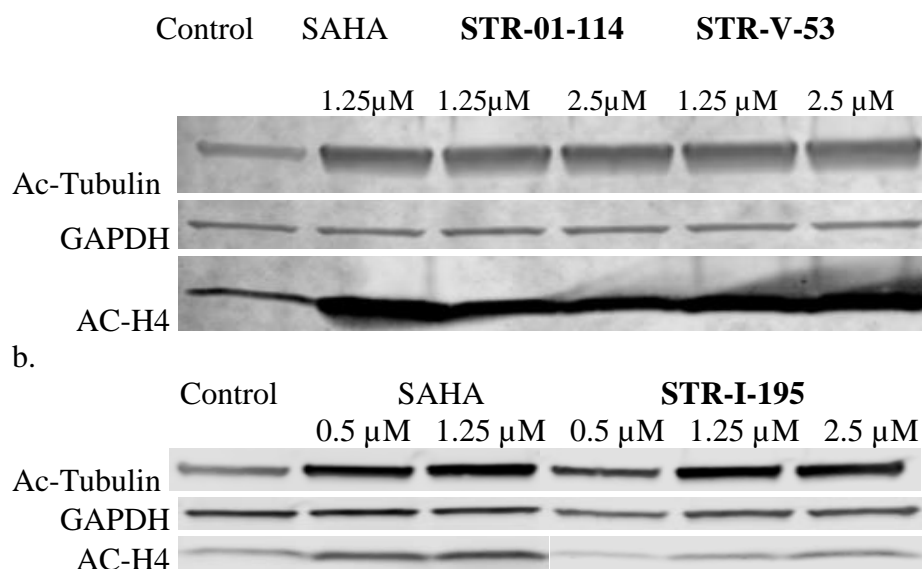


Figure 7. 4. Hep-G2 induced up-regulation of acetylated H4 and acetylated α -Tubulin. (a) Hep-G2 treated with DMSO or 0.1% DMSO solution of SAHA (1.25 μ M), **STR-I-114** (1.25 μ M, 2.5 μ M) and **STR-V-53** (1.25 μ M, 2.5 μ M). (b) Hep-G2 treated with DMSO or 0.1% DMSO solution of SAHA (0.5 μ M, 1.25 μ M) and **STR-I-195** (1.25 μ M, 2.5 μ M). Cell were treated for 5 h before lysis. Data are from two independent experiments.

To determine the contributions of HDAC inhibition to the antiproliferative activities of the glycosylated HDACi compounds, immunoblotting was used to investigate the acetylation status of histone H4 and α -tubulin in Hep-G2 cells in response to exposure to representative compounds **STR-V-53**, **STR-V-114** and **STR-I-195** using SAHA as a positive control for HDAC inhibition. H4 and tubulin acetylation states as biomarkers for HDAC class I and class IIb intracellular inhibition, respectively. GAPDH expression was used as a protein loading control. As expected, the exposure of cells to **STR-V-165** and **STR-V-114** at $\frac{1}{4}$ IC₅₀ and $\frac{1}{2}$ IC₅₀ induced accumulation of acetylated H4 and acetylated tubulin. Similarly, SAHA at 1.25 μ M induced H4 and tubulin hyperacetylation (Fig. 7.4b). On the other hand, **STR-I-195** at 0.5 μ M did not show significant acetylation of H4 and α -Tubulin, but at 1.25 μ M and 2.5 μ M showed significant acetylation (Fig.

7.4b). All these data indicates that compounds **STR-V-53**, **STR-I-195** and **STR-V-114** intracellularly inhibit HDAC isoform I and HDAC 6 at low micromolar concentrations.

7.2.6 Glycosylated HDACi induce selective Hep-G2 cell apoptosis

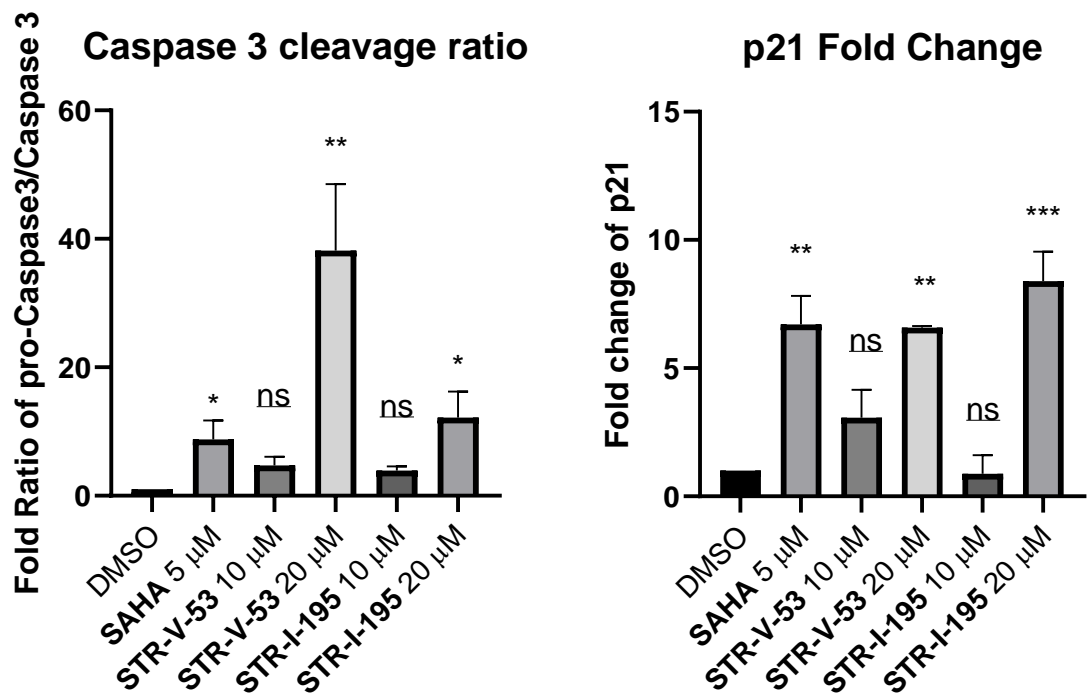
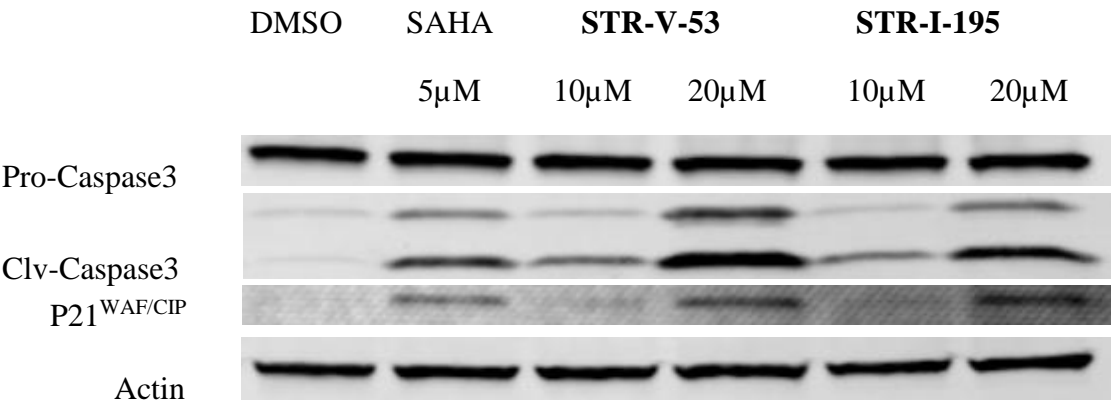
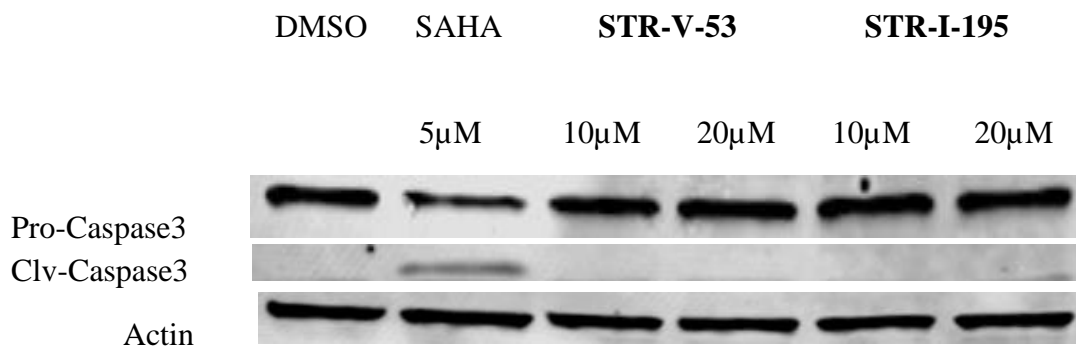


Figure 7. 5. Evidence of caspase 3 cleavage and p21 up-regulation in Hep-G2 cell by glycosylated HDACi. Cells were treated with DMSO or 0.1% DMSO solution of SAHA (5 μ M), **STR-V-53** (10 and 20 μ M), or **STR-I-195** (10 and 20 μ M) for 18 h. (a) Cropped gels with upregulation on p21, pro-caspase3 and clv-caspase 3. (b) Quantification of relative expression of p21 and ratio of clv-caspase 3 vs pro-caspase3. (Bars show mean plus standard deviation; * P < 0.0332; ** P < 0.0021;***P<0.0002; ****P<0.00001).

HDAC inhibition could cause cell apoptosis through Caspase cleavage and p21 upregulation. Typically, SAHA induces the cleavage of Caspase 3 and p21 upregulation in Hep-G2 cell line (Fig. 7.5). To probe if our compounds elicit a similar phenotype, we investigated their effects on the cellular levels of cleaved Caspase 3 and p21 through immunoblotting. Specifically, Hep-G2 cells (1 x10⁶ count/well) were treated with SAHA, **STR-V-53** and **STR-I-195** at IC₅₀ or 2x IC₅₀ for 18 h prior to the cell lysis. Western blotting on the cell lysates revealed that **STR-V-53** caused a significant upregulation of cleave Caspase 3/Pro-caspase 3 ratio, while SAHA and **STR-I-195** also showed cleavage of Caspase 3. p21^{WAF/CIP} was also upregulated significantly at higher concentrations of **STR-V-53** and **STR-I-195**. These data implies that **STR-V-53** and **STR-I-195** act through HDAC inhibition, in similar manner to SAHA, to induce apoptosis in Hep-G2 cells.



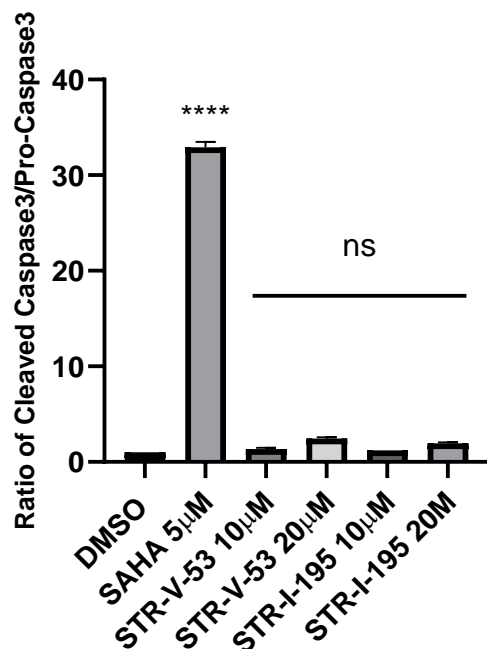


Figure 7. 6. No evidence of cleavage of caspase 3 in Vero cell treated with **STR-V-53** or **STR-I-195**. Cells were treated with DMSO or 0.1% DMSO solution of SAHA (5µM), **STR-V-53** (10 and 20 µM), or **STR-I-195** (10 and 20 µM) for 18 h. (a) Cropped gels with upregulation on Pro-caspase3 and clv-caspase3. (b) Quantification of ratio of pro-caspase3 vs cleaved-caspase3. (Bars show mean plus standard deviation; * P < 0.0332; ** P < 0.0021; ***P<0.0002; ****P<0.00001).

Interestingly, **STR-V-53** or **STR-I-195** did not induce cleavage of caspase 3 in VERO cells even at the same concentrations that would induce caspase 3 activation in Hep-G2 cells (Fig. 7.6). In contrast, the SAHA induced cleavage of caspase 3 (Fig. 7.6). This data shows that glycosylated HDACi are selectively toxic to HCC cell line Hep-G2. This is most likely due to the selective cell uptake mediated by GLUT-2.

7.2.7 STR-V-53 caused cell cycle arrest at S stage

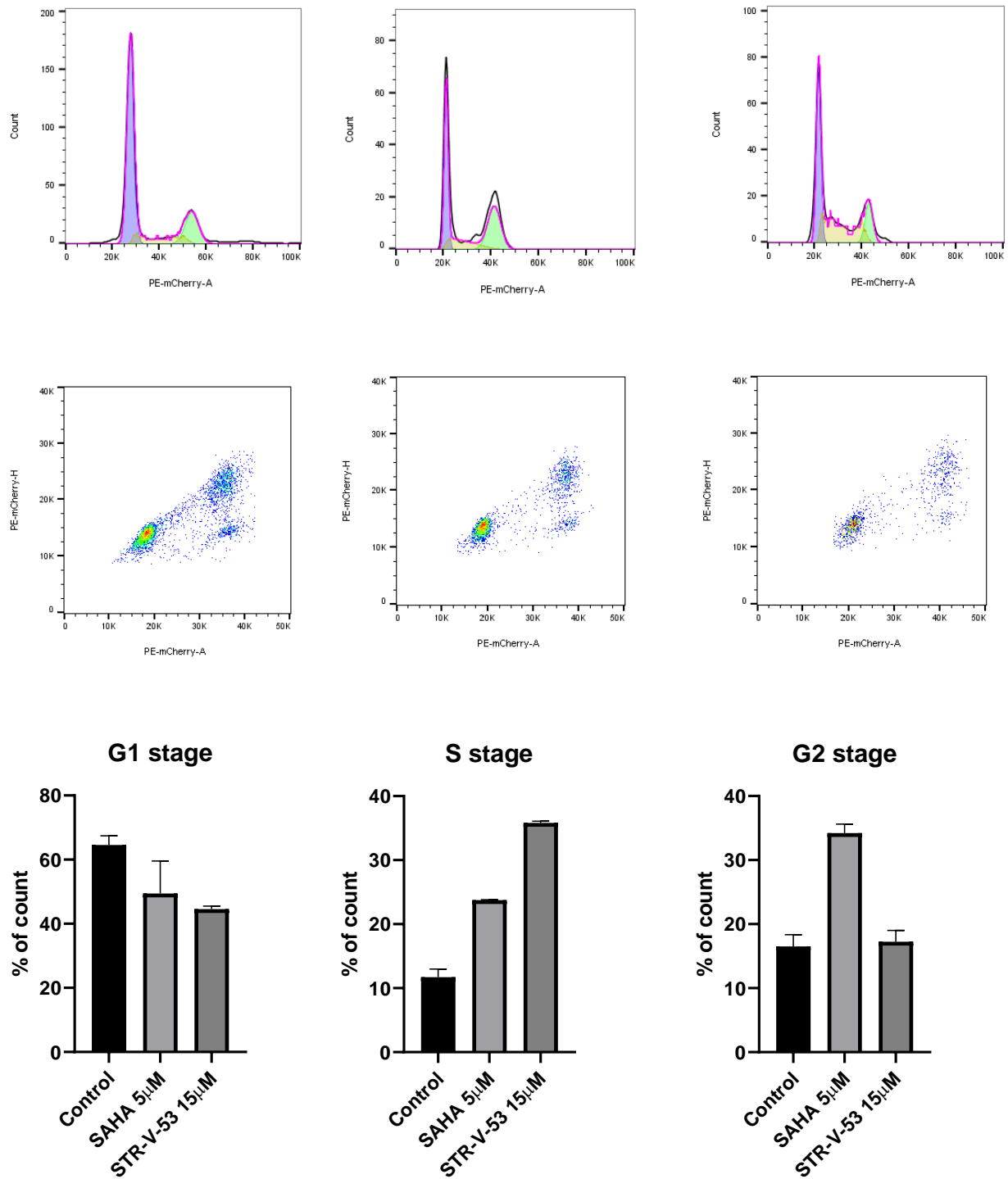


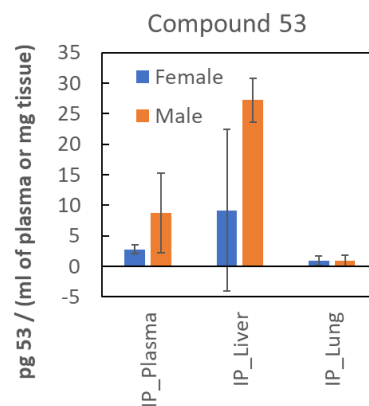
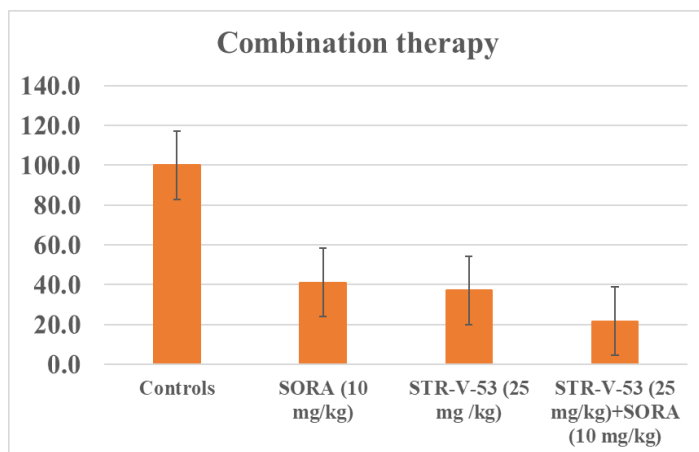
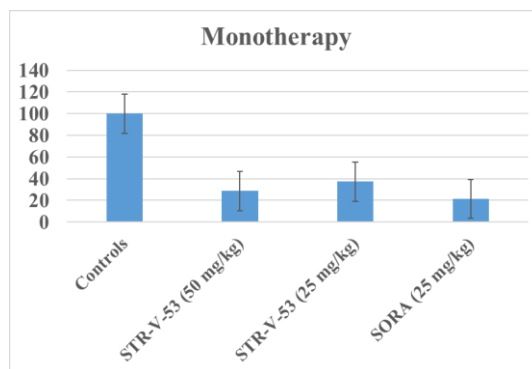
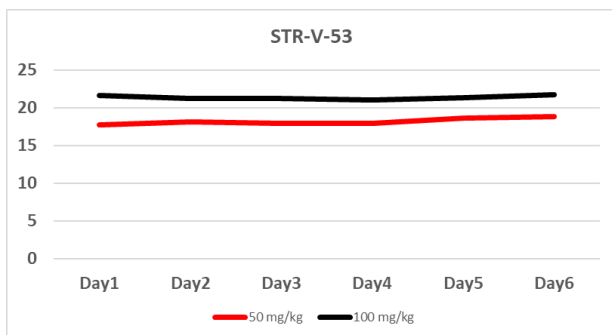
Figure 7.7. The effect of STR-V-53 on cell cycle progression. Hep-G2 cells were cultured until 80% confluence in 10cm petri dish. The cell was serum starved overnight before drug treatment. Then the cell were treated with 10 mL of 0.1% DMSO medium, 0.1% DMSO solution of SAHA

(5 μ M) or **STR-V-53** (15 μ M) respectively for 48 h. (a) The control group. (b) SAHA (5 μ M) treated group. (c) **STR-V-53** (15 μ M) treated group. Data are from two independent experiments. Quantification data is shown above.

To determine if the potent Hep-G2 cell selective cytotoxicity of **STR-V-53** results from its perturbation of the cell cycle pattern, we evaluated the effect of **STR-V-53** on the cycle progression by flow cytometry using SAHA as a control (Fig. 7.7). We observed that both SAHA (5 μ M) and **STR-V-53** (15 μ M) caused significant S phase arrest of Hep-G2 cell after 48 h treatment. This data shows that the **STR-V-53** may act like SAHA to cause cell death.

7.2.8 Glycosylated HDACi suppress tumor growth in murine model (This experiment was performed in collaboration with Petros lab at Emory University)

Based on the data from the aforementioned *in vitro* studies, we selected **STR-V-53** as a candidate for further evaluation in an orthotopic model of Hep-G2-Red-FLuc Bioware® Brite Cell Line (PerkinElmer) in mice.



e.

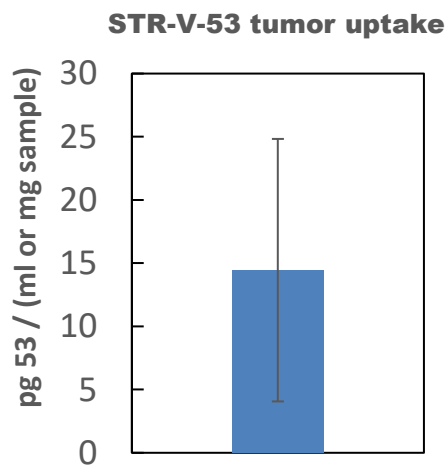


Figure 7. 8. Compound **STR-V-53** significantly suppressed liver tumor growth and liver tissue accumulation with no toxicity based on mice body weight indication. (a) Maximum tolerated dose experiment with mice weight monitor. Mice were treated with 50 mg/kg and 100 mg/kg daily for

6 days through IP injection, and body weights were recorded daily. There are 6 per group, equal number of both sexes. (b) **STR-V-53** (25 and 50 mg/kg daily) and SORA (25 mg/kg) were administrated into tumor bearing mice via i.p. injection for 21 days. (c). Comparison of the monotherapy of **STR-V-53** with that of combination therapy of **STR-V-53** (25 mg/kg) + Sorafenib (SORA) (10 mg/kg). (d). Biodistribution of **STR-V-53** 8 h post i.p. injection. (e). Tumor uptake of STR-V-53 in male and female mice. There are 10 mice (5 male and 5 female) per treatment group.

Prior to embarking on tissue distribution and efficacy studies, we first determined the maximum tolerated dose (MTD) of **STR-V-53** in healthy C57Bl/6 mice. The compound was administered via i.p. injection using a formulation containing excipients found in FDA approved drugs – dimethylacetamide (DMA)/Cremophor RH 40 (CRH)/Water (10%/20%/70%) – that we developed. We exposed cohorts of animals (6 per group, equal number of both sexes) to the drug at two concentrations – 50 mg/kg, 100 mg/kg (limiting injection volume to 100 μ L per dose) – daily for 6 days. Using body weight as an indicator of toxicity, we observed no overt toxicity as **STR-V-53** caused no significant body weight loss at 100 mg/kg (Fig. 7.8a). Based on this MTD data, we investigated the effect of **STR-V-53** on tumor growth at 25 and 50 mg/kg body weight.

Mice (6-8 weeks old) were orthotopically implanted through by a direct intrahepatic artery injection with Hep-G2-Red-FLuc cells according to published protocols.⁴¹ We used the Red-Fluc expression to confirm tumor implantation by bioluminescent imaging using IVIS. Treatment began after imaging confirmed the establishment of intrahepatic tumors (approx. 7 days). Mice were grouped into cohorts with similar average relative chemiluminescence and the treatment groups were injected daily with 200 μ L of solution of **STR-V-53**, SORA and combination of **STR-V-53** and SORA for 21 days via i.p. route. No treatment group received vehicle only. After treatment, mice were imaged again, sacrificed and liver samples were harvested to determine the effects of

treatment on tumor size by measurement with calipers. We found that **STR-V-53** efficiently suppressed HCC tumor growth at 50mg/kg and 25mg/kg to a similar extent as SORA. **STR-V-53** at 25 mg/Kg and 50 mg/Kg induced tumor growth inhibition (TGI) of 60% and 68% respectively (Fig. 7.8b). Moreover, the combination therapy of SORA (10 mg/kg) and STR-V-53 (25 mg/kg) is more efficacious than either drug as standalone agents. Relative to the effect of each agent alone, the combination of **STR-V-53** (25 mg/Kg) and sorafenib (10 mg/Kg) additively reduce tumor volume with TGI of ~ 80% (Fig. 7.8c). This suggest that **STR-V-53** could enhance the efficacy of clinically approved SORA.

Finally, we used mass spectrometry to determine biodistribution of STR-V-53 8h post i.p. administration. We measured the levels of **STR-V-53** in selected tissues – liver, lungs and the plasma – of healthy mice exposed to **STR-V-53** (50 mg/kg, i.p.). In the plasma, the level of **STR-V-53** is relatively low for both the female (2.82 pg/mL) and male (8.76 pg/mL) mice. The levels of **STR-V-53** in the liver tissue of female and male mice are approximately 9.2 pg/mL and 27.2 pg/mL respectively. In lung tissues, the levels of **STR-V-53** in both male and female mice are almost undetectable (Fig. 7.8d). We also measured the STR-V-53 in tumor distribution, and we found that STR-V-53 demonstrated an efficient tumor distribution rate as 15pg/mg of the tumor. This data implies a selective biodistribution of STR-V-53 in HCC tumor.

7.3 Conclusion

HCC as one of the leading lethal cancers in the world and it still lacks efficient treatment. Previous studies have shown that HCC is strongly driven by epigenetic dysregulation that leads to chromatin histone hypoacetylation. HDAC inhibition therapy could be promising treatment option for HCC.

However, HDACi have been ineffective against solid tumors such as HCC. We discovered herein that the integration of glycoside moieties into the prototypical HDACi surface recognition group afforded glycosylated HDACi that are selectively cytotoxic to Hep-G2 cells. A cohort of these demonstrated intracellular on-target effect and selectively induced in Hep-G2 cells. We noticed that a lead compound **STR-V-53** displayed exquisite HCC cell line selectivity, as it is none toxic to cells in the NCI-60 panel and derived a significant part of its Hep-G2 cell penetration through GLUT-2-mediated transport. Furthermore, we found that **STR-V-53** is relatively non-toxic to mice and robustly and selectively suppressed tumor growths in an orthotopic model of HCC as standalone agent. **STR-V-53** also enhanced the potency of SORA in a combination therapy experiment. Others have shown that systemic HDACi could enhance the potency of SORA in murine models of HCC.⁴² However, the benefit of HDACi/SORA combination has not borne out in the clinic due to dose-limiting toxicities which forced the cancelation of clinical trials of the combination of SORA with approved HDACi such as SAHA [NCT01075113] and panobinostat [NCT00873002]. Because these compounds are selectively cytotoxicity to HCC cells, they may be less prone to the toxic side effects observed in the combination of SORA. Collectively, our data revealed that **STR-V-53** is a novel HDACi whose potential as targeted anti-HCC agent merits further evaluation in additional preclinical and/or IND enabling studies.

7.4 Materials and methods

7.4.1 Materials

Anhydrous solvents and reagents were purchased from Sigma-Aldrich (St. Louis, MO, USA), Acros, VWR International (Radnor, PA, USA), Greenfield Chemicals or Thermo Fisher Scientific

(Waltham, MA, USA) and were used without further purification. Analtech silica gel plates (60 F254) were utilized for analytical TLC, and Analtech preparative TLC plates (UV254, 2000 μm) were used for purification. Silica gel (200–400 mesh) was used in column chromatography. TLC plates were visualized using UV light, anisaldehyde, and/or iodine stains. High performance liquid chromatography (HPLC) analyses were performed on a Agilent 1260 Infinity II instrument using a Luna® 5 μm C-18 column 100 Å (100 mm \times 4.6 mm), eluting with solvent A (water) and solvent B (acetonitrile) at a gradient of 5% solvent B for the first 4 min and increase to 40% from 4 to 5 min, then elute with gradient from 40% to 80% for another 20 min, and then constantly eluting with 80% solvent B for 5 min. The detection wavelength is at 280 nm and a flow rate of 0.5 mL/min. Sample concentrations were 250 μM – 1mM, injecting 30 μL . All compounds have $\geq 95\%$ purity as determined by HPLC. Chemicals used LC-MS analyses were obtained from the following sources: acetonitrile (Optima, LCMS, Fischer Scientific, catalog No. A955-4); formic acid (Optima, LCMS, Fischer Scientific, catalog No. A117-50); isopropanol (Optima, LCMS, Fischer Scientific, catalog No. A461-4); water (Optima, LCMS, Fischer Scientific, catalog No. W6-4); methanol (Optima, LCMS, Fischer Scientific, catalog No. A456-4); Phloretin (VWR, Radnor, PA) NMR spectra were obtained on a Varian-Gemini 400 MHz magnetic resonance spectrometer. ^1H NMR spectra were recorded in parts per million (ppm) relative to the residual peaks of CHCl_3 (7.24 ppm) in CDCl_3 or CHD_2OD (4.78 ppm) in CD_3OD or DMSO- d_5 (2.49 ppm) in DMSO- d_6 . ^{13}C spectra were recorded relative to the central peak of the CDCl_3 triplet (81.5 ppm) and were recorded with complete hetero-decoupling. MestReNova (version 11.0) was used to process the original NMR “fid” files. High-resolution mass spectra were recorded at the Georgia Institute of Technology mass spectrometry facility.

Cell lines including Hep-G2, A549, MDA-MB-231, MCF-7, and VERO were purchased from ATCC (Manassas, VA). Cells were cultured the following medium: Dulbecco's Modified Eagle Medium (DMEM) (Corning, 10-017-CV) and phenol red free Minimum Essential Medium (MEM) (Corning, 17-305-CV), supplemented with 10% fetal bovine serum (FBS) (Corning, 35-010-CV). Electrophoresis supplies, TGX MIDI 4–20% gel (cat. # 5671093) and Turbo PDVF membrane (cat. # 1704273), were from Bio-Rad Laboratories, Inc (Hercules, CA, USA). Primary antibodies - Ac-Tubulin (sc-23950), Ac-H4 (sc-515319) were obtained from Santa Cruz Biotechnology (Dallas, TX, USA), caspase 3 and clv-caspase 3 were purchased from Cell signaling Technology (Danvers, MA), anti-p21^{WAF/CLIP} (ThermoFisher, Waltham, MA USA), anti-GAPDH (Sigma, Saint Louis, USA), while secondary antibody (part. IR2173) was from ImmunoReagents (Raleigh, NC, USA). RIPA buffer (VWRVN653-100ML) was from VWR International (Radnor, PA, USA) while phosphatase inhibitor (A32957) and protease inhibitor (A32955) were procured from Thermo Fisher Scientific (Waltham, MA, USA). BCA protein assay kit (K813-2500) was purchased from BioVision, Inc (Milpitas, CA, USA). C57BL/6 and Athymic Nude-Foxn1nu mice (5-7 weeks old; male and female) were purchased from Envigo RMS, Inc (Indianapolis, IN, USA).

7.4.2 *Synthesis*

Published/Reported Agents

STR-V-46 (N-hydroxy-7-[4-(4-methoxyphenyl)triazol-1-yl]heptanamide) was published before. The compound PubChem ID is 25068485. **STR-V-48** (N-hydroxy-7-(4-(6-methoxynaphthalen-2-yl)-1H-1,2,3-triazol-1-yl)heptanamide) have also been synthesized and studied in our lab.³³

Intermediates **STR-V-107** (7-azido-N-((tert-butyldiphenylsilyl)oxy)heptanamide) was available in stock. **STR-V-51** (Pubchem: 102084446), **STR-I-190** (CAS: 677352-87-3), were reported and published in previous study. (2R,3R,4S,5S,6R)-2-(acetoxymethyl)-6-(4-iodophenoxy)tetrahydro-2H-pyran-3,4,5-triyl triacetate (**STR-V-49**) was reported in patent.⁴⁴ Azido linkers: N-(2-amino-4-fluorophenyl)-7-azidoheptanamide, N-(2-amino-5-fluorophenyl)-7-azidoheptanamide, and N-(2-amino-5-(thiophen-2-yl)phenyl)-7-azidoheptanamide were made in published work.²² n-(trityloxy)acrylamide (**STR-V-38**) is a commercially available chemical (CAS: 79-06-1).

Chemical synthesis

4-ethynylphenol (**STR-V-180**). 4-iodophenol (1.09g, 4.95mmol) mixed with Bis(triphenylphosphine)palladium(II) dichloride (104mg, 0.15mmol) and copper iodide (29mg, 0.15mmol) along with TMS-acetylene (1.01mL, 7.18mmol) in triethylamine (15mL). The solution was purged with argon for 5-10 minutes. Then the reaction was heated to 80°C for 3 h followed by suspension. The solution was filtered by Celite and the filtrate was evaporated to dryness by vacuum. The crude solution was purified by column chromatography with Solvent system of EtOAc: hexane=3:7. The purified compound was collected and dried through vacuum and yield in yellow solid. The product was directly dissolved into ice cold THF and mixed with 6mL of TBAF (1M in THF) in ice bath.³² The reaction lasted for 1 h and the crude product was purified again with column under solvent system EtOAc:hexane=1:9. The product was collected and dried with vacuum. The **STR-V-180** was yielded as a brown oil (ambiguous amount).

N-hydroxy-7-(4-(4-hydroxyphenyl)-1H-1,2,3-triazol-1-yl)heptanamide (**STR-V-183**). **STR-V-180** (47mg, 0.4mmol) mixed with **STR-V-107** (167mg, 0.4mmol) and copper iodide (38mg, 0.2mmol) in THF:DMSO (1:1mL) solution. The solution was purged with Argon for 5-10 minutes before Hunig's base (0.2ml, 10v/v%) was added. The reaction ran at room temperature for 1 h and was suspended by adding ammonia hydroxide (1M, 1mL). The reaction was partitioned between DCM (50 mL) and 1M NH₄OH (30ml) and the two layers separated. The organic layer was washed with water (30 mL), dried over Na₂SO₄ and evaporated off to give a crude product. The product was again dissolved into Methanol (4mL) with addition of cesium fluoride (122mg, 0.8mmol) to remove the TBDPS protection group. The reaction was completed in 1 h at room temperature. The final product **STR-V-183** was furnished by preparative TLC under condition with 5% MeOH in DCM. The **STR-V-183** was yielded as brick-red solid (4.5mg, 0.015mmol, 3.8%). ¹H NMR (700 MHz, MeOD) δ 8.08 (s, 1H), 7.54 (d, *J* = 8.5 Hz, 2H), 6.75 (d, *J* = 8.6 Hz, 2H), 4.33 (t, *J* = 7.1 Hz, 2H), 1.99 (t, *J* = 7.4 Hz, 2H), 1.86 (p, *J* = 7.1 Hz, 2H), 1.53 (p, *J* = 7.3 Hz, 2H), 1.34 – 1.24 (m, 2H), 1.20 (d, *J* = 4.8 Hz, 4H). ¹³C NMR (176 MHz, MeOD) δ 157.6, 147.7, 126.7, 119.7, 115.3, 76.8, 49.9, 32.2, 29.7, 28.0, 25.7, 25.1, 13.0.

(2R,3R,4S,5R,6R)-2-(acetoxymethyl)-6-(4-(1-(7-(((tert-butyl)diphenylsilyl)oxy)amino)-7-oxoheptyl)-1H-1,2,3-triazol-4-yl)phenoxy)tetrahydro-2H-pyran-3,4,5-triyl triacetate (**STR-V-167**). **STR-V-51** (1 g, 2.2mmol) was mixed with **STR-V-107** (0.88g, 2.07mmol) in mixture of ethanol and tert-butanol (6:6mL). The copper sulfate (99mg, 0.395mmol) was added to the solution with sodium ascorbate (313mg, 1.58mmol). Followed by 0.5mL water addition, the reaction lasted for 3 h in room temperature and was completed. The crude product was partitioned between DCM (30mL) and water (50mL) and two layers separated. The organic layer was washed by water (30

mL), dried over Na₂SO₄ and vacuum evaporation to gained the crude product. The product was purified through preparative TLC eluting with EtOAc: hexane=8:2 to furnish the TDBPS protected intermediate (1.1g, 1.74mmol, 84%). Then, the intermediate (1.10g, 1.27mmol) was dissolved into methanol and deprotected by cesium fluoride (330mg, 2.2mmol) in room temperature for 15 minutes. The final product was yielded in brown solid (730mg, 1.15mmol, 66.1% after second step reaction).

N-hydroxy-7-(4-(4-(((2R,3R,4S,5S,6R)-3,4,5-trihydroxy-6-(hydroxymethyl)tetrahydro-2H-pyran-2-yl)oxy)phenyl)-1H-1,2,3-triazol-1-yl)heptanamide (**STR-V-53**). The **STR-V-167** (730mg, 1.15mmol) dissolved into MeOH (2mL) with the addition of sodium methoxide (0.5mL, 2.3mmol) for 1 h stirring. The hydrolysis reaction was completed with successful removal of acetate groups. Then, the reaction is neutralized by Ambolite IR120 Plus resin to adjust the pH=1. Noticed that some precipitates may crush out when methoxide was added if the reaction was in larger scale (>500mg), while the addition of Resin could rapidly eliminate the precipitation. The resin was filtered, and the filtrate was collected and evaporated to dryness via vacuum. The final product of crude **STR-V-53** was gained. To purify the final product, STR-V-53 was then re-dissolved into water (5mL) and wash of organic solvents (30mL 15% MeOH solution of DCM). The aqueous layer was collected and evaporated to dryness. To completely dry to final pure product, 1mL Acetonitrile+0.1mL water was applied for lyophilization. Final product in white solid was yielded in 460mg, 0.98mmol, 85.2%. ¹H NMR (700 MHz, DMSO) δ 10.33 (s, 1H), 8.48 (s, 1H), 7.76 (d, J = 8.6 Hz, 2H), 7.16 (d, J = 8.7 Hz, 2H), 5.76 (s, 0H), 5.42 (d, J = 3.5 Hz, 1H), 4.36 (t, J = 7.1 Hz, 2H), 3.63 (t, J = 9.2 Hz, 1H), 3.57 (m, 3.59-3.55, 4.2 Hz, 1H), 3.47 (m, 3.49-3.42, 2H), 3.38 (dd, J = 9.7, 3.5 Hz, 1H), 3.20 (t, J = 9.2 Hz, 1H), 1.93 (t, J = 7.4 Hz, 2H), 1.85 (p,

$J = 7.1$ Hz, 2H), 1.48 (p, $J = 7.3$ Hz, 2H), 1.27 (m, 1.32-1.22, 5H). ^{13}C NMR (176 MHz, MeOD) δ 171.5, 157.3, 147.2, 126.5, 124.5, 120.3, 117.1, 97.9, 73.5, 71.9, 70.1, 61.0, 50.0, 48.5, 48.1, 48.0, 47.6, 32.2, 29.7, 28.0, 25.7, 25.1. HRMS (ESI) m/z Calcd. for $\text{C}_{21}\text{H}_{31}\text{O}_8\text{N}_4$ $[\text{M}+\text{H}^+]$: 467.2136, found 467.2123.

(2R,3R,4S,5R,6R)-2-(acetoxymethyl)-6-((6-bromonaphthalen-2-yl)oxy)tetrahydro-2H-pyran-3,4,5-triyl triacetate (**STR-V-55**). Beta-D-glucose pentaacetate (3.31g, 8.49mmol) was mixed with 6-bromo-2-naphthol (2.34g, 10.18mmol) and dissolved in DCM (25mL) at 0 °C in ice bath. The Boron trifluoride etherate (1.6mL, 12.74mmol) was added drop-wisely into the reaction. The reaction was removed from ice and stir at room temperature for 30 minutes. Then, the reaction was heated up to reflux for 48 h in total. The solution was mixed with water (30mL) and extracted by DCM (30mL). The organic layer was collected and evaporated to dryness. The crude product was furnished via column chromatography (EtOAc: hexane=3:7), where the product should elute in 40% Rf. Final product was yielded as 523mg, 80%. The product **STR-V-55** was directly used for the next reaction. ^1H NMR (400 MHz, cdcl_3) δ 7.95 (d, $J = 2.0$ Hz, 1H), 7.71 (d, $J = 9.0$ Hz, 1H), 7.61 (d, $J = 8.7$ Hz, 1H), 7.53 (dd, $J = 8.8, 2.0$ Hz, 1H), 7.43 (d, $J = 2.5$ Hz, 1H), 7.33 – 7.25 (m, 2H), 5.88 (d, $J = 3.6$ Hz, 1H), 5.75 (t, $J = 10.3$, 1H), 5.19 (t, $J = 9.4$ Hz, 1H), 5.10 (dd, $J = 10.3, 3.6$ Hz, 1H), 4.30-4.23 (m, 1H), 4.13 (ddd, $J = 10.2, 4.6, 2.1$ Hz, 1H), 4.05 (d, $J = 12.3$ Hz, 1H), 2.13 – 2.00 (m, 9H), 1.99 (s, 3H).

(2R,3R,4S,5R,6R)-2-(acetoxymethyl)-6-((6-ethynynaphthalen-2-yl)oxy)tetrahydro-2H-pyran-3,4,5-triyl triacetate (**STR-V-111**). **STR-V-55** (354mg, 0.63mmol), TMS-acetylene (0.13mL,

0.95mmol), Bis(triphenylphosphine)palladium(II) dichloride (9mg, 0.013mmol), copper iodide (3.4mg, 0.02mmol) and TPP (2.5mg, 0.0095mmol) was dissolved into THF (3mL) with TEA addition (0.17mL). The reaction was kept stirring in room temperature for 72 h. The solution was filtered through celite and solution was evaporated. The crude product was purified directly through column with solvents EtOAc: hexane=1:2 to gain purified intermediate 250mg, 0.5mmol, 79.3%. Then, the intermediate product (45mg, 0.08mmol) was immediately dissolved into DCM with addition of TBAF (0.08mL, 0.08mmol) to remove TMS group. The crude product was furnished via column chromatography (EtOAc: hexane=3:7), the final product **STR-V-111** was gained as brown solid 30mg, 0.06mmol, 75%. ¹H NMR (700 MHz, CDCl₃) δ 7.94 (d, *J* = 13.6 Hz, 1H), 7.73 (d, *J* = 9.0 Hz, 1H), 7.67 (dd, *J* = 15.7, 8.7 Hz, 1H), 7.59 (d, *J* = 8.7 Hz, 1H), 7.50 (dd, *J* = 13.6, 8.6 Hz, 1H), 7.41 (t, *J* = 3.3 Hz, 1H), 7.30 – 7.25 (m, 1H), 5.86 (dd, *J* = 10.2, 3.5 Hz, 1H), 5.72 (td, *J* = 9.9, 2.4 Hz, 1H), 5.16 (t, *J* = 9.9 Hz, 1H), 5.08 (dt, *J* = 10.4, 3.4 Hz, 1H), 4.26 – 4.21 (m, 1H), 4.11 (dd, *J* = 10.6, 4.4 Hz, 1H), 4.03 (d, *J* = 12.5 Hz, 1H), 3.11 (s, 1H), 2.06 – 2.01 (m, 9H), 1.96 (s, 3H).

N-hydroxy-7-(4-(6-(((2R,3R,4S,5S,6R)-3,4,5-trihydroxy-6-(hydroxymethyl)tetrahydro-2H-pyran-2-yl)oxy)naphthalen-2-yl)-1H-1,2,3-triazol-1-yl)heptanamide (**STR-V-114**). **STR-V-111** (29mg, 0.06mmol), **STR-V-107** (30mg, 0.07mmol), copper sulfate (1.5mg, 0.006mmol), sodium ascorbate (4.75mg, 0.024mmol), ethanol (1.5mL) and tert-butanol (1.5mL) was used for click reaction. The procedures of reaction setup and work-up was described for **STR-V-166** synthesis. Later, the intermediate **STR-V-113** (53mg, 0.057mmol, 95%) was deprotected by CsF (17mg, 0.114mmol) in MeOH (2mL). Then, the hydroxamate intermediate was worked up with extraction of ethyl acetate and re-dissolved into methanol for deprotection of glucose with NaOMe (25% in

methanol) (0.08mL, 0.342mmol). Followed by the procedure described in **STR-V-53** synthesis, final product was yield as white solid (9mg, 31%). ¹H NMR (700 MHz, DMSO) δ 10.33 (s, 1H), 8.14 (s, 1H), 7.95-7.89 (m, 1H), 7.89-7.76 (m, 3H), 7.58 (d, *J* = 9.6 Hz, 2H), 7.35-7.29 (m, 2H), 5.56 (t, *J* = 2.6 Hz, 1H), 3.67 (t, *J* = 9.5 Hz, 1H), 3.56 (d, *J* = 10.5 Hz, 1H), 3.47 (d, *J* = 9.1 Hz, 2H), 3.42 (dt, *J* = 9.8, 2.7 Hz, 1H), 3.31 (t, *J* = 7.0 Hz, 2H), 3.21 (t, *J* = 9.2 Hz, 1H), 3.17 (d, *J* = 1.9 Hz, 0H), 1.93 (t, *J* = 7.4 Hz, 2H), 1.50 (dp, *J* = 22.8, 7.4 Hz, 4H), 1.28 (dq, *J* = 32.1, 7.7 Hz, 6H). HRMS (ESI) *m/z* Calcd. for C₂₅ H₃₃ O₈ N₄ [M+H⁺]: 517.2293, found 517.2272.

N-(2-amino-5-fluorophenyl)-7-(4-(4-(((2R,3R,4S,5S,6R)-3,4,5-trihydroxy-6-(hydroxymethyl)tetrahydro-2H-pyran-2-yl)oxy)phenyl)-1H-1,2,3-triazol-1-yl)heptanamide (**STR-V-155**). **STR-V-51** (97mg, 0.21mmol) was mixed with N-(2-amino-4-fluorophenyl)-7-azidoheptanamide (75mg, 0.21mmol) and copper iodide (21mg, 0.11mmol) in THF/DMSO (1:1mL) solution. Argon was purged into the solution for 5-10 minutes before 10v/v% addition of Hunig's base. The reaction and work-up procedures were described in synthesis of **STR-V-183**. This clicked intermediate (136mg, 0.19mmol, 90.5%) was re-dissolved into MeOH (2mL) with addition of sodium methoxide (0.34mL, 1.49mmol). The following process of deprotection of acetate group and purification was followed by procedure described for **STR-V-53** synthesis. The final product was yielded 29mg (27.4%). ¹H NMR (700 MHz, DMSO) δ 9.09 (s, 1H), 8.50 – 8.43 (m, 1H), 7.75 (td, *J* = 5.0, 4.5, 2.0 Hz, 2H), 7.18 – 7.13 (m, 2H), 5.42 (d, *J* = 3.5 Hz, 1H), 5.07 (d, *J* = 6.3 Hz, 1H), 4.96 (dd, *J* = 26.6, 5.3 Hz, 2H), 4.76 (s, 1H), 4.48 (t, *J* = 5.7 Hz, 1H), 4.37 (dt, *J* = 15.9, 8.4 Hz, 2H), 3.63 (td, *J* = 9.2, 4.9 Hz, 1H), 3.56 (dt, *J* = 10.2, 5.3 Hz, 1H), 3.46 (dt, *J* = 9.4, 5.8 Hz, 2H), 3.37 (ddd, *J* = 9.8, 6.3, 3.6 Hz, 1H), 3.19 (td, *J* = 9.0, 5.6 Hz, 1H), 2.30 (dt, *J* = 17.5,

9.3 Hz, 1H), 1.86 (tt, $J = 17.0, 7.8$ Hz, 2H), 1.57 (dp, $J = 14.1, 7.4$ Hz, 1H), 1.39 – 1.21 (m, 4H). ^{13}C NMR (176 MHz, MeOD) δ 173.4, 157.3, 156.4, 155.0, 147.2, 137.4, 137.1, 126.5, 124.6, 120.3, 117.8, 117.2, 112.7, 112.6, 111.6, 111.4, 97.9, 73.6, 73.1, 71.9, 70.1, 61.0, 50.0, 48.0, 47.9, 47.7, 47.6, 47.5, 47.4, 47.3, 35.7, 35.7, 29.7, 28.2, 25.7, 25.2, 25.1. HRMS (ESI) m/z Calcd. for $\text{C}_{27}\text{H}_{35}\text{O}_7\text{N}_5\text{F}$ [$\text{M}+\text{H}^+$]: 560.2515, found 560.2503.

N-(2-amino-4-fluorophenyl)-7-(4-(4-(((2R,3R,4S,5S,6R)-3,4,5-trihydroxy-6-(hydroxymethyl)tetrahydro-2H-pyran-2-yl)oxy)phenyl)-1H-1,2,3-triazol-1-yl)heptanamide (**STR-V-157**). **STR-V-51** (104mg, 0.23mmol), N-(2-amino-5-fluorophenyl)-7-azidoheptanamide (81mg, 0.23mmol), CuI (22mg, 0.12mmol) and Hunig's base (0.2mL, 10v/v%) in THF-DMSO solution (1:1mL) was processed for click reaction followed by procedure of **STR-V-183**. The intermediate (137mg, 0.19mmol, 91%) was gained and deprotected by NaOMe (0.34mL, 1.51mmol) in MeOH followed by procedure described in synthesis of **STR-V-53**. The final product yielded as yellow solid (21mg, 20%). ^1H NMR (700 MHz, DMSO) δ 9.00 (s, 1H), 8.48 (s, 1H), 7.88 – 7.61 (m, 2H), 7.15 (d, $J = 8.8$ Hz, 2H), 7.07 (dd, $J = 8.9, 6.6$ Hz, 1H), 6.46 (dd, $J = 11.2, 2.8$ Hz, 1H), 6.28 (td, $J = 8.5, 2.8$ Hz, 1H), 5.41 (d, $J = 3.5$ Hz, 1H), 4.37 (t, $J = 7.1$ Hz, 2H), 3.62 (t, $J = 9.2$ Hz, 1H), 3.58 – 3.53 (m, 1H), 3.46 (dt, $J = 13.9, 5.9$ Hz, 2H), 3.37 (dd, $J = 9.8, 3.6$ Hz, 1H), 3.18 (t, $J = 9.3$ Hz, 1H), 2.27 (t, $J = 7.5$ Hz, 2H), 1.86 (q, $J = 7.3$ Hz, 2H), 1.57 (p, $J = 7.5$ Hz, 2H), 1.32 (dq, $J = 33.2, 7.8$ Hz, 4H). ^{13}C NMR (176 MHz, MeOD) δ 173.9, 157.3, 151.7, 147.2, 127.5, 126.5, 120.2, 119.1, 117.1, 103.6, 102.4, 97.9, 73.5, 70.1, 60.9, 49.9, 48.0, 47.8, 47.7, 47.6, 47.5, 47.4, 47.2, 35.5, 29.7, 25.8, 25.3. HRMS (ESI) m/z Calcd. for $\text{C}_{27}\text{H}_{35}\text{O}_7\text{N}_5\text{F}$ [$\text{M}+\text{H}^+$]: 560.2515, found 560.2511.

(2R,3R,4S,5R,6S)-2-(acetoxymethyl)-6-(4-(1-(7-(hydroxyamino)-7-oxoheptyl)-1H-1,2,3-triazol-4-yl)phenoxy)tetrahydro-2H-pyran-3,4,5-triyl triacetate (**STR-V-176**). **STR-I-190** (67mg, 0.15mmol), **STR-V-107** (67mg, 0.16mmol), copper sulfate (3.73mg, 0.015mmol), Sodium ascorbate (12mg, 0.06mmol), tert-butanol (1.5mL) and ethanol (1.5mL) were used for click reaction follow by the procedure mentioned in synthesis of **STR-V-167**. The protected intermediate (91mg, 0.1mmol, 66.7%) was gained and deprotected by cesium fluoride (32mg, 0.20mmol) in MeOH (2mL), the reaction and work-up procedures were described for **STR-V-53** synthesis. Later, the crude product was then dried and furnished through preparative TLC with condition of DCM:MeOH=9:1. The final product yielded as white solid (15mg, 23.6%). ¹H NMR (700 MHz, CDCl₃) δ 7.81 – 7.68 (m, 3H), 7.12 (d, *J* = 8.1 Hz, 2H), 5.56 – 5.51 (m, 2H), 5.43 (dd, *J* = 3.6, 1.8 Hz, 1H), 5.35 (t, *J* = 10.1 Hz, 1H), 4.34 (t, *J* = 6.6 Hz, 2H), 4.25 (dd, *J* = 12.2, 5.2 Hz, 1H), 4.10 – 4.02 (m, 2H), 2.18 (s, 3H), 2.14 – 2.08 (m, 2H), 2.04 – 1.98 (m, 9H), 1.90 – 1.86 (m, 2H), 1.60 (s, 2H), 1.31 (d, *J* = 26.4 Hz, 6H). ¹³C NMR (176 MHz, MeOD) δ 171.3, 170.2, 155.5, 147.1, 127.0, 125.3, 120.1, 116.9, 95.7, 77.7, 77.5, 77.3, 69.2, 69.1, 65.8, 62.1, 50.2, 49.2, 48.7, 48.6, 48.5, 48.4, 48.2, 48.1, 48.0, 32.4, 29.8, 29.5, 28.1, 25.8, 25.1, 20.3, 20.2. HRMS (ESI) *m/z* Calcd. for C₂₉H₃₉O₁₂N₄ [M+H⁺]: 635.2559, found 635.2552.

N-hydroxy-7-(4-(4-(((2S,3R,4S,5S,6R)-3,4,5-trihydroxy-6-(hydroxymethyl)tetrahydro-2H-pyran-2-yl)oxy)phenyl)-1H-1,2,3-triazol-1-yl)heptanamide (**STR-I-195**). Followed by the procedure of deprotection of acetate groups in synthesis of **STR-V-53**, **STR-V-176** (13mg, 0.02mmol) was deprotected by NaOMe (0.1mL, 0.495mmol) in MeOH (1mL). The final product

was yielded as pale-yellow foam (4.95mg, 0.011mmol, 55%). ^1H NMR (400 MHz, dmso) δ 10.31 (s, 4H), 8.47 (s, 1H), 7.73 (d, J = 8.7 Hz, 2H), 7.13 (d, J = 8.6 Hz, 2H), 5.38 (d, J = 1.8 Hz, 1H), 4.34 (t, J = 7.1 Hz, 2H), 3.82 (s, 1H), 3.71 – 3.53 (m, 2H), 3.53 – 3.20 (m, 4H), 1.94 – 1.76 (m, 4H), 1.46 (d, J = 8.0 Hz, 2H), 1.25 (s, 6H). ^{13}C NMR (100 MHz, MeOD) δ 171.5, 156.6, 147.1, 126.6, 124.5, 120.3, 116.8, 98.7, 74.1, 71.0, 70.5, 66.9, 65.5, 61.3, 49.9, 48.3, 46.4, 32.2, 29.7, 28.0, 25.7, 25.1, 14.1, 7.9. HRMS (ESI) m/z Calcd. for $\text{C}_{21}\text{H}_{31}\text{O}_8\text{N}_4$ $[\text{M}+\text{H}^+]$: 467.2136, found 467.2136.

(2R,3R,4S,5R,6S)-2-(acetoxymethyl)-6-((6-bromonaphthalen-2-yl)oxy)tetrahydro-2H-pyran-3,4,5-triyl triacetate (**STR-II-30**). Mannose pentaacetate (1.48g, 3.8mmol), 6-bromo-2-naphthol (3.5g, 15.21mmol), boron trifluoride etherate (0.72mL, 5.70mmol), were dissolved in DCM as the procedure described in synthesis of **STR-V-55**. TLC condition for the reaction is EtOAc:hexane=4:6. The final product yielded 1.34g (64%) without purification. ^1H NMR (400 MHz, CDCl_3) δ 7.94 (d, J = 2.3 Hz, 1H), 7.77 – 7.66 (m, 1H), 7.63 – 7.38 (m, 3H), 7.31 – 7.23 (m, 1H), 5.67 (d, J = 1.9 Hz, 1H), 5.60 (dd, J = 10.0, 3.5 Hz, 1H), 5.49 (dd, J = 3.6, 1.9 Hz, 1H), 5.39 (t, J = 10.0 Hz, 1H), 4.29 (dd, J = 12.0, 5.2 Hz, 1H), 4.16 – 4.03 (m, 2H), 2.22 (s, 3H), 2.05 (s, 3H), 1.95 (s, 3H). HRMS (ESI) m/z Calcd. for $\text{C}_{24}\text{H}_{25}\text{O}_{10}\text{BrNa}$ $[\text{M}+\text{Na}^+]$: 707.2535, found 707.2515.

(2R,3R,4S,5R,6S)-2-(acetoxymethyl)-6-((6-ethynynaphthalen-2-yl)oxy)tetrahydro-2H-pyran-3,4,5-triyl triacetate (**STR-II-34**). **STR-II-30** (301mg, 0.54mmol), Tetrakis(triphenylphosphine)paladdium(0) (31mg, 0.027mmol), TMS-acetylene (0.14mL,

1.0mmol) were dissolved in Triethylamine (15mL) with DMF (1mL). The reaction was protected with Argon gas and heated to 60°C for 12 h. The crude product was filtered through celite to remove palladium. The filtrate was evaporated to dryness and purified through column with condition of EtOAc:hexane=4:6. This intermediate product (239mg, 0.45mmol, 84%, yellow solid) was gained. Then, the solid (233mg, 0.43mmol) was dissolved into THF (2mL) with addition of 1M TBAF (solution in methanol, 0.43mL, 0.43mmol) in ice bath. The reaction was stirred in room temperature for 24h. The TMS protected group was successfully removed and the final product was yielded as yellow solid (129mg, 0.26mmol, 60.4%). ¹H NMR (400 MHz, cdcl₃) δ 7.96 (t, *J* = 1.1 Hz, 1H), 7.74 (dd, *J* = 8.9, 0.7 Hz, 1H), 7.70 – 7.63 (m, 1H), 7.50 (dd, *J* = 8.5, 1.6 Hz, 1H), 7.45 (d, *J* = 2.5 Hz, 1H), 7.30 – 7.23 (m, 1H), 5.68 (d, *J* = 1.9 Hz, 1H), 5.60 (dd, *J* = 10.0, 3.5 Hz, 1H), 5.50 (dd, *J* = 3.5, 1.8 Hz, 1H), 5.39 (t, *J* = 10.0 Hz, 1H), 4.29 (dd, *J* = 12.1, 5.3 Hz, 1H), 4.15 – 4.03 (m, 2H), 3.13 (s, 1H), 2.22 (s, 3H), 2.05 (d, *J* = 1.7 Hz, 6H), 1.94 (s, 3H). HRMS (ESI) *m/z* Calcd. for C₂₆ H₂₆ O₁₀ Na [M+Na⁺]: 707.2535, found 707.2515.

(2R,3R,4S,5R,6S)-2-(acetoxymethyl)-6-((6-(1-(7-(hydroxyamino)-7-oxoheptyl)-1H-1,2,3-triazol-4-yl)naphthalen-2-yl)oxy)tetrahydro-2H-pyran-3,4,5-triyl triacetate (**STR-V-177**). **STR-II-34** (199mg, 0.4mmol), **STR-V-107** (120mg, 0.4mmol), and CuI (11.4mg, 0.06mmol) was mixed in the solution of THF-DMSO mixture (1.5:1.5mL). The procedure of reaction set-up and work-up was described in synthesis of **STR-V-180**. The intermediate was deprotected through CsF (32mg, 0.2mmol) in 2mL MeOH as described in **STR-V-53**. The product was furnished by DCM:MeOH=10:1 in Prep TLC and yielded as white solid (15mg, 0.03mmol, 7.5% after two steps). ¹H NMR (700 MHz, CDCl₃) δ 8.24 (s, 1H), 7.85 (d, *J* = 9.7 Hz, 2H), 7.80 (d, *J* = 8.8 Hz, 1H), 7.75 (d, *J* = 8.2 Hz, 1H), 7.45 (d, *J* = 2.4 Hz, 1H), 7.23 (s, 3H), 5.58 (dd, *J* = 10.0, 3.6 Hz,

1H), 5.47 (dd, $J = 3.6, 1.8$ Hz, 1H), 5.37 (t, $J = 10.1$ Hz, 1H), 4.38 (s, 2H), 4.27 (dd, $J = 12.3, 5.5$ Hz, 1H), 4.11 (ddd, $J = 10.2, 5.4, 2.3$ Hz, 1H), 4.05 (dd, $J = 12.3, 2.3$ Hz, 1H), 3.21 (t, $J = 6.8$ Hz, 4H), 2.19 (s, 3H), 2.12 (s, 3H), 2.02 (s, 3H), 1.92 (s, 3H), 1.60 (s, 4H), 1.54 (p, $J = 7.1$ Hz, 4H), 1.31 (q, $J = 14.1, 12.6$ Hz, 4H), 1.21 (s, 3H). HRMS (ESI) m/z Calcd. for $C_{33}H_{40}O_{12}N_4Na$ $[M+Na^+]$: 707.2535, found 707.2515.

N-hydroxy-7-(4-(6-(((2S,3R,4S,5S,6R)-3,4,5-trihydroxy-6-(hydroxymethyl)tetrahydro-2H-pyran-2-yl)oxy)naphthalen-2-yl)-1H-1,2,3-triazol-1-yl)heptanamide (**STR-II-36**). **STR-V-177** (219mg, 0.27mmol) was deprotected by NaOMe (0.5mL, 2.19mmol) in MeOH (2mL), and lyophilized to final product **STR-II-36** (90mg, 43%) followed by procedure described for **STR-V-53** synthesis. 1H NMR (400 MHz, dmsO) δ 10.31 (s, 1H), 8.64 (s, 1H), 8.31 (s, 2H), 7.98 – 7.80 (m, 4H), 7.56 (d, $J = 2.4$ Hz, 1H), 7.27 (dd, $J = 8.9, 2.5$ Hz, 1H), 5.53 (s, 1H), 4.39 (t, $J = 6.9$ Hz, 2H), 3.87 (dd, $J = 3.5, 1.8$ Hz, 1H), 3.72 (dd, $J = 9.1, 3.4$ Hz, 1H), 3.59 (d, $J = 10.8$ Hz, 1H), 3.55 – 3.38 (m, 4H), 1.95 – 1.84 (m, 4H), 1.48 (d, $J = 7.3$ Hz, 2H), 1.40 – 1.07 (m, 6H). ^{13}C NMR (101 MHz, cd_3od) δ 154.62, 134.3, 129.7, 129.4, 127.6, 126.1, 123.8, 123.7, 120.9, 119.2, 110.6, 98.8, 74.1, 70.6, 67.0, 61.3, 50.0, 47.8, 47.2, 47.0, 29.7, 28.0, 25.7, 25.0. HRMS (ESI) m/z Calcd. for $C_{25}H_{33}O_8N_4$ $[M+H^+]$: 517.2293, found 517.2283.

(E)-N-hydroxy-3-(4-(6-(((2S,3R,4S,5S,6R)-3,4,5-trihydroxy-6-(hydroxymethyl)tetrahydro-2H-pyran-2-yl)oxy)naphthalen-2-yl)-1H-1,2,3-triazol-1-yl)acrylamide (**STR-V-105**). **STR-II-30** (202mg, 0.365mmol), **STR-V-38** (240mg, 0.73mmol) were mixed with palladium (II) acetate (12.3mg, 0.05mmol) and tri(o-tolyl)phosphine (32.3mg, 0.11mmol) in Acetonitrile (3mL) for 5

minutes with Argon protection. Then, TEA (0.13mL, 0.91mmol) was added to the solution and heated to 90°C for 5 h with stirring. The solution was filtered by celite and the filtrate was evaporated by vacuum. The crude product was purified through column chromatography with solvent EtOAc:hexane=6:4 to collect the intermediate. Then, the intermediate product (87mg, 0.11mmol, 29%) was re-dissolved into DCM (1.5mL) with addition of TFA (0.5mL) and TIPS (0.1mL). The solution turned bright yellow with addition of TFA and returned to pale-yellow followed by adding TIPS dropwisely. The product was evaporated to dryness after 30 minutes stirring in room temperature. Then, the solutes were redissolved by MeOH (2mL) and deprotected by NaOMe followed by procedure described in synthesis of **STR-V-53**. The final product **STR-V-105** was yielded as brownish solid (24mg, 54%). ¹H NMR (700 MHz, DMSO) δ 10.77 (s, 1H), 8.01 (s, 1H), 7.89 (d, *J* = 8.9 Hz, 1H), 7.83 (d, *J* = 8.6 Hz, 1H), 7.67 (dd, *J* = 8.6, 1.7 Hz, 1H), 7.60 – 7.56 (m, 2H), 7.30 (dd, *J* = 8.9, 2.5 Hz, 1H), 6.54 (d, *J* = 15.8 Hz, 1H), 5.56 (d, *J* = 1.8 Hz, 1H), 3.89 (dd, *J* = 3.4, 1.9 Hz, 1H), 3.73 (dd, *J* = 9.2, 3.4 Hz, 1H), 3.60 (dd, *J* = 11.7, 2.1 Hz, 1H), 3.52 (t, *J* = 9.4 Hz, 1H), 3.48 (dd, *J* = 11.7, 6.1 Hz, 1H), 3.43 (m, 3.44-3.41, 1H). ¹³C NMR (176 MHz, MeOD) δ 155.3, 140.5, 135.3, 130.7, 129.8, 129.6, 128.8, 127.6, 123.5, 119.2, 116.4, 110.6, 98.8, 74.2, 71.0, 70.6, 67.0, 61.3, 48.5. HRMS (ESI) *m/z* Calcd. for C₁₉ H₂₂ O₈ N [M+H⁺]: 392.1340, found 392.1338.

(E)-N-hydroxy-3-(4-(6-(((2R,3R,4S,5S,6R)-3,4,5-trihydroxy-6-(hydroxymethyl)tetrahydro-2H-pyran-2-yl)oxy)naphthalen-2-yl)-1H-1,2,3-triazol-1-yl)acrylamide (**STR-V-115**). **STR-V-55** (156mg, 0.28mmol) was dissolved with **STR-V-38** (186mg, 0.56mmol) with Pd(OAc) (9.43mg, 0.042mmol), tri(o-tolyl)phosphine (26.34mg, 0.084mmol) and TEA (0.1mL, 0.74mmol) in Acetonitrile (3mL). The procedure to yield pure intermediate (57mg, 25%) was described in

synthesis of **STR-V-105**. The intermediate product (55mg, 0.07mmol) was deprotected by TFA(0.5mL) and TIPS (0.1mL) in DCM (1.5mL) as mentioned in procedure of **STR-V-105**. The crude product was deprotected again on acetate group of glucose by NaOMe (0.1mL, 0.42mmol) in MeOH (2mL) as described in **STR-V-53**. The final product was yielded as brownish solid (14mg, 52%). ¹H NMR (700 MHz, DMSO) δ 10.74 (s, 1H), 7.99 (s, 1H), 7.83 (dd, J = 45.6, 8.8 Hz, 2H), 7.64 (d, J = 8.6 Hz, 1H), 7.55 (d, J = 17.3 Hz, 2H), 7.29 (dd, J = 8.9, 2.7 Hz, 1H), 6.51 (d, J = 15.7 Hz, 1H), 5.73 (d, J = 2.7 Hz, 1H), 5.55 (d, J = 2.9 Hz, 1H), 3.65 (td, J = 9.3, 2.8 Hz, 1H), 3.56 – 3.52 (m, 1H), 3.46 (d, J = 9.5 Hz, 3H), 3.42 – 3.37 (m, 1H), 3.21 – 3.17 (m, 1H), 3.14 (d, J = 2.8 Hz, 1H). ¹³C NMR (176 MHz, MeOD) δ 156.0, 140.5, 135.3, 130.7, 129.7, 129.6, 128.8, 127.6, 123.5, 119.6, 110.9, 97.9, 73.6, 73.2, 71.9, 70.1, 61.0, 48.5. HRMS (ESI) m/z Calcd. for C₁₉H₂₂O₈N [M+H⁺]: 392.1340, found 392.1340.

(2S,3R,4S,6R)-4-(dimethylamino)-6-methyltetrahydro-2H-pyran-2,3-diyl diacetate (**STR-V-160**) Desosamine (2g, 11.41mmol) was mixed with Acetic anhydride (3.24mL, 34.24mmol) in DCM (60mL). The solution was stirred at room temperature with addition of DMAP (558mg, 4.57mmol). The reaction was completed and washed by water (50mL) and extracted by EtOAc (30mL*2). The EtOAc layer was collected and dried through sodium acetate and vacuum. The product was purified through column chromatography in DCM:MeOH=9.5:0.5 solution and was detected by Anisaldehyde staining. The eluted product was collected and dried. **STR-V-160** was yielded as white solid (2.48g, 80%). ¹H NMR (400 MHz, cdcl₃) δ 6.22 (d, J = 3.6 Hz, 1H), 5.03 (ddd, J = 11.1, 3.7, 0.8 Hz, 1H), 4.04 (dq, J = 12.3, 6.1, 2.2 Hz, 1H), 3.64 (d, J = 0.8 Hz, 1H), 3.13 (td, J = 11.6, 3.9 Hz, 1H), 2.29 (d, J = 0.8 Hz, 6H), 2.13 (d, J = 0.9 Hz, 3H), 2.04 (d, J = 0.8 Hz, 3H), 1.85 (ddd, J = 13.2, 4.2, 2.5 Hz, 1H), 1.48 – 1.33 (m, 1H), 1.21 (dd, J = 6.2, 0.9 Hz, 3H).

(2S,3R,4S,6R)-4-(dimethylamino)-2-(4-iodophenoxy)-6-methyltetrahydro-2H-pyran-3-yl acetate (**STR-V-161**). **STR-V-160** (104mg, 0.4mmol) was mixed with 4-iodophenol (135mg, 0.6mmol) and dissolved with DCM (3mL). The solution was cooled to ice bath for 10 minutes with Argon protection. Then, the Boron trifluoride etherate (1mL, 8mmol) was added slowly and dropwisely. The ice bath was removed after 10 minutes stirring, and the reaction lasted for 12 h at room temperature. The reaction was partitioned between DCM (30 mL) and water (30mL) and the two layers separated. The organic layer was washed with water (30 mL), dried over Na₂SO₄ and evaporated off to give a crude **STR-V-161**. The product was purified through column with ethyl acetate solvent, and the product **STR-V-161** was yielded as white solid (161mg, 95%). H NMR (400 MHz, cdcl₃) δ 7.60 – 7.51 (m, 2H), 6.80 – 6.72 (m, 2H), 5.07 (dd, J = 10.6, 7.5 Hz, 1H), 4.89 (dd, J = 7.5, 2.1 Hz, 1H), 3.83 – 3.54 (m, 1H), 2.82 (ddd, J = 12.3, 10.4, 4.3 Hz, 1H), 2.31 (d, J = 2.3 Hz, 6H), 2.16 – 2.03 (m, 3H), 1.87 – 1.78 (m, 1H), 1.61 (s, 1H), 1.46 (q, J = 12.8, 12.2 Hz, 1H), 0.89 – 0.77 (m, 1H).

(2S,3R,4S,6R)-4-(dimethylamino)-2-(4-ethynylphenoxy)-6-methyltetrahydro-2H-pyran-3-yl acetate (**STR-V-163**). **STR-V-161** (221mg, 0.53mmol) was coupled with TMS-acetylene (0.1mL, 0.65mmol) with catalyst CuI (4mg, 0.02mmol) and Bis(triphenylphosphine)palladium(II) dichloride (7.6mg, 0.01mmol), TEA (1.85mL, 13.25mmol) in THF (3mL). The solution was stirred at room temperature for 15 h and then filtered with celite. The filtrate was evaporated by vacuum to gain the crude product (198mg, 0.51mmol, 96.2%). The crude product was directly

deprotected with potassium carbonate (140mg, 1.02mmol) in MeOH (2mL) as describe in synthesis of STR-V-53. Noted that the acetylated group was also removed in the process. Product **STR-V-163** was yielded as yellow solid (105mg, 0.38mmol, 74%). ¹H NMR (700 MHz, DMSO) δ 7.43 (d, J = 8.7 Hz, 2H), 7.08 (d, J = 8.8 Hz, 2H), 5.53 (d, J = 3.5 Hz, 1H), 4.00 (s, 1H), 3.90 (dq, J = 12.5, 6.2, 2.2 Hz, 1H), 3.72 (d, J = 9.2 Hz, 1H), 2.46 (s, 7H), 2.42 – 2.39 (m, 3H), 1.88 (d, J = 12.8 Hz, 1H), 1.25 (s, 1H), 1.18 (d, J = 6.2 Hz, 1H), 1.09 (d, J = 6.2 Hz, 4H).

(2S,3R,4S,6R)-4-(dimethylamino)-2-(4-(1-(7-(hydroxyamino)-7-oxoheptyl)-1H-1,2,3-triazol-4-yl)phenoxy)-6-methyltetrahydro-2H-pyran-3-yl acetate (**STR-V-165**). Followed by procedure of **STR-V-53**, STR-V-163 (47mg, 0.17mmol) was converted to intermediate product (62mg, 52%) with copper sulfate (4.26mg, 0.017mmol), sodium ascorbate (13mg, 0.068mmol), in tert-butanol (1mL) and methanol (1mL). The product was purified through solution of DCM:MeOH:NH₄OH =8.5:1.5:0.2. The intermediate compound (58mg, 0.08mmol, 47.1%) was deprotected by CsF (25mg, 0.17mmol) in MeOH (2mL) for 30 minutes stirring at room temperature. The final product **STR-V-165** was purified through preparative TLC with solution of 15% MeOH in DCM with 2% NH₄OH (1M) and yielded 18.1mg, (0.04mmol, 48%). ¹H NMR (700 MHz, DMSO) δ 8.48 (s, 1H), 7.76 (dq, J = 8.8, 2.6, 2.1 Hz, 2H), 7.16 – 7.10 (m, 2H), 5.48 (d, J = 3.5 Hz, 1H), 4.35 (t, J = 7.1 Hz, 2H), 3.90 (dq, J = 12.6, 6.2, 2.1 Hz, 1H), 3.60 (dd, J = 10.6, 3.5 Hz, 1H), 3.00 (ddd, J = 12.0, 10.5, 3.9 Hz, 1H), 2.28 (s, 5H), 1.83 (td, J = 7.3, 3.5 Hz, 4H), 1.74 (ddd, J = 12.8, 4.1, 2.3 Hz, 1H), 1.44 (p, J = 7.2 Hz, 2H), 1.29 – 1.21 (m, 6H), 1.06 (d, J = 6.2 Hz, 2H). ¹³C NMR (176 MHz, MeOD) δ 171.7, 157.6, 147.9, 135.8, 134.7, 133.7, 130.7, 128.3, 127.3, 120.3, 117.6, 98.3, 77.9, 69.1, 66.0, 60.7, 53.8, 52.4, 50.7, 49.3, 48.8, 40.6, 32.9, 31.2, 30.3, 28.6, 26.8, 25.6, 21.2, 19.4. HRMS (ESI) m/z Calcd. for C₂₃ H₃₆ O₅ N₅ [M+H⁺]: 462.2711, found 462.2696.

7.4.3 Cell Culture:

The cell culture and viability assay protocol were described in our previous work.⁴³ In brief, VERO, and A549 cell lines were maintained in Dulbecco's Modified Eagle Medium (DMEM) (Corning, 10-017-CV), supplemented with 10% fetal bovine serum (FBS) (Corning, 35-010-CV). Hep-G2 cells were cultured in phenol red free Minimum Essential Medium (MEM) (Corning, 17-305-CV), supplemented with 10% fetal bovine serum (FBS). Cells were seeded into a 96-well plate (2000 counts/100uL) for 24 h prior to treatment and then treated with various drug concentrations for 72 h. All drugs were dissolved in DMEM/DMSO with DMSO concentration maintained at 1%. The effect of compounds on cell viability was measured using the MTS assay (CellTiter 96 Aqueous One Solution and CellTiter 96 Non-Radioactive Cell Proliferation Assays, Promega, Madison, WI) as described by the manufacturer. IC₅₀s were determined using Prism GraphPad 8.

7.4.4 Western blots analysis

The Western blot protocol was described in our previous work⁴³. In brief, Hep-G2 cells were seeded into 6-well plate at 1×10^6 /well in MEM for 24 h-48 h prior to treatment. Various concentrations of SAHA, **STR-V-53**, **STR-V-114**, **STR-I-195** solutions in DMSO were added to the cell culture such that the final DMSO level is 0.1%. Cells were treated for 24 h, washed with cold PBS, and lysed with RIPA buffer (120 μ L) (VWR, VWRVN653-100ML) buffer containing phosphatase inhibitor (Fisher Thermo, A32957) and protease inhibitor (Fisher Thermo, A32955).

The cell lysates were scraped, collected, and vortexed for 15s followed by sonication for 60s. The lysate was then centrifuged at 14000x rpm for 10 min and the supernatants were collected. The total protein concentration was determined using a BCA protein assay kit (BioVision, K813-2500). Based on the results from the BSA assay, the lysates were diluted to make equal protein concentration and 20-40 µg of each lysate was loaded to each well of the TGX MIDI 4-20% gel (Biorad, cat. 5671093) and ran at 150V for 70 min. The gel was then transferred on to the Turbo PDVF membrane (Biorad, 1704273) and after blocking with 5% BSA for 1-2 h, the membrane was incubated overnight with primary antibodies Ac-Tubulin (sc-23950), Ac-H4 (sc-515319) (Santa Cruz Biotechnology), caspase 3 and clv-Caspase 3 (Cell signaling Technology), anti-p21^{WAF/CIP} (ThermoFisher), anti-GAPDH (Aldrich-Sigma). The second day, the membrane was washed with TBST for 3x5 min; secondary antibody (LiCOR) was added, and the membrane was incubated with agitation for 1 h. After washing with TBS-T 3x5 mins, bands were quantified using Odyssey CLx Image system.

7.4.5 *GLUT-2 uptake competition test*

Hep-G2 or VERO cells were seeded (2500 to 4,000counts/well) into 96-well plates, in where each well contains 100 µL medium. The cells were cultured overnight with respective mediums described in section 4.2. Day 2, the cells were treated with 25 µM Phloretin for 24h. In day 3, 200x stock solutions of **STR-V-53** and SAHA were used to prepare 2x treatment solution by adding 1% stock solution in medium. Then, without removal of medium in 96-well plates, the same volumes of drug medium were add directly to the wells with gentle pipetting, to reach 1x drug solution with 25 µM Ph. In detail, the 200x stock solutions with 2.5mM Ph were made with mixture of 50 µL 400x stock solutions and 50 µL of 5 mM Ph solution. For examine, to make 100µM **STR-V-53** treatment solution, 50 µL of 40mM stock solution of **STR-V-53** would be mixed with 50 µL 5

mM Ph solution. Then 4 μ L of this stock solution were added to 396 μ L medium to make 20 μ M medium solution with 25 μ M Ph. Finally, the 100 μ L medium solution was added directly to the wells with gentle pipetting to form 1x medium solution of drug containing 25 μ M Ph. In this way, the original Ph from day 2 will remain inhibit GLUT-2 with no concentration change. After 72h, the medium was removed, and new medium (100 μ L) added to the wells. MTS solution (20 μ L) was added to each well. After 2.5-4 h incubation in incubator, the plates were read by plate reader at 490 nm. The data were processed by GraphPad Prism 8.

7.4.6 Flow cytometry

Hep-G2 cells (5×10^6) were seeded to 10 cm plate with MEM and incubated until 50% confluency prior to drug treatment. Cells were treated with DMSO (control) and DMSO solutions of SAHA (5 μ M) and **STR-V-53** (15 μ M), such that the final DMSO level is 0.1%, for another 48 h. Cells were washed with cold 1X PBS solution twice and trypsinized. Subsequently, cells were collected using 5mL 1x PBS buffer and fixed overnight at -20°C using 70% ethanol. Cells were centrifuged by 1x PBS in the day 2 at 4 °C with spin speed of 3,000g, re-suspended in 1X PBS and centrifuged again in the same condition. The supernatant was removed, and the cell pellets were re-suspended with 500 μ L of 200ug/mL RNase for 30 min. Then cells were treated with another 500 μ L of 100ug/mL PI staining at room temperature for 30 mins. The cell cycle was analyzed with BD FACS Aria Illu analyzer and the data was processed using FlowJo.

7.5 References:

1. Society, A. C., Global Cancer Facts & Figures 4th Edition. *Atlanta: American Cancer Society*.
2. Hopkins, B. D.; Goncalves, M. D.; Cantley, L. C., Obesity and cancer mechanisms: cancer metabolism. *Journal of clinical oncology* **2016**, 34 (35), 4277.
3. Soriano, A.; Varona, A.; Gianchandani, R.; Moneva, M. E.; Arranz, J.; Gonzalez, A.; Barrera, M., Selection of patients with hepatocellular carcinoma for liver transplantation: Past and future. *World journal of hepatology* **2016**, 8 (1), 58.
4. Sahil Mittal, S.; Hashem, B., El-Serag HB (2013) Epidemiology of HCC: Consider the Population. *Clin Gastroenterol* 47, S2-S6.
5. Siegel, A. B.; Conner, K.; Wang, S.; Jacobson, J. S.; Hershman, D. L.; Hidalgo, R.; Verna, E. C.; Halazun, K.; Brubaker, W.; Zaretsky, J., Smoking and hepatocellular carcinoma mortality. *Experimental and therapeutic medicine* **2012**, 3 (1), 124-128.
6. Caldwell, S. H.; Crespo, D. M.; Kang, H. S.; Al-Osaimi, A. M., Obesity and hepatocellular carcinoma. *Gastroenterology* **2004**, 127 (5), S97-S103.
7. Yang, J. D.; Ahmed, F.; Mara, K. C.; Addissie, B. D.; Allen, A. M.; Gores, G. J.; Roberts, L. R., Diabetes is associated with increased risk of hepatocellular carcinoma in patients with cirrhosis from nonalcoholic fatty liver disease. *Hepatology* **2020**, 71 (3), 907-916.
8. Yu, L.-X.; Ling, Y.; Wang, H.-Y., Role of nonresolving inflammation in hepatocellular carcinoma development and progression. *npj Precision Oncology* **2018**, 2 (1).
9. Refolo, M. G.; Messa, C.; Guerra, V.; Carr, B. I.; D'Alessandro, R., Inflammatory mechanisms of HCC development. *Cancers* **2020**, 12 (3), 641.
10. Llovet, J. M.; Fuster, J.; Bruix, J., Intention-to-treat analysis of surgical treatment for early hepatocellular carcinoma: resection versus transplantation. *Hepatology* **1999**, 30 (6), 1434-1440.
11. Kim, R. D.; Reed, A. I.; Fujita, S.; Foley, D. P.; Mekeel, K. L.; Hemming, A. W., Consensus and Controversy in the Management of Hepatocellular Carcinoma. *Journal of the American College of Surgeons* **2007**, 205 (1), 108-123.
12. Mazzaferro, V.; Regalia, E.; Doci, R.; Andreola, S.; Pulvirenti, A.; Bozzetti, F.; Montalto, F.; Ammatuna, M.; Morabito, A.; Gennari, L., Liver transplantation for the treatment of small hepatocellular carcinomas in patients with cirrhosis. *New England Journal of Medicine* **1996**, 334 (11), 693-700.
13. Health Care Rich, Resource Poor: Struggling with the National Shortage of Organs in Liver Transplantation. *AMA Journal of Ethics* **2016**, 18 (2), 95-194.
14. Llovet, J. M.; Ricci, S.; Mazzaferro, V.; Hilgard, P.; Gane, E.; Blanc, J.-F.; De Oliveira, A. C.; Santoro, A.; Raoul, J.-L.; Forner, A., Sorafenib in advanced hepatocellular carcinoma. *New England journal of medicine* **2008**, 359 (4), 378-390.
15. Mossenta, M.; Busato, D.; Baboci, L.; Di Cintio, F.; Toffoli, G.; Dal Bo, M., New insight into therapies targeting angiogenesis in hepatocellular carcinoma. *Cancers* **2019**, 11 (8), 1086.

16. Marisi, G.; Cucchetti, A.; Ulivi, P.; Canale, M.; Cabibbo, G.; Solaini, L.; Foschi, F. G.; De Matteis, S.; Ercolani, G.; Valgiusti, M., Ten years of sorafenib in hepatocellular carcinoma: Are there any predictive and/or prognostic markers? *World journal of gastroenterology* **2018**, *24* (36), 4152.
17. Hilmi, M.; Neuzillet, C.; Calderaro, J.; Lafdil, F.; Pawlowsky, J.-M.; Rousseau, B., Angiogenesis and immune checkpoint inhibitors as therapies for hepatocellular carcinoma: current knowledge and future research directions. *Journal for immunotherapy of cancer* **2019**, *7* (1), 1-13.
18. Freese, K.; Seitz, T.; Dietrich, P.; Lee, S. M.; Thasler, W. E.; Bosserhoff, A.; Hellerbrand, C., Histone deacetylase expressions in hepatocellular carcinoma and functional effects of histone deacetylase inhibitors on liver cancer cells in vitro. *Cancers* **2019**, *11* (10), 1587.
19. Yoon, S.; Eom, G. H., HDAC and HDAC inhibitor: from cancer to cardiovascular diseases. *Chonnam medical journal* **2016**, *52* (1), 1.
20. Yeo, W.; Chung, H. C.; Chan, S. L.; Wang, L. Z.; Lim, R.; Picus, J.; Boyer, M.; Mo, F. K.; Koh, J.; Rha, S. Y., Epigenetic therapy using belinostat for patients with unresectable hepatocellular carcinoma: a multicenter phase I/II study with biomarker and pharmacokinetic analysis of tumors from patients in the Mayo Phase II Consortium and the Cancer Therapeutics Research Group. *Journal of Clinical Oncology* **2012**, *30* (27), 3361.
21. Gryder, B. E.; Akbashev, M. J.; Rood, M. K.; Raftery, E. D.; Meyers, W. M.; Dillard, P.; Khan, S.; Oyeler, A. K., Selectively targeting prostate cancer with antiandrogen equipped histone deacetylase inhibitors. *ACS chemical biology* **2013**, *8* (11), 2550-2560.
22. Tapadar, S.; Fathi, S.; Wu, B.; Sun, C. Q.; Raji, I.; Moore, S. G.; Arnold, R. S.; Gaul, D. A.; Petros, J. A.; Oyeler, A. K., Liver-targeting class I selective histone deacetylase inhibitors potently suppress hepatocellular tumor growth as standalone agents. *Cancers* **2020**, *12* (11), 3095.
23. Liberti, M. V.; Locasale, J. W., The Warburg effect: how does it benefit cancer cells? *Trends in biochemical sciences* **2016**, *41* (3), 211-218.
24. Shang, R.-Z.; Qu, S.-B.; Wang, D.-S., Reprogramming of glucose metabolism in hepatocellular carcinoma: Progress and prospects. *World journal of gastroenterology* **2016**, *22* (45), 9933.
25. Mueckler, M.; Thorens, B., The SLC2 (GLUT) family of membrane transporters. *Molecular Aspects of Medicine* **2013**, *34* (2-3), 121-138.
26. Daskalow, K.; Pfander, D.; Weichert, W.; Rohwer, N.; Thelen, A.; Neuhaus, P.; Jonas, S.; Wiedenmann, B.; Benckert, C.; Cramer, T., Distinct temporospatial expression patterns of glycolysis-related proteins in human hepatocellular carcinoma. *Histochemistry and cell biology* **2009**, *132* (1), 21-31.
27. Leturque, A.; Brot-Laroche, E.; Le Gall, M.; Stolarczyk, E.; Tobin, V., The role of GLUT2 in dietary sugar handling. *Journal of physiology and biochemistry* **2005**, *61* (4), 529.

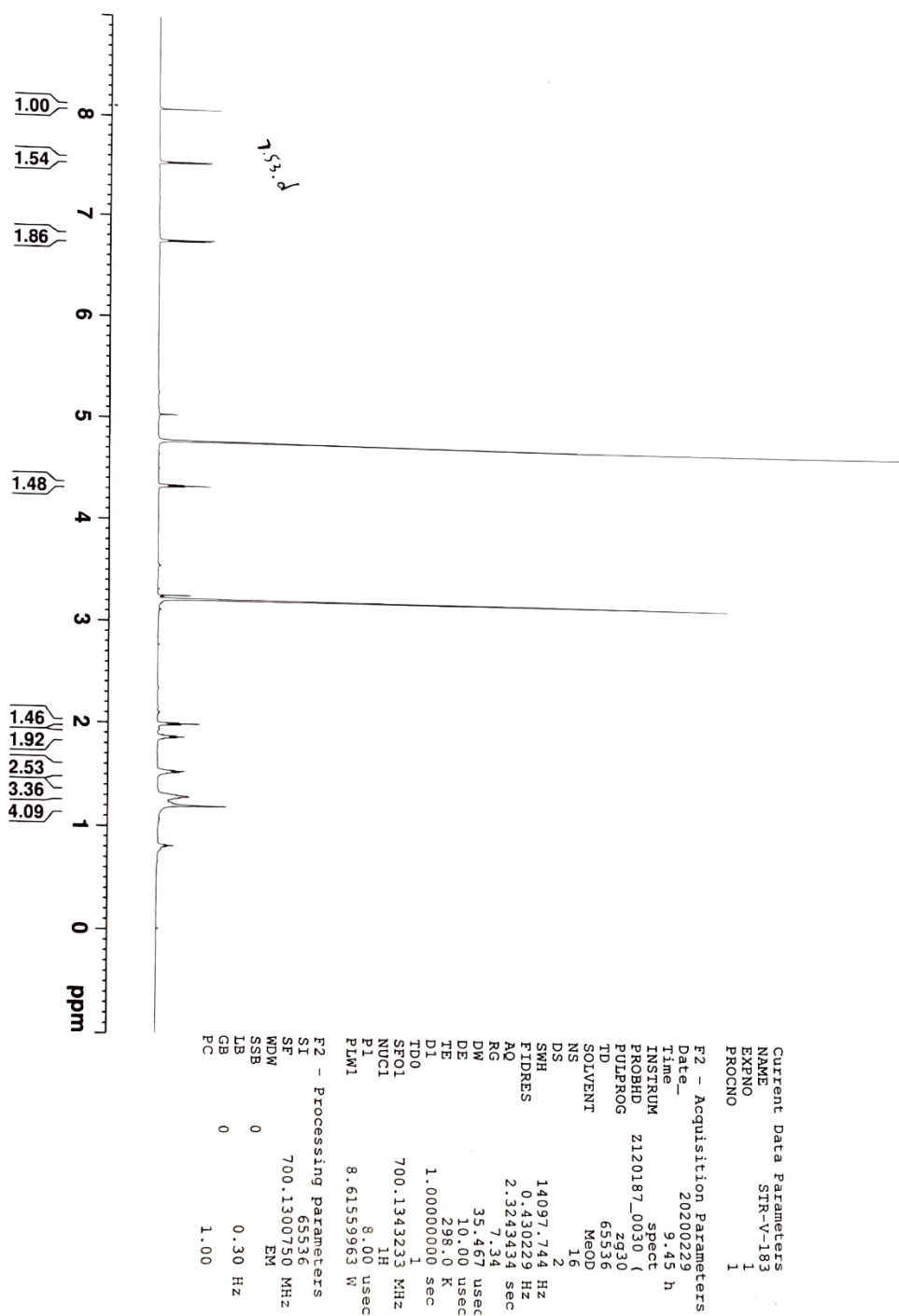
28. Gryder, B. E.; Sodji, Q. H.; Oyelere, A. K., Targeted cancer therapy: giving histone deacetylase inhibitors all they need to succeed. *Future medicinal chemistry* **2012**, *4* (4), 505-524.
29. Rostovtsev, V. V.; Green, L. G.; Fokin, V. V.; Sharpless, K. B., A stepwise Huisgen cycloaddition process: copper(I)-catalyzed regioselective "ligation" of azides and terminal alkynes. *Angew Chem Int Ed Engl* **2002**, *41* (14), 2596-9.
30. Pirali, T.; Pagliai, F.; Mercurio, C.; Boggio, R.; Canonico, P. L.; Sorba, G.; Tron, G. C.; Genazzani, A. A., Triazole-Modified Histone Deacetylase Inhibitors As a Rapid Route to Drug Discovery. *Journal of Combinatorial Chemistry* **2008**, *10* (5), 624-627.
31. Wang, F.; Zhang, Y.; Liu, Z.; Du, Z.; Zhang, L.; Ren, J.; Qu, X., A Biocompatible Heterogeneous MOF–Cu Catalyst for In Vivo Drug Synthesis in Targeted Subcellular Organelles. *Angewandte Chemie International Edition* **2019**, *58* (21), 6987-6992.
32. Pirali, T.; Gatti, S.; Di Brisco, R.; Tacchi, S.; Zaninetti, R.; Brunelli, E.; Massarotti, A.; Sorba, G.; Canonico, P. L.; Moro, L., Estrogenic analogues synthesized by click chemistry. *ChemMedChem: Chemistry Enabling Drug Discovery* **2007**, *2* (4), 437-440.
33. Chen, P. C.; Patil, V.; Guerrant, W.; Green, P.; Oyelere, A. K., Synthesis and structure–activity relationship of histone deacetylase (HDAC) inhibitors with triazole-linked cap group. *Bioorganic & medicinal chemistry* **2008**, *16* (9), 4839-4853.
34. Otsuka, I.; Hongo, T.; Nakade, H.; Narumi, A.; Sakai, R.; Satoh, T.; Kaga, H.; Kakuchi, T., Chiroptical and lectin recognition properties of glycoconjugated poly (phenylacetylene)s featuring variable saccharide functionalities. *Macromolecules* **2007**, *40* (25), 8930-8937.
35. Capicciotti, C. J.; Mancini, R. S.; Turner, T. R.; Koyama, T.; Alteen, M. G.; Doshi, M.; Inada, T.; Acker, J. P.; Ben, R. N., O-aryl-glycoside ice recrystallization inhibitors as novel cryoprotectants: a structure–function study. *ACS omega* **2016**, *1* (4), 656-662.
36. Moradei, O. M.; Mallais, T. C.; Frechette, S.; Paquin, I.; Tessier, P. E.; Leit, S. M.; Fournel, M.; Bonfils, C.; Trachy-Bourget, M.-C.; Liu, J.; Yan, T. P.; Lu, A.-H.; Rahil, J.; Wang, J.; Lefebvre, S.; Li, Z.; Vaisburg, A. F.; Besterman, J. M., Novel Aminophenyl Benzamide-Type Histone Deacetylase Inhibitors with Enhanced Potency and Selectivity. *Journal of Medicinal Chemistry* **2007**, *50* (23), 5543-5546.
37. Liang, L.; Astruc, D., The copper (I)-catalyzed alkyne-azide cycloaddition (CuAAC) "click" reaction and its applications. An overview. *Coordination Chemistry Reviews* **2011**, *255* (23-24), 2933-2945.
38. Trott, O.; Olson, A. J., AutoDock Vina: improving the speed and accuracy of docking with a new scoring function, efficient optimization, and multithreading. *Journal of computational chemistry* **2010**, *31* (2), 455-461.
39. Wu, B.; Fathi, S.; Mortley, S.; Mohiuddin, M.; Jang, Y. C.; Oyelere, A. K., Pyrimethamine conjugated histone deacetylase inhibitors: Design, synthesis and evidence for triple negative breast cancer selective cytotoxicity. *Bioorganic & medicinal chemistry* **2020**, *28* (6), 115345.

40. Caggia, S.; Tapadar, S.; Wu, B.; Venugopal, S. V.; Garrett, A. S.; Kumar, A.; Stiffend, J. S.; Davis, J. S.; Oyelere, A. K.; Khan, S. A., Small Molecule Inhibitors Targeting Gai2 Protein Attenuate Migration of Cancer Cells. *Cancers* **2020**, *12* (6), 1631.
41. Reiberger, T.; Chen, Y.; Ramjiawan, R. R.; Hato, T.; Fan, C.; Samuel, R.; Roberge, S.; Huang, P.; Lauwers, G. Y.; Zhu, A. X., An orthotopic mouse model of hepatocellular carcinoma with underlying liver cirrhosis. *Nature protocols* **2015**, *10* (8), 1264.
42. Lachenmayer, A.; Toffanin, S.; Cabellos, L.; Alsinet, C.; Hoshida, Y.; Villanueva, A.; Minguez, B.; Tsai, H.-W.; Ward, S. C.; Thung, S., Combination therapy for hepatocellular carcinoma: additive preclinical efficacy of the HDAC inhibitor panobinostat with sorafenib. *Journal of hepatology* **2012**, *56* (6), 1343-1350.
43. Wu, B.; Fathi, S.; Mortley, S.; Mohiuddin, M.; Jang, Y. C.; Oyelere, A. K., Pyrimethamine conjugated histone deacetylase inhibitors: Design, synthesis and evidence for triple negative breast cancer selective cytotoxicity. *Bioorg Med Chem* **2020**, *28* (6), 115345.
44. Gallant, M.; Truchon, J.-f.; Reddy, T. J.; Dietrich, E.; Vaillancourt, L.; Vallee, F., Mannose derivatives for treating bacterial infections. Google Patents: 2019.

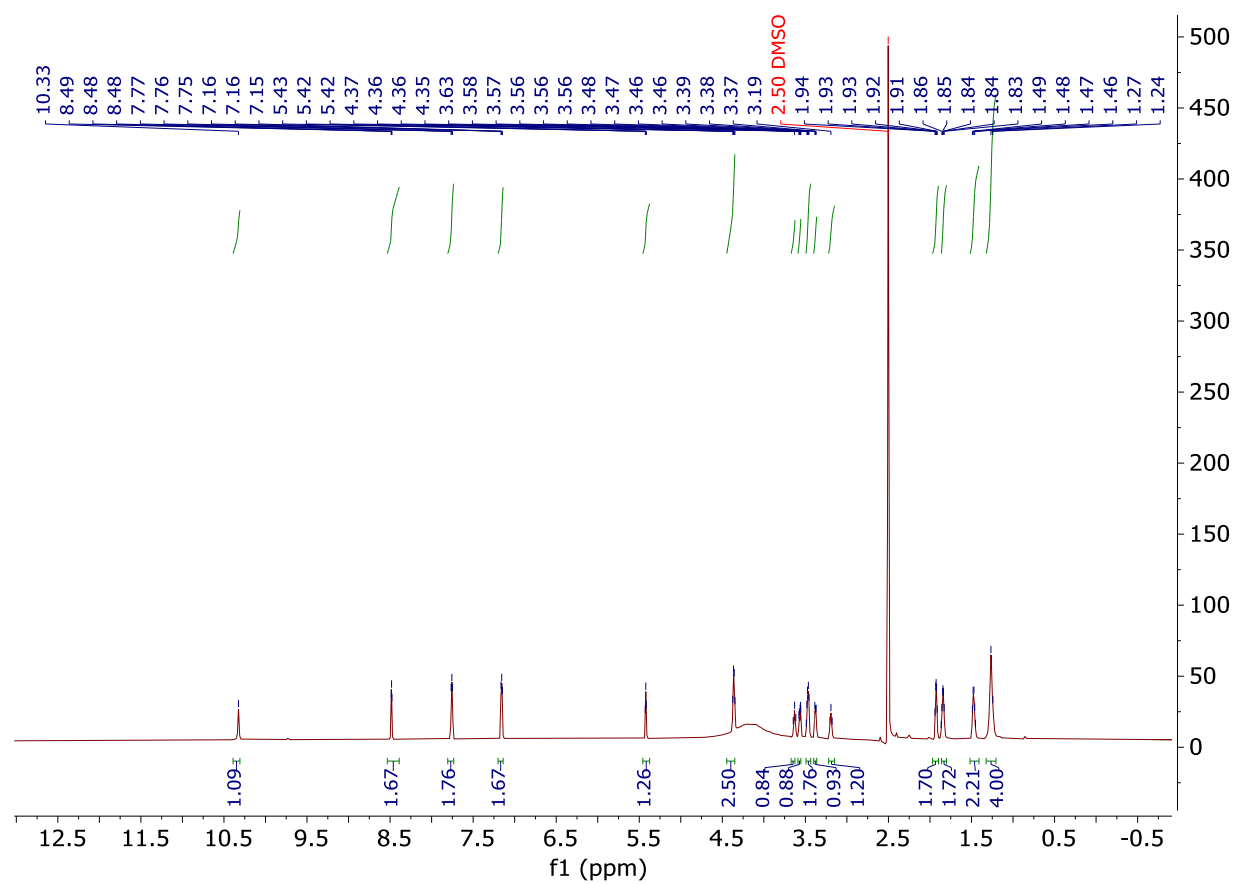
7.6 Supporting information

NMRs

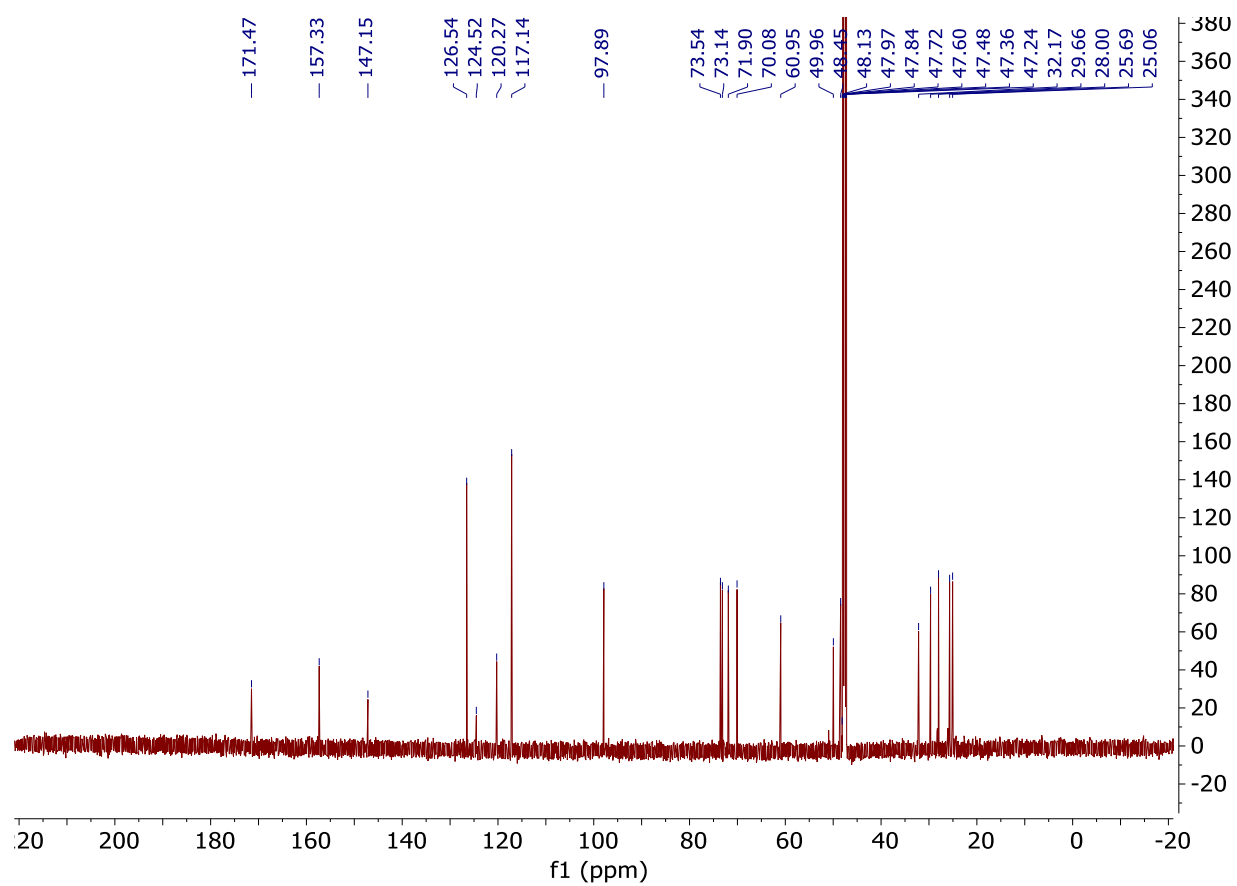
STR-V-183 (^1H)



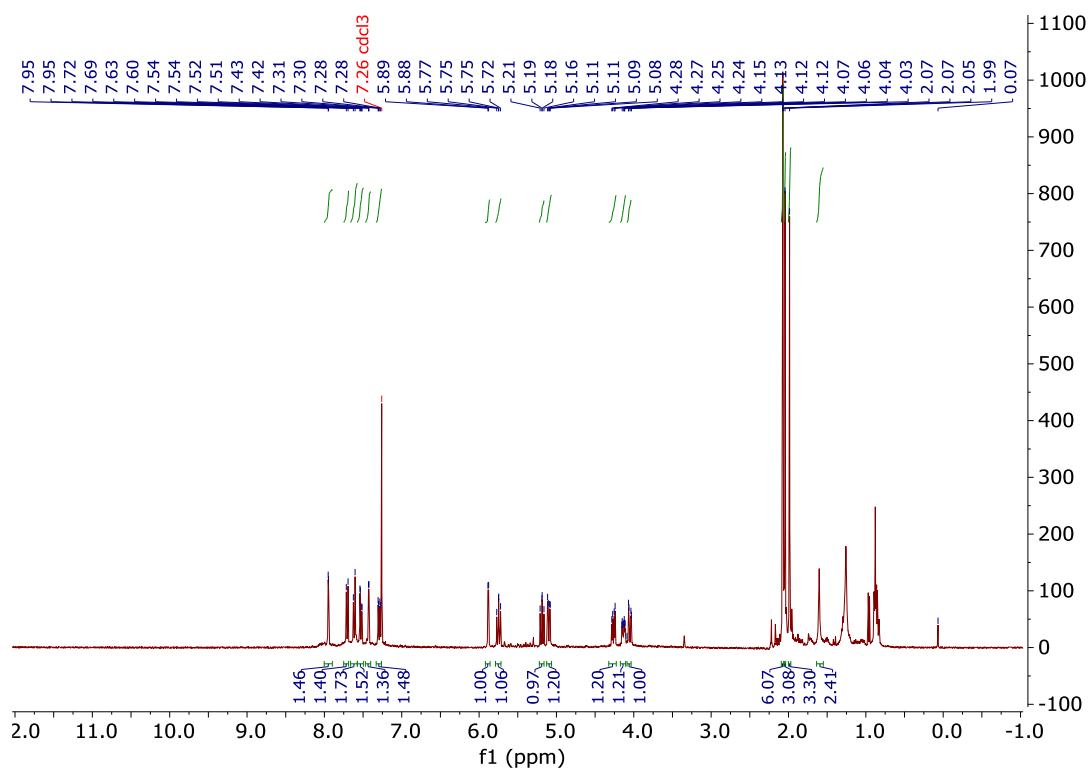
STR-V-53 (¹H)



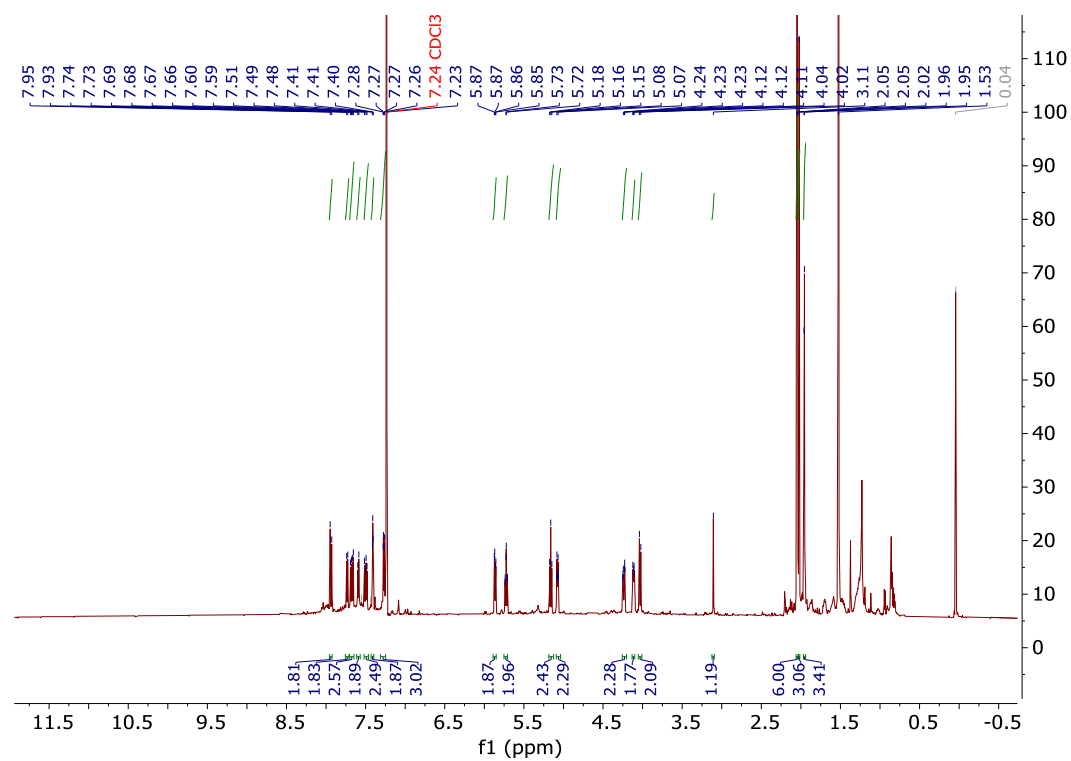
STR-V-53 (¹³C)



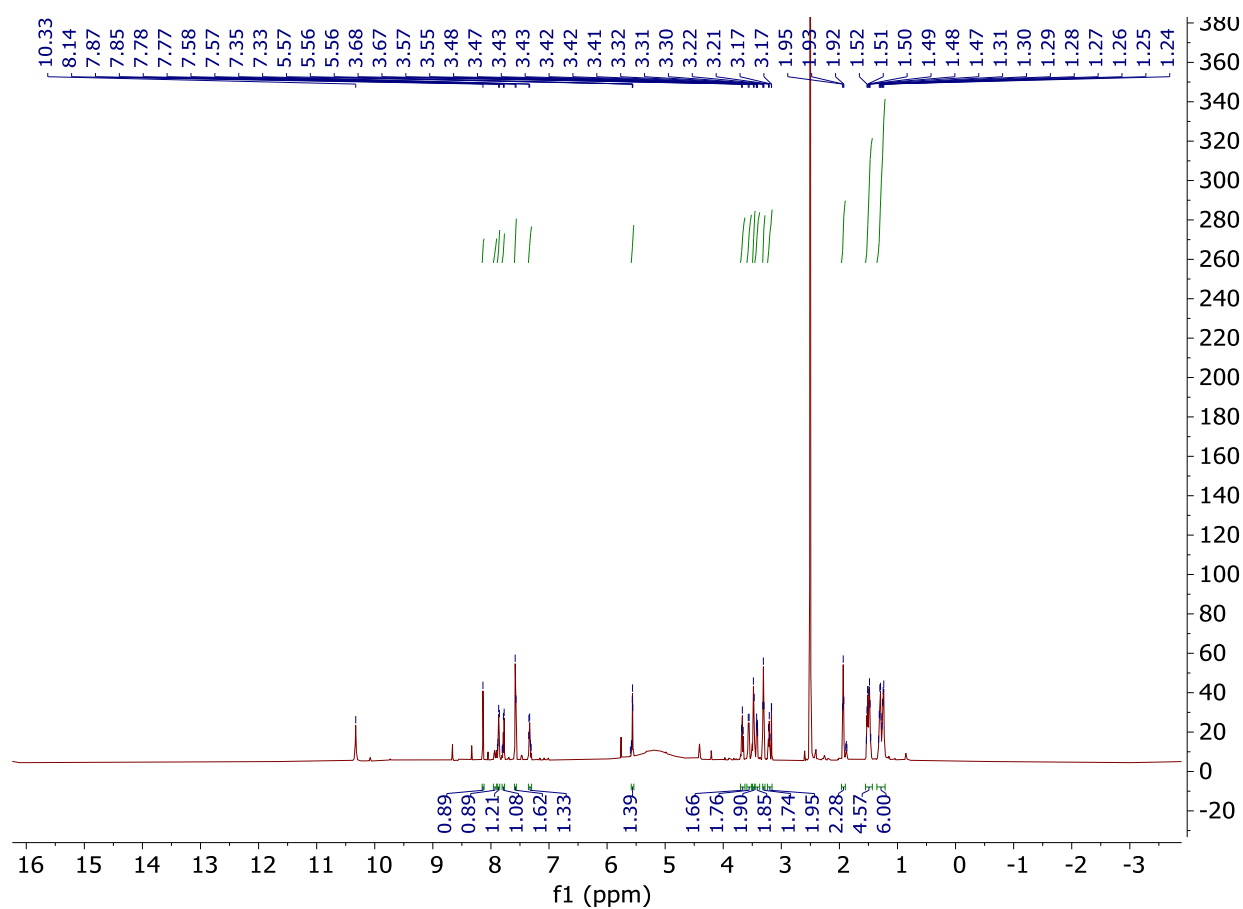
STR-V-55



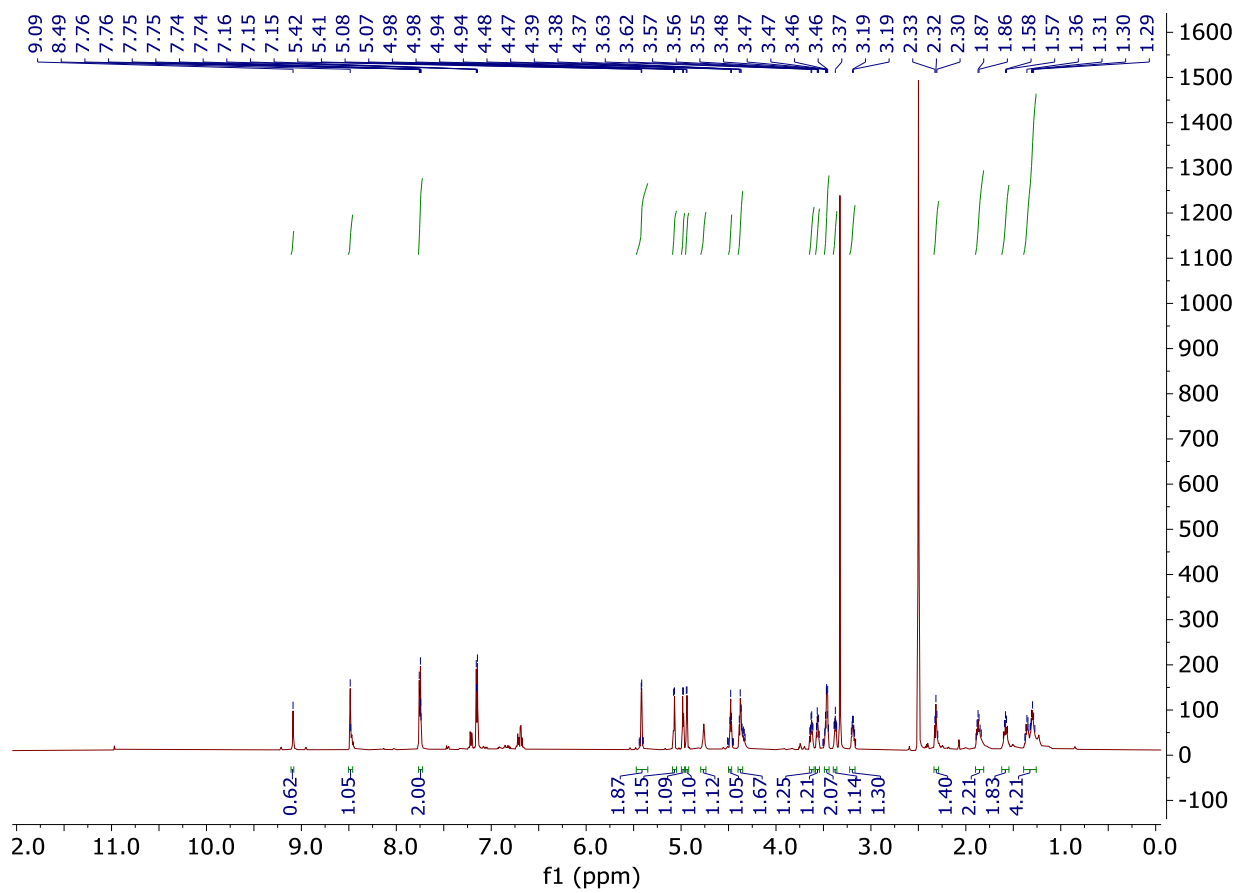
STR-V-111



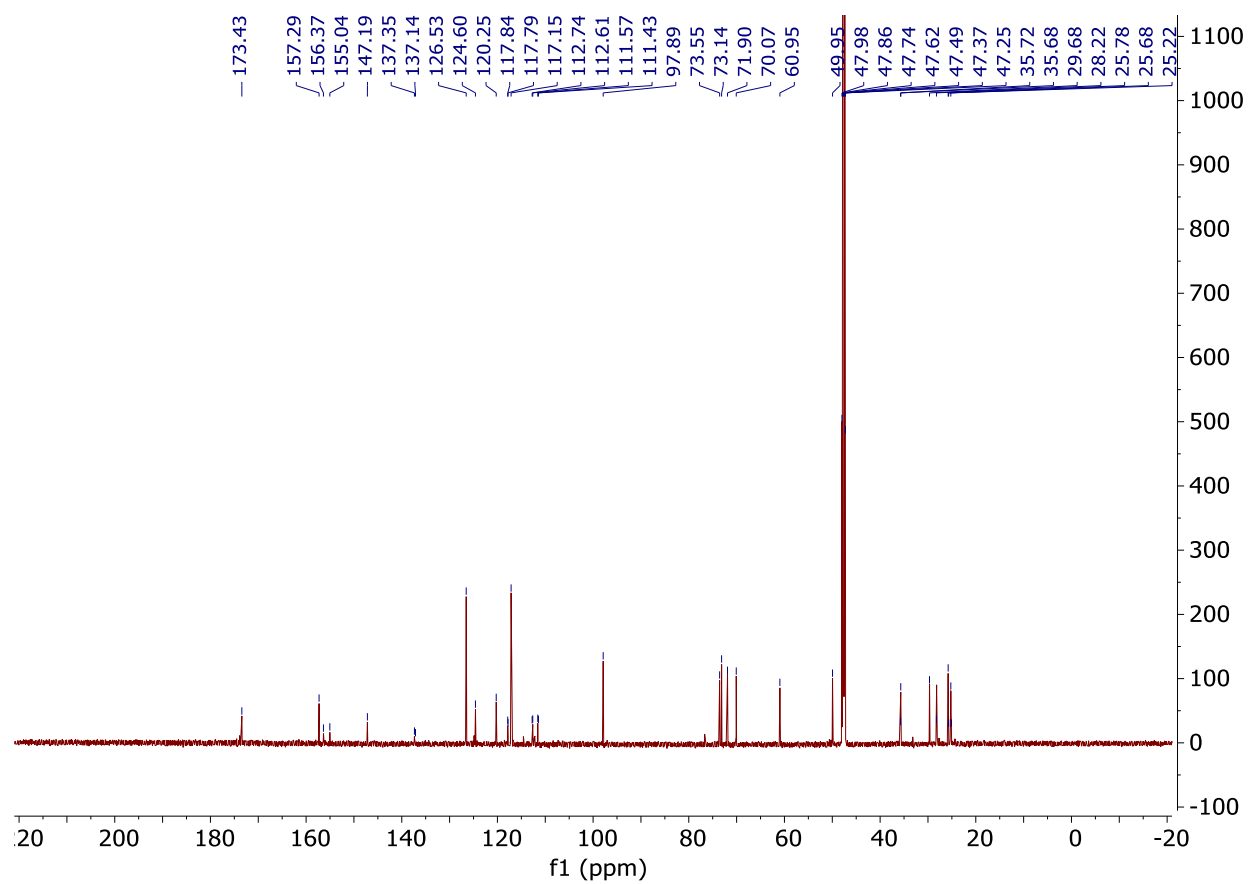
STR-V-114



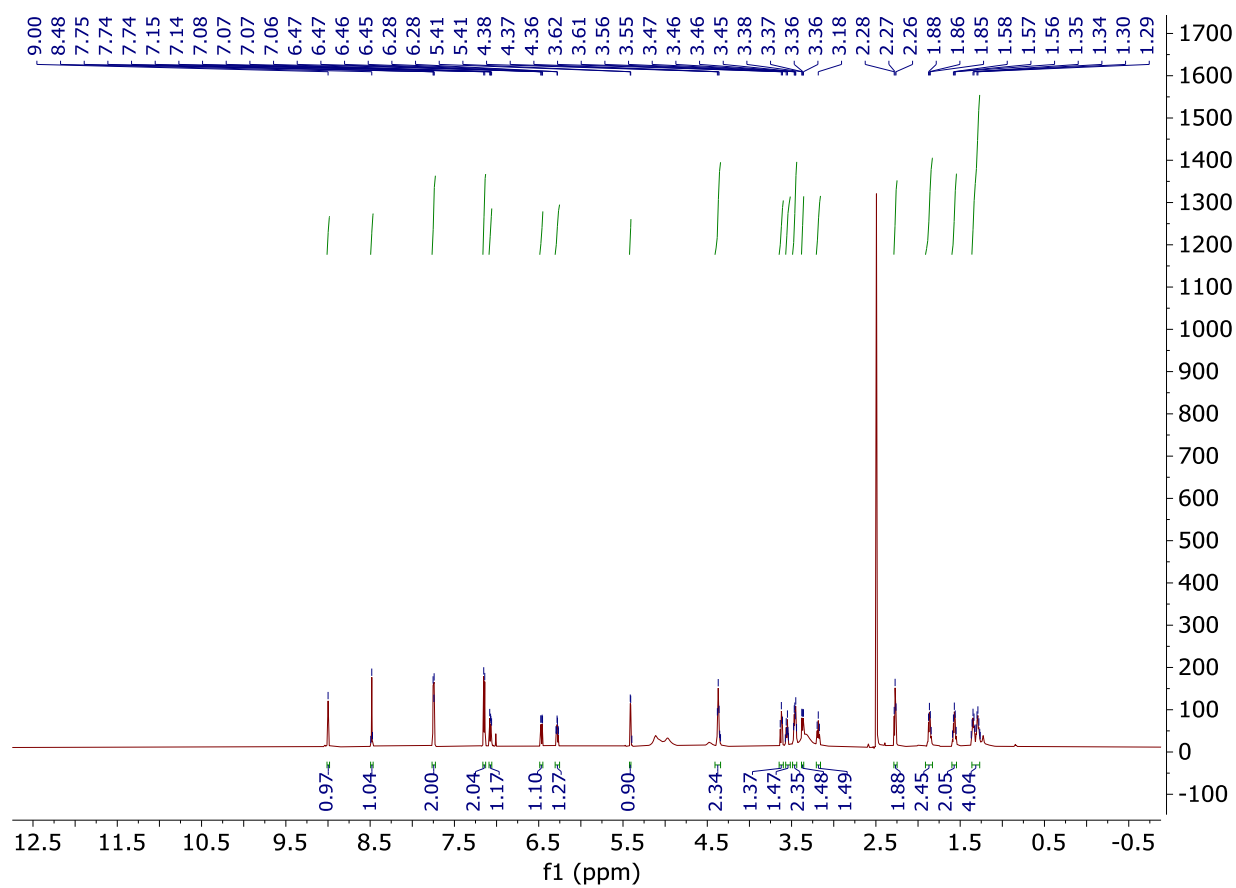
STR-V-155 (¹H)



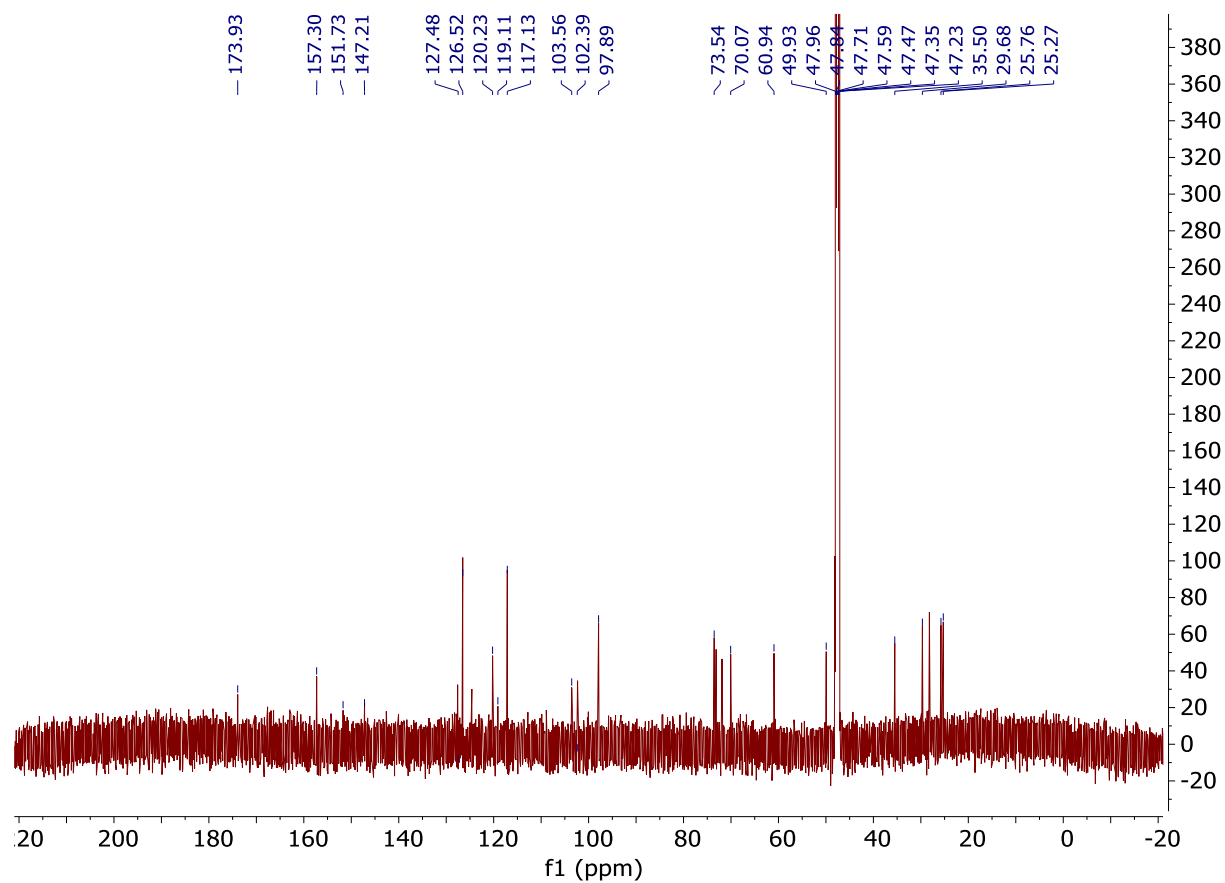
STR-V-155 (¹³C)



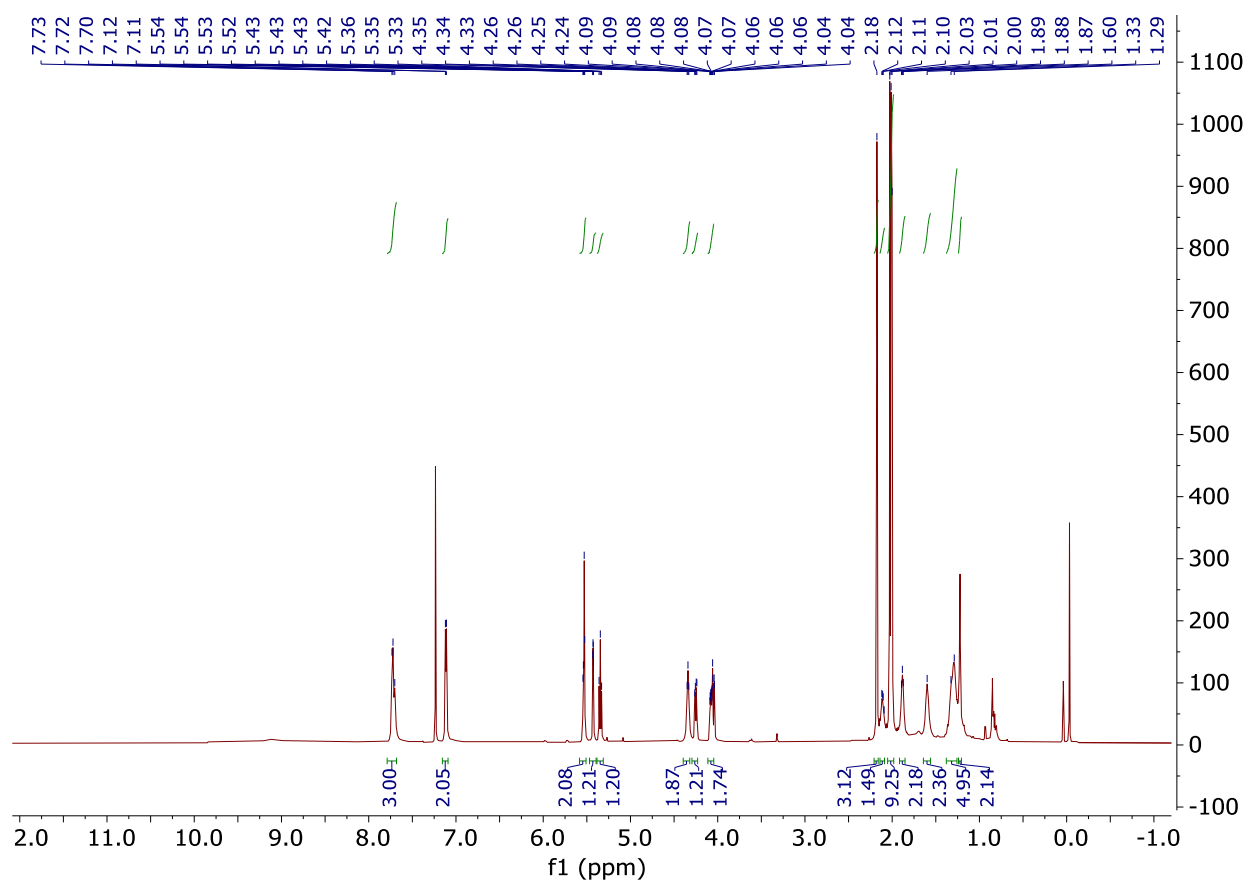
STR-V-157 (^1H)



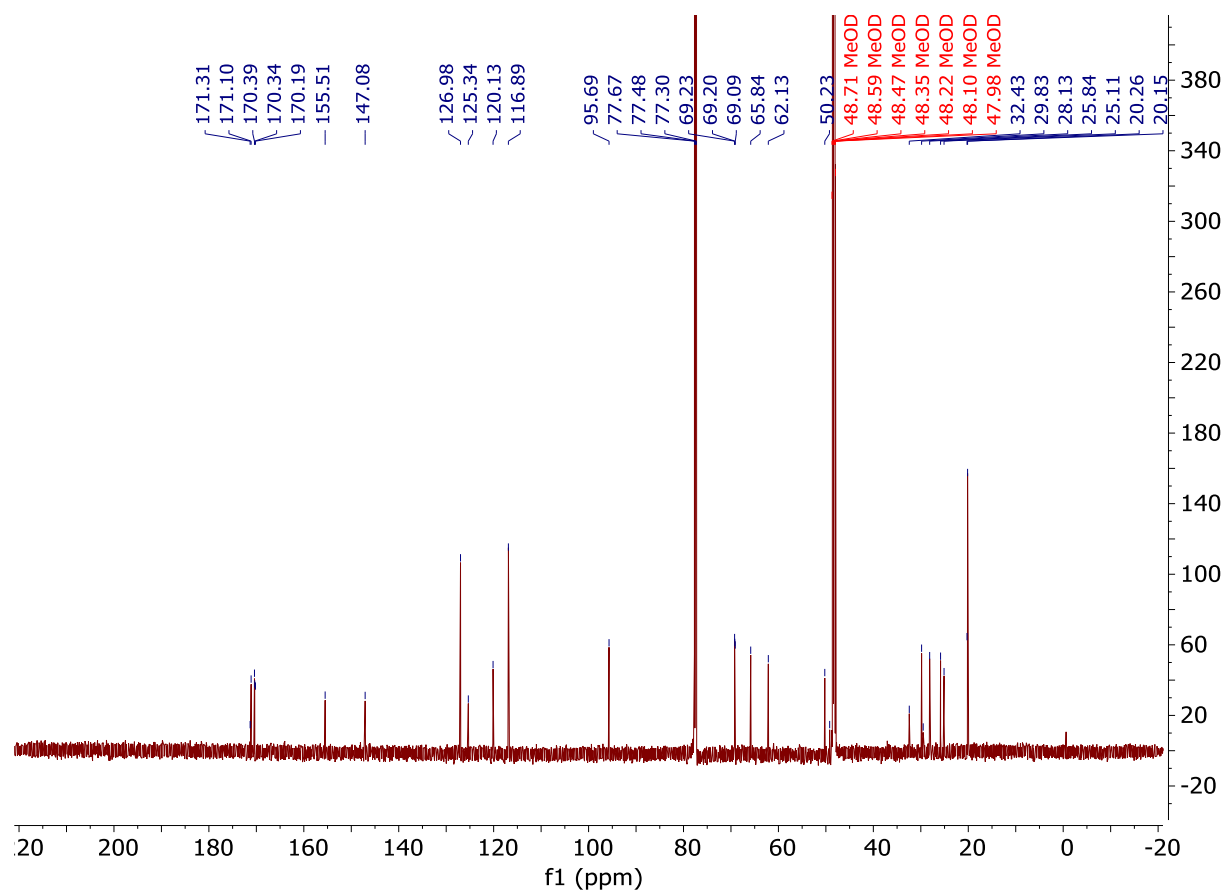
STR-V-157 (^{13}C)



STR-V-176 (^1H)

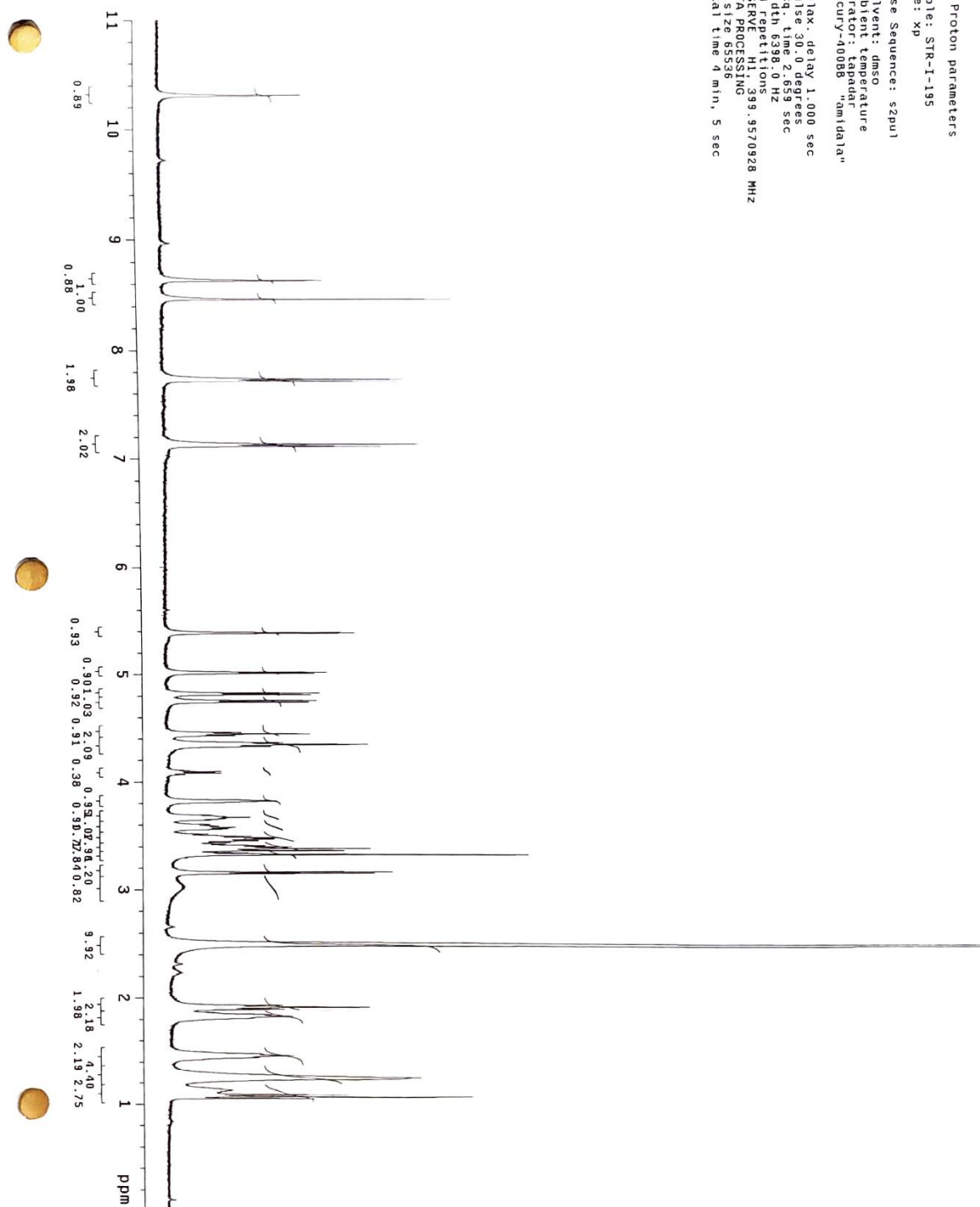


STR-V-176 (^{13}C)

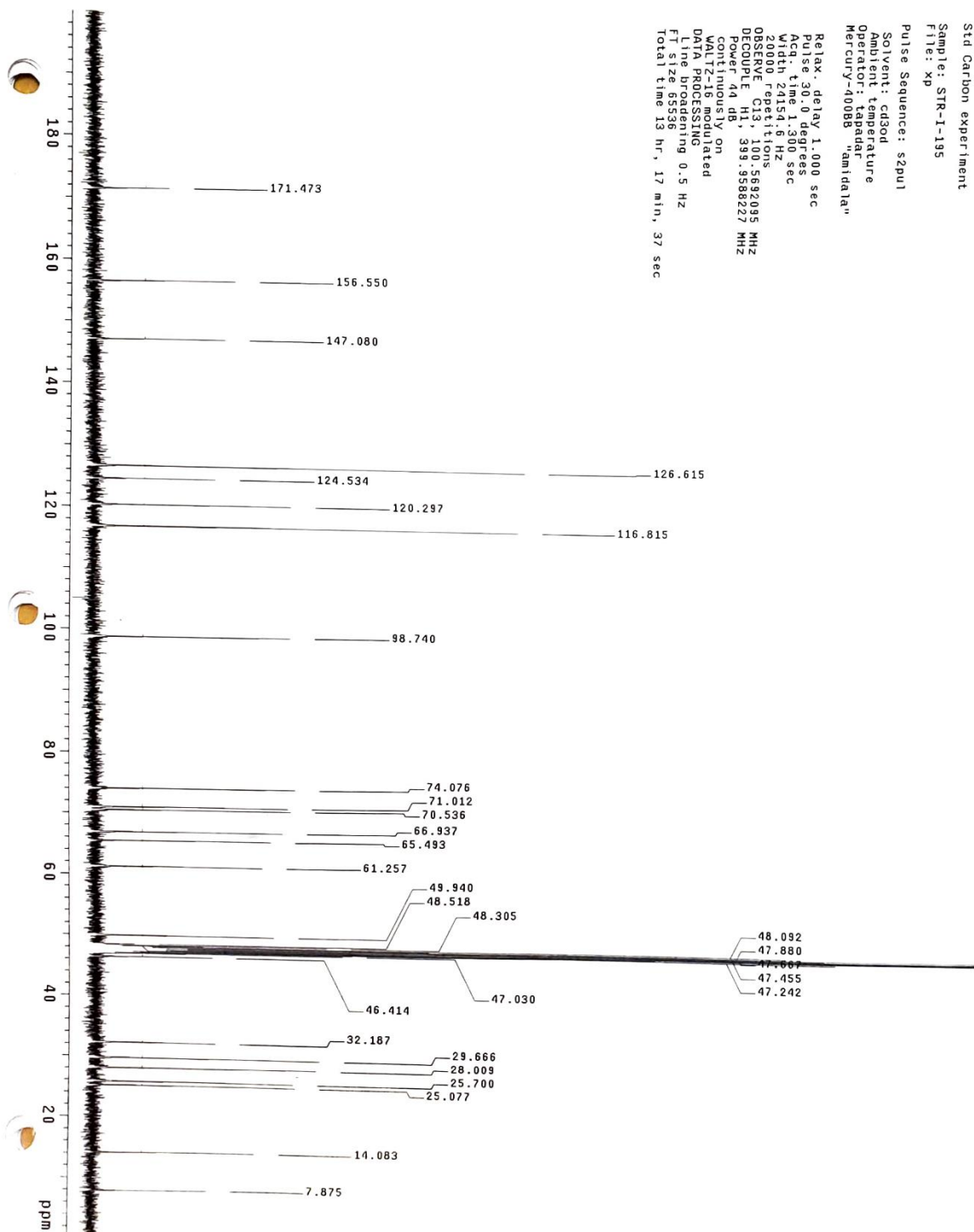


STR-V-195 (¹H)

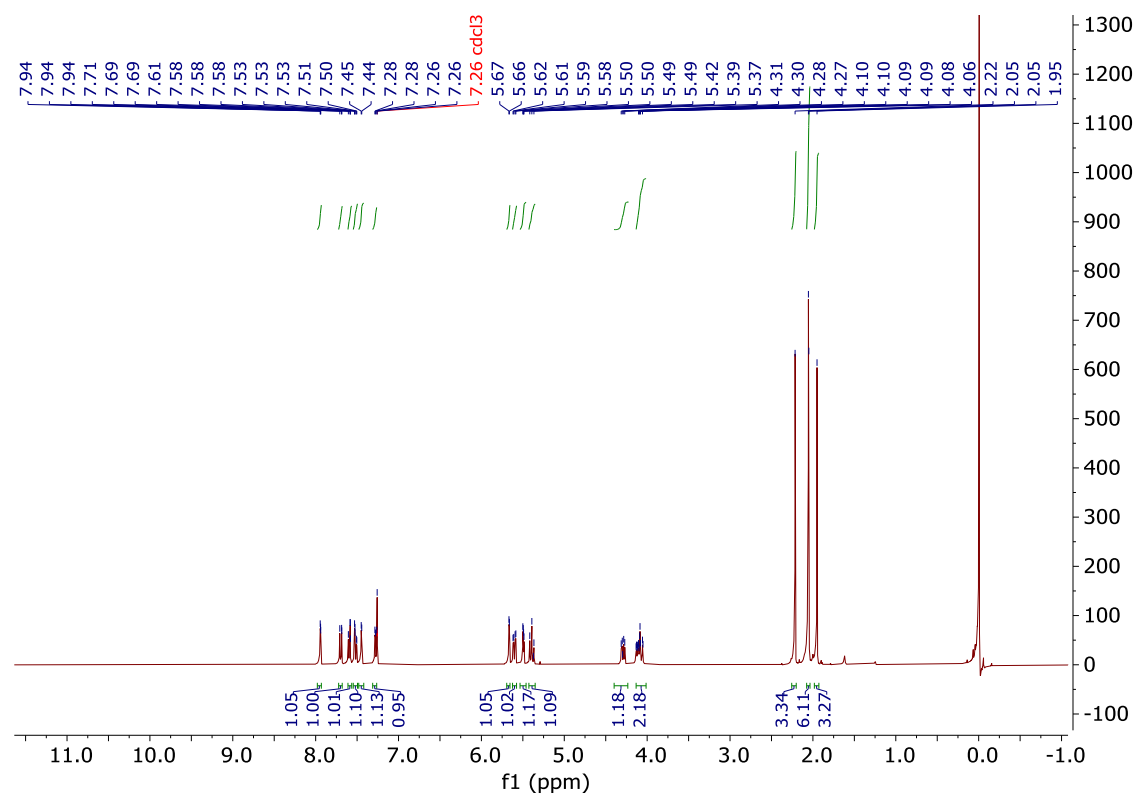
Std Proton parameters
 Sample: STR-I-195
 Title: xp
 Pulse Sequence: szpul
 Solvent: dmsd
 Ambient temperature
 Operator: lapadat
 Mercury-40088 "amidata"
 Relax. delay: 1.000 sec
 Pulse: 30.0 degrees
 Acq. time: 2.659 sec
 Width: 6398.0 Hz
 64 repetitions
 OBSERVE H1: 399.9570928 MHz
 DATA PROCESSING
 FI size: 8536
 Total time: 4 min, 5 sec



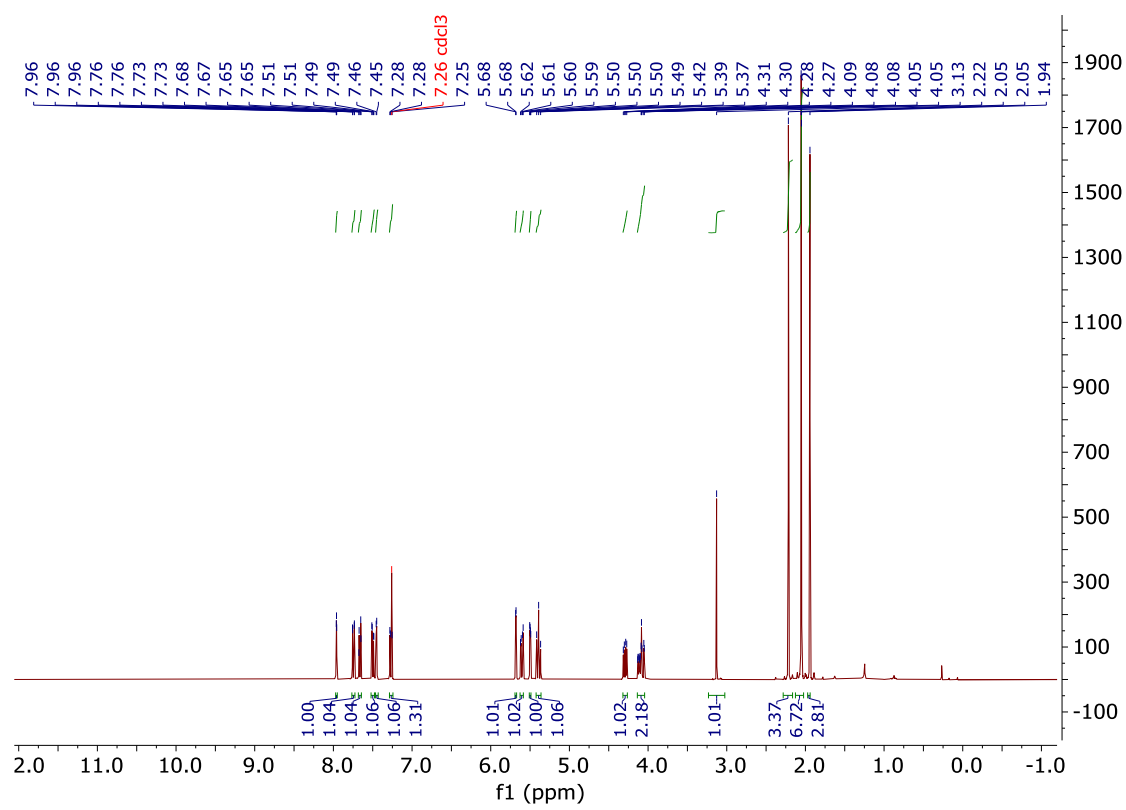
STR-V-195 (¹³C)



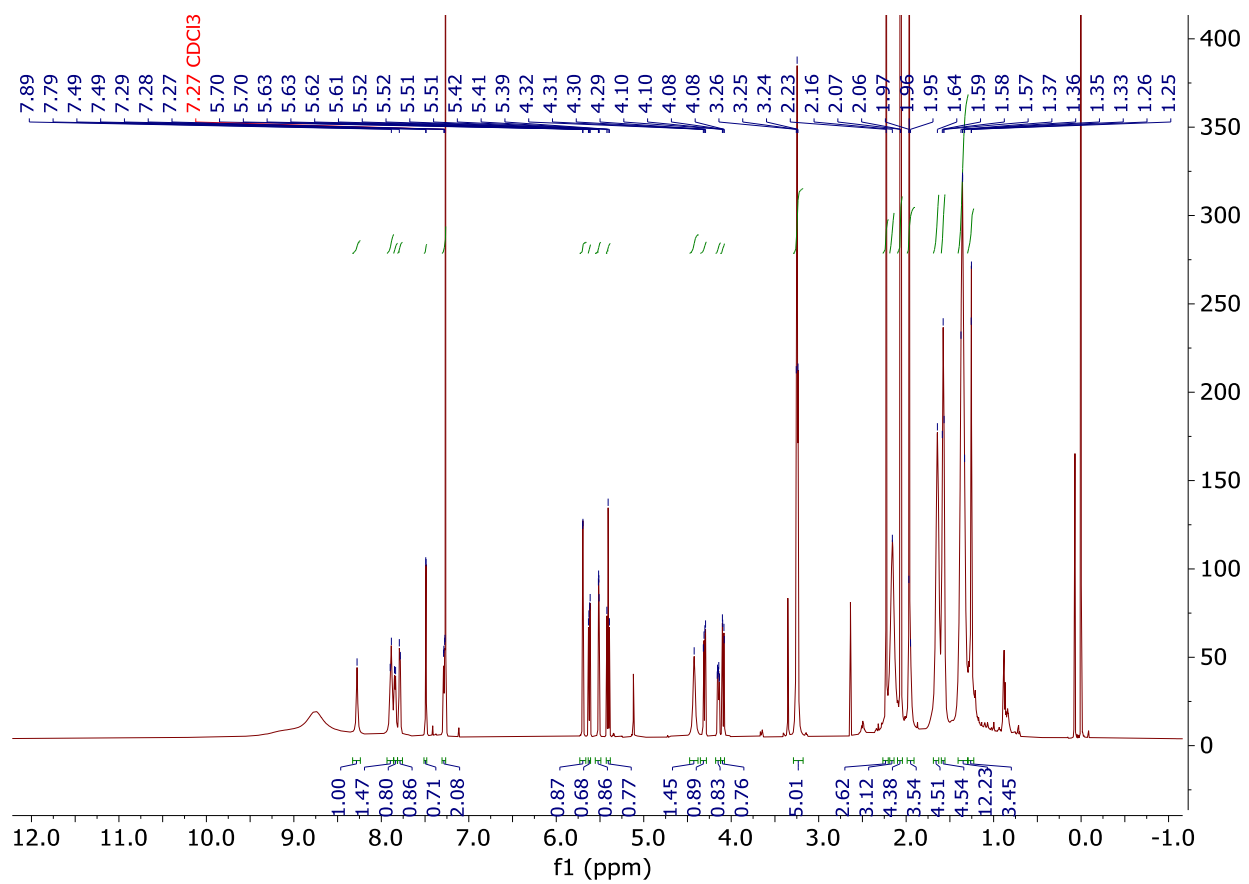
STR-II-30(¹H)



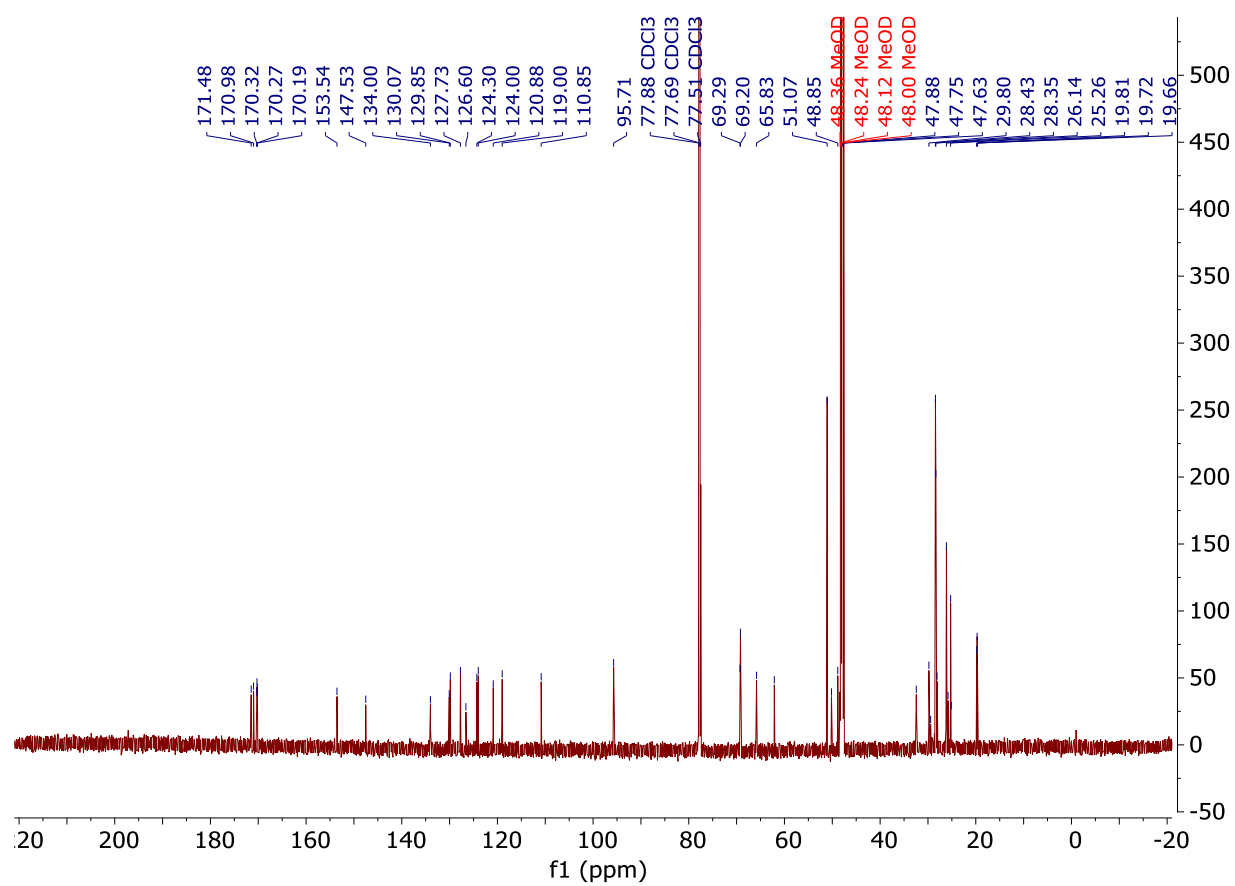
STR-II-34(¹H)



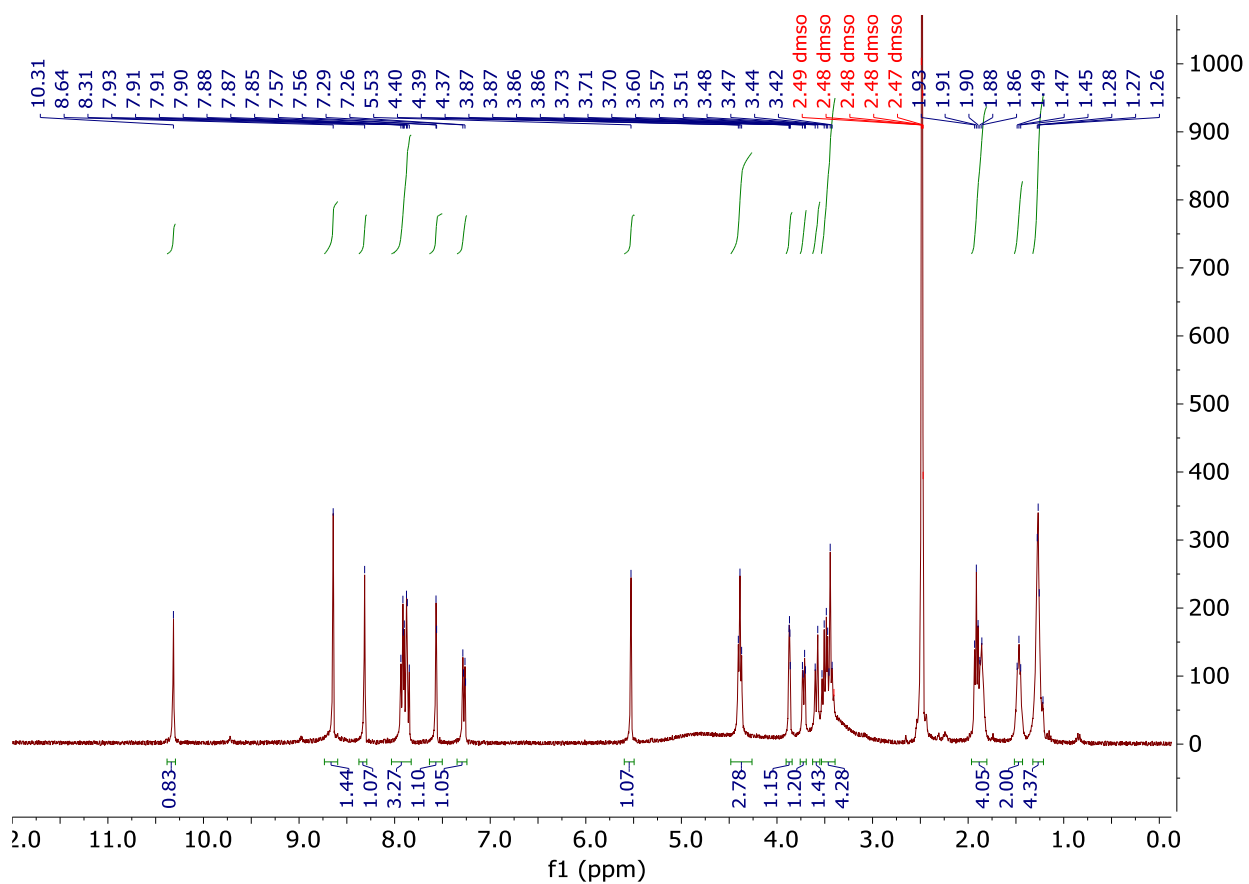
STR-V-177(¹H)



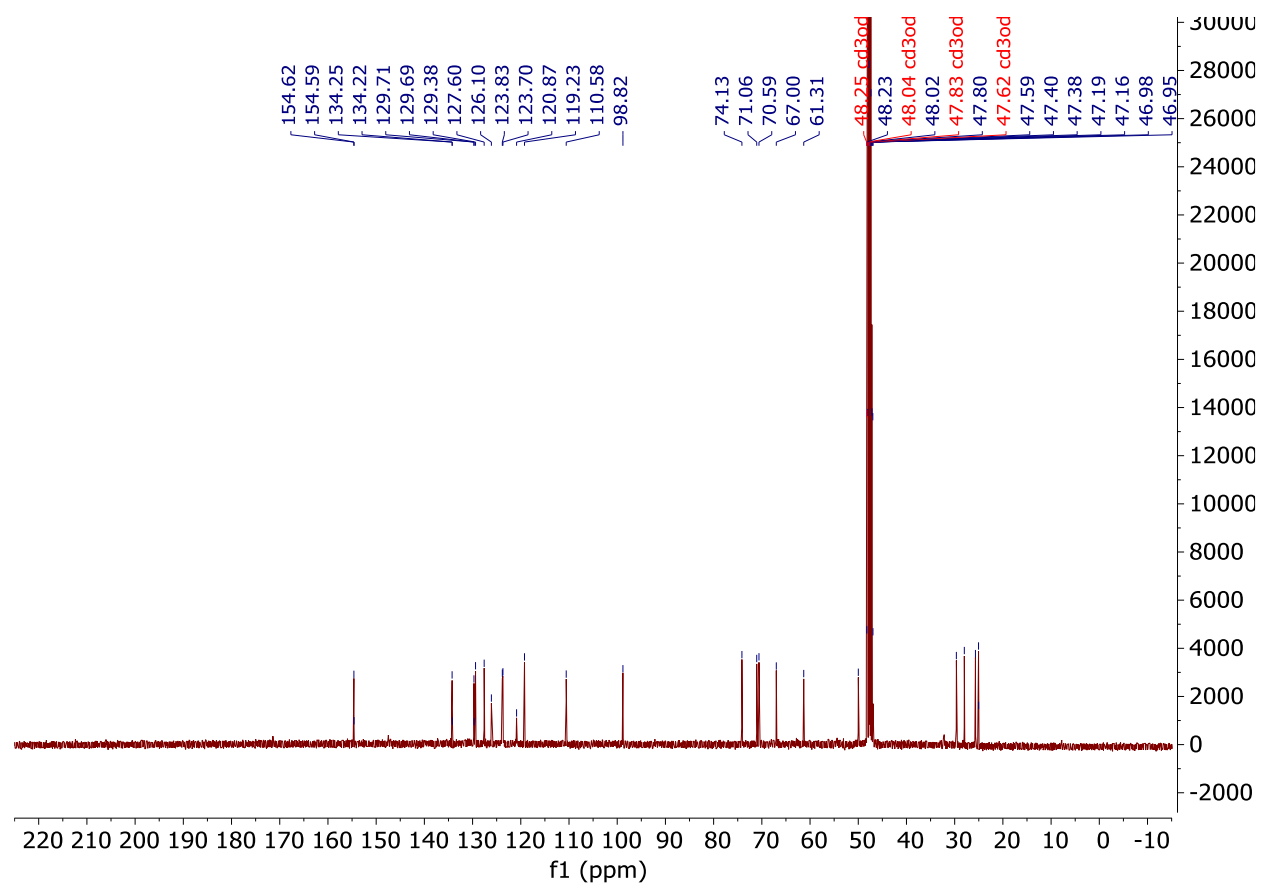
STR-V-177(¹³C)



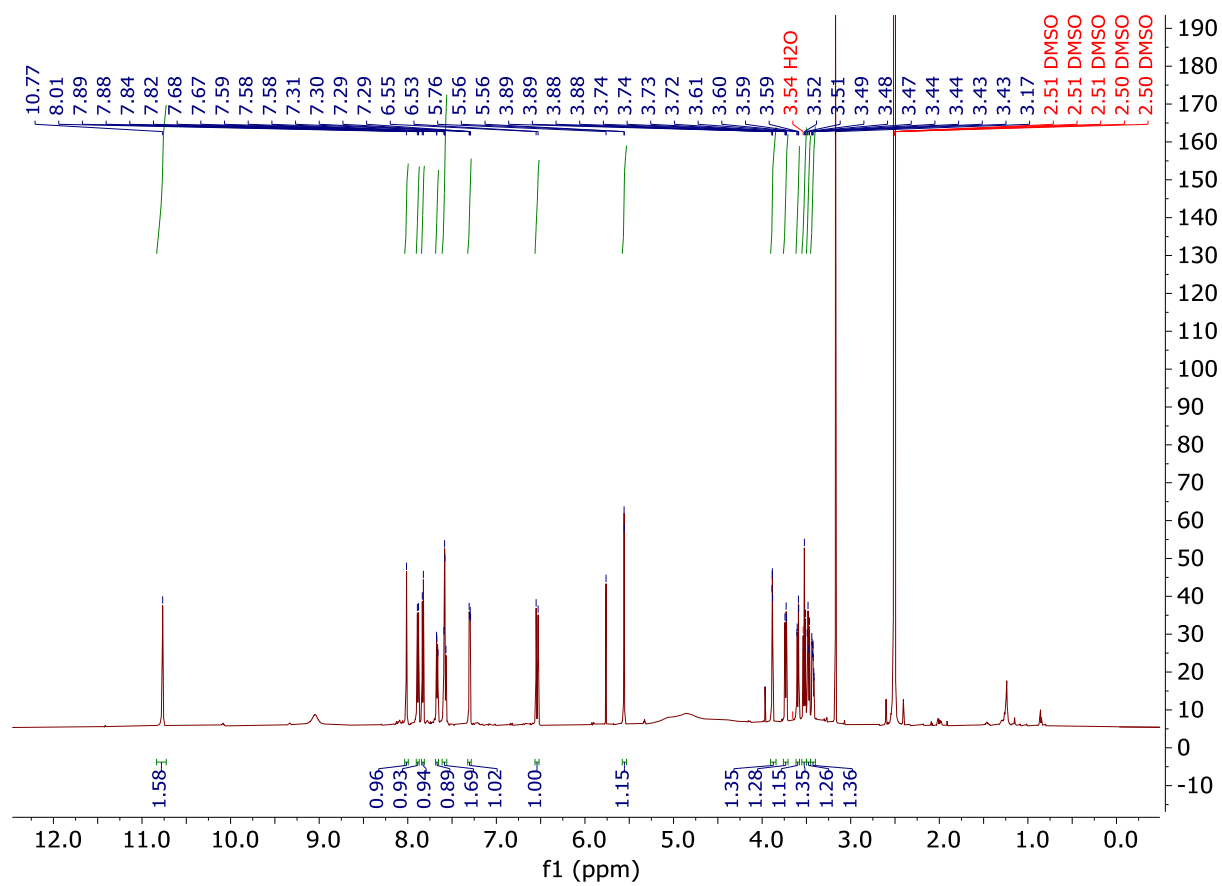
STR-II-36(¹H)



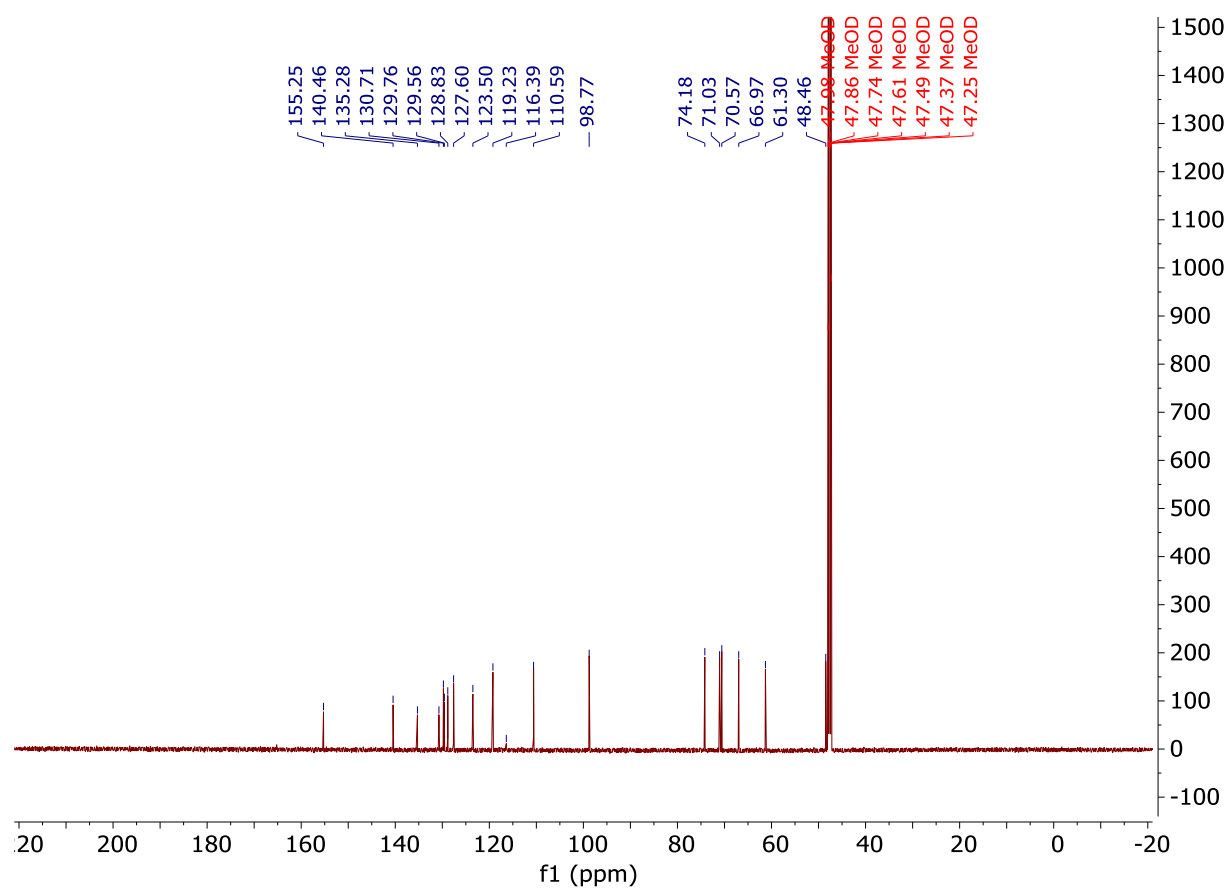
STR-II-36(¹³C)



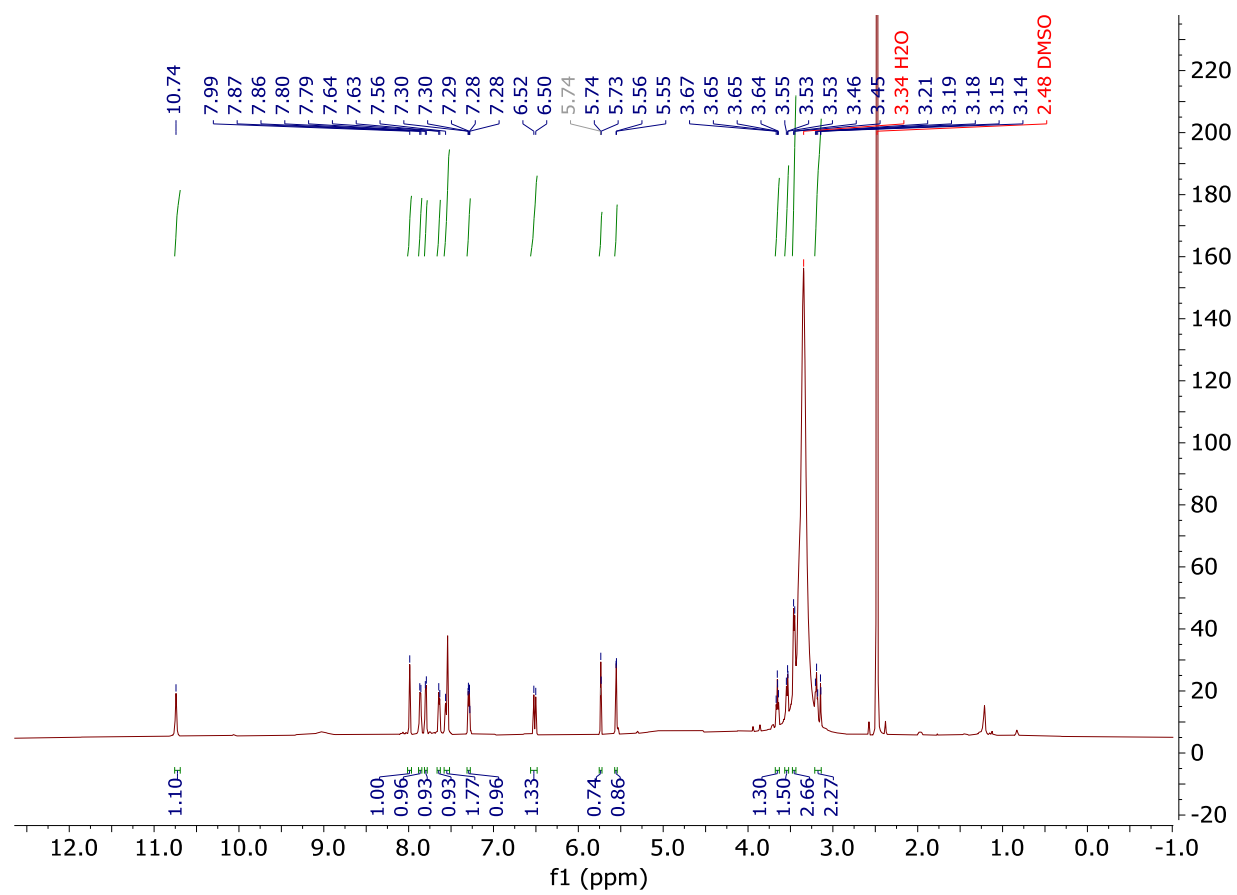
STR-V-105 (¹H)



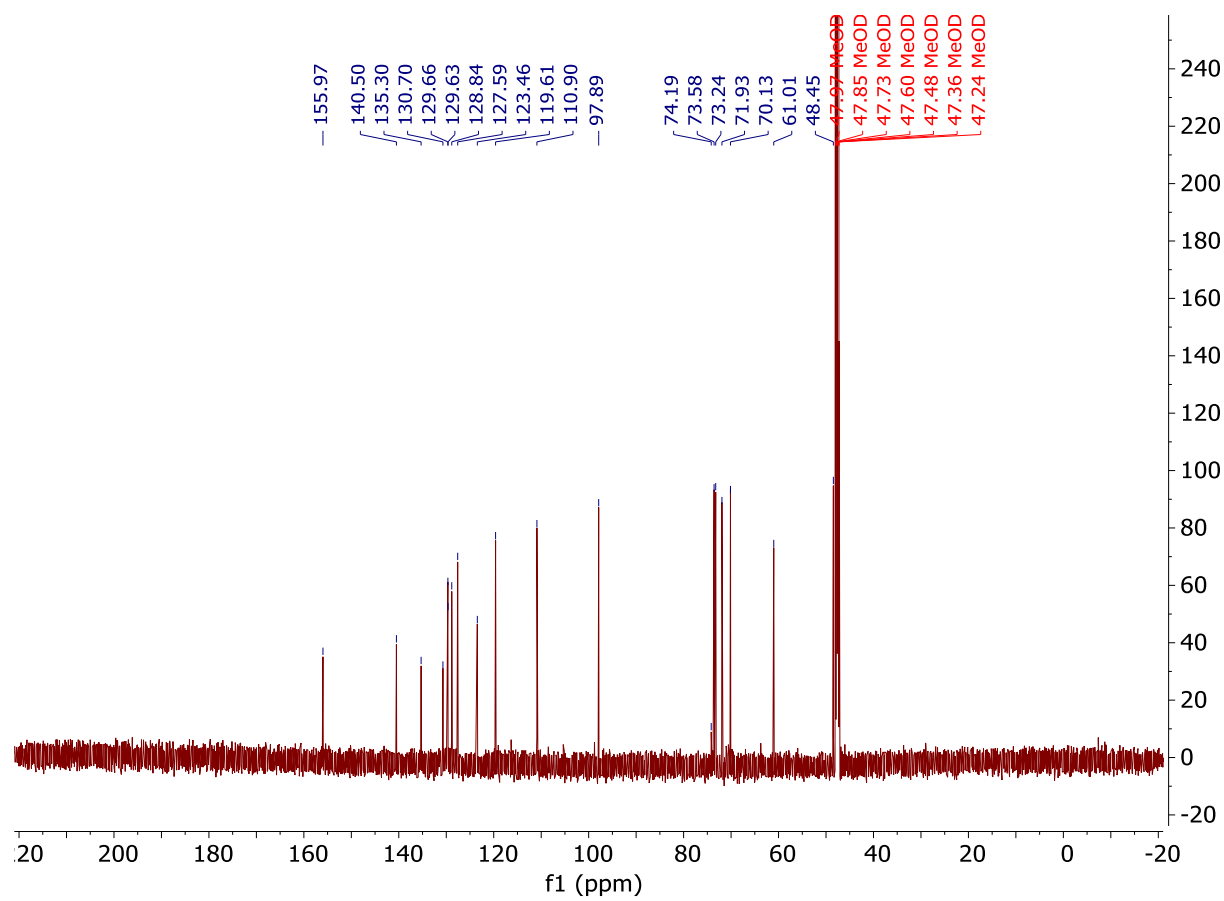
STR-V-105 (^{13}C)



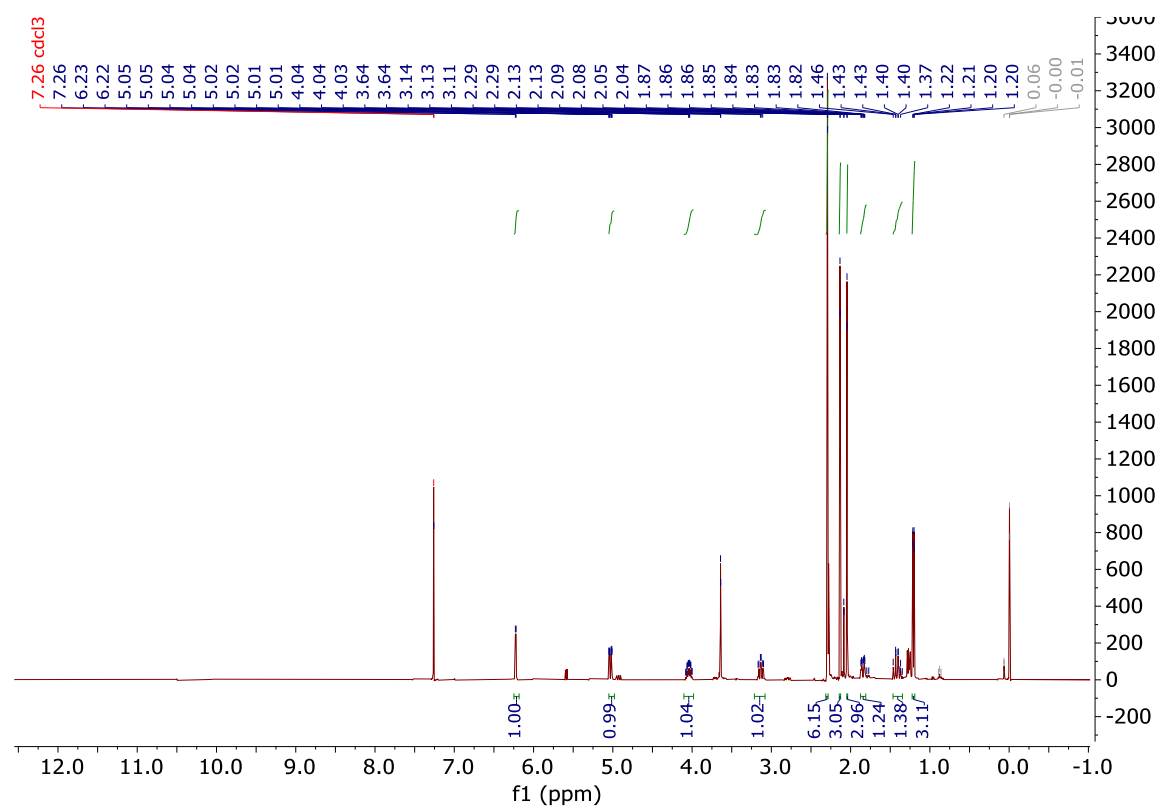
STR-V-115 (^1H)



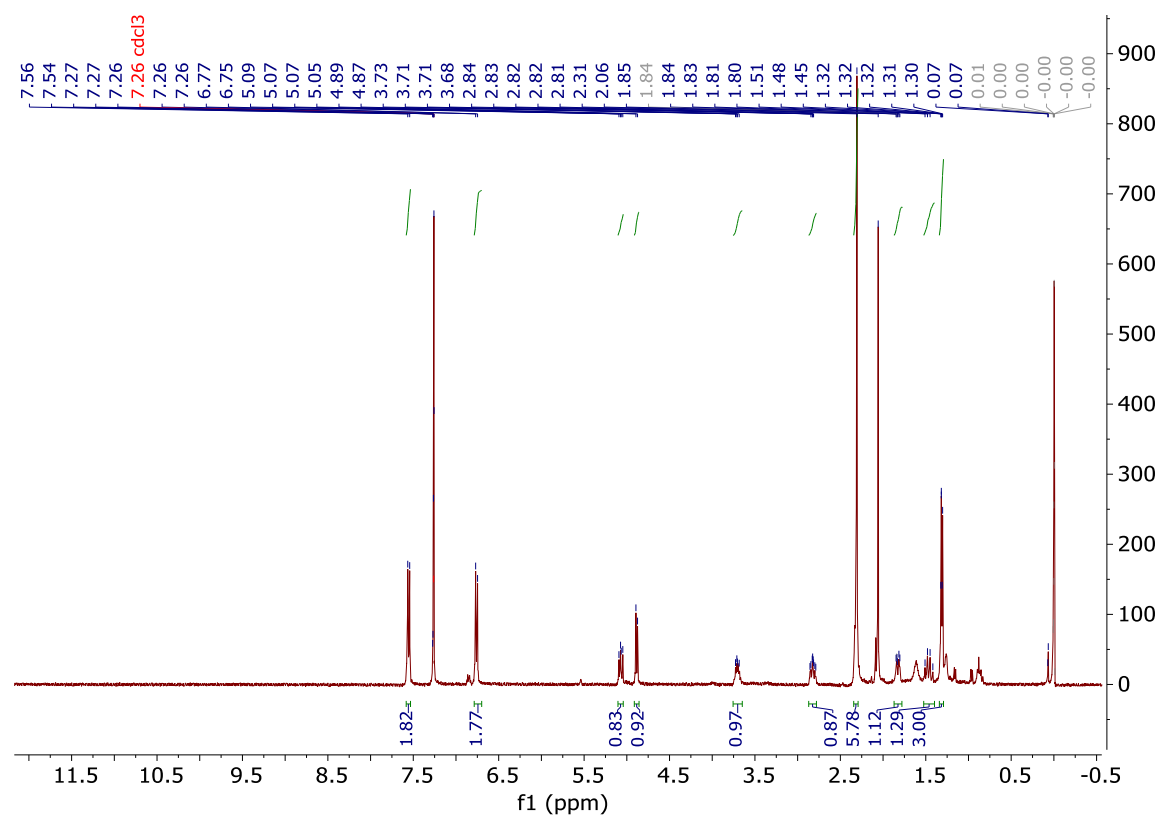
STR-V-115 (^{13}C)



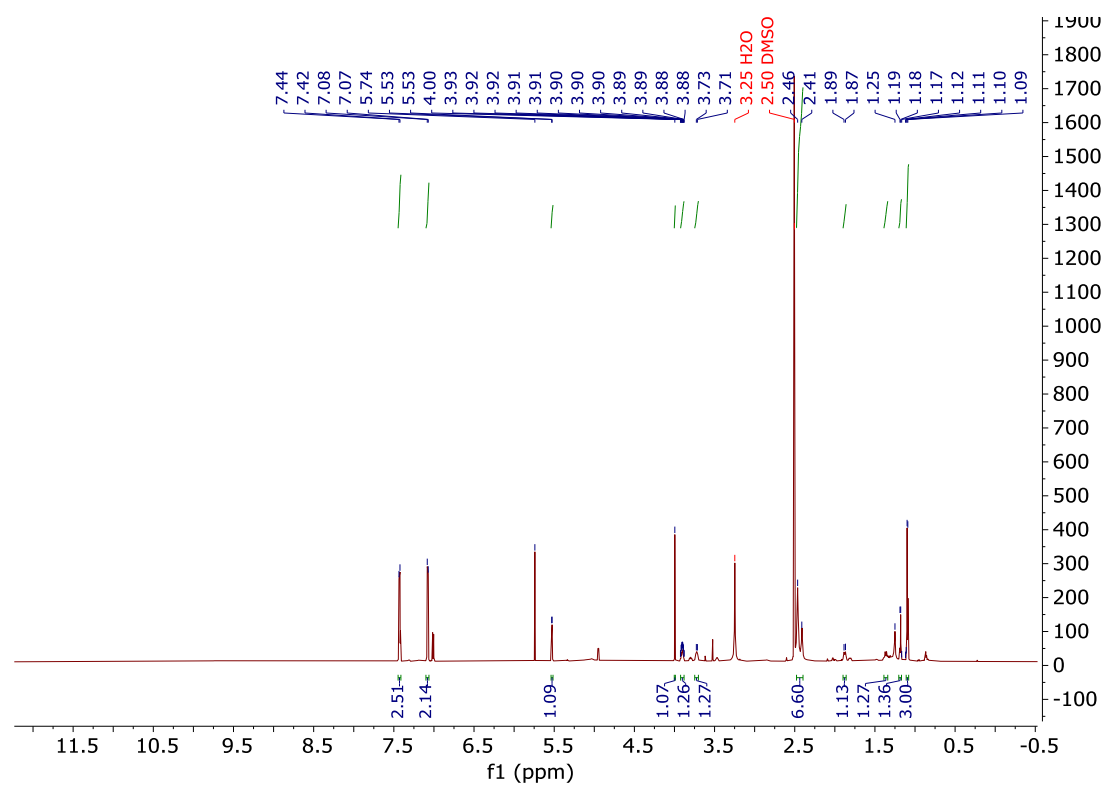
STR-V-160 (¹H)



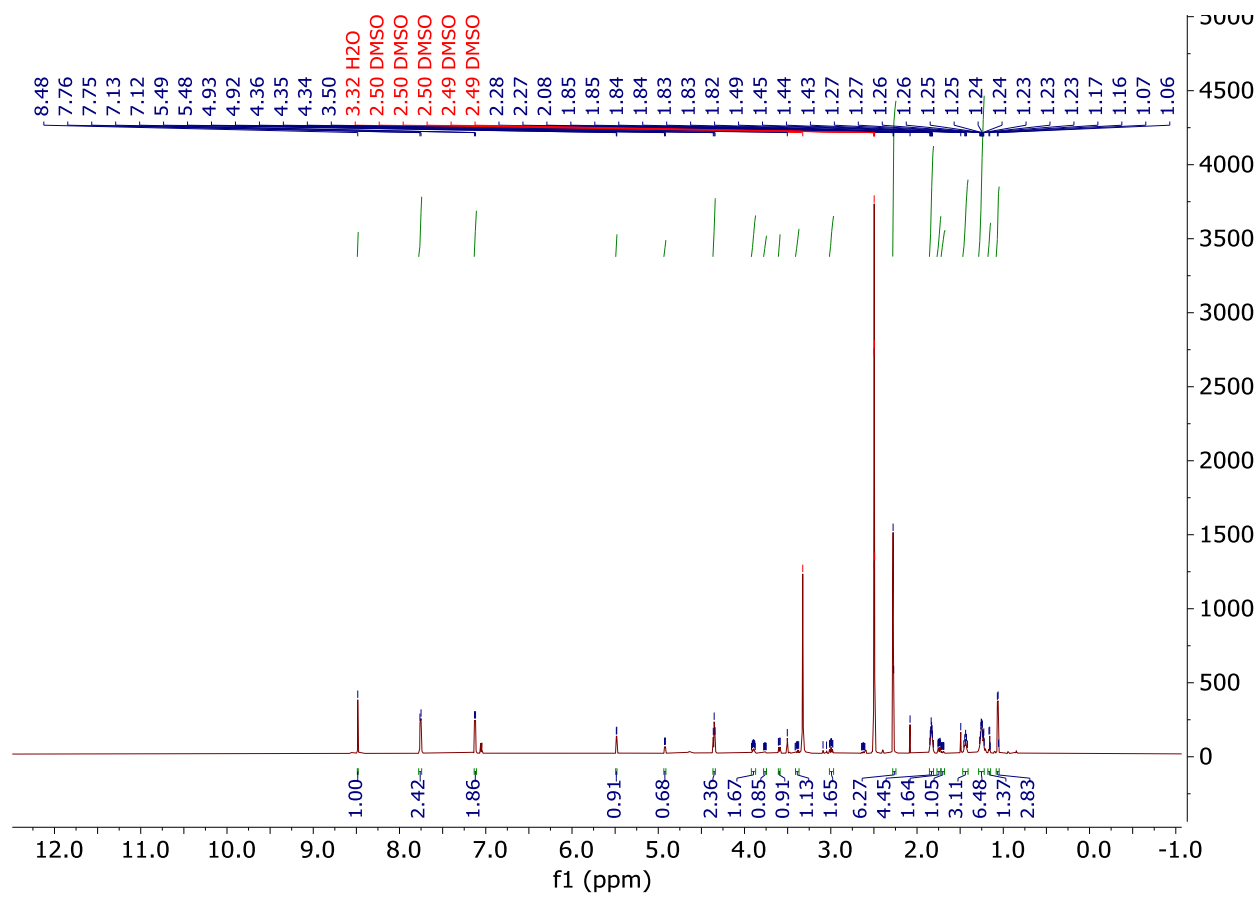
STR-V-161 (^1H)



STR-V-163 (^1H)



STR-V-165 (¹H NMR)



STR-V-165 (¹³C NMR)

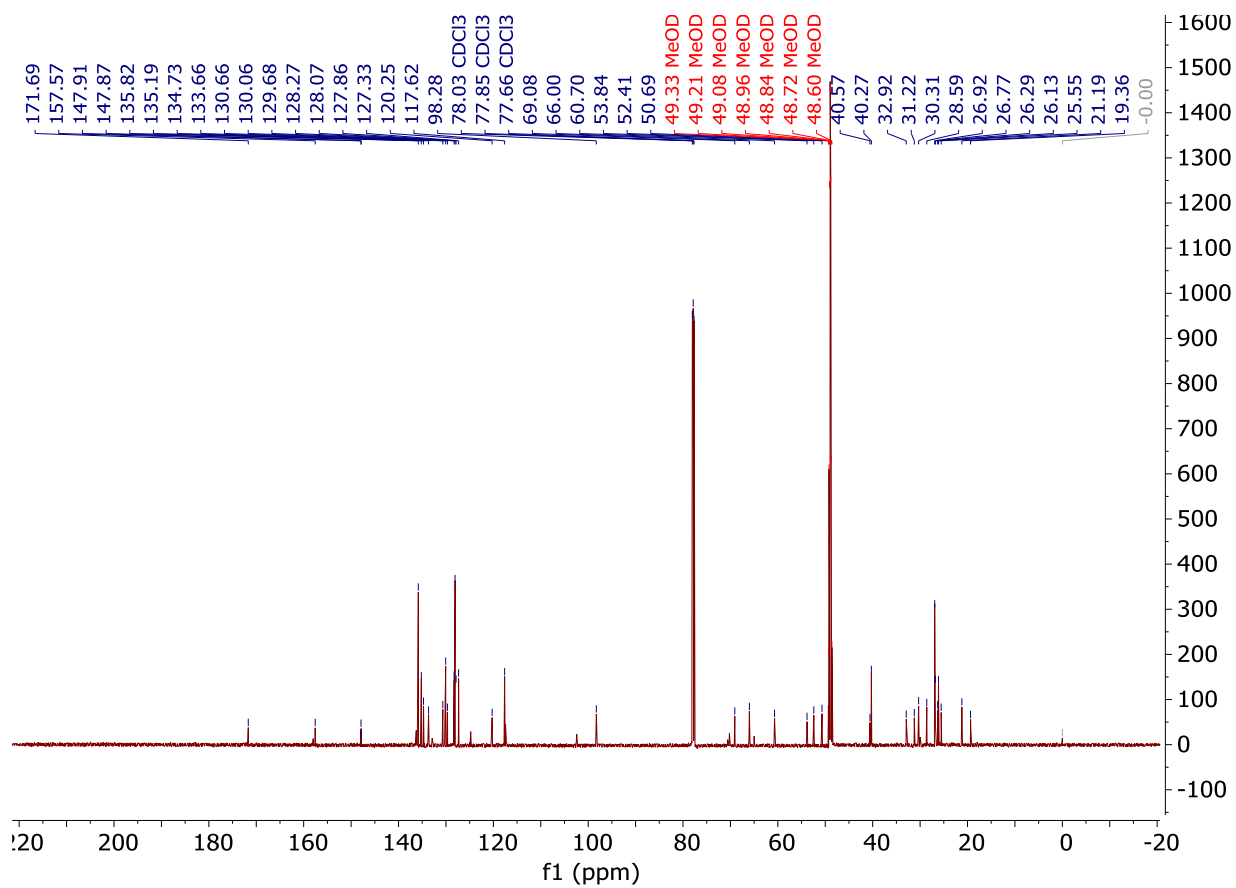
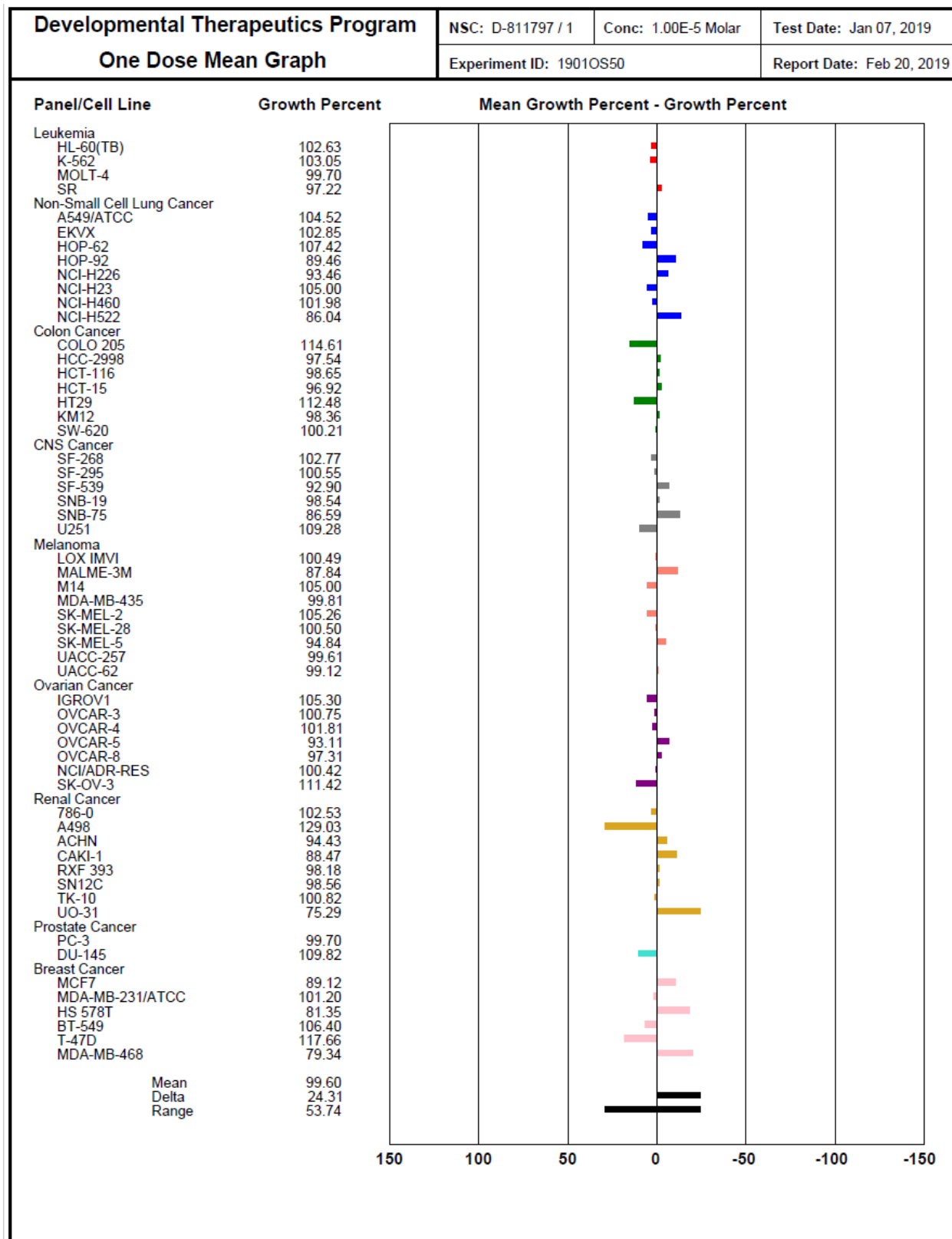


Figure S7. 1. Table of NCI-60 panel of STR-V-53 in 10 μ M dosage screening.



VITA

Bocheng Wu

Scientist/Researcher

Highly skilled medicinal Chemist and Chemical Biologist with a strong educational background and a proven history of innovation and invention, including the drug discovery of novel therapeutic strategies for multiple diseases including tissue fibrosis, inflammation, and cancer. In possession of a unique combination of skills in organic synthesis and biology with 5-year drug discovery experiences.

RESEARCH SUMMARY

Research Goals:

- Drug discovery and modification for tissue inflammatory diseases including Idiopathic pulmonary fibrosis (IPF) and Liver cirrhosis; cancers including Hepatocyte Carcinoma (HCC), Triple Negative Breast Cancer (TNBC), and Prostate cancer (PC); metabolism disorder including diabetes.

Responsibilities:

- Computational drug designs
- Organic synthesis (multi-step modern synthesis strategies)
- Biological tests: *in vitro* bioassays and *in vivo* drug pharmacological profile studies

EDUCATION:

Georgia Institution of Technology (Ph.D. candidate)

Atlanta, GA

Department of Chemistry and Biochemistry

Aug.2015-2021

- Graduation: May 2021 (GPA=3.5)
- Researcher in Dr. Adegboyega K. Oyelere lab

Marquette University (Bachelor Degree)

Milwaukee, WI

Klingler College of Arts and Sciences

Aug. 2011-Dec. 2014

- Bachelor of Science in Chemistry (GPA=3.72)
 - Minor in Mathematics

RELATED EXPERIENCE:

Georgia Tech Chemistry & Biochemistry Department (Ph.D. candidate)

Atlanta, GA

1. Lead for novel anti-fibrotic agents for Idiopathic pulmonary fibrosis (IPF). (*Manuscript in preparation*)
2. Invention of a novel Clarithromycin-derived anti-cancer agent. (*Manuscript in preparation*)
3. Design and invention novel anti-ROS agents for cancer treatment. (*Manuscript in preparation*)

4. Invention of triple negative breast cancer-selective histone deacetylase inhibitors. (Published)
5. Discovery of novel STAT3 inhibitors targeting STAT3 DNA binding domain. (Under Review)
6. Characterization of liver-tissue targeting histone deacetylase inhibitors. (*Published*)
7. Managing and biological investigation of novel indole-based COX-1/2 inhibitors. (*Manuscript in preparation*)
8. Delivery of Virus-Like Particles (VLP) Mediated by Macrolide Antibiotics as drug delivery system. (*Published, collaboration*)
9. Design of novel small molecule Gai2 inhibitors. (*Published, collaboration*)
10. Initiate and design of project on novel TBK1 inhibitors as anti-Diabetes agents. (*Grant submitted*)

Hunan Nucien Pharmaceutical Co., Ltd.

Research scientist (Internship)

Guangzhou, China

Feb, 2015 – Apr, 2015

- Synthesis and purification on anti-allergy compounds

SKILLS

1. Synthesis skills:

- Named synthesis: Sonogashira coupling, Heck coupling, Suzuki coupling, Hoveyda-Grubbs olefin metathesis, Swern Oxidation, Pinnick oxidation, Dess-martin Oxidation, Grignard Reaction, etc.
- Modern synthetic strategies: Heterocyclic synthesis or substitution, acid-base conjugation, Azide-alkyne Huisgen cycloaddition, N- or C- alkylation, Functional group protections and deprotections, etc.
- Modern Purification methods: solvent extraction, Preparative TLC, silica column chromatography, Crystallization, HPLC purification.
- Characterization: Mass spectroscopy, proton and carbon NMR, IR, LC/MS, X-ray crystallography.

2. Biological skills: *in vitro* and *in vivo*

- *In vitro* Target Validation: Western blotting, rtPCR, Bioassay kits
 - Cell cycle studies with use of Cell flowcytometry.
 - Pull-down assay and silver staining for target validation study
 - Experience for *in vivo* studies: Organ harvest, IP injection, Histology and Sectioning on purpose of drug development for PK profile.
3. Professional Academic Software: Prism, Mestrenova, Chemdraw office, Auto-dock Vina, Pyrx, Pymol, Biorender, FlowJo, BD FACSDiva, LI-COR Image Studio.
 4. Lab equipment: HPLC, NMR, GC, UV Spectroscopy, Odyssey Imaging system, PCR, IR spectroscopy.
 5. Editing software: Photoshop, Microsoft offices
 6. Language: English, Chinese.

JOURNAL REVIEWED

- Bioorganic & Medicinal Chemistry 2019-present
- Scientific Report, Nature 2020-present

PROFESSIONAL SOCIETY MEMBERSHIP

ACS trainee member

AACR scholar member

INVITED PRESENTATIONS:

1. Bocheng Wu. 'Pyrimethamine derivatives as novel STAT3 inhibitors disrupt DNA binding and induce cytotoxicity to cancers'. Presented at ACS National meeting 2021. *Poster presentation*
2. Bocheng Wu. 'Novel Macrolide HDACi to suppress Liver cancer tumor growth with HDAC class I selectivity' School of Chemistry and Biochemistry, Annual Retreat. *Oral Presentation*. 2020
3. Bocheng Wu. 'Pyrimethamine derivatives as a novel STAT3 inhibitor' School of Chemistry and Biochemistry Special Summer Seminar Series. *Oral Presentation*. 2020
4. Bocheng Wu. 'HDAC-STAT3 inhibitors that target to Triple Negative Breast Cancer' 2019 Graduate Student Research Symposium. *Poster Presentation*. 2020
5. Bocheng Wu. 'HDAC-STAT3 inhibitors that target to Triple Negative Breast Cancer' Festival of Research Ideas in Cancer Biology and Technology. *Poster Presentation*. 2019
6. Bocheng Wu, Shaghayegh Fathi, Shanee Mortly, Adegboyega Oyelere. *HDAC-STAT3 inhibitors that target to Triple Negative Breast Cancer*. presented at AACR annual meeting. *Poster Presentation*. 2019
7. Bocheng Wu, Stephen N. Crooke, Jiri Schimer, Idris Raji, Adegboyega Oyelere, and M.G. Finn. *Macrolide Mediated Macrophage Uptake of Polymeric Cargoes*. presented at The 70th Southeastern Regional Meeting of American Chemistry Society. *Poster Presentation*. 2018

PEER-REVIEWED JOURNAL PUBLICATIONS:

1. Wu, B., Payero, B., Taylor, S., Oyelere, A. K. (2020). Design, Synthesis, and Biological activities of Novel Pyrimethamine-based DNA Binding Domain STAT3 inhibitors. Under reviewed by *Fut. Med. Chem*
2. Tapadar, S.; Wu, B.; Fathi, S.; Sun, C.Q.; Raji, I.; Moore, S.G.; Arnold, R.S.; Gaul, D.A.; Petros, J.A.; Oyelere, A.K. Liver-Targeting Class I Selective Histone Deacetylase Inhibitors Potently Suppress Hepatocellular Tumor Growth as Standalone Agents. *Cancers* 2020, 12, 3095.
3. Caggia, S., Tapadar, S., Garrett, A., Wu, B., Venugopal, S. V., Garrett, A. S., Kumar, A., Stiffend, J. S., Davis, J. S., Oyelere, A. K., Khan, S. A. Small molecule inhibitors targeting Gai2 protein attenuate migration of cancer cells. *Cancers (Basel)* **2020**, *12*, 1631; doi:10.3390/cancers12061631.
4. Wu, B.; Fathi, S.; Mortley, S.; Mohiuddin, M.; Jang, Y. C.; Oyelere, A. K. Pyrimethamine conjugated histone deacetylase inhibitors: Design, synthesis and evidence

for triple negative breast cancer selective cytotoxicity. *Bioorg. Med. Chem.* **2020**, 28, 115345.

5. Crooke, S. N., Schimer, J., Raji, I., Wu, B., Oyelere, A. K., Finn, M. G. Lung Tissue Delivery of Virus-Like Particles Mediated by Macrolide Antibiotics. *Mol. Pharm.* **2019**, 16, 2947-2955.
-

Teaching Experience

2015-2021

- General Chemistry (Chem 1310)
- General Chemistry (Chem 1211K, Chem 1212K)
- Biochemistry I and II (Chem 4511, Chem 4512)
- Survey of Biochemistry (Chem3511-A)
- Organic Synthesis lab (Chem 2380)

Mentorship (Undergraduate research mentor)

- Shanee Mortley (*in vitro* study) 2017 fall- 2018 Summer
 - Oludamilola T Taiwo (Organic Synthesis) 2018 Summer and Fall
 - Sara Zimmerman (*in vitro* study) 2018 Summer
 - Benny Payero (Organic Synthesis) 2019 Spring and Fall, 2020 Spring
 - Kate Bullock (*in vitro* study) 2019 Spring and Summer
 - Hassan Asif (*in vitro* study and Virtual screening) 2019 Fall to 2020 Spring
 - Mikhil Patel (Organic Synthesis and Virtual Screening) 2019 Fall
 - Justin P. Keener (Drug design) 2020 Fall
 - Andrew W. Frazier (Drug design) 2020 Fall
-

HONORS & AWARDS

- Winner of 2021 Suddath Honorable Mention Award Dec. 2020
- Winner of 2020 ATCC innovative Challenge Dec. 2020
- Winner of Merck Index Award for Top Undergraduate chemistry senior May 2014
- The Best Competitor of Undergraduate Research Presentation Competition May 2014
- Dean's List Recipient fall 2011, spring 2012, fall 2013, spring 2014
- Ignatius Academic Scholarship 2011-2014